

Dear Aunt Julia Garcia

# **TRANSPORT PHENOMENA in MATERIALS PROCESSING**

2710

D.R. Poirier  
G.H. Geiger

A Publication of  
**TMS**  
Minerals • Metals • Materials

660.24  
P674

## PREFACE

A Publication of The Minerals, Metals & Materials Society

420 Commonwealth Drive  
Warrendale, Pennsylvania 15086  
(412) 776-9000

The Minerals, Metals & Materials Society is not responsible for statements or opinions and is absolved of liability due to misuse of information contained in this publication.

Printed in the United States of America  
Library of Congress Catalog Number 94-76335  
ISBN Number 0-87339-272-4

Authorization to photocopy items for internal or personal use, or the internal or personal use of specific clients, is granted by The Minerals, Metals & Materials Society for users registered with the Copyright Clearance Center (CCC) Transactional Reporting Service, provided that the base fee of \$3.00 per copy is paid directly to Copyright Clearance Center, 27 Congress Street, Salem, Massachusetts 01970. For those organizations that have been granted a photocopy license by Copyright Clearance Center, a separate system of payment has been arranged.

**TMS**  
Minerals • Metals • Materials

© 1994

If you are interested in purchasing a copy of this book, or if you would like to receive the latest TMS publications catalog, please telephone 1-800-759-4867.

*Transport Phenomena in Metallurgy* was published more than twenty years ago. The need then was to provide a textbook on transport phenomena (momentum, heat, and mass transport) with metallurgical pedagogy. Many academic programs in metallurgy and metallurgical engineering have since evolved to programs in materials science and engineering, but the need to include transport phenomena in the curricula still remains. Indeed, the importance of transport phenomena in curricula is probably greater today than it was in the early seventies for two reasons: (1) the recognition of the importance of materials processing and synthesis, and (2) the increasing use of sophisticated softwares to simulate materials processes. We hope, therefore, that this textbook provides a teachable and readable approach to transport phenomena and then goes further by providing numerous examples and applications, which are particularly important to metallurgical, ceramic, and materials engineers.

Like its predecessor, this textbook has been designed to utilize the mathematical abilities of upper-class engineering students. In particular, students in materials related programs have studied integral and differential calculus, but often make little use of it again, except in rather trivial applications. Since one can proceed quite a way into the field of transport phenomena without resorting to higher-level mathematics, and because we think that it is important for students and practicing engineers to visualize the physical situations, we have attempted to lead the readers through the development and solution of the relevant differential equations by applying the familiar principles of conservation to numerous situations and by including many worked examples in each chapter. We hope that readers with good mathematical abilities will not feel that we are being condescending but will realize that we have tried to make transport phenomena understandable to a group as large as possible. Also, because of the increased availability of computing power and software utilizing numerical methods to solve the differential equations with more realistic boundary conditions, we believe that it is even more important to be able to recognize and define the problem than to analytically solve a specific equation with the usual attendant limitations on boundary conditions.

The book is organized in a manner characteristic of other texts in transport phenomena. Section I deals with the properties and mechanics of fluid motion; Section II with thermal properties and heat transfer; and Section III with diffusion and mass transfer. We depart from the tradition, however, in that we build on a presumed understanding of the

relationships between the structure and properties of matter, particularly in the chapters devoted to the transport properties (viscosity, thermal conductivity, and diffusion coefficients). In addition, generous portions of the text, numerous examples, and many problems at the ends of the chapters apply transport phenomena to materials processing. Those familiar with *Transport Phenomena in Metallurgy* will see a large carry-over to this textbook. The major and perhaps most welcome change is the use of S.I. units. In a few instances, there are compelling reasons to maintain non-S.I. units, but lest the modern student lose heart we explain our reasons and present the relevant unit conversions. The problem sets have been greatly expanded, which should provide a more than an adequate supply of instructional fodder to build on the reading in the individual chapters. We added a concluding chapter entitled Numerical Methods and Models to serve as a bridge between this textbook and books intended for advanced study and, indeed, for the practice of materials engineering. One chapter from *Transport Phenomena in Metallurgy* was completely eliminated, and all other chapters and the Appendices have been extensively revised to make this textbook an introduction to *materials processing*.

We emphasize that the book is not intended to be a comprehensive review of all the applications and current research in the field. Its aim is rather to present the basic equations and show how they can be applied to a variety of topics, thereby preparing the readers to make use of transport phenomena and to understand and interpret the current literature in the field. We also hope that the book will be useful to those who are already active in seeking better ways to engineer materials processes.

February 1994

David R. Poirier  
Gordon H. Geiger

We express our sincere thanks to Merton Flemings and Morris Cohen of M.I.T. for always rising as champions of materials processing within the materials science and engineering community and for their encouragement to redo *Transport Phenomena in Metallurgy* into the present book. Publication of the manuscript by 'The Minerals, Metals and Materials Society (TMS)' was recommended by the Publication Committee of TMS, under the Chairmanship of Gary Warren of the University of Alabama-Tuscaloosa. We thank the Committee for its endorsement, and Robert Makowski, Wendy McCalip, and the entire publications staff of TMS for working with us on this project.

The text for the manuscript was typed by Patricia Broyles and the illustrations were done by Alison Habel, James Abbot, Patricia Broyles, and Robert Erdmann, all at the University of Arizona. As a "fill-in," one of the authors (DRP) made some of the illustrations with help from Mary Cromwell. We are very grateful that these good people shared their talents with us.

The manuscript readers were Kathryn Soie of the Council of Mineral Technology in South Africa (formerly of the University of Arizona) and Ernest Poirier, a consultant to the metals casting industry and brother of DRP from Gales Ferry, Connecticut. They pointed out many computational errors and typos, and provided ways of improving both the text and problem statements. We are very grateful that they participated so diligently in our undertaking. It was wonderful working with them and knowing that at least two other people have read this book.

## CONTENTS

---

### PART 1 FLUID DYNAMICS

#### **Chapter 1 Viscous Properties of Fluids**

1.1	Types of fluid flow . . . . .	3
1.2	Newtonian fluids . . . . .	4
1.3	Viscosity of gases . . . . .	7
1.4	Viscosity of liquids . . . . .	13
1.5	Non-Newtonian fluids . . . . .	29

#### **Chapter 2 Laminar Flow and the Momentum Equation**

2.1	Momentum balance . . . . .	39
2.2	Flow of a falling film . . . . .	40
2.3	Fully developed flow between parallel plates . . . . .	44
2.4	Fully developed flow through a circular tube . . . . .	46
2.5	Equation of continuity and the momentum equation . . . . .	50
2.6	The momentum equation in rectangular and curvilinear coordinates . . . . .	56
2.7	Application of Navier-Stokes' equation . . . . .	62

#### **Chapter 3 Turbulent Flow and Complex Flows**

3.1	Friction factors for flow in tubes . . . . .	76
3.2	Flow in noncircular conduits . . . . .	81
3.3	Flow past submerged bodies . . . . .	82
3.4	Flow through porous media . . . . .	90
3.5	Fluidized beds . . . . .	101

4.1 Conservation of energy . . . . .	113
4.2 Friction losses in straight conduits . . . . .	117
4.3 Enlargement and contraction . . . . .	119
4.4 Flow through valves and fittings . . . . .	122
4.5 Flow through smooth bends and coils . . . . .	123
4.6 Flow measurement . . . . .	124
4.7 Flow from ladles . . . . .	131
4.8 Flow through piping networks . . . . .	135

**Chapter 5 Flow and Vacuum Production**

5.1 Pumps . . . . .	145
5.2 Fans and blowers . . . . .	151
5.3 Interactions between fans or pumps and systems . . . . .	154
5.4 Supersonic nozzles and jet behavior . . . . .	158
5.5 Vacuum production . . . . .	166

**PART 2 ENERGY TRANSPORT****Chapter 6 Fourier's Law and Thermal Conductivity of Materials**

6.1 Fourier's law and thermal conductivity . . . . .	187
6.2 Thermal conductivity of gases . . . . .	190
6.3 Thermal conductivity of solids . . . . .	191
6.4 Thermal conductivity of liquids . . . . .	193
6.5 Thermal conductivity of bulk materials . . . . .	203
7.1 Heat transfer with forced convection in a tube . . . . .	219
7.2 Heat transfer with laminar forced convection over a flat plate . . . . .	224
7.3 Heat transfer with natural convection . . . . .	228
7.4 Heat conduction . . . . .	233
7.5 The general energy equation . . . . .	236
7.6 The energy equation in rectangular and curvilinear coordinates . . . . .	240

**Chapter 7 Heat Transfer and the Energy Equation**

9.1 The energy equation for conduction . . . . .	281
9.2 Steady-state one-dimensional systems . . . . .	282
9.3 Transient systems, finite dimensions . . . . .	288
9.4 Transient conditions, infinite and semi-infinite solids . . . . .	304
9.5 Simple multidimensional problems . . . . .	312
9.6 Moving sources . . . . .	315
10.1 Solidification in sand molds . . . . .	329
10.2 Solidification in metal molds . . . . .	334
10.3 Continuous casting . . . . .	350
10.4 Crystal growth . . . . .	355
11.1 Basic characteristics . . . . .	369
11.2 The black radiator and emissivity . . . . .	370
11.3 The energy distribution and the emissive power . . . . .	372
11.4 Gray bodies and absorptivity . . . . .	378
11.5 Exchange between infinite parallel plates . . . . .	378
11.6 View factors . . . . .	381
11.7 Electric circuit analog . . . . .	386
11.8 Furnace enclosures . . . . .	390
11.9 Radiation combined with convection . . . . .	395
11.10 Radiation from gases . . . . .	398
11.11 Enclosures filled with radiating gas . . . . .	402
11.12 Radiation in transparent solids . . . . .	404
11.13 Transient conduction with radiation at the surface . . . . .	407
11.14 Transient heating with thermal stresses . . . . .	409
12.1 Definition of fluxes—Fick's first law . . . . .	419
12.2 Diffusion in solids . . . . .	420
12.3 Diffusion in ceramic materials . . . . .	435
12.4 Diffusion in elemental semiconductors . . . . .	442
12.5 Diffusion in liquids . . . . .	444
12.6 Diffusion in gases . . . . .	453
12.7 Diffusion through porous media . . . . .	457
8.1 Heat transfer coefficients for forced convection in tubes . . . . .	248
8.2 Heat transfer coefficients for forced convection past submerged objects . . . . .	254
8.3 Heat transfer coefficients for natural convection . . . . .	258
8.4 Quenching heat transfer coefficients . . . . .	262
8.5 Heat transfer coefficients in fluidized beds . . . . .	268
8.6 Heat transfer coefficients in packed beds . . . . .	272
8.7 Heat transfer coefficients in forging . . . . .	274

**Chapter 9 Conduction of Heat in Solids**

9.1 The energy equation for conduction . . . . .	281
9.2 Steady-state one-dimensional systems . . . . .	282
9.3 Transient systems, finite dimensions . . . . .	288
9.4 Transient conditions, infinite and semi-infinite solids . . . . .	304
9.5 Simple multidimensional problems . . . . .	312
9.6 Moving sources . . . . .	315

**Chapter 10 Solidification of Metals**

10.1 Solidification in sand molds . . . . .	329
10.2 Solidification in metal molds . . . . .	334
10.3 Continuous casting . . . . .	350
10.4 Crystal growth . . . . .	355

**Chapter 11 Radiation Heat Transfer**

11.1 Basic characteristics . . . . .	369
11.2 The black radiator and emissivity . . . . .	370
11.3 The energy distribution and the emissive power . . . . .	372
11.4 Gray bodies and absorptivity . . . . .	378
11.5 Exchange between infinite parallel plates . . . . .	378
11.6 View factors . . . . .	381
11.7 Electric circuit analog . . . . .	386
11.8 Furnace enclosures . . . . .	390
11.9 Radiation combined with convection . . . . .	395
11.10 Radiation from gases . . . . .	398
11.11 Enclosures filled with radiating gas . . . . .	402
11.12 Radiation in transparent solids . . . . .	404
11.13 Transient conduction with radiation at the surface . . . . .	407
11.14 Transient heating with thermal stresses . . . . .	409

**PART III MASS TRANSPORT****Chapter 12 Interphase Mass Transfer**

12.1 Definition of fluxes—Fick's first law . . . . .	419
12.2 Diffusion in solids . . . . .	420
12.3 Diffusion in ceramic materials . . . . .	435
12.4 Diffusion in elemental semiconductors . . . . .	442
12.5 Diffusion in liquids . . . . .	444
12.6 Diffusion in gases . . . . .	453
12.7 Diffusion through porous media . . . . .	457
8.1 Heat transfer coefficients for forced convection in tubes . . . . .	248
8.2 Heat transfer coefficients for forced convection past submerged objects . . . . .	254
8.3 Heat transfer coefficients for natural convection . . . . .	258
8.4 Quenching heat transfer coefficients . . . . .	262
8.5 Heat transfer coefficients in fluidized beds . . . . .	268
8.6 Heat transfer coefficients in packed beds . . . . .	272
8.7 Heat transfer coefficients in forging . . . . .	274

**Chapter 13 Diffusion in Solids**

13.1 Steady-state diffusion experiments . . . . .	463
13.2 Transient diffusion experiments . . . . .	468
13.3 Finite system solutions . . . . .	476
13.4 Microelectronic diffusion processing . . . . .	480
13.5 Homogenization of alloys . . . . .	485
13.6 Formation of surface layers . . . . .	491

**Chapter 14 Mass Transfer in Fluid Systems**

14.1 Diffusion through a stagnant gas film . . . . .	510
14.2 Diffusion in a moving gas stream . . . . .	513
14.3 Diffusion into a falling liquid film . . . . .	516
14.4 The mass transfer coefficient . . . . .	519
14.5 General equation of diffusion with convection . . . . .	523
14.6 Mass transfer with forced convection over a flat plate . . . . .	526
14.7 Correlations of mass transfer coefficients for turbulent flow . . . . .	529
14.8 Models of the mass transfer coefficient . . . . .	535
14.9 Mass transfer in chemical vapor deposition . . . . .	537

**Chapter 15 Interphase Mass Transfer**

15.1 Two-resistance mass transfer theory . . . . .	547
15.2 Mixed control in gas-solid reactions . . . . .	551
15.3 Mass transfer with vaporization . . . . .	560

**Chapter 16 Numerical Methods and Models**

16.1 Finite difference approximations . . . . .	571
16.2 Turbulent flow . . . . .	598
16.3 Discretization in convective flows . . . . .	606

Appendix A Physical Constants . . . . .	611
Appendix B Thermal Properties . . . . .	613
Appendix C Conversion Factors . . . . .	621
Appendix D Description of Particulate Materials . . . . .	631

Appendix E Flow Measurement Instruments . . . . .	637
Appendix F Derivation of Eq. (9.62) for Semi-infinite Solids . . . . .	641
Appendix G Derivation of Eq. (13.53) for Drive-in Diffusion . . . . .	643
Index . . . . .	645

## PART ONE

### FLUID DYNAMICS

The first part of this text deals with fluids, their intrinsic properties, their behavior under various conditions, and the methods by which we can manipulate and utilize them to produce desired results. Most materials processing deals with fluids at one point or another, and although the materials engineer is usually not required to be an "expert" on fluids, he should understand the fundamentals of fluid dynamics as presented in the following chapters, and be able to make intelligent use of the properties of fluids and characteristics of equipment used to manipulate and control fluids.

The behavior of fluids is also intimately related to heat and mass transport processes. For example, if a gas is hotter than a solid past which it is flowing, the solid naturally is heated. The rate at which heat is transferred to the solid's surface is dependent on the fluid's properties and its flow pattern. Similarly, if a piece of graphite is to be dissolved in a bath of molten iron, the rate of dissolution depends on the motion of the liquid iron adjacent to the graphite. Thus, to appreciate transfer of heat and/or mass, an understanding of fluid dynamics is important.

These are just two simple examples which illustrate the necessity for the student to become acquainted with the means of examining and expressing the flow of fluids and to eventually recognize the role of fluid flow in rate processes involving heat and mass transfer. Actually, if we take a fundamental approach to the study of fluid flow, then the subject matter is appropriately designated *momentum transport*. Momentum transport with *energy transport* and *mass transport* make up the subject of *transport phenomena*, which Bird, Stewart, and Lightfoot\* rank as a "key engineering science," along with thermodynamics and mechanics. Transport phenomena as a key engineering science has been well received in both the academic and industrial communities of engineering.

---

\*R. B. Bird, W. E. Stewart, and E. N. Lightfoot, *Transport Phenomena*, Wiley, New York, 1960.

# 1

## VISCOS PROPERTIES OF FLUIDS

### 1.1 TYPES OF FLUID FLOW

When fluids move through a system, either one of two different types of fluid flow may occur. We can most easily visualize the fact that there are two distinctly different types of fluid flow by referring to an experiment performed by Reynolds in 1883. Imagine a transparent pipe with water flowing through it; several threadlike streams of dye are injected parallel to the path of the water's flow. At sufficiently small velocities of water, the dye will flow in parallel, straight lines. When the velocity is increased, a point is reached at which the entire mass of water becomes colored. In other words, hypothetical individual particles of liquid, instead of flowing in an orderly manner parallel to the long axis of the pipe, flow in an erratic manner so as to cause complete mixing of the dye and water.

The first type of dye flow is called *laminar* or *streamline* flow. The significance of these terms is that the fluid's motion seems to be the sliding of laminations of infinitesimal thickness relative to adjacent layers, and that the hypothetical particles in the layers move in predictable paths or streamlines, as depicted in Fig. 1.1.

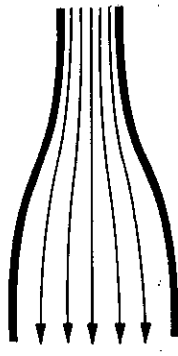


Fig. 1.1 Laminar flow.

The second (erratic) type of flow is described as *turbulent* flow. In turbulent flow, the motion of the fluid particles is irregular, and accompanied by fluctuations in velocity. This type of flow is illustrated in Fig. 1.2, in which part (a) shows the erratic path of a single

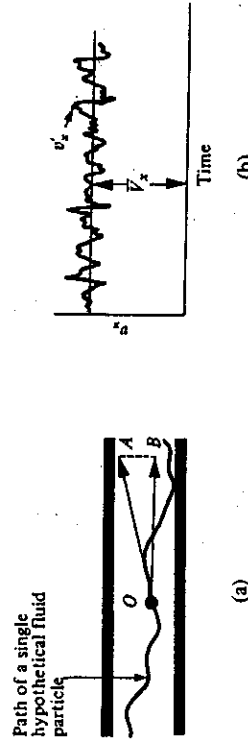


Fig. 1.2. Turbulent flow. (a) The instantaneous velocity  $OA$  varies continually in direction and magnitude. The velocity  $OB$  is the  $x$ -directed component and is designated  $v_x$  in (b). (b) Variation at point  $O$  of  $v_x$  about the temporal mean velocity  $\bar{V}$ .

particle during some time interval and part (b) demonstrates that the velocity at a fixed point in the fluid fluctuates randomly about some mean value, which is called the *temporal mean or time averaged velocity*, and which is given the symbol  $\bar{V}$ .

One of the earliest systematic investigations of turbulent flow was conducted by Reynolds, who suggested the parameter  $\bar{V}D/v$  as the criterion for predicting the type of flow in round tubes, where  $\bar{V}$  is the average fluid velocity,  $D$  is the pipe diameter, and  $v$  is the kinematic viscosity, which is a property of the fluid to be described in the following section. In a consistent set of units, the parameter is dimensionless, and is called the *Reynolds number* ( $Re$ ). The value of  $Re$  at which transition from laminar to turbulent flow occurs is approximately 2100 in the usual engineering applications of flow in pipes. In general, however, the transition Reynolds number varies with different systems, and even for a given system it may vary according to such external factors as surface roughness and initial disturbances in the fluid.

Figure 1.3 shows the distribution of velocity across the radius of a tube, for laminar and turbulent flow. The temporal mean velocity is plotted for turbulent flow. When dealing with turbulent flow, we are usually interested in the temporal mean value, so that, unless otherwise stated, the temporal mean value will be implied. Note that for both cases the velocity is zero at the fluid-wall interface; this is known as the no-slip boundary condition. For laminar flow the velocity profile is parabolic; in turbulent flow, the curve is somewhat flattened in the middle.

## 1.2 NEWTONIAN FLUIDS

Consider a fluid between two parallel plates (Fig. 1.4). The upper plate is stationary and the lower one is set in motion with a velocity  $V$  at time zero. From experience we know that the fluid adjacent to the plates will have the same velocity as the plates themselves. Hence the fluid adjacent to the lower plate moves with a velocity  $V$ , while that adjacent to the upper plate has null velocity. As time proceeds, the fluid gains momentum, and after sufficient time has elapsed a steady state is reached, in which, in order to keep the lower plate in motion with the velocity  $V$ , a force  $F$  must be maintained, and an equal but opposite force is exerted on the stationary plate.

At steady state, for plates of area  $A$ , and laminar flow, the force is expressed by

$$\frac{F}{A} = \eta \frac{V}{Y}, \quad (1.1)$$

where  $Y$  = distance between plates and  $\eta$  = constant of proportionality.

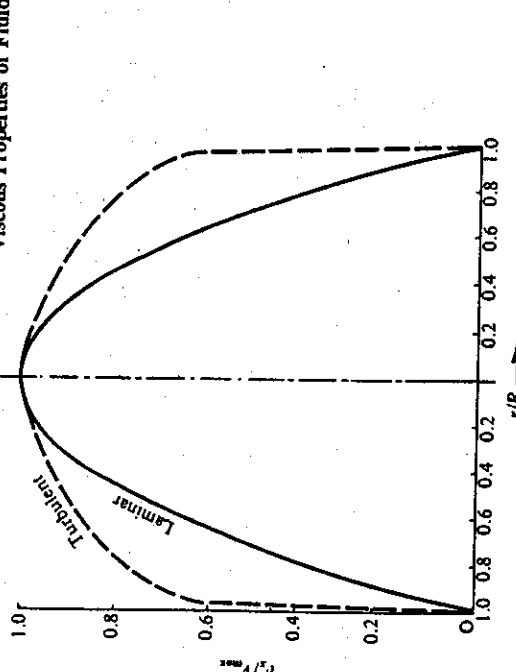


Fig. 1.2 Qualitative distribution of laminar and turbulent velocities in a tube.

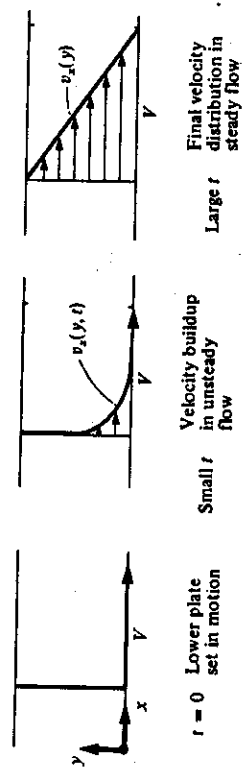


Fig. 1.3 Qualitative distribution of laminar and turbulent velocities in a tube.

The force system as described is pure shear, and the force per unit area ( $F/A$ ) is the shear stress. At steady state, when the velocity profile is linear,  $V/Y$  exactly equals the constant velocity gradient  $dv_z/dy$  and the shear stress  $\tau_{xy}$  between any two thin layers of fluid may be expressed as

$$\tau_{xy} = -\eta \frac{dv_z}{dy}. \quad (1.2)$$

Equation (1.2) may alternatively be interpreted in terms of momentum transport. Picture the fluid as a series of thin layers parallel to the plates. By the shearing action each layer causes the layer directly above it to move. Thus momentum is transported in the  $y$ -direction. The subscripts of  $\tau_{xy}$  refer to this direction of momentum transport ( $y$ ) and the velocity component being considered ( $x$ -direction). The minus sign in Eq. (1.2) reflects the fact that momentum is transferred from the lower layers of fluid to the upper layers, that is, in the positive  $y$ -direction. In this case,  $dv_z/dy$  is negative, so that the minus sign makes  $\tau_{xy}$  positive. This follows the generally accepted convention for heat transfer, in that momentum flows in the direction of decreasing velocity, just as heat flows from hot to cold.

The period between  $t = 0$ , when the lower plate is set into motion, and large  $t$ , when steady state is reached, is called the *transient period*. During the transient period,  $v_t$  is a function of both time and position, so that a more general relationship for  $\tau_{yx}$  is used:

$$\tau_{yx} = -\eta \frac{\partial v_x}{\partial y}. \quad (1.3)$$

This empirical relationship is known as *Newton's law of viscosity*, and defines the constant of proportionality,  $\eta$ , as the *viscosity*.

The dimensions of viscosity are found by referring to Eq. (1.3):

$$\eta = -\frac{\tau_{yx}}{(\partial v_x / \partial y)}.$$

Units of  $\eta$  are:

$$\eta = \frac{N \cdot m^{-2}}{(m \cdot s^{-1})/(m^{-1})} = N \cdot s \cdot m^{-2}.$$

In keeping with the trend to using SI units, the units used in examples will be SI. However, since data are still available in cgs units and English units, the ability to convert back and forth between systems remains important, and some data will also be presented in units other than SI. Accordingly, the English system yields the following units for  $\eta$ :

$$\eta = \frac{(lb_m \cdot ft \cdot hr^{-2})(ft^2)}{(ft \cdot hr^{-1})(ft^{-1})} = lb_m \cdot hr^{-1} \cdot ft^{-1}.$$

In the cgs system of units, the *poise* (P) is used, in which

$$1 \text{ poise (P)} = 1 \text{ dyn s cm}^{-2}.$$

The *centipoise* (cP) is probably the most common unit tabulated for viscosity. It equals 0.01 poise. The viscosity of water at 68.4°F (20.2°C) is 1 cP. Thus the value of the viscosity in centipoises is an indication of the viscosity of the fluid relative to that of water at 68.4°F. Viscosity in  $N \cdot s \cdot m^{-2}$  is  $10^3$  times viscosity in cP. (See Table C.8 in the Appendix for these and other conversion factors.)

In many problems involving viscosity, it is useful to have a value of a fluid's viscosity divided by its density  $\rho$ . Hence we define the *kinematic viscosity*  $\nu$  at this point as

$$\nu = \frac{\eta}{\rho}.$$

The kinematic viscosity is a fundamental quantity, in that it is a measure of *momentum diffusivity*, analogous to thermal and mass diffusivities, which will be presented in later chapters.

In SI units, the kinematic viscosity is measured in  $m^2 \cdot s^{-1}$ , while in the cgs system the units are commonly  $cm^2 \cdot s^{-1}$ , sometimes called the *stoke*.

**Example 1.1** Two parallel plates are 1 mm apart. The lower plate is stationary and the upper plate moves with a velocity of  $2 \text{ m s}^{-1}$ . A stress of  $5 \text{ N m}^{-2}$  is needed to maintain the

upper plate in motion. Find the viscosity of the fluid contained between the plates in (a)  $N \cdot s \cdot m^{-2}$  and (b) cP.

**Solution.** From Eq. (1.1) and referring to Fig. 1.4, we have

$$\eta = \frac{F/A}{V/Y}$$

$$V/Y = \frac{2 \text{ m}}{s} \left| \frac{s}{1 \times 10^{-3} \text{ m}} \right. = 2 \times 10^3 \text{ s}^{-1}.$$

$F/A$  is the stress; then

$$\eta = \frac{5 \text{ N}}{m^2} \left| \frac{2 \times 10^3}{2 \times 10^3} \right. = 2.50 \times 10^{-3} \text{ N} \cdot \text{s} \cdot \text{m}^{-2} = 2.5 \text{ cP}.$$

### 1.3 VISCOSITY OF GASES

For the purpose of explaining momentum transport in gases, we resort to the simplest treatment of the kinetic theory of gases. We utilize the concept of the mean free path, in which the molecules are idealized as billiard balls, and postulate a hypothetical "ideal" gas possessing the following features:

1. The molecules are hard spheres resembling billiard balls, having diameter  $d$  and mass  $m$ .
2. The molecules exert no force on one another except when they collide.
3. The collisions are perfectly elastic and obey the classical laws of conservation of momentum and energy.
4. The molecules are uniformly distributed in a concentration of  $n$  per unit volume throughout the gas. They are in a state of continuous motion and are separated by distances which are large compared to their diameter.
5. All directions of molecular velocities are equally probable. The speed (magnitude of velocity) of a molecule can have any value between zero and infinity.

If we assume that the molecules possess a Maxwellian speed distribution, then the average speed  $\bar{V}$  is given by

$$\bar{V} = \left[ \frac{8\kappa_b T}{\pi m} \right]^{1/2}, \quad (1.4)$$

where  $\kappa_b$  is the Boltzmann constant and  $T$  is absolute temperature.

In addition, for such a collection of molecules, a significant parameter that governs the momentum transfer in gases is the free path, defined as the distance traveled by a molecule between two successive collisions. At the instant of collision, the center-to-center distance of two molecules is  $d$ . Intuitively we know that the *mean free path*  $\lambda$  should be inversely proportional to the collision cross section  $\pi d^2$ , and also inversely proportional to the concentration  $n$  of the molecules. The rigorous analysis for determining  $\lambda$  includes these

terms, along with a coefficient whose numerical value is developed by considering the random fluctuations of the colliding molecules. The final result gives

$$\lambda = \left[ \frac{1}{\sqrt{2}} \right] \left[ \frac{1}{\pi d^2 n} \right]. \quad (1.5)$$

Now consider an imaginary plane at  $y = y_1$ , which is being crossed by molecules in either direction. If we examine the condition of no bulk motion (no macroscopic flow) of the gas in the  $y$ -direction, then the molecules cross the  $y_1$  plane from both sides with equal frequency. This frequency per unit area at which molecules cross the plane at  $y_1$  from one side is given by

$$Z = n \bar{V}/4. \quad (1.6)$$

We may picture the molecules crossing the  $y_1$ -plane as carrying momentum characteristic of an average distance  $\bar{y}$  above and below the  $y_1$  plane at which they made this last collision. Numerically,  $\bar{y}$  is not exactly equal to  $\lambda$ , but rather is given by

$$\bar{y} = 2/3\lambda.. \quad (1.7)$$

Up to this point, no macroscopic flow of the gas has been considered, so that, as stated above, the number of molecules arriving from above and below  $y_1$  is equal, and on the average no net momentum is transferred across the plane  $y_1$ .

To determine the viscosity of the gas, consider the gas under the influence of macroscopic flow in the  $x$ -direction, with a velocity gradient,  $dv_x/dy$ , as depicted in Fig. 1.5.

Now if all the molecules have velocities characteristic of the plane in which they last collided, we may write the  $x$ -momentum above  $y_1$  as

$$mv_x \Big|_{y_1+\bar{y}} = mv_x \Big|_{y_1-\bar{y}} + \frac{2}{3}\lambda m \frac{dv_x}{dy}. \quad (1.8)$$

$$mv_x \Big|_{y_1+\bar{y}} = mv_x \Big|_{y_1-\bar{y}} - \frac{2}{3}\lambda m \frac{dv_x}{dy}. \quad (1.9)$$

Similarly, for below  $y_1$

$$mv_x \Big|_{y_1+\bar{y}} = mv_x \Big|_{y_1-\bar{y}} + \frac{2}{3}\lambda m \frac{dv_x}{dy}. \quad (1.10)$$

A significant conclusion from the above argument is that the viscosity of a gas is independent of pressure and depends only on temperature. This conclusion is in good agreement with experimental data up to about ten atmospheres.<sup>1</sup> However, the temperature dependency is only qualitatively correct, in that  $\eta$  does increase with increasing temperatures; but, quantitatively, the temperature dependency is not satisfactory. Data for real gases indicate that  $\eta$  varies with  $T^m$ , with  $n$  between 0.6 and unity, rather than 0.5, as in Eq. (1.13).

The more up-to-date kinetic theories replace the billiard-ball model with a more realistic molecular force field by considering the force of attraction and repulsion between molecules. These theories, reviewed by Hirschfelder, Curtiss, and Bird,<sup>2</sup> make use of the potential energy of interaction between a pair of molecules in the gas. This function—often referred to as the *Lennard-Jones potential*—displays the behavior of molecular interactions by exhibiting weak attraction at large separation distances and strong repulsion at small separations, as shown in Fig. 1.6.

Where the position of the molecules is  $\delta$ , the potential energy is a minimum at  $-\epsilon$ ;  $\epsilon$  is called the *characteristic energy parameter*. Using the Lennard-Jones potential, Chapman and Enskog have developed the following equation for the viscosity of nonpolar gases at low pressures:

$$\eta = 2.67 \times 10^{-5} \frac{\sqrt{MT}}{\sigma^2 \Omega}. \quad (1.14)$$

We find the net rate of  $x$ -momentum crossing the plane  $y_1$  by summing the  $x$ -momentum of molecules that cross from below and subtracting the  $x$ -momentum of those that cross from above. In this manner, we write

$$\tau_{yx} = Zm \left[ v_x \Big|_{y_1+\bar{y}} - v_x \Big|_{y_1-\bar{y}} \right]. \quad (1.10)$$

By combining Eqs. (1.6), (1.8), and (1.9), we arrive at

$$\tau_{yx} = -\frac{1}{3}\lambda m \bar{V}\lambda \frac{dv_x}{dy}. \quad (1.11)$$

In addition, by utilizing the expressions for  $\bar{V}$  and  $\lambda$ , Eqs. (1.4) and (1.5), respectively, we write

$$\tau_{yx} = -\frac{2}{3\pi^{3/2}} \frac{(mk_B T)^{1/2}}{d^2} \frac{dv_x}{dy}. \quad (1.12)$$

This result corresponds to Newton's law of viscosity (Eq. 1.2), with the viscosity given by

$$\eta = \frac{2}{3\pi^{3/2}} \frac{(mk_B T)^{1/2}}{d^2}. \quad (1.13)$$

<sup>1</sup> standard atmosphere (atm) =  $1.0133 \times 10^5 \text{ N/m}^2$ .

<sup>2</sup>J. O. Hirschfelder, C. F. Curtiss, and R. B. Bird, *Molecular Theory of Gases and Liquids*, Wiley, New York, 1954.

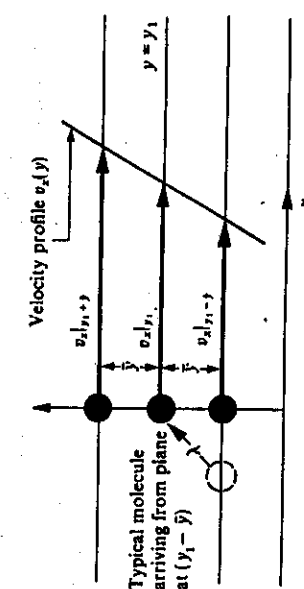
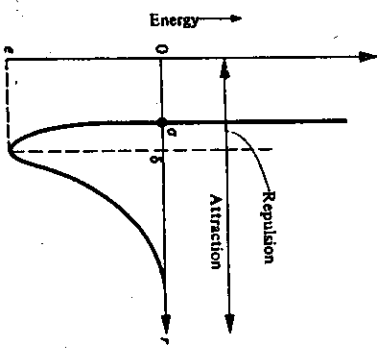


Fig. 1.5 Relation between the macroscopic velocity profile and the plane of interest at  $y_1$ .



**Fig. 1.6** Lennard-Jones potential function describing the interaction of two nonpolar molecules.

Here  $M$  is the gram-molecular weight,  $\eta$  is in poises,  $T$  in K, and  $\sigma$  is a characteristic diameter of the molecule in Å (see Fig. 1.6). The quantity  $\Omega_c$  is the collision integral of the Chapman-Enskog theory, which is a function of a dimensionless temperature parameter  $\kappa_B T / \epsilon$ . In order to use Eq. (1.14), we need values of  $\sigma$  and  $\epsilon/\kappa_B T$ ; these parameters are known for many substances. A partial list of them is given in Table 1.1. We can then determine the collision integral by using Table 1.2.

**Example 1.2** Compute the viscosity of hydrogen at 1 atm and 1364 K.

**Solution.** From Table 1.1, we find that

$$\epsilon/\kappa_B = 59.7 \text{ K}, \sigma = 2.827 \text{ Å}.$$

From Table 1.2,

$$\Omega_c \approx 0.733.$$

Substituting appropriate values into Eq. (1.14), we have

$$\eta = 2.67 \times 10^{-5} \frac{\sqrt{(2)(1364)}}{(2.827)^3(0.733)} = 2.38 \times 10^{-4} \text{ poise.}$$

(Observed viscosity is  $2.44 \times 10^{-4}$  poise.)

Using Eq. (1.14) to calculate  $\eta$  requires knowing  $\sigma$  and  $\epsilon/\kappa_B T$ . When values of  $\sigma$  are not available, one may use a modified form of Eq. (1.14), as presented by Bromley and Wilke<sup>2</sup>:

$$\eta = 3.33 \times 10^{-5} \frac{\sqrt{MT_c}}{V_c^{2/3}} f \left[ \frac{\kappa_B T}{\epsilon} \right]. \quad (1.15)$$

Note: The Angstrom, Å, equals  $0.1 \text{ nm}$  or  $10^4 \text{ cm}$ .  
 \*R. C. Reid, J. M. Prausnitz, and B. E. Poling, *The Properties of Gases and Liquids*, 4th edition, McGraw-Hill Book Co., New York, NY, 1987, Appendices A and B.

**Table 1.2** Values of  $\Omega_c$  integral for viscosity and of the viscosity function  $f(\kappa_B T / \epsilon)$ , based on the Lennard-Jones potential.\*

$\kappa_B T / \epsilon$	$\Omega_c$	$f(\kappa_B T / \epsilon)$	$\kappa_B T / \epsilon$	$\Omega_c$	$f(\kappa_B T / \epsilon)$
0.3	2.785	0.1969	6.0	0.8963	2.751
0.4	2.492	0.2540	8.0	0.8538	3.377
0.5	2.257	0.3134	10	0.8242	3.866
0.6	2.065	0.3751	20	0.7432	6.063
0.7	1.908	0.4384	40	0.6718	9.488
0.8	1.780	0.5025	60	0.6335	12.324
0.9	1.675	0.5666	80	0.6076	14.839
1.0	1.587	0.6302	100	0.5882	17.137
2.0	1.175	1.2048	200	0.5320	26.80
4.0	0.9700	2.0719	400	0.4811	41.90

\*J. O. Hirschfelder, C. F. Curtiss, and R. B. Bird, *Molecular Theory of Gases and Liquids*, Wiley, New York, 1954.

<sup>2</sup>L. R. Bromley and C. R. Wilke, *Ind. Eng. Chem.* 43, 1641 (1951).

Then

$$\eta_{\text{mix}} = \frac{(0.2)(3.37 \times 10^{-3})}{2,040} + \frac{(0.5)(3.43 \times 10^{-3})}{1,284} + \frac{(0.3)(3.82 \times 10^{-3})}{1,980}$$

$$\eta_{\text{mix}} = 3.60 \times 10^{-3} \text{ N s m}^{-2}, \quad 6,361$$

where  $\eta$  is in poises,  $T_c$  (K) and  $\hat{V}_c$  ( $\text{cm}^3/\text{mol}$ ) are the critical temperature and volume, respectively, and  $f(\kappa_B T/e)$  is an empirical function also to be found in Table 1.2.

The Chapman-Enskog theory has been extended to include multicomponent gas mixtures at low density. For most purposes, the semiempirical formula of Wilke<sup>4</sup> is quite adequate:

$$\eta_{\text{mix}} = \sum_{i=1}^n \frac{x_i \eta_i}{\sum_{j=1}^n x_j \Phi_{ij}}, \quad (1.16)$$

in which

$$\Phi_{ij} = \frac{1}{\sqrt{8}} \left[ 1 + \frac{M_i}{M_j} \right]^{-1/2} \left[ 1 + \left( \frac{\eta_i}{\eta_j} \right)^{1/2} \left( \frac{M_j}{M_i} \right)^{1/4} \right]^2.$$

Here  $n$  is the number of chemical species in the mixture;  $x_i$  and  $x_j$  are the mole fractions of species  $i$  and  $j$ ;  $\eta_i$  and  $\eta_j$  are the viscosities of species  $i$  and  $j$  at the system temperature and pressure; and  $M_i$  and  $M_j$  are the corresponding molecular weights. Note that  $\Phi_{ii}$  is dimensionless, and, when  $i = j$ ,  $\Phi_{ii} = 1$ .

**Example 1.3** Estimate the viscosity of a gas comprising 20%  $\text{CO}_2$ , 50%  $\text{CO}$  and 30%  $\text{He}$  at 800 K and  $10^5 \text{ N m}^{-2}$  (approx. 1 atm), given the viscosities of the pure components.

$i$	$j$	$M_i/M_j$	$\eta_i/\eta_j$	$\Phi_{ij}$	$\eta_i$ $\text{N s m}^{-2}$	$\sum_{j=1}^3 x_j \Phi_{ij}$
1 ( $\text{CO}_2$ )	0.2	44.011	3.37 $\times 10^{-3}$	0.404		
2 ( $\text{CO}$ )	0.5	28.011	3.43 $\times 10^{-3}$	( $j = 1, x_j = 0.2$ )		
3 ( $\text{He}$ )	0.3	4.903	3.82 $\times 10^{-3}$			
2	1	0.636	1.018	1.254	1.284	
	2	1.000	1.000	1.000	( $j = 2, x_j = 0.5$ )	
	3	6.998	0.898	0.313		
3	1	0.091	1.133	2.921	1.908	
	2	0.143	1.114	2.440	( $j = 3, x_j = 0.3$ )	
	3	1.000	1.000	1.000		

**Solution.** Calculate values of  $\Phi_{ij}$  first and collect the denominators for Eq. (1.16).

To summarize, Eqs. (1.14), (1.15), and (1.16) are useful equations for computing viscosities of nonpolar gases and gas mixtures at low density from tabulated values of the intermolecular force parameters  $\sigma$  and  $\epsilon$ . They cannot, however, be applied with confidence to gases consisting of polar or highly elongated molecules such as  $\text{H}_2\text{O}$ ,  $\text{NH}_3$ ,  $\text{CH}_3\text{OH}$ , and  $\text{NOCl}$ . A further limitation is that for the most part these equations have been tested only over the temperature range 100 K to 1500 K.

The data on viscosity of several gases as a function of temperature are given in Fig. 1.7. Keep in mind that the data are valid for pressures up to about 10 atmospheres. Note that (1) the viscosity of all gases increases with temperature, and (2) the magnitude of viscosity does not solely depend on the molecular weight of the gas. For example, the data for helium fall in the range of much heavier gases than hydrogen. Sports commentators in particular should heed some of the data and stop propagating the myth that baseballs can be hit farther in dry air than under humid weather conditions. Not only is the viscosity of humid air less than that of dry air, the density is too.

#### 1.4 VISCOSITY OF LIQUIDS

In dealing with transport processes in liquids, we are always faced with the problem that much less is known about the structure of liquids than about the structures of solids or gases. However, there is more similarity between liquids and solids than between liquids and gases. This similarity is based on the small fractional increase in volume on melting (3 to 5% for metals), and the fact that the heat of fusion is quite a bit less than the heat of vaporization. Furthermore, x-ray data tell us that there is at least some degree of short-range order in a liquid. That is, at a short distance from a central atom, the arrangement of nearest neighbors is reasonably predictable. However, as the distance increases, the predictability of atom positions decreases rapidly, unlike in solids. Several theories have been postulated to account for the observed properties of liquids, none without some serious deficiencies. The oldest, in terms of the structural picture involved, is the *hole theory*, which postulates that a liquid contains many holes or vacant areas, distributed throughout the liquid, with these holes having some distribution of sizes about an average. Although this theory does not explain all observations of the changes of properties of materials upon fusion, it has been useful in deriving a relatively simple approach to predicting the temperature dependence of the viscosity of liquids. Other models, based on differing assumptions of where the extra volume associated with a liquid is assumed to reside, are discussed in Chapter 12.

Because liquids near their melting points still represent a dense phase, the concept of transfer of momentum from atom to atom, as utilized in the kinetic theory approach to gas-phase viscosity, is invalid, since the momentum of each atom varies rapidly with the vibration of the atoms within the pseudo-lattice of the liquid. As Frenkel<sup>5</sup> points out, the fact to be explained in the case of liquids is not their resistance to shearing stress, but rather their capability of yielding to stress.

<sup>4</sup>C. R. Wilke, *J. Chem. Phys.* **18**, 517 (1950).

<sup>5</sup>J. Frenkel, *Kinetic Theory of Liquids*, Dover, New York, 1955.

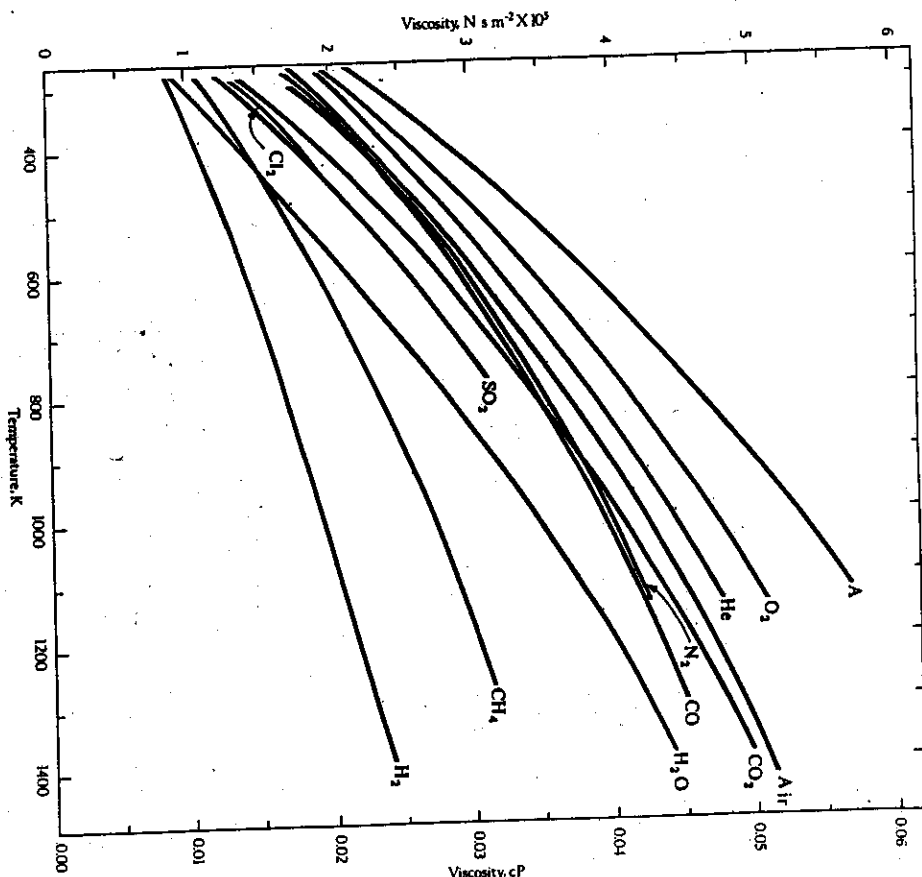


**Fig. 1.7** The viscosity of common gases at 1 atm. (Curves drawn from data given in A. Schack, *Industrial Heat Transfer*, sixth edition, Wiley, New York, 1965, and *Handbook of Chemistry and Physics*, 52nd edition, The Chemical Rubber Co., Cleveland, 1971.)

Without recourse to any specific model of a liquid, but assuming only that viscous flow takes place by movement of particles past other particles, we can start by considering the mobility of an individual particle. Einstein has shown that the mobility  $B$  of a particle under the influence of an external force is related to the diffusion coefficient  $D$  by the relationship

$$D = B k_B T; \quad (1.17)$$

$B$  is the mean velocity divided by the force acting on the particle. Since diffusion appears to be an activated process, i.e., a minimum activation energy  $\Delta G^\ddagger$  must be supplied to the particle to move it from one stable position to the next, then the fluidity, which is proportional to the capability of atoms to move, just as diffusion is, must also be thermally activated.

However, fluidity is the inverse of viscosity, so that, although  $D$  is proportional to  $\exp[-\Delta G^\ddagger/RT]$ ,  $\eta$  must be proportional to  $\exp[+\Delta G^\ddagger/RT]$ . That is, the viscosity of liquids decreases with increasing temperature. Recall that the viscosity of gases increases with temperature. The temperature dependence of  $\eta$  may then be described by an equation of the form

$$\eta = A \exp \left[ \frac{\Delta G_{vis}^\ddagger}{RT} \right], \quad (1.18)$$

where  $\eta$  = viscosity,  $A$  = constant,  $T$  = absolute temperature,  $K$ ,  $R$  = gas constant, and  $\Delta G_{vis}^\ddagger$  = activation energy of viscosity.

The constant  $A$  is the object of much of the theoretical work done on the structure of liquids. None of the theories to date gives satisfactory equations, based on fundamental parameters, which can be used to accurately predict values of  $A$ . The closest is Eyring's theory, which predicts  $A$  according to the equation

$$A \equiv \frac{N_0 \hbar}{\hat{V}}, \quad (1.19)$$

in which  $N_0$  = Avogadro's number,  $\hat{V}$  = molar volume, and  $\hbar$  = Planck's constant.

For molecular liquids in which the bonding force is of a van der Waals type, we can predict the activation energy of viscosity from the vaporization energy  $\Delta E_{vap}$ :

$$\Delta G^\ddagger \approx 0.41 \Delta E_{vap}. \quad (1.20)$$

Equations (1.19) and (1.20) are not valid for liquid metals, which are not molecular, nor are they valid for polymers or other chainlike molecules, and should not be used except as a last resort.

It is surprising that the viscosities of many diverse liquids, in terms of bonding nature in the solid state, are very similar. To illustrate this point, Table 1.3 lists groups of various materials under general ranges of viscosity. The viscosities used are those of the material in the normal temperature range of interest.

**Table 1.3** Viscosity ranges for various liquids

Viscosity range, poise	Materials
1-100	CaO-Al <sub>2</sub> O <sub>3</sub> -SiO <sub>2</sub> slags 50% NaOH, 50% H <sub>2</sub> O Linseed oil Liquid polymer melts
0.1-1.0	H <sub>2</sub> SO <sub>4</sub> Molten salts Heavy metals (Pb, Au, Zn, etc.) Alkaline earth metals (Ca, Mg) Transition metals (Fe, Ni, Co, etc.)
0.01-0.1	Water (22°C) Kerosene (22°C) Acetone Alkali metals
0.001-0.01	

Figure 1.8 gives a nomograph for the viscosity of common liquids. More specific aspects of several classes of liquids of particular interest in materials processing are taken up in the following sections.

#### 1.4.1 Viscosity of liquid metals and alloys

As you are undoubtedly aware, metals are not molecular in nature and neither the constants  $A$  nor  $\Delta G_{\text{vis}}$  can be predicted by using the simplified equations presented above. Metals do, however, show activated behavior. Figure 1.9 plots the viscosities for many of the common metals as  $\log \eta$  versus  $1/T$ .

Chapman<sup>6</sup> analyzed these data in the light of the theory of liquids developed by Kirkwood<sup>7</sup> and by Born and Green.<sup>8</sup> He arrived at a generalized model for the viscosity of liquid metals which involves no assumptions of the structure other than that the atoms are spherical and that the potential between atoms can be expressed by some function  $\phi(r)$  of the distance between atoms and an energy parameter, such as is done in the Lennard-Jones picture of the potential energy well between atoms, in which

$$\phi(r) = 4\epsilon \left[ \left( \frac{\delta}{r} \right)^{12} - \left( \frac{\delta}{r} \right)^6 \right].$$

By obtaining a suitable expression for the time average of the interactions between atoms, when their normal molecular motion is disturbed by imposing a velocity gradient on the liquid, and by attributing virtually all the momentum flux to intermolecular forces (that is, neglecting the very small contribution from the kinetic motion of the atoms), Chapman deduced a relationship between the viscosity, an energy parameter  $\epsilon$ , and a separation distance  $\delta$ . Then, by further assuming that all liquid metals obey the same function  $\phi(r)$  he concluded that all substances with this  $\phi(r)$  should have a reduced viscosity  $\eta^*$ , which is a function of the reduced temperature  $T^*$  and volume  $V^*$ , where the functional relationship is given by

$$(1.21)$$

$$\eta^* (V^*)^2 = f(T^*),$$

and

$$\eta^* = \frac{\eta \delta^2 N_0}{\sqrt{MKT}}, \quad (1.22)$$

$$T^* = \frac{\kappa_B T}{\epsilon}, \quad (1.23)$$

$$V^* = \frac{1}{n\delta^3}. \quad (1.24)$$

and

<sup>6</sup>T. Chapman, *AIChE J.* **12**, 395 (1966).

<sup>7</sup>J. G. Kirkwood, *J. Chem. Phys.* **14**, 180 (1946).

<sup>8</sup>M. Born and H. S. Green, *A General Kinetic Theory of Liquids*, University Press, Cambridge, 1949.

Viscosities of liquids (coordinates for use with Fig. 1.8)

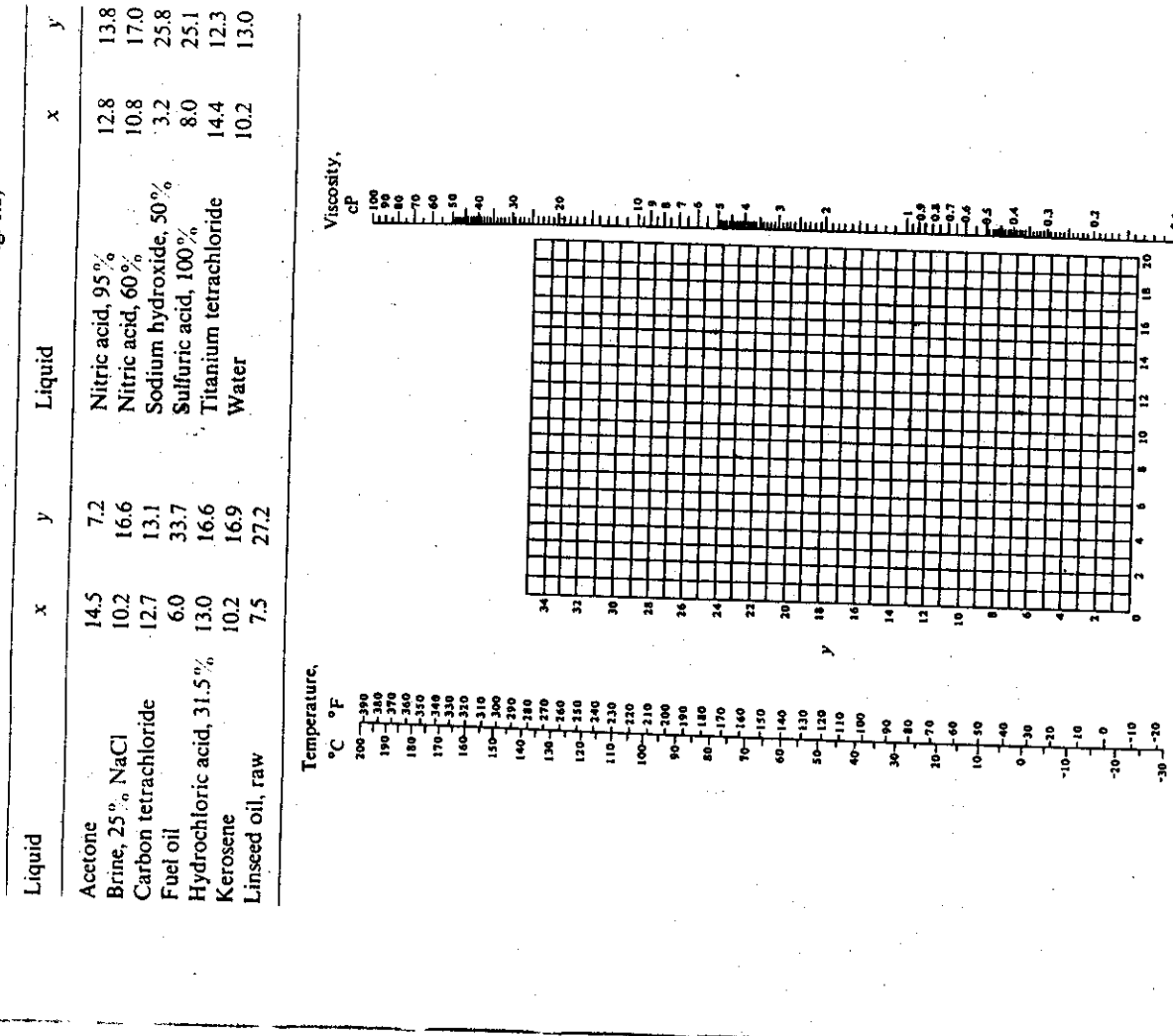


Fig. 1.8 Viscosities of liquids at 1 atm. For coordinates see the table above. (From J. H. Perry (editor), *Chemical Engineers' Handbook*, fourth edition, McGraw-Hill, New York, 1963.)

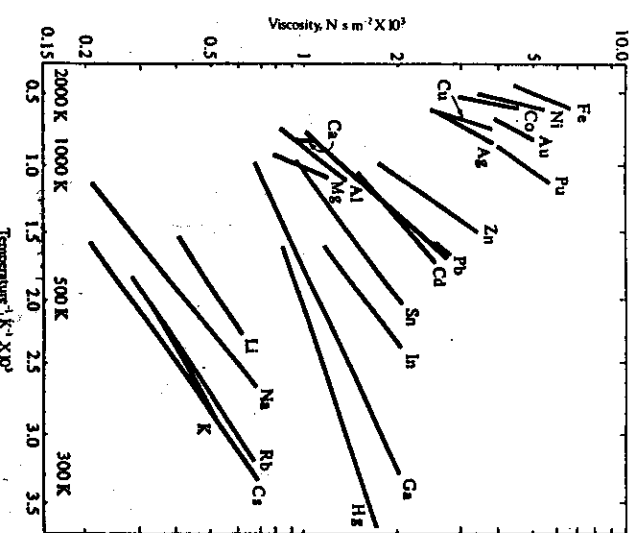


Fig. 1.9 The viscosities of liquid metals and their dependence on temperature. (From Chapman, *ibid.*)

The variables used are:

$\delta$  = interatomic distance in the close-packed crystal at 0 K, Å,

$\varepsilon$  = energy parameter characteristic of specific metal,

$N_0$  = Avogadro's number,

$M$  = atomic weight,

$R$  = gas constant,

$T$  = absolute temperature, K,

$k_B$  = Boltzmann's constant, and

$n$  = number of atoms per unit volume.

The parameter  $\delta$  is taken as the interatomic spacing for the close-packed crystal at 0 K. The energy parameters present the largest difficulty, and have been derived in the following manner. The effective Lennard-Jones parameters for sodium and potassium have been determined.<sup>9</sup> Using these two values, one can plot the reduced viscosity data for sodium and potassium as a function of reduced temperature. The data points fall on a smooth curve, as predicted by Eq. (1.21). Then, assuming that all the rest of the metals in Fig. 1.9 obey the same functional relationship, the viscosity-temperature data for the remainder of the pure metals are correlated by empirically adjusting the parameter  $\varepsilon/k_B$  until all the data for a given metal fall on one point on the curve, given in Fig. 1.10. Table 1.4 shows the resulting values of  $\varepsilon/k_B$  starting with the known (measured) values for sodium and potassium.

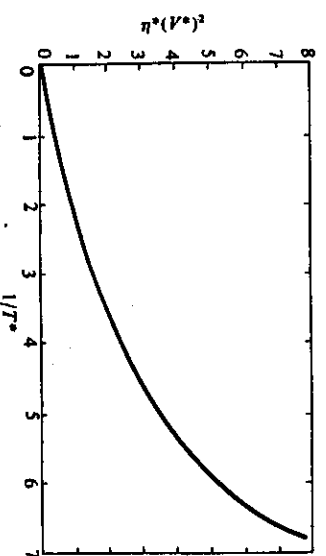


Fig. 1.10 Correlation curve for viscosities of liquid metals. (From Chapman, *ibid.*)

Table 1.4 Empirically determined values of  $\varepsilon/k_B$  (from Chapman, *ibid.*)

Metals	$\delta, \text{\AA}$	$\varepsilon/k_B, \text{K}$	Metals	$\delta, \text{\AA}$	$\varepsilon/k_B, \text{K}$
Na	3.84	1970	Rb	5.04	1600
K	4.76	1760	Ag	2.88	6400
Li	3.14	2350	Cd	3.04	3300
Mg	3.20	4300	In	3.14	2500
Al	2.86	4250	Sn	3.16	2650
Ca	4.02	5250	Cs	5.40	1550
Fe	2.52	10 900	Au	2.88	6750
Co	2.32	9550	Hg	3.10	1250
Ni	2.50	9750	Pb	3.50	2800
Cu	2.56	6600	Pt	3.10	5550
Zn	2.74	4700			

The fact that, by adjusting an unmeasured parameter, it is possible to correlate all these liquid-metal viscosities on a single curve, might not be taken as significant, except for the fact that one theory of melting indicates that the melting point should be proportional to  $\varepsilon$ , and that this relationship has been observed for other classes of materials. The empirically determined values of  $\varepsilon/k_B$  from Table 1.4 have been plotted as a function of the absolute melting temperature, and an excellent correlation has been observed, leading to the equation

$$\frac{\varepsilon}{k_B} = 5.20T_m, \text{ K.} \quad (1.25)$$

For metals with high melting points, this may be used to predict viscosities, as no further data are available.

**Example 1.4** Estimate the viscosity of liquid titanium at 2120 K. The following data are available:  $T_m = 1943 \text{ K}$  ( $1670^\circ\text{C}$ ),  $M = 47.9 \text{ g mol}^{-1}$ ,  $\rho$  (density) =  $4.5 \times 10^3 \text{ kg m}^{-3}$ , and  $\delta = 0.289 \text{ nm}$ .

**Solution.** Using Eq. (1.25), one can estimate  $\varepsilon/k_B$  to be

$$\varepsilon/k_B = (5.20)(1943) = 10 100 \text{ K.}$$

Then  $T^*$  is given by Eq. (1.23), and  $\eta^*(V^*)^2$  is found from Fig. 1.10:

$$T^* = \frac{2120}{10/100} = 0.210,$$

and

$$\eta^*(V^*)^2 = 3.1.$$

From the given data, one can calculate  $V^*$ :

$$V^* = \frac{1}{\left[ \frac{6.023 \times 10^{23} \text{ atoms}}{47.9 \text{ g}} \right] \left[ \frac{4.5 \text{ g}}{\text{cm}^3} \right] (2.89 \times 10^{-3} \text{ cm})^3} = 0.733.$$

Then

$$\eta^* = \frac{3.1}{(0.733)^2} = 5.77.$$

Solving for  $\eta$ , we first obtain

$$(MRT)^{1/2} = \left[ \frac{47.9 \text{ g}}{\text{mol}} \left| \frac{8.3144 \text{ J}}{\text{mol K}} \right| \frac{2120 \text{ K}}{\text{mol}} \right]^{1/2} = 918.9 (\text{J g})^{1/2} \text{ mol}^{-1};$$

then

$$\begin{aligned} \eta &= \frac{\eta^* (MRT)^{1/2}}{\delta^2 N_0} = \frac{5.77}{\text{mol}^2} \left| \frac{918.9 \text{ J}^{1/2} \text{ g}^{1/2}}{\text{mol}^2} \right| \frac{(0.289 \times 10^{-9})^2 \text{ m}^2}{\text{mol}^2} \left| \frac{6.023 \times 10^{23}}{\text{mol}^2} \right. \\ &= \frac{0.1054 \text{ J}^{1/2} \text{ g}^{1/2}}{\text{m}^2} \left| \frac{1 \text{ kg}^{1/2}}{10^{32} \text{ g}^{1/2}} \right| \frac{1 \text{ kg}^{1/2} \text{ m}}{1 \text{ J}^{1/2} \text{ s}} = 3.33 \times 10^{-3} \text{ kg m}^{-1} \text{ s}^{-1}, \end{aligned}$$

or

$$\eta = 3.33 \times 10^{-3} \text{ N s m}^{-2} (3.33 \text{ cP}).$$

Other theories on the viscosity of liquid metals are reviewed in Iida and Guthrie,<sup>10</sup> who estimate the preexponential constant in Eq. (1.18) by

$$A \approx \frac{5.7 \times 10^{-5} (MT_m^{1/2})}{V_m^{2/3} \exp(\Delta G_{\text{vis}}^{\ddagger}/RT_m)}. \quad (1.26)$$

where  $A$  is in  $\text{N s m}^2$ ,  $M$  is the atomic weight,  $T_m$  is the absolute melting point,  $V_m$  is the atomic volume at  $T_m$ ,  $R$  is the gas constant and  $\Delta G_{\text{vis}}^{\ddagger}$  is the activation energy of viscosity. For metals:

$$\Delta G_{\text{vis}}^{\ddagger} = 5.06 T_m^{1/2}, \quad (1.27)$$

and for semi-metals (Hg, Ga, K, In, Sn, Bi and Pb)

$$\Delta G_{\text{vis}}^{\ddagger} \approx 3.14 T_m^{1/2}, \quad (1.28)$$

where  $\Delta G_{\text{vis}}^{\ddagger}$  is in  $\text{kJ mol}^{-1}$ .

Experimental data for the viscosity of binary liquid alloys sometimes show anomalous viscosity changes at compositions corresponding to eutectics and limits of solid solubility. Data that show discontinuous viscosities with respect to composition should be doubted, although there may be some mild indications of structure related to the phase diagram. Iida and Guthrie<sup>11</sup> give a phenomenological equation to estimate viscosity, but it is too lengthy to repeat here. Kucharski<sup>12</sup> put forth a model to relate the viscosity of binary alloys to their structure. Kucharski's predictive equation is

$$\eta = \sum_{i=1}^2 x_i (V_i/V) (\beta/\beta_i)^2 \gamma_i^* \eta_i, \quad (1.29)$$

where  $i$  denotes species 1 and 2,  $V_i$  is molar volume of  $i$ ,  $V$  is molar volume of the alloy,  $\gamma_i^*$  is the thermodynamic activity coefficient of  $i$  and  $\alpha$  is a constant, that varies slightly with temperature. Also

$$\beta_i = x_i V_i^{1/3} + x_j V_j^{4/3}/V_i$$

and

$$\beta = \sum_{i=1}^2 x_i V_i^{1/3}.$$

The use of Eq. (1.29) requires activity coefficients and molar volumes so it cannot be readily applied without first gathering thermodynamic data. At least for the Al-Cu system, the parameter  $\alpha$  was found to vary with both temperature and composition,<sup>13</sup> so in applying Eq. (1.29) this should be carefully checked.

In Fig. 1.11, the viscosities in an important binary system, Fe-C, are superimposed on the phase diagram to illustrate the effect an alloying element may have on viscosity. Viscosity data for many alloys can be found in Elliott *et al.*<sup>14</sup>

<sup>10</sup>T. Iida and R. I. L. Guthrie, *ibid.*, p. 196.

<sup>11</sup>M. Kucharski, *Z. Metallk.* **77**, 393 (1986).

<sup>12</sup>S. Ganeshan, R. Speiser and D. R. Poirier, *Metall. Trans. B* **18B**, 421 (1987).

<sup>13</sup>J. F. Elliott, M. Gleiser and V. Ramakrishna, *Thermochemistry for Steelmaking*, Vol. II, Addison-Wesley, Reading, MA, 1963, Section 9.

<sup>14</sup>J. F. Elliott, M. Gleiser and V. Ramakrishna, *Thermochemistry for Steelmaking*, Clarendon Press, Oxford, 1988, p. 196.

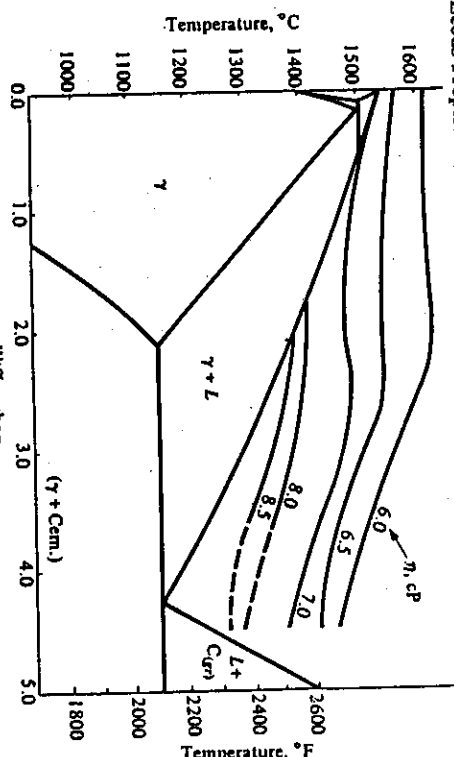


Fig. 1.11 Viscosities of iron-carbon alloys. (From R. N. Barfield and J. A. Kitchener, *J. Iron and Steel Inst.* 180, 324 (1955).)

#### 1.4.2 Viscosity of molten slags, silicates, and salts

The structures of molten slag systems have been studied from many aspects. At this point we will not go into the detail of the various structures, but rather discuss briefly their basic aspects which affect viscosity.

In general, slags consist of cations and anions resulting from ionization of basic and acidic constituents in molten oxide solution. We may consider an acidic component to be an oxide which, when dissolved in the slag, acquires additional oxygen ions to form a complex anion, while a basic oxide contributes an oxygen ion to the melt; the cation then remains dissociated from any other ions, and moves about freely. The most common acidic component is  $\text{SiO}_2$ , and  $\text{Al}_2\text{O}_3$  behaves in a similar manner. Starting with pure  $\text{SiO}_2$ , in which the bonding is both strong and highly directional, and in which viscous flow occurs only by breaking bonds, let us examine what happens if we add a basic oxide, such as  $\text{CaO}$ , to it.

We presume that the structure of pure liquid silica is quite similar to that of solid silica, in which each  $\text{Si}^{4+}$  ion shares one electron with each of four  $\text{O}^{2-}$  ions which form a tetrahedron about the  $\text{Si}^{4+}$  ion. In the solid state, electroneutrality is maintained by each oxygen ion sharing its other electron between two tetrahedra, or  $\text{Si}^{4+}$  ions, and the structure built up is a regular crystalline array of  $\text{SiO}_4^{4-}$  groups. This is illustrated in Fig. 1.12(a). When this substance is melted, the arrangement presumably continues, but the long-range order is destroyed, as indicated in Fig. 1.12(b). However, the same Si-O bonds are present and these high energy bonds need to be broken so that viscous flow could take place. The activation energy for this process is quite high (135 kcal) and the viscosity of pure liquid  $\text{SiO}_2$  at 1940°C is  $1.5 \times 10^5$  poises ( $1.5 \times 10^5 \text{ N s m}^{-2}$ ).

When  $\text{CaO}$ , or another similar divalent basic oxide, is added to the melt, the  $\text{Ca}^{2+}$  ions are accommodated in the interstices of the silicate structure and the  $\text{O}^{2-}$  ions enter into the network (Fig. 1.13). The  $\text{O}^{2-}$  ions cause two of the tetrahedra to separate since each corner of these two can now have an oxygen ion of its own. Increasing additions of base results in a progressive breakdown of the original three-dimensional network.

Table 1.5 shows this progression as a function of total oxygen atoms to silicon atoms. As the breakdown progresses, we may consider the silicate network to be made up of

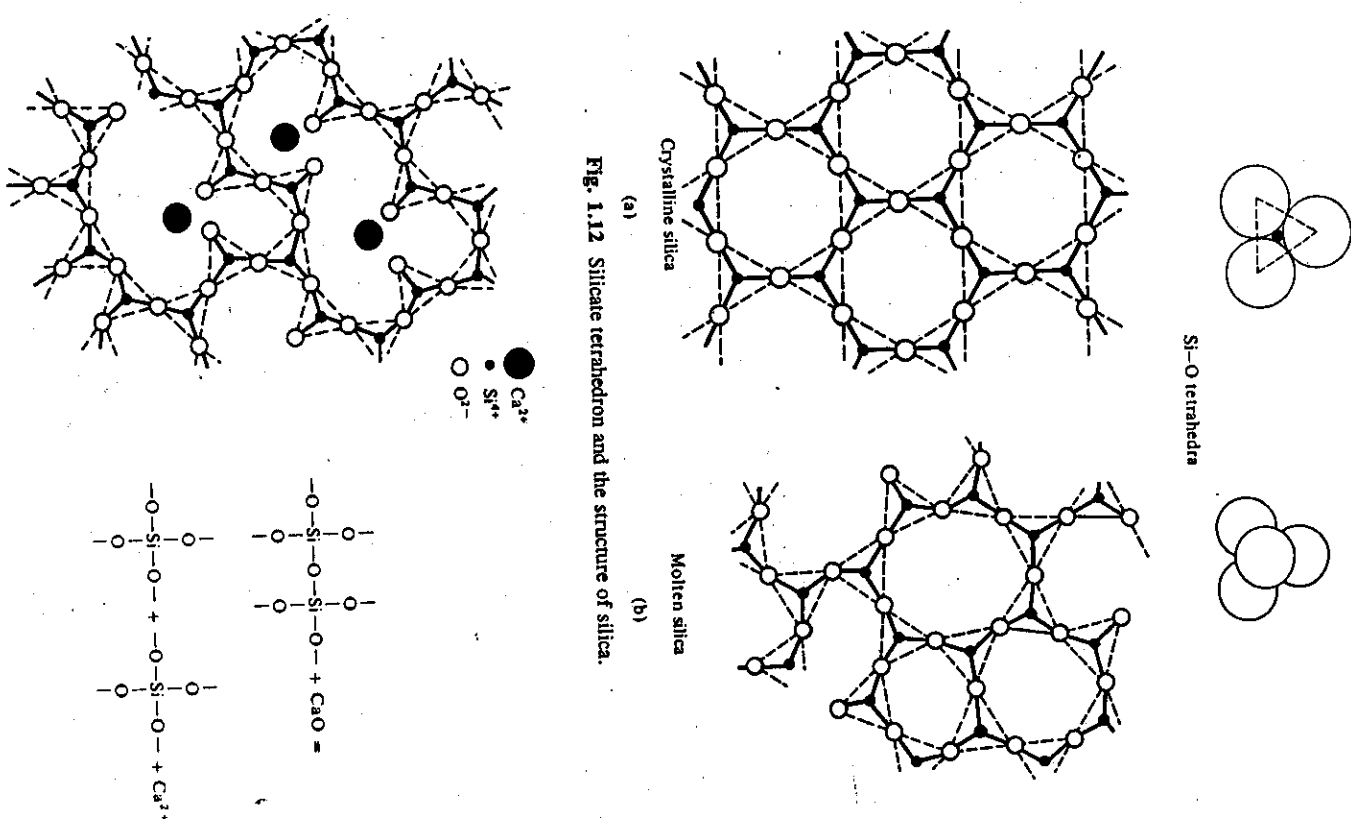


Fig. 1.13 The solution of a divalent metal oxide in molten silica.

Table 1.5 Structural relationships in basic oxide-silicate melts

Total oxygen atoms Silicon atoms	Corresponding binary molecular formula	Structure	Equivalent silicate ion
2:1	$\text{SiO}_2$	All corners of tetrahedra shared	Infinite network
5:2	$\text{MO}-2\text{SiO}_2$	One broken link per tetrahedron	$(\text{Si}_2\text{O}_{13})^6-$ or $(\text{Si}_3\text{O}_{20})^8-$
3:1	$\text{MO}-\text{SiO}_2$	Two broken links per tetrahedron (ring)	$(\text{Si}_3\text{O}_9)^6-$ or $(\text{Si}_4\text{O}_{11})^4-$
7:2	$3\text{MO}-\text{SiO}_2$	Three broken links per tetrahedron (chain)	$(\text{Si}_2\text{O}_7)^6-$
4:1	$2\text{MO}-\text{SiO}_2$ (orthosilicate)	All links broken	Discrete $(\text{SiO}_4)^4-$ tetrahedra

progressively smaller discrete ions. From the original three-dimensional network, we progress to discrete molecules, such as  $(\text{Si}_2\text{O}_7)^6-$  and  $(\text{Si}_4\text{O}_{11})^4-$ , as more and more oxygen ions are contributed by the basic oxide. Actually, it is more probable that rather than only one type of silicate ion existing at any given ratio of base to acid, there exists a statistical distribution of sizes about the average one, as indicated by the number of links broken per tetrahedron.

As the three-dimensional network breaks down, the number of Si-O bonds that need to be broken during viscous flow decreases. The shear process becomes easier as the size of the anions decreases (Fig. 1.14), so that the activation energy  $\Delta G_{vis}^{\circ}$  falls off continuously as basic oxide is added (Fig. 1.14), up to the orthosilicate composition, beyond which no further significant decrease is expected. At that point the network of  $(\text{SiO}_4)^4-$  tetrahedra is completely broken down. For compositions more basic than the orthosilicate, the viscosity changes that do occur are more likely due to changes in the liquidus temperature.

Alumina, which appears to exist in molten oxide solutions as  $(\text{AlO}_4)^3-$  anions, behaves in much the same way as silica. However, silica and alumina are not equivalent on a molar basis, since the basic building block of alumina is  $(\text{AlO}_4)^3-$ , and two  $\text{Al}^{3+}$  ions can replace two  $\text{Si}^{4+}$  ions only if one  $\text{Ca}^{2+}$  ion is available to maintain electrical neutrality. Thus, as far as the  $\text{Al}_2\text{O}_3/\text{CaO}$  ratio and on the total  $\text{Al}_2\text{O}_3$  content, as shown in Fig. 1.15, Turkdogan and Bills,<sup>15</sup> using these data in correlating the viscosity and composition of  $\text{CaO}-\text{MgO}-\text{Al}_2\text{O}_3-\text{SiO}_2$  slags, have found that, for a given temperature, a smooth curve correlates all compositions in the studied range (Fig. 1.16). To utilize this fact, we convert the slag analysis to mole fractions, and determine  $X_a$  from Fig. 1.15. Magnesium oxide ( $\text{MgO}$ ) is equivalent to  $\text{CaO}$ , up to about 10 mole percent  $\text{MgO}$ , and their mole fractions are added together to obtain  $X_{\text{CaO}}$ . Thus, when we add  $X_{\text{SiO}_2}$  and  $X_a$ , and know the temperature, we can find the viscosity from Fig. 1.16. Up to a concentration of 16 mole percent, we may consider  $\text{FeO}$  to be identical to  $\text{CaO}$ , as far as their effect on viscosity is concerned. Above 16%,  $\text{FeO}$  decreases viscosity more than  $\text{CaO}$  or  $\text{MgO}$ , except at lower temperatures.

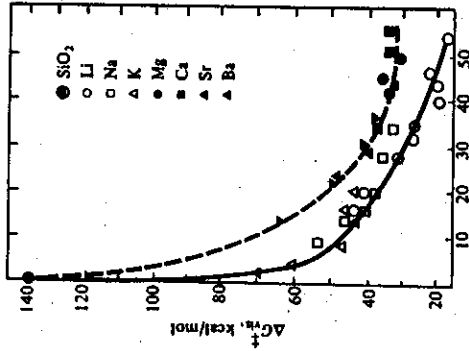


Fig. 1.14 Decrease of the activation energy of viscosity for silica as basic oxides are added. (From P. M. Bills, *J. Iron and Steel Inst.* 201, 133 (1963).)

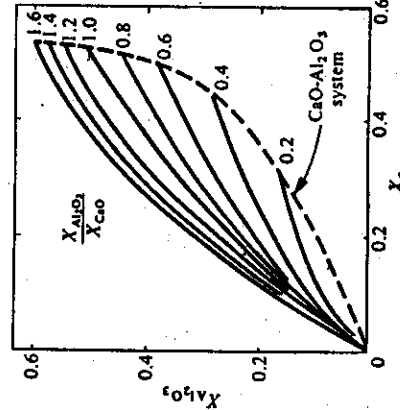


Fig. 1.15 Silica equivalence of alumina related to alumina molar concentrations and alumina: lime molar ratios. (From Bills, *J. Iron and Steel Inst.* 201, 133 (1963).)

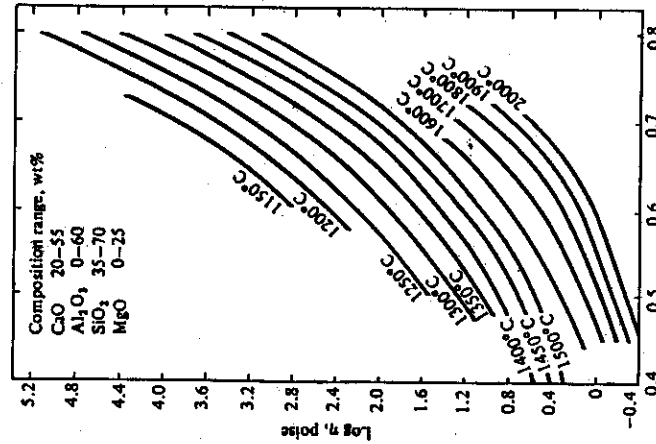


Fig. 1.16 Viscosity of  $\text{CaO}-\text{Al}_2\text{O}_3-\text{SiO}_2-\text{MgO}$  melts. Viscosity is expressed in poises. (From E. T. Turkdogan and P. M. Bills, *Amer. Ceram. Soc. Bull.* 39, 682 (1960).)

<sup>15</sup>E. T. Turkdogan and P. M. Bills, *Amer. Ceram. Soc. Bull.* 39, 682 (1960).

Finally, we should note the ability of the well-known flux  $\text{CaF}_2$  (fluorspar) to decrease the viscosity of oxide slags. Although we do not quite understand the reason, it may be due to the ability of  $\text{CaF}^+$  cations to move between silicate anions that are electrostatically bound together, by mutual attraction to a  $\text{Ca}^{2+}$  cation, thereby decreasing the electrostatic bond and thus lowering the viscosity. The effect is much more pronounced at low rather than at elevated temperatures, and in acidic slags more than in basic slags. Viscosity data for an important class of fluxes used in the continuous casting of steel are available in McCauley and Apelian.<sup>16</sup>

**Example 1.5** Calculate the viscosity of a slag with composition 40%  $\text{CaO}$ , 40%  $\text{SiO}_2$ , 8%  $\text{MgO}$ , 12%  $\text{Al}_2\text{O}_3$ , at 1600°C and at 1500°C.

**Solution.** Converting to mole fractions, we have  $X_{\text{CaO}} = 0.422$ ,  $X_{\text{MgO}} = 0.117$ ,  $X_{\text{SiO}_2} = 0.390$ ,  $X_{\text{Al}_2\text{O}_3} = 0.069$ .

For our purposes, we lump  $X_{\text{CaO}}$  and  $X_{\text{MgO}}$  together, so the effective  $X_{\text{CaO}} = 0.539$ .

Calculating the ratio  $X_{\text{Al}_2\text{O}_3}/X_{\text{CaO}}$  (= 0.128), enter Fig. 1.15 at  $X_{\text{Al}_2\text{O}_3} = 0.069$ , move slightly to the right of  $X_{\text{Al}_2\text{O}_3}/X_{\text{CaO}} = 0.2$ , and go down to find  $X_e = 0.10$ . After calculating  $X_{\text{SiO}_2} + X_e = 0.490$ , move to Fig. 1.16, and go up to the curves for 1600°C and 1500°C. The viscosity values are approximately 2.1 and 3.6 poises, respectively.

Urbain and Boiret<sup>17</sup> have a model of viscosity for a variety of liquid systems, including silicates. They derived a theoretical equation that suggests viscosity varies with temperature as

$$\eta = AT \exp(1000 B/T), \quad (1.30)$$

where  $\eta$  is in poise,  $T$  is in K and  $A$  and  $B$  are empirical constants (Table 1.6). If values of  $A$  and  $B$  are not known, then one may estimate values of  $A$  and  $B$ , depending on the type of liquid and other parameters given in their paper.

The simplest molten salts are those in which we take the bonding to be essentially electrostatic; for example, we consider that molten  $\text{NaCl}$  consists entirely of  $\text{Na}^+$  and  $\text{Cl}^-$  ions. Since there appear to be no large anion or cation complexes analogous to the  $(\text{SiO}_4)^4-$  or  $(\text{AlO}_4)^4-$  ions in molten oxide systems, and since there is a relatively large fraction of nondirectional electrostatic bonding, flow takes place relatively easily in these materials. Figure 1.17 shows viscosities of many molten salts. Note that their viscosities are about 1/100th of those of the molten oxides.

Because of the nondirectionality of the bond forces, the activation energies of viscosity for salts are also lower than those of the slags and silicates. We can also use Eq. (1.30) to estimate viscosities of molten salts. Values of  $A$  and  $B$  can be found in Table 1.7.

Table 1.6 Values of  $A$  and  $B$  for inorganic melts including silicates (from G. Urbain and M. Boiret, *Ironmkg. and Steelmkg.* 17, 255 (1990)).

Type of Melt	Melt	-ln A	B
Network Liquid	$\text{SiO}_2$	23.1	64.1
Ionic Liquids	' $\text{FeO}'$	12.5	6.1
	$\text{Al}_2\text{O}_3$	14.2	13.2
	$\text{B}_2\text{O}_3$	12.3	13.2
	$\text{P}_2\text{O}_5$	16.6	21.7
	$\text{Fe}_2\text{SiO}_4$	13.6	9.2
	$\text{Mg}_2\text{SiO}_4$	14.8	13.3
	$\text{MgCaSiO}_4$	16.9	19.1
	$\text{MgSiO}_3$	17.7	18.8
	$(\text{Mg/Ca})\text{SiO}_3$	17.5	20.8
	$\text{CaSiO}_3$	17.3	19.6
	$\text{MnSiO}_3$	19.6	24
	$\text{Si}_2\text{SiO}_3$	17.4	20.6
	$\text{BaSiO}_3$	17.7	21.1
	$\text{LiAlSiO}_4$	19.8	28.1
	$\text{NaAlSiO}_4$	25.6	43.9
	$\text{KAISiO}_4$	25.3	50.2
	$\text{Ca}(\text{AlSiO}_3)_2$	20.7	30.6
	$\text{Sr}(\text{AlSiO}_3)_2$	21.3	33.2
	$\text{Ba}(\text{AlSiO}_3)_2$	22.6	37.2
	$\text{LiAlSi}_3\text{O}_6$	21.2	34.7
	$\text{LiAlSi}_3\text{O}_6$	21.4	38
	$\text{NaAlSi}_3\text{O}_6$	26	51.5
	$\text{KAISi}_3\text{O}_6$	27.4	55.6
	$\text{LiAlSi}_3\text{O}_6$	23.2	42.5
Binary Silicate	Mole Fraction		
$\text{B}_2\text{O}_3-\text{SiO}_2$	$\text{B}_2\text{O}_3$	21.9	55.1
	0.062	20.1	48.5
	0.100	19.5	44
	0.147	15.5	35
	0.252	12.3	21.9
	0.446	12.04	19.8
	0.516	12.4	15.02
	0.777	13.1	14.2
	0.893	13.1	13.7
	0.940		
Binary Silicate	Mole Fraction		
$\text{Al}_2\text{O}_3-\text{SiO}_2$	$\text{Al}_2\text{O}_3$	21.67	39.21
	0.202	18.54	25.85
	0.500	17.12	21.01

<sup>16</sup>W. L. McCauley and D. Apelian, *Can. Met. Quart.* 20, 247 (1981).

<sup>17</sup>G. Urbain and M. Boiret, *Ironmkg. and Steelmkg.* 17, 255, 1990.

Table 1.6 (continued)

Type of Melt	Melt	-ln A	B
Binary Silicate $\text{PbO-SiO}_2$	Mole Fraction PbO		
	0.429	21.1	20.6
	0.474	18.9	17.8
	0.512	19.2	17.8
	0.603	17.4	12.6
	0.666	17.3	12.6
	0.633	16.7	11.3
	0.641	17.7	12.7
	0.651	17.5	11.9
	0.670	17.1	12
	0.815	15.4	8.6

Table

Melt	$-\ln A$	$B$	Melt	$-\ln A$	$B$
LiCl	15.91	4.52	KI	14.9	3.75
NaCl	16.65	5.85	LiNO <sub>3</sub>	14.9	3.18
KCl	15.63	4.44	NaNO <sub>3</sub>	14.36	2.61
LiBr	15.14	3.65	KNO <sub>3</sub>	14.66	2.88
NaBr	14.84	3.71	Li <sub>2</sub> CO <sub>3</sub>	19.16	9.59
KBr	15.01	3.7	Na <sub>2</sub> CO <sub>3</sub>	22.86	14.41
LiI	14.48	3.04	K <sub>2</sub> CO <sub>3</sub>	24.08	16.06
NaI	15.17	3.88			

15 NON-NEWTONIAN FLUIDS

According to Newton's law of viscosity (Eq. 1.3) the shear stress  $\tau_{xy}$ , plotted versus the velocity gradient  $-d\psi_x/dy$ , should yield a straight line running through the origin. Experimentally, this has been proved true for all gases and for all single-phase nonpolymeric liquids. Fluids that behave in this manner—and most fluids do—are termed *Newtonian fluids*. However, Eq. (1.3) does not describe the behavior of a large number of fluids which are called *non-Newtonian fluids* and include substances such as molten plastics, slurries, and certain gels.

The study of Newtonian flow is part of a larger discipline of science known as *rheology*. Rheology encompasses the mechanical behavior of gases, liquids, and solids, including Newtonian gases and liquids on the one hand and elastic stress-strain behavior of solids on the other. Certain stages.

A large number of non-Newtonian fluids follow one of the behavioral patterns represented in Fig. 1.18, where the shear stress  $\tau_{yx}$  is plotted versus the rate of strain  $\dot{\gamma}$  (i.e.,  $-d\eta/dy$  at steady state). The curve of stress-strain rate is also plotted for Newtonian fluids, demonstrating the obvious fact that  $\tau_{yx}/\dot{\gamma}$  is independent of  $\dot{\gamma}$ ; i.e., the slope of the Newtonian curve is  $\eta$ . On the other hand, non-Newtonian fluids are those in which  $\tau_{yx}/\dot{\gamma}$  is a function of  $\dot{\gamma}$ .

The fluids classified as *Bingham plastics* require a finite shear stress  $\tau_0$  (yield stress) to initiate flow. In other words, the fluid remains rigid when the shear stress is less than  $\tau_0$ , but flows when the shear stress exceeds  $\tau_0$ . An example of a fluid exhibiting Bingham plastic behavior is an aqueous slurry of fine, powdered coal. The following relationship gives the rate of shear stress and shear strain:

(1-31)

Here  $\eta_p$  is a plastic viscosity or coefficient of rigidity. We use the plus sign when  $\dot{\gamma}$  is

*Pseudoplastic fluids*, which are characterized by a decreasing slope of the  $\tau_y$  versus  $\dot{\gamma}$  curve as the stress increases, need, like Newtonian fluids, no yield stress for flow, but, unlike Newtonian fluids,  $\tau_y/\dot{\gamma}$  does depend on  $\tau_y$ . *Dilatant fluids* differ from pseudoplastics in that the  $\tau_y$  versus  $\dot{\gamma}$  curve has an increasing slope as stress increases. For both pseudoplastic and dilatant fluids we can sometimes use the *Ostwald power law* to describe the relationship of the stress, strain rate,

11-22

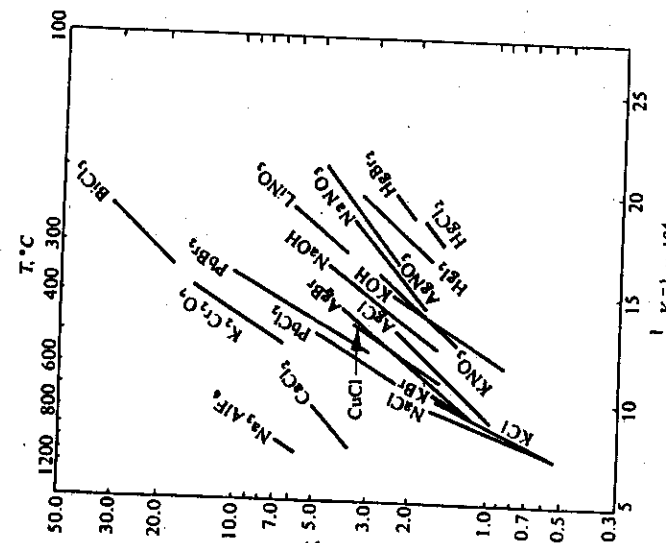


**Fig. 1.17** Viscosities of molten salts. (From C. J. Smithells, *Metals Reference Book*, fourth edition, Vol. 1, Plenum Press, New York, 1967.)

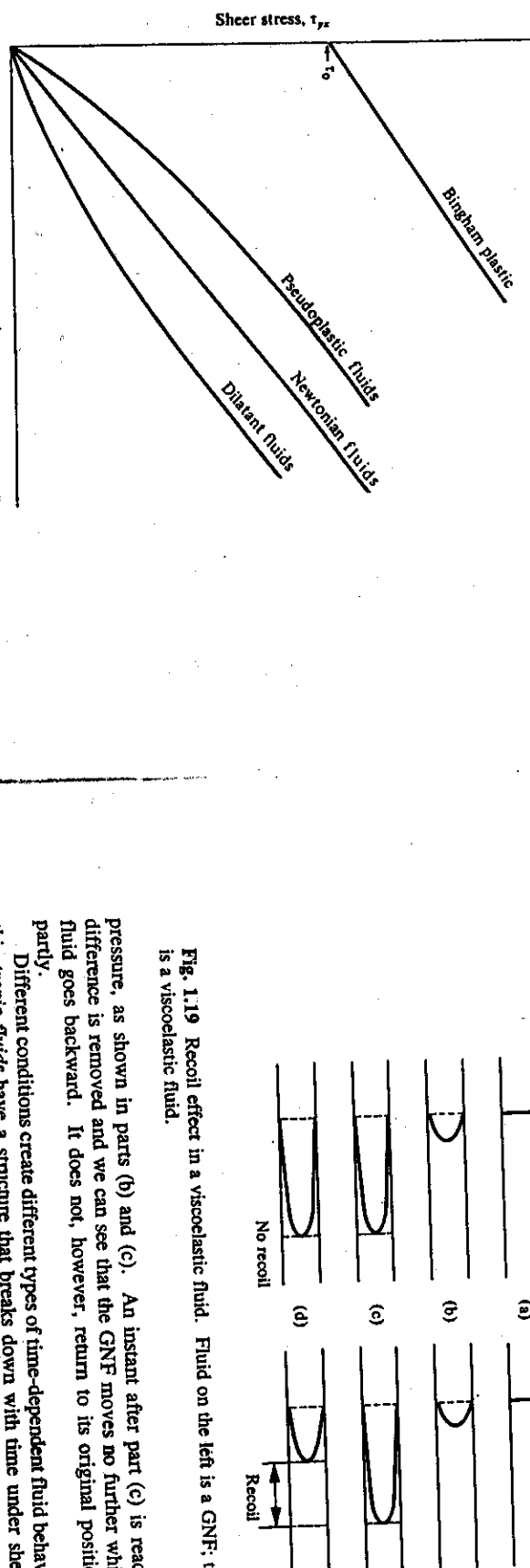


Fig. 1.18 Stress-strain rate curves for time-independent fluids.

Here,  $k$  is a measure of the fluid's consistency, and  $n$  is a measure of the fluid's departure from Newtonian behavior. For  $n = 1$ , Eq. (1.32) reduces to Newton's law of viscosity with  $k = \eta$ . For  $n < 1$ , the behavior is pseudoplastic, whereas if  $n > 1$  it is dilatant. Aqueous suspensions of clay, lime, and cement rock are examples of various fluids described by the power law.

Since the Ostwald power law is the simplest model to describe dilatant and pseudoplastic fluids, it is often applied. However, when using it, we should keep in mind that this model does not give an accurate portrayal of the low-shear-rate region (i.e., low flow rates).<sup>18</sup> In addition to these models, numerous other empirical equations have been proposed to express the relationship between shear stress and strain rate. The models we have been discussing are called *generalized Newtonian Fluids* (GNF). They should not be applied to those fluids or conditions in which viscoelastic effects are present and play an important role, or to the fluids which exhibit *time-dependent properties*. The fluids in which viscoelastic effects are of great importance under certain conditions are *high polymers*.

*Viscoelastic fluids* are fluids which exhibit elastic recovery from deformation, that is, they recoil. This is in contrast with the behavior of GNF's which do not recoil. This difference is illustrated by the experiment depicted in Fig. 1.19. We observe the behavior of a black line made by injecting a charcoal slurry into a transparent tube. In part (a), the line has just been introduced into the tube with the fluid at rest. The fluid starts flowing when the pressure is lowered at the right end of the tube; both fluids flow in the direction of the lower

Fig. 1.19 Recoil effect in a viscoelastic fluid. Fluid on the left is a GNF; that on the right is a viscoelastic fluid.

pressure, as shown in parts (b) and (c). An instant after part (c) is reached, the pressure difference is removed and we can see that the GNF moves no further while the viscoelastic fluid goes backward. It does not, however, return to its original position, recoiling only partly.

Different conditions create different types of time-dependent fluid behavior. For example, *thixotropic fluids* have a structure that breaks down with time under shear. At a constant shear-strain rate, the viscosity decreases with time and approaches an asymptotic value. Under steady-state flow conditions, when the asymptotic value is maintained, thixotropic fluids may be treated as GNF's. *Rheopetric fluids*, in which viscosity increases with time, behave again quite differently from thixotropic fluids.

The purpose of this brief introduction to non-Newtonian fluids has been to make the reader aware of the fact that there are many fluids that do not necessarily obey Newton's law of viscosity, and that a direct application to such fluids of data and concepts in fluid mechanics dealing with Newtonian fluids could lead to serious engineering blunders. In the remainder of the text, we deal usually with Newtonian fluids.

The rheology of polymers, in itself, is a complex science. The viscosity of a polymer is a function of shear stress (or strain rate), temperature and molecular weight. The shear stress dependence at a given temperature is usually given by the power law of Eq. (1.32). The temperature dependence of viscosity can be represented by the exponential function, 'given by Eq. (1.18), provided there is no transition in the temperature range being considered and the temperature is at least  $1.5 T_g$  ( $T_g$  is the glass transition temperature). Equation (1.20) indicates that  $\Delta G^\circ$  increases with the vaporization energy, so we could expect that  $\Delta G^\circ$  would increase with molecular weight. This is true, but at very high degrees of polymerization, the activation energy is independent of molecular weight.

Based on the above, therefore, we represent the viscosity of a particular polymer as a function of degree of polymerization ( $N$ ), temperature ( $T$ ), and strain rate ( $\dot{\gamma}$ ). Generally, the functional dependence of  $\dot{\gamma}$  is separated from the other two so that

$$\eta(N, T, \dot{\gamma}) = f(N, T) g(\dot{\gamma}) \quad (1.33)$$

<sup>18</sup>R. B. Bird, *Can. J. of Chem. Eng.* 43, 161 (Aug. 1965).

Many polymers follow the power law given by Eq. (1.32), where  $k$  can be interpreted as the Newtonian viscosity or zero strain rate viscosity,  $\eta_0$ . In the absence of data, the viscosity can be approximated<sup>19</sup> by

$$\frac{\eta}{\eta_0} = 1 + A_1(\dot{\gamma}\eta_0)^\alpha + A_2(\dot{\gamma}\eta_0)^{2\alpha}, \quad (1.34)$$

with  $A_1 = 6.12 \times 10^{2.645}$ ,  $A_2 = 2.85 \times 10^{-3.645}$ ,  $\alpha = 0.355$  and  $\eta$  and  $\eta_0$  in N s m<sup>-2</sup> and  $\dot{\gamma}$  in s<sup>-1</sup>.

The dependence of the Newtonian viscosity on molecular weight and temperature for many high molecular weight polymers show

$$\log \eta_0 = 3.4 \log N + k(T), \quad (1.35)$$

where  $N$  is the weight-average degree of polymerization and  $k(T)$  is given in Table 1.8. The weight-average degree of polymerization is based on the so-called weight-average molecular weight:

$$\bar{M}_w = \frac{\sum x_i M_i^2}{\sum x_i M_i},$$

Table 1.8 Temperature dependence of  $k$  in Eq. (1.35) for long-chain polymers (from A. T. DiBenedetto, *The Structure and Properties of Materials*, McGraw-Hill, New York, 1967, p. 364).

Polymer	$k(T, K)$	$k$	$T, K$	$N$ greater than
<u>Linear nonpolar polymers</u>				
Polyisobutylene	$5.5 \times 10^3/T^2 - 10.93$	—	—	610
Polystyrene	$2.7 \times 10^{16}/T^6 - 9.51$	—	—	730
<u>Linear polar polymers</u>				
Poly(methyl methacrylate)	$4.5 \times 10^3/T^3 - 7.4$	—	—	208
Polyvinyl acetate	$9.77 \times 10^{10}/T^4 - 10.05$	—	—	—
Decamethylene sebacate	—	—	—	—
Decamethylene adipate	$3.4 \times 10^3/T^2 - 11.2$	-8.2	382	290
Decamethylene succinate	—	—	—	280
Diethyl adipate	$2.1 \times 10^{10}/T^4 - 9.1$	-8.0	382	290
<u>Effect of branching</u>				
Poly( <i>e</i> -caprolactam):	—	—	—	—
Linear	—	-8.0	526	340
Terrachain	—	-8.1	526	390
Octachain	—	-8.7	526	550

where  $x_i$  is the mole fraction of molecules with molecular weight  $M_i$ . After  $\bar{M}_w$  is found, then  $N$  is simply

$$\bar{M}_w = \frac{M_w}{M_m},$$

where  $M_m$  is the molecular weight of a mer.

When  $k(T)$  is not available, then an empirical equation for temperature dependence is recommended. It is

$$\log \frac{\eta_0}{\eta_r} = -\frac{8.86(T - T_r)}{101.6 + T - T_r}, \quad (1.36)$$

where the subscript  $r$  refers to a reference state. Values of  $T_r$  and  $T_i$  for several polymers are in Table 1.9. Equation (1.36) works best in the range  $T_r \leq T < T_i + 100$  K. Since most thermoplastics are formed in the range of 1.3 to 1.5  $T_r$ , Eq. (1.36) is often used for temperature extrapolations. For temperatures above the limit of Eq. (1.36),  $T > 1.5 T_r$ , we can use Eq. (1.18) for extrapolations.

Table 1.9 Reference Temperature,  $T_r$ , and Glass Transition Temperature,  $T_i$ , for Selected Polymers (from DiBenedetto, *Ibid.*, p. 362)

Polymer	$T_r, K$	$T_i, K$
Polyisobutylene	243	202
Polymethyl acrylate	378	324
Polyvinyl acetate	349	301
Polystyrene	408	373
Polymethylmethacrylate	433	378
Polyvinyl acetal	380	—
Butadiene-styrene:	75-25	—
60-40	268	216
50-50	283	235
30-70	296	252
	328	291

Example 1.6 Polystyrene has an average molecular weight ( $\bar{M}_w$ ) of  $10^6$  g mol<sup>-1</sup>. The mer is C<sub>8</sub>H<sub>8</sub>. Estimate its Newtonian viscosity at 450 K.

Solution. We can make use of Eq. (1.35) and Table 1.8. To do so we first calculate the mer weight and the degree of polymerization.

$$M_m = (3)(12.01) + (8)(1) = 104.08 \text{ g mol}^{-1}$$

$$N = \frac{\bar{M}_w}{M_m} = \frac{10^6}{104.08} = 9608$$

Then

$$\log \eta = 3.4 \log 9608 + \frac{2.7 \times 10^{16}}{450^6} - 9.51 = 7.28$$

$$\eta = 1.92 \times 10^7 \text{ poise} = 1.92 \times 10^6 \text{ N s m}^{-2}$$

**Example 1.7** At 50 K above  $T_g$ , the Newtonian viscosity of a polymer is  $10^4 \text{ N s m}^{-2}$ . Estimate the viscosity at 25 K above  $T_g$ .

**Solution.** The given data can be used to represent the reference state in Eq. (1.36). Then

$$\log \frac{\eta_0}{10^4} = -\frac{8.86(-25)}{101.6 - 25} = 2.892$$

$$\eta_0 = 7.80 \times 10^8 \text{ N s m}^{-2}$$

This illustrates very clearly the rapid increase in viscosity as  $T_g$  is approached.

Before we leave this chapter, we must make it abundantly clear that the relationships used to estimate the viscosities of polymers are just that—only estimates. We have not considered situations in which polymers are in solvents and in polymer systems undergoing polymerization. Students of polymers, desirous of more information, should consult the references already presented. In addition, other useful starting sources are Biesenberger and Sebastian,<sup>20</sup> Rodriguez,<sup>21</sup> and Crawford.<sup>22</sup> Viscosities of polymers are used to characterize degree of polymerization and, indeed, as part of specifications in purchasing polymers and in quality control. Practitioners tell us that viscosity can vary from batch to batch, and so it is always better to measure viscosity than it is to rely on an estimate.

## PROBLEMS

- 1.1 Compute the steady-state momentum flux ( $\text{N m}^{-2}$ ) in a lubricating oil, viscosity equal to  $2 \times 10^{-2} \text{ N s m}^{-2}$ , that is contained between a stationary plate and one that is moving with a velocity of  $61.0 \text{ cm s}^{-1}$ . The distance between the plates is 2 mm. Next, show the direction of the momentum flux and the shear stress with respect to the  $x$ - $y$  axis system in the diagram below.



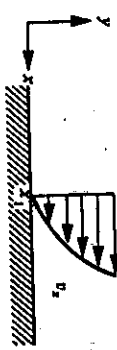
Stationary

- 1.2 Near the surface of a flat plate, water has a velocity profile given by

$$v_r = 3y - y^3$$

with  $y$  in mm,  $v_r$  in  $\text{cm s}^{-1}$ , and  $0 \leq y \leq 1 \text{ mm}$ . The density and the kinematic viscosity of water are  $10^3 \text{ kg m}^{-3}$  and  $7 \times 10^{-7} \text{ m}^2 \text{ s}^{-1}$ , respectively.

- a) What is the shear stress at  $x_1$  on the plate?  
 b) What is the momentum flux in the  $x$ -direction at  $y = 0.8 \text{ mm}$  and  $x = x_1$  in the  $y$ -direction?  
 c) Is there momentum flux in the  $x$ -direction at  $y = 0.8 \text{ mm}$  and  $x = x_1$  in the  $x$ -direction? If so, evaluate.



y

x

v<sub>r</sub>

- 1.3 In fluidized bed processes, operating temperatures can vary from process to process or within the beds itself. Therefore, it is necessary to know how these temperature variations affect the properties, such as viscosity of the fluidizing gas in the reactor. Taking air as the fluidizing gas, estimate its viscosity at 313 K and 1073 K when considered as a one component gas with the parameters given in Table 1.1. Repeat the estimates, only now consider the air to be 79%  $\text{N}_2$ , 21%  $\text{O}_2$ . Compare these results to the experimental values of 0.019 cP and 0.0438 cP at 313 K and 1073 K, respectively.

- 1.4 Consider that the binary gas A-B is such that at a given temperature  $\eta_A = \eta_B$ . Plot the ratio of  $\eta_{\text{mix}}/\eta_A$  versus  $x_A$  if the ratio of the molecular weights of the two species,  $M_A/M_B$ , is:  
 a) 100; b) 10; c) 1.

- 1.5 A quick estimate of the viscosity of a binary gas A-B is

$$\eta_{\text{mix}} = x_A \eta_A + x_B \eta_B$$

What are the maximum errors in the viscosities estimated by the above equation when compared to the results calculated for a), b) and c) in problem 1.4? Briefly discuss the errors.

<sup>20</sup>J. A. Biesenberger and D. H. Sebastian, *Principles of Polymerization Engineering*, John Wiley & Sons, New York, NY, 1983.

<sup>21</sup>F. Rodriguez, *Principles of Polymer Systems*, 2nd ed., Hemisphere Publ. Corp., Washington, DC, 1982.

<sup>22</sup>R. J. Crawford, *Plastics Engineering*, 2nd ed., Pergamon Press, Oxford, England, 1987.

✓ 1.6 At 920 K the viscosity of methane ( $\text{CH}_4$ ) is  $2.6 \times 10^{-3} \text{ N s m}^{-2}$ , and the viscosity of nitrogen is  $3.8 \times 10^{-3} \text{ N s m}^{-2}$ . Plot the viscosity of methane-nitrogen mixtures versus mole fraction methane at 920 K.

✓ 1.7 Estimate the viscosity of liquid beryllium at 1575 K. The following data are available: atomic weight, 9.01 g mol<sup>-1</sup>; melting point, 1550 K; density at 293 K, 1850 kg m<sup>-3</sup>; crystal structure, hex; atomic radius, 0.114 nm.

✓ 1.8 Chromium melts at approximately 2148 K. Estimate its viscosity at 2273 K given the following data: atomic weight, 52 g mol<sup>-1</sup>; density, 7100 kg m<sup>-3</sup>; interatomic distance, 0.272 nm.

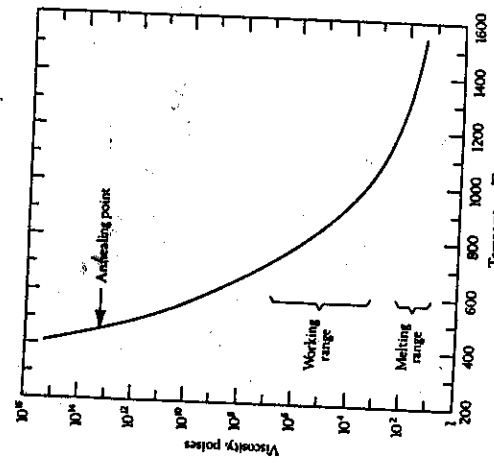
✓ 1.9 At 1273 K a melt of Cu-40% Zn has a viscosity of 5 cP and at 1223 K this same alloy has a viscosity of 6 cP. Using this information, estimate the viscosity of the alloy at 1373 K.

✓ 1.10 Many metal processing operations, such as steelmaking, employ a slag as a means by which impurities are removed from the processing operation. Thus, it becomes necessary to characterize certain properties of the slag, such as viscosity, at temperatures it will encounter in the processing operation. Using Bill's method, estimate the viscosity of a 50 wt. %  $\text{SiO}_2$ , 30 wt. %  $\text{CaO}$ , 20 wt. %  $\text{Al}_2\text{O}_3$  slag at 1773 K.

✓ 1.11 Assume that the viscosity of a glass varies with temperature according to Eq. (1.18). At 1700 K it has a viscosity of  $20 \text{ N s m}^{-2}$ ; at 1500 K it is  $100 \text{ N s m}^{-2}$ . What is the viscosity at 1450 K?

✓ 1.12 When oxides such as  $\text{MgO}$  and  $\text{CaO}$  are added to molten silica, the activation energy of viscosity is reduced from 135 kcal/mol for pure  $\text{SiO}_2$  to approximately 39 kcal/mol for 0.5 mole fraction of  $\text{SiO}_2$ . We can observe even more dramatic effects when oxides such as  $\text{Li}_2\text{O}$  and  $\text{Na}_2\text{O}$  are added to silica. For example, for 0.5 mol fraction  $\text{SiO}_2$ , the activation energy is only 23 kcal/mol. Explain with the aid of any appropriate sketches, why this phenomenon occurs.

✓ 1.13 The glass transition temperature for the soda-lime-silicate glass shown to the right is approximately 720 K. Test the applicability of Eq. (1.18). Does it apply? Explain why or why not.



✓ 1.14 Equation (1.30) differs in form from Eq. (1.18). Based on Eq. (1.30) and Table 1.6, calculate the viscosity of 0.5  $\text{Al}_2\text{O}_3$ -0.5  $\text{SiO}_2$  (mol fraction) in the temperature range of 2100 to 2500 K. Plot your results as  $\ln \eta$  vs.  $T$ . Does Eq. (1.18) adequately represent your results?

✓ 1.15 Estimate the viscosities of LiCl and LiBr at 1000 K. Which is greater? Can you explain your results on the basis of ionic bonding?

✓ 1.16 Estimate the percent change in viscosity of polymer melts on changing the shear strain rate from  $10^4 \text{ s}^{-1}$  to  $10^1 \text{ s}^{-1}$ .

✓ 1.17 Estimate the viscosity of poly( $\epsilon$ -caprolactam) at 526 K (see Table 1.8). Compare its viscosity to that of a branched form (octachain). On the basis of the structure of polymers, explain the effect of branching on the viscosity.

✓ 1.18 Refer to Example 1.6. Estimate the viscosities at the glass transition temperature ( $T_g$ ) and 10 K above  $T_g$ . Comment on the sensitivity of the viscosity with temperature near the glass transition temperature.

## 2

---

## LAMINAR FLOW AND THE MOMENTUM EQUATION

---

In discussing Newton's law of viscosity, we have described fluid motion as flowing parallel layers which, because of viscosity, establish a velocity gradient dependent upon the shear stress applied to the fluid. This velocity gradient has been regarded as a potential or a "reason" for momentum transport from layer to layer.

In this chapter, we shall first derive simple differential equations of momentum for special cases of flow, for example, flow of a falling film, flow between two parallel plates, and flow through tubes. To make it possible for the student to participate in developing complex formulas, these derivations make use of the concept of a momentum balance and the definition of viscosity. These classic examples of viscous flow patterns certainly apply to rather simplified and idealized conditions. You may be tempted, therefore, to disregard the importance of thoroughly understanding these examples; however, we should point out that despite the simplicity of the following calculations, you will gain an appreciation of the variables involved. Also, you will obtain a basic tool for analyzing engineering problems: the ability to arrive at pertinent differential equations.

### 2.1 MOMENTUM BALANCE\*

A momentum balance is applied to a small control volume of fluid to develop a differential equation. The differential equations, when their solutions comply with the physical restrictions (boundary conditions), yield the algebraic relationships which can be used to determine the engineering characteristics of the system. The solutions give the velocity distributions from which other characteristics, including the shear stress at the fluid-solid interface, are developed. As we shall see in Chapter 3, the shear stress at the fluid-solid

---

\*The general aspects of the developments in Sections 2.1-2.6 are similar to those found in Chapters 2-3 in R. B. Bird, W. E. Stewart, and E. N. Lightfoot, *Transport Phenomena*, Wiley, New York, 1960.

interface is very important in analyzing the disposition of energy flowing through a system. For steady state flow, the momentum balance is

$$\left( \text{rate of momentum in} \right) - \left( \begin{array}{l} \text{rate of momentum out} \\ \text{momentum in} \end{array} \right) + \left( \begin{array}{l} \text{sum of forces} \\ \text{acting on system} \end{array} \right) = 0. \quad (2.1)$$

Momentum in (or out) may enter a system by momentum transfer according to Newton's equation of viscosity (if the fluid is Newtonian); otherwise various equations for non-Newtonian fluids are used), or it may enter due to the overall fluid motion. The forces applied to the balance are pressure forces and/or gravity forces.

The momentum balance is actually a force balance because we are concerned with the *rate of momentum* that enters and leaves the unit volume. Units of momentum are  $ML^2T^{-1}$  ( $M$  = mass,  $L$  = length,  $T$  = time), whereas a rate of momentum is  $ML^2T^{-2}$ . Classical physics states clearly that forces ( $F = ma$ ) are involved when we consider momentum rates. Thus, if the term momentum balance confuses the reader, he or she is reassured that a force balance is being applied.

## 2.2 FLOW OF A FALLING FILM

Consider the flow of a liquid at steady state along an inclined plane (Fig. 2.1). The liquid is at a constant temperature, and therefore its density and viscosity are constant. Furthermore, we consider only that portion of the plane where the entrance and exit of the liquid to the plane are sufficiently remote so as not to influence the velocity  $v_z$ . In this situation,  $v_z$  is not a function of  $z$  but obviously a function of  $x$ . Figure 2.1 also depicts the unit volume as a "shell" with a thickness  $\Delta x$  and length  $L$ ; the width of the shell extends a distance  $W$ , perpendicular to the page. The terms used in Eq. (2.1) are as follows:

Rate of momentum in  
across surface at  $x$   
(moment transport due to viscosity)

Rate of momentum out  
across surface at  $x + \Delta x$   
(due to viscosity)

Rate of momentum in  
across surface at  $z = 0$   
(due to fluid motion)

Rate of momentum out  
across surface at  $z = L$   
(due to fluid motion)

Gravity force acting on fluid

In this particular problem, the pressure forces are irrelevant because the pressure does not vary with  $z$ . Also note that all terms in the list, including the first two, are  $z$ -directed forces. Figure 2.1 shows that momentum in by viscous transport is  $x$ -directed, but if we think of

\*In the region where  $v_z = f(x)$  and  $v_z \neq f(z)$ , we say that the flow is *fully developed*.

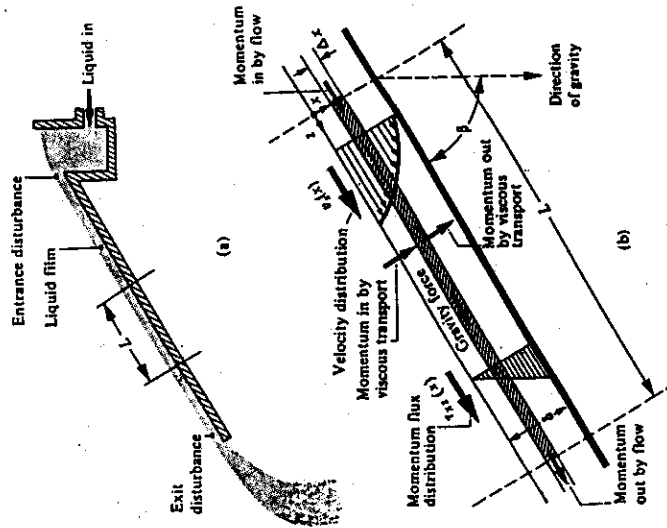


Fig. 2.1 Flow of a falling film.

interpreting  $v_z$  in an alternative way—namely, as a shear stress—we certainly realize that we are dealing with a  $z$ -directed force.

When all these terms are substituted into the momentum balance, we get

$$LW\tau_{xz}|_x - LW\tau_{xz}|_{x+\Delta x} + W\Delta x\rho v_z^2|_{z=0} - W\Delta x\rho v_z^2|_{z=L} + LW\Delta x\rho g \cos \beta = 0. \quad (2.2)$$

Because we are restricted to that part of the inclined plane which does not feel the effects of the exit and entrance,  $v_z$  is independent of  $z$ . Therefore, the third and fourth terms cancel one another out. Equation (2.2) is now divided by  $LW\Delta x$  and, if  $\Delta x$  is allowed to be infinitely small, we obtain

$$\lim_{\Delta x \rightarrow 0} \frac{\tau_{xz}|_x + \tau_{xz}|_L}{\Delta x} = \rho g \cos \beta. \quad (2.3)$$

We have now recognized the definition of the first derivative of  $\tau_{xz}$  with respect to  $x$ , and have thus developed the differential equation pertinent to our system:

$$\frac{d\tau_{xz}}{dx} = \rho g \cos \beta. \quad (2.4)$$

This equation is integrated to yield

$$\tau_{xz} = \rho g x \cos \beta + C_1. \quad (2.5)$$

Equation (2.5) describes the momentum flux (or alternatively the shear-stress distribution), but contains an integration constant  $C_1$ . This constant is evaluated by recognizing that the shear stress in the liquid is very nearly zero at a liquid-gas interface. In other words, the gas phase, in this instance, offers little resistance to liquid flow, which results in a realistic boundary condition:

$$\text{B.C. 1} \quad \text{at } x = 0, \quad \tau_{xz} = 0. \quad (2.6)$$

Substitution of this boundary condition into Eq. (2.5) requires that  $C_1 = 0$ ; hence the momentum flux is

$$\tau_{xz} = \rho g x \cos \beta. \quad (2.7)$$

If the fluid is Newtonian, then we know that the momentum flux is related to the velocity gradient according to

$$\tau_{xz} = -\eta \frac{du}{dx}. \quad (2.8)$$

Substituting this expression for  $\tau_{xz}$  in Eq. (2.7) gives the distribution of the velocity gradient:

$$\frac{du}{dx} = -\frac{\rho g \cos \beta}{\eta} x. \quad (2.9)$$

Integrating Eq. (2.9), we have

$$v_z = -\left[\frac{\rho g \cos \beta}{2\eta}\right] x^2 + C_2. \quad (2.10)$$

Another integration constant has evolved which is evaluated by examining the other boundary condition, namely, that at the fluid-solid interface the fluid clings to the wall; that is,

$$\text{B.C. 2} \quad \text{at } x = \delta, \quad v_z = 0. \quad (2.11)$$

Substituting this into Eq. (2.10), we determine the constant of integration:  $C_2 = (\rho g \cos \beta / 2\eta)\delta^2$ . Therefore the velocity distribution is

$$v_z = \frac{\rho g \delta^2 \cos \beta}{2\eta} \left[1 - \left(\frac{x}{\delta}\right)^2\right]. \quad (2.12)$$

and is parabolic. Once the velocity profile has been found, a number of quantities may be calculated.

- i) The maximum velocity,  $V_z^{\max}$ , is that velocity at  $x = 0$ :

$$V_z^{\max} = \frac{\rho g \delta^2 \cos \beta}{2\eta}. \quad (2.13)$$

- ii) The average velocity,  $\bar{v}_z$ , is simply

$$\bar{v}_z = \frac{1}{\delta} \int_0^\delta v_z dx = \frac{\rho g \delta \cos \beta}{2\eta} \int_0^\delta \left[1 - \left(\frac{x}{\delta}\right)^2\right] dx = \frac{\rho g \delta^2 \cos \beta}{3\eta}. \quad (2.14)$$

- iii) The volume flow rate,  $Q$ , is given by the product of the average velocity and the cross-section of flow:

$$Q = \bar{v}_z (W\delta) = \frac{\rho g W\delta^3 \cos \beta}{3\eta}. \quad (2.15)$$

The foregoing analytical results are valid only when the film is falling in laminar flow (straight streamlines). This condition can easily be satisfied for the slow flow of viscous films, but experimentally, it has been found that as the film velocity increases, the film thickness increases (according to Eq. (2.14)) to a critical value, depending on the liquid's kinematic viscosity, where turbulence replaces laminar flow. Of course, when turbulent flow develops, Eqs. (2.12)-(2.15) are no longer valid.

**Example 2.1** A viscous molten glass covers a molten metal, and together they flow slowly down an inclined plane that makes an angle  $\beta$  with the vertical. The thickness of the glass is  $\delta_1$ , and the combined thickness of both layers is  $\delta_0$ . Of course, each layer has its own viscosity. For a plane of length  $L$ , assume laminar flow that is fully developed and derive an equation for the velocity distribution in each layer.

**Solution.** We should recognize that Eq. (2.4) applies to both layers. In the glass (i.e., the top layer),  $\tau_{xz} = 0$  at  $x = 0$ . Therefore, after integrating Eq. (2.4) the shear stress in the glass is

$$\tau_{xz} = \rho_p x g \cos \beta$$

or

$$\frac{du}{dx} = -\frac{x g \cos \beta}{\rho_p}$$

where the subscript  $g$  is for glass. Another integration gives:

$$u_g = -\frac{x^2 g \cos \beta}{2\rho_p} + c_1, \quad \delta_1 \leq x \leq 0.$$

In the metal, we rewrite Eq. (2.4) as

$$\frac{d^2 u}{dx^2} = -\frac{g \cos \beta}{\rho_m}$$

and integrate twice. The result is

$$u_m = -\frac{x^2 g \cos \beta}{2\rho_m} - c_2 x + c_3, \quad \delta_1 \leq x \leq \delta_2$$

where the subscript  $m$  is for metal.

In order to evaluate the three constants,  $c_1$ ,  $c_2$  and  $c_3$ , we apply the following conditions:

$$\text{B.C. 1: } u_g = 0 \text{ at } x = \delta_2,$$

$$\text{B.C. 2: } u_g \text{ (metal)} = u_g \text{ (glass)} \text{ at } x = \delta_1,$$

$$\text{B.C. 3: } \tau_{xz} \text{ (metal)} = \tau_{xz} \text{ (glass)} \text{ at } x = \delta_1.$$

From these three conditions (and lines and lines of algebra), the three constants can be determined so that the velocity distribution in both layers can be found. The results are

$$c_2 = \frac{(\rho_s - \rho_m) \delta_1 g \cos \beta}{\eta_m},$$

$$c_3 = \frac{\delta_2^2 g \cos \beta}{2 \eta_m} + c_2 \delta_2,$$

and

$$c_1 = \left[ \frac{\delta_2^2 - \delta_1^2}{\eta_m} + \frac{\delta_1^2}{\eta_s} \right] \frac{g \cos \beta}{2} + c_2 (\delta_2 - \delta_1).$$

### 2.3 FULLY DEVELOPED FLOW BETWEEN PARALLEL PLATES

Consider the flow of fluid between parallel plates in Fig. 2.2. The velocity at the entrance is uniform and, as the flow progresses, velocity gradients must form because the fluid clings to the wall. At some distance downstream from the entrance, the velocity profile becomes independent of the distance from the entrance, and the flow is then fully developed. Let this region of fully developed flow start at  $x = 0$  and consider the unit volume in Fig. 2.2 with a thickness  $\Delta y$ , width  $W$ , and length  $L$ .

Rate of momentum in  
across surface at  $y + \Delta y$   
(momentum transport due to viscosity)

Rate of momentum in  
across surface at  $x = 0$   
(due to fluid motion)

Rate of momentum out  
across surface at  $x = L$   
(due to fluid motion)

Pressure force on liquid at  $x = 0$   
Pressure force on liquid at  $x = L$

$$\Delta y W [P(x = L)] = P_0 \Delta y W$$

$$-\Delta y W [P(x = 0)] = -P_L \Delta y W$$

$$Q = \frac{2}{3} \frac{W \delta^3}{\eta} \frac{(P_0 - P_L)}{L}$$

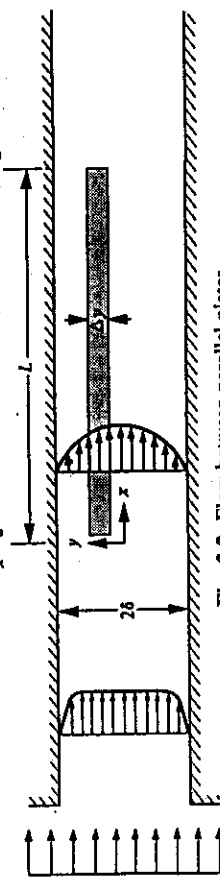


Fig. 2.2 Flow between parallel plates.

Again, the momentum in and out of the system due to the fluid motion are equal. We are left with

$$(LW)(\tau_{yx})|_y - (LW)(\tau_{yx})|_{y + \Delta y} + (P_0 - P_L)\Delta y W = 0. \quad (2.16)$$

Dividing through by  $LW\Delta y$  and letting  $\Delta y$  approach zero, we develop the differential equation

$$\frac{d\tau_{yx}}{dy} = \frac{(P_0 - P_L)}{L}. \quad (2.17)$$

The boundary conditions are described at the centerline ( $y = 0$ ) and at the solid wall ( $y = \delta$ ) as follows:

$$\text{B.C. 1} \quad \text{at } y = 0, \quad \tau_{yx} = 0; \quad (2.18)$$

$$\text{B.C. 2} \quad \text{at } y = \delta, \quad v_x = 0.$$

It is left as an exercise for the reader to show that the shear stress distribution is given by

$$\tau_{yx} = \frac{(P_0 - P_L)}{L} y, \quad (2.19)$$

and the velocity distribution (for a Newtonian fluid) by

$$v_x = \frac{1}{2\eta} (\delta^2 - y^2) \frac{(P_0 - P_L)}{L}. \quad (2.20)$$

We determine other characteristics of the system by the method shown in Section 2.2. These are:

i) The maximum velocity

$$V_x^{\max} = \frac{1}{2\eta} \delta^2 \frac{(P_0 - P_L)}{L}. \quad (2.21)$$

ii) The average velocity

$$\bar{v}_x = \frac{1}{\delta} \int_0^\delta v_x dy = \frac{\delta^2}{3\eta} \frac{(P_0 - P_L)}{L}. \quad (2.22)$$

iii) The volume flow rate

$$Q = \frac{2}{3} \frac{W \delta^3}{\eta} \frac{(P_0 - P_L)}{L}. \quad (2.23)$$

On looking back through this example, we note that in this instance the fluid flows because of the pressure drop ( $P_0 - P_L$ ). For horizontal flow, such a pressure drop would be necessary to make the fluid flow, in contrast to the flow down an inclined plane (Section 2.2) on which gravity exerts the necessary force for fluid motion.

## 2.4 FULLY DEVELOPED FLOW THROUGH A CIRCULAR TUBE

In this section we derive the momentum balance for steady flow through a long cylindrical tube for a Newtonian fluid and then for a non-Newtonian fluid, using an empirical equation that is often applied to polymeric melts.

### 2.4.1 Newtonian Fluids

Consider the fully developed flow of a fluid in a long tube of length  $L$  and radius  $R$ ; we specify fully developed flow so that end effects are negligible. Since we are dealing with a pipe, it is convenient to work with cylindrical coordinates. Therefore the shell in Fig. 2.3 is cylindrical, of thickness  $\Delta r$  and length  $L$ .

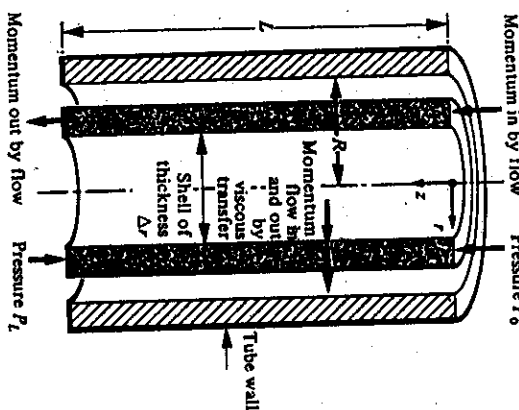


Fig. 2.3 Cylindrical shell chosen for momentum balance in tubes.

Rate of momentum in across surface at  $r$  (due to viscosity)

Note that here we include the area factor  $(2\pi rL)$  in parentheses. This is because the area as well as the shear stress is a function of  $r$ .

Rate of momentum out across surface at  $r + \Delta r$  (due to viscosity)

Since we are considering fully developed flow, the momentum fluxes due to flow are equal; hence these terms are omitted.

Gravity force acting on the cylindrical shell

Pressure force acting on surface at  $z = 0$   
Pressure force acting on surface at  $z = L$

We now add up the contributions to the momentum balance:

$$(2\pi rL\tau_n)|_r - (2\pi rL\tau_n)|_{r+\Delta r} + 2\pi r\Delta rL\log + 2\pi r\Delta r(P_0 - P_L) = 0. \quad (2.24)$$

Note that all terms contain the factor  $r$ ; however, since  $r$  is a variable, it should not be used as a common divisor. By dividing through by  $2\pi r\Delta r$  and taking the limit as  $\Delta r$  goes to zero, we develop the differential equation

$$\frac{d}{dr}(r\tau_n) = \left[ \frac{P_0 - P_L}{L} + \rho g \right] r. \quad (2.25)$$

Integration yields

$$\tau_n = \left[ \frac{P_0 - P_L}{L} + \rho g \right] \frac{r}{2} + \frac{C_1}{r}. \quad (2.26)$$

At  $r = 0$ , the velocity gradient (hence, the shear stress) equals zero; this can be realized because of the symmetry of flow.  
Thus for this case,

$$\text{B.C. 1} \quad \text{at } r = 0, \quad \tau_n = 0. \quad (2.27)$$

Therefore,  $C_1 = 0$ , and the momentum flux is given by

$$\tau_n = \left[ \frac{P_0 - P_L}{L} + \rho g \right] \frac{r}{2}. \quad (2.28)$$

Substituting Newton's law of viscosity

$$\tau_n = -\eta \frac{dv_t}{dr}, \quad (2.29)$$

and noting

$$\text{B.C. 2} \quad \text{at } r = R, \quad v_t = 0, \quad (2.30)$$

we obtain the solution for the velocity distribution:

$$v_t = \left[ \frac{P_0 - P_L}{L} + \rho g \right] \left[ \frac{R^2}{4\eta} \right] \left[ 1 - \left( \frac{r}{R} \right)^2 \right]. \quad (2.31)$$

i) As before:  
The maximum velocity is at  $r = 0$ , and is given by

$$V_t^{\max} = \left[ \frac{P_0 - P_L}{L} + \rho g \right] \frac{R^2}{4\eta}. \quad (2.32)$$

- ii) The average velocity is

$$\bar{v}_z = \frac{1}{\pi R^2} \int_0^{2\pi} \int_0^R v_z r dr d\theta = \left[ \frac{P_0 - P_L}{L} + \rho g \right] \frac{R^2}{8\eta}. \quad (2.33)$$

- iii) The volume flow rate is

$$Q = \left[ \frac{P_0 - P_L}{L} + \rho g \right] \left[ \frac{\pi R^4}{8\eta} \right]. \quad (2.34)$$

This latter result, which is commonly referred to as the *Hagen-Poiseuille law*, is valid for laminar steady-state flow of incompressible fluids in tubes having sufficient length to make end effects negligible. An entrance length given by  $L_e = 0.035 D Re$  is required before we can establish fully developed parabolic velocity distribution.

**Example 2.2** Water at 290 K flows through a horizontal tube of diameter 1.6 mm with a pressure drop of 900 N m<sup>-3</sup>. Find the mass flow rate through the tube.

**Solution.** In this situation, the force of gravity does not act on the fluid in the direction of flow, so according to Eq. (2.34) the volume flow rate is

$$Q = \left[ \frac{P_0 - P_L}{L} \right] \frac{\pi R^4}{8\eta}.$$

The viscosity and density of water at 290 K are  $1.080 \times 10^{-3}$  N s m<sup>-2</sup> and  $10^3$  kg m<sup>-3</sup>, respectively. Substituting in values, we obtain:

$$Q = \frac{900 \text{ N}}{\text{m}^3} \left| \frac{\pi}{8} \right| \frac{(0.8 \times 10^{-3})^4 \text{ m}^4}{1.080 \times 10^{-3} \text{ N s}} = 1.34 \times 10^{-7} \text{ m}^3 \text{ s}^{-1}$$

Thus we see that the mass flow rate is

$$\rho Q = (10^3)(1.34 \times 10^{-7}) = 1.34 \times 10^{-4} \text{ kg s}^{-1}$$

We should then check if the flow is laminar, by evaluating the Reynolds number. As mentioned in Chapter 1, the criterion is  $Re < 2100$ :

$$Re = \frac{D\bar{V}}{\nu} = \frac{D\bar{V}\rho}{\eta}.$$

Also

$$\rho \bar{V} = \frac{\rho Q}{\pi D^2/4}.$$

so that the Reynolds number may be written in the alternative form

$$Re = \frac{D\rho Q}{(\pi D^2/4)\eta} = \frac{4\rho Q}{\pi D\eta}. \quad (2.35)$$

Therefore,

$$Re = \frac{4}{\pi} \left| \frac{1.34 \times 10^{-4} \text{ kg}}{\text{s}} \right| \left| \frac{1.6 \times 10^{-3} \text{ m}}{1.080 \times 10^{-3} \text{ N s}} \right| \left| \frac{1 \text{ N s}^2}{1 \text{ kg m}} \right| \quad (2.36)$$

$$= 77.6$$

Because  $Re < 2100$ , the flow is laminar.

#### 2.4.2 Power law non-Newtonian fluids

Now we consider the isothermal flow of a non-Newtonian fluid through the circular tube of Fig. 2.3. The momentum balance is precisely the same as in Section 2.4.1 up to Eq. (2.28). We assume that the relationship between the shear stress and the shear rate is given by a power law, Eq. (1.32), as is often used for polymeric melts. Then

$$\tau_{rz} = -\eta \frac{\partial v_z}{\partial r} = -\eta_0 \left[ \frac{\partial v_z}{\partial r} \right]^n \quad (2.37)$$

and by combining Eqs. (2.28) and (2.35), we obtain

$$\left[ \frac{\partial v_z}{\partial r} \right] = - \left[ \frac{1}{2\eta_0} \left( \frac{P_0 - P_L}{L} + \rho g \right) \right]^{1/n} r^{1/n}. \quad (2.38)$$

Integrating with  $v_z = 0$  at  $r = R$ , the velocity distribution is obtained:

$$v_z = \left[ \frac{1}{2\eta_0} \left( \frac{P_0 - P_L}{L} + \rho g \right) \right]^{1/n} \left[ \frac{n}{n+1} [R^{(n+1)/n} - r^{(n+1)/n}] \right]. \quad (2.39)$$

The maximum velocity is at  $r = 0$  and is given by

$$v_z^{\max} = \left[ \frac{1}{2\eta_0} \left( \frac{P_0 - P_L}{L} + \rho g \right) \right]^{1/n} \left[ \frac{n}{n+1} \right] R^{(n+1)/n} \quad (2.40)$$

$$v_z = V_z^{\max} \left[ 1 - \left[ \frac{r}{R} \right]^{(n+1)/n} \right]. \quad (2.41)$$

so that Eq. (2.37) can be written in a simpler form:

The volume flow rate is

$$Q = \int_0^R 2\pi r v_z dr = 2\pi V_z^{\max} \int_0^R r \left[ 1 - \left( \frac{r}{R} \right)^{(n+1)/n} \right] dr$$

or

$$Q = \left[ \frac{n+1}{3n+1} \right] \pi R^2 V_z^{\max}. \quad (2.40)$$

The average velocity is simply

$$\bar{v}_z = \frac{Q}{\pi R^2}$$

or

$$\bar{v}_z = \left[ \frac{n+1}{3n+1} \right] V_z^{\max}. \quad (2.41)$$

## 2.5 EQUATION OF CONTINUITY AND THE MOMENTUM EQUATION

In the previous sections of this chapter, we determined velocity distributions for some simple flow systems by applying differential momentum balances. The balances for these systems served to illustrate the application of the momentum equation. In general, when dealing with isothermal fluid systems which do not involve changes in compositions, we can solve problems by starting with general expressions. This method is better than developing formulations peculiar to the specific problem at hand. The general momentum equation is also called the *equation of motion* or the *Navier-Stokes' equation*; in addition the *equation of continuity* is frequently used in conjunction with the momentum equation.

The continuity equation is developed simply by applying the law of conservation of mass to a small volume element within a flowing fluid. The principle of conservation of mass is quite simple to apply and we assume that the reader has used it in developing material balances. We develop the momentum equation by applying the momentum balance which, in its general form, is an extension of Eq. (2.1). With the aid of these two equations, we can mathematically describe the problems encountered in the previous section, as well as more complicated problems. However, as we shall see, these expressions are rather cumbersome, and exact solutions can be found only in very limited cases. Hence these equations are used primarily as starting points for solving problems. The equations of continuity and motion are simplified to fit the problem at hand. Although theoretically these equations are valid for both laminar and turbulent flows, in practice they are applied only to laminar flow.

### 2.5.1 Equation of continuity

Consider the stationary volume element within a fluid moving with a velocity having the components  $v_x$ ,  $v_y$ , and  $v_z$ , as shown in Fig. 2.4. We begin with the basic representation of the conservation of mass:

$$\left( \begin{array}{l} \text{rate of mass} \\ \text{accumulation} \end{array} \right) = \left( \begin{array}{l} \text{rate of} \\ \text{mass in} \end{array} \right) - \left( \begin{array}{l} \text{rate of} \\ \text{mass out} \end{array} \right). \quad (2.42)$$

FIG. 2.4 Volume element fixed in space with fluid flowing through it.

First, look at the faces perpendicular to the  $x$ -axis. The volume flow rate of fluid in across the face at  $x$  is simply the product of the velocity ( $x$ -component) and the cross-sectional area, yielding  $\Delta y \Delta z |v_x|_x$ . The rate of mass in through the face at  $x$  is then  $\Delta y \Delta z (\rho v_x)|_x$ . Similarly, the rate of mass out through the face at  $x + \Delta x$  is  $\Delta y \Delta z (\rho v_x)|_{x+\Delta x}$ . We may write analogous expressions for the other two pairs of faces, and then enter all the terms that account for the fluid entering and leaving the system into the mass balance, and leave the accumulation term to be developed.

The *accumulation* is the rate of change of mass within the control volume

$$\Delta x \Delta y \Delta z \frac{\partial \rho}{\partial t}.$$

The mass balance thus becomes

$$\begin{aligned} \Delta x \Delta y \Delta z \frac{\partial \rho}{\partial t} &= \Delta y \Delta z [\rho v_x|_x - \rho v_x|_{x+\Delta x}] + \Delta x \Delta z [\rho v_y|_y - \rho v_y|_{y+\Delta y}] \\ &\quad + \Delta x \Delta y [\rho v_z|_z - \rho v_z|_{z+\Delta z}]. \end{aligned} \quad (2.43)$$

Then, dividing through by  $\Delta x \Delta y \Delta z$ , and taking the limit as these dimensions approach zero, we get the *equation of continuity*:

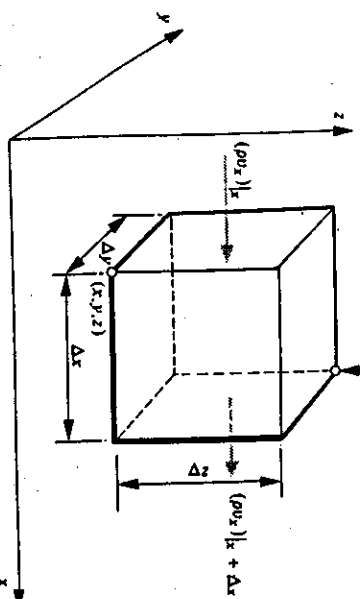
$$\frac{\partial \rho}{\partial t} = - \left[ \frac{\partial}{\partial x} \rho v_x + \frac{\partial}{\partial y} \rho v_y + \frac{\partial}{\partial z} \rho v_z \right]. \quad (2.44)$$

A very important form of Eq. (2.44) is the form that applies to a fluid of constant density. For this case, which frequently occurs in engineering problems, the continuity equation reduces to

$$\frac{\partial v_x}{\partial x} + \frac{\partial v_y}{\partial y} + \frac{\partial v_z}{\partial z} = 0$$

or in vector notation

$$\nabla \cdot v = 0.$$



### 2.5.2 The momentum equation

When Eq. (2.1) is extended to include unsteady-state systems, the momentum balance takes the form:

$$\left[ \begin{array}{c} \text{rate of} \\ \text{momentum} \\ \text{accumulation} \end{array} \right] = \left[ \begin{array}{c} \text{rate of} \\ \text{momentum} \\ \text{in} \end{array} \right] - \left[ \begin{array}{c} \text{rate of} \\ \text{momentum} \\ \text{out} \end{array} \right] + \left[ \begin{array}{c} \text{sum of} \\ \text{forces acting} \\ \text{on system} \end{array} \right] \quad (2.46)$$

For simplicity, we begin by considering only the  $x$ -component of each term in Eq. (2.46); the  $y$ - and  $z$ -components may be handled in the same manner.

Figure 2.5(a) shows the  $x$ -components of  $\tau$  as if they were made up of viscous momentum fluxes rather than shear stresses. On the other hand Fig. 2.5(b) shows the  $x$ -component of  $\tau$  as stresses. Note the appearance of  $\tau_{xx}$ , which by the scheme of subscripts represents the transport of  $x$ -momentum in the  $x$ -direction. Alternatively, we view  $\tau_{xx}$  as the  $x$ -directed *normal stress* on the  $x$ -face, in contrast to  $\tau_{yy}$ , which we view as the  $x$ -directed shear stress on the  $y$ -face.

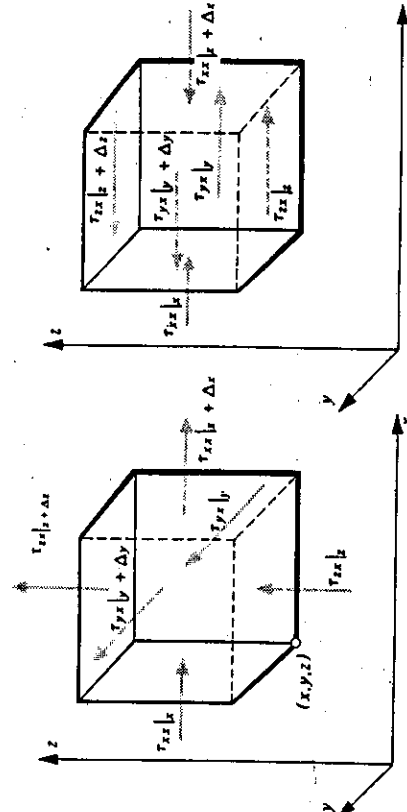


Fig. 2.5 Momentum transport ( $x$ -component) due to viscosity into the volume element. (a) Directions of viscous momentum transport. (b) Directions of stresses.

Let us now develop the terms that enter into Eq. (2.46). First, the net rate at which the  $x$ -component of the convective momentum enters the unit volume, is

$$\begin{aligned} \Delta y \Delta z (\rho v_x v_x|_{x+\Delta x}) & - \rho v_x v_x|_{x+\Delta x} + \Delta x \Delta z (\rho v_y v_x|_y - \rho v_y v_x|_{y+\Delta y}) \\ & + \Delta x \Delta y (\rho v_z v_x|_z - \rho v_z v_x|_{z+\Delta z}). \end{aligned} \quad (2.47)$$

Similarly, the net rate of *viscous* momentum flow into the unit volume across the six faces is

$$\begin{aligned} \Delta y \Delta z (\tau_{xx}|_{x+\Delta x}) & + \Delta x \Delta z (\tau_{yy}|_y - \tau_{yy}|_{y+\Delta y}) \\ & + \Delta x \Delta y (\tau_{zz}|_z - \tau_{zz}|_{z+\Delta z}). \end{aligned} \quad (2.48)$$

The reader who has not come in contact with this development before might find a brief explanation of the meaning of  $\rho v_y v_x$  and  $\rho v_z v_x$  useful. Remember that we are applying the law of conservation of momentum to the  $x$ -component of momentum. Thus  $v_x$  represents the  $x$ -velocity, and the rate at which mass enters the system through the  $y$ -face is given by  $\Delta x \Delta z v_y|_y$ . Hence the rate at which  $x$ -momentum enters through the  $y$ -face is simply the product of mass-flow rate and velocity:

$$\Delta x \Delta z \rho v_y v_x|_y.$$

In most cases, the forces acting on the system are those arising from the pressure  $P$  and the gravitational force per unit mass  $\mathbf{g}$ . In the  $x$ -direction, these forces are

$$\Delta y \Delta z (P|_x - P|_{x+\Delta x}), \quad (2.49)$$

and

$$\rho g_x \Delta x \Delta y \Delta z, \quad (2.50)$$

respectively. Here  $g_x$  is the  $x$ -component of  $\mathbf{g}$ . Finally, the rate of accumulation of  $x$ -momentum within the element is

$$\Delta x \Delta y \Delta z \left[ \frac{\partial}{\partial x} \rho v_x \right]. \quad (2.51)$$

Entering Eqs. (2.47)-(2.51) into the momentum balance, dividing through by  $\Delta x \Delta y \Delta z$ , and taking the limit as all three approach zero, we obtain the  $x$ -component of the momentum equation:

$$\begin{aligned} \frac{\partial}{\partial x} \rho v_x &= - \left[ \frac{\partial}{\partial x} \rho v_x v_x + \frac{\partial}{\partial y} \rho v_y v_x + \frac{\partial}{\partial z} \rho v_z v_x \right] \\ & - \left[ \frac{\partial}{\partial x} \tau_{xx} + \frac{\partial}{\partial y} \tau_{yx} + \frac{\partial}{\partial z} \tau_{zx} \right] - \frac{\partial P}{\partial x} + \rho g_x. \end{aligned} \quad (2.52)$$

The  $y$ - and  $z$ -components, which we obtain in a similar manner, are

$$\begin{aligned} \frac{\partial}{\partial y} \rho v_y &= - \left[ \frac{\partial}{\partial x} \rho v_x v_y + \frac{\partial}{\partial y} \rho v_y v_y + \frac{\partial}{\partial z} \rho v_z v_y \right] \\ & - \left[ \frac{\partial}{\partial x} \tau_{xy} + \frac{\partial}{\partial y} \tau_{yy} + \frac{\partial}{\partial z} \tau_{zy} \right] - \frac{\partial P}{\partial y} + \rho g_y, \end{aligned} \quad (2.53)$$

and

$$\frac{\partial}{\partial t} \rho u_z = - \left[ \frac{\partial}{\partial x} \rho v_x u_z + \frac{\partial}{\partial y} \rho v_y u_z + \frac{\partial}{\partial z} \rho v_z u_z \right] - \frac{\partial P}{\partial z} + \rho g_z. \quad (2.54)$$

To describe the general case, all three Equations (2.52), (2.53), and (2.54) are needed. Vector notation can reduce these to one equation which is just as meaningful as all three. The quantities  $\rho v_x$ ,  $\rho v_y$ , and  $\rho v_z$  are the components of the mass velocity  $\rho v$ ; similarly  $g_x$ ,  $g_y$ , and  $g_z$  are the components of  $\mathbf{g}$ . Vectorial representation of a velocity and an acceleration is familiar to most readers. However, the terms  $\partial P/\partial x$ ,  $\partial P/\partial y$ , and  $\partial P/\partial z$  all represent pressure gradients. By itself, pressure is a scalar quantity, but the gradient of pressure is a vector denoted, in general, by  $\nabla P$  (sometimes written  $\text{grad } P$ ). Therefore

$$\nabla P = \frac{\partial}{\partial x} P + \frac{\partial}{\partial y} P + \frac{\partial}{\partial z} P,$$

and  $\nabla$  can be thought to be an operator, such that

$$\nabla = \frac{\partial}{\partial x} + \frac{\partial}{\partial y} + \frac{\partial}{\partial z}.$$

The terms  $\rho v_x u_x$ ,  $\rho v_y u_y$ ,  $\rho v_z u_z$ , etc., are the nine components of the convective momentum flux  $\rho v v$ , which is the dyadic product of  $\rho v$  and  $v$ . Also,  $\tau_{xx}$ ,  $\tau_{yy}$ , etc., are the nine components of  $\tau$ .

The vector equation representing Eqs. (2.52)-(2.54) is finally written:

$$\frac{\partial}{\partial t} \rho v = -[\nabla \cdot \rho v v] - \nabla P - [\nabla \cdot \tau] + \rho g. \quad (2.55)$$

To interpret the mathematical nature of  $\nabla \cdot \rho v v$  and  $\nabla \cdot \tau$  in physical terms is difficult. However, for sufficient understanding of this text it is enough if the reader accepts them as mathematical shorthands of the appropriate terms in Eqs. (2.52)-(2.54).

So far we have developed a general expression, namely, Eq. (2.55) for the law of conservation of momentum. However, in order to use this equation for the determination of velocity distributions, it is necessary to insert expressions for the various stresses in terms of velocity gradients and fluid properties. The following equations are presented without proof because the arguments involved are quite lengthy. For Newtonian fluids, the nine components of  $\tau$  are written as follows.<sup>1</sup>

$$\begin{cases} \tau_{xx} = -2\eta \frac{\partial u}{\partial x} + \frac{2}{3} \eta (\nabla \cdot v) \\ \tau_{yy} = -2\eta \frac{\partial v}{\partial y} + \frac{2}{3} \eta (\nabla \cdot v) \\ \tau_{zz} = -2\eta \frac{\partial w}{\partial z} + \frac{2}{3} \eta (\nabla \cdot v) \end{cases} \quad (2.56)$$

$$\begin{cases} \tau_{xy} = \tau_{yx} = -\eta \left[ \frac{\partial v_x}{\partial y} + \frac{\partial v_y}{\partial x} \right] \\ \tau_{yz} = \tau_{zy} = -\eta \left[ \frac{\partial v_y}{\partial z} + \frac{\partial v_z}{\partial y} \right] \end{cases} \quad (2.60)$$

$$\begin{cases} \tau_{xz} = \tau_{zx} = -\eta \left[ \frac{\partial v_x}{\partial z} + \frac{\partial v_z}{\partial x} \right] \\ \tau_{yz} = \tau_{zy} = -\eta \left[ \frac{\partial v_y}{\partial z} + \frac{\partial v_z}{\partial y} \right] \end{cases} \quad (2.61)$$

These equations constitute a more general statement of Newton's law of viscosity than that given in Eq. (1.2), and apply to complex flow situations. When the fluid flows between two parallel plates in the  $x$ -direction so that  $v$  is a function of  $y$  alone, where the  $y$ -direction is perpendicular to the plates' surfaces (Fig. 1.4), then Eqs. (2.56)-(2.61) yield

$$\tau_{xx} = \tau_{yy} = \tau_{zz} = \tau_{xy} = \tau_{xz} = 0 \quad \text{and} \quad \tau_{yz} = -\eta \left[ \frac{\partial v_x}{\partial y} \right].$$

which is the same as the simple relationship previously used to describe Newton's law of viscosity. Also in many other problems of physical significance in which  $v$  is recognized as a function of both  $y$  and  $x$ , we find that  $\partial v_x / \partial y \gg \partial v_x / \partial x$ , and the simple rate Eq. (1.2) can be used for  $\tau_{xx}$  as an example with a high degree of accuracy rather than Eq. (2.59).

### 2.5.3 Navier-Stokes' equation, constant $\rho$ and $\eta$

The continuity equation for constant density is given by Eq. (2.45) or in vector notation,

$$\nabla \cdot v = 0. \quad (2.62)$$

Regarding the momentum equation, we can write Eqs. (2.52)-(2.54) with constant  $\rho$  and  $\eta$ :

$$\rho \left[ \frac{\partial u_x}{\partial t} + v_x \frac{\partial u_x}{\partial x} + v_y \frac{\partial u_x}{\partial y} + v_z \frac{\partial u_x}{\partial z} \right] = -\frac{\partial P}{\partial x} + \eta \left[ \frac{\partial^2 u_x}{\partial x^2} + \frac{\partial^2 u_x}{\partial y^2} + \frac{\partial^2 u_x}{\partial z^2} \right] + \rho g_x, \quad (2.63)$$

$$\begin{aligned} \rho \left[ \frac{\partial v_y}{\partial t} + v_x \frac{\partial v_y}{\partial x} + v_y \frac{\partial v_y}{\partial y} + v_z \frac{\partial v_y}{\partial z} \right] &= -\frac{\partial P}{\partial y} + \eta \left[ \frac{\partial^2 v_y}{\partial x^2} + \frac{\partial^2 v_y}{\partial y^2} + \frac{\partial^2 v_y}{\partial z^2} \right] + \rho g_y, \\ \rho \left[ \frac{\partial v_z}{\partial t} + v_x \frac{\partial v_z}{\partial x} + v_y \frac{\partial v_z}{\partial y} + v_z \frac{\partial v_z}{\partial z} \right] &= -\frac{\partial P}{\partial z} + \eta \left[ \frac{\partial^2 v_z}{\partial x^2} + \frac{\partial^2 v_z}{\partial y^2} + \frac{\partial^2 v_z}{\partial z^2} \right] + \rho g_z. \end{aligned} \quad (2.64)$$

$$\begin{aligned} \rho \left[ \frac{\partial u_x}{\partial t} + v_x \frac{\partial u_x}{\partial x} + v_y \frac{\partial u_x}{\partial y} + v_z \frac{\partial u_x}{\partial z} \right] &= -\frac{\partial P}{\partial x} + \eta \left[ \frac{\partial^2 u_x}{\partial x^2} + \frac{\partial^2 u_x}{\partial y^2} + \frac{\partial^2 u_x}{\partial z^2} \right] + \rho g_x, \\ \rho \left[ \frac{\partial v_y}{\partial t} + v_x \frac{\partial v_y}{\partial x} + v_y \frac{\partial v_y}{\partial y} + v_z \frac{\partial v_y}{\partial z} \right] &= -\frac{\partial P}{\partial y} + \eta \left[ \frac{\partial^2 v_y}{\partial x^2} + \frac{\partial^2 v_y}{\partial y^2} + \frac{\partial^2 v_y}{\partial z^2} \right] + \rho g_y, \\ \rho \left[ \frac{\partial v_z}{\partial t} + v_x \frac{\partial v_z}{\partial x} + v_y \frac{\partial v_z}{\partial y} + v_z \frac{\partial v_z}{\partial z} \right] &= -\frac{\partial P}{\partial z} + \eta \left[ \frac{\partial^2 v_z}{\partial x^2} + \frac{\partial^2 v_z}{\partial y^2} + \frac{\partial^2 v_z}{\partial z^2} \right] + \rho g_z. \end{aligned} \quad (2.65)$$

The bracketed terms on the left side of these equations merit attention. Consider a control volume of fluid moving in space with no mass flow across its surface. The change in the  $x$ -component of its velocity with time and position is given by

$$\Delta v_x = \frac{\partial v_x}{\partial t} \Delta t + \frac{\partial v_x}{\partial x} \Delta x + \frac{\partial v_x}{\partial y} \Delta y + \frac{\partial v_x}{\partial z} \Delta z \quad (2.66)$$

and since the  $x$ -component of acceleration is defined as

$$a_x = \lim_{\Delta t \rightarrow 0} \frac{\Delta v_x}{\Delta t} = \lim_{\Delta t \rightarrow 0} \left\{ \frac{\partial v_x}{\partial t} \frac{\Delta t}{\Delta t} + \frac{\partial v_x}{\partial x} \frac{\Delta x}{\Delta t} + \frac{\partial v_x}{\partial y} \frac{\Delta y}{\Delta t} + \frac{\partial v_x}{\partial z} \frac{\Delta z}{\Delta t} \right\}, \quad (2.67)$$

then we obtain

$$a_x = \frac{\partial v_x}{\partial t} + v_x \frac{\partial v_x}{\partial x} + v_y \frac{\partial v_x}{\partial y} + v_z \frac{\partial v_x}{\partial z} = \frac{Dv_x}{Dt}. \quad (2.68)$$

This is the acceleration one would feel if riding with the control volume of fluid. We also refer to this time derivative of velocity,  $Dv_x/Dt$ , as the *substantial derivative*. Analogous expressions exist for the  $y$ - and  $z$ -directions. In general, one notation can represent all three substantial derivatives, so that Eqs. (2.63)-(2.65) become

$$\rho \frac{Dv}{Dt} = -\nabla P + \eta \nabla^2 v + \rho g. \quad (2.69)$$

Equation (2.69), or Eqs. (2.63)-(2.65) which taken together represent the expansion of Eq. (2.69), is often referred to as the *Navier-Stokes' equation*. In the form of Eq. (2.69), we can recognize it as a statement of Newton's law in the form *mass ( $\rho$ )  $\times$  acceleration ( $Dv/Dt$ ) equals the sum of forces*, namely, the pressure force ( $-\nabla P$ ), the viscous force ( $\eta \nabla^2 v$ ), and the gravity or body force  $\rho g$ .

## 2.6 THE MOMENTUM EQUATION IN RECTANGULAR AND CURVILINEAR COORDINATES

Table 2.1: The continuity equation in different coordinate systems

Rectangular coordinates ( $x, y, z$ ):	$\frac{\partial \rho}{\partial t} + \frac{\partial}{\partial x} (\rho v_x) + \frac{\partial}{\partial y} (\rho v_y) + \frac{\partial}{\partial z} (\rho v_z) = 0 \quad (A)$
Cylindrical coordinates ( $r, \theta, z$ ):	$\frac{\partial \rho}{\partial t} + \frac{1}{r} \frac{\partial}{\partial r} (\rho r v_r) + \frac{1}{r} \frac{\partial}{\partial \theta} (\rho v_\theta) + \frac{\partial}{\partial z} (\rho v_z) = 0 \quad (B)$
Spherical coordinates ( $r, \theta, \phi$ ):	$\frac{\partial \rho}{\partial t} + \frac{1}{r^2} \frac{\partial}{\partial r} (\rho r^2 v_r) + \frac{1}{r \sin \theta} \frac{\partial}{\partial \theta} (\rho v_\theta \sin \theta) + \frac{1}{r \sin \theta} \frac{\partial}{\partial \phi} (\rho v_\phi) = 0 \quad (C)$

Tables 2.1-2.7 are from R. B. Bird, W. E. Stewart, and E. N. Lightfoot, *Transport Phenomena*, Wiley, New York, 1960, pages 83-91. Reprinted by permission.

In many instances rectangular coordinates are not useful for analyzing problems. For example, in the Hagen-Poiseuille problem discussed in Section 2.4, we described the axial velocity  $v_z$  as a function of only a single variable  $r$  by employing cylindrical coordinates. If rectangular coordinates had been used instead,  $v_z$  would have been a very complicated function of  $x$  and  $y$ . Similarly, it would have been difficult to describe and apply the boundary condition at the tube wall.

The equations of continuity and motion in Section 2.5 were given in rectangular coordinates and are repeated here, along with spherical or cylindrical coordinates in Tables 2.1-2.7.

Table 2.3 The momentum equation in cylindrical coordinates  $(r, \theta, z)$ 

In terms of  $\tau$ :

$$x\text{-component} \quad \rho \left( \frac{\partial v_x}{\partial t} + v_r \frac{\partial v_x}{\partial r} + v_\theta \frac{\partial v_x}{\partial \theta} + v_z \frac{\partial v_x}{\partial z} \right) = - \frac{\partial P}{\partial x}$$

$$y\text{-component} \quad \rho \left( \frac{\partial v_y}{\partial t} + v_r \frac{\partial v_y}{\partial r} + v_\theta \frac{\partial v_y}{\partial \theta} + v_z \frac{\partial v_y}{\partial z} \right) = - \frac{\partial P}{\partial y} \\ - \left( \frac{1}{r} \frac{\partial}{\partial r} (r \tau_{rr}) + \frac{1}{r} \frac{\partial \tau_{\theta\theta}}{\partial \theta} - \frac{\tau_{\theta\theta}}{r} + \frac{\partial \tau_{zz}}{\partial z} \right) + \rho g_x \quad (\text{A})$$

$$z\text{-component} \quad \rho \left( \frac{\partial v_z}{\partial t} + v_r \frac{\partial v_z}{\partial r} + v_\theta \frac{\partial v_z}{\partial \theta} + v_z \frac{\partial v_z}{\partial z} \right) = - \frac{\partial P}{\partial z} \\ - \left( \frac{\partial \tau_{rz}}{\partial x} + \frac{\partial \tau_{yz}}{\partial y} + \frac{\partial \tau_{xz}}{\partial z} \right) + \rho g_y \quad (\text{B})$$

$$\theta\text{-component} \quad \rho \left( \frac{\partial v_\theta}{\partial t} + v_r \frac{\partial v_\theta}{\partial r} + \frac{v_\theta}{r} \frac{\partial v_\theta}{\partial \theta} + v_z \frac{\partial v_\theta}{\partial z} \right) = - \frac{1}{r} \frac{\partial P}{\partial \theta} \\ - \left( \frac{1}{r^2} \frac{\partial}{\partial r} (r^2 \tau_{rr}) + \frac{1}{r} \frac{\partial \tau_{\theta\theta}}{\partial \theta} + \frac{\partial \tau_{zz}}{\partial z} \right) + \rho g_\theta \quad (\text{B})$$

In terms of velocity gradients for a Newtonian fluid with constant  $\rho$  and  $\eta$ :

$$x\text{-component} \quad \rho \left( \frac{\partial v_x}{\partial t} + v_r \frac{\partial v_x}{\partial r} + v_\theta \frac{\partial v_x}{\partial \theta} + v_z \frac{\partial v_x}{\partial z} \right) = - \frac{\partial P}{\partial x} \\ - \left( \frac{\partial \tau_{xx}}{\partial x} + \frac{\partial \tau_{xy}}{\partial y} + \frac{\partial \tau_{xz}}{\partial z} \right) + \rho g_x \quad (\text{C})$$

$$z\text{-component} \quad \rho \left( \frac{\partial v_z}{\partial t} + v_r \frac{\partial v_z}{\partial r} + \frac{v_\theta}{r} \frac{\partial v_z}{\partial \theta} + v_z \frac{\partial v_z}{\partial z} \right) = - \frac{\partial P}{\partial z} \\ - \left( \frac{1}{r} \frac{\partial}{\partial r} (r^2 \tau_{rr}) + \frac{1}{r} \frac{\partial \tau_{\theta\theta}}{\partial \theta} + \frac{\partial \tau_{zz}}{\partial z} \right) + \rho g_z \quad (\text{D})$$

In terms of velocity gradients for a Newtonian fluid with constant  $\rho$  and  $\eta$ :

$$r\text{-component}^* \quad \rho \left( \frac{\partial v_r}{\partial t} + v_r \frac{\partial v_r}{\partial r} + \frac{v_\theta}{r} \frac{\partial v_r}{\partial \theta} - \frac{v_\theta^2}{r} + v_z \frac{\partial v_r}{\partial z} \right) = - \frac{\partial P}{\partial r}$$

$$\theta\text{-component} \quad \rho \left( \frac{\partial v_\theta}{\partial t} + v_r \frac{\partial v_\theta}{\partial r} + v_\theta \frac{\partial v_\theta}{\partial \theta} + v_z \frac{\partial v_\theta}{\partial z} \right) = - \frac{1}{r} \frac{\partial P}{\partial \theta} \\ + \eta \left[ \frac{\partial}{\partial r} \left( \frac{1}{r} \frac{\partial}{\partial r} (r v_r) \right) + \frac{1}{r^2} \frac{\partial^2 v_r}{\partial \theta^2} - \frac{2}{r^2} \frac{\partial v_\theta}{\partial \theta} + \frac{\partial^2 v_r}{\partial z^2} \right] + \rho g_\theta \quad (\text{D})$$

$$y\text{-component} \quad \rho \left( \frac{\partial v_y}{\partial t} + v_r \frac{\partial v_y}{\partial r} + v_\theta \frac{\partial v_y}{\partial \theta} + v_z \frac{\partial v_y}{\partial z} \right) = - \frac{\partial P}{\partial y} \\ + \eta \left[ \frac{\partial^2 v_y}{\partial x^2} + \frac{\partial^2 v_y}{\partial y^2} + \frac{\partial^2 v_y}{\partial z^2} \right] + \rho g_y \quad (\text{E})$$

$$z\text{-component} \quad \rho \left( \frac{\partial v_z}{\partial t} + v_r \frac{\partial v_z}{\partial r} + \frac{v_\theta}{r} \frac{\partial v_z}{\partial \theta} + v_z \frac{\partial v_z}{\partial z} \right) = - \frac{\partial P}{\partial z} \\ + \eta \left[ \frac{1}{r} \frac{\partial}{\partial r} \left( r v_\theta \right) \right] + \frac{1}{r^2} \frac{\partial^2 v_\theta}{\partial \theta^2} + \frac{2}{r^2} \frac{\partial v_\theta}{\partial \theta} + \frac{\partial^2 v_z}{\partial z^2} \right] + \rho g_z \quad (\text{E})$$

$$z\text{-component} \quad \rho \left( \frac{\partial v_z}{\partial t} + v_r \frac{\partial v_z}{\partial r} + v_\theta \frac{\partial v_z}{\partial \theta} + v_z \frac{\partial v_z}{\partial z} \right) = - \frac{\partial P}{\partial z} \\ + \eta \left[ \frac{\partial^2 v_z}{\partial x^2} + \frac{\partial^2 v_z}{\partial y^2} + \frac{\partial^2 v_z}{\partial z^2} \right] + \rho g_z \quad (\text{F})$$

\*The term  $\rho v_\theta^2/r$  is the *centrifugal force*. It gives the effective force in the  $r$ -direction resulting from fluid motion in the  $\theta$ -direction. This term arises automatically on transformation from rectangular to cylindrical coordinates; it does not have to be added on physical grounds.

**Table 2.4** The momentum equation in spherical coordinates  $(r, \theta, \phi)$ In terms of  $\tau$ :

$$\begin{aligned} r\text{-component} & \rho \left( \frac{\partial v_r}{\partial t} + v_r \frac{\partial v_r}{\partial r} + \frac{v_\theta}{r} \frac{\partial v_r}{\partial \theta} + \frac{v_\phi}{r \sin \theta} \frac{\partial v_r}{\partial \phi} - \frac{v_\theta^2 + v_\phi^2}{r} \right) \\ & = - \frac{\partial P}{\partial r} - \left( \frac{1}{r^2} \frac{\partial}{\partial r} (r^2 \tau_{rr}) + \frac{1}{r \sin \theta} \frac{\partial}{\partial \theta} (\tau_{\theta\theta} \sin \theta) \right. \\ & \quad \left. + \frac{1}{r \sin \theta} \frac{\partial \tau_{\phi\phi}}{\partial \phi} - \frac{\tau_{\theta\phi} + \tau_{\phi\theta}}{r} \right) + \rho g_z. \quad (A) \end{aligned}$$

$$\begin{aligned} \theta\text{-component} & \rho \left( \frac{\partial v_\theta}{\partial t} + v_r \frac{\partial v_\theta}{\partial r} + \frac{v_\theta}{r} \frac{\partial v_\theta}{\partial \theta} + \frac{v_\phi}{r \sin \theta} \frac{\partial v_\theta}{\partial \phi} + \frac{v_r v_\theta}{r} - \frac{v_\theta^2 \cot \theta}{r} \right) \\ & = - \frac{1}{r} \frac{\partial P}{\partial \theta} - \left( \frac{1}{r^2} \frac{\partial}{\partial r} (r^2 \tau_{rr}) + \frac{1}{r \sin \theta} \frac{\partial}{\partial \theta} (\tau_{\theta\theta} \sin \theta) + \frac{1}{r \sin \theta} \frac{\partial \tau_{\phi\phi}}{\partial \phi} \right. \\ & \quad \left. + \frac{\tau_{\theta\phi} - \cot \theta \tau_{\phi\theta}}{r} \right) + \rho g_\theta. \quad (B) \end{aligned}$$

$$\begin{aligned} \phi\text{-component} & \rho \left( \frac{\partial v_\phi}{\partial t} + v_r \frac{\partial v_\phi}{\partial r} + \frac{v_\theta}{r} \frac{\partial v_\phi}{\partial \theta} + \frac{v_\phi}{r \sin \theta} \frac{\partial v_\phi}{\partial \phi} + \frac{v_\theta v_r}{r} + \frac{v_\phi v_r}{r} + \frac{v_\phi v_\theta}{r \cot \theta} \right) \\ & = - \frac{1}{r \sin \theta} \frac{\partial P}{\partial \phi} - \left( \frac{1}{r^2} \frac{\partial}{\partial r} (r^2 \tau_{rr}) + \frac{1}{r} \frac{\partial \tau_{\theta\theta}}{\partial \theta} + \frac{1}{r \sin \theta} \frac{\partial \tau_{\phi\phi}}{\partial \phi} \right. \\ & \quad \left. + \frac{\tau_{\phi\theta} + 2 \cot \theta \tau_{\theta\phi}}{r} \right) + \rho g_\phi. \quad (C) \end{aligned}$$

In terms of velocity gradients for a Newtonian fluid with constant  $\rho$  and  $\eta$ :

$$\begin{aligned} r\text{-component} & \rho \left( \frac{\partial v_r}{\partial t} + v_r \frac{\partial v_r}{\partial r} + \frac{v_\theta}{r} \frac{\partial v_r}{\partial \theta} + \frac{v_\phi}{r \sin \theta} \frac{\partial v_r}{\partial \phi} - \frac{v_\theta^2 + v_\phi^2}{r} \right) \\ & = - \frac{\partial P}{\partial r} + \eta \left( \nabla^2 v_r - \frac{2}{r^2} v_r - \frac{2}{r^2} \frac{\partial v_\theta}{\partial \theta} - \frac{2}{r^2} v_\theta \cot \theta \right. \\ & \quad \left. - \frac{2}{r^2 \sin \theta} \frac{\partial v_\phi}{\partial \phi} \right) + \rho g_z. \quad (D) \end{aligned}$$

$$\begin{aligned} \theta\text{-component} & \rho \left( \frac{\partial v_\theta}{\partial t} + v_r \frac{\partial v_\theta}{\partial r} + \frac{v_\theta}{r} \frac{\partial v_\theta}{\partial \theta} + \frac{v_\phi}{r \sin \theta} \frac{\partial v_\theta}{\partial \phi} + \frac{v_r v_\theta}{r} - \frac{v_\theta^2 \cot \theta}{r} \right) \\ & = - \frac{1}{r} \frac{\partial P}{\partial \theta} + \eta \left( \nabla^2 v_\theta + \frac{2}{r^2} \frac{\partial v_r}{\partial \theta} - \frac{v_\theta}{r^2 \sin^2 \theta} - \frac{2 \cos \theta}{r^2 \sin^2 \theta} \frac{\partial v_\phi}{\partial \phi} \right) + \rho g_\theta. \quad (E) \end{aligned}$$

$$\begin{aligned} \phi\text{-component} & \rho \left( \frac{\partial v_\phi}{\partial t} + v_r \frac{\partial v_\phi}{\partial r} + \frac{v_\theta}{r} \frac{\partial v_\phi}{\partial \theta} + \frac{v_\phi}{r \sin \theta} \frac{\partial v_\phi}{\partial \phi} + \frac{v_\theta v_r}{r} + \frac{v_\phi v_\theta}{r \cot \theta} \right) \\ & = - \frac{1}{r \sin \theta} \frac{\partial P}{\partial \phi} + \eta \left( \nabla^2 v_\phi - \frac{v_\phi}{r^2 \sin^2 \theta} + \frac{2}{r^2 \sin^2 \theta} \frac{\partial v_r}{\partial \phi} \right. \\ & \quad \left. + \frac{2 \cos \theta}{r^2 \sin^2 \theta} \frac{\partial v_\theta}{\partial \phi} \right) + \rho g_\phi. \quad (F) \end{aligned}$$

**Table 2.5** Components of the stress tensor in rectangular coordinates  $(x, y, z)$ 

$$\begin{aligned} \tau_{xx} & = -\eta \left[ 2 \frac{\partial v_x}{\partial x} - \frac{1}{2} (\nabla \cdot v) \right] \quad (A) \\ \tau_{yy} & = -\eta \left[ 2 \frac{\partial v_y}{\partial y} - \frac{1}{2} (\nabla \cdot v) \right] \quad (B) \\ \tau_{zz} & = -\eta \left[ 2 \frac{\partial v_z}{\partial z} - \frac{1}{2} (\nabla \cdot v) \right] \quad (C) \\ \tau_{xy} & = \tau_{yx} = -\eta \left[ \frac{\partial v_x}{\partial y} + \frac{\partial v_y}{\partial x} \right] \quad (D) \\ \tau_{yz} & = \tau_{zy} = -\eta \left[ \frac{\partial v_y}{\partial z} + \frac{\partial v_z}{\partial y} \right] \quad (E) \\ \tau_{zx} & = \tau_{xz} = -\eta \left[ \frac{\partial v_z}{\partial x} + \frac{\partial v_x}{\partial z} \right] \quad (F) \\ (\nabla \cdot v) & = \frac{\partial v_x}{\partial x} + \frac{\partial v_y}{\partial y} + \frac{\partial v_z}{\partial z} \quad (G) \end{aligned}$$

**Table 2.6** Components of the stress tensor in cylindrical coordinates  $(r, \theta, z)$ 

$$\begin{aligned} \tau_{rr} & = -\eta \left[ 2 \frac{\partial v_r}{\partial r} - \frac{1}{2} (\nabla \cdot v) \right] \quad (A) \\ \tau_{\theta\theta} & = -\eta \left[ 2 \left( \frac{1}{r} \frac{\partial v_\theta}{\partial r} + \frac{v_r}{r} \right) - \frac{1}{2} (\nabla \cdot v) \right] \quad (B) \\ \tau_{zz} & = -\eta \left[ 2 \frac{\partial v_z}{\partial z} - \frac{1}{2} (\nabla \cdot v) \right] \quad (C) \\ \tau_{r\theta} & = \tau_{\theta r} = -\eta \left[ r \frac{\partial v_\theta}{\partial r} + \frac{1}{r} \frac{\partial v_r}{\partial \theta} \right] \quad (D) \\ \tau_{\theta z} & = \tau_{z\theta} = -\eta \left[ \frac{\partial v_\theta}{\partial z} + \frac{1}{r} \frac{\partial v_z}{\partial \theta} \right] \quad (E) \\ \tau_{rz} & = \tau_{zr} = -\eta \left[ \frac{\partial v_z}{\partial r} + \frac{1}{r} \frac{\partial v_r}{\partial z} \right] \quad (F) \\ (\nabla \cdot v) & = \frac{1}{r} \frac{\partial}{\partial r} (r v_r) + \frac{1}{r} \frac{\partial v_\theta}{\partial \theta} + \frac{\partial v_z}{\partial z} \quad (G) \end{aligned}$$

Table 2.7 Components of the stress tensor in spherical coordinates ( $r, \theta, \phi$ )

$$\begin{aligned} \tau_{rr} &= -\eta \left[ 2 \frac{\partial v_r}{\partial r} - \frac{1}{r} (\nabla \cdot v) \right] & (A) \\ \tau_{\theta\theta} &= -\eta \left[ 2 \left( \frac{1}{r} \frac{\partial v_\theta}{\partial \theta} + \frac{v_r}{r} \right) - \frac{1}{r} (\nabla \cdot v) \right] & (B) \\ \tau_{\phi\phi} &= -\eta \left[ 2 \left( \frac{1}{r \sin \theta} \frac{\partial v_\phi}{\partial \phi} + \frac{v_r}{r} + \frac{v_\theta \cot \theta}{r} \right) - \frac{1}{r} (\nabla \cdot v) \right] & (C) \\ \tau_{r\theta} &= \tau_{\theta r} = -\eta \left[ r \frac{\partial}{\partial r} \left( \frac{v_\theta}{r} \right) + \frac{1}{r} \frac{\partial v_r}{\partial \theta} \right] & (D) \\ \tau_{r\phi} &= \tau_{\phi r} = -\eta \left[ \frac{\sin \theta}{r} \frac{\partial}{\partial \theta} \left( \frac{v_\phi}{\sin \theta} \right) + \frac{1}{r \sin \theta} \frac{\partial v_r}{\partial \phi} \right] & (E) \\ \tau_{\theta\phi} &= \tau_{\phi\theta} = -\eta \left[ \frac{1}{r \sin \theta} \frac{\partial v_r}{\partial \phi} + r \frac{\partial}{\partial r} \left( \frac{v_\phi}{r} \right) \right] & (F) \\ (\nabla \cdot v) &= \frac{1}{r^2} \frac{\partial}{\partial r} (r^2 v_r) + \frac{1}{r \sin \theta} \frac{\partial v_\theta}{\partial \theta} + \frac{1}{r \sin \theta} \frac{\partial v_\phi}{\partial \phi} & (G) \end{aligned}$$

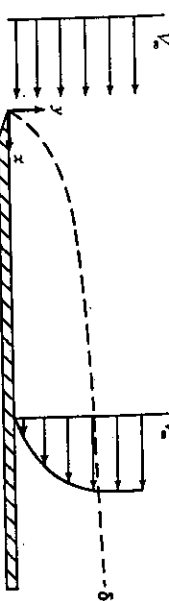


Fig. 2.6 Velocity profile and momentum boundary layer of flow parallel to a flat plate.

due to the fact that in this region  $v_r$  is essentially uniform and constant, being equal to  $V_\infty$ . Since  $v_r$  is uniform and constant for  $y > \delta$ , Eq. (D) in Table 2.2 reveals that the pressure gradient  $\partial P/\partial x$  is zero or, stated differently, pressure everywhere in the bulk stream is uniform. In turn, the pressure within the boundary layer is equal to the pressure in the bulk stream, so that  $\partial P/\partial x$  is also zero within the boundary layer. We are now almost ready to pick out the appropriate equation of motion for the flow pattern in Fig. 2.6, but before we do so, let us examine which velocity components are relevant.

As discussed above,  $v_r$  is a function of  $y$ , and the determination of this functional relationship is indeed a major part of describing the flow and how the fluid and the solid surface interact. Also note that  $v_r$  depends on  $x$ . This results from the fact that, as the fluid progresses down the plate, it is retarded more and more by the drag at the plate's surface. Thus  $\partial v_r / \partial x$  is not zero, and the equation of continuity for steady two-dimensional flow of fluid with constant  $\rho$  and  $\eta$  is

$$\frac{\partial v_r}{\partial x} + \frac{\partial v_y}{\partial y} = 0. \quad (2.70)$$

## 2.7 APPLICATION OF NAVIER-STOKES' EQUATION

In this section, we show how to set up problems of viscous flow, by selecting the appropriate equation of motion that applies to the problem at hand and by simplifying it to manageable proportions so that it still relates to the given problem, and yet is not oversimplified. We do so by discarding those terms which are zero, and then recognizing those terms which can be neglected. To decide this, is, to a certain extent, a matter of experience, but in most instances even the novice can make intelligent decisions by making an order-of-magnitude estimate. For this purpose, we shall discuss below an order-of-magnitude technique that can be used to arrive at a more simplified, but still relevant, equation of motion. We also introduce other topics, such as the *boundary layer* and *drag forces* exerted by fluids on solids.

### 2.7.1 Flow over a flat plate

Figure 2.6 depicts the velocity profile of a fluid flowing parallel to a flat plate. Before it meets the leading edge of the plate, we assume that the fluid has a uniform velocity  $V_\infty$ . At any point  $x$  downstream from the leading edge of the plate, we observe that the velocity increases from zero at the wall to very near  $V_\infty$  at a very short distance  $\delta$  from the plate. The loci of positions where  $v_r/V_\infty = 0.99$ , is  $\delta$ , and it is defined as the *boundary layer*. At the leading edge of the plate ( $x = 0$ ),  $\delta$  is zero, and it progressively grows as flow proceeds down the plate.

Whenever problems of this type are encountered, namely, in the flow of fluid past a stationary solid, the viscous effects are felt only within the fluid near the solid, that is,  $y < \delta$ . Of course, this is exactly where the behavior of the fluid should be analyzed, because for  $y > \delta$ , the happenings from the point of view of this discussion are essentially uneventful,

Thus  $v_r$  exists and we should consider both the  $x$ - and  $y$ -components in Table 2.2. For the steady-state case with constant density and viscosity, Eqs. (D) and (E) in Table 2.2 reduce to

$$v_x \frac{\partial v_x}{\partial x} + v_y \frac{\partial v_x}{\partial y} = \nu \left[ \frac{\partial^2 v_x}{\partial x^2} + \frac{\partial^2 v_x}{\partial y^2} \right], \quad (2.71)$$

and

$$v_x \frac{\partial v_y}{\partial x} + v_y \frac{\partial v_y}{\partial y} = \nu \left[ \frac{\partial^2 v_y}{\partial x^2} + \frac{\partial^2 v_y}{\partial y^2} \right] + g_y. \quad (2.72)$$

When we remember that we are primarily interested in the region  $y \leq \delta$ , at this point it is convenient to define some dimensionless parameters:<sup>1</sup>

$$u^* = \frac{v_x}{V_\infty}, \quad x^* = \frac{x}{L}, \quad \delta^* = \frac{\delta}{L},$$

<sup>1</sup>The Reynolds number  $Re$ , which was briefly introduced in Chapter 1 reappears here again. Also the Froude number  $F_r$ , is introduced. These two dimensionless numbers, which so often occur in engineering studies, have been given names in honor of those two early workers in fluid mechanics.

$$v^* = \frac{y}{V_\infty}, \quad y^* = \frac{y}{L}, \quad \text{Re}_L = \frac{V_\infty L}{\nu},$$

$$\text{Fr}_L = \frac{V_\infty^2}{g L}.$$

Substituting these parameters into Eqs. (2.71), (2.72), and the continuity equation, we get

*Continuity:*

$$\frac{\partial u^*}{\partial x^*} + \frac{\partial v^*}{\partial y^*} = 0. \quad (2.73)$$

*Momentum:*

$$u^* \frac{\partial u^*}{\partial x^*} + v^* \frac{\partial u^*}{\partial y^*} = \frac{1}{\text{Re}_L} \left[ \frac{\partial^2 u^*}{\partial (x^*)^2} + \frac{\partial^2 u^*}{\partial (y^*)^2} \right]; \quad (2.74)$$

$$u^* \frac{\partial v^*}{\partial x^*} + v^* \frac{\partial v^*}{\partial y^*} = \frac{1}{\text{Re}_L} \left[ \frac{\partial^2 v^*}{\partial (x^*)^2} + \frac{\partial^2 v^*}{\partial (y^*)^2} \right] + \frac{1}{\text{Fr}_L}. \quad (2.75)$$

The next step is to make order-of-magnitude estimates of the terms in Eqs. (2.74) and (2.75), realizing that we are interested only in the happenings within the boundary layer.

*Order of magnitudes:*

$$\Delta x^* \approx 0 \text{ to } 1. \quad (2.76)$$

$$\Delta y^* \approx \delta^*. \quad (2.77)$$

$$\Delta u^* \approx 1. \quad (2.78)$$

From (2.76) and (2.78), we get

$$\frac{\partial u^*}{\partial x^*} \approx \frac{1}{1} = 1, \quad \text{and from continuity,} \quad \frac{\partial v^*}{\partial y^*} \approx 1. \quad (2.79)$$

From (2.77) and (2.78), we obtain

$$\frac{\partial u^*}{\partial y^*} \approx \frac{1}{\delta^*}, \quad (2.81)$$

and from (2.79) and (2.80),

$$\frac{\partial v^*}{\partial x^*} \approx \frac{\delta^*}{1} = \delta^*. \quad (2.82)$$

Now we can estimate all the second derivatives:

$$\frac{\partial^2 u^*}{\partial (x^*)^2} = \frac{\partial}{\partial x^*} \left[ \frac{\partial u^*}{\partial x^*} \right] \approx \frac{1}{1} = 1. \quad (2.83)$$

$$\frac{\partial^2 u^*}{\partial (y^*)^2} = \frac{\partial}{\partial y^*} \left[ \frac{\partial u^*}{\partial y^*} \right] \approx \frac{1}{\delta^*} \left[ \frac{1}{\delta^*} \right] = \frac{1}{\delta^{*2}}. \quad (2.84)$$

$$\frac{\partial^2 v^*}{\partial (x^*)^2} \approx \delta^*. \quad (2.85)$$

$$\frac{\partial^2 v^*}{\partial (y^*)^2} \approx \frac{1}{\delta^*}. \quad (2.86)$$

Insertion of the various magnitudes into Eqs. (2.74) and (2.75) reveals two important facts:  $\partial^2 u^*/\partial (y^*)^2 \gg \partial^2 u^*/\partial (x^*)^2$ , and the equation involving the  $x$ -component of the velocity has much larger terms than that for  $y$ . Hence we deal only with

$$v_x \frac{\partial v_x}{\partial x} + v_y \frac{\partial v_x}{\partial y} = v \frac{\partial^2 v_x}{\partial y^2}, \quad (2.87)$$

which is the *boundary layer* equation for a flat plate with zero pressure gradient. We now proceed to solve Eq. (2.87) for the boundary conditions

$$\text{B.C. 1} \quad \text{at } y = 0, \quad v_x = 0, \quad v_y = 0; \quad (2.88)$$

$$\text{B.C. 2} \quad \text{at } y = \infty, \quad v_x = V_\infty. \quad (2.89)$$

In order to simplify Eq. (2.87), we define the *stream function*  $\psi$  as

$$v_x = \frac{\partial \psi}{\partial y} \quad \text{and} \quad v_y = -\frac{\partial \psi}{\partial x}. \quad (2.90)$$

The use of the stream functions simplifies Eq. (2.87) and automatically satisfies continuity (Eq. (2.70)). Substituting Eq. (2.90) into Eq. (2.87) yields:

$$\frac{\partial \psi}{\partial y} \frac{\partial^2 \psi}{\partial x \partial y} - \frac{\partial \psi}{\partial x} \frac{\partial^2 \psi}{\partial y^2} = v \frac{\partial^3 \psi}{\partial y^3}. \quad (2.91)$$

A *similarity argument*<sup>2</sup> shows that the stream function may be expressed as

$$\psi = \sqrt{V_\infty \nu x} f(\beta), \quad (2.92)$$

<sup>2</sup>Blasius showed that Eq. (2.91) could be solved in this manner. (See H. Blasius, *NACA Tech. Mem.*, 1949, page 1217.)

where

$$\beta = \frac{y}{\sqrt{x}} (V_\infty/v)^{1/2}, \quad (2.93)$$

From Eqs. (2.90), (2.92), and (2.93),

$$v_x = \frac{\partial \psi}{\partial y} = \frac{\partial \psi}{\partial \beta} \frac{\partial \beta}{\partial y} = V_\infty \frac{df}{d\beta}, \quad (2.94)$$

$$v_y = -\frac{\partial \psi}{\partial x} = \frac{1}{2} \left[ \frac{vV_\infty}{x} \right]^{1/2} \left[ \beta \frac{df}{d\beta} - f \right]. \quad (2.95)$$

Then Eq. (2.91) becomes

$$2 \frac{d^2 f}{d\beta^2} + f \frac{d^2 f}{d\beta^2} = 0. \quad (2.96)$$

Mathematically, the use of  $\psi$  and  $\beta$  has reduced a partial differential equation to an ordinary differential equation with the boundary conditions also taking equivalent forms:

$$\text{B.C. 1 at } \beta = 0, \quad f = 0, \quad \frac{df}{d\beta} = 0; \quad (2.97)$$

$$\text{B.C. 2 at } \beta = \infty, \quad \frac{df}{d\beta} = 1. \quad (2.98)$$

Equation (2.96) may be solved by expressing  $f(\beta)$  in a power series, that is,  $f = \sum_0^\infty a_k \beta^k$ .

The technique is too involved to develop here, but the solution conforming to the boundary conditions becomes

$$f = \frac{\alpha \beta^2}{2!} - \frac{1}{2} \frac{\alpha^2 \beta^6}{5!} + \frac{11}{4} \frac{\alpha^3 \beta^8}{8!} + \dots \quad (2.99)$$

where  $\alpha = 0.332$ . Then Eqs. (2.94) and (2.95) give expressions for  $v_x$  and  $v_y$ ; the solution for  $v_y$  is shown graphically in Fig. 2.7. The position, where  $v_y/V_\infty = 0.99$ , is located at  $\beta = 5.0$ ; thus the boundary-layer thickness  $\delta$  is

$$\delta = 5.0 \left[ \frac{vx}{V_\infty} \right]^{1/2}. \quad (2.100)$$

Note that if we divide Eq. (2.100) by  $x$ , both sides become dimensionless:

$$\frac{\delta}{x} = 5.0 \left[ \frac{v}{xV_\infty} \right]^{1/2} = \frac{5.0}{\sqrt{Re_x}}. \quad (2.101)$$

Note also that as a result of the analysis, the Reynolds number ( $Re_x = xV_\infty/v$ ) has evolved; in this instance we give  $Re$  the subscript  $x$  in order to emphasize that it is a local value with

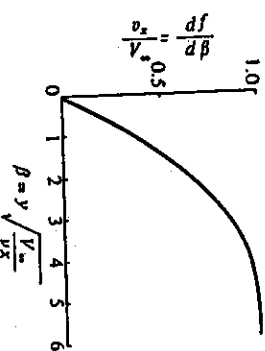


Fig. 2.7 Solution for the velocity distribution in the boundary layer over a flat plate.  
(From L. Howarth, Proc. Roy. Soc., London A164, 547 (1938).)

the characteristic dimension  $x$ . We can also calculate the *drag force*, which is exerted by the fluid on the plate's surface. If the plate has a length  $L$  and width  $W$ , the drag force  $F_K$  is

$$F_K = \int_0^W \int_0^L \left[ \eta \frac{\partial v_x}{\partial y} \right]_{y=0} dx dz. \quad (2.102)$$

In other words, the shear stress at the solid surface is integrated over the entire surface. From Fig. 2.7 we find that

$$\left[ \frac{\partial(v_x/V_\infty)}{\partial \beta} \right]_{\beta=0} = 0.332. \quad (2.103)$$

Knowing the integrand in Eq. (2.102), we can now perform the integration. The result is

$$F_K = 0.664 \sqrt{\rho u L W^2 V_\infty^3}. \quad (2.104)$$

This is the drag force exerted by the fluid on one surface only.

## 2.7.2 Flow in inlet of circular tubes

In Section 2.4, we considered the flow of fluid in a long tube so that end effects were negligible. Now we wish to study the flow conditions at the inlet where the flow is not fully developed. The fluid enters the tube with a uniform velocity  $V_0$  in the  $z$ -direction. The most important component for this system is the  $z$ -component, just as the  $x$ -component is most important for the flow past a flat plate. According to Eq. (F) in Table 2.3, the momentum equation with  $v_y = 0$ ,  $\partial v_z / \partial t = 0$ , and  $g_z = 0$ , reduces to

Again, the viscous effect in the direction parallel to flow is negligible, so that  $\partial^2 v_z / \partial z^2 \approx 0$ , and we are left with

$$v_r \frac{\partial v_z}{\partial r} + v_z \frac{\partial v_r}{\partial z} = -\frac{1}{\rho} \frac{\partial P}{\partial z} + \frac{\nu}{r} \frac{\partial}{\partial r} \left[ r \frac{\partial v_z}{\partial r} \right] \quad (2.105)$$

We can deduce the equation of continuity from Eq. (B) in Table 2.1:

$$\frac{1}{r} \frac{\partial}{\partial r} (rv_r) + \frac{\partial v_z}{\partial z} = 0. \quad (2.106)$$

The method for the solution of Eq. (2.105) is not given here, but one should understand why Eq. (2.105) is the starting point. Langhaar<sup>2</sup> has developed the solution for this problem, as described in Fig. 2.8. His analysis shows that a fully developed flow is not established until  $v_z/R^2 V_0 \approx 0.07$ . Thus an entrance length ( $z = L_e$ ) of approximately  $0.035 (D^2 V_0 \rho) / \eta$  is required for buildup to the parabolic profile of the fully developed flow.

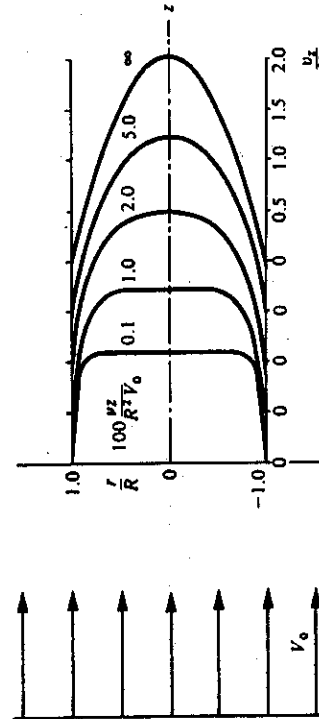


Fig. 2.8 Velocity distribution for laminar flow in the inlet section of a tube.

### 2.7.3 Creeping flow around a solid sphere

Consider the flow of an incompressible fluid about a solid sphere (Fig. 2.9). The fluid approaches the sphere upward along the  $z$ -axis with a uniform velocity  $V_\infty$ . Clearly, the momentum equation for this situation does not involve the  $\phi$ -component. In addition, if the flow is slow enough, the acceleration terms in Navier-Stokes' equation can be ignored. Therefore, in spherical coordinates, from Eqs. (D) and (E) in Table 2.4, we obtain for the  $r$ -component:

$$-\frac{\partial P}{\partial r} + \eta \left[ \nabla^2 v_r - \frac{2}{r^2} v_r - \frac{2}{r^2} \frac{\partial v_\theta}{\partial \theta} - \frac{2}{r^2} v_\theta \cot \theta \right] + \rho g_r = 0, \quad (2.107)$$

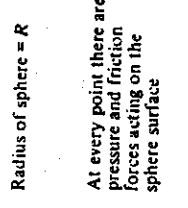


Fig. 2.9 Coordinate system used in describing the flow of a fluid about a rigid sphere.

and for the  $\theta$ -component:

$$-\frac{1}{r} \frac{\partial P}{\partial \theta} + \eta \left[ \nabla^2 v_\theta + \frac{2}{r^2} \frac{\partial v_r}{\partial \theta} - \frac{v_\theta}{r^2 \sin^2 \theta} \right] + \rho g_\theta = 0. \quad (2.108)$$

The continuity equation (Eq. (C) in Table 2.1) is

$$\frac{1}{r^2} \frac{\partial}{\partial r} (r^2 v_r) + \frac{1}{r \sin \theta} \frac{\partial}{\partial \theta} (v_\theta \sin \theta) = 0. \quad (2.109)$$

The momentum flux-distribution, pressure distribution, and velocity components have been found analytically:<sup>3</sup>

$$r_{\text{eff}} = \frac{3}{2} \frac{\eta V_\infty}{R} \left[ \frac{R}{r} \right]^4 \sin \theta, \quad (2.110)$$

$$P = P_0 - \rho g z - \frac{3}{2} \frac{\eta V_\infty}{R} \left[ \frac{R}{r} \right]^2 \cos \theta, \quad (2.111)$$

$$v_r = V_\infty \left[ 1 - \frac{3}{2} \left[ \frac{R}{r} \right]^2 + \frac{1}{2} \left[ \frac{R}{r} \right]^3 \right] \cos \theta. \quad (2.112)$$

<sup>2</sup>H. L. Langhaar, *J. Appl. Mech.*, **9**, A55-58 (1942).

<sup>3</sup>V. L. Streeter, *Fluid Dynamics*, McGraw-Hill, New York, 1948, pages 235-240.

$$v_\theta = -V_\infty \left[ 1 - \frac{3}{4} \left[ \frac{R}{r} \right] - \frac{1}{4} \left[ \frac{R}{r} \right]^3 \right] \sin \theta. \quad (2.113)$$

We can check the validity of the results by showing that Eqs. (2.107)-(2.109) and the following conditions are satisfied:

$$\text{B.C. 1 at } r = R, \quad v_r = 0 = v_\theta,$$

$$\text{B.C. 2 at } r = \infty, \quad v_r = V_\infty.$$

In Eq. (2.111), the quantity  $P_0$  is the pressure in the plane  $z = 0$  far away from the sphere,  $-\rho g z$  is simply the hydrostatic effect, and the term containing  $V_\infty$  results from the fluid flow around the sphere. These equations are valid for a Reynolds number ( $DV_\infty/\nu$ ) less than approximately unity.

With these results, we can calculate the net force which is exerted by the fluid on the sphere. This force is computed by integrating the normal force and tangential force over the sphere surface as follows.

The *normal force* acting on the solid surface is due to the pressure given by Eq. (2.111) with  $r = R$  and  $z = R \cos \theta$ . Thus

$$P(r = R) = P_0 - \rho g R \cos \theta - \frac{3}{2} \frac{\eta V_\infty}{R} \cos \theta.$$

The  $z$ -component of this pressure multiplied by the surface area on which it acts,  $R^2 \sin \theta d\theta d\phi$ , is integrated over the surface of the sphere to yield the net force due to the pressure difference:

$$F_n = \int_0^{2\pi} \int_0^\pi \left[ P_0 - \rho g R \cos \theta - \frac{3}{2} \frac{\eta V_\infty}{R} \cos \theta \right] R^2 \sin \theta d\theta d\phi. \quad (2.114)$$

Equation (2.114), integrated, yields two terms:

$$F_n = \frac{4}{3} \pi R^3 \rho g + 2\pi R V_\infty, \quad (2.115)$$

the *buoyant force* and *form drag*, respectively.

At each point on the surface, there is also a shear stress acting tangentially,  $-\tau_{\theta\theta}$ , which is the force acting on a unit surface area. The  $z$ -component of this force is  $(-\tau_{\theta\theta})(-\sin \theta)R^2 \sin \theta d\theta d\phi$ ; again, integration over the sphere's surface yields

$$F_t = \int_0^{2\pi} \int_0^\pi (\tau_{\theta\theta}|_{r=R} \sin \theta) R^2 \sin \theta d\theta d\phi.$$

From Eq. (2.110), we get

$$\tau_{\theta\theta}|_{r=R} = \frac{3}{2} \frac{\eta V_\infty}{R} \sin \theta,$$

so that the *friction drag* results:

$$F_t = 4\pi \eta R V_\infty.$$

$$(2.116)$$

The total force  $F$  of the fluid on the sphere is given by the sum of Eqs. (2.115) and (2.116):

$$F = \frac{4}{3} \pi R^3 \rho g + 6\pi \eta R V_\infty. \quad (2.117)$$

These two terms are designated as  $F_r$  (the force exerted even if the fluid is stationary) and  $F_K$  (the force associated with fluid movement). Thus these forces are

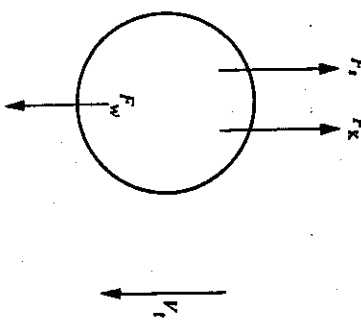
$$F_r = \frac{4}{3} \pi R^3 \rho g, \quad (2.118)$$

$$F_K = 6\pi \eta R V_\infty. \quad (2.119)$$

We use Eq. (2.119), known as *Stokes' law*, primarily for determining the terminal velocity,  $V_t$ , of small spherical particles moving through fluid media. The fluid media are stagnant; the spherical particle moves through the fluid, and  $V_\infty$  is viewed as  $V_t$ . With this in mind, we may use *Stokes' law* as the basis of a *falling-sphere viscometer*, in which the liquid is placed in a tall transparent cylinder and a sphere of known mass and diameter is dropped into it. The terminal velocity of the falling sphere can be measured, and this in turn relates to the fluid's viscosity.

**Example 2.3** Apply Stokes' law to the falling sphere viscometer and write an expression for the viscosity of the liquid in the viscometer.

**Solution.** A force balance on the sphere, as it falls through the liquid, is made according to the diagram:



Here  $F_r$  is the buoyant force exerted by the liquid and is therefore directed upward;  $F_K$  is often called the *drag force* and as such always acts in the opposite direction to that of motion and is therefore directed upward. The only force in the downward direction is the weight of the sphere. The terminal velocity is reached when the force system is in equilibrium. Therefore  $F_r + F_K = F_w$ , and by substituting in expressions for each of these forces, we have

$$\frac{4}{3} \pi R^3 \rho g + 6\pi \eta R V_t = \frac{4}{3} \pi R^3 \rho_s g. \quad (2.120)$$

where  $\rho_s$  is the sphere's density.

By solving Eq. (2.120) for  $\eta$ , we arrive at

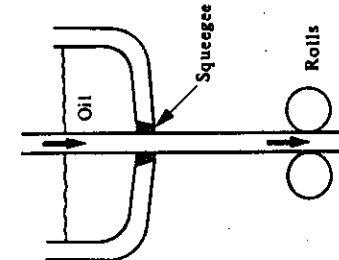
$$\eta = \frac{2R^2(\rho_s - \rho)g}{9V_t}. \quad (2.121)$$

The result is valid only if  $2RV_t/\nu$  is less than approximately unity.

**PROBLEMS**

**2.1** Refer to the results of Example 2.1. The viscosity of the glass is  $1 \text{ N s m}^{-2}$ , and the viscosity of the metal is  $3 \times 10^3 \text{ N s m}^{-2}$ . The densities of the glass and the metal are  $3.2 \text{ kg m}^{-3}$  and  $7.0 \text{ kg m}^{-3}$ , respectively. For  $\beta = \pi/8$  and  $\delta_1 = 1 \text{ mm}$  and  $\delta_2 = 2 \text{ mm}$ , calculate the maximum velocities and average velocities of the glass and the metal.

**2.2** A continuous sheet of metal is cold-rolled by passing vertically between rolls. Before entering the rolls, the sheet passes through a tank of lubricating oil equipped with a squeegee device that coats both sides of the sheet uniformly as it exits. The amount of oil that is carried through can be controlled by adjusting the squeegee device. Prepare a control chart that can be used to determine the thickness of oil (in mm) on the plate just before it enters the roll as a function of the mass rate of oil (in kg per hour). Values of interest for the thickness of the oil film range from 0-0.6 mm. *Data:* Oil density,  $962 \text{ kg m}^{-3}$ ; oil viscosity,  $4.1 \times 10^{-3} \text{ N s m}^{-2}$ ; width of sheet, 1.5 m; velocity of sheet,  $0.3 \text{ m s}^{-1}$ .



**2.3** A Newtonian liquid flows simultaneously through two parallel and vertical channels of different geometries. Channel "A" is circular with a radius  $R$ , and "B" is a slit of thickness  $2b$  and width  $W$ ,  $2b \ll W$ . Assume fully developed flow in both channels and derive an equation which gives the ratio of the volume flow rate through A to that through B.

**2.4** Develop expressions for the flow of a fluid between vertical parallel plates. The plates are separated by a distance of  $2\delta$ . Consider fully developed flow and determine

- the velocity distribution,
- the volume flow rate.

Compare your expressions with Eqs. (2.20) and (2.23).

**2.5** Repeat Problem 2.4 but now orient the plates at an angle  $\beta$  to the direction of gravity and obtain expressions for

- the velocity distribution,
- the volume flow rate.

Compare your expressions with the results of Problem 2.4 and Eqs. (2.20) and (2.23).

**2.6** A liquid is flowing through a vertical tube 0.3 m long and 2.5 mm in I.D. The density of the liquid is  $1260 \text{ kg m}^{-3}$  and the mass flow rate is  $3.8 \times 10^{-5} \text{ kg s}^{-1}$ .

- What is the viscosity in  $\text{N s m}^{-2}$ ?
- Check on the validity of your results.

**2.7** Water (viscosity  $10^{-3} \text{ N s m}^{-2}$ ) flows parallel to a flat horizontal surface. The velocity profile at  $x = x_1$  is given by

$$v_x = 6 \sin \left[ \frac{\pi}{2} \right] y$$

with  $v_x$  in  $\text{m s}^{-1}$  and  $y$  as distance from surface in mm.

- a) Find the shear stress at the wall at  $x_1$ . Express results in  $\text{N m}^{-2}$ .  
b) Farther downstream, at  $x = x_2$ , the velocity profile is given by

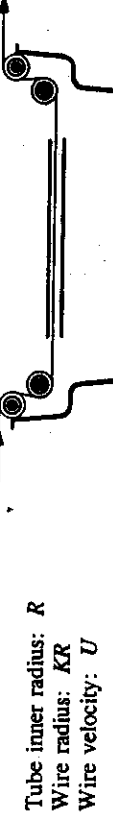
$$v_x = 4 \sin \left[ \frac{\pi}{2} \right] y$$

- c) Is the flow "fully developed"? Explain.  
Is there a  $y$ -component to flow (i.e.,  $v_y$ )? Explain with the aid of the continuity equation.

- 2.8** For a polymeric melt that follows a power law for shear stress versus shear strain rate, derive an equation for the velocity profile and volume flow rate for flow between parallel plates.

- 2.9** The power law polymer of Problem 2.8 has constants  $\eta_0 = 1.2 \times 10^4 \text{ N s m}^{-2}$  and  $n = 0.35$ . It is injected through a gate into a thin cavity, which has a thickness of 2 mm, a width of 10 mm and a length of 20 mm. If the injection rate is constant at  $200 \text{ mm}^3 \text{s}^{-1}$ , estimate the time to fill the cavity and the injection pressure at the gate.

- 2.10** A wire is cooled after a heat treating operation by being pulled through the center of an open-ended, oil-filled tube which is immersed in a tank. In a region in the tube where end effects are negligible, obtain an expression for the velocity profile assuming steady state and all physical properties constant.



- 2.11** Starting with the  $x$ -component of the momentum equation (Eq. (2.52)), develop the  $x$ -component for the Navier-Stokes' equation (constant  $\rho$  and  $\eta$ , (Eq. 2.63)).

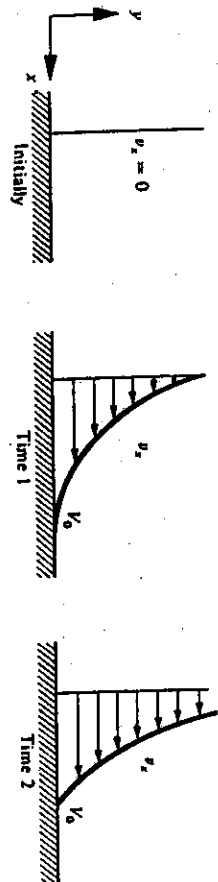
- 2.12** Air at  $289 \text{ K}$  flows over a flat plate with a velocity of  $9.75 \text{ m s}^{-1}$ . Assume laminar flow and a) calculate the boundary-layer thickness 50 mm from the leading edge; b) calculate the rate of growth of the boundary layer at that point; i.e., what is  $d\delta/dx$  at that point? *Properties of air at 289 K:* density:  $1.22 \text{ kg m}^{-3}$ ; viscosity:  $1.78 \times 10^{-5} \text{ N s m}^{-2}$ .

- 2.13** A fluid flows upward through a vertical cylindrical annulus of length  $L$ . Assume that the flow is fully developed. The inner radius of the annulus is  $\alpha R$ , and the outer radius is  $R$ .
- Write the momentum equation in terms of velocity.
  - Solve for the velocity profile.
  - Solve for the maximum velocity.

- 2.14** In steelmaking, deoxidation of the melt is accomplished by the addition of aluminum, which combines with the free oxygen to form alumina,  $\text{Al}_2\text{O}_3$ . It is then hoped that most of these alumina particles will float up to the slag layer for easy removal from the process, because their presence in steel can be detrimental to mechanical properties. Determine the size of the smallest alumina particles that will reach the slag layer from the bottom of the steel two minutes after the steel is deoxidized. It may be assumed that the alumina particles are spherical in nature. For the purpose of estimating the steel's viscosity use the data for Fe-0.5 wt pct C in Fig. 1.11. *Data:* Temperature of steel melt:  $1873 \text{ K}$ ; steel melt depth: 1.5 m; density of steel:  $7600 \text{ kg m}^{-3}$ ; density of alumina:  $3320 \text{ kg m}^{-3}$ .

## 2.15

- a) Consider a very large flat plate bounding a liquid that extends to  $y = +\infty$ . Initially, the liquid and the plate are at rest; then suddenly the plate is set into motion with velocity  $V_0$  as shown in the figure below. Write (1) the pertinent differential equation in terms of velocity, for constant properties, that applies from the instant the plate moves, and (2) the appropriate boundary and initial conditions. The solution to these equations will be discussed in Chapter 9.



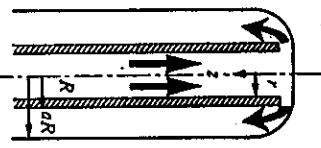
- b) A liquid flows upward through a long vertical conduit with a square cross section. With the aid of a clearly labeled sketch, write (1) a pertinent differential equation that describes the flow for constant properties, and (2) the appropriate boundary conditions. Consider only that portion of the conduit where flow is fully developed and be sure that your sketch and equations correspond to one another.

- 2.16 Molten aluminum is degassed by gently bubbling a 75%  $N_2$ -25%  $Cl_2$  gas through the melt. The gas passes through a graphite tube at a volumetric flow rate of  $6.6 \times 10^{-5} \text{ m}^3 \text{ s}^{-1}$ . Calculate the pressure that should be maintained at the tube entrance if the pressure over the bath is  $1.014 \times 10^5 \text{ N m}^{-2}$  (1 atm). Data: Tube dimensions:  $L = 0.9 \text{ m}$ ; inside diameter = 2 mm. Temperature of aluminum melt is 973 K; density of aluminum is  $2500 \text{ kg m}^{-3}$ .

- 2.17 Glass flows through a small orifice by gravity to form a fiber. The free-falling fiber does not have a uniform diameter; furthermore as it falls through the air it cools so that its viscosity changes. a) Write the momentum equation for this situation. b) Write appropriate boundary conditions.

- 2.18 A liquid flows upward through a tube, overflows, and then flows downward as a film on the outside.

- a) Develop the pertinent momentum balance that applies to the falling film, for steady-state laminar flow, neglecting end effects.
- b) Develop an expression for the velocity distribution.



## TURBULENT AND COMPLEX FLOWS

In Chapter 2 we discussed only laminar flow problems where we knew differential equations describing the flow, and could calculate the velocity distribution for simple systems. But more often than not, the flow is turbulent, and then experimental information must be sought. For example, it is practically impossible for laminar flow to persist in a pipe at values of  $Re$  greater than about 2100. This value of  $Re$  is subject to variations in that laminar flow has been maintained up to values of  $Re$  as high as 50 000. However, in such cases, the flow is extremely unstable, and the least disturbance transforms it instantly into turbulent flow. Also, the transition  $Re$  is higher in a converging pipe and lower in a diverging pipe than in a straight pipe, and even depends to some degree on the inside-surface roughness of the pipe.

If we accept 2100 as the normal transition value of  $Re$  for turbulent flow in pipes with normal roughness, we can easily show that turbulent flow is the usual case. Consider water at 289 K (60°F) which has a kinematic viscosity of  $1.13 \times 10^{-6} \text{ m}^2 \text{ s}^{-1}$ . In a pipe of 25.4 mm diam. the average velocity that still corresponds to laminar flow is

$$V_{cr} = \frac{v}{D} Re_p = \frac{1.13 \times 10^{-6} \text{ m}^2 \text{ s}^{-1}}{25.4 \times 10^{-3} \text{ m}} \times 2100 \\ = 9.34 \times 10^{-2} \text{ m s}^{-1}.$$

Velocities as small as these (in 25 mm pipes) are not often encountered in practical engineering; most problems of engineering importance occur in the region of turbulent flow.

Notwithstanding, many instances in engineering involve laminar flow. In this chapter we examine some empirical information available for various systems. We may classify the flow systems into two groups: flow through closed conduits and flow past submerged bodies. We also introduce the readers to flow through porous media and in fluidized beds.

The fluctuating nature of turbulence and an introduction to turbulence models are reserved for Chapter 16. These models are being increasingly used in commercial software packages that are used for solving industrial flow problems.

### 3.1 FRICTION FACTORS FOR FLOW IN TUBES

As an example of a flow system, consider a length of horizontal pipe between  $z = 0$  and  $z = L$ . We presume that in this length of pipe the fluid is flowing with an average velocity independent of time, and that the flow is fully developed. For flow in such a system, we may write the kinetic force of the fluid on the inner wall as

$$(3.1) \quad F_K = 2\pi RL\tau_0.$$

Here  $\tau_0$  is defined as the shear stress at the wall, or, in terms of previous notation,  $\tau_0 \equiv \tau_{r_1}$  ( $r = R$ ). According to Eq. (2.28), we can express  $\tau_0$  in terms of the pressure drop:

$$(3.2) \quad \tau_0 = \left[ \frac{P_0 - P_L}{L} \right] \frac{R}{2}.$$

Equation (3.2) is also valid for turbulent flow as it specifies conditions only at the wall. Using Eq. (3.2), we may write  $F_K$  in an alternative form:

$$(3.3) \quad F_K = \pi R^2 (P_0 - P_L).$$

Equation (3.3) focuses our attention on what should be considered if we ask the following question: What pressure drop is necessary to deliver a given volume of fluid through a tube? Thus we learn from Eq. (3.3) that  $F_K$  must be determined; for laminar flow, this can be calculated because the velocity distribution is amenable to analysis, and pressure drops can be determined *a priori*. For turbulent flow, the uncertainties involved in parallel analysis have led engineers to take an experimental approach to the problem.

In turbulent flow we may think that the flow pattern starts with a *laminar boundary layer*, in which the flow can be described by Newton's law of viscosity, followed by a transition region in which the degree of turbulence steadily increases and laminar effects diminish, until finally the region of fully developed turbulence is reached. These regions are illustrated in Fig. 3.1. In turbulent flow, therefore, the fluid still clings to the solid wall. Thus Eq. (3.1) is applicable, but, in general, the value of  $\tau_0$  is not determined by analytical means. More often we employ an empirical technique and express the force  $F_K$  as the product of a *characteristic area*  $A$ , a *characteristic kinetic energy*  $K$  (per unit volume), and a dimensionless quantity  $f$ , known as the *friction factor*:

$$(3.4) \quad F_K = AKf.$$

This is a useful definition because  $f$  is a function only of the dimensionless Reynolds number for a given geometrical shape. This is shown in a following discussion, but first let us present how  $f$  is related to  $\tau_0$ .

For flow in conduits,  $A$  is taken to be the wetted surface  $2\pi RL$ , and  $K$  is taken to be the kinetic energy based on the average velocity, that is  $\frac{1}{2}\rho \bar{V}^2$ . Thus for flow in a filled pipe of length  $L$ , we have

$$(3.5) \quad F_K = f(2\pi RL)\left(\frac{1}{2}\rho \bar{V}^2\right).$$

Combining Eqs. (3.1) and (3.5), we see that

$$(3.6) \quad f = \frac{\tau_0}{\left(\frac{1}{2}\rho \bar{V}^2\right)}.$$

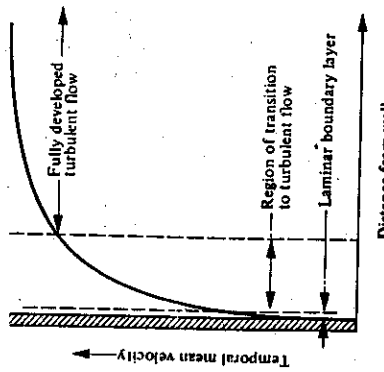


Fig. 3.1 Velocity distribution for turbulent flow in tubes in the region near the wall.

#### 3.1.1 Dimensional analysis for friction factor

Now we resort to *dimensional analysis* which is a method of deducing logical groupings of the variables involved in a process. One of these methods, called the *similarity technique*, is applied to systems which are geometrically similar. For example, in two circular tubes, all comparable lengths have identical ratios. Thus we write

$$(3.7) \quad K_D = \frac{z_1}{z_2} = \frac{r_1}{r_2} = \frac{D_1}{D_2},$$

where  $z_1$  and  $z_2$  are comparable distances along the lengths of tube;  $r_1$  and  $r_2$  are comparable radii in tubes 1 and 2, respectively.

For the flow system in either tube, the differential equation for the conservation of momentum that applies in the steady state is

$$(3.8) \quad \eta \left[ \frac{1}{r} \frac{d}{dr} \left( r \frac{dv_z}{dr} \right) \right] - \frac{dp}{dz} = 0,$$

and a boundary condition is

$$(3.9) \quad \left. \tau_{rz} \right|_{r=R} \equiv \tau_0 = -\eta \left[ \frac{dv_z}{dr} \right]_{r=R}$$

The differential equation and the boundary condition require certain relationships among velocities,  $dp/dz$ , and fluid properties, at corresponding points in the two systems. Thus, in addition to the ratios of Eq. (3.7), we define the ratios for kinematic and dynamic similarity:

$$(3.10) \quad K_v = \frac{v_1}{v_2} = \frac{\bar{V}_1}{\bar{V}_2}, \quad K_p = \frac{dp_1/dz_1}{dp_2/dz_2}, \\ K_\eta = \frac{\eta_1}{\eta_2}, \quad K_o = \frac{\rho_1}{\rho_2}.$$

$$\frac{\tau_{01}}{\rho_1 \bar{V}_1^2} = \frac{\tau_{02}}{\rho_2 \bar{V}_2^2}, \quad (3.16)$$

To investigate the conditions which must be satisfied by these ratios, we write Eq. (3.8) specifically for system 1:

$$\eta_1 \left[ \frac{1}{r_1} \frac{d}{dr_1} \left[ r_1 \frac{dv_{z1}}{dr_1} \right] \right] - \frac{dP_1}{dz_1} = 0. \quad (3.11)$$

Now if we replace  $r_1$ ,  $v_{z1}$ , etc., by their equivalents in Eqs. (3.7) and (3.10), then we can write Eq. (3.11) for system 2:

$$\left[ \frac{K_p K_p}{K_b^2} \right] \eta_2 \left[ \frac{1}{r_2} \frac{d}{dr_2} \left[ r_2 \frac{dv_{z2}}{dr_2} \right] \right] - K_p \frac{dP_2}{dz_2} = 0. \quad (3.12)$$

Multiplying Eq. (3.12) by  $K_b/K_p^2 K_p$ , we finally obtain:

$$\left[ \frac{K_p}{K_b K_p K_p} \right] \eta_2 \left[ \frac{1}{r_2} \frac{d}{dr_2} \left[ r_2 \frac{dv_{z2}}{dr_2} \right] \right] - \left[ \frac{K_p K_p}{K_b K_p^2} \right] \frac{dP_2}{dz_2} = 0. \quad (3.13)$$

It is apparent that Eq. (3.13) written with subscripts 1 would also be valid, and because both systems must obey the original differential equation, then

$$\frac{K_p K_p}{K_b K_p K_p} = 1 \quad \text{and} \quad \frac{K_p K_p}{K_b K_p^2} = 1,$$

or

$$\frac{D_1 \bar{V}_1 \rho_1}{\eta_1} = \frac{D_2 \bar{V}_2 \rho_2}{\eta_2}, \quad (3.14)$$

and

$$\frac{D_1 (dP_1/dz_1)}{\rho_1 \bar{V}_1^2} = \frac{D_2 (dP_2/dz_2)}{\rho_2 \bar{V}_2^2}. \quad (3.15)$$

The group in Eq. (3.14) is the Reynolds number which, of course, is dimensionless. Once again it appears—in fact, in all cases of forced convection, the Reynolds number is a significant dimensionless group. The group in Eq. (3.15) is another dimensionless group and, as shown in the following paragraph, is actually twice the friction factor.

If we define a new ratio as

$$K_r = \tau_{01}/\tau_{02},$$
then the boundary condition, (Eq. 3.9), applied to both systems, yields

$$\frac{K_r K_p}{K_b K_p} = 1 \quad \text{or} \quad \frac{\tau_{01} D_1}{\eta_1 \bar{V}_1} = \frac{\tau_{02} D_2}{\eta_2 \bar{V}_2}.$$

which are equivalent to half the friction factor (Eq. 3.6). Now the dimensional analysis is complete; it has been shown that for flow in the two arbitrary systems having geometric similarity, the friction factors are equal when the Reynolds numbers are equal. Thus for flow in tubes, the friction factor  $f$  may be correlated as a function of the Reynolds number.

### 3.1.2 Experimental results for friction factor

Experimentally,  $f$  can be measured by noting that if  $F_k$  is eliminated between Eqs. (3.3) and (3.5), then

$$f = \frac{1}{4} \left[ \frac{D}{L} \right] \left[ \frac{P_0 - P_L}{\frac{1}{2} \rho \bar{V}^2} \right], \quad (3.17)$$

and the connection with Eq. (3.15) is made apparent. Also, as we have shown, the friction factor is only a function of the Reynolds number:  $f = f(\text{Re}_D)$ . In most designs the pressure drop is not usually known *a priori*; we therefore use  $\text{Re}_D$  to evaluate the friction factor and then the pressure drop developed due to friction. Since  $f$  is only a function of  $\text{Re}_D$ , it is sufficient to plot only a single curve of  $f$  against  $D\bar{V}/\nu$  rather than determine how  $f$  varies for separate values of  $D$ ,  $\bar{V}$ ,  $\rho$ , and  $\eta$ . The lower curve in Fig. 3.2 gives a plot of  $f$  versus  $\text{Re}_D$  for smooth tubes. This curve reflects the laminar and turbulent behavior of fluids in long, smooth, circular tubes. For the laminar region,

$$f = \frac{16}{\text{Re}}, \quad (3.18)$$

which can be derived by using the Hagen-Poiseuille law developed in Chapter 2.

The turbulent region has been established solely by experimental data. The entire turbulent curve closely approximates

$$1/\sqrt{f} = 4.0 \log \left( \text{Re} \sqrt{f} \right) - 0.40, \quad (3.19)$$

and a simpler expression exists for  $2.1 \times 10^3 < \text{Re} < 10^6$ , namely,

$$f = 0.0791 \text{ Re}^{-1/4}. \quad (3.20)$$

If the tubes are rough, then in turbulent flow the friction factor is higher than that indicated for smooth tubes. The relative roughness,  $\varepsilon/D$ , enters the correlation where  $\varepsilon$  is the height of protuberances on the tube wall. For use with Fig. 3.2, we can obtain values of  $\varepsilon$  from Table 3.1. However, the reader should note that these values apply for new, clean pipes, and even then the values may vary. For old pipes, they may be much higher and certainly  $\varepsilon$  varies greatly with age, depending on the fluid being transported. In addition, in small pipes, deposits may substantially reduce the inside diameter. Therefore we must carefully use our judgment in estimating a value of  $\varepsilon$  and consequently of  $f$ .

*First approximation.* In Fig. 3.2,  $f = 0.005$  when  $\epsilon/D = 0.001$  and  $Re = 9 \times 10^5$ . For this friction factor, the velocity is

$$\bar{V} = \left\{ \left( \frac{1}{2f} \right) \left[ \frac{D}{L} \right] \left[ \frac{\Delta P}{\rho} \right] \right\}^{1/2};$$

$$\begin{aligned} \left[ \frac{D}{L} \right] \left[ \frac{\Delta P}{\rho} \right] &= \frac{0.125 \text{ m}}{180 \text{ m}} \left| \frac{3.5 \times 10^4 \text{ N}}{\text{m}^2} \right| \left| \frac{\text{m}^3}{1,000 \text{ kg}} \right| \left| \frac{1 \text{ kg m}}{1 \text{ N s}^2} \right| \\ &= 2.43 \times 10^{-2} \text{ m}^2 \text{ s}^{-2}. \end{aligned}$$

Therefore

$$\bar{V} = \left\{ \left( \frac{1}{0.01} \right) (2.43 \times 10^{-2}) \right\}^{1/2} = 1.56 \text{ m s}^{-1}.$$

Now we make a second estimate of the Reynolds number and the friction factor. The estimated velocity gives the following Reynolds number:

$$\begin{aligned} Re_D &\approx \frac{D\bar{V}\rho}{\eta} = \frac{0.124 \text{ m}}{\text{s}} \left| \frac{1.56 \text{ m}}{\text{s}} \right| \left| \frac{1000 \text{ kg}}{\text{m}^3} \right| \left| \frac{1 \text{ N s}^2}{1 \text{ kg m}} \right| \\ &= 2.28 \times 10^5. \end{aligned}$$

*Second approximation.* This Reynolds number gives  $f = 0.0052$ . Thus, with this  $f$ ,  $\bar{V}$  is corrected slightly.

$$\bar{V} = \left[ \frac{0.0050}{0.0052} \right] (1.56) = 1.53 \text{ m s}^{-1}.$$

Therefore, the mass flow rate  $W$  is

$$W = \left[ \frac{\pi D^2}{4} \right] \rho \bar{V} = \left[ \frac{\pi}{4} \right] (0.125)^2 (1000) (1.53) = 18.8 \text{ kg s}^{-1}.$$

### 3.2 FLOW IN NONCIRCULAR CONDUITS

If the pipes are not circular and turbulent flow exists, then an equivalent diameter  $D_e$  replaces  $D$  in the Reynolds number:

$$D_e = \frac{4 \times \text{flow area}}{\text{wetted perimeter}} = \frac{4A}{P_w}. \quad (3.21)$$

**Example 3.1** Determine the mass flow rate ( $\text{kg s}^{-1}$ ) of water at  $300 \text{ K}$  through  $180 \text{ m}$  of horizontal pipe, having I.D. of  $125 \text{ mm}$ , under a pressure drop of  $3.5 \times 10^4 \text{ N m}^{-2}$ . The relative roughness  $\epsilon/D$  of the pipe is estimated as  $0.001$ .

**Solution.** The solution to this problem can be found by using Eq. (3.17) and solving for the average velocity  $\bar{V}$ . However,  $\bar{V}$  cannot be determined unless  $f$  is known and, because  $= f(Re_D)$ , a trial and error solution is in order.

Many other texts refer to the hydraulic radius  $R_h$  rather than equivalent diameter. In such instances,  $D$  is replaced by  $4R_h$ , where  $R_h = A/P_w$ ; the end result is the same whether  $D_e$  or  $R_h$  is employed.

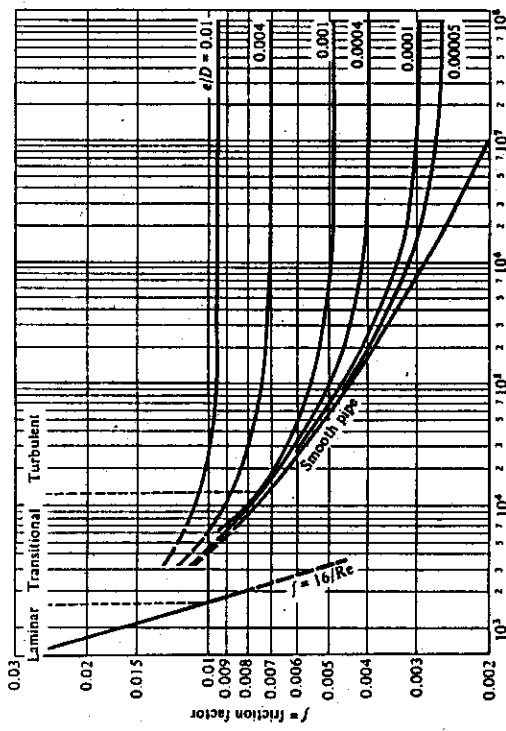


Fig. 3.2 Friction factors for flow in tubes. (Adapted from L. F. Moody, Trans. ASME 66, 671 (1944), and Mech. Eng. 69, 1005 (1947).)

Table 3.1 Values of absolute roughness  $\epsilon$  for new pipes

	$\epsilon, \text{ mm}$
Drawn tubing, brass, lead, glass, centrifugally spun cement, bituminous lining, transite	0.0015
Commercial steel or wrought iron	0.046
Welded-steel pipe	0.046
Asphalt-dipped cast iron	0.12
Galvanized iron	0.15
Cast iron, average	0.26

From Eq. (3.4),

$$f = \frac{F_K}{A K}, \quad (3.4a)$$

With this modification, we can determine the friction factor from Fig. 3.2 where  $\varepsilon/D$  is replaced by  $\varepsilon/D_e$ . Similarly in Eq. (3.17), we replace  $D$  by  $D_e$ , and calculate the pressure drop due to friction in noncircular conduits. This approach gives good results for turbulent flow, but for laminar flow the results are poor. For example, in a thin annulus in which the spacing  $z$  is very much less than the width, laminar flow has a parabolic distribution perpendicular to the walls. This situation closely approximates flow between parallel flat plates, and we can show the friction factor to be

$$f = \frac{24}{\bar{R}e}. \quad (3.22)$$

This expression, of course, differs from Eq. (3.18) which applies to laminar flow in circular pipes.

For laminar flow in a rectangular duct of dimensions,  $z_1 \times z_2$ , the friction factor is

$$f = \frac{16}{\phi \bar{R}e}. \quad (3.23)$$

Here we evaluate the Reynolds number using  $D_e$ , which for rectangular ducts is

$$D_e = \frac{2(z_1 z_2)}{(z_1 + z_2)},$$

and  $\phi$  is given by Fig. 3.3. The laminar-to-turbulent transition for noncircular conduits is still normally taken at a Reynolds number of approximately 2100.

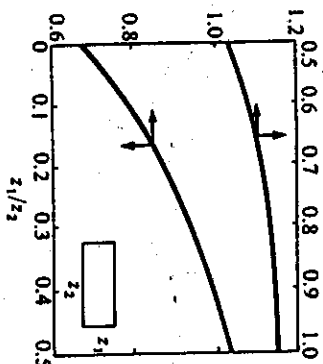


Fig. 3.3 Values of  $\phi$  for laminar flow in rectangular ducts. (From W. M. Rohsenow and H. Y. Choi, *Heat, Mass, and Momentum Transfer*, Prentice-Hall, Englewood Cliffs, New Jersey, 1961, page 63.)

### 3.3 FLOW PAST SUBMERGED BODIES

#### 3.3.1 Turbulent boundary layer on flat plate

In Chapter 2, laminar flow over a flat plate was analyzed. The force exerted by the fluid on one side of the plate (drag force  $F_K$ ) was calculated for laminar flow as

$$F_K = 0.664 \sqrt{\rho \eta L W^2 V_\infty^3}. \quad (2.104)$$

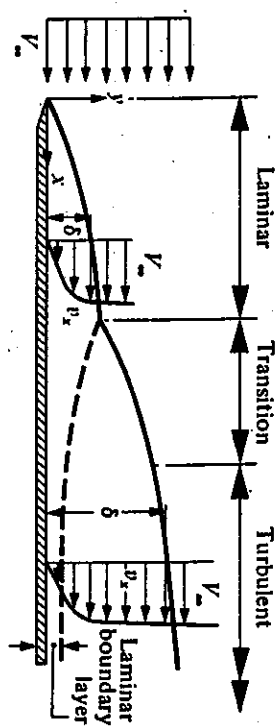


Fig. 3.4 Laminar and turbulent boundary-layers next to a flat plate (the vertical scale is greatly exaggerated).

Using the applicable differential equation, the geometric similarity argument would again indicate that the friction factor is a function of the same dimensionless group,  $\bar{R}e$ . Again, experimental data have been gathered to correlate the friction factor and the Reynolds number. The results in Fig. 3.5 show that the laminar region may extend up to a Reynolds number of about  $10^4$ . However, this condition is only achieved on smooth surfaces, and if the system is protected against minute external vibrations caused by automobiles equipped with those highly amplified sound systems with special woofers that make the silly "boom-boom" sound or by passing trucks. The results for turbulent flow can be represented as

$$f = \frac{0.455}{(\log \bar{R}e)^{1/4}}. \quad (3.25)$$

These equations are valid for a flat plate at zero incidence to the flow, providing separation does not occur.

<sup>Most texts on fluid mechanics use the term *drag coefficient*  $C_D$  rather than friction factor  $f$ , when considering flow past submerged bodies. When the form drag is entirely friction drag, an even more specific term, *skin friction coefficient*  $C_f$ , is sometimes used.</sup>

**Solution.** In this problem it is convenient to choose values of  $Re_L$  and then calculate the corresponding sets of  $F_k$  and  $V_\infty$ . The velocity of the aluminum is found by:

$$V_\infty = \frac{\eta}{L\rho} Re_L,$$

and then we can write the corresponding force exerted by the moving aluminum on both sides of the flag:

$$F_k = 2f(LW)\left(\frac{1}{2}\rho V_\infty^2\right) = fLW\rho \left[\frac{\eta^2}{L^2\rho^2} Re_L^2\right] = f \left[\frac{W}{L}\right] \left[\frac{1}{\rho}\right] (\eta Re_L).$$

For  $Re_L = 10^6$ , Fig. 3.5 gives  $f = 0.0045$ .

$$V_\infty = \frac{1.1 \times 10^{-3} \text{ N s}}{\text{m}^2} \quad | \quad 0.3 \text{ m} \quad | \quad 1 \text{ m}^3 \quad | \quad 2.5 \times 10^3 \text{ kg} \quad | \quad 10^6 \quad | \quad 1 \text{ kg m} \\ = 1.46 \text{ m s}^{-1},$$

and

$$F_k = \frac{0.0045}{0.0045} \quad | \quad 0.3 \text{ m} \quad | \quad 1 \text{ m}^3 \quad | \quad 2.5 \times 10^3 \text{ kg} \quad | \quad (1.1 \times 10^{-3})^2 \text{ N}^2 \text{ s}^2 \quad | \quad 10^{12} \quad | \quad 1 \text{ kg m} \\ = 2.18 \text{ N.}$$

In a similar manner, the corresponding values of  $V_\infty$  and  $F_k$  can be found for other values of  $Re_L$ .

$Re_L$	$f$	$V_\infty, \text{m s}^{-1}$	$F_k, \text{N}$
$10^5$	0.0072	0.146	0.035
$5 \times 10^5$	0.0051	0.73	0.62
$10^6$	0.0045	1.46	2.18
$2 \times 10^6$	0.0039	2.92	7.56
$5 \times 10^6$	0.0034	7.30	41.2

### 3.3.2 Flow past a sphere and other submerged objects

In Chapter 2, we analyzed laminar flow past a sphere, and gave the kinetic force of the fluid exerted on the sphere:

$$F_k = 6\pi\eta RV_\infty. \quad (2.119)$$

We have found that this force, often termed the *drag force*, is composed of two parts: the *friction drag* and the *form drag*. In a well-streamlined body (flow parallel to a flat plate, airplane wing, hull of a boat, etc.), the friction drag not only forms the major part of the total drag, but may even comprise it entirely. In the case of a body with sharp corners, or a sphere, or a cylinder oriented normally to flow, separation occurs, and a turbulent wake forms.

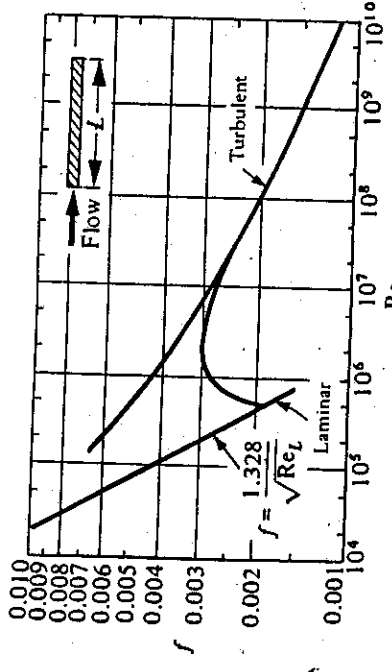
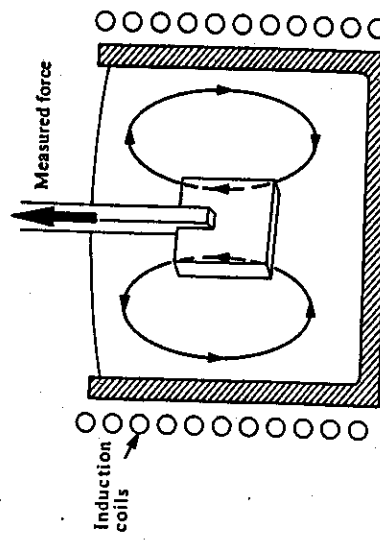


Fig. 3.5 Friction factor for flow parallel to flat plates. (From J. K. Vennard, *Elementary Fluid Mechanics*, Wiley, New York, 1954, page 344.)

**Example 3.2** In order to study the mixing action in a molten bath of aluminum contained in an induction furnace, we use a steel flag. The flag is held in a vertical position, and placed in the central part of the furnace where the metal flows upward, as depicted in the figure below.



Arrows indicate the melt's motion due to the electromagnetic forces.

If provisions are made to measure the added force exerted on the flag due to fluid motion, prepare a control chart that relates this force to the velocity of the molten aluminum in the central portion of the furnace. Assume that turbulent flow encompasses the conditions of interest.

**Data:** Viscosity of aluminum,  $1.1 \times 10^{-3} \text{ N s m}^{-2}$ , Density of aluminum,  $2.5 \times 10^3 \text{ kg m}^{-3}$ , Flag dimensions,  $0.3 \text{ m} \times 0.3 \text{ m} \times 5 \text{ mm}$  thickness.

With a plate oriented perpendicularly to flow, the separation always occurs at the same point, and the wake extends across the full projected width of the body, as shown in Fig. 3.6; this results in almost all form drag comprising the drag force. If the body has curved sides, the location of the separation point is determined according to whether the leading boundary layer is laminar or turbulent, as depicted in Fig. 3.7. In turn, this location determines the size of the wake and the amount of the form drag. After this brief introduction, let us now consider some of the available data.

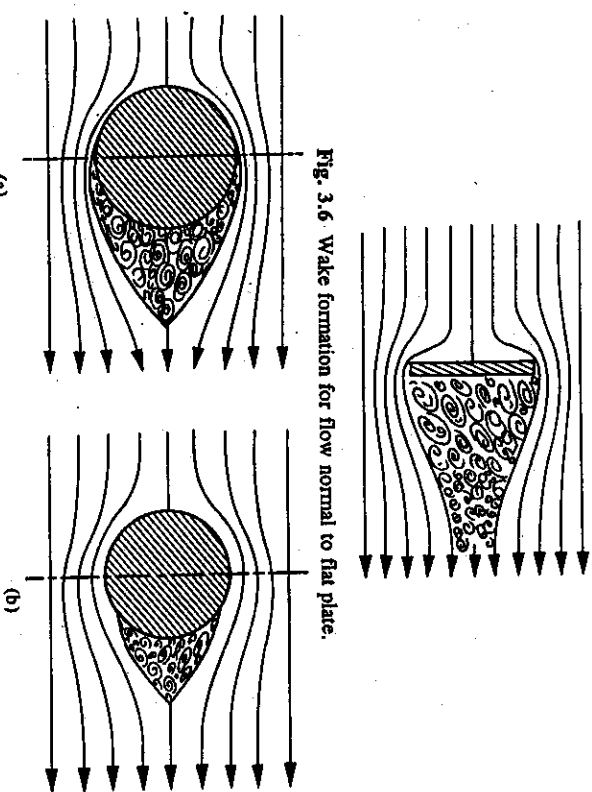


Fig. 3.6. Wake formation for flow normal to flat plate.

Fig. 3.7 Separation of boundary layer and wake formation with a cylinder or sphere immersed in a flowing fluid when (a) the leading boundary layer is laminar, and (b) the leading boundary layer is turbulent.

For the presentation of data, we use Eq. (3.4). As we come across the friction factor again, let us repeat the expression

$$F_K = fAK; \quad (3.4)$$

$K$  still remains  $\frac{1}{2}\rho V_\infty^2$ , but for shapes such as spheres, cylinders, ellipsoids, etc., we choose the area  $A$  as the projected area normal to the flow. For example, for flow past a sphere,  $F_K$  takes the form

$$F_K = (\pi R^2) \left( \frac{1}{2} \rho V_\infty^2 \right) f. \quad (3.26)$$

From Stokes' law, which is the result of an analytical solution for creeping flow around a sphere, we can write the following equation by rearranging Eq. (2.119):

$$F_K = (\pi R^2) \left[ \frac{24}{DV_\infty/\nu} \right]. \quad (3.27)$$

By comparing Eqs. (3.26) and (3.27), we obtain the friction factor (drag coefficient) for laminar flow past a sphere:

$$f = \frac{24}{Re}. \quad (3.28)$$

Once again, the friction factor is a function of the Reynolds number. This is also true for turbulent flow but, as you may suspect, Eq. (3.28) does not apply for all velocities, and experimental correlation is sought in the form of  $f = f(Re)$ . Figure 3.8 shows such a correlation for spheres, as well as for some other geometrical shapes. We also include Fig. 3.9 to indicate other possibilities. Note that Stokes' law applies up to  $Re \approx 1$  for spheres.

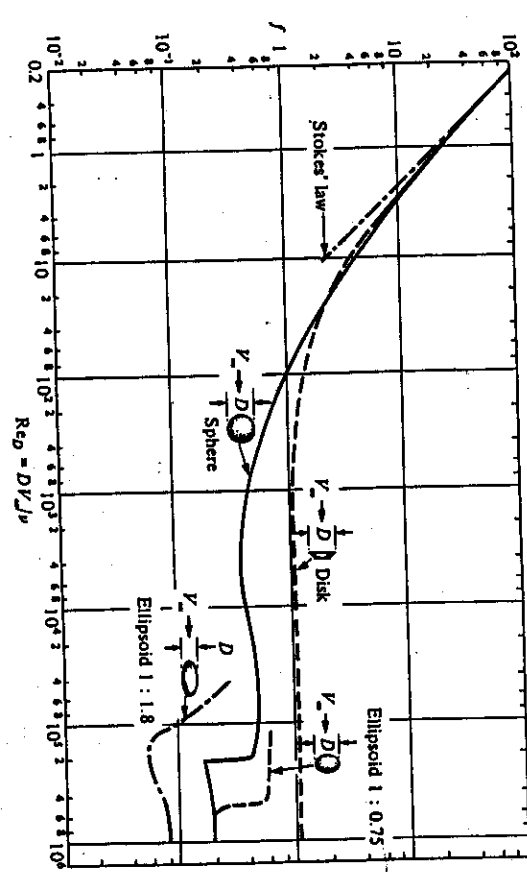


Fig. 3.8 Friction factors for submerged bodies. (Adapted from F. Eissner, Proc. 3rd Intern. Congr. Appl. Mech., 1930, page 32.)

The phenomenon of boundary-layer separation has a major effect on the form drag. This effect is noticeable at large  $Re$  where the form drag comprises most of the total drag. At this high  $Re$ , the transition to turbulent flow occurs before separation, and the separation point is moved farther downstream, as illustrated in Fig. 3.7, thereby reducing the friction factor.

In materials processing, the discussed principles of flow past submerged bodies mostly apply to situations in which the body moves in a fluid. The friction factors are determined experimentally, and it makes no difference whether the body moves in a still fluid or is held stationary while the fluid flows past it. However, when the body is irregularly shaped, friction factors which are measured while the body is stationary may not be applicable when the body moves, because during free motion the orientation of the body may change rapidly and repeatedly.

It is often desirable to separate particulate mixtures of solids. These mixtures may consist of particles of the same material which have different sizes (homogeneous mixtures), or they may consist of particles of different materials and various sizes (heterogeneous mixtures).

**Solution.** To obtain the solution, recognize that particles which have terminal velocities equal to the upward air velocities are those which remain suspended. Further, examine the criterion that Stokes' law applies for  $Re_D < 1$  and that a simple expression for the diameter may be appropriate.

For air at 300 K, the fluid properties are  $\eta = 1.80 \times 10^{-5} \text{ kg m}^{-1} \text{s}^{-1}$  and  $\rho = 1.18 \text{ kg m}^{-3}$ . The largest particle that can be supported by the flow of air can be determined with the aid of a force balance. For upward flowing air:

$$F_k + \frac{4}{3}\pi R^3 \rho g = \frac{4}{3}\pi R^3 \eta g,$$

with  $\rho$  = density of the air and  $\rho_s$  = density of the solid. We substitute Eq. (3.26) for  $F_k$  and solve for  $V_\infty$ ; the result is

$$V_\infty = \left[ \frac{8Rg(\rho_s - \rho)}{3f\rho} \right]^{1/2}.$$

Therefore, we determine  $V_\infty$  by trial and error as a function of  $R$ , because  $f$  depends upon  $V_\infty$  and  $R$  through the Reynolds number.

We can start with the smallest particles,  $D = 2R = 10^{-5} \text{ m}$ , and assume that Stokes' law applies; therefore

$$f = \frac{24\eta}{DV_s \rho} = \frac{12\eta}{RV_s \rho},$$

and

$$V_\infty = \frac{2R^2(\rho_s - \rho)g}{9\eta}.$$

Notice that this is just a rearrangement of Eq. (2.121).

$$V_\infty = \frac{(2)(0.5 \times 10^{-5})^2(4000)(9.8)}{(9)(1.80 \times 10^{-5})} = 1.21 \times 10^{-2} \text{ m s}^{-1}.$$

The corresponding value of  $Re_D$  is

$$Re_D = \frac{DV_\infty \rho}{\eta} = \frac{(10^{-5})(1.21 \times 10^{-2})(1.18)}{(1.80 \times 10^{-5})} \approx 0.008,$$

so that Stokes' law applies, at least for the smallest particles. Similar calculations can be repeated for all particles with diameters up to 50  $\mu\text{m}$ ; Stokes' law is not valid for larger particles.

For larger particles, a trial and error method is used. Starting with  $R = 7 \times 10^{-5} \text{ m}$ , and the first approximation for  $V_\infty$  as 1  $\text{m s}^{-1}$ , we get  $Re_D = 9.2$ . From Fig. 3.8,  $f \approx 4.5$  and we calculate  $V_\infty$

$$V_\infty = \left[ \frac{(8)(7 \times 10^{-5})(9.8)(4000)}{(3)(4.5)(1.18)} \right]^{1/2} = 1.17 \text{ m s}^{-1}.$$

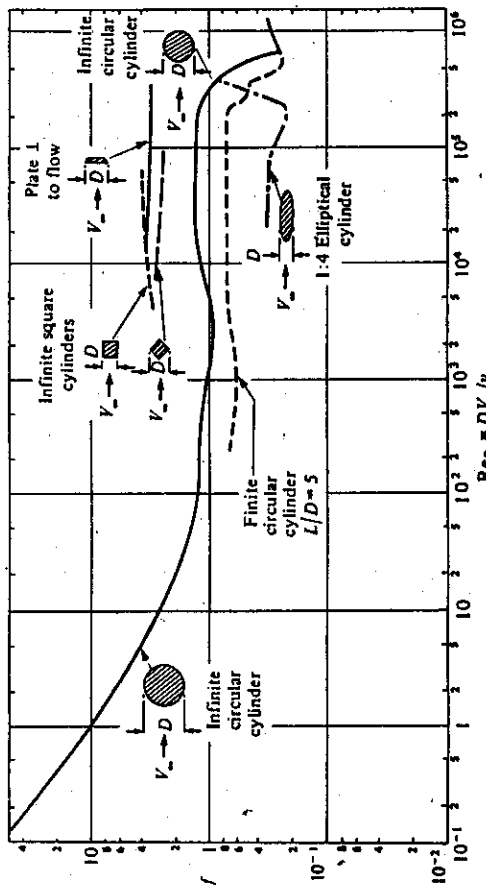
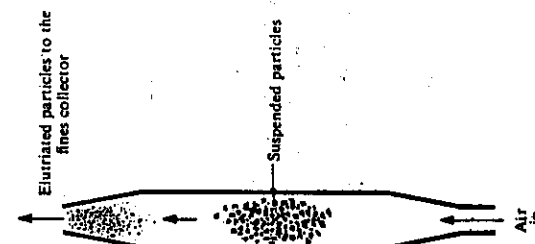


Fig. 3.9 Friction factors for submerged bodies. (Adapted from F. Eisner, Proc. 3rd Intern. Congr. Appl. Mech., 1930, page 32.)

Homogeneous mixtures can be separated by screening, but for separating mixtures of fine sizes, free settling or centrifugal methods are preferred. In general, screening does not work for heterogeneous mixtures, and therefore separation is gained by free settling or centrifugal methods.

**Example 3.3** With either metallic or ceramic powders, it is important to separate homogeneous mixtures in the range of particle sizes from 10 to 250  $\mu\text{m}$ . For this purpose we apply the principle of air elutriation, which is illustrated by the device shown to the right. The force exerted by the air stream is great enough to suspend particles of a given diameter, and all particles of smaller diameter are carried upward and to the collector of fines. Larger particles fall back against the air stream and down into a settling chamber. For the effective operation of this device it is necessary to know the size of particles suspended at a given flow rate.

Assuming that a spherical particle, with a density of  $4000 \text{ kg m}^{-3}$ , applies to a homogeneous mixture of iron powder, draw a graph that relates the diameter of suspended particles to the velocity of the air in the expanded portion of the tube.



We see that a second approximation, at least, is needed. With  $V_\infty = 1.35 \text{ m s}^{-1}$ ,  $Re_b = 12.4$  and  $f = 3.5$ . Another recalculation for  $V_\infty$  yields

$$V_\infty = (1.17) \left[ \frac{4.5}{3.5} \right]^{1/2} = 1.33 \text{ m s}^{-1}$$

which is very close to our assumed velocity of  $1.35 \text{ m s}^{-1}$ . The procedure is repeated for particle diameters up to  $250 \mu\text{m}$ . The results are tabulated below.

Particle diameter, $\mu\text{m}$	Velocity, $\text{m s}^{-1}$
10	0.012
20	0.048
40	0.19
70	0.62
140	1.33
200	2.05
250	2.65

where  $Q$  = volume flow rate,  $\text{m}^3 \text{s}^{-1}$ ,  $A$  = cross-sectional area,  $\text{m}^2$ , and  $k_p$  = permeability coefficient, a constant that depends on the fluid, temperature, and packing characteristics with units of  $\text{m}^4 \text{N}^{-1} \text{s}^{-1}$ . Equation (3.29), which is known as Darcy's law, is based on the experiments of Darcy in the middle of the nineteenth century.<sup>1</sup>

The  $k_p$  in Eq. (3.29) is sometimes called the *permeability*, which is satisfactory provided we carry out the test with the same fluid at the same temperature, but it is more common and better to define a *specific permeability*  $\mathcal{P}$  by means of

$$k_p = \frac{\mathcal{P}}{\eta}, \quad (3.30)$$

where  $\eta$  is the viscosity of the fluid. This makes  $\mathcal{P}$  specific to the geometry of the solid phase only; therefore we can make predictions of the flows of other fluids, regardless of temperature. Actually  $\mathcal{P}$  is almost always used, rather than  $k_p$ , and it is commonly called the permeability instead of the specific permeability.

The units of permeability are  $\text{m}^2$ , but some of the older data are in the unit called *Darcy*, defined as

$$1 \text{ Darcy} = 1 \times 10^{-12} \text{ m}^2.$$

Unfortunately the reader might even encounter a different Darcy in the British Standard Specification (BSS), which is

$$1 \text{ Darcy (BSS)} = 0.987 \times 10^{-12} \text{ m}^2.$$

Granular solids or agglomerates of fine particles occur in many materials processing systems, ranging from sinter plants for agglomerating iron ores to the production of intricate parts via alloy powders or ceramic powders. In solidifying castings, there are regions in which solid and liquid coexist, and at least for a significant fraction of the solidification period the intermingled liquid (i.e., the interdendritic liquid) can convect through the stationary solid network (i.e., the dendritic solid). Convection of this type is a major cause of macrosegregation in cast products. Other applications in materials processing include the production of metal matrix composites by infiltration of alloy melts through ceramic fiber preforms and the use of reticulated ceramic foams as filter media for the refinement of molten metal.

The flow of fluids through porous media is not simple, especially because of the effect of the complex geometry of the solids on the flow. Therefore, we rely largely on empirical measurements of a system parameter, known as the *permeability*, or on measurements of friction factors.

### 3.4.1 Darcy's Law

If the flow occurs under low pressure gradients, that is it is slow enough, then the rate of flow is proportional to a pressure drop per unit length of the porous medium,  $\Delta P'/L'$ :

$$Q = \frac{k_p A \Delta P'}{L'}, \quad (3.29)$$

If the flow is not unidirectional, then the superficial velocity has components  $v_x$ ,  $v_y$ , and  $v_z$ , the pressure gradient has components  $\partial P/\partial x$ ,  $\partial P/\partial y$  and  $\partial P/\partial z$ , and the body force has components  $\rho g_x$ ,  $\rho g_y$ , and  $\rho g_z$ . With vector notation, therefore,

$$\mathbf{v} = -\frac{\mathcal{P}}{\eta} (\nabla P - \rho \mathbf{g}). \quad (3.32)$$

Example 3.4 An important characteristic of foundry molding sands is the allowance for the permeation of gases. Accordingly, the permeability of molding sands is routinely measured for process quality control purposes. Calculate the permeability of a sample of molding sand, 30 mm dia. by 60 mm length, through which  $10^{-3} \text{ m}^3$  of air flows in 15 s under a pressure drop of  $600 \text{ N m}^2$ .

<sup>1</sup>The original paper by Darcy is not readily available, but a reproduction is in M. K. Hubbert, *The Theory of Ground-Water Motion and Related Papers*, Hefner Publishing, New York, NY, 1969, pp. 303-311.

### 3.4.2 Tube-bundle theory and Ergun's equation

Darcy's law is an empirically observed law. However, a semitheoretical approach to the unidirectional flow through a sample is available. The problem yields Darcy's law with more insight into the effect of the packing on  $P$ . The theory, which is known as the *tube-bundle theory*, regards the porous medium as a bundle of tangled tubes with weird cross-sections. It is assumed that the packing is uniform without isolated porosity, that there is no *channeling* of flow, and that the diameter of the column is much greater than that of the particles. To start with, we look to the Hagen-Poiseuille formula for laminar flow in Chapter 2 (Eq. 2.33). By analogy, we say that

$$\bar{V} = K_1 \frac{\Delta P R_h^2}{L\eta}, \quad (3.33)$$

This is integrated with  $\rho$  constant,  $P = P_0$  at  $x = 0$  and  $P = P_L$  at  $x = L$ . The result is

$$v_x = \frac{P}{\eta} \left[ \frac{P_0 - P_L}{L} - \rho g \right].$$

The minus sign results because the flow is antiparallel to gravity; if it is parallel then  $+P_0$  appears. Recall our goal is to calculate  $P$ , so let's gather all of the terms:

$$v_x = \frac{Q}{A} = \frac{(4)(10^{-3}) \text{ m}^3}{(\pi)(0.03)^2 \text{ m}^2} \left| \frac{1}{15 \text{ s}} \right. = 9.43 \times 10^{-2} \text{ m s}^{-1}$$

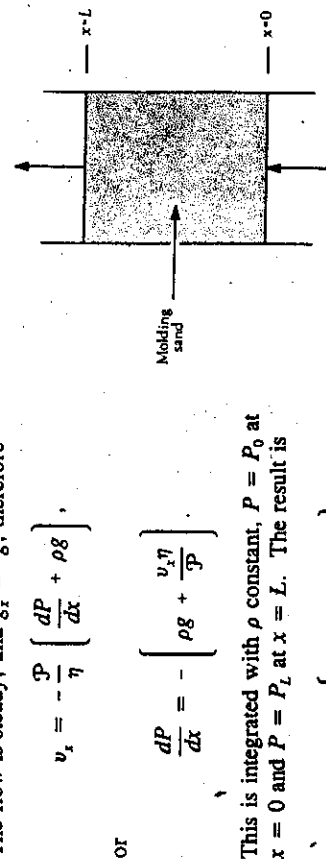
$$\rho g = \frac{1.223 \text{ kg}}{\text{m}^3} \left| \frac{9.8 \text{ m}}{\text{s}^2} \right. = 12 \text{ kg m}^{-2} \text{ s}^{-2}$$

$$\eta = 1.90 \times 10^{-5} \text{ N s m}^{-2} = 1.90 \times 10^{-5} \text{ kg m}^{-1} \text{ s}^{-1}$$

Therefore,

$$\begin{aligned} P &= \frac{\eta v_x}{\left[ \frac{P_0 - P_L}{L} - \rho g \right]} = \frac{1.90 \times 10^{-5} \text{ kg}}{\text{m s}} \left| \frac{9.43 \times 10^{-2} \text{ m}}{\text{s}} \right| \frac{\text{m}^2 \text{s}^2}{10^8 \text{ kg}} \\ &= 17.9 \times 10^{-11} \text{ m}^2. \end{aligned}$$

This permeability is considered to be high for molding sands; a typical value would be  $2 \times 10^{-11}$  to  $4 \times 10^{-11} \text{ m}^2$ .



where  $K_1$  = constant of proportionality, and  $\bar{V}$  = average velocity in the interstices of the porous medium. If flow is unidirectional and in the  $x$ -direction, then let  $V_0 = v_x$ , the superficial velocity.

Engineers usually know  $V_0$  rather than  $\bar{V}$ ; it is defined by

$$V_0 = Q/A,$$

where  $A$  is the cross-sectional area of the column and  $Q$  is the volume flow rate. Since,

$$V_0 = \bar{V}\omega, \quad (3.34)$$

then

$$V_0 = K_1 \frac{\Delta P R_h^2 \omega}{L\eta}. \quad (3.35)$$

where  $\omega$  = void fraction (also called voidage or porosity). The concept of the *hydraulic radius*  $R_h$  was introduced with the equivalent diameter (Eq. 3.21).

For porous media,  $R_h$  is defined as

$$R_h = \frac{\text{average cross section available for flow}}{\text{average wetted perimeter}} = \frac{A_t}{P_w}. \quad (3.36)$$

By the average wetted perimeter, we mean the average total boundary line between the fluid and the packing, viewed by a slice through the column normal to the axis of the column. Thus, in a column of length  $L$ ,

$$R_h = \frac{\text{volume available for flow}}{\text{total wetted perimeter}} = \frac{A_h L}{P_w L}. \quad (3.37)$$

Here  $A_h L$  is also the volume of fluid in the packing, and if both the numerator and denominator of Eq. (3.37) are normalized by the column volume, we obtain

$$R_h = \frac{A_h L/V}{P_w L/V} = \frac{\omega}{S}, \quad (3.38)$$

where  $S = S_0(1 - \omega)$ .

The factor  $S_0$  is the total surface area of solid per unit volume of solid, while  $S$  is the total surface area per unit volume of the column. From this,

$$R_h = \frac{\omega}{S_0(1 - \omega)} \quad (3.39)$$

We may substitute Eq. (3.39) into Eq. (3.35) and obtain

$$V_0 = K_1 \frac{\Delta P'}{L \eta S_0^2} \frac{\omega^3}{(1 - \omega)^2} \quad (3.40)$$

Equation (3.40), which is the form of the pressure-drop relationship for flow through packed columns, is valid for the lower range of Reynolds numbers (creeping flow region), where  $K_1^{-1}$  has been found to equal 4.2.<sup>2</sup> Insertion of this value into Eq. (3.40) gives

$$V_0 = \frac{1}{4.2} \frac{\Delta P'}{L \eta S_0^2} \frac{\omega^3}{(1 - \omega)^2}, \quad (3.41)$$

which is the *Blake-Kozemey* equation. Note that this is the same as the Darcy equation, where

$$k_D = \frac{\omega^3}{4.2 \eta S_0^2 (1 - \omega)^2}, \quad (3.42)$$

or

$$\mathcal{P} = \frac{\omega^3}{4.2 S_0^2 (1 - \omega)^2}. \quad (3.43)$$

These equations emphasize the fact that  $k_D$  depends on the properties of both the fluid and solid, while  $\mathcal{P}$  depends only on the properties of the solid phase.

According to the flow behavior in all forced convection systems, a fluid velocity is eventually reached beyond which laminar flow no longer prevails. Under these conditions, we again resort to the use of a friction factor which can be correlated solely as a function of a Reynolds number. For packed beds, the modified friction factor may be measured by

$$f_t = \frac{\Delta P' \omega^3}{LS_0 \rho V_0^2 (1 - \omega)}. \quad (3.44)$$

This is analogous to Eq. (3.17). We utilize a modified Reynolds number for packed beds in the correlation

$$Re_c = \frac{\rho V_0}{\eta (1 - \omega) S_0}. \quad (3.45)$$

<sup>2</sup>S. Ergun, *Chem. Eng. Prog.* **48**, 93 (1952). The constant 4.2 is not universally selected; some believe the value to be as high as 5.0, based on a paper by P. C. Carman, *Trans. Inst. Chem. Eng.* **15**, 150 (1937). These are reasonable values for granular materials and spherical particles but are certainly not valid for other solid morphologies or for higher values of  $\omega$ . For example, these factors are substantially different for packings that comprise fibers or even for uniform size spheres that are not consolidated.

When the flow exceeds that for  $Re_c \approx 2$ , then Eq. (3.41) no longer applies and we use Fig. 3.10. The equation

$$\frac{\Delta P}{L} = \frac{4.2 n V_0^2 S_0^2 (1 - \omega)^2}{\omega^3} + \frac{0.292 \rho V_0^2 S_0 (1 - \omega)}{\omega^3} \quad (3.46)$$

describes the entire curve analytically; the second term on the right describes the pressure drop under highly turbulent flow conditions. In dimensionless groups,

$$f_t = \frac{4.2}{Re_c} + 0.292. \quad (3.47)$$

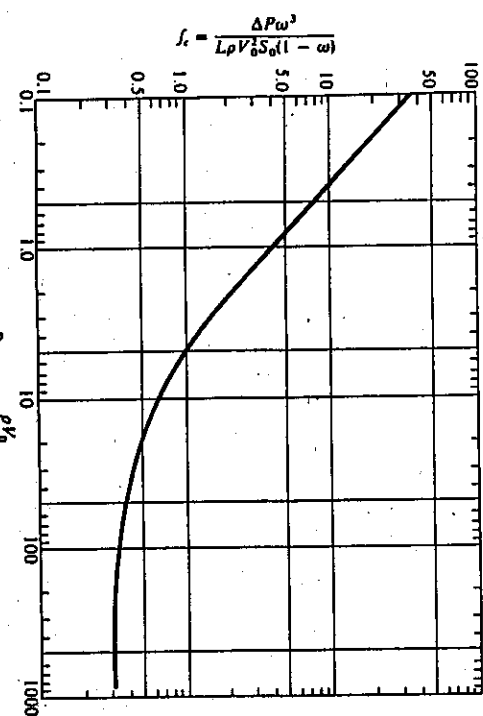


FIG. 3.10 Pressure-drop correlation for flow through packed beds. (Based on S. Ergun, *Chem. Eng. Prog.* **48**, 93 (1952).)

When applying this expression to gases, we take the density of the gas as the arithmetic average of the end densities. For large pressure drops, however, it is better to apply Eq. (3.46), to express pressure gradient in the differential form, and to integrate over the bed thickness, taking into account the variations in density, viscosity, and superficial velocity.

Thus far, we have defined the modified Reynolds number and friction factor in terms of  $S_0$ , the particle surface area per unit particle volume. If the particles in the bed are spheres of uniform size,  $S_0$  may be easily related to the diameter,  $D_p$ , by

$$S_0 = \frac{\pi D_p^2}{(\pi D_p^3/6)} = \frac{6}{D_p}. \quad (3.48)$$

Then Eq. (3.46) becomes

$$\frac{\Delta P}{L} = \frac{150n V_0^2 (1 - \omega)^2}{D_p^2 \omega^3} + \frac{1.75 \rho V_0^2 (1 - \omega)}{D_p \omega^3}, \quad (3.49)$$

which is known as *Ergun's equation*. It is then useful to define a new friction factor which is often associated with Ergun's work:

$$f_E = 6f_c = \frac{D_p \Delta P \omega^3}{L \rho V_0^2 (1 - \omega)}. \quad (3.50)$$

and a new Reynolds number

$$Re_E = 6 RE_c = \frac{D_p \rho V_0}{\eta(1 - \omega)}. \quad (3.51)$$

Now, in dimensionless form, Eq. (3.49) becomes

$$f_E = \frac{150}{Re_E} + 1.75. \quad (3.52)$$

When a bed contains a mixture of different-size particles, the question arises as to what should be used for  $D_p$  in Eqs. (3.49)-(3.51). To this day, the question is still unanswered, but a suggestion commonly put forward (although not adequately tested) is to use the *volume-surface mean diameter*,  $\bar{D}_{vs}$ . This parameter is discussed in the following paragraph.

For a bed containing a mixture of different-size spherical particles,  $S_0$  may be determined from the specific surface of the mixture,  $S_w$  (surface area per mass of particles). If the material is screened, and the diameter of each size fraction,  $D_{r_i}$ , is taken as the arithmetic mean of the openings of the two screens defining the corresponding mass fraction,  $\Delta\phi_i$ , collected between them, then

$$S_w = \frac{6}{\rho_p} \sum_{i=1}^n \frac{\Delta\phi_i}{\bar{D}_{r_i}}, \quad (3.53)$$

where  $n$  is the number of screens used, and  $\rho_p$  is the density of the particulate material. The average particle diameter for this mixture is called the *volume-surface mean diameter*, defined as

$$\bar{D}_{vs} = \frac{6}{S_w \rho_p}. \quad (3.54)$$

Noting that  $S_0 = S_w \rho_p$ , then

$$S_0 = \frac{6}{\bar{D}_{vs}}, \quad (3.55)$$

and, by comparing Eq. (3.55) with Eq. (3.48), the proper value of  $D_p$  to use is  $\bar{D}_{vs}$ .

Finally, the situation arises that we have a bed of nonspherical particles. In this case, we define a shape factor  $\lambda$ , which does not depend on particle size and which is a function of the shape of the particles only, by:

$$S_0 = \frac{6\lambda}{D_p}. \quad (3.56)$$

Table 3.2 Shape factors for screened particles

Substance	Type of measurement	Shape factor, $\lambda$
Sand (jagged)	Permeability	1.68 <sup>1</sup>
Sand (nearly spherical)	Permeability	1.15 <sup>1</sup>
Sand (angular)	Permeability	1.49 <sup>1</sup>
Sand (flakes)	Permeability	2.54 <sup>1</sup>
Sand (rounded)	Metallographic	1.24 <sup>1</sup>
Crushed glass (jagged)	Metallographic	1.54 <sup>1</sup>
Coal (pulverized)	Metallographic	1.37 <sup>1</sup>
Coal dust (up to 10 mm)	Metallographic	1.54 <sup>1</sup>
Tungsten powder	Metallographic	1.12 <sup>1</sup>
Cu hot	Settling techniques	1.00 <sup>2</sup>
Sand	Settling techniques	1.59 <sup>2</sup>
Coal	Settling techniques	1.72 <sup>2</sup>
Silimanite	Settling techniques	1.72 <sup>2</sup>
Limestone	Settling techniques	2.20 <sup>2</sup>
Flake graphite	Settling techniques	7.96 <sup>2</sup>
Crushed and screened ores		1.75 <sup>3</sup>

<sup>1</sup>Values calculated from data presented by P. C. Carman, *Trans. Inst. Chem. Eng.* 15, 155 (1937).

<sup>2</sup>Derived from data in F. A. Zenz and D. F. Othmer, *Fluidization and Fluid Particle Systems*, Reinhold, New York, 1960, pages 184, 213.

<sup>3</sup>Typical value suggested by A. M. Gaudin, *Principles of Mineral Dressing*, McGraw-Hill, New York, 1939, page 132.

Now, replace  $D_p$  in Eq. (3.49) by  $D_p/\lambda$  or  $\bar{D}_{vs}/\lambda$ , and other forms of Ergun's equation evolve:

#### Uniform size particles

$$\frac{\Delta P}{L} = \frac{150\eta V_0^2 \lambda^2}{D_p^2} \frac{(1 - \omega)^2}{\omega^3} + \frac{1.75\rho V_0^2 \lambda}{D_p} \frac{(1 - \omega)}{\omega^3}. \quad (3.57a)$$

#### Nonuniform size particles

$$\frac{\Delta P}{L} = \frac{150\eta V_0^2 \lambda^2}{\bar{D}_{vs}^2} \frac{(1 - \omega)^2}{\omega^3} + \frac{1.75\rho V_0^2 \lambda}{\bar{D}_{vs}} \frac{(1 - \omega)}{\omega^3}. \quad (3.57b)$$

<sup>1</sup>We alert the reader that there are other shape factors used in particle technology. Another often used one is defined as the surface area divided by the surface area of a sphere with the same volume.

We should caution the reader that the literature in this field abounds with confusion concerning the definition of  $D_p$  for nonspherical particles, and the shape factor  $\lambda$ . In general, values of  $\lambda$  are very difficult to obtain, and therefore pressure drop equations utilizing  $D_p$ , such as Eq. (3.49), are not of much use unless the particles are spherical. It is usually more satisfactory to use Eq. (3.46), determining  $S_0$  by means of permeability tests and Eq. (3.43).

**Example 3.5** Sintering of iron ore is an important metallurgical process in which gases must penetrate through a bed of solids. In this process, loosely packed fine particles of ore are sintered into larger particles by passing air through the bed, which in turn reacts with admixed coal to develop very high temperatures in the sinter. It is necessary that large amounts of air can pass through the bed without creating large pressure drops, which would require unduly large fans.

Calculate the pressure drop, prior to ignition, across a bed of sinter 0.305 m deep ( $\omega = 0.39$ ) for air flowing at 289 K and with  $V_0 = 0.25 \text{ m s}^{-1}$ . The surface area  $S$  measures  $8100 \text{ m}^2$ . For air:  $\rho = 1.23 \text{ kg m}^{-3}$  and  $\eta = 1.78 \times 10^{-5} \text{ N s m}^{-2}$ .

*Solution.*

$$\text{Re}_c = \frac{\rho V_0}{\eta S} = \frac{(1.23)(0.25)}{(1.78 \times 10^{-5})(8100)} = 2.13.$$

Using Eq. (3.46), we get

$$\frac{\Delta P}{L} = \frac{\rho V_0^2 S}{\omega^3} \left[ \frac{4.2}{\text{Re}_c} + 0.292 \right] = 2.38 \times 10^4 \text{ N m}^{-3}.$$

$$\Delta P = (2.38 \times 10^4)(0.305) = 7.25 \times 10^3 \text{ N m}^{-2}.$$

### 3.4.3 Wall effect

It is probably obvious to the reader that the container diameter must be a good deal larger than the mean particle diameter of the packing, in order for the above equations to be valid, since the void fraction at the wall will be larger than the bulk value of  $\omega$ . This *wall effect* is demonstrated in Fig. 3.11, which shows that the container diameter should be approximately 20 times the particle diameter in order for Eq. (3.46) to predict the pressure drop to within 10% for  $\text{Re}_c$  between 2 and 150. If necessary, we may first compute the pressure drop using Eq. (3.46), and then use Fig. 3.11 for correction.

### 3.4.4 Applications

With Examples 3.4 and 3.5, we pointed out the application of relationships for flow through porous media to the testing and control of permeability in foundry molding sand and in estimating pressure drop requirements for flow in a sinter bed of iron ore.

In powder metallurgy, the permeability of a sintered metal compact is of importance because it is a measure of the relationship between processing variables and the pore structure developed during sintering, and because, in some instances, the flow of a fluid through a

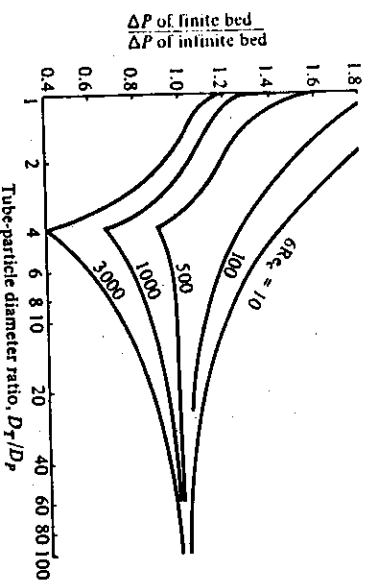


Fig. 3.11 Correction factor for wall effect. (Derived by H. E. Rose and A. M. Rizk, Proc. Inst. Mech. Engrs., London, 60, 493 (1950).)

porous sintered metal part is important. Self-lubricating bearings and porous metal filters for air, water, etc., can serve as examples.

Morgan<sup>3</sup> used the following form of the Ergun equation for steady flow conditions through porous sintered metal:

$$\frac{\Delta P}{L} = \frac{\eta V_0}{\phi} + \frac{\rho V_0^2}{\Phi}, \quad (3.58)$$

where  $\phi$  is called the viscous permeability, and  $\Phi$  the inertial permeability;  $V_0$ ,  $\eta$ , and  $\rho$  are defined as before. We should compare this equation with Eq. (3.46), from which it appears that

$$\phi = \frac{\omega^3}{4.2 S_0 (1 - \omega)^2} = \mathcal{P} \quad \text{and} \quad \Phi = \frac{\omega^3}{0.292 S_0 (1 - \omega)}.$$

Now, at low values of  $\omega$ ,  $S_0$  is the surface area seen by the fluid, and there may be internal porosity which is not connected to any flow channels, and which contributes to the  $\omega$  determined *in situ*. Because the total  $\omega$  is then too large,  $S_0$  measured in this manner will be larger than the true value of  $S_0$ . The  $\omega$  used when the isolated pore volume becomes significant should only be the interconnected void volume fraction. Another complication in the use of the above relationships to estimate  $\phi$  and  $\Phi$  is the use of the constants 4.2 and 0.292, which are only valid for granular type packings with  $0.3 < \omega < 0.6$ . For a variety of particle sizes of partially sintered metal powders, German<sup>4</sup> gives empirical results as

$$\phi = 4.6 \times 10^{-11} \bar{D}_{\alpha}^{0.73} \omega^{6.3}, \quad (3.59)$$

<sup>3</sup>V. T. Morgan, *Symposium sur la Metallurgie des Poudres*, Editions Métaux (sponsored by Société Française de Métallurgie), Paris, June, 1964, page 419.

<sup>4</sup>R. M. German, *Powder Technol.* 30, 81 (1981).

This can be rearranged and put into the exact form of Eq. (3.31). Hence, Darcy's law is certainly adequate when  $\omega$  is small enough. On the other hand, when  $\omega \rightarrow 1$ ,  $P \rightarrow \infty$  and Eq. (3.61) reduces to the  $x$ -component of the Navier-Stokes' equation (see Eq. (D)) in Table 2.2), as it should.

Permeability data for flow through dendritic networks are presented in Poirier.<sup>8</sup> Darcy's law has also been applied to study the infiltration of metal through both particulates<sup>9</sup> and fiber preforms for the production of metal matrix composites.<sup>10</sup> In the latter, the authors gave two useful relationships of permeability for flow through fibrous preforms. In both it is assumed that the fibers are continuous, with parallel axes located on a square grid. The first is

$$\Phi = 3.9 \times 10^{-6} \bar{D}_{vs}^{0.92} \omega^{6.4} \quad (3.60)$$

Equations (3.59) and (3.60) require that the unit of  $\bar{D}_{vs}$  is  $\mu\text{m}$ , with  $59 \leq \bar{D}_{vs} \leq 715 \mu\text{m}$  (measured before sintering) and  $0.25 \leq \omega \leq 0.56$ .

As mentioned above the compressibility of a gas, with flow accompanied by a large pressure drop, should be taken into account. That effect and also the effect of a large mean free path of the gas relative to the pore size can be included with the equations given here. German<sup>11</sup> has presented an excellent exposition of flow of gases through porous materials that includes these added factors.

During the solidification of dendritic alloys, there is a  *mushy zone* comprising dendritic solid and interdendritic liquid. In general the liquid convects, and it is desirable to analyze this convection because it is a major cause of macrosegregation in cast products. The analysis is very complex with one complexity being the fact that  $\omega$  (the volume fraction of liquid) varies spatially and temporally as solidification proceeds.

Because  $\omega \rightarrow 1$  in some parts of the mushy zone, Darcy's law by itself is not a sufficient representation of the momentum equation. Ganesan and Poirier<sup>12</sup> derived the momentum equation and then Nandapurkar et al.<sup>13</sup> used it to analyze convection during solidification.

For illustrative purposes, we give only the  $x$ -component of the momentum equation for the mushy zone with a fixed solid and convecting liquid:

$$\begin{aligned} \omega \frac{\partial(v_x/\omega)}{\partial t} + \frac{1}{\omega} \left[ v_x \frac{\partial v_x}{\partial x} + v_y \frac{\partial v_x}{\partial y} + v_z \frac{\partial v_x}{\partial z} \right] \\ + v_x \left[ v_x \frac{\partial}{\partial x} (1/\omega) + v_y \frac{\partial}{\partial y} (1/\omega) + v_z \frac{\partial}{\partial z} (1/\omega) \right] = +\omega g_x \\ - \frac{\omega}{\rho} \frac{\partial P}{\partial x} + v \left[ \frac{\partial^2 v_x}{\partial x^2} + \frac{\partial^2 v_x}{\partial y^2} + \frac{\partial^2 v_x}{\partial z^2} \right] - \frac{\nu \omega}{P} v_x, \quad (3.61) \end{aligned}$$

where  $v_x$ ,  $v_y$  and  $v_z$  are the components of the superficial velocity. The last term on the right-hand-side of Eq. (3.61) is the Darcy term. The reader can deduce the  $y$ - and  $z$ -components of the momentum equation.

The utility of Eq. (3.61) is that it allows for a transition in the convection in the interior of the mushy zone to the region where there is only liquid remaining in the solidifying mass ( $\omega = 1$ ). In the interior of the mushy zone where  $\omega < 0.6$ , the Darcy term dominates to the extent that it, along with the body force term and the pressure gradient term, comprise the momentum equation; therefore

$$0 = +\omega g_x - \frac{\omega}{\rho} \frac{\partial P}{\partial x} - \frac{\nu \omega}{P} v_x.$$

For an up-draft packed column, an upper limit exists for the fluid flow rate. Let us consider what happens if the flow rate through a static bed steadily increases. The pressure drop across the bed increases steadily with increasing flow rate until, at a certain point, the bed expands slightly, and the individual particles become supported in the fluid stream with freedom to move relative to each other. At this point, the bed is no longer static, and is said to be *fluidized*. The void fraction at this point,  $\omega_{mf}$ , corresponds to the loosest possible packing of the material in a fixed-bed configuration, and this is usually greater than the initial fixed-bed voidage, so that some internal rearrangement of the bed takes place prior to the onset of fluidization, as shown in Fig. 3.12. With increasing velocity, the bed expands, or  $\omega$  increases. If this expansion is uniform, with the interparticle spacing increasing uniformly, then we speak of *particulate fluidization*. Bed expansion continues until the velocity required to balance or support a single particle acting alone is reached, which is the terminal or free-

<sup>8</sup>R. M. German, *Int. J. Powd. Metall. Tech.* **15**, 23 (1979).

<sup>9</sup>S. Ganesan and D. R. Poirier, *Mettal. Trans. B* **21B**, 173 (1990).

<sup>10</sup>J. Nandapurkar, D. R. Poirier and J. C. Heinrich, *Numerical Heat Transfer, Part A* **19**, 101 (1991).

<sup>11</sup>G. W. Jackson and D. F. James, *Can. J. Chem. Eng.* **64**, 364 (1986).

<sup>12</sup>D. R. Poirier, *Mettal. Trans. B* **18B**, 245 (1987).

<sup>13</sup>P. B. Maxwell, G. P. Martins, D. L. Olson and G. R. Edwards, *Mettal. Trans. B* **21B**, 475 (1990).

<sup>14</sup>A. Mortensen, L. J. Masur, J. A. Cornie and M. C. Flemings, *Mettal. Trans. A* **20A**, 2535 (1989).

fall velocity,  $V_f$ . This point is reached when  $\omega$  approaches 1, and from that point on, the pressure drop is determined by the equation for flow through an empty tube. At velocities above  $V_f$ , the particles are entrained and blow out of the reactor. Figure 3.12 shows the various stages of fluidization schematically.

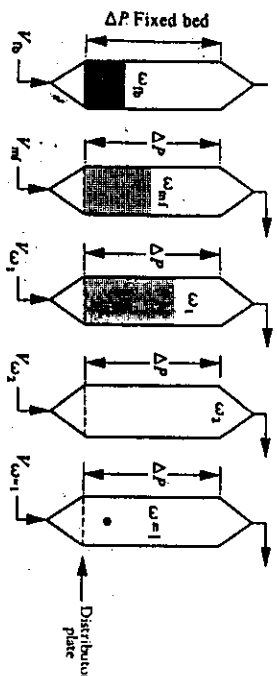


Fig. 3.12 Schematic representation of the relationship between the void fraction in the fluidized bed, the superficial velocity, and the pressure drop across the entire reactor, for particulate fluidization.

In Section 3.3.2 we discussed friction factors for flow past individual particles. In a fluidized bed, the particles, although suspended by the gas stream, exhibit a varying friction factor as the voidage varies, until finally at  $\omega \approx 1$  the friction factor is the same as that for the suspended condition. When Eq. (3.26) is equated to the gravity force exerted on the particle less the buoyancy force, it can be shown that

$$f = \frac{4}{3} \frac{D_p(\rho_p - \rho_f)g}{\rho_f V_0^2}, \quad (3.64)$$

where the subscripts  $p$  and  $f$  represent the particles and fluid, respectively, and  $V_0$  is the velocity of the fluid. In a fluidized bed,  $V_0$  is taken as the superficial velocity which is defined as the volume flow rate of fluid through the bed divided by the cross-sectional area of the bed.

Zenz<sup>12</sup> proposed that for a fluid-solid system there are two operating characteristics that can be established: (1) the velocity-particle size relation at the condition of minimum fluidization (a fluidized bed's minimum possible fixed-bed configuration with  $\omega_{mf}$ ) and (2) the terminal velocity of the largest significant particle in the bed, where  $\omega = 1$ . He then pointed out that since the data of Fig. 3.8 were correlated by a plot of  $f$  versus  $Re$ , it is possible to

form new dimensionless parameters that contain  $D_p$  and  $V_0$  separately and express the same data. These new dimensionless parameters are

$$\left[ \frac{Re}{f} \right]^{1/3} = \frac{V_0}{\left[ \frac{4g\eta_f(\rho_p - \rho_f)}{3D_p^2} \right]^{1/3}}, \quad (3.65)$$

and

$$(fRe^2)^{1/3} = \left[ \frac{D_p}{\frac{3\eta_f^2}{4g\rho_f(\rho_p - \rho_f)}} \right]^{1/3}. \quad (3.66)$$

In Eqs. (3.65) and (3.66),  $f$  is given by Eq. (3.64) and the Reynolds number is defined with  $V_0$  as the characteristic velocity. When the data of Fig. 3.8 are plotted in this way, a single curve corresponding to the terminal velocity at  $\omega = 1$  is found.

Applying this same methodology to the experimental data of Wilhelm and Kwauk<sup>13</sup> and other investigators who determined  $V_{mf}$ , the superficial velocity at minimum fluidization when particulate fluidization occurred, Zenz found a generalized empirical graph that describes the other boundary of the particulate fluid bed regime. For void fractions as the bed expands from  $\omega_{mf}$  to  $\omega = 1$ , other experimental data also can be explained by the same correlation. The resulting set of curves is given in Fig. 3.13 with lines of constant void fraction and  $Re$  given.

Leva et al.<sup>14</sup> give a relation for calculating  $V_{mf}$ :

$$V_{mf} = \frac{0.0007 g (\rho_p - \rho_f) D_p^2}{\eta_f} Re^{-0.003} \quad (3.67)$$

This can be rearranged to

$$\left[ \frac{Re}{f} \right]^{1/3} = \frac{Re^{0.645}}{12.4}, \quad (3.68)$$

which falls essentially on the line for  $\omega = 0.4$  on Fig. 3.13. Their data are for  $0.35 \leq \omega \leq 0.45$  and  $Re \leq 5$ . The data of Frantz<sup>15</sup> can similarly be shown to fit

$$\left[ \frac{Re}{f} \right]^{1/3} = \frac{Re^{2/3}}{9.8}, \quad (3.69)$$

<sup>12</sup>R. H. Wilhelm and M. Kwauk, *Chem. Engr. Prog.* 44, 201 (1948).

<sup>13</sup>M. Leva, T. Shirai and C. Y. Werr, *Genie Chim.* 75, 33 (1956).

<sup>14</sup>J. F. Frantz, *Chem. Engr.* 69, 161 (1962).

<sup>15</sup>F. A. Zenz, *Petrol. Refiner.* 36, 147 (1957).

which differs only slightly from that of Leva et al. Wen and Yu<sup>16</sup> use a Galileo number, which is simply  $(fR^2)$  and again falls in place on Fig. 3.13. Davison and Harrison<sup>17</sup> worked the void fraction into their correlation:

$$V_{mf} = \frac{0.0055 \omega_{mf}^3}{(1 - \omega_{mf})} \cdot \frac{g D_p (\rho_p - \rho_f)}{v}, \quad (3.70)$$

which can be rearranged to

$$\left[ \frac{Re}{f} \right]^{1/3} = \left[ \frac{\omega^3}{1 - \omega} \right]^{1/3} \frac{Re^{2/3}}{5.67}. \quad (3.71)$$

When  $\omega = 0.4687$ , Eq. (3.71) reduces to Eq. (3.69).

There is another mode of fluidization besides *particulate fluidization* (in which the bed is assumed to expand essentially uniformly). The other mode is known as *aggregative fluidization*, in which the fluid tends to rise through the bed in discrete bubbles, and aggregates of particles circulate in the bed. Usually, gas-solid beds exhibit aggregative fluidization, and liquid-solid beds exhibit particulate fluidization.

The expansion of the bed in aggregative fluidization may be estimated using

$$\frac{H}{H_0} = 1 + \frac{V_0 - V_{mf}}{2.21 \sqrt{D_s}}, \quad (3.72)$$

where  $H_0$  = height of bed (m) at minimum fluidization velocity,  $V_{mf}$ , m s<sup>-1</sup>,

$H$  = height of bed (m) at superficial velocity,  $V_0$ , m s<sup>-1</sup>

and

$2.21 \sqrt{D_s}$  = the terminal rate of rise (m s<sup>-1</sup>) of bubbles of diameter,  $D_s$  (m), through a freely bubbling bed.

More accurately,  $D_s$  should be expressed as a function of position in the bed, since as a gas bubble rises it expands as the pressure of the bed above it decreases. This relationship can be expressed as

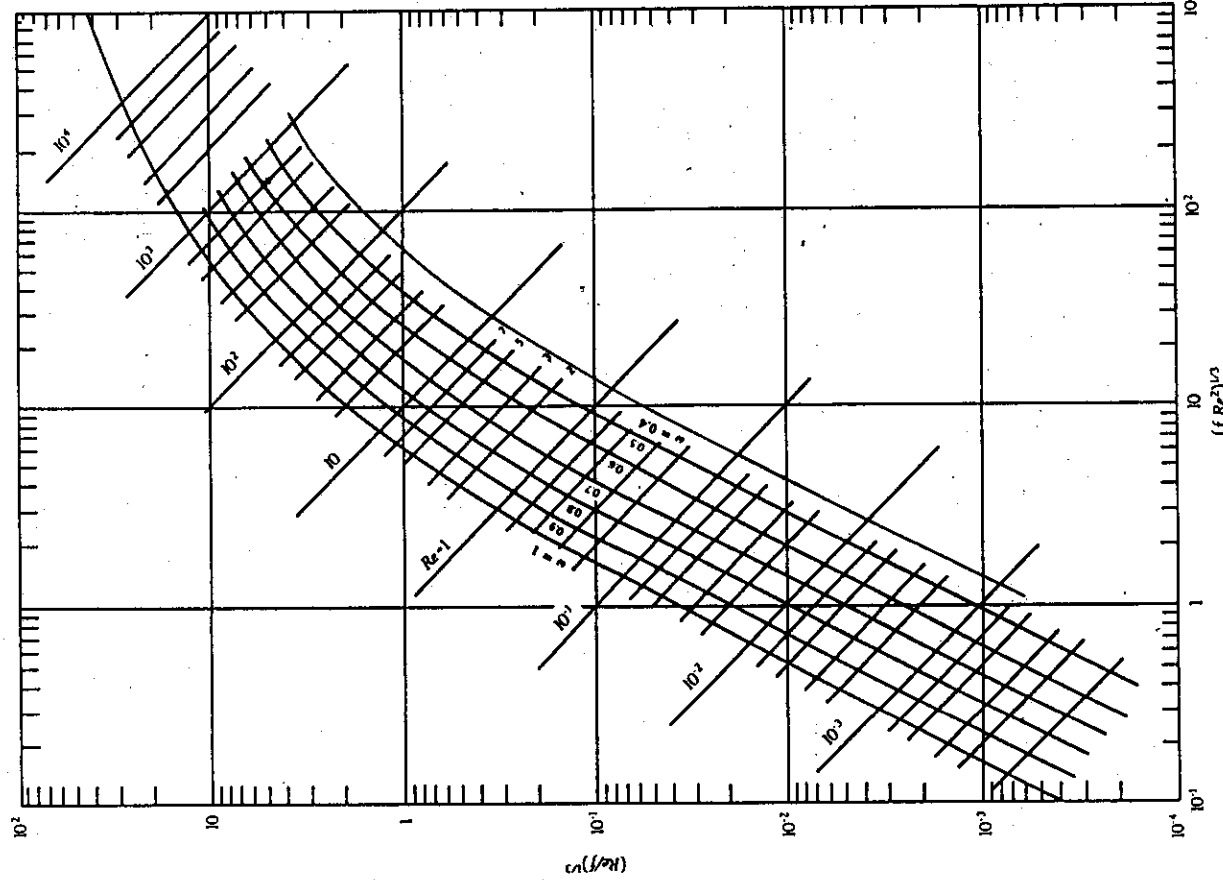
$$\frac{D_s}{D_{Bi}} = 0.15 \frac{L_B}{D_{Bi}} + 0.85, \quad (3.73)$$

where  $D_s$  is the bubble diameter at height  $L_B$  above the distributor, and

$D_{Bi}$  = initial bubble diameter at the distributor  
=  $P/2$  where  $P$  is the penetration of the gas into the bed from the orifice

with diameter  $D_0$  in the distributor, from Fig. 3.14.

In Fig. 3.14,  $V_{or}$  is the average velocity of the gas through the orifice (m) and  $\rho_g$  is the density of the gas (kg m<sup>-3</sup>).



<sup>16</sup>C. Y. Wen, and Y. H. Yu, *Fluid Particle Technology*, Chem. Engr. Prog. Symp. Ser., No. 62, AIChE, New York, 1966.

<sup>17</sup>J. F. Davison and D. Harrison, *Fluidized Particles*, Cambridge University Press, 1963.

Fig. 3.13 Smoothed correlation of particulate fluidization. (From F. A. Zenz and D. F. Othmer, *Fluidization and Fluid Particle Systems*, Reinhold Publ. Corp., New York, NY, 1960, page 236.)

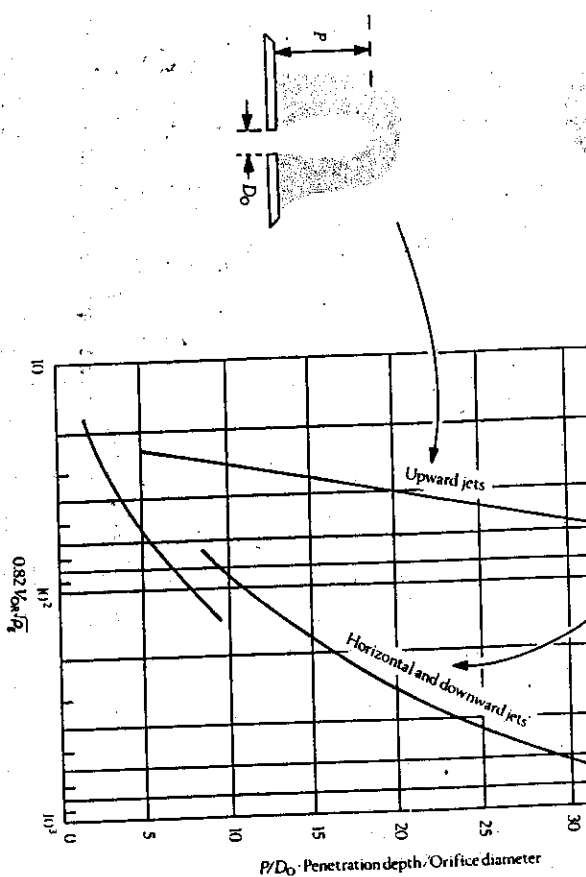


Fig. 3.14 Jet penetration into fluid-particle media. (From F. A. Zenz, *Fluidization and Fluid-Particle Systems*, Vol. II, Penn-Corp. Publ., Nelsonville, NY, 1989, page 114.)

There are many practical problems associated with the design of fluidized beds, particularly the design of distributor plates and tuyeres. For an excellent discussion of this entire topic and much practical advice, the reader is referred to Zenz,<sup>18</sup> to Cheremisinoff and Gupta,<sup>19</sup> and to Kunii and Levenspiel.<sup>20</sup>

Fluidized beds are utilized in materials processing with increasing frequency. They have the ability to provide good gas-solid contact and therefore to carry out gas-solid reactions efficiently. Examples include the roasting of sulfide ores (e.g., ZnS) to oxides; the conversion of oxide particles, such as TiO<sub>2</sub>, to gaseous products, such as TiCl<sub>4</sub>; and the reduction of oxides to metal, such as Fe<sub>3</sub>O<sub>4</sub> to Fe, or to carbides, such as Fe<sub>3</sub>C. They have the additional capability to transfer heat to parts immersed in them more efficiently than

would gas alone, so they are used as heat transfer devices (see Chapter 8). And they make it possible to contact powdered solids evenly onto surfaces of parts immersed in them, so they are used to produce polymeric coatings on unusually shaped parts, and in a similar operation to build up ceramic shell molds for investment castings.

**Example 3.6** Consider the design of a fluid bed to recover uranium from U<sub>3</sub>O<sub>8</sub> nuclear fuel elements by fluorinating it to UF<sub>6</sub>. The U<sub>3</sub>O<sub>8</sub> is fed into a fluidized bed of Al<sub>2</sub>O<sub>3</sub> particles (90% by weight), fluidized with N<sub>2</sub> at 750 K to which a small amount of F<sub>2</sub> has been added. The properties of the materials involved are:

	$\rho$ (kg m <sup>-3</sup> )	$\eta$ (N s m <sup>-2</sup> )	$D_p$ (m)
U <sub>3</sub> O <sub>8</sub>	8.3 × 10 <sup>3</sup>	—	?
Al <sub>2</sub> O <sub>3</sub>	3.9 × 10 <sup>3</sup>	0.48	3.4 × 10 <sup>-5</sup>
N <sub>2</sub> (750 K)	1.2 × 10 <sup>-4</sup>	—	—

Since the bed is primarily Al<sub>2</sub>O<sub>3</sub>, the gas flow must be enough to exceed minimum fluidization velocity for the Al<sub>2</sub>O<sub>3</sub>, yet not be so high as to carry out the U<sub>3</sub>O<sub>8</sub> particles. The question is: What size U<sub>3</sub>O<sub>8</sub> particles will stay in the bed?

**Solution.** Since the Al<sub>2</sub>O<sub>3</sub> particles are uniformly sized, the void fraction at minimum fluidization will be just above that of the bed at rest, which would be about 0.4. Assume  $\omega_{mf} = 0.45$ .

Calculate

$$(fRe^2)^{1/3} = \frac{D_p}{\left[ \frac{3\eta^2}{4g\rho_f(\rho_p - \rho_f)} \right]^{1/3}} = \frac{1.2 \times 10^{-4}}{\left[ \frac{(3)(3.4 \times 10^{-5})^2}{(4)(9.8)(0.48)(3900 - 0.48)} \right]^{1/3}} = 3.32.$$

Entering Fig. 3.13 at  $(fRe^2)^{1/3} = 3.32$  and  $\omega = 0.45$ , obtain a value of  $(Reff)^{1/3} = 0.0095$  from which  $V_{mf}$  can be calculated:

$$(Reff)^{1/3} = \frac{V_{mf}}{\left[ \frac{4g\eta_f(\rho_p - \rho_f)}{3\rho_f^2} \right]^{1/3}}.$$

$$V_{mf} = (0.0095) \left[ \frac{(4)(9.8)(3.4 \times 10^{-5})(3900)}{(3)(0.48)^2} \right]^{1/3} = 0.019 \text{ m s}^{-1}.$$

Now calculate the entrainment velocity of the Al<sub>2</sub>O<sub>3</sub>.  $(Reff)^{1/3}$  is still 3.32, but now enter Fig. 3.13 and, for  $\omega = 1.0$ , obtain  $(Reff)^{1/3} = 0.41$ . The corresponding velocity is now 0.82 m s<sup>-1</sup>. Therefore, the operating velocity of the bed will be between 0.019 and 0.82 m s<sup>-1</sup>. For a void fraction of 0.8,  $V_{mf}$  will be 0.26 m s<sup>-1</sup>.

The entrainment velocity of the reacted U<sub>3</sub>O<sub>8</sub> particles must be calculated to see if it will stay in the reactor. At a bed operating velocity of 0.26 m s<sup>-1</sup>, for the U<sub>3</sub>O<sub>8</sub>,

$$(Reff)^{1/3} = \left[ \frac{(4)(9.8)(3.4 \times 10^{-5})(8300)}{(3)(0.48)^2} \right]^{1/3} = 0.103.$$

<sup>18</sup>F. A. Zenz, *Fluidization and Fluid-Particle Systems*, Vol. II, Penn-Corp. Publ., Nelsonville, NY, 1989.

<sup>19</sup>N. P. Cheremisinoff and R. Gupta (editors), *Handbook of Fluids in Motion*, Butterworths, Boston, 1983, Chaps. 23–26.

<sup>20</sup>D. Kunii and O. Levenspiel, *Fluidization Engineering*, Second Edition, Butterworths-Heinemann, Boston, 1991.

For  $\omega = 1.0$  (elutriation), this gives  $(fRe^2)^{1/3} = 1.5$ . Therefore, the smallest particle of  $U_3O_8$  that will remain in the bed will be

$$D_p = (1.5) \left[ \frac{(3)(3.4 \times 10^{-5})^2}{(4)(9.8)(0.48)(8300 - 0.48)} \right]^{1/3} = 4.2 \times 10^{-5} \text{ m.}$$

Any particles of  $U_3O_8$  smaller than this will be carried out of the bed when they reach the top.

### PROBLEMS

**3.1** Water at 300 K is flowing through a brass tube that is 30.0 m long and 13 mm in diameter (inner). The water is moving through the tube at a rate of  $3.2 \times 10^{-3} \text{ m}^3 \text{ s}^{-1}$ . The density of water is  $1000 \text{ kg m}^{-3}$ , and its viscosity is  $8.55 \times 10^{-4} \text{ N s m}^{-2}$ . Calculate the pressure drop in Pa that accompanies this flow.

**3.2** Evaluate the pressure drop in a horizontal 30 m length of galvanized rectangular duct ( $30.0 \text{ mm} \times 75.0 \text{ mm}$ ) for the following conditions:

- a) An average air flow velocity of  $0.46 \text{ m s}^{-1}$  at 300 K and atmospheric pressure.
- b) An average air flow velocity of  $4.6 \text{ m s}^{-1}$  at 300 K and atmospheric pressure. The density and viscosity are  $1.16 \text{ kg m}^{-3}$  and  $1.85 \times 10^{-5} \text{ N s m}^{-2}$ .

**3.3** For flow in tubes (smooth wall) the friction factor is given by Eq. (3.20) for  $2.1 \times 10^3 < Re < 10^5$ . What is the percent change in the pressure drop if the tube diameter is doubled for the same volume flow rate, same fluid and the same tube length? Assume that Eq. (3.20) for the friction factor applies.

**3.4** Show that for flow through a slit with a spacing that is much less than the width, Eq. (3.22) gives the friction factor for laminar flow.

**3.5** Determine the size of the largest alumina particle in Problem 2.14 that would be expected to obey Stokes' law, remembering that for spheres this law is valid for  $Re \leq 1$ .  
Data: Radius of steel ball, 88.7 mm; terminal velocity of steel ball,  $1.52 \text{ m s}^{-1}$ .

**3.6** A falling-sphere viscometer was used to determine the viscosity of a slag intended for the production of copper. The viscosity of the slag was determined to be 441.2 Poise, using a steel ball as the falling sphere. Is this a valid viscosity? Why or why not? If not, determine the real value of the viscosity and then calculate its kinematic viscosity. The density of the slag may be taken as one-half that of the steel ball.  
Data: Radius of steel ball, 88.7 mm; terminal velocity of steel ball,  $1.52 \text{ m s}^{-1}$ .

**3.7** Two spheres of equal density and different diameters fall through a liquid with an unknown density and an unknown viscosity. The diameter of the larger sphere is twice the diameter of the smaller sphere.

- a) With an appropriate force balance, derive an equation for the terminal velocity of either sphere. Your equation should be valid for any Reynolds number.
- b) Assume that  $10^3 < Re_D < 2 \times 10^5$  for both spheres and calculate the ratio of the terminal velocity of the larger to that of the smaller.
- c) Assume that  $Re_D < 1$  for both spheres, and calculate the ratio of terminal velocities.

**3.8** Bubbles that rise through liquids may be treated as rigid spheres provided they are small enough. Assume that a spherical bubble of air has a diameter of 1 mm at the bottom of a glass melt that is 1 m deep.

- a) Calculate the pressure in the bubble as a function of the distance below the top surface of the glass. Neglect added pressure within the bubble because of the surface tension.
- b) Calculate the diameter of the bubble as a function of the distance below the top surface of the glass.
- c) Neglecting acceleration effects, calculate the velocity of the bubble as a function of distance below the top surface of the glass. Data for melt: Temperature is 1700 K; viscosity is  $2.0 \text{ N s m}^{-2}$ ; density is  $3000 \text{ kg m}^{-3}$ . Assume that air behaves as an ideal gas with a molecular weight of  $28.8 \text{ kg kmol}^{-1}$ .

**3.9** A thermocouple tube lies in a melt that is flowing perpendicular to the axis of the tube. Calculate the force per unit length of tube exerted by the flowing metal. Data: Velocity of the melt is  $3 \text{ m s}^{-1}$ ; viscosity is  $2 \times 10^{-3} \text{ N s m}^{-2}$ ; density of the melt is  $8000 \text{ kg m}^{-3}$ ; diameter of thermocouple tube is 61 mm.

**3.10** A packed bed reduction-reactor, 15.0 m high and 6.0 m in diameter, is packed with spherical metal oxide pellets ( $D_p = 3 \text{ mm}$ ). A reducing gas enters the top of the bed at 800 K and at a rate of  $95 \text{ kg s}^{-1}$  and exits the reactor at the same temperature. What should the pressure at the top of the reactor be if the pressure at the bottom of the reactor is maintained at  $1.4 \times 10^5 \text{ Pa}$ . Data: Bed porosity,  $\omega = 0.40$ ; viscosity of the reducing gas at 800 K is  $4.13 \times 10^{-5} \text{ N s m}^{-2}$ ; density of the gas at atmospheric pressure and 800 K is  $0.5 \text{ kg m}^{-3}$ .

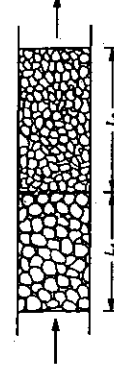
**3.11** In a packed bed reactor (diameter = 4.5 m and height = 18 m), metal oxide A forms a central column within the reactor, having a diameter of 3.0 m, while pellets of metal oxide B fill the annulus between metal oxide A and the wall of the reactor. The pressure at the top of the bed is maintained at  $6.9 \times 10^4 \text{ Pa}$ , while the pressure at the bottom is kept at  $1.72 \times 10^4 \text{ Pa}$ . Calculate the fraction of reducing gas that passes through metal oxide A. It may be assumed that the temperature and reducing gas density are uniform throughout the reactor. Furthermore, turbulent flow conditions prevail.

Data for A:  $\omega = 0.40, D_p = 76 \text{ mm}$ .

Data for B:  $\omega = 0.25, D_p = 19 \text{ mm}$ .

**3.12** Preliminary experimental studies have shown that the porosity in a newly developed packed bed reactor is  $\omega < 0.6$ . The pellets have a diameter of 30.0 mm and the reducing gas flows through the bed at a rate of  $0.025 \text{ kg s}^{-1}$ . The reactor has  $3.0 \text{ m} \times 3.0 \text{ m}$  square cross section and is 15 m in height. A constant pressure difference of  $690 \text{ Pa}$  is maintained between the inlet and outlet nozzles, and it may be assumed that the temperature is uniform throughout the reactor. You are required to evaluate the bed porosity. The properties of the gas are  $\eta = 2.07 \times 10^{-5} \text{ N s m}^{-2}$  and  $\rho = 1.2 \text{ kg m}^{-3}$  (average).

**3.13** Molten aluminum is passed through a horizontal filter bed of  $Al_2O_3$  spheres in order to remove drossy oxides from the aluminum. The filter bed comprises two different packings arranged in series.

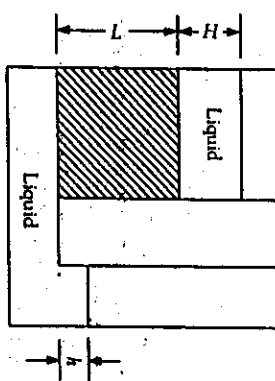


The first packing encountered by the flow captures large drossy particles, and the second packing captures the smaller drossy particles. Given  $L_A = 0.7 L_B$ ,  $\omega_A = \omega_B$ ,  $D_{p,A} = 2D_{p,B}$ , compute the ratio of the pressure drop through  $A$  to the pressure drop through  $B$  for a) very low Reynolds numbers, and b) very high Reynolds numbers.

**3.14** Derive an equation for the pressure drop through an isothermal column of a porous medium, that accompanies the flow of a compressible gas. Assume that the gas follows ideal behavior.

**3.15** For unidirectional flow through a column of a porous medium, show that Eq. (3.61) reduces to Eq. (3.31).

**3.16** In a *falling head permeameter*, the permeability is determined by measuring the difference in height between two liquid columns. In the apparatus depicted below,  $H$  decreases and  $h$  increases as liquid flows by gravity through the porous medium of length  $L$ . Derive an equation that gives  $h$  as a function of time  $t$ , assuming that  $P$  is uniform and constant.



Cross-sectional areas of the larger and smaller columns of liquid are  $A$  and  $a$ , respectively.

### 3.17 The tube bundle theory for permeability predicts

$$\mathcal{P} = \frac{\omega^3}{K S_0^2 (1 - \omega)^2}$$

where  $K$  is a constant. Assuming that Eq. (3.55) applies, does the tube bundle theory compare to the empirical result given by Eq. (3.59)?

**3.18** Consider Eqs. (3.62) and (3.63) and assume that the aspect ratio of the fibers is sufficiently large that the fibers can be assumed to have infinite lengths.

- Derive an equation for the relationship between  $S_0$  and  $a$ .
- Does the equation for permeability given in Problem 3.17 predict the permeabilities for flow through fibrous media?

**3.19** In the production of titanium (Ti), rutile ore ( $TiO_2$ ) is fluidized with gaseous chlorine and the following reaction occurs:



The rate of this reaction is controlled by the removal of the oxygen by reaction with coke particles in the reactor, according to



The rutile ore, prior to being placed in the reactor, was analyzed according to size. The following ranges of particle diameters,  $D_p$ , were found:

$180 \leq D_p < 250 \mu m$	5%
$150 \leq D_p < 180 \mu m$	6.2%
$106 \leq D_p < 150 \mu m$	77.4%
$75 \leq D_p < 106 \mu m$	11.4%

Using the above data, calculate the possible chlorine mass flow rates (at 1223 K) that are needed to fluidize the ore in a reduction reactor that is 1.2 m in diameter and 10 m in height.

**3.20** A bed of particles of uniform size is fluidized such that the bed voidage is 0.6 when the Reynolds number is 10. A second bed, similar to the first, contains particles with a diameter equal to one-half of the diameter of particles in the first bed. Both beds operate with the same superficial velocity. What is the bed voidage in the bed filled with the smaller particles?

**3.21** A fan delivers air to two fluidized beds,  $A$  and  $B$ . Bed  $A$  is operating at a minimum volume (i.e., at minimum fluidization) and bed  $B$  is fluidized to a volume equal to twice its fixed bed volume.

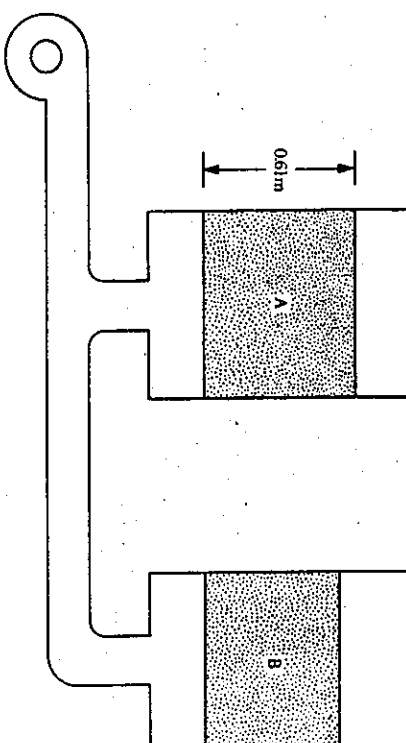
- Calculate the superficial velocity through bed  $A$ .
- Calculate the superficial velocity through bed  $B$ .
- Calculate  $\Delta P$  across bed  $A$ .
- For bed  $B$ , prove that  $\omega = 0.7$  when it is fluidized to twice the fixed bed volume.

Bed  $A$ :  $D_p = 91.4 \mu m$  (uniform);  $\rho$  (solid) =  $4808 \text{ kg m}^{-3}$ ;  $\lambda = 1$ .

Bed  $B$ :  $D_p = 61.0 \mu m$  (uniform);  $\rho$  (solid) =  $4006 \text{ kg m}^{-3}$ ;  $\lambda = 1$ ;

$\omega$  (fixed bed) = 0.4;  $\omega$  (fluidized) = 0.7.

Air:  $\rho = 1.28 \text{ kg m}^{-3}$ ;  $\eta = 2.07 \times 10^{-5} \text{ N s m}^2$ .



**3.22** Metal parts are to be annealed at 800 K in a bed of silica sand fluidized by products of combustion of natural gas with 100% excess air. If the sand has a U.S. Standard screen analysis of 20% -30M+50M, 30% -50M+70M, 40% -70M+10M, and 10% -100M+140M, what superficial velocity of gas is required through the bed? (Hint: Think about at what void volume you want to operate.) What is the minimum superficial velocity that you can operate at?

**3.23** Pellets of polyethylene are to be fluidized in a column 1 meter in diameter and 10 meters high with air at 350 K. A hot steel pipe is lowered into the fluidized bed to bring it into contact with the pellets, which melt onto its surface to form a protective anticorrosion coating. Calculate the total flow of air required, if the pellets are 5 mm in diameter and the desired void fraction of the bed is 0.7. The density of the polyethylene is  $920 \text{ kg m}^{-3}$ .

- 3.24** During the compaction of metal powders into sheet material (powder rolling), as shown in the figure below, the entrapped air is expelled from the loose powder. This expulsion occurs at the line  $AB$ . Below  $AB$ , the powder is coherent, that is, the particles are locked together, but above  $AB$ , the powder is loose, i.e., a normal packed bed.

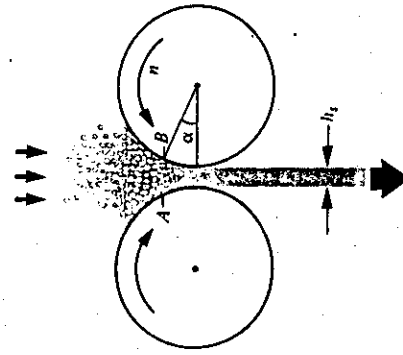
If the velocity of expulsion exceeds the minimum fluidization velocity, the powder does not feed properly into the roll gap and the sheet product is not satisfactory. This, in fact, limits the production rate of the process.

The following equation gives the superficial velocity  $V_0$  ( $\text{cm s}^{-1}$ ) of gas expulsion from the coherent zone:

$$V_0 = \frac{2\pi R^2 n (\alpha - \sin \alpha \cos \alpha)}{\alpha [2R(1 - \cos \alpha) + h_i]},$$

where  $R$  = roll radius, cm,  $n$  = rolling speed, rev  $\text{s}^{-1}$ ,  $\alpha$  = roll-coherent powder contact angle, rad, and  $h_i$  = roll gap, cm. For copper powder,  $\alpha$  has been found to be  $6^\circ$  ( $0.1047$  radians).

- Calculate the rolling speed at which copper powder, with properties given below, will just begin to be fluidized at the plane  $AB$ , for strip thickness 0.5 mm and roll diameter 200 mm.
- Calculate the corresponding speed of the emerging coherent strip.
- Discuss the effect that order-of-magnitude changes in particle size and roll radius would have on production rates. Data are given as follows:  $\eta = 1.8 \times 10^6 \text{ N s m}^{-2}$ ,  $\rho_{\text{air}} = 1.30 \text{ kg m}^{-3}$ ,  $D_{P_c} = 40 \mu\text{m}$ ,  $\rho_{Cu} = 6700 \text{ kg m}^{-3}$ .



## ENERGY BALANCE APPLICATIONS IN FLUID FLOW

One of the most powerful analytical tools available for quantitative problems in engineering is the principle of the conservation of energy. In fluid flow, this principle is most often applied to open systems in the form of the *mechanical energy equation*, which is also commonly called *Bernoulli's equation*. The approach is macroscopic, since we examine the entire flow system with an entrance and an exit. This method is different from the one presented in Chapter 2, where we analyzed the microscopic volume element through which fluid flows as the starting point for solving problems.

### 4.1 CONSERVATION OF ENERGY

The *mechanical energy equation* is the starting point for analyzing many problems involving fluid flow. It can be derived from the first law of thermodynamics, which is usually written for a system (or control volume) with a fixed mass and no mass entering or leaving the system. For an *open system*, however, mass may enter or leave the system, and it is convenient to write the first law of thermodynamics for a control volume that allows for mass flow across its boundaries. Our goal is to apply the first law to engineering systems, in which there can be significant changes in both kinetic energy and potential energy as the fluid flows through the system. Furthermore, the fluid flow may be mechanically forced or assisted through the system by the power of a pump, fan, or blower.\*

When presented the first law of thermodynamics for the first time, most readers were probably given

$$\Delta U = Q - M$$

where  $U$  is the internal energy,  $\Delta U$  is the change in internal energy in going from "state 1" to "state 2" in a closed system,  $Q$  is the heat added to the system, and  $M$  is the work done

\*In other engineering scenarios, the fluid provides power (e.g., a water-wheel, a steam turbine or a gas turbine).

by the system. This statement of the first law is usually adequate because our interest in applying thermodynamics to materials is usually based on principles of chemical thermodynamics. Changes in kinetic energy and potential energy of a substance are not important when our goal is to use thermodynamics to understand the structure and properties of materials. More generally, however, the first law of thermodynamics has far-reaching applications to devices and systems for producing electrical or mechanical power, and for effecting heating or cooling. In this broader context, the *total energy*, which comprises the sum of internal, potential and kinetic energies, and not the internal energy by itself, must be used in the first law of thermodynamics.

In materials processing, fluid flows are often driven through systems by pumps, fans or blowers, so we start with the first law of thermodynamics written for an open system. A derivation of the equation can be found in many engineering textbooks on thermodynamics.<sup>1</sup> With the aid of the symbols in Table 4.1, the conservation of energy can be written

$$\frac{dE}{dt} = -\Delta[H + E_p + E_k]W + Q - M + S_R. \quad (4.1)$$

In this form, the macroscopic energy balance is written for unsteady-state conditions in which the left side of the equation represents the accumulation of total energy in the system. The total energy,  $\Sigma$ , is defined as the sum of internal, potential, and kinetic energy. The operator  $\Delta$  signifies exit minus entrance quantities, and note that the expression  $\Delta H = \Delta U + \Delta(P/\rho)$  has been employed in the usual manner for open systems.

Table 4.1 Symbols used in the general energy balance

	Entering the system	Leaving the system
Mass flow rate	$W_1$	$W_2$
Pressure	$P_1$	$P_2$
Volume per unit mass	$1/\rho_1$	$1/\rho_2$
Energy per unit mass	$E_{p1}$ $E_{k1}$ $U_1$	$E_{p2}$ $E_{k2}$ $U_2$
Potential	$H_1 = U_1 + P_1(1/\rho_1)$	$H_2 = U_2 + P_2(1/\rho_2)$
Kinetic		
Internal		
Enthalpy		
Mechanical power done by the system, $M$		
Net power generation within the system from chemical reactions or other sources, $S_R$		
Net power input by heat transfer, $Q$		

<sup>1</sup>For example, see G. J. Van Wylen and R. E. Sonntag, *Fundamentals of Classical Thermodynamics*, third edition, John Wiley, New York, NY, 1985, pages 113-121.

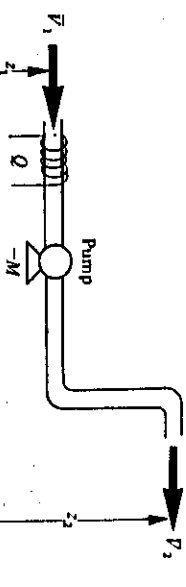


Fig. 4.1 Flow system for the application of the energy balance.

at "2," respectively. After this brief discussion explaining the basis of the problem at hand, namely, the flow of fluids, we now proceed to focus attention on some of the specific terms in Eq. (4.1) for steady-state conditions, namely,

$$\frac{dE}{dt} = 0, \quad W_1 = W_2 = W, \quad \text{and} \quad S_R = 0.$$

#### 4.1.1 Evaluation of the kinetic energy terms

The rate of kinetic energy entering the system through area  $A_1$  (normal to flow) is given by

$$WE_{k1} = \frac{1}{2} \int_0^{A_1} (\rho_1 v_1)^2 dA_1. \quad (4.2)$$

Examine Eq. (4.2) for meaning; one may be tempted at this point to simply write  $\frac{1}{2}(\rho_1 A_1 \bar{V}_1) \bar{V}_1$  to represent the kinetic energy entering the system, where  $\bar{V}_1$  is the average velocity ( $= W_1/\rho_1 A_1$ ). However, because the velocity varies in some manner across the cross-sectional area, the integration indicated by Eq. (4.2) is in order.

To account for the velocity distribution, the kinetic energy term can be written as:

$$WE_{k1} = \frac{1}{2\beta_1} W_1 \bar{V}_1^2, \quad (4.3)$$

where  $\beta_1$  is defined by

$$\frac{1}{\beta_1} = \frac{1}{A_1} \int_0^{A_1} \left[ \frac{v_1}{\bar{V}_1} \right]^2 dA_1. \quad (4.4)$$

We can also use a similar expression for the rate at which kinetic energy leaves the system, so we write the difference between leaving and entering the system

$$WE_{k2} = W \left[ \frac{\bar{V}_2^2}{2\beta_2} - \frac{\bar{V}_1^2}{2\beta_1} \right]. \quad (4.5)$$

For laminar flow in a circular tube,  $\beta = 0.5$ , and for turbulent flow,  $\beta$  is nearly unity, and is usually approximated as such.

#### 4.1.2 Evaluation of the potential energy terms

Potential energy is defined relative to some arbitrary reference plane for the fluid both leaving and entering the system. Therefore, the difference in potential energy of the fluid leaving and entering is simply

$$W\Delta E_p = Wg(z_2 - z_1),$$

or

$$W\Delta E_p = Wg\Delta z. \quad (4.6)$$

#### 4.1.3 Mechanical energy equation, Bernoulli's equation

Substituting Eqs. (4.5) and (4.6) into Eq. (4.1) for steady-state conditions yields

$$\Delta H + \left[ \frac{\bar{V}_2^2}{2\beta_2} - \frac{\bar{V}_1^2}{2\beta_1} \right] + g\Delta z + M^* - Q^* = 0. \quad (4.7)$$

Here  $M^* = M/W$ , and  $Q^* = Q/W$ . In this form, all the terms are now energies per unit mass of fluid flowing through the system. Further, if we express  $H$  by  $U + P/\rho$ , we obtain the *overall energy balance*:

$$\Delta U + \Delta \left[ \frac{P}{\rho} \right] + \left[ \frac{\bar{V}_2^2}{2\beta} \right] + g\Delta z + M^* - Q^* = 0. \quad (4.8)$$

The equation is also commonly found in its differential form for a differential segment of the system:

$$dU + d \left[ \frac{P}{\rho} \right] + \left[ \frac{\bar{V}^2}{2\beta} \right] + gdz - \delta Q^* = 0. \quad (4.9)$$

Here  $\delta$  prefacing  $Q^*$  emphasizes that it is not a true differential but that it merely represents the heat which is transferred across the system boundary.

A more common form of the energy balance for applications to fluid flow is a variation referred to as the *mechanical energy equation*. From Eq. (4.8), we see that the change in the internal energy for the unit mass of fluid as it passes through a short segment of the system is

$$dU = dQ^* - Pd(1/\rho) + \delta E_f, \quad (4.10)$$

where  $\delta E_f$  is the *mechanical energy per unit mass lost as frictional conversion into heat*. Substituting Eq. (4.10) into (4.9) and expanding  $d(P/\rho)$  into

$$\left[ (1/\rho)dP + Pd(1/\rho) \right]$$

yields

$$\frac{1}{\rho} dP + d \left[ \frac{\bar{V}^2}{2\beta} \right] + gdz + \delta E_f = 0. \quad (4.11)$$

The integral of this equation, which applies to the whole system, finally yields (with  $M^*$  reinserted) the mechanical energy equation, which can be applied directly to many problems of fluid flow:

$$\int_{P_1}^{P_2} \frac{dP}{\rho} + \left[ \frac{\bar{V}_2^2}{2\beta_2} - \frac{\bar{V}_1^2}{2\beta_1} \right] + g\Delta z + M^* + E_f = 0. \quad (4.11)$$

This equation is also called Bernoulli's equation. Actually, Bernoulli's equation only applies to the flow of ideal fluids, where  $M^* = E_f = 0$ , but Eq. (4.11), having been used so frequently in engineering, has taken on the connotation of Bernoulli's equation as well. Also note that it is written in terms of unit mass of material flowing.

#### 4.2 FRICTION LOSSES IN STRAIGHT CONDUITS

Due to the utility of Eq. (4.11) in engineering calculations, considerable effort has been made to develop methods for estimating the friction loss  $E_f$  in various flow systems.

If we consider the friction loss in a straight conduit with steady flow of constant-density fluid, we can determine  $E_f$  in terms of the friction factor  $f$ . The control volume is a portion of a conduit with an arbitrary but constant cross-sectional area  $A$  and a length  $L$ . The fluid flows only due to a pressure difference of  $P_2 - P_1$ ; then Eq. (3.3) gives us the force exerted by the fluid on the inside surface of the conduit.

$$F_k = (P_1 - P_2)A. \quad (4.12)$$

Since we are discussing a horizontal control volume with no mechanical work supplied or withdrawn, Eq. (4.11) reduces to

$$E_f = \frac{1}{\rho} (P_1 - P_2). \quad (4.13)$$

By comparing Eqs. (4.12) and (4.13), we see that

$$E_f = \frac{F_k}{\rho A}. \quad (4.14)$$

For circular tubes,  $A = \pi R^2$  and  $F_k = 2\pi RL(\frac{1}{2}\rho \bar{V}^2)f$ . Thus,

$$E_f = 2f \left[ \frac{L}{D} \right] \bar{V}^2. \quad (4.15)$$

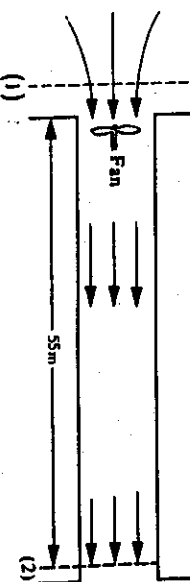
Again, for noncircular conduits,  $D$  may be replaced by the equivalent diameter  $D_e$ , which is discussed in Section 3.2. Equation (4.15) is a form of the well-known *Fanning equation*. Caution must be exercised by the reader in the exact definition of the friction factor; in much of the literature the friction factor is defined such that it is four times the friction factor employed here. Therefore, the Fanning equation may be found in a different form from that in Eq. (4.15).

From Fig. 3.2,  $f = 0.0042$  (smooth). Because

$$E_f = 2 \left[ \frac{L}{D_e} \right] \bar{V}_2^2 f,$$

the energy balance can be written as

**Solution.** Consider the system below that is defined by placing planes 1 and 2 where shown. The mechanical equation includes  $M^*$ , because there is a fan in the system.



Because  $P_1 \approx P_2 = 750 \text{ mm Hg}$ , then  $\int dP = 0$ . Also  $\bar{V}_1 = 0$  and  $\Delta z = 0$ . Under these conditions, Eq. (4.11) reduces to

$$\frac{\bar{V}_2^2}{2\beta_2} + M^* + E_f \approx 0.$$

Now

$$D_e = \frac{2(0.2 \times 0.3) \text{ m}^2}{(0.2 + 0.3) \text{ m}} = 0.24 \text{ m}.$$

At normal atmospheric pressure and 289 K, the density of air is  $1.22 \text{ kg m}^{-3}$ . Therefore,

$$\rho = \left[ \frac{750}{760} \right] (1.22) = 1.20 \text{ kg m}^{-3}.$$

(Why is this an approximation? Just to the right of the fan do you think the pressure is equal to, greater than or less than  $750 \text{ mm Hg}$ ?)

$$\bar{V}_2 = \frac{0.472 \text{ m}^3}{s} \left| \frac{(0.2 \times 0.3) \text{ m}^2}{(0.2 \times 0.3) \text{ m}^2} \right| = 7.87 \text{ m s}^{-1}.$$

The Reynolds number is now determined:

$$Re = \frac{D_e \bar{V}_2 \rho}{\eta} = \frac{(0.24)(7.87)(1.20)}{(1.78 \times 10^{-5})} = 1.27 \times 10^6.$$

By stating that  $P_2 = 750 \text{ mm Hg}$ , we ignore the exit loss which we shall discuss in Section 4.3.

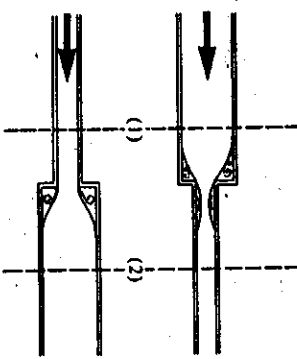


Fig. 4.2: Sudden contraction and enlargement.

The friction loss associated with a *sudden enlargement* or a *sudden contraction* (Fig. 4.2) is calculated by using a *friction-loss factor*  $\epsilon_f$ . The friction loss for the particular geometry that upsets flow in conduits is evaluated in the following manner:

$$E_f = \frac{1}{2} \bar{V}^2 \epsilon_f. \quad (4.16)$$

where  $\bar{V}$  is the velocity of fluid in the smaller cross section. (Since other conventions are also used, the reader should always be certain of which velocity is chosen to define  $e_f$ .) By analogy with Eq. (4.15),  $e_f$  corresponds to a friction factor with built-in geometry effects. Hence,  $e_f$  depends on a Reynolds number and a geometric ratio of the system. We present values of  $e_f$  for enlargements and contractions in circular cross sections in Figs. 4.3 and 4.4, respectively. For both these figures,  $D$  is the smaller diameter,  $R_e$  is calculated using the same  $D$ , and  $L$  is the length of the smaller pipe considered.

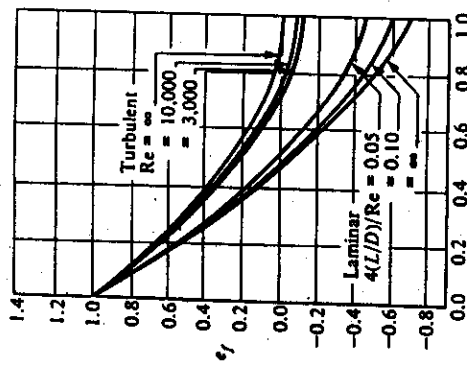


Fig. 4.3 Friction-loss factor for sudden expansion. (From W. M. Kays and A. L. London, Trans. ASME 74, 1179 (1952).)

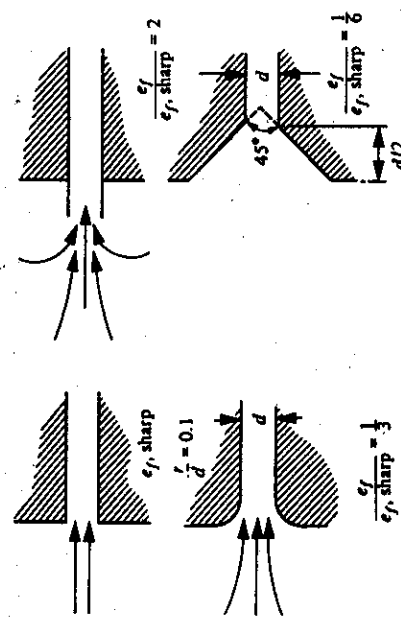


Fig. 4.5 Entrance-loss coefficients.

In flow through *radial enlargements*, the energy losses are significantly reduced due to the elimination of the vortices shown in Fig. 4.2. Experiments on tapered enlargements show that the friction-loss factor  $e_f$  depends on both the taper angle  $\beta$  and the area ratio  $A_1/A_2$  (Fig. 4.6). In reality,  $e_f$  should also depend on a Reynolds number, but this is not given in the figure, since, in turbulent flow, the dependence of  $e_f$  on the Reynolds number is small, as can be seen in Figs. 4.3 and 4.4. Consequently, data presented for  $e_f$  are usually assumed to apply to all Reynolds numbers in the regime of turbulent flow.

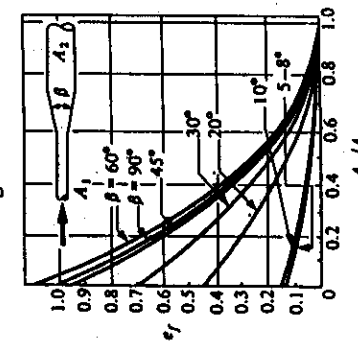


Fig. 4.6 Friction-loss factor for turbulent flow through gradual enlargements. (From Steam—Its Generation and Use, Babcock & Wilcox, New York, 1963, page 8-17.)

The results for  $e_f$  in the case of enlargements apply equally well to all exit shapes (except for gradual expansions discussed in the following paragraphs), as can be seen by viewing the flow in Fig. 4.2. The extent of the region of vortices after the expansion does not depend on whether the corners are rounded. However,  $e_f$  for contraction (entrances) can be modified

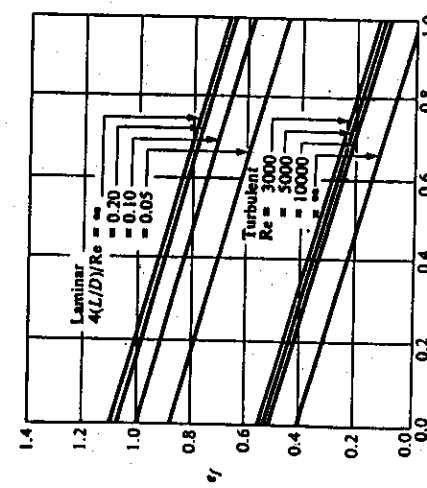


Fig. 4.4 Friction-loss factor for sudden contraction. (From Kays and London, *Ibid.*)

In *gradual contractions*, the converging boundaries have a tendency to steady the flow, and if the included angle of convergence is  $30^\circ$  or less, the energy loss factor can be approximated as 0.05–0.10. Again, when using these data, one must realize that they apply only to turbulent flow.

**Example 4.2** In Example 4.1 the entrance and exit losses were ignored. This time we repeat the calculation and include these losses.

**Solution.** Refer to the figure included with Example 4.1. Keep plane 1 in place, but move plane 2 to the right so that it is just beyond the exit end of the duct. Now  $P_1 = P_2 = 750 \text{ mm Hg}$ , and  $\bar{V}_2 = \bar{V}_1 = 0$ . The latter is true because the air flows at planes 1 and 2 are essentially within very large areas, which makes the average velocities small, and then these small velocities are squared. As before  $\Delta z = 0$ , then Eq. (4.11) reduces to

$$M^* + E_f = 0,$$

where

$$E_f = 2 \left[ \frac{L}{D_e} \right] \bar{V}^2 f + \frac{1}{2} \epsilon_{f1} \bar{V}^2 + \frac{1}{2} \epsilon_{f2} \bar{V}^2,$$

with  $\bar{V}$  the velocity within the duct and  $\epsilon_{f1}$  and  $\epsilon_{f2}$  the energy loss coefficients for the entrance and the exit, respectively. Now, we solve for  $M^*$ :

$$M^* = - \left[ \frac{1}{2} \epsilon_{f1} + \frac{1}{2} \epsilon_{f2} + 2 \left[ \frac{L}{D_e} \right] f \right] \bar{V}^2.$$

Values of the Reynolds number, velocity, friction factor and  $L/D_e$  are all found in Example 4.1. With  $Re = 1.27 \times 10^5$  and  $A_2/A_1 = 0$ , Fig. 4.4 gives  $\epsilon_{f1} = 0.4$ . With  $A_1/A_2 = 0$ , Fig. 4.3 gives  $\epsilon_{f2} = 1.0$ . Then

$$\begin{aligned} M^* &= - \left[ \left[ \frac{1}{2} \right] (0.4) + \left[ \frac{1}{2} \right] (1.0) + (2)(0.0042) \left[ \frac{55}{0.24} \right] \right] 7.87^2 \\ &= -163 \text{ W s kg}^{-1}. \end{aligned}$$

Also

$$\text{Power} = 0.0924 \text{ kW.}$$

By carefully accounting for the additional frictional losses in the system, our estimate of the power has increased by 8.7%.

#### 4.4 FLOW THROUGH VALVES AND FITTINGS

To evaluate flow through valves and fittings, we usually assign an equivalent length to the fixture such that the pressure drop is given by Eq. (4.15), where  $L$  is replaced by  $L_e$ . Therefore

$$E_f = 2f \frac{L_e}{D} \bar{V}^2, \quad (4.17)$$

where  $f$  is evaluated for  $Re$  with the pipe diameter equal to the fitting diameter, and  $L_e/D$  for turbulent flow of various fittings is given in Table 4.2. Thus, when evaluating the friction loss through a system with fittings, the sum of the equivalent lengths of all the fittings is added to the length of the pipe;  $E_f$  is then determined by using Eq. (4.17).

Table 4.2 Equivalent length for various fixtures, turbulent flow\*

Fitting	$L_e/D$	Fitting	$L_e/D$
45° elbow	15	Tee (as el., entering branch)	90
90° elbow, standard radius	31	Couplings, unions	Negligible
90° elbow, medium radius	26	Gate valve, open	7
90° elbow, long sweep	20	Gate valve, $\frac{1}{2}$ closed	40
90° square elbow	65	Gate valve, $\frac{1}{2}$ closed	190
180° close return bend	75	Gate valve, $\frac{1}{2}$ closed	840
Swing check valve, open	77	Globe valve, open	340
Tee (as el., entering run)	65	Angle valve, open	170

\*W. M. Rohsenow and H. Y. Choi, *Heat, Mass, and Momentum Transfer*, Prentice-Hall, Englewood Cliffs, New Jersey, 1961, p. 64. A more complete list is in R. H. Perry and C. H. Chilton (Eds.), *Chemical Engineers' Handbook*, fifth edition, McGraw-Hill, New York, NY, 1973, pages 5-35 to 5-38.

For example, if a pipe network contains 6 m of pipe with an inside diameter of 21 mm, two elbows (90°, medium radius), and a wide open gate valve, then the  $L/D$  ratio to be substituted into Eq. (4.15) would be

$$\begin{aligned} \left[ \frac{L}{D} \right] &= \left[ \frac{L}{D} \right]_{\text{pipe}} + 2 \left[ \frac{L_e}{D} \right]_{\text{elbow}} + \left[ \frac{L_e}{D} \right]_{\text{valve}} \\ &= \frac{6}{0.021} + (2)(26) + 7 = 345. \end{aligned}$$

#### 4.5 FLOW THROUGH SMOOTH BENDS AND COILS

In curved pipes, the friction loss may rise considerably above the values for straight lengths of pipe, and the transition Reynolds number may be much higher than 2100. The maximum Reynolds number for laminar flow, or critical Reynolds number,  $Re_c$ , is given as a function of the coil diameter  $D_c$  and pipe diameter  $D$ :<sup>2</sup>

$$Re_c = 20,000 \left[ \frac{D_c}{D} \right]^{0.32}, \quad 15 < \frac{D_c}{D} < 860. \quad (4.18)$$

The friction loss for laminar flow in a curved pipe can be expressed in terms of the ratio of the friction factor for the curved pipe to that for the same length of straight pipe. This

ratio is a function of  $\text{Re}(D/D_c)^{1/2}$ , which is given in a publication by Babcock and Wilcox.<sup>3</sup> The effect of curvature on the friction factor for laminar flow is negligible for  $\text{Re}(D/D_c)^{1/2} < 10$ .

We can compute the friction loss for turbulent flow by using Eq. (4.15) and applying the ratio of curved-to-straight pipe friction factors,  $f_c/f_s$ , given by<sup>4</sup>

$$\frac{f_c}{f_s} = \left[ \text{Re} \left( \frac{D}{D_c} \right) \right]^{1/20} \quad (4.19)$$

for  $\text{Re}(D/D_c)^2 > 6$ .

## 4.6 FLOW MEASUREMENT

Efficient operation and control of engineering processes and experimental set-ups often require information concerning the quantities of flowing fluids. For measuring flow in closed conduits, there is a variety of measuring devices available; for example, velocity meters, head meters, or area meters. Although all of them can be used to determine the mass-flow rate, which is the information usually needed, none can measure the flow *directly*, so that, particularly in the case of compressible fluids, the meters require careful calibration. The devices described in this section are based on applying Eq. (4.11). Other devices for flow measurement and flow visualization are described in Appendix E.

### 4.6.1 Velocity meters

A commonly encountered velocity meter is the Pitot-static tube which measures local velocities. The Pitot tube consists essentially of a tube with an open end facing the stream, as shown in Fig. 4.7. The velocity of the fluid along the streamline  $x-y$  decreases to zero at  $y$  which corresponds to the tip of the Pitot-tube opening, and is called the stagnation point. Applying Eq. (4.11) between planes (1) and (2) along the streamline  $xy$  we have

$$\frac{P_2}{\rho} + 0 = \frac{P_1}{\rho} + \frac{v_1^2}{2}, \quad (4.20)$$

where  $P_1$  denotes the upstream pressure, and  $v_1$  the approach velocity. The pressure  $P_2$ , which is called the stagnation pressure, is made up of two parts: (1) the pressure to be measured if the fluid were not moving—the static pressure, and (2) the pressure resulting from the sudden cessation of the streamline's kinetic energy—the velocity pressure. In other words,

$$P_2 = P_1 + \frac{\rho v_1^2}{2},$$

which is, in fact, a rearrangement of Eq. (4.20). The construction of the Pitot tube in Fig. 4.7 shows the static holes; at these locations, static pressure is measured, while the pressure differential  $P_2 - P_1$  is measured by the complete assembly. Thus, after including a

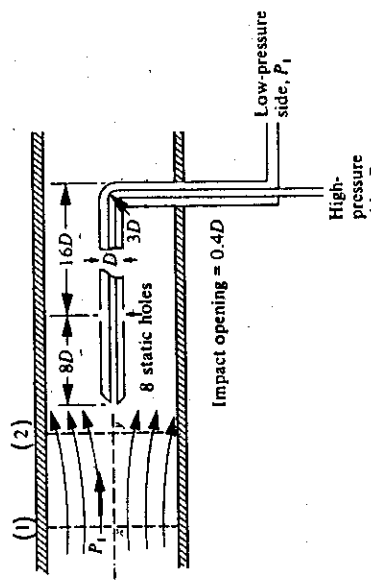


Fig. 4.7 Pitot-static tube and recommended dimensional relationships.

calibration constant  $C_p$  which takes care of nonideal behavior in the system, we rewrite Eq. (4.20) to yield the velocity of the fluid:

$$v_1 = C_p \left[ \frac{2}{\rho} (P_2 - P_1) \right]^{1/2}; \quad (4.21)$$

$C_p$ , which is sometimes called the Pitot-tube coefficient, usually has a value between 0.98 and 1.00.

Because the Pitot tube measures only local velocities, a traverse of the conduit must be made in order to obtain the complete profile, and from it the average velocity  $\bar{V}$ . To obtain the density  $\rho$ , we usually measure the temperature upstream from the probe tip. In the flow in a straight circular pipe at points preceded by a run of at least 50 diameters without obstructions, the ratio of  $V_{\max}$  (the velocity measured at the center line) to  $\bar{V}$  (the average velocity) can be found by relating the ratio to the Reynolds number. For laminar flow, of course,

$$\frac{\bar{V}}{V_{\max}} = \frac{1}{2}, \quad 0 < \text{Re} < 2.1 \times 10^3, \quad (4.22)$$

and for a large region of the turbulent range, namely,  $10^4 < \text{Re} < 10^7$ ,

$$\frac{\bar{V}}{V_{\max}} = 0.62 + 0.04 \log \left[ \frac{DV_{\max}\rho}{\eta} \right]. \quad (4.23)$$

In the range  $2.1 \times 10^3 < \text{Re} < 10^4$ , a traverse must be made because  $\bar{V}/V_{\max}$  is not predictable.

For gases at low flow rates ( $< 60 \text{ m s}^{-1}$ ) and isothermal flow conditions, we may use Eq. (4.21) as it is. However, if there is a substantial temperature rise (high velocity), then an energy balance must be made between the upstream point, at which a temperature is measured, and the tip of the Pitot tube. For this case, Bernoulli's equation should be written

$$\int_{P_1}^P \frac{dP}{\rho} = \frac{v_i^2}{2}. \quad (4.24)$$

<sup>3</sup>Steam—Its Generation and Use, Babcock & Wilcox, New York, NY, 1963, pages 8-17.

<sup>4</sup>H. Ito, *ibid.*

If the fluid is a compressible gas, we may assume that the flow is adiabatic and the gas ideal; thus the equation of state is

$$P \left[ \frac{1}{\rho} \right]^\gamma = \text{constant}, \quad (4.25)$$

where  $\gamma$  is the ratio of the heat capacity at constant pressure to that at constant volume. Integrating Eq. (4.24) by using Eq. (4.25) yields

$$v_1 = C_p \sqrt{\left[ \frac{2\gamma}{\gamma - 1} \right] \left[ \frac{P_1}{\rho_1} \right] \left[ 1 - \left( \frac{P_1}{P_2} \right)^{1-\gamma/\gamma} \right]} \quad (4.26)$$

**Example 4.3** A Pitot-static tube is installed with its impact opening along the centreline of a long pipe with an inside diameter of 300 mm. Air at 339 K and  $8.27 \times 10^4 \text{ N m}^{-2}$  (gauge pressure) passes through the pipe; the barometric pressure is 145 mm Hg ( $9.93 \times 10^4 \text{ N m}^{-2}$ ). The pressure difference measured by the Pitot-static tube is 10.7 mm water. Calculate the mass flow rate in the pipe.

**Solution.** The absolute pressure in the pipe where  $P_1$  is measured is

$$P_1 = 8.27 \times 10^4 + 9.93 \times 10^4 = 1.82 \times 10^5 \text{ N m}^{-2}.$$

At this pressure and 339 K, the gas density is

$$\begin{array}{c|c|c|c|c|c} 1 \text{ mol} & 1.82 \times 10^5 \text{ N m}^{-2} & 273 \text{ K} & 28.8 \text{ g} & 1 \text{ kg} \\ \hline 0.0224 \text{ m}^3 & 1.0133 \times 10^5 \text{ N m}^{-2} & 339 \text{ K} & 1 \text{ mol} & 1000 \text{ g} \\ \hline & & & & & \end{array}$$

$$= 1.86 \text{ kg m}^{-3}$$

The manometer fluid used to measure the pressure drop is water so we need the conversion between height of water and pressure; it is  $1 \text{ N m}^{-2} = 0.1020 \text{ mm water}$ . Therefore

$$P_2 - P_1 = \frac{10.7 \text{ mm H}_2\text{O}}{0.1020 \text{ mm H}_2\text{O}} = 1.049 \times 10^2 \text{ N m}^{-2}.$$

Now we utilize Eq. (4.21) to determine  $V_{\max}$  (assume  $C_p = 1$ ):

$$v_1 = V_{\max} = \left[ \frac{2 \text{ m}^3}{1.86 \text{ kg}} \mid \frac{1.049 \times 10^2 \text{ N}}{\text{m}^2} \mid \frac{1 \text{ kg m}}{1 \text{ N s}^2} \right]^{1/2} = 10.6 \text{ m s}^{-1}.$$

To find the average velocity, we utilize Eq. (4.23):

$$\frac{\bar{V}}{V_{\max}} = 0.62 + 0.04 \log \left[ \frac{(0.3)(10.6)(1.86)}{2.03 \times 10^{-5}} \right] = 0.84$$

Therefore, the mass flow rate  $W$  can finally be determined:

$$W = \frac{(0.84)(10.6) \text{ m}}{\text{s}} \mid \frac{(\pi)(0.3)^2 \text{ m}^2}{4} \mid \frac{1.86 \text{ kg}}{\text{m}^3} = 1.17 \text{ kg s}^{-1}.$$

#### 4.6.2 Head meters

There are essentially three types of head meters. They are so called because all of them place some sort of restriction in the flow line, causing a local increase in the velocity of the fluid and a corresponding decrease in the pressure *head*. The simplest is perhaps the *orifice plate* illustrated in Fig. 4.8; however, the *Venturi meter* and *flow nozzle* (Figs. 4.9 and 4.10) are based on the same principle, and the same group of equations apply to all of them.

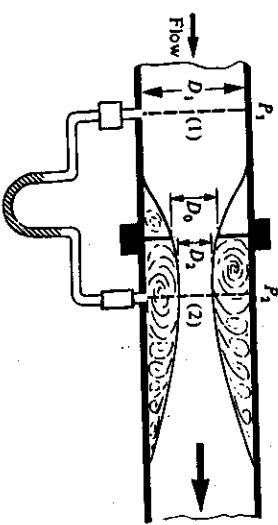


Fig. 4.8 Orifice meter.

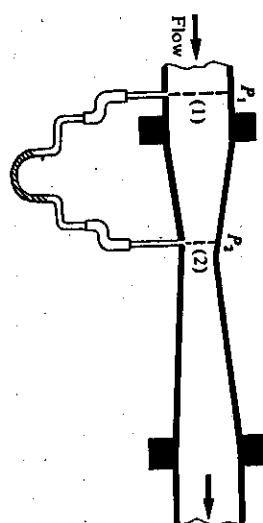


Fig. 4.9 Venturi meter.

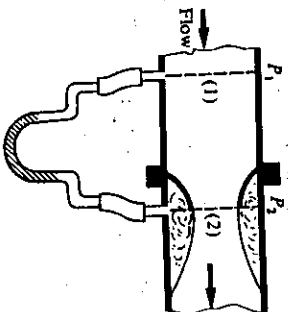


Fig. 4.10 Flow nozzle.

\*We discuss the term *head* in Chapter 5.

Specifically, consider the orifice meter in Fig. 4.8, which is of very simple construction. A thin plate with a centrally located circular hole is inserted into the duct, and, as indicated, the flow contracts before the hole, and continues to contract for a short distance downstream from the orifice to the location of the smallest flow section, known as the *vena contracta*. If we apply Eq. (4.11) to the system between (1) and (2), and neglect friction loss for the time being, then the mechanical energy balance (for incompressible fluids) with  $\beta = 1$  is

$$\frac{P_2 - P_1}{\rho} + \frac{\bar{V}_2^2}{2} - \frac{\bar{V}_1^2}{2} = 0. \quad (4.27)$$

Also, for incompressible fluids (by continuity),

$$\bar{V}_1 = \left[ \frac{D_2}{D_1} \right]^2 \bar{V}_2, \quad (4.28)$$

so that when Eq. (4.27) is solved for  $\bar{V}_2$  in terms of the difference in pressure between the taps, we obtain

$$\bar{V}_2 = \left[ \frac{2(P_1 - P_2)}{\rho \left[ 1 - \left( \frac{D_2}{D_1} \right)^4 \right]} \right]^{1/2}. \quad (4.29)$$

This is the theoretical velocity at the *vena contracta*, which disregards frictional energy losses and can never be achieved in practice. Therefore we utilize a *discharge coefficient*  $C_D$  which accounts for such losses and an additional geometric factor. The largest pressure drop is measured at the *vena contracta*, but it is more convenient to relate the velocity at the orifice plate  $\bar{V}_o$  to the pressure drop,  $(P_1 - P_2)$ , and at the same time use the diameter of the plate opening  $D_o$  instead of the diameter of the *vena contracta*. Thus we get the final form of the expression

$$\bar{V}_o = C_D \left[ \frac{2}{\rho} \frac{(P_1 - P_2)}{(1 - B^4)} \right]^{1/2}, \quad (4.30)$$

in which  $B = D_o/D_1$ , or

$$\bar{V}_o = K \left[ \frac{2}{\rho} (P_1 - P_2) \right]^{1/2}, \quad (4.31)$$

where  $K$  is the *flow coefficient*, defined as  $C_D / \sqrt{1 - B^4}$ .

Equations (4.30) and (4.31) also apply to venturi and nozzle meters as well as to orifice plates, but, as will be discussed below,  $C_D$  and  $K$  are quite different. In addition, for both venturi and nozzle meters, as shown in Figs. 4.9 and 4.10, the minimum flow contraction corresponds to the position where  $P_2$  is measured, hence  $D_2 = D_o$ , and  $\bar{V}_2 = \bar{V}_o$ . For liquids (incompressible fluids), the mass flow rate is

$$W = KA_o \sqrt{2\rho(P_1 - P_2)}. \quad (4.32)$$

For gases, we can modify this equation to a more general form, utilizing the *expansion factor*  $Y$ ,

$$W = KYA_o \sqrt{2\rho(P_1 - P_2)}. \quad (4.33)$$

Expansion factors for gases are different for each type of head meter; these are summarized in Table 4.3. For convenience, Fig. 4.11 shows values of  $Y$  for each of the above meter types. For liquids,  $Y$  is taken to be unity, as it is also for gases when the pressure difference is small compared with the total pressure.

Table 4.3 Expansion factors  $Y$  for flow meters\*

Meter type	$Y$
Venturi and nozzle	$\left[ \frac{\gamma(1 - r^{1-1/\gamma})(1 - B^4)}{(\gamma - 1)(1 - r)r^{-2\gamma} - B^4} \right]^{1/2}$
Orifice (square-edged)	$1 - \left[ \frac{1 - r}{Y} \right] (0.41 + 0.35B^4)$

\*In these expressions for  $Y$ ,  $r = P_2/P_1$  and  $\gamma = C_p/C_v$ .

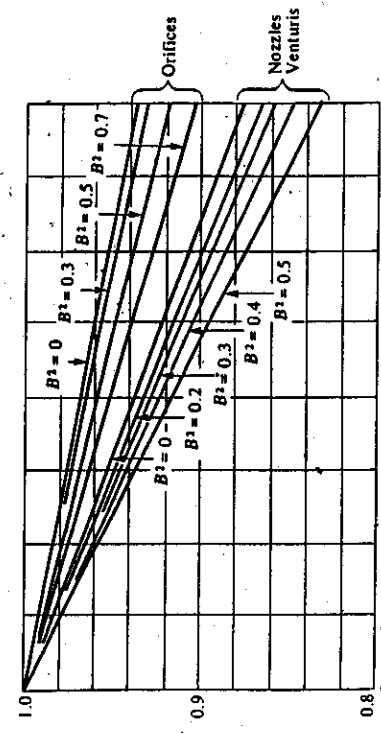


Fig. 4.11 Expansion factors for gases flowing through various head meters. (From Perry and Chilton, *ibid.*, page 5-11.)

For the orifice plate, we have to choose: (1) whether to use a square-edged hole, or one with a 45°-taper and a knife-edge inlet, and (2) where to locate the pressure taps with respect to the plate. Figure 4.12 illustrates the effect of various locations of taps on the flow coefficient, and shows how the stream is narrowed as it leaves the orifice plate, reaching a minimum at the *vena contracta*. In most cases, the upstream tap is located from one to two pipe diameters ahead of the plate, and the downstream tap either one-half of a pipe diameter downstream or exactly at the *vena contracta*, which would have to be found experimentally. As specified in the legend, the data of Fig. 4.12 apply specifically to square-edged circular orifices. Generally, such data depend to some extent on the exact design of the orifice plate.

Orifice plates are the simplest and cheapest types of head meters, but they also cause the largest permanent pressure drop in the system. This refers to the fact that the pressure difference,  $P_1 - P_2$ , across the orifice is not entirely lost, and a partial pressure recovery is experienced downstream. The results of experiments indicate that the permanent loss of pressure for orifice plates is given by

$$\Delta P_{\text{loss}} = (1 - B^2)(P_1 - P_2). \quad (4.34)$$

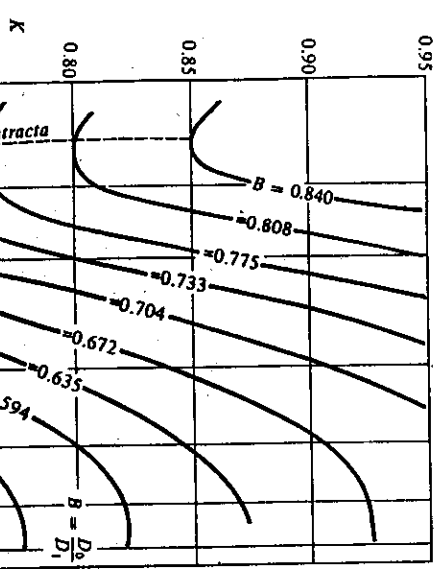


Fig. 4.12 Effect of tap locations on the flow coefficient. Applies to square-edged circular orifices

with  $Re$  (at the orifice) greater than 30 000. (From Perry and Chilton, *ibid.*, page 5-12.)

In metallurgical operations, molten metal is contained in refractory lined vessels (ladles). These ladles transport the metal to various points within a plant where molten metal is required. It is desirable to know the time required to completely or partially empty a ladle.

As a means of applying Bernoulli's equation, consider the vessel depicted in Fig. 4.13. The liquid level is obviously constant if the mass flow rates of the incoming and discharging streams are equal. For this steady-state system,  $P_1 = P_2$ ,  $M^* = 0$ , and  $\bar{V}_2^2 \gg \bar{V}_1^2$ ; thus Eq. (4.11) reduces to

$$\frac{\bar{V}_2^2}{2g} + g\Delta z + E_f = 0. \quad (4.35)$$

The friction loss  $E_f$  for this system is entirely due to the contraction nozzle, and we can evaluate it by the method applied in Section 4.3:

$$E_f = \frac{1}{2} e_f \bar{V}_2^2. \quad (4.36)$$

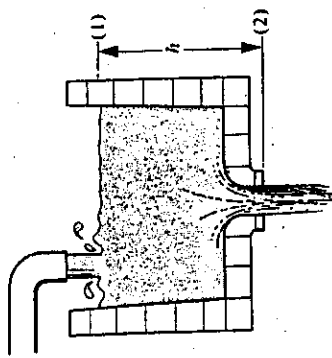
Combining Eqs. (4.35) and (4.36) yields

$$\frac{\bar{V}_2^2}{2} \left[ \frac{1}{\beta_2} + e_f \right] + g\Delta z = 0. \quad (4.37)$$

<sup>5</sup>G. F. Round and V. K. Gorg, *Applications of Fluid Dynamics*, Edward Arnold, London, 1986, page 394.

<sup>6</sup>Fluid Meters: Their Theory and Application, sixth edition, ASME, New York, 1971.

<sup>7</sup>R. H. Perry and C. H. Chilton (Eds.), *Chemical Engineers' Handbook*, fifth edition, McGraw-Hill, New York, NY, 1973, pages 5-12 to 5-15.

Fig. 4.13 Flow from a vessel in which  $h$  can be maintained constant.

For a given nozzle, we can evaluate the term in parentheses, which relates to the flow. As a vessel empties,  $\beta_2$  may change as well as  $\epsilon_f$ , which is a function of the Reynolds number. However, it is common engineering practice to recognize that  $\bar{V}_2 = \sqrt{2gh}$  represents the maximum possible velocity of the exit stream, and then to assign a discharge coefficient  $C_D$  to a real situation:

$$\bar{V}_2 = C_D \sqrt{2gh} \quad (4.39)$$

By comparing Eqs. (4.38) and (4.39), we can compute the discharge coefficient:

$$C_D = \left[ \frac{1}{\beta_2} + \epsilon_f \right]^{-1/2} \quad (4.40)$$

Now consider the case when the mass flow of the incoming stream is reduced so that the liquid level gradually diminishes. Then the velocity of the exit stream changes with time, but the velocity at any instant is still given by Eq. (4.39), where  $h$  is the liquid level at that instant. Finally, if the vessel contains a liquid and no liquid enters at the top, and then a bottom plug is removed, Eq. (4.39) still applies, but  $h$  becomes a function of time. This is the situation that applies to ladles; Fig. 4.14 shows a typical ladle design for molten steel.

The mass flow rate discharging from the ladle with a nozzle of area  $A_N$  is given by

$$\frac{dw}{dt} = A_N \rho \bar{V}_2, \quad (4.41)$$

so that

$$\frac{dw}{dt} = A_N \rho C_D \sqrt{2gh} \quad (4.42)$$

The integration limits at time  $t = 0$ , are  $h = h_0$ , and  $w = w_0$ .

$$\int_{w_0}^{w_h} \frac{dw}{\sqrt{2gh}} = A_N \rho \int_0^t C_D dt. \quad (4.43)$$

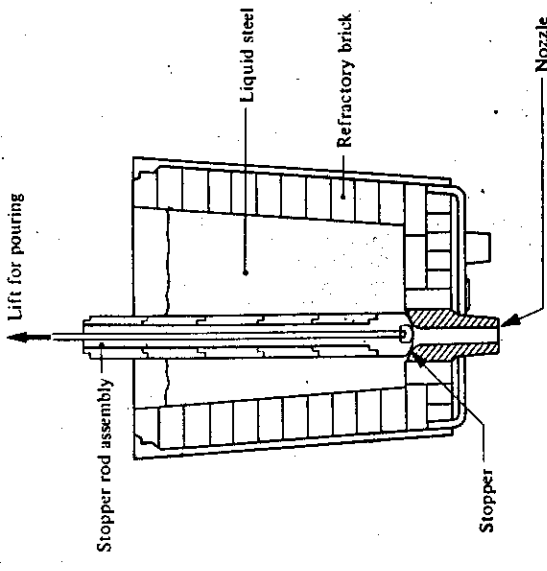


Fig. 4.14 Single-nozzle bottom-pour ladle for steel.

It is usually assumed that  $C_D$  is constant; also, many ladles have a constant circular cross section of  $\pi D_L^2/4$ , so that

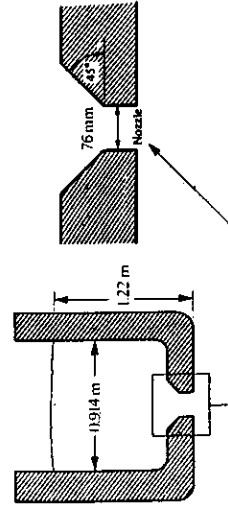
$$dw = -\rho \frac{\pi D_L^2}{4} dh. \quad (4.44)$$

$$t_f = \frac{\pi D_L^2}{2A_N C_D} \left[ \frac{h_0}{2g} \right]^{1/2} \quad (4.45)$$

Thus we obtain the time  $t_f$  to completely empty the ladle by integrating Eq. (4.43):

- Example 4.4** A ladle with an inside diameter of 0.914 m and a capacity height of 1.22 m has a nozzle that tapers  $\pi/4$  radians ( $45^\circ$ ) to a 76 mm exit diameter.  
 a) Calculate the time to empty the ladle if it is filled with Al-7% Si alloy at 977 K.  
 b) Calculate the discharge rate ( $\text{kg s}^{-1}$ ) initially and when the ladle is 75% empty.

Data:  $\eta = 2.75 \times 10^3 \text{ N s m}^{-1}$ ;  $\rho = 2400 \text{ kg m}^{-3}$ .



**Solution.** Equation (4.45) may be utilized if it is reasonable to treat  $C_D$  as a constant. Because  $\epsilon_f$  and  $\beta_2$  both depend on the Reynolds number through the nozzle,  $C_D$  is actually a function of the depth of the melt. Let us first examine the manner in which  $C_D$  varies. This involves calculating the friction loss factor for flow through a contraction; hence we use Figs. 4.4 and 4.5.

### Completely Full

Re is estimated by assuming  $C_D = 1$ .

$$\bar{V}_2 = \sqrt{2gh} = [(2)(9.8)(1.22)]^{1/2} = 4.89 \text{ m s}^{-1}$$

$$Re = \frac{D\bar{V}_2\rho}{\eta} = \frac{(0.076)(4.89)(2400)}{2.75 \times 1.0^{-3}} = 3.24 \times 10^5$$

$$\epsilon_f = (0.4) \left[ \frac{1}{6} \right] = 0.067$$

$$\beta_2 = 1 \text{ (flow is turbulent)}$$

$$C_D = (1 + 0.067)^{-1/2} = 0.97$$

Nearly empty (assume only 4 mm remain)

$$\bar{V}_2 = [(2)(9.8)(0.004)]^{1/2} = 0.28 \text{ m s}^{-1}$$

$$Re = \frac{(0.076)(0.28)(2400)}{2.75 \times 1.0^{-3}} = 1.86 \times 10^4$$

$$\epsilon_f = (0.5) \left[ \frac{1}{6} \right] = 0.083$$

$$C_D = (1 + 0.083)^{-1/2} = 0.96$$

It is certainly reasonable to assume that  $C_D$  is constant, so we can use Eq. (4.45).

a) With  $A_N = \pi D_N^2/4$ , we can write:

$$t_f = \frac{2(D_L/D_N)^2}{C_D} \left[ \frac{h_0}{2g} \right]^{1/2}$$

$$t_f = \frac{2(0.914/0.076)^2}{0.97} \left[ \frac{1.22}{(2)(9.8)} \right]^{1/2}$$

$$t_f = 74.4 \text{ s}$$

b) The discharge rate is calculated with Eq. (4.41).

$$A_N = \frac{\pi D_N^2}{4} = \frac{(\pi)(0.076)^2}{4} = 4.54 \times 10^{-3} \text{ m}^2$$

Initial discharge rate (1.22 m level):

$$\frac{dw}{dt} = A_N \rho \bar{V}_2 = (4.54 \times 10^{-3})(2400)(4.89)(0.97) \\ = 51.7 \text{ kg s}^{-1}.$$

Discharge rate at 75% empty (0.305 m level):

$$\frac{dw}{dt} = 51.6 \left[ \frac{1}{4} \right]^2 = 25.8 \text{ kg s}^{-1}.$$

### 4.8 FLOW THROUGH PIPING NETWORKS

All of the effects of individual fittings, flow devices, pipe diameters, etc., on flow through fluid systems combine and must be considered when total systems involving pumps, valves and nozzles are put together. The goal of such systems is to provide fluid to particular locations at specified rates. In many cases, a single main supply line and pump are used to distribute fluid to a network of pipes that supply several outlets, such as spray cooling or internal cooling of process equipment or products. If the effects of variation of resistance to flow and therefore on flow quantity are not understood, unintended maldistribution of flow can occur.

Consider the system in Fig. 4.15. Let us assume that we want to deliver the same flow rate from each nozzle:

$$Q_1 = Q_2 = Q_3 = \frac{Q_0}{3}$$

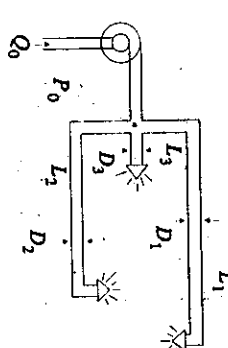


Fig. 4.15 Flow in network.

Since the pressure drop from the branch point, where  $P = P_0$ , to the atmosphere is the same,

$$\Delta P_1 = \Delta P_2 = \Delta P_3 = (P_0 - P_{atm})$$

But the flow through a nozzle (Fig. 4.16) depends on the pressure of the nozzle entrance; see Table 4.4. For a given nozzle, as the pressure in the line behind it decreases, so does the flow. On the other hand, it can be seen that by picking a small orifice, the pressure drop across the nozzle can be very large for a similar flow, e.g., a hollow cone nozzle with a 0.218 in. orifice will deliver 1.25 gal/min at 10 psi pressure, whereas a 0.140 in. orifice will deliver 1.50 gal/min flow with a 100 psi pressure.

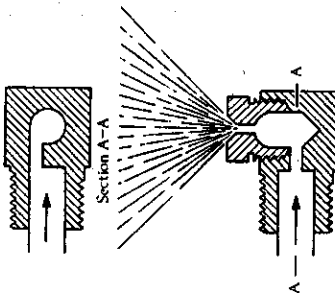


Fig. 4.16 A hollow-cone nozzle of the tangential type. (From R. H. Perry, C. H. Chilton, and S. D. Kirkpatrick, *Chemical Engineers' Handbook*, fourth edition, McGraw-Hill, New York, NY, 1963, page 18-63.)

Table 4.4 Discharge rates and included angle of spray from pressure nozzles. (From R. H. Perry, C. H. Chilton, and S. D. Kirkpatrick, *ibid.*, page 18-65.)

Nozzle type	Orifice diameter, in.	Discharge, gal/min, and included angle of spray					
		10 psi	25 psi	50 psi	100 psi	Angle, deg.	Angle, deg.
Hollow cone	0.046	—	0.10	0.135	0.183	75	
	0.140	0.535	0.81	1.10	1.50	93	
Solid cone	0.218	1.25	1.88	2.55	3.45	92	
	0.375	7.2	11.8	16.5	20		
Fan	0.047	—	0.167	0.235	0.34	70	
	0.188	1.60	5.5	3.42	60	4.78	60
	0.250	3.35	6.5	5.40	7.50	70	75
	0.500	17.5	86	27.5	84	38.7	73
	0.031	0.085	40	0.132	90	0.182	110
	0.093	0.70	70	1.12	76	1.57	80
	0.187	2.25	50	3.70	59	5.35	65
	0.375	9.50	66	15.40	74	22.10	75

Note: 1 gal/min (gallon per minute) =  $6.309 \times 10^{-3} \text{ m}^3 \text{ s}^{-1}$ ; 1 psi ( $\text{lb/in}^2$ ) =  $6895 \text{ N m}^{-2}$ .

If the nozzle pressure at the desired flow is high enough, the pressure drop down the length of feed pipe at that flow rate,  $\Delta P_{\text{pipe}}$ , will be negligible by comparison to the drop across the nozzle. Then, although not exactly the same, the flows out of each nozzle will be close to each other. On the other hand, if the length of pipe is long, so that  $\Delta P_{\text{pipe}}$  is on the same order as  $\Delta P_{\text{nozzle}}$ , the flows will be different unless the pipe diameters are adjusted so that

$$\Delta P_{\text{pipe1}} = \Delta P_{\text{pipe2}} = \Delta P_{\text{pipe3}}$$

For this to be the case with  $Q_1 = Q_2 = Q_3$ , then

$$L_1 D_1^3 = L_2 D_2^3 = L_3 D_3^3 \quad (4.46)$$

because

$$\Delta P_{\text{pipe}} = \left[ \frac{32 f p}{\pi^2} \right] L D^{-5} Q^2, \quad (4.47)$$

Given  $L_1$ ,  $L_2$  and  $L_3$  and the value of one of the pipe diameters to obtain the required  $Q$ , the remaining diameters can be calculated.

### PROBLEMS

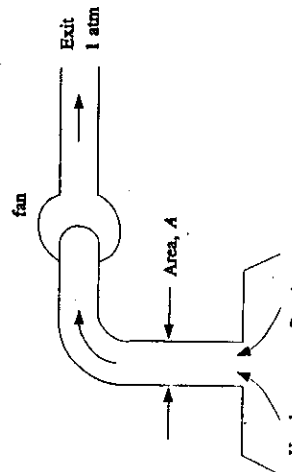
4.1 The reciprocal of  $\beta$ , as defined in Eq. (4.4) is called the kinetic energy correction factor. Derive the kinetic energy correction factors for the following flows:

- a) fully developed, laminar flow between infinite parallel plates;
- b) Hagen-Poiseuille flow in a circular tube;
- c) turbulent flow, in a tube of radius  $R$ , described by

$$\bar{V} = \left[ \frac{r}{R} \right]^n$$

where  $n = 1/7$ .

4.2 A fan is used to draw exhaust gases from a large hood. For highly turbulent flow, write an equation for the system which gives  $-M^* \rho$  as a function of volume flow rate,  $Q$ . Neglect potential energy changes because a gas is being exhausted. For friction include only the contraction ( $e_f = 0.4$ ), the expansion ( $e_f = 1.0$ ) and the elbow ( $L/D_e = 20, f = 20, f = 0.001$ ). Note that  $-M^* \rho$  has units of pressure and represents the "total pressure" against which the fan must operate.

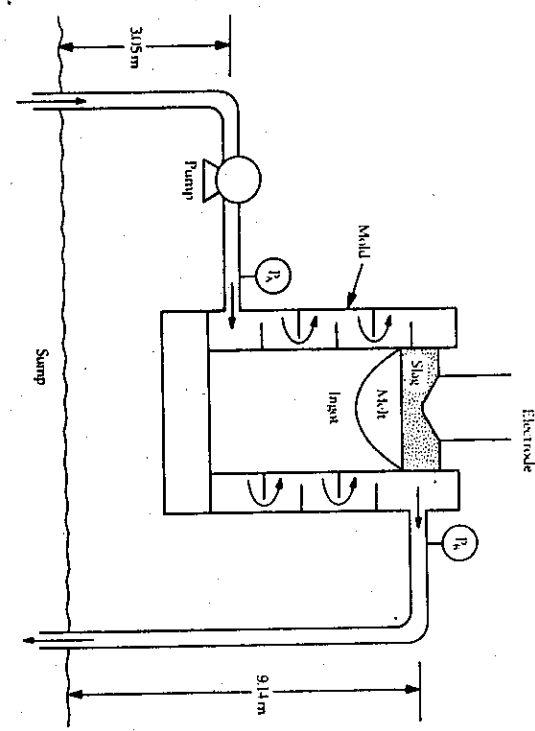


4.3 Cooling water is provided to the mold used in the electroslag remelting process depicted below. For flow through the mold,

$$E_f = K \bar{V}^2$$

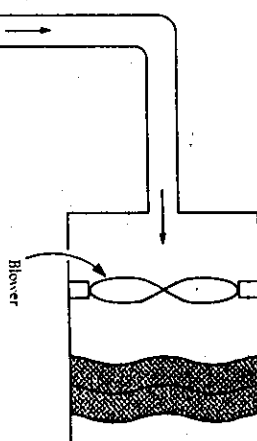
where  $\bar{V}$  is the average velocity of the water in the lines at the entrance and exit of the mold and  $K$  is a turbulent flow constant for the mold. When the pressure gauges read  $P_A = 2.76 \times 10^5 \text{ N m}^{-2}$  and  $P_B = 2.07 \times 10^5 \text{ N m}^{-2}$ , the volume flow rate is  $2.83 \times 10^{-3} \text{ m}^3 \text{ s}^{-1}$ . Calculate  $-M^* \rho$  (in  $\text{N m kg}^{-1}$ ) for the pump when the volume flow rate is  $5.66 \times 10^{-3} \text{ m}^3 \text{ s}^{-1}$ . Assume that friction losses through the straight lengths of pipes can be ignored. Data:  $D$  (pipes) = 15.4 mm;  $f = 0.001$ ;  $L_e/D = 26$  (elbows);  $e_f$  (entrance) = 0.8;  $e_f$  (exit) = 1.

**4.5** Water is pumped from a storage tank to a mold designed to produce nonferrous ingots by the "direct-chill" process. The water supply is at ambient pressure ( $1.0133 \times 10^5 \text{ N m}^{-2}$ ), and the water leaving the mold impinges upon the surface of the ingot which is also at ambient pressure. A pressure gauge mounted in the manifold portion of the mold (pressure gauge  $P$  in the diagram) indicates an absolute pressure of  $1.22 \times 10^5 \text{ N m}^{-2}$ , when the volume flow rate is  $3.93 \times 10^{-3} \text{ m}^3 \text{ s}^{-1}$ . The water level in the tank is 3 m, and the vertical length of the pipe is 3 m. Calculate the theoretical power of the pump. Assume that the tank for the water supply has a very large diameter, and that the kinetic energy of the water within the manifold portion of the mold is negligible. *Piping Information:* total length of straight pipe, 9.14 m; diameter, 30.5 mm;  $L/D = 25$  (elbows);  $f = 0.004$ ;  $e_f$  (contraction) = 0.4;  $e_f$  (expansion) = 0.8.



**4.4** A blower draws air from a melting area and directs the air to a "bag house" where particulates are filtered before the air is discharged to the environment. The melting area and the environment are at ambient temperature and pressure (289 K and  $1.0133 \times 10^5 \text{ N m}^{-2}$ , respectively). When the pressure drop across the bag house ( $\Delta P$ ) in the diagram is  $5.07 \times 10^3 \text{ N m}^{-2}$ , the volume flow rate is  $0.944 \text{ m}^3 \text{ s}^{-1}$ . Calculate the work done by the blower in N m per kg of air delivered by the blower. *Conduit Information:* length before elbow, 61 m; length after elbow, 61 m; diameter, 305 mm;  $L/D = 25$  (elbows);  $f = 0.0043$ ;  $e_f$  (contraction) = 0.4;  $e_f$  (expansion) = 0.8.

Bag house



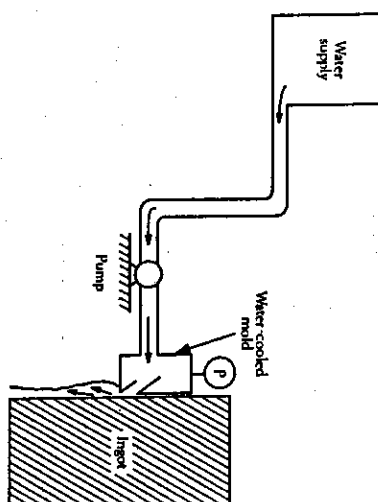
**4.6** Water, maintained at a constant level, is supplied to a long line from a filter tank filled with sand. There are two vertical branches attached to the main line as shown in the accompanying figure; these branches and the tank are open to ambient pressure (i.e.,  $1.0133 \times 10^5 \text{ N m}^{-2}$ ). At the end of the line there is a frictionless valve.

a) When the valve is closed, what are the heights  $h_1$  and  $h_2$  in the vertical branches?

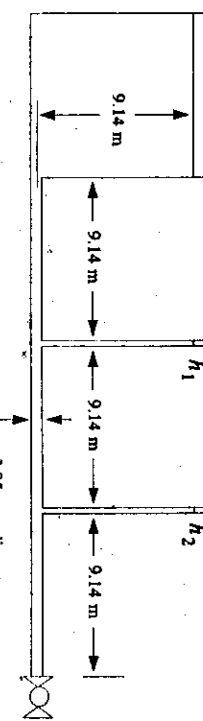
b) When the valve is open, what is the mass flow rate?

c) When the valve is open, what is the difference in height between  $h_1$  and  $h_2$ ?

Data:  $\rho = 1,000 \text{ kg m}^{-3}$ ;  $\eta = 1 \times 10^{-3} \text{ N s m}^{-2}$ ;  $\epsilon/D$  (relative roughness) = 0.01;  $\omega$  (sand) = 0.40;  $D_p$  (sand) =  $152 \mu\text{m}$ .

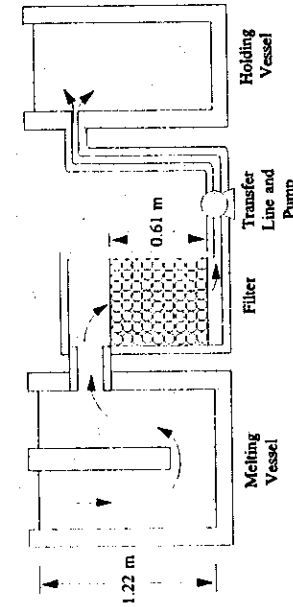


**4.7** Liquid aluminum contains a small fraction of  $\text{Al}_2\text{O}_3$  inclusions which are removed by filtering through a bed of ceramic spheres. The refined aluminum (i.e., filtered aluminum) is pumped to a holding vessel from which liquid metal is drawn to cast ingots. For the equipment arrangement shown below, calculate the theoretical power of the pump to process  $2.52 \text{ kg s}^{-1}$ . The important friction losses are in the filter bed, the transfer line which contains two  $90^\circ$  elbows (medium radius), and the entrance and exit.

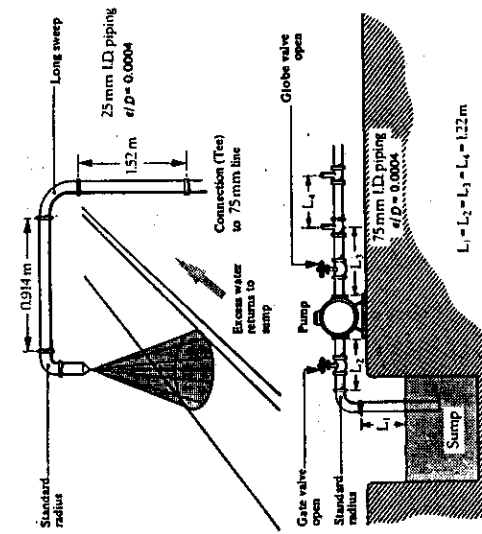


**Data:** Aluminum:  
 $\rho = 2644 \text{ kg m}^{-3}$   
 $\eta = 1.28 \times 10^{-3} \text{ N s m}^{-2}$   
 $\omega = 0.4$   
 $D_p = 0.61 \text{ mm}$   
 $\text{Area (bed)} = 0.292 \text{ m}^2$

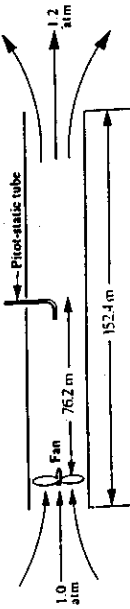
Ceramic spheres:  
 $L(\text{straight portions}) = 1.83 \text{ m}$   
 $D = 9.1 \text{ mm}$   
 $\epsilon(\text{roughness}) = 9.1 \times 10^{-4} \text{ mm}$



**4.8** Hot-rolled steel sheet is quenched by passing under two water sprays as depicted below. Each spray requires  $9.46 \times 10^{-4} \text{ m}^3 \text{ s}^{-1}$  of water at 294 K, and the pressure drop across each nozzle at this flow rate is  $1.72 \times 10^5$ . Calculate the theoretical power required by the pump.



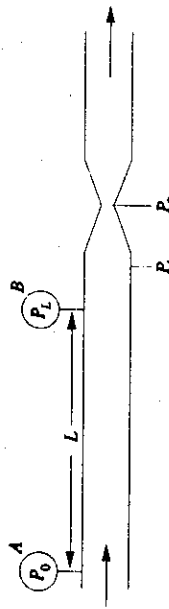
**4.9** A fan draws air at rest and sends it through a straight duct 152 m long. The diam. of the duct is 0.61 m and a Pitot-static tube is installed with its impact opening along the center line. The air enters at 300 K and 1 atm and discharges at 1.2 atm. Calculate the theoretical work (in  $\text{N m kg}^{-1}$ ) of the fan if the Pitot-static tube measures a pressure difference of 25.4 mm of water. (Note: 1 atm =  $1.0133 \text{ N m}^{-2}$ )



- 4.10** Compressed air at  $6.9 \times 10^5 \text{ N m}^{-2}$  and 310 K flows through an orifice plate meter installed in a 75 mm I.D. pipe. The orifice has a 25 mm hole and the downstream pressure tap location is 38 mm from the plate. When the manometer reading is 358 mm Hg,  
 a) What is the flow rate of air?  
 b) What is the permanent pressure drop?

- 4.11** A venturi meter is installed in an air duct of circular cross-section 0.46 m in diameter which carries up to a maximum of  $1.18 \text{ m}^3 \text{ s}^{-1}$  of air at 300 K and  $1.1 \times 10^5 \text{ N m}^{-2}$ . The throat diameter is 230 mm.  
 a) Determine the maximum pressure drop that a manometer must be able to handle, i.e., what range of pressure drops will be encountered? Express the results in mm of water.  
 b) Instead of the venturi meter, an orifice meter is proposed and the maximum pressure drop to be measured is 50 mm of water. Calculate what diameter of sharp-edged orifice should be installed in order to obtain the full scale reading at maximum flow.  
 c) Estimate the permanent pressure drop for the devices in parts a) and b).  
 d) If the air is supplied by a blower operating at 50% efficiency, what is the power consumption associated with each installation?

- 4.12** Liquid flows through a long straight tube and then through a Venturi meter. Pressure gauges A and B measure the pressure drop for a tube length  $L$ , and  $P_1$  and  $P_2$  are the pressures for the manometer used with the Venturi. Derive an equation for the ratio of the two pressure drops,  $(P_0 - P_D)/(P_1 - P_2)$  in terms of  $f$ ,  $K$ ,  $D$ , and  $D_0$  where  $f$  is friction factor for the tube,  $K$  is the flow coefficient of the Venturi,  $D$  is the diameter of the tube, and  $D_0$  is the throat diameter.

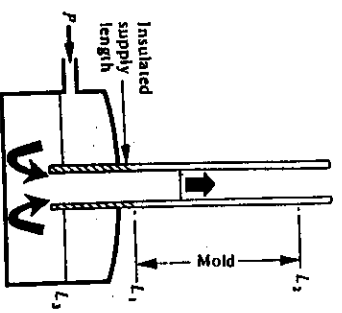


- 4.13** Lacking the funds to purchase a head meter, Mr. Make-do installed a 50 mm dia. tube in a 100 mm dia. line in order to measure flow rate. Pressure taps  $P_1$  and  $P_2$  are connected to a manometer.

- a) For flow which is highly turbulent ( $\text{Re} \rightarrow \infty$ ), derive an equation which gives mass flow rate through the line in terms of the pressure difference  $P_1 - P_2$ .  
 b) Develop an equation which could be used to calculate the permanent pressure drop (i.e.,  $P_1 - P_2$ ).

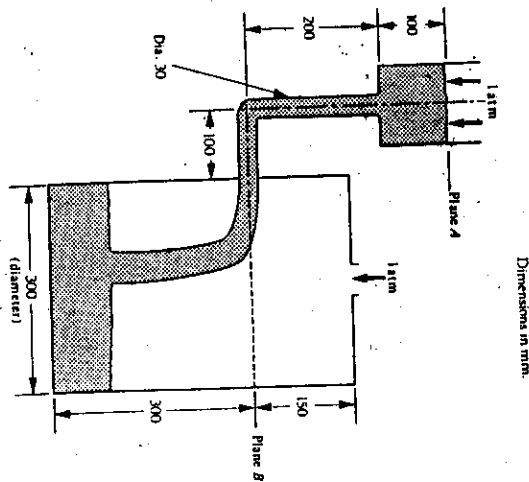
- 4.14 In order to *slush cast* seamless stainless-steel pipe, a *pressure pouring* technique is utilized, as depicted below.

Atmospheric pressure



The mold must be filled rapidly up to level  $L_2$  so that no solidification takes place until the entire mold is filled. Determine an expression that we can use to give the time it takes to fill the mold *only*. Consider the mold to be between  $L_1$  and  $L_2$  and open to atmospheric pressure at the top. Neglect the change of metal height  $L_2$  in the ladle; you may also neglect the friction loss associated with the supply tube and mold tube walls, but the entrance loss may not be neglected.

- 4.15 Calculate the time to fill the mold, as depicted below, with molten metal if the metal level at plane A is maintained constant and the time to fill the runner system (entering piping) is ignored. Data (all may be taken as constant):  $\eta = 1.65 \times 10^3 \text{ N s m}^{-2}$ ;  $\rho = 6410 \text{ kg m}^{-3}$ ;  $f = 0.0025$  (runner);  $e_f$  (contraction) = 0.1;  $e_f$  (enlargement for liquid levels above B) = 1.0;  $L/D(90^\circ \text{ turn}) = 25$ ;  $\beta = 1.0$ .



Dimensions in mm.

- 4.16 In planning continuous casting, we use fluid flow analysis. Consider the illustrated configuration of the equipment, which includes in-line vacuum degassing.

- a) Determine the tundish and degasser nozzle sizes which are necessary to operate the system at a rate of  $6.3 \text{ kg s}^{-1}$  per strand. Suppose that for operational reasons it is desirable to maintain tundish and degasser bath depths of 0.76 and 1.83 m, respectively.

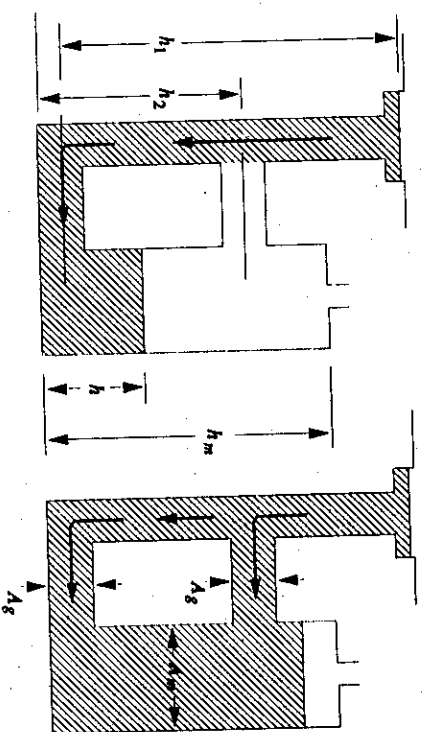
- b) If only 13 mm diameter degasser nozzles are available, how would their use affect the casting operation?

Inside dimensions: tundish,  $2.4 \text{ m} \times 2.4 \text{ m} \times 1.2 \text{ m}$ ; degasser,  $1.2 \text{ m} \times 1.2 \text{ m} \times 2.4 \text{ m}$ .

Liquid-steel density =  $7530 \text{ kg m}^{-3}$ .

Discharge coefficients for tundish and vacuum degasser nozzles:  $C_D = 0.8$ .  
Vacuum pressure =  $10^3 \text{ atm}$  ( $101 \text{ N m}^{-2}$ ).

- 4.17 Liquid metal flows into a permanent mold through a vertical gating-system. If the mold has a uniform area ( $A_m$ ) and the metal flows through gates of equal areas ( $A_g$ ), derive an equation which gives time to fill the mold. Assumptions: (i) no friction, but flow is turbulent; (ii)  $h_1$  is constant; (iii) no flow through the upper gate until  $h$  equals  $h_2$ .



$A_g$

- 4.18 If the pipes in Fig. 4.15 are of lengths  $L_1 = 10 \text{ m}$ ,  $L_2 = 5 \text{ m}$ , and  $L_3 = 1 \text{ m}$  and the nozzles are fan type with a 0.187 inch orifice, and  $D_1$  is 3 cm, determine the diameter of pipes 2 and 3 needed to produce a flow of 3.70 gallons of water per minute through each nozzle. What pressure  $P_0$  needs to be provided? What happens to the flow pattern if a small particle in the water clogs nozzle 1?

**5****FLOW AND VACUUM PRODUCTION**

The materials engineer must know not only how to measure flow, but also how to produce it. Some methods of producing flow and vacuum, such as gravity flow and suction lift, are well known, but there are many types of fans, pumps, and flow devices which are often required and used in materials laboratories and materials processing. Vacuum technology is a crucial part of materials processing and in materials science and engineering. Basic uses of vacuums include removal of gas molecules to permit travel of electrons, atoms, and ions through a required distance, removal of chemically active gases, decreasing the gas density to minimize heat transfer, refinement of melts, and controlled deposition of thin films on substrates. Keeping in mind that this is a textbook on transport phenomena, we have limited our presentation of vacuum technology to only several pages, and at that much of the presentation is qualitative and descriptive. We urge all readers involved in vacuum technology to immerse themselves in books devoted to this subject.<sup>1,2</sup>

Unfortunately the jargon and units used in engineering associated with pumps, fans, blowers and vacuum-producing devices can be rather strange, particularly in the U.S.A. where the use of English units still prevails. Accordingly, along with the working equations, we explain the jargon and non-S.I. units.

**5.1 PUMPS**

In general, pumps may be classified as either positive-displacement pumps or centrifugal pumps. We may subdivide positive-displacement pumps into reciprocal or rotary types, and centrifugal pumps into tangential- or axial-flow types.

Positive-displacement pumps deliver a definite volume of liquid at every stroke or revolution, regardless of the pressure and friction against which they are working. There are two common types of reciprocating positive-displacement pumps—the double-acting piston

<sup>1</sup>M. H. Hablanian, *High-Vacuum Technology*, Marcel Dekker, Inc., New York, NY, 1990.

<sup>2</sup>J. F. O'Hanlon, *A User's Guide to Vacuum Technology*, Second edition, John Wiley & Sons, New York, NY, 1989, pages 35-42.

pump and the single-acting plunger pump—and a large number of different designs of rotary positive-displacement pumps, the gear pump perhaps being the best known.

In general, positive-displacement pumps are employed where delivery of a relatively small volume of liquid against high pressure is required. In reciprocating pumps, as the piston withdraws, the fluid discharge ceases, and so the delivery is in pulses. In double-acting pumps, this pulsating characteristic is lessened.

In centrifugal pumps, the fluid enters axially at the suction connection, accelerates radially out along the blades of the impeller, and leaves the pump tangentially at a high velocity.

Centrifugal pumps can have various types of vane configurations, each with its own combination of power losses due to circulatory flow, fluid friction, shock, and mechanical friction.

When using a positive-displacement pump, the major factor to consider when specifying the pump is the power required. The power (as well as other factors) is also important when specifying a centrifugal pump. To determine the power, we apply Eq. (4.11) to a system.

Consider the system with a pump shown in Fig. 5.1, and write Eq. (4.11) from the plane at level (3) to the discharge plane (1).

$$\left[ \frac{P_1}{\rho_1} - \frac{P_3}{\rho_3} \right] + \left[ \frac{\bar{V}_1^2}{2\beta_1} - \frac{\bar{V}_3^2}{2\beta_3} \right] + g(z_1 - z_3) + E_f = -M^*. \quad (5.1)$$

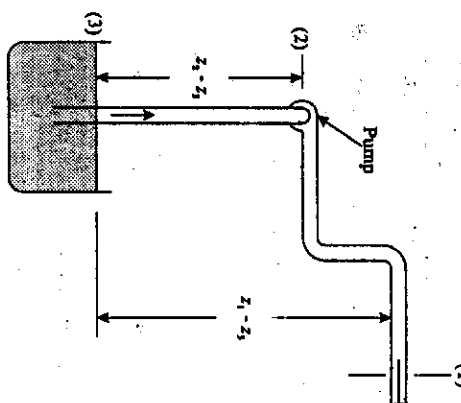


Fig. 5.1 Reference levels for the analysis of pump application.

If the frictional loss within the pump itself is accounted for by a mechanical efficiency  $\Gamma$ , then the work done by the pump is

$$\Gamma M_p^* = \left[ \frac{P_1}{\rho_1} + \frac{\bar{V}_1^2}{2\beta_1} + g z_1 \right] - \left[ \frac{P_3}{\rho_3} + \frac{\bar{V}_3^2}{2\beta_3} + g z_3 \right] + E_f. \quad (5.2)$$

In the nomenclature associated with pumps, the quantities in the brackets are called *heads*,  $h$ ,  $E_f$  is the *friction head*, and so

$$M_p^* = \frac{\Delta h}{\Gamma}, \quad (5.3)$$

where  $\Delta h$  is the total head (i.e., the right side of Eq. (5.2)). Each head, as well as  $M_p^*$ , has the units of  $J kg^{-1}$  so that the power required by the pump from a motor (brake power) is given by

$$P_b = WM_p^* = \frac{W\Delta h}{\Gamma}, \quad (5.4)$$

where  $W$  is the mass flow rate in  $kg s^{-1}$  and  $P_b$  is in  $W$ . The power absorbed by the fluid (fluid power) is

$$P_f = W\Delta h \quad (5.5)$$

and, therefore,

$$\Gamma = \frac{P_f}{P_b}. \quad (5.6)$$

In the U.S.A., power ratings of pumps are given in *horsepower* (hp), whereas the ratings of the motors can be in either kW or hp. The conversion is  $1 \text{ kW} = 1.341 \text{ hp}$ . Often the flow rate is given in gallons per minute (gpm), so the reader should also be familiar with the following conversion:

$$1 \text{ gallon (U.S.)} = 3.785 \times 10^{-3} \text{ m}^3.$$

In pumping liquids, there is a limit on the net positive *suction-head* that cannot be exceeded. This is set by the fact that if the dynamic pressure of the liquid ( $P + \rho\bar{V}^2/2\beta$ ) falls below the vapor pressure of the liquid  $P_v$ , then the liquid vaporizes, and no liquid is drawn into the pump. This phenomenon is called *cavitation*. For example, consider the liquid just before it enters the pump at plane (2) in Fig. 5.1. In order to avoid cavitation,

$$\left[ \frac{\bar{V}_2^2}{2\beta_2} + \frac{P_2}{\rho} \right] > \frac{P_v}{\rho}. \quad (5.7)$$

The pump lifts the liquid from the reservoir through a pipe, and Eq. (4.11), written between the reservoir surface (3), which is open to the atmosphere, and the suction entrance of the pump (2), assuming  $\bar{V}_3 = 0$ , is

$$\left[ \frac{P_2}{\rho} - \frac{P_3}{\rho} \right] + \frac{\bar{V}_2^2}{2\beta_2} + g(z_2 - z_3) + E_f = 0. \quad (5.8)$$

From Eqs. (5.7) and (5.8), we obtain the following requirement in terms of the height of lift and the pressure at the reservoir:

$$\frac{P_3}{\rho} - g(z_2 - z_3) - E_f > \frac{P_v}{\rho}. \quad (5.9)$$

Therefore, the net positive suction-head defined below must indeed be positive:

$$h_{nph} = \left[ \frac{P_3}{\rho} - \frac{P_v}{\rho} \right] - g(z_2 - z_3) - E_f > 0. \quad (5.10)$$

The efficiency of centrifugal pumps is a maximum at the design conditions, falling off on either side of them (Fig. 5.2). In selecting a centrifugal pump, one should consider its head-flow rate characteristic curve. The head is usually given in terms of feet of the fluid flowing through the pump, and indicates the height of a column of the liquid which could be pulled up through a frictionless pipe to the pump itself, assuming the limit imposed by cavitation, Eq. (5.10), is not exceeded. In practice, of course, the friction loss and any fitting or meter losses would have to be subtracted from this height.

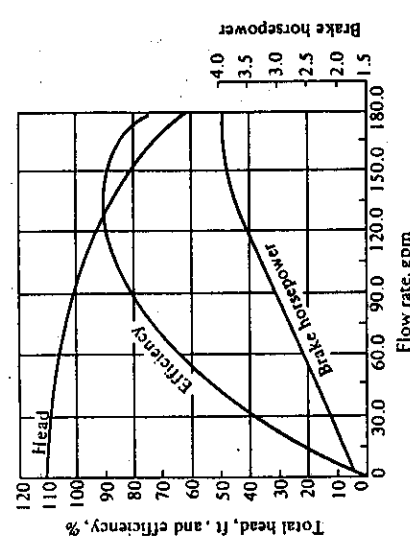


Fig. 5.2 Characteristic curves for a centrifugal pump.

When the head is expressed in feet, in reality the units are  $\text{ft lb}_t \text{lb}_m^{-1}$ , where  $\text{lb}_t$  and  $\text{lb}_m$  are the units for pound force and pound mass from the English system of units. A pound force is the force required to accelerate one pound mass by the acceleration of gravity ( $32.2 \text{ ft s}^{-2}$ ). In the following example, the reader is exposed to these units, as well as conversions to SI units.

**Example 5.1** A strip of metal emerging from a set of rolls is to be cooled by means of a spray of water. If 60 gpm are required, and the pressure drop across the spray nozzle is 15 psi at this flow rate, is it possible to install the pump, as depicted to the right, if the characteristic curves given in Fig. 5.2 apply? Assume 3-in. welded steel-piping up to the pump and 1-in. welded steel-piping to the nozzle. The problem is specified in units commonly encountered in engineering situations involving pumps in the U.S.A.

**Solution.** From Fig. 5.2, we obtain the total head delivered by the pump,  $-M^*$ , which is 107 ft at 60 gpm. In reality, the units of the head are  $\text{ft lb}_t \text{lb}_m^{-1}$ .

$$\begin{aligned} -M^* &= \frac{107 \text{ ft lb}_t}{\text{lb}_m} \left| \frac{1 \text{ lb}_m}{1 \text{ ft lb}_t} \right| \frac{1.356 \text{ N m}}{0.4556 \text{ kg}} = 320 \text{ N m kg}^{-1}. \\ P_1 - P_3 &= \frac{15 \text{ lb}_t}{\text{in}^2} \left| \frac{1^2 \text{ in}^2}{(0.0254)^2 \text{ m}^2} \right| \frac{4.448 \text{ N}}{1 \text{ lb}_t} = 1.034 \times 10^5 \text{ N m}^{-2}. \end{aligned}$$

Thus

$$\frac{P_1 - P_3}{\rho} = \frac{1.034 \times 10^5 \text{ N}}{\text{m}^2} \left| \frac{\text{m}^3}{1,000 \text{ kg}} \right| = 103.4 \text{ N m kg}^{-1}.$$

At 60 gpm, we calculate the velocity in the 1-in. pipe (diameter equals 25.4 mm) as follows:

$$\bar{V}_1 = \frac{60 \text{ gallon}}{\text{min}} \left| \frac{3.785 \times 10^{-3} \text{ m}^3}{1 \text{ gallon}} \right| \frac{1 \text{ min}}{60 \text{ s}} \left| \frac{\pi}{4} \right| \frac{0.0254^2 \text{ m}^2}{\text{m}}$$

$$\bar{V}_1 = 7.47 \text{ m s}^{-1}.$$

Similarly in the 3-in. pipe, we get

$$\bar{V} = 0.829 \text{ m s}^{-1}.$$

For now, we consider  $L$  (in m) to be an unknown. Therefore,

$$gL = \frac{9.807 \text{ m}}{\text{s}^2} \left| \frac{L \text{ m}}{3 \text{-in. pipe loss}} \right| = 9.807 L \text{ m}^2 \text{ s}^{-2} = 9.807 L \text{ N m kg}^{-1}.$$

Next we formulate  $E_f$ :

$$E_f = \frac{1}{2} \epsilon_f \bar{V}^2 + 2f \left[ \frac{L}{D} \right] \bar{V}^2 + 2f \left[ \frac{L}{D} \right] \bar{V}^2.$$

entrance  
loss

3-in. pipe  
loss

1-in. pipe  
loss

From Figs. 4.4 and 4.5, we obtain:

$$\epsilon_f = (2)(0.4) = 0.8.$$

The Reynolds numbers are

$$\text{Re (1-in. pipe)} = \frac{D \bar{V}_1 \rho}{\eta} = \frac{(0.0254)(7.47)(1000)}{(0.001)} = 1.90 \times 10^5$$

and similarly

$$\text{Re (3-in. pipe)} = 6.32 \times 10^4.$$

Now we seek the respective friction factors:

Re	$\epsilon/D$	$f$
1-in. pipe	$1.9 \times 10^5$	0.0018
3-in. pipe	$6.3 \times 10^4$	0.0006

With these friction factors, we calculate  $E_f$ :

$$E_f = \left[ \frac{1}{2} (0.8)(0.829^2) + (2)(0.0055) \left[ \frac{L}{0.0762} \right] (0.829^2) + (2)(0.0050) \left[ \frac{1.829}{0.0254} \right] (7.47^2) \right]$$

$$E_f = 40.46 + 0.09921L, \text{ m}^2 \text{ s}^{-2} \text{ or N m kg}^{-1}.$$

Collecting terms in the mechanical energy equation we have:

$$103.4 + \frac{7.47^2}{2} + 9.807L + 40.46 + 0.09921L = 320.$$

Therefore,  $L = 14.96 \text{ m}$ .

We should be suspect of this result. We know from our everyday experience that when pumps are situated more than 34 ft (10.4 m) above water, there is cavitation and the water cannot be pumped.

In a more formal manner, let's examine the net positive suction head. We use  $E_f$  only between (3) and (2). Also,  $(P_3 - P_v)/\rho = P_3/\rho$  in this case. Therefore

$$h_{\text{ns}} = \frac{P_3}{\rho} - gL - E_f,$$

with

$$\frac{P_3}{\rho} = \frac{1 \text{ atm m}^3}{1000 \text{ kg}} \left| \frac{1.01325 \times 10^5 \text{ N}}{1 \text{ atm m}^2} \right| = 101.32 \text{ N m kg}^{-1}$$

$$gL = (9.807)(14.96) = 146.7 \text{ N m kg}^{-1}$$

and

$$E_f = (2)(0.0055) \left[ \frac{14.96}{0.0762} \right] (0.829^2) = 1.48 \text{ N m kg}^{-1},$$

then

$$h_{\text{ns}} = -46.87 \text{ N m kg}^{-1}.$$

Cavitation will occur because  $h_{\text{ns}} < 0$ , and the installation will not work with  $L = 14.96 \text{ m}$ . A solution is to decrease  $L$  to 6 m and to compensate for the reduction in friction loss,  $E_f$ , by adding a gate valve to the system between the pump and the nozzle.

With the gate valve, the friction losses are

$$E_f = \left[ \frac{1}{2} (0.8)(0.829^2) + (2)(0.0055) \left[ \frac{6}{0.0762} \right] (0.829^2) + (2)(0.0050) \left[ \frac{1.829}{0.0254} \right] (7.47^2) \right]$$

$$+ (2)(0.0050) \left[ \frac{L_e}{D} \right] (7.47^2),$$

where  $(L_e/D)$  is the equivalent length-to-diameter ratio for the gate valve. After collecting terms, we get

$$E_f = 41.05 + 0.558 \left[ \frac{L_e}{D} \right], \text{ N m kg}^{-1}.$$

Since the total head at the desired flow rate is 320 N m kg<sup>-1</sup>, the system will perform as desired when  $(L_e/D)$  is such that

$$320 = 103.4 + \frac{7.47^2}{2} + (9.807)(6) + 41.05 + 0.558 \left[ \frac{L_e}{D} \right]$$

$$\left[ \frac{L_e}{D} \right] = \frac{320 - 231.2}{0.558} = 159.$$

From Table 4.2 we see that the system will work with the gate valve closed about one-half. The reader can check to see whether the net positive suction head is positive.

## 5.2 FANS AND BLOWERS

Fans and blowers are used for moving gases. We employ fans when the pressure drop in the system to overcome is not larger than about 50 in. w.c., although volumes up to several hundred thousand cubic feet per minute (cfm) may be involved. Blowers and turboblowers, on the other hand, are used in situations where larger pressure drops occur.

As in the case of pumps, there are many different designs of fans—axial flow, propeller and cross-flow fans as well as centrifugal types with a variety of blade configurations. All manufacturers of gas-moving equipment supply characteristic curves describing the performance of their equipment under the specified operating conditions at the inlet, as, for example, in Fig. 5.3, which presents curves for both the static and total pressures and the

\*The notation in. w.c., or inches water-column, is often used as the unit for pressure drop. Normal atmospheric pressure is 407.14 in. w.c.

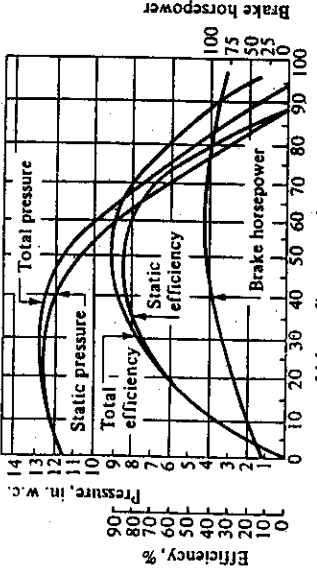


Fig. 5.3 Characteristic curves for a fan.

static and total efficiencies. If one wants to use a fan for moving a specified amount of gas against a given system resistance, it is necessary to know the static pressure developed by the fan at that flow rate.

Blowers are essentially constant-pressure machines with power consumption almost directly proportional to the volume delivered. Characteristic performance curves for a variable speed turboblower are given in Fig. 5.4. Pressure is in psig, which represents a gage pressure\* in  $\text{lb}_\text{f}/\text{in}^2$ , and the speed of the blower is in revolutions per minute (rpm), and the volume flow rate is in cubic feet per minute (cfm). Blowers and turboblowers find their typical applications in large metallurgical processes, such as in producing the air blast for blast furnaces and smelting furnaces.

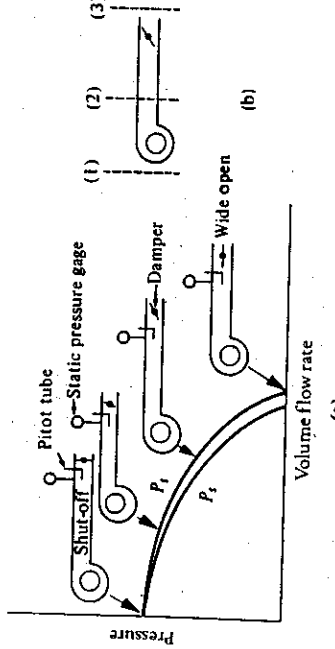


Fig. 5.5 Obtaining characteristic curves of a fan.

generated. Both of these values are relative to the inlet conditions, and are really pressure increases developed by the fan. At any flow rate, a theoretical horsepower may be calculated corresponding to either  $P_1$  or  $P_3$ , so that the definition of the *static efficiency*,  $\Gamma_s$ , as well as of the total efficiency,  $\Gamma$ , is based on the actual, or so-called brake horsepower.

The above statement can also be demonstrated by use of Bernoulli's equation applied to the system shown in Fig. 5.5(b). Between planes (1) and (3), the energy balance is simply

$$M^* + E_f = 0. \quad (5.11)$$

In this case, the system friction is composed of the resistance offered by the damper and the exit losses, that is, the friction between planes (2) and (3). The mechanical energy balance between planes (2) and (3) is then expressed

$$E_f = \left[ \frac{P_2 - P_3}{\rho} \right] + \left[ \frac{\bar{V}_2^2}{2} \right], \quad (5.12)$$

assuming  $\beta = 1$ .

Hence, by combining Eqs. (5.11) and (5.12), and noting  $P_1 - P_3$ , we arrive at

$$-M^* = \left[ \frac{P_2 - P_1}{\rho} \right] + \left[ \frac{\bar{V}_2^2}{2} \right], \quad (5.13)$$

or

$$-M^* \rho = (P_2 - P_1) + \left[ \frac{\rho \bar{V}_2^2}{2} \right]. \quad (5.14)$$

Writing the above expression with the actual or brake horsepower  $P_b$  and the efficiency  $\Gamma$ , we obtain

$$\Gamma P_b = -M^* \rho Q = \left[ (P_2 - P_1) + \frac{\rho \bar{V}_2^2}{2} \right] Q. \quad (5.15)$$

where  $Q$  is the volume flow rate.

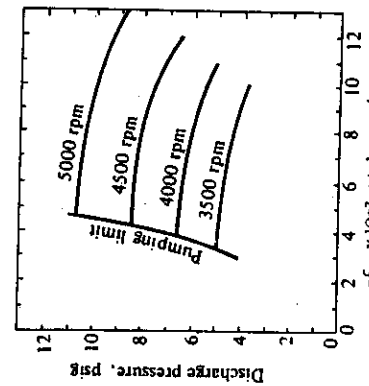


Fig. 5.4 Typical characteristic curves for a variable-speed blower.

Now, consider how the fan characteristics are measured. Figure 5.5(a) illustrates an appropriate system provided with a damper, so that the flow throughput may be varied. The Pitot tube measures the total pressure  $P_t$ , which is made up of the static pressure  $P_s$  (measured by the static pressure gage), and the dynamic pressure  $\frac{1}{2}\rho \bar{V}^2$ . By adjusting the damper to various positions, the values of  $P_t$  and  $P_s$ , corresponding to the various flow rates can be

\*The gage pressure is the pressure in excess of the ambient pressure.

Because a fan is part of an overall system, the system as a whole determines the size of the fan required. For any system, there is a certain curve of volume flow rate versus system resistance or pressure drop (see Fig. 5.6). The reader should realize by now that the resistance usually increases as the square of the volume flow rate for a highly turbulent system. The system may contain any combination of duct work, beds of fluidized or packed solids, dust collectors, flues, etc. There is usually a specific volume throughput  $Q'$ , required for proper operation of the process; this fixes the pressure drop resistance of the system, which in turn must be overcome by the fan or blower. Essentially then, the fan characteristic curve must intersect the system curve at the desired  $Q' - \Delta P$  coordinate (the so-called *operating point*). The efficiency and required horsepower are then fixed. Note that a different fan with a different characteristic curve would place the operating point at a different position on the system curve, resulting in a flow different from  $Q'$ .

### 5.3 INTERACTIONS BETWEEN FANS OR PUMPS AND SYSTEMS

It is not always possible to make desired changes in the operating point of a fan system. Changes in operating temperature or pressure drop require reevaluation of the system resistance curve, and if this changes, the operating point shifts, unless the fan is adjusted to keep  $Q'$  constant. Conversely, if it is desired to change  $Q'$ , then the operating point has to be changed, and consequently the fan characteristic curve must be changed.

In order to estimate the effect of deviations from the specified conditions, or the effect of a change in fan size or speed, on the behavior of the fan or the gas, the so-called *fan laws* are used to adjust from one set of operating variables to another. The variables are given in Table 5.1.

Table 5.1 Variables for fan laws

Speed of rotation	$n$
Impeller diameter	$D$
Gas density	$\rho$
Static pressure	$P_s$
Power	$P_h$
Volume flow	$Q$

The fan laws are:

$$Q = k_1 D^3 n, \quad (5.16)$$

$$P_s = k_2 D^2 n^2 \rho, \quad (5.17)$$

$$P_h = k_3 D^5 n^3 \rho. \quad (5.18)$$

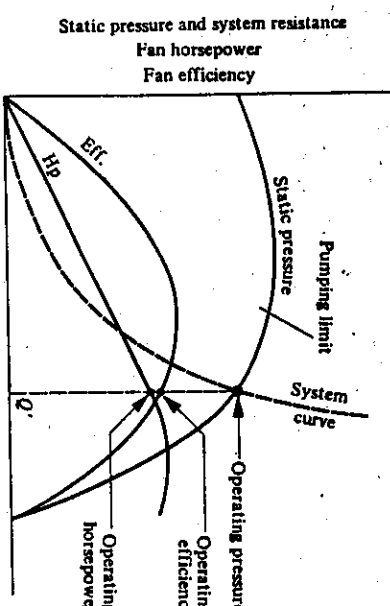


Fig. 5.6 Relationship between the fan curves and system curve. Often only the static pressure curve is supplied, so one assumes it is approximately the same as the total pressure curve.

The normal operating range for a fan is to the right of the peak of its pressure-volume curve. The so-called *pumping limit*, defines the furthest possible left-hand operating point.

*Pumping* occurs when the fan is slowed down to the point where the static pressure created is less than the static pressure in the discharge line. At that point a flow reversal takes place. After this reversal, a momentary drop in the pressure in the discharge line occurs, and flow starts in a normal direction again. This pattern is repeated very rapidly and results in a pumping-type action, which may cause damage to the fan unless flow below this limit is avoided. It usually turns out that this point is reached at the maximum on the fan total pressure curve, which in turn is usually slightly to the right of the maximum of the static pressure curve.

As an example of the use of the fan laws, if the density of the gas varies, and the speed and volume flow remain constant, then Eqs. (5.17) and (5.18) tell us that both the horsepower and the static pressure would be expected to vary directly with the density. The proportionality constants  $k_1$ ,  $k_2$ , and  $k_3$  are constants over a limited range, which should not deviate too far from a given point on the curve of pressure versus flow rate. Changes in the pattern of flow of the gases entering the fan will also change the characteristic curve, since the calibration is performed with gases entering smoothly at right angles to the rotor. If the gases enter otherwise, then their flow through the fan will affect the characteristic curves.

It is best, therefore, to overrate fans somewhat on both the pressure and volume specifications, but not too much, because severe damping, if necessary, decreases the efficiency and wastes the available power. The problems that can arise from errors in matching the system and fan curves are illustrated in the following example.

**Example 5.2** Part of an iron-ore pelletizing plant consists of a moving chain grate (carrying a bed of pellets subjected to a hot gases) and associated gas cleaning and exhaust equipment, as shown schematically in Fig. 5.7. The total pressure drop due to duct work, at the required bed-flow of 320 000 cfm at 394 K, is 3.5 in. w.c., and, when added to the calculated design bed-resistance of 9.5 in. w.c. at the design flow, gives a total system *design resistance* of 13.0 in. w.c. The fan to be used in this system is then specified to meet a 320 000 cfm flow with a 13.0 in. w.c. static pressure drop (point O in Fig. 5.8).

Suppose, however, that when the plant is built, the *actual* pressure drop across the bed of pellets at the required flow is 21.0 in. w.c. This means that the actual system curve (I)

$320'000/280'000 = 1.14$ ; the ratio of the new horsepower required to the old will be  $(1.14)^3 = 1.50$ ; in other words, a motor 50% more powerful is required. This may be quite expensive and could cause many problems in the electrical system. The ultimate solution is to buy a new fan.

If, on the other hand, the actual bed-resistance were, e.g., 7 in. w.c., then the fan would pull too much gas through the system, as at point 1 (Fig. 5.8). This can easily be corrected by increasing the system resistance through the use of dampers, until the system and fan curves coincide at the required flow and pressure drop, point O.

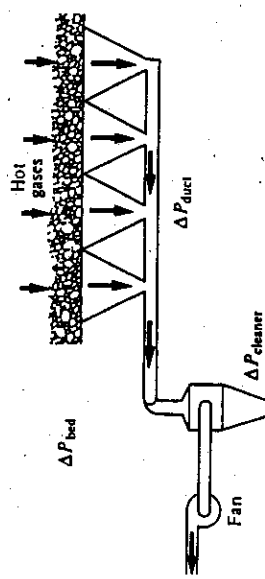


Fig. 5.7 Schematic diagram of an iron-ore pelletizing plant for Example 5.2.

We have seen that the operating point of a system with a fan is given by the intersection of the system curve with the characteristic pressure curve of the fan. The same principle applies to the use of pumps where the operating curve is given by the intersection of the system curve with the characteristic head curve of the pump. In installations with more than one pump, this principle can lead to a rather surprising result; that the use of two equivalent pumps, rather than one, does not double the flow rate through the system. This is illustrated by the following example.

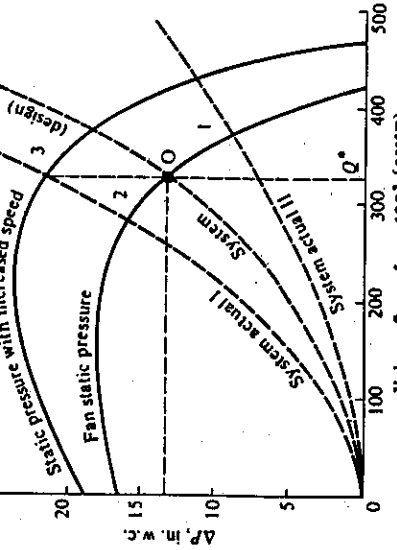


Fig. 5.8 Interaction between the system-resistance curves and fan curves for Example 5.2.

is different from the design system curve. Now the fan operates at point 2 (Fig. 5.8), and it pulls less than the required flow through the system (280 000 cfm). In this case, the only alternatives to regain a flow of 320 000 cfm are either to decrease the system resistance, or to change the characteristic curve by increasing the fan speed. In the first instance, one could decrease the system resistance by decreasing the bed height. If this is done, however, the lateral speed of the bed must be increased in order to keep the production rate at the design value. However, this may not be possible, because there is usually a minimum reaction time for the exposure of the solids to the hot gases, and the original design is usually close to that minimum. Changes in duct work may also be possible, but usually are not practical once the plant is built.

The other alternative—speeding up the fan until the operating condition is at point 3—is easier but may be very expensive. Reference to the fan laws shows us that the power required is proportional to the cube of the flow; that is, for constant fan size and gas density,  $Q \propto n$ , and  $P_f \propto n^3$ , so that  $P_f \propto Q^3$ . Therefore, for an increase of flow in the ratio

$320'000/280'000 = 1.14$ ; the ratio of the new horsepower required to the old will be  $(1.14)^3 = 1.50$ ; in other words, a motor 50% more powerful is required. This may be quite expensive and could cause many problems in the electrical system. The ultimate solution is to buy a new fan.

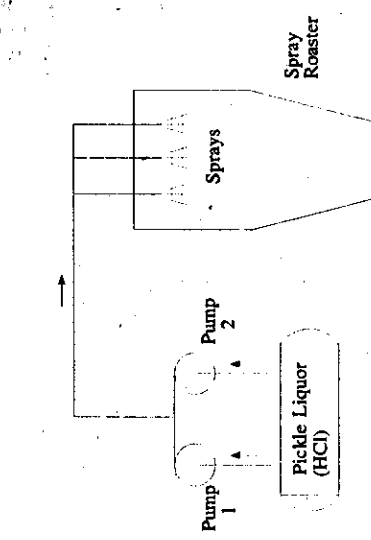


Fig. 5.9 System for Example 5.3.

Solution: With both operating, the pumps work against a head given by

$$h_{12} = E_f = KQ^2,$$

where  $h_{12}$  is the head overcome by both pumps 1 and 2.  $Q$  is the volume flow rate and  $K$  is a constant. We have assumed  $E_f = KQ^2$  because the flow is turbulent. Therefore, the work done by one pump, when both are operating, must be

$$h_1 = \frac{h_{12}}{2} = \frac{KQ^2}{2},$$



Fig. 5.10 Characteristic head curve for the pumps in Example 5.3.

with a flow rate of  $Q/2 = 15 \text{ gpm}$  ( $9.45 \times 10^4 \text{ m}^3 \text{ s}^{-1}$ ) which gives an operating point at  $h_1 = 40.8 \text{ N m kg}^{-1}$  from Fig. 5.10. Therefore,

$$K = \frac{2}{\text{kg}} \frac{40.8 \text{ N m}}{(1.89 \times 10^3)^2 \text{ m}^6} = 2.28 \times 10^7 \text{ N s}^2 \text{ kg}^{-1} \text{ m}^{-5}.$$

With this value of  $K$ , we can plot the system curve on Fig. 5.10 and determine the operating point when one pump operates by itself.

$$h_1 = KQ^2.$$

$Q, \text{m}^3 \text{s}^{-1}$	$h_1, \text{N m kg}^{-1}$
$5 \times 10^{-4}$	5.7
$10 \times 10^{-4}$	22.8
$12.5 \times 10^{-4}$	35.6
$15 \times 10^{-4}$	51.3

The curve generated by these calculated data intersects the characteristic head curve at  $h = 39.2 \text{ N m kg}^{-1}$  and  $Q = 13.2 \times 10^{-4} \text{ m}^3 \text{ s}^{-1}$  (21.0 gpm). Notice that with both pumps operating, the throughput is not doubled; in this example it increases by only 43%.

#### 5.4 SUPERSONIC NOZZLES AND JET BEHAVIOR

During the past three decades, jets of gas have become important in several metallurgical processes; process engineers should therefore have a good understanding of the characteristics and behavior of jets, in order to make the best use of them. Applications of supersonic nozzles include injection of oxygen into molten steel baths for refining purposes, and inert gas jets used to atomize liquid metal streams into metal powders.

Consider the flow nozzle described in Fig. 5.11. If the area of the nozzle opening is considerably smaller than that of the approach pipe, then the velocity in the pipe is negligible (the gas is stagnant) with respect to the velocity at the nozzle opening, as long as the pressure in the pipe is at or above the stagnation pressure. The application of Bernoulli's equation to the adiabatic and frictionless flow of an ideal compressible gas under these conditions yields an equation for the velocity in the nozzle opening  $\bar{V}_t$ :

$$\bar{V}_t = \sqrt{\frac{2P_0}{\rho_0} \left[ \frac{\gamma}{\gamma - 1} \right] \left[ 1 - \left( \frac{P_t}{P_0} \right)^{(\gamma - 1)/\gamma} \right]} \quad (5.19)$$

where reference points are defined in Fig. 5.11 and  $\gamma = C_p/C_v$ . We may use this equation for a flow nozzle operating at subsonic velocities.

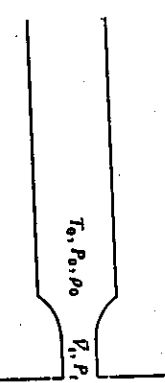


Fig. 5.11 Reference points for flow-nozzle equations.

Now the speed at which a compression-expansion wave passes through a medium, that is, the speed of sound  $V_s$  in that medium, is given by

$$V_s = \left[ \frac{\partial P}{\partial \rho} \right]^{1/2}_s \quad (5.20)$$

where the subscript on the partial derivative indicates constant entropy. For an ideal gas,

$$V_s = \left[ \frac{\gamma P}{\rho} \right]^{1/2} \quad (5.21)$$

The equation of momentum for one-dimensional flow is

$$\frac{dP}{\rho} + \bar{V} d\bar{V} = 0. \quad (5.22)$$

Substituting  $dP = V_t^2 d\rho$  into Eq. (5.22), we get

$$V_t^2 \frac{d\rho}{\rho} + \bar{V} d\bar{V} = 0. \quad (5.23)$$

The continuity equation, which requires that the mass flow rate remain constant at all points in the nozzle

$$\frac{dp}{\rho} + \frac{d\bar{V}}{\bar{V}} + \frac{dA}{A} = 0, \quad (5.24)$$

must be satisfied along with Eq. (5.23), and so

$$\frac{d\bar{V}}{\bar{V}} \left[ \frac{\bar{V}^2}{V_s^2} - 1 \right] = \frac{dA}{A}. \quad (5.25)$$

The Mach number,  $M$ , is defined as  $\bar{V}/V_s$ , so that finally

$$\frac{d\bar{V}}{\bar{V}} (M^2 - 1) = \frac{dA}{A}. \quad (5.26)$$

Now, if the velocity at any point in the nozzle is less than  $M = 1$ , and if the area of the nozzle decreases at that point ( $dA/A$  is negative), then the velocity increases at that point ( $d\bar{V}/\bar{V}$  is positive).<sup>†</sup> At the throat  $dA = 0$ , so either  $M = 1$  or  $d\bar{V}/\bar{V} = 0$ . If  $M < 1$  at the throat, then  $d\bar{V}/\bar{V}$  is zero and no further increase in velocity is possible, i.e., this is the maximum velocity which can be achieved.

If  $M = 1$  at the throat, then we have reached the point at which supersonic flow can take place. By adding a diverging section on the end, and referring to Eq. (5.26), we see that if  $dA/A$  is positive, then either  $d\bar{V}/\bar{V}$  will be positive, and a further increase to higher velocities is achieved in the diverging section, or the flow must come to a stop. The former case occurs as long as  $P_r > P_{\text{exit}}$ . A converging-diverging nozzle is shown in Fig. 5.12. It is usually called a *deLaval nozzle*.

For a converging nozzle, we obtain the conditions required to attain sonic velocity at the throat by using the energy relation for an ideal gas undergoing adiabatic flow:

$$\frac{T_0}{T} = 1 + \frac{\gamma - 1}{2} M^2. \quad (5.27)$$

When  $M = 1$ , sonic conditions exist denoted by an asterisk, and since the flow is also isentropic, substitution of the ideal gas relationship

$$\frac{P}{P_0} = \left[ \frac{T}{T_0} \right]^{\gamma(\gamma-1)} = \left[ \frac{\rho}{\rho_0} \right]^{\gamma} \quad (5.28)$$

gives the *critical pressure ratio*

$$\frac{P^*}{P_0} = \left[ \frac{2}{\gamma + 1} \right]^{\gamma(\gamma-1)}. \quad (5.29)$$

This means that the ratio of throat pressure to reservoir pressure at the sonic flow condition is governed only by the value of  $\gamma$ . For air and oxygen,  $P_r^*/P_0 = 0.528$ . For pressure ratios between 1.00 and 0.528, the mass flow rate of the gas is  $W_t = \rho_r V_r A_r$ , and using Eq. (5.28),

$$W_t = A_r \frac{2\rho_0 P_0 \gamma}{\gamma - 1} \left[ 1 - \left( \frac{P_r}{P_0} \right)^{\gamma(\gamma-1)/\gamma} \right]^{1/\gamma} \quad (5.30)$$

For the nozzle with the additional diverging section, the mass flow at sonic or supersonic conditions is still given by Eq. (5.31). However, since the velocity increases along the length of the diverging portion, the pressure correspondingly decreases from that at the throat. The problem is to determine how long this portion of the nozzle should be made in order to

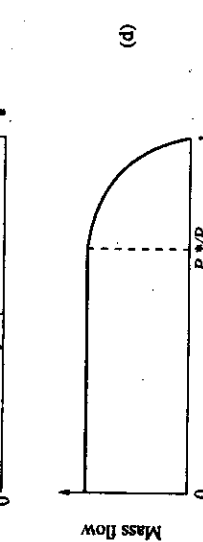
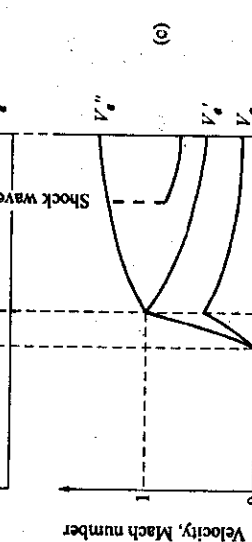
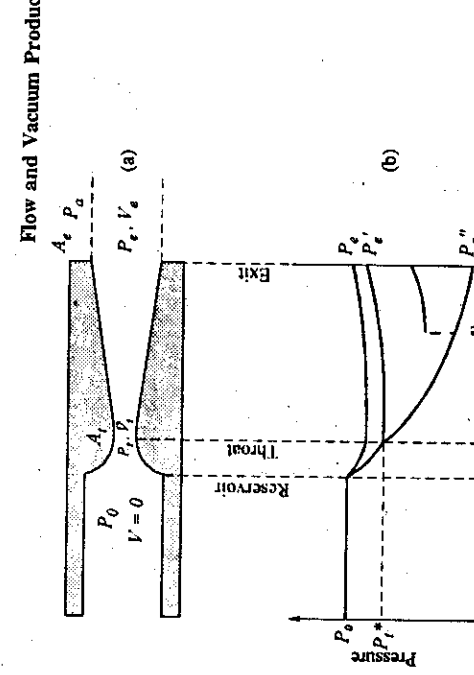


Fig. 5.12 Reference points and schematic internal conditions for various operating pressure ratios for converging-diverging nozzles.

Any further decrease in the ratio  $P_r/P_0$  below that for the  $P_r^*/P_0$ , caused, for example, by increasing the reservoir pressure  $P_0$ , will not cause a further increase in the mass flow rate out of a converging nozzle, since the condition of isentropic flow is no longer satisfied beyond the nozzle. If  $(P_r/P_0) \leq (P_r^*/P_0)$ , then the nozzle is said to be *choked*, and the mass flow rate is

$$W_r^* = A_r \rho_0 P_0 \gamma \left[ \frac{2}{\gamma + 1} \right]^{\gamma(\gamma-1)/\gamma} \quad (5.31)$$

<sup>†</sup>The reader should consider whether or not  $M > 1$  can be achieved in the converging portion of a nozzle.

produce a jet with exit pressure  $P_e'$  equal to ambient pressure. Such a condition establishes the most effective condition for achieving the maximum supersonic jet length.

Up to this point, it has not been established what the absolute pressure at the throat, relative to the exit pressure, is. Several possible solutions arise, depending on the nozzle design. There are two values of  $P_e^*/P_e$ —and therefore two values of  $P_e$ , shown in Fig. 5.12(b), which result in isentropic shockless flow in the diverging portion of the nozzle for the conditions where  $M = 1$  at the throat. The higher pressure  $P_e'$  will cause the flow to become subsonic again immediately at the throat, and will cause a decrease in velocity; the lower pressure  $P_e''$  will allow supersonic flow throughout the nozzle. If the exit pressure is between  $P_e'$  and  $P_e''$ ,  $P_e = P_e^*$ , then somewhere in the nozzle, a discontinuous transition from a lower to higher pressure (and simultaneously from supersonic to subsonic flow) occurs, as shown schematically in Fig. 5.12. This produces a shock wave.

If the nozzle design is such that  $P_e = P_e'$ , then we may proceed to calculate the exit velocity, using the equation

$$V_e = \sqrt{\left[\frac{2}{\gamma - 1}\right] \frac{\gamma P_0}{P_e} \left[1 - \left(\frac{P_e}{P_0}\right)^{\gamma - 1/\gamma}\right]} \quad (5.32)$$

or

$$M_e^2 = \frac{2}{\gamma - 1} \left[ \left(\frac{P_0}{P_e}\right)^{\gamma - 1/\gamma} - 1 \right]. \quad (5.33)$$

The mass flow rate and throat area are still given by Eq. (5.31).

Now that we have the mass flow rate, we may calculate the area of the exit by means of a mass balance, since  $W_e^* = W_e$ .

$$A_e \sqrt{\rho_0 P_0 Y \left[\frac{2}{\gamma + 1}\right]^{\gamma + 1/\gamma(\gamma - 1)}} = A_e \sqrt{\rho_0 P_0 Y \left[\frac{2}{\gamma - 1}\right] \left[1 - \left(\frac{P_e}{P_0}\right)^{\gamma - 1/\gamma}\right]} \cdot \left(\frac{P_e}{P_0}\right)^{1/\gamma}, \quad (5.34)$$

$$\left(\frac{A_e}{A_e'}\right)^2 = \left[\frac{2}{\gamma - 1}\right] \left[\frac{\gamma + 1}{2}\right]^{\gamma + 1/\gamma(\gamma - 1)} \left[1 - \left(\frac{P_e}{P_0}\right)^{\gamma - 1/\gamma}\right]. \quad (5.35)$$

Ideally, we want  $P_e = P_a$  (the ambient pressure), since then the ultimate adiabatic expansion is reached, and the jet issues from the nozzle at atmospheric pressure. If  $P_e$  is less than  $P_a$ , the ambient atmosphere compresses the flowing jet and collapses it in a series of shock waves. If  $P_e > P_a$ , the jet continues to expand beyond the nozzle tip. In both non-ideal situations, the efficiency of conversion of the nozzle velocity to jet momentum decreases.

The angle of divergence of the nozzle is usually about  $7^\circ$  in-order to avoid separation of flow from the nozzle walls.

**Example 5.4** In the basic oxygen steelmaking process, we decarburize a bath of molten iron-carbon alloy with gaseous oxygen which is blown into the bath from a lance held above the bath. Determine the dimensions of the converging-diverging nozzle which are required to achieve a velocity of Mach 2 at the exit with an oxygen flow rate of 15 000 scfm.\* What is the required driving pressure?

**Solution.** From Eq. (5.33), we can obtain  $P_0$  by assuming that  $P_e = 1$  atm to achieve the best behavior of the jet, and noting that  $\gamma$  for O<sub>2</sub> is 1.4:

$$\left(\frac{P_0}{P_e}\right)^{0.286} = \frac{2^2}{\left(\frac{2}{0.4}\right)} + 1.0,$$

and thus

$$\frac{P_0}{P_e} = 7.85.$$

For  $P_e = 1$  standard atmosphere,  $P_0 = 7.95 \times 10^5 \text{ N m}^{-2}$  (7.84 atm). Now we can make use of Eq. (5.35) to find the ratio  $A_e/A_e'$ :

$$\left(\frac{A_e}{A_e'}\right)^2 = \left[\frac{2}{0.4}\right] \left[\frac{2.4}{2}\right]^{2.4/0.4} \left[\frac{1}{7.84}\right]^{2/1.4} \left[1 - \left(\frac{1}{7.84}\right)^{0.4/1.4}\right]$$

$$\left(\frac{A_e}{A_e'}\right)^2 = 0.595.$$

Finally, we can calculate  $A_e$  from Eq. (5.31), since the nozzle is choked, as otherwise supersonic velocities could not be reached.

The mass flow is

$$W_e^* = 15\ 000 \text{ scfm} \times 0.089 \frac{\text{lb}_m}{\text{ft}^3} \times \frac{1 \text{ min}}{60 \text{ s}} = 22.2 \text{ lb}_m \text{ s}^{-1} = 10.1 \text{ kg s}^{-1}$$

$$10.1 = A_e \left\{ (10.41)(7.95 \times 10^5)(1.4) \left[\frac{2}{2.4}\right]^6 \right\}^{1/2} = 1.970 \times 10^3 A_e$$

$$A_e = 5.127 \times 10^{-3} \text{ m}^2$$

and

$$A_e = 8.617 \times 10^{-3} \text{ m}^2.$$

Thus, the throat diameter  $d_t = 80.8 \text{ mm}$ , and the exit diameter  $d_e = 105 \text{ mm}$ .

\*Standard cubic feet per minute.  $1 \text{ m}^3 \text{ s}^{-1} = 2.1189 \times 10^3 \text{ cfm}$ .

As a jet exits from the nozzle, it entrains adjacent air, which in turn acts as a drag, creating turbulence. This slows some of the supersonically flowing gas to sonic and subsonic velocities and the supersonic core of the jet gradually decays, until at some distance from the nozzle the core disappears, and the entire jet is subsonic. Figure 5.13 shows the relationship between the exit velocity (in terms of Mach number) and the length of the supersonic core (in terms of either the ratio  $x/d_t$ , where  $x$  is the distance from the nozzle and  $d_t$  is the throat diameter, or the ratio  $x/d_e$ , where  $d_e$  is the exit diameter).

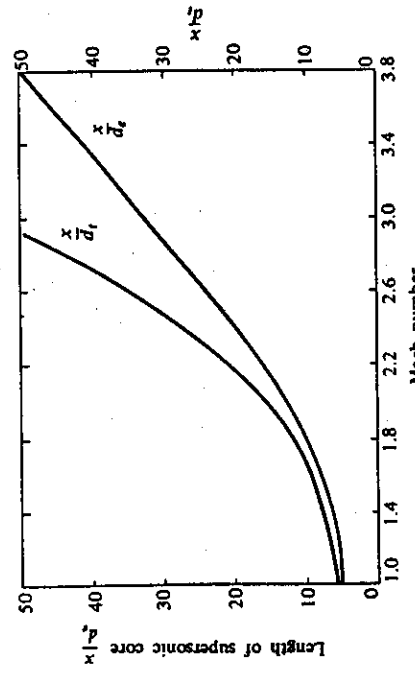


Fig. 5.13 Relationship between the length of supersonic core and exit Mach number.

We measure the overall spreading of the jet by the ratio  $r_0/r$ , where we define  $r_0$  as the radius at which the velocity is one-half that at the center line. The typical velocity or impact pressure profile is that of a normal distribution about the center line. However, the spreading of the jet is minor until the supersonic core has decayed. Once this point has been reached, the jet expands at an included angle of about  $18^\circ$ . Figure 5.14 gives a dimensionless graph for determining the width of the jet as a function of the exit Mach number and the distance from the nozzle. We then take the effective jet radius  $r$  as  $2r_0$  and can calculate it at any distance from the nozzle.

The increase in the mass flow of a subsonic jet due to the entrainment of the surrounding gas has been found to be directly proportional to the distance from the nozzle exit, according to the equation

$$W_x = W_e + k \sqrt{M_e \rho_e} \left[ \frac{x}{d} \right], \quad (5.36)$$

where  $M_e$  = jet momentum at nozzle exit ( $= W_e V_2$ ),  $x/d$  = distance from the nozzle exit,  $W_e$  = jet mass flow rate at nozzle exit,  $W_x$  = jet mass flow at  $x$ ,  $\rho_e$  = density of the ambient gas.

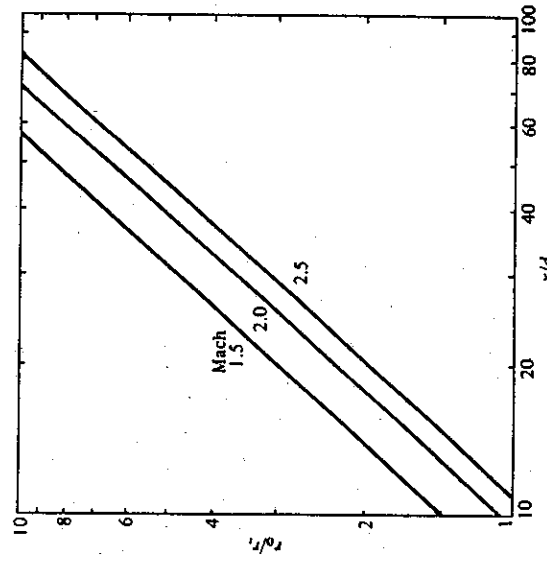


Fig. 5.14 Jet-spreading characteristics as a function of Mach number and distance from the nozzle. (Adapted from A. R. Anderson and F. R. Johns, *Jet Propulsion* 25, 13 (1955).)

In supersonic jets, the entrainment in the region where supersonic flow predominates is less than in the subsonic region, where Eq. (5.36) is satisfactory. A very satisfactory representation of the increased jet mass for supersonic jets with exit velocities between Mach 1 and 2 is given by\*

$$\frac{W_x - W_e}{W_e} = 9 \times 10^{-3} \sqrt{\frac{T_0}{T_e A_e}} \left[ 1 + \frac{(\gamma - 1) M^2}{2} \right] \left[ \left[ \frac{x}{d_e} \right]_{core} - \left[ \frac{x}{d_e} \right] \right], \quad (5.37)$$

where  $T_0$  = stagnation temperature,  $*R$ ,  $T_e$  = ambient temperature,  $R$ , and  $(x/d_e)_{core}$  = length of the supersonic core determined from Fig. 5.13. (Degrees Rankine,  $*R$ , is an absolute temperature scale equal to 9/5 K.) This equation does not describe the increasing entrainment in the region from the nozzle to a distance of about 10 nozzle diameters downstream, but since this is not the region of usual interest and also the rate of increase is not very strong in this region, the equation is still useful. Note that as the ambient temperature increases, the entrainment decreases.

We should point out that the entrainment of the surrounding gases dilutes the jet-gas

concentration. For example, the concentration of oxygen in cold jets of pure oxygen issuing into cold air, at a distance of 6 ft (1.8 m) from the nozzle, is 90% in the case of a Mach 3 nozzle versus 80% in the case of a subsonic nozzle with 25 psig ( $1.7 \times 10^5$  Pa) driving pressure.

\*This equation is derived from data presented in the report by J. D. Kapner and Kun Li, *Mixing Phenomena of Turbulent Supersonic Jets*, American Iron and Steel Inst., June 26, 1967.

## 5.5 VACUUM PRODUCTION

In materials processing, vacuum technology plays an important role in processes such as vacuum annealing, vacuum deposition of coatings, vacuum melting, and vacuum degassing. In addition, vacuum equipment is a standard item in almost every materials laboratory. For these reasons, it is important that materials engineers be acquainted with the principles and operation of vacuum-producing equipment.

The most important variable in the design and specification of equipment for a vacuum system is the pressure which the pumping system must be able to maintain in the work chamber. In the U.S.A., the most commonly used unit of vacuum measure is the torr, which is equivalent to the old millimeters of mercury. In European usage, the pressure is commonly expressed in millibars (mbar), with 1 bar equal to normal atmospheric pressure. Therefore,  $1000 \text{ mbar} = 760 \text{ torr} = 1.0133 \times 10^5 \text{ N/m}^2$ . Figure 5.15 compares the various pressure scales, indicating the ranges of application of various types of vacuum gages and pumps.

*Throughput* ( $Q$ ) is another term that is commonly used in vacuum technology. It is the quantity of gas, expressed as the volume of gas multiplied by its pressure, that passes a plane in a unit time. In SI units, throughput has units of  $\text{Pa m}^3 \text{ s}^{-1}$ . Coincidentally these units are equivalent to  $W$ , so throughput can also be pictured as energy flow. We should keep in mind that throughput is not a mass flow, but of course if the temperature is known then mass flow rate can be calculated from throughput.

Another variable is the speed at which the desired pressure is reached. We define the speed  $S_p$  of any type of vacuum pump by

$$S_p = Q/P \quad (5.38)$$

where  $P$  is the pressure at the inlet to the pump, and  $Q$  is the throughput at that point. Typical units for  $S_p$  are  $\text{m}^3 \text{ s}^{-1}$ . We may use the same definition to express the pump-down speed of a system  $S_s$ , consisting of a working chamber, connecting duct work, and pumps, but the speed depends on the design of the rest of the system as well as on the pump itself.

A system, initially at atmospheric pressure, is first *roughed out* by either mechanical pumps or the first stage of an ejector system until a pressure is reached where vapor diffusion pumps, or further stages of an ejector system, become effective and can be used for final evacuation to the desired limiting pressure. During the initial roughing out, the gas density will be high enough, so that the mean free path of the gas is very small ( $\sim 10^{-4} \text{ mm}$ ) compared with the dimensions of the conduit, and the flow rate of the gas is governed by the viscosity of the gas through the equations developed in previous chapters for turbulent and laminar flows. However, at low pressures, the density eventually reaches a value such that the mean free path is much greater than the conduit dimensions. At this point, viscosity is meaningless in determining the flow rate, and the gas flow becomes *molecular flow*. At an intermediate pressure, a transition flow regime is encountered when the mean free path is of the same order of magnitude as the equipment dimensions.

\*The name torr comes from E. Torricelli, a student of Galileo, who devised the first single stroke pump by inverting a closed tube of mercury into a dish containing mercury, creating a vacuum in the tube.

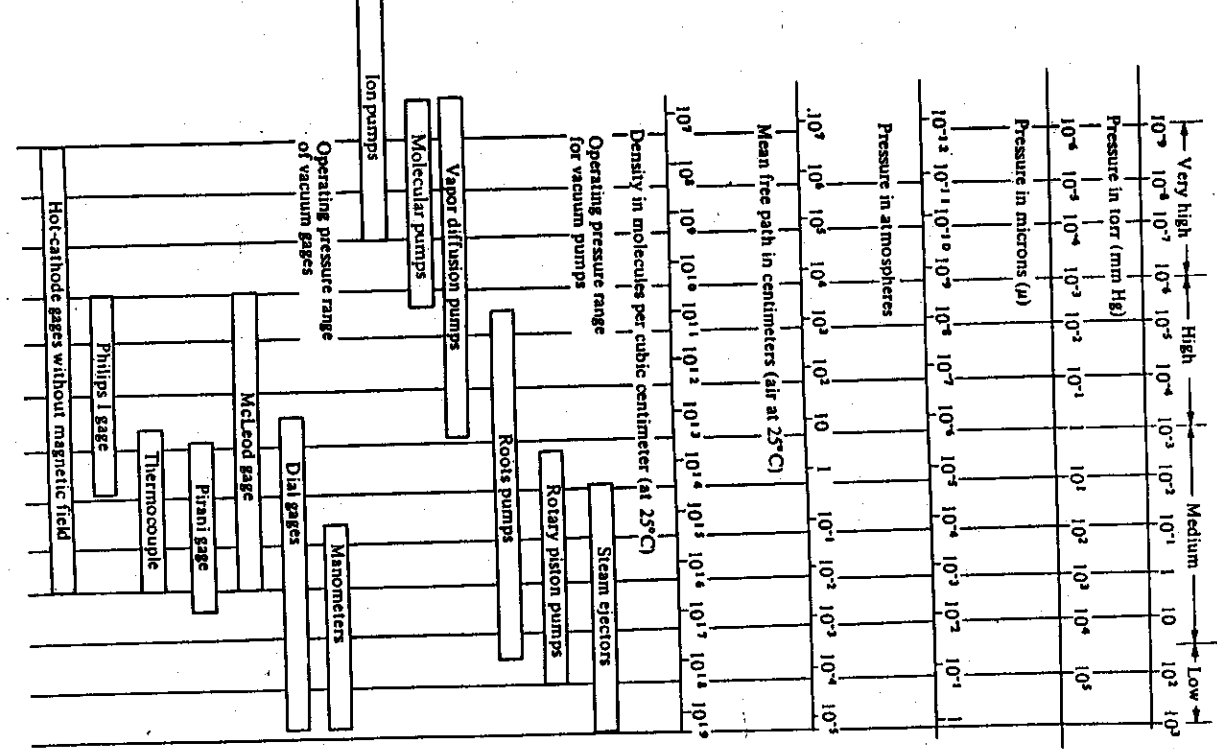
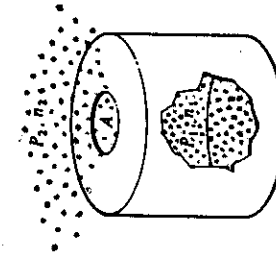


Fig. 5.15 Comparative pressure scales and ranges of application of various vacuum pumps and gages.

### 5.5.1 Molecular flow mechanics

In the *molecular flow* regime, the gas molecules move randomly, with a Maxwell-Boltzmann distribution of velocities, and collisions between molecules are rare compared to collisions with the walls. The only transfer of momentum is between molecules and the wall instead of from molecule to molecule. Net flow results from the statistical effect that the number of molecules leaving a given region is proportional to the number of molecules in the region, and the number reentering will be proportional to the number in the adjacent region. Knudsen developed the equations which govern the flow of gases through various geometries under molecular flow conditions. Consider a chamber with an aperture of area  $A$ , as in Fig. 5.16. The pressure on the downstream side of the aperture is  $P_2$  and that in the chamber is  $P_1$ . If the concentration of gas molecules is given by  $n$  (molecules  $\text{mm}^{-3}$ ), and the number hitting the wall is

$$Z = \frac{n\bar{V}}{4}, \text{ molecules } \text{mm}^{-2} \text{ s}^{-1}, \quad (5.39)$$



**Fig. 5.16** Schematic chamber being evacuated from an internal pressure of  $P_1$  to an external pressure of  $P_2$  through an aperture of area  $A$ .

where  $\bar{V}$  is the average molecular speed given in Eq. (1.4), then the frequency  $Z$  of gas molecules per unit area passing from the high-pressure side of the aperture through it, is

$$Z_1 = \frac{n_1}{2\sqrt{\pi}} \left[ \frac{2\kappa_B T}{m} \right]^{1/2},$$

The frequency from the low-pressure side back through the opening

$$Z_2 = \frac{n_2}{2\sqrt{\pi}} \left[ \frac{2\kappa_B T}{m} \right]^{1/2},$$

yields a net frequency

$$Z_{\text{net}} = Z_1 - Z_2 = \frac{1}{2\sqrt{\pi}} \left[ \frac{2\kappa_B T}{m} \right]^{1/2} (n_1 - n_2). \quad (5.40)$$

For a circular opening, the net rate at which molecules leave the chamber is

$$n = \frac{\pi D^2}{4} Z_{\text{net}} = \frac{\sqrt{\pi}}{8} \left[ \frac{2\kappa_B T}{m} \right]^{1/2} D^2 (n_1 - n_2). \quad (5.41)$$

Because  $n = P/\kappa_B T$ ,

$$n = \left[ \frac{2\pi}{m\kappa_B T} \right]^{1/2} \frac{D^2}{8} (P_1 - P_2), \text{ molecules s}^{-1} \quad (5.42)$$

or

$$n = \left[ \frac{2\pi}{MRT} \right]^{1/2} \frac{D^2}{8} (P_1 - P_2), \text{ kmol s}^{-1} \quad (5.43)$$

where  $M$  is the molecular weight,  $\text{kg kmol}^{-1}$ , and  $R$  is the gas constant ( $R = 8.315 \text{ kJ kmol}^{-1} \text{ K}^{-1}$ ).

The throughput for flow of molecules across the aperture can be written as

$$Q = C(P_1 - P_2), \quad (5.44)$$

where  $C$  is the *conductance* of the aperture. By the definition of throughput and using the ideal gas law, we can also write

$$Q = nRT, \quad (5.45)$$

so that

$$C = \frac{nRT}{P_1 - P_2}. \quad (5.46)$$

By combining Eqs. (5.43) and (5.46), we arrive at the conductance of an aperture:

$$C = \left[ \frac{2\pi RT}{M} \right]^{1/2} \frac{D^2}{8}. \quad (5.47)$$

We can write Eq. (5.47) in a simpler form:

$$C = \frac{\bar{V}}{4} A, \quad (5.48)$$

where  $\bar{V}$  is the Maxwellian speed of the molecules given by Eq. (1.4) and  $A$  is the area of the aperture. For other shapes (e.g., tubes), the conductance is usually given by Eq. (5.48) with a *transmission probability*,  $a$ , which is the probability that a molecule entering the tube will leave the tube at the other end. Thus, the conductance is found from

$$C = \frac{a\bar{V}}{4} A, \quad (5.49)$$

where  $A$  is the cross-sectional area of the tube. The conductance of an aperture of area  $A$  has a maximum value, and tubes and conduits of the same area will have a conductance less than the conductance of the aperture.

To describe molecular flow through long circular tubes, Knudsen derived

$$C = \frac{\pi \bar{V} D^3}{12L}, \quad (5.50)$$

or

$$a = \frac{4D}{3L}.$$

With this result, we can see that we must be careful in how we apply conductances. For example, Eq. (5.50) indicates that the conductance goes to infinity as  $L$  approaches zero, whereas the limit should be the value given by (5.48). In an attempt to deal with short tubes, it has been suggested that the aperture and the tube be considered as two flow resistors in series. When this is done

$$\frac{1}{C} = \frac{1}{C_1} + \frac{1}{C_2}, \quad (5.51)$$

where  $C$  is for the short tube,  $C_1$  is for the aperture, and  $C_2$  is for the "tube," itself, given by Eq. (5.50). As  $L/D \rightarrow 0$  this result reduces to Eq. (5.48), and as  $L/D \rightarrow \infty$ , it reduces to Eq. (5.50). However, it is only approximate for intermediate values of  $L/D$  and can be in error by as much as 15%. Actually, the Monte Carlo method to track molecular motions through various configurations has been applied to calculate the transmission probabilities.

Many of these results are reviewed and presented by O'Hanlon.<sup>3</sup> The conductance of an entire vacuum system composed of several different components may be approximately calculated by analogy with electrical circuits. Specifically,

$$\frac{1}{C_{\text{system}}} = \frac{1}{C_1} + \frac{1}{C_2} + \frac{1}{C_3} + \dots \quad (5.52)$$

for a system with components 1, 2, 3, etc., in series, or, if the components are in parallel, then

$$C_{\text{system}} = C_1 + C_2 + C_3 + \dots \quad (5.53)$$

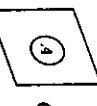
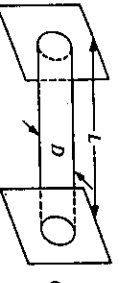
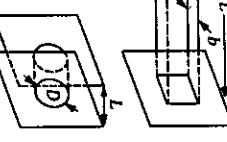
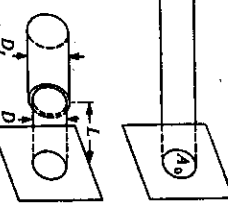
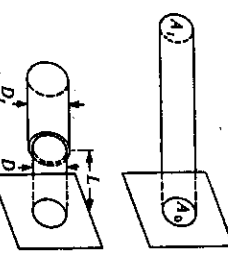
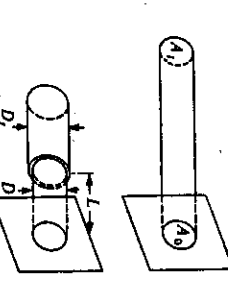
Table 5.2 presents the conductances of several shapes.

**Example 5.4** A 150 mm diameter tube, with a length of 150 mm, connects a vacuum chamber and a vacuum pump. Which of the following modifications will give the greatest increase in conductance? (a) Decrease the length of the tube to 75 mm; (b) increase the diameter to 175 mm; (c) increase the length to 175 mm; (d) decrease the diameter to 125 mm.

**Solution.** We can immediately disregard modifications (c) and (d) because both result in an increase in  $L/D$ . The total conductance of the tube comprises the conductance of the aperture at the chamber-tube connection ( $C_1$ ) and the tube itself ( $C_2$ ). We combine Eqs. (5.48), (5.49) and (5.51):

$$\frac{1}{C} = \frac{4}{VA} + \frac{4}{aVA} = \frac{4}{VA} \left[ 1 + \frac{1}{a} \right].$$

Table 5.2 Conductances of various geometric shapes for molecular flow\*

Shape'	Conductance ( $L \cdot s^{-1}$ )**	$C$ , for air at 298 K
	$C = 3.64A \left( \frac{T}{M} \right)^{1/2}$	$= 11.7A$
	$C = 19.4 \frac{A^2}{BL} \left( \frac{T}{M} \right)^{1/2}$	$= 12.2 \frac{D^3}{L}$
	$C = 3.81 \frac{D^3}{L} \left( \frac{T}{M} \right)^{1/2}$	$= 12.2 \frac{(D_2 - D_1)^2(D_1 + D_2)}{L}$
	$C = 9.70 \frac{b^2 c^2}{(b+c)L} \left( \frac{T}{M} \right)^{1/2}$	$= 31.1 \frac{b^2 c^2}{(b+c)L}$
	$C = 2.85 D^2 \left( \frac{T}{M} \right)^{1/2} \left( \frac{1}{1 + 3L/4D} \right)$	$= 9.14 \frac{D^2}{1 + 3L/4D}$
	$C = 3.64 \left( \frac{T}{M} \right)^{1/2} \left( \frac{1}{1 - A/A_0} \right)$	$= \frac{11.7 A_0}{1 - A_0/A}$
	$C = 3.81 \frac{D^3}{L} \left( \frac{T}{M} \right)^{1/2} \left( \frac{1}{1 + \frac{4D}{3L} \left( 1 - \frac{D^2}{D_t^2} \right)} \right)$	$= \frac{12.2 D^3}{L \left[ 1 + \frac{4D}{3L} \left( 1 - \frac{D^2}{D_t^2} \right) \right]}$

\*This table is taken from J. M. Lafferty, *Techniques of High Vacuum*, General Electric Report No. 64-RL-3791G, 1964.

The variables and their respective dimensions are

$A$  = area,  $\text{cm}^2$ ,

$D$  = diameter,  $\text{cm}$ ,

$L, b, c$  = length dimensions,  $\text{cm}$ ,

$B$  = perimeter,  $\text{cm}$ ,

$T$  = absolute temperature,  $\text{K}$ ,

$M$  = molecular weight,  $\text{g mol}^{-1}$ ,

\*\* $1 \text{ L s}^{-1} = 10^3 \text{ m}^3 \text{ s}^{-1}$ .  $L$  is liter.

With the original dimensions of the tube, the transmission probability is

$$a = \frac{4D}{3L} = \frac{4 \times 150}{3 \times 150} = \frac{4}{3}$$

so that

$$C = 0.571 \left[ \frac{\bar{V}A}{4} \right]$$

For modification (a):

$$a = \frac{4 \times 150}{3 \times 75} = \frac{8}{3}$$

and

$$C_{(a)} = 0.727 \left[ \frac{\bar{V}A}{4} \right]$$

For modification (b):

$$a = \frac{4 \times 175}{3 \times 150} = \frac{14}{9}$$

and

$$C_{(b)} = 0.607 \left[ \frac{\bar{V}A}{4} \right]$$

The greatest increase is achieved by modification (a).

Pumping speed has the same units as conductance, but it should be noted that conductance implies a pressure gradient across a specific geometry. Pumping speed is simply the volume of gas flowing across any plane in a system per second, which is measured at the pressure existing at that particular plane.

The pump-down speed of a system depends on both the pump speed and the conductance of the connections. Refer to the schematic diagram of a vacuum melting system in Fig. 5.17. Because  $P = Q/S$  at the inlet to the duct,  $P_p = Q/S_p$  at the inlet to the pump, and  $(P - P_p) = Q/C$  over the duct length, then

$$\frac{1}{S} - \frac{1}{S_p} = \frac{1}{C}, \quad (5.54)$$

or

$$S = S_p \left[ \frac{1}{1 + S_p/C} \right]. \quad (5.55)$$

This means that the effective pump speed  $S$  of a system being evacuated by a pump with rated speed  $S_p$  cannot exceed  $S_p$  or  $C$ , whichever is smaller. If the conductance of the duct is the same as the pump speed, then  $S = S_p/2$ . This should emphasize why it is desirable to make connections between the working chamber and the pump as short and as wide as possible.

Vacuum induction melting chamber

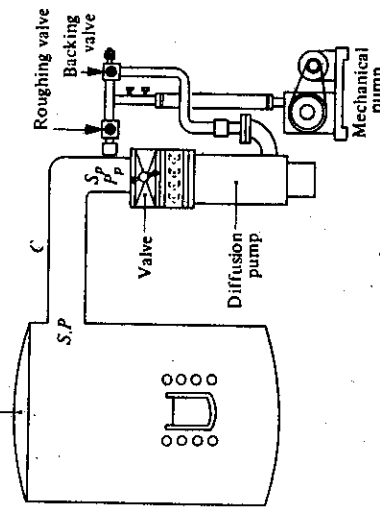


Fig. 5.17 A typical vacuum melting system.

### 5.5.2 Mechanical pumps

Most mechanical vacuum pumps are of the positive-displacement, rotary-piston type with sliding vanes, and sealed with oil. A small quantity of gas from the system is isolated, compressed, and discharged to the atmosphere with each rotation of the piston. These pumps have *intrinsic speeds*,  $S_0$ , ranging in value from  $5 \times 10^4$  to  $0.35 \text{ m}^3 \text{ s}^{-1}$ . There is a lower limit to the pressure that a pump may produce, known as the ultimate pressure  $P_u$ , at which point the speed drops to zero. This limit is determined by the amount of back leakage of a very small quantity of gas  $Q_a$ , which is nearly independent of pressure. At the inlet to the pump,

$$S_p = \frac{Q - Q_a}{P_p} = S_0 \left[ 1 - \frac{Q_a}{Q} \right]. \quad (5.56)$$

At the ultimate pressure,  $Q_a = Q$  and  $S_0 = Q_u/P_u$ . Therefore

$$S_p = S_0 \left[ 1 - \frac{P_u}{P_p} \right]. \quad (5.57)$$

Substitution of Eq. (5.57) into Eq. (5.55), and elimination of  $S_p$  and  $P_p$  by the use of  $PS = Q = (P - P_p)C$ , leads to a more realistic value for the speed of the system

$$S = S_0 \left[ \frac{1 - P_u/P}{1 + S_0/C} \right], \quad (5.58)$$

or

$$S = S' \left[ 1 - \frac{P_u}{P} \right], \quad (5.59)$$

where

$$S' = S_0 \left[ \frac{1}{1 + S_0/C} \right]$$

Single-stage pumps have ultimate pressures in the range from  $10^{-2}$ - $10^{-3}$  torr. Two-stage mechanical pumps can reduce the ultimate pressure to  $10^{-4}$ - $10^{-5}$  torr. In order to remove condensable gases (especially water vapor), a trap, either cold or chemical, should be placed ahead of the pump. If a slightly lower pressure is desired, and if the quantity of gas is large, a so-called Roots pump may be used in conjunction with an oil-sealed mechanical forepump. This combination may produce an ultimate pressure of  $10^{-6}$  torr. Typical characteristic curves for various types of mechanical pumps are shown in Fig. 5.18.

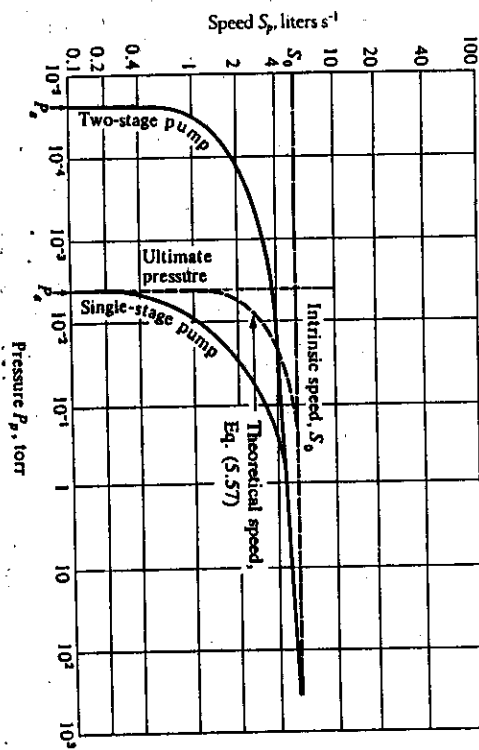


Fig. 5.18 The speed-pressure characteristics curves for a single- and two-stage rotary, oil-sealed, vane-type pump.

**5.5.3 Diffusion pumps**

We apply the term diffusion pump to a jet pump which utilizes the vapor from low vapor-pressure liquids to impart increased momentum to the gas molecules being removed from the system, eventually forcing them out of the mouth of the discharge into a mechanical forepump. Figure 5.19 illustrates a typical diffusion pump. The pump liquid is heated in the boiler until its vapor pressure reaches an optimum value of about 1 torr. This vapor is carried to a nozzle from which it is ejected as a high-velocity jet directed away from the incoming gas and towards the wall of the pump. The gas molecules flow into the annular space between the wall and column by molecular diffusion. Some fraction,  $H$ , of the molecules that encounter the jet in the first stage is entrained into the jet and driven downstream with higher velocities than the molecules would normally have. The jet expands and eventually strikes the water-cooled wall, the working fluid condenses, and flows down the walls back to the boiler. In multiple-jet pumps, the gas molecules being pumped are caught in a succession of jet spray stages, and eventually ejected from the diffusion pump into the foreline.

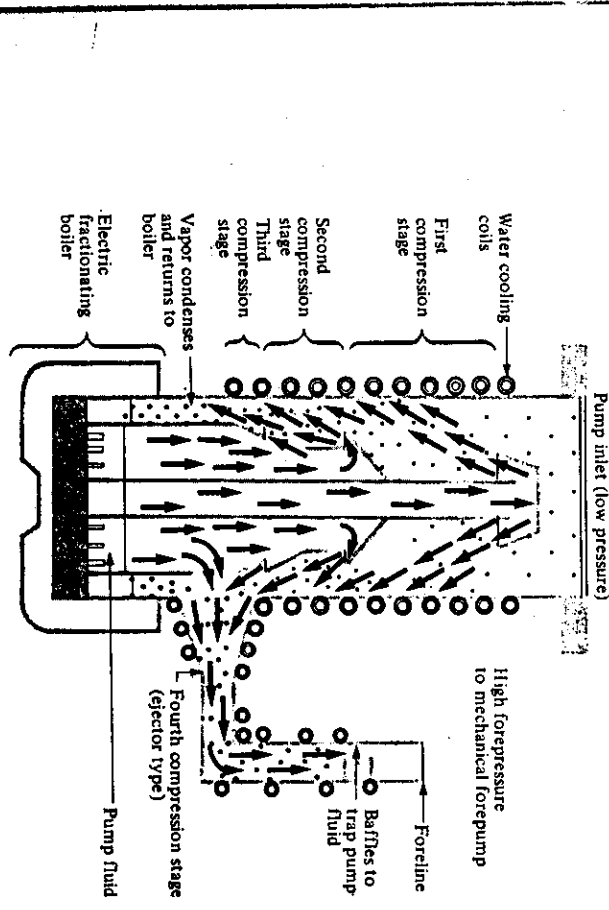


Fig. 5.19 Cross section of a typical vapor diffusion pump.

Since free molecular flow is needed for their successful operation, diffusion pumps usually operate at inlet pressures of  $10^{-3}$  torr, or below. The compression ratios are not great enough to allow direct discharge to the atmosphere, so a relatively low forepressure must be maintained by a mechanical forepump, ultimately discharging to the atmosphere. For any diffusion pump there is a *limiting forepressure*, which is the pressure above which the boundary between the jet of pump vapor molecules and the randomly moving incoming gas molecules does not extend to the cold pump walls. In this situation, there is a direct connection between the high-vacuum and low-vacuum (forepump) sides of the jet, and effective pumping ceases. This pressure is typically of the order of 0.5 torr for multistage diffusion pumps and 0.05 torr for single-stage pumps.

We define the speed of diffusion pumps in the same way as for mechanical pumps. If  $A$  is the area of the pumping annulus, then the rate at which gas molecules are entrained by the jet is

$$HZA = \frac{H\bar{A}nV}{4}, \quad (5.60)$$

using the previously defined nomenclature. Then, the intrinsic pump speed  $S_0$  is

$$S_0 = \frac{HZA}{n} = \frac{Q}{P_p} = \frac{H\bar{A}V}{4}, \quad (5.61)$$

and, substituting Eq. (1.4) for  $\bar{V}$ , we obtain

$$S_0 = \frac{H}{2\sqrt{\pi}} \left[ \frac{2k_a T}{m} \right]^{1/2} A, \quad (5.62)$$

or

$$S_0 = 3.64H \left[ \frac{T}{M} \right]^{1/2} A, \text{ L s}^{-1}. \quad (5.63)$$

Specifically, for air at 293 K,

$$S_0 = 11.6(HA), \text{ L s}^{-1}, \quad (5.64)$$

where  $A$  is measured in  $\text{cm}^2$ . The coefficient  $H$  is a measure of the collection efficiency of the pump and is called the *Ho coefficient* (named after T. L. Ho). For most diffusion pumps the Ho coefficient is about 0.5. These equations imply that  $S_0$  is independent of the pressure for diffusion pumps, and this is nearly true, as shown in Fig. 5.20.

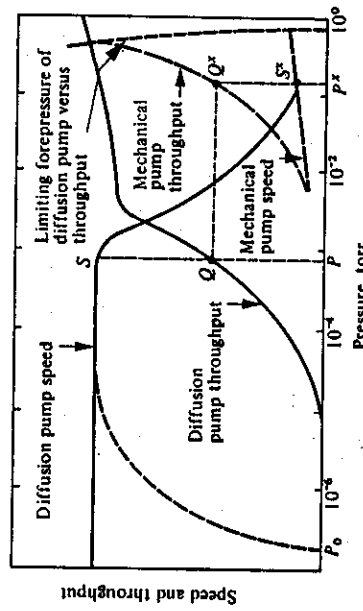


Fig. 5.20 Characteristic curve for a typical vacuum diffusion-pump, with the curves for a matching mechanical forepump included.

The ultimate pressures attainable with diffusion pumps depend on their design, including the number of stages, and also on the working fluid used. If we use mercury, a vapor trap, in the form of a baffle system externally cooled to low temperatures, must be placed between the diffusion pump and the system being evacuated in order to prevent back-diffusion of mercury vapor ( $P_{Hg} = 1 \times 10^{-3}$  torr at 293 K). In this case, the effective speed of the pump is

$$S_p = S_0 \left[ \frac{1}{1 + S_0/C_t} \right], \quad (5.65)$$

where  $C_t$  is the conductance of the trap. For well-designed traps,  $S_p \approx S_0/2$ . The ultimate pressures attainable with *well-trapped* mercury diffusion pumps are of the order of  $10^{-6}\text{--}10^{-7}$  torr. More commonly, low-vapor-pressure hydrocarbon oils or silicone oils are used as the working fluids. They are capable of producing vacuums of  $10^{-6}$  torr without traps.

#### 5.5.4 Pumpdown time

Returning to our vacuum melting unit, the basic equation relating the change in pressure in the tank to the pumping speed of the system, is

$$PS = -V \frac{dP}{dt} + Q_i, \quad (5.66)$$

where  $P$  = pressure measured at a specified point in the system,  $S$  = speed at that point,  $V$  = system volume, and  $Q_i$  = additional gas flow made up of the leak rate, interior surface outgassing, and any process gases. In well-maintained systems with no process gas evolution,  $Q_i$  is eventually brought to a negligible level.

Solving Eq. (5.66) for  $S$  and equating with Eq. (5.59), we obtain

$$\frac{dP}{(P - P_a)} = -\frac{S'}{V} dt. \quad (5.67)$$

We find the pumpdown time by integrating this equation from the initial tank pressure  $P_i$  to the final pressure  $P_2$

$$t = \frac{V}{S'} \ln \left[ \frac{P_i - P_a}{P_2 - P_a} \right]. \quad (5.68)$$

However, because  $S'$  is a function of the conductance, it is also a function of pressure at the higher pressures where viscous flow occurs. Therefore, in order to use Eq. (5.68), our approach will have to be to add several values of  $t$  obtained by incrementing  $S'$  until it is no longer a function of pressure. Equation (5.68) is not completely accurate, but it is a good approximation down to a pressure of the order of 1 torr.

Finally, we must consider the interaction and matching of the forepump and diffusion pump. Figure 5.20 includes the performance curves for a diffusion pump and a mechanical pump. In operation, the forepump is turned on, and run alone until a forepump inlet pressure less than the limiting forepressure of the diffusion pump is reached, at which point the lower stages of the diffusion pump become operative. If the pressure at the diffusion pump inlet is  $P$ , then the throughput is at point  $Q$ , and since the throughput is the same at any instant for both pumps, then the forepump inlet pressure is  $P'$ , its speed is  $S'$ , and its throughput  $Q'$ .

Because the speed and throughput required of mechanical pumps when employed as forepumps are often rather low values, their use in large systems for roughing out would require excessively long pumpdown times. Therefore separate mechanical roughing pumps are often used, and then turned off when the diffusion pump-forepump combination can be applied.

#### 5.5.5 Ejectors

For very large systems, other types of vapor pumps, called *steam ejectors*, are used. Figure 5.21 shows a schematic diagram of such an ejector. The steam is made to pass through a converging-diverging nozzle, designed to reach Mach 2 or higher at the nozzle exit and, correspondingly, a very low pressure  $P_e$ . The inlet port design pressure is then this  $P_e$ , and the steam jet entrains gas molecules at this pressure, as it leaves the nozzle. Flow into the port is again due to statistical molecular flow, at the lower pressures. Once entrained, the gas and steam slow down and are compressed in the diffuser so that they may exit at an

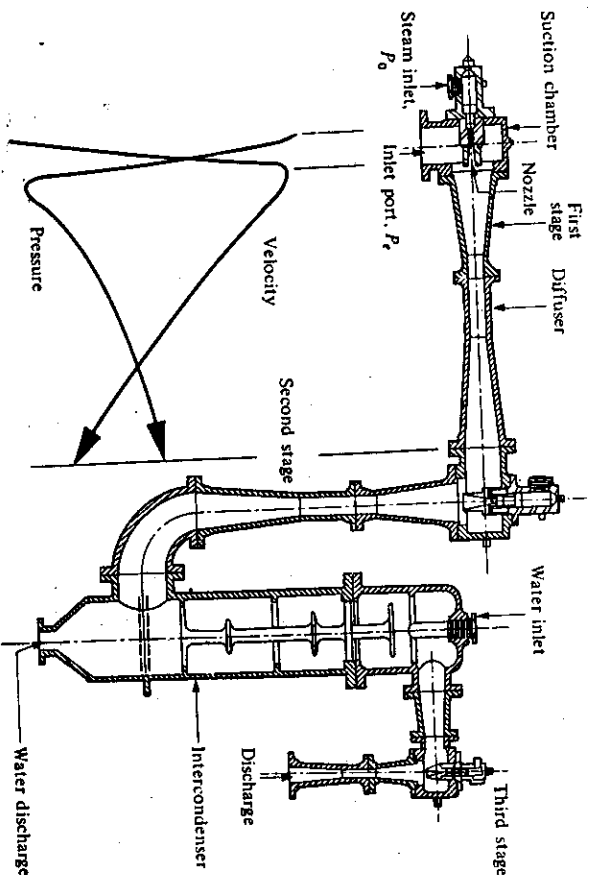


**Fig. 5.21** Three-stage steam ejector with intercondenser. Schematic diagram of pressure-velocity relationships in the first-stage ejector is included.

exhaust pressure equal to the atmosphere, in the case of a single-stage pump, or at the design inlet pressure to the next stage in the case of a multiple-stage ejector. In order to lighten the load on the succeeding stages, condensers are often inserted between stages to remove the steam from the preceding stage.

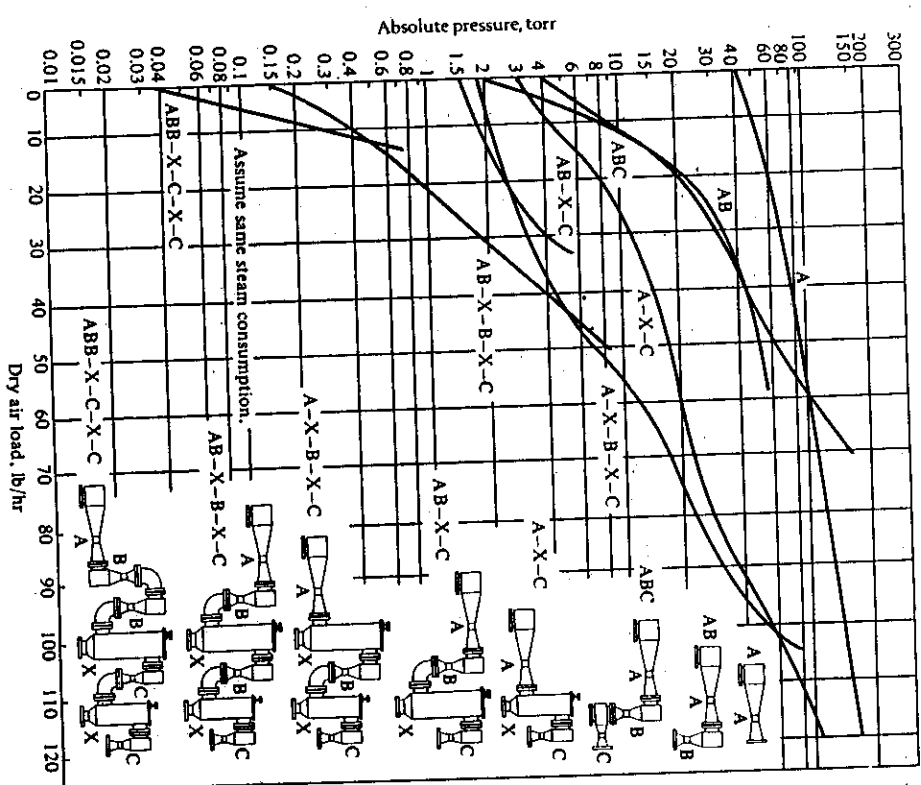
The pumping up of pounds of dry air removed per hour. For comparison purposes

Figure 5.22 illustrates the range of pressures and throughputs obtainable with typical combinations of ejector stages and condensers.

## 5.5.6 Molecular pumps

We saw in Section 5.5.3 that diffusion pumps are often coupled with mechanical roughing pumps to achieve pressures that are typically  $10^{-6}$  torr without traps. Molecular pumps can also be used to achieve similar pressures, although at somewhat more cost.

In molecular pumps, the gas molecules are imparted a velocity by momentum transfer also be used to activate .... from a fast-moving solid surface. In diffusion pumps, the gas molecules are entrapped and carried from the inlet to the discharge by the stream of vapor. In molecular pumps, collisions occur with the fast-moving surface. Pumps of this type can maintain pressures as low as  $10^{-7}$  torr, while discharging at 10 to 40 torr (a considerably higher discharge pressure than tolerated by diffusion pumps).



**Fig. 5.22** Ranges of application of various steam-jetector (A, B, C) nozzles. (From an article by F. Berkeley, *Chem. Eng.* (April 1957), page 255.)

Advantages of molecular pumps include their installation in systems with smaller backing pumps than required when diffusion pumps are used. Backstreaming of oil molecules from the mechanical pump is lessened because the discharge pressure is relatively high. When large throughputs are needed, the turbomolecular pumps that are used are axial-flow turbines.

### 5.5.7 Gettering and ion pumps

The pressure region between  $10^{-9}$  and  $10^{-12}$  torr is often referred to as *ultrahigh vacuum*. At such low pressures, we start thinking about the number of molecules per unit volume rather than pressure as a force per unit area. Consequently, the amount of gas adsorbed on surfaces in the vacuum system is paramount, so maintaining a ultrahigh vacuum system requires the maintenance of ultraclean surfaces.

In an ultrahigh vacuum a surface can hold a large number of molecules compared to the number of molecules in the vacuum space. To effect a pumping action, a chemically active surface can be used to "get" molecules from the vacuum space by physisorption. The most commonly used material is titanium.

In the inset of Fig. 5.23, there is a titanium source that sublimes by electrical heating. The titanium atoms travel to the colder surrounding surface, where they condense and form a large surface of fresh titanium. In turn, the layer of fresh titanium forms stable compounds with chemically active gas molecules that strike the surface. The capture process is continuous so long as new layers are deposited.

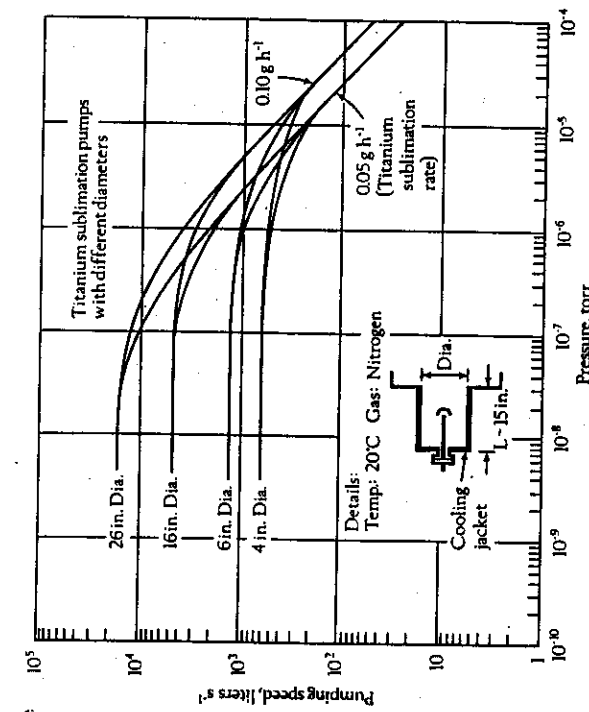


Fig. 5.23 Pumping speeds of gettering pumps of various sizes. (From M. H. Hablanian, *High Vacuum Technology*, Marcel Dekker, Inc., New York, N.Y., 1990.)

So-called sputter-ion pumps can also be used to supply the layer of fresh titanium. The device consists of a cylinder of stainless steel (the anode) and plates of titanium (the cathode) positioned near the open ends of the cylinder. Electrons are emitted from the cathode because 5 to 7 kV are applied between the electrodes. The trajectories of these electrons are controlled by a magnet which causes the electrons to move in very long helical paths in order to improve the chances of collisions between the electrons and gas molecules. These collisions produce positively charged ions that travel to the cathode (titanium). This collision ejects titanium atoms (i.e., sputtering) which deposit on other surfaces in the system and capture other molecules.

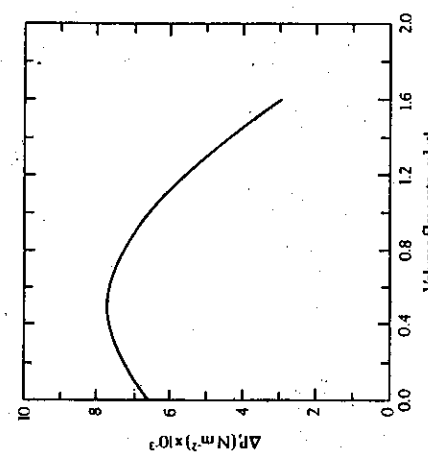
The pumping speed characteristics of a sputter-ion pump are qualitatively similar to that shown for the diffusion pump in Fig. 5.20, with the major advantage of having an ultimate pressure ( $P_o$ ) that is less than  $10^{-11}$  torr. There is a range of intermediate pressures ( $10^{-7}$  to  $10^{-5}$  torr), where the pumping speed is approximately constant. At lower pressures, the speed decreases to zero at  $P_o$ , and it decreases to very low values at higher pressures. Sputter-ion pumps have relatively low throughputs and should only be coupled with roughing pumps that

can achieve  $10^{-3}$  torr. The cathodes are eroded by sputtering, and they must be replaced periodically, which is not a simple matter.

### PROBLEMS

5.1 Refer to Example 3.5 for the system characteristics and the desired operating point for flow through a sinter bed. The bed has a cross-sectional area of  $0.189 \text{ m}^2$ , and  $V_0$  is a superficial velocity. You can select either fan A or fan B to blow the air. Their respective characteristic curves are given to the right.

- If you select fan A, what volume flow rate will be delivered through the sinter bed? Repeat for fan B. You may assume that the pressure drop through the sinter bed is proportional to the square of volume flow rate; i.e.,  $\Delta P = kQ^2$ .
- Which fan, A or B, is better suited for the bed of ore and coal which is discussed? Explain why.
- What adaptation, if any, must be made to use the fan you have selected?



5.2 Refer to Problem 4.4. Suppose the characteristic curve of the fan is as shown to the right.

- Assume that  $\Delta P = kQ^2$  for the entire system and determine the operating point.
- As particulates are collected, the pressure drop across the bag house increases. When the pressure drop increases by twenty percent, what will be the volume flow rate?

- 5.3** Two identical pumps are used to pump water from one reservoir to another whose level is 6.1 m higher than the first. When both pumps are operating the flow rate is  $0.04 \text{ m}^3 \text{s}^{-1}$ . What is the flow rate when only one pump operates? Assume highly turbulent flow. The characteristic head curve for the pump is given by the following table.

Flow rate, $\text{m}^3 \text{s}^{-1}$	Head, $\text{N m kg}^{-1}$
0	208
0.0057	211
0.0113	212
0.0170	211
0.0227	203
0.0340	178
0.0453	141
0.0566	99
0.0680	39
0.0736	15

- 5.4** Derive an equation for the conductance of a long straight tube. Assume viscous flow prevails and that the viscosity is given by Eq. (1.13).

- a) Write the conductance in terms of viscosity.  
b) Show that

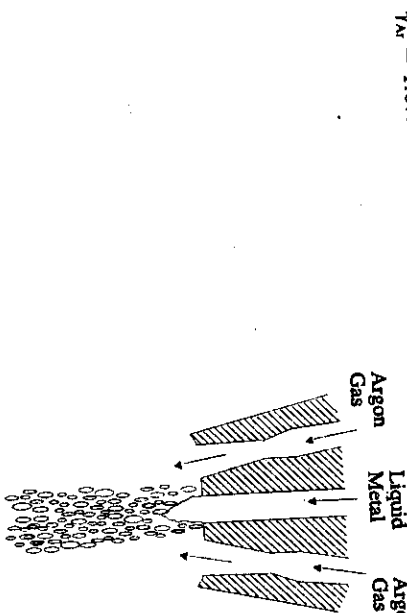
$$\eta = \frac{m\bar{V}}{3\pi^{1/2} d^2},$$

where  $\bar{V}$  is the Maxwellian speed of the molecules.

- c) Write the conductance in terms of  $\bar{V}$ .

- 5.5** Compare the conductance for viscous flow in a long straight tube (from Problem 5.4c) to the conductance for molecular flow.

- a) How does each vary with  $\bar{V}$ ?  
b) How does each vary with temperature?  
c) For nitrogen at 300 K, what is the mean free path (see Eq. (1.5)) at normal atmospheric pressure (760 torr).



- 5.6** For nitrogen at 300 K, what is the minimum diameter of a long tube for viscous conduction at a) standard atmospheric pressure (760 torr). Repeat for b) 100 torr, c) 10 torr, d) 1 torr and e)  $10^{-1}$  torr. [The criterion is  $(\lambda/D) \geq 10$  where  $\lambda$  is the mean free path (see Eq. (1.5)).]
- 5.7** Consult Table 5.2 and obtain the conductance for two chambers connected by a tube with a diameter 250 mm and a length of 750 mm. Compare your result to the approximation given by Eq. (5.52). Assume that the gas is air at 298 K, with a molecular weight of 28.8 kg kmol<sup>-1</sup>.
- 5.8** Consider the use of the two-stage pump of Fig. 5.18 that is connected to a chamber of 1 m<sup>3</sup> volume through a duct with an infinitely high conductance. Calculate the time to pumpdown to a)  $10^{-2}$  torr and b)  $10^{-4}$  torr.

- 5.9** A heat of steel ( $5 \times 10^4 \text{ kg}$ ) is to be vacuum degassed from 5 ppm H<sub>2</sub> to 1 ppm H<sub>2</sub> and from 100 ppm N<sub>2</sub> to 75 ppm N<sub>2</sub> in 15 min. The steel is at 1873 K, and the chamber has 9 m<sup>3</sup> of space occupied by air after the top is closed with the lidle inside. At what pressure would you recommend operating the system? Calculate the throughputs of air, hydrogen and nitrogen that must be removed from the chamber. Consult Fig. 5.22 and specify a steam ejector to do the job.
- 5.10** An ultrahigh vacuum chamber (300 liters) is equipped with two pumping modes, one which liquid metal is fed. The argon gas jets are focused on a point below the exit of the orifice, where they impinge on the metal stream to break it into fine droplets that solidify to microstructures of particular interest. It has been found that nozzle exit velocities on the order of Mach 3 are desirable. For a Mach 3 nozzle calculate the reservoir pressure  $P_0$  needed, if the desired exit pressure is 1.0 atm and the flow rate of argon is  $0.1 \text{ kg s}^{-1}$ . Assume should the throat diameter, exit diameter and length of diverging section be? Assume  $\gamma_{\text{Ar}} = 1.67$ .

- 5.11** Supersonic nozzles are arranged circumferentially around a central orifice through which liquid metal is fed. The argon gas jets are focused on a point below the exit of the orifice, where they impinge on the metal stream to break it into fine droplets that solidify to microstructures of particular interest. It has been found that nozzle exit velocities on the order of Mach 3 are desirable. For a Mach 3 nozzle calculate the reservoir pressure  $P_0$  needed, if the desired exit pressure is 1.0 atm and the flow rate of argon is  $0.1 \text{ kg s}^{-1}$ . Assume should the throat diameter, exit diameter and length of diverging section be? Assume  $\gamma_{\text{Ar}} = 1.67$ .
- 5.12** Derive Eq. (5.20).

## PART TWO

### ENERGY TRANSPORT

In the processing of materials, a situation almost invariably arises that necessitates a change in the temperature of a material, as, for example, in heat treating processes. We assume that the student is aware of the importance of being able to calculate the heat which is produced and used in such processes, by making heat balances. However, it is also desirable to have an understanding of how heat is transferred into, out of, and within materials processes, because many operations take place in such a way that the *rate* of energy transfer becomes the controlling factor in raising and lowering the temperature. Since we usually consider this energy to be virtually all thermal energy, we speak of *heat transfer* as the controlling factor.

There are two basic types of heat-transfer mechanisms: *conduction* and *radiation*. Quite frequently, however, three mechanisms are set forth, namely, conduction, radiation, and convection. To be more specific, convection is rather a process involving mass movement of fluids, than a real mechanism of heat transfer. In regard to this distinction it is better to speak of "heat transfer with convection" rather than of "heat transfer by convection." The term convection implies fluid motion, and mechanisms of heat transfer anywhere within the fluid are only conduction and radiation. We shall discuss conduction and radiation, and present the relationships used for describing heat transfer by each mechanism in the following chapters. Here, as an introduction, we shall consider them in brief.

Conduction is the transfer of heat by molecular motion which occurs between two parts of the same body, or between two bodies which are in physical contact with each other. In fluids, heat is conducted by molecular collisions; in solids, heat is conducted either by lattice waves in nonconductors or by a combination of lattice waves with the drift of the conduction electrons in conducting materials. The macroscopic theory of conduction is merely *Fourier's law*:

$$q_y = -k \frac{\partial T}{\partial y},$$

where  $q_y$  is the heat flux in the  $y$ -direction,  $\partial T/\partial y$  is the temperature gradient in the  $y$ -direction, and  $k$  is the thermal conductivity. Note the analogy with Newton's law of viscosity (Eq. 1.3). In both cases, fluxes are proportional to gradients, and the relationships

186 Energy Transport  
also define the proportionality constants, namely, viscosity by Newton's law and thermal conductivity by Fourier's law.

The nature of heat transfer by radiation is quite different from that by conduction, and consequently the basic rate equation for heat transfer by radiation is in no way similar to Fourier's law. In Chapter 11, we shall analyze radiation problems in detail; here, we state briefly that thermal radiation is part of the electromagnetic spectrum. The energy flux emitted by an ideal radiator is proportional to the fourth power of its absolute temperature.

$$e_b = \sigma T^4,$$

where  $e_b$  is the emissive power (a special term for the thermal emission from an ideal radiator) and  $\sigma$  is the Stefan-Boltzmann constant. The processes of conduction and radiation frequently occur simultaneously, even within certain media. In many practical situations, however, one mode is negligible with respect to the other, and may be ignored.

When a moving fluid at one temperature is in contact with a solid at a different temperature, heat exchanges between the solid and the fluid by conduction at a rate given by Fourier's law where  $k$  is the conductivity of the fluid, and  $\partial T / \partial y$  is the temperature gradient in the fluid normal to the wall at the fluid-solid interface. If the details of the convection are known in a given situation, then we can determine the distribution of temperature within the fluid, and calculate the heat flux at the wall. In many cases, such a detailed analysis is not available; then it is convenient to define the *heat-transfer coefficient*,  $h$ , by the equation

$$h = \frac{q_0}{T_s - T_f} = \frac{-k(\partial T / \partial y)}{T_s - T_f},$$

where  $T_s$  is the surface temperature,  $T_f$  is usually taken as some bulk fluid temperature, and  $q_0$  is the heat flux at the wall. The units of  $h$ , which is a function of the fluid and the flow pattern of the system, are  $\text{W m}^{-2} \text{K}^{-1}$ . Much of the research on heat transfer has been devoted to the determination of  $h$ , since it enters into all problems of heat transfer with convection.

Convection is usually classified as either a *forced* convection or *free* (*natural*) convection. When a pump or other mechanical device causes the fluid to move, we call this process forced convection; when a fluid moves as a result of density difference, then we speak of a free or natural convection. Thus, when a radiator heats the air which rises, displacing colder air in the upper part of a room, the fluid motion is by natural convection.

In Part Two, we shall examine the thermal conductivity of materials and the various modes of heat transfer applied to situations in materials processing.

## 6

### FOURIER'S LAW AND THERMAL CONDUCTIVITY OF MATERIALS

Thermal conductivity is an intrinsic property of materials. In this chapter we consider the thermal conductivity of various materials, such as gases, liquids, and solids, with the emphasis on solids, including porous solids.

#### 6.1 FOURIER'S LAW AND THERMAL CONDUCTIVITY

Consider a slab of area  $A$  bounded by two large parallel surfaces a distance  $Y$  apart (Fig. 6.1). Initially, the slab is at a uniform temperature  $T_0$ . At some instant, the lower surface is suddenly raised to a temperature  $T_1$ , which is maintained. The material above the heated surface becomes heated, and the heat is gradually transferred across the slab toward the colder surface, which is kept at  $T_0$ . A steady-state temperature distribution is attained when a constant rate of heat flow through the slab is required to maintain the temperature difference  $T_1 - T_0$ . It is found that for sufficiently small temperature differences, the rate of heat flow per unit area  $q$  is proportional to the temperature difference and inversely proportional to the distance between the surfaces; hence,

$$q = k \frac{(T_1 - T_0)}{Y}. \quad (6.1)$$

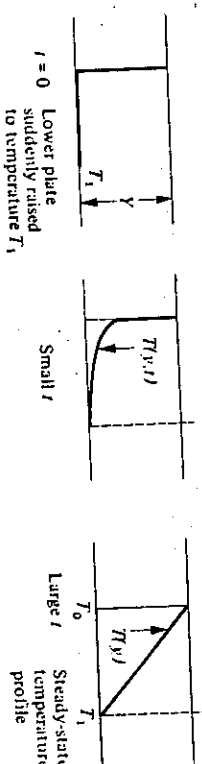


Fig. 6.1 Build-up to steady-state temperature profile for a solid slab.

Equation (6.1) also applies to liquids and gases, provided no convection or heat transfer by radiation is allowed to take place in the fluid. As stated, the temperature difference must be sufficiently small, because the thermal conductivity depends not only on the specific material, but also on the temperature. Equation (6.1) is therefore valid for fixed values of  $T_1$  and  $T_0$  for all values of  $Y$ .

As the temperature difference and the separation distance approach zero, the differential form of Fourier's law of heat conduction arises:

$$q_y = -k \frac{\partial T}{\partial y} \quad (6.2)$$

The flow of heat per unit area (heat flux) in the  $y$ -direction is proportional to the temperature gradient in the  $y$ -direction.

For a three-dimensional situation in which the temperature varies in all three directions in material with an isotropic thermal conductivity, we write

$$q_x = -k \frac{\partial T}{\partial x}; \quad q_y = -k \frac{\partial T}{\partial y}; \quad q_z = -k \frac{\partial T}{\partial z}. \quad (6.3)$$

These three relations form the components of the single equation

$$\mathbf{q} = -k\nabla T. \quad (6.4)$$

Note the similarity between Eq. (6.2) for one-dimensional heat flux and Eq. (1.2) for one-dimensional momentum flux. In each case, the flux is proportional to the gradient of a potential variable, temperature and velocity, respectively. The mathematical similarity ends, however, when we compare the three components for heat flux versus the nine components that express momentum transfer in three dimensions. This is because energy is a scalar quantity whereas momentum is a vector quantity.

The units involved in Fourier's law of heat conduction are

	SI units*	English units
$q_x, q_y, q_z$	$\text{W m}^{-2}$	$\text{Btu h}^{-1} \text{ft}^{-2}$
$T$	$\text{K}$	$^{\circ}\text{F}$ or $\text{R}$
$x, y, z$	$\text{m}$	$\text{ft}$
$k$	$\text{W m}^{-1} \text{K}^{-1}$	$\text{Btu h}^{-1} \text{ft}^{-1} {^{\circ}\text{F}}^{-1}$

Therefore,

$$q_x = -\frac{8k(T_s - T_0)}{\delta} \left( \frac{x}{\delta} \right).$$

Substituting values, we get

$$q_x = -\frac{(8)(600 \text{ K})}{\delta} \left| \frac{10 \text{ W}}{\text{m K}} \right| \left| \frac{(x/\delta)}{0.02 \text{ m}} \right|.$$

$$q_x = -2.4 \times 10^6 \left[ \frac{x}{\delta} \right] \text{ W m}^{-2}.$$

The absolute value of the flux varies from its maximum of  $2.4 \times 10^6 \text{ W m}^{-2}$  at the surface to zero at the centerline.

**Example 6.1** A flat slab of uniform thickness ( $\delta = 0.02 \text{ m}$ ) with an initial temperature of 300 K is placed in a furnace. At 900 s after being placed in the furnace, a series of thermocouples embedded in the slab gives a temperature distribution approximated by a second order polynomial:

$$T = a_0 + a_1 x + a_2 x^2$$

where  $T$  is temperature, K,  $x$  is distance from the centerline of the slab in mm, and the  $a_i$ 's are constants. Assume that  $T(x)$  is symmetrical. a) Solve for the constants in terms of the surface ( $T_s$ ) and centerline ( $T_0$ ) temperatures. b) Solve for the heat flux as a function of  $x$  in the slab if  $T_s = 1000 \text{ K}$  and  $T_0 = 400 \text{ K}$ . The thermal conductivity of the slab is  $10 \text{ W m}^{-1} \text{ K}^1$ .

**Solution.** a)  $T(x)$  is symmetrical. Therefore  $\partial T / \partial x = 0$  at  $x = 0$ , and it is easy to show that  $a_1 = 0$ . The other two specifications give

$$T_s = a_0 + a_2 \left[ \frac{\delta}{2} \right]^2$$

and

$$T_0 = a_0,$$

so that

$$a_2 = \frac{4(T_s - T_0)}{\delta^2}.$$

b) The flux is

$$q_x = -k \frac{\partial T}{\partial x}$$

and

$$\frac{\partial T}{\partial x} = 2a_2 x = \frac{8(T_s - T_0)}{\delta} \left( \frac{x}{\delta} \right).$$

\*  $1 \text{ W m}^{-1} \text{ K}^1 = 0.57782 \text{ Btu h}^{-1} \text{ ft}^{-2} {^{\circ}\text{F}}^{-1}$ .

## 6.2 THERMAL CONDUCTIVITY OF GASES

Conduction of energy in a gas phase is primarily by transfer of translational energy from molecule to molecule as the faster moving (higher-energy) molecules collide with the slower ones.

For a simple, monoatomic gas, we can develop an expression for the thermal conductivity in a similar manner as we did in Eq. (1.13) for viscosity. Assume that the gas in Fig. 1.5 is under the influence of a temperature gradient,  $\partial T/\partial y$ . The temperatures of the molecules at  $y - \bar{y}$  and  $y + \bar{y}$  are, respectively,

$$T|_{y-\bar{y}} = T|_y - \frac{2}{3} \lambda \frac{\partial T}{\partial y}, \quad (6.5)$$

and

$$T|_{y+\bar{y}} = T|_y + \frac{2}{3} \lambda \frac{\partial T}{\partial y}. \quad (6.6)$$

Here the average distance moved in the  $y$ -direction between collisions is  $\bar{y}$ , and  $\bar{y} = \frac{2}{3}\lambda$ , where  $\lambda$  is the mean free path as defined by Eq. (1.7).

If the heat capacity per molecule is  $c$ , then the net flux of thermal energy across the plane at  $y$  is given by the net difference between the energy of the molecules crossing the  $y$ -plane in the positive and in the negative directions:

$$q_y = ZCT|_{y-\bar{y}} - ZCT|_{y+\bar{y}} = Zc(T|_{y-\bar{y}} - T|_{y+\bar{y}}). \quad (6.7)$$

Equation (1.6) gives the expression for  $Z$ , the flux of molecules ( $\text{number m}^2 \text{s}^{-1}$ ) crossing the  $y$ -plane in either the positive or the negative direction; Eqs. (6.5) and (6.6) give the expressions for the temperatures, so that ultimately

$$q_y = -\frac{ncV\lambda}{3} \left[ \frac{\partial T}{\partial y} \right]. \quad (6.8)$$

Denoting  $nc$  as  $C_V$ , the heat capacity per unit volume, and by comparing Eq. (6.8) to Eq. (6.2), we arrive at

$$k = \frac{C_V \bar{V}\lambda}{3}. \quad (6.9)$$

This equation is basic for an understanding of the thermal conductivity of gases. In some cases, it can be extended to aid in theorizing about the thermal conductivity of solids and liquids. For dilute gases with atoms assumed as rigid spheres, Eqs. (1.4) and (1.5) may be substituted for  $\bar{V}$  and  $\lambda$  in Eq. (6.9), with the result that

$$k = \frac{1}{d^2} \left[ \frac{k_B^3 T}{\pi^3 n} \right]^{1/2} \quad (6.10)$$

This result suggests that the thermal conductivity of gases does not depend on pressure, but that it does depend on the square root of the temperature. For pressures to about 10 atm, this lack of dependence on pressure is essentially correct. The thermal conductivity, however, increases with temperature more than predicted by Eq. (6.10).

In the case of polyatomic gases, Eucken<sup>1</sup> developed an equation for the thermal conductivity of these gases at normal pressures:

$$k = \eta \left[ C_p + \frac{1.25R}{M} \right], \quad (6.11)$$

where  $M$  is the molecular weight and  $C_p$  the heat capacity at constant pressure.

In the case of gas mixtures, we can estimate the thermal conductivity within a few percent by

$$k_{\text{mix}} = \frac{\sum_i X_i k_i M_i^{1/3}}{\sum_i X_i M_i^{1/3}}, \quad (6.12)$$

where  $X_i$  is the mole fraction of component  $i$  having molecular weight  $M_i$  and intrinsic thermal conductivity  $k_i$ . A comparison<sup>2</sup> of observed conductivities with calculated values, using Eq. (6.12), for binary gas mixtures involving air, CO, CO<sub>2</sub>, H<sub>2</sub>O, N<sub>2</sub>, N<sub>2</sub>O, NH<sub>3</sub>, CH<sub>4</sub>, C<sub>2</sub>H<sub>2</sub>, He, and Ar, indicates average discrepancies of only 2.7% over the temperature range 273–353 K. Tests at elevated temperatures are not available, but the errors would probably be no larger. There are more complex equations, which reduce the errors to about 1%, but they are not as easy to use.

Figure 6.2 gives the thermal conductivities of several common gases as a function of temperature. The data are valid to at least 10<sup>6</sup> Pa (approx. 10 atm).

**Example 6.2** Calculate the thermal conductivity of a gas containing 40 mol% CH<sub>4</sub> and 60 mol% H<sub>2</sub>, at  $1.5 \times 10^5 \text{ N m}^{-2}$  pressure and 1255 K.

**Solution.** From Fig. 6.2,  $k_{\text{H}_2} = 0.51 \text{ W m}^{-1} \text{ K}^{-1}$  and  $k_{\text{CH}_4} = 0.22 \text{ W m}^{-1} \text{ K}^{-1}$ . Using Eq. (6.12) we get

$$k_{\text{mix}} = \frac{(0.6)(0.51)(2)^{1/3} + (0.4)(0.22)(16)^{1/3}}{(0.6)(2)^{1/3} + (0.4)(16)^{1/3}} = 0.34 \text{ W m}^{-1} \text{ K}^{-1}.$$

The fact that the pressure is  $1.5 \times 10^5 \text{ N m}^{-2}$  has no significance here, since the thermal conductivity is independent of pressure at this pressure level.

## 6.3 THERMAL CONDUCTIVITY OF SOLIDS

Solids transmit thermal energy by two modes, either one of which, or both, may operate. In all solids, energy may be transferred by means of elastic vibrations of the lattice moving through the crystal in the form of waves. In some solids, notably metals, free electrons moving through the lattice also carry energy in a manner similar to thermal conduction in a gas.

<sup>1</sup>A. Eucken, *Physik Z.* 14, 324 (1913).

<sup>2</sup>L. Friend and S. Adler, article in *Transport Properties in Gases*, Northwestern University Press, Evanston, IL, 1958.

If the forces between atoms were perfectly harmonic, two phonons moving through the crystal could collide and combine, with the resulting phonon having the same total energy and momentum, energy transport would continue in the direction of the resultant of the original phonons. If this were the only type of phonon-phonon interaction (Normal or N-type), then the only limit to the mean free-path of the phonons would be the dimensions of the piece of the material itself, since the resultant phonon acts in the same manner as the two original phonons as far as energy transport is concerned. Thermal conduction would thus be extremely easy. But the forces between atoms are not in perfect harmony, and there exists another type of collision between phonons, known as an Umklapp (U-process) collision. In this process, energy is conserved, while phonon momentum is not, and the result of such a collision is that a phonon moves in a direction opposite to the resultant of the original phonons. For these processes, the mean free-path of phonons is extremely short, being of the order of the distance between atoms. Since the number of phonons increases with temperature, the number of the U-processes also increases with temperature and the wavelength of the phonons  $\lambda_{ph}$  is proportional to  $1/T$ . At room temperature and above,  $\hat{C}_v$  for most materials is roughly constant, and if we use Eq. (6.9) to describe the thermal conductivity of a solid which conducts energy only by phonons, then  $k$  must decrease with increasing temperature. This is what happens in most electrically insulating substances, such as the oxides shown in Fig. 6.3 (but not in the form of porous, bulk materials).

When heat enters a crystal, the crystal expands, and this thermal expansion of the lattice is related to the bulk modulus  $B$  by a constant  $\gamma$ , known as Gruneisen's constant

$$\gamma = \frac{\hat{V}}{\hat{C}_v} \left[ \frac{\partial P}{\partial T} \right]_v = \frac{3B\hat{V}\alpha}{\hat{C}_v}, \quad (6.13)$$

where  $\hat{V}$  = molar volume,  $\alpha$  = linear thermal expansion coefficient, and  $\hat{C}_v$  = molar heat capacity. For most solids at ordinary temperatures,  $\gamma \approx 2$ . Combining this result with Lindemann's theory of the melting of solids, Debye showed that

$$\lambda_{ph} = \frac{20T_m d}{\gamma^2 T}, \quad (6.14)$$

where  $T_m$  = melting point,  $T$  = absolute temperature, and  $d$  = crystal-lattice dimension, resulting in the previously mentioned intuitive relation between phonon mean free path and temperature. Note that a high-melting-point material has a large value of  $\lambda$  at low temperatures, and therefore a large value of  $k$  at room temperature. We can observe this in the case of diamond, which has a thermal conductivity at room temperature comparable to that of copper, one of the best conductors known. However, the conductivity of diamond drops very rapidly to a small fraction of that of copper as the temperature increases.

At very low temperatures ( $T < 10$  K),  $\lambda_{ph}$  approaches the dimensions of the crystal, since U-processes diminish rapidly as the temperature approaches absolute zero; consequently, the thermal conductivity rises rapidly. In this case, the larger the crystal, the higher the thermal conductivity, as illustrated in Fig. 6.4; this is an exception to Fourier's law.

Phonons are also scattered by differences in isotopic masses, chemical impurities, dislocations, and second phases. With these imperfections quantitative prediction of thermal conductivity is exceedingly difficult, but we can be sure that the less perfect the crystal is, the lower is the thermal conductivity.

The influence of structure and composition on the thermal conductivity of dielectric materials is difficult to predict. Qualitatively we know that materials with complex structures have a greater tendency toward thermal scattering of phonons (i.e., Umklapp collisions) and accordingly lower thermal conductivities. Mullite ( $\text{Al}_2\text{O}_3\text{-MgO}$ ), for example, has a lower thermal conductivity than either pure  $\text{Al}_2\text{O}_3$  or pure  $\text{MgO}$ . Comparisons between single

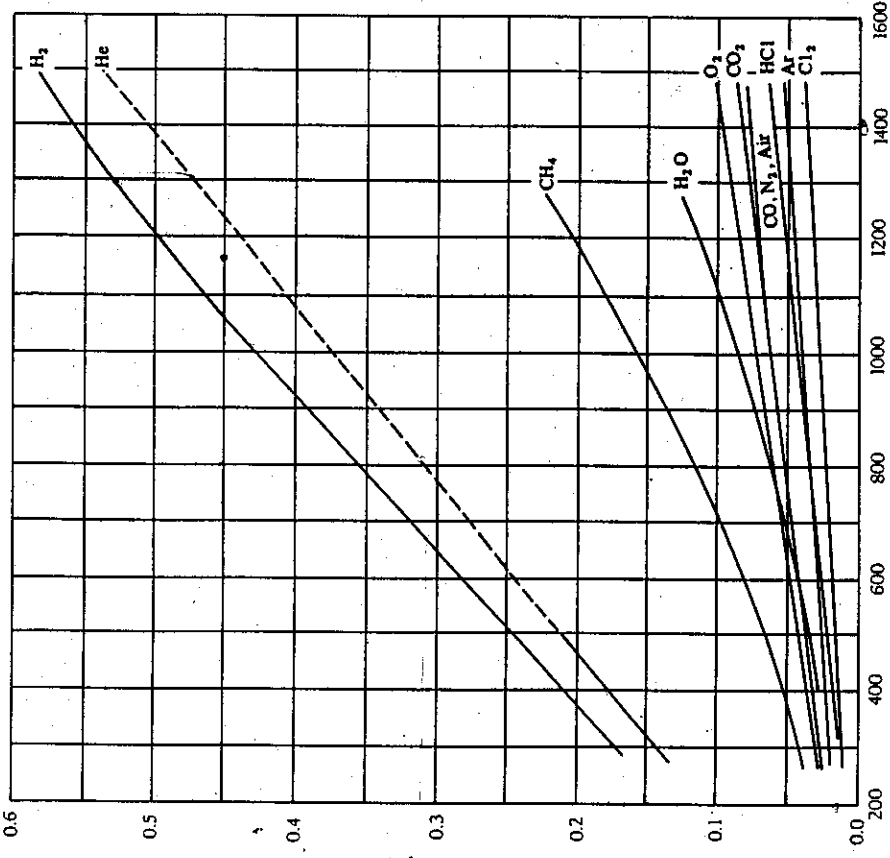
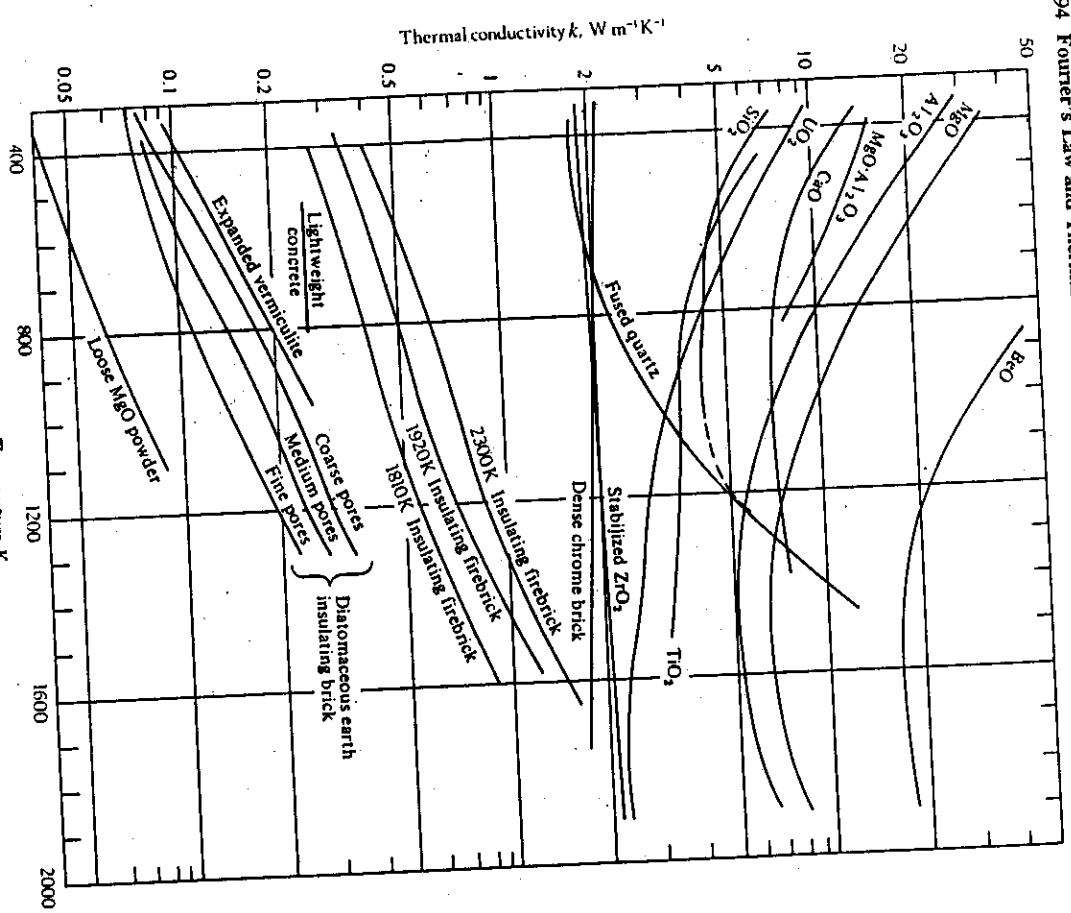


Fig. 6.2 Thermal conductivity of several gases. Data valid for up to  $10^8$  Pa (approx. 10 atm).

Recalling the fundamental treatments of bonding in solids, we remember that at ordinary temperatures all solids store thermal energy as vibratory motion of their atoms, and potential energy in the bonding between atoms. Einstein developed his theory for the heat capacity of solids by assuming that each atom vibrates independently of its neighbors. This, however, results in no conduction via lattice waves, which in fact exists because neighboring atoms do interact and therefore do not vibrate independently. Debye, in the process of improving Einstein's model of heat capacity, assumed that the lattice is made up of independent oscillators, and that these oscillators are simply considered to be elastic waves traveling in different directions with different polarizations and wavelengths, not necessarily associated with the atoms themselves. This led to his theory of specific heat ( $C_v \propto T^3$  at low temperatures) which is more in agreement with experiments than Einstein's theory, and also gives a more satisfactory picture of thermal conductivity of insulating solids. Each lattice vibration (there is always a spectrum of vibrations) may be described as a traveling wave carrying energy and obeying the laws of quantum mechanics. By analogy with light theory, the waves in a crystal exhibit the attributes of particles and are called **phonons**.



**Fig. 6.3** Thermal conductivity of oxides and various insulating materials. (From A. Schack, *Industrial Heat Transfer*, Wiley, New York, NY, 1965, page 189.)

crystals and polycrystalline samples of  $\text{Al}_2\text{O}_3$ ,  $\text{CaF}_2$  and  $\text{TiO}_2$ , show that the thermal conductivities are equal below 500 K (approx.), but at higher temperatures the polycrystalline samples are less conductive. The effect of composition in solid solutions of two oxides,  $\text{MgO}$  and  $\text{NiO}$ , is shown in Fig. 6.5. Numerous examples of the effects of structure and composition in dielectric materials are given by Kingery *et al.*<sup>3</sup>

<sup>3</sup>W. D. Kingery, H. K. Bowen and D. R. Uhlmann, *Introduction to Ceramics*, 2nd ed., John Wiley, New York, NY, 1976, pages 613-642.

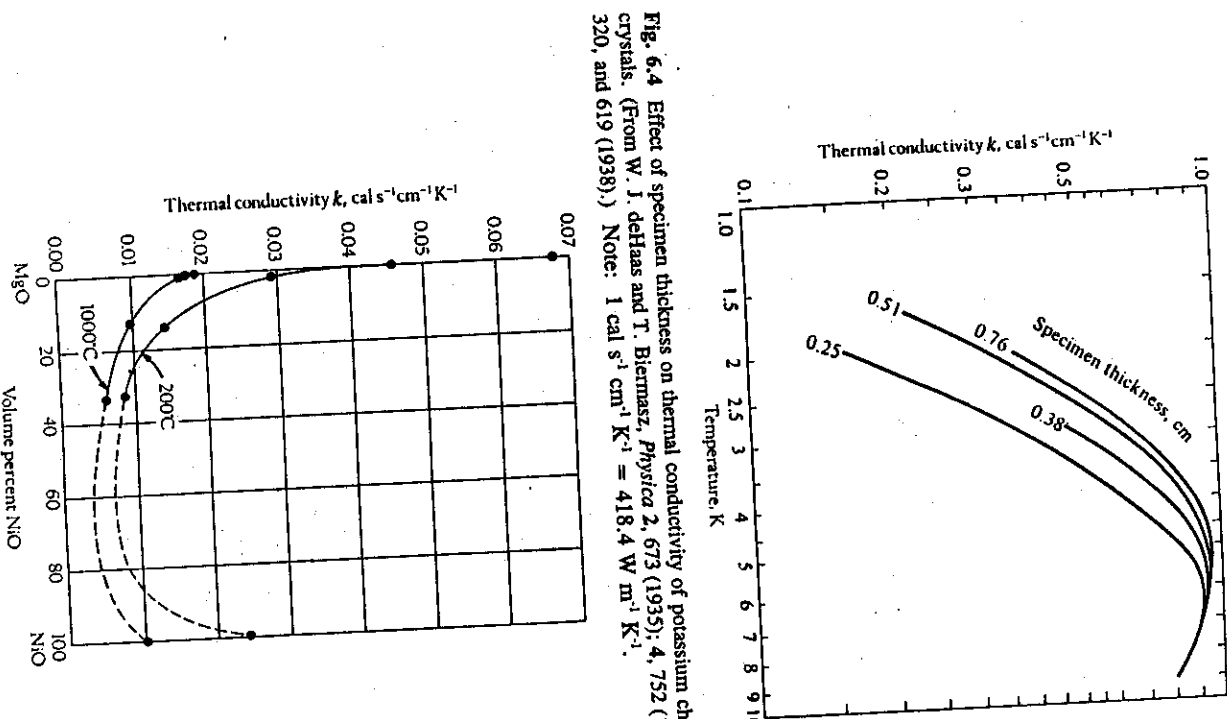


**Fig. 6.4** Effect of specimen thickness on thermal conductivity of potassium chloride single crystals. (From W. J. deHaas and T. Biermasz, *Physica* 2, 673 (1935); 4, 752 (1937); 5, 47, 320, and 619 (1938).) Note:  $1 \text{ cal s}^{-1} \text{cm}^{-1} \text{K}^{-1} = 418.4 \text{ W m}^{-1} \text{K}^{-1}$ .

As we proceed from electrical insulators to conductors, we deal with materials with increasing concentrations of conduction electrons. The conduction electrons in metals form an *electron gas* which obeys the laws of quantum mechanics. The electronic contribution to the volumetric heat capacity of a metal is given by

$$C_{v,\text{el}} = \frac{\pi^2 n_e k_B T}{2e_F} \quad (6.15)$$

Here  $e_F$  is the Fermi energy, and  $n_e$  is the number of free electrons per  $\text{cm}^3$ . The Fermi energy is related to the average velocity of the electrons by

$$\bar{V}_F = \left[ \frac{2e_F}{m_e} \right]^{1/2} \quad (6.16)$$

where  $\bar{V}_F$  = electron velocity at the Fermi surface, and  $m_e$  = electron mass. Using Eq. (6.15) for the heat capacity and Eq. (6.16) for the Fermi energy, Eq. (6.9) becomes

$$k_{\text{el}} = \frac{\pi^2 n_e^2 s T \lambda_e}{3m_e \bar{V}_F} \quad (6.17)$$

where  $k_{\text{el}}$  is now the electronic contribution to the thermal conductivity. This predicts that the electronic contribution in metals *increases* with temperature, provided that  $\lambda_e$  does not decrease just as strongly with temperature.

To prove that the electrons in a metal carry the major portion of the thermal energy, the thermal and electrical conductivities should be proportionally related. This proportionality is known as the Wiedemann-Franz law and the constant of proportionality as the Lorentz number  $L$ :

$$L = \frac{k_{\text{el}}}{\sigma_e T} = \frac{\pi}{3} \left[ \frac{k_B}{e} \right]^2 = 2.45 \times 10^{-8} \text{ W ohm K}^{-2} \quad (6.18)$$

where  $\sigma_e$  = the electrical conductivity,  $\text{ohm}^{-1} \text{cm}^{-1}$ , and  $e$  = the charge on an electron. When the experimental value of  $L$  is close to, or equal to, the theoretical value, then we assume that the electronic contribution to the thermal conductivity predominates. For pure metals near room temperature, experimental values of  $L$  range from  $2.23 \times 10^{-8} \text{ W ohm K}^{-2}$  for copper to  $3.04 \times 10^{-8} \text{ W ohm K}^{-2}$  for tungsten.

The thermal conductivities of pure metals are shown in Fig. 6.6. Since the thermal conductivity of all crystalline materials is made up of contributions from both  $k_{\text{ph}}$  and  $k_{\text{el}}$ , we can only crudely predict the temperature dependence. It is evident that the increase in  $k$  with temperature predicted by Eq. (6.17) does not operate in a strong fashion, and that most metals actually show a decrease in  $k$  with temperature. In the cases of pure nickel and pure iron,  $k$  decreases with temperature at low temperatures; at higher temperatures, the electronic contribution presumably overwhelms the phonon contribution, and  $k$  increases with temperature.

Qualitatively, at least, thermal conductivities in solids and alloys, in particular, can be explained *post facto* by Eq. (6.9) through the mean free path for phonons ( $\lambda_{\text{ph}}$ ) and the mean free path for electrons ( $\lambda_e$ ). In the case of phonons,  $\lambda_{\text{ph}}$  is governed by three interaction processes: the Umklapp collisions, scattering of phonons by crystal imperfections and solute atoms, and interactions between the phonons and the free electrons. Similarly,  $\lambda_e$  is limited

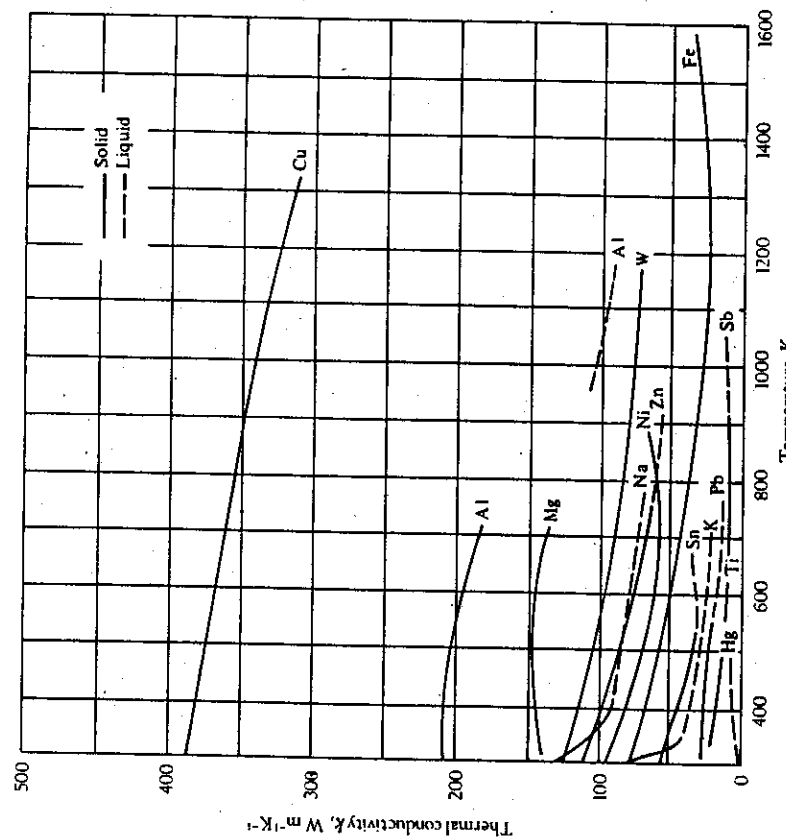


Fig. 6.6 Thermal conductivities of pure, solid, and liquid metals.

by scattering of electrons by crystal imperfections and solute atoms, electron-electron interactions, and the electron-phonon interactions. With the thermal conductivity comprising both  $\lambda_e$  and  $\lambda_{\text{ph}}$ , each involving several different mechanisms, it is not surprising that our ability to predict thermal conductivities in alloys is rather limited.

Figures 6.7 and 6.8 show the effect of alloying. Substitutional alloying and second phases both lower the conductivity from that of the pure metal, although a wide variety of ferrous alloys all reach the same limiting value at temperatures at or above the  $\alpha$ - $\gamma$  transition point.

Note that the alloys in both Figs. 6.7 and 6.8 have absolute values of  $k$  that are about the same as those for the oxides in Fig. 6.3, which clearly are not metallic in nature. This indicates that a substantial portion of the thermal conduction is via phonons in alloys. Klemens and Williams<sup>4</sup> pointed out that the so-called Smith-Palmer equation has been used to describe experimental thermal conductivities in aluminum alloys (with the exception of high Si casting alloys) to within 5%. The Smith-Palmer equation is

$$k = A L \sigma_e T + B \quad (6.19)$$

<sup>4</sup>P. G. Klemens and R. K. Williams, *Int. Met. Rev.* 31, 197 (1986).

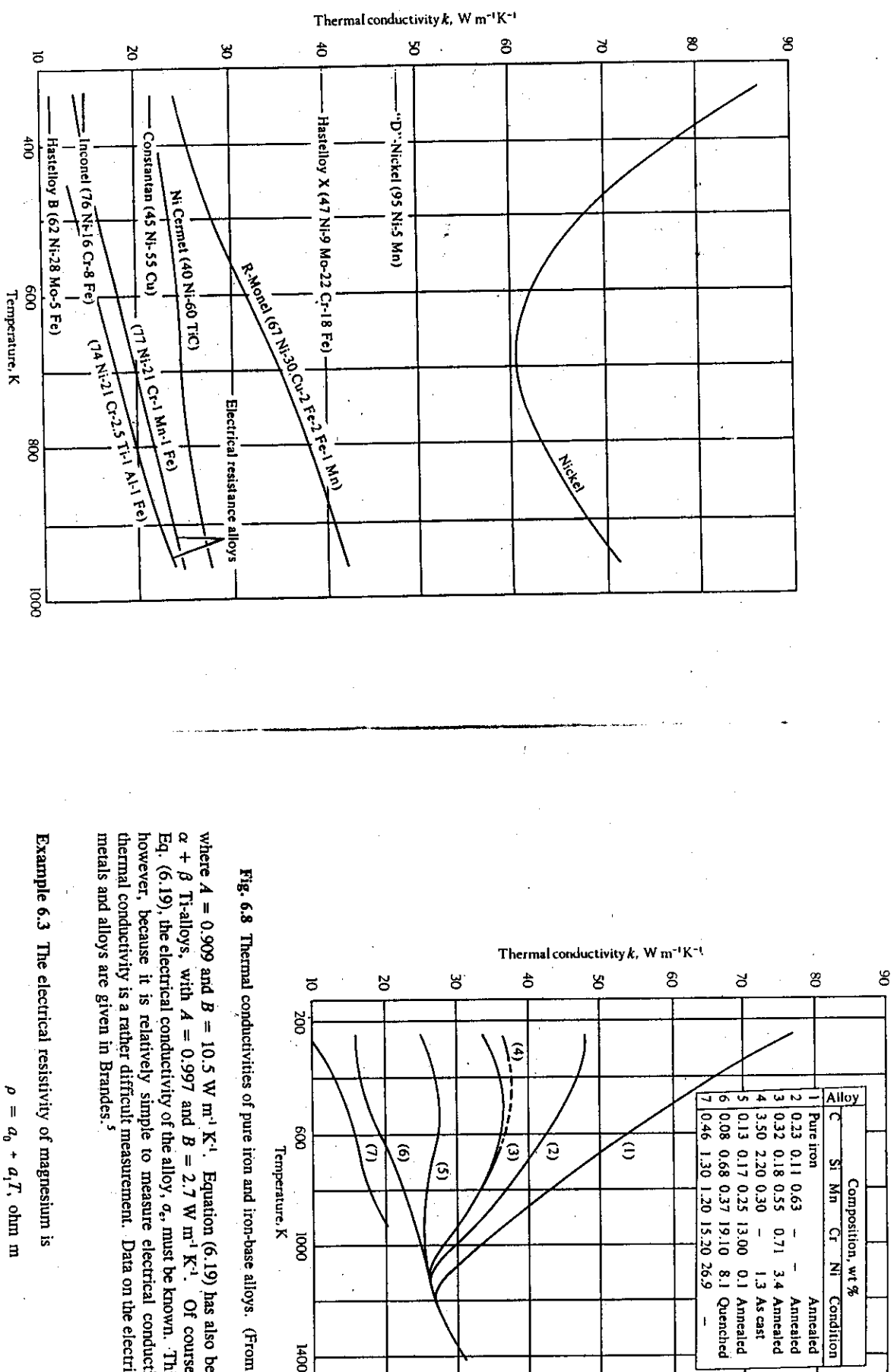


Fig. 6.7 Thermal conductivities of nickel and of nickel-base alloys.

**Fig. 6.8** Thermal conductivities of pure iron and iron-base alloys. (From Schack, *ibid.*)

where  $A = 0.909$  and  $B = 10.5 \text{ W m}^{-1} \text{ K}^{-1}$ . Equation (6.19) has also been used for  $\alpha$  and  $\alpha + \beta$  Ti-alloys, with  $A = 0.997$  and  $B = 2.7 \text{ W m}^{-1} \text{ K}^{-1}$ . Of course, in order to use Eq. (6.19), the electrical conductivity of the alloy,  $\sigma_e$ , must be known. This is advantageous, however, because it is relatively simple to measure electrical conductivity, whereas the thermal conductivity is a rather difficult measurement. Data on the electrical conductivity of metals and alloys are given in Brandes.<sup>5</sup>

**Example 6.3** The electrical resistivity of magnesium is

$$\rho = \sigma_0 + \sigma_1 T, \text{ ohm m}$$

<sup>5</sup>E. A. Brandes (editor), *Smithells Metals Reference Book*, 6th ed., Butterworths, London, U.K., 1983, pages 19-1 to 19-7.

where  $T$  is temperature (K). The constants are  $a_0 = 0.2 \times 10^8 \text{ ohm m}$  and  $a_1 = 1.68 \times 10^{-10} \text{ ohm m K}^{-1}$ , which apply in the range  $150 \leq T \leq 500 \text{ K}$ . Evaluate the Lorentz number for magnesium at 300 and 500 K.

**Solution.** Assume that  $k_e = k$  so that Eq. (6.18) can be used. When we do this, the Lorentz number is

$$L = \frac{k\rho}{T} = k \left[ \frac{a_0}{T} + a_1 \right].$$

From Fig. 6.6,  $k(300 \text{ K}) = 140 \text{ W m}^{-1} \text{ K}^{-1}$ ; therefore

$$L(300 \text{ K}) = 140 \left[ \frac{0.2 \times 10^{-8}}{300} + 1.68 \times 10^{-10} \right] = 2.44 \times 10^{-8} \text{ W ohm K}^{-2}.$$

In a similar manner,  $k(500 \text{ K}) = 148 \text{ W m}^{-1} \text{ K}^{-1}$  and

$$L(500 \text{ K}) = 2.55 \times 10^{-8} \text{ W ohm K}^{-2}.$$

Notice that these values of  $L$  are within 4 pct. of the theoretical value given by Eq. (6.18).

In the case of semiconducting compounds, the thermal conductivity may be strongly influenced by phonon mechanisms at low or at moderate temperatures, but as more electrons are excited from valence to conduction states when the temperature is raised, the electron contribution increases, until  $k_e$  may predominate. In the intrinsic conduction range, the Lorentz number is given by

$$L = 2 \left[ \frac{\kappa_b}{e} \right]^2 + \left[ \frac{\kappa_b}{e} \right]^2 \frac{1}{(\sigma_n + \sigma_p)} \left[ 4 + \frac{E_g}{kT} \right]^2 \quad (6.20)$$

where  $\sigma_n$  = electrical conductivity via electrons in the conduction band,  $\sigma_p$  = electrical conductivity via holes in the valence band, and  $E_g$  = energy gap between bands. It has been shown,<sup>6,7</sup> that this contribution is significant in the case of  $\text{UO}_2$ , and is certainly significant for other semiconducting oxides, such as  $\text{TiO}_2$ ,  $\text{ZrO}_2$ , and  $\text{Nb}_2\text{O}_5$ . Since this contribution increases with temperature ( $\sigma_n + \sigma_p$ ,  $\sigma_n$ , and  $\sigma_p$  all increase with temperature), it must be superimposed on the phonon contribution in order to totally explain the rise in the thermal conductivity at very high temperatures for semiconductors.

Conversely, other oxides, for example,  $\text{SiO}_2$ ,  $\text{Al}_2\text{O}_3$ , and  $\text{MgO}$ , never show significant electronic conduction, and yet their thermal conductivities also increase with temperature at very high temperatures (see Fig. 6.3). This phenomenon has been explained on the basis of the ability of certain materials to transmit radiant energy (a *photon* contribution to thermal conductivity). This occurs when a material is no longer opaque, but translucent to incident radiation. Without going into the details of the interaction of radiation and solids, we can compute the radiant energy conductivity  $k_r$  from

$$k_r = \frac{16}{3} \frac{\sigma V^2 T^3}{a} \quad (6.21)$$

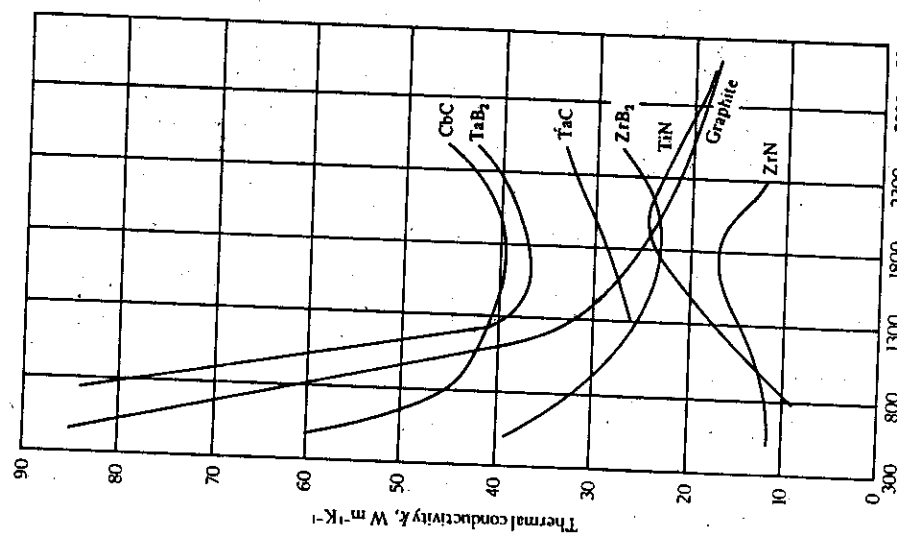


Fig. 6.9 Thermal conductivity of high-temperature materials.

where  $\sigma$  = the Stefan-Boltzmann constant ( $5.670 \times 10^{-8} \text{ W m}^2 \text{ K}^{-4}$ ),  $v$  = the index of refraction, and  $a$  = the absorption coefficient equal to  $1/\lambda_{ph}^2 \text{ m}^{-1}$ . When  $a$  is large (opaque material), the ability to absorb incident radiation is large; thus radiant energy is not transmitted through the solid as photons, but rather is absorbed at the surface and transferred to energy transmitted by the phonon or electron mechanisms.

When  $a$  is small (transparent material),  $k_r$  may be quite significant. In general, the contribution of photon or radiant energy becomes significant for dense oxides at temperatures in the neighborhood of 1750 K.

Figure 6.9 presents thermal conductivity data for a variety of nonmetallic crystalline materials used for high-temperature applications. Some of these exhibit semiconducting electrical properties at elevated temperatures, and the transition in temperature dependence is probably caused by an increasing influence of the electronic conductance over the phonon contribution. The absolute value is again in the same range as that for the alloys in Figs. 6.7 and 6.8.

Finally, for amorphous materials such as high polymers and glasses, thermal conduction is mainly via atomic or molecular migration (or radiation at high temperatures), because the material is too irregular in structure to support a phonon mechanism and the electron contribution is negligible. This results in very low values of conductivity, as indicated in Table 6.1.

Table 6.1 Thermal conductivities of amorphous or molecular solids

Substance	Temperature, K	$k, \text{W m}^{-1} \text{K}^{-1}$
Glass	373	0.76
Lead glass	273	0.87
Pyrex glass	373	1.16
Quartz glass	373	1.42
Asphalt	293	0.76
Polystyrene	293	0.12
Polyvinyl chloride	293	0.26

The thermal conductivity of glass can be explained on the basis of Eq. (6.9) and Eq. (6.21). In this context,  $\lambda$  is the phonon mean free path and  $\bar{V}$  is considered to be the speed of sound in the glass. The phonon mean free path is limited by the noncrystalline structure of the glass, so it is only on the order of interatomic distances and independent of temperature. Therefore, the thermal conductivity depends on temperature in the same way as  $C_V$ . Figure 6.10 shows this behavior for fused silica. The conductivity increases at low temperatures and then reaches a nearly constant value (excluding radiation) beyond approximately 600 K. High temperature conductivities show the expected increases because of the photon conductivity, i.e., Eq. (6.21).

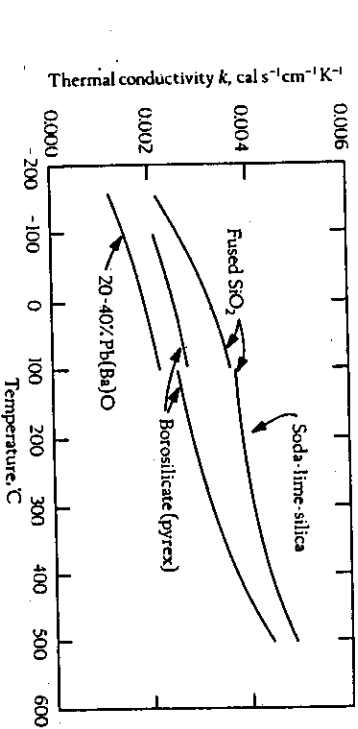
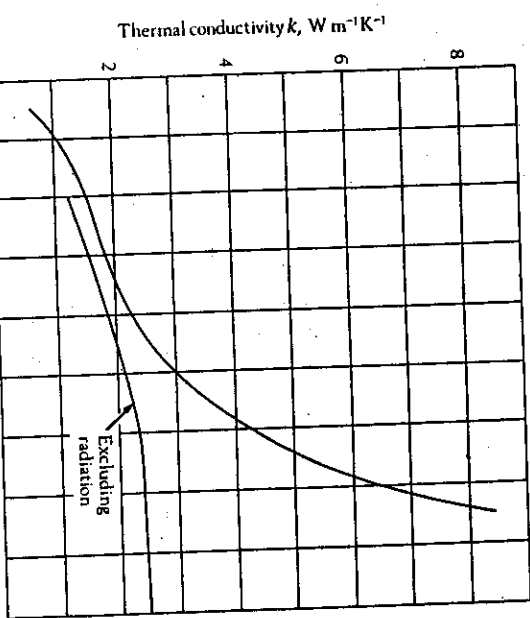


Fig. 6.11. The thermal conductivity in several glasses. (From Kingery *et al.*, page 626.)  
Note:  $1 \text{ cal s}^{-1} \text{cm}^{-1} \text{K}^{-1} = 418.4 \text{ W m}^{-1} \text{K}^{-1}$ .

For polymeric materials the same thermal conduction mechanisms apply as in metallic and ceramic materials. There is no widely accepted quantitative theory to predict thermal conductivity in these materials. Their structure can vary from strongly crystalline to essentially amorphous, in which case the molecular chains are randomly arranged. In the amorphous state, the difficulty of propagating a lattice wave through the structure can be imagined, and since these are not electron-conducting materials, thermal energy has a difficult time being transmitted. Even when there are crystalline (ordered) regions within the polymer, they are usually surrounded by enough amorphous material that their improved conductivity does not significantly change their overall low conductivity. Table 6.2 gives some representative thermal data for polymeric materials.

To summarize, we should remember that the value of the thermal conductivity of solids is determined by the sum of several mechanisms, including those of phonons, electrons, photons, and atomic migration, regardless of the materials, and it is because of this fact that the prediction of this property is so difficult.

#### 6.4 THERMAL CONDUCTIVITY OF LIQUIDS

As usual, when dealing with liquids, we are faced with a lack of knowledge of their structure. Using Eq. (6.9), Bird *et al.*<sup>8</sup> modified a theory due to Bridgman which results in an expression for the thermal conductivity of liquids at densities away from the critical value:

$$k = 2.8\kappa_B V \left[ \frac{N_0}{\bar{V}} \right]^{2/3} \quad (6.22)$$

Fourier's Law and Thermal Conductivity of Materials 203  
The effect of composition on the thermal conductivity of glass is shown in Fig. 6.11. The variation of thermal conductivity in glasses is not as pronounced as it is in crystalline materials because the mean free path for phonon conduction is not affected very much by composition.

Table 6.2 Thermal conductivity and other thermal properties of polymeric materials

Material	Density (kg m <sup>-3</sup> )	Specific heat (kJ kg <sup>-1</sup> K <sup>-1</sup> )	Thermal conductivity (W m <sup>-1</sup> K <sup>-1</sup> )	Coeff. of therm. exp. (μm K <sup>-1</sup> m <sup>-1</sup> )	Thermal diffusivity (m <sup>2</sup> s <sup>-1</sup> × 10 <sup>-3</sup> )	Max. operating temp. (°C)
ABS (high impact)	1040	1.46	0.3	90	1.7	70
Acetal (homopolymer)	1420	1.46	0.2	80	0.7	85
Acetal (copolymer)	1410	1.46	0.2	95	0.72	90
Acrylic	1180	1.46	0.2	70	1.09	50
Cellulose acetate	1280	1.50	0.15	100	1.04	60
CAB	1190	1.46	0.14	100	1.27	60
Epoxy	1200	—	0.23	70	—	130
Modified PPO	1060	—	0.22	60	—	120
Nylon 66	1140	1.7	0.24	90	1.01	90
Nylon 66 (33% glass)	1380	1.2	0.52	30	1.33	100
PEEK	1300	—	—	48	—	204
PEEK (30% carbon)	1400	—	—	14	—	255
PET	1360	—	0.14	90	—	110
PET (36% glass)	1630	—	—	40	—	150
Phenolic (mineral filled)	1690	—	—	22	—	185
Polyamide-imide	1400	—	—	36	—	260
Polycarbonate	1150	1.2	0.2	65	1.47	125
Polyester	1200	—	0.2	100	—	—
Polyetherimide	1270	—	0.22	56	—	170
Polyethersulfone	1370	—	1.18	55	—	180
Polyimide	1420	—	—	45	—	260
Polyphenylene sulfide (30% carbon)	1460	—	—	16	—	200
Polypropylene	905	1.92	0.24	100	0.65	100
Polysulfone	1240	—	—	56	—	170
Polystyrene	1030	1.34	0.15	80	0.6	50
Polythene (LD)	920	2.30	0.33	200	1.17	50
Polythene (HD)	950	2.30	0.63	120	1.57	55
PTFE	2100	—	0.25	140	0.7	50
PVC (rigid)	1400	1.00	0.16	70	1.16	50
PVC (flexible)	1300	1.7	0.14	140	0.7	50
SAN	1080	1.38	0.17	70	0.81	60
DMC (polyester)	1800	—	0.2	20	—	130
SMC (polyester)	1800	—	0.2	20	—	130
Polystyrene foam	32	—	0.032	—	—	—
PV foam	32	—	0.032	—	—	—

(From R. J. Crawford, *Plastics Engineering*, second edition, Pergamon Press, Oxford, U.K., 1987, page 33.)

where  $\hat{V}$  = the molar volume,  $N_0$  = Avogadro's number, and  $V_s$  = the speed of sound through the liquid, given by

$$V_s = \left[ \frac{C_p}{C_v} \left( \frac{1}{\rho \beta} \right) \right]^{1/2},$$

where  $\beta$  = compressibility. This is based on the assumption that the molecules in the liquid are arranged in a cubic lattice and energy transfer is via collisions between molecules. The thermal conductivity of ordinary liquids near room temperature is considerably below that of crystalline solids, as indicated in Table 6.3, emphasizing the fact that energy transfer in ordinary liquids is difficult because of the lack of both phonon and electron conduction. However, liquid metals show much higher conductivities than other liquids, because electronic conduction is possible, and a survey of the Lorentz numbers for liquid metals indicates close agreement with the theoretical value. Data for liquid metals along with solid metals are included in Fig. 6.6 and Fig. 6.12.

Fourier's Law and Thermal Conductivity of Materials 205

Table 6.3 Thermal conductivities of various liquids

Substance	Temperature, K	$k$ , W m <sup>-1</sup> K <sup>-1</sup>
Water	289	0.552
Water	311	0.415
Light oil	289	0.13
Light oil	311	0.14
Benzene	354	0.14
Fluoride salts	755	5.5
Slag	1865	4.0

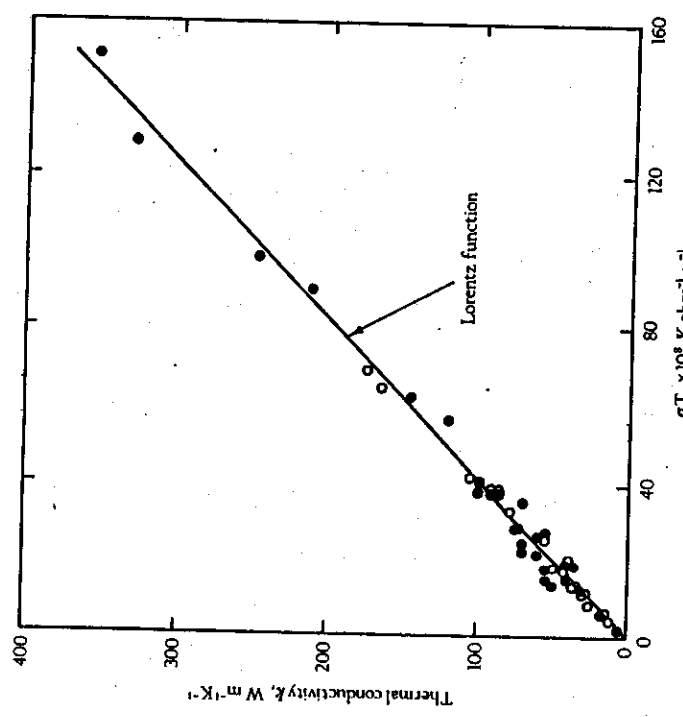


Fig. 6.12 Variation of thermal conductivity with the product of melting temperature and electrical conductivity of solid (●) and liquid (○) metals. (From E. T. Turkdogan, *Physical Chemistry of High Temperature Technology*, Academic Press, New York, N.Y., 1980, page 125.)

When dealing with molten salts, Iida and Guthrie<sup>9</sup> correlated thermal conductivity at the melting point with the speed of sound; their equation is

$$k = 3.3 \times 10^{-7} U_s / \hat{V}^{2/3} \quad (6.23)$$

<sup>9</sup>T. Iida and R. I. L. Guthrie, *The Physical Properties of Liquid Metals*, Clarendon Press, Oxford, U.K., 1988, pages 248-250.

where  $U_s$  is the speed of sound in  $\text{m s}^{-1}$  and  $\hat{V}$  is the molar volume in  $\text{m}^3 \text{mol}^{-1}$ . If the speed of sound is not available, it can be estimated by

$$U_s = 16 \left[ \frac{T_m}{M} \right]^{1/2} \quad (6.24)$$

where  $T_m$  = melting point, K, and  $M$  = formula weight, g  $\text{mol}^{-1}$ . Equation (6.23), by itself, gives values of  $k$  within 20 percent; however,  $U_s$ , estimated by Eq. (6.24) is only within 40 percent so the overall error can be even greater than 20 percent.

The thermal conductivities of highly basic silicate melts, including some that are supercooled, are given as

$$k = a + bT \quad (6.25)$$

where  $a$  and  $b$  can be found in Table 6.4.

Table 6.4 Coefficients for Eq. (6.25)

System (mol %)	Temp., K	$a$ $\text{W m}^{-1} \text{K}^{-1}$	$b$ $\text{W m}^{-1} \text{K}^{-2}$
50SiO <sub>2</sub> -50Na <sub>2</sub> O	1400	1.03	—
60SiO <sub>2</sub> -40Na <sub>2</sub> O	900-1400	-0.063	5.2
70SiO <sub>2</sub> -30Na <sub>2</sub> O	800-1400	0.184	2.4
50SiO <sub>2</sub> -50K <sub>2</sub> O	1310	0.32	—
60SiO <sub>2</sub> -40K <sub>2</sub> O	950-1300	0.19	0.85
70SiO <sub>2</sub> -30K <sub>2</sub> O	900-1300	0.04	2.0

(From H. Ohta, Y. Waseda and Y. Shiraishi in H. A. Fine and D. R. Gaskell (eds.), *Second International Symposium on Metallurgical Slags and Fluxes*, The Metallurgical Society (AIME), Warrendale, PA, 1984, page 863.)

In these silicates, as well as in some metallurgical slags containing CaO-SiO<sub>2</sub>-Al<sub>2</sub>O<sub>3</sub>, thermal conductivity increases with increasing temperature up to about 1000 K to 1300 K and then decreases with increasing temperature in both the solid/glassy state and the liquid state. An exception is the silicate with the composition Na<sub>2</sub>O-SiO<sub>2</sub>, with a thermal conductivity that decreases with increasing temperature. Some data are given in Figs. 6.13 and 6.14. In these materials, the mean free path of the phonons is almost constant with temperature, so the changes in the thermal conductivity are attributed to the variation of the speed of sound with temperature. It is also important to note the "insulating" character of molten silicate slags. The low conductivity of these slags causes considerable difficulty in transferring heat from combustion gases above a slag to a metal phase below it.

From this discussion, we can see that to accurately predict the thermal conductivity of solids and liquids is difficult. One must be able to make intelligent estimates and extrapolations from known data. This in turn requires an understanding of the role of the various conduction mechanisms, and of the effects that structural and chemical variations may have on these mechanisms. Sometimes we can only make order-of-magnitude estimates if experimental data are not available. Figure 6.15 gives a summary of the typical ranges of thermal conductivities for various classes of materials.

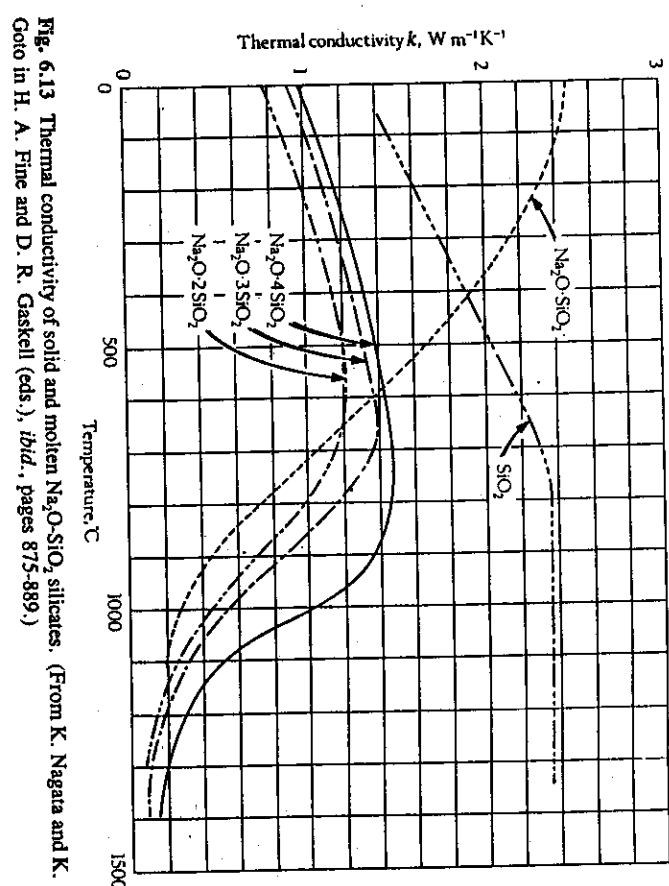


Fig. 6.13 Thermal conductivity of solid and molten Na<sub>2</sub>O-SiO<sub>2</sub> silicates. (From K. Nagata and K. S. Goto in H. A. Fine and D. R. Gaskell (eds.), *ibid.*, pages 875-889.)

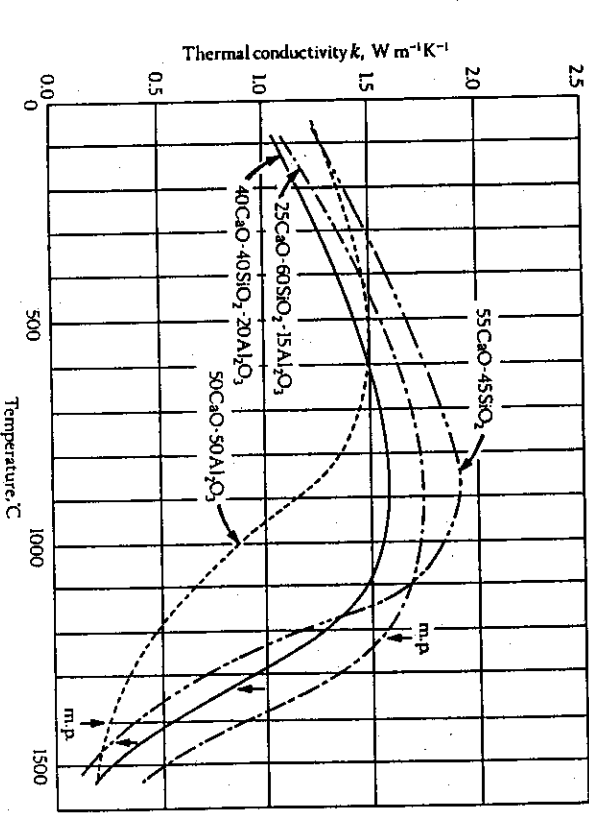


Fig. 6.14 Thermal conductivity of solid and molten CaO-SiO<sub>2</sub>-Al<sub>2</sub>O<sub>3</sub> slags. (From K. Nagata and K. S. Goto in H. A. Fine and D. R. Gaskell (eds.), *ibid.*, pages 875-889.)

Fourier's Law and Thermal Conductivity of Materials 209  
 Data for the thermal conductivity of SAP Al-Al<sub>2</sub>O<sub>3</sub> alloys<sup>10</sup> are plotted in Fig. 6.16 along with  $k_{\text{mix}}$  calculated by using Eq. (6.27) and the data from Figs. 6.3 and 6.6. The agreement is less than satisfactory.

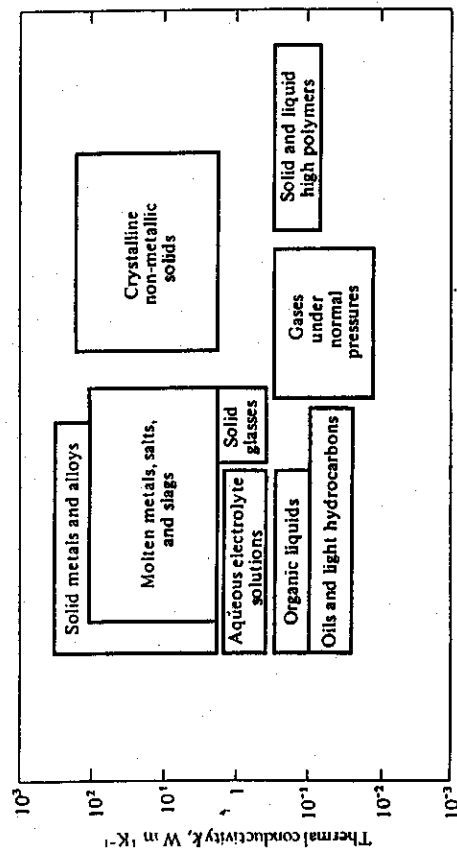


Fig. 6.15 Summary of the ranges of thermal conductivity for various classes of materials.

## 6.5 THERMAL CONDUCTIVITY OF BULK MATERIALS

So far, we have looked at the thermal conductivity of individual phases. We have seen the difficulties of arriving at exact predictions of thermal conductivity for most solids, particularly complex alloys. In most engineering situations, we are often faced with even more complex materials, for example, porous bulk materials. The thermal conductivity of such materials is certainly not equal to the intrinsic thermal conductivity of the solid involved. The question is: What value should be used?

### 6.5.1 Two-phase mixtures

Alloys known as cermets or metal-matrix composites have evolved. These are metallic alloys with a dispersion of a ceramic phase within the matrix. The thermal conductivity of such materials is a function of the volume fraction of each phase. For up to one-tenth volume fraction,  $V_d$ , of a dispersed phase of spherical particles with intrinsic thermal conductivity,  $k_d$ , it has been suggested that the thermal conductivity of the mixture,  $k_{\text{mix}}$ , may be found from the Maxwell equation,

$$\frac{k_{\text{mix}}}{k_c} = \frac{k_d/k_c + 2 - 2V_d(1 - k_d/k_c)}{k_d/k_c + 2 + V_d(1 - k_d/k_c)} \quad (6.26)$$

If the thermal conductivity of the continuous phase,  $k_c$ , is much larger than  $k_d$ , then

$$k_{\text{mix}} \approx k_c \left[ \frac{1 - V_d}{1 + V_d/2} \right] \quad (6.27)$$

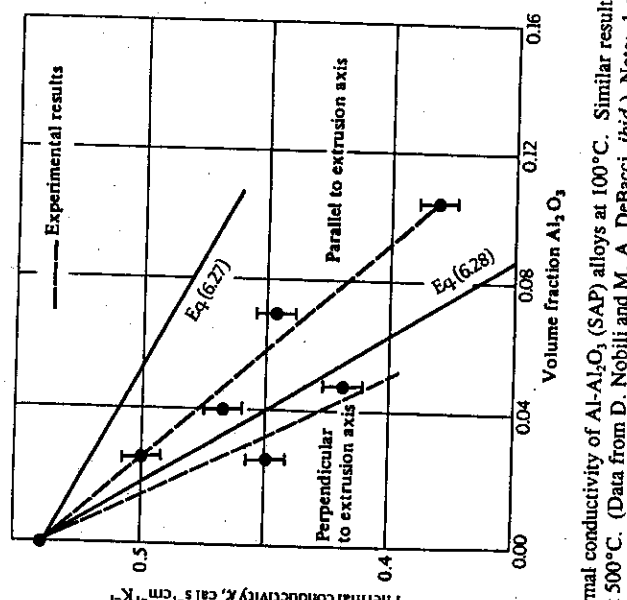


Fig. 6.16 Thermal conductivity of Al-Al<sub>2</sub>O<sub>3</sub> (SAP) alloys at 100°C. Similar results are obtained on data available at 500°C. (Data from D. Nobili and M. A. DeBacci, *Ibid.*) Note: 1 cal s<sup>-1</sup> cm<sup>-1</sup> K<sup>-1</sup> = 418.4 W m<sup>-1</sup> K<sup>-1</sup>.

However, if we assume that the material behaves as if it were a series of plates of Al and Al<sub>2</sub>O<sub>3</sub> normal to the direction of heat flow, then they would be equivalent to a series of resistors in an electric circuit, and

$$\frac{1}{k_{\text{mix}}} = \frac{V_c}{k_c} + \frac{V_d}{k_d} \quad (6.28)$$

Using this equation, we obtain better agreement with the experimental results. We should emphasize, however, that we lack the physical basis for this assumption, and that the purpose in including it at this point is only to stress the difficulty of predicting  $k$  for two-phase materials. Several models for the thermal conductivity of two-phase materials are summarized in Table 6.5.

### 6.5.2 Porous materials

Most ceramic materials and some powder metallurgy products have some low, internal porosity  $\omega$ , as a result of having been sintered from powders. The pores are generally isolated from one another. At temperatures up to and slightly above the room temperature,

<sup>10</sup>D. Nobili and M. A. DeBacci, *J. Nuclear Materials* **18**, 187 (1966).

Table 6.5 Thermal conductivities of two-phase mixtures based on models with various geometric arrangements.

Parallel	$\frac{k_{\text{mix}}}{k_c} = (1 - V_d) + V_d \frac{k_d}{k_c}$	(1)
Series	$\frac{k_{\text{mix}}}{k_c} = \frac{1}{(1 - V_d) + V_d \frac{k_d}{k_c}}$	(2)
Russell model: cubes in a cubic array; linear isotherms	$\frac{k_{\text{mix}}}{k_c} = \frac{1 - V_d^{2/3} + \frac{k_d}{k_c} V_d^{2/3}}{1 - V_d^{2/3} + V_d + \frac{k_d}{k_c} (V_d^{2/3} - V_d)}$	(3)
son Frey model: cubes in a cubic array; linear heat flow	$\frac{k_{\text{mix}}}{k_c} = \frac{1 - V_d^{1/3} + V_d + \frac{k_d}{k_c} (V_d^{1/3} - V_d)}{1 - V_d^{1/3} + \frac{k_d}{k_c} V_d^{1/3}}$	(4)
Rayleigh-DeVries model: regular array of uniform spheres in contact; simple cubic array, $a = 1.31$ ; face-centered cubic, $a = 0.129$ ; face-centered cubic, $a = 0.0752$	$\frac{k_{\text{mix}}}{k_c} = 1 - \frac{3V_d}{\left[ \frac{2 + k_d/k_c}{1 - k_d/k_c} \right] + V_d - a \left[ \frac{1 - k_d/k_c}{4/3 + k_d/k_c} \right] V_d^{10/3} + \dots}$	(5)
Maxwell model: random distribution of spheres; no contact	$\frac{k_{\text{mix}}}{k_c} = \frac{\frac{k_d}{k_c} + 2 - 2V_d \left[ 1 - \frac{k_d}{k_c} \right]}{\frac{k_d}{k_c} + 2 + V_d \left[ 1 - \frac{k_d}{k_c} \right]}$	(6)
Bruggeman model: infinite range of bubble sizes in continuous phase	$1 - V_d = \left[ \frac{k_{\text{mix}}}{k_c} \right]^{1/3} \left[ 1 - \frac{k_d}{k_c} \right]$	(7)

$k_d$  = thermal conductivity of discontinuous phase  
 $k_c$  = thermal conductivity of continuous phase  
 $V_d$  = volume fraction of discontinuous phase

Table provided by courtesy of A. Ortega, University of Arizona, Tucson, Arizona (1992). Also in W. D. Drotning, A. Ortega, and P. E. Havey, *Thermal Conductivity of Aqueous Foam*, Sandia Report SAND82-0742, Sandia National Laboratories, Albuquerque, New Mexico, 1982, pages 5 and 6.

$$k_{\text{eff}} = k_c(1 - \omega) \quad (6.29)$$

At larger porosities, the pores are not isolated and the porosity becomes continuous. Conductivity at room temperature is thus even lower than that predicted by Eq. (6.29). Figure 6.17 illustrates the effect of larger amounts of porosity on the thermal conductivity of partially sintered powder metal compacts.

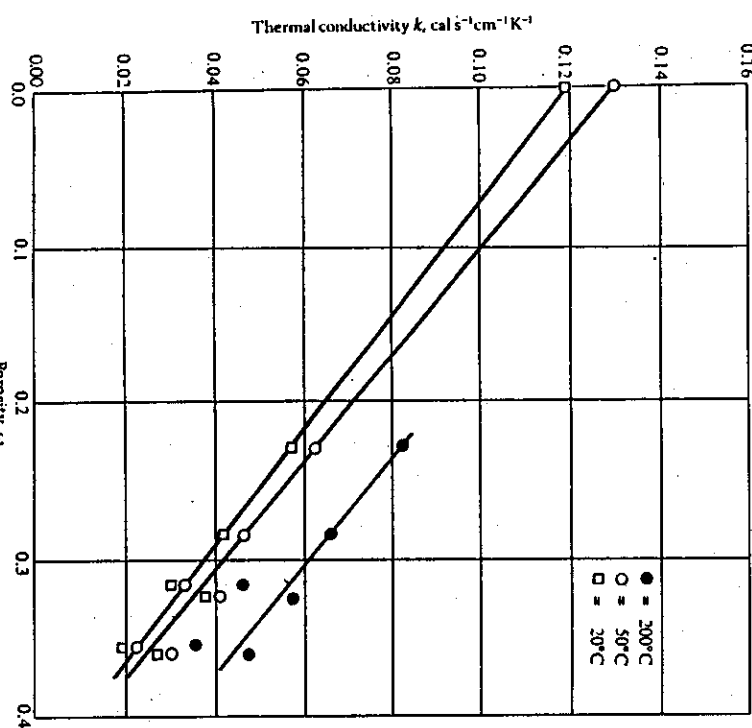


Fig. 6.17 Thermal conductivity of phosphor-bronze powder compacts as a function of porosity  $\omega$ . (From P. Grootenhuis, R. W. Powell, and R. P. Tye, Proc. Phys. Soc. 65, 502 (1952).)

In general, the conductivity of a loose packing, or packed bed, is a function of the thermal conductivity of the gas in the pores, the solid, the void fraction in the bed, and the temperature, because, as the temperature increases, the particle-to-particle thermal radiation also increases. Schotte<sup>11</sup> developed a technique for predicting the conductivity of packed beds, in which the gas phase is continuous; it is outlined below.

Taking the gas first, we can use the methods outlined in Section 6.2 to obtain  $k_g$  except in the following instance. When the effective pore dimensions are of the same order of

magnitude as the mean free path of the gas, the true thermal conductivity of the gas decreases. This occurs when the particle diameter  $D_p$  is about 1000 times the mean free path of the gas. (The mean free path of air at room temperature and 1 atm is  $\sim 10^5$  cm. At 1810 K and 1 atm, it is  $\sim 10^{-4}$  cm. Thus we are talking about situations where  $D_p < 10^2$   $10^{-1}$  cm.) Deissler and Eian<sup>12</sup> developed a correlation for the *break-away* pressure  $P_b$  in  $N/m^2$ , above which no correction for this effect is required:

$$P_b = 4.32 \times 10^{-21} \frac{T}{D_p^2} \quad (6.30)$$

where  $T$  is temperature, K,  $D_p$  = the average particle diameter, m, and  $d$  = the mean diameter of the gas molecules, m. If the actual pressure is greater than  $P_b$ , no correction to the value of  $k_g$  read from Fig. 6.2 is needed, but if the actual pressure is less than  $P_b$ , calculated by Eq. (6.30), then the thermal conductivity of the gas phase should then be calculated according to the equation

$$k_g = \frac{k_g^0}{1 + 4.95 \times 10^{-22} \left[ \frac{C_p/C_v}{1 + C_p/C_v} \right] \left[ \frac{1 - \omega}{\omega} \right] \left[ \frac{T k_g^0}{P D_p d^2 C_p \eta} \right]} \quad (6.31)$$

where  $k_g^0$  is the uncorrected value obtained from Fig. 6.2; SI units are used for the variables. We see that  $k_g$  decreases, at any given temperature, as  $D_p$  decreases, and if the pores are small enough, then  $k_g$  is effectively zero. This effect is illustrated in Fig. 6.3 by the data for the thermal conductivity of porous brick.

Having obtained  $k_g$ , either directly or by using Eq. (6.31) if required, we use  $k_r$ , the intrinsic thermal conductivity of the solid phase, to calculate the ratio  $k_r/k_g$ . Then, using Fig. 6.18 we may find  $k_e$ , the *effective thermal conductivity* of the packed bed, from the ratio  $k_e/k_g$ . This correlation (Fig. 6.18) has been developed from data on many packed beds, and is accurate as given at temperatures less than 200°C.<sup>13</sup> However, Fig. 6.18 should not be used outside the limit  $1 < k_e/k_g < 6000$ . If  $k_e/k_g$  is greater than 6000, then there may be appreciable contact conduction between particles which has not been accounted for in Fig. 6.18. However, this situation does not often arise, except possibly in compacts of powdered metals.

If the temperature is above 200°C we must add another term to  $k_e$ , found in the same manner as above, in order to obtain the true effective thermal conductivity of the bed. At higher temperatures, there is a contribution to the effective thermal conductivity of the bed by radiation heat-transfer from particle to particle. This contribution, for example, is important for 1-mm particles above 400°C and for 0.1-mm particles above 1500°C. Schotte considered the radiation from a plane on one side of a spherical particle to a plane on the other side. First, there is a direct radiation heat-transfer across the void space past the particle, with heat-transfer contribution:

$$Q_1 = -h_r \left[ D_p^2 \frac{\pi}{4} \frac{\omega}{1 - \omega} \right] \left[ D_p \frac{dT}{dx} \right]. \quad (6.32)$$

When  $Q_1$  and  $Q_2$  are added, one obtains the total heat flow

$$Q = -k_r \left[ D_p^2 \frac{\pi}{4} \frac{1}{1 - \omega} \right] \left[ \frac{dT}{dx} \right],$$

where  $k_r$  is the *radiation contribution to the effective thermal conductivity of the bed*:

$$k_r = \frac{1 - \omega}{(1/k_r) + (1/k_e^0)} + \omega k_e^0 \quad (6.34)$$

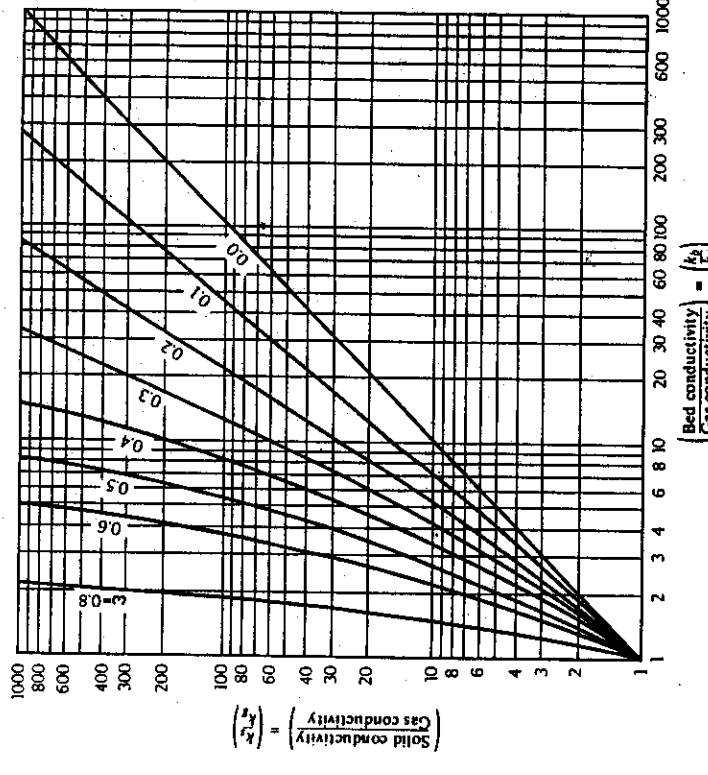


Fig. 6.18 Effect of porosity on packed bed thermal conductivity. (From Deissler and Eian, *ibid*.) Curves outside the range  $0.2 \leq \omega \leq 0.6$  have not been tested as extensively as the others. where  $h_r$  is the radiation heat-transfer coefficient between a particle and its neighbor, given by

$$h_r = 22.91 \varepsilon \frac{T^3}{10^3}, \quad W/m^2 \cdot K^{-1}.$$

Here  $\varepsilon$  is the emissivity of the solid, and  $T$  is the temperature, K. Secondly, there is radiation to and from the particle, in series with conduction through the particle. This is written

$$Q_2 = -D_p^2 \frac{\pi}{4} \left[ \frac{k_r h_r D_p}{k_g + h_r D_p} \right] \left[ \frac{dT}{dx} \right]. \quad (6.33)$$

<sup>12</sup>R. G. Deissler and C. S. Eian, NACA, RM E52C05 (1952).  
<sup>13</sup>For another review, see R. Krupiczka: Analysis of thermal conductivity of granular materials, *Int. Chem. Engr.* 1, 122 (Jan. 1967). He arrives at a graph that is virtually the same as that of Deissler and Eian.

and

$$k_r^0 = 22.91 \varepsilon D_p \left[ \frac{T^3}{10^8} \right].$$

To evaluate the thermal conductivity of a packed bed, we use Fig. 6.18 (if necessary, use Eq. (6.31) to obtain  $k_r$ ), then add  $k_r$  from Eq. (6.34) to obtain the effective thermal conductivity, as illustrated in Example 6.4. The reader will note that even at high temperatures, it is possible for porosity to contribute only slightly to  $k_r$ , provided the pore size is quite small. This is generally true of isolated pores as well as of pores in loose materials.

**Example 6.4** Bearing in mind the importance of the effective thermal conductivity of molding sand in relation to the solidification rate of castings, let us see if we can predict the thermal conductivity of silica sand molds as a function of temperature, using the method described above.

**Solution.** Assume that the material is entirely quartz ( $\text{SiO}_2$ ) with thermal conductivity given in Fig. 6.3, and that the atmosphere is dry air. If the bulk porosity is 40%, the grain size  $D_p$  is  $3.81 \times 10^{-4}$  m (AFS 43), and the emissivity of quartz is as given below, then we can proceed as outlined above.

### 1. Calculate $P_b$ at 278 K

$$P_b = 4.32 \times 10^{-21} \frac{T}{D_p d^2}.$$

Assuming  $d = 0.4$  nm:

$$P_b = \frac{(4.32 \times 10^{-21})(278)}{(3.81 \times 10^{-4})(0.4 \times 10^{-9})^2} = 1.97 \times 10^4 \text{ N m}^{-2},$$

and we need to make no correction to the value read from Fig. 6.2. Subsequent calculations show that this condition holds true up to 1420 K. At 1555 K,  $k_r$  is calculated using Eq. (6.31).

### 2. Using the value of $k_r$ in the table below, we calculate the ratio $k_r/k_t$ at 278 K:

$$\frac{k_r}{k_t} = 384.$$

Then, from Fig. 6.18, we find that for  $\omega = 0.4$ ,  $k_r/k_t = 12$ , or, because  $k_t = 0.0225 \text{ W m}^{-1} \text{ K}^{-1}$ ,  $k_b = 0.270 \text{ W m}^{-1} \text{ K}^{-1}$ . This calculation is carried out at each temperature:

T, K	$k_r \text{ W m}^{-1} \text{ K}^{-1}$	$k_r/k_t$	$k_b \text{ W m}^{-1} \text{ K}^{-1}$
278	0.022	384	12.0
500	0.036	167	9.5
722	0.050	90	7.9
944	0.062	79	7.5
1111	0.069	67	7.0
1389	0.076	136	9.0
1555	0.082	380	11.9
			0.98

Then

$$k_r = \left[ \frac{1}{8.65} \right] + \left[ \frac{1}{0.00154} \right]$$

On the other hand, at 1555 K,  $\varepsilon = 0.27$  and

$$k_r^0 = \frac{(22.91)(0.27)(3.81 \times 10^{-4})(1555^3)}{10^8} = 8.87 \times 10^{-2} \text{ W m}^{-1} \text{ K}^{-1}.$$

The values are added to the  $k_b$  values, given above, to obtain the final result.

Conductivities, $\text{W m}^{-1} \text{ K}^{-1}$					
T, K	$\varepsilon$	$k_r^0$	$k_r$	$+ k_b$	$= k_{eff}$
278	0.82	0.0015	0.0015	0.26	0.26
500	0.75	0.0081	0.0083	0.34	0.35
722	0.68	0.0225	0.0227	0.40	0.42
944	0.58	0.0429	0.0742	0.46	0.53
1111	0.49	0.0587	0.0583	0.48	0.54
1389	0.32	0.0692	0.0689	0.68	0.75
1555	0.27	0.0887	0.0885	0.98	1.07

When these calculated results are compared to experimental measurements, the agreement is surprisingly good.

We remind the reader that the previous calculation of the effective thermal conductivity applies to porous media with interconnected porosity. Mathematical models that predict the effective thermal conductivity with a measure of the degree of continuity of the solid phase are discussed by Marcusen.<sup>14</sup>

<sup>14</sup>L. Marcusen in T. Ashworth and D. R. Smith (eds.), *Thermal Conductivity 18*, Plenum Press, New York, N.Y., 1985, pages 585-598.

**PROBLEMS**

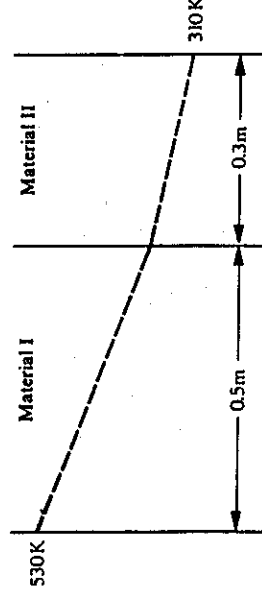
- 6.1 In the same system described in Problem 1.2, the temperature profile at  $x = x_1$  is given by

$$T - T_0 = 6 \sin \left[ \frac{\pi y}{2} \right], \quad 0 \leq y \leq 0.1 \text{ m},$$

where  $T$  is temperature (K) in the water,  $T_0$  is temperature at  $y = 0$ , and  $y$  is distance from the flat plate in m. Find the heat flux  $\dot{q}$  at the wall at  $x = x_1$ . (The thermal conductivity of water is  $0.62 \text{ W m}^{-1} \text{ K}^{-1}$ , and the heat capacity is  $4.19 \times 10^3 \text{ J kg}^{-1} \text{ K}^{-1}$ .)

- 6.2 Determine the thermal conductivity of a test panel  $150 \text{ mm} \times 150 \text{ mm}$  and 12 mm thick, if during a two-hour period  $8.4 \times 10^4 \text{ J}$  are conducted through the panel when the two faces are at  $290 \text{ K}$  and  $300 \text{ K}$ .

- 6.3 At steady state, the temperature profile in a laminated system appears thus:



Determine the thermal conductivity of II if the steady-state heat flux is  $12.6 \times 10^3 \text{ W m}^{-2}$  and the conductivity of I is  $52 \text{ W m}^{-1} \text{ K}^{-1}$ .

- 6.4 Show that Fourier's law can be written (for constant  $\rho C_p$ ) as

$$\dot{q}_y = -\alpha \frac{d}{dy} (\rho C_p T)$$

for one-dimensional heat flow. In addition, show that Newton's law, for constant  $\rho$ , is

$$\tau_{yx} = -v \frac{d}{dy} (\rho v).$$

Discuss the analogies between the fluxes, constants, and gradients as they appear in these equations.

- 6.5 The thermal conductivity of helium at  $400 \text{ K}$  is  $0.176 \text{ W m}^{-1} \text{ K}^{-1}$ . Knowing only this datum, estimate the thermal conductivity of helium at  $800 \text{ K}$ . Compare your estimate to the value obtained from Fig. 6.2. What do you conclude about the equation that you used for your estimate?

- 6.6 Repeat Problem 6.5 but use the following equation to estimate the thermal conductivity of helium at  $800 \text{ K}$ :

$$k = \frac{15R}{4M} \eta$$

where  $R$  is the gas constant,  $M$  is the molecular weight, and  $\eta$  is the viscosity.

- 6.7 Calculate the thermal conductivity of carbon dioxide at  $800 \text{ K}$  and compare your result to that given in Fig. 6.2. The heat capacity of  $\text{CO}_2$  at  $800 \text{ K}$  is  $1.17 \text{ kJ kg}^{-1} \text{ K}^{-1}$ .

- 6.8 a) Calculate the thermal conductivity of a gas containing 40 mol% He, 40 mol% H<sub>2</sub>, and 20 mol% N<sub>2</sub> at  $1400 \text{ K}$ .  
b) Assume that the concentration of He is constant but that the concentrations of H<sub>2</sub> and N<sub>2</sub> vary as much as  $\pm 5$  mol% in a process. What is the variation in the thermal conductivity of the gas?

- 6.9 Refer to Fig. 6.3 and explain the variation of the thermal conductivity of MgO with temperature.

- 6.10 Refer to Fig. 6.5 and comment on the effect of impurity scattering of phonons in dielectric solid solutions. Assume that the inverse mean free path for different scattering processes are additive, so that

$$\frac{1}{\lambda_{ph}} = \frac{1}{\lambda_i} + \frac{1}{\lambda_j}$$

where  $\lambda_i$  is the thermal mean free path and  $\lambda_j$  is the impurity mean free path.

- 6.11 Electrical resistivities of Ti-Al alloys at  $800 \text{ K}$  are given in the table below. Aluminum is an "α-stabilizer."

At. pct. Al	Resistivity $\mu\text{ohm cm}$
0	112
3	140
6	165
11	190
33	210

Estimate the thermal conductivity for each alloy at  $800 \text{ K}$ .

- 6.12 The electrical conductivity of molten Pb-Sn alloys at  $673 \text{ K}$  is

$$\sigma = (100 - 48X)^{-1}$$

where  $\sigma$  is in  $\mu\text{ohm}^{-1} \text{ cm}^{-1}$  and  $X$  is the atom fraction of Sn. Estimate the thermal conductivities of 90Pb-10Sn, 50Pb-50Sn and 10Pb-90Sn alloys (compositions in mol pct.).

- 6.13 Use the Maxwell-Eucken equation and predict the thermal conductivity of a two-phase solid (A plus B) as a function of composition (wt.pct.). A and B are insoluble in each other, and the following data apply:  $k_A = 13 \text{ W m}^{-1} \text{ K}^{-1}$ ,  $k_B = 7 \text{ W m}^{-1} \text{ K}^{-1}$ ,  $\rho_A = 4 \times 10^3 \text{ kg m}^{-3}$ ,  $\rho_B = 3 \times 10^3 \text{ kg m}^{-3}$ .

- 6.14 A flat heater is sandwiched between two solids of equal areas ( $0.1 \text{ m}^2$ ) with different thermal conductivities and thicknesses. The heater operates at a uniform temperature and provides a constant power of 290 W. The external surface temperature of each solid is 300 K, and there is perfect thermal contact at each internal interface.
- Calculate the heat flux through each solid.
  - What is the operating temperature of the heater?

Solid	Thermal Conductivity, $\text{W m}^{-1} \text{K}^{-1}$	Thickness, mm
A	35	60
B	9	30

## HEAT TRANSFER AND THE ENERGY EQUATION

We have designed this chapter to introduce the reader to three interwoven topics. First, we develop differential equations in terms of temperature in space (and with time if transient conditions apply) for several simple problems, by writing energy balances for unit volumes. In order to obtain solutions, we integrate the differential equations to ascertain the temperature and arbitrary constants, and then apply boundary and initial conditions to obtain the particular solution. The general procedure is similar to that followed in Chapter 2 for obtaining the velocity profiles.

Second, several of the examples are concerned with heat transfer to and from moving fluids. We deal only with laminar convection, but this enables the reader to become involved in the fundamentals of heat transfer with convection.

Third, we bring to the reader's attention more general forms of the equation of energy, leading to Tables 7.3-7.5 which may be used in a manner similar to the general momentum equations given in Chapter 2.

### 7.1 HEAT TRANSFER WITH FORCED CONVECTION IN A TUBE

Consider laminar flow in a circular tube of radius  $R$ , as depicted in Fig. 7.1. If the tube and the fluid exchange heat, then clearly the fluid's temperature is a function of both the  $r$ - and  $z$ -directions. A suitable unit volume is a ring-shaped element,  $\Delta r$  thick and  $\Delta z$  high. Energy enters and leaves this ring by thermal conduction; also, a unit mass of fluid, which enters with an enthalpy, must leave with a different enthalpy. Let us now develop the energy balance for the unit volume.

Rate of energy in by conduction across surface at  $r$   $2\pi r \Delta z q_r|_r$

Rate of energy out by conduction across surface at  $r + \Delta r$   $2\pi(r + \Delta r)\Delta z q_r|_{r + \Delta r}$

Rate of energy in by conduction across surface at  $z$   $2\pi r \Delta r q_z|_z$

We can further simplify the energy balance (Eq. (7.5)), since, except for the very slow flow of liquid metals, the term  $(k/\rho C_p) \partial^2 T / \partial z^2$  is negligible even though  $v_z (\partial T / \partial z)$  is not. With this assumption, Eq. (7.5) reduces to

$$v_z \frac{\partial T}{\partial z} = \frac{k}{\rho C_p} \left[ \frac{1}{r} \frac{\partial}{\partial r} \left[ r \frac{\partial T}{\partial r} \right] \right]. \quad (7.6)$$

Equation (7.6) contains  $v_z$ , the factor that ties together heat transfer and convection. Here we consider fully developed laminar flow; the velocity distribution is therefore parabolic, and is given by Eqs. (2.31) and (2.33):

$$v_z = 2\bar{V}_z \left[ 1 - \left( \frac{r}{R} \right)^2 \right].$$

By including this velocity distribution, Eq. (7.6) becomes

$$2\bar{V}_z \left[ 1 - \left( \frac{r}{R} \right)^2 \right] \frac{\partial T}{\partial z} = \frac{k}{\rho C_p} \left[ \frac{1}{r} \frac{\partial}{\partial r} \left[ r \frac{\partial T}{\partial r} \right] \right]. \quad (7.7)$$

We consider the special case where a *fully developed temperature profile* exists. For any set of boundary conditions, a fully developed temperature profile exists when  $(T_R - T)/(T_R - T_m)$  is a unique function of  $r/R$ , independent of  $z$ . Then

$$\frac{T_R - T}{T_R - T_m} = f(r/R), \quad (7.8)$$

or

$$\frac{\partial}{\partial z} \left[ \frac{T_R - T}{T_R - T_m} \right] = 0, \quad (7.9)$$

where  $T_R$  = temperature of fluid at the wall, and  $T_m$  = mean temperature of the fluid. A fully developed temperature profile is analogous to fully developed flow. This is exemplified by Fig. 7.2, where the liquid flowing in the  $z$ -direction encounters the heated section of the tube. Over a finite interval downstream from this point, the temperature profile changes from uniform to fully developed.

For a fully developed temperature profile, an important corollary arises; namely, the heat transfer coefficient is uniform along the pipe. We realize this by employing the definition of the heat transfer coefficient based on the mean temperature of the fluid:

$$h = \frac{q_k}{T_R - T_m} = -\frac{k}{R} \frac{\partial}{\partial(r/R)} \left[ \frac{T_R - T}{T_R - T_m} \right], \quad (7.10)$$

where  $q_k$  is the flux evaluated at the wall ( $r = R$ ). Because the derivative in Eq. (7.10) has a unique value at the wall, independent of  $z$ ,  $h$  is therefore uniform along the pipe under the fully developed temperature conditions.

Now consider the case where  $q_k$  is uniform. This represents a uniform heat flux at the wall, and could be physically obtained by using an electric heater, depicted in Fig. 7.2. Further, since  $h$  and  $q_k$  are constant, Eq. (7.10) specifies that  $T_R - T_m$  is constant, and

$$\frac{\partial T_R}{\partial z} = \frac{\partial T_m}{\partial z}. \quad (7.11)$$

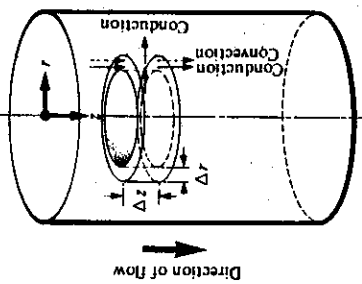


Fig. 7.1 Elemental circular ring used to develop the differential energy balance for laminar tube flow.

Energy out by conduction across surface at  $z + \Delta z$

$$2\pi r \Delta r q_z|_{z+\Delta z}$$

Energy in due to fluid flow (enthalpy) across surface at  $z$

$$\rho v_z 2\pi r \Delta r H|_z$$

Energy out due to fluid flow across surface at  $z + \Delta z$

$$\rho v_z 2\pi r \Delta r H|_{z+\Delta z}$$

Here  $H$  is the enthalpy per unit mass, and  $v_z$  is the velocity in the  $z$ -direction. At steady state, the energy balance requires equal inputs and outputs. If we divide all terms by  $2\pi \Delta r \Delta z$ , we obtain

$$\frac{rq_z|_{r+\Delta r} - rq_z|_r}{\Delta r} + r \frac{q_z|_{z+\Delta z} - q_z|_z}{\Delta z} + r \rho v_z \frac{H|_{z+\Delta z} - H|_z}{\Delta z} = 0. \quad (7.1)$$

Now  $\Delta r$  and  $\Delta z$  are allowed to approach zero.

$$\frac{\partial(q_z)}{\partial r} + r \frac{\partial q_z}{\partial z} + r \rho v_z \frac{\partial H}{\partial z} = 0. \quad (7.2)$$

If  $C_p$  is the heat capacity, then

$$\frac{\partial H}{\partial z} = C_p \frac{\partial T}{\partial z}. \quad (7.3)$$

Also

$$q_z = -k(\partial T / \partial r) \quad \text{and} \quad q_z = -k(\partial T / \partial z). \quad (7.4a,b)$$

Substituting Eqs. (7.3) and (7.4) into Eq. (7.2) yields an energy equation written in terms of temperature:

$$v_z \frac{\partial T}{\partial z} = \frac{k}{\rho C_p} \left[ \frac{1}{r} \frac{\partial}{\partial r} \left[ r \frac{\partial T}{\partial r} \right] + \frac{\partial^2 T}{\partial z^2} \right]. \quad (7.5)$$

Having obtained the temperature profile, we can evaluate  $h$ . From Eq. (7.10),  $(T_R - T_m)$  and  $q_R$  must then be evaluated. First, we find  $(T_R - T_m)$  by performing the integration:

$$T_R - T_m = \frac{\int_0^R v_z(T_R - T) 2\pi r dr}{\int_0^R v_z 2\pi r dr}. \quad (7.17)$$

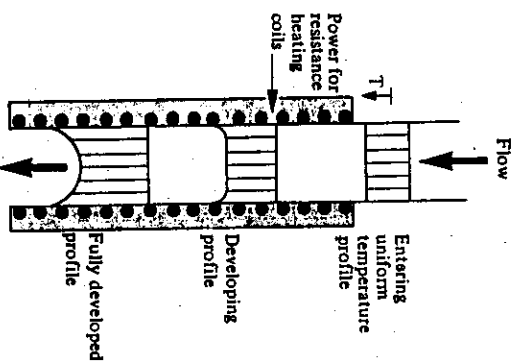


Fig. 7.2 Heating a fluid in a tube showing the development of the temperature profile.

(Note that  $T_R$  and  $T_m$  themselves are not constants.) Now expand Eq. (7.9) in a general sense where each quantity varies as follows:

$$\left[ \frac{\partial T_R}{\partial z} - \frac{\partial T}{\partial z} \right] = \left[ \frac{T_R - T}{T_R - T_m} \right] \left[ \frac{\partial T_R}{\partial z} - \frac{\partial T_m}{\partial z} \right] = 0. \quad (7.12)$$

Then Eq. (7.11) shows that

$$\frac{\partial T_R}{\partial z} = \frac{\partial T}{\partial z} = \frac{\partial T_m}{\partial z}. \quad (7.13)$$

Equation (7.13) is important because it allows Eq. (7.7) to be integrated directly using  $\frac{\partial T}{\partial z} = \frac{\partial T_m}{\partial z}$ :

$$2\bar{V}_z \left[ \frac{\partial T_m}{\partial z} \right] \int_0^r \left[ 1 - \left( \frac{r}{R} \right)^2 \right] dr = \frac{k}{\rho C_p} \int_{\text{wall}}^{\partial T_R} d \left[ r \frac{\partial T}{\partial r} \right]. \quad (7.14)$$

Integrating, we get

$$2\bar{V}_z \left[ \frac{\partial T_m}{\partial z} \right] \frac{r}{2} \left[ 1 - \frac{1}{2} \left( \frac{r}{R} \right)^2 \right] = \frac{k}{\rho C_p} \frac{\partial T}{\partial r}. \quad (7.15)$$

A second integration with  $T = T_R$  at  $r = R$  finally results in

$$T_R - T = \left[ \frac{\bar{V}_z C_p}{8Rk} \right] \left[ \frac{\partial T_m}{\partial z} \right] (3R^4 - 4r^2R^2 + r^4). \quad (7.16)$$

<sup>a</sup>From W. M. Rohsenow and H. Y. Choi, *Heat, Mass and Momentum Transfer*, Prentice-Hall, Englewood Cliffs, New Jersey, 1961, page 141.

<sup>b</sup>Slug flow refers to a flat velocity profile.

<sup>c</sup> $D_e$  is the equivalent diameter, as defined in Chapter 3.

Second, we determine  $q_R$  by evaluating the gradient at the wall using Eq. (7.16):

$$q_R = -k \left[ \frac{\partial T}{\partial r} \right]_{r=R}. \quad (7.18)$$

When these operations have been carried out, we can determine the heat transfer coefficient. The final result, with  $D$  as the diameter, is

$$\frac{hD}{k} = 4.36. \quad (7.19)$$

The dimensionless number resulting from this analysis is the *Nusselt number*. This important dimensionless number for heat flow with *forced* convection reappears as we examine other solutions and correlations. For emphasis, then, the Nusselt number is

$$\text{Nu}_{\infty} = \frac{hD}{k}. \quad (7.20)$$

## 7.2 HEAT TRANSFER WITH LAMINAR FORCED CONVECTION OVER A FLAT PLATE

In Chapter 2, the velocity distribution, within the boundary layer over a flat plate, was determined. Here we consider the case of a plate at a different temperature than that of the fluid, with the plate serving to heat or cool the fluid. Just as a velocity profile continually changes with distance from the leading edge, and results in a *momentum boundary layer* which increases in thickness, there is also a changing temperature profile and development of a *thermal boundary layer* when heat transfer is involved. We depict this situation along with a unit element in Fig. 7.3. With a depth of unity perpendicular to the page, the contributions to the energy balance are:

Energy in by conduction across surface at  $x$

$$q_x|_{x+\Delta x, \Delta y=1}$$

$$q_x|_{x, \Delta x=1}$$

$$q_x|_{y+\Delta y, \Delta x=1}$$

$$q_x|_{y, \Delta x=1}$$

$$\rho v_x \Delta y \cdot 1 \cdot H|_x$$

$$\rho v_x \Delta y \cdot 1 \cdot H|_{x+\Delta x}$$

$$\rho v_y \Delta x \cdot 1 \cdot H|_y$$

$$\rho v_y \Delta x \cdot 1 \cdot H|_{y+\Delta y}$$

Energy out by conduction across surface at  $x + \Delta x$

$$\rho v_x \Delta y \cdot 1 \cdot H|_{x+\Delta x}$$

$$\rho v_y \Delta x \cdot 1 \cdot H|_y$$

$$\rho v_y \Delta x \cdot 1 \cdot H|_{y+\Delta y}$$

Energy in by conduction across surface at  $y$

$$q_x|_{x+\Delta x, \Delta y=1}$$

$$q_x|_{x, \Delta x=1}$$

$$q_x|_{y+\Delta y, \Delta x=1}$$

$$q_x|_{y, \Delta x=1}$$

Energy out by conduction across surface at  $y + \Delta y$

$$q_x|_{x+\Delta x, \Delta y=1}$$

$$q_x|_{x, \Delta x=1}$$

$$q_x|_{y+\Delta y, \Delta x=1}$$

$$q_x|_{y, \Delta x=1}$$

Energy in due to fluid flow (sensible heat) across surface at  $x + \Delta x$

$$\rho v_x \Delta y \cdot 1 \cdot H|_{x+\Delta x}$$

$$\rho v_y \Delta x \cdot 1 \cdot H|_y$$

$$\rho v_y \Delta x \cdot 1 \cdot H|_{y+\Delta y}$$

Energy out due to fluid flow (sensible heat) across surface at  $y + \Delta y$

$$\rho v_x \Delta y \cdot 1 \cdot H|_{x+\Delta x}$$

$$\rho v_y \Delta x \cdot 1 \cdot H|_y$$

$$\rho v_y \Delta x \cdot 1 \cdot H|_{y+\Delta y}$$

Energy in due to fluid flow (sensible heat) across surface at  $y$

$$\rho v_x \Delta y \cdot 1 \cdot H|_{x+\Delta x}$$

$$\rho v_y \Delta x \cdot 1 \cdot H|_y$$

$$\rho v_y \Delta x \cdot 1 \cdot H|_{y+\Delta y}$$

Energy out due to fluid flow (sensible heat) across surface at  $x$

$$\rho v_x \Delta y \cdot 1 \cdot H|_{x+\Delta x}$$

$$\rho v_y \Delta x \cdot 1 \cdot H|_y$$

$$\rho v_y \Delta x \cdot 1 \cdot H|_{y+\Delta y}$$

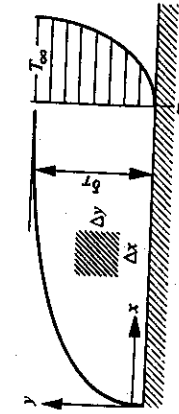


Fig. 7.3 Development of the thermal boundary layer and the temperature distribution over a flat plate.

Adding all these quantities, dividing through by  $\Delta x \Delta y$ , and taking the limits as  $\Delta x \rightarrow 0$  and  $\Delta y \rightarrow 0$ , we obtain

$$\frac{\partial q_x}{\partial x} + \frac{\partial q_y}{\partial y} + \frac{\partial(\rho v_x H)}{\partial x} + \frac{\partial(\rho v_y H)}{\partial y} = 0. \quad (7.21)$$

For constant density and conductivity, Eq. (7.21) becomes

$$\rho H \left[ \frac{\partial v_x}{\partial x} + \frac{\partial v_y}{\partial y} \right] + \rho \left[ v_x \frac{\partial H}{\partial x} + v_y \frac{\partial H}{\partial y} \right] = k \left[ \frac{\partial^2 T}{\partial x^2} + \frac{\partial^2 T}{\partial y^2} \right]. \quad (7.22)$$

Since continuity requires that  $(\partial v_x / \partial x) + (\partial v_y / \partial y) = 0$  and  $dH = C_p dT$ , we finally obtain

$$\rho C_p \left[ v_x \frac{\partial T}{\partial x} + v_y \frac{\partial T}{\partial y} \right] = k \left[ \frac{\partial^2 T}{\partial x^2} + \frac{\partial^2 T}{\partial y^2} \right]. \quad (7.23)$$

The temperature gradient in the  $y$ -direction is much steeper than that in the  $x$ -direction; therefore the  $x$ -directed second derivative term may be neglected. Then Eq. (7.23) simplifies to

$$v_x \frac{\partial T}{\partial x} + v_y \frac{\partial T}{\partial y} = \alpha \frac{\partial^2 T}{\partial y^2}. \quad (7.24)$$

Here  $\alpha = k/\rho C_p$ , which is called the *thermal diffusivity*. It has the same units of kinematic viscosity, which is sometimes called *momentum diffusivity*. In addition, the momentum boundary layer equation, developed in Chapter 2, is

$$\frac{\partial v_x}{\partial x} + v_y \frac{\partial v_x}{\partial y} = \nu \frac{\partial^2 v_x}{\partial y^2}. \quad (2.87)$$

Equations (7.24) and (2.87) are analogous. If  $v = \alpha$ , and if the velocity and thermal boundary conditions are similar, then the temperature and velocity profiles are exactly identical, and the thermal boundary layer  $\delta_T$  equals the momentum boundary layer  $\delta$ .

The method of solution for Eq. (7.24) parallels that for the velocity distribution, as given in Section 2.7.1. For the case of a uniform-temperature plate, the following boundary conditions apply

$$B.C.1 \quad \text{at } y = 0, \quad T = T_0;$$

$$B.C.2 \quad \text{at } y = \infty, \quad T = T_\infty;$$

$$B.C.3 \quad \text{at } x \leq 0, \quad T = T_\infty.$$

We do not present the method of solution here, but Fig. 7.4 gives the temperature  $T$  as a function of  $y$  and  $x$ . The temperature is a part of the dimensionless temperature  $\Theta$  on the ordinate, which includes the wall temperature  $T_0$  and the bulk fluid temperature  $T_\infty$ . Space dimensions  $x$  and  $y$  appear together on the abscissa in exactly the same way, as shown in Fig. 2.7 for describing the velocity profiles. Several curves are shown in Fig. 7.4, each for a different value of the *Prandtl number*,  $Pr$ . This number is the ratio of  $v/\alpha$ , and for  $Pr$  equal to unity, the  $\Theta$  curve in Fig. 7.4 is exactly the same as  $v_y/V_\infty$  in Fig. 2.7. Therefore, the Prandtl number controls the similarity between the velocity profiles and the temperature profiles.

Knowing the temperature profile, we can determine the heat-transfer coefficient. From the results given in Fig. 7.4, the *local* heat transfer coefficient is

$$h_x = -k \left[ \frac{\partial T}{\partial y} \right]_{y=0} = 0.332k \Pr^{0.343} \left[ \frac{V_\infty}{\nu x} \right]^{1/2}, \quad Pr \geq 0.6, \quad (7.25)$$

or, in terms of dimensionless numbers,

$$Nu_x = 0.332 \Pr^{0.343} Re^{0.33}, \quad Nu_x = h_x x / k,$$

where  $Nu_x = h_x x / k$ , which is called the *local Nusselt number*. If we wish to know the average heat-transfer coefficient, then we can find it by averaging  $h_x$  from  $x = 0$  to  $x = L$ :

$$h = \frac{1}{L} \int_0^L h_x dx = 0.664k \Pr^{0.343} \left[ \frac{V_\infty}{\nu L} \right]^{1/2},$$

Equations (7.27)-(7.29) are valid only for  $\text{Pr} > 0.5$ , and thus do not apply to liquid metals. For liquid metals with uniform wall temperatures as a boundary condition, the results are approximated by<sup>2</sup>

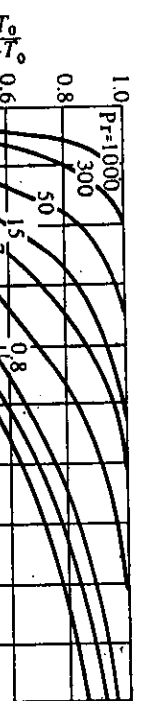


Fig. 7.4 Dimensionless temperature profiles in the laminar boundary layer over a flat plate for various  $\text{Pr}$ . (From E. Z. Pohlhausen, *Z. Angew. Math. Mech.* 1, 115 (1921).)

or

$$\text{Nu}_L = 0.664 \text{Pr}^{0.343} \text{Re}_L^{0.5}, \quad (7.27)$$

Note the general form of either Eq. (7.26) or (7.27). We shall find in Chapter 8 that the Nusselt number is generally a function of the Reynolds and Prandtl numbers in problems of forced convection.

For the case of  $\text{Pr} = 1$  ( $\nu = \alpha$ ), the thermal boundary layer is given by

$$\frac{\delta_T}{x} = \frac{5.0}{\sqrt{V_\infty x / \nu}}, \quad (7.28)$$

which is the same as the momentum boundary layer.

At this point it is instructive to examine Prandtl numbers for various fluids; approximate values are given in Table 7.2. These numbers represent values that include several substances, and cover substantial temperature ranges. The Prandtl numbers of liquids vary significantly with temperature; however, gases show almost no variation in  $\text{Pr}$  with temperature. From Table 7.2, we see that for gases  $\delta_T \approx \delta$ , for common liquids  $\delta_T < \delta$ , and for liquid metals—due to their high thermal conductivity— $\delta_T \gg \delta$ . To a close approximation, the ratio of the boundary layer thicknesses is

$$\frac{\delta_T}{\delta} = 0.975 \text{Pr}^{-1/3}, \quad \text{Pr} > 0.5. \quad (7.29)$$

Table 7.2. Typical Prandtl numbers

Substance	Range of Prandtl number ( $\nu/\alpha$ )
Common liquids (water, alcohol, etc.)	2-50
Liquid metals	0.001-0.03
Gases	0.7-1.0

$$\text{Nu}_x = \sqrt{\text{Re}_x \text{Pr}} \left[ \frac{0.564}{1 + 0.90 \sqrt{\text{Pr}}} \right]. \quad (7.30)$$

$$\text{Pr} > 0.5, \quad \text{Nu}_x = 0.458 \text{Pr}^{0.343} \sqrt{\text{Re}_x}; \quad (7.31)$$

$$0.006 \leq \text{Pr} \leq 0.03, \quad \text{Nu}_x = \sqrt{\text{Re}_x \text{Pr}} \left[ \frac{0.880}{1 + 1.317 \sqrt{\text{Pr}}} \right]. \quad (7.32)$$

For a uniform heat flux at the wall, we present these results.<sup>3</sup>

Example 7.1 Air at 1 atm ( $1.013 \times 10^5 \text{ N m}^{-2}$ ) and 290 K flows parallel to a plate's surface at  $15 \text{ m s}^{-1}$ . The plate, 0.3 m long, is at 360 K. Assume that laminar flow is stable along the entire length.

- Calculate the thicknesses of the velocity and thermal boundary layers 0.15 m from the leading edge of the plate.
- Calculate the rate of heat transfer from the entire plate per 0.1 m of plate width.

Solution.

- We calculate the thickness of the momentum boundary layer using Eq. (2.101).

$$\frac{\delta}{x} = \frac{5.0}{\sqrt{V_\infty x / \nu}}.$$

For air, evaluating  $\nu$  at an average boundary-layer temperature of  $\frac{1}{2}(290 + 360) = 325 \text{ K}$ , the kinematic viscosity is  $18.4 \times 10^{-6} \text{ m}^2 \text{s}^{-1}$ . Then,

$$\frac{V_\infty x}{\nu} = \frac{15 \text{ m}}{\text{s}} \left| \frac{0.15 \text{ m}}{18.4 \times 10^{-6} \text{ m}^2} \right| = 1.22 \times 10^5,$$

and

$$\delta = \frac{(0.15)(5.0)}{\sqrt{1.22 \times 10^5}} = 2.15 \times 10^{-3} \text{ m} = 2.15 \text{ mm}.$$

Next, we use Eq. (7.29)

$$\frac{\delta_T}{\delta} = 0.975 \text{Pr}^{-1/3}.$$

<sup>2</sup>E. M. Sparrow and J. L. Gregg, *J. Aero. Sc.* 24, 852 (1957).

<sup>3</sup>R. J. Nickerson and H. P. Smith, as reported in Rohsenow and Choi, *ibid.*, page 149.

The Prandtl number for air, evaluated at 325 K, is 0.703. Then

$$\delta_T = (2.15)(0.975)(0.703)^{-1/3} = 2.36 \text{ mm.}$$

b) Equation (7.27) is used for the average heat-transfer coefficient, which applies to the whole plate.

$$Nu_L = (0.664)(0.703^{0.343}) \sqrt{2.44 \times 10^5} = 291.$$

The thermal conductivity for air at 325 K is  $28.1 \times 10^{-3} \text{ W m}^{-1} \text{ K}^{-1}$ . Then

$$h = \frac{k}{L} Nu_L = \frac{(28.1 \times 10^{-3})(291)}{(0.3)} = 27.2 \text{ W m}^{-2} \text{ K}^{-1},$$

and finally

$$Q = hA(T_\infty - T) = (27.2)(0.3 \times 0.1)(360 - 290) = 57.1 \text{ W.}$$

### 7.3 HEAT TRANSFER WITH NATURAL CONVECTION

In Sections 7.1 and 7.2 we considered heat transfer with forced convection. In forced convection, the known velocity distribution can be entered into the energy equation. The situation is more complex in problems of heat transfer with natural convection because the velocities are not known *a priori* to solving the energy equation. Hence, the velocity and temperature distributions cannot be treated as separate problems; the temperature distribution, in effect, produces the velocity distribution by causing density differences within the fluid.

Consider the vertical surface in Fig. 7.5; the surface is at  $T_0$ , and it heats the neighboring fluid whose bulk temperature is  $T_\infty$ . In this situation, the velocity component  $v_y$  is quite small; the fluid moves almost entirely upward, and therefore we write the momentum equation for the  $x$ -component only. For steady forced convection over a flat plate, we ignored the gravity force, and no pressure gradient was involved. We cannot ignore these forces in free convection, and therefore the momentum equation for the present case contains these terms

$$v_x \frac{\partial v_x}{\partial x} + v_y \frac{\partial v_x}{\partial y} = -\frac{1}{\rho} \frac{\partial P}{\partial x} + \nu \frac{\partial^2 v_x}{\partial y^2} + g_x. \quad (7.33)$$

We apply the so-called *Boussinesq approximation* in which variations in the density of the fluid are neglected except in the buoyancy force term that drives the natural convection. Thus, in Eq. (7.33) the density is a reference density at the reference temperature,  $T_\infty$ . Therefore, the inertial terms become

$$\rho_\infty \left[ v_x \frac{\partial v_x}{\partial x} + v_y \frac{\partial v_x}{\partial y} \right],$$

and the pressure gradient is approximated as

$$\frac{\partial P}{\partial x} = \frac{dp}{dx} = -\rho_\infty g.$$

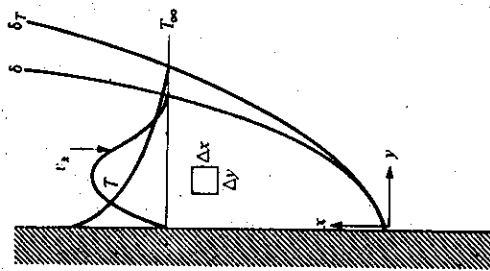


Fig. 7.5 Thermal and momentum boundary layers for vertical plate natural convection.

With  $g_x = -g$ , the buoyancy term is simply

$$\rho g_x = -\rho_\infty g [1 + \beta(T_\infty - T)],$$

where the volume expansion coefficient  $\beta$  is defined as

$$\beta = -\frac{1}{\rho} \left[ \frac{\partial \rho}{\partial T} \right]_P,$$

The momentum balance in the  $x$ -direction then becomes

$$v_x \frac{\partial v_x}{\partial x} + v_y \frac{\partial v_x}{\partial y} = \nu \frac{\partial^2 v_x}{\partial y^2} + g\beta(T_\infty - T), \quad (7.34)$$

which is identical with Eq. (2.87), except for the addition of the buoyancy term. Equation (7.34) shows that the momentum equation must be coupled to an appropriate energy equation, in order to treat the buoyancy term.

The energy equation applied to the control volume  $\Delta x \Delta y$  in this case is identical to that for flow over a flat plate:

$$v_x \frac{\partial T}{\partial x} + v_y \frac{\partial T}{\partial y} = \alpha \frac{\partial^2 T}{\partial y^2}. \quad (7.35)$$

This equation is coupled to Eq. (7.34) by the presence of the velocity terms. The mathematical task at hand is, therefore, to solve the coupled equations with the boundary conditions:

$$\text{B.C.1} \quad \text{at } y = 0, \quad v_x = v_y = 0, \quad T = T_0;$$

$$\text{B.C.2} \quad \text{at } y = \infty, \quad v_x = v_y = 0, \quad T = T_\infty.$$

Analytical solutions of such coupled differential equations are beyond the scope of this text; we simply present the results. First, however, let us examine a dimensional analysis approach in order to bring forth pertinent dimensionless numbers.

The problem is to determine the conditions for which the velocity profile in a natural convection situation is similar to the velocity profile in another natural convection situation. Both systems have the same boundary conditions, i.e., velocity is zero at the surface and within the bulk fluid removed from the surface. Now employ the dynamic similarity argument introduced in Section 3.1.1.

First, Eq. (7.34) is written for system 1:

$$\frac{\partial v_{11}}{\partial x_1} + v_{11} \frac{\partial v_{11}}{\partial y_1} = v_1 \frac{\partial^2 v_{11}}{\partial y_1^2} + g_1 \beta (T - T_{\infty})_1. \quad (7.36)$$

System 2 is related to system 1 by geometrical and dynamic similarities expressed by the ratios:

$$K_u = \frac{x_1}{x_2} = \frac{y_1}{y_2} = \frac{L_1}{L_2} \quad K_v = \frac{v_1}{v_2}$$

$$K_g = \frac{v_{11}}{v_{21}} = \frac{v_{11}}{v_{22}} = \frac{v_1}{v_2} \quad K_s = \frac{g_1}{g_2}$$

$$K_b = \frac{\beta}{\beta_2} \quad K_T = \frac{(T - T_{\infty})_1}{(T - T_{\infty})_2} = \frac{(T_0 - T_{\infty})_1}{(T_0 - T_{\infty})_2}. \quad (7.37)$$

Now, we replace  $v_{11}$ ,  $x_1$ ,  $y_1$ ,  $v_{11}$ ,  $g_1$ , etc. in Eq. (7.36) by their equivalents in Eq. (7.37); then we write Eq. (7.34) for system 2:

$$\frac{K_v^2}{K_L} v_{22} \frac{\partial v_{22}}{\partial x_2} + \frac{K_v^2}{K_L} v_{22} \frac{\partial v_{22}}{\partial y_2} = \frac{K_v K_g}{K_L^2} v_2 \frac{\partial^2 v_2}{\partial y_2^2} + K_s K_g K_T g_2 \beta_2 (T - T_{\infty})_2. \quad (7.38)$$

Equation (7.38) if rewritten without all the  $K$ s would of course be valid, because it would transform back to Eq. (7.34). Hence,

$$\frac{K_v^2}{K_L} = \frac{K_v K_g}{K_L^2} = K_s K_g K_T = 1, \quad (7.39)$$

and therefore

$$\frac{v_1^2}{L_1} = \frac{v_2^2}{L_2}, \quad \frac{v_1 v_1}{L_1^2} = \frac{v_2 v_2}{L_2^2}. \quad (7.40a,b,c)$$

Thus,

$$g_1 \beta_1 (T_0 - T_{\infty})_1 = g_2 \beta_2 (T_0 - T_{\infty})_2.$$

If we combine Eqs. (7.40a) and (7.40b) we get

$$\frac{v_1 L_1}{v_1} = \frac{v_2 L_2}{v_2}, \quad (7.41)$$

which are Reynolds numbers. The combination of Eqs. (7.40b) and (7.40c), yields

$$\frac{g_1 \beta_1 (T_0 - T_{\infty})_1 L_1^2}{v_1 v_2} = \frac{g_2 \beta_2 (T_0 - T_{\infty})_2 L_2^2}{v_2 v_2}. \quad (7.42)$$

The group of variables represented in Eq. (7.42) could be considered a dimensionless number, but by reflecting on the physical aspects, we realize that the velocity of the fluid is not an independent quantity, but that it rather depends on the buoyant force. Hence, the  $v$ 's are eliminated from Eq. (7.42), and substituting their equivalents from Eq. (7.41), we obtain

$$\frac{g_1 \beta_1 (T_0 - T_{\infty})_1 L_1^3}{v_1^2} = \frac{g_2 \beta_2 (T_0 - T_{\infty})_2 L_2^3}{v_2^2}. \quad (7.43)$$

This dimensionless number is important in natural convection problems and is called the *Grashof number*,  $\text{Gr}$ . When buoyancy is the only driving force for convection, the velocity profile is determined entirely by the quantities in the Grashof number, and the Reynolds number is superfluous.

Recall that for forced convection, as discussed in Section 7.2, the Nusselt number is correlated in the general form

$$\text{Nu} = f(\text{Pr}, \text{Gr}), \quad \text{forced convection.}$$

Correspondingly then, for natural convection, the Nusselt number is correlated as

$$\text{Nu} = f(\text{Pr}, \text{Gr}), \quad \text{natural convection.}$$

Returning to the complete solution of Eqs. (7.34), (7.35) and the appropriate boundary conditions, we present the velocity and temperature distributions (see Fig. 7.6). The curves show that for  $\text{Pr} \leq 1$ ,  $\delta_r \approx \delta$ , but for  $\text{Pr} > 1$ ,  $\delta_r < \delta$ . For liquid metals, therefore,  $\delta_r$  is about equal to  $\delta$  in free convection as contrasted to forced convection in which  $\delta_r \gg \delta$ . Corresponding to the temperature profile, shown in Fig. 7.6b, the local Nusselt number is

$$\frac{\text{Nu}_x}{\sqrt[4]{\text{Gr}_x / 4}} = \frac{0.676 \text{ Pr}^{1/2}}{(0.861 + \text{Pr})^{1/4}}. \quad (7.44)$$

Equation (7.44) applies for a wide range of  $\text{Pr}$  numbers ( $0.00835 \leq \text{Pr} \leq 1000$ ) for laminar flow conditions, with  $10^4 < \text{Gr}_x \cdot \text{Pr} < 10^{10}$ .

**Example 7.2.** Calculate the initial heat transfer rate from a plate at 360 K, 0.3 m long  $\times 0.1$  m wide hung vertically in air at 290 K. Contrast the results with those of Example 7.1.

**Solution.** Equation (7.44) should be integrated to obtain the average heat transfer coefficient which can be applied to the whole plate.

In Eq. (7.44), because  $h_r$  varies as  $x^{1/4}$ , then the average  $h$  equals  $\frac{4}{3} h_r$ . Hence  $\text{Nu}_L$  defined as  $hL/k$  is

$$\frac{\text{Nu}_L}{\sqrt[4]{\text{Gr}_L / 4}} = \frac{0.902 \text{ Pr}^{1/2}}{(0.861 + \text{Pr})^{1/4}}. \quad (7.45)$$

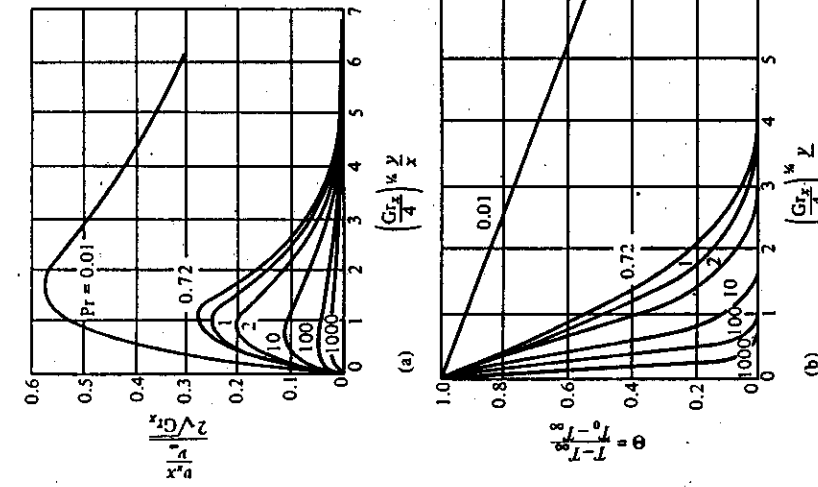


**Fig. 7.6** Laminar natural convection for a vertical plate. (a) Dimensionless velocity profiles.  
(b) Dimensionless temperature profiles. (Calculated by S. Ostrach, *Nat. Advisory Comm. Aeronaut. Tech. Note 2635*, Feb. 1952, as presented in W. M. Rohsenow and H. Y. Choi, *Heat, Mass, and Momentum Transfer*, Prentice-Hall, Englewood Cliffs, New Jersey, 1961, pages 155-159.)

or

$$\text{Nu}_L = 0.902 \sqrt[4]{\frac{\text{Gr}_L \cdot \text{Pr}^2}{4(0.861 + \text{Pr})}} \quad (7.45a)$$

We evaluate the properties at the average boundary temperature of 325 K. For air at 325 K

$$\text{Pr} = 0.703 \quad \text{and} \quad g\beta/\nu^2 = 9.85 \times 10^7 \text{ K}^{-1} \text{ m}^3$$

The Grashof number is

$$\text{Gr}_L = \frac{g\beta}{\nu^2} (T_0 - T_\infty)L^3 = (9.85 \times 10^7)(360 - 290)(0.3^3) = 1.86 \times 10^8$$

Rate of energy in by conduction across surface at  $r$

$$2\pi r q_r|_{r+\Delta r} \quad (7.45c)$$

Rate of energy out by conduction across surface at  $r + \Delta r$

$$2\pi r q_r|_r + \Delta r \quad (7.45d)$$

At steady state, these are the only terms that contribute to the energy balance. Thus

$$2\pi r q_r|_{r+\Delta r} - 2\pi r q_r|_r = 0.$$

Next, we calculate the product  $\text{Gr}_L \cdot \text{Pr}$  to test for laminar flow conditions

$$\text{Gr}_L \cdot \text{Pr} = (1.86 \times 10^8)(0.703) = 1.31 \times 10^8.$$

Since it is between  $10^4$  and  $10^{10}$ , Eq. (7.45a) is valid. When we substitute values of  $\text{Gr}_L$  and  $\text{Pr}$  into Eq. (7.45a),

$$\text{Nu}_L = 55.8,$$

from which,

$$h = \text{Nu}_L \frac{k}{L} = (55.8) \left[ \frac{28.1 \times 10^{-3}}{0.3} \right] = 5.23 \text{ W m}^{-2} \text{ K}^{-1}.$$

Finally, we evaluate the rate of heat transfer  $Q$ .

$$Q = h(T_\infty - T_0)A = (5.23)(360 - 290)(0.1 \times 0.3) = 11.0 \text{ W}.$$

For Example 7.1,  $Q$  was 57.1 W; that is, the rate of heat transfer for forced convection is considerably higher. This is the usual case.

It is instructive to look at special forms of Eq. (7.45a). First, if  $\text{Pr} = 0.7$ , then it reduces to

$$\text{Nu}_L = 0.477 \text{ Gr}^{1/4}. \quad (7.45b)$$

It so happens that for many gases, including air,  $\text{O}_2$ ,  $\text{CO}$ ,  $\text{He}$  (and other inert gases),  $\text{H}_2$  and  $\text{CO}_2$ ,  $\text{Pr}$  is very close to 0.7 and practically constant for temperatures even as high as 1900 K. Thus, we can apply Eq. (7.45b) directly to gases.

Second, if  $\text{Pr} \rightarrow 0$  (liquid metals), then Eq. (7.59a) reduces to

$$\text{Nu}_L = 0.936 \sqrt[4]{\frac{\text{Gr}_L \cdot \text{Pr}^2}{4}}. \quad (7.45c)$$

We consider heat conduction through the wall of a hollow solid cylinder. Figure 7.7 depicts the situation, and also locates a suitable unit volume with a thickness  $\Delta r$ . From a practical point of view, we may visualize a long cylindrical shaped furnace, and it is desirable to calculate the heat loss to the surroundings. Suppose the cylinder is long enough so that end effects are negligible; in addition, the system is at steady state, so that both the inside and outside surfaces of the wall are at some fixed temperatures,  $T_1$  and  $T_2$ , respectively. For such a system, we develop the energy equation.

Rate of energy in by conduction across surface at  $r$

$$2\pi r q_r|_r, \quad (7.45d)$$

Heat Transfer and the Energy Equation 235

Determination of the constants using the boundary conditions yields the temperature distribution

$$\frac{T - T_2}{T_1 - T_2} = \frac{\ln(r/r_2)}{\ln(r_1/r_2)}, \quad (7.51)$$

and the heat flux

$$q_r = -k \frac{dT}{dr} = \frac{k}{r} \left[ \frac{T_1 - T_2}{\ln(r_1/r_2)} \right]. \quad (7.52)$$

As the heat flows through the wall, it encounters larger areas, so that the flux itself decreases. The heat flow  $Q$ , however, is constant (as it must be for steady state), and is given by

$$Q = q_r(2\pi rL) = \frac{2\pi kL}{\ln(r_1/r_2)} (T_1 - T_2). \quad (7.53)$$

This problem, elementary as it is, demonstrates an interesting engineering characteristic. Suppose we use the cylindrical wall as the insulation of a furnace wall. As increasing thicknesses of insulation are added, the outside layer, because of its greater area, offers less resistance to heat flow than an inner layer of the same thickness. Thus, from a cost point of view, the expense of additional insulation can become greater than the savings associated with reduction in heat losses.

**Fig. 7.7** Heat conduction through a solid cylindrical wall. The shaded area depicts the unit volume.

If we divide all terms by  $2\pi r\Delta r$ , and take the limit as  $\Delta r$  approaches zero, we obtain

$$\frac{d(q_r)}{dr} = 0. \quad (7.46)$$

Equation (7.46) requires that

$$rq_r = C_1. \quad (7.47)$$

Note that  $q_r$ , the heat flux, is not constant in itself. Since  $q_r = -k(dT/dr)$ , Eq. (7.47) yields

$$-k \frac{dT}{dr} = \frac{C_1}{r}. \quad (7.48)$$

Integrating once again, we find for constant thermal conductivity that

$$T = -\frac{C_1}{k} \ln r + \frac{C_2}{k}. \quad (7.49)$$

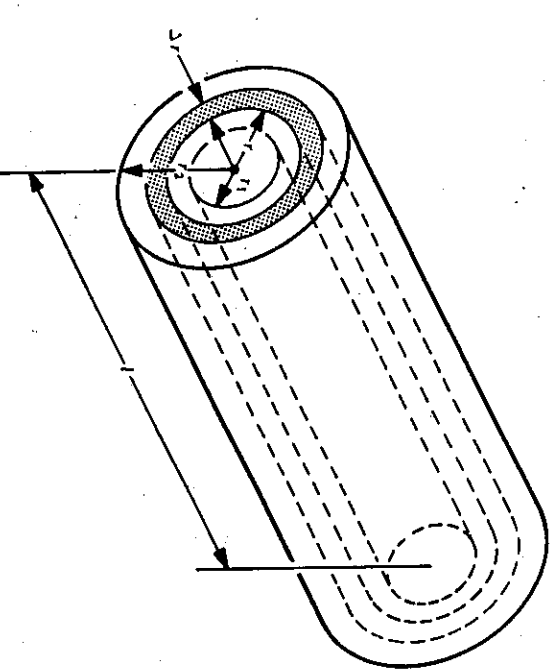
By absorbing  $k$  in new constants, Eq. (7.49) simplifies even more to

$$T = C_3 \ln r + C_4. \quad (7.50)$$

The boundary conditions under consideration are

$$\text{B.C.1} \quad \text{at } r = r_1, \quad T = T_1;$$

$$\text{B.C.2} \quad \text{at } r = r_2, \quad T = T_2.$$



	$k, \text{ W m}^{-1} \text{ K}^{-1}$	Cost, \$ per $\text{m}^3$
Insulation A	0.70	350
Insulation B	0.35	880

**Solution.** Equation (7.53) can be written

$$\ln \left[ \frac{r_2}{r_1} \right] = \frac{2\pi kL}{Q} (T_1 - T_2).$$

For A, then

$$\ln \left[ \frac{r_2}{r_1} \right] = \frac{(2\pi)(0.70)(15.2)(920 - 310)}{(73 \times 10^3)} = 0.559,$$

so that with  $r_1 = 50.5 \text{ mm}$ , we have  $r_2 = 88.3 \text{ mm}$ . Similarly for B, using the ratio of conductivities, we get

$$\ln \left[ \frac{r_2}{r_1} \right] = \left[ \frac{0.35}{0.70} \right] (0.559) = 0.280.$$

so that  $r_i = 66.8$  mm. We calculate the volume of insulation and the corresponding cost.

$$\text{Cost } A = \frac{\pi(88.3^2 - 50.5^2)}{1000^2} \text{ mm}^2 \cdot \frac{1 \text{ m}^2}{1000^2 \text{ mm}^2} \cdot \frac{350 \text{ \$}}{\text{m}^3} = \$87.69.$$

In the same manner, Cost  $B = \$80.34$ . The obvious choice is  $B$ .

## 7.5 THE GENERAL ENERGY EQUATION

In Sections 7.1-7.4, we determined temperature distributions and heat fluxes for some simple systems, by developing pertinent energy balances in differential form. In this section we develop the general energy equation, which can be reduced to solve specific problems.

Consider the stationary unit volume  $\Delta x \Delta y \Delta z$  in Figs. 2.4 and 2.5; we apply the law of conservation of energy to the fluid contained within this volume at any given time

$$\begin{bmatrix} \text{rate of accumulation} \\ \text{of internal and} \\ \text{kinetic energy} \end{bmatrix} = \begin{bmatrix} \text{net rate of internal} \\ \text{heat in by} \\ \text{convection} \end{bmatrix} + \begin{bmatrix} \text{net rate of} \\ \text{heat in by} \\ \text{conduction} \end{bmatrix} - \begin{bmatrix} \text{work done} \\ \text{by fluid} \end{bmatrix}. \quad (7.54)$$

This statement of the law of energy conservation is not completely general, because other forms of energy transport, e.g., radiation, and sources such as electrical Joule heating, are not included.

The rate of accumulation of internal and kinetic energy within the unit volume is simply

$$\Delta x \Delta y \Delta z \frac{\partial}{\partial t} \left( \rho U + \frac{1}{2} \rho v^2 \right), \quad (7.55)$$

where  $U$  is the internal energy per unit mass of fluid and  $v$  is the *magnitude* of the local fluid velocity.

The *net* rate of internal and kinetic energies in by convection is

$$\begin{aligned} \Delta y \Delta z &\left[ v_x \left( \rho U + \frac{1}{2} \rho v^2 \right) \Big|_x - v_x \left( \rho U + \frac{1}{2} \rho v^2 \right) \Big|_{x+\Delta x} \right] \\ &+ \Delta x \Delta z \left[ v_y \left( \rho U + \frac{1}{2} \rho v^2 \right) \Big|_y - v_y \left( \rho U + \frac{1}{2} \rho v^2 \right) \Big|_{y+\Delta y} \right] \\ &+ \Delta x \Delta y \left[ v_z \left( \rho U + \frac{1}{2} \rho v^2 \right) \Big|_z - v_z \left( \rho U + \frac{1}{2} \rho v^2 \right) \Big|_{z+\Delta z} \right]. \end{aligned} \quad (7.56)$$

In a similar manner, the net rate of energy in by conduction is

$$\Delta y \Delta z [q_x|_x - q_x|_{x+\Delta x}] + \Delta x \Delta z [q_y|_y - q_y|_{y+\Delta y}] + \Delta x \Delta y [q_z|_z - q_z|_{z+\Delta z}]. \quad (7.57)$$

The work done by the fluid consists of work against gravity, work against pressure, and work against viscous forces. The rate of doing work against the three components of gravity is

$$-\rho \Delta x \Delta y \Delta z (v_x g_x + v_y g_y + v_z g_z). \quad (7.58)$$

The rate of doing work against the pressure at the six faces of the unit volume is

$$\begin{aligned} \Delta y \Delta z &\left\{ (Pv_y)|_{x+\Delta x} - (Pv_x)|_x \right\} + \Delta x \Delta z \left[ (Pv_y)|_{y+\Delta y} - (Pv_y)|_y \right] \\ &+ \Delta x \Delta y \left[ (Pv_z)|_{z+\Delta z} - (Pv_z)|_z \right]. \end{aligned} \quad (7.59)$$

The rate of doing work against the  $x$ -directed viscous forces is

$$\begin{aligned} \Delta y \Delta z &\left\{ \tau_x v_x|_{x+\Delta x} - \tau_x v_x|_x \right\} + \Delta x \Delta z \left[ \tau_x v_x|_{y+\Delta y} - \tau_x v_x|_y \right] \\ &+ \Delta x \Delta y \left[ \tau_x v_x|_{z+\Delta z} - \tau_x v_x|_z \right]. \end{aligned} \quad (7.60)$$

Similar expressions may be written for the work against the  $y$ - and  $z$ -directed viscous forces

$$\begin{aligned} \Delta y \Delta z &\left\{ \tau_y v_y|_{x+\Delta x} - \tau_y v_y|_x \right\} + \Delta x \Delta z \left[ \tau_y v_y|_{y+\Delta y} - \tau_y v_y|_y \right] \\ &+ \Delta x \Delta y \left[ \tau_y v_y|_{z+\Delta z} - \tau_y v_y|_z \right], \end{aligned} \quad (7.61)$$

and

$$\begin{aligned} \Delta y \Delta z &\left\{ \tau_z v_z|_{x+\Delta x} - \tau_z v_z|_x \right\} + \Delta x \Delta z \left[ \tau_z v_z|_{y+\Delta y} - \tau_z v_z|_y \right] \\ &+ \Delta x \Delta y \left[ \tau_z v_z|_{z+\Delta z} - \tau_z v_z|_z \right]. \end{aligned} \quad (7.62)$$

Substituting all these expressions into Eq. (7.54), dividing by  $\Delta x \Delta y \Delta z$ , and taking the limit as  $\Delta x$ ,  $\Delta y$ , and  $\Delta z$  approach zero, we obtain one form of the energy equation

$$\begin{aligned} \frac{\partial}{\partial t} (\rho U + \frac{1}{2} \rho v^2) &= - \left[ \frac{\partial}{\partial x} v_x (\rho U + \frac{1}{2} \rho v^2) + \frac{\partial}{\partial y} v_y (\rho U + \frac{1}{2} \rho v^2) + \frac{\partial}{\partial z} v_z (\rho U + \frac{1}{2} \rho v^2) \right] \\ &- \left[ \frac{\partial q_x}{\partial x} + \frac{\partial q_y}{\partial y} + \frac{\partial q_z}{\partial z} \right] + \rho (v_x g_x + v_y g_y + v_z g_z) \\ &- \left[ \frac{\partial}{\partial x} Pv_x + \frac{\partial}{\partial y} Pv_y + \frac{\partial}{\partial z} Pv_z \right] \\ &- \left[ \frac{\partial}{\partial x} (\tau_x v_x + \tau_y v_y + \tau_z v_z) + \frac{\partial}{\partial y} (\tau_x v_x + \tau_y v_y + \tau_z v_z) \right. \\ &\left. + \frac{\partial}{\partial z} (\tau_x v_x + \tau_y v_y + \tau_z v_z) \right]. \end{aligned} \quad (7.63)$$

If all the terms involving  $(\rho U + \frac{1}{2}\rho v^2)$  are expanded and combined, we can obtain

$$\rho \left[ \frac{\partial}{\partial t} \left( U + \frac{1}{2}v^2 \right) + v_x \frac{\partial}{\partial x} \left( U + \frac{1}{2}v^2 \right) + v_y \frac{\partial}{\partial y} \left( U + \frac{1}{2}v^2 \right) + v_z \frac{\partial}{\partial z} \left( U + \frac{1}{2}v^2 \right) \right] + \left( U + \frac{1}{2}v^2 \right) \left[ \frac{\partial \rho}{\partial t} + \frac{\partial}{\partial x} \rho v_x + \frac{\partial}{\partial y} \rho v_y + \frac{\partial}{\partial z} \rho v_z \right]. \quad (7.64)$$

Continuity (Eq. A, Table 2.1) requires that the second term in the above expression is zero; the remaining term in the expression is the substantial derivative of  $(U + \frac{1}{2}v^2)$ , so that we may write Eq. (7.63) as

$$\begin{aligned} \rho \frac{D}{Dt} \left( U + \frac{1}{2}v^2 \right) &= \left[ \frac{\partial q_x}{\partial x} + \frac{\partial q_y}{\partial y} + \frac{\partial q_z}{\partial z} \right] + \rho(v_x g_x + v_y g_y + v_z g_z) \\ &\quad - \left[ \frac{\partial}{\partial x} P v_x + \frac{\partial}{\partial y} P v_y + \frac{\partial}{\partial z} P v_z \right] \\ &\quad - \left[ \frac{\partial}{\partial x} (\tau_{xx} v_x + \tau_{xy} v_y + \tau_{xz} v_z) + \frac{\partial}{\partial y} (\tau_{yx} v_x + \tau_{yy} v_y + \tau_{yz} v_z) \right. \\ &\quad \left. + \frac{\partial}{\partial z} (\tau_{zx} v_x + \tau_{zy} v_y + \tau_{zz} v_z) \right]. \end{aligned} \quad (7.65)$$

For most heat flow problems, it is convenient to eliminate internal energy from Eq. (7.65). The manipulation that leads to the following equation is rather lengthy, and is not given here, except to say that with the aid of the conservation of momentum, we can write Eq. (7.65) as

$$\rho \frac{DU}{Dt} = - \left[ \frac{\partial}{\partial x} q_x + \frac{\partial}{\partial y} q_y + \frac{\partial}{\partial z} q_z \right] - P \left[ \frac{\partial v_x}{\partial x} + \frac{\partial v_y}{\partial y} + \frac{\partial v_z}{\partial z} \right] + \eta\Phi, \quad (7.66)$$

where the quantity  $\Phi$  is known as the *dissipation function*,

$$\begin{aligned} \Phi &= 2 \left[ \left[ \frac{\partial v_x}{\partial x} \right]^2 + \left[ \frac{\partial v_y}{\partial y} \right]^2 + \left[ \frac{\partial v_z}{\partial z} \right]^2 \right] + \left[ \left[ \frac{\partial v_x}{\partial y} + \frac{\partial v_y}{\partial x} \right]^2 + \left[ \frac{\partial v_x}{\partial z} + \frac{\partial v_z}{\partial x} \right]^2 + \left[ \frac{\partial v_y}{\partial z} + \frac{\partial v_z}{\partial y} \right]^2 \right] \\ &\quad - \frac{2}{3} \left[ \frac{\partial v_x}{\partial x} - \frac{\partial v_y}{\partial y} + \frac{\partial v_z}{\partial z} \right]^2. \end{aligned} \quad (7.67)$$

From the definition of enthalpy,  $H = U + P/\rho$ , we write

$$\frac{DU}{Dt} = \frac{DH}{Dt} - \frac{1}{\rho} \frac{DP}{Dt} + \frac{P}{\rho^2} \frac{D\rho}{Dt}, \quad (7.68)$$

but from continuity,

$$\frac{1}{\rho} \frac{D\rho}{Dt} + \frac{\partial v_x}{\partial x} + \frac{\partial v_y}{\partial y} + \frac{\partial v_z}{\partial z} = 0,$$

so that

$$\rho \frac{DU}{Dt} = \rho \frac{DH}{Dt} - \frac{DP}{Dt} - P \left[ \frac{\partial v_x}{\partial x} + \frac{\partial v_y}{\partial y} + \frac{\partial v_z}{\partial z} \right] = 0. \quad (7.69)$$

Substitution of Eq. (7.69) into Eq. (7.66) leads to

$$\rho \frac{DH}{Dt} = - \left[ \frac{\partial}{\partial x} q_x + \frac{\partial}{\partial y} q_y + \frac{\partial}{\partial z} q_z \right] + \frac{DP}{Dt} + \eta\Phi. \quad (7.70)$$

From the thermodynamic relations of properties, we can write

$$dH = C_p dT + \frac{1}{\rho} (1 - T\beta)dP, \quad (7.71)$$

where  $C_p$  is the heat capacity, and  $\beta = -(1/\rho)(\partial \rho / \partial T)$ .

From Eq. (7.71), it follows that

$$\rho \frac{DH}{Dt} = \rho C_p \frac{DT}{Dt} + (1 - T\beta) \frac{DP}{Dt}, \quad (7.72)$$

and from the Fourier rate equations, that

$$q_x = -k \frac{\partial T}{\partial x}, \quad q_y = -k \frac{\partial T}{\partial y}, \quad q_z = -k \frac{\partial T}{\partial z}.$$

Substituting Eq. (7.72) and the rate equations into Eq. (7.70) finally gives the energy equation in terms of temperature:

$$\rho C_p \frac{DT}{Dt} = \frac{\partial}{\partial x} \left[ k \frac{\partial T}{\partial x} \right] + \frac{\partial}{\partial y} \left[ k \frac{\partial T}{\partial y} \right] + \frac{\partial}{\partial z} \left[ k \frac{\partial T}{\partial z} \right] + T\beta \frac{DP}{Dt} + \eta\Phi. \quad (7.73)$$

We usually simplify Eq. (7.73). For example, if  $k$  is independent of the space coordinates, we write

$$\rho C_p \frac{DT}{Dt} = k\nabla^2 T + T\beta \frac{DP}{Dt} + \eta\Phi. \quad (7.74)$$

Further, if the system is an *ideal gas*,  $\beta = 1/T$ :

$$\rho C_p \frac{DT}{Dt} = k\nabla^2 T + \frac{DP}{Dt} + \eta\Phi. \quad (7.75)$$

Many problems involve incompressible fluids where the viscous dissipation term is negligible. In this instance,  $\beta = \Phi = 0$ , and

$$\rho C_p \frac{DT}{Dt} = k\nabla^2 T. \quad (7.76)$$

In the conduction of heat through solids, the velocity is zero; the compressibility term is ignored, so that

$$\rho C_p \frac{\partial T}{\partial t} = k\nabla^2 T \quad (7.7)$$

### 7.6 THE ENERGY EQUATION IN RECTANGULAR AND CURVILINEAR COORDINATES

In this section, we give the fluxes and the energy equation—already developed in rectangular coordinates—in cylindrical and spherical coordinates. Tables 7.3, 7.4, and 7.5 may be used for the problems of heat flow by discarding unnecessary terms, rather than setting up problems by means of shell balances.

Table 7.3 Components of the energy flux,  $\dot{q}$

Rectangular	Cylindrical	Spherical
$q_x = -k \frac{\partial T}{\partial x}$ (A)	$q_r = -k \frac{\partial T}{\partial r}$ (D)	$q_r = -k \frac{\partial T}{\partial r}$ (G)
$q_y = -k \frac{\partial T}{\partial y}$ (B)	$q_\theta = -k \frac{1}{r} \frac{\partial T}{\partial \theta}$ (E)	$q_\theta = -k \frac{1}{r} \frac{\partial T}{\partial \theta}$ (H)
$q_z = -k \frac{\partial T}{\partial z}$ (C)	$q_\phi = -k \frac{\partial T}{\partial \phi}$ (F)	$q_\phi = -k \frac{1}{r \sin \theta} \frac{\partial T}{\partial \phi}$ (I)

\*This table and the following two tables are from R. B. Bird, W. E. Stewart, and E. N. Lightfoot, *Transport Phenomena*, Wiley, New York, 1960, pages 317-319.

Table 7.4 The equation of energy in terms of energy and momentum fluxes

Rectangular coordinates

$$\begin{aligned} \rho C_v \left( \frac{\partial T}{\partial t} + v_x \frac{\partial T}{\partial x} + v_y \frac{\partial T}{\partial y} + v_z \frac{\partial T}{\partial z} \right) &= - \left[ \frac{\partial q_x}{\partial x} + \frac{\partial q_y}{\partial y} + \frac{\partial q_z}{\partial z} \right] \\ &- T \left( \frac{\partial P}{\partial T} \right)_p \left( \frac{\partial v_x}{\partial x} + \frac{\partial v_y}{\partial y} + \frac{\partial v_z}{\partial z} \right) - \left\{ \tau_{xx} \frac{\partial v_x}{\partial x} + \tau_{yy} \frac{\partial v_y}{\partial y} + \tau_{zz} \frac{\partial v_z}{\partial z} \right\} \\ &- \left\{ \tau_{xy} \left( \frac{\partial v_x}{\partial y} + \frac{\partial v_y}{\partial x} \right) + \tau_{xz} \left( \frac{\partial v_x}{\partial z} + \frac{\partial v_z}{\partial x} \right) + \tau_{yz} \left( \frac{\partial v_y}{\partial z} + \frac{\partial v_z}{\partial y} \right) \right\}. \end{aligned} \quad (\text{A})$$

Cylindrical coordinates

$$\begin{aligned} \rho C_v \left( \frac{\partial T}{\partial t} + v_r \frac{\partial T}{\partial r} + v_\theta \frac{\partial T}{\partial \theta} + v_z \frac{\partial T}{\partial z} \right) &= - \left[ \frac{1}{r} \frac{\partial}{\partial r} (rq_r) + \frac{1}{r} \frac{\partial q_\theta}{\partial \theta} + \frac{\partial q_z}{\partial z} \right] \\ &- T \left( \frac{\partial P}{\partial T} \right)_p \left( \frac{1}{r} \frac{\partial}{\partial r} (rv_r) + \frac{1}{r} \frac{\partial v_\theta}{\partial \theta} + \frac{\partial v_z}{\partial z} \right) - \left\{ \tau_{rr} \frac{\partial v_r}{\partial r} + \tau_{\theta\theta} \frac{1}{r} \left( \frac{\partial v_\theta}{\partial \theta} + v_r \right) \right. \\ &\quad \left. + \tau_{zz} \frac{\partial v_z}{\partial z} \right\} - \left\{ \tau_{r\theta} \left[ \frac{1}{r} \frac{\partial}{\partial r} \left( \frac{v_\theta}{r} \right) + \frac{1}{r} \frac{\partial v_r}{\partial \theta} \right] + \tau_{rz} \left[ \frac{\partial v_z}{\partial r} + \frac{\partial v_r}{\partial z} \right] \right. \\ &\quad \left. + \tau_{\theta z} \left( \frac{1}{r} \frac{\partial v_z}{\partial \theta} + \frac{\partial v_\theta}{\partial z} \right) \right\}. \end{aligned} \quad (\text{B})$$

Spherical coordinates

$$\begin{aligned} \rho C_v \left( \frac{\partial T}{\partial t} + v_r \frac{\partial T}{\partial r} + v_\theta \frac{\partial T}{\partial \theta} + v_\phi \frac{\partial T}{\partial \phi} \right) &= - \left[ \frac{1}{r^2} \frac{\partial}{\partial r} (r^2 q_r) \right. \\ &\quad \left. + \frac{1}{r \sin \theta} \frac{\partial}{\partial \theta} (q_\theta \sin \theta) + \frac{1}{r \sin \theta} \frac{\partial T}{\partial \phi} \right] - T \left( \frac{\partial P}{\partial T} \right)_p \left( \frac{1}{r^2} \frac{\partial}{\partial r} (r^2 v_r) \right. \\ &\quad \left. + \frac{1}{r \sin \theta} \frac{\partial}{\partial \theta} (v_\theta \sin \theta) + \frac{1}{r \sin \theta} \frac{\partial v_\phi}{\partial \phi} \right) - \left\{ \tau_{rr} \frac{\partial v_r}{\partial r} + \tau_{\theta\theta} \frac{1}{r} \frac{\partial v_\theta}{\partial \theta} + \frac{v_r}{r} \right\} \\ &\quad + \tau_{\theta\theta} \left( \frac{1}{r \sin \theta} \frac{\partial v_\theta}{\partial \phi} + \frac{v_r}{r} + \frac{v_\theta \cos \theta}{r} \right) \left\{ \tau_{rr} \left( \frac{\partial v_\theta}{\partial r} + \frac{1}{r} \frac{\partial v_r}{\partial \theta} - \frac{v_\theta}{r} \right) \right. \\ &\quad \left. + \tau_{\theta\phi} \left( \frac{\partial v_\phi}{\partial r} - \frac{v_\theta}{r} \right) + \tau_{\phi\phi} \left( \frac{1}{r} \frac{\partial v_\theta}{\partial \phi} - \frac{v_r}{r} \right) \right\} \\ &\quad + \tau_{\phi\phi} \left( \frac{\partial v_\phi}{\partial r} + \frac{1}{r \sin \theta} \frac{\partial v_\theta}{\partial \phi} - \frac{v_\phi}{r} \right) + \tau_{\theta\phi} \left( \frac{1}{r} \frac{\partial v_\phi}{\partial \theta} + \frac{1}{r \sin \theta} \frac{\partial v_\theta}{\partial \phi} - \frac{v_\phi}{r} \right). \end{aligned} \quad (\text{C})$$

Note: The terms contained in braces {} are associated with viscous dissipation and may usually be neglected, except for systems with large velocity gradients.

**Table 7.5** The equation of energy in terms of the transport properties (for Newtonian fluids of constant  $\rho$ ,  $\eta$ , and  $k$ ; note that the constancy of  $\rho$  implies that  $C_v = C_p$ )

Rectangular coordinates

$$\begin{aligned} \rho C_v \left( \frac{\partial T}{\partial t} + v_x \frac{\partial T}{\partial x} + v_y \frac{\partial T}{\partial y} + v_z \frac{\partial T}{\partial z} \right) &= k \left[ \frac{\partial^2 T}{\partial x^2} + \frac{\partial^2 T}{\partial y^2} + \frac{\partial^2 T}{\partial z^2} \right] \\ &+ 2\eta \left\{ \left( \frac{\partial v_x}{\partial x} \right)^2 + \left( \frac{\partial v_y}{\partial y} \right)^2 + \left( \frac{\partial v_z}{\partial z} \right)^2 \right\} + \eta \left\{ \left( \frac{\partial v_x}{\partial y} + \frac{\partial v_y}{\partial x} \right)^2 \right. \\ &\quad \left. + \left( \frac{\partial v_x}{\partial z} + \frac{\partial v_z}{\partial x} \right)^2 + \left( \frac{\partial v_y}{\partial z} + \frac{\partial v_z}{\partial y} \right)^2 \right\}. \end{aligned} \quad (\text{A})$$

Cylindrical coordinates

$$\begin{aligned} \rho C_v \left( \frac{\partial T}{\partial t} + v_r \frac{\partial T}{\partial r} + \frac{v_\theta}{r} \frac{\partial T}{\partial \theta} + v_z \frac{\partial T}{\partial z} \right) &= k \left[ \frac{1}{r} \frac{\partial}{\partial r} \left( r \frac{\partial T}{\partial r} \right) + \frac{1}{r^2} \frac{\partial^2 T}{\partial \theta^2} + \frac{\partial^2 T}{\partial z^2} \right] \\ &+ 2\eta \left\{ \left( \frac{\partial v_r}{\partial r} \right)^2 + \left[ \frac{1}{r} \left( \frac{\partial v_\theta}{\partial \theta} + v_r \right) \right]^2 + \left( \frac{\partial v_z}{\partial z} \right)^2 \right\} + \eta \left\{ \left( \frac{\partial v_\theta}{\partial z} + \frac{1}{r} \frac{\partial v_z}{\partial \theta} \right)^2 \right. \\ &\quad \left. + \left( \frac{\partial v_r}{\partial \theta} + \frac{\partial v_\theta}{\partial r} \right)^2 + \left[ \frac{1}{r} \frac{\partial v_r}{\partial \theta} + r \frac{\partial}{\partial r} \left( \frac{v_\theta}{r} \right) \right]^2 \right\}. \end{aligned} \quad (\text{B})$$

and we finally write:

$$v_x \frac{\partial T}{\partial x} + v_y \frac{\partial T}{\partial y} = \alpha \frac{\partial^2 T}{\partial y^2}.$$

$$\rho C_v \left( \frac{\partial T}{\partial t} + v_r \frac{\partial T}{\partial r} + \frac{v_\theta}{r} \frac{\partial T}{\partial \theta} + \frac{v_z}{r \sin \theta} \frac{\partial T}{\partial \phi} \right) = k \left[ \frac{1}{r^2} \frac{\partial}{\partial r} \left( r^2 \frac{\partial T}{\partial r} \right) \right]$$

$$\begin{aligned} &+ \frac{1}{r^2 \sin \theta} \frac{\partial}{\partial \theta} \left( \sin \theta \frac{\partial T}{\partial \theta} \right) + \frac{1}{r^2 \sin^2 \theta} \frac{\partial^2 T}{\partial \phi^2} + 2\eta \left\{ \left( \frac{\partial v_r}{\partial r} \right)^2 \right. \\ &\quad \left. + \left( \frac{1}{r} \frac{\partial v_\theta}{\partial \theta} + \frac{v_r}{r} \right)^2 + \left( \frac{1}{r \sin \theta} \frac{\partial v_\phi}{\partial \phi} + \frac{v_r}{r} + \frac{v_\theta \cot \theta}{r} \right)^2 \right\} \\ &+ \eta \left\{ \left[ r \frac{\partial}{\partial r} \left( \frac{v_\theta}{r} \right) + \frac{1}{r} \frac{\partial v_r}{\partial \theta} \right]^2 + \left[ \frac{1}{r \sin \theta} \frac{\partial v_\phi}{\partial \phi} + r \frac{\partial}{\partial r} \left( \frac{v_\theta}{r} \right) \right]^2 \right. \\ &\quad \left. + \left[ \frac{\sin \theta}{r} \frac{\partial}{\partial \theta} \left( \frac{v_\phi}{\sin \theta} \right) + \frac{1}{r \sin \theta} \frac{\partial v_\phi}{\partial \phi} \right]^2 \right\}. \end{aligned} \quad (\text{C})$$

**Example 7.4** Refer back to Fig. 7.3 and the system described in Section 7.2. Using Table 7.4 or 7.5 derive the energy equation.

**Solution.** Table 7.5 is selected because the fluid has constant properties. Flow is two-dimensional in rectangular coordinates so Eq. (A) is the best choice. Before proceeding, recall that there are two velocity components  $v_x$  and  $v_y$ . Also, it is a good idea to qualitatively sketch the temperature field. Having done so, you should recognize that  $T = T(x, y)$ . Now, we can proceed to simplify Eq. (A) in Table 7.5. Notice that  $C_v = C_p$ .

$$\begin{aligned} u_z \frac{\partial T}{\partial z} &= 0 \quad \text{because } v_z = 0 \text{ and } T = T(x, y). \\ \frac{\partial^2 T}{\partial z^2} &= 0 \quad \text{because } T = T(x, y). \end{aligned}$$

All terms in {} are zero because we neglect viscous heating. We are left with

$$\rho C_p \left[ v_x \frac{\partial T}{\partial x} + v_y \frac{\partial T}{\partial y} \right] = k \left[ \frac{\partial^2 T}{\partial x^2} + \frac{\partial^2 T}{\partial y^2} \right].$$

Except for fluids with very low Pr numbers, we can ignore conduction in the direction of flow; hence

$$\frac{\partial^2 T}{\partial x^2} = 0$$

### PROBLEMS

7.1 For laminar flow, calculate the results given in Table 7.1 for  $\text{Nu}_\infty$  for slug flow ( $v_x$  = uniform) and uniform heat flux in a circular tube.

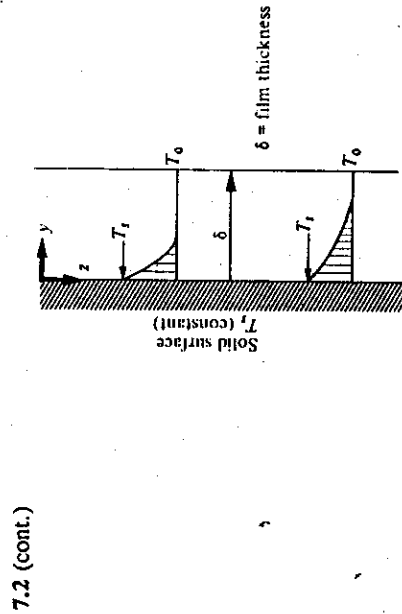
7.2 A liquid film at  $T_0$  flows down a vertical wall at a higher temperature  $T_w$ . Consider heat transfer from the wall to the liquid for such contact times that the liquid temperature changes appreciably only in the immediate vicinity of the wall. (See figure on next page.)

- a) Show that the energy equation can be written (state assumptions):

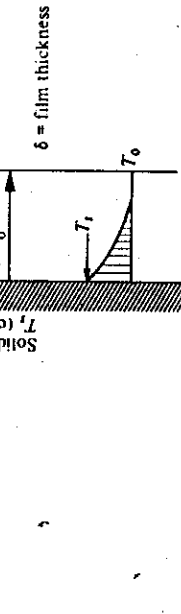
$$\rho C_p v_z \frac{\partial T}{\partial z} = k \frac{\partial^2 T}{\partial y^2}.$$

- b) The energy equation contains  $v_z$ . What would you use for  $v_z$ ?
- c) Write appropriate boundary conditions.

Note: The terms contained in braces {} are associated with viscous dissipation and may usually be neglected, except for systems with large velocity gradients.



- 7.6** Consider natural convection between parallel vertical plates maintained at  $T_1$  and  $T_0$ , respectively. Assume that the plates are very long and the convection is fully developed. For constant properties: a) Write the energy equation and boundary conditions for temperature. b) Write the momentum equation with the Boussinesq approximation and boundary conditions for velocity.



- 7.3** A gap of thickness  $L$  exists between two parallel plates of porous solids. Fluid is forced to flow through the bottom plate, across the gap, and then through the upper plate. Assume that the fluid flows with a constant velocity  $V$  in laminar flow with straight streamlines across the gap. The system is at steady state with the upper and lower plates at  $T_L$  and  $T_0$ , respectively. a) Write an appropriate energy equation and boundary conditions for the fluid in the gap. b) Solve for the temperature in the gap. c) Derive an equation for the heat flux across the gap.

- 7.4** A liquid of constant density and viscosity flows upward in the annulus ( $R_1 \leq r \leq R_2$ ) between two very long and concentric cylinders. Assume that both the flow and the temperature are fully developed. The inner cylinder is electrically heated and supplies a constant and uniform flux,  $q_i$ , to the liquid. The outer cylinder is maintained at a constant temperature,  $T_0$ .

- Solve for  $v_r$ .
- Write the energy equation and state your assumptions.
- Write appropriate boundary conditions.

- 7.5** Air at  $0.3 \text{ m s}^{-1}$  and  $365 \text{ K}$  flows parallel to a flat plate at  $310 \text{ K}$ . a) Calculate the distance from the leading edge to where the momentum boundary layer thickness is  $6 \text{ mm}$ . b) At the same distance from the leading edge, what is the thermal boundary layer thickness? c) Up to the same distance from the leading edge, how much heat is transferred to the plate (one side) in  $600 \text{ s}$ , if the plate is  $100 \text{ mm}$  wide?

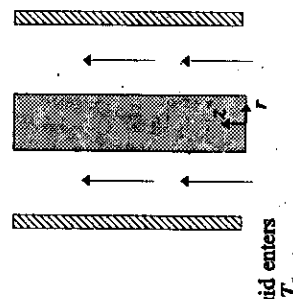
- 7.7** The surface temperature of a vertical plate is maintained at  $390 \text{ K}$ . At  $0.24 \text{ m}$  from the bottom of the plate, calculate the heat transfer coefficient to: a) air at  $290 \text{ K}$ , b) helium at  $290 \text{ K}$ .

- 7.8** Liquid metal flows through a channel with a rectangular cross-section. Two walls are perfectly insulated and two are at a constant temperature of  $T_w$ . The metal has temperature  $T_0$  as it enters the channel, and  $T_w > T_0$ . Assume steady state, fully developed flow and no solidification.



- a) Write the energy equation in terms of temperature for constant thermal properties.  
b) Write the boundary conditions.

- 7.9** Consider the creeping flow of a fluid about a rigid sphere as illustrated by Fig. 2.9. The sphere is maintained at  $T_0$  and the fluid approaches from below with a temperature  $T_\infty$  and velocity  $V_\infty$ . a) Write the energy equation which applies to the fluid in the vicinity of the sphere. Assume steady-state conditions. b) Write appropriate boundary conditions for part a). c) What other equations or results would you use in order to solve the system described by parts a) and b)?



- 7.10** A very long fiber of glass (radius =  $R$ ) is extracted from a hole in the bottom of a crucible. It is extracted with a constant velocity  $V$  into a gas at  $T_\infty$ ; assume slug flow.

- For uniform properties write the energy equation for temperature in the fiber. Do not ignore conduction in the direction of flow.
- Write boundary conditions. [Hint: At  $r = R$ , the flux to the surface must equal the flux to the surrounding gas "via  $h$ ."]

- 7.11** Starting with Eq. (7.44), derive Eq. (7.45) and define the dimensionless numbers in Eq. (7.45).

7.12

- a) Determine an expression that gives the heat flow  $Q$  (W) through a solid spherical shell with inside and outside radii of  $r_1$  and  $r_2$ , respectively.
- b) Examine the results regarding what happens as the shell thickness becomes larger compared with the inside radius.

7.13 A sphere of radius  $R$  is in a motionless fluid (no forced or natural convection). The surface temperature of the sphere is maintained at  $T_R$  and the bulk fluid temperature is  $T_\infty$ .

a) Develop an expression for the temperature in the fluid surrounding the sphere.

b) Determine the Nusselt number for this situation. Such a value would be the limiting value for the actual system with convection as the forces causing convection become very small.

- 7.14 For the system in Fig. 2.1 develop an expression for the temperature distribution in the falling film. Assume fully developed flow, constant properties, and fully developed temperature profile. The free liquid surface is maintained at  $T = T_0$  and the solid surface at  $T = T_s$ , where  $T_0$  and  $T_s$  are constants. a) Ignore viscous heating effects. b) Include viscous heating effects.

Answer b)

$$\frac{T - T_0}{T_s - T_0} = \frac{x}{\delta} \left\{ 1 + \frac{3}{4} Br \left[ 1 - \left( \frac{x}{\delta} \right)^3 \right] \right\},$$

where  $Br = \frac{\eta V^2}{k(T_s - T_0)}$ , Brinkman number.

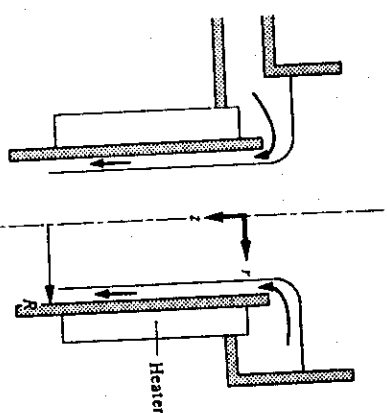
- 7.15 Consider heat conduction through a plane wall of thickness  $\Delta x$ , and  $T_1$  and  $T_2$  are the surface temperatures. Derive the steady-state heat flux in terms of  $T_1$ ,  $T_2$  and  $\Delta x$  if the thermal conductivity varies according to

$$k = k_0 (1 + aT)$$

where  $k_0$  and  $a$  are constants.

- 7.16 A liquid at a temperature  $T_0$  continuously enters the bottom of a small tank, overflows into a tube, and then flows downward as a film on the inside. At some position down the tube ( $z = 0$ ) when the flow is fully developed, the pipe heats the fluid with a uniform flux  $q_F$ . The heat loss from the liquid's surface is sufficiently small so that it may be neglected.

- a) For steady-state laminar flow with constant properties, develop by shell balance or show by reducing an equation in Table 7.5 the pertinent differential energy equation that applies to the falling film.
- b) Write the boundary conditions for the heat flow.
- c) What other information must complement parts a) and b) in order to solve the energy equation?



The problems of heat flow with convection, discussed in the preceding chapter, pertain to simple systems with laminar flow. Despite the simplicity of laminar flow problems, they should not be underestimated. Many simple solutions have been applied to real systems with approximating assumptions and, besides, the simpler systems provide models for interpretation of complex systems. The more complex nature of turbulent flow and its limited accessibility to mathematical treatment requires, however, an empirical approach to heat transfer. On the other hand, the study of turbulent transfer processes is possible to establish certain theoretical bases for the analyses of turbulent transfer processes and an introduction to this complex area is given in Chapter 16.

Figure 8.1 illustrates heat transfer in a bounded fluid. The fluid is artificially subdivided into three regions: the turbulent core, the transition zone, and the laminar sublayer near the surface. In the turbulent core, thermal energy is transferred rapidly due to the eddy (mixing) action of turbulent flow. Conversely, within the laminar sublayer, energy is transferred by conduction alone—a much slower process than the eddy process. In the transition zone, energy transport by both conduction and by eddies is appreciable. Hence, most of the total temperature drop between the fluid and the surface is across the laminar sublayer and the transition zone. Within the turbulent core, the temperature gradients are quite shallow.

In Chapter 3, it was convenient to define a friction factor to deal with momentum transport in fluids in contact with surfaces. Similarly, for energy transport between fluids and surfaces, it is convenient to define a heat transfer coefficient by

$$h = \frac{q_0}{T_0 - T_f} = \frac{-k(\partial T/\partial y)_0}{T_0 - T_f}, \quad (8.1)$$

where the subscript "0" refers to the respective quantities evaluated at the wall, and  $T_f$  is some temperature of the fluid. If the fluid is infinite in extent, we take  $T_f$  as the fluid temperature far removed from the surface, and designate it  $T_\infty$ . If the fluid flows in a confined space, such as inside a tube,  $T_f$  is usually the *mixed mean temperature*, denoted by  $T_m$ ; it is a temperature that would exist if the fluid at a particular cross section were removed and allowed to mix adiabatically.

## 8

### CORRELATIONS AND DATA FOR HEAT TRANSFER COEFFICIENTS

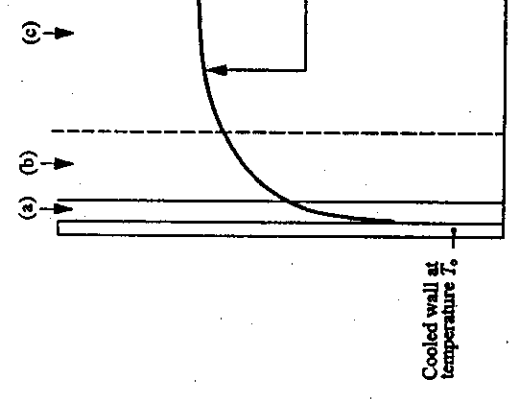


Fig. 8.1 Temperature profile of a flowing fluid bounded by a cooler wall; (a) laminar sublayer, (b) transition zone, and (c) turbulent core.

As explained in Chapter 7,  $h$  is a function of the fluid's properties ( $k, \eta, \rho, C_p$ ), the system geometry, the flow velocity, and the value of the defining temperature difference. We deal in the remainder of this chapter with predicting the dependence of  $h$  on these quantities, by presenting experimental data for various systems in the form of correlations based on dimensional analysis.

### 8.1 HEAT TRANSFER COEFFICIENTS FOR FORCED CONVECTION IN TUBES

In Section 3.1, we presented a method of dimensional analysis utilizing a rearrangement of differential equations in order to show that the friction factor was a function of the Reynolds number. We used the same method in Section 7.3 for natural convection. Here we bring the reader's attention to a different technique of dimensional analysis, while deriving those dimensionless numbers which are pertinent to the heat transfer system of forced convection within a tube.

#### 8.1.1 Dimensional analysis—Buckingham's $\pi$ theorem

We may obtain pertinent dimensionless numbers without reference to the basic differential equations, if we can identify the variables sufficient to specify a given situation. A systematic way of determining the groups is known as *Buckingham's  $\pi$  theorem*.<sup>1</sup> Simply stated, it reads: *The functional relationship among  $q$  quantities, whose units may be given in terms of  $u$  fundamental units, may be written as a function of  $q - u$  dimensionless groups (the  $\pi$ 's).*

In the application of the  $\pi$  theorem, these rules are helpful:

- a) Compile a list of the  $q$  significant quantities and their respective fundamental units. The fundamental units are  $L$  (length),  $M$  (mass),  $\Theta$  (time), and  $T$  (temperature).
- b) Select the primary quantities or primary  $q$ 's. The number of primary  $q$ 's should equal  $u$ , the number of fundamental units.
- c) Form each  $\pi$  term by expressing the ratio of the remaining  $q$ 's (one at a time) to the product of the primary  $q$ 's, each raised to an unknown power determined as shown below.

We now illustrate the method for heat transfer in forced convection. We presume that the heat transfer coefficient for fully developed forced convection in a tube is a function of the variables

$$h = f(\bar{V}, \rho, k, \eta, C_p, D). \quad (8.2)$$

We can express all these quantities in terms of the four fundamental dimensions  $M, L, \Theta$ , and  $T$ . Specifically,

$$\begin{aligned} \bar{V} &= L\Theta^{-1}, & \eta, M L^{-1}\Theta^{-1}, \\ \rho &= M L^{-3}, & C_p, L^2\Theta^{-2}T^{-1}, \\ k &= M L\Theta^{-3}T^{-1}, & h, M\Theta^{-3}T^{-1}. \end{aligned}$$

Note that energy is given the units of work (force  $\times$  distance), namely,  $ML^2\Theta^{-1}$ .

The number of fundamental units in this case is four. Thus, since  $u = 4$ , select as the four primary  $q$ 's,  $\bar{V}, D, \rho$ , and  $k$ , leaving  $h, \eta$ , and  $C_p$ . Proceed to form the first  $\pi$  term.

$$\pi_1 = \frac{h}{\bar{V}^a D^\rho k^k} = \frac{M\Theta^{-3}T^{-1}}{(L\Theta^{-1})^a (M L^{-3})^\rho (M L^2\Theta^{-2}T^{-1})^k}.$$

Equating the exponents of each dimension to zero, so that the  $\pi$  group is dimensionless, we obtain

$$M: 1 = c + d,$$

$$L: 0 = a + b - 3c + d,$$

$$\Theta: -3 = -a - 3d,$$

$$T: -1 = -d.$$

Solving these four equations simultaneously, we obtain  $a = 0, b = -1, c = 0$ , and  $d = 1$ . Thus

$$\pi_1 = \frac{hD}{k} \equiv Nu \quad (\text{Nusselt number}).$$

Similarly, the following  $\pi$  groups can be obtained:

$$\pi_2 = \eta/\rho \bar{V} D \equiv \frac{1}{Re},$$

$$\pi_3 = C_p \eta/k \equiv Pr \quad (\text{Prandtl number}).$$

Thus, heat transfer data in forced convection can be correlated in terms of these three groups or dimensionless numbers:

$$Nu = Nu(Re, Pr).$$

We superimpose the plot of  $f/2$  on Fig. 8.2 for long, hydraulically smooth tubes, where

$$j_H = St_m \left[ \frac{C_{pm} \eta_f}{k_m} \right]^{2/3} = \frac{f}{2}. \quad (8.6)$$

$St_m$  is the Stanton number, and  $j_H$  is often referred to as a  $j$ -factor. The Stanton number is defined

$$St = \frac{Nu}{Re \cdot Pr} = \frac{h}{C_p \rho V}. \quad (8.4)$$

This dimensional analysis is of great use in experimental work involving heat transfer. For example,  $h$  depends on eight physical quantities:  $D$ ,  $\bar{V}$ ,  $\rho$ ,  $\eta_m$ ,  $\eta_0$ ,  $C_p$ ,  $k$ , and  $L$ . To study all combinations of eight independent variables for ten values of each would require  $10^8$  tests, whereas, by giving  $Nu$  as a function of only four groups ( $Re, Pr, L/D, \eta_m/\eta_0$ ),  $10^4$  tests would suffice. Thus, a graduate student would require only five years of research instead of 50,000 years!

### 8.1.2 Correlations for forced convection in tubes

For fully developed flow in tubes, a correlation for flow in smooth tubes with nearly constant wall temperature is presented in Fig. 8.2. The Reynolds number used here,  $Re_m = DV\rho/\eta_m$ , is convenient because the laminar-to-turbulent transition is at about 2100 (the same as in Fig. 3.2), even when  $\eta_0$  differs appreciably from  $\eta_m$ . For highly turbulent flow ( $Re_m > 10,000$ ), the equation

$$Nu_m = 0.026 Re_m^{0.8} Pr_m^{1/3} \left[ \frac{\eta_m}{\eta_0} \right]^{0.14} \quad (8.5)$$

reproduces experimental data to within about  $\pm 20\%$  in the range  $10^4 < Re_m < 10^5$ ,  $0.6 < Pr < 100$ , and  $L/D > 10$ . As we discuss later, the data need not be restricted to the situations of constant wall temperature.

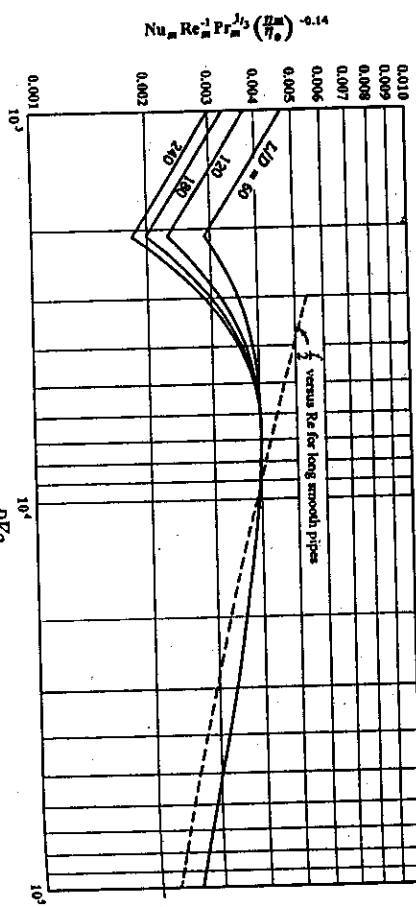


Fig. 8.2. Heat transfer coefficients for fully developed flow in smooth tubes. (From E. N. Seider and G. E. Tate, *Ind. Eng. Chem.* 28, 1429 (1936).)

For liquid metals, where  $0.005 < Pr < 0.05$ , the following equation represents available experimental data with  $Re > 10,000$  and for a uniform heat flux:<sup>2</sup>

$$Nu_q = 6.7 + 0.0041(Re \cdot Pr)^{0.791} \exp(41.8 \cdot Pr). \quad (8.7)$$

Because of the very high values of  $h$  in liquid metals,  $(T_w - T_m)$  is not very large, so that the mixed mean temperature properties can be used without significant error.

Equation (8.7) for liquid metals applies to uniform heat flux along the tube. For uniform wall temperature, the difference between  $Nu_T$  (uniform wall temperature) and  $Nu_q$  (uniform heat flux) is significant for liquid metals (Fig. 8.4); for  $Pr > 0.5$  the difference between  $Nu_T$  and  $Nu_q$  is small, and hence Eq. (8.5) is also approximately valid for constant heat flux boundary conditions.

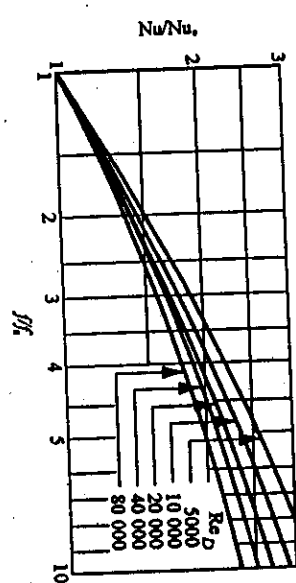


Fig. 8.3. Effect of roughness on heat transfer in turbulent flow. (From W. Nummer, VDI-Forschungsheft No. 455/1956 (VDI-Verlag GmbH-Düsseldorf).)

For liquid metals, where  $0.005 < Pr < 0.05$ , the following equation represents available experimental data with  $Re > 10,000$  and for a uniform heat flux.<sup>2</sup>

$$Nu_q = 6.7 + 0.0041(Re \cdot Pr)^{0.791} \exp(41.8 \cdot Pr). \quad (8.7)$$

<sup>2</sup>W. M. Rohsenow and H. Y. Choi, *Heat, Mass, and Momentum Transfer*, Prentice-Hall, Englewood Cliffs, NJ, 1961, page 193.

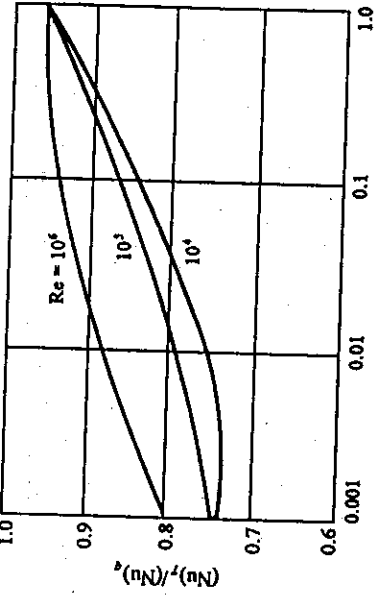


Fig. 8.4 Comparison of uniform wall temperature and uniform heat flux in tubes.  
(From R. A. Seban and T. T. Shimazaki, *Trans. ASME* 73, 803 (1951).)

**Example 8.1** A 5 ton (4536 kg) heat of steel must be decarburized from 0.40 to 0.20% C in 5 min. A convenient method for accomplishing this is to blow oxygen through a submerged lance. A low carbon steel pipe of 12.7 mm I.D. is used as the lance, despite the fact that the end of the pipe gradually melts. If we estimate the portion of the lance within the furnace to be at 1744 K, calculate the temperature at which the oxygen enters the liquid steel. Neglect the pressure drop through the pipe and assume that the pressure in the pipe equals  $1.22 \times 10^5$  N/m<sup>2</sup> (1.2 atm).

**Solution.** The oxygen requirement, for  $C + \frac{1}{2}O_2(g) \rightarrow CO(g)$ , is

$$\bar{V}_p = \frac{(4536)(0.20) \text{ kg } C}{(100)(300) \text{ s}} \left| \begin{array}{c} 1 \text{ kmol } C \\ 12.011 \text{ kg } C \end{array} \right| \left| \begin{array}{c} 0.5 \text{ kmol } O_2 \\ 1 \text{ kmol } C \end{array} \right| \left| \begin{array}{c} 32 \text{ kg } O_2 \\ 1 \text{ kmol } O_2 \end{array} \right| \left| \begin{array}{c} 4 \\ \pi(12.7)^2 \text{ mm}^2 \end{array} \right| \left| \begin{array}{c} 1000^2 \text{ mm}^2 \\ 1 \text{ m}^2 \end{array} \right| = 318 \text{ kg m}^2 \text{ s}^{-1}$$

The oxygen enters the tube at 300 K, and as it proceeds through the pipe its temperature rises. Consequently, the properties of the oxygen vary with distance down the tube. A commonly employed estimation is to evaluate the properties of the fluid at its average temperature along the heated pipe. The heat transfer coefficient corresponding to these properties is then calculated, assumed to be constant along the pipe, and used to determine the heat transferred to the gas.

First, arbitrarily assume that the gas leaves the pipe at 820 K. Then take the average  $T_m$  as  $(820 + 300)/2 = 560$  K for the last 1.2 m of pipe. At 560 K, the properties of  $O_2$  are  $\eta = 32.4 \times 10^{-6}$  kg m<sup>-1</sup>s<sup>-1</sup>;  $k = 45.8 \times 10^{-3}$  W m<sup>-2</sup>K<sup>-1</sup>;  $C_p = 991 \text{ J kg}^{-1}\text{K}^{-1}$ ;  $\rho = 0.701$ .

At 820 K,  $\eta = 41.5 \times 10^{-6}$  kg m<sup>-1</sup>s<sup>-1</sup>, which we use for  $\eta_0$ . Now calculate  $Re_m$ :

$$Re_m = \frac{D\bar{V}_p}{\eta_m} = \frac{(12.7 \times 10^{-3})(318)}{(32.4 \times 10^{-6})} = 1.25 \times 10^5.$$

Thus, Eq. (8.5) applies, so that

$$\begin{aligned} Nu_m &= 0.026 Re_m^{0.8} Pr_m^{1/3} \left[ \frac{\eta_m}{\eta_0} \right]^{0.14} = (0.026)(1.25 \times 10^5)^{0.8} (0.701)^{1/3} \left[ \frac{32.4 \times 10^{-6}}{41.5 \times 10^{-6}} \right]^{0.14} \\ &= 267. \end{aligned}$$

Therefore

$$h = \frac{k_m Nu_m}{D} = \frac{(45.8 \times 10^{-3})(267)}{12.7 \times 10^{-3}} = 963 \text{ W m}^{-2} \text{ K}^{-1}.$$

An energy balance applied to the fluid over a differential length of pipe,  $dx$ , can be written where  $W$  = mass flow rate, kg s<sup>-1</sup>, and  $T_0$  = temperature of pipe wall. Integrating for a length of pipe  $L$ , with  $h$ ,  $C_p$ , and  $T_0$  taken as constants, yields

$$WC_p dT_m = h(T_0 - T_m)(\pi D dx),$$

or

$$h \int_0^L dx = - \frac{WC_p}{\pi D} \int_{T_0}^{T_L} d \ln (T_m - T_0),$$

Substituting numerical values yields

$$\ln \frac{\Delta T_L}{\Delta T_0} = - \frac{hL \pi D}{WC_p} = - \frac{4hL}{\rho V C_p D},$$

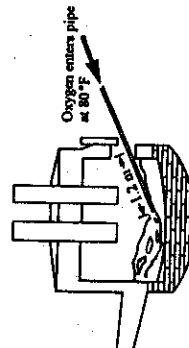
from which

$$\Delta T_L = 164 \text{ K} \quad \text{or} \quad T_m = 984 \text{ K} \quad (\text{at } x = L = 1.2 \text{ m}).$$

Recalling our initial guess of 820 K, we see that in terms of estimating properties we have selected reasonably good values.

As a second guess, assume that the gas leaves the pipe is 940 K. Then, we take the average  $T_m$  as  $(940 + 300)/2 = 620$  K. At 620 K, the properties of  $O_2$  are  $\eta = 35.1 \times 10^{-6}$  kg m<sup>-1</sup>s<sup>-1</sup>;  $k = 48.4 \times 10^{-3}$  W m<sup>-2</sup>K<sup>-1</sup>;  $C_p = 1010 \text{ J kg}^{-1}\text{K}^{-1}$ ;  $\rho = 0.732$ .

When we repeat the method of calculation using these new values, we get  $Re_m = 1.15 \times 10^5$ ,  $Nu_m = 256$ , and  $h = 976 \text{ W m}^{-2} \text{ K}^{-1}$ . The difference between the first and the second estimates of  $h$  is only 1.3%. Finally,  $\Delta T_L = 165 \text{ K}$ , or  $T_m = 985 \text{ K}$  (at  $x = L = 1.2 \text{ m}$ ). We could repeat the process, but of course our second result is practically the same as the first. Hence, it is not necessary to do so.



The conclusion that the gas temperature is lower than the metal temperature when it exits from the lance becomes significant when the bubble size is calculated in order to obtain the surface area and residence time for calculations of mass transfer. Since the gas is not fully expanded when it exits from the pipe, the bubble size, calculated on the basis of the pipe size, is smaller than the ultimately expanded bubble size, and the rate of rise is faster than anticipated on the basis of the pipe size.

## 8.2 HEAT TRANSFER COEFFICIENTS FOR FORCED CONVECTION PAST SUBMERGED OBJECTS

In the following correlations, the heat transfer coefficient  $h$  is defined for the total surface area of the submerged object, and the defining fluid temperature is that far removed from the surface. We evaluate all the properties, however, at the *film temperature*,  $T_f = (T_0 + T_\infty)/2$ . In Fig. 8.5,  $j_H = \text{Nu}_f \text{Re}_f^{0.3} \text{Pr}_f^{0.3}$  is plotted versus  $\text{Re}$  for a long cylinder perpendicular to the fluid. The figure also shows a plot of  $f/2$  versus  $\text{Re}$  to illustrate that  $i_H < f/2$ , which is usually the case in flows with curved streamlines. Colburn's analogy breaks down here because of the form drag which has no counterpart in heat transfer.

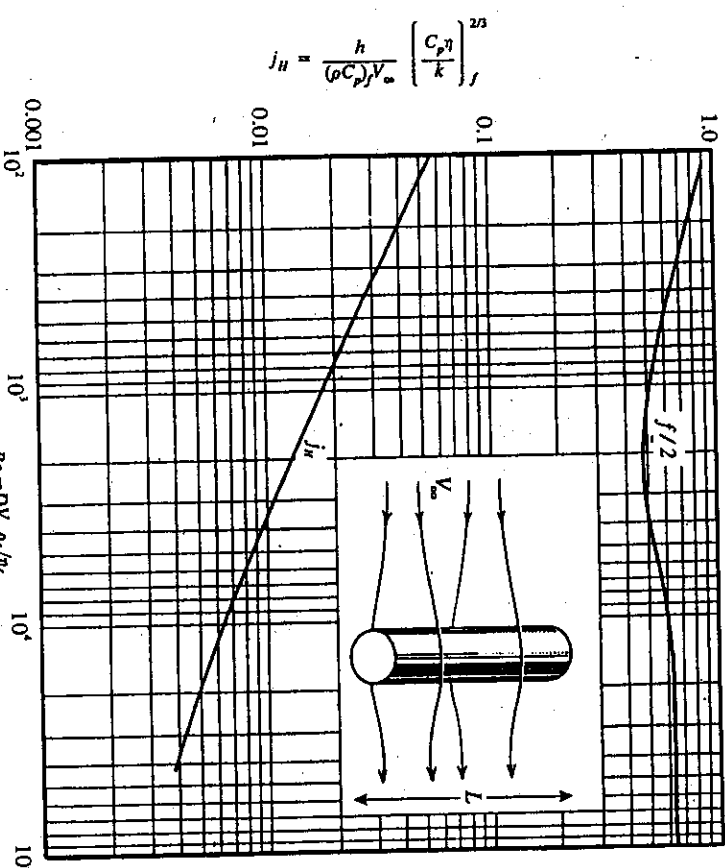


Fig. 8.5 Heat and momentum transfer for a cylinder perpendicularly oriented to flow.  $j_H$  from T. K. Sherwood and R. L. Pigford, *Absorption and Extraction*, second edition, McGraw-Hill, New York, 1952, page 70;  $f$  from F. Eisner, see Fig. 3.9.)

More recent correlations are summarized by Holman,<sup>4</sup> among which the most comprehensive is that given by Churchill and Bernstein:<sup>5</sup>

$$\text{Nu}_f = 0.3 + \frac{0.62 \text{Re}_f^{1/2} \text{Pr}_f^{1/3}}{\left[ 1 + (0.4/\text{Pr}_f)^{2/3} \right]^{1/4}} \left[ 1 + \left[ \frac{\text{Re}_f}{2.82 \times 10^5} \right]^{5/8} \right]^{4/5} \quad (8.10)$$

These results agree closely with McAdams' correlation<sup>3</sup> which is based on experiments with water, oils, and air. Over the range  $1 < \text{Re}_f < 10^3$ , McAdams specifies

$$\text{Nu}_f \text{Pr}_f^{-0.3} = 0.35 + 56 \text{Re}_f^{0.53} \quad (8.8)$$

$$\text{Nu}_f \text{Pr}_f^{-0.3} = 0.26 \text{Re}_f^{0.60} \quad (8.9)$$

For higher Reynolds numbers,  $10^3 < \text{Re} < 5 \times 10^4$ , data collected for air are correlated by

for  $10^2 < \text{Re}_f < 10^7$  and  $\text{Re}_f \text{Pr}_f > 0.2$ . Equation (8.10) was tested against data for air, water, and liquid sodium so it has a wide range of applicability. Notice, however, that it is not useful for very small Reynolds numbers ( $\text{Re}_f < 100$ ); furthermore it underestimates data somewhat in the range  $2 \times 10^4 < \text{Re}_f < 4 \times 10^5$ . For this range, the second brackets on the right-hand-side of Eq. (8.10) should be replaced with

$$1 + \left[ \frac{\text{Re}_f}{2.82 \times 10^5} \right]^{1/2} \quad (8.10)$$

Holman<sup>4</sup> also gives correlations, based on empirical data, for heat transfer between fluids and noncircular cylinders.

Figure 8.6 gives  $\text{Nu}_f$  for the flow past a sphere. The relationship plotted is

$$hD/k_f = 2.0 + 0.60(DV_\infty \rho_f / \eta_f)^{1/2} (C_p \eta_f / k_f)^{1/3}. \quad (8.11)$$

This equation predicts that  $\text{Nu}$  approaches 2 as  $\text{Re}$  approaches zero; we can calculate this result for pure conduction, from a sphere at a uniform temperature in an infinite stagnant medium. Another correlation for heat transfer between fluids and spheres is that given by Whitaker:<sup>6</sup>

$$\text{Nu}_s = 2 + (0.4 \text{Re}_\infty^{1/2} + 0.06 \text{Re}_\infty^{2/3}) \text{Pr}_\infty^{0.4} \left[ \frac{\eta_\infty}{\eta_s} \right]^{1/4}. \quad (8.12)$$

where the properties are evaluated at the temperature of the free stream, except  $\eta_s$ , which is the viscosity at the temperature of the sphere. The ranges for Eq. (8.12) are  $0.71 < \text{Pr}_\infty < 380$ ,  $3.5 < \text{Re}_\infty < 7.6 \times 10^4$ , and  $1.0 < (\eta_\infty / \eta_s) < 3.2$ . Neither Eq. (8.11) nor (8.12) should be used for liquid metals.

<sup>3</sup>W. H. McAdams, *Heat Transmission*, third edition, McGraw-Hill, New York, 1954, page 268.

<sup>4</sup>J. P. Holman, *Heat Transfer*, sixth edition, McGraw-Hill, New York, 1986, pages 292-296.

<sup>5</sup>S. W. Churchill and M. Bernstein, *J. Heat Transfer* 99, 300 (1977).

<sup>6</sup>S. Whitaker, *AIChE J.* 18, 361 (1972).

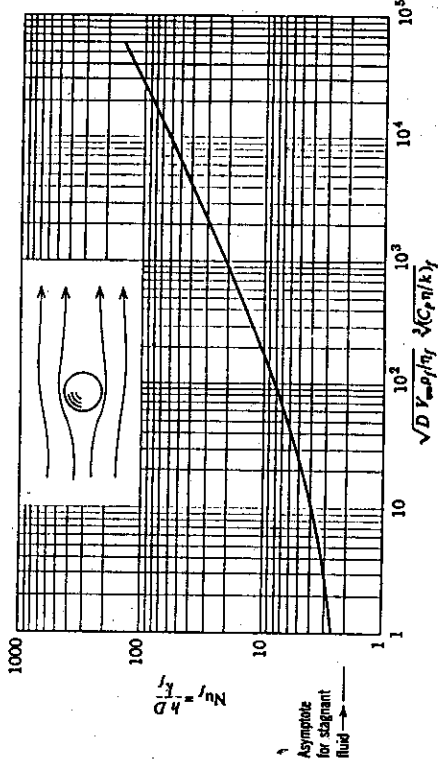


Fig. 8.6 Heat transfer from a sphere to a flowing fluid. (From W. E. Ranz and W. R. Marshall, Jr., *Chem. Eng. Prog.* 48, 141-146, 173-180 (1952).)

Figure 8.7 shows results for the flow parallel to an isothermal semi-infinite flat plate. For this flow system, the Colburn analogy holds very well because there is no form drag; therefore, the local heat transfer coefficient is related to the friction factor by

$$\frac{h_x}{C_p \rho V_\infty} \text{Pr}^{2/3} = \frac{f_x}{2}. \quad (8.13)$$

For turbulent flow (from Fig. 3.5),  $f_t = 0.0592 \text{ Re}_x^{1/5}$ ; then Eq. (8.13) is

$$\frac{h_x}{C_p \rho V_\infty} \text{Pr}^{2/3} = 0.0296 \text{ Re}_x^{-1/5}, \quad (8.14)$$

*Solution.* Assume that Eq. (8.9) applies:

$$\text{Nu}_f \text{Pr}_f^{-0.3} = 0.26 \text{ Re}_f^{0.60},$$

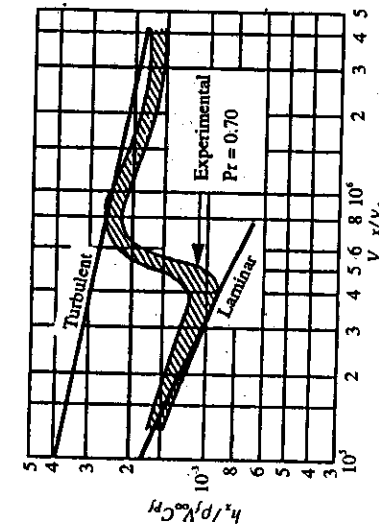


Fig. 8.7 Heat transfer coefficient for flow over flat plate with turbulent boundary layer and uniform heat flux. Experimental data collected for air, and compared to the analysis for turbulent flow (Eq. (8.12)), and laminar flow (Eq. (7.27)). (From R. A. Seban and D. L. Doughty, *Trans. ASME* 78, 217 (1956).)

or

$$\frac{h_x x}{k} = \text{Nu}_x = 0.0296 \text{ Re}^{0.8} \text{ Pr}^{1/3}. \quad (8.15)$$

The average coefficient  $h$  between  $x = 0$  and  $x = L$  is

$$hL/k = \text{Nu}_L = 0.037 \text{ Re}_L^{0.8} \text{ Pr}^{1/3}. \quad (8.16)$$

(Here the initial part of the plate where laminar flow could exist has been ignored.) Equation (8.15) overestimates the experimental data by approximately 4 to 19 pct. The agreement can be improved simply by modifying Eq. (8.15), so it becomes

$$\text{Nu}_x = 0.026 \text{ Re}^{0.8} \text{ Pr}^{1/3}. \quad (8.17)$$

The data agree with the laminar boundary layer result (Eq. (7.27)). Note that Eqs. (8.13)-(8.17) are valid for  $\text{Pr} > 0.5$ , but not for liquid metals; the equations are valid for either uniform wall temperature or uniform heat flux.

**Example 8.2** A hot-wire anemometer is a device which indirectly measures the velocity of a moving fluid. It is usually a platinum wire which is heated electrically and positioned normal to the motion of the fluid. At a steady power input to the wire, its temperature reaches a steady value which can be related to the fluid velocity. The temperature of the wire is determined by measuring current, voltage drop, and hence electrical resistance, and by knowing how the resistance varies with the temperature. Thus, both the heat flux—from the wire to the fluid—and the wire temperature are measured electrically. Given air at 290 K flowing normal to the wire (3 mm in diameter) at 330 K, with a heat flux of 6300 W m<sup>-2</sup>, determine the velocity of the air.

$$\begin{aligned} \text{Nu}_f \text{Pr}_f^{-0.3} &= 0.26 \text{ Re}_f^{0.60}, \\ h &= \frac{q_0}{\Delta T} = \frac{6300}{(330 - 290)} = 157.5 \text{ W m}^{-2} \text{ K}^{-1}. \end{aligned}$$

Use the properties of air at  $T_f = 310 \text{ K}$ :  $\rho = 1.13 \text{ kg m}^{-3}$ ;  $C_p = 1.01 \times 10^3 \text{ J kg}^{-1} \text{ K}^{-1}$ ;  $k = 27.0 \times 10^{-3} \text{ W m}^{-1} \text{ K}^{-1}$ ;  $\eta = 1.89 \times 10^{-5} \text{ kg m}^{-1} \text{ s}^{-1}$ ;  $\text{Pr}_f = 0.705$ .

$$\text{Nu}_f = \frac{hD}{k} = \frac{(157.5)(0.003)}{(27.0 \times 10^{-3})} = 17.5,$$

$$\text{Re}_f^{0.60} = \frac{(17.5)}{(0.705)^{0.3}(0.26)} = 74.75,$$

$$\text{Re}_f = 1326.$$

Thus, Eq. (8.9) applies as assumed, and

$$V_a = \left[ \frac{\eta}{\rho_f} \right] \left[ \frac{\text{Re}_f}{D} \right] = \left[ \frac{1.89 \times 10^{-5}}{1.13} \right] \left[ \frac{1326}{0.003} \right] = 7.40 \text{ m s}^{-1}.$$

## 8.3 HEAT TRANSFER COEFFICIENTS FOR NATURAL CONVECTION

In Chapter 7, the discussion of natural convection in laminar flow led to a dimensionless equation of the form

$$\text{Nu} = \text{Nu}(\text{Gr}, \text{Pr}).$$

This corresponds to the results of dimensional analysis in this chapter if the Reynolds number, the important number for forced convection, is replaced by the Grashof number, the important number for natural convection.

Figure 8.8 shows the results of correlating experimental data for free convection from vertical plates and horizontal cylinders to gases and liquids with Prandtl numbers ranging from about 0.5 to 10. The effect of the variation of properties with temperature is included by evaluating properties at  $T_f = \frac{1}{2}(T_0 + T_\infty)$ . The dimensionless numbers are then defined as  $\text{Nu}_L = \frac{\nu L}{k_f}$ ,  $\text{Pr} = \frac{\alpha_f}{\nu_f}$ , and  $\text{Gr}_L = g \frac{L^3 \rho_f \beta_f (T_0 - T_\infty)}{\eta_f^2}$ .

The characteristic dimension  $L$  is the plate length. For cylinders, the characteristic dimension is one-half the circumference, that is,  $\pi D/2$ ; by defining  $L$  as such, note how closely the curves for the two different correlations lie. In fact, very often no distinction is made between these two cases, and a third case, namely, that of vertical cylinders with characteristic dimension taken as length, is included in the correlations.\*

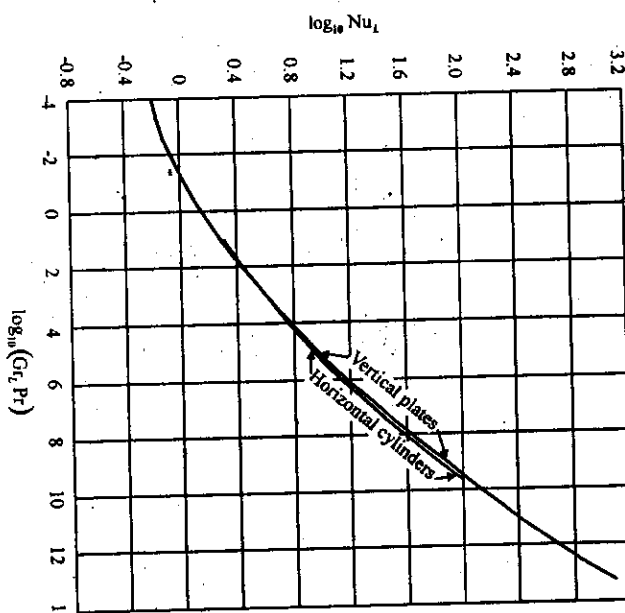


Fig. 8.8 Heat transfer coefficients for natural convection. (From W. H. McAdams, *ibid.*, pages 173-176.)

\*This procedure can be followed when  $(D/L) \geq 35/(\text{Gr}_L^{1/4})$  and  $L$  is vertical length.

Correlations and Data for Heat Transfer Coefficients 259

In Chapter 7, Ostrach's analysis of laminar natural convection past vertical plates led to Eq. (7.45). This relationship holds in the laminar flow region  $10^4 < \text{Gr Pr} < 10^8$  for a wide range of Prandtl numbers ( $0.00835 \leq \text{Pr} \leq 1000$ ). For the sake of completeness, let us repeat it:

$$\frac{\text{Nu}_L}{\sqrt[4]{\text{Gr}_L / 4}} = \frac{0.902 \text{ Pr}^{1/2}}{(0.861 + \text{Pr})^{1/4}}. \quad (7.45)$$

In the range of  $0.6 < \text{Pr} < 10$ , the data can be represented by a much simpler equation (still for laminar flow):\*

$$\text{Nu}_L = 0.56(\text{Gr}_L \text{Pr})^{1/4}. \quad (8.18)$$

For liquid metals, the data in the laminar range for horizontal cylinders were correlated by<sup>7</sup>

$$\text{Nu}_D = 0.53 \left[ \frac{\text{Pr}}{0.952 + \text{Pr}} \right]^{1/4} (\text{Gr}_D \text{Pr})^{1/4}. \quad (8.19)$$

The expression is of the same form as Eq. (7.45), and also closely corresponds numerically if the characteristic dimension  $D$  (diameter) is replaced by  $L$  taken as  $\pi D/2$ .

In the turbulent range of  $10^9 < \text{Gr Pr} < 10^{12}$ , the following equation has been proposed as possibly valid for a wide range of  $\text{Pr}$  for vertical plates<sup>8</sup> and horizontal cylinders with  $L$  replaced by  $\pi D/2$ :

$$\text{Nu}_L = 0.0246 \text{ Gr}_L^{2/5} \text{ Pr}^{7/15} (1 + 0.494 \text{ Pr}^{2/3})^{-2/5}. \quad (8.20)$$

We use a much simpler form of Eq. (8.20) for  $0.6 < \text{Pr} < 10$ :

$$\text{Nu}_L = 0.13 (\text{Gr}_L \text{Pr})^{1/3}. \quad (8.21)$$

Perhaps the most encompassing correlation for natural convection heat transfer from long horizontal cylinders is that of Churchill and Chu<sup>9</sup>; it is

$$\text{Nu}_D = \left\{ 0.60 + \frac{0.387 (\text{Gr}_D \text{Pr})^{1/6}}{[1 + (0.559 \text{Pr})^{9/16}]^{8/27}} \right\}^2, \quad (8.22)$$

which applies for  $10^5 < \text{Gr}_D \text{Pr} < 10^{12}$ . In situations involving natural convection and mixed convection (forced convection plus natural convection) from very small diameter ( $< 0.01$  mm) cylinders, the results of Gebhart *et al.*<sup>10</sup> can be consulted.

\*To make a distinction between plates and cylinders in Fig. 8.8, the coefficient 0.56 in Eq. (8.18) should be replaced by 0.59 and 0.53, respectively.

<sup>7</sup>Reactor Handbook 2; Engineering, AECD-3646 (May, 1955), page 283.

<sup>8</sup>W. M. Rohsenow and H. Y. Choi, *ibid.*, page 204.

<sup>9</sup>S. W. Churchill and H. H. S. Chu, *Int. J. Heat Mass Transfer* 18, 1049 (1975).

<sup>10</sup>B. Gebhart, T. Andanson and L. Pera, in *Heat Transfer 1970*, U. Grigull and E. Hahne (editors), Elsevier Publishing, Amsterdam, 1970, Session NC3.2.

For a single sphere of diameter  $D$  in a body of fluid, the relationship

$$\text{Nu}_D = 2 + 0.060 \text{Gr}_D^{1/3} \text{Pr}^{1/3}. \quad (8.23)$$

agrees with available data for  $\text{Gr}_D^{1/3} \text{Pr}^{1/3} < 200$ . In most instances, if the fluid is a gas, this restriction means that the equation applies to small particles. Note that the relationship yields  $\text{Nu}_D = 2$  when the fluid is motionless, as in Problem 7.14 where free convection is neglected.

Churchill<sup>11</sup> gives the following correlation for spheres in fluids with  $\text{Pr} \geq 0.7$  and  $\text{Gr}_D \text{Pr} \leq 10^6$ :

$$\text{Nu}_D = 2 + \frac{0.589 \text{Gr}_D^{1/4} \text{Pr}^{1/4}}{\left[1 + (0.469 \text{Pr})^{9/16}\right]^{4/9}}. \quad (8.24)$$

**Example 8.3** Write an expression to relate the growth rate of a single spherical nucleus of solid as it develops in a pure supercooled liquid. Express the result in terms of  $dR/dt$  as a function of supercooling  $\Delta T$  and the properties of the metal. The thermal profile is depicted below; the temperature of the solid may be assumed as the freezing point  $T_M$ .

**Solution.** The rate at which heat of fusion evolves is equal to the rate at which heat flows from the interface into the bulk liquid

$$4\pi\rho_s H_f R^2 \frac{dR}{dt} = 4\pi R^2 h \Delta T,$$

where  $\rho_s$  = density of the solid,  $H_f$  = latent heat of fusion, and  $\Delta T = T_M - T_\infty$  = amount of undercooling;

$$\frac{dR}{dt} = \frac{h}{\rho_s H_f} \Delta T.$$

From Eq. (8.23),

$$\frac{hD}{k} = 2 + 0.060 \left[ \frac{D^3 \rho^2 g \beta \Delta T}{\eta^2} \right]^{1/4} \left[ \frac{\eta C_p}{k} \right]^{1/3}.$$

When this is substituted into the expression for  $dR/dt$ , we obtain

$$\frac{dR}{dt} = \frac{k \Delta T}{\rho_s H_f} \left[ \frac{1}{R} + 0.0504 \left( \frac{\rho^2 g \beta \Delta T}{R \eta^2} \right)^{1/4} \left( \frac{\eta C_p}{k} \right)^{1/3} \right].$$

Students of phase transformations are invited to use this as a basis for further discussion and/or refinement.

In the previous discussion of this section, heat transfer took place in the presence of convection mostly in the vertical direction. The convection behavior in the vicinity of horizontal surfaces is quite different, as shown in Fig. 8.9, and the correlations of Eqs. (8.18)-(8.21) do not apply. McAdams<sup>12</sup> recommends the following equations for some situations of natural convection from horizontal surfaces:

1. For a square plate with a surface warmer than the fluid facing upward, or cooler surface facing downward:

$$\text{Nu}_L = 0.14 (\text{Gr}_L \text{Pr})^{1/3}, \quad (8.25)$$

in the turbulent range,  $2 \times 10^7 < \text{Gr}_L < 3 \times 10^{10}$ ; and

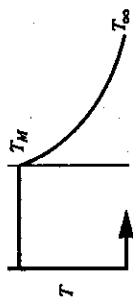
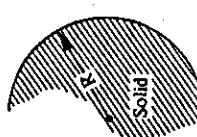
$$\text{Nu}_L = 0.54 (\text{Gr}_L \text{Pr})^{1/4}, \quad (8.26)$$

in the laminar range,  $10^5 < \text{Gr}_L < 2 \times 10^7$ .

2. For a square plate with a surface warmer than the fluid and facing downward, or cooler surface facing upward:

$$\text{Nu}_L = 0.27 (\text{Gr}_L \text{Pr})^{1/4}, \quad (8.27)$$

for  $10^6 < \text{Gr}_L \text{Pr} < 10^{11}$ .



In Eqs. (8.25)-(8.27),  $L$  is the length of the side of the square. As approximations, we can also apply the equations to horizontal circular disks with  $L$  defined as  $0.9 D$  ( $D$  being the disk diameter). The characteristic length, for a surface other than a square or a circle, should be taken as  $L = A/P$  where  $A$  is the surface area and  $P$  is the perimeter.

In this very brief exposition of correlations used to estimate heat transfer coefficients, we have omitted many different geometrical and flow configurations. We recommend that

Fig. 8.9 The convection pattern over a horizontal surface which is warmer than the fluid.

In Eqs. (8.25)-(8.27),  $L$  is the length of the side of the square. As approximations, we can also apply the equations to horizontal circular disks with  $L$  defined as  $0.9 D$  ( $D$  being the disk diameter). The characteristic length, for a surface other than a square or a circle, should be taken as  $L = A/P$  where  $A$  is the surface area and  $P$  is the perimeter.

In this very brief exposition of correlations used to estimate heat transfer coefficients, we have omitted many different geometrical and flow configurations. We recommend that

<sup>11</sup>S. W. Churchill, "Free Convection Around Immersed Bodies," in E. U. Schlünder, Ed.-in-Chief, *Heat Exchanger Design Handbook*, Section 2.5.7, Hemisphere Publishing Corp., New York, 1993.

<sup>12</sup>W. H. McAdams, *ibid.*, page 180.

<sup>262</sup> Correlations and ~~heat transfer~~ heat transfer coefficients for various fluids and geometries are available in the literature. Interested readers consult heat transfer texts, such as Holman,<sup>13</sup> Incropera and DeWitt,<sup>14</sup> Azbel,<sup>15</sup> and Kandlikar and Desmond.<sup>16</sup>

## 8.4 QUENCHING HEAT TRANSFER COEFFICIENTS

In the next chapter, we present analytical expressions which describe the temperature during heating or cooling as a function of time and position within a solid. The most difficult variable to ascribe to such unsteady-state situations is probably the heat transfer coefficient governing the energy transport between the solid's surface and the surroundings. The methods of estimating  $h$  for some convection systems, which were presented in previous sections of this chapter, can be applied satisfactorily to certain problems of unsteady-state heat flow. For the most part, however, correlations of  $h$ -values applicable to quenching operations have not been obtained because of the complexity of the convection systems.

engineers have not considered nearly enough of the quantitative aspects of boiling heat transfer, which is strongly linked to boiling heat transfer. Historically, the primary purpose of boiling heat transfer has been simply the conversion of liquid into vapor, and perhaps this is the reason why it has not been studied enough by materials engineers. On the other hand, engineers who are involved with the development of nuclear reactors, rocket nozzles, and spacecraft have conducted considerable research into the boiling process.

Although boiling is a familiar phenomenon, from the point of view of energy transport it is a complicated process. Figure 8.10 illustrates the complexities of boiling in which several regimes exist. If a heated metal surface is submerged in a pool of liquid at its saturation temperature,  $T_{ss}$ , the following events take place. As the surface temperature  $T_s$  increases above  $T_{ss}$ , convection currents circulate within the superheated liquid. Heat transfer with convection takes place, and the correlations discussed for natural convection in Section 8.3 apply. However, the liquid cannot be indefinitely superheated so that further increases of  $(T_s - T_{ss})$  above approximately 2 K are accompanied by vapor bubbles forming at preferred sites on the surface. This is regime II, in which most of the bubbles do not exceed a certain size necessary for their escape. In regime III,  $(T_s - T_{ss})$  is large enough so that larger and more stable bubbles grow, and at the same time more bubbles form because more nucleation sites become active on the solid's surface. This mechanism, which is called nucleate boiling, can generate very high heat fluxes. As the bubbles rapidly form and detach themselves from the surface, fresh liquid rushes to the former bubble site, and the very rapid process of bubble formation and detachment repeats itself over and over again. The net result is that all the bubble sites act as micropumps and create a large degree of convection at the surface.

If  $(T_s - T_{ss})$  is raised to even higher values, for example, 40 K in water, then the nucleation sites on the surface become so numerous that the bubbles coalesce, and tend to

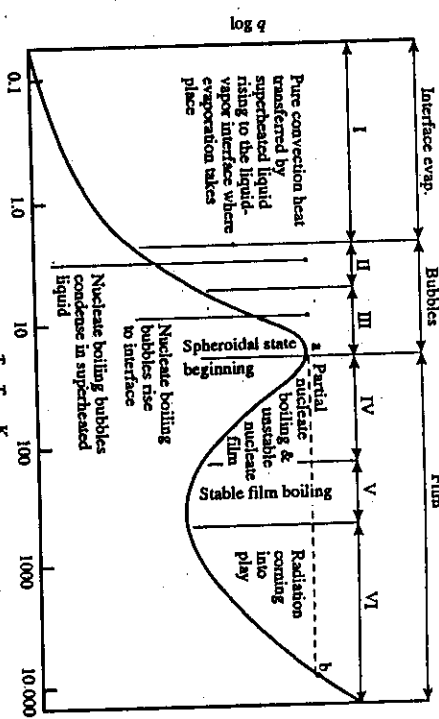


**FIG. 8-10** Characteristic boiling curve. (From W. M. Rohsenow, *Developments in Heat Transfer*, MIT Press, Cambridge, MA, 1964, Chapter 8.)

form a vapor blanketing layer. Beyond this point, the heat flux decreases with increasing  $(T_w - T_{\text{sat}})$  because of the vapor's insulating nature. Regime IV encompasses this effect wherein an unstable vapor film forms but collapses and reforms rapidly. For values of  $(T_w - T_{\text{sat}})$  greater than about 480 K (for water), a stable film exists (regime V). This is called *film boiling*, with which rather low heat fluxes are associated (contrasted to nucleate boiling); for values of  $(T_w - T_{\text{sat}})$  greater than 920 K, radiation across the vapor blanket becomes important, and the rate of heat transfer increases accordingly.

Returning to quenching, we see that Fig. 8.11 shows a typical cooling curve of a metal part plunged into water. Note the three distinct stages during the cooling process. Stage A, called the vapor cooling stage, occurs immediately upon immersing the part in the water. Liquid vaporizes adjacent to the surface and forms a continuous vapor film. Cooling during this stage proceeds by film boiling and, if the part is at a sufficiently high temperature (i.e., steel), also by radiation. The second stage, B, is often denoted as the "vapor transport stage." This term is not really appropriate because during this stage there is a transition from

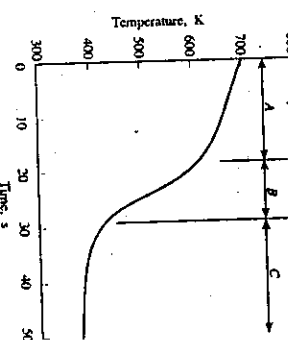


Fig. 8.11 Cooling curve of a metal part quenched in water.

<sup>13</sup>J. P. Holman, *Ibid.* Chapters 6 and 7.

<sup>14</sup>F. P. Incropera and D. P. DeWitt, *Fundamentals of Heat and Mass Transfer*, third edition, John Wiley, New York, NY, Chapters 7, 8, and 9, 1990.

<sup>15</sup>D. Azele, *Fundamentals of Heat Transfer for Process Engineering*, 1992, NJ, Chapter 3, 1984.

<sup>16</sup>B. V. Kailekar and R. M. Desmond, *Engineering Heat Transfer*, West Publishing Co., St. Paul, Minnesota, 1977.

Heated solid surfaces are subjected to *burnout*, unless the heating is reduced, because the operating point of the system will jump from point a to point b on the boiling curve.

partial nucleate boiling and unstable film boiling to entirely nucleate boiling. During stage C, referred to as the liquid cooling stage, there is less vapor formation, and eventually cooling occurs by only natural convection. Thus we see that as the metal cools from its initial elevated temperature to the fluid's temperature, it passes through all the regimes of the boiling curve (Fig. 8-10).

For these and other reasons, no comprehensive body of engineering correlations has evolved and been applied to quenching problems. Rather, most of the literature give some average values of  $h$  which apply to specific cases.

For example, we can find the values of a parameter  $H$ , known as the *severity of quench*, and defined as  $h/k$ , which represent quenching practices for steel. Table 8.1 gives some typical values of  $H$ .

Table 8.1 Severity of assault

Table 6.1 Severity of quench values and heat transfer coefficients for steel			
Quench media	H-value, m <sup>-1</sup>	$h$ , W m <sup>-2</sup> K <sup>-1</sup>	
Oil, no agitation	7.9	270	
Oil, moderate agitation	13.8	480	
Oil, good agitation	19.7	680	
Oil, violent agitation	27.6	970	
Water, no agitation	39.4	1400	
Water, strong agitation	59.0	2000	
Brine, no agitation	78.7	2700	
Brine, violent agitation	196	6800	

Data from this table should be applied only to conditions for which the values are derived. For example,  $h$  can depend strongly on the temperature of the liquid media alone. The values shown above are for quenchants at room temperature. In addition, during quenching  $h$  varies with the temperature of the solid itself. The values in Table 8.1 are derived specifically to predict the time to cool steel from its austenizing temperature to a temperature midway between the austenizing and original quench temperatures. Therefore all that we can say about the above  $h$ -values is that they are average and apply during cooling from about 1090 K to 690 K. It is left to the reader to comprehend the "political" terms—moderate agitation, good circulation and violent circulation.

For precipitation-hardenable aluminum alloys, an important step in their heat treatment is the cooling rate during quenching from the homogenization temperature. If the cooling rate is too low through a critical range of about 700 to 530 K, then precipitation occurs, and subsequent aging cannot be controlled. On the other hand, if the cooling rate during quenching is too great, then intolerable distortion in many parts occurs. In practice, therefore, heat treaters usually quench aluminum alloys in heated water to slow cooling and minimize distortion.

Brines, quenching oils, polymer solutions, and emulsions are used for quenching, in addition to water. Technological aspects, as well as heat transfer characteristics, of various quenchants are discussed in *Morris' Handbook*<sup>17</sup> and in *Surf. & Fin.*<sup>18</sup>.

*Metals Handbook*, Ninth edition, vol. 4, American Society for Metals, Metals Park, OH, 1981.

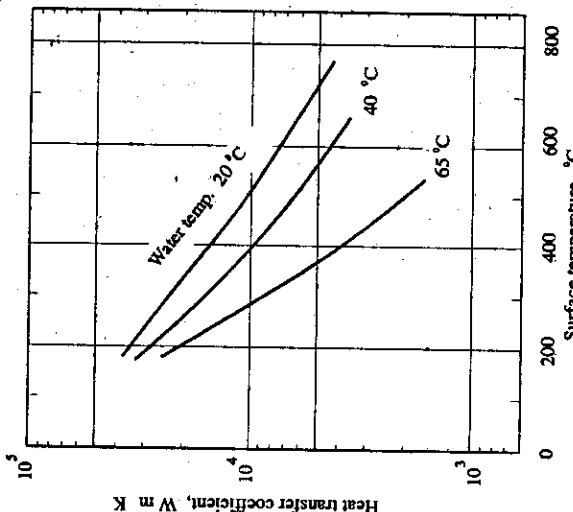


**Fig. 8.12** Heat transfer coefficients for immersion of copper billets in water. (From M. Bamberger and B. Prinz, *Mat. Sci. Tech.* 2, 410-415 (1986))

Stoltz<sup>19</sup> devised a numerical technique for obtaining heat transfer coefficients during quenching from measurements of interior temperatures of a solid sphere. By means of this technique heat transfer coefficients for quenching oils were evaluated as a function of the surface temperature of the solid. Figure 8.14 shows these data for oils designated as slow, intermediate, and fast. The figure also shows that between 1140 K and 895 K the heat transfer coefficients of all three types of oils are similar; over this range all three oils form continuous vapor film on the solid's surface, and  $h$  is only about  $570 \text{ W m}^{-2} \text{ K}^{-1}$ . From 895 K to 325 K, similar heat transfer coefficients are found for all three oils. The main differences among these oils lie in the regions where the heat transfer coefficients are greater

G. Stoltz, Jr. / Heat Transfer 82 20-26 (1980)

than  $570 \text{ W m}^{-2} \text{ K}^{-1}$ , showing that the stable vapor film breaks down first (at a higher surface temperature) for the fast oil, and last for the slow oil.

The results for water and aqueous solutions of 1% NaOH and 5% NaOH are given in Fig. 8.15; all three solutions have a bulk temperature of 316 K. For these aqueous solutions,  $h$  is initially between 1700 and 5100  $\text{W m}^{-2} \text{ K}^{-1}$ . In a quench, these initial values of  $h$  represent the rapid vaporization of water as the solid plunges into the water. This period is only a fraction of a second, after which  $h$  drops to values indicative of the vapor film stage, but this is short-lived, especially for the 5% NaOH solution. The marked increase in heat transfer in the presence of NaOH over the range 1050 K-500 K is due to exploding salt crystals that make the vapor film unstable. All three solutions, however, reach the same peak value of  $h$  at approximately 480 K.

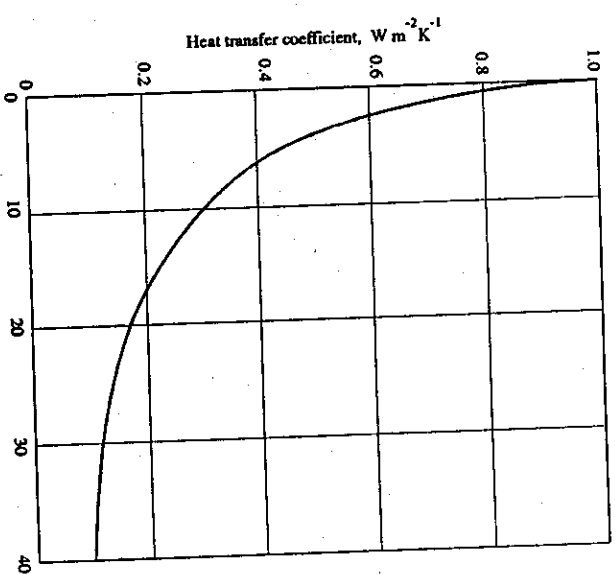


Fig. 8.13 Heat transfer coefficients for cooling aluminum through the critical range of 700-530 K in water and water-polyalkylene glycol (PAG) solutions. (Reproduced by permission of Progressive Metallurgical Industries, Gardena, CA.)

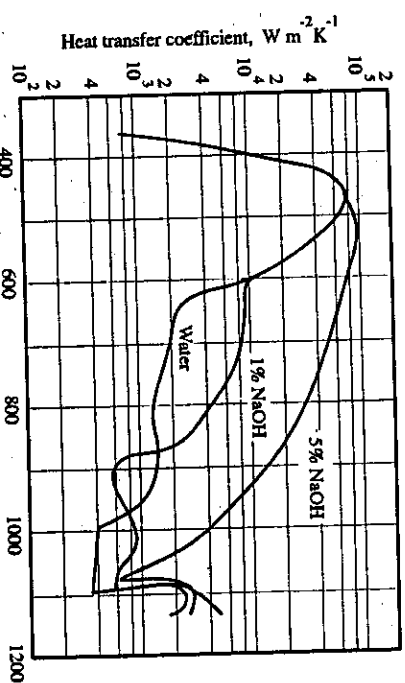


Fig. 8.15 Heat transfer coefficients in aqueous quenching media. (From V. Paschakis and G. Stoltz, Heat and Mass Flow Analyzer Laboratory, Columbia University, New York.)

In order to quench very long metal shapes, such as the strip from a hot strip mill or a continuously cast slab, we often use a multiplicity of water sprays. Figure 8.16 shows cooling data with a fan-type spray of water at 294 K which impinges on a hot horizontal surface from above. There is a sharp increase in the heat flux at about 900-750 K, which represents a transition from boiling with a vapor film to nucleate boiling.

When the vapor film is present during spray cooling, the rate of heat transfer depends on the degree to which the steam film can be broken down by the impinging droplets. With sprays, the droplets approaching the hot metal surface encounter the vapor film, and their success in penetrating this film depends on their kinetic energy. If the sprays are placed closer to the metal surface or the water velocity is increased, thereby increasing the droplets' kinetic energy, then the probability that the droplets will penetrate the film increases and so does the rate of heat removal.

With this in mind, it has been argued that a continuous stream of water, because of its high kinetic energy associated with its large mass, should penetrate the vapor film and bring about an increase in heat transfer rates.<sup>20</sup> For this reason, large nozzles in combination with low water pressure have been utilized to produce a falling stream, or jet, of water which does not break into droplets. For such a jet, an increase in the flow rate of water increases

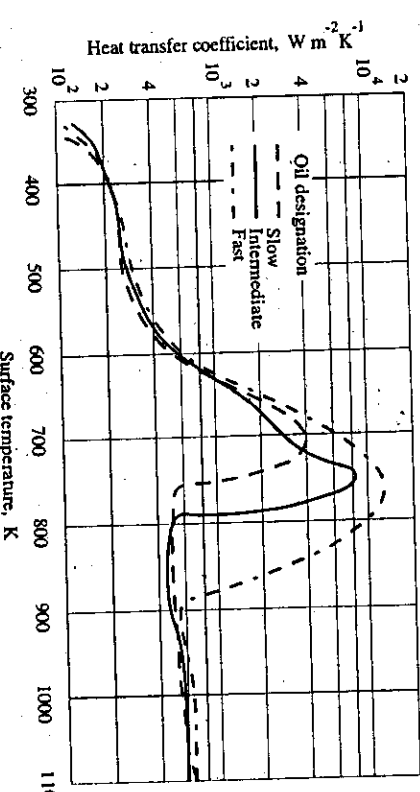


Fig. 8.14 Heat transfer coefficients in quenching oils. (From G. Stoltz, V. Paschakis, C. F. Bonilla, and G. Acevedo, *JISI* 193, 116-123 (1959).)

<sup>20</sup>E. R. Morgan, T. E. Dancy, and M. Korchynsky, *J. Metals* 17, No. 8, 829-831 (1965).

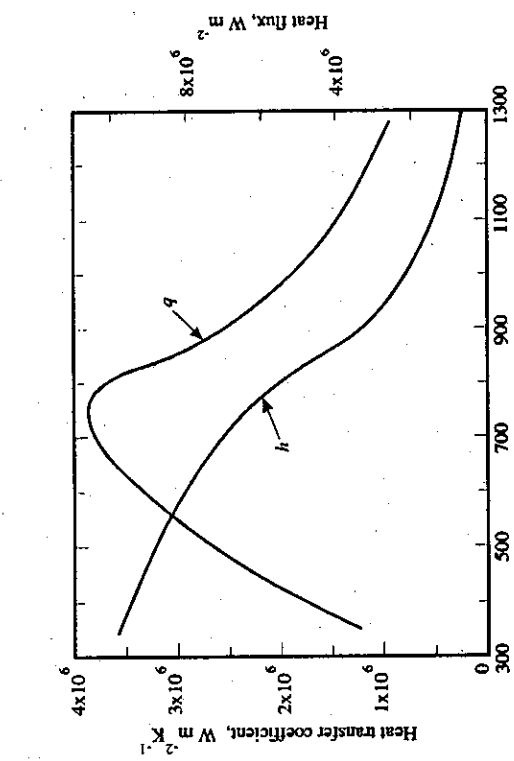


Fig. 8.16 Heat flux and heat transfer coefficients for cooling a horizontal surface from above with a fan-type spray of water at 294 K. (Adapted from P. M. Auman, D. K. Griffiths, and D. R. Hill, *Iron Steel Engineer*, Sept., 1967.)

In addition to water sprays, oil sprays have been used for quenching. It was found in a study,<sup>21</sup> that the cooling rate due to properly applied oil sprays was three to five times the cooling rate by immersing in oil in the conventional manner. Figure 8.17 shows some of these data.

Heat transfer coefficients for water spray cooling with slight overlapping of the spray cones are given in Fig. 8.18. Notice that results for immersion in water are also shown and that only the lines for the two highest spray intensities lie above the line for immersion in water.

### 8.5 HEAT TRANSFER COEFFICIENTS IN FLUIDIZED BEDS

Heat transfer in fluidized beds is of interest mainly because of a relatively new technology pertaining to combustion and gasification of solid fuels. Fluidized beds also are used extensively as dryers and chemical reactors. Here, however, we consider the fluidized bed as a possible medium for effecting the heating or cooling of immersed solids, as in heat treatment or quenching of metallic alloys.

Heat transfer between a fluidized bed and a solid surface immersed in the bed involves the convective heat transfer associated with the gas and the heat transfer associated with the contact between the fluidized particles and the immersed surface. The contact, itself, results in very little conduction and most of this heat transfer is associated with the complex

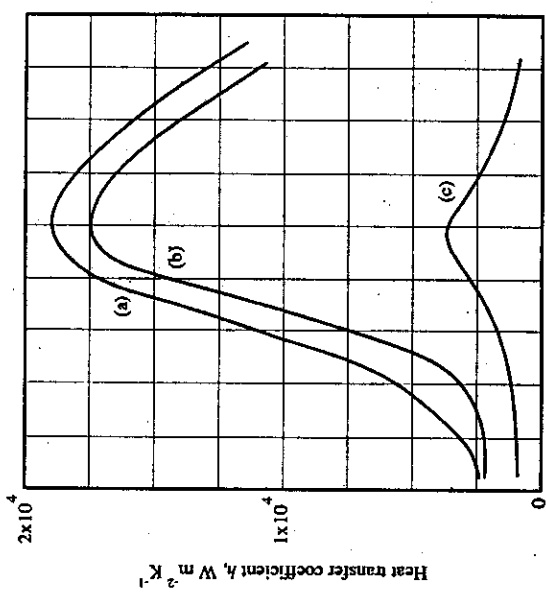


Fig. 8.17 Heat transfer coefficients for oil-spray quenching and immersion in oil. (a) Very strong spray, flow rate  $> 0.70 \text{ m}^3 \text{ s}^{-1} \text{ m}^{-2}$ . (b) Strong spray, flow rate  $= 0.60 \text{ m}^3 \text{ s}^{-1} \text{ m}^{-2}$ . (c) Still oil. (From Zimin, *ibid.*)

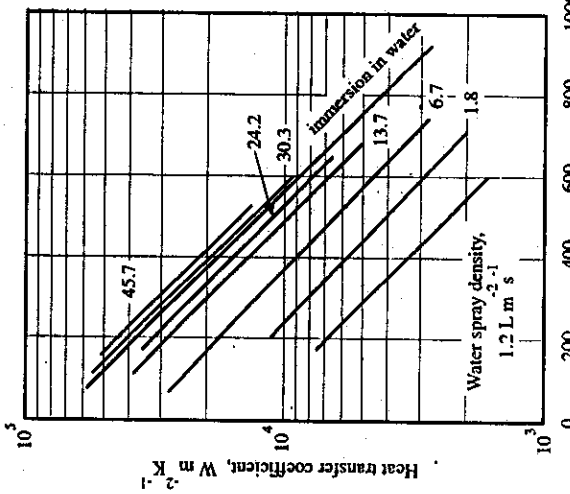


Fig. 8.18 Heat transfer coefficient as function of surface temperature during spray cooling with various spray intensities. (From M. Bamberger and B. Prinz, *ibid.*)

<sup>21</sup>N. V. Zimin, UDC 621.784.06, pages 854-858, Plenum Press, New York, 1968. Translated from *Metallovedenie i Termicheskaya Obrabotka Metallov*, No. 11, 62-68 (Nov., 1967).

convection between the contacting solids. In addition, heat transfer by radiation can be significant, so that correlations for heat transfer coefficients can be quite complicated. One such equation is the following:<sup>22</sup>

$$\text{Nu} = 0.85 \text{ Ar}_{\infty}^{0.1} \left[ \frac{\rho_p}{\rho_s} \right]^{0.14} \left[ \frac{C_p}{C_s} \right]^{0.24} (1 - \omega)^{23} + 0.046 \text{ RePr} \frac{(1 - \omega)^{23}}{\omega} + \frac{\bar{D}}{k_s} \sigma^* (T_{\infty}^2 + T_i^2) / (T_{\infty} + T_i), \quad (8.28)$$

Thermophysical properties are evaluated at  $(T_{\infty} + T_i)/2$ , and Nu has an error of  $\pm 16$  percent. Equation (8.28) contains the usual Nusselt, Reynolds and Prandtl numbers for the fluid, as well as the Archimedes number, Ar, which is defined as

$$\text{Ar} = \frac{g \bar{D}^3 \rho_s (\rho_p - \rho_s)}{\eta_g^2}, \quad (8.29)$$

where  $g$  is gravitational acceleration, the subscripts  $g$  and  $p$  are for the gas and particles making up the bed, and  $\bar{D}$  is the mean diameter of the particles.  $\bar{D}$  is defined as

$$\bar{D} = \left[ \sum_i \frac{\phi_i}{D_i} \right]^{-1}, \quad (8.30)$$

where  $\phi_i$  is the mass fraction of particles with diameter of  $D_i$ . The Nusselt and Reynolds numbers are

$$\text{Nu} = \frac{h \bar{D}}{k_g},$$

and

$$\text{Re} = \frac{\bar{D} V_0}{\nu_g},$$

Finally, the last term in Eq. (8.28) accounts for radiation with  $T_{\infty}$  taken as the temperature of the fluidized bed core (analogous to a free stream temperature in a single phase fluid) and  $T_i$  is the temperature of the surface of the immersed solid. The factor  $\sigma^*$  depends on the emissivities of the immersed solid,  $\varepsilon_s$ , and the effective emissivity of the bed,  $\varepsilon_b$ , according to

$$\sigma^* = \frac{\sigma}{\left[ \frac{1}{\varepsilon_s} + \frac{1}{\varepsilon_b} - 1 \right]}, \quad (8.31)$$

and

$$\frac{\varepsilon_b}{\varepsilon_p} = A + (1 - A) \left[ \frac{T_i}{T_{\infty}} \right]^4, \quad (8.32)$$

where  $\sigma = 5.670 \times 10^{-8} \text{ W m}^{-2} \text{ K}^4$ ,<sup>23</sup> where  $\varepsilon_p$  is calculated below and  $\text{Ar}_{\infty}$  is evaluated at  $T_{\infty}$ . As if all of the above has not yet buried us completely, we must finally evaluate  $\varepsilon_b$  as follows:

$$\varepsilon_b = 1.63 \frac{\omega - \omega_{mf}}{1 - \omega_{mf}} \varepsilon_p^{0.310} + \left[ 1 - 1.63 \frac{\omega - \omega_{mf}}{1 - \omega_{mf}} \right] \varepsilon_p^{0.485}, \quad (8.34)$$

where  $\varepsilon_p$  is the intrinsic emissivity of the particles. Equation (8.28) is valid within the ranges:  $0.1 \leq \bar{D} \leq 6 \text{ mm}$ ;  $0.1 \leq P \leq 10 \text{ MPa}$ ;  $293 \leq T_{\infty} \leq 1473 \text{ K}$ ;  $293 \leq T_i \leq 1373 \text{ K}$ ;  $1.4 \times 10^2 \leq \text{Ar} \leq 1.1 \times 10^7$ .

**Example 8.6** A bed of alumina particles (1 mm) is fluidized ( $\omega = 0.6$ ) with air at 700 K and a superficial velocity of 3.5 m s<sup>-1</sup>. Assume that the emissivity of the bed is 0.8 and the following data for the alumina particles apply:  $C_p = 830 \text{ J kg}^{-1} \text{ K}^{-1}$ ,  $\rho_p = 3900 \text{ kg m}^{-3}$ . Calculate the heat transfer coefficient for heating nickel alloy parts ( $\varepsilon_s = 0.5$ ) in the bed when  $T_i = 300 \text{ K}$  and  $T_{\infty} = 600 \text{ K}$ .

**Solution.** First let's collect properties for air, with the bed operating at 1 standard atmosphere.

$T, \text{K}$	$\rho_g, \text{kg m}^{-3}$	$C_p, \text{J kg}^{-1} \text{ K}^{-1}$	$k_g, \text{W m}^{-1} \text{ K}^{-1}$	$\eta_g, \text{N s m}^{-2}$
500	0.696	1030	$40.7 \times 10^{-3}$	$270 \times 10^{-7}$
600	0.584	1051	$46.9 \times 10^{-3}$	$306 \times 10^{-7}$
700	0.498	1075	$52.4 \times 10^{-3}$	$339 \times 10^{-7}$

With  $T_{\infty} = 700 \text{ K}$ ,

$$\text{Ar}_{\infty} = \frac{g \bar{D}^3 \rho_s (\rho_p - \rho_s)}{\eta_g^2} = \frac{(9.81)(1 \times 10^{-3})^3 (0.498)(3900)}{(3.39 \times 10^{-7})^2} = 16.580$$

and from Eq. (8.33)

$$A = 1 - \exp [ - (0.16)(16.580)^{0.25}] = 0.865.$$

The effective emissivity is calculated with Eq. (8.32); this gives

$$\frac{\varepsilon_b}{\varepsilon_p} = 0.865 + (1 - 0.865) \left[ \frac{300}{700} \right]^4 = 0.870$$

<sup>22</sup>V. A. Borodulya, Y. S. Teplytsky, I. I. Markevich, A. F. Hassan and T. P. Veryomenko, *Int. J. Heat Mass Transfer* 34, 47-53 (1991).

<sup>23</sup>This is the Stefan-Boltzmann constant. Radiation heat transfer is the subject of Chapter 11, where this constant is discussed and used repeatedly.

and

$$\varepsilon_r = 0.870 \quad \varepsilon_b = (0.870)(0.8) = 0.696.$$

With Eq. (8.31), we have

$$\sigma^* = \frac{5.670 \times 10^{-8}}{\left[ \frac{1}{0.5} + \frac{1}{0.696} - 1 \right]} = 2.33 \times 10^{-8} \text{ W m}^{-2} \text{ K}^{-4}.$$

Now we can evaluate the last term of Eq. (8.28); with  $k_g(500 \text{ K}) = 0.0407 \text{ W m}^{-1} \text{ K}^{-1}$ ,

$$\frac{\bar{D}}{k_g} \sigma^* (T_{\infty}^2 + T_s^2) (T_{\infty} + T_s) = \frac{(1 \times 10^{-3})(2.33 \times 10^{-8})(700^2 + 300^2)(700 + 300)}{0.0407} = 0.33.$$

This calculation tells us that radiation heat transfer cannot be neglected at these temperatures. With  $T_s = 300 \text{ K}$ , the properties of the gas are evaluated at  $(700 + 300)/2 = 500 \text{ K}$ :

$$\text{Ar} = \frac{(9.81)(1 \times 10^{-3})^3 (0.696)(3900)}{(2.70 \times 10^{-3})^2} = 3.65 \times 10^4; \quad \frac{\rho_p}{\rho_s} = \frac{3900}{0.696} = 5600;$$

$$\frac{C_p}{C_s} = \frac{830}{1030} = 0.806; \quad \text{Re} = \frac{(1 \times 10^{-3})(3.5)(0.696)}{2.70 \times 10^{-3}} = 90.2;$$

$$\text{Pr} = 0.684 \quad \text{and} \quad \omega = 0.6.$$

We substitute these values into Eq. (8.28):

$$\begin{aligned} \text{Nu} &= (0.85)(3.65 \times 10^4)^{0.1} (5600)^{0.14} (0.806)^{0.24} (1 - 0.6)^{23} \\ &\quad + (0.046)(90.2)(0.684) \frac{(1 - 0.6)^{23}}{0.6} + 0.33 \\ &= 4.19 + 2.57 + 0.33 = 7.09. \end{aligned}$$

Therefore,

$$h = \frac{k_g \text{Nu}}{\bar{D}} = \frac{(0.0407)(7.09)}{(1 \times 10^{-3})} = 289 \text{ W m}^{-1} \text{ K}^{-1}.$$

When  $T_s = 600 \text{ K}$ , the properties are evaluated at 650 K; otherwise the same procedure is followed. The results are  $\text{Nu} = 6.07$  and  $h = 301 \text{ W m}^{-1} \text{ K}^{-1}$ . The heat transfer coefficient changes by only 4.3 percent.

## 8.6 HEAT-TRANSFER COEFFICIENTS IN PACKED BEDS

The heat transfer coefficient for flow through packed beds could be given by an expression of the form  $\text{Nu} = A \text{Re}^\alpha \text{Pr}^\beta$ . Here we are dealing exclusively with gases as the fluid phase, and since the Prandtl numbers of gases are all about equal over a wide range of temperatures, there is not any strong dependence of Nu or Pr for gas-solid heat transfer. So we are left with finding the relationship between Nu and Re. However, this is much easier said than

done, as most of the experimental work on this subject has been confined to much lower temperatures than those of most metallurgical processes.

The highest temperatures— $1100^\circ\text{C}$ —were employed by Furnas<sup>23</sup> in 1932. Kitaev and coworkers<sup>24</sup> summarized the results of the pertinent studies at elevated temperatures, and also some at lower temperatures. Their review includes a complete reanalysis of Furnas' data. They present the results with the volumetric heat-transfer coefficient,  $h_v$ , in a dimensional equation

$$h_v = \frac{AV_g^{0.9} T^{0.3} f(\omega)}{D_p^{0.75}}, \quad (8.35)$$

where  $h_v = hS$  = volumetric heat transfer coefficient,  $\text{kcal m}^{-3} \text{ h}^{-1} \text{ K}^{-1}$

$A$  = a coefficient dependent on bed material,

$T$  = temperature,  $^\circ\text{C}$ ,

$D_p$  = particle diameter, mm,

$V_g$  = superficial gas velocity,  $\text{m s}^{-1}$ ,

$f(\omega)$  = function of void fraction.

For natural, lump materials,  $A = 160$  and  $f(\omega) = 0.5$ , so that

$$h_v = \frac{80V_g^{0.9} T^{0.3}}{D_p^{0.75}}. \quad (8.36)$$

A nomogram was developed, Fig. 8.19, which facilitates the determination of  $h_v$ . Paper et al.<sup>25</sup> experimentally confirmed the predictions of Fig. 8.19 up to  $1100^\circ\text{C}$  for 10 mm pellets. For spheres, the equation

$$h_v = \frac{12V_g T^{0.3}}{D_p^{1.35}}. \quad (8.36)$$

agrees with Furnas' results and those of Saunders and Ford,<sup>26</sup> when  $D_p$  is in meters. The gas velocity

*Solution.* Entering the nomograph at  $1.0 \text{ m s}^{-1}$ , going up to  $1200^\circ\text{C}$ , across to 25 mm, and down, we find that  $h_v = 12,500 \text{ kcal m}^{-3} \text{ h}^{-1} \text{ °C}^{-1}$ . This becomes

$$h_v = \frac{12,500 \text{ kcal}}{\text{m}^3 \text{ h} \text{ °C}} \quad | \quad \frac{4.184 \times 10^3 \text{ J}}{1 \text{ kcal}} \quad | \quad \frac{1 \text{ h}}{3600 \text{ s}} \quad | \quad \frac{1^\circ\text{C}}{1 \text{ K}}$$

<sup>23</sup>C. C. Furnas, U.S. Bureau Mines Bull., No. 261 (1932).

<sup>24</sup>B. I. Kitaev, Y. G. Yaroshenko, and V. D. Suchkov, *Heat Exchange in Shaft Furnaces*, Pergamon Press, New York, 1968.

<sup>25</sup>P. O. Paper, R. Frans and G. H. Geiger, *Ironmaking and Steelmaking*, 138 (1976).

<sup>26</sup>O. H. Saunders and H. Ford, *JSI* I, 292 (1940).

where  $q$  is the flux ( $\text{W m}^{-2}$ ) and  $\Delta T$  is the temperature difference at the interface of the two pieces in contact. Figure 8.20 gives some data for the contact heat transfer coefficient of an aluminum alloy (Al 6061-O) at various temperatures of the die (H-12 tool steel). The contact heat transfer coefficient varies with both forging pressure (i.e., the normal stress at the surface) and temperature of the workpiece, as well as the surface roughness, the type of lubricant, and the temperature of the die material. These factors should be considered in using contact heat transfer coefficients for estimating temperature distributions during forging.

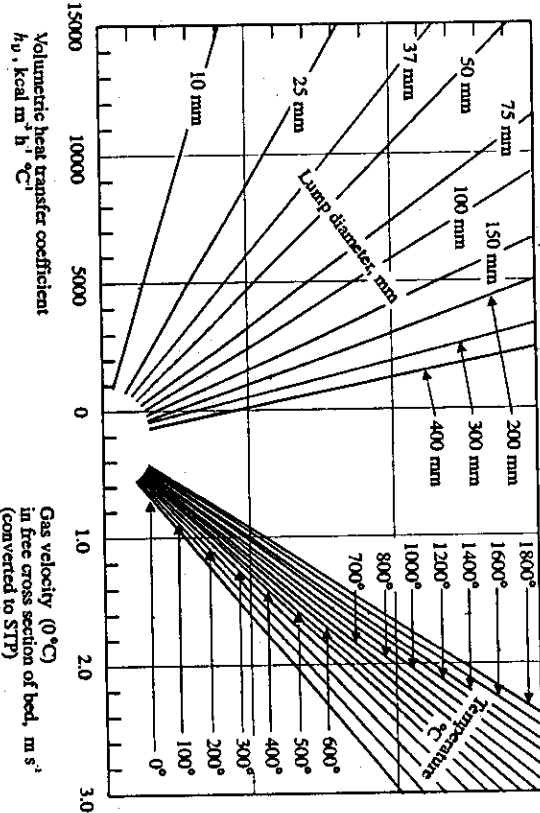


Fig. 8.19 Nomograph for the volumetric heat transfer coefficient  $h_S$  or  $h_v$ , based on knowledge of the superficial gas velocity,  $V_g$ , the gas temperature, and the particle diameter  $D_p$ . (Adapted from B. I. Kitaev et al., *ibid.*)

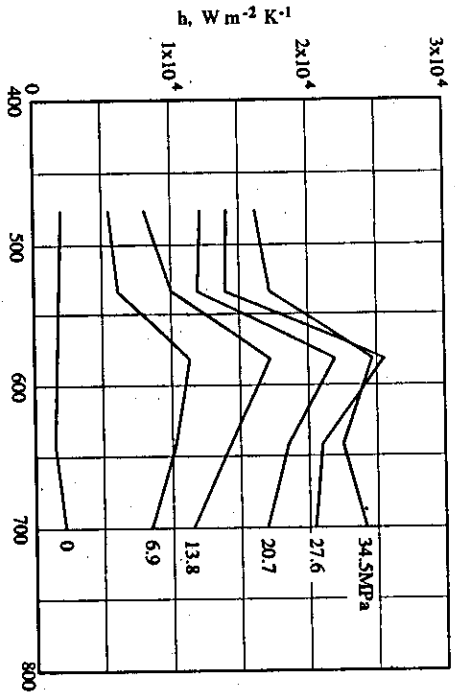


Fig. 8.20 Contact heat transfer coefficient as a function of die temperature and the forging pressure. Test conditions: workpiece Al 6061-O; lubricant MoS<sub>2</sub>; surface roughness of workpiece =  $0.74 \mu\text{m}$ ; surface roughness of die =  $0.93 \mu\text{m}$ . (From V. K. Jain, *J. Mater. Shaping Technol.* 8, 193 (1990).)

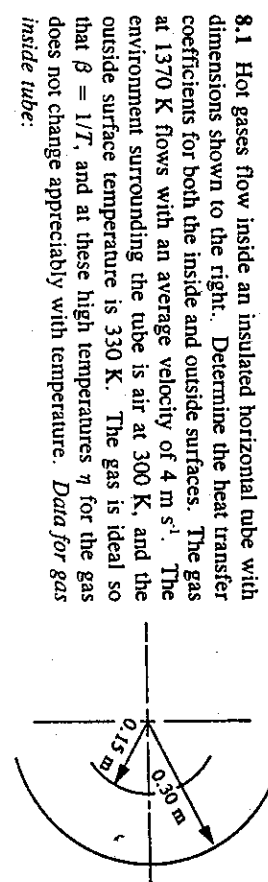
### PROBLEMS

**8.7 HEAT TRANSFER COEFFICIENTS IN FORGING**

Forging involves deformation of alloys at a temperature where the stresses to strain the material are relatively low. As an alloy is forged it loses heat to the forging die, which causes a decrease in the workpiece temperature and an increase in the deformation stresses. Thus, it is important to predict the heat transfer from the workpiece to the die because this has a direct bearing on the power required to carry out the forging operation and on the ability of the metal to plastically deform and fill the die cavity. We must also realize that the heat loss from the workpiece represents a heat gain by the die. For one thing, there is a softening of the surface of the die making it more subject to plastic deformation and wear. The die is also subject to thermal fatigue because the temperature at the die surface fluctuates cyclically. Knowledge of the heat transfer between the workpiece and the die is, therefore, important, and in order to model the forging process we should have data on the so-called *contact heat transfer coefficient*.

It is the rule rather than the exception that, when two solids of a different temperature are brought into contact, there is a discontinuity of temperature at the contact interface. At the microscopic level some of the asperites on the two surfaces touch each other to form paths for energy conduction, but otherwise the energy is transferred by radiation across the tiny depressions and by conduction through fragmented oxide layers and lubrication films. The actual heat transfer process is so complex that we normally rely on empirical measurements of the contact heat transfer coefficient, which is defined as

$$h = \frac{q}{\Delta T} \quad (8.37)$$

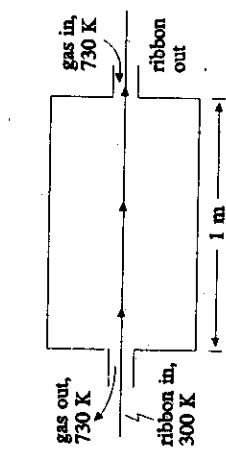


**8.2** Molten aluminum is preheated while being transferred from a melting furnace to a casting tundish by pumping through a heated tube, 50 mm in diameter, at a flow rate of  $1.3 \text{ kg s}^{-1}$ . The tube wall is kept at a constant temperature at  $1030 \text{ K}$ . a) Calculate the heat transfer coefficient between the tube wall and the aluminum. b) Using this value of the heat transfer coefficient, how long would the tube have to be to heat the aluminum from  $950 \text{ K}$  to  $1025 \text{ K}$ ? *Data for aluminum:*  $k = 86 \text{ W m}^{-1} \text{K}^{-1}$ ;  $C_p = 1050 \text{ J kg}^{-1} \text{K}^{-1}$ ;  $\eta = 1.2 \times 10^{-3} \text{ kg s}^{-1} \text{m}^{-1}$ .

**8.3** A sheet of glass (1 m length) is cooled from an initial temperature of  $1250 \text{ K}$  by blowing air at  $300 \text{ K}$  parallel to the surface of the glass. The free stream velocity of the air is  $30 \text{ m s}^{-1}$ . Calculate the initial heat transfer coefficient and when the glass has cooled to  $400 \text{ K}$ .

**8.4** A long cylindrical bar of steel (30 mm diameter) is heated in a tempering furnace to  $810 \text{ K}$ . It is then cooled in a cross-stream of moving air at  $300 \text{ K}$  with a free stream velocity of  $30 \text{ m s}^{-1}$ . Calculate the heat transfer coefficient that applies when the bar begins to cool.

**8.5** Refer to Example 8.1, in which a tube with a uniform surface temperature was considered. Now consider flow through a tube which is electrically heated so that the heat flux along the length of the tube is uniform. The fluid has a mixed mean temperature of  $T_0$  as it enters the heated length of the tube. Assume constant and uniform thermal properties and steady state. a) For a small length of tube,  $\Delta x \rightarrow 0$ . c) Integrate part b) and obtain an equation which gives the mixed mean temperature of the fluid as it leaves the heated section of the tube.



**8.6** A rapidly solidified ribbon is annealed by continuously passing it through a tube with countercurrent hot gas, which flows at  $30 \text{ m s}^{-1}$  and  $730 \text{ K}$ . Estimate the heat transfer coefficient, and calculate the temperature of the ribbon leaving the tube. *Data and thermal properties:* Ribbon thickness, 1 mm; ribbon width, 150 mm; ribbon velocity,  $0.17 \text{ m s}^{-1}$ .

	$\rho, \text{kg m}^{-3}$	$C_p, \text{J kg}^{-1} \text{K}^{-1}$	$k, \text{W m}^{-1} \text{K}^{-1}$
Gas	0.64	2000	0.04
Ribbon	6400	500	30

**8.7** In order to reduce the amount of dissolved hydrogen, dry helium is bubbled through molten copper. In order to prevent clogging of the submerged end of the lance, the helium must enter the melt at a temperature greater than the freezing point of copper ( $1356 \text{ K}$ ). What is the maximum mass flow rate of helium which can be employed if the supply of helium is at  $300 \text{ K}$ ?

**8.8** Calculate the initial rate of losing energy (W) of an aluminum plate ( $1.2 \text{ m} \times 1.2 \text{ m} \times 10 \text{ mm}$ ) and heated uniformly to  $370 \text{ K}$  when it is a) cooled in a horizontal position by a stream of air at  $290 \text{ K}$  with a velocity of  $2 \text{ m s}^{-1}$ ; b) suspended vertically in stagnant air at the same temperature.

**8.9** Oil flows in a long horizontal 50 mm I.D. copper tube at an average velocity of  $3 \text{ m s}^{-1}$ . If the oil has a bulk temperature of  $370 \text{ K}$  and the air surrounding the tube is at  $290 \text{ K}$ , calculate a) the "liquid side" heat transfer coefficient; b) the "vapor-side" heat transfer coefficient; c) the temperature of the copper tube; d) the rate of heat transfer to the air. *Data for oil:*

$T, \text{K}$	$\rho, \text{kg m}^{-3}$	$C_p, \text{J kg}^{-1} \text{K}^{-1}$	$\eta \cdot 10^2, (\text{N s m}^{-2})$	$\nu \cdot 10^6, (\text{m}^2 \text{s}^{-1})$	$k \cdot 10^3, (\text{W m}^{-1} \text{K}^{-1})$	$\alpha \cdot 10^3, (\text{m}^2 \text{s}^{-1})$	$\beta \cdot 10^3, (\text{K}^{-1})$
290	890.0	1.868	99.9	1120	145	0.872	12.900
300	884.1	1.909	48.6	550	145	0.859	6400
320	871.8	1.993	14.1	161	143	0.823	1963
340	859.9	2.076	5.31	61.7	139	0.779	793
360	847.8	2.161	2.52	29.7	138	0.753	395
370	841.8	2.206	1.86	22.0	137	0.738	300

**8.10** Replace the oil with sodium and repeat Problem 8.5. Compare or contrast the results of the two problems.

**8.11** A heat treating furnace is 6 m long, 3 m wide and 6 m high. If a check with thermocouples indicates that the average wall temperature is  $340 \text{ K}$  and the top is  $365 \text{ K}$ , calculate the heat loss from the furnace in W. A quick estimate can be made by using the simplified equations given in Problem 8.14.

**8.12** In flow past a flat plate, a laminar boundary layer exists over the forward portion between 0 and  $L_{\tau}$ , and the turbulent boundary layer exists beyond  $L_{\tau}$ . With this model, the average  $h$  over a plate of length  $L$  (with  $L > L_{\tau}$ ) can be determined as indicated

$$h = \frac{1}{L} \left[ \int_0^{L_{\tau}} h_{x(\text{lam})} dx + \int_{L_{\tau}}^L h_{x(\text{turb})} dx \right].$$

Take  $Re_{\tau} = 3.2 \times 10^5$  and show that

$$\frac{hL}{k} = 0.037 Re_{\tau}^{1/3} (Re_{\tau}^{0.8} - 15500).$$

[Hint:  $L_{\tau}/L = Re_{\tau}/Re_L$ .]

**8.13** A steel plate, 2.5 m by 2.5 mm, is removed from an oven at  $420 \text{ K}$  and hung horizontally in a laboratory at  $295 \text{ K}$ . a) Calculate the initial heat loss (W) from the steel. b) Repeat if the plate is hung vertically.

**8.14** Repeat Problem 8.13 using one of the following simplified equations, which apply reasonably well to air,  $\text{CO}_2$ ,  $\text{N}_2$ , and  $O_2$  in the range  $310\text{--}1090 \text{ K}$ .  $L$  and  $D$  are in m,  $\Delta T$  in K, and  $h$  in  $\text{W m}^{-2} \text{K}^{-1}$ .  $L = A/P$  with  $A$  = surface area and  $P$  = perimeter of the surface.

Vertical plates of length  $L$ :

$$h = 1.42 (\Delta T/L)^{1/4}, \quad 5 \times 10^6 < L^3 \Delta T < 50$$

$$h = 1.45 (\Delta T)^{1/3}, \quad 50 < D^3 \Delta T < 5 \times 10^4$$

Horizontal pipes of diameter  $D$ :

$$h = 1.22 (\Delta T/D)^{1/4}, \quad 5 \times 10^3 < D^3 \Delta T < 50$$

$$h = 1.24 (\Delta T)^{1/3}, \quad 50 < D^3 \Delta T < 10^5$$

Horizontal plate, \* hot surface up or cold surface down:

$$h = 1.32 (\Delta T/L)^{1/4}, \quad 5 \times 10^5 < L^3 \Delta T < 0.30$$

$$h = 1.52 (\Delta T)^{1/3}, \quad 0.30 < L^3 \Delta T < 470$$

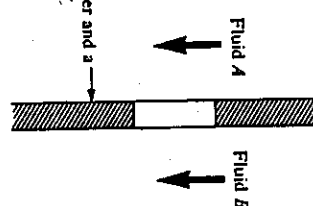
Horizontal plate, \* hot surface down or cold surface up:

$$h = 0.59 (\Delta T/L)^{1/4}, \quad 0.005 < L^3 \Delta T < 470$$

Are the results for the heat transfer coefficients within 20 pct of the results using the more complete correlations (as in Problem 8.13)?

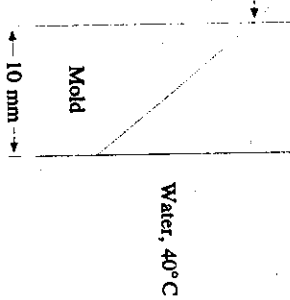
- 8.15** Two fluids are separated by a solid with a thickness of 10 mm and a thermal conductivity of  $22 \text{ W m}^{-1}\text{K}^{-1}$ . For each of the following scenarios, estimate the heat transfer coefficient on each side of the solid and the surface temperatures of the solid.

Fluid	Free stream velocity, $\text{m s}^{-1}$	Free stream temperature, K
a) A air	15.2	300
B air	0	650
b) A air	0	300
B sodium	0	650
c) A air	15.2	300
B sodium	0	650
d) A sodium	15.2	365
B sodium	0	650



- 8.16** A wire with a diameter of 0.03 mm and 0.3 m in length is heated by an electrical current and placed in helium at 280 K. a) If the surface temperature of the wire is 600 K, calculate the electric power. b) Calculate the electric power, for the same wire temperature, if there is a cross flow of helium with a free stream velocity of  $20 \text{ m s}^{-1}$ .

- 8.17** A copper mold is used to make a casting of a nickel-base alloy. During most of the solidification period, the temperature profile in the copper is linear, with the surface on the casting side maintained constant at 1000 K. The other side of the mold contacts the water at  $40^\circ\text{C}$  ( $313 \text{ K}$ ). What is the surface temperature on the water side of the mold?



- 8.18** Glass plate can be made stronger by inducing compressive residual surface stresses. This is done by a process called thermal tempering. The glass is heated to a temperature between the softening point ( $\sim 750 \text{ K}$ ) and the glass transition temperature ( $\sim 600 \text{ K}$ ). It is then cooled to room temperature in a stream of air, or in some cases immersed in an oil bath. Compare the heat transfer coefficients, as the glass cools from 700 K to 300 K, in air ( $V_\infty = 30 \text{ m s}^{-1}$ ) and in "fast" oil.

- 8.19** Polymeric fibers are formed by heating the polymer to its viscous liquid state and then pumping it through small, round orifices. From each orifice, a single fiber is formed which solidifies almost immediately upon passing into air. Compare the heat transfer coefficients that can be obtained by forming the fibers (0.1 mm diameter) in air and in helium. The fibers are formed at  $50 \text{ m s}^{-1}$ .

- 8.20** A steel rod (25 nun diameter and 0.6 m length) is heated vertically in a large bath of molten salt at 920 K. Calculate the heat transfer coefficient when the bar is at 640 K.   
Data for molten salt:  $k = 86 \text{ W m}^{-1}\text{K}^{-1}$ ;  $C_p = 870 \text{ J kg}^{-1}\text{K}^{-1}$ ;  $\rho = 3200 \text{ kg m}^{-3}$ ;  $\beta = 2 \times 10^{-5} \text{ K}^{-1}$ ;  $\eta(920 \text{ K}) = 1.03 \times 10^{-3} \text{ N s m}^{-2}$ ;  $\eta(780 \text{ K}) = 1.24 \times 10^{-3} \text{ N s m}^{-2}$ ;  $\eta(640 \text{ K}) = 1.65 \times 10^{-3} \text{ N s m}^{-2}$ .

- 8.21** Consider a vertical surface (1.5 m) at 600 K that loses heat by natural convection to nitrogen at 300 K. Using the simplified equations given in Problem 8.14, calculate and plot the heat transfer coefficient as the surface temperature decreases from 600 K to 300 K.

- 8.22** We can maximize the heat transfer coefficient in a fluidized bed by selecting the optimum superficial velocity. Start with Eq. (8.28), neglect the term for radiation, and assume that the thermophysical properties are constant. With these assumptions, the correlation is of the form:

$$\text{Nu} = \text{Nu}(\text{Re}, \omega)$$

$\text{Re}$  and  $\omega$  are interrelated, so  $\text{Nu}$  can be optimized with respect to  $\text{Re}$ . Carry out the optimization with

$$\omega^{4/7} \text{Ar} = 18 \text{ Re} + 2.70 \text{ Re}^{1.67}.$$

(This equation is from C. Y. Wen and Y. H. Yu, *Fluid Particle Technology*, Chem. Eng. Prog. Symposium Series, No. 62, AIChE, New York, 1966.)

- 8.23** Bars (50 mm diameter) of steel, on cooling beds, cool from a rolling temperature ( $1150 \text{ K}$ ) to a shearing temperature ( $650 \text{ K}$ ) in a horizontal position with all surfaces exposed to ambient air. The air temperature can vary from  $250 \text{ K}$  to  $310 \text{ K}$ . Calculate the convective heat transfer coefficients that apply to the two extremes of ambient conditions.

## 9

## CONDUCTION OF HEAT IN SOLIDS

Materials engineers easily recognize that the conduction of heat within solids is fundamental to understanding and controlling many processes. We could cite numerous examples to emphasize the importance of this topic. Some important applications that fall in this category include estimating heat losses from process equipment, quenching, or cooling operations where the cooling rate of a part actually controls its microstructure and hence its application, and solidification.

### 9.1 THE ENERGY EQUATION FOR CONDUCTION

The general equation for the conduction of heat in a solid free of heat sources or sinks can be written

$$\nabla \cdot k \nabla T = \rho \frac{\partial (C_p T)}{\partial t}. \quad (9.1)$$

The more common form of this equation is written for conductivity independent of position in space and heat capacity independent of temperature:

$$\frac{\partial T}{\partial t} = \alpha \nabla^2 T = \alpha \left[ \frac{\partial^2 T}{\partial x^2} + \frac{\partial^2 T}{\partial y^2} + \frac{\partial^2 T}{\partial z^2} \right], \quad (9.2)$$

where the thermal diffusivity, as defined in Chapter 7, is  $\alpha = k/\rho C_p$ . Equation (9.2), although not as rigorous as Eq. (9.1), is used when analytical solutions are sought.

When the temperature is not a function of time but only depends upon position in space, then Eq. (9.2) becomes

$$\nabla^2 T = \frac{\partial^2 T}{\partial x^2} + \frac{\partial^2 T}{\partial y^2} + \frac{\partial^2 T}{\partial z^2} = 0. \quad (9.3)$$

Equation (9.3) therefore applies to steady-state conduction in systems free of heat sources and sinks. It is often referred to as the *Laplace equation*.

## 9.2 STEADY-STATE ONE-DIMENSIONAL SYSTEMS

### 9.2.1 Infinite flat plate

Equation (9.3) for an infinite flat plate, such as that in Fig. 9.1, reduces to

$$\frac{d^2T}{dx^2} = 0. \quad (9.4)$$

Boundary conditions are

$$\text{B.C. 1. at } x = 0, \quad T = T_1; \quad (9.5)$$

$$\text{B.C. 2. at } x = L, \quad T = T_2. \quad (9.6)$$

We can solve Eq. (9.4) quite simply, in accordance with the boundary conditions, to yield the temperature profile:

$$\frac{T - T_1}{T_2 - T_1} = \frac{x}{L}. \quad (9.7)$$

In addition, the heat flux through the slab may be described as follows:

$$q = -k \frac{dT}{dx} = \frac{k}{L} (T_1 - T_2). \quad (9.8)$$

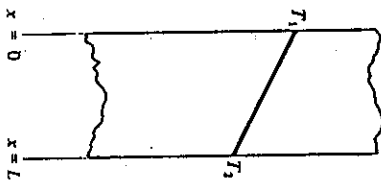


Fig. 9.1 Steady-state temperature distribution in a plate.

### 9.2.2 Series composite wall

Consider a simple series wall made up of two different materials whose thermal conductivities are  $k_1$  and  $k_2$  (Fig. 9.2). There is a flow of heat from the gas at temperature  $T_1$  through its boundary layer, the composite wall, and the boundary layer of the gas at  $T_0$ .

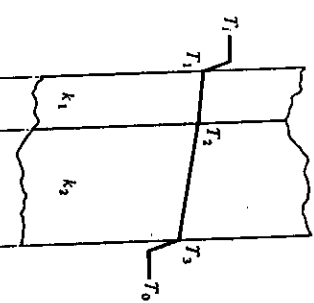


Fig. 9.2 Steady-state temperature distribution in a composite wall.

The unidirectional heat flux through the four parts of the entire circuit is constant because steady state prevails. Thus

$$Q = Ah_1(T_1 - T_1) = \frac{k_1 A}{L_1} (T_1 - T_2) = \frac{k_2 A}{L_2} (T_2 - T_3) = Ah_0(T_3 - T_0). \quad (9.9)$$

We can build up a solution based on the four equalities in Eq. (9.9). However, this procedure is rather tedious, and it is much easier to make use of the *resistance concept*.

The flow of heat  $Q$  through material, subject to a temperature difference  $T_j - T_k$ , is analogous to the flow of current  $I$ , as a result of a potential difference  $E_j - E_k$  through an electrical conductor. From Ohm's law for electricity, the thermal resistance  $R_i$  for heat flow is visualized:

$$R_i = \frac{T_j - T_k}{Q}. \quad (9.10)$$

Thus for the composite wall, the four thermal resistances are  $1/Ah_1$ ,  $L_1/k_1 A$ ,  $L_2/k_2 A$ , and  $1/Ah_0$ . The total resistance for the whole circuit is simply their sum, so that the heat flow is

$$Q = \frac{T_1 - T_0}{\frac{1}{Ah_1} + \frac{L_1}{k_1 A} + \frac{L_2}{k_2 A} + \frac{1}{Ah_0}}. \quad (9.11)$$

With Eq. (9.11), we only need to know the total temperature drop across the system to calculate the heat flux, which we can use to determine the temperature at any position within the composite wall.

**Example 9.1** A furnace wall is constructed of 230 mm of fire brick ( $k = 1.04 \text{ W m}^{-1} \text{ K}^{-1}$ ), 150 mm of insulating brick ( $k = 0.70 \text{ W m}^{-1} \text{ K}^{-1}$ ), 50 mm of glass-wool insulation ( $k = 0.07 \text{ W m}^{-1} \text{ K}^{-1}$ ), and 3 mm thick steel plate ( $k = 45 \text{ W m}^{-1} \text{ K}^{-1}$ ) on the outside. The heat transfer coefficients on the inside and outside surfaces are 28 and  $5.7 \text{ W m}^{-2} \text{ K}^{-1}$ , respectively. The gas temperature inside the furnace is 1365 K and the outside air temperature is 305 K.

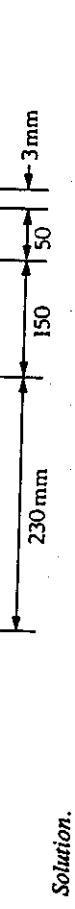
- Calculate the heat flux through the wall.
- Determine the temperatures at all interfaces.

In addition to the resistances discussed in this section, composite walls often have another type of thermal resistance. When two elements of the composite are in contact, a resistance occurs which depends on the roughness of the two surfaces, the fluid between the surfaces, and the contact pressure. For furnace walls, it is customary to ignore the additional resistance because of the very high thermal resistance of the refractories; for metallic composite walls, however, it is wise to include it. Unfortunately, each individual situation is different, and so experimental information must be obtained.

### 9.2.3 Infinite cylinder

For steady radial flow of heat through the wall of the hollow cylinder depicted in Fig. 9.3, the Laplace equation still applies. The Laplace equation written in cylindrical coordinates can be deduced from Eq. (B), Table 7.5.

$$\frac{1}{r} \frac{\partial}{\partial r} \left[ r \frac{\partial T}{\partial r} \right] + \frac{1}{r^2} \frac{\partial^2 T}{\partial \theta^2} + \frac{\partial^2 T}{\partial z^2} = 0. \quad (9.12)$$



Solution.

$$a) \quad q = \frac{T_i - T_o}{AR_i}$$

and

$$AR_i = \frac{1}{28} + \frac{0.230}{1.04} + \frac{0.150}{0.70} + \frac{0.050}{0.07} + \frac{0.003}{45} + \frac{1}{5.7} = 1.361 \text{ W}^{-1} \text{ m}^2 \text{ K}.$$

Therefore,

$$q = \frac{(1365 - 305)}{1.361} = 778.8 \text{ W m}^{-2}$$

$$b) \quad T_i - T_1 = \frac{q}{h_i} = \frac{778.8}{28} = 27.8 \text{ K}$$

$$T_1 = 1337.2 \text{ K.}$$

Similarly,

$$T_1 - T_2 = \frac{q}{(k_i/L_i)} = \frac{(778.8)(0.230)}{1.04} = 172.2 \text{ K}$$

$$T_2 = 1165.0 \text{ K.}$$

The remaining temperatures are determined in the same manner, yielding  $T_3 = 998.2 \text{ K}$  and  $T_4 = T_3 = 441.8 \text{ K}$ .

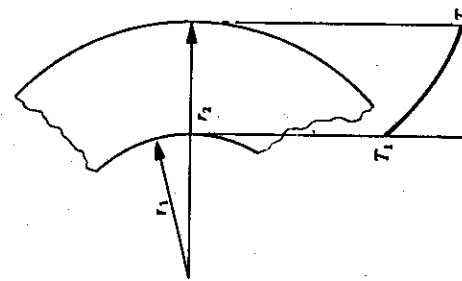


Fig. 9.3 Steady-state temperature distribution in a hollow cylinder.

For the case at hand, temperature depends only on the radial coordinate; therefore, Eq. (9.12) reduces to:

$$c) \quad \frac{1}{r} \frac{d}{dr} \left[ r \frac{dT}{dr} \right] = 0. \quad (9.13)$$

The boundary conditions under consideration are

$$B.C. 1 \quad \text{at } r = r_1, \quad T = T_1, \quad (9.14)$$

$$B.C. 2 \quad \text{at } r = r_2, \quad T = T_2. \quad (9.15)$$

286 Conduction of Heat in Solids  
At this point, the reader should note that this problem and the one discussed in Section 7.4 are identical. By way of illustration, we have used a different starting point here. In any event, the temperature profile is given by

$$\frac{T_i - T_2}{T_1 - T_2} = \frac{\ln(r/r_2)}{\ln(r_1/r_2)} \quad (7.51)$$

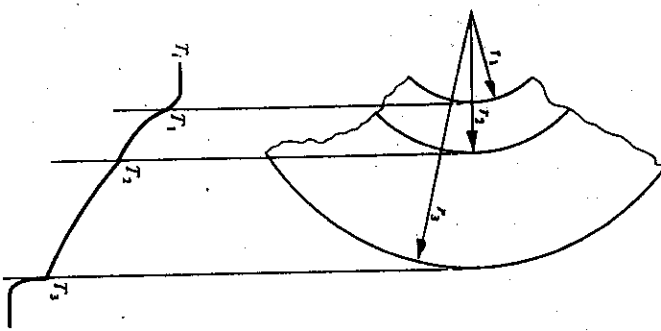
It then follows that the heat flux  $q_r$  ( $\text{W m}^{-2}$ ) and the heat flow  $Q$  (W) are given by Eqs. (7.52) and (7.53), respectively.

#### 9.2.4 Composite cylindrical wall

Consider the cylindrical composite wall shown in Fig. 9.4. By referring to Eq. (7.53), we can see for steady-state conditions, that  $Q$  is constant. For a length  $L$ , we have

$$Q = h_i(2\pi r_1 L)(T_1 - T_2) = \frac{2\pi k_i L}{\ln(r_1/r_2)} (T_1 - T_2) = \frac{2\pi k_i L}{\ln(r_3/r_2)} (T_2 - T_3)$$

$$= h_0(2\pi r_3 L)(T_3 - T_0).$$



Again, the series concept is the most convenient method to relate the heat flow to the overall temperature drop:

$$Q = \frac{2\pi L(T_i - T_0)}{\frac{1}{h_i r_1} + \frac{\ln(r_2/r_1)}{2\pi L k_1} + \frac{\ln(r_3/r_2)}{2\pi L k_2} + \frac{1}{h_0 r_3}} \quad (9.16)$$

Note that the form of the thermal resistance attributed to the cylindrical wall differs from that of the slab. By comparing Eq. (9.16) to Eq. (9.11), we can contrast the thermal resistances as follows:

$$\text{Infinite slab: } R_i = \frac{L}{kA},$$

$$\text{Infinite cylinder: } R_i = \frac{\ln(r_2/r_1)}{2\pi L k}, \quad (9.17)$$

$$\text{Surface to fluid: } R_i = \frac{1}{A h_i}.$$

As an application of Eq. (9.16), consider the design of a single-wall tube furnace to operate at  $T_i$  internally while placed in some environment at  $T_0$ . The radial heat flow through the furnace wall is then given by Eq. (9.16) written for a tube composed of a single layer with conductivity  $k$ :

$$Q = \frac{2\pi L(T_i - T_0)}{\frac{1}{h_i r_1} + \frac{1}{k} \ln \frac{r_2}{r_1} + \frac{1}{h_0 r_2}} \quad (9.18)$$

If we examine Eq. (9.18), then we see that as  $r_2$  (the outer radius) increases, there is an increasing resistance to radial heat conduction as embodied in the  $1/k$  term. Simultaneously, however, as  $r_2$  increases, the outer cooling surface area increases as well. This dual effect suggests that there exists a particular outer radius for which the heat loss (or gain) is a maximum. To examine this proposed effect, fix  $r_1$ , and determine that particular value of  $r_2$  for which  $dQ/dr_2 = 0$ :

$$\frac{dQ}{dr_2} = \frac{-2\pi L(T_i - T_0)(1/k r_2 - 1/h_0 r_2^2)}{\left[ \frac{1}{h_i r_1} + \frac{1}{k} \ln \frac{r_2}{r_1} + \frac{1}{h_0 r_2} \right]^2} = 0.$$

From this, we obtain the critical outer radius

$$r_{2c} = k/h_0. \quad (9.19)$$

The existence of a critical radius shows that under some conditions, and contrary to common expectations, the heat loss through a tube furnace can actually be decreased by decreasing the insulating wall thickness.

Fig. 9.4 Steady-state temperature distribution in a composite cylindrical wall.

In this section, we consider conduction heat transfer in solids, in which the temperature varies not only with position in space, but also undergoes a continuous change with time at any position.

### 9.3.1 Newtonian heating or cooling

When a solid such as a flat plate, initially at a uniform temperature  $T_i$ , is cooled by a fluid at temperature  $T_f$ , the temperature distribution varies with time, as shown in Fig. 9.5(a). If the plate is thin (Fig. 9.5(b)), and/or its thermal conductivity high, then the temperature gradients within the plate are negligible, and we may consider the temperature only as a function of time. In the next section, we examine the conditions under which this criterion is met; we find that if  $hL/k \leq 0.1$ , then the analysis that follows is valid.

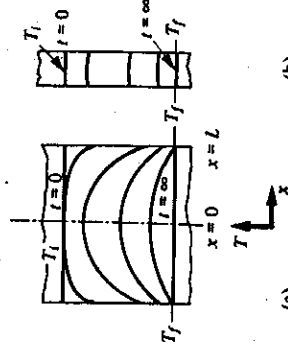


Fig. 9.5 Transient temperature distributions during cooling  
of (a) a thick plate, and (b) a thin plate.

For this situation, we equate the rate of heat lost by the plate to the rate of heat transfer to the fluid:

$$-V_p C_p \frac{dT}{dt} = hA(T - T_f), \quad (9.20)$$

where  $V$  = volume of the plate, and  $A$  = area of the plate exposed to the fluid. Rearranging for integration and taking  $T = T_i$  at  $t = 0$ , we have

$$\frac{T - T_f}{T_i - T_f} = \exp \left[ \frac{-hAt}{\rho C_p V} \right]. \quad (9.21)$$

The analysis applies only to the cases in which internal gradients are negligible. If this requirement is met, we speak of Newtonian cooling. Note that no geometric restrictions are imposed, since Eq. (9.21) just specifies  $A$  and  $V$ ; also note that the solution does not contain the conductivity.

The temperature history of such objects during cooling is illustrated in Fig. 9.6, which shows that for the same surface radius,  $R$ , or semithickness,  $L$ , the time it takes an infinite cylinder (or infinite square rod) to cool within 1% of thermal equilibrium with its surrounding fluid is almost 50% longer than for a sphere (or cube) of the same material. On the other hand, an infinite plate of the same material and semithickness equal to the cylinder radius requires 100% more time.

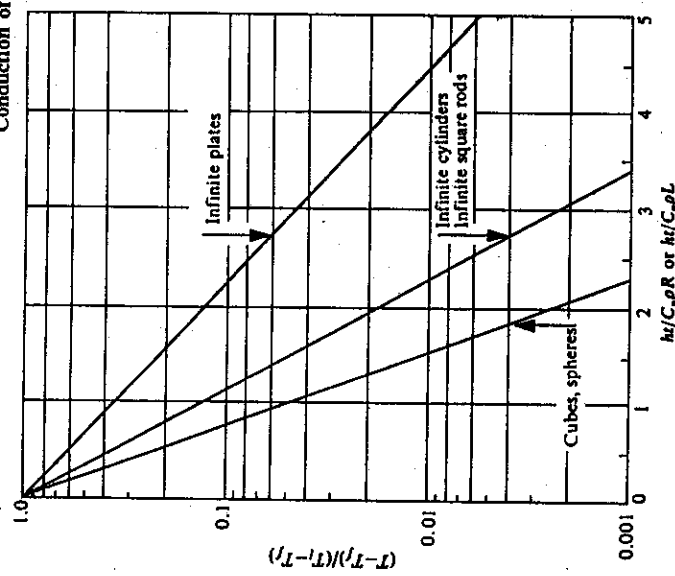


Fig. 9.6 Cooling (or heating) of bodies with negligible temperature gradients.  $R$  is radius, and  $L$  is semithickness.  
Example 9.2 A plate of aluminum alloy with dimensions 6 mm  $\times$  300 mm  $\times$  300 mm is solutionized at 810 K, and then quenched into water at 365 K. Over the temperature range 810–530 K, the heat transfer coefficient for quenching may be assumed constant as  $510 \text{ W m}^{-2} \text{ K}^{-1}$ . In the range 530–365 K, the heat transfer coefficient may be approximated as  $2550 \text{ W m}^{-2} \text{ K}^{-1}$ . a) Calculate the cooling rate during quenching at that instant when the plate is at 590 K. b) Repeat, when the plate is at 420 K. c) Determine the time it takes the plate to cool to 390 K. The properties of the aluminum are:  $k = 78 \text{ W m}^{-1} \text{ K}^{-1}$ ,  $C_p = 1000 \text{ J kg}^{-1} \text{ K}^{-1}$ ,  $\rho = 2880 \text{ kg m}^{-3}$ .

*Solution.* We can write an expression for the cooling rate by simply rearranging Eq. (9.20):

$$\frac{dT}{dt} = -\frac{h}{\rho C_p} \frac{A}{V} (T - T_f).$$

For a plate or slab whose thickness is much less than its width and length,  $A/V$  may be assumed equal to  $A/V$  for an infinite plate. Therefore

$$\frac{A}{V} = \frac{1}{L} = \frac{1}{0.003 \text{ m}} = 333.3 \text{ m}^{-1}.$$

a)	$\frac{dT}{dt} = -\frac{510 \text{ W}}{\text{m}^2 \text{ K}} \frac{333.3 \text{ m}^3}{\text{m}} \frac{\text{kg K}}{2880 \text{ kg}} \frac{(590 - 365) \text{ K}}{1000 \text{ J}} \frac{1 \text{ J}}{1 \text{ W s}}$
----	---

$$\frac{dT}{dt} = -13.3 \text{ K s}^{-1} \text{ at } 590 \text{ K.}$$

$$\text{b) } \frac{dT}{dt} = -\frac{(2550)(333.3)(420 - 365)}{(2880)(1000)} = -16.4 \text{ K s}^{-1} \text{ at } 420 \text{ K.}$$

- c) First we calculate time  $t_1$  to cool to 530 K. Use Eq. (9.21):

$$\frac{T - T_f}{T_i - T_f} = \exp \left[ -\frac{h}{\rho C_p} \frac{A}{V} t_1 \right],$$

and

$$\frac{\partial T}{\partial x} (\text{boundary}) \pm \frac{h}{k} T (\text{boundary}) = 0. \quad (9.26c)$$

Solving for  $t_1$ , we have  $t_1 = 16.81 \text{ s}$ . Second, we calculate time  $t_2$  to cool from 530 to 390 K; during this period  $T$ , is interpreted as 530 K.

$$\frac{390 - 365}{530 - 365} = \exp \left[ -\frac{(2550)(333.3)t_2}{(2880)(1000)} \right].$$

Solving for  $t_2$ , we get  $t_2 = 6.39 \text{ s}$ . Therefore, total time to cool to 390 K is  $t = t_1 + t_2 = 23.2 \text{ s}$ . The reader is assured that the assumption that the internal temperature gradients are non-existent, as applied to this particular example, is valid.

### 9.3.2 Bodies with internal temperature gradients

For the flat plate of Fig. 9.5(a), the applicable differential equation by reference to Eq. (9.2)

$$\frac{\partial T}{\partial t} = \alpha \frac{\partial^2 T}{\partial x^2}. \quad (9.22)$$

We find the solution  $T(x,t)$  of this equation for the boundary conditions

$$T(x,0) = T_i \quad (\text{uniform}), \quad (9.23)$$

$$\frac{\partial T(0,t)}{\partial x} = 0, \quad (9.24)$$

$$\frac{\partial T(L,t)}{\partial x} + \frac{h}{k} [T(L,t) - T_f] = 0, \quad (9.25)$$

by employing the method of separation of variables.

The boundary condition in time (Eq. (9.23)) is usually referred to as the initial condition. For this case, the initial condition is a uniform temperature; we could, however, consider some arbitrary temperature distribution,  $f(x)$ , existing at time zero. Equation (9.24) results from the symmetry of the problem, and we develop the final boundary condition (Eq. (9.25)) by equating the heat flux at the surface to the rate of heat transfer to the fluid. Before proceeding, we give some attention to the boundary conditions.

When applying the method of separation of variables, there are three basic types of boundary conditions that can be treated analytically. They are:

$$T(\text{boundary}) = 0, \quad (9.26a)$$

$$\frac{\partial T}{\partial x} (\text{boundary}) = 0, \quad (9.26b)$$

$$\frac{\partial T}{\partial x} (\text{boundary}) \pm \frac{h}{k} T (\text{boundary}) = 0. \quad (9.26c)$$

Comparing Eqs. (9.24) and (9.25) to Eqs. (9.26b) and (9.26c), respectively, we see that we must make a modification because  $T_f$  is not necessarily zero. The modification, however, is easily recognized; specifically, let  $\theta = T - T_f$ , so that the differential equation and boundary conditions become

$$\frac{\partial \theta}{\partial t} = \alpha \frac{\partial^2 \theta}{\partial x^2}, \quad (9.27)$$

$$\theta(x,0) = T_i - T_f = \theta_i, \quad (9.28)$$

$$\frac{\partial \theta}{\partial x}(0,t) = 0, \quad (9.29)$$

$$\frac{\partial \theta(L,t)}{\partial x} + \frac{h}{k} \theta(L,t) = 0. \quad (9.30)$$

The method of separation of variables consists of seeking a product solution of the form,

$$\theta(x,t) = X(x)G(t). \text{ Then Eq. (9.27) becomes} \quad (9.31)$$

$$\frac{1}{X} \frac{d^2 X}{dx^2} = \frac{1}{\alpha G} \frac{dG}{dt} = -\lambda^2,$$

from which

$$\frac{d^2 X}{dx^2} + \lambda^2 X = 0, \quad (9.32)$$

and

$$\frac{dG}{dt} + \alpha \lambda^2 G = 0. \quad (9.33)$$

We write the solution for Eq. (9.32)

$$X = c_1 \cos \lambda x + c_2 \sin \lambda x, \quad (9.34)$$

---

$\lambda^2$  is called the separation constant. Consider the possibilities of using either  $+\lambda^2$  or  $\lambda = 0$  in Eq. (9.31).

and for Eq. (9.33), the solution is

$$G = \exp(-\lambda^2 \alpha t). \quad (9.35)$$

Boundary condition (9.29) requires that  $c_2 = 0$ , and Eq. (9.30) can be shown to require that

$$\cot \lambda_n L = \frac{1}{(h/k)L} (\lambda_n L), \quad (9.36)$$

where  $\lambda_n$  takes on an infinite number of eigenvalues. Figure 9.7 indicates this for the first three eigenvalues.

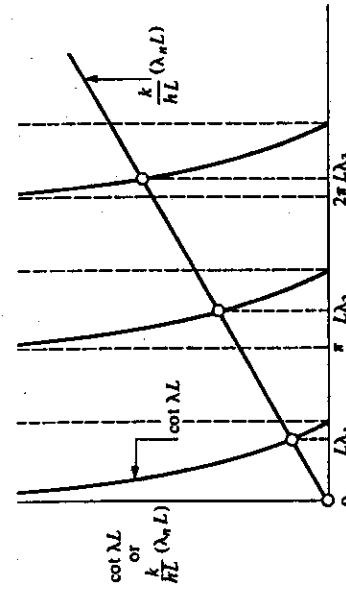


Fig. 9.7 Solutions of  $\lambda_n$  roots of Eq. (9.36).

Taking the product of Eqs. (9.34) and (9.35) with  $c_2 = 0$ , and realizing that all values of  $\lambda_n$  satisfying Eq. (9.36) are suitable, we have

$$\theta = \sum_{n=1}^{\infty} A_n \exp(-\lambda_n^2 \alpha t) \cos \lambda_n x, \quad (9.37)$$

where the  $A_n$ s have absorbed the constants involved. The initial condition (9.28) still remains to be satisfied. When Eq. (9.28) is substituted into Eq. (9.37), we get

$$\theta_i = \sum_{n=1}^{\infty} A_n \cos \lambda_n x. \quad (9.38)$$

Multiplying both sides of this equation by  $\cos \lambda_m x dx$ , and integrating from  $x = 0$  to  $x = L$ , we obtain

$$\theta_i \int_0^L \cos \lambda_n x dx = \int_0^L \sum_{n=1}^{\infty} A_n \cos \lambda_n x \cos \lambda_m x dx. \quad (9.39)$$

When  $m \neq n$ , all integrals on the right-hand side of Eq. (9.39) are zero, and when  $m = n$  the integral has the nonzero value

$$A_n \left[ \frac{L}{2} + \frac{1}{2\lambda_n} \sin \lambda_n L \cos \lambda_n L \right].$$

The integral on the left-hand side of Eq. (9.39) is  $(1/\lambda_n) \sin \lambda_n L$ . Therefore

$$A_n = \frac{2\theta_i \sin \lambda_n L}{\lambda_n L + \sin \lambda_n L \cos \lambda_n L}. \quad (9.40)$$

The final solution is then

$$\frac{\theta}{\theta_i} = \frac{T - T_f}{T_i - T_f} = 2 \sum_{n=1}^{\infty} \frac{\sin \lambda_n L}{\lambda_n L + \sin \lambda_n L \cos \lambda_n L} \exp(-\lambda_n^2 \alpha t) \cos(\lambda_n x), \quad (9.41)$$

where the  $\lambda_n$ s are the roots of Eq. (9.36), given in Table 9.1.

Table 9.1 The first four roots of Eq. (9.36)\*

Bi	$k/hL$	$\lambda_1 L$	$\lambda_2 L$	$\lambda_3 L$	$\lambda_4 L$
100	0.01	1.5552	4.6658	7.7764	10.8871
10	0.10	1.4289	4.3058	7.2281	10.2003
1	1.0	0.8603	3.4256	6.4373	9.5293
0.1	10.0	0.3111	3.1731	6.2991	9.4354

\*A more comprehensive table can be found in H. S. Carslaw and J. C. Jaeger, *Conduction of Heat in Solids*, second edition, Oxford University Press, Oxford, UK, 1959, page 491.

Evaluations of Eq. (9.41) and the analogous solutions for infinitely long cylinders and spheres have been presented in many graphical forms for practical use. They are in terms of a relative temperature as a function of the Fourier number, Biot number, and relative position. These four dimensionless variables are defined as follows:

1. relative temperature  $= \frac{T - T_f}{T_i - T_f}$ ,
2. Fourier number (Fo)  $= \frac{\alpha t}{L^2} = \frac{k t}{\rho C L^2}$ ,
3. Biot number (Bi)  $= \frac{hL}{k}$ ,
4. relative position  $= \frac{x}{L}$ .

For plates,  $L$  is the semithickness, and  $x$  is the distance from the center. For cylinders and spheres, the radius  $R$  replaces  $L$ , and  $r$  replaces  $x$  in the above definitions. Among the earliest graphs prepared were the so-called Gurney-Lurie charts.<sup>1</sup> These charts are still referred to in engineering. However, the charts are limited to a small range of Fo and Bi values. Other diagrams commonly used are the Heisler charts<sup>2</sup> for  $0.01 \leq Bi < \infty$  and  $Fo > 0.2$ . For more convenience, Figs. 9.8, 9.9 and 9.10 have been constructed for the temperature response of infinite plates, infinite cylinders, and spheres, respectively.

<sup>1</sup>H. P. Gurney and J. Lurie, *Ind. Eng. Chem.* 15, 1170-1172 (1923).

<sup>2</sup>M. P. Heisler, *Trans ASME* 69, 227-236 (1947).

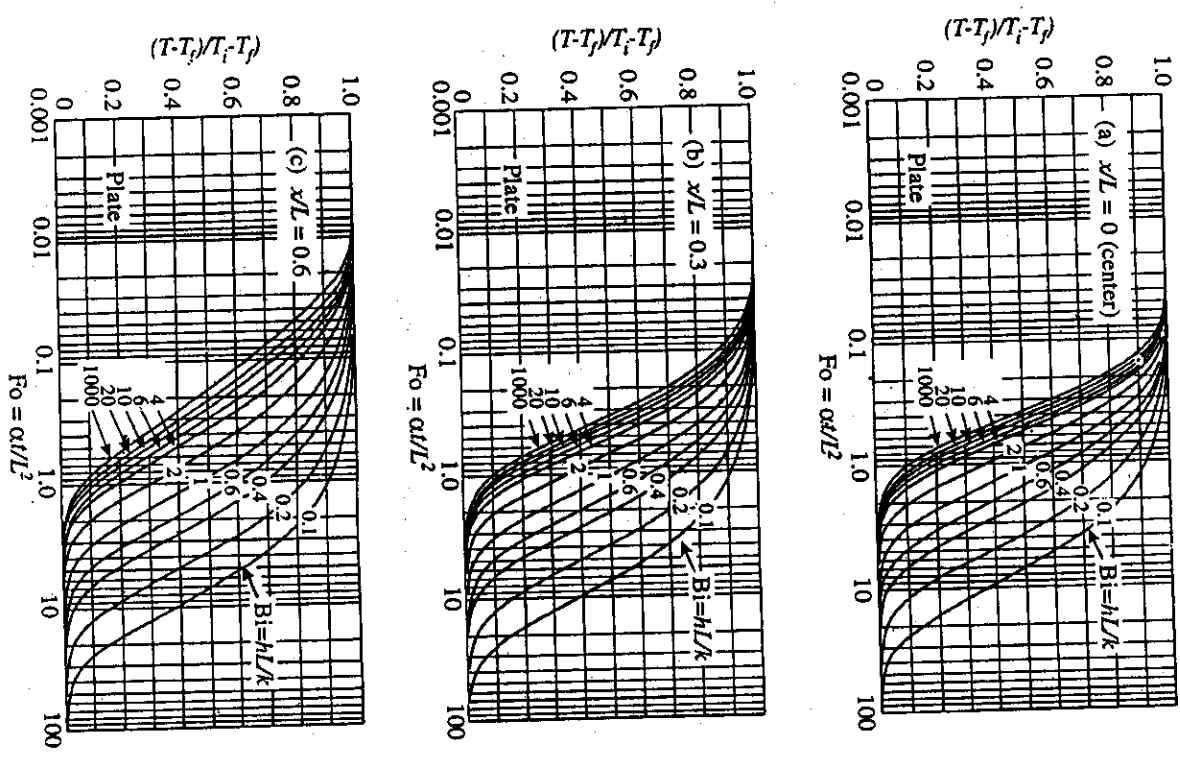


Fig. 9.8 Temperature response of an infinite plate initially at a uniform temperature  $T_i$ , and then subjected to a convective environment at  $T_f$ .

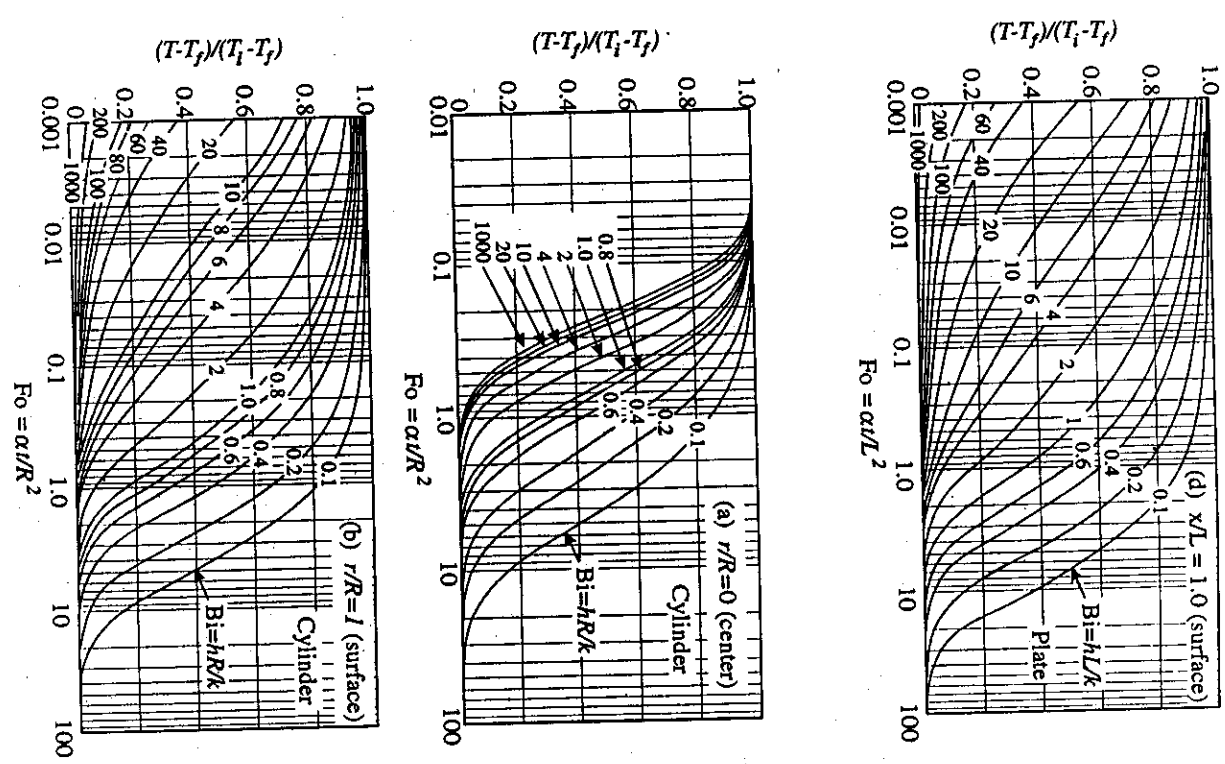


Fig. 9.9 Temperature response of an infinite cylinder initially at a uniform temperature  $T_i$ , and then subjected to a convective environment at  $T_f$ .

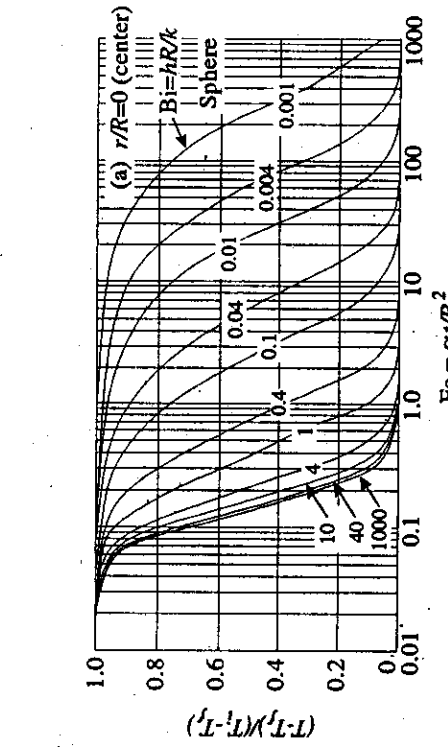


Fig. 9.10 (continued)

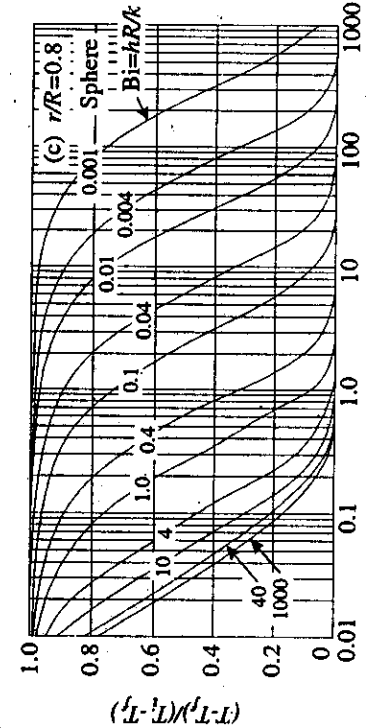
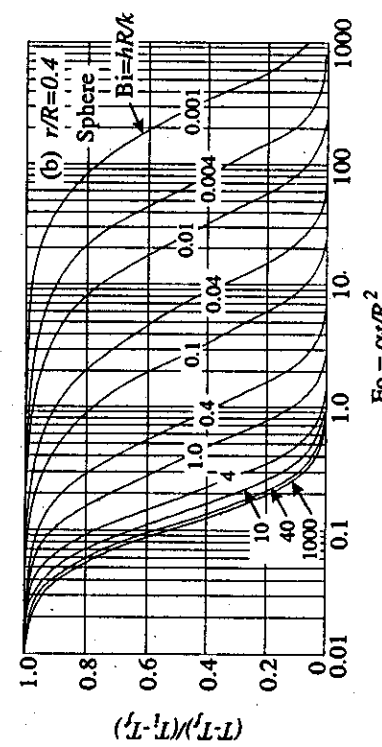
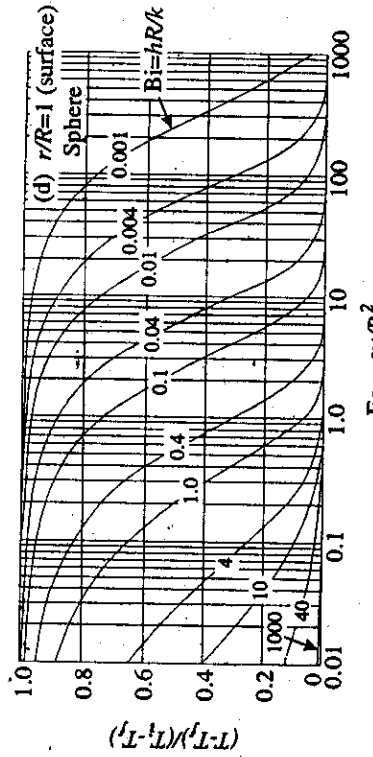
Fig. 9.10 Temperature response of a sphere initially at a uniform temperature  $T_i$ , and then subjected to a convective environment at  $T_f$ .

Fig. 9.10 (continued)

**Example 9.3** As an example of the use of Fig. 9.9, consider a very long cylindrical stainless steel bar, 1.27 mm in diameter, which is heated to 478 K uniformly across its diameter. The bar is then cooled in a blast of fan forced air at 300 K with  $h = 142 \text{ W m}^{-2} \text{ K}^{-1}$ . a) Find the time it takes for the center to reach 310 K. b) When the center reaches 310 K, what is the surface temperature? c) What would be the minimum possible time for the center of the bar to reach 310 K if it were cooled in an ideal quenchant ( $H = \infty$ ) at 300 K. The thermal properties of the stainless steel are  $k = 16 \text{ W m}^{-1} \text{ K}^{-1}$  and  $\alpha = 4.08 \times 10^{-6} \text{ m}^2 \text{ s}^{-1}$ .

*Solution.*

a) When  $T = 310 \text{ K}$  at the center, we have

$$\frac{T - T_f}{T_i - T_f} = \frac{310 - 300}{478 - 300} = 0.056.$$

Also

$$\text{Bi} = \frac{hR}{k} = \frac{(142)(0.0635)}{(16)} = 0.563.$$

From Fig. 9.9(a),  $\alpha t/R^2 = 3.2$ . Then

$$t = \frac{(3.2)(0.0635)^2}{4.08 \times 10^{-6}} = 3.16 \times 10^3 \text{ s}.$$

b) For the surface temperature, we refer to Fig. 9.9(b). When  $Fo = 3.2$  and  $\text{Bi} = 0.563$ , we find that

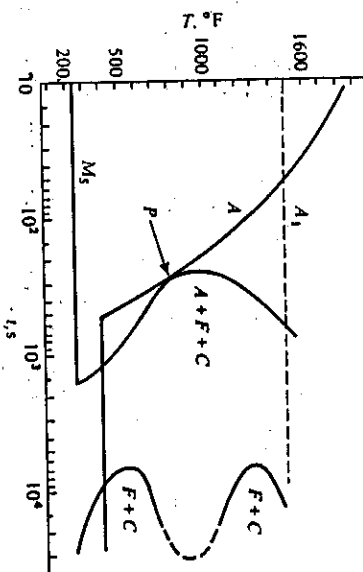
$$\frac{T - T_f}{T_i - T_f} \approx 0.040.$$

Therefore,  $T = 0.040(478 - 300) + 300 = 303 \text{ K}$ .

- c) The minimum possible time would correspond to the situation in which the surface temperature is equal to the temperature of the cooling medium; that is,  $Bi \rightarrow \infty$ . It is sufficient to use Fig. 9.9(a) with  $Bi = 1000$ . Thus,  $\alpha t/R^2 = 0.60$ , and

$$t = \frac{(0.60)(0.0635)^2}{4.08 \times 10^{-6}} = 593 \text{ s.}$$

**Example 9.4** The process of austempering requires that a steel be quenched to just above its  $M_s$  temperature, and then isothermally transformed to a lower bainite structure that resembles tempered martensite. For a steel with the continuous cooling diagram below, estimate the maximum thickness of plate that can be completely austempered by quenching into molten salt at  $400^\circ\text{F}$  from a  $1600^\circ\text{F}$  austenitizing temperature with  $h = 50 \text{ Btu h}^{-1} \text{ ft}^{-2} \text{ }^\circ\text{F}^{-1}$ . For the steel, assume  $\alpha = 0.46 \text{ ft}^2 \text{ h}^{-1}$  and  $k = 20 \text{ Btu h}^{-1} \text{ ft}^{-1} \text{ }^\circ\text{F}^{-1}$ . English units are commonly used in the metal processing industry in the U.S.A., so let's work this example with them.



**Solution.** Since we must cool at such a rate as to bring the center of the plate past the "nose" of the curve without undergoing any transformation, we start by assuming that point  $P$  is the critical point. Since point  $P$  is at  $800^\circ\text{F}$ , then

$$\frac{T - T_f}{T_i - T_f} = \frac{800 - 400}{1600 - 400} = 0.333.$$

Figure 9.8(a) is used for the calculation. What is needed is the value of the semithickness  $L$  that will result in agreement among  $Bi$ ,  $Fo$ , and reduced temperature. Point  $P$  is at  $t_c \approx 400 \text{ s}$ , or  $0.111 \text{ hr}$ , then

$$Fo = (0.46)(0.111)/L^2 = 0.0511/L^2$$

and

$$Bi = \frac{50}{20} L = 2.5L,$$

with  $L$  in ft.

Try  $L = 0.1 \text{ ft}$ . In this case,  $Bi = 0.25$  and, from Fig. 9.8(a),  $Fo$  should be 5.3. However, with  $L = 0.1 \text{ ft}$ ,  $Fo = 5.11$ , so that this value of  $L$  does not satisfy  $Fo$  and  $Bi$  simultaneously.

Try  $L = 0.05 \text{ ft}$ . Now  $Bi = 0.125$ , and  $Fo$  from Fig. 9.8(a) is 10. With  $L = 0.05 \text{ ft}$ ,  $Fo$  is calculated as 20.4.

We have bracketed the actual value, and after more trial and error, the value of  $L = 0.095 \text{ ft}$  leads to agreement between  $Bi = 0.24$  and  $Fo = 5.6$ . Thus we can say that a plate 2.28 in. thick can be fully austempered.

It is important to indicate when limiting cases are valid, such as Newtonian cooling. This, of course, simplifies our work, as Fig. 9.11 demonstrates.

Figure 9.11 presents the solution for the infinite plate in the form of temperature distributions for different times during cooling in media of various Biot numbers. Examination of Fig. 9.11 shows that the temperature gradients within the slab decrease as  $Bi$  decreases. A low value of  $Bi$ , physically interpreted, reflects low resistance to heat flow

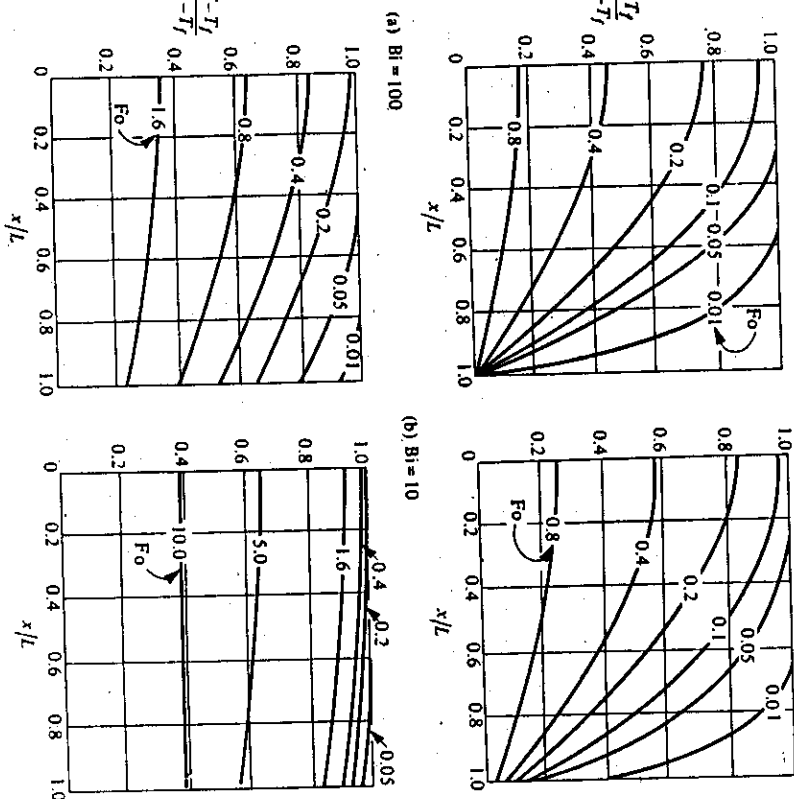


Fig. 9.11 Temperature profiles for infinite plates when cooled under conditions of various Biot numbers.

Table 9.2 Coefficients for the first two terms in Eq. (9.41).

Bi	$\lambda L$	$\lambda L$	$\xi_1$	$\xi_2$
0.01	0.0998	3.1448	0.5008	-0.001019
0.02	0.1410	3.1479	0.5017	-0.002000
0.04	0.1987	3.1543	0.5033	-0.004012
0.06	0.2425	3.1606	0.5049	-0.005978
0.08	0.2791	3.1668	0.5065	-0.007862
0.1	0.3111	3.1731	0.5080	-0.009830
0.2	0.4328	3.2039	0.5155	-0.01906
0.4	0.5932	3.2636	0.5290	-0.03596
0.6	0.7051	3.3204	0.5407	-0.05088
0.8	0.7910	3.3744	0.5508	-0.06411
1.0	0.8603	3.4256	0.5596	-0.07584
1.5	0.9882	3.5422	0.5768	-0.09996
2.0	1.0769	3.6436	0.5892	-0.1184
4.0	1.2646	3.9352	0.6144	-0.1607
6.0	1.3496	4.1116	0.6239	-0.1802
8.0	1.3978	4.2264	0.6285	-0.1906
10.0	1.4289	4.3058	0.6310	-0.1967
15	1.4729	4.4255	0.6338	-0.2042
20	1.4961	4.4915	0.6350	-0.2074
40	1.5325	4.5979	0.6362	-0.2109
60	1.5451	4.6353	0.6364	-0.2116
80	1.5514	4.6543	0.6365	-0.2119
100	1.5552	4.6658	0.6365	-0.2120
$\infty$	1.5708	4.7124	0.6366	-0.2122

Examination of Fig. 9.11 shows that the criterion,  $T(L,t) = T_f$ , is closely approximated when  $Bi = 100$ . Thus when  $Bi \geq 100$ , Eq. (9.41) can be very closely approximated by Eq. (9.42).

### 9.3.3 Long-time and short-time solutions

The solutions to many problems of unsteady-state heat conduction are in the form of infinite series, such as Eqs. (9.41) and (9.42). This type of series converges rapidly for large Fourier numbers. For short times (small  $at/L^2$ ), however, the convergence is very slow, requiring an expansion of a great number of terms in the series to obtain sufficiently accurate answers. If we require a solution for short times, alternative series that evolve by the method of Laplace transforms when solving Eq. (9.22) are more convenient. These alternative series have the advantage of converging rapidly for small  $at/L^2$ , but the disadvantage of converging very slowly for large  $at/L^2$ . Thus the two kinds of solutions complement each other, depending on what value of  $at/L^2$  is of interest. These considerations are important when we wish to use the actual equations, rather than the graphical solutions, as might be the case in computer programming, for example.

If we desire a long-time solution, rather than the complete series of Eq. (9.41), it is convenient to use only the first one or two terms of the series. For this case, we write

$$\frac{T - T_f}{T_i - T_f} = 2 \sum_{n=1}^2 \xi_n \exp[-(\lambda_n L)^2 F_0] \cos \left[ (\lambda_n L) \left[ \frac{x}{L} \right] \right]. \quad (9.43)$$

Here

$$\xi_n = \frac{\sin(\lambda_n L)}{\lambda_n L + \sin(\lambda_n L) \cos(\lambda_n L)}.$$

The value of  $\lambda_n L$  depends on the value of the index  $n$  and the Biot number; hence  $\xi_n$  is also a function of the same. Values of  $(\lambda_n L)$  and  $\xi_n$  for  $n = 1$  and  $n = 2$  are given in Table 9.2.

$$\begin{aligned} a) \quad Bi &= \frac{\hbar L}{k} = \frac{(11,000)(0.050)}{78} = 7.05. \\ b) \quad Fo &= \frac{at}{L^2} = \frac{(2.71 \times 10^{-5})(30)}{(0.050)^2} = 0.325. \end{aligned}$$

The first two terms in the infinite series are probably adequate because  $Fo > 0.25$ . From Table 9.2,  $\lambda L = 1.375$ ,  $\xi_1 = 0.6263$  and  $\lambda_2 L = 4.1719$ ,  $\xi_2 = -0.1856$ . Substituting values into Eq. (9.43) with  $x/L = 0$ :

$$\frac{T - T_f}{T_i - T_f} = 2 \left\{ 0.6263 \exp \left[ -(1.375^2)(0.325) \right] - 0.1856 \exp \left[ -(4.1719^2)(0.325) \right] \right\}$$

$$\frac{T - T_f}{T_i - T_f} = 2 \left\{ 0.3388 - 0.00064 \right\}.$$

The absolute value of the first term is much larger than the second; this indicates that Eq. (9.41) is converging rapidly, and therefore a good answer results by the use of Eq. (9.43). Solving, we have

$$\frac{T - T_f}{T_i - T_f} = 0.6764,$$

and

$$T = 0.6764(800 - 300) + 300 = 638 \text{ K}.$$

- b) By reading Fig. 9.8(a), the result is

$$\frac{T - T_f}{T_i - T_f} = 0.68,$$

which is very close to the result by calculation. This difference would have been smaller if we had considered longer times, but would have been larger for shorter times. Usually, Eq. (9.43) suffices for problems of this type if  $Fo > 0.25$ ; it is wise, however, to compare results with those obtained by using Figs. 9.8-9.10.

When the long-time solution is not appropriate, we may utilize the alternative series mentioned above. Here we only present the first several terms of the series without going through the analysis of solving the differential equation. We may deduce the following expression from an equation given by Carslaw and Jaeger<sup>3</sup>

$$\frac{T - T_f}{T_i - T_f} = 1 - \left[ \operatorname{erfc} \frac{(1 - x/L)}{2\sqrt{Fo}} + \operatorname{erfc} \frac{(1 + x/L)}{2\sqrt{Fo}} \right] \\ + \exp [Bi(1 - x/L) + Bi^2 Fo] \cdot \operatorname{erfc} \left[ Bi\sqrt{Fo} + \frac{1 - x/L}{2\sqrt{Fo}} \right] \\ + \exp [Bi(1 + x/L) + Bi^2 Fo] \cdot \operatorname{erfc} \left[ Bi\sqrt{Fo} + \frac{1 + x/L}{2\sqrt{Fo}} \right]. \quad (9.44)$$

Equation (9.44) contains the *complementary error function*,  $\operatorname{erfc}$ . The  $\operatorname{erfc} N$  is related to the  $\operatorname{erf} N$  (the error function) simply by

$$\operatorname{erfc} N = 1 - \operatorname{erf} N.$$

and the  $\operatorname{erf} N$  is defined as the value of a definite integral. The definite integral is

$$\operatorname{erf} N = \frac{2}{\sqrt{\pi}} \int_0^N e^{-\beta^2} d\beta.$$

The error function is commonly encountered, and hence it has been tabulated. An abbreviated compilation is given in Table 9.3.

Table 9.3 Tabulation of the error function

$N$	$\operatorname{erf} N$						
0.00	0.00000	0.40	0.4284	0.80	0.7421	1.40	0.9523
0.05	0.05637	0.45	0.4755	0.85	0.7707	1.50	0.9661
0.10	0.1125	0.50	0.5205	0.90	0.7969	1.60	0.9763
0.15	0.1680	0.55	0.5633	0.95	0.8209	1.70	0.9838
0.20	0.2227	0.60	0.6039	1.00	0.8427	1.80	0.9891
0.25	0.2763	0.65	0.6420	1.10	0.8802	1.90	0.9928
0.30	0.3286	0.70	0.6778	1.20	0.9103	2.00	0.9953
0.35	0.3794	0.75	0.7112	1.30	0.9340		

#### Notes

- a)  $\operatorname{erf} 0 = 0$ ;  $\operatorname{erf} \infty = 1$ ,
- c)  $N > 2.0$ ,  $\operatorname{erfc} N \cong \frac{e^{-N^2}}{\sqrt{\pi}N}$ ,
- b)  $N < 0.2$ ,  $\operatorname{erf} N \cong \frac{2N}{\sqrt{\pi}}$ ,
- d)  $\operatorname{erf} (-N) = -\operatorname{erf} (N)$ .

As the reader probably suspects, long-time and short-time solutions are also available for cylinders and spheres. These solutions can be deduced by reference to Carslaw and Jaeger.<sup>4</sup>

In materials processing, the rates of heating and/or cooling are often more important than the determination of the temperature itself. For cases where Newtonian cooling applies, the determination of cooling rates is not too difficult; we discussed this in Section 9.3.1, and illustrated it in Example 9.2. However, when Newtonian cooling does not apply, it is necessary to resort to other means. If analytical expressions are desired, then solutions such as those discussed in Section 9.3.2 and this section may be used to determine  $\partial T/\partial t$ . If approximate and graphical solutions are needed, then charts given by Paschakis<sup>5</sup> may be consulted. Surprisingly enough, cooling or heating rates at the surfaces of cylinders and spheres are only 3-4% higher than for plates, when the cooling rates are compared at the same Fourier number. In the internal positions, however, the cooling or heating rates of plates, cylinders and spheres do differ greatly.

**Example 9.6** Continuous anneal and continuous quench and temper processes for steel have been installed worldwide over the last decade. In order to achieve the same properties in the commercial product as in the laboratory, the cooling rates in a continuous line must be the same as for the specimens processed in the laboratory. This scale-up is not always understood by materials engineers who are accustomed to working with very thin specimens in the laboratory. Consider a steel that must be cooled from austenitizing temperature (1200 K) to 810 K at an average cooling rate of 3600 K s<sup>-1</sup> to achieve the required microstructure. Various thicknesses in the range of 1.0 mm to 2.0 mm are to be processed. Determine whether the desired cooling rate can be achieved throughout the thicknesses if the quenchant has a heat transfer coefficient of  $3 \times 10^5 \text{ W m}^{-2} \text{ K}^{-1}$ . In order to obtain the necessary production rate in the process, the strip must be in the quenchant (at 285 K) for no more than 0.5 s, and the strip should be no hotter than 400 K when it leaves the quench tank.

H. S. Carslaw and J. C. Jaeger, *Conduction of Heat in Solids*, second edition, Oxford University Press, Oxford, UK, 1959, page 310.

V. Paschakis, *Welding Research Supplement*, Sept. 1946, pages 497-502.

**Solution.** The thermal properties are  $C_p = 600 \text{ J kg}^{-1} \text{ K}^{-1}$ ,  $k = 21.5 \text{ W m}^{-1} \text{ K}^{-1}$  and  $\rho = 7700 \text{ kg m}^{-3}$ . For the thinner section, we calculate the Biot number.

$$\text{Bi} = \frac{hL}{k} = \frac{(3 \times 10^4)(0.5 \times 10^{-3})}{(21.5)} = 0.698.$$

We refer to Fig. 9.8(a) to determine the Fo and the time to achieve 810 K.

$$\frac{T - T_f}{T_i - T_f} = \frac{810 - 285}{1200 - 285} = 0.574.$$

This gives  $\text{Fo} = 1.2$ , which happens at

$$t = \frac{L^2 \text{Fo}}{\alpha} = \frac{\rho C_p L^2 \text{Fo}}{k} = \frac{(7700)(600)(0.5 \times 10^{-3})^2(1.2)}{(21.5)} = 6.45 \times 10^{-2} \text{ s},$$

so the average cooling rate from 1200 to 810 K is

$$\frac{\Delta T}{\Delta t} = \frac{1200 - 810}{6.45 \times 10^{-2}} = 6050 \text{ K s}^{-1}.$$

We should also estimate the time required to cool the strip to 400 K.

$$\frac{T - T_f}{T_i - T_f} = \frac{400 - 285}{1200 - 285} = 0.126.$$

This corresponds to  $\text{Fo} = 4$ , which happens at  $t = 0.215 \text{ s}$ . Therefore, strip of 1 mm thickness can be successfully processed.

We now repeat the calculations for the thicker strip.

$$\text{Bi} = \frac{(3 \times 10^4)(1 \times 10^{-3})}{(21.5)} = 1.40.$$

$$\frac{T - T_f}{T_i - T_f} = 0.574.$$

From Fig. 9.8(a),  $\text{Fo} = 0.75$  and

$$t = \frac{(7700)(600)(1 \times 10^{-3})^2(0.75)}{(21.5)} = 0.161 \text{ s}.$$

Therefore, the average cooling rate to cool from 1200 to 810 K is

$$\frac{\Delta T}{\Delta t} = \frac{1200 - 810}{0.161} = 2.42 \times 10^3 \text{ K s}^{-1},$$

which is much less than the specified cooling rate of  $3600 \text{ K s}^{-1}$ . The thicker strip cannot be quenched rapidly enough in this process.

#### 9.4 TRANSIENT CONDITIONS, INFINITE AND SEMI-INFINITE SOLIDS

In Section 9.3, all the solids we considered had at least one dimension of finite extent. In this section, we consider the so-called infinite and semi-infinite solids. The solutions for the

semi-infinite solids can be applied when the time involved in transient situations is very short, or during the time of interest the depth of material affected by the boundary condition is less than the thickness of material itself. There are many applications of these solutions, such as heat transfer in certain solidification problems, and also in diffusion problems which are discussed in Part III, Mass Transport. We start by looking at a stationary source in an infinite solid. A moving source with steady power will be considered in Section 9.6; this has application in materials processes such as laser heating and welding.

##### 9.4.1 Infinite solid

Consider the infinite solid in Fig. 9.12(a) where at time zero a thin slice of material  $\Delta x'$  thick at  $x = x'$  is at some temperature  $T_i$ . This temperature peak decays with time, as shown in Fig. 9.12(b). Again for transient heat conduction, Eq. (9.22) applies, and the solution is

$$T(x,t) = \frac{T_i}{2\sqrt{\pi\alpha t}} \exp \left[ -\frac{(x - x')^2}{4\alpha t} \right] \Delta x'. \quad (9.45)$$

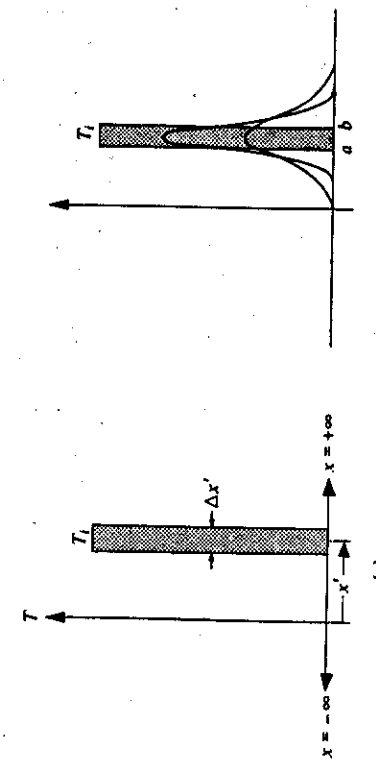


Fig. 9.12 Temperature distribution in an infinite solid showing (a) an initial temperature peak, and (b) the decay of the peak with time.

If another slice of the same thickness exists at time zero with a different temperature  $T_{i'}$ , then the temperature at  $x$  and  $t$  is the sum of contributions from both peaks. For this case then, Eq. (9.45) is applied to the peaks at  $x'_i$  and  $x'_{i'}$  and the temperature is

$$T(x,t) = \sum_{i=1}^2 \frac{T_{i'}}{2\sqrt{\pi\alpha t}} \exp \left[ -\frac{(x - x'_{i'})^2}{4\alpha t} \right] \Delta x'. \quad (9.46)$$

Now think of many such slices side by side occupying the whole space. If the thicknesses of the individual slices are allowed to approach zero, then all the various  $T_{i'} \Delta x'$  can be considered to form a function  $f(x')$ . In this case, examine the series in the limit as the slices all approach zero thickness

$$T(x,t) = \lim_{\Delta x' \rightarrow 0} \sum_{i=1}^{\infty} \frac{f(x')}{2\sqrt{\pi\alpha t}} \exp \left[ -\frac{(x - x')^2}{4\alpha t} \right] \Delta x'. \quad (9.47)$$

As  $\Delta x' \rightarrow 0$ , the infinite summation becomes an integral

$$T(x,t) = \int_{x'-\infty}^x \frac{f(x')}{2\sqrt{\pi\alpha t}} \exp \left[ -\frac{(x-x')^2}{4\alpha t} \right] dx'. \quad (9.48)$$

As an example consider an initial distribution (Fig. 9.13). For this case, we develop the solution by recognizing that  $f(x') = 0$  for all  $x'$  except  $a < x' < b$  where  $f(x') = T_i$ . Substituting this information into Eq. (9.48) yields

$$T = \int_{-\infty}^0 0 dx + \int_a^b \frac{T_i}{2\sqrt{\pi\alpha t}} \exp \left[ -\frac{(x-x')^2}{4\alpha t} \right] dx' + \int_b^{\infty} 0 dx. \quad (9.49)$$

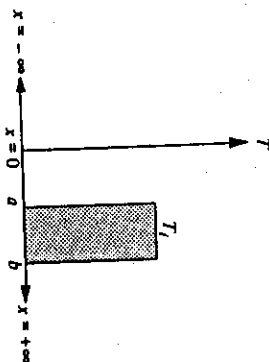


Fig. 9.13 The initial distribution of uniform temperature  $T_i$  between  $x = a$  and  $x = b$ .

Let  $\beta = (x' - x)/2\sqrt{\alpha t}$ ; this transforms Eq. (9.49) into

$$T = \frac{T_i}{\sqrt{\pi}} \int_{(b-x)/2\sqrt{\alpha t}}^{(a-x)/2\sqrt{\alpha t}} e^{-\beta^2} d\beta = \frac{T_i}{2} \left[ \frac{2}{\sqrt{\pi}} \int_0^{(b-x)/2\sqrt{\alpha t}} e^{-\beta^2} d\beta - \frac{2}{\sqrt{\pi}} \int_0^{(a-x)/2\sqrt{\alpha t}} e^{-\beta^2} d\beta \right]. \quad (9.50)$$

Therefore we write Eq. (9.50) as

$$T = \frac{T_i}{2} \left[ \operatorname{erf} \left[ \frac{b-x}{2\sqrt{\alpha t}} \right] - \operatorname{erf} \left[ \frac{a-x}{2\sqrt{\alpha t}} \right] \right]. \quad (9.51)$$

#### 9.4.2 Semi-infinite solid

A semi-infinite solid has an extent of  $0 \leq x < \infty$ , that is, a very thick solid with a surface at  $x = 0$ . At this surface the transient is put into effect. For example, we solve the problem with the following conditions for the region  $0 \leq x < \infty$ :

$$T(x,0) = f(x), \quad (9.52)$$

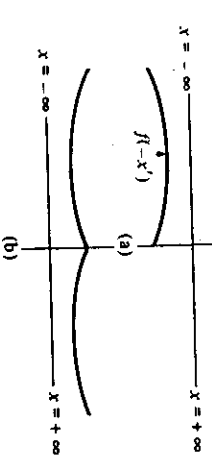


Fig. 9.14 Temperature distribution in infinite solids that satisfy boundary conditions for semi-infinite solids. (a) Odd function,  $T(0,t) = 0$ . (b) Even function,  $\partial T(0,t)/\partial x = 0$ .

The problem with the flux equal to zero at the surface is set up in a similar manner. For this case, the conditions for the region  $0 \leq x < \infty$  become

$$T(x,0) = f(x), \quad (9.55)$$

$$\frac{\partial T}{\partial x}(0,t) = 0. \quad (9.56)$$

We indicate the method of setting up this situation in Fig. 9.14(b), where an even function,  $f(x') = f(-x')$ , gives symmetry to the temperature field about  $x = 0$ , so that condition (9.56) is automatically satisfied. Thus we use Eq. (9.48) in the following form

$$T = \int_{-\infty}^0 \frac{f(-x')}{2\sqrt{\pi\alpha t}} \exp \left[ -\frac{(x-x')^2}{4\alpha t} \right] dx' + \int_0^{\infty} \frac{f(x')}{2\sqrt{\pi\alpha t}} \exp \left[ -\frac{(x-x')^2}{4\alpha t} \right] dx'. \quad (9.57)$$

Finally as an application of Eq. (9.54), consider the important and often encountered problem of the semi-infinite solid with the conditions

$$T(x,0) = T_i, \quad T(0,t) = 0. \quad (9.58)$$

This situation is depicted in Fig. 9.15. Initially the semi-infinite solid is at a uniform temperature  $T_i$ , and its surface is abruptly brought to a temperature that is maintained at  $T_s$ . Thus, we can think of the temperature field in the vicinity of the surface of a thick solid, even a solid with a finite thickness, provided certain conditions are met, as will be discussed.

We develop the solution to this problem by referring to an infinite solid with the initial condition depicted in Fig. 9.14(a). For the odd function where  $f(-x') = -f(x')$ , the boundary condition (9.53) is automatically satisfied; therefore we use Eq. (9.48) as follows to satisfy this boundary condition:

$$T = \int_{-\infty}^0 \frac{-f(-x')}{2\sqrt{\pi\alpha t}} \exp \left[ -\frac{(x-x')^2}{4\alpha t} \right] dx' + \int_0^{\infty} \frac{f(x')}{2\sqrt{\pi\alpha t}} \exp \left[ -\frac{(x-x')^2}{4\alpha t} \right] dx'. \quad (9.54)$$

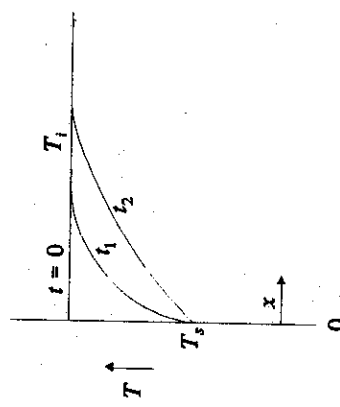


Fig. 9.15 Temperature in a semi-infinite solid with its surface temperature constant for  $t > 0$ .

If we define  $\theta = T - T_s$ , the conditions become

$$\theta(x, 0) = T_i - T_s = \theta_i \quad (9.60)$$

$$\theta(0, t) = 0. \quad (9.61)$$

Thus Eq. (9.54) applies for  $\theta$ , where  $f(x') = \theta_i$  (uniform initial distribution). Even so, after we look at Eq. (9.54) we might hesitate to use it because it involves integrating to  $x = \infty$ . This is done in Appendix F. Here, we give the final equation, which is

$$\frac{T - T_s}{T_i - T_s} = \operatorname{erf} \left[ \frac{x}{2\sqrt{\alpha t}} \right]. \quad (9.62)$$

To summarize, Eq. (9.62) describes the temperature as a function of position and time in a semi-infinite solid initially at a uniform temperature  $T_i$ , with its surface temperature suddenly raised or lowered to  $T_s$  at  $t = 0$  and maintained for  $t > 0$ . In practice, we consider a solid to be semi-infinite until such time as all of the solid differs appreciably from  $T_i$ .

Equation (9.62) is applied to many problems in materials processing. Another important problem of heat flow for a semi-infinite solid remains to be discussed. For the cooling (or heating) of slabs, Eq. (9.41) was developed; however, as mentioned previously, this equation is unwieldy for "short times." For short times we found that Eq. (9.44) was more appropriate. Here, we present a solution that is a slightly simplified version of Eq. (9.44), which applies for the very short times when the center of the slab has not yet felt the effects of the changing temperature field. For such a situation, we may consider the solid to be semi-infinite, and the following initial and boundary conditions must be satisfied:

$$T(x, 0) = T_i, \quad (9.63)$$

$$k \frac{\partial T(0, t)}{\partial x} = h [T(0, t) - T_s]. \quad (9.64)$$

We present only the final solution:

$$\frac{T - T_s}{T_i - T_s} = \operatorname{erfc} \left[ \frac{x}{2\sqrt{\alpha t}} \right] - e^r \operatorname{erfc} \left[ \frac{x}{2\sqrt{\alpha t}} + \frac{h}{k} \sqrt{\alpha t} \right], \quad (9.65)$$

where

$$\gamma = \frac{h}{k} \sqrt{\alpha t} \left[ \frac{x}{\sqrt{\alpha t}} + \frac{h}{k} \sqrt{\alpha t} \right].$$

The solution given by Eq. (9.65) is also shown in Fig. 9.16.

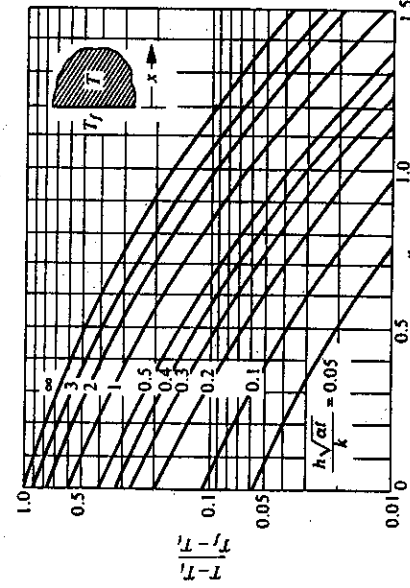
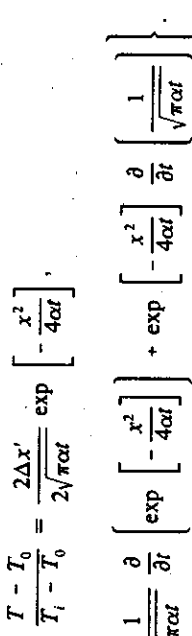


Fig. 9.16 Temperature history in a semi-infinite solid with surface resistance. (From P. J. Schneider, *Conduction Heat Transfer*, Addison-Wesley, Reading, MA, 1955, page 266.)

**Example 9.7** Lasers can be used in several materials processing schemes including the rapid heating and subsequent quenching of surface layers. Suppose a laser is pulsed once at the surface and heats a very thin layer of thickness  $\Delta x'$  to temperature  $\Delta x'$  to temperature  $\Delta x'$ . Derive an equation that gives cooling rate,  $\partial T / \partial t$ , versus distance from the surface and time after the single pulse of energy from the laser.

**Solution.** If we neglect the small heat loss from the surface, then the solution is twice the relative temperature (also called dimensionless temperature) given by Eq. (9.45) with  $x' = 0$ .



$$\frac{T - T_0}{T_i - T_0} = \frac{2\Delta x'}{2\sqrt{\pi\alpha t}} \exp \left[ -\frac{x'^2}{4\alpha t} \right],$$

$$\frac{\partial T}{\partial t} = (T_i - T_0) \Delta x' \left\{ \frac{1}{\sqrt{\pi\alpha t}} \frac{\partial}{\partial x} \left[ \exp \left[ -\frac{x'^2}{4\alpha t} \right] \right] + \exp \left[ -\frac{x'^2}{4\alpha t} \right] \frac{\partial}{\partial t} \left[ \frac{1}{\sqrt{\pi\alpha t}} \right] \right\}.$$

This simplifies to

$$\frac{\partial T}{\partial t} = \left[ \frac{T - T_0}{t} \right] \left[ \frac{x^2}{4\alpha t} - \frac{1}{2} \right].$$

**Example 9.8** Aluminum oxide at 300 K is pulsed with a laser such that 0.1  $\mu\text{m}$  of its surface is raised to 3600 K. Calculate the cooling rate at a depth of 0.3  $\mu\text{m}$  as a function of temperature. The thermal diffusivity of the aluminum oxide is  $1.6 \times 10^{-6} \text{ m}^2 \text{ s}^{-1}$ .

**Solution.** The equation derived in Example 9.7 applies. We need temperature versus time first. This is found from

$$T - T_0 = (T_i - T_0) \frac{\Delta x'}{\sqrt{\pi\alpha t}} \exp \left[ -\frac{x^2}{4\alpha t} \right],$$

with  $(T_i - T_0) = 3300 \text{ K}$ ,  $\Delta x' = 1 \times 10^{-7} \text{ m}$ , and  $x = 3 \times 10^{-7} \text{ m}$ . Temperature and time are tabulated below in the first two columns. The corresponding heating and cooling rates are in the third column.

Time, s	$(T - T_0)$ , K	$\partial T / \partial t$ , K $\text{s}^{-1}$
$1 \times 10^0$	0.004	$4.93 \times 10^7$
$5 \times 10^{-9}$	125.0	$5.78 \times 10^{10}$
$1 \times 10^{-8}$	360.7	$3.27 \times 10^9$
$2 \times 10^{-8}$	515.2	$5.23 \times 10^8$
$3 \times 10^{-8}$	531.8	$-5.54 \times 10^8$
$5 \times 10^{-8}$	496.9	$-2.17 \times 10^8$
$1 \times 10^{-7}$	404.4	$-1.45 \times 10^9$
$5 \times 10^{-7}$	202.4	$-1.91 \times 10^8$
$1 \times 10^{-6}$	145.1	$-7.05 \times 10^7$
$5 \times 10^{-6}$	65.6	$-6.53 \times 10^6$
$1 \times 10^{-5}$	46.5	$-2.32 \times 10^6$

Before leaving this example, it is instructive to point out some features of the temperature field. At a depth of  $0.3 \mu\text{m}$ , there is a heating period of somewhat less than  $3 \times 10^{-8} \text{ s}$ , during which a maximum temperature of more than 832 K is achieved. Heating is followed by cooling at rates less than the heating rates, and the material returns to within 50 K of the base temperature in only  $1 \times 10^{-5} \text{ s}$ . This example demonstrates that extremely high heating and cooling rates are achievable in the surface layers of solids when they are pulsed with lasers.

**Example 9.9** The Jominy end-quench test is commonly used to assess the hardenability of steels. The temperature near the quenched end can be approximated as that in a semi-infinite solid with its surface (i.e., the end of the Jominy bar) quenched by a spray of 295 K water with  $h \rightarrow \infty$ .

In an eutectoid steel, a microstructure of 50% martensite-50% pearlite is achieved at a distance of 9 mm from the end-quench when the steel is initially heated to 1090 K before the quench. Assume that the achievable microstructure depends on the time to cool to 840 K. Knowing this, predict the maximum thickness of a plate in which a 50% martensite-50% pearlite microstructure can be achieved when the plate is quenched in brine with no agitation

( $h = 2700 \text{ W m}^{-2} \text{ K}^{-1}$ ). The thermal properties of the steel are  $k = 21.5 \text{ W m}^{-1} \text{ K}^{-1}$ ,  $C_p = 600 \text{ J kg}^{-1} \text{ K}^{-1}$ , and  $\rho = 7700 \text{ kg m}^{-3}$ .

**Solution.** Starting with our knowledge of the Jominy end-quench, we calculate the time to achieve 840 K at  $x = 9 \text{ mm}$ .

$$\frac{T - T_s}{T_i - T_s} = \operatorname{erf} \left[ \frac{x}{2\sqrt{\alpha t}} \right]$$

$$\frac{840 - 295}{1090 - 295} = 0.6635 = \operatorname{erf} \left[ \frac{x}{2\sqrt{\alpha t}} \right].$$

From Table 9.3 and  $\alpha = 4.65 \times 10^{-6} \text{ m}^2 \text{ s}^{-1}$ :

$$\frac{x}{2\sqrt{\alpha t}} = \frac{(0.009)^2}{(0.7115^2)(4)(4.65 \times 10^{-6})} = 8.60 \text{ s}.$$

and

$$t = \frac{x^2}{(0.7115^2)(4\alpha)} = \frac{(0.009)^2}{(0.7115^2)(4)(4.65 \times 10^{-6})} = 8.60 \text{ s}.$$

In order to deal with the plate, we make use of Fig. 9.8(a). The semithickness of the plate, however, appears in both  $F_o$  and  $B_i$  so that a trial-and-error solution is sought. We fix the relative temperature at 0.6855 and read corresponding values of  $F_o$  and  $B_i$  from the curves in Fig. 9.8(a). The length derivable from  $F_o$  is  $L_1$ :

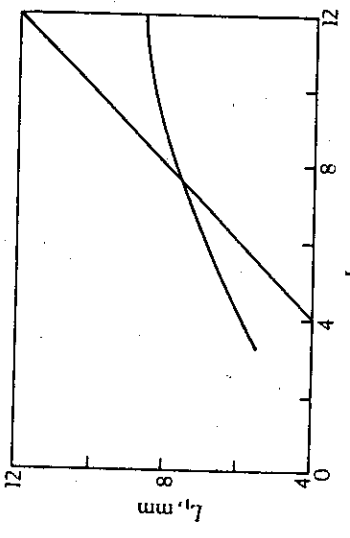
$$L_1 = \left[ \frac{\alpha t}{F_o} \right]^{1/2} = \left[ \frac{4.65 \times 10^{-6} \times 8.60}{F_o} \right]^{1/2},$$

and the length from  $B_i$  is  $L_2$ :

$$L_2 = \frac{k B_i}{h} = \left[ \frac{21.5 B_i}{2700} \right].$$

The solution is when  $L = L_1 = L_2$ . By some trial-and-error, we find that the solution is in the region  $0.4 \leq B_i \leq 1.5$ ; so we plot several values in this range.

$F_o$	$B_i$	$L_1$ , mm	$L_2$ , mm
1.3	0.4	5.55	3.18
1	0.6	6.32	4.78
0.65	1.0	7.84	7.96
0.52	1.5	8.77	11.94



The solution is  $L = 7.7$  mm so that the thickness of the plate is 15.4 mm.

### 9.5 SIMPLE MULTIDIMENSIONAL PROBLEMS

In this section we present methods of obtaining solutions for solid shapes such as cubes, rectangular bars, and short cylinders. These solutions can be obtained directly by simply combining solutions for the semi-infinite solid, the infinitely long cylinder, and the infinite slab, which are given in Sections 9.3 and 9.4.

As an example, consider an infinitely long bar with a rectangular cross-section  $2L$  by  $2l$ , using coordinates as illustrated by Fig. 9.17. The bar is initially at the uniform temperature  $T_i$ , and then it is suddenly exposed to a convective environment at  $T_f$ . In such a bar,  $T(x,y,t)$  must satisfy the partial differential equation

$$\frac{\partial T}{\partial t} = \alpha \left[ \frac{\partial^2 T}{\partial x^2} + \frac{\partial^2 T}{\partial y^2} \right]. \quad (9.66)$$

Recall that the temperature in solids is best represented by the relative temperature; here, we assign  $\Theta$  so that

$$\Theta = \frac{T - T_f}{T_i - T_f}.$$

We can prove that the solution  $\Theta(x,y,t)$  is the product

$$\Theta(x,y,t) = X(x,t) \cdot Y(y,t). \quad (9.67)$$

Here,  $X(x,t)$  is the solution for the temperature response in the infinite slab of thickness  $2L$ , and  $Y(y,t)$  is the solution for the infinite slab of thickness  $2l$ . The reader is invited to pursue Problem 9.22 at the end of this chapter to satisfy himself of the validity of Eq. (9.67).

We may also make use of the solution for the semi-infinite solid in combination with solutions to solids such as the infinite plate or semi-infinite cylinder. For example, consider the semi-infinite cylinder for which we seek the solution of  $\Theta(r,y,t)$ . If  $S(y,t)$  represents the solution to the semi-infinite solid in the regime  $0 \leq y < \infty$ , and  $C(r,t)$  is the solution for the infinitely long cylinder, then the solution we seek is simply their product, that is,

$$\Theta(r,y,t) = S(y,t) \cdot C(r,t). \quad (9.68)$$

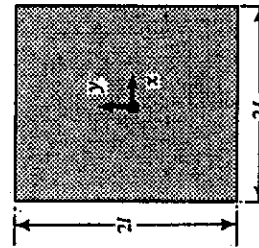
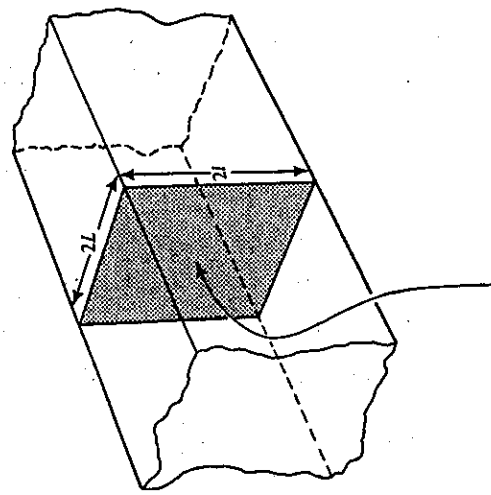


Fig. 9.17 Rectangular bar showing the system of coordinates.

By means of this method, many so-called *product solutions* can be developed for a large number of solid shapes, some of which are depicted in Fig. 9.18, with their respective solutions indicated.

**Example 9.10** A cylindrical polyethylene preform (at 300 K) is to be preheated for 100 s in a bath of hot oil at 500 K with  $h = 200 \text{ W m}^{-2} \text{ K}^{-1}$ . The polyethylene has a thermal diffusivity of  $1 \times 10^{-7} \text{ m}^2 \text{ s}^{-1}$  and a thermal conductivity of  $0.34 \text{ W m}^{-1} \text{ K}^{-1}$ . The preform has a diameter of 10 mm and a length of 8 mm. a) Calculate the temperature at its geometrical center. b) What is the surface temperature at one-half of the distance between the ends?

*Solution.*

$$\text{a)} \quad \text{Bi}_R = \frac{hR}{k} = \frac{(200)(0.005)}{0.34} = 2.94,$$

$$\text{Fo}_R = \frac{\alpha t}{R^2} = \frac{(1 \times 10^{-7})(100)}{(0.005)^2} = 0.400.$$

$$F_0 L = \frac{\alpha t}{L^2} = \frac{(1 \times 10^{-7})(100)}{(0.004)^2} = 0.625.$$

From Fig. 9.8(a),

$$X(0,t) = \left[ \frac{T_0 - T_f}{T_i - T_f} \right]_{\infty \text{ plate}} = 0.552.$$

To get the solution, we take the product

$$\frac{T - T_f}{T_i - T_f} = C(0,t) \cdot X(0,t) = (0.407)(0.552) = 0.225,$$

and

$$T = (0.225)(300 - 500) + 500 = 455 \text{ K}.$$

b) For this case we use Fig. 9.9(b):

$$C(R,t) \approx 0.545.$$

Now the product is

$$\frac{T - T_f}{T_i - T_f} = C(R,t) \cdot X(0,t) = (0.545)(0.552) = 0.300,$$

and

$$T = (0.300)(300 - 500) + 500 = 440 \text{ K}.$$

In Example 9.10, we were given the time and asked to determine the temperature so that the method of solution was direct. Given a specified temperature to be achieved and asked to determine the time, however, is not so simple and requires trial-and-error iterations. Some of the problems at the end of this chapter are posed in the latter scenario.

## 9.6 MOVING SOURCES

Processes that utilize concentrated power sources in materials processing include processes for surface modification, cutting, and joining. Power sources include laser beams, electron beams, and electric arcs. Here we present and discuss analytical solutions to two types of mathematical sources that are used to estimate the temperature field in processes involving moving sources. The solutions are presented again in the next chapter where they are applied to thermal aspects of welding.

### 9.6.1 Moving point source

Additionally,

$$Bi_L = \frac{hL}{k} = \frac{(200)(0.004)}{0.34} = 2.35,$$

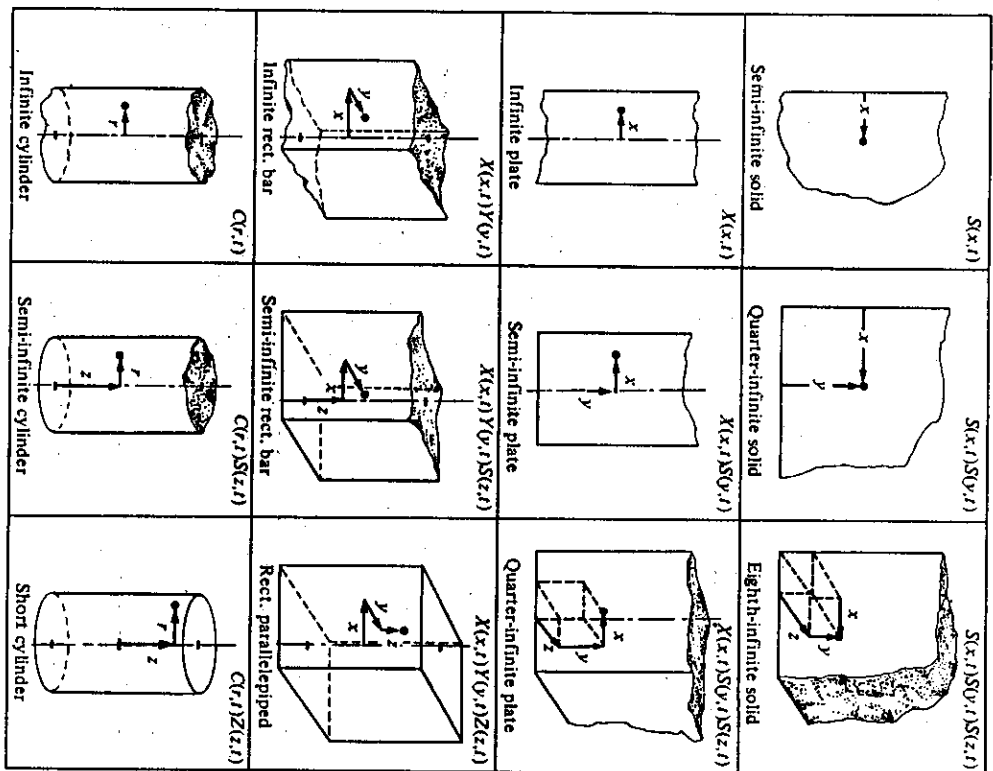


Fig. 9.18 The composition of product solutions.

From Fig. 9.9(a),

$$C(0,t) = \left[ \frac{T_0 - T_f}{T_i - T_f} \right]_{\infty} = 0.407.$$

A power source that is approximated as a point source moves with a constant velocity on the surface of a thick plate. The situation is depicted in Fig. 9.19, where an isotherm is shown. In front of the source, the thermal gradients are steeper than the gradients behind

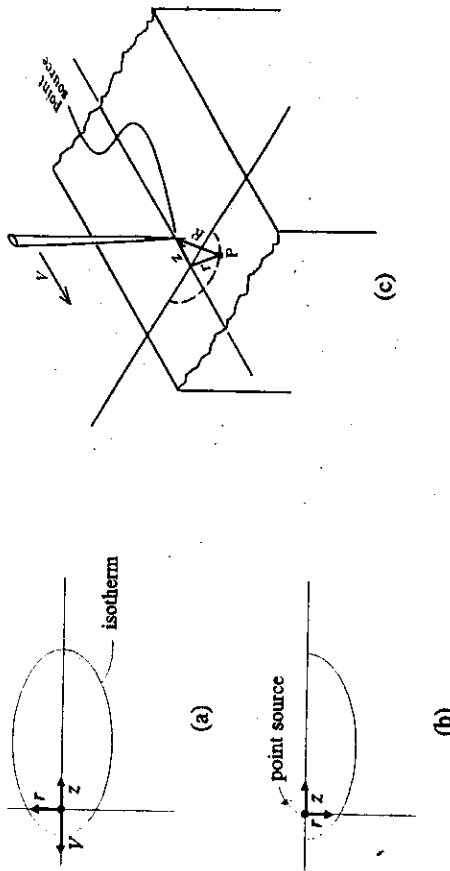


Fig. 9.19 Moving point source and an isotherm on the surface of a thick plate. The point source is moving to the left with velocity  $V$ . (a) View from the top; (b) view of transverse section; (c) perspective showing coordinates of point  $P$  on an isotherm in terms of the cylindrical coordinates  $r$  and  $z$  or in terms of the spherical coordinate  $R = (z^2 + r^2)^{1/2}$ .

the source. Therefore, the front of any isotherm is closer to the source than it is behind the source.

In cylindrical coordinates, the energy equation can be deduced from Eq. (B) in Table 7.5. For constant and uniform thermal properties, we have

$$\frac{\partial T}{\partial r} = \alpha \left[ \frac{1}{r} \frac{\partial}{\partial r} \left[ r \frac{\partial T}{\partial r} \right] + \frac{\partial^2 T}{\partial z^2} \right]. \quad (9.69)$$

This equation gives  $\partial T / \partial r$  experienced by any stationary unit element in the solid. Suppose, however, that we choose an element that moves with the same constant velocity,  $V$ , of the source. If we do this, it becomes convenient to work with a moving coordinate system with the origin at the source, as depicted in Fig. 9.19. With respect to the moving coordinate system, Eq. (9.69) transforms to

$$V \frac{\partial T}{\partial z} = \alpha \left[ \frac{1}{r} \frac{\partial}{\partial r} \left[ r \frac{\partial T}{\partial r} \right] + \frac{\partial^2 T}{\partial z^2} \right]. \quad (9.70)$$

Furthermore, it is convenient to also think in terms of a spherical distance from the moving origin. This spherical coordinate is denoted  $R$  to avoid confusion with the cylindrical coordinate  $r$ . The spherical coordinate is related to  $z$  and  $r$  by

$$R^2 = z^2 + r^2. \quad (9.71)$$

With source strength given as power,  $Q$ , in  $W$ , the temperature must satisfy two boundary conditions:

$$\text{B.C. 1: } T = T_\infty \quad \text{at } R = \infty, \quad (9.72)$$

$$\text{B.C. 2: } Q = \left[ (2\pi R^2) \left[ -k \frac{\partial T}{\partial R} \right] \right]_{R=0}. \quad (9.73)$$

Equation (9.72) can be satisfied by assuming

$$T = T_\infty + \theta(z, r) \exp \left[ \frac{Vz}{2\alpha} \right], \quad (9.74)$$

then Eq. (9.70) becomes

$$\frac{\partial^2 \theta}{\partial z^2} + \frac{\partial}{\partial r} \left[ r \frac{\partial \theta}{\partial r} \right] + \frac{V^2}{4\alpha^2} \theta = 0. \quad (9.75)$$

A solution to Eq. (9.75) is

$$\theta = \frac{A}{R} \exp \left[ -\frac{VR}{2\alpha} \right], \quad (9.76)$$

in which  $A$  is an arbitrary constant. (Remember  $R$  is single variable that represents both  $r$  and  $z$ , Eq. (9.71).) With the solution in this form, Eq. (9.73) requires

$$A = \frac{Q}{2\pi k};$$

therefore, the temperature in the thick plate is

$$T - T_\infty = \frac{Q}{2\pi k R} \exp \left[ \frac{Vz}{2\alpha} \right] \exp \left[ -\frac{VR}{2\alpha} \right]. \quad (9.77)$$

This result was originally given by Rosenthal.<sup>6</sup> Equation (9.77) can also be written

$$T - T_\infty = \frac{QV}{4\pi k \alpha} (Pe_z^2 + Pe_r^2)^{-1/2} \exp \left[ Pe_z - (Pe_z^2 + Pe_r^2)^{1/2} \right], \quad (9.78)$$

where  $Pe_z$  and  $Pe_r$  are Peclot numbers defined as

$$Pe_z = \frac{Vz}{2\alpha} \quad \text{and} \quad Pe_r = \frac{Vr}{2\alpha}.$$

Notice that in Eq. (9.78) we have resorted to cylindrical coordinates,  $z$  and  $r$ . With cylindrical coordinates, it is more convenient to derive an equation for the so-called *peak temperature*. Suppose we insert a thermocouple into the plate and measure temperature versus time. Of course, the thermocouple is fixed so it experiences the temperature of a stationary observer. Temperature increases as the source moves toward the vicinity of the thermocouple but then decreases as the source passes by. Hence, at a given distance  $r$  from the path of the source, a unique peak temperature is achieved. In materials processing,

<sup>6</sup>D. Rosenthal, *Weld. J.* 20, 220s (1941).

knowledge of the peak temperature is important because it pertains to the likelihood of a transformation occurring during the heating and cooling cycle.

The peak temperature can be found by finding the following extremum in Eq. (9.78):

$$\frac{\partial Pe_r}{\partial Pe_z} = 0.$$

The result of this operation is

$$Pe_z^2 + Pe_r^2 = Pe_z \left[ 1 + (Pe_z^2 + Pe_r^2)^{1/2} \right]. \quad (9.79)$$

Except in the immediate vicinity of the point source, Eq. (9.79) is closely approximated with

$$Pe_z^2 \approx 2Pe_r. \quad (9.80)$$

Equation (9.80)<sup>7</sup> is a good approximation only if  $Pe_r > 5$ ; otherwise the following approximations can be consulted to obtain values of  $Pe_z$  and  $Pe_r$  that satisfy Eq. (9.79):

$$\log_{10} Pe_r = 0.505 \log_{10} Pe_z + 0.02, \quad 10^{-2} \leq Pe_r \leq 10^{-1}$$

and

$$\log_{10} Pe_z = 0.547 \log_{10} Pe_r + 0.100, \quad 10^{-1} \leq Pe_r \leq 5.$$

If  $Pe_r > 5$  applies, then the peak temperature,  $T_p$ , can be obtained by substituting  $T_p = T$  and Eq. (9.80) into Eq. (9.78). The final result is

$$T_p - T_\infty = \left[ \frac{QV}{2\pi k \epsilon} \right] \left[ \frac{1}{2 + Pe_z^2} \right], \quad Pe_r > 5. \quad (9.81)$$

where  $\epsilon = 2.7183$ . Equation (9.81) was first derived by Adams.<sup>7</sup>

If Eq. (9.81) cannot be used, then a set of values of  $Pe_z$  and  $Pe_r$  that satisfy Eq. (9.79) should be obtained and then substituted into Eq. (9.78) with  $T = T_p$ , the peak temperature. This procedure is illustrated in the following example.

### 9.6.2 Moving Line Source

When the plate is thin enough, it is better to assume that the power source is a *line source*, Fig. 9.20. Equation (9.70) applies; the solution<sup>8</sup> is

$$T - T_\infty = \frac{Q}{2\pi k \delta} \exp(Pe_z) K_0 \left( \sqrt{Pe_z^2 + Pe_r^2} \right), \quad (9.82)$$

Example 9.11 Estimate the peak temperature as a function of  $r$ , the radial distance from the path of a moving laser. Aluminum oxide at 300 K is subjected to a 1 kW laser beam, moving at 1 mm s<sup>-1</sup>. Assume that the efficiency of the laser energy is 30 percent. The thermal diffusivity of the aluminum oxide is  $1.6 \times 10^{-6}$  m<sup>2</sup> s<sup>-1</sup>, and its thermal conductivity is 6 W m<sup>-1</sup> K<sup>-1</sup>.

*Solution.* Let us start with  $r = 0.05$  mm.

$$Pe_r = \frac{Vr}{2\alpha} = \frac{(1 \times 10^{-3})(5 \times 10^{-5})}{(2)(1.6 \times 10^{-6})} = 1.562 \times 10^{-2}.$$

$$K_0 \left( \sqrt{Pe_z^2 + Pe_r^2} \right) = \left[ \frac{\pi}{2} \right]^{1/2} \frac{\exp(-\sqrt{Pe_z^2 + Pe_r^2})}{\sqrt[4]{Pe_z^2 + Pe_r^2}}, \quad (9.83)$$

so that Eq. (9.78) with  $T = T_p$  can be used:

$$T_p - 300 = \frac{(300)(0.001) \exp[2.42 \times 10^{-4} - 1.562 \times 10^{-2}]}{(4\pi)(6)(1.6 \times 10^{-6})(1.562 \times 10^{-2})} = 1.57 \times 10^5 \text{ K}.$$

and with  $Pe_r = 1.562 \times 10^{-2}$ , we calculate  $Pe_z = 2.42 \times 10^{-4}$ . These values give

$$\left[ Pe_z^2 + Pe_r^2 \right]^{1/2} = 1.562 \times 10^{-2},$$

and

$r$ , mm	$Pe_r$	$T_p$ , K
0.05	$1.562 \times 10^{-2}$	$1.57 \times 10^5$
0.10	$3.125 \times 10^{-2}$	$7.75 \times 10^4$
0.5	$1.562 \times 10^{-1}$	$1.41 \times 10^4$
1	$3.125 \times 10^{-1}$	6349
2	0.625	2722
3	0.938	1638
4	1.25	1152
6	1.875	732
8	2.5	559
10	3.125	472

Obviously any real material melts at this temperature. The peak temperatures at other values of  $r$  are determined in the same way, provided the appropriate estimates for  $Pe_z$  are used. The results are tabulated below.

<sup>7</sup>C. M. Adams, *Weld J.* 37, 210s (1958).

<sup>8</sup>D. Rosenthal, *ibid.*

<sup>9</sup>C. M. Adams, *ibid.*

The results are tabulated below.

$\delta, \text{ mm}$	$T_p, \text{ K}$
5	4172 (metals)
10	2236
20	1268
30	945
40	784

### PROBLEMS

(For practice in manipulating units, some of the problems are in English units.)

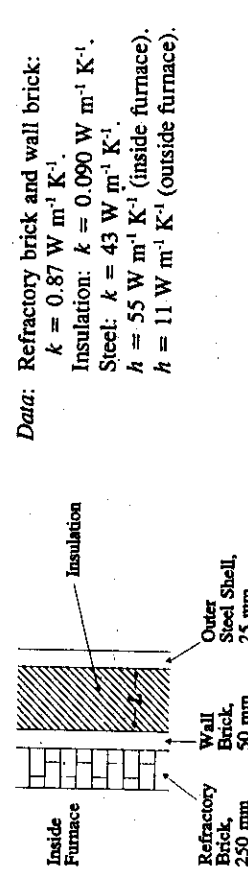
- 9.1 A furnace wall is constructed of 7 in. of fire brick ( $k = 0.60 \text{ Btu h}^{-1} \text{ ft}^{-1} {^{\circ}\text{F}}^{-1}$ ), 4 in. of red brick ( $k = 0.40$ ), 1 in. of glass-wool insulation ( $k = 0.04$ ), and  $\frac{1}{4}$  in. steel plate ( $k = 26.3 \text{ Btu h}^{-1} \text{ ft}^{-2} {^{\circ}\text{F}}^{-1}$ ), respectively. The heat transfer coefficients on the inside and outside surfaces are 9 and outside air temperature is  $90^{\circ}\text{F}$ . The gas temperature inside the furnace is  $2500^{\circ}\text{F}$ , and the outside air temperature is  $90^{\circ}\text{F}$ .

- a) Calculate the heat-transfer rate through the wall ( $\text{Btu h}^{-1} \text{ ft}^2$ ).  
 b) Determine the temperatures at all interfaces.

- 9.2 Consider the flow of heat through a spherical shell. For steady-state conditions, the inside surface ( $r = R_1$ ) is at temperature  $T_1$ , and the outside surface ( $r = R_2$ ) is at  $T_2$ .

- a) Write the pertinent differential energy equation that applies.  
 b) Write the boundary conditions and develop an expression for the temperature distribution in the shell.  
 c) Develop an expression for the heat flow ( $Q, \text{ W}$ ) through the shell.  
 d) Determine the thermal resistance of the spherical shell.

- 9.3 In order to reduce the heat loss through a large furnace wall, the decision has been made to add external insulation. Calculate the thickness of insulation required to reduce the heat loss by 75%. Before the change is made, no outer steel shell is used.



$$T - T_\infty = \frac{Q}{\sqrt{8\pi k}} \frac{\exp(Pe_z) - \sqrt{Pe_z^2 + Pe_r^2}}{\sqrt{Pe_z^2 + Pe_r^2}} \quad (9.84)$$

$$\frac{\partial Pe_r}{\partial Pe_z} = 0.$$

The final result, based on the approximation of Eq. (9.83), is

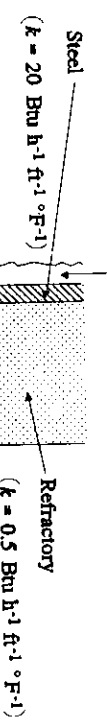
$$T_p - T_\infty = \frac{Q}{\sqrt{8\pi k} \delta Pe_z} \quad (9.85)$$

**Example 9.12** Select  $r = 1 \text{ mm}$ , use the conditions specified in Example 9.11 and determine peak temperature versus the thickness of the plate.

$$Pe_z = \frac{V_t}{2\alpha} = \frac{(0.001)(0.001)}{(2)(1.6 \times 10^{-6})} = 0.3125.$$

$$T_p - 300 = \frac{(300)}{(\sqrt{8\pi k})(6)(0.3125)\delta} = \frac{19.36}{\delta}.$$

- 9.4 The wall of a blast furnace is water-cooled. Given the inside- and outside-surface temperatures ( $2400^{\circ}\text{F}$  and  $180^{\circ}\text{F}$ ), what is the heat transfer coefficient for the water? The water, itself, is at  $80^{\circ}\text{F}$ . Assume steady-state conditions.



9.5 Consider steady-state heat conduction through a cylindrical wall. The fluid on the inside

is at 590 K with a heat transfer coefficient of 23 W m<sup>-2</sup> K<sup>-1</sup>. The temperature on the outside surface of the wall is known and maintained at 420 K. The heat flow rate through the cylindrical wall is 200 W per 1 m length of the cylinder. If the wall has a thermal conductivity of 0.17 W m<sup>-1</sup> K<sup>-1</sup>, what are the inside and outside radii of the cylindrical wall? The ratio of the outside radius to inside radius is 2.

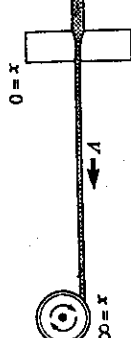
9.6 Small droplets of a molten glass maintain their amorphyticity if they cool at a rate of at least 10 K s<sup>-1</sup>, measured at 1070 K. For a spherical droplet with 0.1 mm diameter, what is the required heat transfer coefficient to achieve the minimum cooling rate? The quench environment is maintained at 293 K. Data for the glass:  $\rho = 3000 \text{ kg m}^{-3}$ ,  $C_p = 840 \text{ J kg}^{-1} \text{ K}^{-1}$ ,  $k = 17 \text{ W m}^{-1} \text{ K}^{-1}$ .

9.7 A small sphere (diameter = 0.30 mm), initially at 1365 K, drops through a gas layer of 150 mm with an average velocity of 3 m s<sup>-1</sup> and then through a liquid layer of 30 mm with an average velocity of 3 mm s<sup>-1</sup>. Data for the sphere:  $\rho = 2560 \text{ kg m}^{-3}$ ,  $C_p = 840 \text{ J kg}^{-1} \text{ K}^{-1}$ ,  $k = 0.86 \text{ W m}^{-1} \text{ K}^{-1}$ . Heat transfer coefficients:  $h$  (gas) = 40 W m<sup>-2</sup> K<sup>-1</sup>,  $h$  (liquid) = 280 W m<sup>-2</sup> K<sup>-1</sup>.

- a) What is the temperature of the droplet just before it impacts the liquid?
- b) What is the temperature of the droplet when it reaches the bottom of the liquid layer?

9.8 A thin wire is extruded at a fixed velocity  $v$  through dies, and the wire temperature at the die is a fixed value  $T_0$ . The wire then passes through the air for a long distance before it is rolled onto large spools. It is desired to investigate the relationship between wire velocity and the distance from the extrusion nozzle for specific values of  $T_0$ .

- a) Derive the differential equation for determining wire temperature as a function of distance from the nozzle. [Hint: Since temperature gradients across the wire are certainly negligible, a slice between  $x$  and  $x + \Delta x$  may be chosen that includes the wire surface. The heat balance then includes heat lost to the surroundings at  $T_\infty$ .]
- b) State boundary conditions and solve for the temperature in the extended wire.



9.9 A very long crystal (dia. =  $D$ ) is slowly withdrawn with a velocity  $v$  from a melt maintained at only a few degrees above the freezing point. The diameter of the crystal is small enough so that radial temperature gradients can be ignored. There is heat loss from the crystal to the surroundings, maintained at  $T_\infty$ ; the heat transfer coefficient is  $h$ . Assume steady-state conditions.

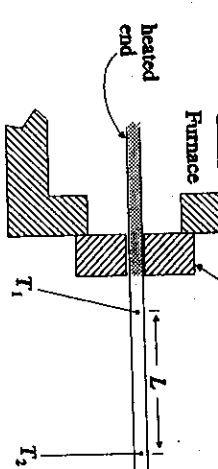
- a) Distance in the crystal and measured from the interface is  $z$ . Derive the energy equation in terms of temperature.
- b) Write appropriate boundary conditions and solve for temperature in the crystal.

- c) If  $h = 110 \text{ W m}^{-2} \text{ K}^{-1}$ , what is the maximum diameter of the crystal so that the radial temperature gradient can be ignored?

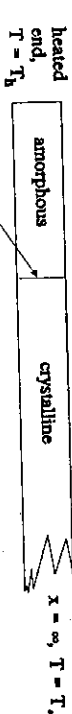
[Note: If you have solved Problem 9.8, then you can write the equation for temperature by inspection.]

9.10 One end of a long thin rod is inserted into a furnace through a hole in the furnace door. Two thermocouples are inserted along the length of the bar and indicate steady-state temperatures of  $T_1$  and  $T_2$ , respectively. Assume that the temperature in the bar only varies

along its length and derive an equation which can be used to calculate  $h$  of the surrounding air as a function of  $T_1$ ,  $T_2$ ,  $P$  (perimeter),  $A$  (area),  $L$ ,  $T_\infty$ , and  $k$  (thermal conductivity of the bar).



9.11 One end of an amorphous rod is heated so that a portion crystallizes. Derive an equation that can be used for finding the position of the interface after steady state is achieved. The interface temperature is  $T^*$ . Assume one-directional conduction along the length of the rod and heat loss to the surroundings at  $T_\infty$  with a uniform heat transfer coefficient.



- a) Assume equal thermal properties in the amorphous and crystalline states.
- b) Assume  $k$  (crystal) =  $4k$  (amorphous).

9.12 Consider the Newtonian cooling of a thin plate (15 mm thick) with a length and width of 1.2 m each. Initially the plate is at 530 K, and then it is cooled by natural convection as it is suspended vertically in air at 300 K. Use the simplified equations given in Problem 8.14 and answer the following questions.

- a) Early in the cooling process, does  $h$  vary with  $(\Delta T)^{1/4}$  or  $(\Delta T)^{1/3}$ ?

- b) Near the end of the cooling process, does  $h$  vary with  $(\Delta T)^{1/4}$  or  $(\Delta T)^{1/3}$ ? Determine the temperature at which the transition occurs.
- c) Derive (an) equation(s) which give(s) the temperature of the bar consistent with the assumption of Newtonian cooling and  $h$  varying with  $(\Delta T)^{1/3}$  and/or  $(\Delta T)^{1/4}$ .

**9.13** In some alloys, grain refinement can be achieved by cycling the alloy above and below a transformation temperature.

Suppose an alloy sphere, initially at a uniform temperature  $T_0$ , is immersed in a bath of heated oil. The electric heaters are controlled so that the temperature of the oil ( $T$ ) follows a cyclic variation given by

$$T_f - T_m = A \sin \omega t$$

where

$$\begin{aligned} T_m &= \text{time average mean oil temperature (constant),} \\ A &= \text{amplitude of variation, and} \\ \omega &= \text{frequency.} \end{aligned}$$

Derive an expression for the temperature of the sphere as a function of time and the heat transfer coefficient. Assume that the temperature of the sphere is uniform.

**9.14** Ball bearings (12 mm diameter spheres) are austenitized at 1145 K and then quenched into a large tank of oil at 310 K. Calculate:

- The time to cool the center of a bearing to 480 K.
- The surface temperature when the center is at 480 K.
- The space-mean temperature when the center is at 480 K.
- If 10,000 balls are quenched per hour, calculate the rate of heat removal from the oil that is needed to maintain its temperature at 310 K.

*Data for ball bearings:*  $h = 1700 \text{ W m}^{-2} \text{ K}^{-1}$ ;  $\rho = 7210 \text{ kg m}^{-3}$ ;  $C_p = 630 \text{ J kg}^{-1} \text{ K}^{-1}$ ;  $k = 43 \text{ W m}^{-1} \text{ K}^{-1}$ .

**9.15** Rapid solidification of Cu is effected by dropping molten droplets into water at 310 K. The droplets may be approximated as spheres with a diameter of 5 mm. Calculate the time for the droplets to cool to 365 K if they enter the water at 1450 K.

*Data for Cu in S.I. units:* Freezing point = 1358,  $C_p$  (solid) = 377;  $C_p$  (liquid) = 502; heat of fusion =  $2.07 \times 10^5 \text{ J kg}^{-1}$ ;  $\rho$  (solid) = 8970;  $\rho$  (liquid) = 8490;  $k$  (solid) = 346;  $k$  (liquid) = 311.

*Data for water quench:*

Temperature range	$h, \text{W m}^{-2} \text{ K}^{-1}$
1450-920 K	450
920-360 K	2270

**9.16** Steel ball bearings (60 mm in diameter) are austenitized at 1089 K and then quenched in fluid X at 310 K. It is known by utilizing a thermocouple that a continuous vapor film surrounds the bearings for 72 s until the surface temperature drops to 530 K and at the same time the center temperature is 645 K. Knowing these results, determine the time it takes for the center of smaller bearings (6 mm in diameter) of the same steel to reach 920 K when quenched from 1089 K into fluid X at 310 K.

**9.17** An open-ended cylindrical section of a steel pressure vessel 10 ft in diameter with 8-in. thick walls is being heat-treated. The wall temperature is brought to a uniform value of 1750°F. Then the vessel is quenched into slow oil at 70°F. Gather the data and work the problem in English units.

- How long does it take for the surface to reach 1000°F?
- What is the temperature at the center of the wall at that time?

**9.18** A cylindrical piece of steel, 50 mm in diameter and initially at 1145 K, is quenched in water at 295 K ( $H = 59 \text{ m}^3$ ). Calculate the temperature at the surface of the piece after 60 s, 120 s, and 300 s. Compare your results with the temperature at the same location if the piece had been quenched in oil ( $H = 20 \text{ m}^3$ ). *Data:*  $\alpha = 6.4 \times 10^{-6} \text{ m}^2 \text{ s}^{-1}$ .

**9.19** Compute the temperature, as a function of time, across a slab of steel 100 mm thick, cooled from 1145 K by water sprays from both sides. *Data:*  $\alpha = 6.2 \times 10^{-6} \text{ m}^2 \text{ s}^{-1}$ .

**9.20** Consider a short cylinder 150 mm high and with a diameter of 150 mm. The cylinder is initially at a uniform temperature of 530 K and cools in ambient air at 300 K. Assume  $\alpha = 6.2 \times 10^{-6} \text{ m}^2 \text{ s}^{-1}$  and  $k = 35 \text{ W m}^{-1} \text{ K}^{-1}$ .

- Write the differential equation that describes the temperature within the cylinder.
- Calculate the temperature at the geometric center after 3600 s of cooling.
- Calculate the temperature on the cylindrical surface midway between the end faces after 3600 s of cooling. Estimate heat transfer coefficients by consulting Problem 8.14.
- In answering parts b) and c), show why your calculation procedure was justified, that is, demonstrate that the differential equation in part a) is satisfied.

**9.21** A steel blank, 300 mm in diameter and 600 mm long, is heated in a preheating furnace maintained at 1410 K as the first step in a forging operation.

- Calculate the temperature in the center of the blank after the blank has been heated for 5400 s from an initial temperature of 295 K.
- Calculate the time required to heat a smaller blank, 150 mm in diameter and 300 mm long, to the same center temperature as the larger blank in part a).

*Data:*  $h = 110 \text{ W m}^{-2} \text{ K}^{-1}$ ;  $k = 35 \text{ W m}^{-2} \text{ K}^{-1}$ ;  $C_p = 500 \text{ J kg}^{-1} \text{ K}^{-1}$ ;  $\rho = 7690 \text{ kg m}^{-3}$ .

**9.22** The temperature field  $T(x,y,t)$  in an infinitely long rectangular ( $2L \times 2l$ ) bar must satisfy the partial differential equation

$$\frac{\partial^2 T}{\partial x^2} + \frac{\partial^2 T}{\partial y^2} = \frac{1}{\alpha} \frac{\partial T}{\partial t}.$$

Prove that  $T(x,y,t)$  can be found by the product

$$T(x,y,t) = T_l(x,t) \cdot T_L(y,t),$$

where  $T_l(x,t)$  is the solution for the temperature history in the semi-infinite plate bounded by  $l < x < +l$ , and  $T_L(y,t)$  is the solution for the temperature history in the semi-infinite plate bounded by  $-L < y < L$ .

**9.23** A strip of spring steel (0.5 mm thick) is heated to 1090 K and quenched in "slow oil" maintained at 310 K. Using Fig. 8.14, calculate the cooling rate at 1090 K, 755 K, and 385 W m<sup>-1</sup> K<sup>-1</sup>;  $k$  (1090 K) = 26 W m<sup>-1</sup> K<sup>-1</sup>;  $k$  (755 K) = 35 W m<sup>-1</sup> K<sup>-1</sup>;  $k$  (385 K) = 628 J kg<sup>-1</sup> K<sup>-1</sup>;  $C_p$  = 7840 kg m<sup>-3</sup>;  $\rho$  = 7840 kg m<sup>-3</sup>.

## 326 Conduction of Heat in Solids

**9.24** A thermoplastic (polypropylene) at 500 K is injected into a mold at 300 K to form a plate that is 4 mm thick. The plastic may not be ejected until the center-line temperature is 360 K. Estimate the time required so that the plastic can be ejected (this is called the "freeze-off" time).

**9.25** A very long cylinder is cooled in a fluid in which the heat transfer coefficient is constant but its value is unknown. At the center, the temperature does not noticeably decrease until the relative temperature at the surface cools to 0.5. Based on this information, deduce the heat transfer coefficient. *Data for solid:* radius = 80 mm;  $\rho = 2000 \text{ kg m}^{-3}$ ;  $C_p = 480 \text{ J kg}^{-1} \text{ K}^{-1}$ ;  $k = 0.246 \text{ W m}^{-1} \text{ K}^{-1}$ .

**9.26** The end ( $z = 0$ ) of very long cylindrical bar is heated uniformly with a constant flux of  $q_0$ . The side of the bar loses heat to the surroundings at  $T_\infty$  with a uniform and constant value of  $h$ . Before heating, the bar is at a uniform temperature of  $T_0$ .

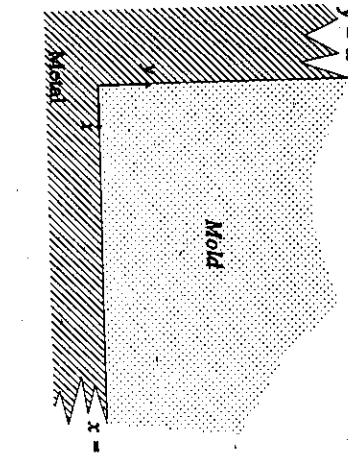
- For constant thermal properties, write an appropriate form of the equation of energy for temperature within the bar during the transient period.
- Give appropriate boundary conditions and an initial condition for part a).
- Is it possible to reach a steady state? Give a reason for your answer.

**9.27** A very large and thick slab of copper is initially at a uniform temperature of 600°F. The surface temperature is suddenly lowered to 100°F by a water spray.

- What is the temperature at a depth of 3 in., 4 min. after the surface temperature has changed?
- If it is necessary to predict the temperature in the slab for a period of 5 minutes, what must be the thickness of the slab so that it can be approximated as a semi-infinite solid?

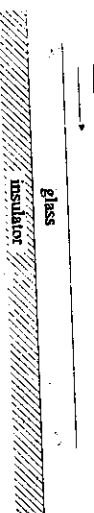
**Data for copper:**  $\rho = 552 \text{ lb}_m \text{ ft}^3$ ;  $C_p = 0.100 \text{ Btu lb}_m^{-1} \text{ }^\circ\text{F}^{-1}$ ;  $k = 215 \text{ Btu h}^{-1} \text{ ft}^{-1} \text{ }^\circ\text{F}^{-1}$ . Work this out in English units.

**9.28** Initially the mold for a junction-shaped casting is at a uniform temperature,  $T_0$ . Then liquid metal at its freezing point,  $T_f$ , is poured into the mold. During the period of time it takes for the metal to solidify, the surface of the mold is maintained at  $T_s$ . Assume constant thermal properties of the mold. For the upper right quadrant of the mold which extends to  $\infty$  for both  $x$  and  $y$ , write a solution that yields temperature as a function of coordinates in the mold and time.



**9.30** A solid circular cylinder of steel, with a diameter of 240 mm and a length of 183 mm, is initially at 300 K. A treatment to transform retained austenite requires cooling in liquid nitrogen (78 K). For a cooling time of 2520 s, it is known (by measurement) that a point in the center of a circular face is at 100 K. What is the temperature at the geometric center of the cylinder. *Data:*  $\rho = 7690 \text{ kg m}^{-3}$ ;  $C_p = 795 \text{ J kg}^{-1} \text{ K}^{-1}$ ;  $k = 35 \text{ W m}^{-1} \text{ K}^{-1}$ ;  $h = 230 \text{ W m}^{-2} \text{ K}^{-1}$ .

**9.31** A sheet of glass, 0.02 ft thick, is cooled from an initial temperature of 1800°F by air flowing over the top surface of the glass. The convective heat transfer coefficient for the air is 8  $\text{Btu h}^{-1} \text{ ft}^{-2} \text{ }^\circ\text{F}^{-1}$ , and the glass rests on a perfect insulator.



- What time is required for the bottom surface of the glass to cool to 400°F?
- When the bottom surface is at 400°F, what is the temperature of the top surface?

Do this problem in English units. Thermal properties of the glass are  $k = 0.32 \text{ Btu h}^{-1} \text{ ft}^{-1} \text{ }^\circ\text{F}^{-1}$ ,  $\rho = 200 \text{ lb}_m \text{ ft}^{-3}$  and  $C_p = 0.2 \text{ Btu lb}_m^{-1} \text{ }^\circ\text{F}^{-1}$ .

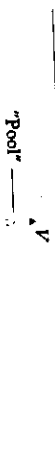
**9.32** A cylinder, initially at 300°F, is plunged into a large melt of a low melting point metal maintained at 810 K; the heat transfer coefficient may be taken to be infinity. The dimensions of the cylinder are 230 mm diameter and 150 mm length.

- After 100 s of heating in the melt, what is the temperature in the geometric center of the cylinder?
- After 5 s, what is the temperature at the centers of the circular surfaces?

*Data:*  $k = 5.2 \text{ W m}^{-1} \text{ K}^{-1}$ ;  $\rho = 4810 \text{ kg m}^{-3}$ ;  $C_p = 420 \text{ J kg}^{-1} \text{ K}^{-1}$ .

**9.33** A laser beam is used as a moving point source to harden the surface of a thick piece of steel by multiple passes (i.e., rapid scanning) across the surface; no melting occurs. To what depth is it possible to produce martensite with one pass if the critical cooling rate for the steel is 280 K s<sup>-1</sup> at 810 K. For this steel it is known that austenite exists at  $T \geq 1090$  K. *Data for steel:*  $\alpha = 7.2 \times 10^{-6} \text{ m}^2 \text{ s}^{-1}$ ;  $k = 35 \text{ W m}^{-1} \text{ K}^{-1}$ ; initial temperature = 300 K. *Laser conditions:* Power = 4 kW at 50 percent efficiency; speed = 420 mm s<sup>-1</sup>.

**9.34** A laser beam is used to remelt silicon in a process to produce material for solar cells. The silicon is 100 mm wide and 2 mm thick. The molten pool passes across the width of the silicon, as shown in the diagram, with a velocity  $V = 400 \text{ m s}^{-1}$ . The bulk of the silicon is at 293 K. Assume that the pool can be treated as a moving source.



- Calculate the maximum cooling rate in the silicon. At what location is this cooling rate achieved?
- At what distances from the centerline of the path left by the laser beam, is a peak temperature of 1280 K achieved?

**Data:** Beam conditions, 5 kW at 50% efficiency. Silicon: melting temperature is 1700 K; heat of fusion is  $1.41 \times 10^3 \text{ kJ kg}^{-1}$ ; thermal conductivity is  $100 \text{ W m}^{-1} \text{ K}^{-1}$ ; diffusivity is  $5.2 \times 10^{-5} \text{ m}^2 \text{ s}^{-1}$ .

## SOLIDIFICATION OF METALS

The production of most metal parts, including articles produced by powder-metallurgy techniques, involves solidification. Castings obviously entail solidification; forgings and wrought products are also castings that have been hot worked, and their behavior in many cases can be traced back to the method of solidification. In particular, the solidification rate of alloys is an extremely important processing variable. The solidification rate relates directly to the coarseness—or fineness—of dendritic structures and hence controls the spacing and distribution of microsegregates, such as coring, second phases, and inclusions. Thermal gradients during freezing are also of great significance, being related to the formation of macrosegregation and porosity in alloys. For these metallurgical reasons and from a process engineering viewpoint, solidification heat transfer should be recognized as an important topic.

### 10.1 SOLIDIFICATION IN SAND MOLDS

The following analysis applies when the metal solidifies in sand molds, or more generally, when the predominant resistance to heat flow is within the mold itself, e.g., the mold is made of plaster, granulated zircon, mullite, or various other materials that are poor conductors of heat, such as ceramic shell-molds in investment casting processes.

Consider pure liquid metal with no superheat poured against a flat mold wall of a poor conductor. Figure 10.1 shows the temperature distribution in the metal and the mold at some time during solidification. Because all the resistance to heat flow is almost entirely within the mold, the surface temperature  $T_s$  nearly equals the melting temperature of the metal  $T_M$ . This means that during freezing the temperature drop through the solidified metal is small, and at the metal-mold interface a constant temperature of  $T_s \approx T_M$  is maintained. Under these conditions, the temperature history in the mold is given by Eq. (9.64) (i.e., the solution for a semi-infinite body):

$$\frac{T - T_M}{T_0 - T_M} = \operatorname{erf} \frac{x}{2\sqrt{\alpha t}} \quad (10.1)$$

which gives

$$M = \frac{2}{\sqrt{\pi}} \left[ \frac{T_M - T_0}{\rho' H_f} \right] \sqrt{k_p C_p} \sqrt{t}. \quad (10.7)$$

Thus, we see that the amount of solidification depends on certain metal characteristics,  $(T_M - T_0)/\rho' H_f$ , and the mold's heat diffusivity,  $k_p C_p$ .

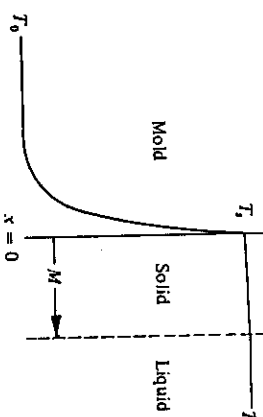


Fig. 10.1 The temperature distribution during solidification of a metal in a sand mold.

where  $x$  is the distance into the mold,  $\alpha$  is its thermal diffusivity, and  $T_0$  is the initial uniform temperature (usually  $T_0$  is room temperature). The use of this equation implies that the mold is sufficiently thick to satisfy the boundary condition  $T(\infty, t) = T_0$ ; in practice, this requirement is often met.

Of primary interest is the rate at which heat is extracted from the solidifying metal, which ultimately leads to a determination of the total solidification time. Equation (10.1) is used to obtain the amount of heat which flows into the mold, and this quantity of heat must equal the latent heat evolved during solidification.

The heat flux into the mold follows from Eq. (10.1):

$$q|_{x=0} = -k \left[ \frac{\partial T}{\partial x} \right]_{x=0} = \frac{k(T_M - T_0)}{\sqrt{\pi \alpha t}}. \quad (10.2)$$

Remembering that  $\alpha = k/\rho' C_p$ , we rewrite Eq. (10.2) as

$$q|_{x=0} = \frac{\sqrt{k\rho' C_p}}{\sqrt{\pi t}} (T_M - T_0). \quad (10.3)$$

The product  $k\rho' C_p$  represents the ability of the mold to absorb heat at a certain rate and is called the *heat diffusivity*.<sup>\*</sup>

The rate at which latent heat is evolved per unit area can be written

$$q|_{x=0} = \rho' H_f \frac{dM}{dt}, \quad (10.4)$$

where  $\rho'$  = density of solidifying metal,  $H_f$  = latent heat of fusion of the metal,  $\text{J kg}^{-1}$ , and  $M$  = thickness of metal solidified.

Equating Eq. (10.3) to Eq. (10.4) yields the rate at which the interface advances into the liquid:

$$\frac{dM}{dt} = \frac{(T_M - T_0)\sqrt{k\rho' C_p}}{\rho' H_f \sqrt{\pi t}}. \quad (10.5)$$

Integration follows, with the limit

$$M = 0 \quad \text{at } t = 0, \quad (10.6)$$

Freezing from a planar mold wall, as discussed above, is not the usual problem engineers encounter in practice. It is often important to evaluate the freezing times of complex shapes, in which the contour of the mold wall has some influence on solidification time. For example, contrast heat flow into the convex and concave walls to the plane mold wall situation shown in Fig. 10.2. Heat flow into the convex surface is divergent and, therefore, more rapid than into the plane mold. In contrast, heat flow into the concave surface is convergent and less rapid than into the plane mold wall.

### 10.1.1 Effect of contour on solidification time

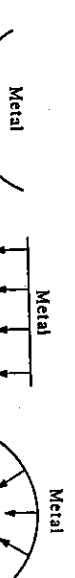


Fig. 10.2 Effect of contour on the heat flux into molds.

As a first approximation, such effects are sometimes neglected because the heated zone in the mold is shallow, and the difference in heat flow between a plane mold wall and a contoured wall is small. As such, we visualize that a given mold surface area has the ability to absorb a certain amount of heat in a given time regardless of its contour. Thus, we generalize Eq. (10.3) for all contours, and for a given surface area  $A$ , the mold absorbs an amount of heat  $Q$  in time  $t$ :

$$Q = \int_0^t A q|_{x=0} dt = \frac{Ak(T_M - T_0)}{\sqrt{\pi \alpha t}} \int_0^t \frac{dt}{\sqrt{t}} = \frac{2Ak(T_M - T_0)}{\sqrt{\pi \alpha}} \sqrt{t}. \quad (10.8)$$

For a casting of volume  $V$  to completely solidify, all its latent heat must be removed; hence, the total latent heat  $Q$  evolved is

$$Q = \rho' VH_f. \quad (10.9)$$

Equations (10.8) and (10.9) are then combined to yield the solidification time of a casting in terms of its volume-to-surface area ratio:

$$t = C \left[ \frac{V}{A} \right]^2. \quad (10.10)$$

\*The heat diffusivity has units of  $\text{J}^2 \text{m}^{-4} \text{K}^{-2} \text{s}^{-1}$  and should not be confused with thermal diffusivity.

where

$$C = \frac{\pi}{4} \left[ \frac{\rho' H_f}{T_m - T_0} \right]^2 \left[ \frac{1}{k_p C_p} \right]$$

Equation (10.10) is often referred to as Chvorinov's rule, and  $C$ , as Chvorinov's constant. It permits comparison of freezing times of castings with different shapes and sizes. The relationship works best for casting geometries in which none of the mold material becomes saturated with heat, such as in internal corners or internal cores. The success of this relationship hinges on the mold material absorbing the same amount of heat per unit area exposed to the metal. This is strictly true only for castings which have similar shapes but different sizes.

In applications when more precision is required, it is necessary to account for the effect of mold contour on solidification. To quantify some contour effects, let us examine differences among castings of three basic shapes, namely, the infinite plate, the infinitely long cylinder, and the sphere. First, we define two dimensionless parameters,  $\beta$  and  $\gamma$ :

$$\beta = \frac{V/A}{\sqrt{\alpha t}},$$

and

$$\gamma = \left[ \frac{T_m - T_0}{\rho' H_f} \right] \rho C_p.$$

With these parameters, the freezing times for the three basic shapes are calculated by

$$\beta = \gamma \left[ \frac{2}{\sqrt{\pi}} + \frac{1}{a\beta} \right], \quad (10.11)$$

where  $a = \infty$  for infinite plates,  $a = 4$  for infinite circular cylinders and  $a = 3$  for spheres.

We can deduce Eq. (10.11) from Eq. (10.10) by a rearrangement. The values of  $a$  for the cylinder and spheres have resulted by rearranging expressions presented by Adams and Taylor;<sup>1</sup> their expression for the cylinder is approximate while that for the sphere is exact.

Equation (10.11) shows the error of using Chvorinov's rule without regard to the mold contours. For example, let us calculate the value of  $\beta$  for  $\gamma = 1$ , which is typical of metal-silica sand combinations.

$$\beta \text{ (plate)} = 1.13,$$

$$\beta \text{ (cylinder)} = 1.32,$$

$$\beta \text{ (sphere)} = 1.37.$$

We see that if we treat the three cases all as plates (i.e., neglecting the contour), then we would make an error of as much as 40-50% in freezing time for equivalent values of  $V/A$ .

The value of  $a$  for spheres may be used for other chunky shapes such as cubes. Similarly, the expression for solidification time of a cylinder may be used to approximate the freezing time of bars of square cross section.

**Example 10.1** Determine the solidification time of the following iron castings, both poured with no superheat into sand molds:

- a) a slab-shaped casting 100 mm thick;
  - b) a spherically shaped casting 100 mm in diameter.
- Iron Data:  $T_m = 1808 \text{ K}$ ;  $H_f = 2.27 \times 10^3 \text{ J kg}^{-1}$ ;  $\rho' = 7210 \text{ kg m}^{-3}$ .  
Sand Data:  $k = 0.865 \text{ W m}^{-1} \text{ K}^{-1}$ ;  $\rho = 1600 \text{ kg m}^{-3}$ ;  $C_p = 1170 \text{ J kg}^{-1} \text{ K}^{-1}$ .

**Solution.** Assume the mold is initially at 300 K.

$$\gamma = \frac{(1808 - 300)(1600)(1170)}{(7210)(2.72 \times 10^3)} = 1.44.$$

$$\alpha = \frac{0.865}{(1600)(1170)} = 4.62 \times 10^{-7} \text{ m}^2 \text{ s}^{-1}.$$

- a) For the slab, with thickness  $\delta = 100 \text{ mm}$ ,  $a = \infty$  and

$$\frac{V}{A} = \frac{\delta}{2} = \frac{0.100}{2} = 0.050 \text{ m.}$$

Equation (10.11) gives:

$$\beta = \frac{2}{\sqrt{\pi}} \gamma = \frac{(2)(1.44)}{\sqrt{\pi}} = 1.62,$$

so that

$$\frac{V/A}{\sqrt{\alpha t}} = 1.62.$$

Therefore,

$$t = \frac{(V/A)^2}{1.62^2 \alpha} = \frac{(0.050)^2}{(1.62^2)(4.62 \times 10^{-7})} = 2060 \text{ s.}$$

- b) For the sphere,  $D$  (diameter) = 100 mm,  $a = 3$  and

$$\frac{V}{A} = \frac{D}{6} = \frac{0.100}{6} = 0.0167 \text{ m.}$$

Equation (10.11) becomes:

$$\beta = 1.44 \left[ \frac{2}{\sqrt{\pi}} + \frac{1}{3\beta} \right],$$

<sup>1</sup>C. M. Adams and H. F. Taylor, *Trans. AFS* **65**, 170-176 (1957).

from which  $\beta = 1.88$ . Therefore,

$$t = \frac{(0.0167^2)}{(1.88^2)(4.62 \times 10^{-7})} = 171 \text{ s.}$$

The sphere solidifies in less than one-tenth the time required for the slab to solidify.

### 10.1.2 Effect of superheat on solidification time

We can assess the effect of superheat on the solidification time by realizing that, in addition to absorbing latent heat, the sand must also absorb the superheat. Again, we assume that the temperature gradients within the casting are negligible, and at the time solidification is complete, the entire casting is close to its freezing point. In this case, the total quantity of heat to be removed from the casting is

$$Q = \rho' V H_f + \rho'_l V C_p \Delta T_s \quad (10.12)$$

The subscript  $l$  denotes liquid phase properties, and  $\Delta T_s$  is the amount of superheat in degrees.

We now consider infinite plate castings, and in order to make the analysis simple, yet sufficiently accurate, we assume that Eq. (10.8) is valid even though the interface temperature of the mold is not constant while the liquid phase loses its superheat. In view of this approximation, it is certainly acceptable not to distinguish differences in the density of the liquid and solid phases. Thus  $\rho'_l \approx \rho$ , and when Eq. (10.12) is set equal to Eq. (10.8), we obtain

$$t = \frac{\pi}{4} \frac{1}{k_p C_p} \left[ \frac{\rho' H_f'}{T_m - T_0} \right]^2 \left[ \frac{V}{A} \right]. \quad (10.13)$$

In this expression,  $H_f'$  is the *effective heat of fusion*, and represents the sum of the latent heat of fusion and the liquid's superheat, that is,

$$H_f' = H_f + C_{p,l} \Delta T_s. \quad (10.14)$$

Note that the solidification time is still proportional to  $(V/A)^2$ .

## 10.2 SOLIDIFICATION IN METAL MOLDS

When poured into metal molds, castings freeze rapidly, and temperatures change drastically in both the mold and the casting. An understanding of the variables affecting solidification in metal molds is important because most ingots, all permanent mold castings, and all die castings are made in metal molds. Also many sand castings are made in molds that incorporate metal inserts called chills at strategic positions to increase the rate of solidification.

The analysis of heat transfer when metal is poured against a chill wall is more complicated than that when metal is poured into a sand mold; this is due to the fact that metal molds are much better heat conductors than sand molds. The added complexities are illustrated by the casting-mold situation shown in Fig. 10.3. At the solidified metal-mold interface, a temperature drop exists, due to thermal contact resistance. The condition of no contact resistance would exist only if the mold-casting contact were so intimate that wetting would occur, that is, the casting would become soldered to the mold.

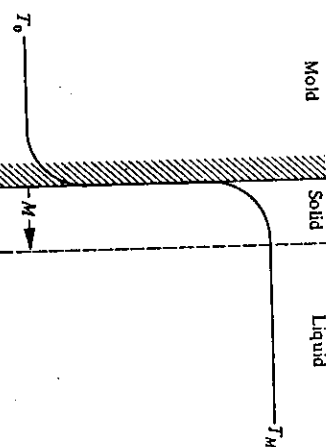


Fig. 10.3 The temperature distribution during the solidification of a metal from a chill wall.

In addition to the contact resistance, there are other differences between solidification in sand and in chill molds:

- The thermal conductivity of the metal being cast forms an important portion of the overall resistance to heat flow. This results in the surface temperature being well below the melting point, while appreciable thermal gradients exist within the solidifying metal.
- More total heat is removed during solidification because of the solidified metal which is subcooled. Thus, the heat capacity of the solidifying metal is important.

In the following sections, we discuss selected problems of solidification, each of practical importance.

### 10.2.1 Constant casting surface temperature

Consider a mass of pure liquid metal, initially at its freezing temperature, which has its surface suddenly cooled to a constant temperature,  $T_r$ . After some solidification has occurred, the temperature profile in the solidifying metal will appear as the solid profile (Fig. 10.4(a)). The temperature profile is identical to the temperature profile in the semi-infinite solid depicted in Fig. 10.4(b), except that the temperature field in the solidifying metal is between  $T_m$  and  $T_r$ , rather than actually extending to  $T_\infty$ . However, the temperature "reactes" for  $T_\infty$  just as in the semi-infinite solid, and the temperature distribution within the solidified metal takes the form

$$\frac{T - T_r}{T_\infty - T_r} = \operatorname{erf} \frac{x}{2\sqrt{\alpha t}}. \quad (10.15)$$

In Fig. 10.4(a),  $T_\infty$  is not known *a priori*. It is an imaginary temperature which makes the temperature distribution analogous to the case of the semi-infinite solid, or it may be thought of as an integration constant. To distinguish the thermal transport properties of the solidifying metal, primes are used. The thermal transport properties of the mold have no primes.

We now develop an expression for the rate of solidification by applying the boundary condition

$$T(M, t) = T_m, \quad (10.16)$$

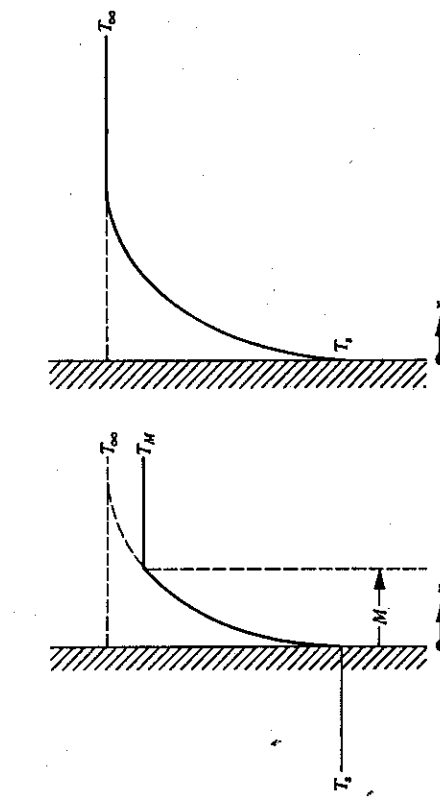


Fig. 10.4 Analogous temperature distributions in (a) solidifying metal, and (b) a semi-infinite solid.

i.e., the temperature at the solid-liquid interface is the freezing point. In addition, we recognize that the rate of evolution of latent heat of fusion equals the heat flux into the solid at the interface; that is

$$k' \frac{\partial T}{\partial x} (M, t) = H_f \rho' \frac{dM}{dt}. \quad (10.17)$$

When applied to the temperature distribution, Eq. (10.16) yields

$$\frac{T_M - T_s}{T_\infty - T_s} = \operatorname{erf} \frac{M}{2\sqrt{\alpha' t}}. \quad (10.18)$$

Since the left-hand side of this equation is constant, the argument of the error function must also be constant. Hence

$$M = 2\beta\sqrt{\alpha' t}. \quad (10.19)$$

Once again the thickness solidified is proportional to  $\sqrt{t}$ .

To evaluate the constant  $\beta$ , we evaluate the heat flux at the solid-liquid interface which we obtain from Eq. (10.17):

$$\begin{aligned} k' \frac{\partial T}{\partial x} (M, t) &= \frac{(T_\infty - T_s)\sqrt{k' \rho' C_p}}{\sqrt{\pi} \sqrt{t}} \exp \left[ -\frac{M^2}{4\alpha' t} \right] \\ &= \frac{(T_M - T_s)\sqrt{k' \rho' C_p}}{\sqrt{\pi} \sqrt{t} \operatorname{erf} \beta} \exp(-\beta^2). \end{aligned} \quad (10.20)$$

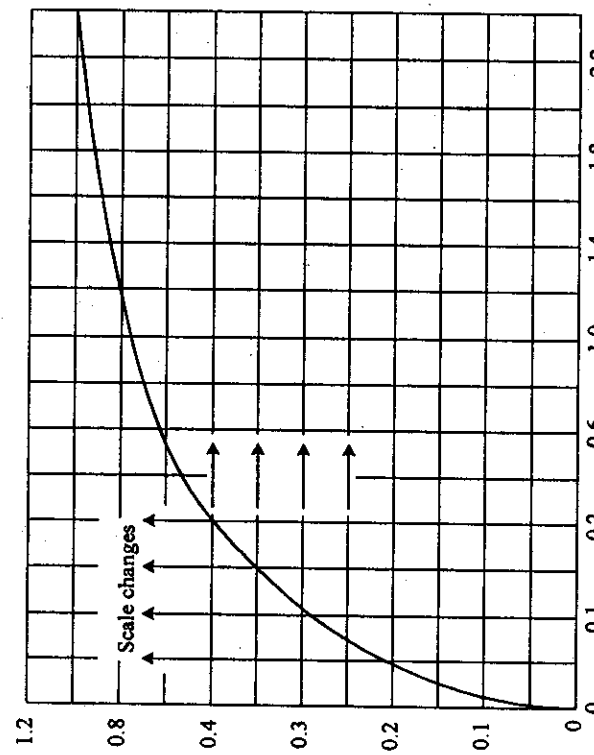
The latent heat evolved at the interface is written

$$H_f \rho' \frac{dM}{dt} = H_f \rho' \beta \frac{\sqrt{\alpha'}}{\sqrt{t}}. \quad (10.21)$$

Substituting Eqs. (10.20) and (10.21) into Eq. (10.17), and simplifying, we have

$$\beta e^\beta \operatorname{erf} \beta = (T_M - T_s) \frac{C_p}{H_f \sqrt{\pi}}. \quad (10.22)$$

We now have an expression to calculate  $\beta$ . We may use Fig. 10.5 to evaluate  $\beta$ , rather than using Eq. (10.22) which entails trial and error.

Fig. 10.5 Evaluation of  $\beta$  for Eq. (10.22).

To summarize,  $\beta$  can be determined from Fig. 10.5. Thus the thickness solidified is known (Eq. (10.19)),  $T_s$  can be determined (Eq. (10.18)), and the temperature distribution can be computed (Eq. (10.15)), if so desired.

This analysis is, of course, valid for unidirectional heat flow; its results can be applied to slab-shaped castings. If the solidification time is sought, then evaluate  $\beta$  and use Eq. (10.19) with  $M = L$ , the semithickness of the slab.

The above method of solution is not systematic and cannot be extended to the solidification of other shapes. However, Adams<sup>2</sup> presented a method utilizing a power series that can be extended to the freezing of spheres and cylinders. His results for solidification

<sup>2</sup>C. M. Adams, "Thermal Considerations in Freezing," *Liquid Metals and Solidification*, ASM, Cleveland, OH, 1958.

times of spheres and cylinders freezing with a constant surface temperature,  $T_s$ , are given in Fig. 10.6.

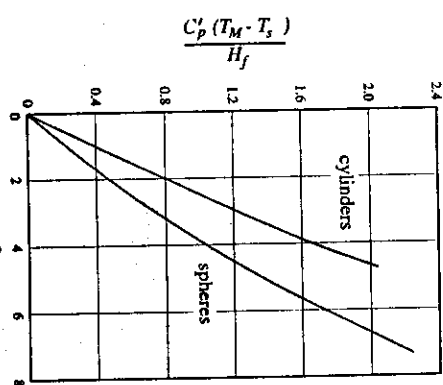


Fig. 10.6 Solidification times for spheres and cylinders with constant surface temperature. (From C. M. Adams, "Thermal Considerations in Freezing," *Liquid Metals and Solidification*, ASM, Cleveland, OH, 1958.)

While application of the foregoing is limited because it is difficult to imagine practical situations in which a constant surface temperature is maintained, an example of a case of practical importance is the determination of the solidification rate in a large steel ingot poured against a copper, water-cooled mold wall,<sup>1</sup> except for the initial stage of solidification. The solutions are also useful for indicating the maximum freezing rate that can be obtained by direct cooling, since the boundary condition of constant surface temperature corresponds to a case of  $h \rightarrow \infty$  at the surface.

### 10.2.2 Gradients within mold and casting, no interface resistance

We depict this case in Fig. 10.7. Both mold and metal form barriers to heat flow. The mold is initially at room temperature, and the liquid metal is at its melting point. The mold is thick enough so that no temperature rise occurs on its exterior surface, and we can consider it to be semi-infinite. This case is applicable, for example, in determining the solidification rate of a large ingot in a thick metal mold; it applies after sufficient material has frozen so that interface resistance is no longer important. This analysis is also useful in deciding if a particular metal-sand mold combination is such that  $T_s$  does, or does not, approximate  $T_M$ .

In the previous problem,  $T_s$  was fixed as the boundary condition of the situation. In the case at hand,  $T_s$  is established at a particular level, depending upon the thermal properties of both the mold and the solidifying metal.

We now proceed to develop the solution which satisfies the requirements

$$\lim_{t \rightarrow 0} \left[ k \left[ \frac{\partial T}{\partial x} \right]_{x=0-t} - k' \left[ \frac{\partial T}{\partial x} \right]_{x=0+t} \right] = 0; \quad (10.23)$$

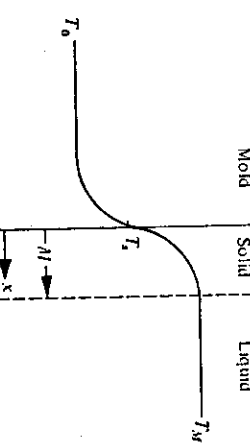


Fig. 10.7 Temperature distribution during solidification with no interface resistance.

that is, the heat flux into the casting-mold interface from the solidifying metal must equal the flux away from the interface into the mold. We repeat the two additional boundary conditions that must be satisfied at the freezing interface:

$$T(M,t) = T_M, \quad (10.16)$$

$$k' \frac{\partial T}{\partial x} (M,t) = \rho' H_f \frac{dT}{dt}. \quad (10.17)$$

The mold is semi-infinite in the negative  $x$ -domain with some unknown surface temperature  $T_s$ . Thus

$$\frac{T - T_s}{T_0 - T_s} = \operatorname{erf} \frac{-x}{2\sqrt{\alpha t}}, \quad (10.24)$$

where  $T_0$  is the initial uniform temperature of the mold. For the solidifying metal, Eq. (10.15) applies again; however, note at this point that  $T_\infty$  and  $T_s$  are both unknown,

$$\frac{T - T_s}{T_\infty - T_s} = \operatorname{erf} \frac{x}{2\sqrt{\alpha t}}. \quad (10.15)$$

When we apply Eq. (10.16) to Eq. (10.15), we realize that the argument of the error function is constant, and again defined as  $\beta$ , so that Eq. (10.19) applies.

On differentiating Eqs. (10.24) and (10.15), and applying Eqs. (10.23), (10.16), and (10.17), we obtain

$$\frac{(T_M - T_s)C_p}{H_f \sqrt{\pi}} = \beta e^\beta \operatorname{erf} \beta, \quad (10.22)$$

$$\frac{(T_M - T_s)C_p}{H_f \sqrt{\pi}} = \beta e^\beta \left[ \sqrt{\frac{k' \rho C_p}{k \rho C_p}} + \operatorname{erf} \beta \right], \quad (10.25)$$

$$\frac{(T_\infty - T_s)C_p}{H_f \sqrt{\pi}} = \beta e^\beta, \quad (10.26)$$

<sup>1</sup>Such processes would include electroslag remelting and vacuum arc melting.

$$\frac{T_s - T_0}{T_\infty - T_s} = \sqrt{\frac{k' \rho' C_p'}{k \rho C_p}} \quad (10.27)$$

To summarize the results of this section, we calculate the temperature profiles in both the mold and the solidifying metal; we also determine the thickness solidified. As a reminder, remember that the thermal transport properties with primes are for the solidifying metal.

We calculate the temperature profile in the mold by completing the following steps:

- 1) Calculate the mold-casting interface temperature  $T_i$ , from the known thermal properties

$$(T_M - T_0) \left[ \frac{C_p}{H_f} \right] \quad \text{and} \quad \sqrt{\frac{k' \rho' C_p'}{k \rho C_p}},$$

and Fig. 10.8, which was derived by calculating  $\beta$  on a trial-and-error solution of Eq. (10.25), and then determining  $T_i$ , from Eq. (10.22).

2) The value of  $T_i$ , thus obtained can be used in Eq. (10.24) for the temperature profile in the mold.

We calculate the temperature profile in the solidifying metal by performing these steps:

- 1) Calculate  $T_i$ , from Fig. 10.8.
- 2) Determine  $T_\infty$ , using either Eq. (10.26) or Eq. (10.27).
- 3) The values of  $T_\infty$  and  $T_i$ , thus obtained can be used in Eq. (10.15) for the temperature profile in the metal.

If we wish to calculate the thickness of the solidified metal, then we determine  $T_s$ , from Fig. 10.8 and use Fig. 10.5 for a value of  $\beta$ . With this value of  $\beta$ , Eq. (10.19) can be applied.

**Example 10.2** Determine the freezing time of an iron slab-shaped casting which is 100 mm thick. Assume no interface resistance, and consider the cases of pure iron poured at its freezing point into a) a sand mold, and b) a very thick copper mold with no resistance to heat transfer at the casting-mold interface.

**Mold Data:**

Material	$k$ , W m <sup>-1</sup> K <sup>-1</sup>	$\rho$ , kg m <sup>-3</sup>	$C_p$ , J kg <sup>-1</sup> K <sup>-1</sup>
Sand	0.865	1600	1170
Copper	398	8970	380

**Iron Data:**  $T_M = 1808$  K;  $H_f = 2.72 \times 10^5$  J kg<sup>-1</sup>;  $\rho' = 7210$  kg m<sup>-3</sup>;  $k' = 83$  W m<sup>-1</sup> K<sup>-1</sup>;  $C_p' = 670$  J kg<sup>-1</sup> K<sup>-1</sup>;  $T_0 = 300$  K.

**Solution:**

$$a) \quad (T_M - T_0) \frac{C_p'}{H_f} = (1808 - 300) \frac{670}{2.72 \times 10^5} = 3.71,$$

$$\sqrt{\frac{k' \rho' C_p'}{k \rho C_p}} = \sqrt{\frac{(83)(7210)(670)}{(0.865)(1600)(1170)}} = 15.7.$$

From Fig. 10.8, we obtain  $T_i$ :

$$\frac{T_i - T_0}{T_M - T_0} = 1.$$

Therefore,  $T_i = T_M$ , and the analysis used in Example 10.1 is valid, so that  $t$  (sand) = 2060 s.

$$b) \quad (T_M - T_0) \frac{C_p'}{H_f} = 3.71, \text{ as in part a),}$$

$$\sqrt{\frac{k' \rho' C_p'}{k \rho C_p}} = \sqrt{\frac{(83)(7210)(670)}{(398)(8970)(380)}} = 0.544.$$

From Fig. 10.8, we get

$$\frac{T_i - T_0}{T_M - T_0} = 0.42$$

$$T_i = (0.42)(1808 - 300) + 300 = 933 \text{ K.}$$

Now we resort to Fig. 10.5 to obtain the value of  $\beta$ :

$$(T_M - T_i) \frac{C_p'}{H_f \sqrt{\pi}} = (1808 - 933) \left[ \frac{670}{2.72 \times 10^5 \sqrt{\pi}} \right] = 1.22,$$

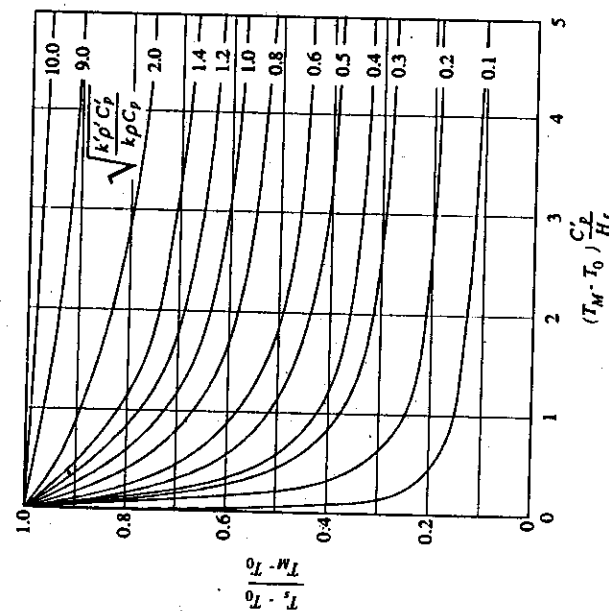


Fig. 10.8 Relative mold-casting interface temperatures for unidirectional freezing with no interface resistance. (From C. C. Reynolds, *Trans. AFS* 72, 343 (1964).)

and  $\beta = 0.87$ . Finally, we use Eq. (10.19), with  $M = 0.050$  m and  $\alpha' = 1.72 \times 10^{-5}$   $\text{m}^2 \text{s}^{-1}$ .

$$t = \frac{M^2}{4\beta^2\alpha'} = \frac{(0.050)^2}{(4)(0.87^2)(1.72 \times 10^{-5})}$$

$$t (\text{copper mold}) = 48 \text{ s.}$$

### 10.2.3 Interface resistance

In the previous sections, we depicted situations in which the surface temperature  $T_s$  remained constant. When we examine the more likely situation of some interface resistance, then the surface temperature of the casting varies with time, and the analysis becomes more complex.

Before analyzing the temperature history in the mold and casting in a general case (Fig. 10.3), let us first consider a simpler case (Fig. 10.9). In Fig. 10.9, the mold is kept at a constant and uniform temperature,  $T_m$ , by internal water cooling. The interface resistance to heat transfer is much greater than the resistance of the solidifying metal. It applies in continuous casting in lower portions of the mold where the solidified shell pulls away from the mold wall and an air gap forms a significant resistance to heat transfer. Practical importance is also attached to this case for estimating the thickness solidified in small thin-section parts cast in conductive metal molds, when the solidification time is small.

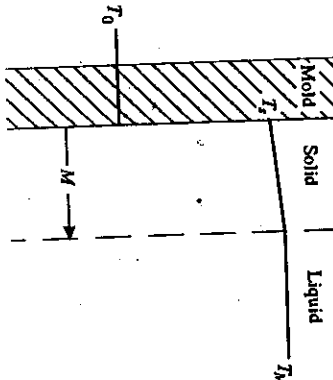


**Fig. 10.9** Temperature distribution during solidification with a predominating interface resistance.

Notice  $T_s \neq T_m$ , and the heat leaves the casting via  $h$  at the surface to a water-cooled mold maintained at  $T_m$ . Here we simplify the analysis by approximating the temperature profile within the solidifying metal as a linear function. Then we write the heat flux at the casting-mold interface as

$$q|_{x=0} = k' \frac{T_m - T_s}{M}. \quad (10.28)$$

Also

$$q|_{x=0} = h(T_s - T_0). \quad (10.29)$$

We then eliminate the surface temperature  $T_s$ , which varies, by combining Eqs. (10.28) and (10.29); because of the linear temperature profile, we express the flux at the solid-liquid interface simply as

$$q|_{x=0} = q|_{x=M} = \frac{T_m - T_0}{1/h + M/k'}. \quad (10.30)$$

In addition, at  $x = M$ , the latent heat is evolved so that

$$q|_{x=M} = \rho' H_f \frac{dM}{dt}. \quad (10.31)$$

By combining Eqs. (10.30) and (10.31) and integrating with  $M = 0$  at  $t = 0$ , we obtain

$$M = \frac{h(T_m - T_0)}{\rho' H_f} t - \frac{h}{2k'} M^2. \quad (10.32)$$

Adams<sup>3</sup> solved the problem approximately but in a more rigorous manner in which the temperature profile is not assumed to be linear as above. The more refined analysis is similar to Eq. (10.32) with an additional factor,  $a$ :

$$M = \frac{h(T_m - T_0)}{\rho' H_f a} t - \frac{h}{2k'} M^2. \quad (10.33)$$

In this expression

$$a = \frac{1}{2} + \sqrt{\frac{1}{4} + \frac{C_p(T_m - T_0)}{3H_f}}.$$

Equation (10.33) is almost exact for  $hM/k \geq 1/2$ . For  $hM/k < 1/2$ , the thickness solidified is overestimated by approximately 10-15%.

**Example 10.3** When Eq. (10.33) applies show that  $M$  varies linearly with time for small times and parabolically with time for large times.

**Solution.** Small times:  $t \rightarrow 0$ ,  $M^2 \rightarrow 0$  and Eq. (10.33) gives

$$M = \frac{h(T_m - T_0)}{\rho' H_f a} t.$$

The result is linear because the heat transfer is limited by the resistance across  $x = 0$ .

Large times:  $t \rightarrow \infty$ ,  $T_s \rightarrow T_0$  and the system behaves as though  $h \rightarrow \infty$ . In this case Eq. (10.33) reduces to

$$M = \left[ \frac{2k'(T_m - T_0)}{\rho' H_f a} \right]^{1/2} t^{1/2}.$$

The result is parabolic because the heat transfer is limited by the conduction through the increasing thickness of solidified metal.

**Example 10.4** Estimate thickness solidified versus time when iron freezes against a mold maintained at 300 K. For iron use the data in Example 10.2. a) Assume  $h = 10^3 \text{ W m}^{-2} \text{ K}^{-1}$ . b) Assume  $h = 10^4 \text{ W m}^{-2} \text{ K}^{-1}$ .

**Solution.** It is easier to rearrange Eq. (10.33), so we can calculate  $t$  as a function of  $M$ ; then

$$t = \frac{\rho' H_f a}{h(T_M - T_0)} \left[ M + \frac{h}{2k'} M^2 \right].$$

$$a = \frac{1}{2} + \sqrt{\frac{1}{4} + \frac{(670)(1808 - 300)}{(3)(2.72 \times 10^5)}} = 1.72$$

$$\frac{\rho' H_f a}{h(T_M - T_0)} = \frac{(7210)(2.72 \times 10^5)(1.72)}{(1000)(1808 - 300)} = 2237$$

$$\frac{h}{2k'} = \frac{1000}{2(83)} = 6.02.$$

Therefore,

$$t = 2237 M + 1.347 \times 10^4 M^2 \quad (t \text{ in s}; M \text{ in m}).$$

b) With  $h = 10^4 \text{ W m}^{-2} \text{ K}^{-1}$ , the relationship is

$$t = 223.7 M + 1.347 \times 10^4 M^2.$$

The results for both cases are shown in the following figure. As expected solidification is faster with the greater heat transfer coefficient; in addition the linearity of  $M(t)$  extends to about twice the thickness solidified.

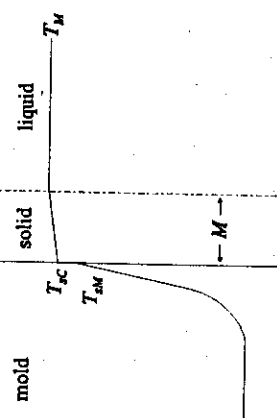
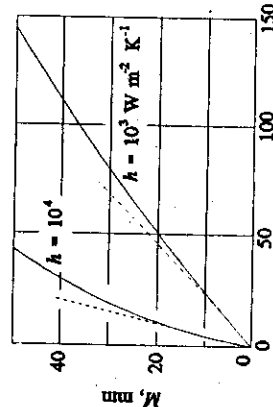


Fig. 10.10 Temperature distribution during solidification with interface resistance to heat transfer.

To start this approximate analysis, we deduce a time-dependent thermal resistance,  $R$ , for heat transfer into the very thick mold of an insulating material. Thus, from Eq. (10.3):

$$R = \frac{\sqrt{\pi t}}{\sqrt{k\rho C_p}}.$$

With the thermal resistance across the interface taken as  $1/h$ , we get the total thermal resistance

$$R_T = \frac{M}{k'} + \frac{1}{h} + \frac{\sqrt{\pi t}}{\sqrt{k\rho C_p}}, \quad (10.34)$$

and Eq. (10.30) can be replaced with

$$q|_{r=0} = \frac{T_M - T_0}{\frac{1}{h} + \frac{M}{k'} + \sqrt{\frac{\pi t}{k\rho C_p}}}. \quad (10.35)$$

To keep the problem tractable, we ignore the sensible heat extracted from the solidifying metal. Further, we neglect  $M/k'$  and thereby restrict this approximate analysis to solidification in relatively insulating molds. With these restrictions in mind, we equate Eqs. (10.31) and (10.35) and arrive at

$$\frac{dM}{dt} = \left[ \frac{T_M - T_0}{\rho' H_f} \right] \left[ \frac{1}{h} + \sqrt{\frac{\pi t}{k\rho C_p}} \right]^{-1}. \quad (10.36)$$

Equation (10.36) is integrated with  $M = 0$  at  $t = 0$ ; the result is Eq. (10.7) corrected by a factor of  $\phi$ :

$$M = \frac{2\phi}{\sqrt{\pi}} \left[ \frac{T_M - T_0}{\rho' H_f} \right] \sqrt{k\rho C_p} \sqrt{t}, \quad (10.37)$$

Now we consider a case that differs somewhat from Fig. 10.9. In addition to the resistance to heat transfer at the mold-metal interface, the mold also offers a comparable resistance to heat transfer. The temperature distribution is shown in Fig. 10.10. At the mold-metal interface, the temperature on the casting side is  $T_{sc}$  and on the mold-side it is

where

$$\phi = 1 - \frac{\sqrt{k\rho C_p}}{h\sqrt{\pi t}} \ln \left[ 1 + \frac{h\sqrt{\pi t}}{\sqrt{k\rho C_p}} \right].$$

This factor accounts for resistance to heat transfer across the metal-mold interface. For small times (i.e., thin section castings), the interface resistance retards solidification significantly. The retarding effect is greater in less insulating molds (i.e., an increased heat diffusivity).

Before we leave discussion of this type of problem, we repeat that the analysis is approximate. An exact solution could be obtained by determining the flux at the surface of the mold on the basis of the temperature distribution given by Eq. (9.67).

**Example 10.5** Recalculate the solidification time of the iron casting, 100 mm thick, in Example 10.1. Assume that  $h = 2800 \text{ W m}^{-2} \text{ K}^{-1}$ .

**Solution.** A trial-and-error solution is required because  $\phi$  depends upon solidification time. From Example 10.1,  $t = 2060 \text{ s}$ . Let's assume, for our first estimate, that  $t = 2300 \text{ s}$ .

$$\begin{aligned} \phi &= 1 - \frac{\sqrt{(0.865)(1600)(1170)}}{(2800)\sqrt{2300}\pi} \ln \left[ 1 + \frac{(2800)\sqrt{2300}\pi}{\sqrt{(0.865)(1600)(1170)}} \right] \\ &= 1 - 5.346 \times 10^{-3} \ln [1 + 187.0] = 0.972. \end{aligned}$$

Notice that  $\phi \sim 1$ ; typically  $0.8 < \phi \leq 1$ , unless  $t < 100 \text{ s}$  when  $0.5 < \phi < 0.9$ .

From the result of Example 10.1, we can write

$$t = \left[ \frac{1}{0.972} \right]^2 (2060) = 2180 \text{ s}.$$

We overestimated the solidification time, so that  $\phi$ , itself, is closer to unity. One or more iterations could be done, but in view of the approximations involved, it might not be worth the added effort. Go ahead and do it anyway!

#### 10.2.4 Gradients within mold and casting with interface resistance

In tackling this situation, we extend the concept of the mold-metal interface temperature introduced in Section 10.2.2. However, in this case there is no constant temperature at the casting-mold interface; rather, there are two surface temperatures, neither of which is constant. To handle this problem, consider an imaginary reference plane between the mold and casting which is at  $T_s$ , where  $T_s$  is constant and determined by the method of Section 10.2.2 using Eq. (10.27). The contact resistance is then apportioned on both sides of the imaginary plane in accordance with the equations

$$h_M = \left[ 1 + \sqrt{\frac{k\rho C_p}{k'\rho' C_p}} \right] h, \quad (10.38)$$

In these expressions,  $h$  is the total heat transfer coefficient across the interface,  $h_M$  is the coefficient on the mold side of the lane, and  $h_c$  is the coefficient on the casting side of the plane.

Figure 10.11 depicts the entire situation, showing the surface temperatures,  $T_{sc}$  and  $T_{sm}$ , of the casting and the mold, respectively. We handle the problem as follows:

- 1) We first solve for  $T_s$  as if there were no interface resistance.
- 2) Using  $T_s$  obtained in (1) and applying Eq. (10.39), we isolate the casting half and study it by using the analysis given in Section 10.2.3. For the casting side, heat is transferred from  $T_{sc}$  to  $T_s$  via  $h_c$ .
- 3) If we wish to study the mold half, we resort to the results of Section 9.4.2 and use Eq. (9.65) or Fig. 9.16. For the mold side, heat is supplied to the mold from a source at  $T_s$  to the surface at  $T_{sm}$  via  $h_M$ .

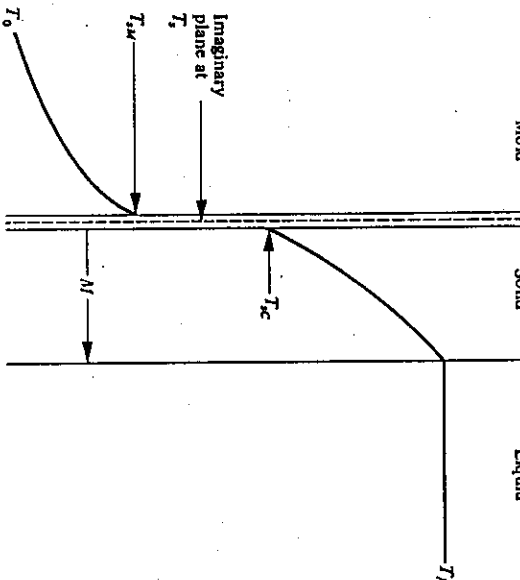


Fig. 10.11 Temperature distribution in the casting and mold when the interface resistance does not predominate.

We present Fig. 10.12 to illustrate the effect of the contact thermal resistance. First, in order to solidify the same amount of metal, it takes more time with some resistance. Note, also, that the two curves become parallel after the early stages of solidification, and  $M$  varies linearly with  $\sqrt{t}$  for both cases. For the early stage of solidification,  $M$  does not vary linearly with  $\sqrt{t}$  when there is some contact resistance.

- b) To solve for the surface temperature of the mold, we may use Eq. (9.63) or Fig. 9.16 with  $h$  replaced by  $h_M$ ,  $T_f$  replaced by  $T_s$ , and  $T_i$  replaced by  $T_0$ . We obtain  $h_M$  by using Eq. (10.38):

$$h_M = \left[ 1 + \sqrt{\frac{(398)(8970)(380)}{(83)(7210)(670)}} \right] (1400) = 3975 \text{ W m}^{-2} \text{ K}^{-1}$$

Then

$$\frac{h_M}{k} \sqrt{\alpha t} = \frac{3975}{398} \sqrt{\frac{(398)(91.9)}{(8970)(380)}} = 1.035.$$

From Fig. 9.16, for the surface we have

$$\frac{T_{sM} - T_0}{T_s - T_0} \approx 0.60,$$

so that

$$T_{sM} = (0.60)(933 - 300) + 300 = 680 \text{ K.}$$

Fig. 10.12 Rate of solidification in metal molds with and without contact resistance.

**Example 10.6** a) Determine the freezing time of the 100 mm thick slab of iron discussed in Example 10.2 when it is cast in a very thick copper mold. The total heat transfer coefficient across the casting-mold interface may be taken as  $1400 \text{ W m}^{-2} \text{ K}^{-1}$ . b) When the casting has completely solidified, what is the surface temperature of the mold?

*Solution.*

a) First solve the problem as if there were no interface resistance, and obtain  $T_f$ . This was done in Example 10.2(b), with the result  $T_f = 933 \text{ K}$ . Using Eq. (10.39), determine the coefficient on the casting side of the interface:

$$h_c = \left[ 1 + \sqrt{\frac{(83)(7210)(670)}{(398)(8970)(380)}} \right] (1400) = 2161 \text{ W m}^{-2} \text{ K}^{-1}.$$

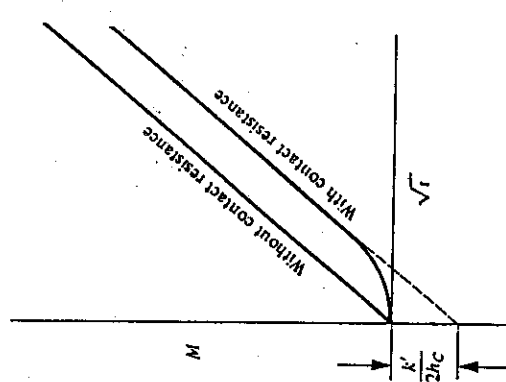
Now use Eq. (10.33), but be sure to substitute  $h_c$  for  $h$  and  $(T_M - T_i)$  for  $(T_s - T_0)$ . Substituting properties and  $M = 0.050 \text{ m}$ , we have

$$0.050 = \frac{(2161)(1808 - 933)}{(7210)(2.72 \times 10^6)a} t - \frac{(2161)(0.050^2)}{(2)(83)},$$

in which

$$a = \frac{1}{2} + \sqrt{\frac{1}{4} + \frac{(670)(1808 - 933)}{(3)(2.72 \times 10^6)}} = 1.484.$$

Solving for  $t$  yields  $t = 127 \text{ s}$ .



Up to this point, we have recognized that a thermal resistance exists at the mold-casting interface in all cases unless soldering occurs. Since no bonding takes place at the interface, the casting and the mold are free to move due to thermal-physical effects. In fact, it is well known that when a metal is cast against a metal mold, a gap forms at the interface. This gap is formed as a result of the mold expanding due to its absorption of heat, and to the solid skin of metal shrinking due to its lowering temperature. Usually, the prediction of the rate of heat transfer across the gap is not reliable, and so we rely upon empirical measurements of surface temperatures and the heat absorbed by the mold to deduce appropriate heat transfer coefficients. Some heat transfer coefficients for various casting situations are given in Table 10.1. Such values are strongly dependent on specific processes and geometrical situations, so the data in Table 10.1 should serve only as general guidelines.

Reference to Table 10.1 indicates that the heat transfer coefficients can be time

dependent in static castings and position dependent in continuous castings.

Nishida et al.<sup>4</sup> give time-temperature solutions for cylindrical and slab castings in molds where the air gap

forms during solidification, and methods to calculate the resulting heat transfer coefficients.

Kelly et al.<sup>5</sup> show how the heat transfer coefficient (or the surface heat flux) may be calculated for continuous casting in a round billet mold. Kim et al.<sup>6</sup> give an inverse method for estimating the heat transfer coefficient as a function of time from temperature measurements inside the casting.

<sup>4</sup>Y. Nishida, W. Drosté, and S. Engler, *Metall. Trans. B* 17B, 833 (1986).

<sup>5</sup>J. E. Kelly, K. P. Michalek, T. G. O'Connor, B. G. Thomas and J. A. Dantzig, *Metall. Trans. A* 19A, 2589 (1987).

<sup>6</sup>W. S. Kim, M. N. Ozisik, and L. G. Hector, "Inverse Problem of Solidification for Determining Air-Gap Resistance to Heat Flow during Metal Casting," in *Proceedings of XXII ICHMT Conference on Heat and Mass Transfer in Manufacturing Processes*, Dubrovnik, Yugoslavia, August 27-31, 1990.

Table 10.1 Heat transfer coefficients across casting-mold interfaces

Casting situation	Heat transfer coefficient W m <sup>-2</sup> K <sup>-1</sup>	Reference listed below
Steel in continuous casting mold	280-2300	(a)
Steel in continuous casting mold, 4 × 4 in. withdrawal rate of 20 in./min withdrawal rate of 100 in./min withdrawal rate of 175 in./min	480 790 1080	(b)
Ductile iron in gray iron mold (coated with amorphous carbon)	1700	(c)
Steel in static cast iron mold	1020	(c)
Copper in centrifugal steel mold	230-340	(d)
Aluminum alloy in small permanent copper molds	1700-2600	(e)
Steel against chill mold in vacuum (decreases with time)	400-130	(f)
Steel in continuous casting meniscus below meniscus	2800 2800-1000	(g)
Uranium in graphite molds	2000	(h)

Steel in continuous casting mold, 4 × 4 in.

withdrawal rate of 20 in./min  
withdrawal rate of 100 in./min  
withdrawal rate of 175 in./min

Water-cooled mold  
water withdrawal rate of 20 in./min  
water withdrawal rate of 100 in./min  
water withdrawal rate of 175 in./min

Ductile iron in gray iron mold (coated with  
amorphous carbon)

Steel in static cast iron mold

Copper in centrifugal steel mold

Aluminum alloy in small permanent copper molds

Steel against chill mold in vacuum  
(decreases with time)

Steel in continuous casting  
meniscus  
below meniscus

Uranium in graphite molds

- a) A. W. D. Hills and M. R. Moore, *Heat and Mass Transfer in Process Metallurgy*, Inst. Min. and Met., London, 1967.
- b) E. Y. Kung and J. C. Pollock, *Simulation* 29-36 (Jan. 1968).
- c) C. C. Reynolds, *ibid.*
- d) R. W. Ruddle, *The Solidification of Castings*, second edition, The Institute of Metals, London, 1957.
- e) B. Bardes and M. C. Flemings, *Trans AFS* 74, 406 (1966).
- f) H. Jacobi, *Proceedings Fifth International Conference on Vacuum Metallurgy and ESR*, Munich, 1976.
- g) K. P. Michalek, J. E. Kelley and J. A. Dantzig, in *Modelling and Control of Casting and Welding Processes*, S. Kou and R. Mehrabian (editors), The Metallurgical Society-AMSE, Warrendale, PA, 1986, pages 497-516.
- h) A. D. Rollett, H. D. Lewis and P. S. Dunn, in S. Kou and R. Mehrabian (editors), *ibid.*, pages 565-575.

### 10.3 CONTINUOUS CASTING

The basic features of a continuous casting machine are depicted in Fig. 10.13. The metal passes through a water-cooled metal mold forming a thin solidified skin (6 to 18 mm), and is then subjected to a water spray for the remainder of solidification. Figure 10.14 schematically shows the temperature distribution within the partially frozen casting as it moves downward with a velocity  $u$  in the  $y$ -direction. While in the mold, the conduction of heat in the thin shell of solid is much greater in the  $x$ -direction than in the  $y$ -direction. Therefore the conduction of heat in the withdrawal direction may be ignored. Under these

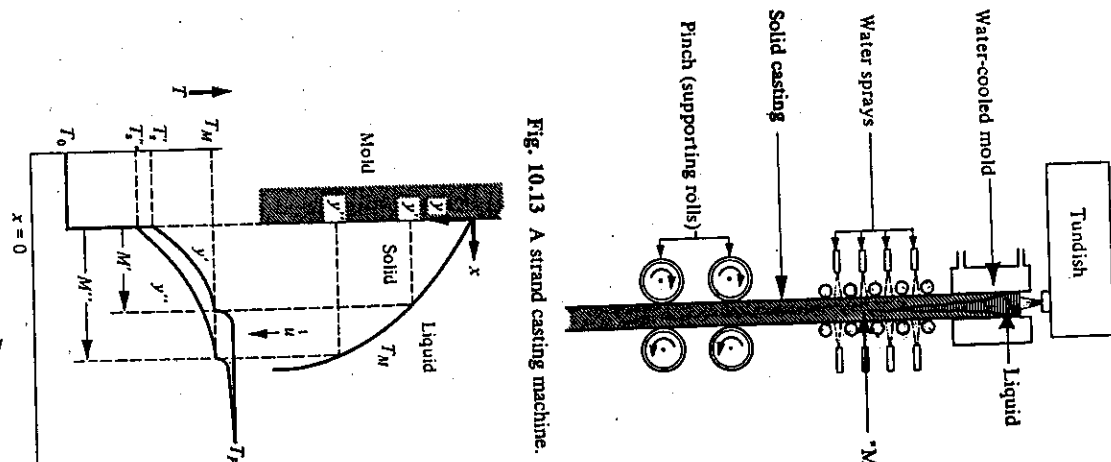


Fig. 10.13 A strand casting machine.

Fig. 10.14 The partially frozen portion of a continuous casting and the temperature profile as a function of the distance down the mold.

circumstances, the analysis used for static casting as presented in Section 10.2.3 may be applied with only minor modifications.

As the metal passes through the mold, we assume that a constant heat transfer coefficient applies at the mold-casting interface, while the heat is removed by the water-cooled mold maintained at  $T_0$ . Equation (10.33) applies if the time  $t$  is recast as the distance down the

mold wall  $y$ , divided by the casting velocity  $u$ . We account for the effect of liquid superheat by realizing that on passing down from the tundish, enough turbulence prevails in the liquid core, at least between the mold walls, so that we may assume that the liquid temperature is constant in the  $y$ -direction, at  $T_p$ . Then, at the solid-liquid interface, latent heat plus the liquid superheat is conducted toward the mold wall through the solid skin, and in the formulation the effective latent heat of fusion  $H_f'$  applies in which

$$H_f' = H_f + C_{p,i}(T_p - T_M)$$

The results are convenient when presented in dimensionless variables. From Eq. (10.33), we deduce the variables

$$\frac{h^2 y}{u k' \rho' C_p}, \quad \frac{C_p(T_M - T_0)}{H_f'}, \quad \text{and} \quad \frac{hM}{k'}$$

These variables and others are used in Figs. 10.15-10.17 to present the results. We can determine the thickness of solid metal at various positions down the mold from Fig. 10.15. Figure 10.16 shows how the surface temperature  $T_s$  of the cast metal varies with the mold position, and we use Fig. 10.17 to calculate the total rate of heat removal entering the mold of length  $L$ . Skin thickness and surface temperature are important parameters, since the solid skin on exit from the mold must be of some minimum strength. The rate of heat removal is useful when computing cooling water requirements.

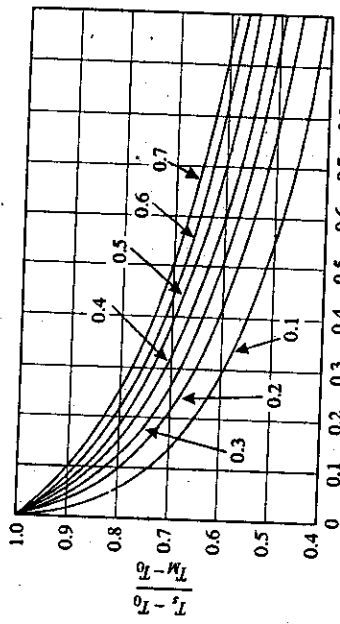


Fig. 10.15 Thickness solidified,  $M$ , versus distance down the mold. (Figures 10.15-10.17 are from A. W. D. Hills and M. R. Moore, *ibid.*)

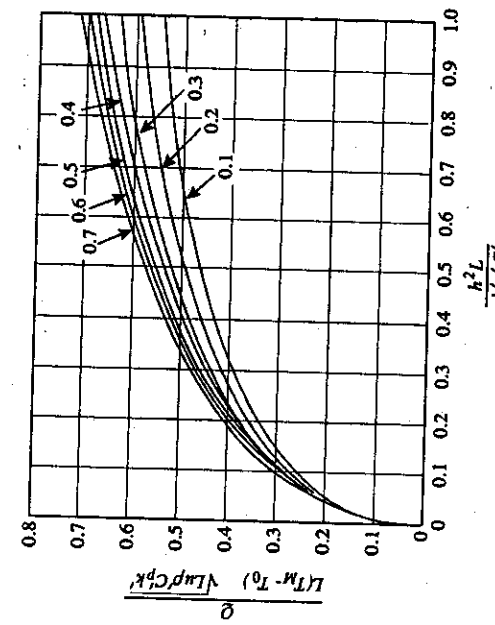


Fig. 10.16 Surface temperature versus distance down the mold. Numbers on the curves are the same as in Fig. 10.15.

Data for steel:  
Freezing temperature = 1770 K,  
Pouring temperature (from tundish) = 1800 K,  
Latent heat of fusion =  $2.67 \times 10^5 \text{ J kg}^{-1}$ ,

**Example 10.7** Determine a) the mold length, and b) the cooling water requirements to produce steel slab (0.61 m wide by 75 mm thick) at a withdrawal rate of 50 mm s<sup>-1</sup>. The solid skin on exit from the mold should be 13 mm thick, and a heat transfer coefficient of 2000 W m<sup>-2</sup> K<sup>-1</sup> may be assumed. To minimize the cooling of the recirculated water, only a 6 K temperature rise of the water is allowed.

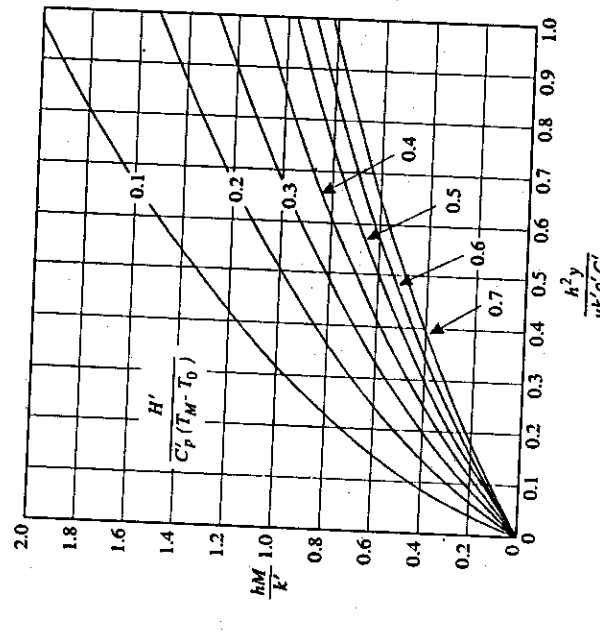


Fig. 10.17 Rate of heat removal by mold cooling water  $Q$  versus mold length  $L$ . Numbers on the curves are the same as in Fig. 10.15.

$$\begin{aligned}\text{Solid density} &= 7690 \text{ kg m}^{-3}, \\ \text{Solid heat capacity} &= 670 \text{ J kg}^{-1} \text{ K}^{-1}, \\ \text{Liquid heat capacity} &= 596 \text{ J kg}^{-1} \text{ K}^{-1}, \\ \text{Solid thermal conductivity} &= 60 \text{ W m}^{-1} \text{ K}^{-1}.\end{aligned}$$

*Solution.*

a)  $\frac{hM}{k'} = \frac{(2000)(0.013)}{60} = 0.433,$

$$\begin{aligned}H'_f &= H_f + C_p(T_p - T_w) = 2.67 \times 10^5 + 596(1800 - 1770) \\ &= 2.85 \times 10^5 \text{ J kg}^{-1},\end{aligned}$$

and

$$\frac{H'_f}{C_p(T_M - T_0)} = \frac{2.85 \times 10^5}{670(1770 - 294)} = 0.288.$$

From Fig. 10.15, we get

$$\frac{h^2 y}{uk' \rho' C_p} \approx 0.20.$$

Therefore,

$$y = L = \frac{(0.20)(0.050)(60)(7690)(670)}{2000^2} = 0.77 \text{ m.}$$

b) From Fig. 10.17,

$$\frac{Q}{L(T_M - T_0) \sqrt{L u \rho' C_p k'}} \approx 0.38,$$

$$Q = (0.38)(0.77)(1770 - 294) \sqrt{(0.77)(0.050)(7690)(670)(60)} = 1.49 \times 10^6 \text{ W.}$$

Now we calculate the flow rate of water (the specific heat of water is  $4184 \text{ J kg}^{-1} \text{ K}^{-1}$ ).

$$\text{Flow rate} = \frac{1.49 \times 10^6 \text{ J}}{\text{s}} \left| \frac{\text{kg K}}{4184 \text{ J}} \right| \left| \frac{6 \text{ K}}{1 \text{ m}^3} \right| = 59.4 \text{ kg s}^{-1},$$

$$\begin{aligned}\text{or,} \\ &= \frac{59.4 \text{ kg}}{\text{s}} \left| \frac{\text{m}^3}{1000 \text{ kg}} \right| \left| \frac{264.2 \text{ gal}}{1 \text{ m}^3} \right| \left| \frac{60 \text{ s}}{1 \text{ min}} \right| \\ &= 942 \text{ gallons per minute (gpm).}\end{aligned}$$

Below the mold in a continuous casting, heat extraction is continued by means of water sprays. Under these conditions, the heat flux at the surface of the solidified metal is

$$q_{x=0} = h_{spray}(T_{surf} - T_{amb}).$$

Finally, below the spray zone, heat extraction continues by radiation, so that

$$q_{x=0} = \varepsilon \sigma (T_{surf}^4 - T_{amb}^4),$$

where  $\varepsilon$  = emissivity of the scale on the surface, and  $\sigma$  = Stefan-Boltzmann constant, which are both defined in the next chapter. The overall result is that the position of the solidified front moves at varying rates, depending on the heat flux at the surface, but as  $M$  increases, the rate becomes less and less influenced by the surface condition and is instead influenced by the rate of conduction of energy through the solidified shell.

A severe problem can arise when the cooling flux provided by water sprays is not high enough compared to the flux in the mold. As the solid skin moves from the mold to the spray zone, the temperature gradient in the solid may be quite steep, providing a strong flux of energy to the surface. If the spray heat transfer coefficient is not high enough, or the sprays do not properly cover the surface, this energy will not be extracted from the metal as fast as it arrives and the temperature at the surface of the metal will therefore increase. If this increase is too large (100 K is considered the allowable maximum), the strength of the metal degrades to the point where it might crack, causing surface quality problems during subsequent rolling. Computations to illustrate this problem are not easily done analytically, but are best handled numerically, using techniques discussed in Chapter 16.

Because of these complications, the reader is cautioned against using the often-quoted "metallurgical length" equation

$$L = k'uD^2,$$

(where  $k'$  is a constant for a given metal and casting shape,  $u$  is the casting speed and  $D$  is the outer dimension of the cast section), except for qualitative estimates of where the final solidification occurs. This equation does, however, point out that the final solidification point does increase directly with casting speed.

#### 10.4 CRYSTAL GROWTH

It is possible to obtain crystals of several hundreds of materials for applications as electronic, optical or magnetic materials, dielectrics, piezoelectrics, etc. The crystal growth processes are probably more numerous than the applications, themselves, and so here we restrict our discussion to melt-grown crystals. An excellent perspective on crystal growth technology is given by Brice.<sup>7</sup>

Actually, heat transfer during crystal growth is only one part of the transport phenomena which should be considered. In fact, it is the mass transfer that is most consequential in determining the success or failure in achieving suitable crystals.

Clearly, semiconductor crystals constitute the greatest portion of crystals produced in the world, and silicon dominates this portion. A sketch of a Czochralski-type crystal grower, which is the most common technique for growing silicon, is shown in Fig. 10.18(a). Another technique makes use of the floating-zone process, which is shown in Fig. 10.18(b).

Solidification of Metals 357

steady state is achieved with respect to coordinates that also move with velocity  $U$ . With these assumptions, Eq. (10.40) reduces to

$$\frac{d^2T}{dz^2} + \frac{U}{\alpha} \frac{dT_L}{dz} = 0. \quad (10.41)$$

We write the same equation for the liquid using the subscript  $L$ :

$$\frac{d^2T_L}{dz^2} + \frac{U}{\alpha_L} \frac{dT_L}{dz} = 0. \quad (10.42)$$

The interface is at  $z = 0$ , the solid is in the region  $z \leq 0$ , and the liquid is in  $z \geq 0$ . We can solve these equations with the following boundary conditions:

$$T = T_L = T_M \quad \text{at} \quad z = 0, \quad (10.43)$$

and

$$\frac{dT}{dz} = G_S \quad \text{at} \quad z = 0, \quad (10.44)$$

$$\frac{dT_L}{dz} = G_L \quad \text{at} \quad z = 0, \quad (10.45)$$

where  $G_S$  and  $G_L$  are the thermal gradients in the solid and liquid, respectively, at the interface. The results are

$$T = T_M + \frac{\alpha G_S}{U} \left[ 1 - \exp \left[ -\frac{zU}{\alpha} \right] \right], \quad (10.46)$$

and

$$T_L = T_M + \frac{\alpha_L G_L}{U} \left[ 1 - \exp \left[ -\frac{zU}{\alpha_L} \right] \right]. \quad (10.47)$$

Keep in mind that the utility of Eqs. (10.46) and (10.47) is that they represent the steady-state temperature profiles in the vicinity of the interface. Actually, Eqs. (10.46) and (10.47) give unrealistic results for the far-field conditions. Specifically,

$$T_L \rightarrow T_M + \frac{\alpha G_L}{U} \quad \text{as} \quad z \rightarrow \infty,$$

and

$$T \rightarrow -\infty \quad \text{as} \quad z \rightarrow -\infty.$$

It is understood, therefore, that Eqs. (10.46) and (10.47) provide asymptotic solutions for  $z = 0$ , which are approximately true at finite values of  $z$ .

Finally, we point out that  $G_S$ ,  $G_L$  and  $U$  are not all independent variables because at the interface, the heat carried by the solid comprises the heat conducted to the interface in the liquid plus the heat of fusion generated at the moving interface. Therefore,

$$kG_S = k_L G_L + \rho U H_f, \quad (10.48)$$

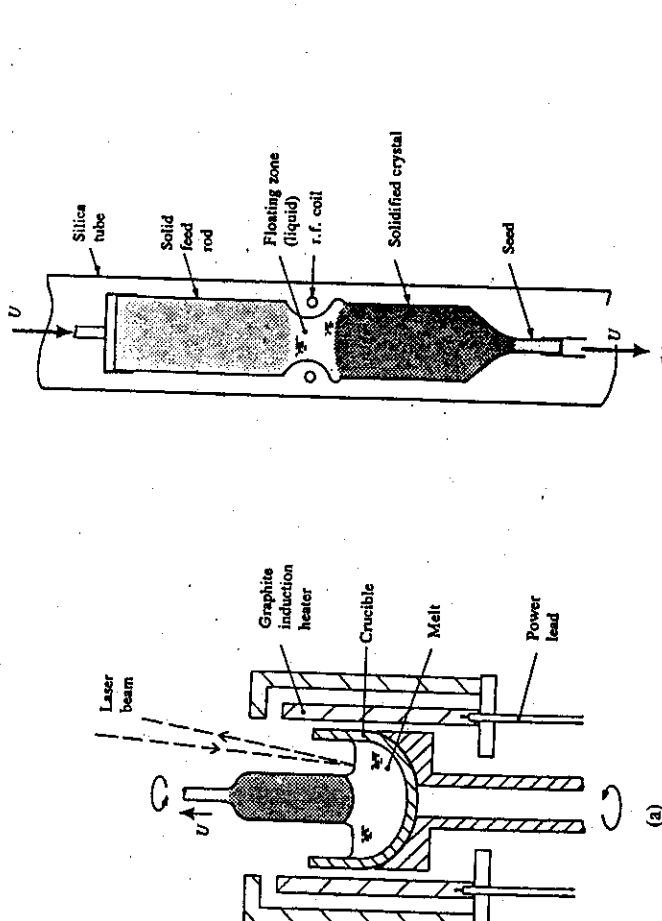


Fig. 10.18 Crystal growing processes: (a) Czochralski grower; (b) floating-zone.

In a Czochralski grower, the charge material is placed in a crucible and melted. A seed crystal is attached to a vertical *pull* rod, lowered until it touches the melt, allowed to melt back slightly, and then raised slowly so that crystallization proceeds from the seed crystal. The crystal is rotated slowly as it is pulled, and the crystal diameter is controlled by adjusting the pull-rate and/or heat input to the melt. The reflected laser beam senses the exact position of the surface of the melt for the control of the pull-rates.

The floating-zone is used in zone melting, in which only a portion of the charge is melted, and this zone is slowly moved through the charge. Many types of heat sources are used for zone melting, including induction, resistance, electron beam, and laser beam. The zone is moved either by mechanically moving the power source with respect to the crystal or vice versa. Zone melting is usually done without a crucible (i.e., *floating zone* melting) for reactive and high-melting-point materials. The molten zone is held in place by surface tension forces sometimes aided by a magnetic field.

The conduction heat transfer in the solidified crystal is described by the energy equation, written in cylindrical coordinates:

$$\frac{\partial T}{\partial r} - U \frac{\partial T}{\partial z} = \alpha \left[ \frac{\partial^2 T}{\partial z^2} + \frac{1}{r} \frac{\partial}{\partial r} \left( r \frac{\partial T}{\partial r} \right) \right], \quad (10.49)$$

where  $U$  = velocity of the crystal. For simplicity, we assume that conduction is one-dimensional, and the solid-liquid interface is flat. Also, the crystal is long enough that

and by fixing any two among  $G_s$ ,  $G_t$  and  $U$ , then the third variable is established. Normally,  $G_t$  and  $U$  are taken to be the process variables, so  $G_s$  follows.

**Example 10.8** In the growth of silicon, the maximum gradient in the solid that can be tolerated is  $0.5 \text{ K mm}^{-1}$  (so that the dislocation number density is not excessive).

a) If the crystal must be grown with  $G_t \geq 0$ , what is the maximum growth rate that can be used?

b) What happens to the growth velocity if  $G_s$  does not change, but  $G_t$  is increased abruptly by 10 pct? This could happen by a fluctuation in the power source or by spurious convection in the liquid.

**Data for silicon:**  $k = 31 \text{ W m}^{-1} \text{ K}^{-1}$ ;  $k_t = 50 \text{ W m}^{-1} \text{ K}^{-1}$ ;  $\alpha = 1.32 \times 10^{-5} \text{ m}^2 \text{ s}^{-1}$ ;  $c_t = 1.94 \times 10^{-5} \text{ m}^2 \text{ s}^{-1}$ ;  $T_M = 1683 \text{ K}$ ;  $H_f = 1.80 \times 10^6 \text{ J kg}^{-1}$ ;  $\rho = 2500 \text{ kg m}^{-3}$ .

**Solution.** a) We use Eq. (10.48) and solve for  $U$ .

$$U = \frac{kG_s - k_t G_t}{\rho H_f}$$

In order that  $U$  be positive (i.e., there is solidification and not melting), then  $kG_s > k_t G_t$  or  $G_t < (k/k_t)G_s$ . Therefore,

$$G_t < \left[ \frac{31}{50} \right] 500$$

To be safe, let's select  $G_t = 200 \text{ K m}^{-1}$ . Then,

$$U = \frac{(31)(500) - (50)(200)}{(2300)(1.80 \times 10^6)} = 1.33 \times 10^{-6} \text{ m s}^{-1} = 1.33 \mu\text{m s}^{-1}$$

This is an extremely small velocity, which resulted because we specified such a very low value of  $G_s$ , resulting in a low number of dislocations. Commercial silicon crystals are grown at an order of magnitude higher rate (approximately  $1.4 \times 10^{-5}$  to  $2 \times 10^{-5} \text{ m s}^{-1}$ ).

b)  $U = \frac{(31)(50) - (50)(200 \times 1.1)}{(2300)(1.80 \times 10^6)} = 1.09 \times 10^{-6} \text{ m s}^{-1} = 10^9 \mu\text{m s}^{-1}$ .

The 10 pct. increase in  $G_t$  causes a decrease of 11 pct. in  $U$ . If the silicon melt was doped, this change in  $U$  would be reflected as a decrease in the concentration of dopant in the crystal as the system adjusts to the new growth velocity.

Equations (10.41)-(10.47) were presented so that we could study the dynamics of the interface. Suppose our interest is to take a more global approach, so that we want the temperature distribution in the crystal while taking into account the power loss from the crystal to the surroundings. The case of a uniform heat transfer coefficient along the length of the crystal was presented as Problem 9.9. If you did not solve this problem, we invite you to do so now. Here, we present a more realistic case in which the heat loss from a floating-

zone crystal and its feed rod is by radiation. Our presentation is based on the work of Donald.<sup>8</sup>

The information we seek comprises the temperature distribution and the power loss from the crystal. The crystal is grown at a high temperature so that the radiant heat flux is

$$q_r = \sigma \varepsilon T^4. \quad (10.49)$$

Equation (10.49) is introduced and utilized extensively in Chapter 11. The variable  $\sigma$  is the Stefan-Boltzmann constant ( $\sigma = 5.670 \times 10^{-8} \text{ W m}^{-2} \text{ K}^{-4}$ ), and  $\varepsilon$  is a material-surface property called emissivity. Typically, in this process the growth rate is so small that it can be neglected, insofar as the temperature distribution in the solid is hardly affected and in the overall power distribution, its contribution is negligible. We make the additional simplification that the temperature is only a function of  $z$ , where  $z$  is the distance coordinate along the length of the crystal. The steady-state energy balance on a length  $\Delta z$  in a crystal with a uniform radius  $R$  is

$$\frac{d^2T}{dz^2} = \frac{2\varepsilon\sigma T^4}{kR}. \quad (10.50)$$

As the solution to Eq. (10.50), Donald gives

$$\frac{T}{T_M} = \frac{1}{\left[ 1 + \frac{z}{\lambda_0} \right]^{2/3}}, \quad (10.51)$$

where

$$\lambda_0 = \left[ \frac{5kR}{9\varepsilon\sigma T_M^3} \right]^{1/2},$$

and  $T_M$  is the melting temperature of the crystal.

The power radiated from the crystal and the feed rod is obtained by an integration over the entire length,

$$Q = 2\pi R \int_{-\infty}^{\infty} \varepsilon\sigma T^4 dz = 2\pi R\varepsilon\sigma T_M^4 \left[ \frac{6}{5} \lambda_0 \right]. \quad (10.52)$$

This integration does not include the power loss from the zone, itself. When this is included, Donald recommends

$$Q = 2\pi\varepsilon\sigma T_M^4 \lambda_0 \left[ \frac{6}{5} + \frac{L}{\lambda_0} \right], \quad (10.53)$$

where  $L$  is the length of the floating zone. Calculated and experimentally measured power requirements for many elements are shown in Fig. 10.19.

In recent years, the mathematical modeling and computer simulation of Czochralski crystal growth (and related processes) have received much attention because of the enormous technological importance of single crystal materials. A good start in understanding the many complexities involved can be gained by reading a short paper by Derby.<sup>9</sup>

### PROBLEMS

Data for Problems 10.1-10.8 and Problems 10.27 and 10.28.

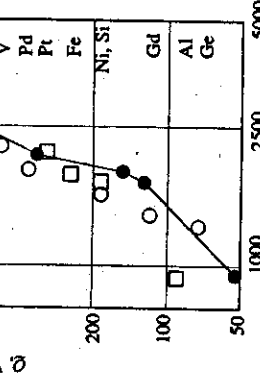


Fig. 10.19 Power required for floating zones in rods of several elements (radius = 12.7 mm). (From D. K. Donald, *ibid.*)

**Example 10.9** Estimate the thermal gradients in silicon at the solid-liquid interface in the floating zone process. The crystal (10 mm dia.) is grown at  $5 \times 10^{-5} \text{ m s}^{-1}$ . Assume that the emissivity of silicon is 0.2. Other properties of silicon are given in Example 10.5.

*Solution.*

$$\lambda_0 = \left[ \frac{SKR}{9\epsilon\sigma T_M^3} \right]^{1/2} = \left[ \frac{(5)(3)(0.005)}{(9)(0.2)(5.670 \times 10^{-8})(1683)^3} \right]^{1/2} = 0.0399 \text{ m.}$$

The temperature gradient is obtained by differentiating Eq. (10.51):

$$\frac{dT}{dz} = -\frac{2T_M}{3\lambda_0} \left[ 1 + \frac{z}{\lambda_0} \right]^{-5/3},$$

$$G_s = \left| \left[ \frac{\partial T}{\partial z} \right]_{z=0} \right| = \frac{2T_M}{3\lambda_0} = \frac{(2)(1683)}{(3)(0.0399)} = 2.81 \times 10^4 \text{ K m}^{-1},$$

$$G_t \text{ is obtained from Eq. (10.48):}$$

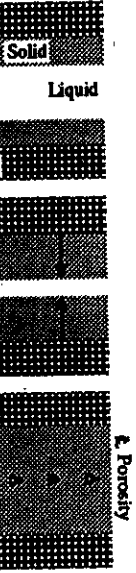
$$G_t = \frac{k}{k_L} G_s - \frac{\rho U H_f}{k_L} = \frac{(31)(2.81 \times 10^4)}{(50)} - \frac{(2300)(5 \times 10^{-5})(1.80 \times 10^6)}{(50)} = 1.328 \times 10^4 \text{ K m}^{-1}$$

Mold material*	$k, \text{W m}^{-1} \text{K}^{-1}$	$\rho, \text{kg m}^{-3}$	$C_p, \text{J kg}^{-1} \text{K}^{-1}$
Silica sand	0.52	1600	1170
Mullite	0.38	1600	750
Plaster	0.35	1120	840
Zircon sand	1.0	2720	840
Ceramic shell	0.70	1800	1100
Copper	390	9000	380

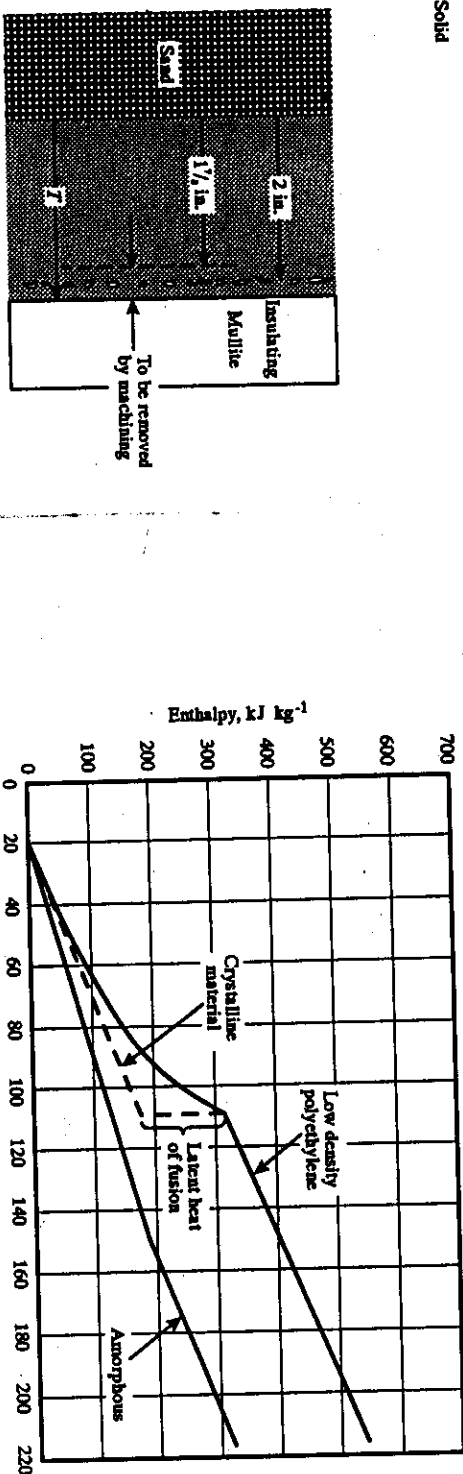
  

Casting material	$T_M, \text{K}$	$H_f, \text{J kg}^{-1}$	$\rho', \text{kg m}^{-3}$	$C_p', \text{J kg}^{-1} \text{K}^{-1}$	$k, \text{W m}^{-1} \text{K}^{-1}$
Iron	1808	$2.72 \times 10^3$	7210	750	40
Nickel	1728	$2.91 \times 10^3$	7850	670	35
Aluminum	933	$3.91 \times 10^3$	2400	1050	260

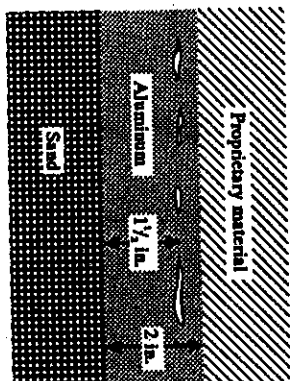
- \*Note: Only typical values can be given here. Actual properties depend on temperature, particle size, binders, porosity, etc.
- 10.1 Plot distance solidified versus the square root of time for the following metals (in each case the pure metal is poured at its melting point against a flat mold wall): a) iron in a silica sand mold, b) aluminum in a silica sand mold, c) iron in a mullite mold heated to 1260 K.
- 10.2 How long does it take to freeze a 100 mm diameter sphere of pure iron in a silica sand mold, assuming: a) no superheat and neglecting the heat flow divergence? b) no superheat and realizing that a sphere is being cast? c) 110 K superheat and realizing that a sphere is being cast?
- 10.3 Plot distance solidified versus time for iron poured at its melting point into a heavy copper mold, assuming that a) there is a large flat mold wall and no resistance exists to heat flow at the mold-metal interface; b) interface resistance to heat flow is finite ( $h = 570 \text{ W m}^{-2} \text{K}^{-1}$ ).
- 10.4 Show whether iron can be cast against a very thick aluminum mold wall without causing the aluminum to melt.
- 10.5 Slab-shaped steel castings are prone to center-line porosity, which—for our purposes—is simply an alignment of defects along the plane of last solidification. The sketch on the next page shows the solidification of a slab cast in silica sand and the location of the centerline porosity.



**10.9** Low density polyethylene is injected into a water-cooled copper mold. The temperature of the melt entering the mold is 465 K. The polyethylene is molded to form a plate that is 10 mm thick. Estimate the time required for all of the polyethylene reach less than 335 K, when it can be safely ejected from the mold. Assume that the heat transfer coefficient at the polyethylene-copper interface is relatively high ( $h = 4000 \text{ W m}^{-2} \text{ K}^{-1}$ ) because cooling occurs while the molding is under pressure. The enthalpy of polyethylene is given below. Other properties of low density polyethylene are  $k = 0.26 \text{ W m}^{-1} \text{ K}^{-1}$  and  $\rho = 920 \text{ kg m}^{-3}$ .



The solidification time for the 2-in. slab cast in sand is known to be 6 min; when cast in an insulating mullite mold, the time is 60 min. If a casting is made in the composite mold depicted to the right, determine the thickness  $T$  the casting should have to yield  $1\frac{1}{2}$  in. of sound metal after machining.



**10.6** A 2-in. thick slab of aluminum is cast in a mold made of silica sand (forming one face) and a proprietary material (forming the other face). The aluminum is poured with no superheat, and the as-cast structure of the slab is examined after solidification and cooling. The examination shows that the plane of last solidification (i.e., the plane where the two solidification fronts meet) is located  $1\frac{1}{2}$  in. from the sand side. Knowing this, calculate the *heat diffusivity* (not the thermal diffusivity) of the proprietary material.

**10.7** Consider solidification in a flat ceramic shell mold with a thickness  $L$ . There is heat loss from the outside surface to the surroundings with a constant heat transfer coefficient ( $h = 150 \text{ W m}^{-2} \text{ K}^{-1}$ ). Except for very early times, the temperature in the mold is at steady state. a) Derive an equation for thickness solidified versus time. b) A plate of nickel (38 mm thick) is cast in a ceramic shell mold (10 mm thick). Calculate the solidification time.

**10.8** Repeat Problem 10.7, but replace the flat mold with a cylindrical shell of thickness  $L$ . A cylinder of nickel (38 mm diameter) is cast into the mold with a thickness of 10 mm.

**10.10** Repeat Problem 10.9 for amorphous polyethylene ( $\rho = 970 \text{ kg m}^{-3}$ ). This polymer can be safely ejected at 315 K. Compare the achievable production rates of the two forms of polyethylene.

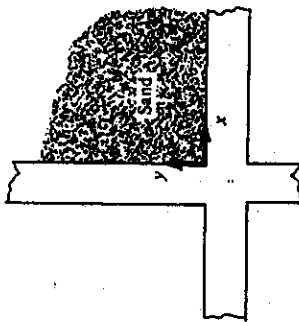
**10.11** Aluminum oxide is solidified in a water-cooled molybdenum mold to form continuous fibers with a diameter of  $200 \mu\text{m}$ . Estimate the length of the mold required to completely solidify the aluminum oxide as it exits from the mold, as a function of the fiber velocity. Assume that  $h = 4000 \text{ W m}^{-2} \text{ K}^{-1}$  in the mold. Data for  $\text{Al}_2\text{O}_3$ :  $k = 11 \text{ W m}^{-1} \text{ K}^{-1}$ ;  $C_p = 1230 \text{ J kg}^{-1} \text{ K}^{-1}$ ;  $\rho = 3016 \text{ kg m}^{-3}$ ;  $T_w = 2327 \text{ K}$ ;  $H_f = 1.07 \times 10^6 \text{ J kg}^{-1}$ .

**10.12** A continuous casting machine forms molten steel into a slab, 1.93 m wide and 229 mm thick, at a production rate of  $25.5 \text{ kg s}^{-1}$ . Assume that  $h = 1135 \text{ W m}^{-2} \text{ K}^{-1}$ . a) Determine the vertical length of the mold if the solid shell must be 12 mm thick at the mold exit. b) Calculate the cooling water requirement ( $\text{kg s}^{-1}$ ) if its temperature rise is from 300 to 307 K. Data for low carbon steel:  $k = 35 \text{ W m}^{-1} \text{ K}^{-1}$ ;  $C_p = C_{p,s} = 670 \text{ J kg}^{-1} \text{ K}^{-1}$ ;  $\rho = 7690 \text{ kg m}^{-3}$ ;  $H_f = 2.79 \times 10^6 \text{ J kg}^{-1}$ ;  $T_w = 1790 \text{ K}$ .

**10.13** The dwell time in the mold of a continuous casting machine is defined as the period which the metal spends in the mold during solidification, that is,  $t = L/u$ , in which  $t$  = dwell time,  $L$  = length of mold over which solidification is occurring, and  $u$  = velocity of metal through the mold. Since the skin solidified in the mold is thin, a simple analysis might be expected to apply. a) Neglect conduction in the withdrawal direction and write an expression

for thickness solidified versus time. b) Compare the results for dwell time in Problem 10.12 and the dwell time calculated from part a) for the same conditions.

- 10.14 A junction-shaped casting, as depicted to the right, is made in a sand mold. The junction may be considered infinitely long in the  $z$ -direction. For the upper right quadrant of sand:
- Write a differential equation for temperature.
  - Write the boundary conditions (for time and space) that apply.
  - Write the solution yielding temperature as a function of position in the sand and time.
  - Derive an equation for the heat absorbed by the sand as a function of time and the lengths of the junction legs.



- 10.15 Equations (10.32) and (10.33) are approximations for the case depicted in Fig. 10.9. The exact solution for the temperature in the solidified skin is

$$\frac{T - T_0}{T_M - T_0} = \left[ \frac{1}{\operatorname{erf} \beta} \right] \operatorname{erf} \left[ \beta \frac{M_0 + x}{M_0 + M} \right],$$

where  $\beta$  satisfies

$$\beta t^{\alpha} \operatorname{erf} \beta = (T_M - T_0) \frac{C_p}{H_f \sqrt{\pi}}.$$

and  $M_0$  satisfies

$$\frac{2k \beta^2}{h M_0} = (T_M - T_0) \frac{C_p}{H_f}.$$

- a) Show that the above relationships are exact.  
b) If  $t_0$  is a time defined as

$$t_0 = \frac{M_0^2}{4 \beta^2 \alpha},$$

show that the thickness solidified is

$$M = 2\beta \sqrt{\alpha'} \left[ [t_0 + t]^{1/2} - t_0^{1/2} \right].$$

- 10.16 Usually when Eq. (10.48) is invoked, the solid-liquid interface is considered to be at the freezing temperature (i.e., at the equilibrium temperature). In rapid solidification processing, however, the interface can be significantly undercooled. If  $H_f$  is the latent heat at the equilibrium temperature: a) rewrite Eq. (10.48) in a more precise manner, taking into account that  $C_p$  of the solid and liquid phases are not necessarily equal; b) rewrite Eq. (10.48) in accordance with part a) and also account for the densities not being equal.

- 10.17 Is it possible that  $G_L < 0$  during crystal growth? Can there be solidification? Do you think the planar interface will be stable?

- 10.18 A single crystal in the form of a long thin rod is grown by the Czochralski method (Fig. 10.18(a)). Assume that the heat conduction is one dimensional and that the heat transfer coefficient is uniform along the length of rod. a) Write the energy equation for temperature along the length of the crystal and obtain the solution for the temperature distribution. b) Use the properties given in Example 10.8 for silicon and assume that  $h = 100 \text{ W m}^{-2} \text{ K}^{-1}$  (uniform). Calculate  $G_s$  for growth rates of  $10^{-6}$ ,  $10^{-5}$  and  $10^{-4} \text{ m s}^{-1}$ . c) Calculate the corresponding values of  $G_L$  and briefly discuss your results.

- 10.19 The properties of aluminum near the melting point are given:  $T_M = 933 \text{ K}$ ;  $k = 210 \text{ W m}^{-1} \text{ K}^{-1}$ . Consult Chapter 11 for emissivity. Calculate the power loss to maintain a floating zone in aluminum. Compare your results to Fig. 10.19 and discuss.

- 10.20 Welding of a "thin plate" can be analyzed by starting with Eq. (9.85) for the peak temperature around a moving line source. With  $r$  as the cylindrical radius from the line source, we can set  $T_p = T_M$  (the melting point of the base metal) at  $r = r_M$ ; then

$$\frac{T - T_0}{T_M - T_0} = \frac{Q}{\rho C_p \delta V r_M \sqrt{2\pi r}}.$$

Show that

$$\frac{1}{T_p - T_0} = \frac{V r' \delta \rho C_p \sqrt{2\pi r}}{Q} + \frac{1}{T_M - T_0},$$

where  $r' = r - r_M$ . For  $r' \geq 0$  this gives the peak temperature in the base metal next to the weld.

- 10.21 Welding of a "thick plate" can be analyzed by starting with Eq. (9.81) for the peak temperature around a moving point source. As in Problem 10.20, set  $T_p = T_M$  at  $r = r_M$  and show that

$$\frac{1}{T_p - T_0} = \frac{2\pi k a e \left( \frac{V r'}{2a} \right)^2}{Q V} + \frac{1}{T_M - T_0},$$

where  $r' = (r^2 - r_M^2)^{1/2}$ , provided  $r' \geq 0$ .

- Problems 10.22-10.26 should be attempted after Problems 10.20 and 10.21 have been solved.

- 10.22 Sketch temperature versus time at  $r = 0$ ,  $r = r_M$  and  $r > r_M$  in a thin plate that is welded.

- 10.23 A very thick steel plate is welded with 5 kW and 75 pct. efficiency at a welding speed of  $4.2 \text{ mm s}^{-1}$ . Prior to welding the plate is preheated to 480 K. Assume that the fusion zone (i.e., the edge of the molten weld metal) corresponds to the 1644 K isotherm. a) Calculate the peak temperature at a distance of 1 mm from the fusion zone. b) What is the cooling rate at that location when the temperature is 1070 K? Data for steel:  $k = 35 \text{ W m}^{-1} \text{ K}^{-1}$ ,  $\rho = 7690 \text{ kg m}^{-3}$ ;  $C_p = 754 \text{ J kg}^{-1} \text{ K}^{-1}$ .

- 10.24** Derive an equation for the thermal gradient,  $\partial T/\partial r$ , at the edge of a weld pool ( $r = r_w$ ) of a material with a freezing point of  $T_w$ . The plate is steel and very thick. Thermal properties are given in Problem 10.23.

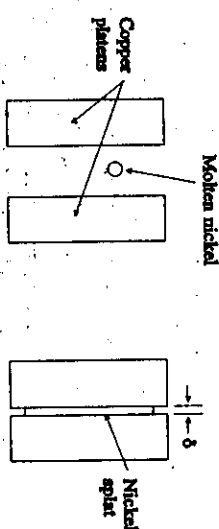
**10.25** The surface of damaged silicon can be annealed by passing a laser beam over the surface in order to effect melting to a depth below the damaged layer. When the silicon resolidifies, it does so epitaxially so that the crystal structure of the underlying single crystal is maintained.

Assume that the silicon is at 293 K and is "thick." The molten pool is 1 mm thick, and the laser beam moves at a velocity of  $20 \text{ cm s}^{-1}$  with a power of  $8 \text{ kW}$  at 75% efficiency.

- a) Calculate the distance from the edge of the molten pool where a peak temperature of 1273 K is achieved. b) Calculate the maximum cooling rate directly behind the molten pool. [Hint: Start with the steady-state temperature associated with a moving point source (Chapter 9) and make a transformation from moving to stationary coordinates.] Consult Example 10.8 for properties of silicon.

**10.26** Steel plate, 19 mm thick, is welded with 4 kW at 80 pct. efficiency with a welding speed of  $2.5 \text{ mm s}^{-1}$ . Assume that the edge of the molten pool corresponds to the isotherm of 1700 K. For this steel it is known that some martensite is found in the vicinity of the weld when the cooling rate exceeds  $4.6 \text{ K s}^{-1}$  at 866 K. a) If the plate is not preheated, would you expect to produce a weld with martensite? b) What is the peak temperature at 0.3 mm from the edge of the weld metal? Problem 10.24 gives properties of the steel.

- 10.27** Nickel is "splat cooled" between two plates of copper which are rapidly accelerated toward each other. The process is sketched below.



#### Before splatting

The splat thickness ( $\delta$ ) is 0.1 mm. Neglect superheat in the nickel droplet. a) Calculate the minimum freezing time of the splat by assuming no interfacial resistance to heat flow.

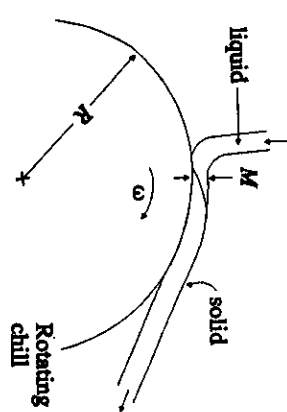
- b) Calculate the freezing time assuming that  $h = 2000 \text{ W m}^{-2} \text{ K}^{-1}$ , and the temperature of the copper plates is 293 K. Properties are listed at the beginning of this section.

Assume that initially the die and the lead frame are at 423 K and that the solder is molten with no superheat ( $T_w = 456 \text{ K}$ ). The ambient above the die is at 293 K. a) What is the temperature at the solder/lead frame interface during solidification of the solder? b) What is the temperature at the solder/die interface early during the solidification of the solder? c) Estimate the time required for the top surface of the die to achieve 428 K. d) Has the solder completely solidified in the time calculated for part c)?

Data:

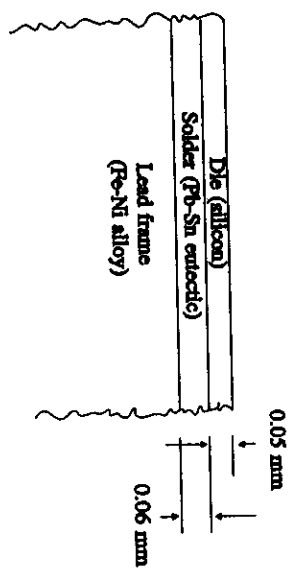
	$T_w, \text{ K}$	$H_f, \text{ J kg}^{-1}$	$k, \text{ W m}^{-1} \text{ K}^{-1}$	$\rho, \text{ kg m}^{-3}$	$C_p, \text{ J kg}^{-1} \text{ K}^{-1}$
Fe-Ni alloy	—	—	12.6	8700	670
Pb-Sn eutectic	456	$54 \times 10^3$	33.6	9200	209
Si	(See Example 10.8)				

- 10.28** In melt spinning, a jet of molten metal is directed to the surface of a rotating chill. Solidification takes place very rapidly, and a very thin ribbon of metal with thickness  $\delta$  is produced. The process is shown on the next page.



Calculate the rate of solidification ( $dM/dt$  in  $\text{mm s}^{-1}$ ) when  $M$  is one-half of  $\delta$ . Assume one-dimensional heat flow in the solidified metal and in the rotating chill, with  $h = 1.7 \times 10^4 \text{ W m}^{-2} \text{ K}^{-1}$ . The metal ribbon is aluminum with a thickness of  $50 \mu\text{m}$ , and the rotating chill is copper. Properties are listed at the beginning of this section.

- 10.29** Silicon dies are attached to the lead frames in microelectronic devices by soldering (see sketch below).



## 11

## RADIATION HEAT TRANSFER

In Chapter 6, we alluded to energy transfer by radiation as a mechanism for heat flow, but due to the entirely different natures of conduction and radiation, only a limited discussion of radiation appeared prior to this chapter. Energy transport by conduction depends on the existence of a conducting material. On the other hand, radiation is electromagnetic energy in transport; therefore, energy travels through space via radiation. The rate equations for conduction and radiation reflect their very different characters, and show no similarity. The energy flux by conduction is proportional to the thermal gradient, that is,  $q_r = -k(\partial T/\partial x)$ . In radiant heat transfer, the energy flux—so-called emissive power—is proportional to the fourth power of the absolute temperature; that is,  $e \propto T^4$ .

Solids, liquids, and some gases emit radiant energy composed of many wavelengths in the spectrum of electromagnetic radiation. The excitation process causing radiation may vary and can be classified as fluorescence, x-radiation, radio waves, etc. The thermal radiation is of primary interest here, and its range of wavelengths is taken to be 0.1-100  $\mu\text{m}$ .

## 11.1 BASIC CHARACTERISTICS

Thermal radiation is defined as the energy transferred by electromagnetic waves that originate from a body because of its molecular motion which characterizes temperature. The rate at which energy is emitted depends on the substance itself, its surface condition, and its surface temperature.

Figure 11.1 depicts a surface emitting and receiving thermal radiation. The total emissive power  $e$  is the flux of thermal radiation energy *emitted* into the entire volume above the surface. In terms of electromagnetic waves, the total emissive power is the sum of all the energy carried by all wavelengths emitted from the surface per unit area per unit time. The quantity  $e$  is also called *emissive power*, *emittance*, *total hemispherical radiation intensity*, *radiance*, or *radiant-flux density*. We use the terminology of emissive power.

---

<sup>a</sup>To add to the confusion, emittance is also used as a synonym for *emissivity*, which is a surface property presented in Section 11.2.

By utilizing Eq. (11.3), we can also write

$$q_{1,\text{net}} = \varepsilon_1 e_b - \alpha_1 e_b. \quad (11.5)$$

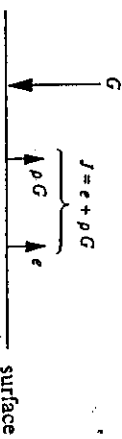


Fig. 11.1 The distribution of thermal radiation at a surface.

We define the *total irradiation*,  $G$ , of a body as the flux of thermal radiant energy incoming to the surface, and the *total radiosity*,  $J$ , as the total flux of radiant energy leaving the surface of a body. The total radiosity includes both the energy emitted and the energy reflected by the surface. As fluxes, the units of  $G$  and  $J$  are in  $\text{W m}^{-2}$ .

The incoming energy (total irradiation) can be absorbed, reflected, or transmitted, so that

$$G = \alpha G + \rho G + \tau G,$$

or

$$\alpha + \rho + \tau = 1, \quad (11.1)$$

where  $\alpha$  = absorptivity (fraction of  $G$  absorbed),  $\rho$  = reflectivity (fraction of  $G$  reflected), and  $\tau$  = transmissivity (fraction of  $G$  transmitted). Most liquids and solids are opaque to thermal radiation, so that  $\tau = 0$ , and

$$\alpha + \rho = 1. \quad (11.2)$$

The principal exceptions to this are glasses and silicate melts.

## 11.2 THE BLACK RADIATOR AND EMISSIVITY

In the study of real surfaces, it is convenient to define a hypothetical ideal surface called a black radiator. A black radiator is a surface which absorbs all incoming radiation; thus  $\alpha = 1$ , and  $\rho = 0$ . Another important characteristic of the black radiator is that it is a perfect emitter, since it emits radiation of all wavelengths, and its total emissive power is theoretically the highest that can be achieved at a given temperature. It follows that any real body emitting thermal radiation has a total emissive power of some fraction of the emissive power of a black radiator, which is often called a black body. This fraction is defined as the emissivity  $\varepsilon$ . Therefore,

$$\varepsilon = \varepsilon e_b. \quad (11.3)$$

Imagine a region in a space completely filled with black body radiation. A real body 1 emitting radiation at a rate of  $e_1$  is placed in this region; the net rate of energy transferred from the body is

$$q_{1,\text{net}} = e_1 - \frac{\alpha_1 e_b}{\text{energy emitted}} \quad (11.4)$$

If the body is in thermal equilibrium with the black body radiation, then  $q_{1,\text{net}} = 0$ , and  $\alpha_1 = \varepsilon_1$ . The same result can be obtained for any other body placed in this space, and thus the absorptivity and emissivity of any body at thermal equilibrium are equal.

It is important to note that although black body radiation is hypothetical, radiation very closely approximating that of a black radiator can be realized. Figure 11.2 depicts radiation emanating from a hollow space having nonblack walls at a uniform temperature. Since the hole is small, only a very small fraction of the radiation entering the hole and diffusely reflecting off the nonblack walls escapes; hence the escaping energy is entirely representative of the radiation within the cavity.

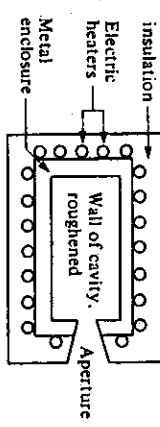


Fig. 11.2 Laboratory black body.

The energy emitted from any point on the walls of the enclosure is  $\varepsilon e_b$ ; when this radiation strikes other parts of the enclosure, a certain fraction is reflected, namely,  $\rho \varepsilon e_b$ . Similarly, a second reflection equals  $\rho(\rho \varepsilon e_b)$ , and the third one is  $\rho^3 \varepsilon e_b$ . Since the hole is small, probability favors radiation that ultimately passes through the hole to be made up of an infinite number of such reflections. Therefore

$$e(\text{hole}) = \varepsilon e_b (1 + \rho + \rho^2 + \rho^3 + \dots). \quad (11.6)$$

or

$$e(\text{hole}) = \varepsilon e_b \frac{1}{1 - \rho}, \quad (11.7)$$

and since  $\alpha = 1 - \rho$ , and thermal equilibrium exists within the cavity, then  $\varepsilon = 1 - \rho$  for the isothermal cavity. Therefore Eq. (11.7) reduces to

$$e(\text{hole}) = e_b. \quad (11.8)$$

Since radiation from a cavity is very nearly black, the *hohlraum* (heated cavity), shown in Fig. 11.2, is normally used as a radiation standard. Such an enclosure may be constructed with heavy metal internal walls that are roughened and oxidized to provide a surface of high emissive power. The walls are heated electrically, and the exterior is well insulated.

The thermal radiation from a solid body is composed of a continuous spectrum of wavelengths forming an energy distribution. Figure 11.3 depicts the spectrum of a black body at various temperatures. For most engineering calculations, the total emissive power of a black body at a particular temperature is an important quantity, which is given by the area under the curve applied at that temperature. Therefore

$$e_b = \int_0^{\infty} e_{b,\lambda} d\lambda, \quad (11.9)$$

where  $\lambda$  is the wavelength, and  $e_{b,\lambda}$  is the *monochromatic emissive power*. *Planck's equation* or *Planck's distribution law* relates  $e_{b,\lambda}$  to the wavelength and the absolute temperature:

$$e_{b,\lambda} = \frac{2\pihc^2\lambda^{-5}}{\exp\left[\frac{ch}{\kappa_b\lambda T}\right] - 1}, \quad (11.10)$$

where  $h$  = Planck's constant,  $c$  = velocity of light, and  $\kappa_b$  = Boltzmann's constant. Substituting Eq. (11.10) into Eq. (11.9) and integrating for all wavelengths results in the *Stefan-Boltzmann equation* for black body radiation, which is

$$e_b = \sigma T^4, \quad (11.11)$$

where the constant  $\sigma$  is

$$\sigma = \frac{2\pi^5\kappa_b^4}{15c^2h^3} = 5.669 \times 10^{-8} \text{ W m}^{-2} \text{ K}^4. \quad (11.12)$$

In view of the Stefan-Boltzmann equation, the total emissive power  $e$  of a real surface is

$$e = \varepsilon e_b T^4. \quad (11.13)$$

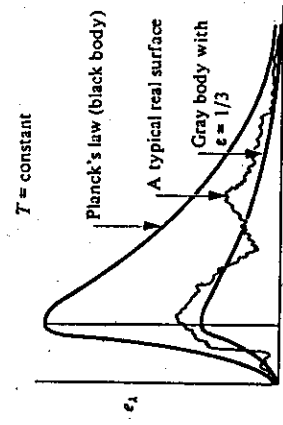


Fig. 11.4 Comparison of black, gray, and real surfaces.

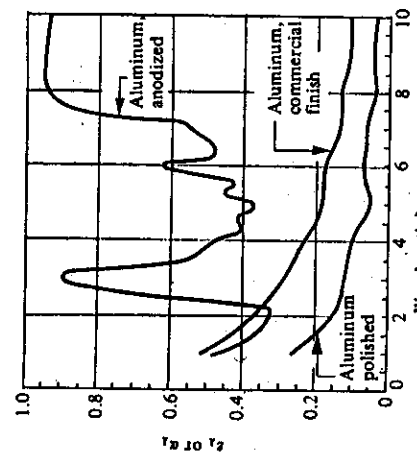


Fig. 11.5 Typical wavelength dependence of  $\varepsilon_\lambda$  and  $\alpha_\lambda$  for metals.

\*Spectral emissivity is sometimes called monochromatic emissivity.

<sup>a</sup>Relative to the depth of participating material which is only a fraction of a micron for metals.

According to Fig. 11.4, the ratio  $e/e_b$  of a real surface varies with wavelength; thus the quantity  $\varepsilon$  used in Eq. (11.13) is in fact the mean value of  $\varepsilon_\lambda$ , the spectral emissivity. Qualitatively, the spectral emissivity for metals decreases with increasing wavelength. In contrast, the spectral emissivity of electric nonconductors has a tendency to increase with increasing wavelength, but the variation of  $\varepsilon_\lambda$  with  $\lambda$  can be quite irregular. Figure 11.5 depicts experimental results showing these trends for aluminum having three different surface finishes. For the bare metal surface (commercial finish), the emissivity decreases almost steadily with increasing wavelength. The anodized aluminum behaves as a nonmetal, since the anodizing process produces a thick oxide coating on the surface. Furthermore, by comparing the commercial surface finish with the polished surface, we see that roughness increases emissivity. But since the descriptions such as polished, rough, or commercial finish are rather vague, emissivity data should be used judiciously with regard to the surface description.

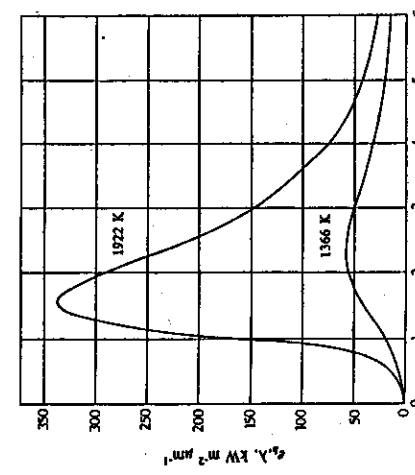
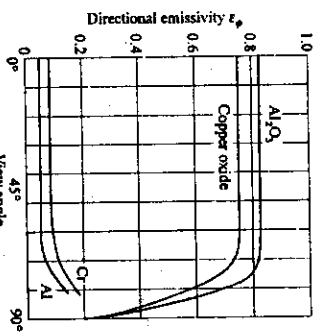


Fig. 11.3 Black body spectral emissive power.

Not only does emissivity vary with wavelength, but in the case of well-polished surfaces, it is also a function of the view angle from the normal to the surface (Fig. 11.6). Therefore, a directional emissivity  $\epsilon_\theta$  exists, but for our purposes the  $\epsilon$  used for calculations is the average value for a substance emitting radiation in all directions as well as all wavelengths. In this sense,  $\epsilon$  used for most calculations is properly called the *total hemispherical emissivity*; usually, however, it is simply called emissivity.



**Fig. 11.6** Variation of directional emissivity. The surfaces are well polished.

The curves in Fig. 11.6 illustrate the characteristics of electrical conductors and electrical insulators. Conductors emit somewhat more energy at high angles with respect to the observer, whereas the insulators have an opposite behavior. As a result, two different spheres, heated to the same incandescent temperature, appear as sketched in Fig. 11.7. Keep in mind that Fig. 11.7 is for highly polished surfaces, called *specular* surfaces; the differences are not so great for rough surfaces (*diffuse* surfaces).



**Fig. 11.7** Effect of directional emissivity on the appearance of radiating spheres: (a) electrical conductor with brighter periphery; (b) electrical insulator with dimmer periphery.

Figures 11.8 and 11.9 give the emissivity of several substances including polished metals. Additional data are given in Table 11.1; several oxides and some refractory materials are listed. More extensive listings of emissivity data are available in texts on radiation heat transfer,<sup>1-3</sup> as well as in compilations such as used for Figs. 11.8 and 11.9 and by Wood

<sup>1</sup>H. C. Hottel and A. F. Sarofim, *Radiative Transfer*, McGraw-Hill, New York, NY, 1967.

<sup>2</sup>E. M. Sparrow and R. D. Cess, *Radiation Heat Transfer*, Brooks/Cole, Belmont, CA, 1966.

<sup>3</sup>T. J. Love, *Radiative Heat Transfer*, Merrill, Columbus, OH, 1968.

<sup>4</sup>R. Siegel and J. Howell, *Thermal Radiation Heat Transfer*, second edition, McGraw-Hill, New York, NY, 1980.

<sup>5</sup>M. Q. Brewster, *Thermal Radiative Transfer and Properties*, John Wiley, New York, NY, 1991.

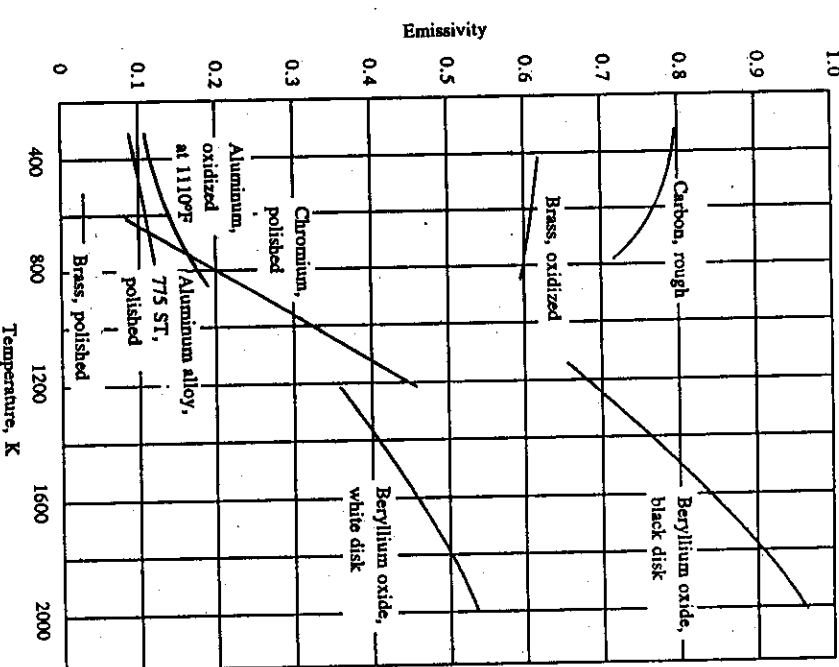


**Fig. 11.8** The emissivity of several materials. (From G. G. Gabareff, J. E. Janssen, and R. H. Torborg, *Thermal Radiation Properties Survey*, Honeywell Research Center, Minneapolis, MN, 1960.)

et al.<sup>6</sup> and Touloukian and DeWitt.<sup>7</sup> In metals, emissivity increases with electrical resistance, and, correspondingly, with temperature. For electric nonconductors, the emissivities are much higher than for clean metal surfaces, and they often, but not always, decrease with temperature.

When searching for emissivity data, the reader should be cognizant that many ceramic materials and coatings transmit considerable amounts of the incident radiation and must be

<sup>6</sup>W. D. Wood, H. W. Deem and C. F. Lucks, *Thermal Radiative Properties of Selected Materials*, DMC Report 177, Volumes 1 and 2, Defense Metals Information Center, Battelle, Columbus, OH, 1962.

<sup>7</sup>Y. S. Touloukian and D. P. DeWitt, *Thermal Radiative Properties*, IFI/Plenum, New York, NY, 1970.

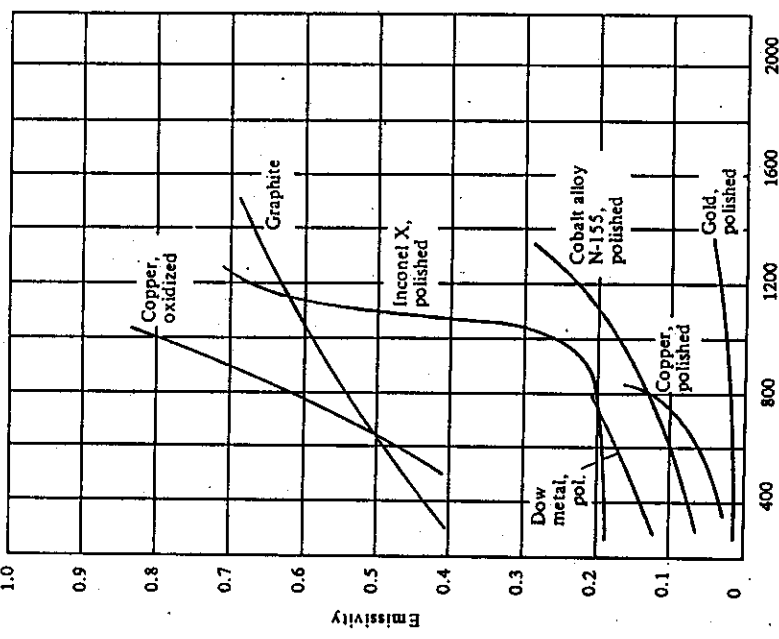
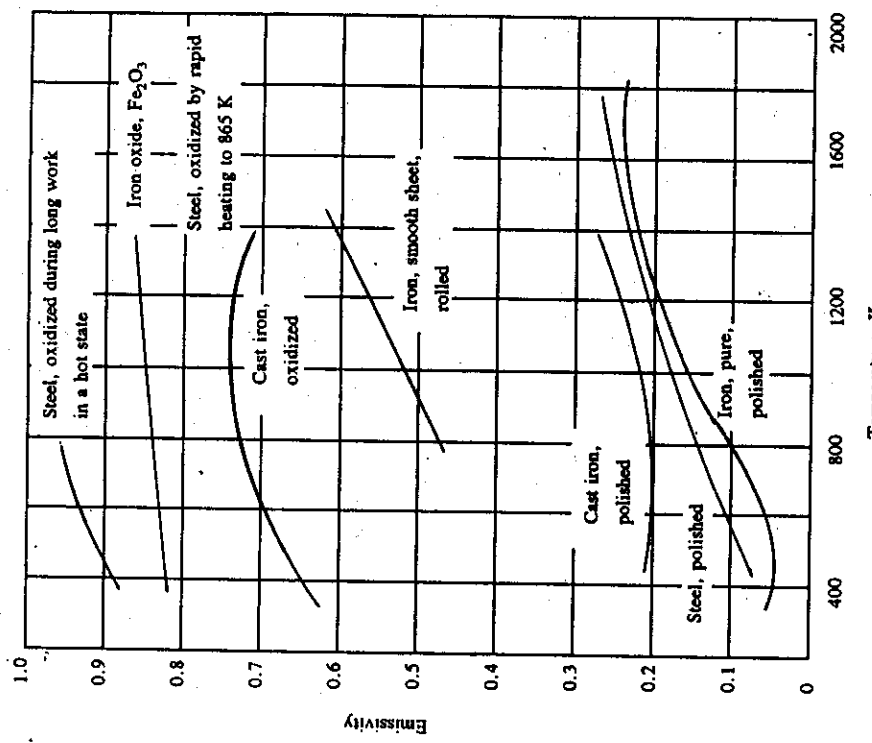


Fig. 11.8 (continued).

Table 11.1 The emissivity of some ceramic materials. (From H. C. Hotel and A. F. Sarofim, *ibid.*)

Material	Temperature, K	Emissivity
Cuprous oxide	1070-1370	0.66-0.54
Magnesium oxide	550-1100	0.55-0.20
Nickel oxide	1170-1980	0.20
Thorium oxide	920-1530	0.59-0.86
	550-770	0.58-0.36
	770-1100	0.36-0.21
Alumina-silica-iron oxide	1280-1840	0.61-0.43
58-80% $\text{Al}_2\text{O}_3$ , 16-38% $\text{SiO}_2$ , 0.4% $\text{Fe}_2\text{O}_3$	1280-1840	0.73-0.62
26-36% $\text{Al}_2\text{O}_3$ , 50-60% $\text{SiO}_2$ , 1.7% $\text{Fe}_2\text{O}_3$	1280-1840	0.78-0.68
61% $\text{Al}_2\text{O}_3$ , 35% $\text{SiO}_2$ , 3% $\text{Fe}_2\text{O}_3$	1273	0.75
Fireclay brick	1273	0.38
Magnesite refractory brick	570-1110	0.92-0.80
Quartz (opaque)	510-770	0.92-0.80
Zirconium silicate	770-1105	0.80-0.52

Fig. 11.9 Variation of emissivity with temperature and conditions of ferrous materials. (From G. G. Gabareff *et al.*, *ibid.*)

relatively thick to be effectively opaque. The emissivity of a coating, or thick film, therefore, reported by one investigator might vary considerably from that for the same coating material reported by another. Reasons for such a variance are differences in the surface conditions (including the underlying material) and in the thicknesses of the coatings. Absorption coefficients ( $\alpha$ ) can vary strongly with wavelength. For example, many glasses of 3 mm thickness are effectively infinitely thick to thermal radiation emanating at room temperature. At elevated temperatures, however, a large fraction of the energy of the total spectrum has wavelengths less than 2.5  $\mu\text{m}$  (see Fig. 11.3) and in this range the absorption coefficient of glass is so low that the energy can be transmitted up to 300 to 400 mm through the glass. Nevertheless, even if transparent thick films are applied to opaque substrates, the surfaces are treated as though they have emissivities. Usually the emissivity of a metal substrate coated with a nonmetallic is significantly greater than the emissivity of the substrate, itself, but somewhat less than the inherent emissivity of the coating. In Section 11.12, we discuss briefly the combined roles of phonon conduction and photon transmission in semitransparent materials at elevated temperatures.

#### 11.4 GRAY BODIES AND ABSORPTIVITY

The absorptivity of a real surface is even more difficult to evaluate with precision than its emissivity. In addition to the factors which affect emissivity, the absorptivity depends on the character of the incoming radiation; therefore, in general, we cannot regard the absorptivity as dependent on the surface alone. Hence, we assign two subscripts to  $\alpha$ , the first to represent the temperature of the absorbing surface, and the second—the source temperature of the incoming radiation. We have already seen in Section 11.2 that the emissivity  $e_1$  of a surface at  $T_1$  is equal to the absorptivity  $\alpha_{11}$  which the surface exhibits for black radiation from a source at the same temperature  $T_1$ ; for this reason, it is customary in a wide variety of engineering problems to assume that  $\alpha = e$ . We shall now discuss the conditions for which it is permissible to deduce  $\alpha$ -values from  $e$ -values.

If  $\alpha_{11}$  is independent of  $\lambda$ , the surface is said to be *gray*, and its total absorptivity is independent of the incoming spectral energy distribution; then for a surface at  $T_1$  receiving radiation from an emitter at  $T_2$ ,  $\alpha_{12} = \alpha_{11}$ . Since  $\alpha_{11} = e_1$ , we see that the emissivity may be substituted for  $\alpha$ , even though the temperatures of the source radiation and the receiver are not the same. There are very few substances with  $\alpha_{11}$  independent of  $\lambda$ , but many real surfaces may be considered gray. For example, look at the emissivity of polished Inconel X in Fig. 11.8. The emissivity is almost constant in the range 300 to 900 K, and if this surface were in an enclosure with temperatures in this range, then the gray assumption would be good. However, if either the enclosure temperature or the Inconel surface temperature was between 900 and 1300 K, where the emissivity of the Inconel varies rapidly with temperature, the material would be very much nongray. Thus, when available, a convenient criterion for grayness versus nongrayness is the emissivity versus temperature curve.

Under conditions of radiation from a source at  $T_1$  incident on a *metallic* surface at a lower temperature  $T_2$ , we prefer to evaluate the absorptivity of the metallic surface as

$$\alpha_{21} = e_2(T^*), \quad (11.14)$$

in which  $T^* = \sqrt{T_1 T_2}$ . We illustrate the use of these approximations in the following section.

#### 11.5 EXCHANGE BETWEEN INFINITE PARALLEL PLATES

When a system is of simple geometry such as infinite parallel plates, concentric cylinders, or concentric spheres, the evaluation of radiant heat transfer is simplified because all of the radiation leaving one of the surfaces is completely intercepted by the other surface. We shall treat more complex geometrical aspects in the next section, but here we consider a case of simple geometry to show the utilization of the system properties. Specifically, consider the two parallel surfaces of infinite extent in Fig. 11.10. In this schematic representation, the energy is viewed as two parts: the radiation originating from surface 2 is shown in Fig. 11.10(a); radiation originating from surface 1 is shown in Fig. 11.10(b).

The irradiation of surface 1 from surface 2 consists of all the upward pointing arrows in Fig. 11.10(a), or

$$e_2 + \rho_{12}\rho_{22}e_2 + \rho_{12}^2\rho_{22}^2e_2 + \dots + \rho_{12}^n\rho_{22}^ne_2. \quad (11.15)$$

We write this infinite series as

$$\frac{e_2}{1 - \rho_{12}\rho_{22}}. \quad (11.16)$$

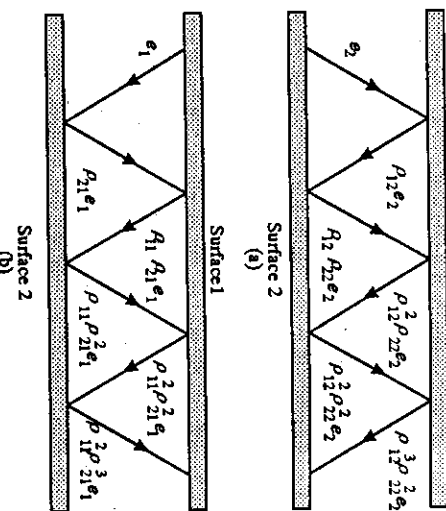


Fig. 11.10 Radiation exchange between parallel surfaces. (a) Irradiation originating from surface (1). (b) Irradiation originating from surface (2).

In a similar manner, the summation of the upward pointing arrows in Fig. 11.10(b) is

$$\frac{\rho_{21}e_1}{1 - \rho_{11}\rho_{21}}. \quad (11.17)$$

The sum of these two terms is the total irradiation of surface 1; thus

$$G_1 = \frac{e_1}{1 - \rho_{12}\rho_{22}} + \frac{\rho_{21}e_1}{1 - \rho_{11}\rho_{21}}. \quad (11.18)$$

The net heat flux from surface 1 is

$$q_{1,\text{net}} = J_1 - G_1, \quad (11.19)$$

but the radiosity  $J_1$  comprises the radiation emitted at surface 1 plus that reflected,

$$J_1 = e_1 + \rho_{11}G_1. \quad (11.20)$$

(The second subscript of  $\rho$  is not denoted at this point.) By combining Eqs. (11.18)-(11.20), we find that the net heat flux from surface 1 is

$$q_{1,\text{net}} = e_1 - (1 - \rho_{11})G_1 = e_1 - \alpha_{11}G_1$$

or

$$q_{1,\text{net}} = e_1 - \left[ \frac{\alpha_{12}e_2}{1 - \rho_{12}\rho_{22}} + \frac{\alpha_{11}\rho_{21}e_1}{1 - \rho_{11}\rho_{21}} \right]. \quad (11.21)$$

Here  $\alpha_{11}$  is denoted  $\alpha_{12}$  and  $\alpha_{11}$  for the first and second terms on the right side of Eq. (11.21) because it is associated with the radiations originating at surfaces 2 and 1, respectively.

The basic practical difficulty in the analysis of systems with nonblack surfaces is what absorptivity value should be used. In the light of this problem, discussed in Section 11.4, let us analyze the various forms that Eq. (11.21) takes depending on the manner in which we evaluate  $\alpha_{11}$ . The gray assumption which would apply for Inconel-X plates, if both were between 300 and 900 K, makes  $\alpha_{12} = \alpha_{11} = \varepsilon_1$ ,  $\alpha_{21} = \alpha_{22} = \varepsilon_2$ , and  $\rho_{12} = \rho_{11} = 1 - \varepsilon_1$ , and  $\rho_{21} = \rho_{22} = 1 - \varepsilon_2$ . In this case, Eq. (11.21) simplifies to

$$q_{1,\text{net}} = (\varepsilon_{b1} - \varepsilon_{b2}) \frac{1}{1/\varepsilon_1 + 1/\varepsilon_2 - 1}. \quad (11.22)$$

For metal plates, we can improve Eq. (11.22) by the approximation of Eq. (11.14); we evaluate the emissivity of the cooler surface at  $T^* = \sqrt{T_1 T_2}$ . For example, if surface 2 is hotter than 1, we write Eq. (11.22) as

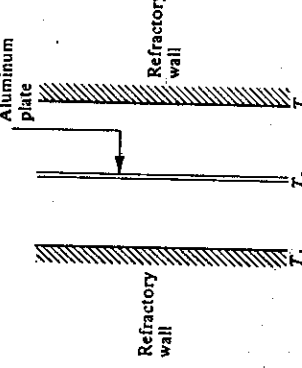
$$q_{1,\text{net}} = (\varepsilon_{b1} - \varepsilon_{b2}) \frac{1}{1/\varepsilon_1(T^*) + 1/\varepsilon_2 - 1}. \quad (11.23)$$

We accomplish the evaluation of radiant heat transfer between nongray surfaces with the most precision only by considering the best approximation for their absorptivities, and also the variation in properties with direction. Fortunately, many industrial materials, especially refractories used in furnaces, behave as gray diffuse radiators so that these details may be omitted from analysis. We shall consider nonblack surfaces as gray in this chapter. More details regarding nongray surfaces and directional properties can be found in the more advanced treatments of radiation heat transfer listed in Section 11.3. The presentations of radiation heat transfer in Holman<sup>8</sup> and Incropera and DeWitt<sup>9</sup> are also more comprehensive and should be consulted when it is apparent that the surfaces under consideration cannot be assumed gray and diffuse.

**Example 11.1** We can use the above results to illustrate the principle of *radiation shields*.

Multiple shields are very effective when used as high-temperature insulation against thermal radiation. To illustrate the principle, develop an expression for the reduction in radiant heat transfer between two infinite and parallel refractory walls, when a thin plate of aluminum is placed between them. Assume that all surfaces are gray; the emissivity of the walls is 0.8 and the emissivity of the aluminum is 0.2.

The system with appropriate subscripts is shown to the right.



**Solution.** First, we examine the case in the absence of the aluminum sheet, that is, direct radiant transfer from surface 1 to surface 3. Equation (11.22) applies with appropriate change of subscripts. Therefore

$$q_{1,\text{net}} (\text{no shield}) = (\varepsilon_{b1} - \varepsilon_{b3}) \frac{1}{1/\varepsilon_1 + 1/\varepsilon_3 - 1}.$$

Now in the presence of the shield, we apply Eq. (11.22) to the net radiant flux from surface 1 to surface 2. Hence

$$q_{1,\text{net}} = (\varepsilon_{b1} - \varepsilon_{b2}) \frac{1}{1/\varepsilon_1 + 1/\varepsilon_2 - 1}.$$

Similarly, we write the radiant flux from surface 2 to surface 3 as

$$q_{2,\text{net}} = (\varepsilon_{b2} - \varepsilon_{b3}) \frac{1}{1/\varepsilon_2 + 1/\varepsilon_3 - 1}.$$

Since  $q_{2,\text{net}} = q_{1,\text{net}}$  (steady state), we eliminate  $\varepsilon_{b2}$  from these equations:

$$q_{1,\text{net}} = \frac{(\varepsilon_{b1} - \varepsilon_{b3})}{(1/\varepsilon_1 + 1/\varepsilon_2 - 1) + (1/\varepsilon_2 + 1/\varepsilon_3 - 1)}.$$

The ratio of radiant flux with the shield to that without the shield is

$$\frac{q_{1,\text{net}} (\text{with shield})}{q_{1,\text{net}} (\text{no shield})} = \frac{(1/\varepsilon_1 + 1/\varepsilon_3 - 1)}{(1/\varepsilon_1 + 1/\varepsilon_2 - 1) + (1/\varepsilon_2 + 1/\varepsilon_3 - 1)}.$$

With  $\varepsilon_1 = \varepsilon_3 = 0.8$ , and  $\varepsilon_2 = 0.2$ , this ratio equals 0.143. Insertion of more shields would lower the ratio even more considerably.

## 11.6 VIEW FACTORS

Having discussed the complexities of property evaluation, we now consider geometric arrangements in radiation heat transfer. In this connection, we introduce the *view factor*. In the engineering literature different terms are used for this factor, such as *configuration factor*, *direct-exchange factor*, *angle factor*, or simply *factor*, and perhaps others which are unknown to us.

The simplest case for calculating the net loss of energy from a body due to radiation is to visualize a body at temperature  $T_1$  which is completely surrounded by an environment at  $T_2$ . Since the environment completely surrounds the body, the radiation impinging on surface 1 is black (as in a cavity). The thermal flux (or emissive power) from the body is  $\varepsilon_1 = \varepsilon_1 \sigma T_1^4$ , and that absorbed by the body from the large isothermal cavity is  $\alpha_{12} \varepsilon_{22} = \alpha_{12} \sigma T_2^4$ . Then

$$q_{1,\text{net}} = \sigma [\varepsilon_1 T_1^4 - \alpha_{12} T_2^4], \quad (11.24)$$

and when we assume that the body is gray,  $\alpha_{12} = \varepsilon_1$ , and we write Eq. (11.24) as

$$q_{1,\text{net}} = \sigma \varepsilon_1 (T_1^4 - T_2^4). \quad (11.25)$$

The more general case of radiation exchange is a system composed of several surfaces at different temperatures and of different emissivities. Such a situation involves the use of the

<sup>8</sup>J. P. Holman, *Heat Transfer*, sixth edition, McGraw-Hill, New York, NY, 1986, Chapter 8.

<sup>9</sup>F. P. Incropera and D. P. DeWitt, *Fundamentals of Heat and Mass Transfer*, third edition, John Wiley, New York, NY, 1990, Chapters 12 and 13.

view factor,  $F_{ij}$ . We define it as the fraction of the radiation which leaves surface  $i$  in all directions and is intercepted by surface  $j$ .

To evaluate  $F_{12}$ , imagine the two black surfaces, of areas  $A_1$  and  $A_2$ , shown in Fig. 11.11. A small surface element  $dA_1$  emits radiation in all directions (from one side), and a small surface element  $dA_2$  on the other surface intercepts some of this radiation. Let  $r$  be the distance between the surface elements, and  $\phi_1$  and  $\phi_2$  the angles that  $r$  makes with the two normals, as depicted in the figure. The intensity of the radiation transferred from  $dA_1$  to  $dA_2$ , called  $E_{12}$ , is proportional to:

1. The apparent area of  $dA_1$  viewed from  $dA_2$ ,  $\cos \phi_1 dA_1$ .
2. The apparent area of  $dA_2$  viewed from  $dA_1$ ,  $\cos \phi_2 dA_2$ .
3. The reciprocal of the distance squared,  $1/r^2$ , between the two surface elements, as in all radiation problems.

or

$$dE_{12} (\text{hemisphere}) = \pi I. \quad (11.27)$$

Note that

$$dE_{12} (\text{hemisphere}) = \frac{dE_{12}}{dA_1} = e_b. \quad (11.28)$$

Since we have been discussing a black body, the result states that the emissive power of a black body  $e_b$  is the product of  $\pi$  and the intensity of the emitted black body radiation per steradian:

$$e_b = \pi I. \quad (11.29)$$

Thus, by combining Eqs. (11.26) and (11.29), we return to the major argument, and express the general equation for the transfer of radiant energy from one black body to another as

$$E_{12} = \int_A dE_{12} = \frac{e_b}{\pi} \int_A \int_A \frac{\cos \phi_1 \cos \phi_2}{r^2} dA_2 dA_1. \quad (11.30)$$

Thus

$$dE_{12} = I \frac{\cos \phi_1 dA_1 \cos \phi_2 dA_2}{r^2}, \quad (11.26)$$

where  $I$  is a proportionality constant. By inspecting Eq. (11.26),  $I$  must be the intensity leaving  $dA_1$  in a particular direction; it has units of  $\text{W m}^{-2}$  per steradian.

At this point, it may appear that  $I$  and  $e_b$  (the emissive power of a black body) are identical. This is not the case, and here we digress from the major argument. Consider the radiation received from the entire field of view to  $dA_1$ , that is, the hemisphere in Fig. 11.12. Visualize  $dA_2$ , as the unit surface described by the ring on the hemisphere. Since the normals to a spherical surface are coincident to the radii,  $\phi_2$  in Eq. (11.26) must be 0, so that  $\cos \phi_2 = 1$ . The elemental area  $dA_2$  is given by the product of  $r d\phi_1$  and its length,  $2\pi \sin \phi_1 r$ . If we integrate over the entire hemisphere, Eq. (11.26) yields (for isotropic  $I$ ) per unit area  $dA_1$ :

$$dE_{12} (\text{Hemisphere}) = 2\pi I \int_0^{\pi/2} \frac{\cos \phi_1 \sin \phi_1 r^2 d\phi_1}{r^2},$$

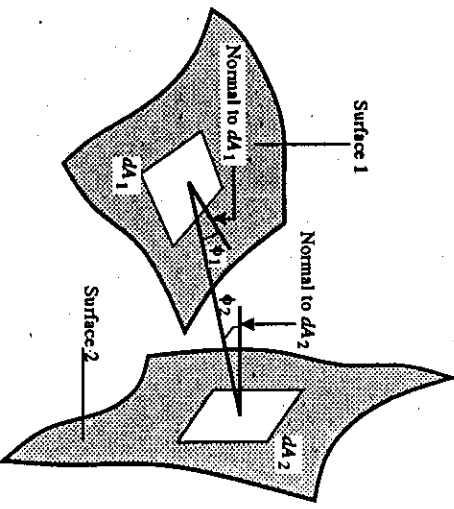


Fig. 11.11 Exchange of radiation between elemental areas.

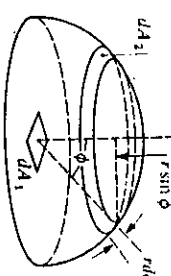


Fig. 11.12 Hemispherical radiation intensity.

This integral contains nothing but geometrical aspects of radiant exchange, and has fortunately been evaluated for many geometries. Usually, one does not have to perform the integration oneself. Now we can write a simple equation to express the energy emitted by a black surface 1 and intercepted by surface 2, using the definition of  $F_{12}$ ,

$$E_{12} = e_b A_1 F_{12}. \quad (11.32)$$

In exactly the same manner, we could have developed an analogous expression for the energy originating at 2 and arriving at 1.

$$E_{21} = e_b A_2 F_{21}. \quad (11.33)$$

Then, the net exchange of energy from 1 to 2 is  $A_1 q_{1,\text{net}}$  or  $Q_{1,\text{net}}$ :

$$Q_{1,\text{net}} = E_{12} - E_{21}. \quad (11.34)$$

At thermal equilibrium,  $Q_{1,\text{net}} = 0$ , and from Eqs. (11.32) and (11.33) and the fact that the emissive power of a black body depends only upon temperature, we see that  $A_1 F_{21} = A_1 F_{12}$ . In general, we can say that

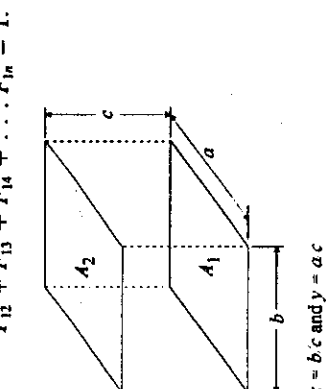
$$A_i F_{ij} = A_j F_{ji}. \quad (11.35)$$

Equation (11.35), though simple, is very useful, and the reader should keep it in mind.

Values of  $F_{12}$  have been calculated for various geometric arrangements of two surfaces. Figures 11.13–11.15 provide such view factor charts. More extensive listings can be found in texts on radiation heat transfer. Although we have restricted the discussion leading up to the view factor charts to black surfaces, it is apparent that for nonblack surfaces, with emissivities independent of emission angles,  $F_{12}$  can be calculated by the method discussed above and again represents the fractional radiation from  $A_1$  intercepted by  $A_2$ . Thus such a calculation is exact for black surfaces, and very useful for most nonmetallic, oxidized or rough metal surfaces which exhibit nearly isotropic surface properties.

Since the view factor is the fraction of radiation emitted by a surface and intercepted by another surface, then all the radiation from any surface must be ultimately intercepted when there are many surfaces involved. For example, if surface 1 is seen by surfaces 2, 3, 4 . . .  $n$ , then

$$F_{12} + F_{13} + F_{14} + \dots + F_{1n} = 1. \quad (11.36)$$



$$x = b/c \text{ and } y = a/c$$

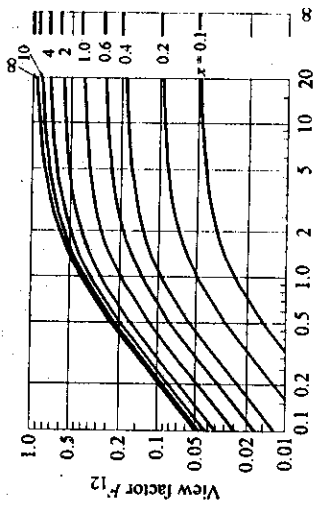


Fig. 11.13 View factors for two rectangles with a common edge. (From T. J. Love, *ibid.*)

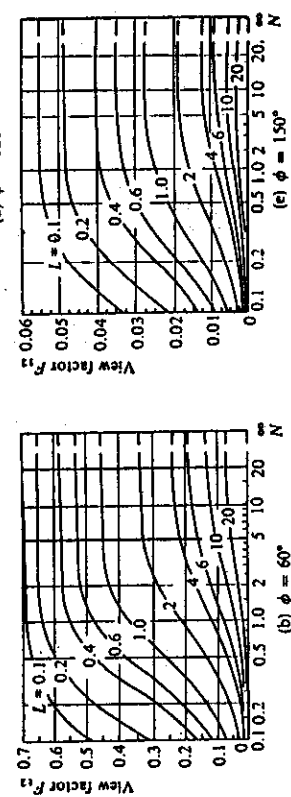
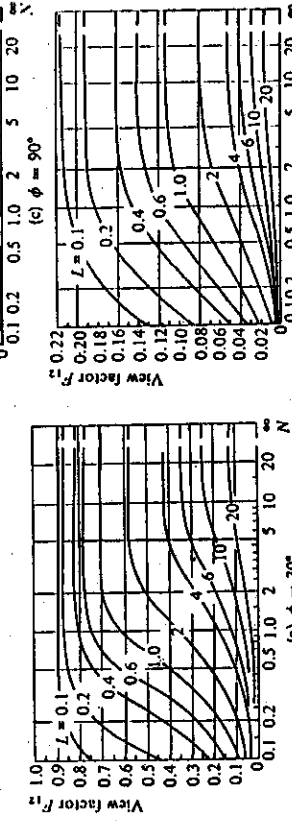
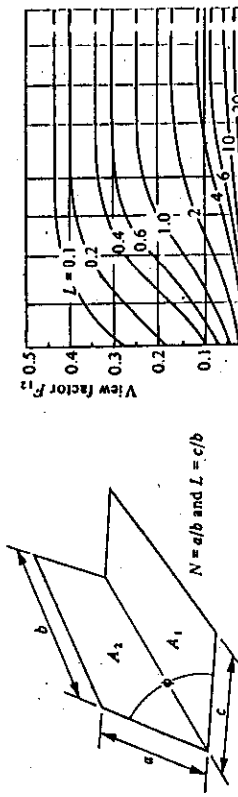


Fig. 11.14 View factors for two rectangles with parallel edges. (From T. J. Love, *ibid.*)

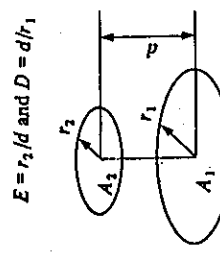
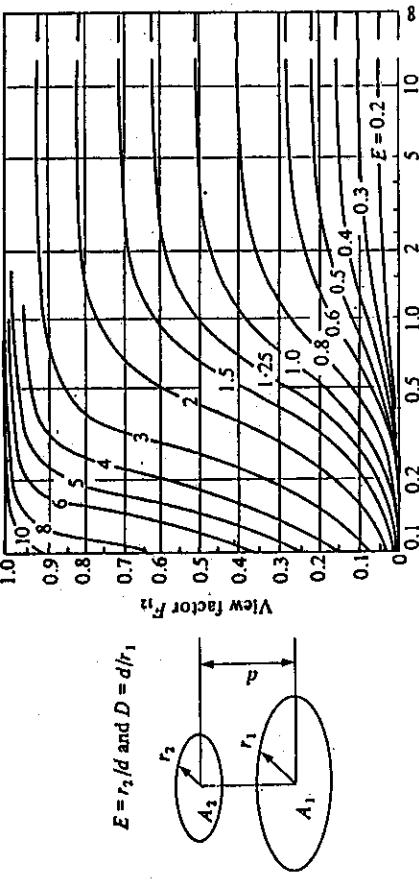
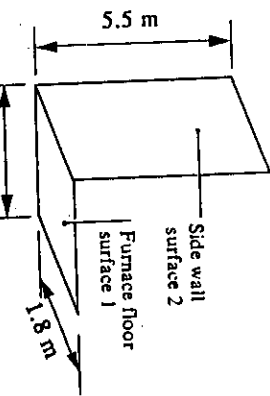


Fig. 11.15 View factors for parallel, directly opposed disks. (From T. J. Love, *ibid.*)

**Example 11.2** Calculate the net heat flow by radiation to the furnace wall at 530 K from the furnace floor at 810 K. Both surfaces can be considered to be black radiators.



**Solution.** The energy emitted by the black surface 1 and intercepted by 2 is  $E_{12} = \epsilon_{b1}A_1F_{12}$ .

Similarly, the energy emitted by surface 2 and intercepted by surface 1 is  $E_{21} = \epsilon_{b2}A_2F_{21}$ . The net exchange of energy from surface 1 to surface 2 is  $Q_{1,\text{net}} = E_{12} - E_{21}$ , and, since  $A_2F_{21} = A_1F_{12}$ , we can finally write the net exchange of energy from surface 1 to surface 2 as

$$Q_{1,\text{net}} = A_1F_{12}(\epsilon_{b1} - \epsilon_{b2}) = A_1F_{12}\sigma[T_1^4 - T_2^4].$$

Figure 11.14(c) is used to evaluate  $F_{12}$  with  $N = 5.5/1.8 = 3.06$ ,  $L = 3.7/1.8 = 2.06$ , and  $\phi = 90^\circ$ . The view factor  $F_{12}$  is approximately 0.16. Recalling that  $\sigma = 5.699 \times 10^{-8} \text{ W m}^{-2} \text{ K}^{-4}$ , we determine that

$$Q_{1,\text{net}} = (1.8 \times 3.7)(0.16)(5.699) \left[ \left[ \frac{810}{100} \right]^4 - \left[ \frac{530}{100} \right]^4 \right] = 21,240 \text{ W}.$$

### 11.7 ELECTRIC CIRCUIT ANALOG

Consider an all-black surface enclosure (Fig. 11.16(a)) in which

$$F_{12} + F_{13} + F_{14} = 1. \quad (11.37)$$

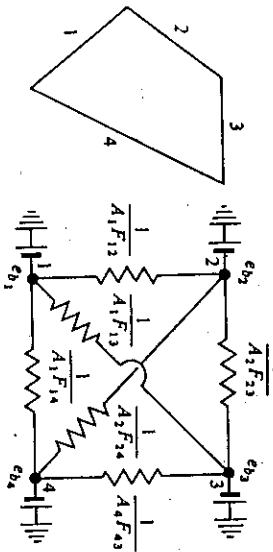


Fig. 11.16 (a) A black enclosure. (b) Its electrical analog.

The net power (W) from surface 1 is

$$\begin{aligned} Q_{1,\text{net}} &= (E_{12} - E_{21}) + (E_{13} - E_{31}) + (E_{14} - E_{41}) \\ &= A_1F_{12}(\epsilon_{b1} - \epsilon_{b2}) + A_1F_{13}(\epsilon_{b1} - \epsilon_{b3}) + A_1F_{14}(\epsilon_{b1} - \epsilon_{b4}). \end{aligned} \quad (11.38)$$

We can also develop Eq. (11.38) by analyzing the situation with an electric analog. We think of each surface as a node in the electric analog (Fig. 11.16(b)) and represent the potential at each node by  $e_{bi}$ , the current by the heat flow, and the resistance between two potential nodes  $i$  and  $j$  by  $1/A_{ij}\sigma$ . We draw the circuit, and connect each node to all the other nodes. We can then easily recognize the net heat flow from any surface. For example, we obtain the net heat flow from surface 4 by simply summing the analog currents through the three resistors connected to node 4:

$$Q_{4,\text{net}} = A_1F_{14}(\epsilon_{b4} - \epsilon_{b1}) + A_2F_{24}(\epsilon_{b4} - \epsilon_{b2}) + A_3F_{34}(\epsilon_{b4} - \epsilon_{b3}).$$

It may be desirable to express the net heat flow only in terms of  $A_i$ . In this case, we utilize Eq. (11.35) to yield

$$Q_{4,\text{net}} = A_4F_{41}(\epsilon_{b4} - \epsilon_{b1}) + A_4F_{42}(\epsilon_{b4} - \epsilon_{b2}) + A_4F_{43}(\epsilon_{b4} - \epsilon_{b3}). \quad (11.39)$$

The electric analog for a gray surface is also very useful in solving many problems. The total energy flux radiating from a surface is its radiosity, or

$$J = \rho G + \varepsilon e_b, \quad (11.40)$$

where  $G$  is the irradiation. The net heat flux transferred from the surface is

$$q_{\text{net}} = J - G, \quad (11.41)$$

and by eliminating  $G$  from these last two equations, we get

$$q_{\text{net}} = \frac{\varepsilon}{1-\varepsilon} (\epsilon_b - J).$$

Therefore, for the net heat flow from a surface of area  $A$ , we can write

$$Q_{\text{net}} = \frac{\varepsilon}{1-\varepsilon} A(\epsilon_b - J). \quad (11.42)$$

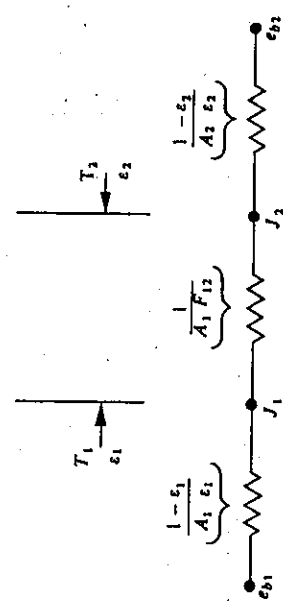
Thus, we can represent a gray surface with a potential of a black surface reduced by a resistance  $(1-\varepsilon)/\varepsilon$ , as in Fig. 11.17. The use of an electric analog is particularly useful when dealing with gray surfaces. We illustrate this in Example 11.3.



Fig. 11.17 Electric analog of a gray surface.

**Example 11.3** Consider the exchange of energy between two parallel and gray plates. For infinitely long plates, 1 and 2, use the method of electric analogs and develop an expression for the heat flux if the plates are at  $T_1$  and  $T_2$ , and have emissivities of  $\epsilon_1$  and  $\epsilon_2$ , respectively.

**Solution.** The system and the appropriate analog are shown below.



By examining the analog circuit, the reader can see that each surface is represented by the nodes shown in Fig. 11.17. The analog circuit is completed by connecting the radiosity nodes with the resistance between the surfaces. Therefore, when dealing with gray surfaces, connect the radiosities; when dealing with black surfaces, connect the black body emissive powers, as shown in Fig. 11.16(b).

To solve the problem, simply determine the total resistance between  $e_{b1}$  and  $e_{b2}$ . The total resistance is

$$\frac{1 - \epsilon_1}{A_1 \epsilon_1} + \frac{1}{A_1 F_{12}} + \frac{1 - \epsilon_2}{A_2 \epsilon_2}.$$

Then by using Ohm's law, we can immediately write an expression for the net heat flow from 1 to 2:

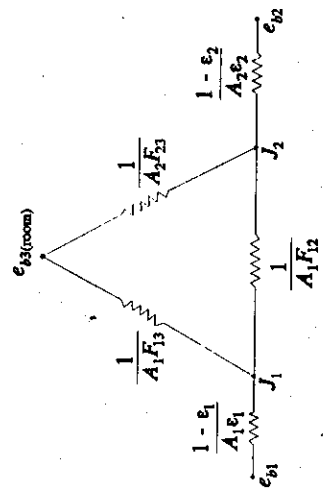
$$Q_{1,\text{net}} = \frac{(e_{b1} - e_{b2})}{\frac{1 - \epsilon_1}{A_1 \epsilon_1} + \frac{1}{A_1 F_{12}} + \frac{1 - \epsilon_2}{A_2 \epsilon_2}}.$$

In this case,  $A_1 = A_2$ , and  $F_{12} = 1$ . Therefore

$$q_{1,\text{net}} = \frac{Q_{1,\text{net}}}{A_1} = \frac{(e_{b1} - e_{b2})}{1/\epsilon_1 - 1 + 1/\epsilon_2}.$$

This expression is the same as Eq. (11.22). After having treated a few situations by using electric analogs, the reader will become quite apt at developing expressions involving radiation exchange between gray and/or black surfaces.

**Example 11.4** In Example 11.2, we were very careful to say that the calculation was "the net exchange of energy from surface 1 to surface 2." But with other surfaces in the radiation circuit, the result we obtained would not have been the total power delivered to surface 2. With this in mind, let us consider the two surfaces in Example 11.2 to be plates with gray surfaces, while insulating the bottom side of plate 1 and the left side of plate 2. The plates are placed in a large room at 300 K. Calculate the net power gain or loss to each plate. Data:  $\epsilon_1 = \epsilon_2 = 0.5$ .



Let's take care of the view factors first. From Example 11.2,  $F_{12} = 0.16$ . Thus,  $F_{13} = 1 - F_{12} = 0.84$ . Also,

$$F_{21} = \frac{A_1 F_{12}}{A_2} = \frac{(3.7 \times 1.8)(0.16)}{(5.5 \times 1.8)} = 0.108,$$

so that  $F_{31} = 1 - F_{21} = 0.892$ .

The resistances in the circuit are calculated as

$$\frac{1 - \epsilon_1}{A_1 \epsilon_1} = \frac{(1 - 0.5)}{(3.7 \times 1.8)(0.5)} = 0.150 \text{ m}^{-2},$$

$$\frac{1 - \epsilon_2}{A_2 \epsilon_2} = \frac{(1 - 0.5)}{(5.5 \times 1.8)(0.5)} = 0.101 \text{ m}^{-2},$$

$$\frac{1}{A_1 F_{12}} = \frac{1}{(3.7 \times 1.8)(0.84)} = 0.179 \text{ m}^{-2},$$

$$\frac{1}{A_2 F_{23}} = \frac{1}{(5.5 \times 1.8)(0.892)} = 0.113 \text{ m}^{-2}.$$

Now we apply Kirchhoff's law at nodes  $J_1$  and  $J_2$ ,

$$\frac{e_{b1} - J_1}{0.150} + \frac{J_2 - J_1}{0.938} + \frac{e_{b3} - J_1}{0.179} = 0,$$

$$\frac{e_{b2} - J_2}{0.101} + \frac{J_1 - J_2}{0.938} + \frac{e_{b3} - J_2}{0.113} = 0.$$

After substituting the values of  $e_{b1}$ ,  $e_{b2}$  and  $e_{b3}$ , we have two equations, with two unknowns  $J_1$  and  $J_2$ , which are solved to give

$$e_{b1} = \sigma T_1^4 = (5.669)(8.10)^4 = 24400 \text{ W m}^{-2},$$

$$e_{b2} = (5.669)(5.30)^4 = 4470 \text{ W m}^{-2},$$

$$e_{b3} = (5.669)(3.0)^4 = 459 \text{ W m}^{-2},$$

$$J_1 = 12600 \text{ W m}^{-2},$$

$$J_2 = 3120 \text{ W m}^{-2}.$$

The power losses of plates 1 and 2 are

$$E_{1,\text{net}} = \frac{e_{b1} - J_1}{(1 - \varepsilon_1)/\varepsilon_1 A_1} = \frac{24400 - 12600}{0.150} = 78300 \text{ W},$$

and

$$E_{2,\text{net}} = \frac{e_{b2} - J_2}{(1 - \varepsilon_2)/\varepsilon_2 A_2} = \frac{4470 - 3120}{0.101} = 13400 \text{ W}.$$

As a check, we calculate the power received by the room.

$$E_{3,\text{net}} = \frac{J_2 - e_{b3}}{1/A_2 F_{23}} + \frac{J_1 - e_{b2}}{1/A_1 F_{13}} = \frac{3120 - 459}{0.113} + \frac{12600 - 459}{0.179} = 91700 \text{ W}.$$

The overall energy balance must satisfy

$$E_{3,\text{net}} = E_{1,\text{net}} + E_{2,\text{net}},$$

and we are within 0.01%.

## 11.8 FURNACE ENCLOSURES

As an application of radiant heat transfer, consider furnace design. We often encounter a situation in which energy is transferred from a *heat source* to a *heat sink* with intermediate refractory walls. For example, the heat source might be a row of electric resistors to heat a metal part placed in a furnace. In normal furnaces, the radiation incident on the refractory walls is so large compared to the heat conduction through the walls that we may approximate the conduction as zero when calculating radiant fluxes. Such walls are examples of *no-net-flux surfaces*. This assumption greatly simplifies the problem of transferring radiant heat from a source to a sink.

As an example, consider the transfer from face 1 (the source) to the opposite face 2 (the sink) with intermediate refractory walls (Fig. 11.18(a)). All surfaces are assumed to be gray, and the electric analog is given in Fig. 11.18(b). First, simplify the circuit by combining all the resistances between  $J_1$  and  $J_2$ , remembering that in parallel circuits conductances are

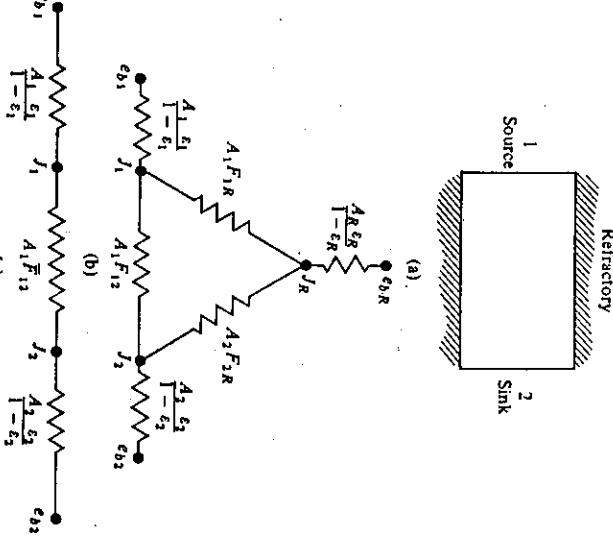


**Fig. 11.18** (a) Furnace enclosure. (b) and (c) Its electric analogs. (In this case, conductances rather than resistances are indicated.)

directly additive, and in series circuits the sample applies to resistances. The equivalent conductance between  $J_1$  and  $J_2$  is

$$A_1 \bar{F}_{12} = A_1 F_{12} + \frac{1}{1/A_1 F_{1R} + 1/A_2 F_{2R}}, \quad (11.43)$$

and the circuit reduces to Fig. 11.18(c). The symbol  $\bar{F}_{12}$  is often used when the several view factors in a system are all combined, as illustrated here. Finally, the equivalent resistance for the entire circuit is

$$\frac{1}{A_1 \bar{F}_{12}} = \frac{1}{A_1} \frac{1 - \varepsilon_1}{\varepsilon_1} + \frac{1}{A_2} \frac{1 - \varepsilon_2}{\varepsilon_2}. \quad (11.44)$$

The symbol  $\bar{F}_{12}$  is used when the entire circuit has been reduced to one equivalent resistance; thus  $\bar{F}_{12}$  depends not only on the individual view factors of the elements in the system but also on the individual emissivities. Since we are approximating the refractory walls as *no-net-flux surfaces*, then the current from  $J_k$  to  $\epsilon_{bR}$  is zero, and the current that goes from  $\epsilon_{b1}$  to  $\epsilon_{b2}$  in the equivalent circuit of Fig. 11.18(c) represents the net flow of energy from the source to the sink. In this sense, we refer to  $\bar{F}_{12}$  as the *total exchange factor* because it takes into account reradiating surfaces between the two surfaces (source and sink) of primary interest.

In this case, then

$$Q_{1,\text{net}} = A_1 \bar{F}_{12} (e_{b1} - e_{b2}) = A_1 \bar{F}_{12} \sigma (T_1^4 - T_2^4), \quad (11.45)$$

in which  $A_1 \bar{F}_{12}$  is given by Eq. (11.44).

In furnaces, electric resistors very often provide the source of heat, and can be mounted on a back-insulated refractory wall in a parallel array, as shown in Fig. 11.19. It is convenient to replace such a system by an equivalent continuous gray plane, having an effective emissivity  $\epsilon_p$ , and a temperature equal to that of the resistors. The gray plane is imaginary, and we show it by the dotted line in Fig. 11.19. To calculate  $\epsilon_p$ , we make use of Fig. 11.20 to determine  $\bar{F}_{pe}$ ; this is equivalent to  $\bar{F}_{12}$  in Eq. (11.43). Then, by rearranging Eq. (11.44) with  $\epsilon_p = 1$ , we can determine  $\mathcal{F}_{pe}$  from the expression

$$\mathcal{F}_{pe} = \frac{1}{\bar{F}_{pe}} + \frac{C}{\pi D} \left[ \frac{1}{\epsilon_p} - 1 \right] \quad (11.46)$$

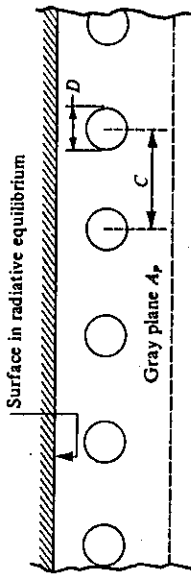


Fig. 11.19 A refractory-backed row of cylindrical elements.

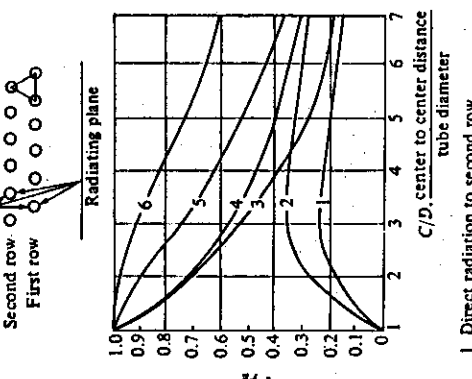


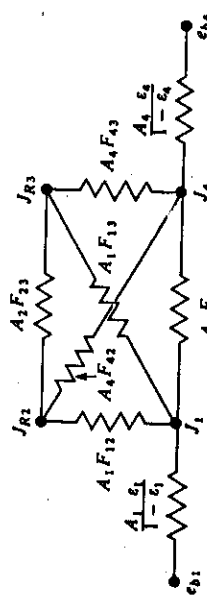
Fig. 11.20 Total exchange factors  $\bar{F}_{pe}$  between a black plane ( $P$ ) and one or two rows of cylindrical elements ( $E$ ) backed by a no-net-flux refractory wall. Direct view factors  $F_{pe}$  are also shown for comparison. Note that the elements form an array of equilateral triangles. (From H. C. Hottel and A. F. Sarofim, *ibid.*, page 114.)

where  $C/D$  is defined in Fig. 11.20. If no reradiating surface (no back-insulated refractory wall) exists, then  $\mathcal{F}_{pe} = \bar{F}_{pe}$  in this expression. Finally, we can consider the elements equivalent to the plane  $A_p$  with an emissivity  $\epsilon_p = \mathcal{F}_{pe}$  at the operating temperature of the elements.

**Example 11.5** A furnace has a floor  $1 \text{ m} \times 2 \text{ m}$ , and located at the top,  $1.5 \text{ m}$  away, are heating elements,  $50 \text{ mm}$  in diameter,  $1 \text{ m}$  long on  $100 \text{ mm}$  centers backed by a well-insulated refractory roof. The heating elements are Nichrome IV ( $\epsilon = 0.74$ ), which operate at a surface temperature of  $1370 \text{ K}$ . The side walls are insulated refractory (no-net-flux) surfaces. Find the rate at which heat can be transferred to a sheet of aluminum at  $300 \text{ K}$  ( $1 \text{ m} \times 2 \text{ m}$ ,  $\epsilon = 0.15$ ) placed on the floor of the preheated furnace.

**Solution.** To demonstrate only the aspects of radiant heating, we shall ignore convective heating on the upper surface of the aluminum sheet and heat transfer that might occur by conduction across minute contact points between the sheet and the furnace floor.

To calculate the rate at which heat is transferred by radiation to the upper surface of the sheet, we divide the system into four zones: (1) an equivalent gray plane to represent the elements, (2) the side walls of dimensions  $1.5 \text{ m} \times 2 \text{ m}$ , (3) the side walls of dimensions  $1.5 \text{ m} \times 1 \text{ m}$ , and (4) the upper surface of the aluminum sheet. The analog circuit (showing conductances) is shown below.



In this particular example, to solve for  $A_1 \bar{F}_{14}$ , the equivalent conductance for the entire circuit between  $J_1$  (source) and  $J_4$  (sink), would be a messy task if done by algebraic means. A  $4 \times 4$  matrix could be set up and solved on a computer rather easily, or one could set up an actual analog circuit. For our purposes, we refer the reader to Fig. 11.21, from which  $\bar{F}_{14}$  can be found directly. In Fig. 11.21, the total exchange factor is presented for several geometries of source-sink combinations connected by perfect reradiating walls (i.e., no-net-flux surfaces). Naturally, we have selected a geometry represented on the figure!

By using Fig. 11.21, we find, for the geometry of a 2:1 rectangular opening with  $D = 1 \text{ m}$  and  $X = 1.5 \text{ m}$ , that



Using Fig. 11.21, we find, for the geometry of a 2:1 rectangular opening with  $D = 1 \text{ m}$  and  $X = 1.5 \text{ m}$ , that

$$\bar{F}_{14} = 0.51.$$

Next we proceed to determine  $\varepsilon_1$ . From Fig. 11.20 (curve 5) with  $C/D = 2$ , we obtain  $\frac{F_{pe}}{F_{pe}} = 0.88$ . Then, from Eq. (11.46),

$$\varepsilon_1 = \varepsilon_p = \mathcal{F}_{pe} = \frac{1}{0.88} + \frac{2}{\pi} \left[ \frac{1}{0.74} - 1 \right] = 0.735.$$

Now using Eq. (11.44) with  $A_1 = A_4$ , we get

$$\frac{1}{\mathcal{F}_{14}} = \frac{1 - \varepsilon_1}{\varepsilon_1} + \frac{1}{F_{14}} + \frac{1 - \varepsilon_4}{\varepsilon_4} = \frac{1 - 0.735}{0.735} + \frac{1}{0.51} + \frac{1 - 0.15}{0.15}$$

$$\mathcal{F}_{14} = 0.125.$$

Therefore,

$$\begin{aligned} Q_{1,\text{net}} &= A_1 \mathcal{F}_{14} \sigma (T_1^4 - T_4^4) = (1 \times 2)(0.125)(5.669) \left[ \left( \frac{1370}{100} \right)^4 - \left( \frac{300}{100} \right)^4 \right] \\ &= 49800 \text{ W}. \end{aligned}$$

To this, we could add the heat transferred to the bottom of the plate; assume that the furnace floor had been preheated to 1370 K prior to the insertion of the aluminum plate, and that all the heat transferred across the furnace floor-aluminum sheet interface is via radiation across a gap of two infinitely long parallel plates. Using Eq. (11.22), and assuming that the emissivity of the refractory floor is 0.8, we obtain

$$Q = \frac{(2 \times 1)(5.669) \left[ \left( \frac{1370}{100} \right)^4 - \left( \frac{300}{100} \right)^4 \right]}{1/0.8 + 1/0.15 - 1} = 57600 \text{ W}.$$

$$Q(\text{total}) = 49800 + 57600 = 107400 \text{ W}.$$

The heat flow rates calculated above are the initial values, and apply only when the cold sheet has been inserted in the oven. We deal with the more general problem of describing the transient heating of a sheet in Section 11.12.

### 11.9 RADIATION COMBINED WITH CONVECTION

In the preceding sections of this chapter we considered energy transfer by radiation as an isolated phenomenon. Indeed, in many high-temperature applications, problems should be tackled in this manner because, at high temperatures, radiation can completely dominate since radiant heat flow depends on the fourth power of the absolute temperature. In many practical situations, however, we cannot neglect convective heat transfer, and it is necessary to consider both modes of energy transport.

When we include radiation in a calculation of a situation which also involves convection, we realize that the total heat flow is the sum of the convective heat flow and the radiant heat

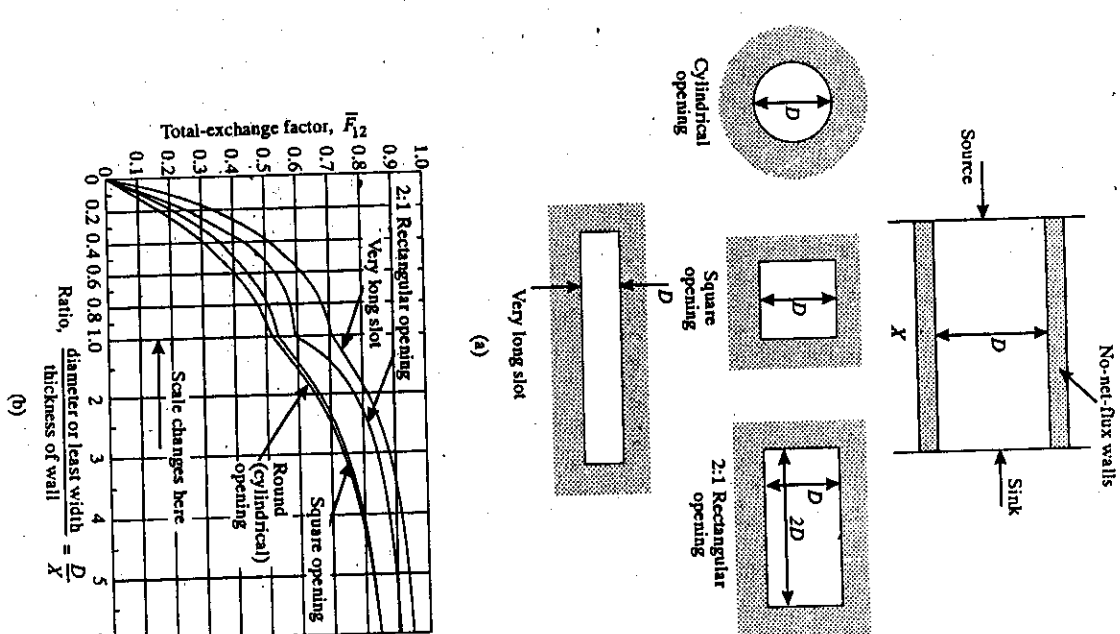


Fig. 11.21 Total exchange factors between parallel source and sink connected by no-net-flux walls. (a) Various geometries included, and (b) values of the total exchange factor. (From H. C. Hottel and A. F. Sarofim, *ibid.*, page 110.)

flow. Thus, we conveniently use the total heat transfer coefficient  $h_r$ , which comprises the heat transfer coefficient  $h$ , in the usual sense, and the radiant heat transfer coefficient  $h_r$ :

$$h_r = h + h_r \quad (11.47)$$

We define the radiant heat transfer coefficient as

$$h_r = \frac{q_{1,\text{net}}}{(T_1 - T_2)} = \mathcal{F}_{12} \left[ \frac{\sigma(T_1^4 - T_2^4)}{T_1 - T_2} \right], \quad (11.48)$$

in which  $T_1 - T_2$  is a temperature difference and  $T_2$  is chosen as a convenient temperature in the system.

We often encounter the situation in which surface 1 is completely surrounded by or exposed only to some fluid whose bulk temperature is at  $T_f$ . In this case, it is convenient to select  $T_2$  as  $T_f$ , and since  $\mathcal{F}_{12} = \varepsilon_1$ , we write

$$h_r = \varepsilon_1 \left[ \frac{\sigma(T_1^4 - T_2^4)}{T_1 - T_2} \right]. \quad (11.49)$$

The square-bracketed part of Eqs. (11.48) and (11.49) is sometimes called the temperature factor,  $F_r$ .

**Example 11.6** A thermocouple with an emissivity of 0.7 measures the temperature of a gas flowing in a long duct whose internal wall surfaces are at 533 K. The temperature indicated by the thermocouple is 811 K, and the convective heat transfer coefficient between the gas and the surface of the thermocouple is  $110 \text{ W m}^{-2} \text{ K}^{-1}$ . Determine the true temperature of the gas.

**Solution.** The temperature of the thermocouple is less than that of the gas because the thermocouple radiates to the wall. We can write an energy balance for the steady state in which the radiant heat flow from the thermocouple to the wall equals the convective heat flow from the gas to the couple. Assuming that the thermocouple can be approximated as a gray surface, we write

$$hA_1(T_f - T_1) = A_1 F_{12} \varepsilon_1 \sigma(T_1^4 - T_2^4),$$

where  $A_1$  is the thermocouple surface area;  $T_f$ ,  $T_1$ , and  $T_2$  are the temperatures of the fluid, thermocouple, and duct walls, respectively. Since the thermocouple is completely surrounded by the duct walls,  $F_{12} = 1$ . The gas temperature is then found by

$$T_f - T_1 = \frac{\varepsilon_1 \sigma}{h} (T_1^4 - T_2^4) = \frac{(0.7)(5.669)}{110} \left[ \left( \frac{811}{100} \right)^4 - \left( \frac{533}{100} \right)^4 \right] = 127 \text{ K},$$

and  $T_f = 938 \text{ K}$ .

Errors such as those indicated by the above example have induced engineers to pursue thermocouple designs which incorporate radiation shields and/or means of increasing  $h$  between the fluid and the thermocouple. Some devices are illustrated in Fig. 11.22.

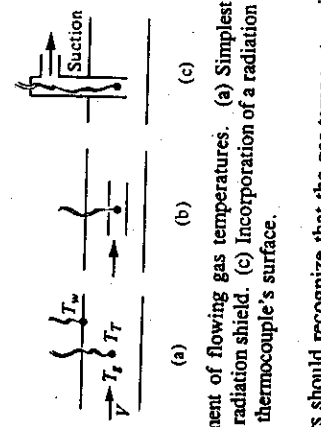
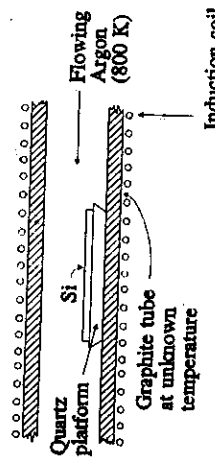


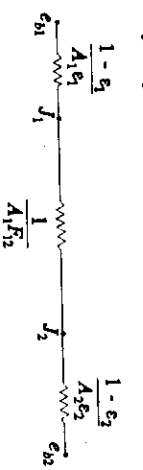
Fig. 11.22 Measurement of flowing gas temperatures. (a) Simplest device most liable to errors. (b) Incorporation of a radiation shield. (c) Incorporation of a radiation shield and use of the increased fluid velocity past the thermocouple's surface.

Process engineers should recognize that the gas temperature in an oven or furnace might not be equal to the temperature of a major source of radiation. If this is overlooked, serious problems of overheating in materials processing can develop. The source of the heat for the process can be a combustion flame, an electric arc, or a resistance-heating element; consequently, the source is often at a very high temperature, where radiation from the source to any surface at a lower temperature is significant. For example, it may be that a gas-fired combustion chamber for a tempering furnace produces a gas that is not too hot by adding excess air to the combustion gases, but if the piece to be tempered "sees" the flame, the radiation from the flame at its temperature will tend to raise the temperature of the piece above that of the gas alone. This can result in "burned" material. Sometimes material can be accidentally melted in this way, as in annealing lines for aluminum. Failed water-cooling jackets, whose surfaces are subjected to radiation from an arc, are not uncommon.

**Example 11.7** Ribbon silicon, 25 mm  $\times$  150 mm, intended for a photovoltaic application, is to be stress-relieved at 800 K by heating in flowing argon. The set-up shown below is used. The graphite tube is heated by an induction coil. Before the ribbon is introduced, care is taken to measure the true gas temperature, and it is found to be 800 K at a given flow rate. During a few trial runs, the temperature of the ribbon is found to be 850 K, even though the argon is maintained at 800 K. Estimate the temperature of a graphite tube. The convective heat transfer coefficient is  $50 \text{ W m}^{-2} \text{ K}^{-1}$ .



**Solution.** We make a radiation circuit to get started. Assume that the area of the graphite tube (node  $J_2$ ) is infinitely larger than that of the silicon ribbon (node  $J_1$ ).



The total equivalent resistance is

$$\frac{1}{A_1 F_{12}} = \frac{1 - \varepsilon_1}{A_1 \varepsilon_1} + \frac{1}{A_1 F_{12}} + \frac{1 - \varepsilon_2}{A_2 \varepsilon_2}$$

or

$$\frac{1}{F_{12}} = \frac{1 - \varepsilon_1}{\varepsilon_1} + \frac{1}{F_{12}} + 0.$$

But  $F_{12} = 1$  so that  $F_{12} = \varepsilon_1$ , and

$$q_{1,\text{rad}} = \frac{Q_{1,\text{rad}}}{A_1} = \sigma \varepsilon_1 (T_1^4 - T_2^4).$$

We could have recognized this immediately because the silicon "sees" only graphite by the assumption that  $A_1/A_2 = 0$ . As written,  $q_{1,\text{rad}} < 0$  because  $T_1 < T_2$ . For convenience, let  $q_{\text{rad}} = -q_{1,\text{rad}}$ . For simplicity, we ignore the energy conducted through the quartz, which supports the silicon; then at steady state:

$$q_{\text{rad}} = q_{\text{conv}},$$

$$\sigma \varepsilon_1 (T_2^4 - T_1^4) = h_{\text{conv}} (T_1 - T_2).$$

With  $\varepsilon_1 = 0.15$ , we have

$$T_2^4 = \frac{h_{\text{conv}} (T_1 - T_2)}{\sigma \varepsilon_1} + T_1^4 = \frac{50(850 - 800)}{(5.669 \times 10^{-8})(0.15)} + 850^4 = 8.16 \times 10^{11} \text{ K}^4.$$

Therefore,  $T_2 = 950 \text{ K}$ .

## 11.10 RADIATION FROM GASES

The methods given in the preceding sections are applicable only to systems involving gases which are transparent to radiation. Gases with simple symmetrical molecules, such as  $\text{H}_2$ ,  $\text{He}$ ,  $\text{O}_2$ , and  $\text{N}_2$ , are essentially transparent to radiation, but heteropolar gases ( $\text{CO}$ ,  $\text{CO}_2$ ,  $\text{H}_2\text{O}$ ,  $\text{SO}_2$ ,  $\text{NH}_3$ ,  $\text{HCl}$ ), which interact with radiation sufficiently, must sometimes be made part of the system for calculations.

Solids emit radiation at all wavelengths, whereas gases emit and absorb radiation only between narrow regions of wavelengths called bands. Analysis of radiation participation should be made for each band, and the total effect can be obtained by summation. However,

it is more convenient to solve the problems in terms of the total radiation and emission characteristics of the gases.

As a first approximation, the total number of radiating gas molecules present in a space determines the emissivity and absorptivity of the gas. This approximation works best at lower pressures with corresponding large mean free paths permitting each molecule to radiate as though it is alone, with a minimal shielding effect by the other molecules present in space. Gas radiation differs from the radiation of solids whose emission and absorption are surface phenomena, because when calculating emission and absorption for a gas layer at a particular temperature, its thickness and pressure must be taken into account. In fact, the emissivity and absorptivity of a gas are functions of the active gas species, temperature, thickness and shape, total pressure, and the partial pressure of the gas. To handle all these complexities, a series of charts based on experimental data has been developed for evaluating the emissivities and absorptivities of various gases.

Consider a hemisphere of radius  $L$ , containing a heteropolar gas of a given partial pressure; the problem is to determine the radiant heat exchange between the gas at temperature  $T_g$  and a unit element at the center of the base of the hemisphere. The emission of the gas to the surface is  $\varepsilon_g \sigma T_g^4$  per unit surface area, where  $\varepsilon_g$  denotes gas emissivity. Specifically, the reduced emissivity  $\varepsilon_g'$  for  $\text{CO}_2$  is presented as a function of the absolute temperature and the product of  $L$  and partial pressure in Fig. 11.23. These values are called reduced emissivities because they are plotted for a reduced pressure; that is, all data are at near-zero partial pressure and at a total pressure of 1 standard atm. The graphs apply strictly to the hemispherical body of gas defined above; we discuss briefly how to treat other shapes. The effect of total pressure on  $\varepsilon_g'$  for  $\text{CO}_2$  is given in Fig. 11.24, where the ratio of the actual emissivity, at the state being considered, to the reduced emissivity is presented as  $C_e$ . For shapes other than hemispheres, we take  $L$  as the effective beam length, and calculate it for use with Figs. 11.23 and 11.24. Table 11.2 lists  $L$  for shapes other than hemispheres. For approximate calculations of shapes which are not listed, we can take  $L$  as  $3.4 \times$  volume/surface area.

For a presentation and discussion of radiation data for other gas species and interactions between species that account for radiation in overlapping wavelength bands, the reader should consult the text by Hottel and Sarofim.<sup>10</sup> The charts were originally developed in the 1940s and 1950s when English units were the preferred system. To convert from absolute temperature in degrees Rankine ( $^{\circ}\text{R}$ ) to kelvins, simply use  $9^{\circ}\text{R} = 5 \text{ K}$ . The pressure-length units on the curves are converted according to

$$1 \text{ atm ft} = 3.0886 \times 10^4 \text{ Pa m} = 3.0886 \times 10^4 \text{ N m}^{-1}.$$

<sup>10</sup>H. C. Hottel and A. F. Sarofim, *ibid.*, Chapter 6.

Radiation Heat Transfer 401  
 Table 11.2 Beam lengths for gas radiation. (From H. C. Hottel, Chapter IV in *Heat Transmission*, by W. H. McAdams, McGraw-Hill, 1954.)

Shape	Characterizing dimension, $X$	Factor by which $X$ is multiplied to obtain mean beam length, $L$	
		When $P_e L = 0$	For average values of $P_e L$
Sphere	Diameter	2/3	0.60
Infinite cylinder	Diameter	1	0.90
Semi-infinite cylinder, radiating to center of base	Diameter	—	0.90
Right-circular cylinder, height = diameter, radiating to center of base	Diameter	—	0.77
Same, radiating to whole surface	Diameter	—	0.77
Infinite cylinder of half-circular cross section, radiating to spot on middle of flat side	Radius	2/3	0.60
<i>Rectangular parallelepipeds</i>			
1:1:1 (cube)	Edge	2/3	—
1:1:4, radiating to 1 × 4 face	Shortest edge	0.90	—
radiating to 1 × 1 face	Shortest edge	0.86	—
radiating to all faces	Shortest edge	0.89	—
1:2:6, radiating to 2 × 6 face	Shortest edge	1.18	—
radiating to 1 × 6 face	Shortest edge	1.24	—
radiating to 1 × 2 face	Shortest edge	1.18	—
radiating to all faces	Distance between planes	1.20	—
1: $\infty$ : $\infty$ (infinite parallel planes)	Distance between planes	2	—
<i>Space outside</i>			
Space outside infinite bank of tubes with centers on equilateral triangles; tube diameter = clearance	Clearance	3.4	2.8
Same as preceding, except tube diameter = one-half clearance	Clearance	4.45	3.8
Same, except tube centers on squares, diameter = clearance	Clearance	4.1	3.5

**Example 11.8** Determine the emissivity of a gas containing 50% N<sub>2</sub> and 50% CO<sub>2</sub> at a total pressure of 2 atm with  $T_s = 1110$  K. The gas is contained in a very long cylindrical space having a 0.6 m diameter.

**Solution.** From Table 11.2, assuming radiation to its base:

$$L = (0.90)(0.6) = 0.54 \text{ m (1.77 ft)}$$

and

$$P_e L = (0.50)(2)(1.77) = 1.77 \text{ atm ft.}$$

From Fig. 11.23, the reduced emissivity of CO<sub>2</sub>, with  $T = 1110$  K = 1998 °R, is  $\epsilon'_e = 0.17$ . Fig. 11.24 gives  $C_e = 1.10$ . Finally,  $\epsilon_e = C_e \epsilon'_e = (1.10)(0.17) = 0.19$ .

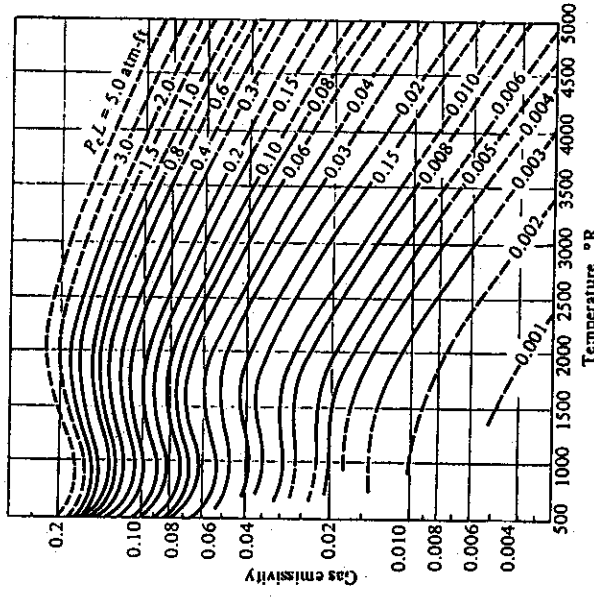


Fig. 11.23 Reduced emissivity of carbon dioxide. (From H. C. Hottel and A. F. Sarofim, *ibid.*, Chapter 6.)

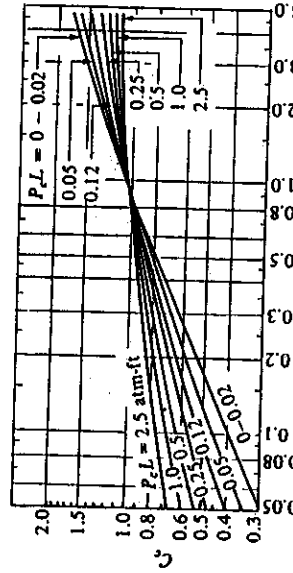


Fig. 11.24 Correction factor for CO<sub>2</sub> emissivity. (From F. Kreith, *Principles of Heat Transfer*, second edition, International Textbook Co., 1965, page 231.)

### 11.11 ENCLOSURES FILLED WITH RADIATING GAS

By evaluating the emissivity and absorptivity of a gas by the method outlined in Section 11.10, we now evaluate the interchange of radiant energy between a gas and the surface of its enclosure. First, consider a black bounding surface. The gas emits energy which is entirely absorbed by the black surface, but, on the other hand, the gas absorbs only a fraction of the radiation from the surface. Thus we write the flux of energy from the gas  $g$  to the surface 1 as

$$q_{g \rightarrow 1} = \epsilon_g - \alpha_g \epsilon_{b1} = \epsilon_g \epsilon_{bg} - \alpha_g \epsilon_{b1} = \sigma (\epsilon_g T_g^4 - \alpha_g T_1^4). \quad (11.50)$$

When the bounding surface is gray, it reflects part of the energy emitted by the gas which is partially absorbed in successive passes back through the gas. In this case, we give the flux of energy by the right side of Eq. (11.50) multiplied by a factor between  $\epsilon_1$  and 1. For surfaces with  $\epsilon_1$  of 0.7 or greater, it is sufficient to use the following equation:

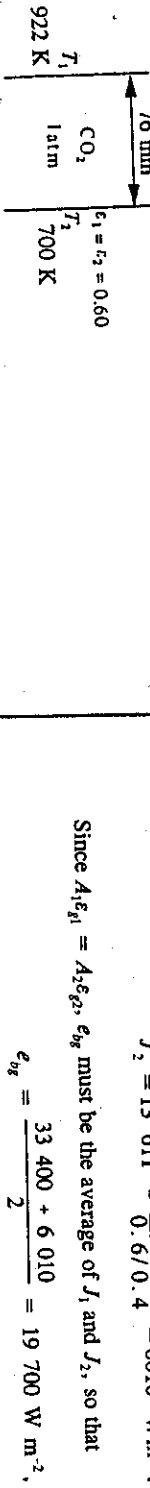
$$q_{g \rightarrow 1} = \sigma \left[ \frac{\epsilon_1 + 1}{2} \right] (\epsilon_g T_g^4 - \alpha_g T_1^4), \quad (11.51)$$

where the factor is simply  $(\epsilon_1 + 1)/2$ .

In order to incorporate participating gases into a system containing surfaces, the gas is a floating node of potential  $\epsilon_{bg}$  and there is a conductance  $A_i \epsilon_{bg}$  between the gas node and the surface  $i$ . Due to the presence of the gas which absorbs some of the radiation between transmissivity; for example, the conductance between surfaces  $i$  and  $j$  is  $A_i F_{ij} T_{bg}$ . The following example demonstrates the use of such an electric analog for a system with a participating gas.

**Example 11.9** Two large parallel plates (with emissivity of 0.6) at temperatures of 922 K and 700 K, transfer radiation across a 76 mm gap filled with CO<sub>2</sub> at 1 atm pressure. Calculate the rate of heat transfer from the hot plate to the cold plate.

**Solution.** We show the system and its electrical analog below.



and

$$J_1 = \epsilon_{b1} - \frac{q_{1 \rightarrow 2}}{\epsilon_1(1 - \epsilon_1)} = 40967 - \frac{11400}{0.6/0.4} = 33400 \text{ W m}^{-2},$$

and

$$J_2 = 13611 - \frac{11400}{0.6/0.4} = 6010 \text{ W m}^{-2}.$$

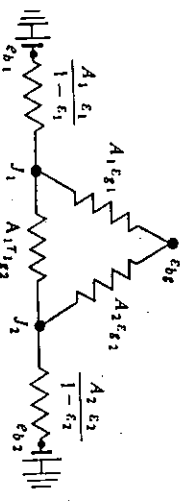
Since  $A_1 \epsilon_{b1} = A_2 \epsilon_{b2}$ ,  $\epsilon_{bg}$  must be the average of  $J_1$  and  $J_2$ , so that

$$\epsilon_{bg} = \frac{33400 + 6010}{2} = 19700 \text{ W m}^{-2},$$

and

$$T_g = \left[ \frac{\epsilon_{bg}}{\sigma} \right]^{1/4} = \left[ \frac{19700}{5.669 \times 10^{-8}} \right]^{1/4} = 767 \text{ K}.$$

The problem could be solved again with this as the gas temperature; in this case, however, 767 K is sufficiently close to the assumed 810 K, so that no significant improvement in the result would be gained.



In order to evaluate the emissivities and transmissivities of the gas, we must know its temperature. Assume the gas temperature is 810 K (this can be checked later). From Table 11.2,  $L = (2)(0.076) = 0.152 \text{ m}$  (0.499 ft). Next, Figs. 11.23 and 11.24, with  $P_c L = 0.499 \text{ atm ft}$ , give  $\epsilon'_c = 0.125$  and  $C_c = 1.05$ , respectively. Thus  $\epsilon_{g1} = \epsilon_{g2} = (0.125)(1.05) = 0.131$ ,

and

$$\tau_{1g2} = 1 - \epsilon_{g1} = 1 - 0.131 = 0.869.$$

It is instructive to extend the above example, by comparing it to the case of no participating gas (see Example 11.3). In this case

$$\frac{1}{\mathcal{F}_{12}} = \frac{1}{\varepsilon_1} + \frac{1}{\varepsilon_2} - 1 = \frac{1}{0.6} + \frac{1}{0.6} - 1 = 2.33.$$

This is hardly different from the factor (2.40) determined in Example 11.9. Therefore, even though we have selected an example involving an atmosphere of 100% CO<sub>2</sub>, we could still consider the atmosphere to be transparent for many calculations. Only at partial pressures greater than about 4 atm of the participating species and/or with very large enclosure dimensions, would the effect of the gas be more evident.

The likely application of these principles to processes, which might involve combustion gases at 1 atm total pressure, requires only small corrections to heat fluxes. For example, a typical combustion gas at 1670 K could contain 12% CO<sub>2</sub>. From Fig. 11.23, the reduced emissivity for a rather large  $L$  (e.g., 1 m) is only 0.08.

## 11.12 RADIATION IN TRANSPARENT SOLIDS

In Chapter 6 we saw that an important contribution to the effective thermal conductivity in transparent ceramics and glasses at high temperatures is the radiation heat transfer. Now we examine the transfer of radiant energy through such a medium.

Consider two surfaces with the space between them occupied by a solid that is transmitting and absorbing. For the solid we use the subscript  $s$  and assume that  $\alpha_s = \varepsilon_s$ , so that

$$\alpha_s + \tau_s = \varepsilon_s + \tau_s = 1. \quad (11.52)$$

The power leaving surface 1 is  $J_1 A_1 F_{12} \tau_s$ , and that leaving surface 2 is  $J_2 A_2 F_{12} \tau_s$ ; therefore, the net power from 1 to 2 is

$$Q_{1,2} = A_1 F_{12} \tau_s (J_1 - J_2), \quad (11.53)$$

or

$$Q_{1,2} = A_1 F_{12} (1 - \varepsilon_s) (J_1 - J_2). \quad (11.54)$$

Inspection of Eq. (11.54) reveals that  $A_1 F_{12} (1 - \varepsilon_s)$  is the conductance or  $[A_1 F_{12} (1 - \varepsilon_s)]^{-1}$  is the resistance between  $J_1$  and  $J_2$ , as indicated by Fig. 11.25.

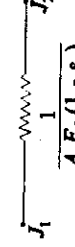


Fig. 11.25 Resistance for partially transmitted radiation between nodes  $J_1$  and  $J_2$ .

Now at the surface itself, there is an exchange process with the partially transmitting solid, which we assume is nonreflecting. A power balance at surface 1 is

$$Q_{1,s} = A_1 F_{12} \varepsilon_s e_{bs} - J_1 A_1 F_{12} \varepsilon_s,$$

$$\mathcal{F}_{12} = 1 - \frac{\varepsilon_s}{2},$$

where the first term on the right hand side is the power emitted by the solid and the second is the radiation emanating from surface 1 that is absorbed by the solid (recall  $\alpha_s = \varepsilon_s$ ). With  $A_1 F_{12} = A_1 F_{12}$  we have

$$Q_{1,s} = \frac{e_{bs} - J_1}{1/A_1 F_{12} \varepsilon_s}. \quad (11.55)$$

This exchange between the partially transmitting solid and surface 1 is represented by Fig. 11.26.

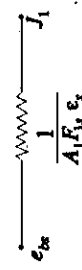
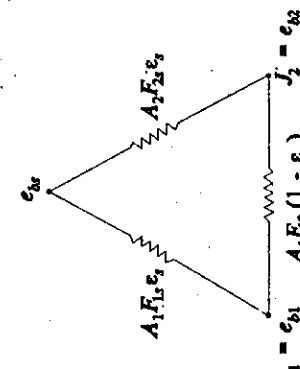


Fig. 11.26 Resistance between a partially transmitting solid and a surface with a radiosity of  $J_1$ .

**Example 11.10** Two large plates with emissivity of 1 are at 1001 K and 999 K, respectively. They are separated by 1 mm of glass with an absorption coefficient of 0.1 mm<sup>-1</sup>. Calculate the "radiation" thermal conductivity of the glass.

**Solution.** The radiation circuit, with conductances, is constructed:



The *absorption coefficient* is not the same as the absorptivity,  $\alpha_s$ , but it is used to estimate  $\alpha_s$ . From basic optics, the fraction of energy absorbed by a solid of thickness  $\delta$  with an absorption coefficient  $\lambda$  is  $\exp(-\lambda\delta)$ . Therefore,

$$\alpha_s = \exp(-\lambda\delta) = \exp(-0.1 \times 1) = 0.905.$$

We assume  $\varepsilon_s = \alpha_s$ . The equivalent resistance for the circuit is

$$A_1 \mathcal{F}_{12} = A_1 F_{12} (1 - \varepsilon_s) + \left[ \frac{1}{A_1 F_{12} \varepsilon_s} + \frac{1}{A_2 F_{12} \varepsilon_s} \right]^{-1},$$

or

because  $A_1 = A_2$  and  $F_{12} = F_{11} = F_{22} = 1$ . The radiant flux is

$$q = \frac{Q_{12}}{A_1} = \mathcal{F}_{12}\sigma(T_1^4 - T_2^4),$$

but also

$$q = k_{\text{rad}} \frac{(T_1 - T_2)}{\delta}.$$

By comparing the two equations, we get

$$k_{\text{rad}} = \frac{\mathcal{F}_{12}\sigma(T_1^4 - T_2^4)\delta}{T_1 - T_2} = \frac{\left[1 - \frac{0.905}{2}\right](5.669)(10.01^4 - 9.99^4)(1)}{(1001 - 999)} = 125 \text{ W m}^{-1} \text{ K}^{-1}.$$

Before you leave this example, you should also show that, if  $T_1 \rightarrow T_2$ , then

$$k_{\text{rad}} \rightarrow 4\sigma \left[1 - \frac{\varepsilon_s}{2}\right] T^3.$$

The spectral absorptivity of several glasses can be found in Hottel and Sarofim.<sup>11</sup> From these data the total hemispherical emissivity of glass of different thicknesses over a wide temperature range has been obtained (Fig. 11.27). As the glass thickness goes to infinity, the limiting value of  $\varepsilon$  is 0.91 (and not 1.0), because some of the energy emitted within the glass is reflected internally at the glass surface.

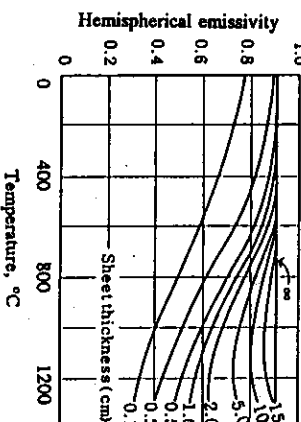


Fig. 11.27 Total hemispherical emissivity of window glass as a function of thickness and temperature. (From H. C. Hottel and A. F. Sarofim, *ibid.*, page 243.)

### 11.13 TRANSIENT CONDUCTION WITH RADIATION AT THE SURFACE

In Chapter 9, we discussed some solutions to transient problems involving solids with heat applied to, or withdrawn from, the surface via convective  $h$ . In several operations, notably heat treating processes, stock is heated with radiation. The condition of heat input at the receiver (stock) surface from a heat source at constant temperature  $T_s$  is

$$\mathcal{F}_{s1}\sigma(T_s^4 - T(0,t)) = -k \frac{\partial T(0,t)}{\partial x} \quad (11.56)$$

We determine  $\mathcal{F}_{s1}$  according to the methods discussed in previous sections, depending on the spatial relationship between the source and stock and their respective emissivities. We can put Eq. (11.56) in a dimensionless form

$$M[\theta_s^4 - \theta^4(0,\text{Fo})] = -\frac{\partial \theta(0,\text{Fo})}{\partial(x/l)}, \quad (11.57)$$

where

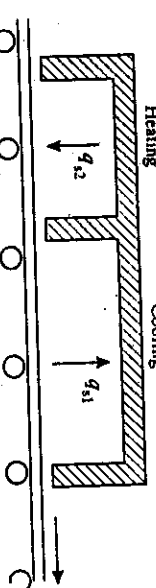
$$M = \frac{\mathcal{F}_{s1}\sigma T_0^3 l}{k}, \quad \text{Fo} = \frac{\alpha l}{l^2},$$

$$\theta = \frac{T}{T_0}, \quad \theta_s = \frac{T_s}{T_0}.$$

$T_0$  is the initial temperature of the stock, and  $l$  is its characteristic dimension.

Consider specifically the temperature response of a sheet,  $0 \leq x \leq l$ , thin enough for Newtonian conditions (no internal gradients) to apply, which is heated at  $x = 0$  by a radiation heat source at constant temperature. The back face ( $x = l$ ) loses a negligible amount of heat so that  $[\partial T(l,t)/\partial x] = 0$ . We give the solution to this problem in Figs. 11.28(a) and (b) for heating and cooling, respectively. For other closely related situations we refer the reader to Schneider.<sup>12,13</sup>

**Example 11.11** (from Schneider) We heat treat a continuous sheet of steel (1 mm thick) by passing it through a radiant furnace designed to provide a heat and cool cycle. The furnace consists of 3.05 m long ceiling heat-source section ( $\mathcal{F}_{s1} = 0.72$ ) at 1478 K followed by a ceiling heat-sink section ( $\mathcal{F}_{s2} = 0.86$ ) at 144 K. If the sheet enters the furnace at 294 K, must be heated to 1367 K, and then cooled to 533 K before leaving the oven, calculate a) the required feed velocity, and b) the length of the cooling section. Data: density of steel = 7788 kg m<sup>-3</sup>; heat capacity = 460 J kg K<sup>-1</sup>.



<sup>11</sup>H. C. Hottel and A. F. Sarofim, *ibid.*, pages 240-241.

<sup>12</sup>P. J. Schneider, *Temperature Response Charts*, Wiley, New York, NY, 1963, pages 143-149.

<sup>13</sup>P. J. Schneider, *J. Aero/Space Sciences* 27, No. 7, 546-548 (1960).

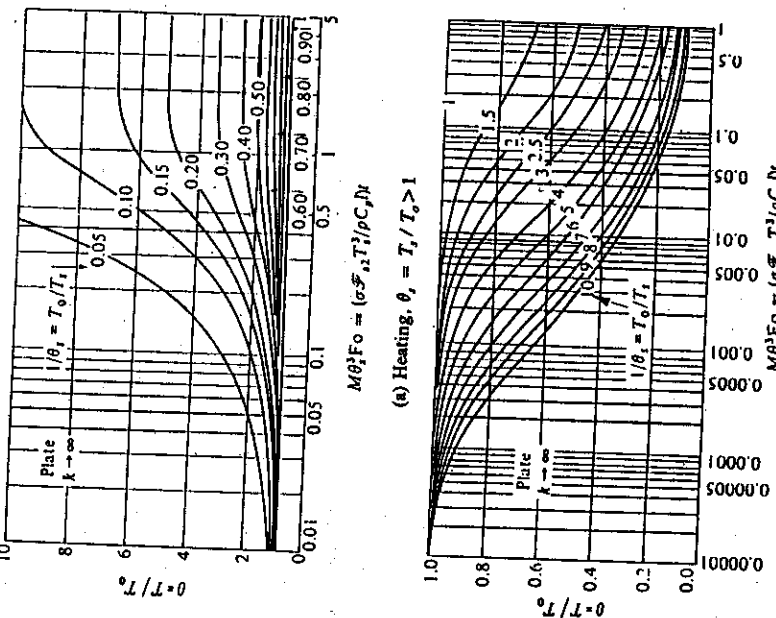


**Fig. 11.28** Temperature of a plate,  $0 \leq x \leq l$ , with no internal thermal gradients and an insulated back face, at  $x = l$ , after sudden exposure to (a) a radiation heat source (heating) or (b) a radiation heat sink (cooling). (From P. J. Schneider, *Temperature Response Charts*, John Wiley, New York, NY, 1963, pages 147 and 148.)

*Solution.*

- a) For the heating section, we apply Fig. 11.28(a) with

$$\frac{1}{\theta_r} = \frac{T_0}{T_r} = \frac{294}{1478} = 0.199$$

$$\theta = \frac{T \text{ (leaving)}}{T_0} = \frac{1367}{294} = 4.65.$$

From Fig. 11.28(a)

$$M \theta_r^3 F_0 = \frac{\mathcal{F}_r \sigma T_0^3}{k} \left( \frac{T_r}{T_0} \right)^3 \frac{k \epsilon}{\rho C_p l^2} = \frac{\mathcal{F}_r \sigma T_0^3 l}{\rho C_p l^2} = 0.980.$$

Then the heating exposure time is

$$t = \frac{0.980 \rho C_p l}{\mathcal{F}_r \sigma T_r^3} = \frac{(0.980)(7788)(460)(0.001)}{(0.72)(5.669 \times 10^{-8})(1478^3)} = 26.6 \text{ s.}$$

Thus, the feed velocity is  $(3.05/26.6) = 0.115 \text{ m s}^{-1}$ .

- b) Figure 11.28(b) is used for the cooling section with

$$\frac{1}{\theta_r} = \frac{T_0}{T_r} = \frac{1367}{144} = 9.49$$

$$\theta = \frac{T \text{ (leaving)}}{T_0} = \frac{533}{1367} = 0.390.$$

Then from Fig. 11.28(b)

$$M \theta_r^3 F_0 = 0.0072,$$

from which we determine the cooling exposure time:

$$t = \frac{(0.0072)(7788)(460)(0.001)}{(0.86)(5.669 \times 10^{-8})(144^3)} = 177 \text{ s.}$$

Thus, the required length of the cooling section is

$$(0.115)(177) = 20.4 \text{ m.}$$

#### 11.14 TRANSIENT HEATING WITH THERMAL STRESSES

In the case of heating material with large cross-sections for subsequent hot-working, such as forging, extrusion, piercing, etc., blooms or ingots are heated in large furnaces, which are usually gas-fired by radiant burners. If placed cold into a hot furnace enclosure, the surface of the piece is immediately subjected to intense radiant heat and increases in temperature rapidly, governed by Eqs. (9.43) and (11.49). As the surface is heated, it expands. During the period when the interior is still at a low temperature, this causes a constraint on the expansion of the hot surface region, and a compressive stress develops at and near the surface, while a tensile stress develops in the interior.

Sun<sup>14</sup> calculated the principal stresses and determined that the maximum tensile stresses were found to be at the center after 4.2 hours of heating an ingot with a diameter of 100 cm. The calculated principal stress in the axial direction ( $\sigma_z$ ) is shown in Fig. 11.29, where it can be seen that the tensile stress is a maximum at the center of the ingot, neutral near the surface, and compressive at the surface.

Sun hypothesized that if  $\sigma_z$  at the center exceeds 90 percent of the yield strength of the material, then internal cracks result. To avoid reaching these stress levels, the heating must be controlled so that thermal stresses are limited to below the yield strength of the material.

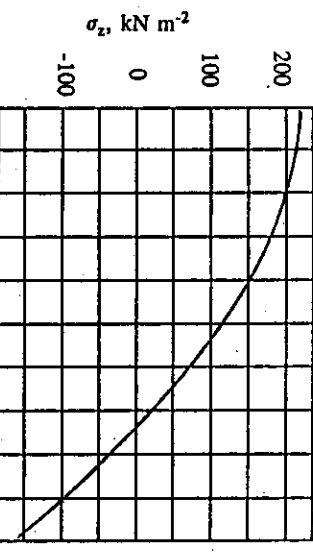


Fig. 11.29 Distribution of  $\sigma_z$  in 100 cm diameter ingot of Hastelloy X placed cold into furnace at 1500 K, after 4.2 hours in the furnace. (From R. C. Sun, *Metall. Trans.* 1, 1883-1887, 1970.)

The point of this discussion is to make the reader aware of this problem, which usually occurs when radiation is the predominant heat transfer mechanism. Radiative heating can also cause thermal shock in ceramic materials very easily, because of their relatively low thermal conductivities.

### PROBLEMS

11.1 A radiation heat transfer coefficient is often defined as  $q = h_r(T_1 - T_2)$ .

- a) For a gray solid at  $T_1$ , completely surrounded by an environment at  $T_2$ , show that  $h_r$  is given by

$$h_r = \sigma\epsilon_1(T_1^2 + T_2^2)(T_1 + T_2)$$

b) Calculate the rate of heat transfer (by radiation and convection) from a vertical surface, 1.5 m high, and the percentage by radiation for the following cases:

Surface ( $\epsilon = 0.8$ ) at:

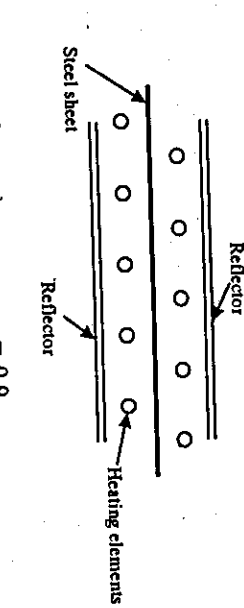
Air at:

500 K	300 K
800 K	300 K
1100 K	300 K

11.2 A metal sphere at 1255 K is suddenly placed in a vacuum space whose walls are at 355 K. The sphere is 50 mm in diameter, and we may assume that its surface is perfectly black.

- a) Calculate the time it takes to cool the sphere to 420 K. Assume that a uniform temperature exists in the sphere at each instant. *Data for sphere:*  $\rho = 7000 \text{ kg m}^{-3}$ ;  $C_p = 1000 \text{ J kg}^{-1} \text{ K}^{-1}$ . b) Discuss the validity of the assumption in part a) with quantitative reasoning using a conductivity of  $50 \text{ W m}^{-1} \text{ K}^{-1}$ .

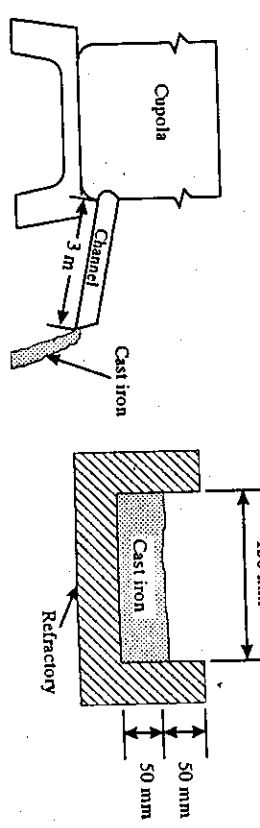
- 11.3 Steel sheet is preheated in vacuum for subsequent vapor deposition. The steel sheet is placed between two sets of cylindrical heating elements (25 mm in diameter). The heating efficiency is kept high by utilizing radiation reflectors of polished brass. The steel sheet and radiation reflectors may be considered to be infinite parallel plates. a) Calculate the rate of heat transfer from the heating elements (maintained at 1810 K) to the steel when the steel is at 300, 390, 530, 670 and 810 K. The reflectors may be assumed to be at 310 K. b) Plot the results of part a) and determine by graphical integration the average value of the heat transfer rate as the steel is heated from 300 to 810 K. c) From part b) determine the time it takes to heat a steel sheet 6 mm thick from 300 to 810 K.



Data: $\epsilon$ (heating elements)	= 0.9
$\epsilon$ (steel sheet)	= 0.3
$\epsilon$ (reflectors)	= 0.03
$\rho$ of steel	= $7690 \text{ kg m}^{-3}$
$C_p$ of steel	= $628 \text{ J kg}^{-1} \text{ K}^{-1}$
Area of steel to area of elements	= 10/1.

- 11.4 A large furnace cavity has an inside surface temperature of 1090 K. The walls of the furnace are 0.3 m thick. A hole 150 mm  $\times$  150 mm is open through the furnace wall to the room at 295 K. a) Calculate the power loss by radiation through the open hole. b) Calculate the power loss if a sheet of nickel covers the hole on the outside surface. *Data:* emissivity of furnace refractories = 0.9; emissivity of nickel sheet = 0.4.

- 11.5 Cast iron is continually tapped from the bottom of a cupola into an open refractory channel. The metal enters at 1810 K and runs down the channel at a rate of  $0.50 \text{ kg s}^{-1}$ . The dimensions of the channel are shown below. Neglect the heat loss by conduction through the refractory and estimate the metal discharge temperature. *Data for molten cast iron:*  $C_p = 830 \text{ J kg}^{-1} \text{ K}^{-1}$ ;  $\rho = 6890 \text{ kg m}^{-3}$ ;  $\epsilon = 0.30$ .



**11.6** A method of melting metal so as to avoid crucible contamination is levitation melting. A metal sample is placed in an electromagnetic field from a coil wound as a cone. The field not only supplies power to melt the metal but also to levitate it. But with this setup, the strength of field necessary to keep the sample levitated is sometimes such that the metal is overheated. A means of preventing this is to flow cooling gas past the sample. Develop an expression that relates the steady-state temperature of the metal to the heating power supplied by the field ( $Q_p$ ), the gas temperature  $T_0$ , the gas velocity  $V$ , and any other parameters which you think are essential. Metal temperatures of interest are 1360–1920 K, and the convection heat transfer coefficient can be expressed as

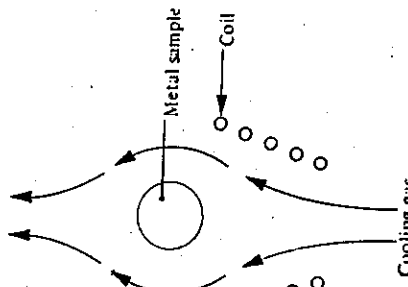
$$h_c = KV^{0.7}$$

in which  $K$  is a known constant.

**11.7** A steel sheet, 12.5 mm thick and having the shape of a square  $1.5 \text{ m} \times 1.5 \text{ m}$ , comes out of a heat-treating furnace at 1090 K. During heat treatment its surface was oxidized so that its emissivity is 0.8.

- Calculate its initial cooling rate ( $\text{K s}^{-1}$ ) if it is suspended freely by a wire in a room at 300 K. Neglect all heat transfer with convection, i.e., deal only with radiation heat transfer.
  - Calculate its initial cooling rate if it is supported vertically on a horizontal surface (also at 300 K) which has an emissivity of 0.2. Again deal only with radiation heat transfer.
- Data (all units in SI):

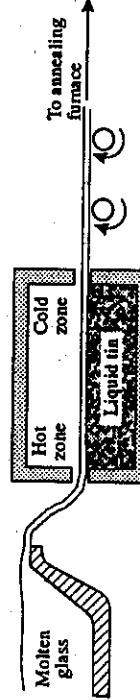
	Supporting surface	Steel sheet
Thermal conductivity	50	20
Density	600	8010
Heat capacity	630	600
Emissivity	0.2	0.8



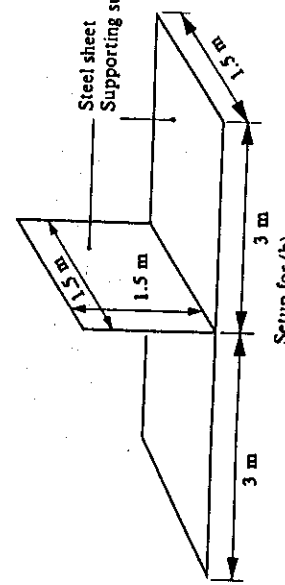
**11.8** Brass sheet, 1.6 mm thick, passes through a continuous tempering surface. The first portion of the furnace is filled with gases at 920 K, moving against the strip direction at a speed of  $0.3 \text{ m s}^{-1}$ . The strip itself moves at a speed of  $0.05 \text{ m s}^{-1}$ . The walls are of  $\text{SiO}_2$  brick, each 0.3 m from the brass sheet as it moves vertically, and the gases are 40%  $\text{H}_2\text{O}$ , 10%  $\text{CO}_2$ , and 50%  $\text{N}_2$ . How many meters of strip would have to be in the first portion of the furnace so that the strip could exit into the second section at a temperature of 700 K? Data:

$$\begin{aligned} C_{p_{\text{brass}}} &= 428 \text{ J kg}^{-1} \text{ K}^{-1} & C_{p_{\text{gas}}} &= 1110 \text{ J kg}^{-1} \text{ K}^{-1} \\ \rho_{\text{brass}} &= 9200 \text{ kg m}^{-3} & \rho_{\text{gas}} &= 0.48 \text{ kg m}^{-3} \\ k_{\text{brass}} &= 170 \text{ W m}^{-1} \text{ K}^{-1} & k_{\text{gas}} &= 0.086 \text{ W m}^{-1} \text{ K}^{-1} \end{aligned}$$

**11.9** Estimate the length of the furnace, shown below, that is used for forming sheet glass (3 mm thick). The glass enters the furnace at 1500 K, and it should leave at 1100 K. The liquid tin and the furnace are kept at 1000 K. Assume that the heat transfer coefficient at the tin-glass interface is infinite. The emissivity of the glass is shown in Fig. 11.27. Other properties of the glass are  $k = 4.2 \text{ W m}^{-1} \text{ K}^{-1}$ ;  $C_p = 420 \text{ J kg}^{-1} \text{ K}^{-1}$ ;  $\rho = 3320 \text{ kg m}^{-3}$ . The emissivity of the molten tin is 0.1.



**11.10** A slab of steel is placed into a reheat furnace so that it can be heated to 1500 K and subsequently hot-rolled to plate. The gas temperature in the furnace has been carefully measured and found to be 1520 K. Energy to the furnace is by burning gas, and its flame behaves as though it is a gray surface ( $\epsilon = 0.9$ ) at 2000 K. The convective heat transfer coefficient is  $85 \text{ W m}^{-2} \text{ K}^{-1}$  and the emissivity of the steel is 0.8. Estimate the temperature of the slab after the system comes to thermal equilibrium. For simplicity assume that the flame and slab surface are parallel planes that are  $5 \text{ m} \times 5 \text{ m}$ , and the gas is transparent. Consider only heat exchange among the slab, flame and gas.



**11.11** One side of a flat ceramic shell mold (30 mm thick) is maintained at 1500 K while the opposite side radiates into a large room at 300 K. The emissivity of the radiating surface is 0.5, and the thermal conductivity of the ceramic mold material is  $0.7 \text{ W m}^{-1} \text{ K}^{-1}$ . Calculate the steady-state flux and the surface temperature of the mold.

**11.12** A plate is heated uniformly to 810 K, and then it is suspended vertically next to and parallel to a cooler plate in a large room. Both plates are  $1.3 \text{ m} \times 1.3 \text{ m} \times 12.5 \text{ mm}$  thick, and they are separated by 0.3 m. The cooler plate and the room are at 300 K. What is the initial cooling rate ( $\text{K s}^{-1}$ ) of the hotter plate? Data:  $\epsilon = 0.7$  and  $\rho C_p = 8 \times 10^6 \text{ J m}^{-3} \text{ K}^{-1}$  for both plates.

11.13 A light bulb (100 watts) can be approximated to be a sphere. It is held at the top level of a large amount of snow; after steady state is achieved, a hole with the form of a hemisphere of radius  $R$  is made in the snow. Consider only radiation heat transfer from the bulb to the snow and to the surroundings. Within the snow, however, there is conduction heat transfer. The snow and the surroundings are at  $0^{\circ}\text{F}$ . The surface of the snow forming the hole is at  $32^{\circ}\text{F}$ . Thermal properties of snow:  $k = 0.2 \text{ Btu h}^{-1} \text{ ft}^{-1} \text{ }^{\circ}\text{F}^{-1}$ ;  $\rho C_p = 10 \text{ Btu ft}^{-3} \text{ }^{\circ}\text{F}^{-1}$ ;  $\epsilon = 0.7$ . a) Calculate the radius of the hole. b) Calculate the surface temperature of the light bulb. Assume that this surface is black and that the radius of the spherical bulb is 0.2 ft.

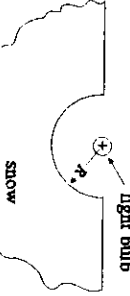
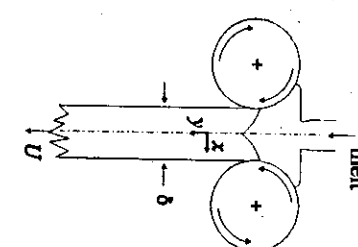
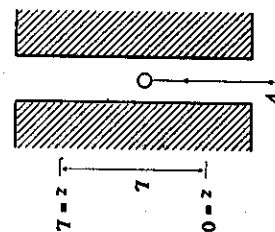
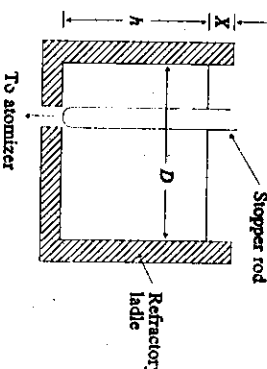
11.14 Thin sheet of alloy is prepared by "roller casting." In this process, a melt solidifies between two rolls that are water-cooled to produce sheet of thickness  $\delta$ . Assume: (1) that temperature in the sheet is independent of  $x$ ; (2) that conduction in the  $y$ -direction cannot be ignored; (3) heat loss from the surface is only by radiation; (4) the sheet temperature at  $y = 0$  is  $T_0$  and the room temperature is  $T_r$ , and (5) sheet velocity is  $U$ . a) Give a differential equation for the temperature,  $T$ , in the sheet that applies for  $x \geq 0$ . Be sure that your equation is consistent with the assumptions.

b) Write appropriate boundary conditions for  $T$ . c) If this had been presented as a numerical problem, how would you solve it?

11.15 A sphere is suspended by a wire and is lowered at a constant velocity into a very long cylindrical tube as indicated in the sketch. Assume that, over the length  $L$ , the view factor is constant, the tube wall has a constant temperature  $T_w$ , and the rate of descent ( $V$ ) is constant. If the sphere has an emissivity  $\epsilon$  and enters the length  $L$  with a temperature  $T_0$ , derive an equation which gives its temperature as it leaves the length  $L$ .  $T_w \gg T_0$  and the sphere radius is  $R$ ; consider only radiation heat transfer.

11.16 A ladle of hot metal is used to feed an atomizer to produce metal powder. By means of a controlled stopper rod, the metal slowly leaves the ladle at a constant mass flow rate,  $W$ . Assume that the ladle refractory can be treated as a "no-net-flux surface" and that the only heat loss from the ladle is by radiant heat transfer.

- a) When the ladle is full (i.e.,  $X = 0$ ), write an equation that gives the radiant heat loss ( $Q$ , energy/time) from the top surface of the melt.



- b) When the ladle is  $3/4$  empty and  $D/X = 4$ , write an equation for  $Q$ . Use the following variables:  $T_1$  = temperature of metal;  $T_2$  = temperature of surroundings;  $h$  = depth of melt;  $D$  = inside diameter of ladle;  $A = \pi D^2/4$  = area of top surface of melt;  $\epsilon_1$  = emissivity of melt surface; and  $X$  = distance from top of ladle to top of melt (see diagram).

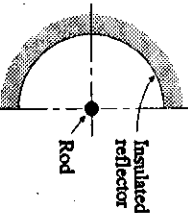
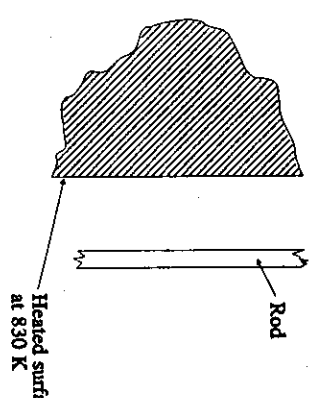
In your answers give numerical values for view factors and total exchange factors.

11.17 A long rod ( $\epsilon = 0.8$ ) is heated to  $1255 \text{ K}$  and is placed near a well insulated reflector ( $\epsilon = 0.01$ ) as shown. The purpose of the reflector is to retard the cooling of the rod. The diameter of the rod is  $75 \text{ mm}$ , and the diameter of the reflector is  $500 \text{ mm}$ . The room surrounding the reflector and the rod are at  $300 \text{ K}$ . a) Calculate the radiant power loss per unit length of the rod when its temperature is  $1255 \text{ K}$ .

b) Repeat if there is no reflector.

11.18 Two parallel plates,  $0.3 \times 0.6 \text{ m}$ , are spaced  $0.3 \text{ m}$  apart in a large heat treating furnace and heated uniformly to  $810 \text{ K}$ . They are then removed from the furnace and cooled in a room maintained at  $300 \text{ K}$ . The emissivities of the plates are  $0.4$  and  $0.8$ , respectively. Other thermal properties are equal. Calculate the ratio of the initial cooling rates ( $\text{K s}^{-1}$ ) of the plates. Consider only radiation heat transfer.

11.19 A long rod, with a diameter of  $3 \text{ mm}$ , is placed in a vacuum parallel to a large and flat heated surface. The other side of the rod is exposed to vacuum chamber walls at  $300 \text{ K}$ . Assume that the heated surface and the surface of the rod are both gray with equal emissivities of  $0.7$ . The rod has a volumetric heat capacity of  $\rho C_p = 6.7 \times 10^6 \text{ J m}^{-3} \text{ K}^{-1}$ . Calculate the heating rate of the rod at  $335 \text{ K}$ ,  $500 \text{ K}$ ,  $700 \text{ K}$ , and  $800 \text{ K}$ .



11.20 For a cylindrical ingot of steel,  $1 \text{ m}$  diameter by  $2 \text{ m}$  long, placed in a refractory-lined furnace at  $1500 \text{ K}$ , calculate the radiation heat transfer coefficient to the steel surfaces. Repeat when the surface of the steel has reached  $500 \text{ K}$  and  $1000 \text{ K}$ .

## PART THREE

### MASS TRANSPORT

The rate at which many processes occur is determined by diffusion, and it is most desirable to treat these processes in a quantitative manner when possible. The carburizing of steel, the oxidation of silicon, and solid-state sintering are just a few examples of diffusion-controlled processes.

On the other hand, there are processes whose rate is determined by the rate of reaction at an interface between two phases. Kinetics describes the rates of reactions in contrast to Fick's law of diffusion. As you may suspect, many processes are of mixed control, that is, neither the reaction rate nor the diffusional transport process alone controls the overall transfer of material.

In general, most processes involve a variety of different steps occurring in gaseous, solid, or liquid phases, and at different phase boundaries. When one step is much slower than the others, a limiting condition is reached and this *rate determining step* determines the overall reaction rate; if none of the steps is much slower than the others, a more general condition—*mixed control*—is achieved. This parallels heat flow problems in that the overall diffusion of heat into or out of a body may be controlled entirely by its thermal diffusivity or by the heat transfer coefficient at its surface, depending on their relative magnitudes. A good example of this is the cooling of solids which, as limiting conditions, either obey Newton's law of cooling, or, if the heat transfer coefficient approaches infinity, cool at a rate entirely controlled by the solid's ability to diffuse heat.

In this part, we introduce the materials engineer to basic equations and analyses that describe the various mechanisms of mass transport through and between phases. Materials engineers constantly deal with these phenomena, and learning these basics is critical to understanding, controlling, and developing processes to produce materials.

## 12

### FICK'S LAW AND DIFFUSIVITY OF MATERIALS

In Chapter 1, we introduced Newton's law of viscosity describing momentum transport due to a velocity gradient, and in Chapter 6 Fourier's law of heat conduction was described as energy transfer due to a temperature gradient. In Chapter 12, we present Fick's law of diffusion which describes the transport of a chemical species through a phase due to the concentration gradient of the species.

#### 12.1 DEFINITION OF FLUXES—FICK'S FIRST LAW

Diffusion is the movement of a species from a region of high concentration to a region of low concentration. Consider Fig. 12.1, which depicts a plate of iron of thickness  $L$ . Initially, both sides of the plate are exposed to the same pressure of hydrogen, which means that the concentration of hydrogen dissolved in the iron is uniform across the plate. At some instant,  $t = 0$ , the upper surface is subjected to a much higher pressure of the gas, which establishes a new hydrogen concentration at that surface. The material beneath this surface is gradually enriched as the hydrogen diffuses from the high concentration at the upper surface into the low concentration region. A steady-state concentration profile is eventually reached when a constant rate of hydrogen mass is required from the gas phase at  $x = 0$ , in order to maintain the concentration difference across the plate.

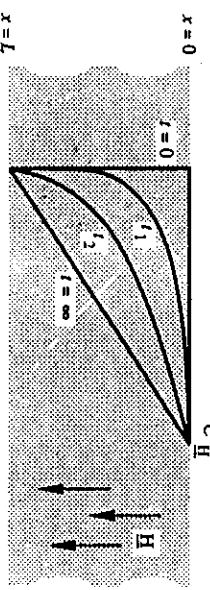


Fig. 12.1 Establishment of steady-state concentration gradient; Fick's first law.

If the concentration of component  $A$  (hydrogen in this example) is given in mass units, then the rate equation for diffusion may be written

$$W_{Ax} = -D_A \left[ \frac{\partial \rho_A}{\partial x} \right], \quad (12.1)$$

where  $W_{Ax}$  = mass flux of  $A$  in the  $x$ -direction, kg (of  $A$ )  $\text{m}^{-2} \text{s}^{-1}$ ,  $\rho_A$  = mass concentration of  $A$ , kg (of  $A$ )  $\text{m}^{-3}$  (of total material), and  $D_A$  = diffusion coefficient, or diffusivity of  $A$ ,  $\text{m}^2 \text{s}^{-1}$ .

In the materials field, the rate equation is usually written in terms of molar concentrations:

$$j_{Ax} = -D_A \left[ \frac{\partial C_A}{\partial x} \right], \quad (12.2)$$

where  $j_{Ax}$  = molar flux of  $A$  in the  $x$ -direction, mol (of  $A$ )  $\text{m}^{-2} \text{s}^{-1}$ , and  $C_A$  = molar concentration of  $A$ , mol (of  $A$ )  $\text{m}^{-3}$  (of total material).

Equations (12.1), (12.2), and other alternative statements of the rate equation are all referred to as *Fick's first law of diffusion* which states that species  $A$  diffuses in the direction of decreasing concentration of  $A$ , similarly as heat flows by conduction in the direction of decreasing temperature, and momentum is transferred in viscous flow in the direction of decreasing velocity.

Equations (12.1) and (12.2) are convenient forms of the rate equation when the density of the total solution is uniform; that is, in solid or liquid solutions, or in a dilute gaseous mixture. When the density is not uniform, other forms of Fick's first law may be preferable. For example, the mass flux may be given by

$$W_{Ax} = -\rho D_A \left[ \frac{\partial \rho_A^*}{\partial x} \right], \quad (12.3)$$

where  $\rho$  is the density of the entire solution,  $\text{kg m}^{-3}$ , and  $\rho_A^*$  is the mass fraction of  $A$ . Similarly, the molar flux may take the form

$$j_{Ax} = -CD_A \left[ \frac{\partial X_A}{\partial x} \right], \quad (12.4)$$

in which  $C$  is the local molar concentration in the solution at the point where the gradient is measured, mol (of all components)  $\text{m}^{-3}$  (of total solution), and  $X_A$  is the mole fraction of  $A$  ( $C_A/C$ ) in the solution.

The diffusivities  $D_A$ , appearing in Eqs. (12.1)-(12.4) are of a particular type, known as the *intrinsic diffusion coefficient*, since they are defined in the presence of a concentration gradient of  $A$ .

## 12.2 DIFFUSION IN SOLIDS

It behoves materials engineers to understand diffusion mechanisms, and especially the implications of the terms self-diffusion, intrinsic diffusion, interdiffusion, interstitial diffusion, vacancy diffusion, etc., so that they can make intelligent estimates of diffusivities for practical uses. In the following sections, we consider the various types of diffusion coefficients and mechanisms of diffusion.

### 12.2.1 Self-diffusion

If we could stand inside the lattice of a solid, we would see a continual motion of the atoms, each vibrating about its normal lattice point. Furthermore, we would see occasional unoccupied sites called vacancies. If we focus on a vacancy, we will eventually see the site suddenly become occupied and one of its neighboring sites become vacant. In this way, a particular atom can slowly progress through the lattice. Alternatively, the vacancy wanders randomly through the lattice. Either way, the net effect is a random motion of the atoms themselves.

The rate at which an atom meanders through the lattice of a pure metal is the *self-diffusion rate*. We can measure it using radioactive atoms (tracers), as illustrated in Fig. 12.2, which depicts self-diffusion between a central region initially with a uniform concentration  $C_A^*$  of radioactive atoms and two adjoining regions initially containing only normal atoms. It is assumed that the diffusion behavior of normal and of radioactive atoms is virtually the same, and by using a scheme as in Fig. 12.2 we can measure the rate at which the atoms diffuse among themselves, that is, self-diffusion.

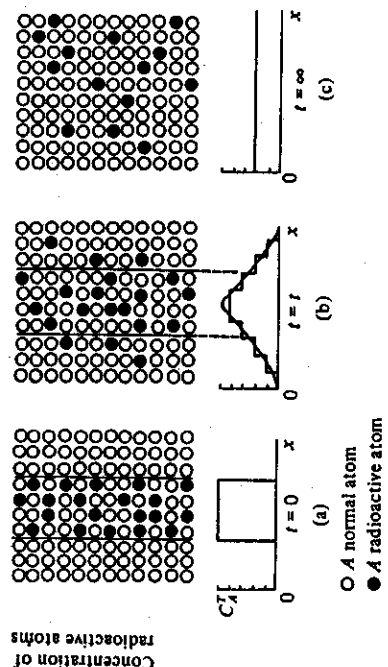


Fig. 12.2 Self-diffusion in materials. (a) Condition before diffusion. (b) Condition after some diffusion. (c) Uniform condition after prolonged diffusion.

We can also speak of self-diffusion rates in homogeneous materials in the same manner as we do for pure metals. In an alloy of gold and nickel, for example, we can determine the self-diffusion coefficient of gold atoms  $D_{Au}^*$  if the central layer of the homogeneous alloy initially contains radioactive gold atoms in the same proportion to Ni atoms as in the outer layers (Fig. 12.3). Similarly, if radioactive nickel atoms are initially present in the central layer, then we can determine its self-diffusion coefficient,  $D_{Ni}^*$ . Figure 12.4 gives self-diffusion data for the entire range of compositions in the gold-nickel system. It should be emphasized that *self-diffusion data apply to homogeneous alloys in which there is no gradient in chemical composition*. Also,  $D^*$ , values depend on the composition of the material and the temperature.

You may recall from Chapter 1 that Einstein proposed the equation

$$D^* = B^* k_B T \quad (1.17)$$

The probabilistic approach has shown that the self-diffusion coefficient in a simple cubic lattice may be expressed as<sup>1</sup>

$$D^* = \frac{1}{6} \delta^2 v, \quad (12.5)$$

where  $\delta$  is the interatomic spacing, and  $v$  is the jump frequency. From measurements of  $D^*$  and  $\delta$ , the jump frequency appears to be approximately  $10^8\text{--}10^{10}\text{ s}^{-1}$ , which is 1 in every  $10^4$  or  $10^5$  vibrations per atom. Most studies of self-diffusion are concerned with this sort of information, that is, with the structure and motion within the lattice of a solid. Some data for pure solid metals are given in Fig. 12.5 and for dilute solid alloys, in Fig. 12.6.

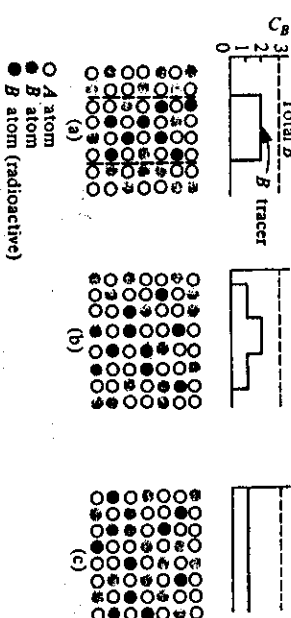
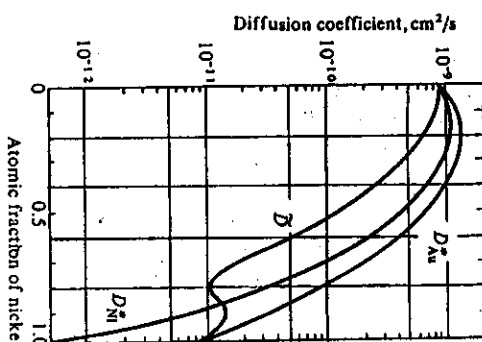


Fig. 12.3 Self-diffusion in an alloy



### Atomic fraction of nickel

**Fig. 12.4** Diffusion coefficients in gold-nickel alloys.  $D$  is the interdiffusion coefficient and  $D^*$  the self-diffusion coefficient. (From J. E. Reynolds, B. L. Averbach, and M. Cohen, *Acta Met.*, **5**, 29 (1957).)

to describe self-diffusion, where  $B^*$  is the self-diffusion "mobility," a measure of the ability of an atom to migrate within the structure without any external field or chemical free energy gradient providing a driving force.

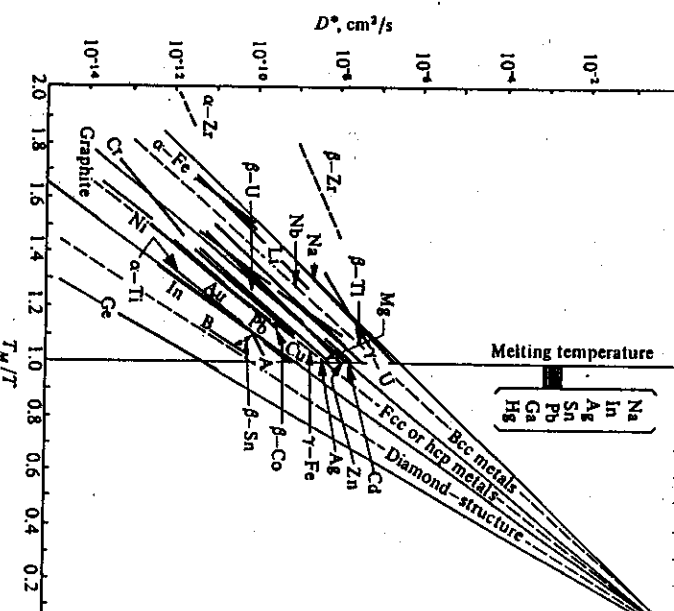


**Fig. 12.5** Self-diffusion coefficients for pure metals, plotted as  $\log D$  versus  $T_M/T$ , where  $T_M$  is the melting temperature. (From O. D. Sherby and M. T. Sinnad, *Trans. ASM* **54**, 227 (1961).)

In the development leading to Eq. (12.5), we assume that the atom jumps are completely random and uncorrelated, meaning that any of the atoms surrounding a vacancy may exchange places with the vacancy. However, if we follow the motion of tracer atoms moving via vacancies, we must realize that the tracer atom is only one of the many atoms around a vacancy and that the tendency for that particular atom (the tracer) to exchange places with the vacancy is not as great as for any atom in general to exchange. This means that the vacancy is often likely to move away from the tagged atom, with diffusion then actually

[See, for example, P. G. Shewmon, *Diffusion in Solids*, second edition, The Minerals, Metals & Materials Soc., Warrendale, PA, 1999, pages 53-68, or R. E. Reed-Hill and R. Abbaschian, *Physical Metallurgy Principles*, third edition, PWS-Kent, Boston, 1992, pages 360-364.

### 12.2.2 Diffusion under the influence of a composition gradient

In most materials processing situations, diffusion occurs because a concentration gradient or driving force is provided. When this force is present, the diffusion coefficient used to calculate the flux of atoms is *not* the self-diffusion coefficient, except under special circumstances.

Consider the diffusion of interstitial atoms through a lattice via interstitial sites, for example, the diffusion of carbon through iron. In this instance, carbon is in dilute concentration, and it diffuses through the stationary iron lattice without displacing the iron atoms from their own sites. Thus, if we treat a problem involving the diffusion of carbon in iron, we can safely use a value for carbon's diffusivity in iron from a handbook, even though it is not clearly specified what type of diffusion coefficient is given. We presume that the interstitial mechanism dominates if the solute atoms are considerably smaller in size than the solvent atoms. If the solute radius begins to approach that of the solvent, this mechanism no longer operates, and movement of the solvent atoms as well as motion of the solute atoms takes place. In this case, then, diffusion involves interchange of solute and solvent atoms on sites in the alloy. In substitutional alloys, the influence of a chemical gradient is such that we must clearly recognize the right type of diffusion coefficient: either the *intrinsic diffusion coefficient* or *interdiffusion coefficient*. Both types are discussed below, but first it seems appropriate to discuss briefly the various mechanisms by which substitutional alloy elements are thought to diffuse. More detailed discussions of diffusion mechanisms in solids are available in many sources on materials science or physical metallurgy.<sup>2</sup>

**Vacancy mechanism.** This is a mechanism by which an atom on a site adjacent to a vacancy jumps into the vacancy. While some distortion of the lattice is required for the atom to pass between neighboring atoms, the energy associated with this distortion is not prohibitive, and this mechanism is well established as the predominant one in many metals

**Ring mechanism.** In some bcc metals, it is thought there might exist a mechanism of diffusion in which a ring of three atoms may rotate, resulting in diffusion. This possibility is considered to be more plausible than an exchange of two atoms, since it involves less strain energy than a two-atom exchange. However, direct evidence of either of these mechanisms and ionic compounds.

operating in metals is lacking.

*Interstitiality mechanism.* This mechanism involves the addition of an extra solute atom to the lattice, by pushing an adjacent atom out of its normal site and into an interstitial site. The motion continues as the new, oversized interstitial atom pushes a further atom out of its normal site in a chain-reaction type of process. This mechanism is believed to operate in some compounds in which one atom is smaller than the other, for example, in AgBr, where silver diffuses via this mechanism. In most metals, however, this mechanism seems unlikely to operate. We find a possible exception in materials subjected to bombardment by radiation, in which case high energy particles may knock atoms out of their normal sites and into

Thinking of diffusion in general, we can see now the basic difference between diffusion and heat flow quite clearly. Heat flow in a medium does not cause the medium to move while diffusion, in itself, involves the movement of the medium, and thus contributes to the hydrology of the medium. Refer to Fig. 12.7 and consider a diffusion couple made by joining gold and a nickel bar together so that there is diffusion across the marked interface. The interstitial positions.

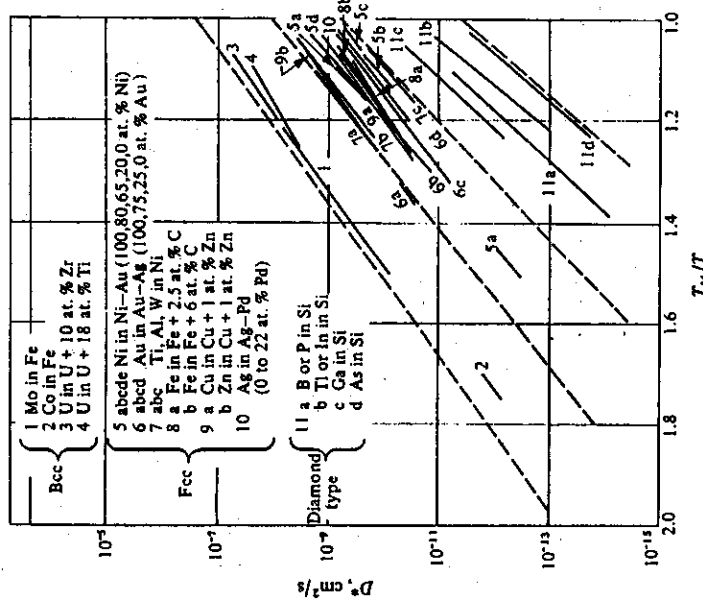


**Fig. 12.6** Effect of dilute alloying on self-diffusion and rate of solute substitutional diffusion for a number of metallic systems.  $T_{\text{M}}$  is the temperature halfway between the liquidus and solidus of the alloy. (From O. D. Sherby and M. T. Simnad, *ibid.*)

1126

Structure	<i>f</i>	Correlation coefficients for various structures*
Diamond	0.500	
Simple cubic	0.655	
Body-centered cubic	0.721	
Face-centered cubic	0.781	

Table 12.1 gives  $f$  calculated for several different crystal structures. For interstitial diffusion,

<sup>22</sup>See, for example, S. Mrowec, *Defects and Diffusion in Solids—An Introduction*, Elsevier Scienti<sup>ific</sup> Publ., Amsterdam, 1980, pages 174–196, or R. J. Borg and G. J. Dienes, *An Introduction to Solid State Diffusion*, Academic Press, Boston, 1999, pages 5–62.

in the plane of joining. During a diffusion anneal of many hours, interdiffusion of the gold and nickel occurs and changes the concentration distribution as shown. But, because gold diffuses more rapidly than nickel, more gold atoms than nickel atoms diffuse past the inert markers. Figure 12.7(b) shows in an exaggerated form the transfer of gold atoms across the plane of markers without any nickel atoms crossing over. If the vacancy concentration remains uniform, that is, the volume is constant, this transfer of gold atoms requires that the bar of pure gold must shorten while the nickel bar (now containing the transferred gold atoms) lengthens by the same amount. In the same manner, the transfer of nickel atoms across the plane of markers without any gold atoms crossing over is shown, producing the shift due to Ni. The net result of these two simultaneous processes is that the side that was originally pure gold is somewhat shorter, and the other side is correspondingly longer. An alternative description is that the inert markers have moved from their original position toward the gold end of the specimen. This is the viewpoint taken if one end of the specimen is the reference plane, and the movement is called the Kirkendall shift or the *Kirkendall effect*. The differences between the various "types" of diffusion coefficients mentioned above are related to the Kirkendall effect, and are pointed out below.

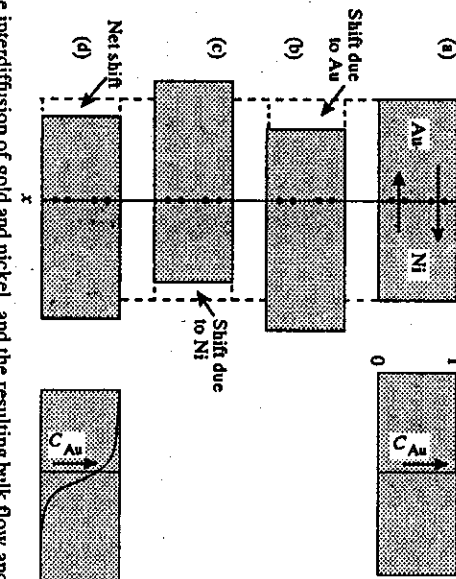


Fig. 12.7 The interdiffusion of gold and nickel, and the resulting bulk flow and composition profiles.

Due to bulk motion in the gold-nickel diffusion couple, we note that the solid bar moves with a velocity depending on the difference between the rates of diffusion of gold and nickel.

An observer sitting on a lattice plane moving with the solid's velocity would notice a flux of gold atoms past that plane given by

$$j_{Au} = -D_{Au} \frac{\partial C_{Au}}{\partial x}$$

However, an observer sitting on an unattached plane in space, would see the total flux of gold atoms passing by as

$$N_{Au} = -D_{Au} \frac{\partial C_{Au}}{\partial x} + v_x C_{Au}, \quad (12.7)$$

where the flux is expressed by  $N_{Au}$ , rather than by  $j_{Au}$ , to emphasize that it is relative to the stationary plane. The accumulation of gold as a function of time within a unit volume ( $\Delta x$ )

$$\Delta x \left[ \frac{\partial C_{Au}}{\partial t} \right] = N_{Au,\Delta x} - N_{Au,\Delta x + \Delta x}, \quad (12.8)$$

When the  $\lim_{\Delta x \rightarrow 0}$  is taken, we obtain

$$\frac{\partial C_{Au}}{\partial t} = -\frac{\partial N_{Au}}{\partial x}, \quad (12.9)$$

which, on substituting Eq. (12.7), becomes

$$\frac{\partial C_{Au}}{\partial t} = \frac{\partial}{\partial x} \left[ D_{Au} \frac{\partial C_{Au}}{\partial x} - v_x C_{Au} \right]. \quad (12.10)$$

Similarly, we can obtain the accumulation of nickel in the same unit volume:

$$\frac{\partial C_{Ni}}{\partial t} = -\frac{\partial}{\partial x} \left[ D_{Ni} \frac{\partial C_{Ni}}{\partial x} - v_x C_{Ni} \right]. \quad (12.11)$$

If the vacancy concentration within the unit volume is constant, then the volume is approximately constant and

$$\frac{\partial C}{\partial t} = \frac{\partial C_{Ni}}{\partial t} + \frac{\partial C_{Au}}{\partial t} = 0, \quad (12.12)$$

which requires, by Eqs. (12.10) and (12.11), that

$$v_x = \frac{1}{(C_{Au} + C_{Ni})} \left[ D_{Au} \left[ \frac{\partial C_{Au}}{\partial x} \right] + D_{Ni} \left[ \frac{\partial C_{Ni}}{\partial x} \right] \right]. \quad (12.13)$$

Only in terms of the gold concentration gradient, this takes the form

$$v_x = \frac{1}{C} [D_{Au} - D_{Ni}] \left[ \frac{\partial C_{Au}}{\partial x} \right]. \quad (12.14)$$

Having obtained an expression for  $v_x$ , we can now write the rate of accumulation of gold solely in terms of diffusion coefficients and concentration gradients, by substituting Eq. (12.14) into (12.10):

$$\frac{\partial C_{Au}}{\partial t} = \frac{\partial}{\partial x} \left[ (X_{Ni} D_{Au} + X_{Au} D_{Ni}) \frac{\partial C_{Au}}{\partial x} \right]. \quad (12.15)$$

We developed Eq. (12.15) from the viewpoint of a stationary observer. However, this requires that the position of a reference plane fixed in space can be determined. In the experimental set-up of Fig. 12.7, the inert markers could provide such a reference plane. But

in applying diffusion data to a commercial process, we cannot expect to be provided with inert markers. In addition, Eq. (12.15) is useful for determining  $D_{Au}$  and  $D_{Ni}$ , but is of no value in the sense that analytical solutions to practical diffusion problems cannot be conveniently developed from it. Instead, the basic complexity that arises from the bulk motion is avoided by merely using Fick's first law in its simplest form, that is, for gold

$$(12.16) \quad j_{Au} = -\bar{D} \left[ \frac{\partial C_{Au}}{\partial x} \right].$$

Note that the diffusion coefficient is written differently;  $\bar{D}$  includes the basic concept that the flux is proportional to the concentration gradient but side-steps the issue of bulk flow. With  $\bar{D}$  defined in this way, the accumulation of gold within the unit volume is

$$(12.17) \quad \Delta x \left[ \frac{\partial C_{Au}}{\partial t} \right] = [j_{Au}]_x - [j_{Au}]_{x+dx}.$$

When taking the  $\lim_{\Delta x \rightarrow 0}$ , we obtain the unsteady-state equation for unidirectional diffusion in solids:

$$(12.18) \quad \frac{\partial C_{Au}}{\partial t} = \frac{\partial}{\partial x} \left[ \bar{D} \frac{\partial C_{Au}}{\partial x} \right].$$

We use this equation, which is often called *Fick's second law*, to obtain analytical solutions for diffusion problems. By comparing Eqs. (12.15) and (12.18), the relation between the more fundamental quantities,  $D_{Au}$  and  $D_{Ni}$ —called *intrinsic diffusion coefficients*—and the more useful quantity,  $\bar{D}$ —called the *interdiffusion, mutual diffusion, or chemical diffusion coefficient*\*—is evident

$$(12.19) \quad \bar{D} = X_{Ni} D_{Au} + X_{Au} D_{Ni}.$$

Figure 12.4 shows  $\bar{D}$  for the gold-nickel system.

### 12.2.3 Darken's equations

Fick's laws contain the implicit assumption that the driving force for diffusion is the concentration gradient. A more fundamental viewpoint assumes that the driving force is a chemical free energy gradient. There is usually a direct correspondence between the two gradients, but occasionally the relationship becomes inverted and so-called "up-hill" diffusion, that is, diffusion against a concentration gradient, occurs. Darken<sup>1</sup> provided an analysis of this situation.

The flux of  $A$  atoms passing through an unit area in the  $x$ -direction is  $n_{Ax}$ , defined by

$$(12.20) \quad n_{Ax} = \frac{-n_A B_A}{N_0} \left[ \frac{\partial \bar{G}_A}{\partial x} \right],$$

\* $\bar{D}$  as the quantity used in diffusion calculations is often called simply the diffusion coefficient and denoted  $D$ .

where  $n_A$  is the number of  $A$  atoms per unit volume,  $B_A$  is the mobility of  $A$  atoms in the presence of the energy gradient,  $N_0$  is Avogadro's number, and  $\bar{G}_A$  is the partial molar free energy of  $A$  (also called the chemical potential of  $A$ ). Recalling from thermodynamics that

$$\bar{G}_A = G_A^0 + RT \ln a_A,$$

then Eq. (12.20) can be written as

$$(12.21) \quad n_{Ax} = \frac{-n_A B_A RT}{N_0} \left[ \frac{\partial \ln a_A}{\partial x} \right],$$

where  $a_A$  is the activity of  $A$ . Now comparing Eq. (12.21) to Fick's first law (Eq. (12.2)), we find that

$$(12.22) \quad D_A = B_A k_B T \left[ \frac{\partial \ln a_A}{\partial \ln X_A} \right],$$

where  $k_B$  (Boltzmann's constant) =  $R/N_0$ , and  $X_A$  is the mole fraction of  $A$ . Examine this expression as applied to a thermodynamically ideal solution with  $a_A = X_A$ . It reduces to

$$(12.23) \quad D_A = B_A k_B T,$$

which is known as the *Nernst-Einstein equation*. If the mobility  $B_A$ , in the presence of a driving force, is independent of composition, then  $D_A$  in an ideal solution alloy is independent of composition. However, it is reasonable to expect  $B_A$  to be a function of composition in alloys and non-stoichiometric compounds and so, even if the solutions are thermodynamically ideal,  $D_A$  may still be a function of composition. In addition, due to the fact that  $D_A^* = B_A^* k_B T$  for self-diffusion, it is often stated that Eq. (12.23) may be written as  $D_A^* = B_A^* k_B T$  for an ideal solution. However, this is *not* true, unless fortuitously  $B_A^* = B_A$ , for there is no reason to think that  $B_A$  under the influence of an energy gradient should be the same as  $B_A^*$  with no energy gradient present. Figure 12.4 shows clearly that  $D_A^*$  is not a constant with composition; at best, one would have to know  $B_A^*$  as a function of composition, and since mobilities are usually computed *from* diffusion coefficient measurements, this becomes an exercise in rhetoric.

Only in one instance—in nonmetallic stoichiometric compounds—may  $B_A^*$  and  $B_A$  be the same, and  $D_A^*$  be calculated from an independent measurement (such as ionic electrical conductivity) of  $B_A$ . We shall learn more about this subject in Section 12.3.

Returning to Eq. (12.19), we can modify the expression. From the Gibbs-Duhem equation, we know that

$$(12.24) \quad \left[ \frac{\partial \ln a_A}{\partial \ln X_A} \right] = \left[ \frac{\partial \ln a_B}{\partial \ln X_A} \right],$$

and only if  $B_A = B_A^*$  and  $B_B = B_B^*$ , then Eq. (12.19) can be written as

$$(12.25) \quad \bar{D} = (X_A D_A^* + X_B D_B^*) \left[ \frac{\partial \ln a_A}{\partial \ln X_A} \right].$$

<sup>1</sup>L. S. Darken, *Trans. AIME* 180, 430 (1949).

If we know the self-diffusion coefficients and the way in which the activity of  $A$  varies with composition, then we can calculate the interdiffusion coefficient, which is the useful value for engineering calculations. If the system is ideal, only then does Eq. (12.25) become

$$\bar{D} = X_A D_A^* + X_B D_B^*. \quad (12.26)$$

But since the restrictions that  $B_A$  equals  $B_A^*$  and  $B_B$  equals  $B_B^*$  apply, Eqs. (12.25) and (12.26) are of limited application.

Equation (12.25) does give insight into the conditions where diffusion may occur from the point of view of an uphill concentration gradient. The best-known example is the experiment carried out by Darken.<sup>4</sup> He welded two pieces of carbon steel together and studied the diffusion of carbon, as schematically shown in Fig. 12.8. One of the bars contained 3.80% Si and 0.48% C, while the other contained only 0.44% C. Figure 12.8(a) shows the initial carbon distribution and we might expect that the carbon distribution would simply have evened out at 0.46% C. However, because silicon greatly increases the activity

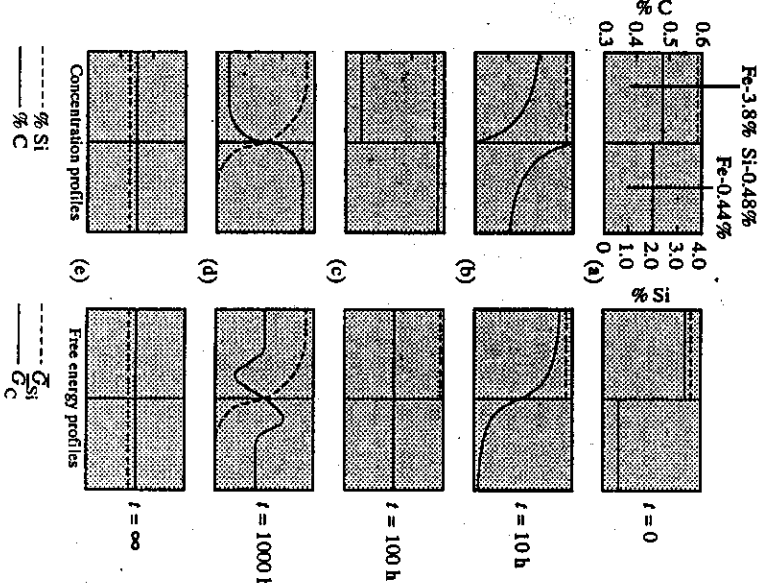


Fig. 12.8 Concentration and partial molar free-energy curves at various times for Fe-C and Fe-C-Si alloys welded together and annealed.

<sup>4</sup>L. S. Darken, *Trans. AIME*, Inst. Met. Div., Tech. Pub. 2443 (1948).

of carbon in iron, the carbon in the left-hand bar was at a much higher chemical potential than it would have been at if no silicon had been present. The result was that a sizeable amount of carbon diffused from left to right, and after a short time, the carbon gradient was as shown in Fig. 12.8(b). If the silicon did not diffuse, the final profile would look as in Fig. 12.8(c). If diffusion continues until both chemical potential curves are flat, not only for carbon but also for silicon, then the silicon will eventually diffuse to the right-hand side. The diffusion of silicon will be much slower than that of carbon, since it involves substitutional diffusion rather than the interstitial mechanism by which carbon diffuses. This means that the higher carbon concentration (created on the right-hand side before appreciable silicon diffusion occurred) will then decrease until ultimately both the silicon and carbon gradients become flat (Fig. 12.8(e)).

A formalism for treating diffusion in multicomponent solids can be found in Kirkaldy and Young<sup>5</sup>; they also discuss many examples of diffusion in ternary metallic solids.<sup>6</sup>

## 12.2.4 Temperature dependence of diffusion in solids

Temperature has a tremendous influence on diffusion in solids. Specifically, the Arrhenius equation adequately describes the relationship between any type of diffusion coefficient and temperature:

$$D = D_0 e^{-Q/kT}, \quad (12.27)$$

in which  $Q$  is the activation energy, and  $D_0$  is sometimes called the frequency factor, both essentially constant over a wide temperature range.

Much effort has gone into the development of theoretical expressions for  $D_0$ . Recall Eq. (12.5), in which the self-diffusion coefficient  $D^*$  is expressed in terms of the jump frequency  $\nu$  and the interatomic distance  $\delta$ . According to Zener,<sup>7</sup> if the jump process is an activated one, then  $\nu$  can be described by

$$\nu = \nu_0 Z e^{-\Delta G^*/kT}, \quad (12.28)$$

where  $\nu_0$  = vibrational frequency of the atom in the lattice,  $Z$  = coordination number, and  $\Delta G^*$  = free energy of activation required for the atom to jump from one site into the next.

Since

$$\Delta G^* = \Delta H^* - T\Delta S^*,$$

then

$$D^* = D_0 e^{-(\Delta H^*/kT)}, \quad (12.29)$$

in which

$$D_0 = \frac{\delta^2 \nu_0 Z}{6} e^{(\Delta S^*/k)}.$$

<sup>5</sup>J. S. Kirkaldy and D. J. Young, *Diffusion in the Condensed State*, The Institute of Metals, London, 1986, pages 140-148.

<sup>6</sup>J. S. Kirkaldy and D. J. Young, *ibid.*, Chapter 7.

<sup>7</sup>C. Zener, *J. Applied Physics* 22, 372 (1951).

$\Delta H^\circ$  is synonymous with  $Q$ , the activation energy for diffusion;  $\delta$ ,  $v_0$ , and  $\Delta S^\circ$  do not vary significantly with temperature, so the result is that  $D_0$  varies with temperature only slightly. This is somewhat different from saying that  $D_0$  is a constant, but for practical purposes it is a close approximation.

There are many data available on metallic systems, and some of these are presented in Figs. 12.9, 12.10, and 12.11. In addition, there are several rules that may be used to estimate  $Q$  and  $D_0$  if data are completely missing. Sherby and Simnad<sup>8</sup> developed a correlation equation for predicting self-diffusion data in pure metals:

$$D^* = D_0 e^{-\frac{Q}{RT} \cdot \ln(\frac{V}{V_0})}, \quad (12.30)$$

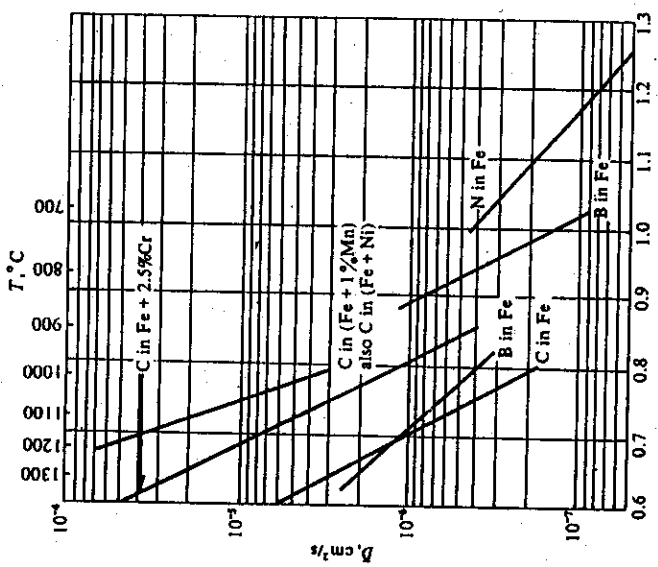


Fig. 12.10 Interdiffusion coefficients of interstitial elements through ferrous materials.

where  $K_0$  depends only on the crystal structure,  $V$  is the normal valence of the metal, and  $T_M$  is the absolute melting point. The values of  $K_0$  are

Crystal structure	$K_0$
bcc	14
fcc	17
hcp	17
Diamond	21

For estimation purposes,  $D_0$  is approximated as  $1 \times 10^{-4} \text{ m}^2 \text{ s}^{-1}$ , as shown for most metals in Fig. 12.5. Furthermore,  $Q$  is predicted by

$$Q = RT_M(K_0 + V). \quad (12.31)$$

This correlation has been tested for self-diffusion in alloys, in which case  $T_M$  is taken as the temperature halfway between the liquidus and solidus for the alloy; it also applies to intrinsic diffusivities of solutes in dilute concentrations in a variety of solvent hosts, with reasonably satisfactory results.

By now the reader has surely surmised that diffusion in metals and alloys is of substantial scientific interest and engineering importance. In the limited space herein, we have only discussed *volume* diffusion effects, but we would be remiss not to at least alert the readers that *grain boundary* diffusion and *surface* diffusion are also very important. In most circumstances, volume diffusion dominates, but grain boundary diffusion (and hence the effect

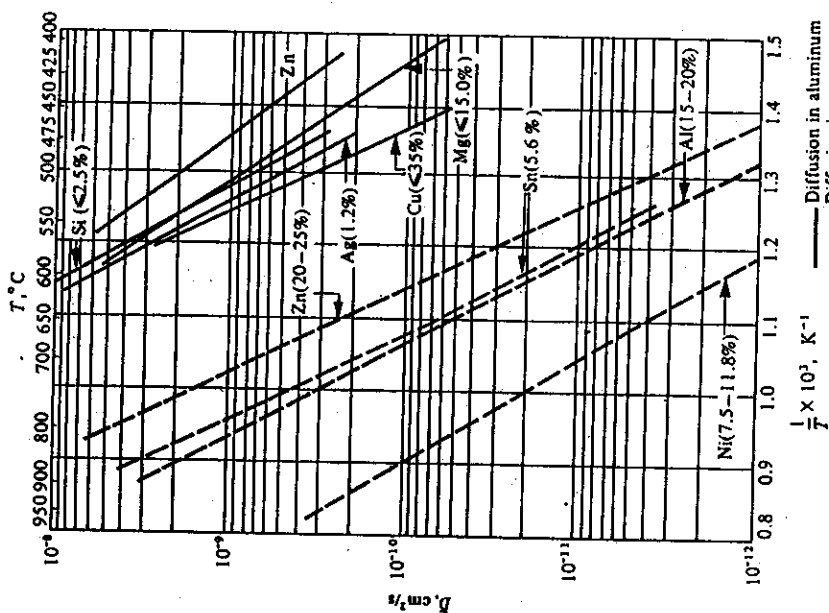


Fig. 12.9 Interdiffusion coefficients in nonferrous metals.

<sup>8</sup>O. D. Sherby and M. T. Simnad, *ASM Trans. ASM 54*, 227 (1961).

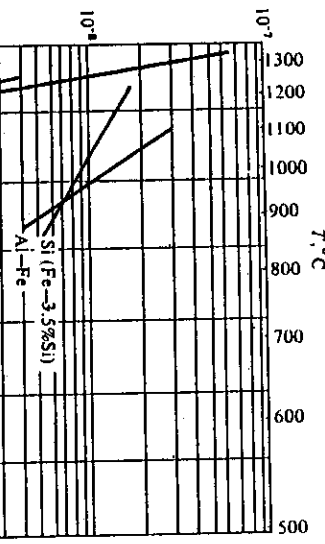


Fig. 12.11 Interdiffusion coefficients in ferrous materials.

of grain size) can be important in polycrystalline metals at relatively low temperatures and in thin films. Surface diffusion is important in sintering and in the growth of some thin films. Many of the references devoted to diffusion phenomena discuss grain boundary diffusion and surface diffusion.<sup>9,10,11,12</sup>

Diffusing ion	Crystal in which diffusion takes place	$D_0$ , m <sup>2</sup> /s	$D$ , J/mol·s
Ag <sup>+</sup>	$\alpha$ -Cu <sub>3</sub> S	38	$\times 10^9$
Cu <sup>+</sup>	$\alpha$ -Ag <sub>2</sub> S	12	$\times 10^{-9}$
Ag <sup>+</sup>	$\alpha$ -Cu <sub>3</sub> Te	2.4	$\times 10^{-4}$
Cu <sup>+</sup>	$\alpha$ -AgI	16	$\times 10^{-9}$
Li <sup>+</sup>	$\alpha$ -AgI	50	$\times 10^{-9}$
Se <sup>2-</sup>	$\alpha$ -Ag <sub>2</sub> S	17	$\times 10^{-9}$
Pb <sup>++</sup>	PbCl <sub>2</sub>	7.8	$\times 10^{-4}$
Pb <sup>++</sup>	PbI <sub>2</sub>	10.6	$\times 10^{-4}$
O <sup>2-</sup>	Fe <sub>2</sub> O <sub>3</sub>	1	$\times 10^{-11}$
Fe <sup>+++</sup>	Fe <sub>2</sub> O <sub>3</sub>	4	$\times 10^{+1}$
Co <sup>++</sup>	CoO	2.15 $\times 10^{-7}$	144 000
Ni <sup>++</sup>	NiO	1.83 $\times 10^{-7}$	192 000
O <sup>2-</sup>	NiO	1.0 $\times 10^{-9}$	226 000
Cr <sup>+++</sup>	Cr <sub>2</sub> O <sub>3</sub>	1.37 $\times 10^{-5}$	256 000

Stoichiometric AB crystals may contain several different types of point defects. The Schottky defect refers to equal numbers of cation and anion vacancies, that is,  $[V_A] = [V_B]$ .<sup>1</sup> The Frenkel defect may occur on either the cation or anion sublattice, when equal numbers of vacancies are balanced by interstitials of the same species, that is,  $[V_A] = [A]$ . An example of a material that exhibits Schottky defects is NaCl, in which  $[V_{Na}] = [V_{Cl}]$ . Frenkel defect concentrations expressed on a fractional basis.

<sup>1</sup>W. Jost, *Diffusion in Solids, Liquids, Gases*, Academic Press, New York, 1960.

K. Hauffe, *Oxidation of Metals*, Plenum Press, New York, 1965.

O. Kubaschewski and B. E. Hopkins, *Oxidation of Metals and Alloys*, Plenum Press, New York, 1962.

P. Kofstad, *High Temperature Oxidation of Metals*, Wiley, New York, 1966.

F. A. Kroger, *Impurities in Crystals*, North-Holland, New Amsterdam, 1964.

R. J. Borg and G. J. Dienes, *ibid.*

J. S. Kirkaldy and D. J. Young, *ibid.*

G. E. Murch and A. S. Nowick, Editors, *ibid.*

<sup>9</sup>S. Mrowec, *ibid.*, pages 275-283.

<sup>10</sup>R. W. Balluffi in *Diffusion in Crystalline Solids*, G. E. Murch and A. S. Nowick, Editors, Academic Press, Orlando, 1984, Chapter 6.

<sup>11</sup>J. S. Kirkaldy and D. J. Young, *ibid.*, pages 27-34.

<sup>12</sup>R. J. Borg and G. J. Dienes, *ibid.*, pages 139-144, 151-156.

defects predominate in AgBr, in which  $[V_{A,i}] = [\text{Ag}]$ . If diffusion is via vacancies, any chemical additions that increase the concentration of vacancies will tend to increase the diffusion coefficient. For example, if  $\text{CdCl}_2$  is added to NaCl, then, since the cadmium cation has a +2 charge, electrical balance in the crystal can only be maintained if one cation site is left vacant for every cadmium atom added, thus increasing  $[V_{\text{Na}}]$ .

Many ceramic materials show deviations from stoichiometry, which may be due to unequal concentrations of cation and anion defects. This is particularly true of transition metal oxides, such as  $\text{TiO}_2$ ,  $\text{Nb}_2\text{O}_5$ ,  $\text{NiO}$ ,  $\text{CoO}$ , and wustite,  $\text{Fe}_2\text{O}$ . In the latter case, the defects are predominantly cation vacancies  $[V_{\text{Fe}}]$ , with charge neutrality maintained by the creation of  $\text{Fe}^{2+}$  ions according to the equation



Some of the trivalent iron ions may be ionized according to\*

$$\text{Fe}^{2+} \rightarrow \text{Fe}^{2+} + h^*, \quad (12.37)$$

which results in an increase in electronic conduction via electron holes as further deviations from stoichiometry occur.

Because of the electrical nature of the defects and of the diffusing species (ions), ionic electrical conduction and diffusion are inseparable processes. Consider an ionic material in which one ionic species makes the predominant contribution to electrical conduction (for example,  $\text{Na}^+$  cations in NaCl). The general equation for the transport of the species in the  $x$ -direction under the influence of an electric field and a concentration gradient in the  $x$ -direction is:

$$\dot{n}_{ix} = -D_i \left[ \frac{\partial n_i}{\partial x} \right] - B_i n_i z_i e \left[ \frac{\partial \phi}{\partial x} \right], \quad i \text{ ions m}^{-2} \text{s}^{-1}, \quad (12.32)$$

where  $z_i$  = number of charges on the diffusing species,

$n_i$  = concentration of diffusing species, ions  $\text{m}^{-3}$   
 $B_i$  = mobility of species  $i$  (steady-state velocity of the particle under the influence of a unit force),  $\text{m}^2 \text{s}^{-1} \text{V}^{-1} \text{C}^{-1}$ ,  
 $D_i$  = the diffusion coefficient of species  $i$ ,  $\text{m}^2 \text{s}^{-1}$   
 $e = 1.6 \times 10^{-19} \text{ C}$  charge  
 $\phi$  = electrical potential,  $\text{V}$ .

In the absence of a concentration gradient, the flux is

$$\dot{n}_{ix} = -B_i n_i z_i e \left[ \frac{\partial \phi}{\partial x} \right], \quad i \text{ ions m}^{-2} \text{s}^{-1}. \quad (12.33)$$

Note that in the physics and electrical engineering literature,  $\sigma = ne\mu$ , where  $\mu$  is called the mobility. Since this is applied to electron or electron-hole conduction,  $z = -1$  or +1, and therefore,  $\mu = Be$ . In this case, the units of  $\sigma$  are  $\text{ohm}^{-1} \text{m}^{-3}$ ,  $n$  are  $\text{m}^{-3}$ ,  $e = 1.6 \times 10^{-19} \text{ C}$ , and  $\mu = \text{m}^2 \text{s}^{-1} \text{V}^{-1}$ .

Since the current density  $I$  is given by

$$I = \dot{n}_{ix} z_i e, \quad \text{A m}^{-2}, \quad (12.34)$$

then

$$I = -B_i n_i (z_i e)^2 \left[ \frac{\partial \phi}{\partial x} \right]. \quad (12.35)$$

The electrical conductivity  $\sigma$  is defined by

$$\sigma_i = \frac{1}{-B_i n_i (z_i e)^2} = -\frac{\partial \phi}{\partial x}, \quad \text{ohm}^{-1} \text{m}^{-1}. \quad (12.36)$$

Now by recalling Eq. (12.23), we can relate the electrical conductivity and diffusivity by the expression:

$$\frac{\sigma_i}{D_i} = \frac{n_i (z_i e)^2}{\kappa_B T}, \quad (12.37)$$

This equation is known as the "extended" Nernst-Einstein equation.

In order to predict  $D_i$  from conductivity measurements, we must know the fraction of the total conductivity due to species  $i$ ; this fraction is called the transference number of species  $i$ , denoted  $f_i$ . This number, obtained from electrolysis experiments, gives the fraction of the total current carried by a particular species, and the total of all transference numbers must equal one. Therefore

$$\sum_{\text{cation species}} f_{\text{cation},i} + \sum_{\text{anion species}} f_{\text{anion},i} + f_{\text{electron}} = 1. \quad (12.38)$$

Thus

$$\sigma_i = f_i \sigma_{\text{total}}, \quad \text{ohm}^{-1} \text{m}^{-1}. \quad (12.39)$$

Equation (12.37) has been tested for several compounds. For example, in NaCl,  $f_{\text{Na}^+} \equiv 1$ , so that  $\sigma_{\text{measured}} \equiv \sigma_{\text{Na}^+}$ . Therefore, if we assume that all of the sodium ions in the crystal participate in the conduction process, then

$$D_{\text{Na}} = \frac{\sigma_{\text{measured}} \kappa_B T}{n_{\text{Na}} e^2}, \quad (12.40)$$

where  $n_{\text{Na}}^+$  is the number of sodium ions per cubic meter. In order to test this, Mapother *et al.*<sup>13</sup> measured the conductivity of NaCl and then, using radioactive sodium, measured diffusion coefficients of sodium,  $D_{\text{Na}}$ , both as functions of temperature. The values of  $D_{\text{Na}}$  calculated by means of Eq. (12.37) and the  $D_{\text{Na}}^T$  values are compared in Fig. 12.12. The agreement between the two values is excellent at the higher temperatures. The discrepancy at the lower temperatures points out the effect of  $\text{CdCl}_2$  present as an impurity in NaCl in dilute concentration. By adding  $\text{CdCl}_2$ ,  $[V_{\text{Na}}]$  increases, thereby increasing  $D_{\text{Na}}$  over that in the pure material. However, the conductivity expression does not include this added effect, and the values differ when the concentration of vacancies due to  $\text{CdCl}_2$  is significant, compared to the intrinsic concentration of vacancies.

\*The notation  $h^*$  is used to represent an electron hole in the valence band, contributing to *p*-type, or hole conduction; similarly,  $e'$  is the symbol for electrons in the conduction band.

<sup>13</sup>D. Mapother, H. N. Crooks, and R. Mauer, *J. Chem. Phys.* **18**, 1231 (1950).

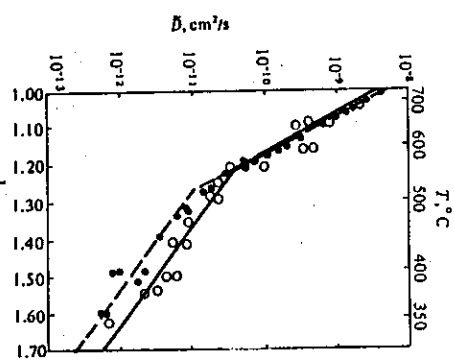
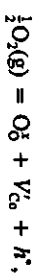


Fig. 12.12 Log  $D$  versus  $1/T$  for sodium in NaCl as determined with radioactive sodium ( $\circ$ ), and as calculated from the conductivity ( $\bullet$ ). (From D. Mapother, H. N. Crooks, and R. Mauer, *J. Chem. Phys.* **18**, 1231 (1950).)

Non-stoichiometry, resulting in vacancies on the cation sublattice, can also have an effect on  $D_i^*$  (and through Eq. (12.25) or (12.26) on  $\bar{D}$ ) in the same manner as impurities. For example, CoO exists as a non-stoichiometric oxide with defects on the cation sublattice in the form of vacancies.<sup>14</sup> This amounts to the addition of an oxygen anion without addition of a cation, according to the reaction:



where  $\text{O}_\text{G}^\ddagger$  indicates an excess oxygen ion on a regular oxygen site,  $V_{\text{Co}}^\ddagger$  a singly-ionized cation vacancy, and  $h^\ddagger$  a free electron hole. The notation for building the superscripts is  $x$  means neutral (for example,  $\text{Na}^+$  substituting for  $\text{Li}^+$ ),  $+$  means positive (and multiple dots means multiple positive), and  $-$  means negative (and again, multiple  $-$  define multiple negative).

Presumably, diffusion of  $\text{Co}_{x+}^\ddagger$  ions should be via a vacancy mechanism on the cation sublattice, with diffusivity increasing as the concentration of cation vacancies increases. The phase diagram (Fig. 12.13) shows the Co-CoO equilibrium. When  $P_{\text{O}_2}$  is increased above that existing at this lower boundary of the CoO phase field, the molar concentration of CoO decreases as oxygen is added to the oxide, until finally an oxygen pressure is reached at which  $X_{\text{Co}} = 0.492$  (corresponding to  $\text{Co}_{0.998}\text{O}$ ) beyond which  $\text{Co}_3\text{O}_4$  forms. This occurs at  $P_{\text{O}_2} = 0.53$  atm at 1000°C. Price and Wagner measured chemical diffusion coefficients in  $\text{CoO}$  by equilibrating a single crystal of  $\text{CoO}$  with an atmosphere at low  $P_{\text{O}_2}$  ( $4.7 \times 10^{-2}$  atm); then, at time zero, they changed the oxygen potential to a higher level, near the  $\text{CoO}-\text{Co}_3\text{O}_4$  boundary. The change in  $X_{\text{O}}$  ( $= -X_{\text{Co}}$ ) is measured as a function of time by following the change in electrical conductivity, since the conductivity in this material is proportional to the concentration of electron holes, which is dependent, in turn, on the oxygen content through the equilibrium constant for the reaction shown above:

$$K = \frac{[h^\ddagger][V_{\text{Co}}^\ddagger]}{P_{\text{O}_2}^{1/2}}.$$

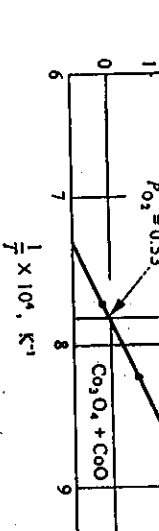


Fig. 12.13 The stable phase field of cobaltous oxide with respect to oxygen pressure and temperature.

Although  $\bar{D}$  is generally composition-dependent in non-stoichiometric crystals, in this case the deviations from non-stoichiometry are small, and  $\bar{D}$  is found to be essentially constant with composition:

$$\bar{D} = 4.33 \times 10^{-7} \exp(-24,000/RT), \text{ m}^2 \text{ s}^{-1}$$

Since the cobalt cation is much smaller than the oxygen anion,  $D_{\text{Co}}$  is very much greater than  $D_{\text{O}}$  in  $\text{CoO}$ . Then we may use Eq. (12.25), neglecting the term  $D_{\text{O}}^* X_{\text{Co}}$ , if we further assume that  $B_{\text{Co}} = B_{\text{O}}^*$  in order to calculate  $D_{\text{Co}}^*$  from the  $\bar{D}$  data:

$$\bar{D} \approx D_{\text{Co}}^* X_{\text{O}} \left[ \frac{\partial \ln a_{\text{Co}}}{\partial \ln X_{\text{Co}}} \right].$$

<sup>14</sup>J. B. Price and J. B. Wagner, Jr., *Zeit. f. physik. Chemie, Neue Folge* **49**, 3-4 (1966).

We may calculate the thermodynamic factor by noting that

$$\left[ \frac{\partial \ln a_{\text{Co}}}{\partial \ln X_{\text{Co}}} \right] = - \left[ \frac{\partial \ln a_0}{\partial \ln X_0} \right],$$

and that

$$a_0 = \left[ \frac{P_{O_2}}{P_{O_2}^0} \right]^{1/2},$$

where  $P_{O_2}^0$  is the standard oxygen pressure, 1 atm. We obtain the slope of the  $\log a_0$  versus  $\log X_0$  plot from the data of Eror and Wagner,<sup>15</sup> who measured  $[V_{\text{Co}}]$  as a function of  $P_{O_2}$  across the CoO phase field:

$$\begin{aligned} - \left[ \frac{\partial \ln a_0}{\partial \ln X_{\text{Co}}} \right] &\approx - \left[ \frac{\Delta \log a_0}{\Delta \log X_{\text{Co}}} \right] = - \left[ \frac{\frac{1}{2} (\log P_{O_2, \text{initial}} - \log P_{O_2, \text{final}})}{\log X_{\text{Co}, \text{initial}} - \log X_{\text{Co}, \text{final}}} \right] \\ &= - \left[ \frac{\frac{1}{2} (\log 4.7 \times 10^{-2} - \log 5.1 \times 10^{-1})}{\log (0.4963) - \log (0.4936)} \right] = +1.45 \times 10^2. \end{aligned}$$

At  $1000^\circ\text{C}$ ,  $\bar{D} = 2.16 \times 10^{-11} \text{ m}^2 \text{ s}^{-1}$ , and  $X_0 \approx 0.50$ . Substituting into Eq. (12.25) as simplified above, we find  $D_{\text{Co}}^T$  to be  $2.98 \times 10^{-13} \text{ m}^2 \text{ s}^{-1}$ . Applying the correlation coefficient,  $f = 0.78$  for the fcc cation sublattice, then

$$D_{\text{Co}}^T = 0.78 D_{\text{Co}}^* = 2.33 \times 10^{-13} \text{ m}^2 \text{ s}^{-1} \quad (\text{calculated}),$$

which is in good agreement with Carter and Richardson's<sup>16</sup> measured value

$$D_{\text{Co}}^T = 2.60 \times 10^{-13} \text{ m}^2 \text{ s}^{-1} \quad (\text{measured}).$$

In some oxides, ionic conduction is unusually high; these are called *super ionic conductors*. These oxides have unusually high concentrations of charge carriers and vacancies or interstitial ions. One example is  $\beta$ -alumina, which is a sodium aluminate of variable composition between  $(\text{Al}_2\text{O}_3)_{0.53}\text{Na}_2\text{O}$  and  $(\text{Al}_2\text{O}_3)_{0.55}\text{Na}_2\text{O}$ . The sodium atoms are the fast-diffusing species, because they occupy sites in a crystal plane that is sparsely populated and can therefore diffuse easily via the large number of vacant sites in that plane. Another material that exhibits fast ionic transport is zirconia, which is stabilized with either calcia ( $\text{CaO}$ ) or yttria ( $\text{Y}_2\text{O}_3$ ). In this case, the oxygen anions diffuse six orders of magnitude faster than the cations because there is a very large concentration of  $\text{O}^{2-}$  vacancies, which is controlled by the concentration of  $\text{Ca}^{2+}$  or  $\text{Y}^{3+}$ .

When molten silicate is cooled to form a rigid glass, there remain spaces, where the monovalent and divalent metallic ions reside amongst the network structure. This is discussed in more detail in Chapter 1. The silicon ions are integral to the covalently bonded network so their mobility is extremely limited. On the other hand, the ions in the spaces diffuse readily.

The diffusion coefficient of sodium ions in a silicate glass is shown in Fig. 12.14. In the range of 870 to 910 K, there is a transition in the diffusion coefficient. At temperatures above the transition, the silicate can be regarded as supercooled liquid, whereas below the transition the silicate is a rigid glass, which affords considerably less mobility of the sodium ions.

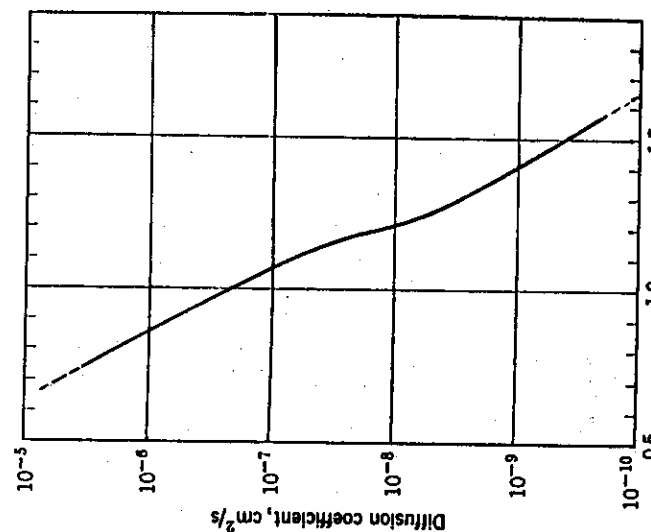


Fig. 12.14 Diffusion of  $\text{Na}^+$  in a sodium silicate glass. (From W. D. Kingery, *Introduction to Ceramics*, John Wiley, New York, 1960, page 239.)

The spaces in the silicate structure also allow for diffusion of many other ions and small atoms; notable are hydrogen and water vapor. Depending on the composition of the glass, diffusion of molecular  $\text{H}_2$  can be accompanied by  $\text{OH}^-$  ions, which result from the formation of  $(\text{Si}^{4+}\text{O}^{2-}\text{OH}^-)^{+1}$  groups. Water vapor probably diffuses as both  $\text{H}_2\text{O}$  and  $\text{OH}^-$  ions, which are part of  $(\text{SiOH})^{+1}$  groups.

Typically diffusion coefficients in glasses are several orders of magnitude greater than they are in crystalline solids. This has the consequence that the presence of a small amount of a glassy phase in a ceramic has a very strong effect on diffusion-controlled processes in a multiphase system.<sup>17</sup>

A good review of the mechanisms of diffusion in oxide glasses and extensive listings of diffusion data are given by Frischat.<sup>17</sup>

<sup>15</sup>N. Eror and J. B. Wagner, Jr., *J. Phys. Chem. Solids* **29**, 1597 (1968).

<sup>16</sup>R. E. Carter and F. D. Richardson, *J. Metals* **20**, 1244 (1948).

<sup>17</sup>G. H. Frischat, *Ionic Diffusion in Oxide Glasses*, Trans Tech Publications, Aedermannsdorf, Switzerland, 1975.

## 12.4 DIFFUSION IN ELEMENTAL SEMICONDUCTORS

Because of their technological importance, and the sophistication of their processing, almost all of which involves diffusion treatments, it is important to know something about the diffusion of alloying elements (dopants) and impurities in silicon and germanium. Both of these elements are intrinsic semiconductors; that is, they have energy band gaps that are small enough that thermal excitation of electrons into a conduction band occurs. Their intrinsic conductivities increase with increasing temperature.

Germanium is tetravalent; the four outer electrons form covalent bonds with four neighboring Ge atoms. If a pentavalent impurity, such as phosphorous, is substituted for germanium, the extra outer electron associated with phosphorous is easily activated into the conduction band, increasing the material's electronic, or *n*-type conductivity. Conversely, if a trivalent impurity, such as boron, is substituted for a germanium atom, the band is short of one electron, which may be provided from the electrons in the valence band, leaving behind a hole or positive conduction charge and contributing to *p*-type conductivity, when the number of such atoms is greater than the number of intrinsic conduction electrons.

Diffusion in germanium is primarily by a vacancy mechanism. Table 12.3 gives the constants that can be used with Eq. (12.27) to calculate diffusion coefficients for various elements in Ge, and Fig. 12.15 shows that the diffusion of pentavalent elements is faster than for Ge self-diffusion, leading to the conclusion that vacancies are electron acceptors, stimulating the diffusion of the *n*-type dopants. The converse appears to be true of Group III elements.

Silicon, on the other hand, exhibits more complex mechanistic behavior. At temperatures below 1440 K, self-diffusion is thought to take place via the vacancy mechanism; above that temperature, interstitial motion dominates. Table 12.4 and Fig. 12.16 give diffusion coefficients for impurities in silicon. In this case, all of the elements diffuse faster than the silicon itself.\*

Table 12.3 Diffusion constants in Ge

Element	$D_0, \text{m}^2 \text{s}^{-1}$	$\mathcal{Q}, \text{kJ mol}^{-1}$
Ge	$1.85 \times 10^{-3}$	296
B	$1.1 \times 10^{-3}$	438
Al	$1.6 \times 10^{-2}$	313
Ga	$4.0 \times 10^{-3}$	304
In	$3.3 \times 10^{-3}$	292
P	$2.5 \times 10^{-4}$	240
As	$1.03 \times 10^{-3}$	242
Sb	$3.2 \times 10^{-4}$	234
Li	$3.1 \times 10^{-7}$	49
Cu	$4.0 \times 10^{-7}$	32

(From R. J. Borg and G. J. Dienes, *ibid.*, page 197.)

The elements Li and Cu diffuse as interstitials so their activation energies are much lower than the energies of the other elements, which are substitutional. This relates to a potential processing problem in microelectronics. That is, extraneous interstitial impurities that diffuse very quickly can poison or modify intentionally doped regions in semiconductors and kill devices. This emphasizes one reason that microelectronic processing must be done in a very clean environment.

\*For a more detailed discussion of the mechanism, refer to R. J. Borg and G. J. Dienes, *ibid.*, pages 198-202.

Fig. 12.15 Diffusion coefficients for Group III and Group V elements in Ge. (From R. J. Borg and G. J. Dienes, *ibid.*, page 196.)

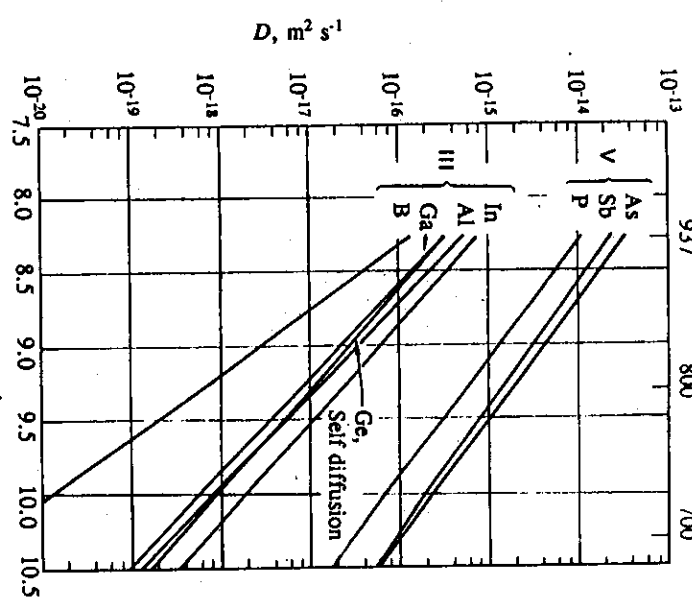


Table 12.4 Diffusion constants in Si

Element	$D_0, \text{m}^2 \text{s}^{-1}$	$\mathcal{Q}, \text{kJ mol}^{-1}$
B	$5.1 \times 10^{-4}$	357
Al	$8.0 \times 10^{-4}$	335
Ga	$3.6 \times 10^{-4}$	339
In	$16.5 \times 10^{-4}$	377
P	$10.5 \times 10^{-4}$	356
As	$60.0 \times 10^{-4}$	405
Sb	$12.9 \times 10^{-4}$	384
Bi	$1.03 \times 10^{-1}$	447

(From R. J. Borg and G. J. Dienes, *ibid.*, page 201.)

Fick's Law and Diffusivity of Materials 445  
 steady-state velocity  $V_\infty$ . According to Eq. (2.119), the force on a sphere moving at steady-state in laminar flow is

$$F = 6\pi R\eta V_\infty, \quad (2.119)$$

and since the definition of the mobility  $B$  is  $V_\infty/F$ , we have

$$B = \frac{1}{6\pi R\eta}. \quad (2.119)$$

Combining this result with Eq. (12.23), we get

$$D = \frac{\kappa_b T}{4\pi R\eta}, \quad (12.41)$$

which is known as the Stokes-Einstein equation. This was then modified by Sutherland,<sup>19</sup> who adopted a slightly different form of the drag force, with the result that

$$D = \frac{\kappa_b T}{4\pi R\eta}. \quad (12.42)$$

This equation is known as the Sutherland-Einstein equation.

Although the use of Stokes' law for this purpose may seem unjustified, since it neglects interatomic forces and considers only form drag, the results, in terms of predicted data, are remarkable. For example, in liquid metals, if we substitute the measured values of  $D^*$  and  $\eta$  into Eq. (12.42) and then calculate the radii of the diffusing species, we obtain very good agreement between these predicted radii and the radii of ions, as shown in Table 12.5.

Table 12.5 Comparison of calculated and Pauling radii for self-diffusion in liquid metals

Element	Temperature range, °C	Sutherland model, nm	Pauling radii, nm
Na	110-630	0.151-0.453	0.157
Hg	274-364	0.120-0.124	0.139
In	448-1013	0.136-0.306	0.142
Ag	977-1397	0.137-0.137	0.134
Zn	394-837	0.129-0.075	0.121
Sn	575-956	0.130-0.222	0.142

The radii used for comparison are those reported by Pauling for single-bond metallic situations. See L. Pauling, *Nature of the Chemical Bond*, Cornell University Press, Ithaca, NY, 1960, page 403.

In the comparisons shown in Table 12.5, self-diffusion data of pure elements were used to calculate the radii in the third column. Equations (12.41) and (12.42) have also been used to explain diffusing particles that differ in size from the host.<sup>20</sup> When the radius of the diffusing particle is large compared to the host, Eq. (12.41) is the better choice. When the radius of the diffusing particle is approximately equal to that of the host, then Eq. (12.42) is better. In spite of the shortcomings of the hydrodynamic assumptions leading to Eqs. (12.41)

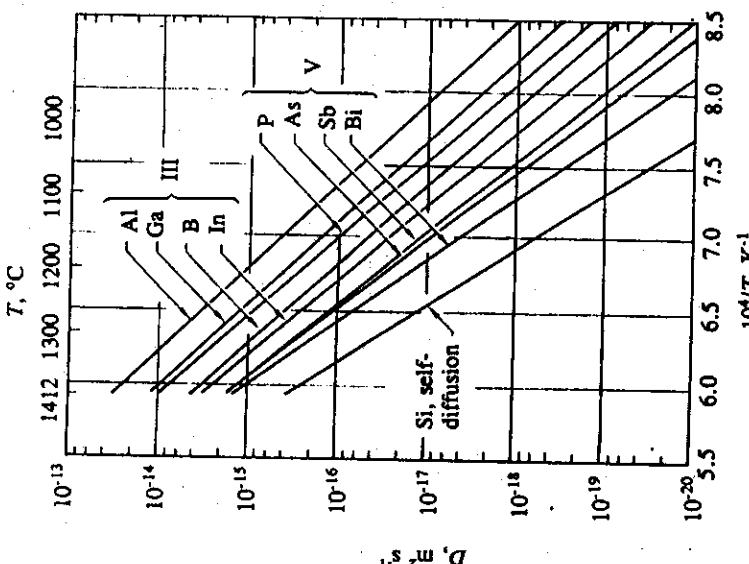


Fig. 12.16 Diffusion coefficients for Group III and Group V elements in Si. (From R. J. Borg and G. J. Dienes, *Ibid.*, page 201.)

## 12.5 DIFFUSION IN LIQUIDS

As in the previous chapters, in which the transport properties of liquids were discussed, the predicting, correlating, and extrapolating of diffusion data in liquids are difficult because of our lack of understanding of the structure of liquids. The difficulties of making accurate experimental determinations of diffusion coefficients in liquids due to natural convection, and the problems of sampling, further complicate the diffusion problem. In the following sections, we discuss various theories of the liquid state as they relate to diffusion, and then present data for a variety of liquids.

### 12.5.1 Liquid state diffusion theories

**Hydrodynamical theory.** The earliest theoretical equation for prediction of self-diffusion in a liquid is that of Einstein.<sup>18</sup> In this theory, the diffusing species are non-reacting spherical particles of radius  $R$  moving through a continuous medium of viscosity  $\eta$  with

<sup>18</sup>A. Einstein, *Ann. Phys. (Leipzig)* 17, 549 (1905).

<sup>19</sup>W. Sutherland, *Philosophical Magazine* 9, 781 (1905).

<sup>20</sup>T. Iida and R. I. L. Guthrie, *The Physical Properties of Liquid Metals*, Clarendon Press, Oxford, 1988, pages 214-215.

and (12.42), they have proven to be useful in that they have been used as the basis for semiempirical equations of the form

$$D^* = A \left[ \frac{T_M}{M} \right]^{1/2} V_M^{1/3}, \quad (12.43)$$

where  $A$  is a constant,  $M$  is the atomic weight or molecular weight,  $T_M$  is the melting point, and  $D^*$  and  $V_M$  are self-diffusion coefficient and molar (or atomic) volume, respectively, each evaluated at  $T_M$ . For liquid metals, Turkdogan<sup>21</sup> recommends  $A = 3.27 \times 10^{-6}$  and Iida and Guhrie<sup>22</sup> recommend  $3.5 \times 10^{-6}$ , when the variables in Eq. (12.43) are in c.g.s. units.

The Sutherland-Einstein equation is useful in predicting self-diffusion data for a wide variety of other substances, including molten semiconductors, polar liquids, associated liquids, and molten sulfur. If we assume that the atoms in the liquid are in a cubic array, then for materials generally the simple theory predicts that

$$2R = (\hat{V}/N_0)^{1/3},$$

and

$$D^* = \frac{k_B T}{2\pi} \left[ \frac{N_0}{\hat{V}} \right]^{1/3}, \quad (12.44)$$

where  $\hat{V}$  is the molar volume and  $N_0$  is Avogadro's number.

**Hole theory.** The oldest structural picture of a liquid is the hole theory which presumes the existence of holes or vacancies randomly distributed throughout the liquid and providing ready diffusion paths for atoms or ions. The concentration of these holes would have to be very great in order to account for the volume increase upon melting, thus resulting in much higher diffusion rates in liquids than in solids just below the melting point. Thus jump in  $D$  on melting is obvious in Fig. 12.5. The hole theory, however, does not result in a prediction of diffusion coefficients by itself, although it has been used to estimate the activation energy for self-diffusion in a liquid, by assuming that this energy is equal to that required to form a hollow sphere (hole) of a diameter on the order of a nanometer.

**Eyring theory.** Eyring *et al.*<sup>23</sup> applied their activated state theory of diffusion, which works reasonably well in solids, to liquid diffusion, assuming that the migrating atoms move from hole to hole in the liquid by a process of discrete jumps. If the liquid is considered quasi-crystalline, and the atoms are in a cubic configuration, then an expression relating  $D^*$  and  $\eta$  results:

$$D^* = \frac{k_B T}{2R\eta}. \quad (12.45)$$

Reynik proposed a small fluctuation model which also predicts a linear temperature dependence of  $D^*$  on  $T$  (K):

$$D^* = a + bT, \quad \text{cm}^2 \text{ s}^{-1}, \quad (12.46)$$

where  $a = 1.72 \times 10^{-4} ZX_K K$ ,  $b = 2.08 \times 10^{-9} ZX_K$ ,  $Z$  = number of nearest neighbors,  $X_0$  = maximum diffusive displacement due to normal vibrations, Å, and  $K$  = a force constant.

Since

$$X_0 = \bar{d} - 2R, \quad (12.47)$$

where  $\bar{d}$  = average interatomic distance in the liquid, Å, and  $R$  = ion radius, Å, the evaluation of this theory relies on the use of x-ray data for  $\bar{d}$  and  $Z$ , and  $b$ -values obtained from correlations to fit an equation of the form of Eq. (12.46). From the calculated values of  $X_0$  and Eq. (12.47),  $R$ -values are obtained which agree quite closely with Pauling's neutral atom radii, suggesting that in liquid metals the diffusing ion core carries its valence electrons with it.

The problem of all the theoretical approaches is that the tests of the theories rely on the functional relationship between  $D$  and  $T$ . For example, while Reynik can reasonably fit liquid

This expression obviously predicts  $D^*$  values six times larger than that given by the Sutherland-Stokes equation. Subsequent revisions of this equation by Li and Chang,<sup>24</sup> and by Eyring *et al.*<sup>25</sup> improved the agreement with the Sutherland-Stokes equation, but do not shed any more light on the structure of liquids, nor are they any more useful from a prediction standpoint.

**Fluctuation theory.** Because the ideas of a well-defined "activated state" as well as of discrete "holes" in the liquid have been difficult to accept, Cohen and Turnbull,<sup>26</sup> and later, Swalin<sup>27</sup> and Reynik<sup>28</sup> developed the fluctuation theory. In this theory, the "extra" volume in the liquid (over that of the solid) is distributed evenly throughout the liquid, making the average nearest neighbor distance increase. One may imagine a diffusing atom contained in a cage whose dimensions are constantly fluctuating. Local fluctuations in density then occasionally open up holes or openings in the cage large enough to allow the atom to diffuse out of the cage. In their approach, Cohen and Turnbull consider that a critical fluctuation must occur before diffusion occurs, whereas Swalin and Reynik both think that a spectrum of fluctuations occurs, with cooperative motion of the neighboring atoms resulting in diffusive motion of an atom. No activation energy is required, since there is virtually no difference between an atom moving forward as a result of cooperative movements and an atom not moving. The result of Swalin's theory<sup>29,30</sup> is that  $D^*$  exhibits a linear dependence on temperature.

Reynik proposed a small fluctuation model which also predicts a linear temperature dependence of  $D^*$  on  $T$  (K):

$$D^* = a + bT, \quad \text{cm}^2 \text{ s}^{-1}, \quad (12.46)$$

<sup>21</sup>E. T. Turkdogan, *Physical Chemistry of High Temperature Technology*, Academic Press, New York, 1980, page 115.

<sup>22</sup>T. Iida and R. I. L. Guhrie, *ibid.*, page 212.

<sup>23</sup>H. Eyring, S. Glasstone, and K. Laidler, *Theory of Rate Processes*, McGraw-Hill, New York, 1941.

<sup>24</sup>J. C. M. Li and P. Chang, *J. Chem. Physics* **23**, 518 (1955).

<sup>25</sup>H. Eyring, T. Ree, D. Grant, and R. Hirst, *Z. Elektrochem.* **64**, 146-152 (1962).

<sup>26</sup>M. H. Cohen and D. Turnbull, *J. Chem. Physics* **31**, 1164 (1959).

<sup>27</sup>R. A. Swalin, *Acta Met.* **7**, 736 (1959).

<sup>28</sup>R. J. Reynik, *Trans. AIME* **245**, 75 (1969).

<sup>29</sup>R. J. Reynik, *Applied Physics Letters* **9**, 239 (1966).

<sup>30</sup>R. Swalin and V. G. Leak, *Acta Met.* **13**, 471 (1965).

metal diffusion data to a linear relationship, Saxton and Sherby<sup>31</sup> concluded that diffusion in liquid metals is a thermally activated process, obeying an Arrhenius relationship (Eq. (12.27)), which is clearly at odds with a linear relationship with  $T$ . The activation energies  $Q$  are apparently not large, and so, when the  $RT$  term is on the same order of magnitude as  $Q$ ,  $D$  is not a strong function of temperature. Thus critical tests of these models is difficult.

It should also be stated that the methods of molecular dynamics and computer simulations have recently shown that the concepts of "holes" and activated rate theory do not physically represent diffusion in non-ionic liquids.<sup>32</sup> The reason becomes quite clear if we look at the results of simulations of trajectories of molecules in a solid, liquid, and gas, which are shown in Fig. 12.17.

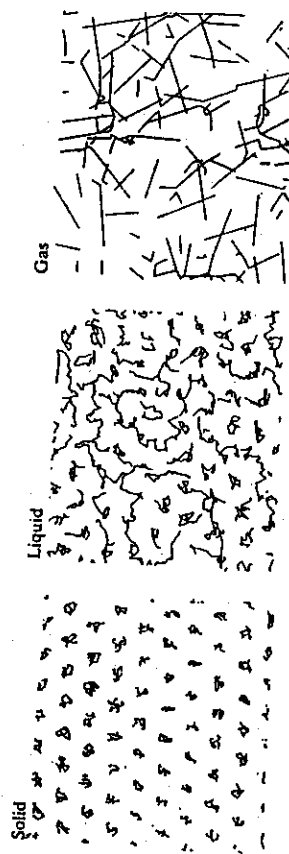


Fig. 12.17 Simulations of trajectories of molecules in solid, liquid, and gas. (Reproduced from T. Iida and R. I. L. Guthrie, *ibid.*, page 5.)

In the solid, the molecules are constrained to highly localized positions in the crystal, whereas the molecules in the liquid and the gas are free to wander. The major differences between the two fluids are the mean free path between collisions and the average velocity of the particles. Therefore, activated rate theory, which has proven to be quite useful in understanding diffusion in solids, does not appear to be applicable for diffusion in liquids.

### 12.5.2 Liquid diffusion data

The remarkable characteristic of diffusion in liquid metals, and in liquids in general, is the fact that the values of  $D$  are almost all approximately the same order of magnitude,  $10^{-9}\text{--}10^{-8} \text{ m}^2 \text{ s}^{-1}$ , even though their solid-state properties differ widely. Furthermore, the activation energies are also approximately equal, usually in the range 4 to 16 kJ mol<sup>-1</sup>. Because the data are still presented in the Arrhenius form, we present the data in this section in the same way.

**Diffusion in liquid metals.** Figure 12.18 gives some data for self-diffusion in pure liquid metals, Fig. 12.19 for interdiffusion in common nonferrous binary alloys, and Fig. 12.20 for

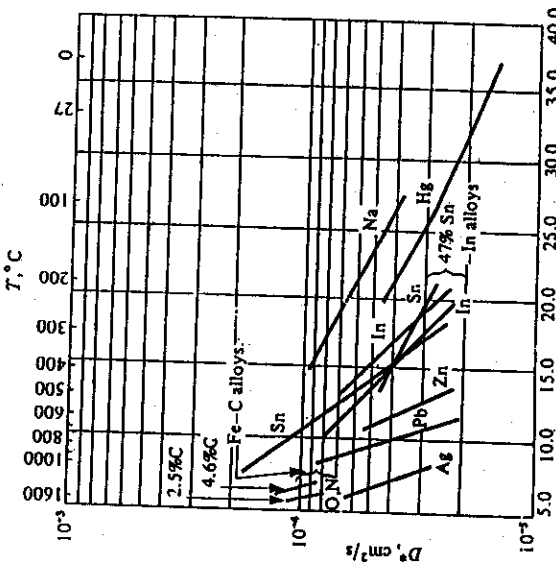


Fig. 12.18 Self-diffusion data in liquid metals.

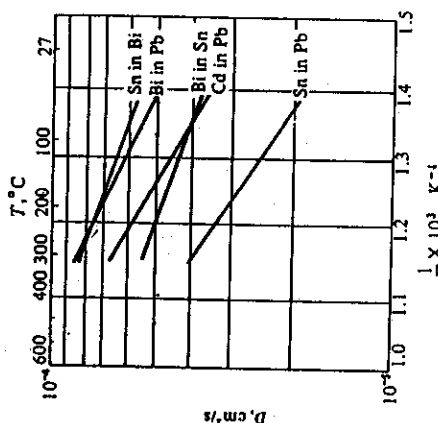


Fig. 12.19 Interdiffusion coefficients in liquid nonferrous alloys.

<sup>31</sup>H. Saxton and O. Sherby, *Trans. ASM* **55**, 826 (1962).

<sup>32</sup>J. S. Kirkaldy and D. J. Young, *ibid.*, page 90.

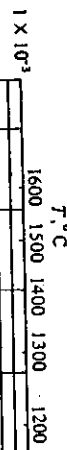


Fig. 12.20 Interdiffusion coefficients in ferrous liquid alloys  
 (—) carbon-saturated; (---) pure Fe.

ferrous alloys. We refer the reader to Edwards *et al.*,<sup>33</sup> Yang and Derge,<sup>34</sup> Elliott *et al.*,<sup>35</sup> or Brandes<sup>36</sup> for listings of data.

**Diffusion in molten salts and silicates.** Again, we know so little of the detailed structure of molten halides, sulfides, oxides, and silicates, that no really satisfactory quantitative expression is available for predicting diffusivities in these materials. However, if we refer

to Chapter 1 in which we discussed the relationship between bonding and viscosity, we realize that the same semiquantitative arguments can be used with regard to diffusion in these materials, particularly in light of the Stokes-Einstein model of diffusion.

Consider first the molten salts. We may describe their structure as holes within a molecular assembly that has density fluctuations and short-range order, but with the added restriction of electroneutrality, so that the cation and anion charge densities must remain equal in any region of the melt. Diffusion coefficients measured in molten salts are remarkably close to values observed in liquid metals, even though there is an obvious difference in bonding. Molten salts have highly polarized ionic bonds, in contrast to the metallic bond. Table 12.6 gives some typical data for self-diffusion in molten salts. Note that the activation energies for the salts are, however, larger than the activation energies for self-diffusion in metals.

Table 12.6 Self-diffusivities in molten salts<sup>1</sup>

Diffusate	Melt	Temp range, °C	$D_0 \times 10^6$ , $\text{m}^2/\text{s}$	$Q$ , $\text{kJ/mol}$	Typical $D^*$ value, $\text{m}^2/\text{s}$	°C
Na	NaCl	845-916	8	16.7	$14.2 \times 10^{-9}$	906
Cl	NaCl	825-942	23	29.7	$8.8 \times 10^{-9}$	933
Na	NaNO <sub>3</sub>	315-375	12.88	20.8	$2.00 \times 10^{-9}$	328
NO <sub>3</sub>	NaNO <sub>3</sub>	315-375	8.97	21.2	$1.26 \times 10^{-9}$	328
Tl	TlCl	487-577	7.4	19.2	$3.89 \times 10^{-9}$	502
Zn	ZnBr <sub>2</sub>	394-650	790	67.2	$0.22 \times 10^{-9}$	500

<sup>1</sup>Data from L. Yang and G. Derge, *ibid.*

In molten silicates, the picture is more complicated; from the relation between the degree of polymerization of the silicates and their viscosity, we can postulate that the diffusivity of oxygen, for example, is lower in the more acid silicates, and increases rapidly as the concentration of free oxygen ions increases near the orthosilicate composition. On the other hand, the diffusivity of basic cations should not depend on the slag composition to such an extent.

There are relatively few diffusion data available for molten silicates; some, which are relevant to metallurgical slags and mattes, are presented in Table 12.7. The curious result, which has not yet been satisfactorily explained, is that the tracer self-diffusion coefficient of oxygen in a basic slag is greater than that of silicon and aluminum, but we may explain this on the basis that silicon is tied up in  $\text{SiO}_4^{4-}$  ions, which clearly do not diffuse as easily as the smaller  $\text{O}^{2-}$  ions; aluminum is probably tied up in  $\text{AlO}_4^{3-}$  ions, which diffuse only a fraction more easily than the  $\text{SiO}_4^{4-}$  ions. Note also that the activation energies are now quite large, in correspondence to the increased difficulty of movement of these complex molecules, presumably requiring much more complicated relative movements of nearest neighbor ions in order to affect any net movement of a molecule. Diffusion data for slags and liquid glasses are also reviewed and presented by Turkdogan.<sup>37</sup>

<sup>33</sup>J. B. Edwards, E. E. Hucke, and J. J. Martin, *Metallurgical Reviews* 13, No. 120, 1 (1968).

<sup>34</sup>L. Yang and G. Derge, paper in *Physical Chemistry of Process Metallurgy*, AIME 7, 195 (1961).

<sup>35</sup>J. F. Elliott, M. Gleiser, and V. Ramachandra, *Thermochemistry for Steelmaking II*, Addison-Wesley, 1963.

<sup>36</sup>E. A. Brandes (Editor), *Smithells Metals Reference Book*, Sixth Edition, Butterworths, London, 1983, Chapter 13.

<sup>37</sup>T. T. Turkdogan, *Physicochemical Properties of Molten Slags and Glasses*, The Metals Society, London, England, 1983, pages 40-51.

Table 12.7 Self-diffusivities in molten silicates and sulfides<sup>a</sup>

System	Temp. range, °C	$D_0 \times 10^8$ , $\text{m}^2 \text{s}^{-1}$	$Q$ , $\text{kJ mol}^{-1}$	$D^*$ , $\text{m}^2 \text{s}^{-1}$
Ca in CaO-Al <sub>2</sub> O <sub>3</sub> -SiO <sub>2</sub> (39/21/40)	1350-1540	—	290	$6.7 \times 10^{-11}$ (1673 K)
Ca in CaO-Al <sub>2</sub> O <sub>3</sub> -SiO <sub>2</sub> (40/20/40)	1350-1450	—	290	$6.2-6.7 \times 10^{-11}$ (1673 K)
Si in CaO-Al <sub>2</sub> O <sub>3</sub> -SiO <sub>2</sub> (40/20/40)	1350-1460	—	290	$1 \times 10^{-11}$ (1703 K)
O in CaO-Al <sub>2</sub> O <sub>3</sub> -SiO <sub>2</sub> (40/20/40)	1370-1520	—	40	$4 \times 10^{-10}$ (1703 K)
Fe in CaO-Al <sub>2</sub> O <sub>3</sub> -SiO <sub>2</sub> (30/15/55)	1500	—	—	$2.4-3.1 \times 10^{-10}$
Fe in CaO-Al <sub>2</sub> O <sub>3</sub> -SiO <sub>2</sub> (43/22/35)	1500	—	—	$2.1-5.0 \times 10^{-10}$
Fe in FeO-SiO <sub>2</sub> (61/39)	1250-1305	—	170	$9.6 \times 10^{-9}$ (1548 K)
P in CaO-Al <sub>2</sub> O <sub>3</sub> -SiO <sub>2</sub> (40/21/39)	1300-1500	—	195	$2 \times 10^{-10}$ (1673 K)
Fe in Fe-S (33.5%)	1150-1238	65.7	56.9	
Fe in Fe-S (31.0%)	1164-1234	298	71	
Fe in Fe-S (29.0%)	1158-1254	20200	116	
Fe in Fe (48.1%) - Cu (20.5%) - S (31.9%)	1160-1250	1440	90.0	
Fe in Fe (32.0%) - Cu (40.0%) - S (28.0%)	1168-1244	35.7	57.3	
Cu in Cu-S (19.8%)	1160-1256	69.3	53.6	
Cu in Fe (32.0%) - Cu (40.0%) - S (28.0%)	1160-1245	564	82.4	

<sup>a</sup>Data from L. Yang and G. Derge, *ibid.*

Table 12.8 Diffusivities in common liquids at 298 K

Solute	Solvent	Concentration	$D, \text{m}^2 \text{s}^{-1}$
HCl	Water	0.1 M	$3.05 \times 10^{-9}$
NaCl	Water	0.1 M	$1.48 \times 10^{-9}$
CaCl <sub>2</sub>	Water	0.1 M	$1.10 \times 10^{-9}$
H <sub>2</sub>	Water	Dilute	$5.0 \times 10^{-9}$
O <sub>2</sub>	Water	Dilute	$2.5 \times 10^{-9}$
SO <sub>2</sub>	Water	Dilute	$1.7 \times 10^{-9}$
NH <sub>3</sub>	Water	Dilute	$2.0 \times 10^{-9}$
Cl <sub>2</sub>	Water	Dilute	$1.44 \times 10^{-9}$
H <sub>2</sub> SO <sub>4</sub>	Water	Dilute	$1.97 \times 10^{-9}$
Na <sub>2</sub> SO <sub>4</sub>	Water	0.01 M	$1.12 \times 10^{-9}$
K <sub>2</sub> Fe(CN) <sub>6</sub>	Water	0.01 M	$1.18 \times 10^{-9}$
Ethanol	Water	X = 0.05	$1.13 \times 10^{-9}$
Glucose	Water	0.39%	$0.67 \times 10^{-9}$
Benzene	CCl <sub>4</sub>	Dilute	$1.53 \times 10^{-9}$
CCl <sub>4</sub>	Benzene	Dilute	$2.04 \times 10^{-9}$
B <sub>2</sub>	Benzene	Dilute	$2.7 \times 10^{-9}$
CCl <sub>4</sub>	Kerosene	Dilute	$0.96 \times 10^{-9}$
CO <sub>2</sub>	Ethanol	Dilute	$4.0 \times 10^{-9}$
CCl <sub>4</sub>	Ethanol	Dilute	$1.50 \times 10^{-9}$
Phenol	Ethanol	Dilute	$0.89 \times 10^{-9}$

In common liquids, Table 12.8 gives some data for diffusivities in aqueous and organic solvents. Again, note that they are all on the order of  $10^{-9} \text{ m}^2 \text{s}^{-1}$ , even though there are obvious differences in bonding between these liquids and liquid metals or slags.

## 12.6 DIFFUSION IN GASES

In gases, we are not faced with the problem of Kirkendall shift phenomena, since any tendency for more A molecules to go in one direction than B molecules in the opposite direction is immediately counteracted by the fact that a pressure gradient cannot build up; thus in gases,  $D_A = D_B = D_{AB}$ . Of course, one must still superimpose the bulk flow term in Eq. (12.7) onto Fick's first law to obtain the total flux if there is convection.

Chemists and chemical engineers have spent a great deal of time and effort in developing equations which predict diffusion coefficients in gases. For example, based on the kinetic theory of gases, the following equation applies to prediction of self-diffusivity of spherical A atoms diffusing in pure A:

$$D_A^* = \frac{2}{3} \left[ \frac{\kappa_B^3}{\pi m_A} \right]^{1/2} \frac{T^{3/2}}{P^{1/2}} \quad (12.48)$$

For the interdiffusivity of two unequal size spherical atoms A and B, kinetic theory predicts

$$\Omega_{AB} = \frac{2}{3} \left[ \frac{\kappa_B^3}{\pi m_A} \right]^{1/2} \left[ \frac{1}{2m_A} + \frac{1}{2m_B} \right]^{1/2} \left[ \frac{T^{3/2}}{P \left[ \frac{d_A + d_B}{2} \right]^2} \right] \quad (12.49)$$

where  $\kappa_B$  = Boltzmann's constant,  $1.38 \times 10^{-16}$  ergs molecule<sup>-1</sup> K<sup>-1</sup>,  $d$  = molecular diameter, cm,  $m$  = molecular mass, g molecule<sup>-1</sup>,  $P$  = pressure, dyn cm<sup>-2</sup>, and  $T$  = temperature, K.

Equations (12.48) and (12.49) give the proper pressure dependence up to about 10 atm; the predicted temperature dependency is only qualitatively correct in that  $D_{AB}$  actually varies more with temperature.<sup>38</sup>

To predict  $D_{AB}$  more accurately, it is better to apply the Chapman-Enskog theory than the above equations. For monoatomic gases, which act ideally, we have

$$D_{AB} = \frac{0.0018553 T^{3/2}}{P (\sigma_{AB})^2 \Omega_{D,AB}} \left[ \frac{1}{M_A} + \frac{1}{M_B} \right]^{1/2} \quad (12.50)$$

where  $\sigma_{AB} = \frac{1}{2}(\sigma_A + \sigma_B)$  = collision diameter, Å,  $\Omega_{D,AB}$  = collision integral for A-B mixture at dimensionless temperature,  $T_{AB}^*$ , for the Lennard-Jones potential.

<sup>a</sup>Chemical engineers often use the notation  $D_{AB}$  to refer to the diffusion of A in an A-B mixture. This is the same as  $\bar{D}$ , which, if  $D_A = D_B$ , is also equal to  $D_A$  and to  $D_B$ .

<sup>38</sup>R. B. Bird, W. E. Stewart, and E. N. Lightfoot, *ibid.*

Table 12.9 Estimated collision diameters for metal vapors\*

Metal	Melting point, °C	Boiling point, °C	Molar volume, cm³ mol⁻¹	$\sigma, \text{Å}$
			$\hat{V}(\text{sol})$	$\hat{V}(\text{liq})$
Ag	960.8	2163	11.02	11.60
Al	660	2057	10.49	11.36
Bi	271	1477	—	20.76
Cd	321	765	13.34	14.01
Co	1493	2877	7.14	7.68
Cu	1083	2570	7.58	8.01
Fe	1535	2833	7.60	7.94
Ga	29.8	1983	—	11.43
Hg	-38.9	357	14.09	14.65
In	156.4	2087	15.94	16.33
K	63.7	760	46.0	47.10
Li	186	1317	13.27	13.40
Mg	651	1103	14.66	15.47
Na	97.9	883	24.04	24.79
Ni	1453	2816	7.11	7.57
Pb	327.4	1717	18.35	19.39
Pt	637	3300	14.20	14.49
Sb	630.5	1440	18.59	18.74
Sn	231.9	2770	16.41	17.04
Tl	303	1457	—	18.10
Zn	419.5	906	9.56	9.45
			10.19	2.59
				2.51

The values of the force parameters and the collision diameters for common gases are given in Table 1.1, and the collision integral can be calculated<sup>39</sup>:

$$\Omega_{AB} = \frac{A}{T_{AB}^{*B}} + \frac{C}{\exp DT_{AB}^{*B}} + \frac{E}{\exp FT_{AB}^{*B}} + \frac{G}{\exp HT_{AB}^{*B}}, \quad (12.51)$$

where  $A = 1.06036$ ,  $B = 0.15610$ ,  $C = 0.19300$ ,  $D = 0.47635$ ,  $E = 1.03587$ ,  $F = 1.52996$ ,  $G = 1.76474$ , and  $H = 3.89411$ . Note that the collision integral values for diffusion are only slightly different from those for gas viscosity calculations.

The force parameters for metal vapors are not well known, but Turkdogan<sup>40</sup> has estimated many of them. For  $\varepsilon/k_B$ , he recommends

$$\varepsilon/k_B = 1.15 T_b, \text{ K}, \quad (12.52)$$

and

$$\varepsilon/k_B = 1.92 T_M, \text{ K}, \quad (12.53)$$

where  $T_b$  and  $T_M$  are the boiling and melting temperatures, respectively. Although Eqs. (12.52) and (12.53) give somewhat different values of  $\varepsilon/k_B$ , the errors in  $D_{AB}$ , particularly at temperatures greater than  $T_M$ , are not great. Melting points, boiling points, molar volumes, and Turkdogan's estimates of collision diameters are given in Table 12.9.

Example 12.1 Calculate the diffusion coefficient for iron vapor diffusing through argon, at 1600°C, assuming that pure iron is the source of the vapor.

**Solution.** Using the Chapman-Enskog equation, we obtain

$$D_{Fe-At} = \frac{0.001858(1873)^{3/2}}{(1)(\sigma_{Fe-At})^2} \left[ \frac{1}{55.85} + \frac{1}{39.54} \right]^{1/2}$$

We evaluate  $\sigma_{Fe-At}$  from the data in Tables 1.1 and 12.9:

$$\sigma_{Fe-At} = \frac{\sigma_{Fe} + \sigma_{At}}{2} = \frac{2.43 + 3.42}{2} = 2.92 \text{ Å.}$$

which gives  $\Omega_{Fe-At} = 0.92$ . Finally,

$$\left[ \frac{\varepsilon}{k_B} \right]_{Fe-At} = \left[ \frac{\varepsilon}{k_B} \right]_{Fe}^{1/2} \left[ \frac{\varepsilon}{k_B} \right]_{At}^{1/2} = \sqrt{3521 \times 124} = 655 \text{ K.}$$

Then

$$T^* = \left[ \frac{\varepsilon}{k_B} \right]_{Fe-At} T = \frac{1873}{655} = 2.86,$$

$$D_{Fe-At} = \frac{0.001858(1873)^{3/2}}{(1)(2.92)^2(0.92)} \left[ \frac{1}{55.85} + \frac{1}{39.54} \right]^{1/2} = 4.00 \text{ cm}^2 \text{ s}^{-1}$$

$$= 4.00 \times 10^{-4} \text{ m}^2 \text{ s}^{-1}.$$

<sup>39</sup>R. C. Reid, J. M. Prausnitz, and T. K. Sherwood, *The Properties of Gases and Liquids*, third edition, McGraw-Hill, New York, NY, 1977, pages 549 and 550.

<sup>40</sup>E. T. Turkdogan, paper in *Steelmaking, The Chapman Conference*, J. F. Elliott (ed.), Addison-Wesley, Reading, Massachusetts, 1962.

Many other correlations have been developed for nonmetallic gases. The most successful correlation, which makes the prediction of  $D_{AB}$  over a wide range of binary gas systems and

temperatures possible, is that of Fuller *et al.*<sup>41</sup>. They correlated 340 data points in a theoretically justified form, predicted  $D_{AB}$  to within 10% of the measured values 92.6% of the time, and had an average error of only 4.3% and a standard deviation of 6.17%. Their equation is

$$D_{AB} = \frac{(1 \times 10^{-3})T^{1.75}}{P(v_B^{1/3} + v_A^{1/3})^2} \left[ \frac{1}{M_A} + \frac{1}{M_B} \right]^{1/2}, \quad \text{cm}^2 \text{s}^{-1}, \quad (12.54)$$

where  $T$  = temperature, K,  $P$  = pressure, atm,  $M_A$ ,  $M_B$  = molecular weight of species A and B, g mol<sup>-1</sup>, and  $v_A$ ,  $v_B$  = diffusion volumes, given for simple molecules in Table 12.10. This approach is relatively simple and avoids the necessity to evaluate the collision integral.

Table 12.10 Diffusion volumes for simple molecules\*

Molecule	$v$	Molecule	$v$	Molecule	$v$
H <sub>2</sub>	7.07	Ne	5.59	NH <sub>3</sub>	14.9
D <sub>2</sub>	6.70	Ar	16.1	H <sub>2</sub> O	12.7
He	2.88	Kr	22.8	Cl <sub>2</sub>	37.7
N <sub>2</sub>	17.9	CO	18.9	Br <sub>2</sub>	67.2
O <sub>2</sub>	16.6	CO <sub>2</sub>	26.9	SO <sub>2</sub>	41.1
Air	20.1	N <sub>2</sub> O	35.9		

\*From E. N. Fuller, P. D. Schettler, and J. C. Giddings, *ibid.*

Values of  $D_{AB}$  in gas phases are usually in the range  $10^{-5}$  to  $10^{-3}$  m<sup>2</sup> s<sup>-1</sup>. Figure 12.21 gives some representative data.

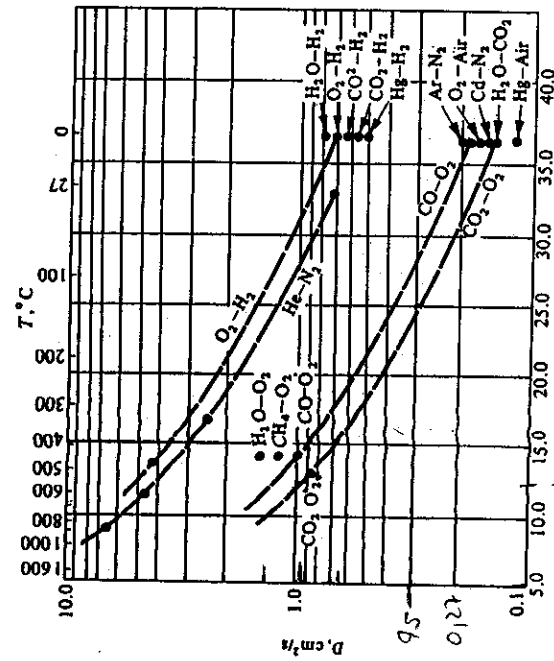


Fig. 12.21 Diffusion coefficients in gas mixtures.

As we have pointed out in previous chapters, materials engineers often encounter situations where they must deal with the properties of solids containing some degree of porosity. Gas diffusion through porous media is important in such fields as ore reduction or roasting, vapor penetration into foundry sands, outgassing of powder metallurgy and ceramic compacts, gas phase alloying of powders, and catalysis.

In general, gas phase diffusion through porous media occurs by one of two mechanisms: ordinary diffusion or Knudsen diffusion. (A third mechanism, surface diffusion, may be important at low temperatures, but for most elevated temperature processes, it is negligible.) The size of the pores through which diffusion is taking place determines whether ordinary or Knudsen diffusion predominates. With ordinary diffusion, the pores are large *relative to the mean free path* of the gas molecules. Knudsen diffusion is important when the pores are small in relation to the mean free path.

When ordinary diffusion prevails, the total diffusion path, from one plane in the porous media to a parallel plane, is longer than when no aggregate is present, because of the irregularity of the porosity. Even after correcting for the decrease in cross-sectional area available for diffusion, using the void fraction,  $\omega$ , we must make a further decrease in the  $D_{AB}$  value, in order to yield the *effective interdiffusivity*. We accomplish this by introducing a new factor, the *tortuosity*,  $\tau$ , so that

$$D_{AB,\text{eff}} = \frac{D_{AB}\omega}{\tau}. \quad (12.55)$$

The tortuosity is a number greater than one, ranging from values of 1.5-2.0 for unconsolidated particles, to as high as 7 or 8 for compacted particles. It is not a function of the void fraction, but does depend on the particle size, particle size distribution, and particle shape. Estimates of the tortuosity may be made by comparisons with previous results using similar materials, such as presented in Fig. 12.22.

When the gas density is low, or the pore size small, then the molecules have a higher probability of collision with the pore walls than with each other, similarly as in the flow of molecules in a vacuum system. An analysis of the flow of molecules through a cylindrical pore of radius  $r$  under a concentration gradient yields

$$j_A = \frac{2}{3} r \bar{V} \left[ \frac{\partial C_A}{\partial x} \right].$$

By using Eq. (1.4) for  $\bar{V}$ , the average speed of the molecules, and comparing it with Fick's first law, we obtain the Knudsen diffusion coefficient:

$$D_K = 9700r \sqrt{T/M}, \quad \text{cm}^2 \text{s}^{-1}, \quad (12.56)$$

where  $r$  = pore radius, cm,  $T$  = temperature, K, and  $M$  = molecular weight of the diffusing species, g mol<sup>-1</sup>. Since collisions between species are negligible at low pressures, this equation applies equally to any component present.

There are two tests that we may use to determine when ordinary diffusion no longer predominates and Knudsen diffusion becomes important. In the first test, we may estimate the pore radius and compare it to the mean free path of the gas  $\lambda$ , given by

$$\lambda = (\sqrt{2} \pi d^2 n)^{-1}, \quad (1.5)$$

Table 12.11 Knudsen diffusion and flow in porous media\*

Material	Gases	T, K	r, Å	$\tau$
Alumina pellets	N <sub>2</sub> , He, CO <sub>2</sub>	303	96	0.85
Fresh and regenerated silica-alumina cracking catalyst	H <sub>2</sub> , N <sub>2</sub>	298	31.50	2.1
Water-gas shift catalyst	O <sub>2</sub> , N <sub>2</sub>	298	177	2.7
Ammonia synthesis catalyst	O <sub>2</sub> , N <sub>2</sub>	298	203	3.8
Vycor glass	He, Ne, H <sub>2</sub> , A, N <sub>2</sub> , O <sub>2</sub> , Kr	292-298	30.50	5.9
Silica-alumina cracking catalyst	CH <sub>4</sub> , C <sub>2</sub> H <sub>6</sub>	273-323	16	0.725
Silica-alumina cracking catalyst	He, Ne, A, N <sub>2</sub>	273-323	24	0.285
Silica-alumina cracking catalyst	He, Ne, N <sub>2</sub>	420	(24)	5.6

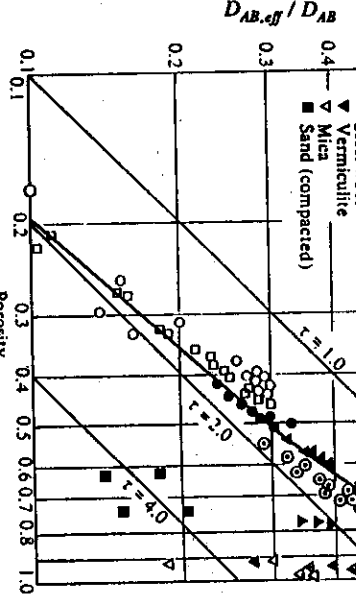
From L. N. Satterfield and T. K. Sherwood, *ibid.*

Fig. 12.22 Hydrogen-air diffusion in various unconsolidated porous media. (Adapted from L. N. Satterfield and T. K. Sherwood, *The Role of Diffusion in Catalysis*, Addison-Wesley, Reading, MA, 1963.)

where  $d$  = collision diameter of the molecule, cm, and  $n$  = concentration of the molecules,  $\text{cm}^{-3}$ . If  $r$  and  $\lambda$  are of the same order of magnitude, or if the pore diameter is only one order larger, then Knudsen diffusion is presumably important. At elevated temperatures, this may occur when pore diameters are on the order of  $10 \mu\text{m}$  or less.

The other test involves comparing the calculated values of  $D_{AB}$  and  $D_r$ . If the ratio  $D_{AB}/D_r$  is small, then we take ordinary diffusion as the rate determining step. Conversely, if  $D_{AB}/D_r$  is large, then we presume that Knudsen diffusion controls.

Since even the micropores are not straight and smooth, we must also define tortuosity for those systems where Knudsen diffusion predominates:

$$D_{K,\text{eff}} = \frac{D_r \omega}{\tau}. \quad (12.57)$$

The results of a large number of tests at relatively low temperatures where tortuosity has been calculated for systems in which Knudsen diffusion predominates are shown in Table 12.11.

**Example 12.2** Consider the diffusion of metal vapors into molding sand when steel is cast. Calculate the diffusion coefficient for manganese vapor through silica sand at 1600°C, assuming that the only other gas present is argon. The pore radius is 0.005 cm, and the porosity is 0.45.

**Solution.** The first step is to test for the importance of Knudsen diffusion. Calculating  $D_{Mn-Ar}$ , as in Example 12.1, we obtain  $3.4 \text{ cm}^2 \text{s}^{-1}$  for Mn at 1600°C. Then we calculate  $D_{K,\text{eff}}$  using Eq. (12.56).

$$D_K = (9700)(0.005) \left[ \frac{1873}{55} \right]^{1/2} = 283 \text{ cm}^2 \text{s}^{-1}.$$

which implies that in this situation ordinary diffusion controls.

As a further check, we calculate the mean free path of Mn vapor where  $n = 4.48 \times 10^{14} \text{ atoms}/\text{A}^3$ ,  $d = 2.4 \text{ \AA}$ , and  $\lambda = 1/\sqrt{2} \pi (4.48 \times 10^{14})(5.76) = 87 \text{ \AA}$ . Based on the fact that the pore size is on the order of  $10^5 \text{ \AA}$ , and  $\lambda_{Mn}$  is much less than that, we conclude that Knudsen diffusion is unimportant in this instance, and that we may analyze the problem in terms of ordinary diffusion.

The tortuosity  $\tau$  for metal vapor diffusion through porous compacts has a range 3-6, with 4 considered to be an average value.<sup>42</sup> Therefore, for a sand mold with a void fraction of 0.45, we have

$$D_{Mn-Ar,\text{eff}} = \frac{D_{Mn-Ar}\omega}{\tau} = \frac{(3.4)(0.45)}{(4.0)} = 0.383 \text{ cm}^2 \text{s}^{-1},$$

or

$$D_{Mn-Ar,\text{eff}} = 3.83 \times 10^{-5} \text{ m}^2 \text{s}^{-1},$$

which is approximately one-tenth the value in the gas phase alone.

### PROBLEMS

- 12.1 Show that the units in Eq. (12.1) are as indicated. Do the same for Eqs. (12.2) and (12.3).

- 12.2 Discuss the reasons why self-diffusion data must apply to homogeneous materials only.

- 12.3 Read one of the references of Footnote 1 and derive Eq. (12.5).

<sup>42</sup>J. M. Svoboda and G. H. Geiger, *Trans. AIME* **245**, 2363 (1969).

12.4 Look up the article by Compaan and Haven (Table 12.1) and summarize the method used to derive the correlation coefficients in Table 12.1.

12.5 Work out the units in Eq. (12.20).

12.6 Derive Eq. (12.28), after reading Zener's article.

12.7 / Using the method of Fuller, Schettler, and Giddings, estimate the diffusion coefficient for a  $\text{CO}_2\text{-O}_2$  gas mixture at 1 atm pressure and 700 K and compare the result to the data in Fig. 12.21.

12.8 Given a tortuosity of 2.0, a void fraction of 0.25, and  $r = 5 \times 10^{-3}$  cm, calculate the effective diffusion coefficient for  $\text{CO-CO}_2$  in a reduced iron oxide pellet at 800 K.

12.9 PbS has a NaCl-type structure. Would you expect the self-diffusion coefficient of Pb or S to be higher? How would you expect the addition of  $\text{Ag}_2\text{S}$  to affect the diffusion coefficient of Pb, knowing that the defects in PbS are predominantly Frenkel defects on the Pb sublattice, and that the undoped PbS is an n-type semiconductor? How would  $\text{Bi}_2\text{S}_3$  additions affect it? [Ref.: G. Simovich and J. B. Wagner, Jr., *J. Chem. Phys.* 38, 1368 (1963).]

12.10 / Describe the conditions under which the following terms are applicable: (1) self-diffusion, (2) tracer diffusion, (3) chemical diffusion, (4) interstitial diffusion, (5) substitutional diffusion, (6) interdiffusion coefficient, and (7) intrinsic diffusion.

12.11 Calculate the self-diffusion coefficient in liquid lead using the Sutherland hydrodynamical model, and the Eyring activated state model. Data for viscosity of liquid metals is given in Fig. 1.9. Calculate  $D^*$  at 873 K, 1073 K, and 1273 K. a) Do the calculated diffusion coefficients vary linearly with temperature according to the fluctuation model of Reynik? according to the Arrhenius relation (Eq. (12.27))? b) What is the error in the calculated values? Experimental results for liquid lead are given in Fig. 12.18.

12.12 The self-diffusion coefficients of gold and nickel in Au-Ni alloys are shown in Fig. 12.4. Show that the alloys of Au and Ni are not ideal solutions.

12.13 The diffusion coefficient of acetone vapor in air is  $1.1 \times 10^{-5} \text{ m}^2 \text{ s}^{-1}$  at 273 K and 1 atm. What is the diffusion coefficient at 500 K and 0.5 atm?

12.14 / The diffusion coefficient of He in Pyrex® is  $2.6 \times 10^{-16} \text{ m}^2 \text{ s}^{-1}$  at 373 K and  $1.6 \times 10^{-14} \text{ m}^2 \text{ s}^{-1}$  at 873 K. What is it at 1000 K? \*Pyrex® is a type of glass commonly used in laboratories.

12.15 The diffusion coefficient of oxygen in liquid copper is not linear with temperature. The following data are available:  
 at 1150°C,  $D = 7 \times 10^{-9} \text{ m}^2 \text{ s}^{-1}$   
 at 1250°C,  $D = 10^{-8} \text{ m}^2 \text{ s}^{-1}$ .  
 Predict the diffusion coefficient at 1350°C.

12.16 What is the diffusivity of Mg vapor in helium gas at 1200 K? The gas has a composition of 90 He and 10 Mg (by volume).

12.17 At 1500°C, the diffusivity of Cr in molten nickel is  $5 \times 10^{-9} \text{ m}^2 \text{ s}^{-1}$ . At 1600°C, it is  $7 \times 10^{-9} \text{ m}^2 \text{ s}^{-1}$ . Estimate the diffusivity at 1700°C.

12.18 Calculate the diffusion coefficient  $D_{AB}$  for zinc vapor diffusing through helium at 773 K.

12.19 At 1 atm. pressure and 1900 K, the diffusion coefficient for a gaseous suboxide ( $\text{Al}_2\text{O}$ ) in argon is  $5 \times 10^{-4} \text{ m}^2 \text{ s}^{-1}$ . Predict the diffusion coefficient for  $\text{Al}_2\text{O}$  in argon at 1900 K and  $10^{-6}$  atm.

12.20 At 273 K and 1 atm. the diffusion coefficient for cadmium vapor in nitrogen is  $1.5 \times 10^{-5} \text{ m}^2 \text{ s}^{-1}$ . Calculate the diffusion coefficient for cadmium vapor in helium at 1500 K and 0.5 atm.

12.21 To quantify the nucleation theory of the liquid to solid transformation, it is necessary to have a value of the self-diffusion coefficient for the liquid at temperatures significantly less than the freezing point. Given that  $D^*$  of liquid metal A is  $5 \times 10^{-9} \text{ m}^2 \text{ s}^{-1}$  at 1200 K and  $10^{-8} \text{ m}^2 \text{ s}^{-1}$  at 1500 K, estimate  $D^*$  at 900 K. Use two distinctly different methods and compare the two estimates.

12.22 At 1500°C the diffusion coefficient of Mo in an Fe melt is  $3 \times 10^{-9} \text{ m}^2 \text{ s}^{-1}$  and at 1600°C it is  $3.5 \times 10^{-9} \text{ m}^2 \text{ s}^{-1}$ . Predict the diffusion coefficient of Mo in an Fe melt which has been supercooled to 1200°C.

12.23 A binary gas of A and B molecules has a diffusion coefficient of  $10 \text{ cm}^2 \text{ s}^{-1}$  at 0°C and 1 atm. Predict the diffusion coefficient in the same gas at 500°C and 10 atm.

12.24 A chamber containing  $\text{O}_2(\text{g})$  and  $\text{N}_2(\text{g})$  is divided by a porous solid, 1 cm thick. On one side of the porous solid, there is continuous flow keeping the composition at 80 mole percent  $\text{O}_2$ . On the other side, there is also continuous flow which maintains the composition of  $\text{O}_2$  at 40 mole percent. The pressures and temperatures in both parts of the chamber are uniform and constant at 1 atm. and 1000 K, respectively. The porous solid has pores with an average radius of  $1 \mu\text{m}$ , a porosity of 0.2 and a tortuosity of 5. Calculate the flux of oxygen which diffuses through the porous solid.

## 13

### DIFFUSION IN SOLIDS

This chapter, in which the primary aim is to obtain solutions to Fick's laws of diffusion, is similar to Chapter 9 where we presented solutions to heat conduction problems. Therefore, much of the groundwork laid in Chapter 9 reappears in the following discussions. We begin by presenting some classical approaches used for determining diffusion coefficients in solids, and then consider some applied problems involving diffusion in solids as the rate-limiting step.

#### 13.1 STEADY-STATE DIFFUSION EXPERIMENTS

As an example of the application of Fick's first law, consider an iron tube held in the isothermal part of a furnace. A carburizing gas is passed through the inside of the tube, and a gas of a different composition is passed over the outside. The carbon activity, thus has a gradient from the inside surface to the outside surface. Steady state is reached when the carbon concentration at each point in the tube wall no longer changes with time. By this time, the appropriate differential equation for steady-state diffusion through a cylinder can be derived from shell balances. If the diffusion coefficient of carbon in iron is a constant, independent of composition, then by analogy with Eq. (9.13),

$$\frac{1}{r} \frac{d}{dr} \left[ r \frac{dC}{dr} \right] = 0. \quad (13.1)$$

The solution to this equation is given by its heat transfer analog from Eq. (7.51):

$$\frac{C - C_2}{C_1 - C_2} = \frac{\ln(r/r_2)}{\ln(r_1/r_2)}, \quad (13.2)$$

where  $r_1$  and  $r_2$  are the inside and outside radii of the tube, and  $C_1$  and  $C_2$  are the corresponding concentrations of carbon at these surfaces. Thus a plot of  $C$  versus  $\ln r$  should be a straight line. However, for carbon diffusing in  $\gamma$ -iron, the slope of such a plot, as shown in Fig. 13.1, becomes smaller on passing from the low-carbon side to the high-carbon side. Therefore, the diffusion coefficient must be a function of composition, Eqs. (13.1) and (13.2) do not apply, and we must approach the problem somewhat differently.

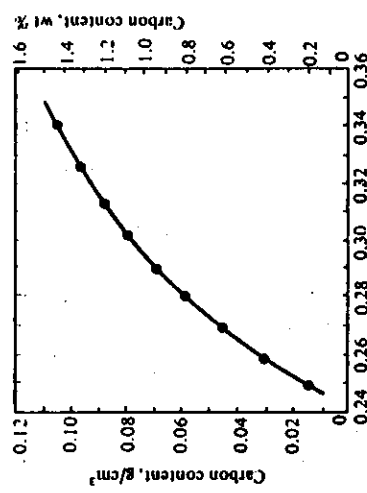


Fig. 13.1 Steady-state carbon concentration profile through a hollow cylinder of iron at 1000°C. (From R. P. Smith, *Acta Met.* 1, 578 (1953).)

In addition to the fact that  $\partial C/\partial t = 0$ , steady state also means that the quantity of carbon passing through the tube per unit time is constant and independent of  $r$ . Thus

$$J = 2\pi rl j_r, \quad (13.3)$$

where  $l$  = length of the cylinder,  $j_r$  = local flux, and  $J$  = quantity of carbon passing through the tube wall per unit time. Since

$$j_r = -D \frac{dC}{dr}, \quad (13.4)$$

we may express Eq. (13.3) as

$$r \left[ -D \frac{dC}{dr} \right] = \frac{J}{2\pi l},$$

or

$$\frac{dC}{d \ln r} = \frac{-J}{2\pi l D}. \quad (13.5)$$

For a given experiment, we can measure  $J$  and  $l$ , and if the carbon concentrations within the tube wall are determined by chemical analyses, then we can determine  $D$  from the slope of the plot of  $C$  versus  $\ln r$ .

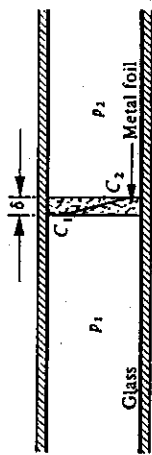


Fig. 13.2 Experiment for diffusion of hydrogen through metal foils.

The foils are very thin, and so it is extremely difficult to determine the concentration as a function of distance through the foil. The experimental results therefore consist of a measured steady-state flux, the hydrogen pressure drop across the foil, and the foil's thickness. To obtain  $D$  from the data, we take the value of  $C$  in the metal at each gas-metal interface as the solubility  $S$  that would exist in equilibrium with the gas.\* From Sievert's law, we know that for equilibrium between gas and the metal

$$S_1 = Kp_1^{1/2}, \quad (13.7a)$$

and

$$S_2 = Kp_2^{1/2}, \quad (13.7b)$$

in which  $K$  is the equilibrium constant for the reaction

$$\frac{1}{2}H_2(g) = H \text{ (in solution)}, \quad (13.8)$$

and  $p_1$  and  $p_2$  are the partial pressures of hydrogen on both sides of the foil with a thickness  $\delta$ , as shown in Fig. 13.2.

The gradient  $dC/dx$  can then be expressed in terms of the pressures:

$$\frac{dC}{dx} = \frac{S_1 - S_2}{\delta} = \frac{K}{\delta} (\sqrt{p_1} - \sqrt{p_2}). \quad (13.9)$$

Combining Eqs. (13.6) and (13.9), we obtain the flux:

$$j_x = \frac{-DK}{\delta} (\sqrt{p_1} - \sqrt{p_2}). \quad (13.10)$$

\*This is true under the conditions when the solution of gas in the surface of the metal occurs much more rapidly than the rate at which the diffusing species leaves the surface and enters the bulk metal. Experimentally, we check this assumption by determining the fluxes for two thicknesses of foil under the same pressure drop and temperature. If equilibrium does exist at the interface, then  $\Delta C$  is the same for both cases, and the flux is inversely proportional to the thickness.

In relation to the diffusion of gases through solids, the term *permeability*,  $P$ , is often used and defined by

$$P = DS = DK\sqrt{p}, \quad (13.11)$$

so that

$$j_x = \frac{-(P_1 - P_2)}{\delta}, \quad (13.12)$$

and permeability is then given by an equation of the form

$$P = Ap^{1/2}e^{-Q_p/RT}, \quad (13.13)$$

which includes the temperature dependence of both  $S$  and  $D$ , with  $A$  and  $Q_p$  as constants. Unfortunately, there are also other ways to define permeability, which is rather confusing. For example, using a different definition, we obtain the flux:

$$j_x = -\frac{P^*}{\delta} (\sqrt{p_1} - \sqrt{p_2}), \quad (13.14)$$

so that  $P^* = P = DS$  only at 1 atm pressure, or 1.013 MPa:

$$P^* = DK. \quad (13.15)$$

In this case, we have

$$P^* = P_0^* e^{-Q_p/RT}. \quad (13.16)$$

The units given to  $P^*$  and  $P_0^*$  are not typically S.I. units; rather  $P_0^* = \text{cm}^3(\text{STP}) \text{s}^{-1} \text{cm}^{-2}$  measured for 1 cm thickness and at 1 atm pressure, and  $Q_p = \text{cal mol}^{-1}$  (activation energy for permeation).

There are other sets of units which apply to  $P_0^*$  as well, and therefore one should be extremely careful of the term *permeability* because different definitions and units are used. Table 13.1 gives some representative data for various systems, using Eqs. (13.15) and (13.16) to define permeability. For data on permeability of gases through polymers, refer to Pauly.<sup>1</sup>

Table 13.1 Permeability data for gas-metal systems

Gas	Metal	$P_0^*$ , $\text{cm}^3(\text{STP}) \text{s}^{-1} \text{cm}^{-2} \text{atm}^{-1/2}$	$Q_p$ , $\text{cal mol}^{-1}$
H <sub>2</sub>	Ni	$1.2 \times 10^{-3}$	13 850
H <sub>2</sub>	Cu	$1.5-2.3 \times 10^{-4}$	16 000-18 700
H <sub>2</sub>	$\alpha$ -Fe	$2.9 \times 10^{-3}$	8400
H <sub>2</sub>	Al	$3.3-4.2 \times 10^{-1}$	30 800
N <sub>2</sub>	Fe	$4.5 \times 10^{-3}$	23 800
O <sub>2</sub>	Ag	$2.9 \times 10^{-3}$	22 550

<sup>1</sup>The units in Eq. (13.14) are:  $\delta = \text{cm}$ ,  $p = \text{atm}$ , and  $j_x = \text{cm}^3(\text{STP}) \text{s}^{-1} \text{cm}^{-2}$ .

**Example 13.1** The solubility of hydrogen dissolved in aluminum at 873 K is  $2.5 \times 10^{-4} \text{ cm}^3(\text{STP}) \text{g}^{-1}$ . Assume that Sievert's law holds. a) Calculate the equilibrium constant, b) the solubility in  $\text{g cm}^{-3}$ ; and c) the diffusion coefficient for hydrogen in aluminum at 873 K.

**Solution.** a) When solubility data are given in this manner, it is assumed that the condensed phase has been equilibrated with the gas at 1 standard atm of pressure. Then, according to Eq. (13.8), the equilibrium constant is

$$K = \frac{S}{p^{1/2}}.$$

Therefore,  $K$  is simply

$$K = \frac{2.5 \times 10^{-4} \text{ cm}^3(\text{STP})}{1 \text{ atm}^{1/2} \text{ g}} = 2.5 \times 10^{-4} \text{ cm}^3(\text{STP}) \text{ atm}^{-1/2} \text{ g}^{-1}.$$

b) Notice the curious units for the atomic hydrogen dissolved in the aluminum (i.e., the solubility). The solubility is the mass of *molecular* hydrogen, expressed as a volume at standard temperature and pressure (STP). We did not invent these units, but they are the units most often given. Let's calculate a concentration in more familiar units. The density of Al at 873 K is  $2.55 \text{ g cm}^{-3}$ .

$$S = \frac{2.5 \times 10^{-4} \text{ cm}^3(\text{STP})}{\text{g (Al)}} \quad | \quad \begin{array}{c} 1 \text{ mol (H}_2\text{)} \\ 22.400 \text{ cm}^3(\text{STP}) \end{array} \quad | \quad \begin{array}{c} 2 \text{ g (H)} \\ 1 \text{ mol (H}_2\text{)} \end{array} \quad | \quad \begin{array}{c} 2.55 \text{ g (Al)} \\ \text{cm}^3(\text{Al}) \end{array}$$

$$= 5.69 \times 10^{-8} \text{ g cm}^{-3}.$$

c) From Table 13.1,  $P_0^* = 0.37 \text{ cm}^3(\text{STP}) \text{s}^{-1} \text{cm}^{-1} \text{atm}^{-1/2}$  and  $Q_p = 30 800 \text{ cal mol}^{-1}$ . Then with Eq. (3.16) we calculate

$$P^* = 0.37 \exp \left[ -\frac{30 800}{(1.987)(873)} \right] = 7.19 \times 10^{-9} \text{ cm}^3(\text{STP}) \text{s}^{-1} \text{cm}^{-1} \text{atm}^{-1/2},$$

and

$$D = \frac{P^*}{K} = \frac{7.19 \times 10^{-9} \text{ cm}^3(\text{STP})}{\text{s cm atm}^{1/2}} \quad | \quad \begin{array}{c} \text{g(AI) atm}^{1/2} \\ 2.5 \times 10^{-4} \text{ cm}^3(\text{STP}) \end{array} \quad | \quad \begin{array}{c} \text{cm}^3 \\ 2.55 \text{ g(AI)} \end{array}$$

$$= 1.13 \times 10^{-5} \text{ cm}^2 \text{s}^{-1},$$

or  $D = 1.13 \times 10^{-9} \text{ m}^2 \text{s}^{-1}$ .

**Example 13.2** A pilot plant for hydrogenation of hydrocarbon vapor is to be constructed of a low-alloy steel. In designing, the question of the effect of wall thickness on the rate of hydrogen loss through the wall is raised. If the inside diameter of a vessel 1 m long is 10 cm, calculate the rate of hydrogen loss as a function of wall thickness at 723 K and a pressure of 75 atm hydrogen, assuming that the gas diffusing through the wall is collected and removed at 1 atm.

<sup>1</sup>S. Pauly, "Permeability and Diffusion Data," in J. Brandrup and E. H. Immergut, editors, *Polymer Handbook*, third edition, John Wiley & Sons, New York, NY, 1989, pages VI/435 to VI/449.

**Solution:** Combining Eqs. (13.2), (13.3), and (13.4), and assuming that  $D$  is constant, we have

$$J = -2\pi l D \frac{C_1 - C_2}{\ln(r_1/r_2)}.$$

In terms of permeability

$$j = \frac{-2\pi l D K \left( \sqrt{P_1} - \sqrt{P_2} \right)}{\ln(r_1/r_2)} = \frac{-2\pi l P^* \left( \sqrt{P_1} - \sqrt{P_2} \right)}{\ln(r_1/r_2)}.$$

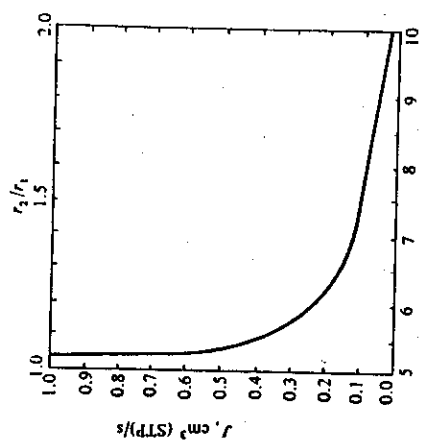
From Table 13.1 and Eq. (13.16),  $P^* = 8.4 \times 10^{-6} \text{ cm}^3(\text{STP}) \text{ s}^{-1} \text{ atm}^{-1/2}$ . Therefore

$$J = \frac{-2\pi(100)(8.4 \times 10^{-6}) \left( \sqrt{75} - \sqrt{1} \right)}{\ln r_1 - \ln r_2} = \frac{-0.0404}{1.609 - \ln r_2},$$

with the outside radius given in cm. In more general terms, where  $r_1$  is not specified, but  $l$  is still 1 m,

$$J = \frac{-0.0404}{\ln(r_1/r_2)}, \text{ cm}^3(\text{STP}) \text{ s}^{-1}.$$

Both results are shown below:



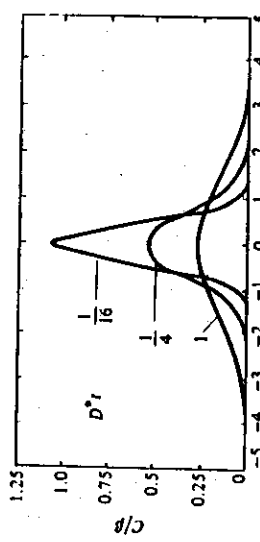
It probably makes sense to design the vessel with a 6 or 7 cm wall thickness.

### 13.2 TRANSIENT DIFFUSION EXPERIMENTS

Under many circumstances it is not possible to carry out steady-state experiments in order to determine diffusion coefficients in solids. This means that we must use the results of transient experiments and solve Eq. (12.18) in its general form

$$\frac{\partial C}{\partial t} = \nabla(D\nabla C) \quad (13.17)$$

Fig. 13.3 Spreading of concentration from a plane source at  $x = 0$ .



\*Extensive compilations of solutions are presented in J. Crank, *The Mathematics of Diffusion*, Oxford University Press, London, 1956; and W. Jost, *Diffusion in Solids, Liquids, and Gases*, Academic Press, 1960. With appropriate change of variables, one can also refer to H. S. Carslaw and J. C. Jaeger, *Conduction of Heat in Solids*, second edition, Oxford University Press, 1959.

Note that we may determine  $D^*$  without measurement or control of  $\beta$ , since a plot of  $\log C$  versus  $x^2$  at time  $t$  yields  $D^*$  directly.

Now suppose that the second bar has not been welded to the first. Then a *semi-infinite* bar would extend over the region  $x > 0$  with an impermeable barrier at  $x = 0$ . In either case, infinite or semi-infinite,

$$\frac{\partial C}{\partial x} = 0 \quad \text{at } x = 0. \quad (13.21)$$

If diffusion is allowed, the material that would normally diffuse in the negative  $x$ -direction is *reflected* at the  $x = 0$  plane, and moves in the positive  $x$ -direction. The concentration at any  $x$  in the  $+x$  domain is then given by the superposition of the original solution for  $x > 0$  and the reflected solution for  $x < 0$ , or

$$C(x,t) = \frac{\beta}{\sqrt{\pi D^* t}} \exp \left[ \frac{-x^2}{4D^* t} \right]. \quad (13.22)$$

### 13.2.2 Diffusion couple with constant $\tilde{D}$

This case is exemplified in Fig. 13.4(a) by butt-welding two bars of  $A-B$  alloy of concentrations  $C_1$  and  $C_2$ . If  $\tilde{D}$  is independent of composition, and the bars extend far enough in the positive and negative domains to be considered infinite, then Eq. (13.18) applies with the boundary conditions:

$$C(x,0) = C_1 \quad \text{at } x < 0, \quad (13.23a)$$

$$C(x,0) = C_2 \quad \text{at } x > 0, \quad (13.23b)$$

$$C(-\infty,t) = C_1, \quad (13.23c)$$

$$C(\infty,t) = C_2. \quad (13.23d)$$

Due to symmetry, the concentration at  $x = 0$  immediately takes on the average value of  $C_1$  and  $C_2$ . Let this average be  $C_s$ ; then it is easy to see that in the positive  $x$ -domain, the solution is directly analogous to the temperature distribution of the semi-infinite solid, as discussed in Section 9.4.2 culminating in Eq. (9.62). Appropriately changing the symbols, we can write the solution:

$$\frac{C - C_s}{C_2 - C_1} = \operatorname{erf} \frac{x}{2\sqrt{\tilde{D}t}}. \quad (13.24)$$

Figure 13.4(b) illustrates this result in a general form, from which one may obtain  $\tilde{D}$ -values from measurements of  $C$ ,  $x$ , and  $t$ . Since  $\operatorname{erf} x = -\operatorname{erf}(-x)$ , the concentration profile given by Eq. (13.24) is symmetrical about  $x = 0$ . This is known as the *Grube solution*, and applies when  $\tilde{D}$  is not a function of concentration. Since  $\tilde{D}$  is usually a function of composition, the use of Eq. (13.24) is restricted to small differences between  $C_1$  and  $C_2$ . For example, a good value for the diffusion coefficient of  $A$  in 50A-50B alloy could be determined from a couple of 45%  $A$  alloy welded to a 55%  $A$  alloy.

Apart from application to diffusion couples, we can use Eq. (13.24) to predict concentration-time curves for situations where the part in which diffusion occurs is thick enough so that, within the time for diffusion, there is still a region of the part unchanged in composition.

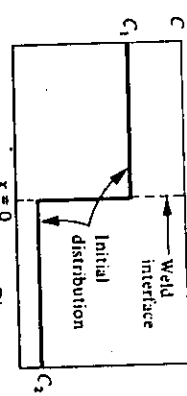


**Fig. 13.4** Interdiffusion between an alloy of composition  $C_1$  and an alloy of composition  $C_2$ .  
a) Initial distribution. b) Diffusion profile when the initial distribution is as in a).

**Example 13.3** A piece of AISI 1020 steel is heated to 1255 K (in the austenite region) and subjected to a carburizing atmosphere such that the reaction



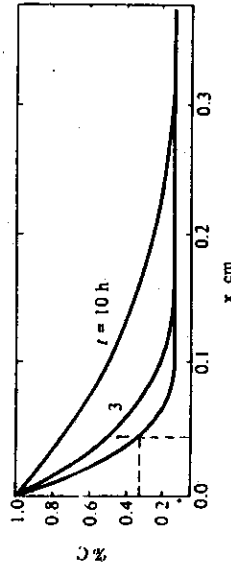
is in equilibrium with 1.0% C in solution at the surface. Calculate the carbon profile after 1, 3, and 10 hours, assuming that diffusion within the solid is the rate-limiting step.

**Solution.** The initial condition is  $C_2 = 0.2\% C$ , and the boundary condition at the surface is  $C_s = 1.0\% C$ .

At 1255 K,  $D_c = 2.0 \times 10^{-11} \text{ m}^2 \text{ s}^{-1}$ . Therefore, Eq. (13.24) for the distribution after 1 hour is

$$C(x,3600) = 1.0 + (0.2 - 1.0) \operatorname{erf} \frac{x}{2\sqrt{(2 \times 10^{-11})(3.6 \times 10^3)}}.$$

Specifically at  $x = 5 \times 10^{-4}$  m,  $C = 0.35\%$  C. The results for various locations as well as for the longer times are:



### 13.2.3 Diffusion couple with variable $\bar{D}$

The analysis in Section 13.2.2 is valid only for  $\bar{D}$  independent of concentration. In general, however, the diffusion coefficient varies with composition, and since there is a concentration gradient, this means that  $\bar{D}$  changes with position. This variation in  $\bar{D}$  is particularly evident in diffusion couple experiments in which pure A is joined to pure B, and a continuous solid solution is formed. Fick's second law must be written over all compositions between A and B, and for such situations this is

$$\frac{\partial C}{\partial t} = \frac{\partial}{\partial x} \left[ \bar{D} \frac{\partial C}{\partial x} \right]. \quad (13.25)$$

The solution to Eq. (13.25) that follows is useful for obtaining  $\bar{D}$  over a range of compositions, but not for the *a priori* task of predicting a concentration profile for a diffusion anneal. In other words, it does not give a solution  $C(x,t)$ , which is usually sought, but rather allows  $\bar{D}(C)$  to be calculated from an experimental plot of  $C(x)$ . This method of analyzing experimental data is called the Boltzmann-Matano technique.

We combine the position variable  $x$  and the time variable  $t$  into one variable  $\lambda = x/\sqrt{t}$ , so that we consider  $C$  to be a function of only one variable,  $\lambda$ . Using this definition of  $\lambda$ , we transform Eq. (13.25) into an ordinary differential equation:

$$\frac{\partial C}{\partial t} = \frac{\partial \lambda}{\partial t} \left[ \frac{dC}{d\lambda} \right] = -\frac{1}{2} \frac{x}{t^{1/2}} \left[ \frac{dC}{d\lambda} \right] = -\frac{\lambda}{2t} \left[ \frac{dC}{d\lambda} \right], \quad (13.26a)$$

and

$$\frac{\partial C}{\partial x} = \frac{\partial \lambda}{\partial x} \left[ \frac{dC}{d\lambda} \right] = \frac{1}{t^{1/2}} \left[ \frac{dC}{d\lambda} \right]. \quad (13.26b)$$

Substituting into Eq. (13.25), we obtain

$$-\frac{\lambda}{2t} \left[ \frac{dC}{d\lambda} \right] = \frac{\partial}{\partial x} \left[ \frac{\bar{D}}{t^{1/2}} \left( \frac{dC}{d\lambda} \right) \right] = \frac{1}{t} \frac{d}{d\lambda} \left[ \bar{D} \frac{dC}{d\lambda} \right],$$

or finally we can get

$$-\frac{\lambda}{2} \frac{dC}{d\lambda} = \frac{d}{d\lambda} \left[ \bar{D} \frac{dC}{d\lambda} \right]. \quad (13.27)$$

Consider the diffusion couple depicted in Fig. 13.5(a). Then for  $C(\lambda)$ , we recognize that

$$C = C_1, \quad \text{for } \lambda = -\infty, \quad (13.28a)$$

$$\text{and} \quad C = C_2, \quad \text{for } \lambda = +\infty, \quad (13.28b)$$

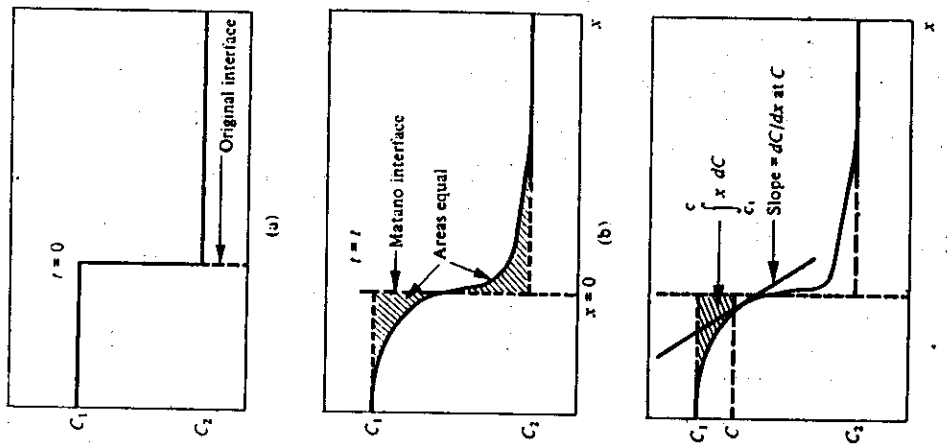


Fig. 13.5 a) Initial conditions. b) Definition of location of Matano interface after diffusion has taken place for a time  $t$ . c) The integral and the slope obtained in order to calculate  $D$  at composition  $C$ .

We then solve Eq. (13.27) by integrating between  $C = C_1$  and  $C = C$ :

$$-\frac{1}{2} \int_{C_1}^C \lambda dC = \tilde{D} \left. \frac{dC}{d\lambda} \right|_{C_1}^C \quad (13.29)$$

Since the concentration gradient goes to zero as  $C$  approaches  $C_1$ , the right-hand side of Eq. (13.29) is simply  $\tilde{D}(dC/d\lambda)$ . Then

$$\tilde{D} = -\frac{1}{2} \left[ \frac{dC}{d\lambda} \right]_{C_1}^C \int_{C_1}^C \lambda dC. \quad (13.30)$$

From Eq. (13.29), we obtain the definition of the *Matano interface*; since the concentration gradient also goes to zero as  $C$  approaches  $C_2$ , Eq. (13.29) gives us the additional condition that

$$\int_{C_1}^{C_2} \lambda dC = 0. \quad (13.31)$$

Since experimental data are available only at some constant time  $t$ , Eqs. (13.30) and (13.31) can be written in terms of  $x$  and  $t$ , and the relationships used for calculating  $\tilde{D}$  from the measured concentration profile are

$$\tilde{D} = -\frac{1}{2t} \left[ \frac{dC}{dx} \right]_{C_1}^C \int_{C_1}^C x dC, \quad (13.32)$$

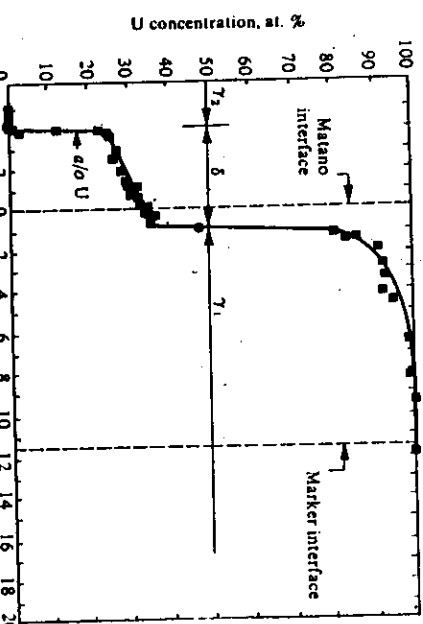
and we choose the plane defining  $x = 0$  such that

$$\int_{C_1}^{C_2} x dC = 0. \quad (13.33)$$

In Fig. 13.5(b), the plane  $x = 0$  is given by the line that makes the two hatched areas equal. We calculate the value of  $\tilde{D}$  at a given  $C$  by measuring the cross-hatched area, which is the integral in Eq. (13.32), and the reciprocal slope at that point,  $dC/dx$ . The diffusion coefficient  $\tilde{D}$ , found by applying Eq. (13.32) in this manner, is the interdiffusion coefficient discussed in Section 13.2.3.

In addition, if we place inert markers at the original plane of welding, we can also determine the intrinsic diffusion coefficients. This is left for the reader to do in Problem 13.9. Furthermore, Jost<sup>2</sup> pointed out that it is not necessary for a single phase to exist over the entire range of the diffusion region. A discontinuity in  $C(x)$  and  $\tilde{D}(C)$  exists where an intermediate phase is formed. The only condition required when applying the Boltzmann-Matano technique is that the concentrations in both phases on either side of the interface between the phases are independent of time.

**Example 13.4** A diffusion couple made of pure Nb welded to pure U is held at 800°C for 49 days. The resulting concentration profile, shown below, is obtained with a microprobe analyzer. Note that an intermediate phase  $\delta$  is formed between the two solid solution,  $\gamma_1$  and  $\gamma_2$ . Calculate  $\tilde{D}$  at 90 at. % U.



(From N. L. Peterson and R. F. Ogilvie, *Trans. AIME* 218, 439 (1960).)

**Solution.** Let  $C$  represent the composition of U. First, the Matano interface is chosen, such that

$$\int_{C_1}^0 x dC = \int_{C_2}^{\infty} x dC.$$

This is found by trial and error, and placed on the figure as shown. At 90% U,  $dC/dx$  is evaluated:

$$dC/dx = 4.60 \times 10^3 \text{ at. \% in}^{-1} = 1.81 \times 10^3 \text{ at. \% m}^{-1}.$$

Also

$$\int_{C=100}^{C=90} x dC = -1.32 \times 10^{-3} \text{ m at. \%}, \text{ by graphical means;}$$

$$t = \frac{49 \text{ days}}{\frac{(-1.32 \times 10^{-3})}{2(4.23 \times 10^6)(1.810 \times 10^3)}} = 8.6 \times 10^{-16} \text{ m}^2 \text{ s}^{-1}.$$

Thus

$$\tilde{D} (90\% \text{ U}) = \frac{(-1.32 \times 10^{-3})}{2(4.23 \times 10^6)(1.810 \times 10^3)} = 8.6 \times 10^{-16} \text{ m}^2 \text{ s}^{-1}.$$

<sup>2</sup>W. Jost, *Diffusion in Solids, Liquids, and Gases*, Academic Press, New York, 1960, page 76, and also W. Jost, *Z. Physik* 127, 163 (1950).

### 13.3 FINITE SYSTEM SOLUTIONS

The solutions to Fick's laws presented thus far represent useful cases in many situations when the sink cannot be considered infinite or semi-infinite. On the other hand, there are many situations in which the effect of the diffusion process on the composition is felt at the furthest point in the material prior to the end of the diffusion treatment. This condition can arise quite often when small parts are exposed to a gaseous environment, and there is diffusion of the gas species into the part. Conversely, metal and ceramic parts must often be degassed. When dealing with these situations, it is usually safe to assume that the rate-limiting step of the overall mass transfer is the diffusion of the gas species into the solid. Hence, we seek solutions of Fick's second law with a surface concentration imposed at time zero and maintained constant.

To illustrate this case, consider the diffusion into or out of a slab of infinite length and thickness  $2L$ . Initially the slab has a uniform concentration  $C_i$ , and then its surfaces are raised or lowered to  $C_s$  and maintained constant. Hence, we are seeking a solution to Fick's second law with constant  $\bar{D}$  (or simply  $D$ ):

$$\frac{\partial C}{\partial t} = D \frac{\partial^2 C}{\partial x^2}. \quad (13.34)$$

The initial and boundary conditions of interest are

$$C(x,0) = C_i, \quad (13.35a)$$

$$\frac{\partial C}{\partial x}(0,t) = 0, \quad (13.35b)$$

and at the slab center,

$$C(L,t) = C_s, \quad (13.35c)$$

and at the surface,

$$\frac{\theta}{\theta_i} = \sum_{n=1, \text{odd}}^{\infty} A_n \cos \left( \frac{(2n+1)\pi}{2} \frac{x}{L} \right). \quad (13.39)$$

If we apply Fourier's analysis to Eq. (13.39) as we demonstrated previously for Eq. (9.38), then we obtain

$$A_n = \frac{(-1)^n}{(2n+1)} \frac{4}{\pi} \theta_i. \quad (13.40)$$

Thus the solution we seek is

$$\frac{\theta}{\theta_i} = \frac{C - C_s}{C_i - C_s} = \frac{4}{\pi} \sum_{n=0}^{\infty} \frac{(-1)^n}{2n+1} \exp \left[ -\frac{(2n+1)^2 \pi^2}{4} \frac{Dt}{L^2} \right] \cos \left( \frac{(2n+1)\pi}{2} \frac{x}{L} \right). \quad (13.41)$$

Equation (13.41) is useful for describing concentration profiles as a function of time. However, the total amount of material that diffuses into or out of the slab is often of more interest, particularly when this is the only measurable quantity. So, the average concentration  $\bar{C}$  is required:

$$\bar{C} = \frac{1}{L} \int_0^L C dx. \quad (13.42)$$

Carrying out this operation, using Eq. (13.41) for  $C$ , we obtain the relative change in average composition for diffusion into a slab:

$$\frac{\bar{C} - C_s}{C_i - C_s} = \frac{8}{\pi^2} \sum_{n=0}^{\infty} \frac{1}{(2n+1)^2} \exp \left[ -\frac{(2n+1)^2 \pi^2}{4} \frac{Dt}{L^2} \right]. \quad (13.43)$$

This expression is good for diffusion into or out of a slab. If we take the first term in the series, then

$$\frac{\bar{C} - C_s}{C_i - C_s} = \frac{8}{\pi^2} \exp \left( -\frac{Dt}{\tau} \right), \quad (13.44)$$

where  $\tau$  is the time constant for the diffusion process ( $\tau = 4L^2/\pi^2 D$ ). It is apparent that a graph of  $\log \frac{\bar{C} - C_s}{C_i - C_s}$  versus  $t/\tau$  is a straight line and that we can obtain  $D$  from the slope. We plot Eq. (13.43) in Fig. 13.6, along with diffusion into or out of cylinders and spheres (see Table 13.2). For long times ( $Dt/L^2 > 0.05$ ), the first term of the series is sufficient, and a straight line relationship is obeyed.

For diffusion into or out of simple multidimensional shapes other than the infinite plate, infinite cylinder, or sphere, we handle the problem in the same manner as we treated heat transfer to or from these shapes in Section 9.5. We can combine product solutions to yield the solution for the shape of interest.

$$\theta = \sum_{n=0}^{\infty} A_n \exp \left[ -\frac{(2n+1)^2 \pi^2}{4} \frac{Dt}{L^2} \right] \cos \left[ \frac{(2n+1)\pi}{2} \frac{x}{L} \right], \quad (13.38)$$

Table 13.2 The relative change in average composition for the basic shapes

*Diffusion in a slab of semithickness, L*I.C.:  $C(x,0) = C_0$ B.C.:  $C(L,t) = C_0$ 

$$\frac{\partial C}{\partial x}(0,t) = 0.$$

Solution:

$$\frac{\bar{C} - C_0}{C_i - C_0} = \frac{8}{\pi^2} \sum_{n=0}^{\infty} \frac{1}{(2n+1)^2} \exp \left[ \frac{-(2n+1)^2 \pi^2}{4} \frac{Dt}{L^2} \right]. \quad (13.43)$$

*Diffusion in solid circular cylinder of radius, R*I.C.:  $C(r,0) = C_0$ B.C.:  $C(R,t) = C_0$ 

$$\frac{\partial C}{\partial r}(0,t) = 0.$$

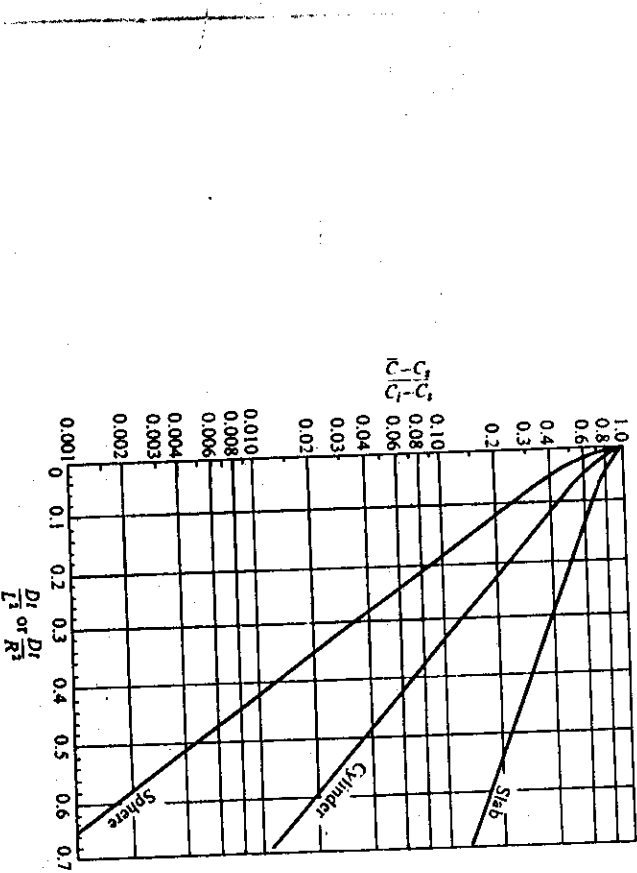
Solution:

$$\frac{\bar{C} - C_0}{C_i - C_0} = \sum_{n=1}^{\infty} \frac{4}{\xi_n^2} \exp \left[ -\frac{\xi_n^2 D t}{R^2} \right], \quad (13.45)$$

where  $\xi_n = 2.405, 5.520, 8.654, 11.792, 14.931$ , when  $n = 1, 2, 3, 4, 5$ , etc.\**Diffusion in spheres of radius, R*

The same set of initial and boundary conditions as for the cylinder above:

$$\frac{\bar{C} - C_0}{C_i - C_0} = \frac{6}{\pi^2} \sum_{n=1}^{\infty} \frac{1}{n^2} \exp \left[ -\frac{n^2 \pi^2 D t}{R^2} \right]. \quad (13.46)$$

\* $\xi_n$  are roots of the equation  $J_0(x) = 0$ , where  $J_0(x)$  is the Bessel function of zero order.Fig. 13.6 The relative change in average composition for the basic shapes;  $R$  = radius, and  $L$  = semithickness.

**Example 13.5** Calculate the fraction of hydrogen remaining in a) a 100 mm thick slab of steel, 3 m long  $\times$  1.2 m wide, b) a 100 mm square billet of steel, 4 m long, and c) a 100 mm square billet of steel, 200 mm long, after 40 hours of vacuum outgassing treatment at a temperature where  $D_H = 1.0 \times 10^{-9} \text{ m}^2 \text{ s}^{-1}$ , assuming an initially uniform distribution.

Solution. a) Consider this to be an infinite plate. Then

$$\frac{Dt}{L^2} = \frac{(1 \times 10^{-9})(40 \times 3600)}{(5 \times 10^{-2})^2} = 5.76 \times 10^{-2}.$$

From Fig. 13.6, we have

$$\frac{\bar{C} - C_0}{C_i - C_0} = 0.74.$$

- b) The desired solution can be obtained as the product of the infinite plate solutions for the two 100 mm dimensions:

$$\frac{\bar{C} - C_s}{C_i - \bar{C}_s} = (0.74)(0.74) = 0.55.$$

c) In this case, first evaluate  $Dt/L^2$  for the 200 mm dimension:

$$\frac{Dt}{L^2} = \frac{(1 \times 10^{-9})(40 \times 3600)}{0.1^2} = 1.44 \times 10^{-2}.$$

From Fig. 13.6, we get

$$\left[ \frac{\bar{C} - C_s}{C_i - \bar{C}_s} \right]_{200 \text{ mm}} = 0.90.$$

Therefore,

$$\frac{\bar{C} - C_s}{C_i - \bar{C}_s} = (0.90)(0.74)(0.74) = 0.49.$$

### 13.4 MICROELECTRONIC DIFFUSION PROCESSING

Some materials result from processes in which alloying elements or *dopants* are diffused into a hot matrix to change electronic or magnetic properties. This is particularly true of silicon processed into devices. Frequently, a junction is fabricated by using two steps, each involving diffusion. The two steps are *predeposition* and *drive-in* diffusion.

In predeposition, a silicon wafer is placed in a high-temperature furnace and exposed to a gas that contains the dopant. Depending on the gas and the temperature, a constant concentration of the dopant is established at the surface. The goal of the predeposit step is to diffuse a small amount of the dopant into a fraction of a micrometer at the surface. Obviously, the silicon matrix is semi-infinite so the concentration profile of the dopant is

$$\frac{C - C_s}{C_0 - \bar{C}_s} = \operatorname{erf} \left[ \frac{x}{2\sqrt{Dt}} \right], \quad (13.47)$$

where  $C_s$  is the constant surface concentration,  $C_0$  is the initial concentration (assumed to be uniform),  $x$  is distance measured from the surface at  $x = 0$ ,  $D$  is the diffusion coefficient of the dopant in the silicon, and  $t$  is time. The situation is depicted in Fig. 13.7.

The amount of dopant predeposited, usually expressed in terms of the number of dopant atoms, is

$$J = A \int_0^{x=0} j_{x=0} dt, \quad (13.48)$$

where  $A$  is the surface area of the silicon wafer and  $j_{x=0}$  is the flux of dopant atoms at the surface ( $x = 0$ ). It can be shown that the flux at the surface is

$$j_{x=0} = (C_s - C_0) \left( \frac{D}{\pi r} \right)^{1/2}; \quad (13.49)$$

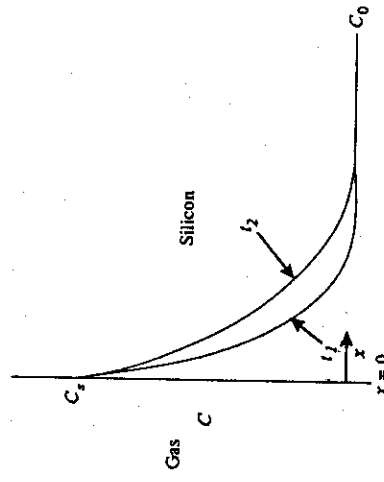


Fig. 13.7 The concentration of dopant at the surface of a silicon wafer during the predeposition step;  $t_2 > t_1$ .

then by combining Eqs. (13.48) and (13.49) and carrying out the integration, we get the amount predeposited. It is

$$J = \frac{2A}{\pi r^2} (C_s - C_0) (Dt)^{1/2}. \quad (13.50)$$

During predeposition, we also calculate the diffusion depth of the dopant profile; it is

$$t = (Dt)^{1/2}. \quad (13.51)$$

Values of diffusion coefficients and approximate surface concentrations for two dopants, boron and phosphorus, are given in Table 13.3. The units are those most likely to be encountered in device fabrication technology.

Table 13.3 Surface concentrations and diffusion coefficients for boron and phosphorus			
T, K	Boron		Phosphorus
	$C_s$ , atoms $\text{cm}^{-3}$	$D$ , $\mu\text{m}^2 \text{h}^{-1}$	$C_s$ , atoms $\text{cm}^{-3}$
1223	$4.5 \times 10^{20}$	$1.6 \times 10^{-3}$	$9 \times 10^{20}$
1273	$4.8 \times 10^{20}$	$5.2 \times 10^{-3}$	$1.0 \times 10^{21}$
1323	$5.0 \times 10^{20}$	$1.7 \times 10^{-2}$	$1.1 \times 10^{21}$
1373	$5.1 \times 10^{20}$	$5.8 \times 10^{-2}$	$1.2 \times 10^{21}$
1423	$5.2 \times 10^{20}$	$1.6 \times 10^{-1}$	$1.2 \times 10^{21}$

**Example 13.6** Boron is predeposited on a silicon wafer with an initial concentration of  $5 \times 10^{15}$  atoms  $\text{cm}^{-3}$ . Conditions are 30 minutes at 1223 K. Calculate a) the amount deposited; b) the diffusion length; c) the concentration at the diffusion length.

*Solution.* a) From Table 13.3,  $C_s = 4.5 \times 10^{20}$  atoms  $\text{cm}^{-3}$  and  $D = 1.6 \times 10^{-3} \mu\text{m}^2 \text{ h}^{-1}$ . Equation (13.50) applies, so that

$$\begin{aligned}\frac{J}{A} &= \frac{2}{\pi^{1/2}} (C_s - C_0)(Dt)^{1/2} = \frac{2}{\pi^{1/2}} (4.5 \times 10^{20} - 5 \times 10^{15})(1.6 \times 10^{-3})^{1/2} (0.5)^{1/2} \\ &= \frac{1.44 \times 10^{19} \text{ atoms } \mu\text{m}}{\text{cm}^3} \quad \left| \frac{1 \text{ cm}}{10^4 \mu\text{m}} \right. = 1.44 \times 10^{15} \text{ atoms } \text{cm}^{-2}.\end{aligned}$$

b) Equation (13.51) is used.

$$\ell = (1.6 \times 10^{-3} \times 0.5)^{1/2} = 2.83 \times 10^{-2} \mu\text{m} = 2.83 \times 10^{-6} \text{ cm}.$$

Notice how small  $\ell$  is; this is typical.

c) Equation (13.47) applies with  $x = \ell = (Dt)^{1/2}$ . Thus, with Table 9.3 we get

$$\frac{C - C_s}{C_0 - C_s} = \text{erf} \left[ \frac{1}{2} \right] = 0.5205,$$

and

$$\begin{aligned}C &= (0.5205)(5 \times 10^{15} - 4.5 \times 10^{20}) + 4.5 \times 10^{20} \\ &= 2.16 \times 10^{20} \text{ atoms } \text{cm}^{-3}.\end{aligned}$$

From the above example we see that a very thin layer of the dopant is deposited on to the surface of the silicon matrix. This was done by the chemical reaction with the gas and allowing a small amount of diffusion to occur. Another method of producing a high concentration of dopant at the surface is *ion implantation*. In this method a beam of ions is accelerated into a mass-separating magnetic field, which selects the dopant ions from unwanted ions, similar to the separation in a mass spectrometer. The beam of dopant ions is aimed at the silicon target, where the ions come to rest after colliding with the nuclei and electrons in the surface layer of the target, which also tends to create vacancies in the host lattice. Ion implantation can be controlled better than predeposition through the gas, both in terms of minimizing lateral spread and in establishing a very sharp definition of the dopant at the surface. A very high density of crystalline defects, especially vacancies, however, is a disadvantage because they can reduce the electronic performance of the device.

After the predeposition step, drive-in diffusion is done to allow diffusion from the surface further into the silicon. This is illustrated by Fig. 13.8. To prevent escape of the dopant, a very thin layer of silica ( $\text{SiO}_2$ ) is made on the surface. During the drive-in, the boundary conditions and the initial condition for  $C(x, t)$  are

$$\frac{\partial C(0, t)}{\partial x} = 0, \quad (13.52a)$$

$$C(\infty, t) = C_0, \quad (13.52b)$$

$$\text{and} \quad C(x, 0) = f(x). \quad (13.52c)$$

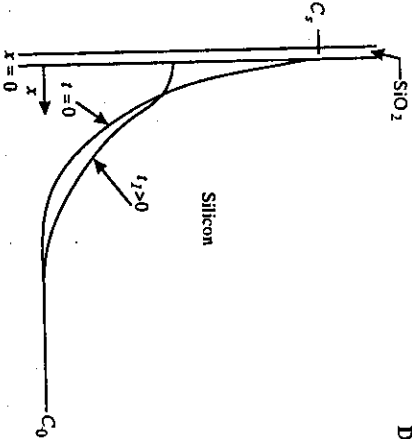


Fig. 13.8 The concentration of dopant near the surface of a silicon wafer during the drive-in step. The distribution at  $t = 0$  is that from the predeposition step.

Equation (13.52a) applies at the surface, Eq. (13.52b) simply gives the concentration in the interior, and Eq. (13.52c) represents the distribution of dopant that results from the predeposition.

The solution which satisfies Fick's second law of diffusion and Eqs. (13.52a,b,c) can be deduced from Appendix G. Then

$$C - C_0 = \int_{x'=0}^x \frac{f(x') - C_0}{2\sqrt{\pi Dt}} \left\{ \exp \left[ \frac{-(x-x')^2}{4Dt} \right] - \exp \left[ \frac{-(x+x')^2}{4Dt} \right] \right\} dx', \quad (13.53)$$

where  $f(x')$  is the distribution of the solute from the predeposition step and given by Eq. (13.47). By combining Eqs. (13.47) and (13.53), we get

$$\frac{C - C_0}{C_s - C_0} = \int_{x'=0}^x \frac{\text{erfc}(x'/2\ell)}{2\sqrt{\pi Dt}} \left\{ \exp \left[ \frac{-(x-x')^2}{4Dt} \right] - \exp \left[ \frac{-(x+x')^2}{4Dt} \right] \right\} dx'. \quad (13.54)$$

Equation (13.54) is the solution, but, unfortunately, it is cumbersome and requires a numerical integration. Therefore, an approximate solution is often invoked.

The dopant taken up by the silicon in the predeposit step is approximated to be a thin source on the surface of the silicon. The strength of the source is given by the amount deposited per unit area. Thus, Eq. (13.22) applies with  $C$  relative to  $C_0$  and the source strength ( $\beta$ ) given by  $J/A$ , Eq. (13.50).

$$\frac{C - C_0}{C_s - C_0} = \frac{2}{\pi} \left[ \frac{\ell^2}{Dt} \right]^{1/2} \exp \left[ -\frac{x^2}{4Dt} \right]. \quad (13.55)$$

Notice that  $C_s$  and  $\ell$  are from the predeposit step, but  $D$  and  $t$  are for the drive-in step.

The so-called "junction depth" ( $x_j$ ) is important because it is a measure of the depth of diffusion after drive-in diffusion. The junction depth is defined as follows.

Since  $C_s \gg C_0$ , Eq. (13.55) is approximated by

$$\frac{C}{C_s} \approx \frac{2}{\pi} \left[ \frac{\ell^2}{Dt} \right] \exp \left[ -\frac{x^2}{4Dt} \right]. \quad (13.56)$$

## 13.5 HOMOGENIZATION OF ALLOYS

During solidification of alloys, *coring* occurs, because the rate of diffusion for most alloying elements in the solid state is too slow to maintain a solid of uniform concentration in equilibrium with the liquid. A cast structure is exemplified in Fig. 13.9 showing the repetitive pattern of microsegregation. In the case at hand we presume the alloy to be a single phase.

$$x_j = \left\{ 4D_r \ln \left[ \left( \frac{2}{\pi} \right) \left( \frac{C_s}{C_0} \right) \left( \frac{t^{1/2}}{D_r} \right) \right] \right\}^{1/2} \quad (13.57)$$

**Example 13.7** After the predeposit step, the wafer of Example 13.6 is subjected to drive-in at 1423 K for 2 h. Calculate: a) the junction depth; b) the concentration at that depth; and c) the surface concentration.

**Solution.** a) Equation (13.57) applies with  $t$ ,  $C_s$ , and  $C_0$  given in Example 13.6. From Table 13.3  $D = 1.6 \times 10^{-1} \mu\text{m}^2 \text{ h}^{-1} = 4.44 \times 10^{-13} \text{ cm}^2 \text{ s}^{-1}$ ; also  $t = 7200 \text{ s}$ .

$$\begin{aligned} x_j &= \left\{ 4 \times 4.44 \times 10^{-13} \right. \\ &\quad \times 7200 \ln \left[ \left( \frac{2}{\pi} \right) \left( \frac{4.5 \times 10^{10}}{5 \times 10^{15}} \right) \left( \frac{2.83^2 \times 10^{-12}}{4.44 \times 10^{-13} \times 7200} \right)^{1/2} \right] \left. \right\}^{1/2} \\ x_j &= 3.19 \times 10^{-4} \text{ cm} = 3.19 \mu\text{m}. \end{aligned}$$

b)  $C = C_0 = 5 \times 10^{15} \text{ atoms cm}^{-3}$ . We obtain an exact result by using Eq. (13.55).

$$\begin{aligned} \frac{C - C_0}{C_s - C_0} &= \frac{2}{\pi} \left[ \frac{2.83^2 \times 10^{-12}}{4.44 \times 10^{-13} \times 7200} \right]^{1/2} \exp \left[ - \frac{3.19^2 \times 10^{-8}}{4 \times 4.44 \times 10^{-13} \times 7200} \right]^{1/2} \\ &= 1.115 \times 10^{-5}. \end{aligned}$$

Therefore,

$$\begin{aligned} C &= (1.115 \times 10^{-5})/(4.5 \times 10^{10} - 5 \times 10^{15}) + 5 \times 10^{15} \\ &\approx 1.00 \times 10^{16} \text{ atoms cm}^{-3}. \end{aligned}$$

c) We use Eq. (13.55) with  $x = 0$ .

$$\frac{C - S \times 10^{15}}{4.5 \times 10^{10} - 5 \times 10^{15}} = \frac{2}{\pi} \left[ \frac{2.83^2 \times 10^{-12}}{4.44 \times 10^{-13} \times 7200} \right]^{1/2} = 0.0319.$$

$$C = 1.43 \times 10^{19} \text{ atoms cm}^{-3}.$$

$$(C_L - C_s^*) df_s = (1 - f_s) dC_L, \quad (13.58)$$

where

$C_L$  = weight percent of solute in the interdendritic liquid;

$C_s^*$  = weight percent of solute in the dendritic solid at the solid-liquid interface;

and  
 $f_s$  = local weight fraction of solid.

Fig. 13.9 A dendritic structure showing the *coring* or microsegregation of the alloying element.  $L$  is one-half of the dendrite arm spacing.

The dendrite arms develop during solidification and their spacing depends upon the alloy and the rate of cooling from the liquidus temperature to the nonequilibrium solidus temperature. Depending on the cooling rate, the *dendritic arm spacing* can be between 5  $\mu\text{m}$  and 400  $\mu\text{m}$ , with typical values ranging from 50  $\mu\text{m}$  to 200  $\mu\text{m}$ .

Dendritic structures occur in cast products that encompass ingots, shaped castings, continuous castings, and weldments. The coring, or microsegregation, is coincident with the growth of the dendrites. Imagine a local region in a solidifying casting that comprises several to many dendrite arms. As solidification proceeds within the local region, solute is rejected to the *interdendritic* liquid, when the concentration of solute in the solid is less than that of the interdendritic liquid. The microsegregation can be closely approximated by a simple solute balance.<sup>3</sup> That is, the solute rejected from the dendritic solid equals the increase of solute in the interdendritic liquid. Therefore, within a local region undergoing solidification we have

<sup>3</sup>M. C. Flemings, *Solidification Processing*, McGraw-Hill, New York, NY, 1974, pages 34-36, 142.

When we use Eq. (13.58), it is assumed that there is sufficient diffusion of solute in the liquid so that it is uniform. This is usually valid because the diffusion length in the liquid is many times greater than the dendrite arm spacing. On the other hand, the diffusion coefficient of the solute in the solid is typically 5 or 6 orders of magnitude less than in the liquid, so we assume no diffusion in the solid. Consequently, as a layer of solid with a concentration  $C_s^*$  forms, its concentration never changes as subsequent solid of different  $C_s^*$  grows from the interdendritic liquid.

To get a quantitative picture of the microsegregation, we integrate Eq. (13.58). Then

$$\int_{C_L - C_0}^{C_L} \frac{dC_L}{C_L - C_s^*} = \int_{f_s=0}^{f_s} \frac{df_s}{1 - f_s},$$

or

$$1 - f_s = \exp \left[ - \int_{C_L - C_0}^{C_L} (C_L - C_s^*)^{-1} dC_L \right], \quad (13.59)$$

where  $C_0$  is the concentration of solute in the unsolidified melt (i.e., the alloy composition). In dendritically freezing alloys, the solid-liquid interface is very close to equilibrium so that  $C_s^*$  can be taken as the solid in equilibrium with the liquid. Many binary alloys have phase diagrams in which the ratio  $C_s^*/C_L = k$  can be approximated as a constant, called the equilibrium partition ratio. With a constant  $k$ , we can substitute  $C_s^* = kC_L$  into Eq. (13.59) and carry out the integration. The result is

$$\frac{C_L}{C_0} = (1 - f_s)^{k-1},$$

or

$$\frac{C_s^*}{C_0} = k(1 - f_s)^{k-1}. \quad (13.60)$$

As an example, suppose  $k = 0.3$ ; then the microsegregation according to Eq. (13.60) is shown in Fig. 13.10. The first solid that forms has a concentration  $C_s^* = kC_0$  and then succeeding solid has progressively higher values of  $C_s^*$ . But with no diffusion in the solid, the microsegregation, which develops, remains.

As  $f_s \rightarrow 1$ , Eq. (13.60) predicts  $C_s^* \rightarrow \infty$ . In reality, a reaction, such as a eutectic reaction, takes place near the end of solidification when the interdendritic liquid becomes sufficiently enriched in solute. In any event, after solidification is complete there is microsegregation, and in many applications it is necessary to subsequently heat treat the alloy to reduce the microsegregation by diffusion. This process is called homogenization.

During homogenization, the alloy naturally tends toward a uniform concentration (Fig. 13.11). We need only examine what happens within one dendritic element since the profile is periodic, and there is no net flow of solute from any dendritic region to the next.

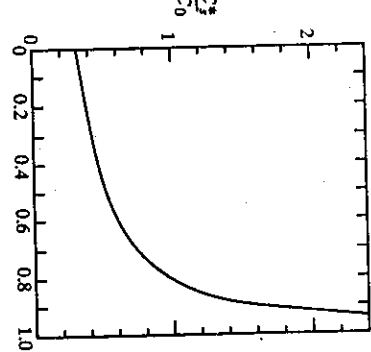


Fig. 13.10 Microsegregation in a dendritic solid with  $k = 0.3$ .

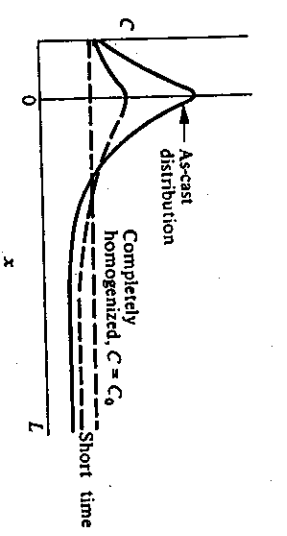


Fig. 13.11 Dendritic element,  $0 < x < L$ , used for describing homogenization kinetics.

To describe the homogenization kinetics, a solution to Fick's second law is needed that satisfies

$$\text{I.C.: } C(x,0) = f(x), \quad (13.61a)$$

$$\text{B.C.: } \frac{\partial C}{\partial x}(0,t) = 0, \quad (13.61b)$$

$$\frac{\partial C}{\partial x}(L,t) = 0, \quad t > 0. \quad (13.61c)$$

The solution can be obtained by applying the method of separation of variables. Here we simply present the solution as given by Crank:<sup>4</sup>

$$C(x,t) = C_0 + \sum_{n=1}^{\infty} A_n \exp \left[ -n^2 \pi^2 \frac{Dt}{L^2} \right] \cos \frac{n\pi x}{L}, \quad (13.62)$$

<sup>4</sup>J. Crank, *The Mathematics of Diffusion*, Oxford University Press, London, 1957, page 58.

with

$$A_n = \frac{2}{L} \int_0^L f(x) \cos \frac{n\pi x}{L} dx \quad (13.63)$$

In Eq. (13.62),  $C_0$  is the overall or average alloy content, and we evaluate the  $A_n$ s by Eq. (13.63) using  $f(x)$  as the initial solute distribution.

A useful parameter to describe the homogenization kinetics is the *residual segregation index*  $\delta$ , which is defined as

$$\delta = \frac{C_M - C_m}{C_M^0 - C_m^0}, \quad (13.64)$$

where  $C_M$  = maximum concentration, that is,  $C_M = C(0, t)$ ;  $C_M^0$  = initial maximum concentration, that is,  $C_M^0 = C(0, 0)$ ;  $C_m$  = minimum concentration, that is,  $C_m = C(L, t)$ ; and  $C_m^0$  = initial minimum concentration, that is,  $C_m^0 = C(L, 0)$ . For no homogenization,  $\delta = 1$ , and after complete homogenization,  $\delta = 0$ .

We can find  $C_M - C_m$  by applying Eq. (13.62) to  $x = 0$  and  $x = L$ , and performing the indicated subtraction. The residual segregation index can then be written as

$$\delta = \frac{2 \sum_{n=1,3,\dots,\text{odd}}^{\infty} A_n \exp \left[ -n^2 \pi^2 \frac{Dt}{L^2} \right]}{C_M^0 - C_m^0} \quad (13.65)$$

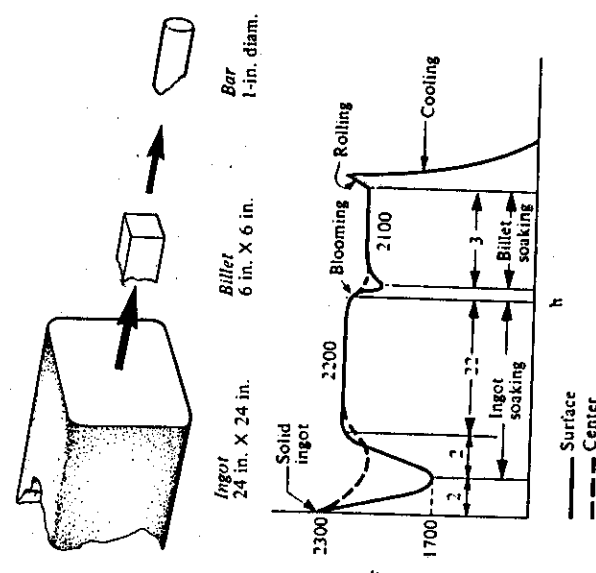
Equation (13.65) has been used to analyze the homogenization of chromium in cast 52100 steel (1%Cr-1.5%Cr). Figure 13.12 shows the results. The practical conclusions of such studies show that:

1. In commercial material, with relatively large dendrite arm spacing (200-400  $\mu\text{m}$ ), substitutional elements do not homogenize unless excessively high temperatures and long diffusion times are employed. For example, in laboratory-cast 52100 ingots the dendrite arm spacing could typically be 300  $\mu\text{m}$ , which would have to be held at 1450 K for about 20 hours to reduce  $\delta$  to 0.2 for chromium. In large commercial ingots, dendrite arm spacings are larger and homogenization is even more difficult to achieve.
2. Significant homogenization of substitutional elements is possible at reasonable temperatures and times only if the material has fine dendrite arm spacings ( $< 50 \mu\text{m}$ ), which result from rapid solidification.
3. Interstitial elements (such as carbon in steel) diffuse very rapidly at austenizing temperatures.

Homogenization studies have also been carried out for 4340 low-alloy steel<sup>5</sup> and 7075 aluminum alloy.<sup>6</sup> In Reference 6, the analysis and discussion of homogenization emphasizes the dissolution of a nonequilibrium second phase during solutionizing.

**Example 13.7** An ingot of 52100 steel goes through the processing schedule indicated below. Estimate the residual segregation index of chromium for the material in the center and the outside surface of the finished bar. Neglect the small amount of diffusion that occurs during blooming, rolling, and final cooling. Near the surface of the original cast ingot, the dendrite arm spacing is 40  $\mu\text{m}$ , and in the center, it is 800  $\mu\text{m}$ . The diffusion coefficient of chromium in this steel at these temperatures is given by

$$D = 2.35 \times 10^{-5} \exp [-17.300/T(\text{K})], \text{ cm}^2 \text{ s}^{-1}$$



Reduction schedule for 52100 alloy steel bars.

**Solution.** Before proceeding directly to the solution of this problem, we should recognize that, although the basis for Eq. (13.65) assumes a constant diffusion coefficient (hence isothermal treatment), we can apply it to non-isothermal conditions.

For example, if a part is subjected to  $n$  heat treatment steps, each at a different temperature and for different times, we can compute the total magnitude of  $Dt/L^2$  as

$$\frac{Dt}{L^2} = \frac{1}{L^2} \sum_{i=1}^n D_i t_i.$$

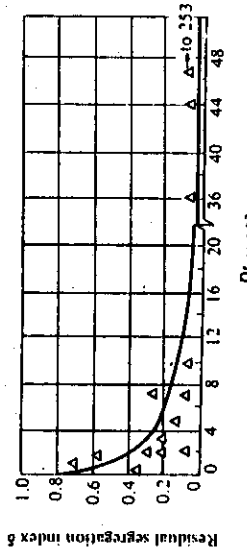


Fig. 13.12 The residual segregation index for chromium in cast 52100 steel. (From M. C. Flemings, D. R. Poirier, R. V. Barone, and H. D. Brody, *JISI*, 371, April 1970.)

<sup>5</sup>T. F. Kattamis and M. C. Flemings, *Trans. TMS-AIME* 233, 992 (1965).

<sup>6</sup>S. N. Singh and M. C. Flemings, *Trans. TMS-AIME* 245, 1803 (1969).

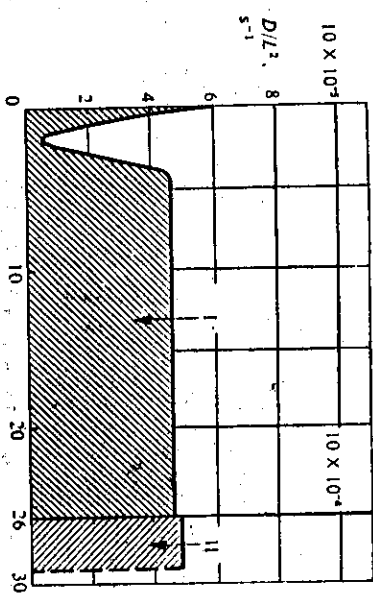
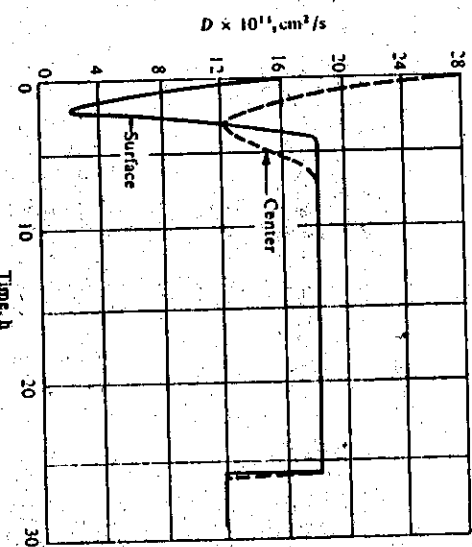
We can then use this value of  $Dt/L^2$  in Eq. (13-65). For a continuous nonisothermal situation, we compute the total magnitude of  $Dt/L^2$  to be used as

$$\frac{Dt}{L^2} = \frac{1}{L^2} \int_0^t D(t) dt.$$

For hot-working in which  $D$  and  $L$  are both time dependent,  $Dt/L^2$  should be evaluated as

$$\frac{Dt}{L^2} = \int \frac{D(t)}{[L(t)]^2} dt.$$

Now we determine  $D(t)$ , given the thermal process schedule and  $D(T)$ .



According to Fig. 13.12, this value of  $Dt/L^2$  indicates that the surface material would be homogeneous since  $\delta \approx 0$ . In the center of the ingot, since the dendrite spacing is 20 times the spacing of the surface, then (neglecting small differences in the thermal history)

$$\frac{Dt}{L^2} (\text{center}) = \frac{Dt}{L^2} (\text{surface}) \times \frac{1}{20^2} = \frac{9.10}{400} = 0.0228.$$

From Fig. 13.12, we see that  $\delta \approx 0.27$ , and a significant amount of microsegregation remains in the material.

During the processing, assume that the dendrite spacing decreases in proportion to the changes of linear dimensions. Based on this,  $L(t)$  is given in the table below.

Time	Center of ingot, $L, \text{cm}$	Surface of ingot $L, \text{cm}$
0-26 h	0.040	0.0020
26-29 h	0.010	0.0005

The rate of formation of oxide (sulfide) layers on metals and alloys exposed to oxidizing (sulfidizing) conditions is a matter of considerable technological importance. In general, it is not possible to say *a priori* that the rate of formation of a nonmetallic layer will be controlled by diffusion. For example, the initial rate of formation of the layer is often determined by the rate of an interface reaction between the gas and solid. As growth proceeds, if the specific volume of the oxide is much larger than that of the metal substrate, separation of the two phases may occur, causing an interruption in the growth of the oxide layer. However, in many cases this separation does not occur, and growth continues by diffusion of either the metal out through the oxide layer, or diffusion of oxygen into the metal-oxide interface, or a combination of both. In the case of adherent oxides, eventually

the diffusion flux slows down to the point where it is considerably slower than the interface reaction, and diffusion controls the rate of growth of the layer from then on.

If we consider the situation in Fig. 13.13, we can derive an expression for the rate of increase in the oxide thickness  $M$ . In this example, the metal is divalent, and the oxygen anions, having a large ionic radius, diffuse only at a negligible rate through the oxide layer so that  $j_{O^2} = 0$ . Thus the oxide thickens because the metal cations diffuse through the oxide so that the oxidation reaction can proceed. At any instant, the flux of cations through the oxide is given by Fick's law (Eq. (12.2)):

$$j = (j_{A^2+}) = -D \left[ \frac{\partial C}{\partial x} \right].$$

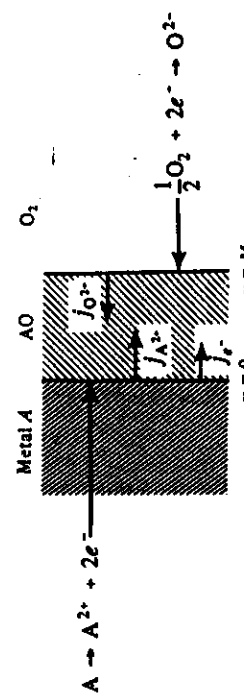


Fig. 13.13 The oxide layer on a metal showing the direction of flow of ions and electrons.

Here  $D$  is the diffusivity of the cation, and  $C$  is the cation concentration. If the oxide layer is thin, then we approximate the concentration profile of the cation as linear, and can integrate Fick's law as

$$j \int_0^M dx = - \int_{C_0}^{C_M} D dC.$$

Here,  $C_0$  is the cation concentration at  $x = 0$ , and  $C_M$  is that at  $x = M$ . If the boundary conditions  $C_M$  and  $C_0$  are unchanged with time (that is, with  $M$ ), then the instantaneous flux at any thickness  $M$  is

$$j = \frac{1}{M} \int_{C_0}^{C_M} D dC, \quad (13.66)$$

or

$$j = \frac{k}{M},$$

where  $k$  is a constant, and has the units of  $\text{mol m}^{-1} \text{s}^{-1}$ .

The flux is proportional to the rate of growth of the thickness of the oxide layer:

$$j \propto \frac{dM}{dt}.$$

or

$$\frac{k}{M} \propto \frac{dM}{dt}, \quad (13.67)$$

so that

$$\int_0^M M dM = \int_0^t k' dt,$$

or

$$M^2 = 2k't, \quad (13.68)$$

where  $k'$  is a constant with units  $\text{m}^2 \text{s}^{-1}$ , known as the *Tammann scaling constant*<sup>7</sup> or the *Pilling and Bedworth constant*.<sup>8</sup> The parabolic nature of the rate of change of the oxide thickness with time is apparent.

Experimentally, it is usually more convenient to measure mass gain rather than the oxide thickness. Then

$$\frac{\Delta m}{A} = M\rho_0, \quad (13.69)$$

where  $\Delta m/A = \text{kg}$  (mass gained)  $\text{m}^{-2}$  (surface area), and  $\rho_0$  = concentration of oxygen in the oxide,  $\text{kg}$  of oxygen  $\text{m}^{-3}$  of oxide.

If we substitute Eq. (13.69) into Eq. (13.68), we obtain

$$\left[ \frac{\Delta m}{A} \right]^2 = \frac{2k'}{\rho_0^2} t,$$

or

$$\left[ \frac{\Delta m}{A} \right]^2 = k_p t, \quad (13.70)$$

where  $k_p$  is the *practical parabolic scaling constant*,  $(\text{kg O}_2)^2 \text{m}^{-4} \text{s}^{-1}$ . Usually, we obtain experimental data by mass gain measurements, and take straight-line behavior when we plot  $(\Delta m/A)^2$  versus  $t$  as an indication of diffusion-controlled oxidation.

Such data alone, however, do not indicate which species is responsible for the major material flow, that is, whether the metal is diffusing out from the oxide-metal interface or the oxygen is diffusing in. Wagner<sup>9</sup> has extended this simple expression to express  $k_p$  in terms of diffusion coefficients of the migrating species.

Combining Eqs. (12.23), (12.37), and (12.39), we obtain the relation

$$n_i B_i = \frac{t_i \sigma}{(\zeta_i e)^2}, \quad (13.71)$$

<sup>7</sup>G. Tammann, *Z. Anorg. u. Allgem. Chem.* 111, 78 (1920).

<sup>8</sup>N. B. Pilling and R. E. Bedworth, *J. Inst. Metals* 29, 529 (1923).

<sup>9</sup>C. Wagner, *Atom Movements*, Amer. Soc. for Metals, Cleveland, OH, 1951, page 153.

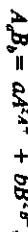
where  $n_i$  = concentration of the migrating species,  $B_i$  = mobility of the species,  $\sigma$  = total electrical conductivity of the compound,  $t_i$  = transference number of species  $i$ ,  $z_i$  = valence, and  $e$  = electronic charge. Now, using Eq. (12.32) and substituting Eqs. (12.37) and (13.71), we obtain the flux  $\dot{n}_i$ :

$$\dot{n}_i = -\frac{t_i \sigma}{(z_i e)^2} \left[ k_B T \left[ \frac{\partial \ln n_i}{\partial x} \right] + z_i e \left[ \frac{\partial \phi}{\partial x} \right] \right], \quad (13.72)$$

or in terms of the free energy for an ideal solution

$$\dot{n}_i = -\frac{t_i \sigma}{(z_i e)^2} \left[ \frac{\partial \mu_i}{\partial x} + z_i e \frac{\partial \phi}{\partial x} \right]. \quad (13.73)$$

where  $\mu_i$  is the chemical potential (per atom) of species  $i$ . If the compound formed has the stoichiometric composition  $A_x B_b$ , where  $A$  is the cation, then the scale consists of ions according to the dissociation reaction:



where the  $z$ s are the respective valences. Since the scale cannot have a net charge, the fluxes of individual species are related by

$$z_a \dot{n}_{A^+} = z_b \dot{n}_{B^-} + \dot{n}_e. \quad (13.74)$$

Using Eq. (13.73) for each flux and recalling Eq. (12.38), we obtain an expression for  $\partial \phi / \partial x$ :

$$\frac{\partial \phi}{\partial x} = \frac{1}{e} \left[ -\frac{t_a}{z_a} \frac{\partial \mu_{A^+}}{\partial x} + \frac{t_b}{z_b} \frac{\partial \mu_{B^-}}{\partial x} + t_e \frac{\partial \mu_e}{\partial x} \right]. \quad (13.75)$$

In order to obtain an expression for the total flux in terms that we can measure, we must replace the expressions involving  $\mu_{A^+}$ ,  $\mu_{B^-}$ , and  $\mu_e$ . We first consider the equilibria

$$A = A^{x+} + z_e e, \quad (13.76a)$$

and

$$B + z_B e = B^{x-}. \quad (13.76b)$$

At equilibrium

$$\mu_A = \mu_{A^+} + z_A \mu_e, \quad (13.76c)$$

and

$$\mu_B = \mu_{B^-} - z_B \mu_e. \quad (13.76d)$$

For the compound in general, we get

$$d\mu_A = - \left| \frac{z_A}{z_B} \right| d\mu_B, \quad (13.77)$$

from the Gibbs-Duhem relationship. Then, eliminating  $\mu_{A^+}$ ,  $\mu_{B^-}$ , and  $\mu_e$  from Eqs. (13.75) and (13.73) and using Eqs. (13.76a,b) and (13.77), we obtain expressions for the particle fluxes:

$$\dot{n}_A^+ = \frac{z_B t_A t_e \sigma}{z_A e^2 z_B} \left[ \frac{\partial \mu_B}{\partial x} \right], \quad A \text{ ions m}^{-2} \text{ s}^{-1} \quad (13.78)$$

and

$$\dot{n}_B^- = - \frac{t_B t_e \sigma}{e^2 z_A^2} \left[ \frac{\partial \mu_B}{\partial x} \right], \quad B \text{ ions m}^{-2} \text{ s}^{-1}. \quad (13.79)$$

Since the growth rate of the compound is the sum of the particle fluxes (although either may go to zero), we obtain

$$\dot{n}_{A_x B_b} = \frac{n_A^+}{a} - \frac{\dot{n}_B^-}{b} = \frac{\dot{\sigma}(t_A + t_B)t_e}{e^2 z_A^2 z_B} \left[ \frac{\partial \mu_B}{\partial x} \right], \quad \text{molecules } A_x B_b \text{ m}^{-2} \text{ s}^{-1}. \quad (13.80)$$

If we use, for some reason, Eq. (13.80), we usually convert the units to give the flux in g-equivalents  $\text{m}^{-2} \text{ s}^{-1}$ . Denoting the number of equivalents per mole by the symbol  $r$ , we obtain the growth rate:

$$\dot{n}_{A_x B_b} = \frac{r \sigma (t_A + t_B) t_e}{e^2 z_A^2 N_0} \left[ \frac{\partial \mu_B}{\partial x} \right], \quad \text{g-equivalents } A_x B_b \text{ m}^{-2} \text{ s}^{-1}. \quad (13.81)$$

We define the *reaction rate constant*,  $k_r$ , as  $\int_0^x \dot{n}_{A_x B_b} dx$ ; then

$$k_r = \frac{r}{e^2 N_0 z_B^2} \int_{\mu_B^0}^0 \sigma (t_A + t_B) t_e d\mu_B, \quad (13.82)$$

where  $\mu_B^0$  and  $\mu_B^0$  are the chemical potentials of  $B$  at the inside and outside (metal and gas) interfaces of the oxide, respectively;  $k_r$  has the units of g-equivalents  $\text{m}^{-1} \text{ s}^{-1}$  and is related to the parabolic rate constant  $k_p$  by

$$k_p = \frac{2 \rho_0 (\text{at. wt } B)^2}{r (\text{mol. wt } A_x B_b)} k_r. \quad (13.83)$$

The Tammann scaling constant is related to  $k_r$  by

$$k' = \frac{2(\text{at. wt } B)}{\rho_0 \bar{z}_B} k_r. \quad (13.84)$$

\*Note that numerically  $r = z_B$ , but that their units differ.

If we assume that the anion exists as  $B_2$  in the gaseous state, and there is ideal gas behavior, we can substitute

$$d\mu_B = \frac{1}{2} k_B T d \ln P_{B_2}$$

into Eq. (13.82) and obtain

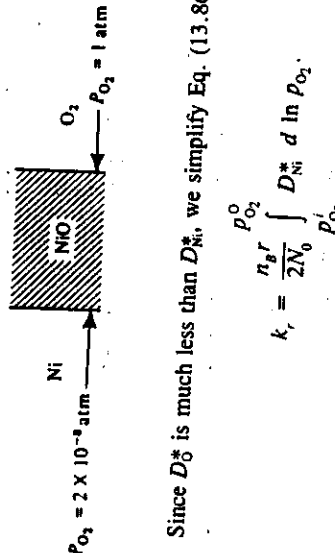
$$k_r = \frac{r k_B T}{2e^2 N_0 z_s^2} \int \frac{t_e(t_e + t_s)\sigma}{P_{B_2}} d \ln P_{B_2} \quad (13.85)$$

We note that although  $t_e$  may approach 1.0, and  $(t_e + t_s)$  may approach zero, the expression  $(t_e + t_s)$  cannot equal zero even for an electronic oxide conductor because it would cause a charge imbalance. In an electronic semiconductor, the product  $t_e(t_e + t_s)$  is a very small number, and  $k_r$  is small. In this case, where  $t_e = 1.0$ , if we assume that mobilities  $B_A$  and  $B_B$  are equal to  $B_A^*$  and  $B_B^*$ , respectively, we can substitute Eq. (12.37) into Eq. (13.85) and obtain

$$k_r = \frac{n_s r}{2N_0} \int \left[ \left| \frac{z_s}{z_s} \right|^2 \frac{n_s}{n_s} D_A^* + D_B^* \right] d \ln P_{B_2} \quad (13.86)$$

When  $D_A^*$  or  $D_B^*$  are very different in magnitude, we may further simplify this expression as shown in the following example.

**Example 13.8** Given the diffusion data for self-diffusion of  $\text{Ni}^{2+}$  and  $\text{O}^{2-}$  ions in  $\text{NiO}$  at 1190°C, calculate the rational rate constant and the parabolic rate constant for the oxidation of Ni in pure oxygen. It is known that  $D_O^* \ll D_{\text{Ni}}^*$ .



**Solution.** Since  $D_O^*$  is much less than  $D_{\text{Ni}}^*$ , we simplify Eq. (13.86) to

$$k_r = \frac{n_s r}{2N_0} \int \frac{D_{\text{Ni}}^*}{P_{O_2}} d \ln P_{O_2}$$

The term  $n_s r / N_0$  has the units of equivalents  $\text{m}^{-3}$ . In this case, we have

$$\begin{aligned} \frac{n_s r}{N_0} &= \frac{2\rho_{\text{NiO}}}{\text{mol. wt}_{\text{NiO}}} = \frac{2(7.44 \times 10^3)}{74.69} = 1.99 \times 10^2 \text{ equivalents m}^{-3} \\ &= 9.33 \times 10^{-8} (\text{kg O}_2)^2 \text{ m}^{-4} \text{ s}^{-1}. \end{aligned}$$

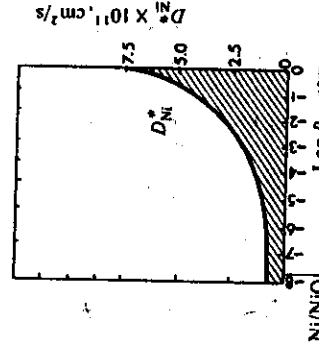
Diffusion in Solids 497  
Alternatively, if we take  $z_s$  as electronic charges per  $B$  atom, and  $n_s$  is the concentration of  $B$  atoms  $\text{m}^{-3}$ , then we must divide by Faraday's constant, 96,487 coulombs/equivalent, and multiply by the charge on an electron,  $1.602 \times 10^{-19}$  coulombs per charge. In this case, we get

$$\begin{aligned} k_r &= \frac{n_s z_s e}{F^2} \int \frac{D_{\text{Ni}}^*}{P_{O_2}} 2.3 d \ln P_{O_2} \\ &= \frac{(6.00 \times 10^{28})(2)(1.602 \times 10^{-19})}{2 \times 96,487} \int \frac{D_{\text{Ni}}^*}{P_{O_2}^0} d \ln P_{O_2}. \end{aligned}$$

Thus either way

$$k_r = \frac{1.99 \times 10^2}{2} \int \frac{D_{\text{Ni}}^*}{P_{O_2}^0} d \ln P_{O_2}.$$

We evaluate the integral graphically. The figure below gives  $D_{\text{Ni}}^*$  as a function of  $P_{O_2}$  in  $\text{NiO}$ . The area under the curve is equal to the integral/2.303. The area is:



equal to  $16 \times 10^{-15} \text{ m}^2 \text{ s}^{-1}$ . Therefore

$$k_r = \left[ \frac{1.99 \times 10^2}{2} \right] (2.303)(16 \times 10^{-15}) = 3.66 \times 10^{-12} \text{ equivalents m}^{-1} \text{ s}^{-1}.$$

From Eq. (13.83), the parabolic rate constant is

Many metals exhibit parabolic oxidation kinetics, among them iron, nickel, cobalt, manganese, copper, and aluminum. Table 13.4 lists some typical values of  $k_p$ . Some, however, do not form compact, adherent oxides, and the kinetics of their oxidation are governed by either gas-solid reaction rates or gas-phase transport. For example, both molybdenum and tungsten form oxides that volatilize immediately upon reaction, and continually expose fresh metal to further oxidation, with no limit by solid-state diffusion on the rate.

Table 13.4 Parabolic oxidation constants for various metals

Metal	Oxide	$k_p$ , $\text{kg O}_2 \text{m}^{-2} \text{s}^{-1}$	Conditions	
			Temp., °C	$P_{\text{O}_2}$ , atm
Co	CoO	$2.43 \times 10^{-6}$	1000	1.0
Cu	Cu <sub>2</sub> O	$6.3 \times 10^{-7}$	1000	0.083
Ni	NiO	$3.8 \times 10^{-4}$	1000	1.0
Fe	FeO	$1.6 \times 10^{-5}$	1000	$3 \times 10^{-14}$
Fe	FeO/Fe <sub>3</sub> O <sub>4</sub> /Fe <sub>2</sub> O <sub>3</sub>	$1.4 \times 10^{-4}$	1000	1.0
Ni-10%Cr	Complex	$5.0 \times 10^{-5}$	1000	1.0
Cr	Cr <sub>2</sub> O <sub>3</sub>	$1.3 \times 10^{-5}$	900	0.1
Fe-1%Ti	Complex	$1.6 \times 10^{-5}$	1000	1.0
Al	Al <sub>2</sub> O <sub>3</sub>	$8.5 \times 10^{-14}$	600	1.0

\*There is a considerable variation in this number, since the surface condition appears to have a strong effect.

Certain metals absorb a significant amount of oxygen in solid solution during the process of oxidation; zirconium, for example, can dissolve up to 29 at. % oxygen in solid solution prior to the formation of ZrO<sub>2</sub>. Once the oxide layer has formed, its thickness increases in proportion to  $\sqrt{k_p t}$ , according to Eq. (13.79), and the thickness of the oxide as measured from the original surface is

$$M = \frac{2\hat{V}_{\text{Zr}}}{\hat{V}_{\text{ZrO}_2}} \sqrt{k_p t}, \quad (13.87)$$

where  $\hat{V}_{\text{Zr}}$  is the molar volume of Zr and  $\hat{V}_{\text{ZrO}_2}$  is the molar volume of ZrO<sub>2</sub>. The diffusing species in the oxide is the oxygen anion moving in from the gas phase to the ZrO<sub>2</sub>-Zr interface. At the interface, some of the oxygen dissolves in the metal, and some reacts to form more ZrO<sub>2</sub>. Beyond the interface and into the metallic phase, for  $x > M$ , we have

$$\frac{\partial T}{\partial t} = D_0 \frac{\partial^2 C}{\partial x^2}, \quad (13.88)$$

where  $C$  is the oxygen concentration, mol m<sup>-3</sup>. If equilibrium is established at all times at the interface, and  $C_i$  is the oxygen content of the metal in equilibrium with ZrO<sub>2</sub>, then

$$C(M, T) = C_i, \quad (13.89a)$$

$$C(\infty, t) = 0, \quad (13.89b)$$

$$(13.89c)$$

The solution to Eq. (13.88) subject to Eqs. (13.87) and (13.89a,b,c) is

$$C = C_i \frac{\operatorname{erfc} \left[ \frac{x'}{2\sqrt{D_0 t}} + \frac{\hat{V}_{\text{Zr}}}{\hat{V}_{\text{ZrO}_2}} \sqrt{k_p / D_0} \right]}{\operatorname{erfc} \left[ \frac{\hat{V}_{\text{Zr}}}{\hat{V}_{\text{ZrO}_2}} \sqrt{k_p / D_0} \right]}, \quad (13.90)$$

where  $x$  is the distance from the original interface, and  $x' = x - M$ , where  $x'$  is the distance from the oxide-metal interface. Thus

$$C = C_i \frac{\operatorname{erfc} \left[ \frac{x'}{2\sqrt{D_0 t}} + \frac{\hat{V}_{\text{Zr}}}{\hat{V}_{\text{ZrO}_2}} \sqrt{k_p / D_0} \right]}{\operatorname{erfc} \left[ \frac{\hat{V}_{\text{Zr}}}{\hat{V}_{\text{ZrO}_2}} \sqrt{k_p / D_0} \right]}, \quad (13.91)$$

### PROBLEMS

- 13.1 One side of an iron sheet, 0.01 cm thick, is subjected to a carburizing atmosphere at 1200 K such that a surface concentration of 1.2% carbon is maintained. The opposite face is maintained at 0.1% carbon. At steady state, determine the flux (mol cm<sup>-2</sup> s<sup>-1</sup>) of carbon through the sheet: a) if the diffusion coefficient is assumed to be independent of concentration ( $D = 2 \times 10^{-7}$  cm<sup>2</sup> s<sup>-1</sup>); b) if the diffusion coefficient varies as shown to the right.
- 

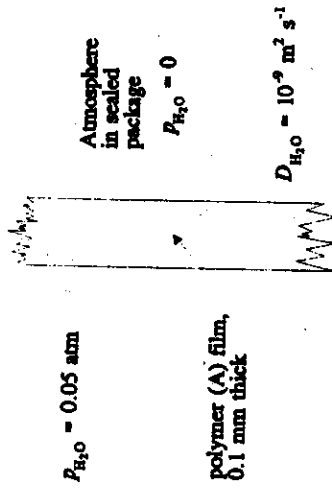
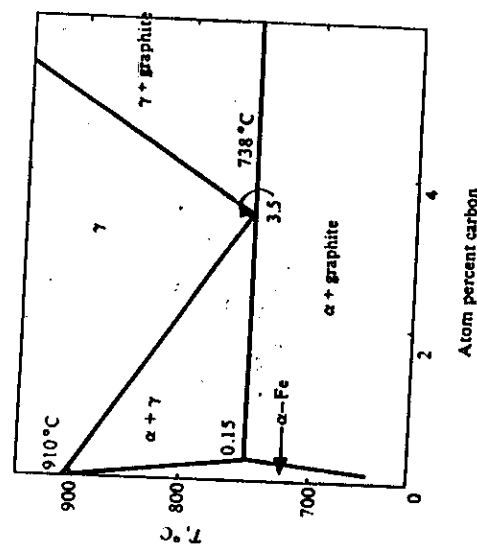
- 13.2 A composite foil made of metal A bonded to metal B, each 0.01 cm thick, is subjected to 0.5 atm of pure hydrogen on metal A's face; the other side, metal B's face, is subjected to a perfect vacuum. At the temperature of interest and 1 atm of hydrogen, the solubility of hydrogen in metal A is  $4 \times 10^{-5}$  g per cm<sup>3</sup> of A and in B it is  $1 \times 10^{-4}$  g per cm<sup>3</sup> of B. It is also known that hydrogen diffuses four times faster in A than B and that A and B do not diffuse in each other. Draw the concentration profile of hydrogen across the composite foil at steady state.

13.3 A thin sheet of iron at 800°C is subjected to different gaseous atmospheres on both of its surfaces such that the composition of one face is at 4 atom percent carbon and the other is at zero atom fraction carbon. At steady state, make a plot of the composition profile in the sample indicating clearly compositions and respective distances.

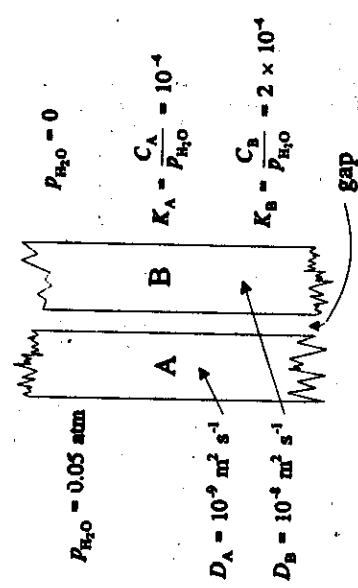
The thickness is 1 mm and density changes during the experiment may be neglected. At 800°C, it is known that the diffusion coefficient of carbon in iron is given by:

$$D = 10^{-6} \text{ cm}^2 \text{ s}^{-1} \text{ in ferrite } (\alpha),$$

$$D = 10^{-8} \text{ cm}^2 \text{ s}^{-1} \text{ in austenite } (\gamma).$$



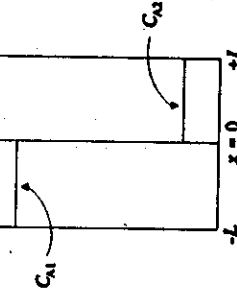
b) Now two films, polymer A and B, are used. Each is 0.1 mm thick.



Assume steady state and equilibrium at all interfaces. What is the pressure of H<sub>2</sub>O(g) in the gap?

13.5 Hydrogen gas is maintained at 3 bar and 1 bar on opposite sides of a plastic membrane which is 0.3 mm thick. The temperature is 25°C, and the diffusion coefficient of hydrogen in the plastic is  $8.7 \times 10^{-10} \text{ m}^2 \text{ s}^{-1}$ . The solubility of hydrogen in the membrane is  $1.5 \times 10^{-3} \text{ kmol m}^{-3} \text{ bar}^{-1}$ . What is the mass diffusion flux of hydrogen through the membrane? Give your result in  $\text{kmol s}^{-1} \text{ m}^{-2}$ .

13.6 The Grube solution is used to analyze diffusion data for a diffusion couple in which the solid is semi-infinite on both sides and when the chemical diffusion coefficient is uniform. Now consider a diffusion couple made from two thin solids so that the Grube solution for semi-infinite solids is not applicable. Such a couple is shown to the right with the initial condition for C<sub>A</sub> shown. a) Assume that D is uniform. Write a partial differential equation for C<sub>A</sub>(x,t) where x is the space coordinate and t is time.



b) For  $0 \leq x \leq L$ , write appropriate boundary conditions and an appropriate initial condition for C<sub>A</sub>. You may assume that component A is not volatile; i.e., no A is lost from the diffusion couple.

13.4 Often electronic packages are hermetically sealed with polymers, but after being put in service corrosion is sometimes observed. This happens because H<sub>2</sub>O molecules can diffuse through polymers. Assume that the equilibrium between water vapor and water dissolved (or absorbed) by the polymer is simply represented by the reaction:

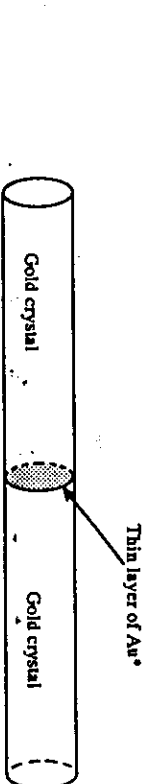


with the equilibrium constant

$$K = \frac{C}{P_{\text{H}_2\text{O}}} = 10^{-4},$$

where C is the concentration of H<sub>2</sub>O in the polymer (moles cm<sup>-3</sup>) and P<sub>H<sub>2</sub>O</sub> is the pressure of H<sub>2</sub>O(g) in atm.  
a) Assume equilibrium at the surfaces and calculate the flux of H<sub>2</sub>O through the polymer (in moles cm<sup>-2</sup> s<sup>-1</sup>); assume steady state.

13.7 An unknown amount of radioactive gold is deposited as a thin layer on the ends of two rods of gold. The two rods are then joined to form a specimen having a planar source of radioactive gold ( $Au^+$ ) atoms at the origin  $x = 0$ . After diffusion for 100 hours at  $920^\circ C$ , the distribution of  $Au$  is as shown below. Calculate the self-diffusion coefficient of gold in pure gold, based on the data at 0.3 mm and 0.6 mm as indicated in the plot of the relative concentration of gold.



13.8 Silicon is exposed to a gas that establishes a concentration of  $10^{18}$  atoms ( $Al$ )  $cm^{-3}$  on the surface of the silicon. The process is carried out at  $1473\text{ K}$ .

- a) After 30 min, at what depth below the surface of the Si will the concentration be  $10^{16}$  atoms  $cm^{-3}$ ? b) Calculate the amount of Al (in atoms  $cm^{-2}$ ) that diffuses into the Si after 30 min of treatment at  $1473\text{ K}$ .

13.9 The Matano-Boltzmann analysis is used to calculate the interdiffusion coefficient,  $\bar{D}$ , from diffusion couple data. It can also be used to determine the intrinsic diffusion coefficients in a binary by inserting inert markers at the original interface.

- a) The distance moved by the markers is proportional to the square root of time. Show that  $v_t$  in Eq. (12.14) is given by

$$v_t = \frac{S}{2t},$$

where  $S$  is the distance moved by the markers and  $t$  is the diffusion time.

- b) Assuming that  $\bar{D}$  and  $S$  are determined in a diffusion-couple, what two equations are needed to simultaneously solve for the intrinsic diffusion coefficients in the binary.

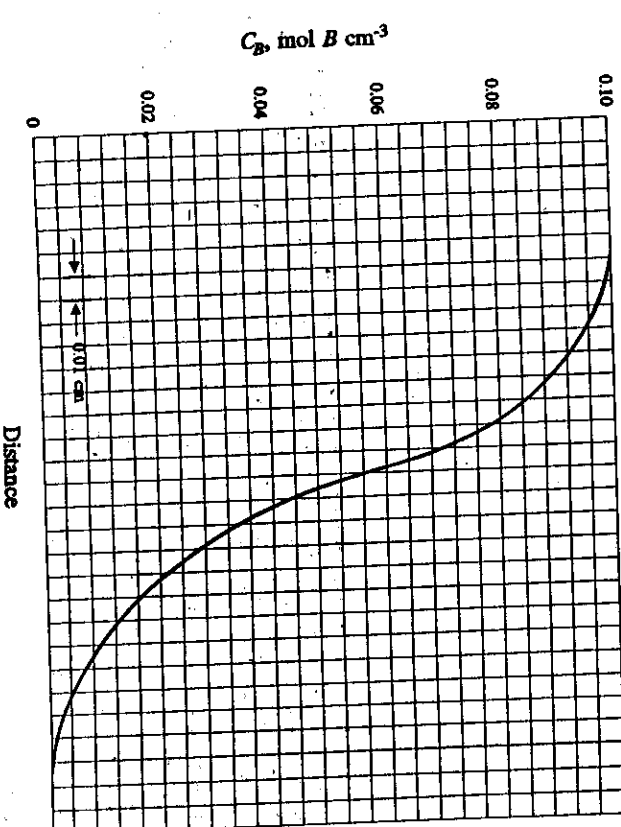
[Hint: Review Section 12.2.2.]

13.10 A gold-nickel diffusion couple of limiting compositions  $X_{Ni} = 0.0974$  and  $X_{Ni} = 0.4978$  is heated at  $925^\circ C$  for  $2.07 \times 10^6$  s. Layers 0.003 in. (0.0762 mm) thick and parallel to the original interface are machined off and analyzed. a) Using the data tabulated

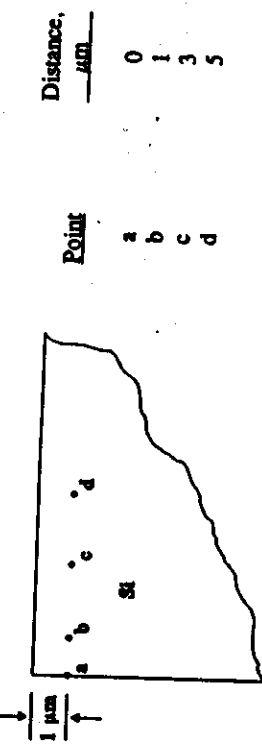
below, calculate the diffusion coefficient at 20, 30, and 40 at. % nickel. b) Suppose that markers are inserted at the original interface and move along during the diffusion process at a composition of 0.30 atom fraction nickel. From this, determine the intrinsic coefficients of gold and nickel at 0.30 atom fraction nickel.

Slice No.	at % Ni						
11	49.73	21	35.10	29	21.38	38	13.26
12	49.59	22	33.17	30	20.51	39	12.55
14	47.45	23	31.40	31	19.12	41	11.41
16	44.49	24	29.74	32	17.92	43	10.48
18	40.58	26	25.87	33	16.86	45	9.99
19	38.01	27	24.11	35	15.49	47	9.74
20	37.01	28	22.49	37	13.90		

13.11 Metals A and B form alloys of fcc structure at  $1200^\circ C$ . They are allowed to interdiffuse as a diffusion couple for  $10^5$  s, and the concentration profile obtained is given in the accompanying figure. Determine the value of the interdiffusion coefficient,  $D$ , at a concentration  $C_B = 0.02$  mol  $cm^{-3}$ .

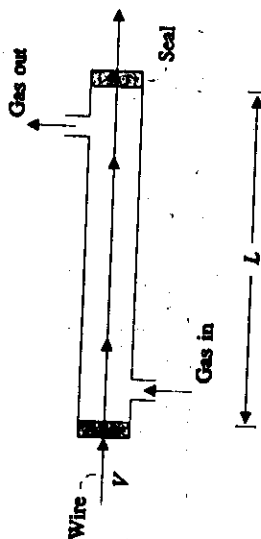


13.12 Intrinsic silicon (i.e., pure Si) is processed in a gas which establishes a concentration of 10 ppm (1 ppm =  $10^{-4}$  wt. %) of boron at the surface of the silicon. Distances from the left vertical face are given in the following table.



After 10 h exposure to the gas, what are the concentrations of boron at points a, b, c and d?  
At the process temperature, the diffusion coefficient for B in Si is  $D = 10^{-11} \text{ cm}^2 \text{ s}^{-1} = 10^{-4} \frac{\mu\text{m}^2}{\text{s}}$ .

13.13 A fine steel wire of 0.2 wt. % C is passed through a tube furnace at 1200°C which contains a carburizing gas. The composition of the carburizing gas is adjusted so that it fixes 0.8 wt. % C on the surface of the wire. By neglecting diffusion in the axial direction of the wire, calculate the average composition of the wire after it passes through the tube. At this temperature the steel is a single phase (austenite). Data: diameter of wire, 0.01 cm; length of furnace,  $L$ , 1.5 m; velocity of wire,  $V$ , 15 cm  $\text{s}^{-1}$ .



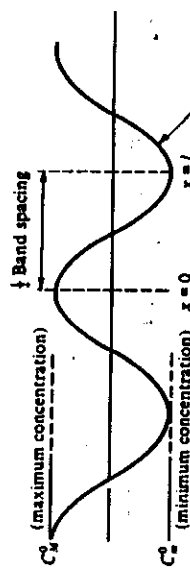
13.14 A thin layer of Au is plated on to the end of a Ni bar. The bar is annealed at 900°C for 10 h; at 900°C the interdiffusion coefficient of Au in Ni is  $10^{-11} \text{ cm}^2 \text{ s}^{-1}$ . It is known that Au and Ni are completely soluble at 900°C. After the treatment, the concentration of Au at a distance of 0.05 cm from the end is 0.1 atom fraction of Au. At what distance from the end is the atom fraction of Au equal to 0.05?

13.15 A long cylindrical bar of steel which contains 3 ppm of hydrogen is dehydrogenated by a two-step vacuum process. The first step is treatment at 150°C for time period  $t_1$ , followed by the second step at 300°C for time period  $t_2$ . If  $t_1 = 2t_2$ , calculate: a) the total time ( $t = t_1 + t_2$ ) to reduce the average composition to 1.5 ppm of hydrogen, and b) the center composition after the two-step treatment. Data:  $D_H = 1.0 \exp(-4000/T)$  with  $D_H$  in  $\text{cm}^2 \text{ s}^{-1}$  and  $T$  in K. The diameter of the bar is 2 cm.

13.16 The solubility of hydrogen in solid copper at 1000°C is 1.4 ppm (by mass) under a pressure of hydrogen of 1 atm. At 1000°C,  $D_H = 10^{-6} \text{ cm}^2 \text{ s}^{-1}$ . a) Determine the time for hydrogen to reach a concentration of 1.0 ppm at a depth of 0.1 mm in a large chunk of copper initially with null hydrogen if the copper is subjected to 2 atm pressure of  $\text{H}_2$  at

1000°C. b) Copper foil, 0.2 mm thick, is equilibrated with hydrogen at a pressure of 4 atm at 1000°C. The same foil is then placed in a perfect vacuum at 1000°C and held for 60 s. Calculate the concentration of hydrogen at the center of the foil after the 60 s period.

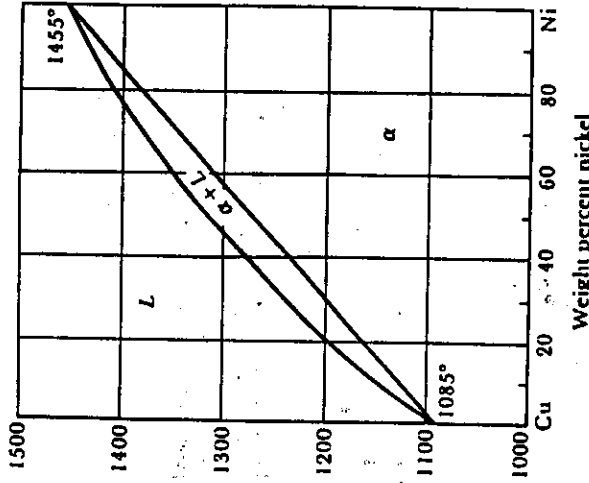
13.17 The term "banding" is used to describe chemical heterogeneity in rolled alloys that shows up as closely spaced light and dark bands in the microstructure of steel. These bands represent areas of segregation of alloying elements that formed during freezing of the ingot. During rolling the segregated areas are elongated and compressed into narrow bands. Assume that the alloy concentration varies sinusoidally with distance after rolling according to the sketch below.



$$C = C_0 + (C_M^0 - C_0) \cos \frac{\pi x}{l}$$

If the steel is now heated to the austenitic range and held at some constant temperature, then a) schematically sketch the concentration profile as time passes; b) write a differential equation for concentration (state assumptions) and c) write the boundary conditions (for time and space) that apply; d) solve for the concentration as a function of time and x; e) derive an equation for the residual segregation index.

13.18 Assume that the banding in a wrought cupronickel alloy (single phase) is described by the cosine function in Problem 13.17. The average composition of the alloy is 10% Ni-90% Cu, and the segregation ratio before homogenization is 1.4. Segregation ratio is defined as  $S = C_M^0/C_m^0$ . a) What are the maximum and minimum compositions of nickel? b) In order to homogenize the alloy in the shortest time possible, what temperature would you select? c) If the average distance between maximum compositions is  $10^{-2}$  cm, determine the time to achieve a residual segregation ratio of 0.1 at 950°C. A diffusion coefficient can be obtained from Fig. 12.9. d) The alloy is given a "step" homogenization treatment which consists of 10 hours at 700°C, 10 hours at 800°C and 10 hours at 900°C. What is the residual segregation index after this treatment?



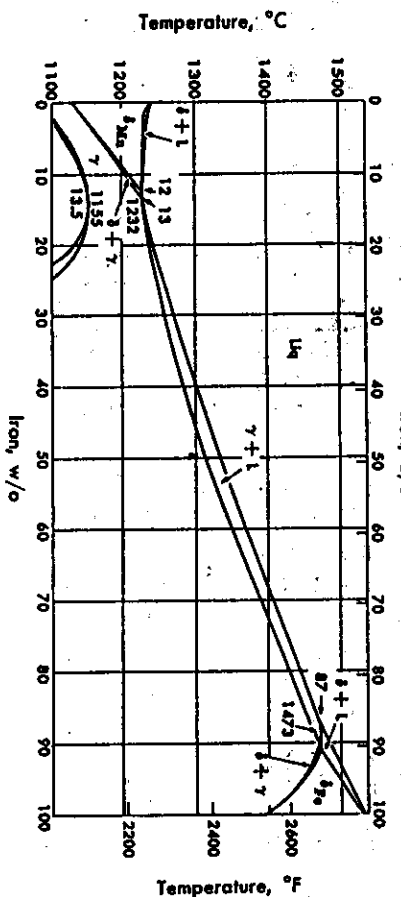
**13.19** A junction in silicon is made by doping with boron using predeposition followed by drive-in diffusion. a) Five minutes at  $1100^{\circ}\text{C}$  are required to deposit the dopant. At what distance from the surface is the concentration of boron raised to  $3 \times 10^{11} \text{ atoms cm}^{-3}$ ? Assume that the silicon is initially pure. b) How much boron (per  $\text{cm}^2$  of silicon surface) will have been taken up by the silicon during the deposition step? c) To prevent loss of boron during the drive-in step, the surface is masked with silica ( $\text{SiO}_2$ ). Now calculate the time required to achieve a concentration of boron equal to  $3 \times 10^{18} \text{ atoms cm}^{-3}$  at a depth of 6  $\times 10^{-4} \text{ cm}$  if the drive-in treatment is carried out at  $1150^{\circ}\text{C}$ .

**13.20** By ion implantation, lithium can be concentrated in a very thin surface layer ( $10^{-6} \text{ cm}$ ) on a nickel substrate. After implanting the surface layer, it has a lithium concentration of  $10^{20} \text{ atoms cm}^{-3}$ . Determine the time at  $1000 \text{ K}$  for reducing the surface concentration to  $10^{19} \text{ atoms cm}^{-3}$ . At  $1000 \text{ K}$ , the interdiffusion diffusion coefficient of lithium in nickel is  $5 \times 10^{-8} \text{ cm s}^{-1}$ .

**13.21** A cylindrical bar of Fe (dia. of 1 cm) is suspended in a well mixed and small melt of Mn maintained at  $1300^{\circ}\text{C}$ . Assume that there is local equilibrium at the solid-liquid interface and calculate the time required to raise the manganese composition at the center of the bar to 1 wt. %. The interdiffusion coefficient of Mn in Fe is given by

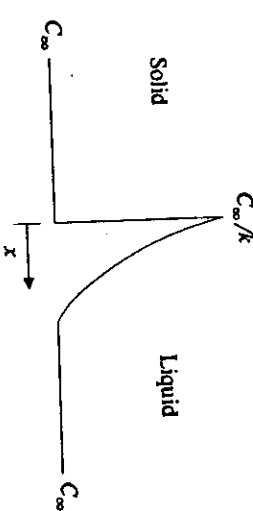
$$D = 0.49 \exp \left[ -\frac{33,200}{T} \right]$$

with  $T$  in K and  $D$  in  $\text{cm}^2 \text{ s}^{-1}$ .



**13.23** A batch of steel exhibits "banding," which is a form of microsegregation in the wrought condition. The spacing between the bands is  $50 \mu\text{m}$ . After 10 h of a high temperature homogenization treatment, the residual segregation index is 0.2 (determined by electron beam microanalysis). A second batch of the same type of steel has a band spacing of  $100 \mu\text{m}$ . How long must this batch be maintained at the high temperature to achieve the same residual segregation index of 0.2?

**13.24** A melt with uniform concentration of solute,  $C_\infty$ , is solidified with a planar interface. Chemical equilibrium is maintained at the interface, which moves with a constant velocity  $V$ . The concentration profile at steady state, with no convection in the liquid, is as depicted:



- Use a moving coordinate system with the origin ( $x = 0$ ) at the solid-liquid interface and derive the differential equation for the concentration profile in the liquid.
- Write appropriate boundary conditions and solve for  $C(x)$ .
- Determine the concentration gradient in the liquid at  $x = 0$ . How does the concentration gradient relate to the velocity of the interface?
- The characteristic length,  $\delta$ , defined by

$$j_0 = \frac{D}{\delta} \left[ \frac{C_\infty}{k} - C_\infty \right],$$

where  $j_0$  is the diffusional flux at the interface ( $x = 0$ ). Determine  $\delta$  in terms of the solidification velocity and the concentration gradient at the interface.

**13.25** A powder-ceramic compact is outgassed at  $500^{\circ}\text{C}$  in a chamber filled with pure argon in order to remove air before sintering. The tortuosity of the compact is 4, its porosity is 0.2, and the average pore radius is  $200 \text{ \AA}$ . The compacts are  $50 \text{ mm long} \times 25 \text{ mm diameter}$ . Calculate the fraction of air remaining after 1 h of outgassing treatment.

**13.26** In order to make a transformer steel with the proper hysteresis loop, a low silicon steel sheet (2 mm thick) is to be exposed on both sides to an atmosphere of  $\text{SiCl}_4$  which dissociates to  $\text{Si(g)}$  and  $\text{Cl}_2(\text{g})$ . The  $\text{Si(g)}$  dissolves in the steel up to 3 wt. % at equilibrium. a) Indicate what partial differential equation and what boundary and initial conditions would apply in order to calculate the diffusion of Si into the sheet. b) Using the data in Fig. 12.11, calculate the time to achieve an average concentration of 2.85 wt. % Si at  $1255 \text{ K}$ .

**13.22** A very thin sheet of Fe-0.2 atom fraction B is "sandwiched" between two large pieces of iron, and then the entire assembly is heated to  $1000^{\circ}\text{C}$ . The sheet is only  $5 \times 10^{-3} \text{ cm}$  thick and at  $1000^{\circ}\text{C}$  diffusion bonding occurs as the boron diffuses into the iron. Assume that the boron is completely soluble and that there is only a single phase. a) Calculate the time required for the concentration of B to achieve its maximum at a distance of 1 mm from the original joint. b) What is the maximum concentration at 1 mm? c) At the time corresponding to part a), what is the atom fraction of B at the original joint?

---

## MASS TRANSFER IN FLUID SYSTEMS

---

In Chapters 2 and 7, we demonstrated the development of differential equations pertinent to momentum and energy transport in simple fluid systems. In this chapter, we consider how to formulate and describe elementary diffusion and mass transfer problems in fluid systems. We use practically the same procedure in this situation as we did previously; we develop a differential equation, and a solution containing arbitrary constants evolves. These constants are evaluated by applying boundary conditions that specify the concentration or the mass flux at the bounding surfaces. Again, we demonstrate the principles involved by considering specific examples, but first let us reconsider the general situation.

Species A in a gas stream moving in the  $x$ -direction is under the influence of a concentration gradient, also in the  $x$ -direction. The molar flux of A relative to stationary coordinates is then made up of two parts:  $C_A v_x^*$  which is the molar flux of A resulting from the bulk motion, and  $j_{Ax} = -CD_A(\partial X_A / \partial x)$  which is the diffusive contribution. Thus

$$N_{Ax} = -CD_A \frac{\partial X_A}{\partial x} + C_A v_x^* = C_A v_{Ax}. \quad (14.1)$$

Here  $v_x^*$  is the local *molar average velocity* in the  $x$ -direction, and  $v_{Ax}$  is the velocity of A in the  $x$ -direction with respect to stationary coordinates, and  $C$  is the total molar concentration in the solution. Thus, we define  $v_x^*$  so that the *total molar flux* of all components in the  $x$ -direction is made up of the sum of the  $n$  component fluxes in the same direction:

$$Cv_x^* = \sum_{i=1}^n C_i v_{Ax}. \quad (14.2)$$

For a binary A-B system, we write

$$v_x^* = \frac{1}{C} (C_A v_{Ax} + C_B v_{Bx}) = \frac{1}{C} (N_{Ax} + N_{Bx}). \quad (14.3)$$

When we combine Eq. (14.3) with Eq. (14.1), we obtain a form of Fick's first law for a binary solution:

$$N_A = X_A(N_{A\text{g}} + N_{A\text{l}}) - CD_A \frac{\partial X_A}{\partial x}. \quad (14.4)$$

#### 14.1 DIFFUSION THROUGH A STAGNANT GAS FILM

Consider the system shown in Fig. 14.1 where liquid *A* is evaporating into gas *B*, and a constant liquid level at  $x = 0$  is maintained. At the liquid-gas phase interface ( $x = 0$ ), the gas phase concentration of *A* is that corresponding to the vapor pressure of *A* at that temperature. For simplicity, also assume that the solubility of *B* in liquid *A* is negligible and that the entire system is maintained at a constant temperature and pressure. At the top of the tube, a stream of *A-B* gas flows past slowly, thereby maintaining a constant concentration of *A* at  $x = l$  which is less than the liquid-gas interface concentration. Therefore, a concentration difference of *A* exists between  $x = 0$  and  $x = l$ , which causes diffusion. When the system attains a steady state, there is a net motion of *A* away from the evaporating surface and the vapor *B* in the tube is stationary.

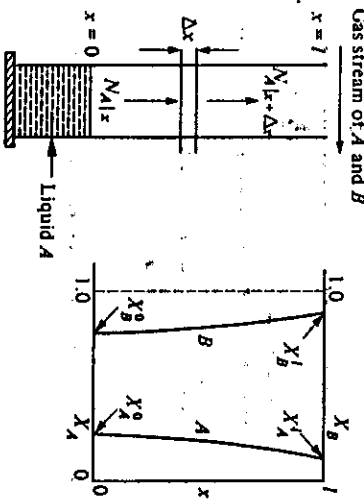


Fig. 14.1 Diffusion of *A* and *B* at steady state. *B* is not in motion, but note that the graph shows how its concentration profile is not linear because of the motion of *A*.

This implies that equilibrium is maintained at the interface. From a simplified mechanistic viewpoint, atoms (or molecules) can readily leave the liquid state and enter the gas phase. This assumption is valid except at very high diffusion rates where the rate of transfer of atoms across the liquid-gas interface is not able to keep pace with the exhaustion of the atoms away from the interface.

Under these conditions, despite the fact that gas *B* is stationary, there is bulk motion of fluid since *A* itself is moving, and its motion contributes to the average velocity. Thus we refer to Eq. (14.4) for the flux of *A* with  $N_{B\text{g}} = 0$ . Solving for  $N_{A\text{g}}$ , we obtain

$$N_{A\text{g}} = -\frac{CD_A}{1-X_A} \frac{dX_A}{dx}. \quad (14.5)$$

A mass balance on a unit volume  $\Delta x$  of column height (see Fig. 14.1) for steady state is

$$SN_{A\text{g}\Delta x} - SN_{A\text{l}\Delta x} = 0, \quad (14.6)$$

in which  $S$  is the cross-sectional area. In the expected manner, we divide by  $\Delta x$  and take the limit as  $\Delta x \rightarrow 0$ :

$$\frac{dN_{A\text{g}}}{dx} = 0. \quad (14.7)$$

Substitution of Eq. (14.6) for  $N_{A\text{g}}$  yields

$$\frac{d}{dx} \left[ \frac{CD_A}{1-X_A} \frac{dX_A}{dx} \right] = 0. \quad (14.8)$$

As pointed out in Chapter 12, diffusion coefficients for isothermal gas solutions are very nearly independent of concentration; also,  $C$  is constant for an ideal gas mixture at constant temperature and pressure. Hence we simplify the derivative further:

$$\frac{d}{dx} \left[ \frac{1}{1-X_A} \frac{dX_A}{dx} \right] = 0. \quad (14.9)$$

Two successive integrations can be made directly, resulting in

$$-\ln(1-X_A) = c_1 x + c_2, \quad (14.10)$$

and we determine the constants by use of the boundary conditions:

$$\text{B.C.1: } \text{at } x = 0, \quad X_A = X_A^0; \quad (14.11a)$$

$$\text{B.C.2: } \text{at } x = l, \quad X_A = X_A^l. \quad (14.11b)$$

When we evaluate the constants and substitute them into Eq. (14.10), we obtain the concentration profile:

$$\ln \left[ \frac{1-X_A}{1-X_A^0} \right] = \frac{x}{l} \ln \left[ \frac{1-X_A^l}{1-X_A^0} \right], \quad (14.12)$$

or

$$\ln \left[ \frac{X_A}{X_A^0} \right] = \frac{x}{l} \ln \left[ \frac{X_A^l}{X_A^0} \right]. \quad (14.13)$$

Figure 14.1 shows these solutions, where the slope of  $dX_A/dx$  is not uniform with  $x$  although the flux  $N_{A\text{g}}$  is. A gradient of *A* in the gas must be accompanied by a gradient of *B*. Consequently, *B* has a tendency to diffuse down the column, but this diffusive tendency is

exactly compensated by the opposing bulk motion of the gas in the direction of diffusion of gas A.

The information that is most often sought is the rate of mass transfer at the liquid-gas interface. We obtain this by using Eq. (14.5):

$$N_{A|z=0} = -\frac{CD_A}{1-X_A^0} \left[ \frac{dX_A}{dx} \right]_{z=0} = \frac{CD_A}{l} \ln \left[ \frac{1-X_A'}{1-X_A^0} \right], \quad (14.14)$$

or

$$N_{A|z=0} = -\frac{CD_A}{(X_B)_{in}} \left[ \frac{X_A^0 - X_A'}{l} \right], \quad (14.15)$$

where  $(X_B)_{in}$  is the *log mean* of the terminal values of  $X_B$ , defined as

$$(X_B)_{in} = \frac{X_B' - X_B^0}{\ln \left[ X_B'/X_B^0 \right]}. \quad (14.16)$$

Equation (14.15) is somewhat more appealing than Eq. (14.14) because a characteristic concentration difference  $X_A^0 - X_A'$  over a distance  $l$  is evident. For a gas in which species A is dilute, Eq. (14.15) reduces to

$$N_{A|z=0} = D_A \left[ \frac{C_A^0 - C_A'}{l} \right], \quad (14.17)$$

which could have resulted from originally ignoring bulk motion and expressing the flux of A simply as

$$J_A = -D_A \frac{dC_A}{dx}. \quad (14.18)$$

Typical applications of Eqs. (14.14) and (14.15) are evaporation and sublimation processes which involve diffusion of the vapor being created (gas A) through a stationary gas (gas B). Also, a method for measuring diffusion coefficients is to measure the rate of fall of liquid A in a small glass tube as gas B passes by the top. Furthermore, these results find use in the "film theories" of mass transfer.

**Example 14.1** In order to determine the diffusivity of Mn in the gas phase, a melt of pure Mn is held in a chamber at 1600°C through which pure Ar flows. The level of the Mn is 2.0 cm below the edge of the crucible. The weight of the crucible is monitored continuously, and when the rate of weight loss is steady with time, that rate is found to be  $2.65 \times 10^{-7} \text{ mol cm}^{-2} \text{ s}^{-1}$ . Calculate  $D_{\text{Mn-Ar}}$ .

**Solution.** At 1600°C,  $P_{\text{Mn}}^0 = 0.03 \text{ atm}$ , which may be taken as the pressure just above the liquid surface. The pressure of manganese may be taken as zero at the crucible edge, as the argon flowing across the opening removes it immediately.

Since the concentration of manganese is clearly dilute,  $D_{\text{Mn-Ar}}$  is obtained directly from Eq. (14.17). The concentration is expressed in  $\text{mol cm}^{-3}$ :

$$\frac{d^2X_A}{dz^2} - \frac{v_A^*}{D_A} \frac{dX_A}{dz} = 0. \quad (14.21)$$

$$C_A^0 = \frac{P_A^0}{RT} = \frac{0.03 \text{ atm}}{0.082051 \text{ atm}} \left| \frac{\text{mol K}}{10^3 \text{ cm}^3} \right| \left| \frac{1}{1873 \text{ K}} \right| \\ = 1.61 \times 10^{-7} \text{ mol cm}^{-3},$$

and

$$D_{\text{Mn-Ar}} = \frac{2.65 \times 10^{-7} \times 2.0}{1.61 \times 10^{-7}} = 3.3 \text{ cm}^2 \text{ s}^{-1}.$$

#### 14.2 DIFFUSION IN A MOVING GAS STREAM

Figure 14.2 illustrates one technique used to determine the vapor pressure of a metal (liquid or solid). Argon, as a carrier gas, passes over the sample which is at the temperature corresponding to the vapor pressure being determined. This gas, containing the saturation concentration of the metal vapor, enters the exit tube at  $z = 0$ , and at the cool end of the exit tube the metal condenses, so we can collect it for a mass determination.

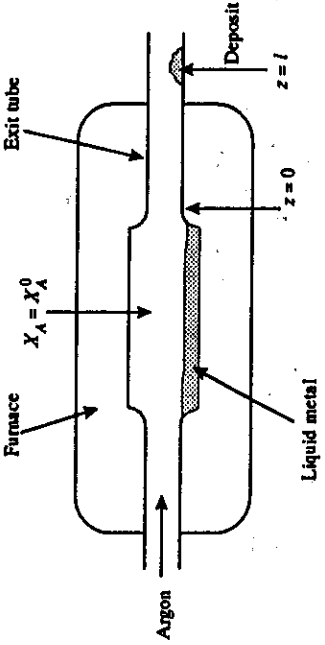


Fig. 14.2 Diffusion in a moving gas stream.

A mass balance applied to a section  $\Delta z$  long for steady state yields

$$\frac{dN_A}{dz} = 0. \quad (14.19)$$

We may choose either Eq. (14.1) or Eq. (14.4) to represent  $N_A$ ; here we select Eq. (14.1) from which we write

$$v_A^* \frac{dC_A}{dz} - \frac{d}{dz} \left[ CD_A \frac{dX_A}{dz} \right] = 0. \quad (14.20)$$

We can certainly consider that the argon-metal gas solution is ideal, and if the temperature between  $z = 0$  and  $z = l$  is uniform, then  $C$  and  $D_A$  are constants, and Eq. (14.20) takes the form

The boundary conditions can be represented as:

$$\text{B.C.1: at } z = 0, \quad X_A = X_A^0 \text{ (saturation value)}; \quad (14.21\text{a})$$

$$\text{B.C.2: at } z = l, \quad X_A = 0. \quad (14.21\text{b})$$

The second boundary condition implies that the temperature at  $l$  is low enough so that the vapor pressure of  $A$  is negligible. We can obtain the solution to Eq. (14.21) directly by integrating twice, or by treating it as a linear homogeneous differential equation with constant coefficients. Applying the latter method, the solution is

$$X_A = c_1 e^{r_1 z} + c_2 e^{r_2 z},$$

where  $r_1$  and  $r_2$  are the roots of

$$r^2 - \frac{v_i^*}{D_A} r = 0. \quad (14.23)$$

Thus,  $r_1 = 0$  and  $r_2 = v_i^*/D_A$ , and the solution is

$$X_A = c_1 + c_2 \exp \left[ \frac{v_i^*}{D_A} z \right]. \quad (14.24)$$

We evaluate the arbitrary constants by using Eqs. (14.24) and (14.21a and b):

$$c_2 = - \frac{X_A^0}{\exp \left[ \frac{v_i^* l}{D_A} \right] - 1}. \quad (14.25)$$

$$X_A = X_A^0 \left[ 1 + \frac{\exp \left[ \frac{v_i^* l}{D_A} \right] - 1}{\exp \left[ \frac{v_i^* l}{D_A} \right] - 1} \right]. \quad (14.26)$$

and

$$\frac{P_A^0}{P} = X_A^0 = \frac{S N_{A|z=0}}{S C v_i^*} \left[ \frac{\exp \left[ \frac{v_i^* l}{D_A} \right] - 1}{\exp \left[ \frac{v_i^* l}{D_A} \right]} \right], \quad (14.29)$$

where  $P_A^0$  is the vapor pressure of  $A$ , and  $P$  is the total pressure. Preferably, the effect of diffusion should be negligible for best experimental results due to the uncertainty of the diffusion coefficient and because we would have to assume an experimental set up that corresponds to the mathematical formulation.

The real value of the analysis lies in the group  $v_i^*/l D_A$ , which indicates how to set up the experiment, so that the effects of diffusion may be ignored. If  $v_i^*/l D_A \geq 5$ , the effect of diffusion may be ignored because the last term in Eq. (14.29) is  $\geq 0.993$  and  $< 1.0$ . To insure sufficiently high values of  $v_i^*/l D_A$ , the experimentalist should provide a small diameter tube between  $z = 0$  and  $z = l$ , and use argon or nitrogen as the carrier gas, rather than hydrogen or helium, since  $D$  in the lighter gases is larger than in the heavier gases.

**Example 14.2** An experimental apparatus is being constructed to study the thermodynamics of Mn-Cu alloys by measuring the Mn vapor pressure over the molten alloys at 1400 K. In order to use the transport technique, what exit tube dimensions and argon gas flow rates should be used?

**Solution.** The criterion that provides the most direct experimental measurement of  $P_{\text{Mn}}^0$  (the equilibrium pressure over the alloy) is

$$\frac{X_A}{X_A^0} = \frac{\exp \left[ \frac{v_i^* l}{D_A} \right] - \exp \left[ \frac{v_i^* z}{D_A} \right]}{\exp \left[ \frac{v_i^* l}{D_A} \right] - 1}. \quad (14.27)$$

where  $N_{\text{Mn}}$  is the number of moles of Mn condensed and  $N = N_{\text{Mn}} + N_A =$  total moles of gas passing through the exit tube over some period of time. This is essentially true when  $v_i^*/l D_{\text{Mn-Ar}} \geq 5.0$ .

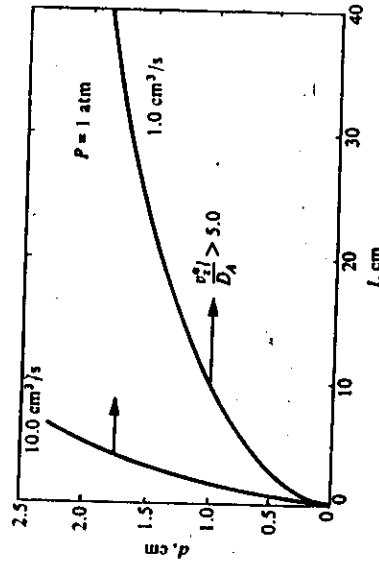
We evaluate  $D_{\text{Mn-Ar}}$  at 1400 K as  $2.6 \times 10^{-4} \text{ m}^2 \text{ s}^{-1}$ . Therefore,  $v_i^*/l$  must be greater than  $13.0 \times 10^{-4} \text{ m}^2 \text{ s}^{-1}$ . Since  $v_i^* \approx 4\pi RT/\sigma d^2 P$ , and  $\dot{n} \equiv \dot{n}_{\text{Ar}}$  (mol Ar s $^{-1}$ ), then

$$\frac{4\dot{n}_{\text{Ar}}RT}{\pi P} \geq 13.0 \text{ } d^2.$$

or

$$N_{\text{Mn}|z=0} = C v_i^* X_A^0 \left[ 1 - \frac{1}{1 - \exp \left[ \frac{v_i^* l}{D_A} \right]} \right]. \quad (14.28)$$

where  $d$  is the tube diameter. The figure below shows the results, with the preferred designs to the right of each curve.



At temperatures where  $P_{Ma}^0$  is greater than negligible values, and  $n > n_A$ , the curves should be shifted even further to the right for better results.

### 14.3 DIFFUSION INTO A FALLING LIQUID FILM

In this section, we consider a fluid system moving in such a way that the velocity distribution is unaffected by diffusion into the fluid. Figure 14.3 shows a film of liquid *B* falling in laminar flow down a wall. Gas *A* is absorbed at the liquid-gas interface; we restrict the situation to that where the penetration distance of *A* into *B* is small relative to the film thickness. We wish to calculate the amount of gas absorbed after the film travels a distance  $L$ .

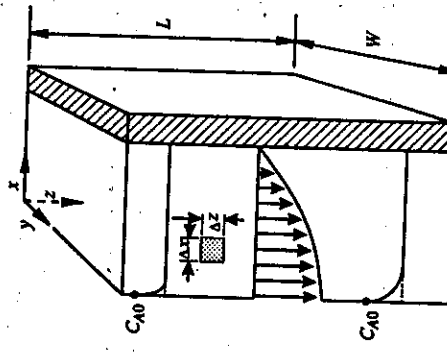


Fig. 14.3 Absorption into a falling film.

First, we develop a mass balance on component *A*. The gas-liquid interface concentration of *A*, at all values of  $z$ , is the saturation concentration  $C_A^0$ ; thus *A* diffuses into the liquid which initially contains less than the saturation amount of *A*. As the film drops, the liquid is exposed to  $C_A^0$  for a longer time, and more penetration of *A* into the film results. We see, therefore, that  $C_A$  changes both with  $x$  and  $z$ , and we select as the unit volume  $\Delta x$  by  $\Delta z$  by unity in the  $y$ -direction.

Then the mass balance for *A* is simply

$$N_{Ae|x} \Delta x - N_{Ae|x+\Delta z} \Delta x + N_{Ae|x} \Delta z - N_{Ae|x+\Delta z} \Delta z = 0. \quad (14.30)$$

Dividing by  $\Delta x \Delta z$ , and performing the usual limiting process, we get

$$\frac{\partial N_{Ae}}{\partial z} + \frac{\partial N_{Ae}}{\partial x} = 0. \quad (14.31)$$

We now have to insert into this equation the expressions for  $N_{Ae}$  and  $N_{Ae}$ . For the molar flux in the  $z$ -direction, we write

$$N_{Ae} = -CD_A \frac{\partial X_A}{\partial z} + C_A v_z^*, \quad (14.32)$$

and neglect the diffusive contribution, realizing that *A* moves in the  $z$ -direction primarily due to bulk flow. In addition, for a small increase in the concentration of *A*,  $v_z^* \equiv v_z$ . Finally, we give  $N_{Ae}$  by the simplified expression

$$N_{Ae} = C_A v_z. \quad (14.33)$$

For the molar flux in the  $x$ -direction, we write

$$N_{Ae} = -D_A \frac{\partial C_A}{\partial x} + C_A v_x^*. \quad (14.34)$$

That is, in the  $x$ -direction, *A* is transported primarily by diffusion, there being almost no bulk flow in the  $x$ -direction due to the small solubility of *A* in *B*. Substitution of Eqs. (14.32) and (14.34) into Eq. (14.31) yields the differential equation for  $C_A(x, z)$ :

$$\frac{\partial C_A}{\partial z} = D_A \frac{\partial^2 C_A}{\partial x^2}. \quad (14.35)$$

When dealing with energy transport in a convective system, it is necessary to obtain the velocity profile  $v(x)$ ; similarly, we need to describe the velocity for the analogous situation of mass transfer in a convective system. For a falling film, we have already worked this out in Chapter 2, and we know that the result for fully developed flow is

$$v_z = v_{max} \left[ 1 - \left( \frac{x}{\delta} \right)^2 \right],$$

where  $\delta$  is the film thickness, and  $x$  is the distance into the film from the gas-liquid surface.

If, as indicated in Fig. 14.3, *A* has penetrated only a slight distance into the film, then for the most part species *A* sees only  $v_{max}$ . Further, since it does not penetrate very far, we can consider that the liquid is semi-infinite. These conditions would hold, for example, for short

contact times. With these approximations we write the differential equation and the boundary conditions as follows:

$$v_{\max} \frac{\partial C_A}{\partial z} = D_A \frac{\partial^2 C_A}{\partial x^2}; \quad (14.36)$$

$$\text{at } z = 0, \quad C_A = C_A^i, \quad x \geq 0; \quad (14.37a)$$

$$\text{at } x = 0, \quad C_A = C_A^0, \quad L \geq z \geq 0; \quad (14.37b)$$

$$\text{at } x = \infty, \quad C_A = C_A^i, \quad L \geq z \geq 0. \quad (14.37c)$$

Note that we may alternatively view  $z/v_{\max}$  as the time  $t$  over which a moving slice of liquid has been subjected to the surface concentration  $C_A^0$ . Thus, we recognize the solution to Eq. (14.36), subject to Eqs. (14.37a), (14.37b), and (14.37c), as the solution for the temperature distribution in a semi-infinite solid, initially at a uniform temperature, which is suddenly subjected to a new constant surface temperature. Then, referring to Eq. (9.62), we have

$$\frac{C_A - C_A^0}{C_A^i - C_A^0} = \operatorname{erf} \frac{x}{2\sqrt{D_A z/v_{\max}}}. \quad (14.38)$$

Now knowing the concentration profile, we proceed to determine the local diffusion mass flux at the surface,  $x = 0$ :

$$N_{A,x=0} = -D_A \left[ \frac{\partial C_A}{\partial x} \right]_{x=0} = (C_A^0 - C_A^i) \frac{D_A v_{\max}}{\pi z^2}, \quad (14.39)$$

which gives the average rate of  $A$  transferred per unit across the entire surface between  $z = 0$  and  $z = L$  as

$$\bar{N}_{A,x=0} = \frac{1}{L} \int_0^L N_{A,x=0} dz = 2(C_A^0 - C_A^i) \frac{D_A v_{\max}}{\pi L}. \quad (14.40)$$

Pigford<sup>1</sup> solved the complete equation

$$v_{\max} \left[ 1 - \left[ \frac{x}{\delta} \right]^2 \right] \frac{\partial C_A}{\partial z} = D_A \frac{\partial^2 C_A}{\partial x^2}, \quad (14.41)$$

and obtained the result:

$$\frac{\bar{C}_A^L - C_A^0}{C_A^i - C_A^0} = 0.7857 e^{-5.1213 \eta} + 0.1001 e^{-39.318 \eta} + \dots, \quad (14.42)$$

where  $\eta = D_A L / \delta^2 v_{\max}$ , and  $\bar{C}_A^L$  = bulk average composition of the liquid at  $L$ .

For small values of  $\eta$ , corresponding to short contact times or very thick films, we obtain

$$\frac{\bar{C}_A^L - C_A^0}{C_A^i - C_A^0} = \frac{6D_A L}{\pi \delta^2 V}, \quad (14.43)$$

and for long times, we have

$$\frac{\bar{C}_A^L - C_A^0}{C_A^i - C_A^0} = 0.7857 e^{-5.1213 \eta}. \quad (14.44)$$

#### 14.4 THE MASS TRANSFER COEFFICIENT

In Chapter 7, we analyzed simple problems of heat transfer with laminar convection, and formulated the temperature distribution from which we calculated heat transfer rates by evaluating the heat fluxes at the fluid-solid boundary. With the fluxes, we wrote expressions for the heat transfer coefficients, and we saw that  $\text{Nu} = f(\text{Re}, \text{Pr})$ , and gained insight into what was to follow in Chapter 8, where we presented the correlations for heat transfer in convective systems.

Having considered diffusion in the presence of forced convection in Section 14.3, it is convenient to introduce the *mass transfer coefficient*. As we mentioned, we may treat the movement of a species as the sum of a diffusional contribution and a bulk flow contribution (see Eq. (14.1)). To be analogous with heat transfer, a mass transfer coefficient for transfer of  $A$  into or out of a phase is defined in terms of the diffusive contribution normal to the interface:

$$k_M = \frac{j_A^0}{C_A^0 - C_{A,\infty}} = -\frac{D_A (\partial C_A / \partial x)_{x=0}}{C_A^0 - C_{A,\infty}}. \quad (14.45)$$

Here, the superscript 0 refers to quantities evaluated at the interface, and  $C_{A,\infty}$  to some concentration of  $A$  within the fluid, usually the bulk concentration. Note that, while  $k_M$  in Eq. (14.45) is defined in terms of the diffusion flux at the surface, in general, at interfaces involving a fluid phase, there is the additional contribution to mass transfer caused by bulk flow. We define the mass transfer coefficient here only in terms of the diffusive contribution, rather than of the total flux  $N_A^0$ . This is because the coefficient so defined is somewhat more fundamental, since we might expect the diffusion flux to be approximately proportional to a characteristic concentration difference as indicated by Eq. (14.45), whereas the bulk flow contribution can be relatively independent of any concentration difference. Similarly, when both heat and mass transfer occur, it is advantageous to retain the definition of the heat transfer coefficient given by Eq. (8.1), which considers only the conduction flux. In the limit of low mass transfer rates, as is often the case, we may neglect the distortion of the velocity and concentration profiles by mass transfer, and the bulk flow term is negligible. Then

$$k_M = \frac{N_A^0}{C_A^0 - C_{A,\infty}}. \quad (14.46)$$

This equation is definitional only, and we must evaluate it by means of various analytical expressions for the flux. As the first example of applying Eq. (14.46), consider the results of diffusion into a falling film in Section 14.3. We evaluate the *local* mass transfer coefficient relating the rate of mass transfer of A into the liquid when the time of contact is short, by substituting Eq. (14.39) into Eq. (14.46).

$$k_{Mz} = \frac{N_A v_{max}}{C_A^0 - C_{A\infty}} = \frac{D_A v_{max}}{\pi z}, \quad (14.47)$$

or in terms of dimensionless groups, and recalling that  $v_{max} = \frac{1}{2}\bar{V}$ ,

$$\frac{k_{Mz} z}{D_A} = \frac{3\bar{V}z\nu}{2\pi\nu D_A}. \quad (14.48)$$

The group  $k_{Mz} z/D_A$  is called the *Sherwood number*,  $Sh$ , or alternatively the *mass transfer Nusselt number*,  $Nu_N$ . The Reynolds number should be easily recognized. The Schmidt number,  $Sc$ , which is defined by

$$Sc = \frac{\nu}{D_A}, \quad (14.49)$$

is the analog of the Prandtl number encountered in heat transfer.

Most available forced-convection mass transfer correlations are in the form:

$$Sh = f(Re, Sc, \text{geometry}), \quad (14.50)$$

as, for example, in the situation above. Specifically, we could write Eq. (14.48) as

$$Sh_z = \frac{3}{2\pi} Re_L^{1/2} Sc^{1/2}. \quad (14.51)$$

In this case, by subscripting with  $z$ , we emphasize that local values are being considered. If we used Eq. (14.40) instead of Eq. (14.39), we would define an *average* mass transfer coefficient over the film length  $L$ .

$$k_M = \frac{(C_A^0 - C_A^I) \left[ \frac{4D_A v_{max}}{\pi L} \right]^{1/2}}{(C_A^0 - C_A^I)} = \frac{6D_A \bar{V}}{\pi L}. \quad (14.52)$$

We can then write this in dimensionless form as

$$Sh_L = \frac{6}{\pi} Re_L^{1/2} Sc^{1/2}, \quad (14.53)$$

where the subscript  $L$  indicates that the quantities are averaged over the entire film length.

In the case of long contact times, where Eq. (14.44) applies, the rate at which A is absorbed in the distance  $dz$  is

$$\bar{V}d\bar{C}_A = k_M(C_A^0 - \bar{C}_A) dz.$$

Over the entire length of the film, the absorption rate of A is

$$\bar{V} \int \frac{d\bar{C}_A}{C_A^0 - \bar{C}_A} = k_M \int_0^L dz.$$

The integration yields

$$\bar{V} \int \frac{d\bar{C}_A}{C_A^0 - \bar{C}_A} = k_M \ln \frac{C_A^0 - C_A^I}{C_A^0 - \bar{C}_A}. \quad (14.54)$$

Substituting Eq. (14.44), we obtain

$$k_M = \frac{\bar{V}\delta}{L} [\ln(e^{5.1213\eta} - \ln 0.7857)] = \frac{\bar{V}\delta}{L} [5.1213\eta + 0.241] \approx 3.42 \frac{D_A}{\delta}. \quad (14.55)$$

By rearranging this expression, we get

$$\frac{k_M D}{D_A} = Sh \approx 3.42, \quad (14.56)$$

which is similar to the results given in Table 7.1, where the Nusselt number was found to be a constant for fully developed laminar flow. This equation is applicable when  $Re(\Gamma/\eta) \leq 25$ , where  $\Gamma$  is the mass flow rate per unit width of film.

Having been tested for absorption of gases into liquids flowing down wall columns, Eq. (14.56) sometimes underestimates the actual mass transfer coefficient. At low Reynolds numbers, this is now understood to be partly due to the so-called *Marangoni effect*, in which upward-directed surface tension forces counteract the downward-directed gravitational forces, causing rippling and turbulence on the surface and an increase in mass transfer, which is not anticipated in the simplified development described above.

**Example 14.3** A method for degassing molten metals involves exposing a thin film of metal to vacuum, by allowing it to flow continuously over an inclined plate. Calculate the average hydrogen concentration of an alloy, with an initial concentration of  $1 \text{ m}^3 \text{ H}_2(\text{STP}) \text{ per m}^3$  of alloy, flowing down a plate 1 m long and 0.15 m wide, which is inclined at an angle of  $10^\circ$  from the horizontal. The concentration of hydrogen at the surface exposed to the vacuum may be taken as zero. The desired film thickness is  $1 \times 10^{-3} \text{ m}$ . Data are as follows:  $\rho = 8.32 \times 10^3 \text{ kg m}^{-3}$ ,  $\eta = 6 \times 10^{-3} \text{ N s m}^{-2}$ ,  $D_H = 1.3 \times 10^{-8} \text{ m}^2 \text{s}^{-1}$ .

*Solution.* Using Eq. (2.14), we find the average velocity:

$$\bar{V} = \frac{(8.32 \times 10^3 \text{ kg m}^{-3})(9.8 \text{ m s}^{-2})(1 \times 10^{-3} \text{ m})^2 (\cos 80^\circ)}{3(6 \times 10^{-3} \text{ N s m}^{-2})} = 7.86 \times 10^{-1} \text{ m s}^{-1}.$$

The product  $ReSc$ , which we often encounter in mass transfer, is sometimes called the Peclét number,  $Pe$ .

The contact time is

$$\frac{L}{\bar{V}} = \frac{1}{0.786 \text{ m s}^{-1}} = 1.27 \text{ s.}$$

Since this is very short, we make use of Eq. (14.52) to calculate an average  $k_M$ :

$$k_M = \frac{6D_s \bar{V}}{\pi L} = \frac{6(1.3 \times 10^{-6})(0.786)}{(3.14)(1)} = 1.4 \times 10^{-4} \text{ m s}^{-1}.$$

Then

$$j_{H_2} = 1.4 \times 10^{-4} \text{ m s}^{-1} (1 \text{ m}^3 \text{ H}_2 \text{ m}^{-3} \text{ alloy}) = 1.4 \times 10^{-4} \text{ m}^3 \text{ H}_2 \text{ m}^{-2} \text{ s}^{-1}.$$

Total content removed per  $\text{m}^2$  of exposed surface is  $= j_{H_2} \text{ (contact time)}$

$$= 1.78 \times 10^{-4} \text{ m}^3 \text{ H}_2 \text{ m}^{-2} \text{ film.}$$

Initial total content =  $(1 \text{ m}^3 \text{ H}_2 \text{ m}^{-3} \text{ alloy})(1.0 \times 10^{-3} \text{ m}^3 \text{ alloy m}^{-2} \text{ film})$

$$= 1.0 \times 10^{-3} \text{ m}^3 \text{ H}_2 \text{ m}^{-2} \text{ film.}$$

Final total content =  $0.0010 - 0.000178 = 0.000822 \text{ m}^3 \text{ H}_2 \text{ m}^{-2} \text{ film, or the average content}$  of the metal is reduced to  $0.822 \text{ m}^3 \text{ H}_2 \text{ m}^{-3} \text{ alloy.}$

Under many circumstances encountered in interphase mass transfer, the bulk flow term is not important, and the diffusive contribution in the mass flux equation is all that we need to consider. On the other hand, there may be occasions, particularly where transfer to and from gas phases is involved, in which this contribution is not negligible. In this case, we write

$$N_A = \theta k_M (C_A^0 - C_A^i), \quad (14.57)$$

where  $N_A$  is the total interphase flux, and  $\theta$  is a correction factor that depends on  $N_A$ ,  $N_B$ , and  $k_M$  according to

$$\theta = \frac{N_A + N_B}{k_M \left[ \exp \left[ \frac{N_A + N_B}{k_M} \right] + 1 \right]}. \quad (14.58)$$

Figure 14.4 gives a graph of  $\theta$  as a function of  $(N_A + N_B)/k_M = \phi$ . A limiting case is equimolar countercurrent diffusion, in which  $N_A = -N_B$  and  $\phi = 0$ , so that  $\theta = 1.0$  and no correction is involved.

In case we do not know  $N_A$  and  $N_B = 0$ , the expression

$$1 + \frac{C_A^0 - C_A^i}{\frac{N_A + N_B}{N_A + N_B} - C_A^0} = \exp \left[ \frac{N_A + N_B}{k_M} \right] \quad (14.59)$$

may be used to evaluate  $N_A$  at high mass transfer rates.

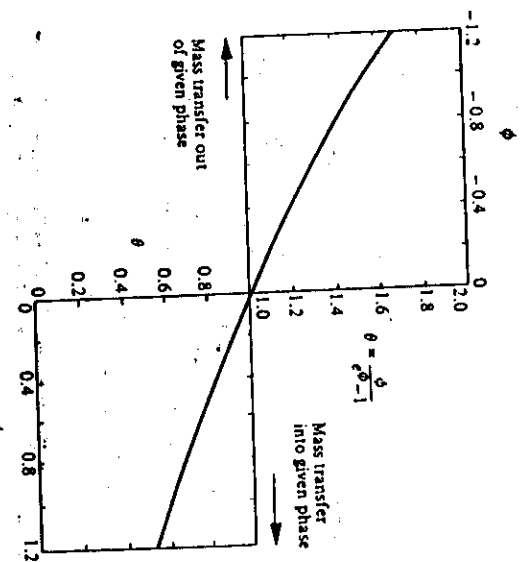


Fig. 14.4 The variation of coefficients with mass transfer rate. (From R. B. Bird, W. E. Stewart, and E. N. Lightfoot, *Transport Phenomena*, Wiley, New York, 1960, page 664.)

Thus, forced convection mass transfer at high mass transfer rates (large  $N_A$  and/or  $N_B$ ) is generally correlated by

$$Sh = f(Re, Sc, N_A \text{ and geometry}). \quad (14.60)$$

For the most part, we do not make use of this form in materials processing.

#### 14.5 GENERAL EQUATION OF DIFFUSION WITH CONVECTION

In this section, we summarize the general approach to the law of mass conservation in the volume element  $\Delta x \Delta y \Delta z$ , depicted in Fig. 2.4, through which a fluid containing  $A$  in solution is flowing. In the following expressions,  $\rho_A$  is the mass concentration (for example, kg of  $A$   $\text{m}^{-3}$  of total solution) as defined by Eq. (12.3);  $W_A$  is the total mass flux of  $A$  in the  $x$ -direction and is composed of a diffusive term and a convective term. Specifically

$$W_A = -\rho D_A \left[ \frac{\partial \rho_A^*}{\partial x} \right] + \rho_A v_x = \rho_A v_A, \quad (14.61)$$

where  $\rho$  is the density of the entire solution,  $\rho_A^*$  is the mass fraction of  $A$ , and  $v_x$  is the local mass average velocity in the  $x$ -direction; thus, we define  $v_x$  such that the total mass flux of all components in the  $x$ -direction is made up of the sum of the  $n$  component fluxes in the same direction:

$$\rho v_x = \sum_{i=1}^n \rho_i v_{x,i} \quad (14.62)$$

$$v_x = \frac{1}{\rho} (\rho_A v_A + \rho_B v_B) = \frac{1}{\rho} (W_{Ax} + W_{Bx}).$$

Now we can proceed to develop a mass balance for the volume element. The various contributions to the mass balance of component A are

$$\text{Accumulation of mass of } A \text{ in the volume element} \quad \Delta x \Delta y \Delta z \frac{\partial \rho_A}{\partial t},$$

$$\text{Input of } A \text{ across face at } x \quad \Delta y \Delta z W_{Ax|x},$$

$$\text{Output of } A \text{ across face at } x + \Delta x \quad \Delta y \Delta z W_{Ax|x+\Delta x}.$$

There are also input and output terms in the y- and z-directions. When we write the entire mass balance for species A, divide through by  $\Delta x \Delta y \Delta z$ , and take the limits in the usual manner, we obtain the *general equation of continuity for component A*:

$$\frac{\partial \rho_A}{\partial t} + \frac{\partial W_{Ay}}{\partial x} + \frac{\partial W_{Az}}{\partial y} + \frac{\partial W_{Ax}}{\partial z} = 0. \quad (14.63)$$

The quantities  $W_{Ax}$ ,  $W_{Ay}$ ,  $W_{Az}$  are the rectangular components of the *mass flux vector*,  $W_A = \rho_A v_A$ , which includes motion of A due to diffusion and bulk flow:

$$W_A = -\rho D_A \nabla \rho_A^* + \rho_A v = \nabla \rho D_A \nabla \rho_A^*. \quad (14.64)$$

Finally, by combining Eqs. (14.63) and (14.64), we develop the *diffusion equation for component A*:

$$\frac{\partial \rho_A}{\partial t} + \nabla \cdot \rho_A v = \nabla \cdot \rho D_A \nabla \rho_A^*. \quad (14.65)$$

As is usually the case, simplifications are utilized more frequently than general equations. Often, one can assume constant mass density and  $D_A$ , and make some simplification. For constant  $\rho$  and  $D_A$ , Eq. (14.65) becomes

$$\frac{\partial \rho_A}{\partial t} + v \nabla \rho_A = D_A \nabla^2 \rho_A, \quad (14.66)$$

or if divided by  $M_A$  (molecular weight of A), we get

$$\frac{\partial C_A}{\partial t} + v \nabla C_A = D_A \nabla^2 C_A, \quad (14.67)$$

The left side of this equation is  $DC_A/Dt$ , showing direct similarity with Eq. (7.76) which is the basis for the numerous analogies between heat and mass transport in fluids with constant  $\rho$ .

The above analysis could have been made equally well in terms of molar fluxes such as we have used previously. Then the equation of continuity for component A becomes:

$$\frac{\partial C_A}{\partial t} + \nabla \cdot N_A = 0, \quad (14.68)$$

and the diffusion equation for A in solution becomes:

$$\frac{\partial C_A}{\partial t} + \nabla \cdot C_A v^* = \nabla \cdot CD_A \nabla C_A. \quad (14.69)$$

For constant  $C$  and  $D_A$ , Eq. (14.69) takes the form

$$\frac{\partial C_A}{\partial t} + v^* \nabla C_A = D_A \nabla^2 C_A. \quad (14.70)$$

This equation is usually applied to low-density gases at constant temperature and pressure.

The left side of this equation cannot be written as  $DC_A/Dt$  because of the appearance of  $v^*$  rather than of  $v$ . A more simplified form of the above equations, which is used for diffusion in solids or stationary liquids ( $v = 0$  in Eq. (14.67)), or for equimolar countercurrent diffusion in gases ( $v^* = 0$  in Eq. (14.70)), is Fick's second law of diffusion:

$$\frac{\partial C_A}{\partial t} = D_A \nabla^2 C_A. \quad (14.71)$$

In Tables 14.1 and 14.2, we summarize the most important equations of this discussion in rectangular, cylindrical, and spherical coordinates. Fick's second law of diffusion can be obtained by setting the velocity components in Table 14.2 equal to zero.

Table 14.1 The equation of continuity of A in various coordinate systems

$$\frac{\partial C_A}{\partial t} + \left[ \frac{\partial N_A}{\partial x} + \frac{\partial N_A}{\partial y} + \frac{\partial N_A}{\partial z} \right] = 0 \quad (A)$$

$$\frac{\partial C_A}{\partial t} + \left[ \frac{1}{r} \frac{\partial}{\partial r} (r N_A) + \frac{1}{r^2} \frac{\partial N_A}{\partial \theta} + \frac{\partial N_A}{\partial z} \right] = 0 \quad (B)$$

$$\frac{\partial C_A}{\partial t} + \left[ \frac{1}{r^2} \frac{\partial}{\partial r} (r^2 N_A) + \frac{1}{r^2} \frac{\partial N_A}{\partial \theta} + \frac{\partial N_A}{\partial z} \right] = 0 \quad (C)$$

Table 14.2 The equation of diffusion of A for constant  $\rho$  and  $D_A$

Rectangular coordinates:

$$\frac{\partial C_A}{\partial t} + \left[ v_x \frac{\partial C_A}{\partial x} + v_y \frac{\partial C_A}{\partial y} + v_z \frac{\partial C_A}{\partial z} \right] = D_A \left[ \frac{\partial^2 C_A}{\partial x^2} + \frac{\partial^2 C_A}{\partial y^2} + \frac{\partial^2 C_A}{\partial z^2} \right] \quad (A)$$

Cylindrical coordinates:

$$\frac{\partial C_A}{\partial t} + \left[ v_r \frac{\partial C_A}{\partial r} + v_\theta \frac{1}{r} \frac{\partial C_A}{\partial \theta} + v_z \frac{\partial C_A}{\partial z} \right] = D_A \left[ \frac{\partial^2 C_A}{\partial r^2} + \frac{1}{r^2} \frac{\partial^2 C_A}{\partial \theta^2} + \frac{\partial^2 C_A}{\partial z^2} \right] \quad (B)$$

Spherical coordinates:

$$\frac{\partial C_A}{\partial t} + \left[ v_r \frac{\partial C_A}{\partial r} + v_\theta \frac{1}{r} \frac{\partial C_A}{\partial \theta} + v_\phi \frac{1}{r \sin \theta} \frac{\partial C_A}{\partial \phi} \right]$$

$$= D_A \left[ \frac{1}{r^2} \frac{\partial}{\partial r} \left[ r^2 \frac{\partial C_A}{\partial r} \right] + \frac{1}{r^2 \sin \theta} \frac{\partial}{\partial \theta} \left[ \sin \theta \frac{\partial C_A}{\partial \theta} \right] + \frac{1}{r^2 \sin^2 \theta} \frac{\partial^2 C_A}{\partial \phi^2} \right] \quad (C)$$

#### 14.6 MASS TRANSFER WITH FORCED CONVECTION OVER A FLAT PLATE

As an application of the above equations, consider the flow system in which a thin, semi-infinite plate of solid A dissolves very slowly under steady-state conditions, into an unbounded fluid of stream of A and B. The flow is initially at uniform velocity, concentration, and temperature. For constant properties of the fluid, we may write the boundary layer equations of momentum, energy, mass, and continuity as follows:

$$\text{Continuity, } \frac{\partial u_x}{\partial x} + \frac{\partial u_y}{\partial y} = 0, \quad (14.72)$$

$$\text{Momentum, } v_x \frac{\partial v_x}{\partial x} + v_y \frac{\partial v_x}{\partial y} = v \frac{\partial^2 v_x}{\partial y^2}, \quad (14.73)$$

$$\text{Energy, } v_x \frac{\partial T}{\partial x} + v_y \frac{\partial T}{\partial y} = \alpha \frac{\partial^2 T}{\partial y^2}, \quad (14.74)$$

$$\text{Mass, } v_x \frac{\partial C_A}{\partial x} + v_y \frac{\partial C_A}{\partial y} = D_A \frac{\partial^2 C_A}{\partial y^2}. \quad (14.75)$$

Equations (14.72)-(14.75) were obtained in Chapter 7 for zero mass transfer. The assumption that the same equations are valid in the presence of mass transfer means that any additional momentum and energy fluxes associated with mass transfer are negligible. Equation (14.75) is derived from Eq. (A) in Table 14.2 with  $\partial C_A / \partial t = 0$ ,  $\partial^2 C_A / \partial z^2 = 0$ ,  $v_z = 0$ , and by neglecting the negligible amount of diffusion in the  $x$ -direction.

A typical set of boundary conditions that may be specified is:

$$\begin{aligned} \text{B.C.1: } & x \leq 0, \quad v_x = V_\infty, \quad v_y = 0, \quad T = T_\infty, \\ & C_A = C_{A\infty} \quad \text{for all } y, \end{aligned} \quad (14.76a)$$

$$\begin{aligned} \text{B.C.2: } & y = \infty, \quad v_x = V_\infty, \quad v_y = 0, \quad T = T_\infty, \\ & C_A = C_{A\infty} \quad \text{for } x > 0, \end{aligned} \quad (14.76b)$$

$$\begin{aligned} \text{B.C.3: } & y = 0, \quad v_x = 0, \quad v_y = v_0, \quad T = T_0, \\ & C_A = C_A^0 \quad \text{for } x > 0. \end{aligned} \quad (14.76c)$$

The fact that  $v_y = v_0$  at the wall accounts for the bulk motion accompanying diffusion from the wall. The method of solving Eqs. (14.72)-(14.75) subject to the conditions (Eqs. (14.76a, b, and c)) is not given here, but Fig. 14.5 presents the results for certain values of  $\text{Pr}$  and  $\text{Sc}$ . Note that the differential equations and boundary conditions for temperature and concentration are analogous; therefore, when  $\text{Pr} = \text{Sc} = 1$ , the velocity, temperature, and concentration profiles within the boundary layer must coincide. Figure 14.5 shows these results, along with the results for  $\text{Pr} = \text{Sc} = 0.7$ ; velocity profiles remain unchanged.

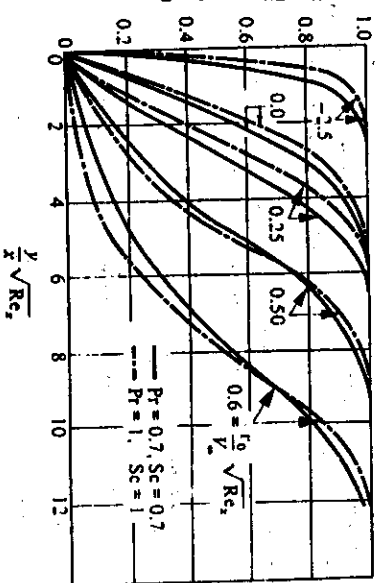


Fig. 14.5 Temperature and concentration profiles in a laminar boundary layer on a flat plate for  $\text{Pr} = \text{Sc} = 0.7$ , and  $\text{Pr} = \text{Sc} = 1$ . Curves for  $\text{Pr} = \text{Sc} = 1$  also represent velocity profiles. (From J. P. Hartnett and E. R. G. Eckert, Trans. ASME 79, 247 (1957).)

These profiles show a dependency on the mass flux  $(v_0 \sqrt{\text{Re}_x} / V_\infty)$ . Mass transfer away from the plate (positive  $v_0$ ) gives flatter profiles as would be true if the solid surface were porous and a gas diffused upward through the plate, or if a liquid passed through the porous plate and evaporated. On the other hand, mass transfer toward the plate (negative  $v_0$ ) gives

steeper profiles; this situation can be obtained if condensation occurs at the surface, or suction is applied to a porous membrane. Figure 14.6 shows the local heat and mass transfer coefficients plotted against the parameter  $v_0/\text{Re}_L / V_\infty$ . For  $v_0 = 0$  (no mass transfer, or, more realistically, at low mass transfer rates), the local mass transfer coefficient is given by Eq. (7.26) with simple changes of notations, namely:  $h_t \rightarrow k_{h,t}$ ,  $k \rightarrow D_A$ , and  $\text{Pr} \rightarrow \text{Sc}$ . Then, the local Sherwood number is

$$\text{Sh}_t = 0.332 \text{ Sc}^{0.343} \text{ Re}_L^{1/2}, \quad (14.77)$$

and the average Sherwood number is

$$\text{Sh}_L = 0.664 \text{ Sc}^{0.343} \text{ Re}_L^{1/2}. \quad (14.78)$$

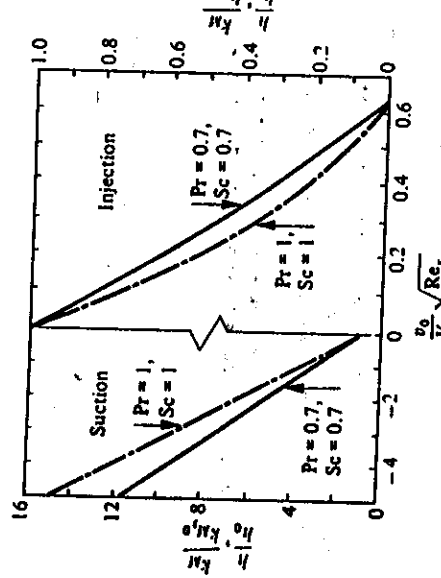


Fig. 14.6 Heat and mass transfer coefficients for laminar flow over a flat plate. Subscript zero indicates the respective coefficients for zero bulk flow normal to wall. (From J. P. Hartnett and E. R. G. Eckert, *ibid.*)

These solutions are valid for most fluids, including liquid metals. Table 14.3 gives typical magnitudes of Prandtl and Schmidt numbers for fluids.

Table 14.3 Typical magnitudes of Prandtl numbers and Schmidt numbers

	Pr	Sc
Gases	0.6-1.0	0.1-2.0
Liquids	1-10	$10^2-10^3$
Liquid metals	$10^{-2}$	$10^3$

It can be shown that the expression for the ratio of the concentration boundary layer to the momentum boundary layer is:

$$\frac{\delta_c}{\delta} = \frac{1}{1.026 \sqrt{\text{Sc}}} \quad (14.79)$$

and in turbulent flow:

$$j_H = j_M = \frac{f}{2} = \frac{0.664}{\sqrt{\text{Re}_L}} \quad (14.80)$$

$$(14.81)$$

$$j_H = j_M = \frac{f}{2} = \frac{0.037}{\text{Re}_L^{0.2}} \quad (14.82)$$

## 14.7 CORRELATIONS OF MASS TRANSFER COEFFICIENTS FOR TURBULENT FLOW

We have seen in the previous sections that many forced-convection mass transfer situations are analogous to heat transfer situations, and the appropriate heat transfer solutions apply with simple changes of notations, namely:  $\alpha \rightarrow D_A$ ,  $T \rightarrow C_A$ ,  $\text{Pr} \rightarrow \text{Sc}$ , and  $\text{Nu} \rightarrow \text{Sh}$ . In addition, we may assume that the results for natural convection resulting from density differences caused by mass transfer may be correlated by a mass transfer Grashof number,

$$\text{Gr}_M = g \xi (X_A - X_{A_\infty}) L^3 / v^2,$$

where  $\xi$  is the concentration coefficient of volumetric expansion defined as:

$$\xi = \frac{1}{\rho} \left[ \frac{\partial \rho}{\partial X_A} \right]_T$$

In this case, we may use correlations for heat transfer to yield mass transfer data if the substitution  $\text{Gr} \rightarrow \text{Gr}_M$  is made. The flow parameters such as  $\text{Re}$  and position parameters such as  $L/D$  remain the same.

We noted in Chapter 8 that in turbulent flow there is an analogy between the friction factor  $f$  for turbulent flow in tubes and heat transfer, which is given as the Chilton-Colburn "j-factor,"  $j_H$ :

$$j_H = \frac{\text{Nu}}{\text{Re} \text{Pr}} (\text{Pr})^{2/3} = \frac{f}{2}. \quad (8.6)$$

Continuing the analogy, we define a mass transfer j-factor,  $j_M$ , for fully developed flow in round tubes:

$$j_M = \frac{\text{Sh}_L}{\text{Re} \text{Sc}} (\text{Sc})^{2/3} = \frac{f}{2}. \quad (14.80)$$

If the temperature profile is not fully developed, then we use Fig. 8.2 where we take  $L/D$  into account, and substitute  $j_M$  for  $j_H$ .

In the case of flow parallel to a flat surface, from the results of Chapter 8, we write for average values in laminar flow:

$$j_H = j_M = \frac{f}{2} = \frac{0.664}{\sqrt{\text{Re}_L}}, \quad (14.81)$$

This relationship has been found to adequately describe the rate of deposition of metallic solutes from liquid to solid,<sup>2</sup> and the rate of dissolution of carbon into iron melts.<sup>3</sup>

In flow around curved surfaces, such as spheres and cylinders,  $f/2$  greatly exceeds  $j_H$  and  $j_M$ . However, the analogy still holds between heat and mass transfer, so that  $j_H$  and  $j_M$  should be equivalent. To illustrate this, consider the heat transfer correlation given in Chapter 8 for forced convection around a sphere of radius  $R$ :

$$2h/R_f = 2.0 + 0.60 \text{ Re}_f^{1/2} \text{ Pr}_f^{1/3}. \quad (8.11)$$

Translated into the  $j_M$  form it becomes

$$j_M = \frac{2.0}{\text{Re} \text{Pr}^{1/3}} + \frac{0.60}{\text{Re}^{1/2}}. \quad (14.83)$$

By analogy we get

$$j_M = \frac{2.0}{\text{Re} \text{Sc}^{1/3}} + \frac{0.60}{\text{Re}^{1/2}}. \quad (14.83)$$

Figure 14.7 illustrates the results of experiments where  $j_M$  is plotted as a function of  $\text{Re}$  for dissolution of uranium spheres in flowing cadmium,<sup>4</sup> cinnamic acid spheres in flowing water,<sup>5</sup> 2-naphthol spheres in flowing water,<sup>6</sup> and for comparison purposes,  $j_H$ ,<sup>7</sup> and  $f/2$ .<sup>8</sup> Note that the data from the liquid metal experiments show lower values of  $j_M$  at low  $\text{Re}$  values than those observed in the organic system experiments. This may be partially corrected for by the presence of the Schmidt number in the expression given in Eq. (14.83), which is not plotted in Fig. 14.7. No equation accounts for the peak in  $j_M$  near Reynolds numbers of  $10^3$ , so usually the graph is preferred rather than an equation in this range.

For natural convection, the mass transfer analog of

$$\text{Nu}_L = 0.13 (\text{Gr}_L \text{Pr})^{1/3} \quad (8.18)$$

has been applied to both the rate of dissolution of carbon in molten iron<sup>9</sup> and the rate of dissolution of steel in molten iron-carbon alloys,<sup>9</sup> and found to be quite reasonable as an approximation, with the best fit of the data yielding the equation

$$\text{Sh}_L = 0.11 (\text{Gr}_{ML} \text{Sc})^{1/3}. \quad (14.84)$$

The velocity in the Reynolds number is the velocity of the gas bubble relative to the liquid velocity. When an expression for the velocity in terms of the density difference,  $\rho_f - \rho_g$ , is substituted, the final result depends on the Grashof number,  $\text{Gr}_M$ , instead. Without the third group that shows up in Hugmark's correlation, the result is

$$\text{Sh} = f \left[ \text{Re}, \text{Sc}, \left[ \frac{\rho_f^{1/3} d}{D^{2/5}} \right] \right].$$

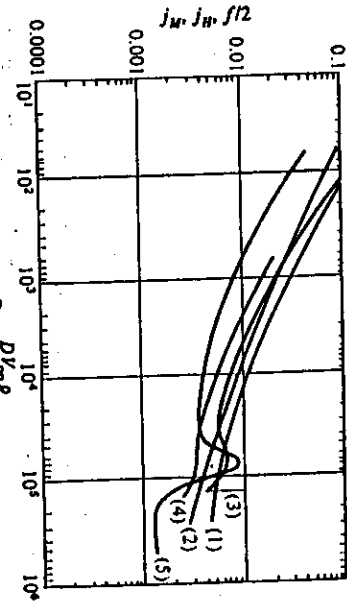


Fig. 14.7 Comparison of mass, heat, and momentum transfer to spheres. (1)  $f/2$ ; (2) Chilton-Colburn factor  $j_H$ ; (3)  $j_M$  for cinnamic acid-water system; (4)  $j_M$  for 2-naphthol-water system; (5)  $j_M$  for uranium dissolving in cadmium.

Many processes depend on gas-liquid contact and mass transfer between the phases. Although this is a very complex area,<sup>10</sup> several relationships have been found that describe the process of mass transfer on the liquid side of a gas bubble-liquid interface. One of the most useful is that of Hugmark.<sup>11</sup> His expression is

$$\frac{k_M d}{D} = 2.0 + a \left[ \left( \frac{V_t d}{v} \right)^{0.48} \left( \frac{v}{g^{1/2} d} \right)^{0.072} \left( \frac{D}{D^{2/5}} \right)^b \right], \quad (14.85)$$

where  $d$  is the bubble diameter,  $V_t$  is the terminal velocity of the rising bubble, and  $a$  and  $b$  are constants that depend on whether the bubbles act singly or in swarms. For single bubbles,  $a = 0.061$  and  $b = 1.61$ . This relationship has been tested in molten copper-carbon monoxide systems, and was found satisfactory for describing the rate of transfer of oxygen in the copper to the interface.<sup>12</sup>

Equation (14.85) is of the form

<sup>2</sup>W. N. Gill, R. P. Vanek, R. V. Jelinek, and C. S. Grove, *AICHEJ* **6**, 139 (1960).  
<sup>3</sup>M. Kosaka and S. Minowa, *Trans. Japan Iron and Steel Inst.* **8**, 393 (1968).  
<sup>4</sup>F. D. Taylor, L. Burris, and C. J. Geankoplis, *I. & E. C. Fundamentals* **4**, 119 (1965).  
<sup>5</sup>L. R. Steele and C. K. Geankoplis, *AICHEJ* **5**, 178 (1959).  
<sup>6</sup>T. K. Sherwood, *Ind. Eng. Chem.* **42**, 2077 (1950).  
<sup>7</sup>F. H. Garner and R. D. Suckling, *AICHEJ* **4**, 114 (1958).  
<sup>8</sup>M. Kosaka and S. Minowa, *ibid.*  
<sup>9</sup>M. Kosaka and S. Minowa, *Tetsu-to-Hagane* **53**, 983 (1967).  
<sup>10</sup>For reviews, see P. H. Calderbank, *Trans. Inst. Chem. Engrs.* **212**, 209 (1967); F. H. H. Valentin, *Absorption in Gas-Liquid Dispersions*, Spon Ltd., London, 1967.  
<sup>11</sup>G. A. Hugmark, *I. & E. C. Process Design and Development* **6**, 218 (1967).  
<sup>12</sup>C. R. Nanda and G. H. Geiger, *Metall. Trans.* **2**, 1101 (1971).

Accordingly, some mass transfer correlations involving gas bubbles in liquid are presented in this way. In bubble swarms, we can use<sup>13</sup>

$$\text{Sh} = 0.31 \text{ Gr}'^{1/3} \text{ Sc}^{1/3} \quad (14.86)$$

for  $d < d_c$ , and

$$\text{Sh} = 0.42 \text{ Gr}'^{1/3} \text{ Sc}^{1/2} \quad (14.87)$$

for  $d > d_c$ . Equations (14.86) and (14.87) apply to two distinct regimes, which are divided by a critical bubble diameter,  $d_c = 2.5$  mm. The Grashof number is defined as

$$\text{Gr}'_M = \frac{8d^3\rho_f(\rho_l - \rho_g)}{\eta_l^2}, \quad (14.88)$$

where the subscripts  $f$  and  $g$  refer to the liquid and gas, respectively.

In applying Eqs. (14.85)-(14.87), one must have a way to estimate the surface area of the bubbles in the swarm. For bubble swarms, this is problematic; furthermore, the ultimate goal is to quantify the relationship between the mass transfer and the flow rate of the gas. With this attitude, Freuhan and Martonik<sup>14</sup> recommend combining  $Ak_M$ , when dealing with bubble swarms, where  $A$  is the surface area. Their result is

$$Ak_M = 0.008 Q^{0.75} H^{0.69}, \quad (14.89)$$

where  $Ak_M$  has units of  $\text{cm}^3 \text{s}^{-1}$ ,  $Q$  is the flow rate of the gas in  $\text{cm}^3 \text{s}^{-1}$ , and  $H$  is the depth of the liquid above the injection nozzle (called a tuyere) in cm.

**Example 14.4** Small individual bubbles of diameter  $d$  are often approximated as nonrotating spheres rising in liquids. Starting with the mass transfer form of Eq. (8.11), show that the correlation can be put in the form

$$\text{Sh} = f(\text{Gr}_M, \text{Sc}).$$

**Solution:** Equation (8.11) in mass transfer form is

$$\text{Sh} = \frac{k_M d}{D} = 2.0 + 0.60 \text{ Re}^{1/2} \text{ Sc}^{1/3},$$

where

$$\text{Re} = \frac{dV_f \rho_f}{\eta_f}.$$

The terminal velocity can be found from Section 3.3.2, from which it can be shown that

$$V_t = \left[ \frac{4dg(\rho_f - \rho_g)}{3f\rho_s} \right]^{1/2}.$$

<sup>13</sup>P. H. Calderbank and M. Yoo-Young, *Chem. Eng. Sci.* **16**, 39 (1961).

<sup>14</sup>R. J. Freuhan and L. J. Martonik, in *Proceedings of the Third International Iron and Steel Congress*, American Society for Metals, Metals Park, OH, 1978, pp. 229-238.

where  $f$  is the friction factor. Using this terminal velocity, the Reynolds number can be written as

$$\text{Re} = \frac{2d\rho_f}{\eta_f} \left[ \frac{dg(\rho_f - \rho_g)}{3f\rho_s} \right]^{1/2},$$

or, with the definition of the Grashof number, Eq. (14.88), as

$$\text{Re} = 2 \left[ \frac{\text{Gr}'_M}{3f} \right]^{1/2}.$$

If  $f$  is constant, which is approximately valid for  $2 \times 10^2 \leq \text{Re} \leq 2 \times 10^5$ , then we get the result

$$\text{Sh} \approx 2.0 + 0.77 (\text{Gr}'_M)^{1/4} \text{ Sc}^{1/3}.$$

In the Stokes' law regime ( $\text{Re} \leq 1.0$ ),  $f = 24/\text{Re}$ ; thus

$$\text{Re} = \frac{\text{Gr}'_M}{18},$$

and

$$\text{Sh} = 2.0 + 0.14 \text{ Gr}'_M^{1/2} \text{ Sc}^{1/3}.$$

Note that the Chilton-Colburn analogy is applicable only at relatively low mass transfer rates, and that the best results are obtained when similar materials are utilized in both the heat and analogous mass transfer situations. Turbulent flow mass transfer correlations based on studies using common liquids appear to be directly translatable into liquid metal systems, but heat transfer data are not quite as accurate in predicting mass transfer, although usually satisfactory to within an order of magnitude.

Also, many of the tests of applicability of heat transfer correlations to mass transfer involving the gas phase have not been made at conditions likely to be of interest to materials engineers, particularly at elevated temperatures and high rates of transfer, so they should be used with caution.

**Example 14.5** Graphite particles are often added to molten cast iron in order to increase the carbon content when scrap steel is used as starting material. The time required to dissolve the particles is of interest. Determine the time to dissolve particles of graphite as a function of the bath's carbon content.

The particles float, and are swept to the side of the surface of the melt by the magnetically induced stirring action, where the metal velocity relative to the graphite is approximately  $25 \text{ cm s}^{-1}$ . Due to the displacement of metal by graphite, the surface area of an individual particle in contact with the melt is calculated as  $\frac{1}{8}$  of the total particle surface area. In addition, a portion of the particle exposed to the atmosphere is burned to CO due to the air circulating over the bath surface. Thus, the recovery of carbon in the melt is less than 100%, and experience shows that, in fact, the recovery is only 50%. Therefore, the mass of an individual particle (of density  $\rho_p$ ) that dissolves in the melt is

$$m = \frac{1}{2} \left[ \frac{\pi}{6} D_p^3 \rho_p \right].$$

and its surface area exposed to the melt is

$$A = \frac{3}{8} \pi \bar{D}_p^2 \lambda.$$

**Solution.** The mass flow, in terms of g (carbon) s<sup>-1</sup> is

$$\frac{dm}{dt} = -k_w A \rho_l (C_0 - C_\infty),$$

where  $\rho_l$  is liquid density, g cm<sup>-3</sup>,  $C_0$  is weight fraction of carbon in the bulk melt interface, and  $C_\infty$  = weight fraction of carbon at the particle-melt interface, and  $C_\infty$  = weight fraction of carbon in the bulk melt.

We evaluate the mass transfer coefficient from Fig. 14.8, which has been developed by several investigators for the dissolution of rotating carbon rods in Fe-C melts. For a velocity of 25 cm s<sup>-1</sup>,  $k_w$  for graphite is 0.02 cm s<sup>-1</sup>. Now, since

$$\frac{dm}{dt} = -\frac{1}{4} \pi \bar{D}_p^2 \rho_l \frac{d\bar{D}_p}{dt},$$

and the area is as given above, we can determine the time to dissolve a particle:

$$\int_{\bar{D}_p}^0 d\bar{D}_p = \frac{3}{2} k_w \lambda \frac{\rho_l}{\rho_s} (C_0 - C_\infty) \int_0^t dt,$$

or

$$t = \frac{2\rho_s \bar{D}_p}{3\rho_l \lambda k_w (C_0 - C_\infty)}, \text{ s.}$$

The results are plotted on the next page.

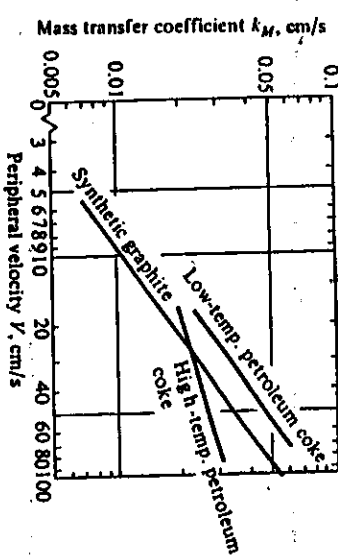
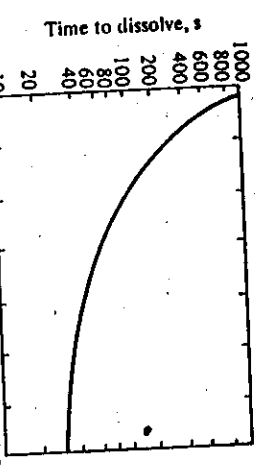


Fig. 14.8 Mass transfer coefficients for carbon dissolution in Fe-C melts. (From

R. G. Olsson, V. Kourmp, and T. F. Petzak, *Trans. AIME* 236, 426 (1965); O. Angeles, G. H. Geiger, and C. R. Loper, *Trans. AFS* 76, 629 (1968); and M. Kosaka and S. Minowa, *Trans. Japan Iron Steel Inst.* 8, 393 (1968).)



**14.8 MODELS OF THE MASS TRANSFER COEFFICIENT**

Since most conditions in which mass transfer is important involve fluids undergoing turbulent motion, we must usually rely on the preceding correlations, with experimental studies giving the necessary empirical coefficients. However, there are situations when test data are outside the experimental scope of variables, and it is desirable to know whether and how the experimental data can be extended to the new situation. Several theories of the process of mass transfer have been developed, which attempt to present models of what actually happens at the interface between two fluids or between a fluid and solid from a fundamental viewpoint, in order to aid in intelligent extrapolation of data.

The oldest theory is the film theory of Lewis and Whitman,<sup>15</sup> who suggested that there is an unmixed layer or film in the fluid next to the actual interface, continuously exposed to the completely mixed bulk fluid on one side and to the other phase on the other. This layer, devoid of any fluid motion, is supposed to offer all the resistance to the transfer of component A from the interface into the bulk solution, as depicted in Fig. 14.9. The transfer takes place purely by atomic or molecular diffusion through the film. Figure 14.9 indicates the concentration profile assumed in the model. Since the entire concentration change from  $C_\infty$  to  $C_A^0$  is assumed to take place within the film in a steady-state manner, and since the mass transfer coefficient is defined by

$$j_A = k_w (C_A - C_{A\infty}),$$

we can compare this to

$$j_A = -D \frac{dC_A}{dx} = +D \frac{(C_A^0 - C_{A\infty})}{\delta_{eff}},$$

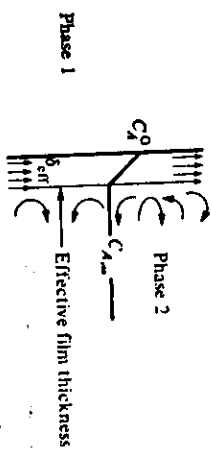


Fig. 14.9 The "effective film thickness" model.

with the result that  $k_w = D/\delta_{eff}$ , where  $\delta_{eff}$  is the effective film thickness. This result often appears in cases where the flux is measured and the overall concentration change ( $C_1^0 - C_{1\infty}$ ) is known, and then either the diffusivity is known (or more often assumed) and  $\delta_{eff}$  is calculated, or vice versa. As noted below, the significance of  $\delta_{eff}$  is dubious, at best.

From a fluid mechanics standpoint, it was recognized at an early stage that interfaces between fluids are bound to be unstable with time, and that any given element of fluid at the interface does not remain there for long. Thus, the film theory is much too crude to be really meaningful. Higbie<sup>16</sup> proposed a model to describe the contact between two fluids, in which  $\theta$ , which is taken to be extremely short, such that the packet is subject only to unsteady-state diffusion or "penetration" by the transferred species during its contact time with the other phase. The packet is assumed to be stagnant internally during this time, and well mixed before and after. Figure 14.10 gives a schematic picture of the situation. This theory results in a prediction that

$$k_w = 2\sqrt{D/\pi\theta} \quad (14.90)$$

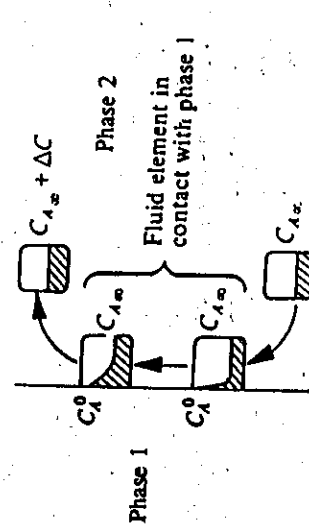


Fig. 14.10 Schematic diagram of fluid motion in penetration theory.

The logical extension of this theory was performed by Danckwerts<sup>17</sup> who suggested that the idea of a constant time of exposure  $\theta$  ought to be replaced by an average time of exposure calculated from an assumed distribution of residence times of the packets at the surface. The result of this "surface renewal" theory is again a relationship of the form

$$k_w \propto \sqrt{D} \quad (14.91)$$

The constants in his equation, like the constant  $\theta$  in Higbie's equation, are not readily obtainable with the exception of bubbles rising through a liquid, in which case we may estimate  $\theta$  to be the time required for a bubble to rise a distance equal to its diameter. When considering the three theories, it is apparent that the dependence of  $k_w$  on  $D$  is different. Experimentally, it has been found that  $k_w$  is proportional to  $D^n$  where  $n$  varies from 0.5 to 1.0, depending on the fluids and the circumstances. In order to resolve this

discrepancy, Dobbins<sup>18</sup> and Toor and Marchello<sup>19</sup> proposed a combined *film penetration theory* in which the residence time of the surface elements (Higbie model) is long enough to allow the concentration gradient to approach a steady state across the finite thickness of the element (film model). This theory approaches each of the other theories as limiting cases. When  $D$  is large or the rate of surface renewal is small ( $\theta$  is large), then  $n$  approaches 1.0 and so the film theory is applicable. When  $D$  is small or  $\theta$  is small (rapid surface renewal rate),  $n$  approaches 0.5, and the penetration theory results. In any case, there are still parameters that must be specified in order to use the theory for predictive purposes, and they are not readily obtainable.

#### 14.9 MASS TRANSFER IN CHEMICAL VAPOR DEPOSITION

If we want to consider chemical vapor deposition, we should be prepared to deal with complex phenomena involving thermodynamics, reaction rates, convection patterns, and mass transfer in systems that are nonisothermal and far from equilibrium. The reactions involved can be extremely complex and multifold. All of this aside, we present a relatively simple scenario in order to illustrate the role of mass transfer in the kinetics of forming a film via chemical vapor deposition.

Titanium tetraloxide ( $Ti_{4(g)}$ ) is used as a feed gas to a reactor which contains a suitable substrate. The substrate is heated and the  $Ti_{4(g)}$  decomposes according to



and the titanium film is deposited. Excess  $Ti_{4(g)}$  and  $I_{2(g)}$  leave the reactor.

At the gas-solid interface, we assume that reaction (14.92) is at equilibrium. The standard free energy change of the reaction is

$$\Delta G^\circ = 402\ 000 - 118\ T, \text{ kJ kmol}^{-1}$$

for  $653 \leq T \leq 1943$  K. The equilibrium constant is

$$\ln K = -\frac{\Delta G^\circ}{RT} \quad (14.93)$$

or

$$\ln K = -\frac{48\ 300}{T} + 14.2 \quad (14.94)$$

We use the equilibrium constant to determine the concentrations of the gas species at the gas-solid interface. Assuming an ideal gas mixture, the equilibrium constant gives

$$K = \frac{X_1^2}{X_2}, \quad (14.94)$$

<sup>18</sup>W. E. Dobbins, *Int. Conference on Water Pollution Research*, London, 1962, Pergamon Press, New York, 1964, page 61.

<sup>19</sup>H. L. Toor and J. M. Marchello, *AIChE J.* 4, 97 (1958).

<sup>16</sup>R. Higbie, *Trans. AIChE* 31, 365 (1935).

<sup>17</sup>P. U. Danckwerts, *Ind. Eng. Chem.* 43, 1460 (1951).

<sup>18</sup>For another discussion of the various models of mass transfer refer to E. L. Cussler, *Diffusion: Mass Transfer in Fluid Systems*, Cambridge University Press, Cambridge, UK, 1984, pages 281-296.

where  $X_1$  and  $X_2$  are the mole fractions of  $\text{I}_2$  and  $\text{Ti}_4$ , respectively. For mass transfer calculations, it is convenient to express the concentrations in  $\text{kmol m}^{-3}$ , so with  $P$  as the reactor pressure we write

$$C_1 = \frac{X_1 P}{RT}, \text{ kmol } \text{I}_2 \text{ m}^{-3} \text{ gas}, \quad (14.95)$$

$$C_2 = \frac{X_2 P}{RT}, \text{ kmol } \text{Ti}_4 \text{ m}^{-3} \text{ gas}. \quad (14.96)$$

After substituting Eqs. (14.95) and (14.96) into Eq. (14.94), we get the equilibrium concentrations at the gas-solid interface; namely

$$\frac{C_1^2}{C_2} = \frac{PK}{RT}, \quad (14.97)$$

and

$$j_1 = k_M(C_1 - C_{\infty 1}). \quad (14.99)$$

**Example 14.6** Calculate (a) the concentration of gas molecules in the  $\text{TiI}_4\text{-Ti}$  reactor and (b) the equilibrium concentrations of  $\text{TiI}_4$  and  $\text{I}_2$  at the solid-gas interface. The reactor operates at 1 standard atmosphere of pressure and 1500 K.

**Solution.** a) The total concentration of gas molecules is

$$C = \frac{P}{RT} = \frac{1 \text{ atm}}{8.205 \times 10^{-2} \text{ m}^3 \text{ atm}} = \frac{\text{kmol K}}{1500 \text{ K}}$$

$$= 8.125 \times 10^{-3} \text{ kmol m}^{-3}.$$

b) At 1500 K, Eq. (14.93) gives

$$K = \exp \left[ -\frac{43,800}{T} + 14.2 \right] = 3.059 \times 10^{-7},$$

and then from Eq. (14.97), we compute

$$\frac{C_1^2}{C_2} = \frac{PK}{RT} = \frac{(1)(3.059 \times 10^{-7})}{(8.205 \times 10^{-3})(1500)} = 2.485 \times 10^{-9}.$$

Also,  $C = C_1 + C_2$ ; therefore

$$\frac{C_1^2}{C - C_1} = 2.485 \times 10^{-9}.$$

With  $C = 8.125 \times 10^{-3} \text{ kmol m}^{-3}$ , we get  $C_1 = 4.492 \times 10^{-6} \text{ kmol I}_2 \text{ m}^{-3}$  and  $C_2 = 8.121 \times 10^{-3} \text{ kmol Ti}_4 \text{ m}^{-3}$ .

The above example is a quick review of using thermodynamics to calculate the equilibrium interface concentrations. We proceed to analyze the mass transfer, which

controls the overall kinetics of the growth of the titanium film. The flux of  $\text{TiI}_4$  from the bulk gas to the interface is

$$j_2 = k_M(C_{\infty 2} - C_2).$$

and the flux of  $\text{I}_2$  from the interface to the bulk gas is

$$j_1 = k_M(C_1 - C_{\infty 1}).$$

In these equations, concentrations in the bulk gas are  $C_{\infty 2}$  and  $C_{\infty 1}$ , the interfacial concentrations are  $C_1$  and  $C_2$ , and the fluxes are in  $\text{kmol m}^{-2} \text{ s}^{-1}$ . If we proceed to evaluate the mass transfer coefficients, we will quickly realize that  $D_{M,0} = D_1 = D_2$  and  $k_M = k_M = k_M$ . Hence,

$$j_2 = k_M(C_{\infty 2} - C_2) \quad (14.98)$$

Notice now the problem is over-specified, because the fluxes calculated by Eqs. (14.98) and (14.99) may not satisfy the stoichiometry of reaction (14.92) (specifically  $j_1 = 2j_2$ ). We must decide, therefore, whether the flux of the reactant ( $\text{TiI}_4$ ) to the surface or the flux of the product ( $\text{I}_2$ ) away from the surface controls the overall mass transfer. The slower of the two is called the *rate limiting step*.

**Example 14.7** For the conditions of Example 14.6, determine the *rate limiting step*.

**Solution.**

$$j_2 = k_M(8.125 - 8.121) \times 10^{-3} = 4 \times 10^{-6} k_M,$$

$$j_1 = k_M(4.492 - 0) \times 10^{-6} = 4.492 \times 10^{-6} k_M.$$

It is obvious that  $j_1 \ll j_2$ , so the flux of  $\text{I}_2$  away from the surface is the rate limiting step.

We are ready to make use of the mass transfer coefficient to estimate the growth kinetics of the titanium film. According to reaction (14.92) for every 2 kmol of  $\text{I}_2$  formed, we deposit 1 kmol of  $\text{Ti}$ . Therefore,

$$2j_1 = j_{\text{Ti}} = \frac{\rho}{M} \frac{d\delta}{dt}, \quad (14.100)$$

where  $\rho$  is the density of the film,  $\delta$  is the thickness,  $M$  is the atomic weight ( $\text{kg kmol}^{-1}$ ), and  $t$  is time. After combining Eqs. (14.99) and (14.100), the growth rate is obtained: it is

$$\frac{d\delta}{dt} = 2M\rho^{-1} k_M(C_1 - C_{\infty 1}). \quad (14.101)$$

With  $\delta = 0$  and  $t = 0$ , we get

$$\delta = 2M\rho^{-1} k_M(C_1 - C_{\infty 1})t. \quad (14.102)$$

**Example 14.8** Estimate the mass transfer coefficient for the film growth of Ti from Ti<sub>4</sub> at 1 atm, and compute the growth rate at 1500 K. The gas flows parallel to the substrate (3 cm long) with a speed of 5 m s<sup>-1</sup>.

**Solution.** We consult Bird *et al.*<sup>20</sup> for the Lennard-Jones parameters of I<sub>1</sub>:  $\sigma_1 = 4.982 \text{ \AA}$  and  $(\varepsilon/\kappa_B)_1 = 550 \text{ K}$ . The Lennard-Jones parameters of Ti<sub>4</sub> are estimated, again from Bird *et al.*,<sup>21</sup> from the boiling point (653 K) and molar volume. These two estimates are  $(\varepsilon/\kappa_B)_2 = 751 \text{ K}$  and  $\sigma = 5.805 \text{ \AA}$ . Therefore,

$$\sigma_{12} = \frac{\sigma_1 + \sigma_2}{2} = \frac{4.982 + 5.805}{2} = 5.394 \text{ \AA};$$

$$\left[ \frac{\varepsilon}{\kappa_B} \right]_{12} = \left[ \frac{\varepsilon}{\kappa_B} \right]_1 \left[ \frac{\varepsilon}{\kappa_B} \right]_2 = \sqrt{(550)(751)} = 643 \text{ K}.$$

Then

$$T^* = \left[ \frac{\kappa_B}{\varepsilon} \right]_{12} T = \frac{1500 \text{ K}}{643 \text{ K}} = 2.33$$

and Eq. (12.51) gives  $\Omega_{D,12} = 1.022$ . By making use of Eq. (12.50), we finally estimate  $D_{12}$ .

$$D_{12} = \frac{(1.858 \times 10^{-3})(1500^{0.7})}{(1)(5.394^2)(1.022)} \frac{1}{253.8} + \frac{1}{555.5}$$

$$= 0.270 \text{ cm}^2 \text{ s}^{-1} = 2.70 \times 10^{-5} \text{ m}^2 \text{ s}^{-1}.$$

We must also estimate the viscosity of the gas, which is practically all Ti<sub>4</sub>. For this we use Eq. (1.14).

$$T^* = \left[ \frac{\kappa_B}{\varepsilon} \right]_{12} T = \frac{1500}{751} = 1.997.$$

Table 1.2 gives  $\Omega_v = 1.175$ , and with  $\sigma = \sigma_2 = 5.805 \text{ \AA}$  we have

$$\eta_z = 2.67 \times 10^{-5} \frac{\sqrt{(555.5)(1500)}}{(5.805)^2(1.175)} = 6.16 \times 10^{-4} \text{ Poise}$$

$$= 6.16 \times 10^{-7} \text{ N s m}^{-2}.$$

The Reynolds number ( $\rho_2 = 1.50 \text{ kg m}^{-3}$ ) is

$$Re_L = \frac{LV_0\rho_2}{\eta_2} = \frac{(0.03)(5)(1.50)}{(6.16 \times 10^{-7})} = 3.65 \times 10^5.$$

For flow parallel to a flat plate, this is laminar so we can use Eq. (14.78). Therefore

$$Sh = 0.664 Sc^{0.343} Re_L^{1/2} = 0.664 \left[ \frac{6.16 \times 10^{-7}}{1.50 \times 2.70 \times 10^{-3}} \right]^{0.343} (3.65 \times 10^5)^{1/2}$$

$$= 94.45,$$

and

$$k_M = 94.45 \frac{D_{12}}{L} = \frac{(94.45)(2.70 \times 10^{-7})}{0.03} = 0.0875 \text{ m s}^{-1}.$$

The growth rate is given by Eq. (14.101):

$$\frac{d\delta}{dt} = 2M\rho^{-1} k_M (C_1 - C_\infty)$$

$$= \frac{2}{2} \frac{47.90 \text{ kg}}{\text{kmol}} \frac{\text{m}^3}{4400 \text{ kg}} \frac{0.0875 \text{ m}}{\text{s}} \frac{4.492 \times 10^{-6} \text{ kmol}}{\text{m}^3}$$

$$= 8.558 \times 10^{-9} \text{ m s}^{-1} = 30.81 \mu\text{m h}^{-1}.$$

Before leaving this section, we remind the reader that a rather simple case was considered. Only one reaction was considered, and we analyzed the mass transfer. Reaction rate kinetics were not included. The gas flow was isothermal, and simple flow parallel to a flat plate was used to estimate the mass transfer coefficient. In most chemical vapor deposition processes, the conditions in the reactor are not so simple. Modern day simulations rely on simultaneously solving the momentum, energy, and species conservation equations along with realistic boundary conditions. A review that discusses the complexities involved is that of Jensen.<sup>22</sup>

#### PROBLEMS

**14.1** A solute is being desorbed from the surface of a melt. The concentration of the solute varies according to

$$\frac{C - C_s}{C_\infty - C_s} = a \left[ \frac{x}{\delta_c} \right]^2 + b \left[ \frac{x}{\delta_c} \right],$$

where  $C$  = concentration, moles cm<sup>-3</sup>;  $C_s$  = concentration at the surface;  $C_\infty$  = bulk concentration;  $a, b$  = constants;  $x$  = distance from the surface; and  $\delta_c$  = thickness of the concentration boundary layer. What is the mass transfer coefficient?

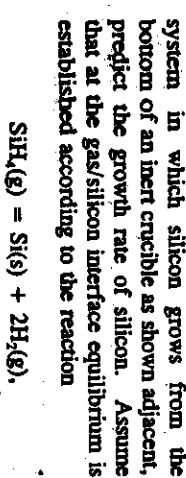
<sup>20</sup>R. B. Bird, W. E. Stewart and E. N. Lightfoot, *Transport Phenomena*, John Wiley & Sons, New York, NY, 1960, page 744.

<sup>21</sup>R. B. Bird *et al.*, *Ibid.*, page 22.

<sup>22</sup>K. F. Jensen, *Chem. Eng. Sci.* 42, 923 (1987).

- 14.2** a) Calculate the diffusion coefficient  $D_{A,B}$  for zinc vapor diffusing through helium at 773 K. The atomic weight of Zn is 65.4 g mol<sup>-1</sup>.  
 b) Calculate the flux of Zn evaporation if the vapor pressure of Zn at 773 K is 0.1 atm. Express the flux in mol s<sup>-1</sup> cm<sup>-2</sup>.

**14.3** Silicon can be grown by the chemical vapor deposition of silane (SiH<sub>4</sub>). Given a system in which silicon grows from the bottom of an inert crucible as shown adjacent, predict the growth rate of silicon. Assume that at the gas/silicon interface equilibrium is established according to the reaction



It is also known that  $D_{\text{H}_2-\text{SiH}_4} = 1 \text{ cm}^2 \text{ s}^{-1}$ .

**14.4** Consider diffusion through a stagnant gas as in Section 14.1; however, in this case the gas is not isothermal, but rather temperature varies according to

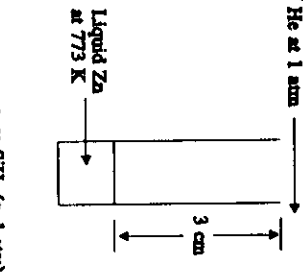
$$\frac{T - T_0}{T_t - T_0} = \frac{x}{l},$$

where  $x$  and  $l$  are indicated in Fig. 14.1,  $T$  is temperature,  $T_0$  is the temperature at  $x = 0$ , and  $T_t$  is the temperature at  $x = l$ . Assume that  $D_{A,B}$  varies with temperature according to Eq. (12.49); i.e.,  $D_{A,B} = A T^{m,n}$  and  $A$  is constant. Obtain the concentration profile which gives the mole fraction of  $A$  ( $X_A$ ) as a function of distance up the tube ( $x$ ).

**14.5** Derive expressions for diffusion through a spherical shell that are analogous to Eq. (14.12) (concentration profile) and Eq. (14.14) (molar flux).

**14.6** Liquid flows in one direction, from  $x = 0$  to  $x = L$ , with a velocity  $V_L$ . Because of the "no-slip" condition, the velocity of the gas along the surface  $y = 0$  is also  $V_L$ . When the gas crosses the plane at  $x = 0$ , its concentration of  $A$  is uniform and constant,  $C_{A,0}$ . However, at  $y = 0$  and  $0 \leq x \leq L$ , its concentration is  $C_A^*$ . Assume steady state. a) Write a partial differential equation for  $C_A(x,y)$  in the gas. b) Write boundary conditions for  $C_A$  that are needed to solve part a). c) Solve for  $C_A(x,y)$ .

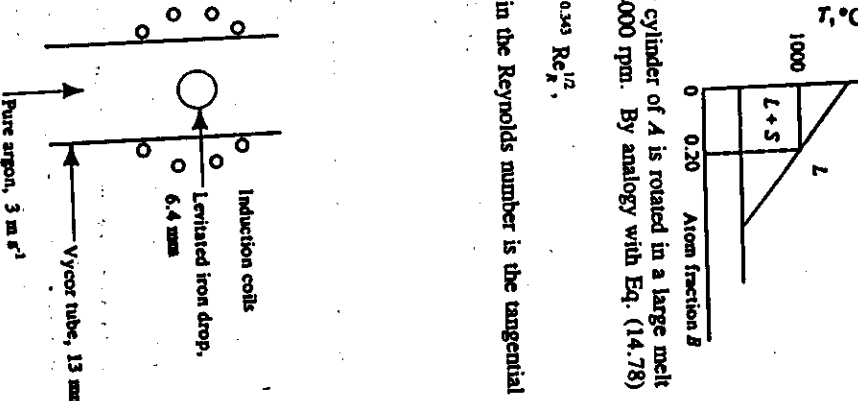
- 14.7** At 1000°C metal  $A$  is soluble in liquid  $B$  but  $B$  is not soluble in solid  $A$  as shown in the pertinent part of the phase diagram. A 5 cm diameter cylinder of  $A$  is rotated at 1000 revolutions per minute (rpm) in a large melt of 0.5 atom fraction  $B$  at 1000°C, and it is noted that after 15 minutes the bar diameter is 4.8 cm. For the same temperature, estimate the bar diameter after 15 minutes if another 5 cm diameter cylinder of  $A$  is rotated in a large melt of the same composition, but now it is rotated at 4000 rpm. By analogy with Eq. (14.78) assume that



- 14.8** Use dimensional analysis to show:  
 a)  $\text{Sh} = f(\text{Re}, \text{Sc})$  for forced convection;  
 b)  $\text{Sh} = f(\text{Gr}, \text{Sc})$  for natural convection.
- 14.9** Levitation melting is a means of supporting a metallic melt by an electromagnetic field. No impurities are added in melting and operation under an inert atmosphere removes dissolved gases. At 1920 K and 1 atm hydrogen pressure, the solubility of hydrogen in iron is 31 cm<sup>3</sup> per 100 g of iron. Estimate the rate at which hydrogen can be removed from a levitated drop of iron that initially contains 10 ppm in the set-up shown to the right. Assume that vigorous convection occurs within the iron drop, the gas temperature is 1920 K, and Eq. (8.11), in mass transfer form, applies.

**14.10** Hydrogen gas is being absorbed from a gas in an experimental set-up shown in the figure to the right. The absorbing liquid is aluminum at 1030 K, which is falling in laminar flow with an average velocity of 2.5 mm s<sup>-1</sup>.

What is the hydrogen content of the aluminum leaving the tube if it enters with no hydrogen? At  $T = 1030$  K and 1 atm hydrogen pressure, the solubility of hydrogen is 1 cm<sup>3</sup> per 100 g of aluminum. The density of Al = 2.3 g cm<sup>-3</sup>, and  $D_H = 1 \times 10^{-9} \text{ m}^2 \text{ s}^{-1}$ .



14.11 When ceramic oxides are used to contain molten metals, they can dissolve and add undesirable impurities to the melt. This is especially true when melting is done under vacuum. For example, magnesium oxide decomposes (slowly) according to

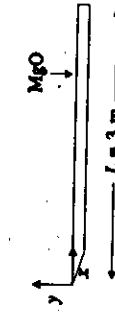


where the underlines indicate that the elements are dissolved in the melt. The equilibrium constant for the reaction is

$$K = C_{\text{Mg}} C_0 = 10^{-6},$$

where  $C_{\text{Mg}}$  and  $C_0$  are the concentrations (moles per  $\text{cm}^3$  of melt) of Mg and O<sub>2</sub>, respectively.

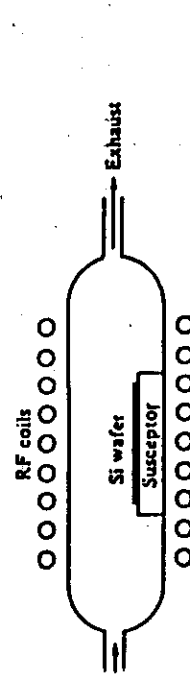
a) For flow parallel to a plate of MgO, calculate the average mass transfer coefficient for Mg dissolving in the melt. Assume that  $C_{\text{Mg}} = C_0$ . For  $x < 0$ ,  $C_{\text{Mg}} = 0$  in the melt and  $V_\infty = 3 \text{ m s}^{-1}$ .



b) What is the average flux of MgO dissolving in the melt? Melt properties:  $\rho = 8000 \text{ kg m}^{-3}$ ;  $k = 50 \text{ W m}^{-1} \text{ K}^{-1}$ ;  $C_p = 840 \text{ J kg}^{-1} \text{ K}^{-1}$ ;  $\eta = 1.24 \times 10^{-3} \text{ N s m}^{-2}$ ; and  $D_{\text{Mg}} = D_{\text{O}_2} = 5 \times 10^{-9} \text{ m}^2 \text{ s}^{-1}$ .

14.12 A common procedure for decreasing the hydrogen content of a melt is to allow bubbles of an inert gas (viz., He) to rise through the melt. Assume that Eq. (8.11), in a form suitable for mass transfer, applies. a) Estimate the mass transfer coefficient from the melt to a single bubble for the removal of dissolved hydrogen. b) Will the overall kinetics of hydrogen removal from the melt depend on mass transfer in the liquid, in the bubble, or both? Justify your answer. c) Derive an equation that can be used to calculate the concentration of dissolved hydrogen as a function of time. Data: bubble diameter, 2 mm; melt density, 7000 kg m<sup>-3</sup>; melt viscosity,  $2 \times 10^{-3} \text{ N s m}^{-2}$ ; diffusivity (hydrogen in melt),  $5 \times 10^{-9} \text{ m}^2 \text{ s}^{-1}$ ; and diffusivity (hydrogen in gas bubble),  $10^{-4} \text{ m}^2 \text{ s}^{-1}$ .

14.13 Consider an electrodeposition process that is controlled by mass transfer at the anode. Calculate the average mass transfer coefficient for the dissolution of the copper anode assuming that the process is controlled by the flux of cupric ions. Assume natural convection and an isothermal solution. Data: Mole fraction of Cu<sup>2+</sup> ions at surface is 0.05; in the bulk it is 0.01. Properties of solution:  $\rho = 1200 \text{ kg m}^{-3}$ ,  $\eta = 2 \times 10^{-3} \text{ N s m}^{-2}$ ,  $D = 5 \times 10^{-9} \text{ m}^2 \text{ s}^{-1}$ , and  $\xi = 4$ .



14.14 A schematic diagram of a vapor-phase epitaxial growth system is shown.

- a) Sketch the concentration of each gas species as a function of the vertical distance from the silicon surface. b) Assume two dimensional flow (rectangular coordinates) and constant  $\rho$  and  $D$  for all species in the gas phase. Give an appropriate equation of diffusion for HCl(g) in an isothermal system. Also give the momentum equation. c) Select an origin and write boundary conditions that are appropriate for the equation of diffusion, with the intent of predicting the growth rate of the epitaxial silicon.

14.15 Boron fibers for composites can be

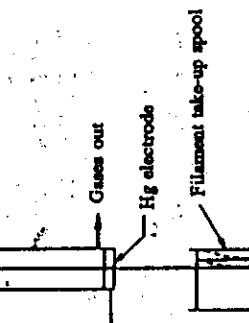
made by running a very fine tungsten wire (12.5  $\mu\text{m}$  dia.) through a reactor tube that is continuously fed with a gas comprising 20% BCl<sub>3</sub> and 80% H<sub>2</sub>. The substrate wire is heated electrically and causes the gases to react and deposit boron. Assume that the reaction is



and is controlled solely by mass transfer. The variables do supply

$$\Delta G^\circ(\text{HCl}) = -22240 + 1.53 T, \text{ cal gmol}^{-1}$$

$$\Delta G^\circ(\text{BCl}_3) = -96560 - 12.35 T, \text{ cal gmol}^{-1}$$



- a) Pick a substrate temperature for depositing the boron. b) Estimate the mass transfer coefficients for the reactants and products. Which species will control the overall deposition rate? (For a discussion of the technology and applications of these fibers see M. E. Buck, *Advanced Materials and Progress In Metal Processes*, 9/87, pp. 61-65.)

## 15

### INTERPHASE MASS TRANSFER

In Chapter 14 we undertook much of the analytical presentation to familiarize ourselves with mass transfer coefficients as they arise from considerations of diffusion with convection in a single phase only. There are many situations, however, in which two fluids or a solid and fluid are in contact, and interphase transfer by diffusion with convection takes place in one or both phases. In some cases, convective mass transfer may be important in controlling the overall rate; in others it is not important. If there is a reaction at the interface, it may very well be the controlling step.

Experimentally, it is difficult to study interphase transfer, and at the same time separate the individual phase resistances; so an *overall transfer coefficient* is usually measured. Having determined this coefficient, we then attempt, via a mathematical model, to deduce the individual phase coefficients, such as those presented in Chapter 14. In some cases the results are clear cut, and we are then able to adjust process conditions to optimize the process. In other cases, however, we cannot differentiate between models even though they may be based on important differences in basic assumptions, because their predictions can be numerically similar within experimental error. Then we deal with the overall coefficients and utilize them, but only if the fluid conditions are similar in both the prototype and model cases.

The objective of this chapter is to indicate the relationships between the individual phase transfer coefficients and the overall coefficients, and to examine several cases in detail, showing how different fluid conditions can influence the overall coefficient through their effects on the individual coefficients.

#### 15.1 TWO-RESISTANCE MASS TRANSFER THEORY

Let us investigate the situation as it might exist in a gas-liquid physical reaction. Figure 15.1 depicts the phases in contact and the concentration profiles in each phase. The mole fraction of  $A$  in the bulk gas phase is  $Y_{A,\infty}$ , and it decreases to  $Y_A^*$  at the interface. In the liquid, the mole fraction drops from  $X_A^*$  at the interface to  $X_{A,\infty}$  in the bulk liquid. The bulk

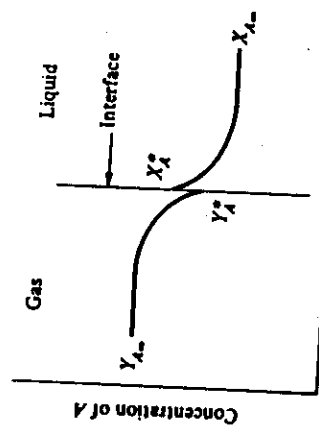


Fig. 15.1 The two-resistance mass transfer concept.

concentrations  $X_{A\infty}$  and  $Y_{A\infty}$  are obviously not in equilibrium, otherwise diffusion of the solute would not occur. To determine the rate of mass transfer between the phases, it is necessary to consider the sequential "steps" in the process.

For example, assume that the only resistances to the overall process are diffusional resistances within the fluids themselves, and that there is no resistance to the transfer of *A* across the interface. Consequently, the interface concentrations,  $X_A^*$  and  $Y_A^*$ , are equilibrium values. In some instances, of course, the atoms or molecules cannot be accommodated into the new phase as rapidly as they might jump from their original phase across the interface. If the accommodation process is slow relative to the diffusional processes, then  $X_A^*$  and  $Y_A^*$  would not represent equilibrium concentrations. In most situations,  $X_A^*$  and  $Y_A^*$  are the equilibrium values, and we proceed with the "two-resistance" theory.

For steady-state transfer, the rate at which *A* reaches the interface from the gas must equal

$$N_A = k_{M,g}(Y_{A\infty} - Y_A^*) = k_{M,l}(X_A^* - X_{A\infty}). \quad (15.1)$$

In this instance, since  $N_A$  is given in  $\text{mol m}^{-2} \text{s}^{-1}$ , and the concentrations are expressed as mole fractions, the mass transfer coefficients ( $k_{M,g}$  and  $k_{M,l}$ ) have the units of  $\text{mol m}^{-2} \text{s}^{-1}$ . The units of the mass transfer coefficients, as presented in Chapter 14 and found within the Sherwood number, are  $\text{m s}^{-1}$ . Of course,  $k_S$  are derivable from  $k_S$ ; specifically, we have  $k_S = k_A C$ , recalling that  $C$  is the total molar concentration ( $\text{mol m}^{-3}$ ) of the solution in question.

In experimental determinations of the rate of mass transfer, it is usually possible to determine solute concentrations in the bulk fluids by sampling. But, because the concentration boundary layers are usually extremely thin, it is physically impossible to approach the interface sufficiently closely to measure  $X_A^*$  and  $Y_A^*$ . Under these circumstances, only the overall effect in terms of either  $X_{A\infty}$  or  $Y_{A\infty}$  can be determined.

Consider the equilibrium of solute *A* as partitioned between the gas phase and a solvent, depicted in Fig. 15.2. The curve for the system is unique at fixed temperature and partial pressure of *A* in the gas phase. On the curve, we identify the four concentrations referred to in Eq. (15.1), specifically  $X_A^*$ ,  $Y_A^*$ ,  $X_{A\infty}$ , and  $Y_{A\infty}$ . In addition, we show  $X_{A,r}$  and  $Y_{A,r}$  which represent equilibrium concentrations corresponding to  $Y_{A\infty}$  and  $X_{A\infty}$ , respectively.  $Y_{A,r}$  in

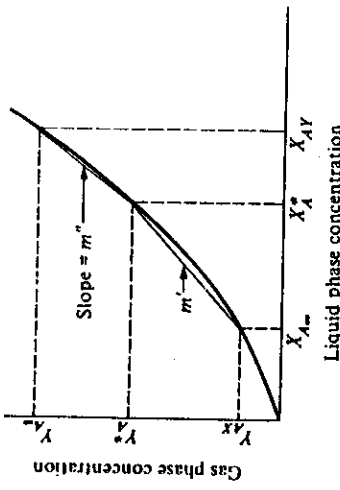


Fig. 15.2 The equilibrium curve for solute *A* partitioned between gas and liquid phases.

equilibrium with  $X_{A\infty}$ , is as good a measure of  $X_{A\infty}$  as  $X_{A\infty}$  itself, and moreover it is on the same basis as  $Y_{A\infty}$ . We may then measure the entire two-phase mass transfer effect in terms of an overall mass transfer coefficient,  $K_g$ :

$$N_A = K_g(Y_{A\infty} - Y_{A,r}). \quad (15.2)$$

From the geometry of the figure, we can show that the relationship among the individual phase coefficients and the overall coefficient is

$$N_A/K_g = N_A/k_{M,g} + m'N_A/k_{M,l},$$

or

$$1/K_g = 1/k_{M,g} + m'/k_{M,l}. \quad (15.3)$$

In a similar manner,  $X_{A,r}$  is a measure of  $Y_{A\infty}$ , and we may use it to define another overall coefficient  $K_i$ :

$$N_A = K_i(X_{A,r} - X_{A\infty}). \quad (15.4)$$

It readily follows that

$$1/K_i = 1/m''k_{M,g} + 1/k_{M,l}. \quad (15.5)$$

Equations (15.3) and (15.5) lead to the following relationships among the mass-transfer resistances:

$$\frac{\text{gas phase resistance}}{\text{total resistance}} = \frac{1/k_{M,g}}{1/K_g}. \quad (15.6)$$

and

$$\frac{\text{liquid phase resistance}}{\text{total resistance}} = \frac{1/k_{M,l}}{1/K_g}. \quad (15.7)$$

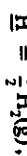
If the individual phase coefficients,  $\kappa_{M,r}$  and  $\kappa_{M,l}$ , have roughly the same values, then we can demonstrate the importance of the shape of the equilibrium partition curve. If  $m'$  is small (equilibrium partition curve is fairly flat and solute A is very soluble in the liquid), then Eq. (15.3) shows that the major resistance is really  $1/\kappa_{M,r}$ , and the rate of mass transfer is gas-phase controlled.

Under such circumstances, even large increases in  $\kappa_{M,l}$  do not significantly change  $K_r$ , and efforts to increase the mass transfer rate are best directed toward decreasing the gas-phase resistance. Conversely, when  $m''$  is large (solute A is relatively insoluble in the liquid) and  $\kappa_{M,r}$  and  $\kappa_{M,l}$  are nearly equal, the major resistance is in the liquid. In these instances, efforts to bring about substantial increases in the rate of mass transfer are best directed toward increasing the liquid coefficient  $\kappa_{M,l}$ .

When overall coefficients are used in calculations, they are frequently synthesized through the correlations developed (such as those in Chapter 14) for the individual coefficients of the phases in contact. It is important to recognize the limitations in this procedure. For example, the hydrodynamic circumstances must be the same as those for which the correlations were developed. This is especially true in the case of two fluids, where motion in one may influence motion in the other. In other situations, absorption of surface-active substances at the interface may slow down reactions (chemical or physical) to such an extent that the estimated overall coefficient in no way reflects the magnitudes of the individual phase coefficients.

On the other hand, most experimental studies of reaction rates measure overall coefficients, from which attempts are often made to deduce individual phase resistances. Again, if experimentally measured overall coefficients are to be used in practice, the conditions with respect to fluid motion and reactant supply must also be similar, unless it is clear that the controlling resistance of the overall transfer lies in a nonfluid phase.

**Example 15.1** In order to remove hydrogen from molten copper at 1150°C, the copper is brought in contact with pure argon at 1 atm pressure. Hydrogen diffuses to the argon, and undergoes the reaction



in which H represents hydrogen dissolved in liquid copper. At 1150°C and 1 atm hydrogen pressure, the solubility of hydrogen in molten copper is 7.0 cm<sup>3</sup> H<sub>2</sub>(STP)/100 g of copper. Assuming that the mass transfer coefficients ( $\kappa_s$ ) within the individual phases are roughly equal in any process involving contact of argon and the copper, determine whether the rate of mass transfer would be gas-phase or liquid-phase controlled.

**Solution.** We proceed by examining the equilibrium of hydrogen between the gas phase (Ar-H<sub>2</sub>) and the liquid (Cu-H). We ignore the presence of Cu in the gas phase because its vapor pressure is very low at this temperature. To examine the relative values of the mass transfer rates, we need to express the concentrations in mole fractions. In the liquid phase, we convert the solubility to the mole fraction of H in the liquid as follows

$$X_H = \frac{7.0 \text{ cm}^3 \text{ H}_2(\text{STP})}{0.1 \text{ kg Cu}} \left| \frac{1 \text{ mol H}_2}{22,400 \text{ cm}^3 \text{ H}_2(\text{STP})} \right| \left| \frac{1 \text{ kmol H}_2}{1000 \text{ mol H}_2} \right| \left| \frac{0.5 \text{ kmol H}_2}{1 \text{ kmol Cu}} \right| = 3.97 \times 10^{-4}.$$

We can express the equilibrium constant for the reaction as

$$K_{eq} = \frac{X_H}{\sqrt{Y_{H_2}}}.$$

where  $Y_{H_2}$  is the mole fraction of hydrogen in the gas; it follows that  $K_{eq} = 3.97 \times 10^{-4}$  at 1150°C. Therefore, we can express the equilibrium partition of hydrogen between the phases as

$$X_H = 3.96 \times 10^{-4} \sqrt{Y_{H_2}}.$$

By referring to Fig. 15.2, we can estimate  $m'$  and  $m''$  with  $Y_{H_{eq}} = 0$  and  $X_{H_{eq}} = 3.97 \times 10^{-4}$ . In addition, because we are assuming  $\kappa_{M,r} = \kappa_{M,l}$ , Eq. (15.1) indicates that

$$Y_{H_{eq}} - Y_H^* \equiv X_H^* - X_{H_{eq}}.$$

Therefore

$$Y_H^* \equiv X_{H_{eq}} - X_H^* \equiv 10^{-4},$$

$$m' = \frac{Y_{H_2}^* - Y_{H_{eq}}}{X_H^* - X_{H_{eq}}} \equiv \frac{10^{-4} - 1}{0 - 4 \times 10^{-4}} \equiv 2.5 \times 10^3,$$

$$m'' = \frac{Y_{H_{eq}} - Y_H^*}{X_{H'} - X_H^*} = \frac{0 - Y_H^*}{0 - X_H^*} = \frac{\sqrt{Y_H^*}}{K_{eq}} = \frac{10^{-2}}{4 \times 10^{-4}} \equiv 25.$$

If we now examine Eq. (15.3) or Eq. (15.5), with these values of  $m'$  and  $m''$ , it is easy to see that major resistance to mass transfer is in the liquid phase and the overall rate of mass transfer is liquid-phase controlled.

## 15.2 MIXED CONTROL IN GAS-SOLID REACTIONS

In Chapter 13 we examined several solutions for diffusion within solids; we found that some of these solutions were appropriate to situations involving gas-solid reactions at the solid surface. Specifically, we examined those cases in which the solute surface concentration in the solid could be considered to be in equilibrium with the gas-phase environment. In many processes, this is indeed the case, because most reactions do proceed readily at the high temperatures. There are situations, however, in which exceptions to this generalization should be made, as the next two subsections demonstrate.

### 15.2.1 Carburization of iron with surface reaction and diffusion as controlling factors

If an iron plate is exposed to a CH<sub>4</sub>-H<sub>2</sub> atmosphere, then carburization occurs at the surface according to



and consequently carbon diffuses into the plate. The objective is to describe the kinetics of the carburization.

It has been proposed<sup>1</sup> that the surface reaction proceeds at a rate given by

$$\frac{1}{A} \frac{dn_c}{dt} = r_1 \frac{P_{\text{CH}_4}}{P_{\text{H}_2}} - r_2 P_{\text{H}_2}^2 C, \quad (15.9)$$

where  $dn_c/dt$  is the amount of carbon in mol taken up by the surface area  $A$  per unit time,  $r_i$  and  $r_s$  are reaction rate constants,  $P_{CH_4}$  and  $P_{H_2}$  are the partial pressures in the gas phase, presumed to be constants,  $C_s$  is the surface concentration of carbon in  $\text{mol m}^{-2}$ , and  $v$  is a number between zero and two, depending on the details of the reaction mechanism.

At equilibrium,  $dn_c/dt = 0$ ; therefore, from Eq. (15.9) we can obtain the equilibrium concentration of carbon

$$C_s = \frac{r_i P_{CH_4}}{r_s P_{H_2}^2}. \quad (15.10)$$

Substitution of Eq. (15.10) into Eq. (15.9) gives

$$\frac{1}{A} \frac{dn_c}{dt} = r(C_s - C_s), \quad (15.11)$$

where

$$r = r_s P_{H_2}^{2-v}.$$

We can incorporate Eq. (15.11) into one of the boundary conditions for the diffusion of carbon in the plate. Consider the region  $0 \leq x \leq L$  in which  $x = 0$  is the center of the plate, and  $x = L$  is the semithickness of the plate. The appropriate differential equation is

$$\frac{\partial C}{\partial t} = D \frac{\partial^2 C}{\partial x^2}, \quad (15.12)$$

where  $C$  is the carbon concentration and  $D$  is the diffusion coefficient of carbon in iron. We assume that only a single phase of iron exists. Therefore, the initial and boundary conditions are

$$C(x, 0) = C_i \text{ (uniform)}, \quad (15.13a)$$

$$\frac{\partial C}{\partial x}(0, t) = 0, \quad (15.13b)$$

$$\text{and } \frac{\partial C}{\partial x}(L, t) + \frac{r}{D}(C_s - C_i) = 0. \quad (15.13c)$$

Condition (15.13c) states that the amount of carbon furnished by the surface reaction must equal the amount diffusing into the interior. Note that Eq. (15.13c) is exactly the same condition existing at the surface of a solid losing heat to a surrounding environment at  $T_f$  at a rate dependent on the heat transfer coefficient. In fact, Eq. (15.12) and its boundary conditions, Eqs. (15.13a), (15.13b), and (15.13c), are exactly the same as Eq. (9.22) and its boundary conditions, Eqs. (9.23)-(9.25). Hence, Eq. (9.43) and Fig. 9.9 are proper solutions to the problem at hand if we merely replace

$$\frac{T - T_f}{T_i - T_f} \text{ by } \frac{C - C_i}{C_s - C_i},$$

$$\frac{\partial C}{\partial t} \text{ by } \frac{rL}{D},$$

$$hL/k \text{ by } rL/D,$$

$$C(x, 0, t) = X_{CH_4}(x, t) \frac{K_{eq}}{P} = C_s, \quad (15.16)$$

In this section, we examine a situation in which the gas phase composition does not remain constant, because the reaction rate at the surface of the solid is so rapid that the gas cannot be replenished instantaneously by the incoming fresh gas. As an example, suppose we wish to carburize the surface of low-carbon sheet steel with a  $\text{CH}_4\text{-H}_2$  atmosphere. The steel is in the form of an open coil so that the gas can flow between parallel layers as depicted in Fig. 15.3. We assume that the thickness of the sheet in the  $y$ -direction is sufficiently large so that diffusion into a semi-infinite solid holds. However, there is a depletion of methane with increasing  $x$  because it is consumed by reaction. Hence, the concentration of carbon in the steel varies with  $x$  as well as with  $t$  (time).

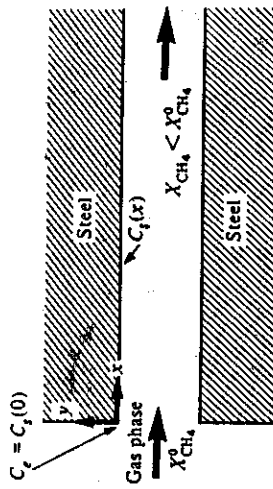


Fig. 15.3 Carburization of steel by gas flowing between parallel sheets.

To simplify the problem considerably, we may disregard the variation of the methane concentration normal to the flow direction; in the solid, the diffusion of carbon in the  $x$ -direction is ignored since the diffusive component in the  $y$ -direction is so much greater. Therefore, Fick's second law for diffusion in the steel applies, and is written

$$\frac{\partial C}{\partial t} = D \frac{\partial^2 C}{\partial y^2}, \quad (15.14)$$

where  $C$  is the carbon concentration, and  $D$  is its diffusion coefficient in the steel. Initially, the steel contains  $C_i$  of carbon; hence

$$C(x, y, 0) = C_i, \quad (15.15)$$

Along the plane  $y = 0$ , we presume that equilibrium exists between the surface carbon and the atmosphere according to

$$K_{eq} = \frac{C_s P_{H_2}^2}{P_{CH_4}},$$

where  $K_{eq}$  is the thermodynamic equilibrium constant for the reaction (15.8). Thus, we can represent the relationship between the local methane mole fraction,  $X_{CH_4}$ , and the local surface concentration as

where  $X_{\text{CH}_4}$  is the mole fraction of methane,  $P$  is the total pressure, and  $X_{\text{CH}_4} \ll 1$ . At the entrance, we have the original mole fraction,  $X_{\text{CH}_4}^0$ ; thus

$$C(0,0,t) = X_{\text{CH}_4}^0 \frac{K_{\text{eq}}}{P} = C_r, \quad (15.17)$$

where  $C_r$  equals the equilibrium concentration for the original gas composition.

As the gas flows between the parallel plates from  $x$  to  $x + dx$ , the loss of methane per unit time equals

$$-n \left[ \frac{\partial X_{\text{CH}_4}}{\partial x} \right] dx,$$

where  $\partial X_{\text{CH}_4}/\partial x$  is negative, and  $n$  is the flow rate of the gas in  $\text{mol s}^{-1}$ . The amount of carbon diffusing from the surface,  $b dx$ , per unit time into the two surfaces equals

$$-2b dx D \left[ \frac{\partial C}{\partial y} \right]_{y=0},$$

where  $b$  is the sheet width normal to the plane of Fig. 15.3, and  $C$  is given in  $\text{mol m}^{-3}$ . Equating this value to the loss of methane per unit time, and substituting Eq. (15.16), we get

$$\left[ \frac{\partial C}{\partial y} \right]_{y=0} = \frac{n P}{2b D K_{\text{eq}}} \left[ \frac{\partial C}{\partial x} \right]_{y=0} \quad (15.18)$$

for  $x > 0$ . To summarize, we wish to solve Eq. (15.14), subject to Eqs. (15.15), (15.17), and (15.18). A method of accomplishing this was presented by Wagner,<sup>2</sup> and is as follows:

Assuming that  $C$  depends only on  $x/\sqrt{t}$  and  $y/\sqrt{t}$ , we define the dimensionless variables:

$$\xi = \frac{2b D K_{\text{eq}}}{n P} \frac{x}{2\sqrt{Dt}}; \quad \eta = \frac{y}{2\sqrt{Dt}}$$

Substitution of  $\xi$  and  $\eta$  into Eq. (15.14) gives

$$\frac{\partial^2 C}{\partial \eta^2} + 2 \left[ \xi \frac{\partial C}{\partial \xi} + \eta \frac{\partial C}{\partial \eta} \right] = 0. \quad (15.19)$$

Substitution of  $\xi$  and  $\eta$  into Eqs. (15.17), (15.15), and (15.18), respectively, yields

$$C = C_r \quad \text{for } \xi = 0, \eta = 0; \quad (15.20a)$$

$$C = C_r \quad \text{for } \xi = \infty, \eta = \infty; \quad (15.20b)$$

$$\left[ \frac{\partial C}{\partial \xi} \right]_{\eta=0} = \left[ \frac{\partial C}{\partial \eta} \right]_{\eta=0}. \quad (15.20c)$$

We can transform Eq. (15.19) into an ordinary differential equation if we consider  $C$  a function of the sum  $\sigma = \xi + \eta$ :

$$\frac{d^2 C}{d \sigma^2} + 2\sigma \frac{dC}{d\sigma} = 0. \quad (15.21)$$

The solution to Eq. (15.21), subject to Eqs. (15.20a, b, and c), is

$$\frac{C - C_r}{C_r - C_i} = \operatorname{erfc} \left[ \frac{\frac{2b D K_{\text{eq}}}{n P} x + y}{2\sqrt{Dt}} \right]. \quad (15.22)$$

**Example 15.2** Calculate the distance  $x$  over which the surface concentration  $C$  does not vary excessively after carburizing. Specifically, it is required that the ratio  $(C_r - C)/(C_r - C_i) \geq 0.75$ . Surface carburization is carried out with dilute methane/argon-hydrogen at 1000°C and 1 atm, and the appropriate equilibrium constant is 0.7 atm mol cm<sup>-3</sup>. The gas flows at a linear velocity of 0.1 m s<sup>-1</sup> through a separation of 2 cm between steel sheets for 5 h. At 1000°C, the diffusion coefficient of carbon in γ-iron is  $3 \times 10^{-11} \text{ m}^2 \text{ s}^{-1}$ .

**Solution.** Seeking the surface concentration  $C_r$ , we obtain from Eq. (15.22) with  $y = 0$ :

$$\frac{C_r - C}{C_r - C_i} = 1 - \operatorname{erf} \left[ \frac{\frac{2b D K_{\text{eq}}}{n P} x}{2\sqrt{Dt}} \right].$$

We require the left-hand side of the equation to be 0.75. Hence

$$0.25 = \operatorname{erf} \left[ \frac{\frac{2b D K_{\text{eq}}}{n P} x}{2\sqrt{Dt}} \right].$$

We find the argument of the error function to be 0.225 (Table 9.3), so that

$$x = 0.450 \sqrt{Dt} \frac{n}{2b} \frac{P}{K_{\text{eq}}}.$$

Next we evaluate  $n/2b$  and  $K_{\text{eq}}$ :

$$n = \frac{0.1 \text{ m}}{\text{s}} \left| \frac{0.02b \text{ m}^2}{22.4 \text{ m}^3 (\text{STP})} \right| \frac{1 \text{ kmol}}{1273 \text{ K}} = 1.915b \times 10^{-5} \text{ kmol s}^{-1};$$

therefore

$$\frac{n}{2b} = \frac{1.915b \times 10^{-5} \text{ kmol}}{2b \text{ m}} = 9.574 \times 10^{-6} \text{ kmol s}^{-1} \text{ m}^{-1}.$$

Also,

$$K_{\text{eq}} = \frac{0.7 \text{ atm mol}}{\text{cm}^3} \left| \frac{10^6 \text{ cm}^3}{1 \text{ m}^3} \right| \frac{1 \text{ kmol}}{10^3 \text{ mol}} = 700 \text{ atm kmol m}^{-3}.$$

Then, by substituting  $t = 18000 \text{ s}$ ,  $D = 3 \times 10^{-11} \text{ m}^2 \text{ s}^{-1}$ , and  $P = 1 \text{ atm}$ , we calculate  $x$  to be 0.15 m.

Of practical significance, this section shows that excessive nonuniformity of the surface concentration can only be prevented by a sufficient concentration of the reactant species in the exit gas phase. For example, we saw in the above problem that there was a limit to the distance that could be properly carburized for the specifications put forth. If the specifications had been more severe, for example,  $|C_i - C_j|/C_i \geq 0.90$ , then a higher velocity of carburizing gas would have had to be supplied to achieve the same value of  $x$ , thus raising the concentration of the reactant species in the exit gas. If the active species is valuable, recovery of this component or recirculation of the exit gas must be used. This is an important economic consideration in chromizing steel with CrCl<sub>2</sub>(g).

### 15.2.2 Oxidation of silicon

Silicon dioxide (SiO<sub>2</sub>) is used to protect the surface of silicon against unwanted reactions and diffusion. Specifically, the diffusivities of boron and phosphorus in SiO<sub>2</sub> are much smaller than they are in silicon. So if a region of a silicon substrate is covered with SiO<sub>2</sub>, the SiO<sub>2</sub> effectively serves as a mask when the substrate is placed in a furnace for diffusion processing.

The SiO<sub>2</sub> mask is also used for selective diffusion in conjunction with photolithography.



The overall mass transfer of oxygen is shown in Fig. 15.4, where there is mass transfer in the gas, diffusion through the SiO<sub>2</sub>, and finally the reaction at the SiO<sub>2</sub>-Si interface. We assume that the concentration of the diffusing species in the oxide is linear.

The oxidation rate is low enough that the flux through the gas, the flux through the oxide, and the reaction flux are all equal.

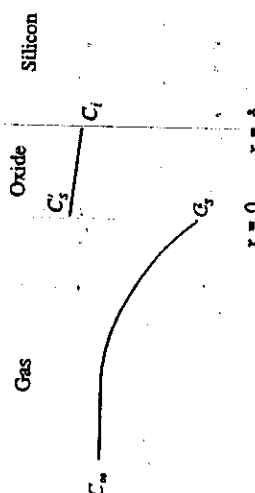


Fig. 15.4 Model for oxidation of silicon.

Hence,  $j_G = j_o = r$  with

$$j_G = k_M(C_\infty - C_i), \quad (15.24)$$

$$j_o = \frac{D}{\delta}(C_i - C_0), \quad (15.25)$$

$$r = k_r C_i, \quad \text{and} \quad (15.26)$$

The subscripts  $G$  and  $O$  are for gas and oxide, respectively. At  $x = \delta$ , the reaction flux,  $r$ , is first order with the reaction rate constant  $k_r$ , and  $k_M$  is the mass transfer coefficient in the gas.

The concentrations in the gas are

$$C_\infty = \frac{P_{O_2}^*}{k_B T},$$

and

$$C_i = \frac{P_{O_2}'}{k_B T}.$$

where  $k_B$  the Boltzmann's constant, is used rather than the customary gas constant because the concentrations of O<sub>2</sub> in the gas have units of molecules m<sup>-3</sup>. At the gas-oxide interface,  $C_i$  and  $C'$  are at equilibrium; hence

$$C' = K P_{O_2}' ,$$

where  $K$  is the equilibrium constant. It is also convenient to express  $C_i$  in terms of its equivalent partial pressure of oxygen; hence

$$C_i = K P_{O_2}' .$$

Now we can express the fluxes given by Eqs. (15.24)-(15.26) in terms of pressure gradients, as follows:

$$j_G = \frac{k_M}{k_B T} (P_{O_2}^* - P_{O_2}'), \quad (15.27)$$

$$j_o = \frac{DK}{\delta} (P_{O_2}' - P_{O_2}), \quad (15.28)$$

and

$$r = k_r K (P_{O_2} - 0). \quad (15.29)$$

It is convenient to use an analog with three resistances in series and an overall potential of  $P_{O_2}^* - 0$ . We get

$$j = \frac{P_{O_2}^*}{\frac{k_M}{k_B T} + \frac{1}{K_r K} + \frac{\delta}{DK}} \quad (15.30a)$$

If we prefer to use concentrations, rather than pressures, the equivalent result is

$$j = \frac{k_r K' C_\infty}{\frac{k_r K'}{k_M} + 1 + \frac{\delta}{D}} \quad (15.30b)$$

where  $K' = K k_B T$ . Keep in mind that this flux has units of O<sub>2</sub> molecules m<sup>-2</sup> s<sup>-1</sup>.

The film thickens by reaction (15.23), so the mass per unit area is  $\rho db/dt$ , with  $\rho$  the density of the oxide. Therefore, the flux of adding oxygen molecules to the film is

$$j = \frac{\rho}{M} \frac{d\delta}{dt}, \quad (15.31)$$

where  $m$  is the mass per molecule ( $O_2$ ). We equate Eqs. (15.30b) and (15.31); this results in

$$\frac{k_r K' C_\infty}{k_r \delta + 1 + \frac{D}{k_r}} = \frac{\rho}{M} \frac{d\delta}{dt}. \quad (15.32)$$

With  $\delta = \delta_i$  at  $t = 0$ , the integrated result (in dimensionless form) is

$$\frac{\delta^2 - \delta_i^2}{2Dt} + \left[ \frac{1}{k_r} + \frac{K'}{k_r} \right] \frac{(\delta - \delta_i)}{t} - \frac{mK' C_\infty}{\rho} = 0. \quad (15.33)$$

If dry oxidation is done, then the gas is pure  $O_2$  and  $C_r = C_\infty$  (see Fig. 15.4). Effectively, this is the same as making  $k_r \rightarrow \infty$ , and Eq. (15.33) reduces to

$$\delta = \frac{A}{2} \left[ \left\{ 1 + \frac{4B(t + \tau)}{A^2} \right\}^{1/2} - 1 \right], \quad (15.34)$$

where

$$A = \frac{2D}{k_r}, \quad B = \frac{2DC_r m}{\rho}, \quad \tau = \frac{\delta_i^2 + A\delta_i}{B}.$$

Oxidation in steam is by the reaction:



Consequently,  $H_2O$  diffuses from the gas and through the film to the reaction site at the oxide-silicon interface, and  $H_2$  leaves the reaction site by diffusing through the film in the opposite direction. At 1273 K, the diffusivity of hydrogen through  $SiO_2$  is more than 1000 times that of steam, so the oxidation rate is controlled by the diffusion of steam.

The oxidation rate is much faster in steam than it is in dry oxygen, largely because  $C'_r$  in steam is much greater than it is in dry oxygen, whereas  $C'_r$ (oxygen) =  $5 \times 10^{16}$  molecules  $cm^{-3}$ , whereas  $C'_r$ (steam) =  $3 \times 10^{19}$  molecules  $cm^{-3}$ .

Equation (15.34) also applies for oxidation in either dry oxygen or steam. The oxidation constants depend on temperature according to the following equations:

dry oxygen

$$A = 1.18 \times 10^{-10} \exp \left[ \frac{8840}{T} \right], \quad m$$

$$B = 1.81 \times 10^{-13} \exp \left[ -\frac{14050}{T} \right], \quad m^2 s^{-1}$$

### steam

$$A = 3.32 \times 10^{-12} \exp \left[ \frac{14170}{T} \right], \quad m$$

$$B = 4.95 \times 10^{-14} \exp \left[ -\frac{7920}{T} \right], \quad m^2 s^{-1}$$

The equations for the oxidation constants were derived from a figure given by Yang,<sup>3</sup> who also gives more discussion on the oxidation of silicon and oxide and nitride masks.

**Example 15.3** Assume  $\delta_i = 20$  nm. a) Calculate the time required to grow a 150 nm-thick oxide on silicon in dry oxygen at 1300 K. b) Suppose you want to achieve the same thickness of oxide in less time. Using dry oxygen again, determine the required time at 1400 K. c) For the same thickness and time as part b), determine the temperature if the oxidation is carried out in steam.

**Solution.** a)  $A = 1.18 \times 10^{-10} \exp \left[ \frac{8840}{1300} \right] = 1.06 \times 10^{-7} \text{ m};$

$$B = 1.81 \times 10^{-13} \exp \left[ -\frac{14050}{1300} \right] = 3.66 \times 10^{-10} \text{ m}^2 s^{-1};$$

$$\tau = \frac{\delta_i^2 + A\delta_i}{B} = \frac{(20 \times 10^{-9})^2 + (1.06 \times 10^{-7})(20 \times 10^{-9})}{3.66 \times 10^{-10}} = 688 \text{ s.}$$

Next, we calculate  $t$  from Eq. (15.34):

$$\begin{aligned} t + \tau &= \frac{A^2}{4B} \left\{ \left[ 1 + \frac{2\delta}{A} \right]^2 - 1 \right\} \\ &= \frac{(1.06 \times 10^{-7})^2}{(4)(3.66 \times 10^{-10})} \left\{ \left[ 1 + \frac{(2)(1.50 \times 10^{-9})}{(1.06 \times 10^{-7})} \right]^2 - 1 \right\} \\ &= 10491 \text{ s} \end{aligned}$$

and

$$t = 10491 - 688 = 9793 \text{ s.}$$

- b) For less time, a higher temperature is required. With  $T = 1400$  K, we follow the same procedure of part a) and calculate:  $A = 6.52 \times 10^{-10} \text{ m}; B = 7.93 \times 10^{-13} \text{ m}; \tau = 215 \text{ s};$  and  $t = 3856 \text{ s.}$  We see that raising the temperature by 100 K decreases the time by 63%.

c) For the same time as part b),  $t = 3856$  s, we expect a lower temperature in steam. For the first trial, we try 1200 K. Then

$$A = 3.32 \times 10^{-12} \exp \left[ \frac{14,170}{1200} \right] = 4.46 \times 10^{-7} \text{ m},$$

$$B = 4.95 \times 10^{-14} \exp \left[ -\frac{7926}{1200} \right] = 6.70 \times 10^{-17} \text{ m}^2 \text{ s}^{-1},$$

and

$$\tau = \frac{(20 \times 10^{-9})^2 + (4.46 \times 10^{-7})(20 \times 10^{-9})}{6.70 \times 10^{-17}} = 139 \text{ s.}$$

From these values, we get  $t = 1195$  s. This time is much less than the 3856 s found in part b), so we can select a lower temperature. After a few more trials, we get  $T = 1118$  K.

Wen<sup>4</sup> discussed in detail the mathematical solutions to the kinetic equations for many different models of gas-solid reactions; he showed how similar some of the results are in terms of experimental weight loss versus time data for models differing widely in terms of assumptions made. His theme is that misleading conclusions concerning rate-controlling mechanisms can easily be made, unless much care is taken to ensure that experimental conditions eliminate control by steps being ignored in the analysis. However, it should be kept in mind that overall coefficients can be useful information from the design engineering standpoint.

### 15.3 MASS TRANSFER WITH VAPORIZATION

As pointed out in Chapter 5, there are many processes that involve heating materials in a vacuum. In vacuum melting or heat treating of ferrous alloys, valuable elements, such as manganese or chromium, may be lost, or undesirable impurities, such as zinc or lead, may be removed. In Knudsen effusion cells, use is made of the measured rate of vaporization of an element to determine thermodynamic properties of the material.

In all of these cases, there are several steps involved in the overall mass transfer process:

1. transport of the volatile species to the surface of the condensed phase;
2. formation of volatile compounds at the surface;
3. evaporation from the surface into the gas or vacuum;
4. transport away from the surface into the gas or vacuum. Depending on conditions, any one of these steps may be rate limiting, or several may make a mixed-control process.

#### 15.3.1 Knudsen effusion cells

The Knudsen cell is used to study thermodynamic properties of alloys by taking advantage of the high volatility of one component relative to the others, and determining the vapor pressure of this species as a function of alloy content. The vapor pressure is determined by measuring the force exerted by a molecular stream emanating into a vacuum from a very small hole in the end of a hollow cell containing the alloy. Under these conditions, free molecular diffusion occurs; then, by referring to Section 5.5.1, we have

$$Z_{\text{ex}} = \left[ \frac{r_{\text{s}} T}{2\pi m} \right]^{1/2} (n_1 - n_2), \text{ molecules m}^{-2} \text{ s}^{-1},$$

or

$$J = \frac{A_e (P_1 - P_2)}{\sqrt{2\pi MRT}}, \text{ mol s}^{-1},$$

where  $P_1$  and  $P_2$  are in  $\text{N m}^{-2}$ , and  $R$  has units of  $\text{N m mol}^{-1} \text{ K}^{-1}$ .

These expressions give the net rate at which atoms or molecules leave the cell through an infinitely thin orifice opening. Because of the difficulty of constructing an infinitely thin opening, that is with no walls, there is a correction to the theoretical flux accounting for the small probability of molecules rebounding and not passing through the opening. The Clausing factor,  $W_r$ , gives the probability of passing and is a function of the ratio of the orifice thickness to radius,  $l/r$ , as given in Table 15.1. When this factor is included, then

$$J = \frac{A_e W_r (P_1 - P_2)}{\sqrt{2\pi MRT}} \quad (15.36)$$

Table 15.1 Clausing factors for effusion cells\*

$l/r$	$W_r$
0	1.00
0.1	0.9524
0.2	0.9092
0.3	0.8699
0.4	0.8341

\*From P. Clauzing, *Annalen der Physik* 12, 976 (1932).

At the same time as vapor leaves through the orifice, the solid within the cell loses alloy from its surface initially having an alloy concentration of  $C_A^0$ . If the area of the orifice,  $A_e$ , is small relative to the exposed surface area of the alloy,  $A_s$ , then we may take the partial pressure within the cell,  $P_1$ , as uniform. Furthermore,  $P_1$  is the pressure of the volatile component in equilibrium with its concentration on the surface of the solid,  $C_A^*$ . Therefore, Fig. 15.5 gives the situation, and the diffusive flux within the solid to the surface equals the effusive flux

$$J = +DA_s \left[ \frac{\partial C_A}{\partial x} \right]_{x=0} = \frac{A_e W_r (P_1 - P_2)}{\sqrt{2\pi MRT}}, \quad (15.37)$$

where  $C_A$  is in  $\text{mol m}^{-3}$ .

In order for free molecular diffusion to occur,  $P_2$  must be very low ( $< 10^{-6}$  atm). In fact, a gradient at the surface is obtained more quickly if the cell is placed in a vacuum, especially since  $P_1$  is on the order of only  $10^{-3}\text{-}10^{-4}$  atm;  $P_1$  is related to the surface mole fraction  $X_A$ ,

$$P_1 = \gamma X_A P_A^0,$$

<sup>4</sup>C. Y. Wen, I. & E. C. 60, No. 9, 34 (1968).

The surface concentration of the solid  $C_s^*$  obtained by letting  $x = 0$  in Eq. (15.41), is

$$C_s^*/C_A^0 = \exp(Y^2 D_t) \operatorname{erfc}(Y\sqrt{D_t}). \quad (15.42)$$

Figure 15.6 gives times allowable in order to limit the surface depletion to 5% in Fe-Mn alloys, based on Eq. (15.42).

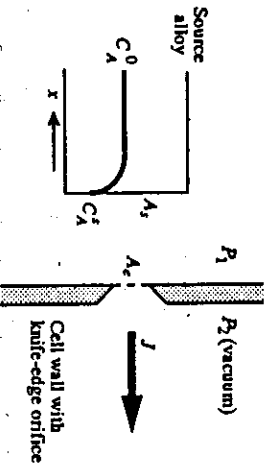


Fig. 15.5 The conditions in a Knudsen effusion cell.

where  $\gamma_A$  is the activity coefficient relative to the pure component, and  $P_A^0$  is the vapor pressure of the pure component at the temperature in question. Thus, with  $P_2 = 0$  in a vacuum,

$$D_A \left[ \frac{\partial C_A}{\partial x} \right]_{x=0} = \frac{A_r W \gamma_A P_A^0 C_A^*}{\rho \sqrt{2\pi M RT}}, \quad (15.38)$$

where  $\rho$  = mol alloy  $\text{m}^{-3}$ , the molar density of the alloy. Fick's second law describes diffusion within the solid; the boundary condition at the surface of the solid is Eq. (15.38). If we consider the alloy as a semi-infinite solid, then we seek a solution to

$$\frac{\partial C_A}{\partial t} = D \frac{\partial^2 C_A}{\partial x^2}, \quad (15.39)$$

with

$$C_A(x, 0) = C_A^0, \quad (15.40a)$$

$$\frac{\partial C_A(0, t)}{\partial x} - Y C_A(0, t) = 0, \quad (15.40b)$$

and

$$C(\infty, t) = C_A^*, \quad (15.40c)$$

where

$$Y = A_r W \gamma_A P_A^0 / A_r D \rho \sqrt{2\pi M RT}, \text{ m}^{-1}.$$

Carslaw and Jaeger<sup>5</sup> give the solution to Eq. (15.39) satisfying Eqs. (15.40a, b, and c):

$$\frac{C_A}{C_A^0} = \operatorname{erf} \frac{x}{2\sqrt{D_t}} + \exp(Yx + Y^2 D_t) \operatorname{erfc} \left[ \frac{x}{2\sqrt{D_t}} + Y\sqrt{D_t} \right]. \quad (15.41)$$

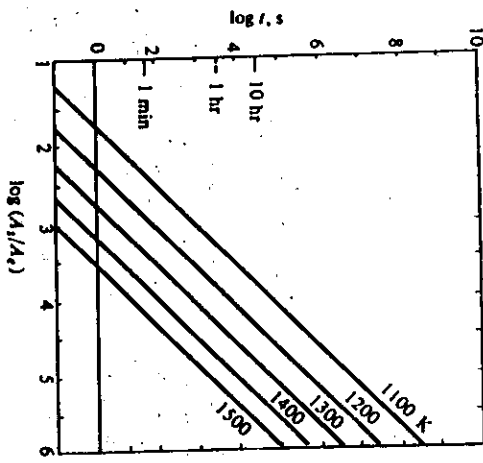


Fig. 15.6 Calculated times for 5% depletion of the surface of 5 wt % Mn-Fe alloys.  
(Adapted from D. L. Schroeder and J. F. Elliott, Trans. AIME 236, 1091 (1967).)

### 15.3.2 Alloy vaporization during melting

In general, vaporization from liquid metals is not very different than that from solid metals. If the melting is carried out under a vacuum, there are again two steps: mass transfer to the free surface, and vaporization from the surface into the vacuum. If there is an inert gas pressure above the surface, there is an additional resistance to mass transfer, and as the gas density increases (or vacuum decreases), this may become significant relative to the resistance of the other transport steps.

Consider the first step. Mass transfer within the liquid to the surface could be calculated from a correlation of the form  $S_h = f(R_e, Sc)$  if this were available for the particular physical arrangement and stirring conditions involved. In the case of induction melting, there is no general correlation available, so we shall make use of an hypothesis by Machlin,<sup>6</sup> which states that flow across the surface of an inductively stirred melt may be considered to be slug flow without any velocity gradients within the surface layer. The volatile solute is supplied to the surface solely by diffusion from within this surface layer. This hypothesis is exactly the same as Higbie's "penetration theory" discussed in Section 14.8. The only new assumption is that the "lifetime"  $\theta$  of a surface element is equal to the average distance from the center of the melt to the edge of the crucible, divided by the average velocity of the melt at the surface. In the induction stirring case,  $\theta$  is of the order of 1 s or less.

<sup>5</sup>H. S. Carslaw and J. C. Jaeger, *Conduction of Heat in Solids*, second edition, Oxford University Press, New York, NY, 1959, page 71.

<sup>6</sup>E. S. Machlin, *Trans. AIME* 218, 314 (1960).

$$k_{M,I} = \frac{2\sqrt{D/\pi\theta}}{\rho}, \text{ mol m}^{-2} \text{ s}^{-1},$$

and the flux to the surface from the bulk liquid is

$$j_A = k_{M,I}(C_{A\infty} - C_A^*), \text{ mol m}^{-2} \text{ s}^{-1}, \quad (14.90)$$

where  $C_{A\infty}$  is the bulk concentration and  $C_A^*$  is the surface concentration.

The second step is the evaporation itself. Returning to Section 15.3.1 and assuming that no chemical reactions are involved,<sup>\*</sup> we have

$$j_A = \frac{\gamma_A P_A^0 C_A^*}{\rho \sqrt{2\pi MRT}}, \quad (15.44)$$

or

$$k_{M,e} = \frac{\gamma_A P_A^0}{\rho \sqrt{2\pi MRT}}, \quad (15.45)$$

where  $k_{M,e}$  is the evaporation mass transfer coefficient.

The final step in the sequence involves mass transfer within the vapor phase, as influenced either by convection (when the gas pressure is  $> 10^{-2}$  atm), or by molecular flow mechanics, as in a vacuum. In the former case, since  $k_{M,e} \propto D$ , and since Eqs. (12.49) and (12.50) indicate that  $D$  increases directly with reciprocal pressure, it is apparent that with a good vacuum,  $k_{M,e}$  becomes very large.

Now consider the overall process in a good vacuum where the gas phase resistance is negligible. The fluxes due to liquid phase mass transfer (Eq. (15.43)), and evaporation (Eqs. (15.44) and (15.45)) are equal:

$$j_A = k_{M,I}(C_{A\infty} - C_A^*) = k_{M,e} C_A^*.$$

Solving for  $C_A^*$ , we get

$$C_A^* = \frac{k_{M,I}}{k_{M,I} + k_{M,e}} C_{A\infty}. \quad (15.46)$$

Substituting, we obtain

$$j_A = \left[ \frac{k_{M,I} k_{M,I}}{k_{M,I} + k_{M,e}} \right] C_{A\infty} = K C_{A\infty}, \quad (15.47)$$

$$K = 8.8 \times 10^{-5} \text{ m s}^{-1}$$

It is apparent that when there is a good vacuum, liquid-phase mass transfer offers 82% of the total resistance; thus we may say that it essentially controls the rate.

This changes, however, if the stirring is increased to decrease  $\theta$ . For example, if  $\theta$  decreases to 0.1 s, then

$$k_{M,I} = 3.39 \times 10^{-4} \text{ m s}^{-1},$$

<sup>\*</sup>We often see an additional multiplier on the right-hand side of Eq. (15.44). This is the condensation coefficient  $\alpha$ , which is a measure of the proportion of atoms leaving a surface that do not return to the surface, but are condensed instead on cool surfaces away from the melt. Typically,  $\alpha$  is taken as unity for high temperature vaporization.

and

$$\frac{1}{k_{M,I}} = 2.95 \times 10^3 \text{ m}^{-1} \text{ s}.$$

Now the liquid-phase mass transfer and the evaporation process are almost equivalent in their contribution to  $K$ , and there is mixed control. Furthermore,  $K$  has increased to  $1.97 \times 10^{-1} \text{ m s}^{-1}$ .

Since neither  $k_{M,I}$  nor  $k_{M,s}$  depend on the external pressure,  $K$  is independent of vacuum pressure as long as  $k_{M,s}$  remains very large. When  $k_{M,s}$  becomes about an order of magnitude smaller than  $k_{M,I}$  or  $k_{M,s}$ , it is rate controlling. Since  $k_{M,s}$  is proportional to  $P^{1/2}$ , then  $K$  decreases with  $P$ , as long as  $\delta_m$  in the gas phase remains constant. When the gas phase is dense, then  $k_{M,s}$  is controlled by natural or forced convection. Figure 15.7 illustrates the effect of system pressure on  $K$  for vaporization of manganese from steel. Figure 15.8 gives the results of the application of Eq. (15.47) to calculate the rate of loss of manganese at 1580°C for various  $(A_f/V)$  and  $K$  values. One apparent result is that the use of an argon atmosphere to increase pressure decreases  $K$  to the point where the loss of manganese is negligible.

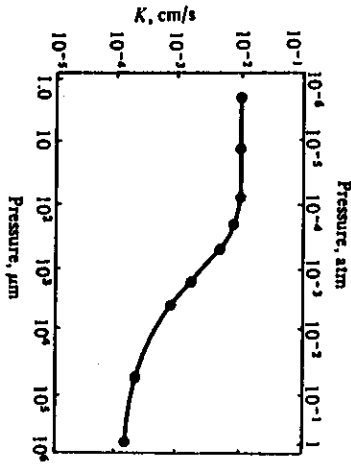


Fig. 15.7 Overall mass transfer coefficients for Mn vaporization from 0.25% C steel at 1580°C as a function of the pressure of Ar over the melt. (From R. G. Ward, JISI 201, 11 (1963).)

Some other experimental values of  $K$  for the loss of various elements from iron-base melts into good vacuums are given in Table 15.2.

Laser welding, using high power beams focused on small areas, has introduced new problems of composition control in the weld zone. Volatile elements can be lost and the integrity of the weld can be compromised. Collur *et al.*<sup>7</sup> analyzed the problem and demonstrated the role of Knudsen vaporization in controlling the rate of compositional changes.

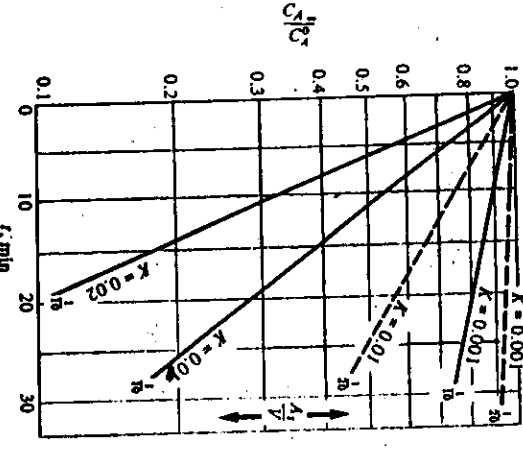


Fig. 15.8 Decrease in concentration of alloying element as a function of mass transfer coefficient and  $A_f/V$  ratio. Units of  $K$  are  $\text{cm s}^{-1}$ , and units of  $A_f/V$  are  $\text{ft}^{-1}$ .

Table 15.2 Overall evaporation constants for iron-base melts at 1600°C

Element	$K, \text{m s}^{-1}$
Mn	$8.4 \times 10^{-5}$
Cu	$4.8 \times 10^{-5}$
Sn	$2.3 \times 10^{-5}$
Cr	$2.1 \times 10^{-6}$
S	$7.0 \times 10^{-6}$

From R. Ohno and T. Ishida, JISI, London 206, 904 (1968).

## PROBLEMS

- 15.1 Argon containing 2 volume percent of hydrogen is bubbled through a melt of aluminum at 970 K. The bubbling is continued to equilibrium with this gas at 1 atm. Initially the melt contains  $5 \times 10^{-6} \text{ m}^3$  (STP) of hydrogen per kg of aluminum. It is known that the solubility of hydrogen is  $10 \times 10^{-6} \text{ m}^3$  (STP)  $\text{kg}^{-1}$ . Determine whether the rate of mass transfer is gas-phase or liquid-phase controlled, a) at the beginning of degassing and b) near the end of degassing.

- 15.2 Iron wire (4 mm dia.) is boronized at 1200°C in a gas that establishes an equilibrium concentration of  $15 \times 10^{-3}$  wt.pct. boron. The transfer of boron is partly controlled by the reaction kinetics between the gas and the iron, as given by Eq. (15.11) with  $r = 5 \times 10^{-3} \text{ m s}^{-1}$  at the surface. a) Make a plot of the concentration of boron (in wt.pct.) at the surface, b) When the concentration at the surface is 90% of the equilibrium value, what is the concentration in the center of the wire?

**15.3 Refer to Example 15.2.** a) Plot the distance  $x$  that satisfies the specification in Example 15.2 as a function of the gas velocity up to  $1 \text{ m s}^{-1}$ . b) Repeat if the separation between the sheets is reduced to 5 mm.

**15.4** Assume that the initial thickness of an oxide layer on silicon is 10 nm. Determine the thickness of the oxide after oxidation in dry oxygen at 1350 K for 7000 s.

**15.5** The standard free energy of formation of  $\text{SiO}_2(\text{s})$  is

$$\Delta G^\circ = -215 \text{ } 600 + 41.5 T, \text{ cal mol}^{-1},$$

for  $700 \leq T \leq 1700 \text{ K}$ . Suppose the pure oxygen in Problem 15.4 is replaced with 90% Ar-10%  $\text{O}_2$ . Would this appreciably change the oxidation kinetics?

**15.6** The vapor pressure of  $\text{Zn}(\text{s})$  is

$$\log_{10} P(\text{mm Hg}) = -\frac{6850}{T} - 0.755 \log_{10} T + 11.24.$$

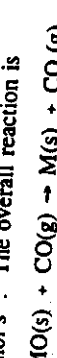
(Note: 760 mm Hg = 1 standard atm =  $1.0133 \times 10^5 \text{ N m}^{-2}$ .) Thermodynamic data at 1200 K give

$$\ln \gamma_{\text{Zn}} = \frac{6850}{(1 - X_{\text{Zn}})} = 3.875 X_{\text{Zn}} - 3.425.$$

For other temperatures, assume that the regular solution model applies so that  $T \ln \gamma_{\text{Zn}}$  = constant. a) Calculate the initial flux of Zn from 70-40 brass by sublimation into a vacuum with sublimation into the vacuum at 1200 K.

**15.7** Ferritic stainless steel parts are vacuum heat-treated in order to maintain a shiny surface finish. If AISI 410 (12% Cr) parts are heat treated in a vacuum of  $10 \mu\text{m}$  of Hg at 1140 K for 2 hours, what will the concentration of chromium on the surface of the parts be? At 1140 K, the vapor pressure of pure Cr is  $1.33 \times 10^{-5} \text{ Pa}$ , and  $D_{\text{Cr}}$  in iron is approximately  $10^{-16} \text{ m}^2 \text{ s}^{-1}$ .

**15.8** A model for the reduction of a spherical oxide is illustrated to the right. Assume mixed control, with mass transfer in the gas and diffusion through the porous product layer controlling the overall kinetics. A reducing gas flows past the sphere with a concentration  $C_\infty$ , and at the product-oxide interface its concentration is  $C^*$ . Derive an equation that gives the rate at which the oxide is reduced in  $\text{kmol s}^{-1}$ . The overall reaction is



where MO is the metal oxide.

**15.9** Using data in Table 15.2, plot the change in concentration with time (up to 3600 s) of a melt of iron containing 1% Mn, 1% Cr, and 0.05% S. The melt is contained in a nonreacting crucible, which has the dimensions 0.5 m dia. by 1 m height.

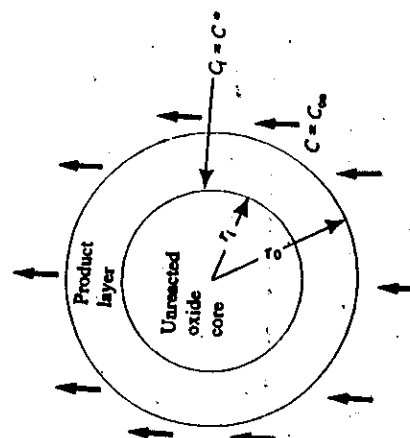
**15.10** The melt of Problem 15.9 also contains carbon, which reacts with the magnesia crucible according to the overall reaction:



Assume that evaporation can only occur at the surface of the well-mixed melt.

- a) Hypothesize the reduction reaction at the melt-crucible interface.
- b) Hypothesize vaporization reactions at the melt surface.
- c) What are the mass transfer steps for oxygen for magnesium? for carbon? For each mass transfer step, make a schematic concentration profile.

**15.11** In vacuum laser welding, it is difficult to measure the temperature of the molten pool. One estimate of the temperature can be made from collecting a sample of vapor evaporated from the weld pool. The ratio of elements in the sample is the ratio of vaporization rates of the elements. If 201 stainless steel is welded and the ratio of Cr/Mn in the condensed vapor sample is 0.56, estimate the pool temperature, assuming that the pool is an ideal thermodynamic solution.



# 16

## NUMERICAL METHODS AND MODELS

Our major goal in this introductory text is to present fundamentals. We hope that has been accomplished in Chapters 1-15. We also tried to orient our pedagogy to materials science and engineering by including many examples and problems in order to instill the necessity of applying transport phenomena in designing and operating processes, intelligently and economically.

Very often, however, materials processing is so complex that transport phenomena can only be applied if materials engineers resort to numerical methods and models. In this chapter, an introduction is given to a numerical method and some models.

### 16.1 FINITE DIFFERENCE APPROXIMATIONS

Finite difference approximations are indispensable in solving problems involving multidimensional transport, nonhomogeneous or nonlinear boundary conditions, or variable properties. Although the majority of practical problems entail such complexities, it is still important to be familiar with at least the analytical solutions found in this text. In setting up the more complex problems using finite difference approximations, the analytical solutions often provide a convenient check on the computations. We start by considering two problems with simple geometry and constant transport properties.

#### 16.1.1 Euler method

The first problem, often encountered in metal casting, is that of a thermally insulating material that forms the internal mold (called a core) that is surrounded on both sides by a solidifying metal. The situation is depicted in Fig. 16.1.

The semithickness of the core is  $L$ , and it is thin enough that after a relatively short time into the solidification period, the region  $0 \leq x \leq 2L$  can become saturated with heat and lose its ability to further extract energy from the solidifying metal. This could lead to a "hot spot" in the solidifying metal near the core resulting in a porous casting. The problem to be solved, therefore, is the computation of the time-temperature history of the core to determine its adequacy to absorb heat.

At any particular time, the gradient between nodes  $m$  and  $m+1$  is

$$\left[ \frac{\partial T}{\partial x} \right]_{m+1/2} = \frac{T_{m+1} - T_m}{\Delta x}.$$

Similarly,

$$\left[ \frac{\partial T}{\partial x} \right]_{m-1/2} \approx \frac{T_m - T_{m-1}}{\Delta x}.$$

For the conduction equation, the second derivative is required; this is

$$\frac{\partial}{\partial x} \left[ \frac{\partial T}{\partial x} \right]_m = \frac{1}{\Delta x} \left[ \left[ \frac{\partial T}{\partial x} \right]_{m+1/2} - \left[ \frac{\partial T}{\partial x} \right]_{m-1/2} \right].$$

Therefore,

$$\left[ \frac{\partial^2 T}{\partial x^2} \right]_m = \frac{1}{(\Delta x)^2} [T_{m+1} - 2T_m + T_{m-1}], \quad (16.5)$$

and Eq. (16.1) for an interior node becomes

$$\frac{\partial T_m}{\partial t} = \frac{\alpha}{(\Delta x)^2} [T_{m+1} - 2T_m + T_{m-1}]. \quad (16.6)$$

At the centerline ( $m = N$ ), the finite difference equation is derived in a different manner.

The flux to the centerline is

$$-\frac{k}{\Delta x} [T_N - T_{N-1}],$$

and the accumulation of energy is

$$\frac{\partial T_N}{\partial t} = \frac{\alpha}{(\Delta x)^2} [T_{N-1} - 2T_N + T_{N+1}]. \quad (16.7)$$

where  $\Delta x/2$  is the volume associated with node  $N$ . Then at this *insulated surface*, the finite difference equation is written as

$$\frac{\partial T_N}{\partial t} = \frac{2\alpha}{(\Delta x)^2} [T_{N-1} - T_N]. \quad (16.8)$$

For convenience, *normalized variables* are introduced. The normalized temperature ( $u$ ), time ( $t$ ) and position ( $x'$ ) are defined as follows:

$$u = \frac{T - T_i}{T_N - T_i}, \quad \theta = \frac{\alpha t}{L^2}, \quad \text{and} \quad x' = \frac{x}{L}.$$

With the normalized coordinates, Eqs. (16.1)-(16.4) are replaced by

$$\frac{\partial u}{\partial \theta} = \frac{\partial^2 u}{\partial x'^2}, \quad \frac{\partial u}{\partial x'} (1, \theta) = 0. \quad (16.9)$$

<sup>a</sup>In Chapter 9,  $x = 0$  was at the centerline. The two different coordinate systems can be reconciled with a simple coordinate transformation.

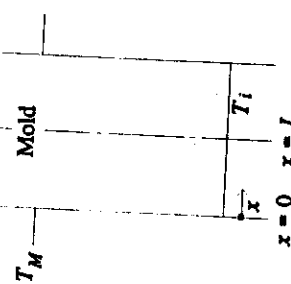


Fig. 16.1 Mold material surrounded by solidifying metal.

Formally presented, the situation is described by

$$\frac{\partial T}{\partial t} = \alpha \frac{\partial^2 T}{\partial x^2}; \quad (16.1)$$

the boundary conditions are

$$\frac{\partial T}{\partial x} (L, t) = 0 \quad t \geq 0, \quad (16.2)$$

$$T(0, t) = T_M \quad t \geq 0, \quad (16.3)$$

and the initial condition is

$$T(x, 0) = T_i. \quad (16.4)$$

To determine the temperature as a function of location and time, the domain  $0 \leq x \leq L$  is subdivided into small segments of length  $\Delta x$ , as shown in Fig. 16.2. Nodes are numbered consecutively 0 to  $N$  from left to right.

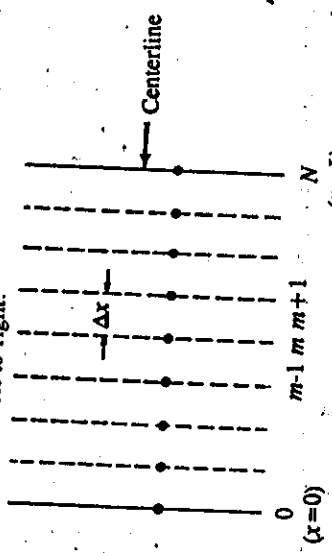


Fig. 16.2 The domain  $0 \leq x \leq L$  subdivided into segments.

$$u(0, \theta) = 1, \quad (16.10)$$

and

$$u(x', 0) = 0. \quad (16.11)$$

For the interior nodes the finite difference equation, Eq. (16.6), becomes

$$\frac{\partial u_m}{\partial \theta} \approx \frac{1}{(\Delta x')^2} [u_{m-1} - 2u_m + u_{m+1}], \quad (16.12)$$

and at the insulated surface ( $m = N$ ) Eq. (16.7) becomes

$$\frac{\partial u_N}{\partial \theta} \approx \frac{2}{(\Delta x')^2} [u_{N-1} - u_N]. \quad (16.13)$$

In an actual application the number of nodes should be large, but in order to illustrate the calculation process we take  $N = 4$ . Equation (16.10) requires  $u_0 = 1$ ; then the difference equations for nodes  $1, \dots, N$  are as follows:

$$\frac{\partial u_1}{\partial \theta} = \frac{1}{(\Delta x')^2} [u_0 - 2u_1 + u_2] = \frac{1}{(\Delta x')^2} [1 - 2u_1 + u_2], \quad (16.14a)$$

$$\frac{\partial u_2}{\partial \theta} = \frac{1}{(\Delta x')^2} [u_1 - 2u_2 + u_3], \quad (16.14b)$$

$$\frac{\partial u_3}{\partial \theta} = \frac{1}{(\Delta x')^2} [u_2 - 2u_3 + u_4], \quad (16.14c)$$

$$\frac{\partial u_4}{\partial \theta} = \frac{1}{(\Delta x')^2} [2u_3 - 2u_4]. \quad (16.14d)$$

The initial temperatures are  $u_1 = u_2 = u_3 = u_4 = 0$ .

There are several methods for proceeding; here the so-called Euler method is used, in which

$$u_m^{i+1} = u_m^i + \frac{\partial u_m^i}{\partial \theta} \Delta \theta. \quad (16.15)$$

It is necessary to add superscripts to indicate time; e.g.,  $u_m^i$  is the present temperature and  $u_m^{i+1}$  is the future temperature after one time step of duration  $\Delta \theta$ .

By combining Eqs. (16.14) through (16.15) for  $m = 1, \dots, N$  with the appropriate superscripts, we get

$$u_1^{i+1} = P + (1 - 2P) u_1^i + P u_2^i \quad (16.16a)$$

$$u_2^{i+1} = P u_1^i + (1 - 2P) u_2^i + P u_3^i \quad (16.16b)$$

$$u_3^{i+1} = P u_2^i + (1 - 2P) u_3^i + P u_4^i \quad (16.16c)$$

$$u_4^{i+1} = 2P u_3^i + (1 - 2P) u_4^i \quad (16.16d)$$

where  $P = \Delta \theta / (\Delta x')^2$ . Initially each  $u_m^i$  is known (starting with  $u_m^0 = 0$ ), so that Eqs. (16.16a,b,c,d) comprise four equations with the four unknowns,  $u_m^{i+1}$ . After the simultaneous equations are solved, the temperatures at  $m = 1, \dots, 4$  are known for time step  $i+1$  ( $\theta = \Delta \theta$ ) and then the process is repeated for as many time steps ( $\theta = v \Delta \theta$ ) as desired.

Table 16.1 gives calculated temperatures at the insulated surface for  $N = 5$  ( $\Delta x' = 0.2$ ) and  $N = 10$  ( $\Delta x' = 0.1$ ) with  $P = 0.25$ . Also shown are the temperatures based on the exact solution (Eq. (9.42)). With more nodes the results are closer to the exact solution. With even more nodes, the agreement between the approximated temperatures and the exact temperatures would be even closer. However, with smaller values of  $\Delta x'$ , we must be careful because the Euler method can result in unstable numerical oscillations in the solution if either  $\Delta \theta$  is too large or  $\Delta x'$  is too small. Specifically, the Euler method requires that  $P = \Delta \theta / (\Delta x')^2 \leq 0.5$ , in order to prevent unstable numerical oscillations. Thus, if we choose to reduce  $\Delta x'$ ,  $\Delta \theta$  has to be correspondingly reduced in order to meet the criterion of  $P \leq 0.5$ . Accordingly, more computer time would be required to execute the calculations.

Table 16.1 Normalized temperature,  $u$ , at the center (insulated surface) with  $P = 0.25$  (Euler method)

$\theta$	With $\Delta x' = 0.2$	With $\Delta x' = 0.1$	Exact Solution, Eq. (9.42)
0.2	0.225	0.229	0.235
0.4	0.525	0.527	0.531
0.6	0.710	0.711	0.714
0.8	0.822	0.824	0.826
1.0	0.892	0.893	0.894

The numerical results can also be used to estimate the amount of energy taken up by the core as a function of time. There are two methods for carrying out this estimate.

The first method is to track the gradient at the core surface in contact with the metal. This surface is at  $x = 0$  in Fig. 16.2. For each time step the energy absorbed by the core can be approximated as the product of the flux and the duration of the time step. By summing these products for all of the time steps, the integrated or total energy absorbed by the core can be estimated. The accuracy of this method depends on the accuracy of the estimate of the gradient at  $x = 0$ .

The second method is based upon calculations of the average temperature in the core. For this particular problem, this method is more accurate than the first because the estimates of temperature are more exact than the estimates of the gradient at  $x = 0$ . We can show this by attacking the problem both ways.

In the first method the estimated gradient, in terms of normalized variables, is  $(u_1^i - u_0^i)/\Delta x'$ . In terms of the original dimensional variables, this is

$$\left[ \frac{\Delta u}{\Delta x'} \right]^i = \frac{L}{T_M - T_i} \frac{T_1^i - T_0^i}{\Delta x'}$$

Therefore, the flux at the metal/core interface is approximated as

$$q_0^i = -k \frac{T_1^i - T_0^i}{\Delta x'} = -k \left[ \frac{T_M - T_i}{L} \right] \left[ \frac{\Delta u}{\Delta x'} \right]^i$$

and the energy absorbed by the area A of the core for one time step is  $q'_c \Delta t$ . Therefore,

$$\hat{Q}_m = \left| A \sum_i q'_c \Delta t \right| = Ak \left[ \frac{T_m - T_i}{L} \right] \frac{L^2}{\alpha} \sum_i \left| \left[ \frac{\Delta u}{\Delta x'} \right]'_0 \right| \Delta \theta \quad (16.17)$$

As before, the energy given up by the solidified portion of the casting (assumed to be pure metal) is

$$\hat{Q}_c = V \rho' H_f \quad (16.18)$$

where  $V$  is the volume solidified next to the casting-core surface. With  $\hat{Q}_c = \hat{Q}_m$ , Eqs. (16.17) and (16.18) finally give

$$\frac{(V/A)}{L\gamma} = \sum_i \left| \left[ \frac{\Delta u}{\Delta x'} \right]'_0 \right| \Delta \theta, \quad (16.19)$$

where  $\gamma$ , as defined in Chapter 10, is

$$\gamma = \left[ \frac{T_m - T_i}{\rho' H_f} \right] \rho C_p \quad (16.20)$$

In the second method, the average normalized temperature at a given time is calculated. The volume of material associated with the nodes  $m = 0$  and  $m = N$  is  $0.5 \Delta x'$ , so the average normalized temperature is

$$\bar{u}' = \frac{1}{N} \left[ \frac{1}{2} (u'_0 + u'_N) + \sum_{m=1}^{N-1} u'_m \right]. \quad (16.21)$$

The average dimensional temperature is

$$\bar{T}' = \bar{u}' (T_m - T_i) + T_i, \quad (16.22)$$

so that the energy absorbed by one-half of the core must be

$$\hat{Q}_m = AL\rho C_p (\bar{T}' - T_i) = AL\rho C_p (T_m - T_i) \bar{u}'. \quad (16.23)$$

With  $\hat{Q}_m = \hat{Q}_c$ , we combine Eqs. (16.18) and (16.21); the result is

$$\frac{(V/A)}{L\gamma} = \bar{u}'. \quad (16.24)$$

Of course, Eq. (16.22) is another approximate counterpart to the exact solution of Eqs. (16.8)-(16.11).

Table 16.2 Amount of solidification as  $V/AL\gamma$  versus  $\theta$  with  $P = 0.25$  and  $N = 10$

$\theta$	Finite Difference Approximations		
	Therm. Grad., Eq. (16.19)	Avg. Temp., Eq. (16.22)	Exact Solution
0.04	0.163	0.231	0.229
0.2	0.434	0.506	0.505
0.4	0.626	0.699	0.698
0.6	0.742	0.817	0.817
0.8	0.814	0.886	0.886
1.0	0.857	0.932	0.930

Approximations of  $V/AL\gamma$  based on Eqs. (16.19) and (16.22), with  $P = 0.25$  and  $N = 10$ , are given in Table 16.2. Also shown are exact values of  $V/AL\gamma$ . The table shows that the estimates based on calculating the average temperature are more accurate than are those based on estimating the gradient at the core-casting interface.

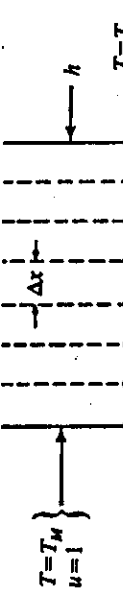


Fig. 16.3 - Shell mold of thickness  $L$  subdivided into segments for estimating temperature during heat conduction.

Also, the normalized temperature is selected so that  $u = 1$  and  $u = 0$  correspond to  $T = T_m$  and  $T = T_\infty$ , respectively; thus

$$u = \frac{T - T_\infty}{T_m - T_\infty}. \quad (16.23b)$$

By selecting  $\theta = \alpha t/L^2$  and  $x' = x/L$ , then the heat conduction equation is Eq. (16.8). The boundary conditions and initial condition are as follows:

$$u(0, \theta) = 1, \quad (16.23a)$$

$$\frac{\partial u}{\partial x'} (1, \theta) + Bi u(1, \theta) = 0, \quad (16.23b)$$

$$u(x', 0) = \frac{T_i - T_\infty}{T_m - T_\infty} = u_i, \quad (16.23c)$$

where  $T_i$  is the initial temperature of the shell mold. Since the mold is often preheated, the effect of the preheat temperature on the solidification time is of particular interest.

The temperatures at nodes 1 through  $N-1$  are approximated by Eq. (16.12). By writing an energy balance for node  $N$  (with a volume of  $\Delta x'/2$ ), we get

$$\frac{\partial u_N}{\partial \theta} = \frac{1}{(\Delta x')^2} [-2(1 + Bi \Delta x) u_N + 2 u_{N-1}], \quad (16.24)$$

with  $Bi = hL/k$ .

In order to advance the solution in time, we again utilize the Euler method and combine Eq. (16.15) with Eqs. (16.12) and (16.24). For nodes 1 through  $N-1$ , we get

$$u_m^{v+1} = P u_{m-1}^v + (1 - 2P) u_m^v + P u_{m+1}^v, \quad (16.25)$$

and for node  $N$

$$u_N^{v+1} = .2P u_{N-1}^v + [1 - 2P(1 + Bi \Delta x')] u_N^v. \quad (16.26)$$

As before  $P = \Delta \theta / (\Delta x')^2$ , and the superscripts  $v$  and  $v+1$  represent the present and next time, respectively.

By selecting  $P = 0.25$  and  $\Delta x' = 0.1$ , then  $\Delta \theta = 0.0025$ ; with  $u_0 = 1$  the set of equations becomes:

$$u_1^{v+1} = 0.25 + 0.5 u_1^v + 0.25 u_2^v, \quad m = 1$$

$$u_m^{v+1} = 0.25 u_{m-1}^v + 0.5 u_m^v + 0.25 u_{m+1}^v, \quad m = 2, 3, \dots, 9$$

$$u_{10}^{v+1} = 0.5 u_9^v + (0.5 - 0.125 Bi) u_{10}, \quad m = N = 10. \quad (16.27)$$

Some calculated temperature distributions are shown in Fig. 16.4 for two mold preheat temperatures and two Bi numbers. Notice that steady state is achieved in a relatively short period of  $\theta = 1$ , which corresponds to a real time of only a few or several minutes. Notice, too, that the temperature of the exterior surface of the mold can decrease and then increase to its steady state value in some circumstances (e.g., Fig. 16.4a).

The thermal gradients at  $x' = 0$ , derived from the temperature distributions, can be used to calculate the total energy extracted from the casting. Hence to estimate the thickness solidified from the mold wall, Eq. (16.19) applies. These estimates are shown in Fig. 16.5.

The previous examples were selected with the intention of introducing the numerical method; hence, the examples were kept simple. The thermal properties of the mold and the heat transfer coefficient at the exterior surface of the mold were constants. In practice, however, these properties depend on temperature.

It should be noted that variable properties can be included in the finite difference approximation (FDA) method by updating the properties with the current temperatures as the calculation proceeds from one time step to the next. The FDA method can also be extended to two-dimensional and three-dimensional heat conduction problems so that complex casting geometries can be analyzed.

Alloys solidify over a temperature range; in such cases, nodes are assigned in the solidifying casting as well as in the mold. Sophisticated computer codes can be used to show positions of isotherms in both the mold and casting, to assist the casting engineer in locating "hot spots," designing and locating risers, estimating solidification times, and in predicting microstructural features and physical properties that depend upon the temperature history during solidification.

Fig. 16.4 Calculated temperature profiles in a shell mold of finite thickness with heat loss from the surface. (a) Preheat temperature  $u_m^0 = 0.536$  and  $Bi = 0.5$ ; (b)  $u_m^0 = 0.536$  and  $Bi = 2$ ; (c)  $u_m^0 = 0.778$  and  $Bi = 0.5$ ; (d)  $u_m^0 = 0.778$  and  $Bi = 2$ .

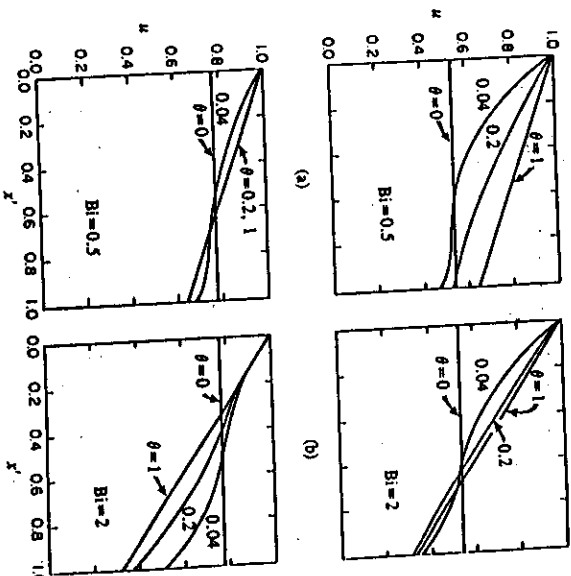
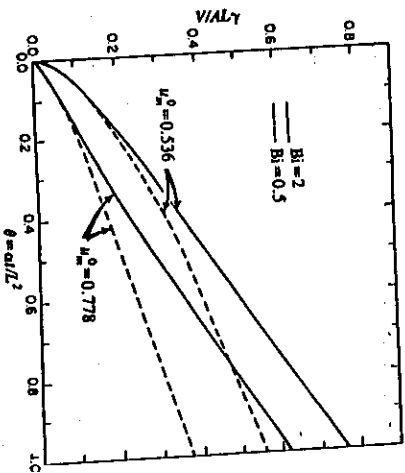


Fig. 16.5 Estimate of thickness solidified ( $V/A$ ) versus time in shell mold of finite thickness with heat loss from the exterior surface.



### 16.1.2 The Crank-Nicolson method

In the Euler method, the time derivative at the beginning of the time step is used to estimate the temperature at the next time. The Euler method is said to be *explicit* for this reason. A method with better accuracy is the Crank-Nicolson method, which is *implicit*.

In the Crank-Nicolson method an average of the time derivative is used. That is, instead of using Eq. (16.15), we use

$$u_m^{v+1} = u_m^v + \frac{1}{2} \left[ \frac{\partial u}{\partial \theta} \Big|_m + \frac{\partial u}{\partial \theta} \Big|_{m+1} \right] \Delta \theta. \quad (16.28)$$

But, Eq. (16.12) tells us that

$$\frac{\partial u}{\partial \theta} \Big|_m = -\frac{1}{(\Delta x')^2} [u_{m-1}^v - 2u_m^v + u_{m+1}^v],$$

and

$$\frac{\partial u}{\partial \theta} \Big|_{m+1} = -\frac{1}{(\Delta x')^2} [u_{m-1}^{v+1} - 2u_m^{v+1} + u_{m+1}^{v+1}],$$

so that ultimately we can write Eq. (16.28) as follows:

$$u_m^{v+1} = u_m^v + \frac{P}{2} \left[ (u_{m-1}^v - 2u_m^v + u_{m+1}^v) + (u_{m-1}^{v+1} - 2u_m^{v+1} + u_{m+1}^{v+1}) \right], \quad (16.29)$$

where  $P = \Delta \theta / (\Delta x')^2$  as before. Notice that the unknown values of  $u^{v+1}$  now appear on both sides of the equation, so this method is *implicit*. We find it necessary to deal with simultaneous equations in order to get a solution.

To see how this is applied, let's return to the problem pertaining to Figs. 16.1 and 16.2. The temperature at  $m = 0$  is fixed by the boundary condition of Eq. (16.10). At  $m = N$ , we use Eq. (16.13) again. Therefore,

$$u_N^{v+1} = u_N^v + P \left[ (u_{N-1}^v - u_N^v) + (u_{N-1}^{v+1} - u_N^{v+1}) \right]$$

or

$$-Pu_{N-1}^{v+1} + (1 + P)u_N^{v+1} = Pu_{N-1}^v + (1 - P)u_N^v. \quad (16.30)$$

We set up the system as matrices for  $N = 4$ ; remember  $u_0^v = u_0^{v+1} = 1$ .

$$\begin{bmatrix} (1 + P) & -P/2 & & \\ -P/2 & (1 + P) & -P/2 & \\ & -P/2 & (1 + P) & -P/2 \\ & & -P & (1 + P) \end{bmatrix} \begin{bmatrix} u_1^{v+1} \\ u_2^{v+1} \\ u_3^{v+1} \\ u_4^{v+1} \end{bmatrix} = \begin{bmatrix} u_1^v \\ u_2^v \\ u_3^v \\ u_4^v \end{bmatrix}$$

The right hand side can be computed directly because all of the components are known. Of course, we simply get a column matrix of constants. To the first element in the column matrix of constants, we must remember to add  $P$  because  $u_0^v = u_0^{v+1} = 1$  in this example.

The left side contains the unknowns, which must be solved as a system of algebraic equations. The process is repeated for each time step.

The computational effort appears to be greater with the Crank-Nicolson method than it appears with the Euler method. Keep in mind, however, that the accuracy of the estimate for the time derivative is improved so that larger time steps can be taken. Furthermore, unstable numerical oscillations are avoided so we are not restricted to  $P \leq 0.5$ .

With the explicit method, we used  $P = 0.25$  for the problem at hand (Table 16.1), so that for the case of  $\Delta x' = 0.2$ , the time steps were of duration  $\Delta \theta = P(\Delta x')^2 = 0.01$ . In order to achieve the normalized temperature at  $\theta = 1$ , 100 time steps were required. Now to demonstrate the advantage of the Crank-Nicolson method, let's double  $P$  ( $P = 0.5$ ) with  $\Delta x'$  kept at 0.2. Then  $\Delta \theta = 0.02$ , and 50 time steps are required to arrive at  $\theta = 1$ . These results are given in Table 16.3, which compare favorably with Table 16.1. Although we have used larger time steps, the accuracy of the results is better than found in Table 16.1 for  $\theta = 0.2$  and comparable for larger values of  $\theta$ .

Table 16.3 Normalized temperature,  $u$ , at the center (insulated surface) with  $P = 0.5$  and  $\Delta x' = 0.2$  (Crank-Nicolson method)

$\theta$	Numerical Solution	Exact Solution
0.2	0.232	0.235
0.4	0.526	0.531
0.6	0.709	0.714
0.8	0.822	0.826
1.0	0.891	0.894

The code used for the results is given below. It is written in BASIC so that a matrix inversion (statement 180) could be used. For very large matrices as encountered in practice, this cannot be done. With tridiagonal matrices, a very efficient algorithm can be devised (e.g., see Carnahan *et al.*<sup>1</sup> or Guthrie<sup>2</sup>). Commonly employed algorithms to solve matrices are based upon the Gauss-Siedel method.<sup>3</sup>

```

11 REM *** VAX BASIC PROGRAM
12 REM *** FOR
13 REM *** SOLVING EQUATION(16.31)
14 REM *** (P = 0.5, delta x' = 0.2) ***
15 DIM A(5,5),B(5,1),C(5,5),D(5,1)
16 DIM E(5,1),F(5,5)
17 REM *** read the matrices
18 MAT READ A(5,5)
19 MAT READ C(5,5)
20 MAT READ D(5,1)
21 MAT READ E(5,1)
22 MAT READ F(5,5)
23 REM *** read the matrices
24 MAT B = ZER(5,1)
25
```

<sup>1</sup>B. Carnahan, H. A. Luther and J. O. Wilkes, *Applied Numerical Methods*, John Wiley & Sons, New York, 1969, pages 441-442.

<sup>2</sup>R. I. L. Guthrie, *Engineering in Process Metallurgy*, Clarendon Press, Oxford, UK, 1989, page 382.

<sup>3</sup>R. E. Serafin, *Basic Numerical Methods*, Edward Arnold, London, UK, 1984, pages 50-51.

```

90      SUBT = 0
100     FOR I = 1 TO 50
110       REM --- compute the time step
120       T = I + 0.02
130       SUBT = SUBT + 1
140       REM --- compute the right hand side
150       MAT E = C * D
160       E(1,1) = E(1,1) + 0.5
170       REM --- compute the inverse matrix of A
180       MAT F = INV(A)
190       REM --- compute the temperature
200       REM --- for next time step
210       MAT B = F * E
220       REM --- print out the results
230       IF SUBT = 10 THEN PRINT "Time = "; T &
240           \ MAT PRINT B \ SUBT = 0
250       NEXT I
410       REM MATRIX --- A (for P = 0.5)
420       DATA 1.5, -0.25, 0, 0
430       DATA -0.25, 1.5, -0.25, 0
440       DATA 0, -0.25, 1.5, -0.25
450       DATA 0, 0, -0.25, 1.5
460       DATA 0, 0, 0, -0.5, 1.5
470       REM MATRIX --- C (for P = 0.5)
480       DATA 0.5, 0.25, 0, 0, 0
490       DATA 0.25, 0.5, 0.25, 0, 0
500       DATA 0, 0.25, 0.5, 0.25, 0
510       DATA 0, 0, 0.25, 0.5, 0.25
520       DATA 0, 0, 0, 0.5, 0.5
530       DATA MATRIX --- D (temperature)
540       DATA 0
550       DATA 0
560       DATA 0
570       DATA 0
580       DATA 0
999       END

```

### 16.1.3 Two-dimensional formulation

For the sake of some variety, let us consider the mass diffusion of solute in a single-phase material. Suppose we want to study the homogenization kinetics in an as-cast alloy with microsegregation. The microstructure is shown in Fig. 16.6 as a transverse section through a columnar dendritic alloy with a primary dendrite arm spacing of 180  $\mu\text{m}$ . The microstructure is periodic so we can study the domain of the smaller square with sides of 90  $\mu\text{m}$ . This problem is an extension of the one-dimensional case of homogenization in Section 13.5. Formally presented we have

$$\frac{\partial C}{\partial t} = D \left[ \frac{\partial^2 C}{\partial x^2} + \frac{\partial^2 C}{\partial y^2} \right] \quad (16.32)$$

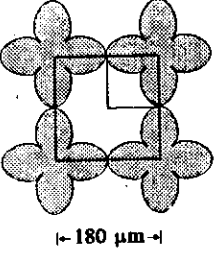


Fig. 16.6 Transverse section through columnar dendritic structure.

Let  $L$  and  $\ell$  be the dimensions of the smaller domain in Fig. 16.6; then the boundary conditions are

$$\frac{\partial C}{\partial x}(L, y, t) = 0 \quad t \geq 0, \quad (16.33)$$

$$\frac{\partial C}{\partial x}(0, y, t) = 0 \quad t \geq 0, \quad (16.34)$$

$$\frac{\partial C}{\partial y}(x, \ell, t) = 0 \quad t \geq 0, \quad (16.35)$$

and

$$\frac{\partial C}{\partial y}(x, 0, t) = 0 \quad t \geq 0, \quad (16.36)$$

and the initial condition is

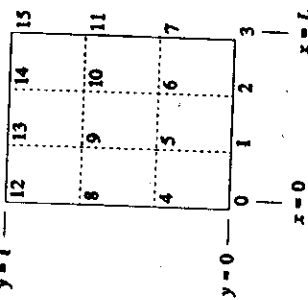
$$C(x, y, 0) = f(x, y). \quad (16.37)$$

Equations (16.32) through (16.37) represent a mathematical formulation of the problem. Before we proceed, let's think about the situation in a less formal manner. We have an inhomogeneous single-phase solid with the initial concentration of the solute arbitrarily disposed in the rectangular region  $L \times \ell$ . If the solid is heated, then diffusion takes place so we must also satisfy some boundary conditions. In this case we require no mass flux of the solute across the system boundaries. Hence, we write the four boundary conditions as Eqs. (16.33) through (16.36).

Following the reasoning that led us to Eq. (16.5), we divide the domain into nine rectangles shown in Fig. 16.7. We select a relatively small number of nodes for the sake of illustrating the method. With two-dimensional transport, double indexing of the nodes is often done, but here we simply number the nodes consecutively in order to simplify the notation. It is also somewhat easier to see the development of the resulting matrices when each node has a single index.

First we write approximations for the second derivatives at an internal node. In this example, we only have four internal nodes (5, 6, 9 and 10), but typically the internal nodes form the largest proportion of the total. At internal node  $n$ , we have

$$\left[ \frac{\partial^2 C}{\partial x^2} \right]_n = \frac{1}{(\Delta x)^2} (C_{n+1} - 2C_n + C_{n-1}). \quad (16.38)$$

Fig. 16.7 The domain  $L \times t$  subdivided into areas of  $(\Delta x) \times (\Delta y)$ .

and

$$\left[ \frac{\partial^2 C}{\partial y^2} \right]_n = \frac{1}{(\Delta y)^2} (C_{n-1} - 2C_n + C_{n+1}). \quad (16.39)$$

To be more general, the subscripts  $(n-4)$  and  $(n+4)$  could be replaced by  $(n-I)$  and  $(n+I)$ , respectively, where  $I$  is the number of vertical columns. With these approximations, Eq. (16.32) becomes

$$\left[ \frac{\partial C}{\partial t} \right]_n = \frac{D}{(\Delta x)^2} (C_{n-1} - 2C_n + C_{n+1}) + \frac{D}{(\Delta y)^2} [C_{n-4} - 2C_n + C_{n+4}]. \quad (16.40)$$

As before we must now decide how to treat the time derivative. Usually, the Crank-Nicolson method is used because, after the added work in setting up the problem is invested, the resulting algorithms are generally more useful than if we had used the simpler Euler method. Proceeding with the Crank-Nicolson method, the time derivative is

$$\left[ \frac{\partial C}{\partial t} \right]_n = \frac{1}{2} \left[ \frac{\partial C}{\partial t} \right]_{n-1} + \frac{1}{2} \left[ \frac{\partial C}{\partial t} \right]_n. \quad (16.41)$$

where now we have added the superscript  $v$  for the present time and  $v+1$  for the next time. You can see that we are proceeding with the method of Section 16.1.2, except now the bookkeeping is a little more tedious. The concentration at time  $v+1$  is

$$C_n^{v+1} = C_n^v + \left[ \frac{\partial C}{\partial t} \right]_n \Delta t, \quad (16.42)$$

and after Eqs. (16.40)-(16.42) are combined, we get

$$C_n^{v+1} = C_n^v + \frac{\Delta \theta_x}{2} [C_{n-1}^{v+1} - 2C_n^{v+1} + C_{n+1}^{v+1}] + \frac{\Delta \theta_y}{2} [C_{n-4}^{v+1} - 2C_n^{v+1} + C_{n+4}^{v+1}] \\ + \frac{\Delta \theta_z}{2} [C_{n-1}^v - 2C_n^v + C_{n+1}^v] + \frac{\Delta \theta}{2} [C_{n-4}^v - 2C_n^v + C_{n+4}^v], \quad (16.43)$$

where  $\Delta \theta_x = D \Delta t / (\Delta x)^2$  and  $\Delta \theta_y = D \Delta t / (\Delta y)^2$ .

Ultimately we must deal with simultaneous equations and solve for the unknowns  $C_n^{v+1}$ . With this in mind, Eq. (16.43) is rearranged into the following form for setting up the matrices:

$$-\frac{\Delta \theta_x}{2} C_{n-4}^{v+1} - \frac{\Delta \theta_x}{2} C_{n-1}^{v+1} + (1 + \Delta \theta_x + \Delta \theta_y) C_n^{v+1} - \frac{\Delta \theta_y}{2} C_{n+1}^{v+1} - \frac{\Delta \theta_z}{2} C_{n+4}^{v+1} = \frac{\Delta \theta_x}{2} C_n^v \\ + \frac{\Delta \theta_x}{2} C_{n-1}^v + (1 - \Delta \theta_x - \Delta \theta_y) C_n^v + \frac{\Delta \theta_y}{2} C_{n+1}^v + \frac{\Delta \theta_z}{2} C_{n+4}^v, \quad (16.44)$$

where  $n = 5, 6, 9, 10$ .

Nodes along the boundaries are considered next; e.g., a solute balance at either node 1 or 2 gives

$$\frac{\Delta y}{2} \left[ -D \frac{C_{n-1} - C_{n+1}}{\Delta x} \right] = \frac{\Delta y}{2} \left[ -D \frac{C_{n-1} - C_n}{\Delta x} \right] + \Delta x \left[ -D \frac{C_{n+4} - C_n}{\Delta y} \right] \\ + \frac{1}{2} \Delta x \Delta y \left[ \frac{\partial C}{\partial t} \right]_n. \quad (16.45)$$

where the area associated with the node is  $\Delta x$  by  $\Delta y/2$ . Again, we take the Crank-Nicolson average for the time derivative. The result is

$$-\frac{\Delta \theta_x}{2} C_{n-1}^{v+1} + (1 + \Delta \theta_x + \Delta \theta_y) C_n^{v+1} - \frac{\Delta \theta_y}{2} C_{n+1}^{v+1} - \Delta \theta_z C_{n+4}^{v+1} = \frac{\Delta \theta_x}{2} C_n^v \\ + (1 - \Delta \theta_x - \Delta \theta_y) C_n^v + \frac{\Delta \theta_y}{2} C_{n+1}^v + \Delta \theta_z C_{n+4}^v, \quad (16.46)$$

where  $n = 1, 2$ .

Along the top boundary, Eq. (16.46) does not apply because in place of diffusion from node  $n$  to node  $n+4$ , there is instead diffusion from  $n-4$  to  $n$ . This results in

$$-\Delta \theta_y C_{n-4}^{v+1} - \frac{\Delta \theta_x}{2} C_{n-1}^{v+1} + (1 + \Delta \theta_x + \Delta \theta_y) C_n^{v+1} - \frac{\Delta \theta_y}{2} C_{n+1}^{v+1} = \Delta \theta_z C_{n+4}^v \\ + \frac{\Delta \theta_x}{2} C_{n-1}^v + (1 - \Delta \theta_x - \Delta \theta_y) C_n^v + \frac{\Delta \theta_y}{2} C_{n+1}^v, \quad (16.47)$$

where  $n = 13, 14$ .

For the left and right boundaries, the procedure gives

$$-\frac{\Delta \theta_y}{2} C_{n-4}^{v+1} + (1 + \Delta \theta_y + \Delta \theta_z) C_n^{v+1} - \Delta \theta_x C_{n+1}^{v+1} - \frac{\Delta \theta_y}{2} C_{n+4}^{v+1} = \frac{\Delta \theta_x}{2} C_n^v \\ + (1 - \Delta \theta_y - \Delta \theta_z) C_n^v + (1 + \Delta \theta_y + \Delta \theta_z) C_{n+1}^v - \Delta \theta_x C_{n+4}^v, \quad (16.48)$$

for the left boundary where  $n = 4, 8$ , and

$$-\frac{\Delta \theta_y}{2} C_{n-4}^{v+1} - \Delta \theta_x C_{n-1}^{v+1} + (1 + \Delta \theta_x + \Delta \theta_y) C_n^{v+1} - \frac{\Delta \theta_y}{2} C_{n+1}^{v+1} = \frac{\Delta \theta_x}{2} C_n^v \\ + \Delta \theta_x C_{n-1}^v + (1 - \Delta \theta_x - \Delta \theta_y) C_n^v + (1 + \Delta \theta_x + \Delta \theta_y) C_{n+1}^v - \frac{\Delta \theta_y}{2} C_{n+4}^v, \quad (16.49)$$

for the right boundary where  $n = 7, 11$ .

Each corner node has an area of  $(\Delta x/2) \times (\Delta y/2)$ . Then a solute mass balance at node  $n = 0$  is

$$\theta = \frac{\Delta y}{2} \left[ -D \frac{C_{n+1} - C_n}{\Delta x} \right] + \frac{\Delta x}{2} \left[ -D \frac{C_{n+4} - C_n}{\Delta y} \right] + \frac{\Delta x \Delta y}{4} \left[ \frac{\partial C}{\partial t} \right]_n. \quad (16.50)$$

After the Crank-Nicolson average for the time derivative is set up, the resulting equation is substituted into Eq. (16.50) and rearranged. The result is

$$(1 + \Delta\theta_x + \Delta\theta_y) C_n^{v+1} - \Delta\theta_x C_{n+1}^{v+1} - \Delta\theta_y C_{n+4}^{v+1} = \\ (1 - \Delta\theta_x - \Delta\theta_y) C_n^v + \Delta\theta_x C_{n+1}^v + \Delta\theta_y C_{n+4}^v. \quad (16.51)$$

with  $n = 0$ . Similarly at  $n = 3$ :

$$-\Delta\theta_x C_{n+1}^{v+1} + (1 + \Delta\theta_x + \Delta\theta_y) C_n^{v+1} - \Delta\theta_y C_{n+4}^{v+1} = \\ -\Delta\theta_x C_{n+1}^v + (1 - \Delta\theta_x - \Delta\theta_y) C_n^v + \Delta\theta_y C_{n+4}^v. \quad (16.52)$$

At  $n = 12$ :

$$-\Delta\theta_y C_{n+4}^{v+1} + (1 + \Delta\theta_x + \Delta\theta_y) C_n^{v+1} - \Delta\theta_x C_{n+1}^{v+1} = \\ -\Delta\theta_y C_{n+4}^v + (1 - \Delta\theta_x - \Delta\theta_y) C_n^v + \Delta\theta_x C_{n+1}^v. \quad (16.53)$$

At  $n = 15$ :

$$-\Delta\theta_y C_{n+4}^{v+1} - \Delta\theta_x C_{n+1}^{v+1} + (1 + \Delta\theta_x + \Delta\theta_y) C_n^{v+1} = \\ -\Delta\theta_y C_{n+4}^v - \Delta\theta_x C_{n+1}^v + (1 - \Delta\theta_x - \Delta\theta_y) C_n^v + \Delta\theta_x C_{n+1}^v. \quad (16.54)$$

We finally have an equation for each of the 16 nodes in our system, so the matrices can be written. We take  $\Delta x = \Delta y = 30 \mu\text{m}$  and assume that  $D = 10^{-11} \text{ m}^2 \text{ s}^{-1} = 10^{-1} \mu\text{m}^2 \text{ s}^{-1}$ . With  $\Delta\theta_x = \Delta\theta_y = 0.01$ , the time steps are  $\Delta t = 0.01(\Delta x)^2/D = 900 \text{ s}$ . In one day (not an unreasonable time for homogenization), there are 96 time steps. In reality, it would be better to have more spatial resolution so  $\Delta\theta_x$  and  $\Delta\theta_y$  could be greater than 0.01. We continue with our rather coarse grid, however, for illustrative purposes in setting up the matrices that result in Eq. (16.55) on the next page.

Examination of Eq. (16.55) reveals that a pattern has emerged. The coefficients for the concentrations all fall on the diagonals in the coefficient matrices, and they are equal. In this example, the coefficient matrix on the left side of Eq. (16.55) has all diagonal elements equal to 1.02.

Figure 16.8 illustrates other aspects of the matrices. Each internal node has four neighbors, and the concentrations of the four neighbors are weighted evenly by their respective coefficients of  $-\Delta\theta/2$ , when  $\Delta\theta = \Delta\theta_x = \Delta\theta_y$ . At a boundary, where one of the four neighbors is missing, the coefficient of its opposite counterpart is doubled. Where two of the four neighbors are missing, as at a corner, then each coefficient of the two neighboring concentrations is doubled.

$$\begin{bmatrix} 1.02 & -0.01 & 0 & 0 & -0.005 & 0 & 0 & 0 & -0.005 & 0 & 0 & 0 & 0 & 0 & 0 & 0 & 0 \\ -0.01 & 1.02 & -0.005 & 0 & 0 & 0 & 0 & 0 & 0 & 0 & 0 & 0 & 0 & 0 & 0 & 0 & 0 & 0 \\ 0 & 0 & 1.02 & -0.01 & 0 & 0 & 0 & 0 & 0 & 0 & 0 & 0 & 0 & 0 & 0 & 0 & 0 & 0 \\ 0 & 0 & 0 & 1.02 & -0.005 & 0 & 0 & 0 & 0 & 0 & 0 & 0 & 0 & 0 & 0 & 0 & 0 & 0 \\ -0.005 & 0 & 0 & 0 & 1.02 & -0.005 & 0 & 0 & 0 & 0 & 0 & 0 & 0 & 0 & 0 & 0 & 0 & 0 \\ 0 & 0 & 0 & 0 & 0 & 1.02 & -0.005 & 0 & 0 & 0 & 0 & 0 & 0 & 0 & 0 & 0 & 0 & 0 \\ 0 & 0 & 0 & 0 & 0 & 0 & 1.02 & -0.005 & 0 & 0 & 0 & 0 & 0 & 0 & 0 & 0 & 0 & 0 \\ -0.005 & 0 & 0 & 0 & 0 & 0 & 0 & 1.02 & -0.005 & 0 & 0 & 0 & 0 & 0 & 0 & 0 & 0 & 0 \\ 0 & 0 & 0 & 0 & 0 & 0 & 0 & 0 & 1.02 & -0.005 & 0 & 0 & 0 & 0 & 0 & 0 & 0 & 0 \\ 0 & 0 & 0 & 0 & 0 & 0 & 0 & 0 & 0 & 1.02 & -0.005 & 0 & 0 & 0 & 0 & 0 & 0 & 0 \\ 0 & 0 & 0 & 0 & 0 & 0 & 0 & 0 & 0 & 0 & 1.02 & -0.005 & 0 & 0 & 0 & 0 & 0 & 0 \\ 0 & 0 & 0 & 0 & 0 & 0 & 0 & 0 & 0 & 0 & 0 & 1.02 & -0.005 & 0 & 0 & 0 & 0 & 0 \\ 0 & 0 & 0 & 0 & 0 & 0 & 0 & 0 & 0 & 0 & 0 & 0 & 1.02 & -0.005 & 0 & 0 & 0 & 0 \\ 0 & 0 & 0 & 0 & 0 & 0 & 0 & 0 & 0 & 0 & 0 & 0 & 0 & 1.02 & -0.005 & 0 & 0 & 0 \\ 0 & 0 & 0 & 0 & 0 & 0 & 0 & 0 & 0 & 0 & 0 & 0 & 0 & 0 & 1.02 & -0.005 & 0 & 0 \\ 0 & 0 & 0 & 0 & 0 & 0 & 0 & 0 & 0 & 0 & 0 & 0 & 0 & 0 & 0 & 1.02 & -0.005 & 0 \\ 0 & 0 & 0 & 0 & 0 & 0 & 0 & 0 & 0 & 0 & 0 & 0 & 0 & 0 & 0 & 0 & 1.02 & -0.005 \end{bmatrix} \quad (16.55)$$



```

    910 DATA 1.2
    920 DATA 1.4
    930 DATA 1.0
    940 DATA 1.03
    950 DATA 1.06
    960 DATA 1.1
    999 END
  
```

Table 16.4 Concentrations during homogenization

	Initial	8 hours	16 hours	24 hours	
C <sub>0</sub>	1.1	1.214	1.277	1.313	
C <sub>1</sub>	1.4	1.400	1.403	1.399	
C <sub>2</sub>	2	1.818	1.675	1.578	
C <sub>3</sub>	2.5	2.059	1.820	1.671	Maximum
C <sub>4</sub>	1.06	1.156	1.225	1.269	
C <sub>5</sub>	1.2	1.296	1.329	1.343	
C <sub>6</sub>	1.8	1.640	1.556	1.498	
C <sub>7</sub>	2	1.818	1.675	1.578	
C <sub>8</sub>	1.03	1.080	1.135	1.186	
C <sub>9</sub>	1.1	1.146	1.196	1.237	
C <sub>10</sub>	1.2	1.296	1.329	1.343	
C <sub>11</sub>	1.4	1.400	1.403	1.399	
C <sub>12</sub>	1	1.043	1.094	1.146	Minimum
C <sub>13</sub>	1.03	1.080	1.135	1.186	
C <sub>14</sub>	1.06	1.156	1.225	1.269	
C <sub>15</sub>	1.1	1.214	1.277	1.313	
Avg.	1.374	1.363	1.360	1.358	

A figure of merit of the process is the residual segregation index,  $\delta$ , defined in Eq. (13.64). The calculated values of  $\delta$  versus dimensionless time are plotted in Fig. 16.10. Even after 24 hours, complete homogenization is not effected.

As mentioned before, a code such as given here may not be capable of solving the problem except for a rather limited number of nodes. In order to treat a larger multi-modal situation, the reader might consider an algorithm based on the *alternating direction implicit (ADI)* method,<sup>4</sup> which involves taking a half-time step at nodes in the vertical direction followed by a half-time step at the nodes in the horizontal direction. The resulting matrices for the half-time steps are tridiagonal, which can be solved very efficiently. With full-time steps as done here, the implicit method leads to a banded matrix that is not tridiagonal (e.g., Eq. (16.55)).

In Sections 16.1.1-16.1.3 the coefficient matrices remained constant as time marched forward because the heat transfer coefficient and transport properties were constant. The finite difference approximation, however, enables us to use heat transfer coefficients or transport properties that vary. Here we illustrate the use of radiation heat transfer at the surface, which must be treated accordingly because of its  $T^4$  behavior.

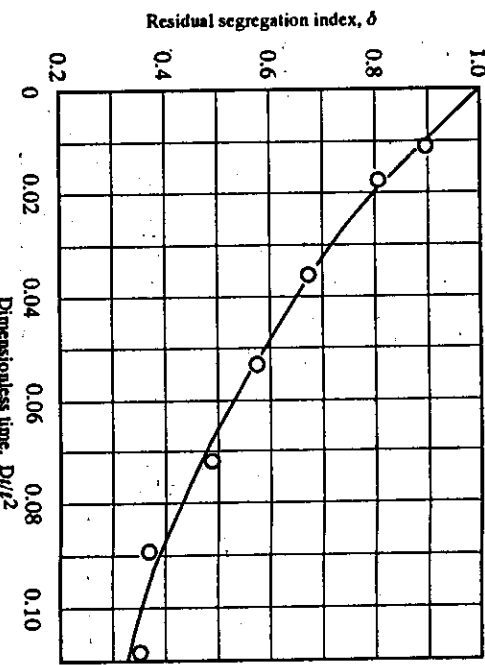


Fig. 16.10 Homogenization kinetics for two-dimensional diffusion.

#### 16.1.4 Radiation heat transfer at a surface

Consider a green ceramic slab that is placed into a high temperature furnace for sintering at 2000 K. Our goal is to estimate the temperature distribution within the green slab as it is heated by radiation emanating from the walls of the furnace. The thermal conductivity of the porous ceramic varies with temperature, but the volumetric heat capacity is constant. Both surfaces of the slab are equally heated by radiation so that the temperature is symmetrical on both sides of  $x = 0$ .

The energy equation is

$$\frac{\partial T}{\partial t} = \frac{\partial}{\partial x} \left[ \alpha \frac{\partial T}{\partial x} \right]. \quad (16.56)$$

At the surface exchanging radiant energy ( $x = L$ ), the power balance is

$$-k \frac{\partial T}{\partial x}(L, t) = \mathcal{F}_o (T^*(L, t) - T^*(L, t)), \quad (16.57)$$

or

$$\frac{\partial T}{\partial t}(0, t) = 0, \quad (16.58)$$

where  $T^*$  is the temperature of the radiating furnace walls. At the plane of symmetry, we have

and the initial condition is

$$T(x, 0) = T_i \text{ (uniform).} \quad (16.59)$$

For the sake of minimizing the algebra involved, let's formulate the finite difference approximation with the Euler method. The internal points will have to be treated differently than they were in Section 16.1.1 because the thermal diffusivity varies with temperature. At a node  $m$ , the energy balance in finite difference form is

$$-k_+ \frac{T_m - T_{m-1}}{\Delta x} = -k_- \frac{T_{m+1} - T_m}{\Delta x} + \Delta x \rho C_p \left[ \frac{\partial T}{\partial t} \right]_m, \quad (16.59)$$

where  $k_+$  is the average thermal conductivity between nodes  $m$  and  $m-1$  and  $k_-$  is the average between nodes  $m+1$  and  $m$ . After rearranging, we get

$$\left[ \frac{\partial T}{\partial t} \right]_m = \frac{\alpha_+}{(\Delta x)^2} (T_{m+1} - T_m) - \frac{\alpha_-}{(\Delta x)^2} (T_m - T_{m-1}).$$

With the Euler method,

$$T_m^{*+1} = T_m^* + \left[ \frac{\partial T}{\partial t} \right]_m^* \Delta t$$

or

$$T_m^{*+1} = T_m^* + \Delta \theta_+ (T_{m+1}^* - T_m^*) - \Delta \theta_- (T_m^* - T_{m-1}^*),$$

where  $\Delta \theta_+ = \alpha_+ \Delta t / (\Delta x)^2$  and  $\Delta \theta_- = \alpha_- \Delta t / (\Delta x)^2$ . The form suitable for setting up the matrix is

$$T_m^{*+1} = +\Delta \theta_- T_{m-1}^* + (1 - \Delta \theta_+ - \Delta \theta_-) T_m^* + \Delta \theta_+ T_{m+1}^*, \quad (16.60)$$

for  $0 < m < N$ .

An energy balance at  $m = 0$  can be written as follows:

$$0 = -k_+ \left[ \frac{T_1 - T_0}{\Delta x} \right] + \frac{\Delta x}{2} \rho C_p \left[ \frac{\partial T}{\partial t} \right]_0$$

or

$$\left[ \frac{\partial T}{\partial t} \right]_0 = \frac{2\alpha_+}{(\Delta x)^2} (T_1 - T_0). \quad (16.61)$$

The Euler method gives

$$T_0^{*+1} = T_0^* + 2\Delta \theta_+ (T_1^* - T_0^*)$$

or

$$T_0^{*+1} = (1 - 2\Delta \theta_+) T_0^* + 2\Delta \theta_+ T_1^*. \quad (16.62)$$

At the surface exchanging radiant energy, the energy balance is

$$-k_+ \left[ \frac{T_N - T_{N-1}}{\Delta x} \right] + \mathcal{F}\sigma [T_N^* - T_N^*] = \frac{\Delta x}{2} \rho C_p \left[ \frac{\partial T}{\partial t} \right]_N$$

or

$$\left[ \frac{\partial T}{\partial t} \right]_N = \frac{2\alpha_-}{(\Delta x)^2} (T_{N-1}^* - T_N^*) + \frac{2\mathcal{F}\sigma}{\rho C_p \Delta x} (T_N^* - T_N^*). \quad (16.63)$$

With the Euler method this gives

$$T_N^{*+1} = T_N^* + 2\Delta \theta_- (T_{N-1}^* - T_N^*) + A$$

or

$$T_N^{*+1} = 2\Delta \theta_- (T_{N-1}^*) + (1 - 2\Delta \theta_-) T_N^* + A, \quad (16.64)$$

where

$$A = \frac{2\mathcal{F}\sigma \Delta t}{\rho C_p \Delta x} (T_N^* - (T_N^*)^*).$$

We cannot include  $T_N^*$  in the matrices for the variables because the elements can only be linear terms. Therefore,  $A$  in the right side of Eq. (16.64) must be evaluated at every time step  $v$  and treated as a constant.

For illustrative purposes, we consider a green ceramic slab that has a thickness of 60 mm and a thermal conductivity that varies with temperature according to

$$k = 5 \times 10^{-4} T + 0.40,$$

with  $T$  in K and  $k$  in  $\text{W m}^{-1} \text{K}^{-1}$ . The volumetric heat capacity of the ceramic,  $\rho C_p$ , is  $2.3 \times 10^6 \text{ J m}^{-3} \text{K}^{-1}$ , and its emissivity is 0.5. The ceramic slab has been preheated uniformly to 1000 K, before we insert it into the high temperature furnace with its walls at 2020 K.

We set up the matrices for the first three time steps. To keep the problem relatively simple, let  $N = 4$  so that  $\Delta x = 1.5 \times 10^{-2}$  m. Recall  $\Delta \theta \leq 0.5$  because we are using the Euler method. The radiation boundary condition is highly nonlinear so we should take small time steps to get reasonably good values of  $A$ . Suppose,  $\Delta \theta_- = 0.025$  at  $m = N$  then each time step will be of a different duration. Notice too that  $\Delta \theta_+$  will not be exactly 0.025 except at the beginning.

Initially  $v = 0$  and  $t = 0$ . We have the following properties and coefficients:

$$k_+ = k_- = k(1000 \text{ K}) = 0.90 \text{ W m}^{-1} \text{K}^{-1},$$

$$\alpha_+ = \alpha_- = \alpha(1000 \text{ K}) = 3.91 \times 10^{-7} \text{ m}^2 \text{s}^{-1},$$

$$\Delta \theta_- = \Delta \theta_+ = 0.025;$$

$$\Delta t = \frac{\Delta \theta_+ (\Delta x)^2}{\alpha_-} = \frac{(0.025)(1.5 \times 10^{-2})^2}{3.91 \times 10^{-7}} = 14.39 \text{ s}.$$

The view factor for the radiating surface is unity, so that  $\mathcal{F} = \epsilon = 0.5$ ; therefore

$$A = \frac{2\mathcal{F}\sigma\Delta t}{\rho C_p \Delta x} (T_w^4 - (T_k^*)^4) = \frac{(2)(0.5)(5.669 \times 10^{-8})(14.39)}{(2.3 \times 10^6)(1.5 \times 10^{-2})} (2020^4 - 1000^4)$$

$$= 370 \text{ K.}$$

Now we set up the matrix to solve for the temperatures at time step  $v+1$  when  $t = 14.39 \text{ s}$ :

$$\begin{bmatrix} T_0^1 & 0.95 & 0.05 \\ T_1^1 & 0.025 & 0.95 & 0.025 \\ T_2^1 & - & 0.025 & 0.95 & 0.025 \\ T_3^1 & 0.025 & 0.95 & 0.025 \\ T_4^1 & 0.05 & 0.95 & 1000 \\ T_4^1 - 370 & 1000 & 1000 & 1000 & 1000 \end{bmatrix}$$

The solution is tabulated, along with new values of  $k_+$ ,  $k_-$ ,  $\alpha_+$  and  $\alpha_-$  (all in SI units) for next time step.

$$\begin{bmatrix} k_+ & k_- & \alpha_+ \times 10^7 & \alpha_- \times 10^7 \\ T_0^1 & 1000 & 0.90 & - \\ T_1^1 & 1000 & 0.90 & 0.90 \\ T_2^1 & 1000 & 0.90 & 0.90 \\ T_3^1 & 1000 & 0.992 & 0.90 \\ T_4^1 & 1370 & - & 0.992 \end{bmatrix}$$

Remember we decided to fix  $\Delta\theta_-$  at  $m = N = 4$ , so that for the second time step

$$\Delta t = \frac{(0.025)(1.5 \times 10^{-2})^2}{4.31 \times 10^{-7}} = 13.05 \text{ s.}$$

and  $t_2 = 14.39 + 13.05 = 27.44 \text{ s.}$

$$A = \frac{(2)(0.5)(5.669 \times 10^{-8})(13.05)}{(2.3 \times 10^6)(1.5 \times 10^{-2})} (2020^4 - 1370^4) = 281 \text{ K.}$$

Now we calculate and tabulate  $\Delta\theta_-$  and  $\Delta\theta_+$  for each node.

With these values we can set up the matrix for the next time step:

$$\begin{bmatrix} T_0^2 & 0.9547 & 0.0453 \\ T_1^2 & 0.02267 & 0.9547 & 0.02267 \\ T_2^2 & - & 0.02267 & 0.9547 & 0.02267 \\ T_3^2 & 0.02267 & 0.9523 & 0.0250 & 1000 \\ T_4^2 - 281 & 0.05 & 0.95 & 1370 \end{bmatrix}$$

The new temperatures and values of thermal conductivities and diffusivities are tabulated below.

$$\begin{bmatrix} k_+ & k_- & \alpha_+ \times 10^7 & \alpha_- \times 10^7 \\ T_0^2 & 1000 & 0.90 & - \\ T_1^2 & 1000 & 0.90 & 0.90 \\ T_2^2 & 1000 & 0.90 & 0.90 \\ T_3^2 & 1000 & 0.902 & 0.90 \\ T_4^2 & 1633 & - & 0.902 \end{bmatrix}$$

For the third time step

$$\Delta t = \frac{(0.025)(1.5 \times 10^{-2})^2}{4.58 \times 10^{-7}} = 12.28 \text{ s.}$$

and  $t_3 = 27.44 + 12.28 = 39.72 \text{ s.}$

$$A = \frac{(2)(0.5)(5.669 \times 10^{-8})(12.28)}{(2.3 \times 10^6)(1.5 \times 10^{-2})} (2020^4 - 1653^4) = 192.$$

Again we calculate and tabulate  $\Delta\theta_-$  and  $\Delta\theta_+$  for each node.

	$\Delta\theta_+$	$\Delta\theta_-$
$T_0^*$	—	0.02134
$T_1^*$	0.02134	0.02134
$T_2^*$	0.02134	0.02139
$T_3^*$	0.02139	0.0250
$T_4^*$	0.0250	—

Now the matrices for the next time step are set up:

$$\begin{bmatrix} T_0^3 \\ T_1^3 \\ T_2^3 \\ T_3^3 \\ T_4^3 - 192 \end{bmatrix} = \begin{bmatrix} 0.9573 & 0.0427 \\ 0.02134 & 0.9573 & 0.02134 \\ 0.02134 & 0.9573 & 0.02139 & 1000 \\ 0.02139 & 0.9536 & 0.0250 & 1009 & 1000 \\ 0.05 & 0.95 & 1633 \end{bmatrix}$$

The new temperatures at  $t = 39.72$  s are 1000, 1000, 1000, 1024 and 1794 K. Having gone through three time steps, we stop here. After almost 40 s the surface is at 1794 K, but very little of the slab has heated. Very steep thermal gradients have developed near the surface, yet the center has not begun to heat.

A computer code to simulate complete heating of the slab, defined as heating the center coefficient matrix for the unknowns at each time step. Calculated temperatures are plotted in Fig. 16.11. The surface attains 2000 K in 30 minutes, but at that time the center is only at 1300 K. It requires 184 minutes for the center to reach 2000 K.

```

180  AlphaP(I) = KP(I) / (2.3E6)
190  KN(I+1) = (0.5 * (5E-4) * T(I,1) + T(I+1,1)) + 0.4
200  Alphan(I+1) = KN(I+1) / (2.3E6)
NEXT I

220  REM --- compute the time step
230  ThetaP(4) = 0.025
240  ThetaN(5) = 0.025
250  dT = ThetaP(4) * (dX**2) / Alphan(5)
260  SumTime = SumTime + dT
265  SubSumTime = SubSumTime + dT

270  REM --- compute 'A'
280  A = (2 * (0.5) * (5.663E-8) * dT) * ((FurTemp**4) - (T(5,1)**4)) / ((2.36E6) * dX)

290  REM --- obtain the matrix
300  FOR I = 1 TO 3
310    ThetaP(I) = Alphan(I) * dT / (dX**2)
320    ThetaN(I+1) = Alphan(I+1) * dT / (dX**2)
NEXT I

340  REM --- compute the temperatures for next step
350  MAT C = ZER(5,5)
360  C(1,1) = 1 - (2 * ThetaP(1))
370  C(1,2) = 2 * ThetaP(1)
380  FOR I = 2 TO 4
390    C(I,I-1) = ThetaN(I)
400    C(I,I) = 1 - ThetaN(I)
410    C(I,I+1) = ThetaN(I) - ThetaP(I)
420  C(5,4) = 2 * ThetaN(5)
430  C(5,5) = 1 - (2 * ThetaN(5))
440  REM --- compute the temperatures for next step
450  MAT NewT = C * T
460  NewT(5,1) = NewT(5,1) + A
470  MAT T = NewT
480  IF (SubSumTime >= 600) THEN GOSUB 800
NEXT I

510  GOSUB 800
500  REM MATRIX ---- T (Initial Temperatures)
700  PRINT "K+", "K-", "Alpha+", "Alpha-"
710  DATA 1000
720  DATA 1000
730  DATA 1000
740  DATA 1000
750  DATA 1000
790  STOP

800  PRINT "K+", "K-", "Alpha+", "Alpha-"
810  FOR I = 1 TO 5
820  PRINT KP(I), KN(I), AlphaP(I), Alphan(I)
830  NEXT I
840  PRINT "Theta+", "Theta-"
850  FOR I = 1 TO 5
860  PRINT ThetaP(I), ThetaN(I)
870  PRINT "R:"; A
880  PRINT "MATRIX is "
890  SumTime = SumTime / 60
900  PRINT "Total Time is ", SumTime, " (min)"
910  PRINT "Iteration : ", ITER
920  PRINT "R:"; A
930  MAT PRINT C,
940  PRINT "Temperatures for next step"
950  MAT PRINT T
960  SubSumTime = SubSumTime - 600
970  RETURN
980
END

```

```

11  REM *** VAX-BASIC PROGRAM
12  REM *** FOR ****
13  REM *** SOLVING RADIATION PROBLEM ****
20  DIM C(5,5),T(5,1),NEWT(5,1)
30  DIM KP(5),KN(5),AlphaP(5),Alphan(5)
40  DIM ThetaP(5),ThetaN(5)
50  REM --- read the initial temperatures
60  MAT READ T(5,1)
70  PRINT "Initial Temperatures"
80  MAT PRINT T
90  dX = 1.5E-2
100  SumTime = 0
105  FurTemp = 0
110  dT = 0.001
120  ITER = 0
130  WHILE (T(1,1) <= 2000)
140  ITER = ITER + 1
150  REM --- compute the thermal conductivities
160  FOR I = 1 TO 4
170  KP(I) = (0.5 * (5E-4) * (T(I,1) + T(I+1,1))) + 0.4

```



Fig. 16.11 Calculated temperatures in green ceramic slab (60 mm thick).

## 16.2 TURBULENT FLOW

Turbulent conditions, rather than laminar, usually prevail in materials processing. Accordingly, we make use of empirically based correlations for friction factors, heat transfer coefficients and mass transfer coefficients, such as presented in Chapters 3, 8 and 15. Even if those respective chapters were complete in summarizing all that has been studied and categorized, materials engineers encounter situations not previously analyzed and presented in such neat packages. For example, many processes involve recirculating flows: flows driven by electromagnetic forces; flows associated with the filling of vessels, ladles and molds; and flows driven by the injection of gas jets or large bubble swarms to effect reactions and mixing.

We know that sometimes even small disturbances of the fluid streamlines in laminar flow can cause turbulence. In forced convection, flows with small Reynolds numbers involve fluids in which the inertial forces are small relative to the viscous forces. For large Reynolds numbers, however, the inertial forces overcome the viscous forces (which tend to dissipate the inertial forces to neighboring streamlines), and the disturbances amplify or at least persist. Turbulent flow can be advantageous in that it enhances heat and mass transfer rates. In some processes, however, its fluctuating and rather unpredictable nature is deleterious. For example, crystals grown in turbulently convecting melts exhibit segregation in the form of striations that are approximately parallel to the overall interface. Whether turbulence is to be desired or avoided depends upon the specific process under consideration, but for certain it can be said that the convection is complicated and difficult to describe and predict.

### 16.2.1 Fluctuation nature of turbulence

The dependent variables ( $v_x$ ,  $v_y$ ,  $v_z$ ,  $T$  and  $C$ ) have instantaneous values in turbulent flow; it is impossible to predict their exact values at any instant. Fortunately, the time-averaged quantities are by far more important and used in analyzing turbulence. The two are simply related; e.g., the  $x$ -component of velocity at a point in the flow field is

$$v_x = \bar{v}_x + v'_x,$$

$$(16.65)$$

where  $v_x$  = instantaneous velocity component,  $\bar{v}_x$  = time-averaged quantity (see Fig. 1.2), and  $v'_x$  = fluctuation. Likewise, instantaneous pressure, temperature and concentrations can be expressed in the same manner; e.g., the pressure is

$$P = \bar{P} + P' \quad (16.66)$$

Consider the continuity equation for an incompressible fluid in a two-dimensional flow field; specifically Eq. (A) in Table 2.1 reduces to

$$\frac{\partial \bar{v}_x}{\partial x} + \frac{\partial \bar{v}_y}{\partial y} = 0. \quad (16.67)$$

When Eq. (16.67) is combined with Eq. (16.65) and a similar equation for  $v_y$ , the result is

$$\left[ \frac{\partial \bar{v}_x}{\partial x} + \frac{\partial \bar{v}_y}{\partial y} \right] + \left[ \frac{\partial v'_x}{\partial x} + \frac{\partial v'_y}{\partial y} \right] = 0. \quad (16.68)$$

The  $x$ -component of the momentum equation (Eq. (D) in Table 2.2) is

$$\frac{\partial \bar{v}_x}{\partial t} + \bar{v}_x \frac{\partial \bar{v}_x}{\partial x} + \bar{v}_y \frac{\partial \bar{v}_x}{\partial y} = -\frac{1}{\rho} \frac{\partial \bar{P}}{\partial x} + \nu \left[ \frac{\partial^2 \bar{v}_x}{\partial x^2} + \frac{\partial^2 \bar{v}_x}{\partial y^2} \right] + g_x. \quad (16.69)$$

In order to simplify our presentation somewhat, we assume that  $\partial^2 v_x / \partial x^2$  can be neglected. We also rewrite Eq. (16.69) in the following equivalent form by adding  $v'_x$  times Eq. (16.67) to it:

$$\frac{\partial \bar{v}_x}{\partial t} + \frac{\partial}{\partial x} (\bar{v}_x v_x) + \frac{\partial}{\partial y} (\bar{v}_y v_x) = -\frac{1}{\rho} \frac{\partial \bar{P}}{\partial x} + \frac{1}{\rho} \frac{\partial}{\partial y} \left[ \eta \frac{\partial v_x}{\partial y} \right] + g_x. \quad (16.70)$$

Our goal is to rewrite Eq. (16.70) in terms of the time-averaged variables,  $\bar{v}_x$ ,  $\bar{v}_y$ , and  $\bar{P}$ . For two-dimensional flow, the quantities  $v_x$ ,  $v_y$ , and  $P$  vary as  $(x, y, t)$ , but the fluctuating quantities  $v'_x$ ,  $v'_y$  and  $P'$  vary as  $(x, y, z, t)$ . Even though the time-averaged flow is two-dimensional, the turbulent fluctuations are still three-dimensional.

The substitution of Eqs. (16.65) and (16.66) into Eq. (16.70) yields

$$\begin{aligned} \frac{\partial}{\partial t} (\bar{v}_x + v'_x) + \frac{\partial}{\partial x} [(\bar{v}_x + v'_x)(\bar{v}_x + v'_x)] + \frac{\partial}{\partial y} [(\bar{v}_x + v'_x)(\bar{v}_y + v'_y)] &= \\ -\frac{1}{\rho} \frac{\partial}{\partial x} (\bar{P} + P') + \frac{1}{\rho} \frac{\partial}{\partial y} \left[ \eta \frac{\partial}{\partial y} (\bar{v}_x + v'_x) \right] + g_x. & \end{aligned} \quad (16.71)$$

We want to use Eq. (16.71) in the time-average sense, and the time averages of the fluctuations, themselves, are zero. Thus,  $v'_x = 0$ ,  $v'_y = 0$ , and  $\bar{P}' = 0$ . With this in mind, we now examine the time averaging of the product of the factors involving  $v_x$ :

$$(\bar{v}_x + v'_x)(\bar{v}_x + v'_x) = \bar{v}_x \bar{v}_x + 2\bar{v}_x v'_x + v'_x v'_x = \bar{v}_x \bar{v}_x + 0 + 0 = \bar{v}_x \bar{v}_x$$

\*Also called the temporal mean velocity or mean velocity.

Numerical Methods and Models 601  
turbulent flow equation for the  $x$ -component of momentum, that compares to Eq. (D) in Table 2.2, is

$$\begin{aligned} (\bar{v}_x + v'_x)(\bar{v}_y + v'_y) &= \bar{v}_x \bar{v}_y + \bar{v}_x v'_y + v'_x \bar{v}_y + v'_x v'_y = \bar{v}_x \bar{v}_y + 0 + 0 + v'_x v'_y \\ &= \bar{v}_x \bar{v}_y + v'_x v'_y. \end{aligned} \quad (16.76)$$

Even though  $\bar{v}_x$  and  $\bar{v}_y$  are each zero, we can use continuity and show that the time average of their product  $(v'_x v'_y)$  must always be negative and never zero in a turbulent flow. Suppose  $v'_x$  is positive, then  $v'_y$  must be negative to compensate for the fluid leaving the unit element in the positive  $y$ -direction. On the other hand, if  $v'_y$  is negative, then  $v'_x$  must be positive. Hence,  $v'_x v'_y$  is always negative and its time average can never be zero. The instantaneous continuity equation is Eq. (16.68), and when the equation is time averaged we get

$$\left[ \frac{\partial \bar{v}_x}{\partial x} + \frac{\partial \bar{v}_y}{\partial y} \right] = 0. \quad (16.72)$$

When we time average Eq. (16.71) and combine it with Eq. (16.72), the result is

$$\frac{\partial \bar{v}_x}{\partial t} + \bar{v}_x \frac{\partial \bar{v}_x}{\partial x} + \bar{v}_y \frac{\partial \bar{v}_x}{\partial y} = -\frac{1}{\rho} \frac{\partial \bar{P}}{\partial x} + \frac{1}{\rho} \frac{\partial}{\partial y} \left[ \eta \frac{\partial \bar{v}_x}{\partial y} - \rho v'_x v'_y \right] + g_x. \quad (16.73)$$

The form of Eq. (16.73) is exactly the same as our original equation for  $v_x$ , Eq. (16.70), with the exception of the term  $v'_x v'_y$ , and it is this term that is at the heart of turbulent flow models.

If at the same time we had considered the temperature field of the flow, then the derived energy equation for the turbulent flow would be

$$\frac{\partial \bar{T}}{\partial t} + \bar{v}_x \frac{\partial \bar{T}}{\partial x} + \bar{v}_y \frac{\partial \bar{T}}{\partial y} = \frac{1}{\rho C_p} \frac{\partial}{\partial y} \left[ k \frac{\partial \bar{T}}{\partial y} - \rho C_p v'_y \bar{T} \right]. \quad (16.74)$$

Added to the familiar form of the energy equation is the term containing  $v'_y \bar{T}$ . This term and the previous  $v'_x v'_y$  account for the effect of the turbulence on the energy and momentum transport, respectively.

We can add species conservation to the presentation by simply referring to Eq. (A) in Table 15.3. The equation of diffusion that goes with the two-dimensional flow of Eq. (16.73)

$$\frac{\partial \bar{C}_A}{\partial t} + \bar{v}_x \frac{\partial \bar{C}_A}{\partial x} + \bar{v}_y \frac{\partial \bar{C}_A}{\partial y} = \frac{\partial}{\partial y} \left[ D_A \frac{\partial \bar{C}_A}{\partial y} - \frac{\partial \bar{v}_x}{\partial y} \bar{v}_y \bar{C}_A \right], \quad (16.75)$$

where we simply replaced  $C_A$  with  $\bar{C}_A$  and added  $\bar{v}_y \bar{C}_A$  to account for the effect of turbulence on the transport of species  $A$ .

Equations (16.73)-(16.75) are for those two-dimensional flow fields in which the 'diffusional' terms in the  $x$ -direction are negligible and can be neglected. This was done to keep the presentation short, but at the same time show the essential connection between the equations used for laminar flow and those used for turbulent flow. The full three-dimensional

$$\begin{aligned} (\bar{v}_x + v'_x)(\bar{v}_y + v'_y) &= \bar{v}_x \bar{v}_y + \bar{v}_x v'_y + v'_x \bar{v}_y + v'_x v'_y = \bar{v}_x \bar{v}_y + 0 + 0 + v'_x v'_y \\ &= \bar{v}_x \bar{v}_y + v'_x v'_y. \end{aligned}$$

For the instantaneous variables, these terms are  $\eta(\partial^2 v/\partial x^2)$ ,  $\alpha(\partial^2 T/\partial x^2)$ , and  $D_A(\partial^2 C_A/\partial x^2)$ . They are often referred to as diffusional terms because they are momentum diffusion, heat diffusion and mass diffusion, respectively.

$$\frac{\partial \bar{v}_x}{\partial t} + \bar{v}_x \frac{\partial \bar{v}_x}{\partial x} + \bar{v}_y \frac{\partial \bar{v}_x}{\partial y} + \bar{v}_z \frac{\partial \bar{v}_x}{\partial z} = -\frac{1}{\rho} \frac{\partial \bar{P}}{\partial x} + \frac{1}{\rho} \left\{ \frac{\partial}{\partial x} \left[ \eta \frac{\partial \bar{v}_x}{\partial x} - \rho \frac{\partial \bar{v}_x}{\partial x} \right] \right\}, \quad (16.77)$$

$$\begin{aligned} \frac{\partial \bar{v}_y}{\partial t} + \bar{v}_x \frac{\partial \bar{v}_y}{\partial x} + \bar{v}_y \frac{\partial \bar{v}_y}{\partial y} + \bar{v}_z \frac{\partial \bar{v}_y}{\partial z} &= -\frac{1}{\rho} \frac{\partial \bar{P}}{\partial y} + \frac{1}{\rho} \left\{ \frac{\partial}{\partial y} \left[ \eta \frac{\partial \bar{v}_y}{\partial y} - \rho \frac{\partial \bar{v}_y}{\partial y} \right] \right\} + g_y, \quad (16.78) \end{aligned}$$

$$\begin{aligned} \frac{\partial \bar{v}_z}{\partial t} + \bar{v}_x \frac{\partial \bar{v}_z}{\partial x} + \bar{v}_y \frac{\partial \bar{v}_z}{\partial y} + \bar{v}_z \frac{\partial \bar{v}_z}{\partial z} &= -\frac{1}{\rho} \frac{\partial \bar{P}}{\partial z} + \frac{1}{\rho} \left\{ \frac{\partial}{\partial z} \left[ \eta \frac{\partial \bar{v}_z}{\partial z} - \rho \frac{\partial \bar{v}_z}{\partial z} \right] \right\} + g_z, \quad (16.79) \end{aligned}$$

Again for brevity, consider transport in the  $y$ -direction. The total fluxes are

$$\begin{aligned} \tau_{xy} &= - \left[ \eta \frac{\partial \bar{v}_x}{\partial y} - \rho v'_y \bar{v}_x \right], \\ q_y &= - \left[ k \frac{\partial \bar{T}}{\partial y} - \rho C_p \bar{v}_y \bar{T} \right], \end{aligned}$$

$$\begin{aligned} j_{xy} &= - \left[ D_A \frac{\partial \bar{C}_A}{\partial y} - v'_y \bar{C}_A \right], \\ \tau_{xy} &= -(\nu + \epsilon_M) \frac{\partial \bar{v}_x}{\partial y}, \\ q_y &= -\rho (v + \epsilon_H) \frac{\partial \bar{T}}{\partial y}, \\ j_{xy} &= -(\nu + \epsilon_C) \frac{\partial \bar{C}_A}{\partial y}, \end{aligned}$$

where  $\epsilon_M$ ,  $\epsilon_H$  and  $\epsilon_C$  are the momentum, heat and species eddy diffusivities, respectively. We see that the diffusivities are defined such that

$$\begin{aligned} \bar{v}'_y \bar{v}_x &= -\epsilon_M \frac{\partial \bar{v}_x}{\partial y}, \\ \bar{v}'_y \bar{T} &= -\epsilon_H \frac{\partial \bar{T}}{\partial y}, \end{aligned}$$

$$\bar{v}'_y \bar{C}_A = -\epsilon_C \frac{\partial \bar{C}_A}{\partial y}. \quad (16.83)$$

$$\bar{v}'_y \bar{T} = -\epsilon_H \frac{\partial \bar{T}}{\partial y}. \quad (16.84)$$

and

$$\overline{v' C_A} = -\varepsilon_C \frac{\partial \overline{C_A}}{\partial y}, \quad (16.85)$$

Life would be simpler if the eddy diffusivities were only fluid properties, but they are properties of both the fluid and the fluid motion. Herein lies the difficulty in modelling turbulent flow.

### 16.2.3 Prandtl mixing length

In this model small packets of the fluid fluctuate normal to the direction of the mean flow. The Prandtl mixing length,  $\ell$ , is the average distance travelled by these packets normal to the mean flow. According to the model, the fluctuations are

$$u'_x = u'_y = -\ell \frac{\partial \bar{u}_x}{\partial y},$$

so the turbulent component of the total momentum is

$$-\rho \overline{u'_x u'_y} = \rho \varepsilon_M \frac{\partial \bar{u}_x}{\partial y} = \rho \ell^2 \left[ \frac{\partial \bar{u}_x}{\partial y} \right]^2$$

Thus, the eddy momentum diffusivity becomes

$$\varepsilon_M = \ell^2 \frac{\partial \bar{u}_x}{\partial y}. \quad (16.86)$$

With only Eq. (16.86) nothing is gained because all we have done is to replace our ignorance of the behavior of  $\varepsilon_M$  with the behavior of  $\ell$ .

For boundary layer flow, Prandtl made a second hypothesis that  $\ell$  is proportional to distance from the wall:

$$\ell = Ky, \quad (16.87)$$

where  $K$  is a constant. In addition near the wall (but beyond the laminar sublayer), the shear stress is approximately constant ( $\tau_w = \tau_\infty$ ) and  $\varepsilon_M \gg v$  so that

$$\tau_w = \rho \ell^2 \left[ \frac{\partial \bar{u}_x}{\partial y} \right]^2 = \rho K^2 y^2 \left[ \frac{\partial \bar{u}_x}{\partial y} \right]^2,$$

or, after integration,

$$\bar{u}_x = \frac{\tau_w^{1/2}}{\rho^{1/2} K} \ln y + C, \quad (16.88)$$

where  $C$  is an integration constant. So far we have an equation of the form that compares to experimental measurements except in the region extremely close to the wall where the laminar sublayer persists.

In the laminar sublayer,  $u_x = \bar{u}_x$ , and

$$\bar{u}_x = -\tau_w = \eta \frac{\partial \bar{u}_x}{\partial y},$$

so with  $\bar{u}_x = 0$  at  $y = 0$ , we get

$$\bar{u}_x = \frac{\tau_w}{\eta} y. \quad (16.89)$$

We have characterized two regions: the laminar sublayer where  $v \gg \varepsilon_M$  and Eq. (16.89) applies, and the turbulent layer where  $\varepsilon_M \gg v$  and Eq. (16.88) applies. There is also a buffer layer (sometimes called the transitional layer) where  $\varepsilon_M \sim v$ .

The so-called *universal velocity profile* is a three-part equation for these three layers that is based upon the forms of Eqs. (16.88) and (16.89). Before giving the universal velocity profile, we define a dimensionless velocity  $u^+$  and a dimensionless coordinate  $y^+$ . They are

$$u^+ = \frac{\rho^{1/2}}{\tau_w^{1/2}} \bar{u}_x$$

and

$$y^+ = \frac{\tau_w^{1/2}}{\rho^{1/2} v} y.$$

With these definitions, Eq. (16.89) becomes

$$u^+ = y^+, \quad (16.90)$$

and Eq. (16.88) becomes

$$u^+ = \frac{1}{K} \ln y^+ + C. \quad (16.91)$$

The buffer layer has an equation of the same form as Eq. (16.88). By comparing these equations with empirical data, the set of equations that describe the universal velocity profile is as follows:

laminar sublayer:	$0 < y^* < 5$	$u^+ = y^*$ ,
-------------------	---------------	---------------

buffer layer:	$5 < y^* < 30$	$u^+ = 5.0 \ln y^* - 3.05$ ,
---------------	----------------	------------------------------

turbulent layer:	$30 < y^* < 400$	$u^+ = 2.5 \ln y^* + 5.5$ .
------------------	------------------	-----------------------------

We emphasize that the final result was determined from experimental data. The Prandtl mixing length model gave the form of the equation for fitting the data.

Prandtl's mixing length model has been found to be quite useful for analyzing two-dimensional boundary layer flows. Here we used the model to show how it forms the basis for the universal velocity profile. Launder and Spalding review the model and include empirical estimates of the mixing length,  $\ell$ , for various applications.

Within at least the materials processing community, the two-equation models of Spalding and Launder<sup>6</sup> have been extensively applied to assist in analyzing a variety of flows, including recirculating flows. Equation (16.80) can be written

$$\tau_{xy} = -(\eta + \eta_i) \frac{\partial \bar{v}_x}{\partial y}, \quad (16.92)$$

where  $\eta_i = \rho \dot{e}_M$  = the turbulent viscosity. In the so-called  $K-\epsilon$  model,<sup>7</sup> the dependent variables are the *turbulence energy*,  $K$ , and the *dissipation rate of turbulence energy*,  $\epsilon$ . The quantities  $K$  and  $\epsilon$  are determined by transport equations, which are differential equations to be described below. After  $K$  and  $\epsilon$  are determined, the turbulent viscosity is calculated by

$$\eta_i = \frac{C_\epsilon \rho K^2}{\epsilon}, \quad (16.93)$$

where  $C_\epsilon$  is an empirical constant. The transport equation for  $K$  is

$$\rho \frac{DK}{Dt} = \frac{1}{\sigma_K} \left\{ \frac{\partial}{\partial x} \left[ \eta_i \frac{\partial K}{\partial x} \right] + \frac{\partial}{\partial y} \left[ \eta_i \frac{\partial K}{\partial y} \right] + \frac{\partial}{\partial z} \left[ \eta_i \frac{\partial K}{\partial z} \right] \right\} + \eta_i G_K - \epsilon, \quad (16.94)$$

where  $\sigma_K$  is another empirical constant and  $\eta_i G_K$  is the turbulent counterpart to the viscous dissipation given in Eq. (A) of Table 7.5; i.e.,

$$\eta_i G_K = 2\eta_i \left\{ \left( \frac{\partial \bar{v}_x}{\partial x} \right)^2 + \left( \frac{\partial \bar{v}_y}{\partial y} \right)^2 + \left( \frac{\partial \bar{v}_z}{\partial z} \right)^2 \right\} + \left\{ \eta_i \left( \frac{\partial \bar{v}_x}{\partial y} + \frac{\partial \bar{v}_y}{\partial x} \right)^2 + \left( \frac{\partial \bar{v}_x}{\partial z} + \frac{\partial \bar{v}_z}{\partial x} \right)^2 + \left( \frac{\partial \bar{v}_y}{\partial z} + \frac{\partial \bar{v}_z}{\partial y} \right)^2 \right\}.$$

For laminar flows, we normally ignore viscous dissipation. With turbulent flows, however,  $\eta_i$  can be as much as 1000  $\eta$  so that the turbulent dissipation is kept in Eq. (16.94). The transport equation for  $\epsilon$  is

$$\rho \frac{D\epsilon}{Dt} = \frac{1}{\sigma_\epsilon} \left\{ \frac{\partial}{\partial x} \left[ \eta_i \frac{\partial \epsilon}{\partial x} \right] + \frac{\partial}{\partial y} \left[ \eta_i \frac{\partial \epsilon}{\partial y} \right] + \frac{\partial}{\partial z} \left[ \eta_i \frac{\partial \epsilon}{\partial z} \right] \right\} + \frac{\epsilon}{K} (C_1 G_K - C_2 \rho \epsilon), \quad (16.95)$$

where  $\sigma_\epsilon$ ,  $C_1$  and  $C_2$  are yet more empirical constants. For most turbulent flows Launder and Spalding recommend  $C_\epsilon = 0.09$ ,  $\sigma_\epsilon = 1.0$ ,  $\sigma_K = 1.3$ ,  $C_1 = 1.44$  and  $C_2 = 1.92$ . These values are normally selected or used as a starting point when calculated results are to be

<sup>6</sup>B. E. Launder and D. B. Spalding, *Comp. Meth. in Appl. Mech.*, 3, 269-289 (1974).

<sup>7</sup>We use  $K$  to avoid confusion with thermal conductivity,  $k$ .

compared to experiment. Equations (16.94) and (16.95), in conjunction with the components of the turbulent momentum equation, must all be solved simultaneously. The procedure is complex and requires an efficient computational scheme, such as that described by Gosman *et al.*<sup>8</sup> Furthermore, modifications to some of the constants used in determining  $K$  and  $\epsilon$  are required if axisymmetric jets or wakes are to be studied.<sup>9</sup>

Energy and mass transport can also be included by rewriting Eqs. (16.78) and (16.79) in the following forms:

$$q_y = -(k + k_t) \frac{\partial T}{\partial y} \quad (16.96)$$

and

$$j_{xy} = -(D_A + D_M) \frac{\partial C_A}{\partial y}, \quad (16.97)$$

where we show the fluxes in the  $y$ -direction as examples to introduce the *turbulent thermal conductivity*,  $k_t$ , and the *turbulent mass diffusivity*,  $D_M$ . After the turbulent viscosity is known, these quantities may be estimated<sup>10</sup> from

$$k_t = C_p \eta_i, \quad (16.98)$$

$$D_M = \frac{\eta_i}{\rho}, \quad (16.99)$$

where  $C_p$  is the heat capacity of the fluid.

Fortunately there are software packages for solution of fluid flow problems that include options for turbulence. Some of these are PHOENICS, FLUENT, TEACH-2E, and FIDAP. Numerous examples involving materials processing can be found in Szekely *et al.*<sup>10</sup> Here, we give Fig. 16.12 as an example of applying the  $K-\epsilon$  model to simulations of the temperature and velocity fields in the direct chill (DC) casting process for producing aluminum alloy ingots. The simulations were for a cylindrical ingot (550 mm diameter) of Al-4 wt. pct. Cu cast at a rate of 0.833 mm s<sup>-1</sup>. In Fig. 16.12a, the simulation was based upon using the conservation equations for laminar flow with no added terms to account for the effect of turbulence. In Fig. 16.12b, the  $K-\epsilon$  model was employed. Turbulence enhances thermal conduction so that the thermal gradients in the melt are lessened and the melt pool ("liquid sump") is less deep with a smoother profile. The latter is thought to be more realistic of the actual process.

<sup>8</sup>A. D. Gosman, W. M. Pun, A. K. Runchal, D. B. Spalding, and M. Wolfstein, *Heat and Mass Transfer in Recirculating Flows*, Academic Press, New York, 1969, pages 18-112.

<sup>9</sup>B. E. Launder and D. B. Spalding, *Ibid.*

<sup>10</sup>J. Szekely, J. W. Evans and J. K. Brimacombe, *The Mathematical and Physical Modelling of Primary Metals Processing Operations*, John Wiley & Sons, New York, 1988, pages 166-167.

<sup>10</sup>J. Szekely, J. W. Evans and J. K. Brimacombe, *Ibid.*

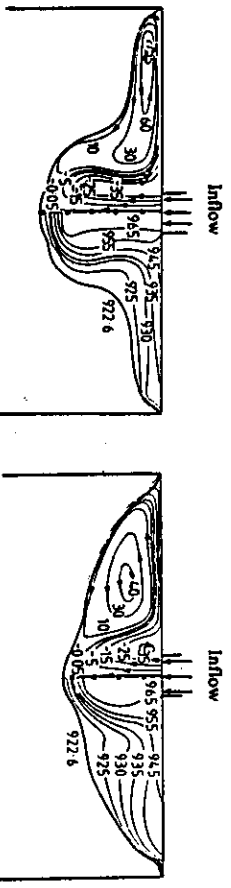


Fig. 16.12. Simulations of the temperature (right side) and streamlines (left side) in the liquid pool of a DC ingot: (a) modeled with laminar flow; (b) modeled with turbulent flow. (Adapted from S. C. Flood, L. Kagerman, A. H. Langille, S. Rogers and C. M. Read in *Light Metals 1989*, P. G. Campbell (editor), The Minerals, Metals and Materials Society, Warrendale, PA, pages 943-947.)

### 16.3 DISCRETIZATION IN CONVECTIVE FLOWS

In Section 16.1 we dealt exclusively with finite difference approximations of diffusive fluxes. It is worthwhile to also be acquainted with approximations of the convective terms in the conservation equations because there are some potential pitfalls. To keep our discussion simple we start with only two terms from the energy equation. From Eq. (A) in Table 7.4, we select one of the convective terms and one of the diffusive terms:

$$\rho C_p v_x \frac{dT}{dx} = \frac{d}{dx} \left[ k \frac{dT}{dx} \right], \quad (16.100)$$

where we have substituted the usual Fourier's rate law for the flux.

Consider three internal nodes shown in Fig. 16.13 for discretizing the temperature. An energy balance at steady state takes on the following terms:

$$(\rho C_p v_x)_L T_L + \left[ -k_L \frac{T_m - T_{m-1}}{\Delta x} \right] = (\rho C_p v_x)_R T_R + \left[ -k_R \frac{T_{m+1} - T_m}{\Delta x} \right], \quad (16.101)$$

where the subscripts *L* and *R* refer to properties and variables that are evaluated at the intermediate left (*L*) and right (*R*) positions shown in Fig. 16.13. Therefore,

$$T_L = \frac{T_m}{2} + \frac{T_{m-1}}{2},$$

and

$$T_R = \frac{T_{m+1}}{2} + \frac{T_m}{2}.$$

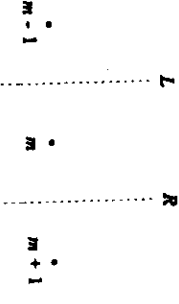


Fig. 16.13. Three internal nodes with left (*L*) and right (*R*) intermediate positions for averaging.

which give

$$\frac{(\rho C_p v_x)_L}{2} (T_m + T_{m-1}) - \frac{(\rho C_p v_x)_R}{2} (T_{m+1} + T_m) =$$

$$k_L \frac{(T_m - T_{m-1})}{\Delta x} - k_R \frac{(T_{m+1} - T_m)}{\Delta x}. \quad (16.102)$$

Next we collect terms for each of the three temperatures and get

$$a_m T_m = a_L T_{m-1} + a_R T_{m+1}, \quad (16.103)$$

where the coefficients are defined as

$$a_m = \frac{(\rho C_p v_x)_L}{2} - \frac{(\rho C_p v_x)_R}{2} - \frac{k_L}{\Delta x} - \frac{k_R}{\Delta x},$$

$$a_L = \frac{(\rho C_p v_x)_R}{2} - \frac{k_L}{\Delta x},$$

and

$$a_R = -\frac{(\rho C_p v_x)_L}{2} - \frac{k_R}{\Delta x}.$$

Equation (16.103) is perfectly adequate provided we realize that there are severe limitations on the grid spacing  $\Delta x$  in order to guarantee numerical stability. This is the potential pitfall because we have discretized a differential equation with an advective term by central differencing.

To illustrate the pitfall, remember that continuity requires

$$(\rho v_x)_R = (\rho v_x)_L.$$

Also let us assume  $k_L = k_R = k$  and  $(C_{p,R}) = (C_{p,L}) = C_p$ , then Eq. (16.103) becomes

$$-\frac{2k}{\Delta x} T_m = \left[ \frac{\rho C_p v_x}{2} - \frac{k}{\Delta x} \right] T_{m+1} + \left[ -\frac{\rho C_p v_x}{2} - \frac{k}{\Delta x} \right] T_{m-1}$$

or

$$4T_m = (2 - P)T_{m+1} + (2 + P)T_{m-1}, \quad (16.104)$$

where  $P = \rho C_p v_x \Delta x / k$ . The instability is associated with the coefficient  $(2 - P)$ . If we allow  $P > 2$ , we get a nonsensical result. This can be seen by a simple example. Suppose  $P = 4$ ,  $T_{m+1} = 100$  K, and  $T_{m-1} = 200$  K. A sensible result would give  $100 < T_m < 200$  K, but Eq. (16.103) gives  $T_m = 250$  K, which is clearly nonsensible. Suppose  $P = 1$ , and  $T_{m+1}$  and  $T_{m-1}$  are 100 K and 200 K, as before. Now Eq. (16.104) gives  $T_m = 175$  K, which is sensible. If we are willing to accept that  $P$  must be less than two, then our calculations will be stable, but this can severely restrict us because  $(v_x \Delta x) < 2\alpha$ . So either we restrict ourselves to situations with convective speeds that are rather small, or we must select  $\Delta x$  to be small and thereby sacrifice computational efficiency. This disadvantage in discretizing the equation with the central differencing scheme has led to the *upwind finite difference method*.

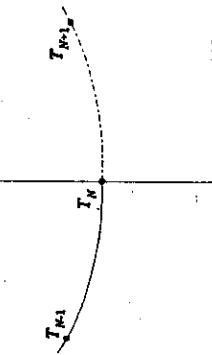
In the upwind method, we focus on the advection terms which form the left side (L.S.) of Eq. (16.102). To simplify our notation somewhat, let  $u = \rho C_p v_x$ . Then the L.S. is replaced<sup>11</sup> with

$$\begin{aligned} \text{L.S.} = \frac{1}{2} & \{ (u_L + |u_L|) T_{m+1} - (u_r - |u_R|) T_{m-1} \\ & - (u_R + |u_R| - u_L + |u_L|) T_m \}. \quad (16.105) \end{aligned}$$

The diffusion terms in Eq. (16.102) are evaluated with the usual central differencing so no change in the right side is needed. Equation (16.105) is based upon always evaluating the advected energy into or out of the unit element at the *upstream* node.

## PROBLEMS

- 16.1 Derive an alternative to Eq. (16.7) for an insulated surface, in a way which is different than that in the text. The insulated surface is at node  $N$ , and there is an imaginary node at  $N+1$  with the same temperature as  $T_{N-1}$ .



16.2 Use finite difference approximations and set up the one-dimensional heat conduction problem that is specified as follows:

$$\frac{\partial T}{\partial t} = \alpha \frac{\partial^2 T}{\partial x^2},$$

with

$$T(L,t) = T_L \quad t > 0,$$

$$T(0,t) = T_0 \quad t > 0,$$

and

$$T(x,0) = T_i.$$

Divide the domain  $0 \leq x \leq L$  into four segments so that  $\Delta x = L/4$ . a) Write the set of algebraic equations in matrix form using the Euler method. b) Repeat using the Crank-Nicolson method.

16.3 Write a computer program that can be used to solve for  $T(x,t)$  in Problem 16.2a.

16.4 Write a computer program that can be used to solve for  $T(x,t)$  in Problem 16.2b.

16.5 Consider the problem in Fig. 16.1 and the VAX-BASIC program for solving Eq. (16.31). Modify and use the program to solve for the time required for the center of the core to heat to 873 K, when molten aluminum encapsulates a plaster core. Thermal data can be found with the problems of Chapter 10.

16.6 Consider one-dimensional homogenization as in Section 13.5. The following microsegregation data in an Fe-Ni alloy are reported.

$x, \mu\text{m}$	% Ni	$x, \mu\text{m}$	% Ni	$x, \mu\text{m}$	% Ni
0	12	30	16	60	29
10	13	40	18.5	70	37
20	14	50	23	80	45

a) Plot the data and determine the average concentration of nickel.  
b) Set up the set of algebraic equations that result from making finite difference approximations. For simplicity, use  $\Delta x = 20 \mu\text{m}$  and the Euler method.

16.7 Extend the one-dimensional homogenization model of Problem 16.6 to the two-dimensional model considered in Section 16.1.3. For  $L = \ell = 80 \mu\text{m}$ , the following microsegregation data are given (see Fig. 16.7 for identification of the nodes).

Nodes	% Ni	Nodes	% Ni
0,15	14	5,10	16
1,11	23	6	29
2,7	37	8,13	13
3	45	9	14
4,14	13	12	12
		Average	20.25

<sup>11</sup>Equation (16.105) is from D. Pouliktas and S. Kimura in A. Bejan, *Convection Heat Transfer*, John Wiley & Sons, New York, 1984, pages 440-446.

- a) The diffusion coefficient for nickel in  $\gamma$ -iron at  $1273 \leq T \leq 1560$  K is

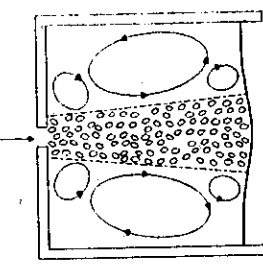
$$D = \exp(0.0519 X_{Ni} + 1.51) \exp\left[-\frac{38.380 + 5.85 X_{Ni}}{T}\right],$$

where  $D$  = diffusion coefficient,  $\text{cm}^2 \text{ s}^{-1}$ ;  $X_{Ni}$  = atom percent Ni;  $T$  = temperature, K. Calculate an appropriate diffusion coefficient for homogenizing the alloy at 1350 K.

- b) Determine the residual segregation index as a function of time for homogenization at 1350 K.

- 16.8 Consider radiant heating of a poorly conducting slab as described in Section 16.1.4. Using the same thermal properties and furnace temperature (2020 K), determine the time to heat the center to 2000 K as a function of the thickness of the slab, in the range of 30 mm to 90 mm.

- 16.9 Gas is injected into the bottom of a melt contained in a large cylindrical vessel; the recirculating flow is turbulent. Assume axisymmetric flow and write an appropriate momentum equation for the liquid.



## APPENDIX A

### Physical Constants

Quantity	Symbol	Value
Gas constant	$R$	$8.31441 \text{ J K}^{-1} \text{ mol}^{-1}$ $1.985857 \text{ Btu lbmol}^{-1} \text{ }^{\circ}\text{R}^{-1}$ $8.205 \times 10^{-2} \text{ m}^3 \text{ atm kmol}^{-1} \text{ K}^{-1}$
Boltzmann constant	$k_B$	$1.3807 \times 10^{-23} \text{ J K}^{-1} \text{ molecule}^{-1}$
Avogadro's number	$N_A$	$6.02204 \times 10^{23} \text{ molecules mol}^{-1}$ $6.02204 \times 10^{26} \text{ molecules kmol}^{-1}$
Planck constant	$\hbar$	$6.62618 \times 10^{-34} \text{ J s molecule}^{-1}$
Stefan-Boltzmann constant	$\sigma$	$5.6703 \times 10^{-8} \text{ W m}^{-2} \text{ K}^{-4}$ $0.1714 \times 10^{-8} \text{ Btu h}^{-1} \text{ ft}^{-2} \text{ }^{\circ}\text{R}^{-4}$
Gravitational acceleration at sea level	$g$	$9.80665 \text{ m s}^{-2}$ $32.174 \text{ ft s}^{-2}$
Standard atmospheric pressure	$P$	$1.01325 \times 10^5 \text{ N m}^{-2}$ $14.69595 \text{ lb in}^{-2} (\text{psi})$ $2116.22 \text{ lb ft}^{-2}$

## APPENDIX B

### Thermal Properties

The compilations given in Tables B.1-B.3 are only samplings of thermal data. More comprehensive sources for data are listed here.

1. Y. S. Touloukian and C. Y. Ho (eds.), *Thermophysical Properties of Matter*, IFI/Plenum, New York, NY.
  - Volume 1. Thermal Conductivity-Metallic Elements and Alloys (1970).
  - Volume 2. Thermal Conductivity-Nonmetallic Solids (1970).
  - Volume 3. Thermal Conductivity-Nonmetallic Liquids and Gases (1970).
  - Volume 4. Specific Heat-Metallic Elements and Alloys (1970).
  - Volume 5. Specific Heat-Nonmetallic Solids (1970).
  - Volume 6. Specific Heat-Nonmetallic Liquids and Gases (1970).
  - Volume 7. Thermal Radiative Properties-Metallic Elements and Alloys (1970).
  - Volume 8. Thermal Radiative Properties-Nonmetallic Solids (1972).
  - Volume 9. Thermal Radiative Properties-Coatings (1972).
  - Volume 10. Thermal Diffusivity (1973).
  - Volume 11. Viscosity (1975).
  - Volume 12. Thermal Expansion-Metallic Elements and Alloys (1975).
  - Volume 13. Thermal Expansion-Nonmetallic Solids (1977).
2. J. Brandrup and E. H. Immergut (eds.), *Polymer Handbook*, third edition, John Wiley, New York, NY (1989).
3. V. Shah, *Handbook of Plastics Testing Technology*, John Wiley, New York, NY (1984).
4. ASM International Handbook Committee, *Engineered Materials Handbook*, Metals Park, OH.
  - Volume 1. Composites (1987).
  - Volume 2. Engineering Plastics (1988).

**Table B.1 Thermal Properties of Selected Metallic Materials**

Material	Composition wt.pct.	$T$ K	$\rho$ $\text{kg m}^{-3}$	$C_p$ $\text{J kg}^{-1} \text{K}^{-1}$	$k$ $\text{W m}^{-1} \text{K}^{-1}$	$H_f$ $\text{J kg}^{-1}$
Aluminum	Al	300	2698	0.90	237	
		600	2636	1.04	232	
		933 (S)	2555	1.19	211	398
		933 (T)	2368	1.09	91	
		1200	2296	1.09	99	
P. D. Desai, R. K. Chu, R. H. Bogaard, M. W. Ackermann and C. Y. Ho, Part I: <i>Thermophysical Properties of Carbon Steels; Part II: Thermophysical Properties of Low Chromium Steels; Part III: Thermophysical Properties of Nickel Steels; Part IV: Thermophysical Properties of Stainless Steels</i> , CINDAS Special Report, Purdue University, West Lafayette, IN, September 1976.						
N. B. Vargaftik, <i>Tables of Thermophysical Properties of Liquids and Gases</i> , 2nd edition, Hemisphere Publishing Corp., New York, 1975.						
L. M. Sheppard and G. Geiger (eds.), <i>Ceramic Source</i> , vol. 6, The American Ceramic Society, Westerville, OH (1991).						
Brass	Cu-40Zn	300	8400	0.39	127	
		600	8240	0.42	158	
		900	8080	0.45	150	
		1356 (T)	8000	0.49	166	
		1600	7800	0.49	174	
Iron	Fe	300	7860	0.43	79.6	
		600	7780	0.58	54.6	
		900	7670	0.76	37.4	
		1033	7620	1.26 (max)	—	
		1040	7620	1.16	—	
		1184 (C)	7570	0.72	28.2	
		1184 (T)	7660	0.61	28.2	
		1400	7515	0.64	30.6	
		1673 (C)	7597	0.68	33.7	
		1673 (T)	7544	0.73	33.4	
		1809 (B)	7257	0.76	34.6	277
		1809 (T)	7022	0.79	40.3	
		2000	6866	0.79	42.6	
AISI 1026	Fe-0.23C-0.63Mn	300	7860	0.48	52.4	
		700	7730	0.61	41.2	
		1000	7645	0.84	29.7	
		1023	7640	1.44 (max)	28.6	
		1100 (T)	7620	0.64	25.9	
		1300	7550	0.64	27.8	
AISI 304	Fe-19Cr-10Ni	300	8260	0.50	15.2	
		600	8150	0.56	19.7	
		900	8030	0.65	24.0	
		1200	7890	0.65	27.9	
		1500	—	0.67	31.9	
Nickel	Ni	300	8900	0.44	89.2	
		600	8780	0.60	65.3	
		631	8770	0.67 (max)	63.8	
		702	8740	0.52	65.3	
		1728 (S)	(8280)	0.65	87.5	
		1728 (T)	7905	0.66	—	
		1900	7700	0.66	—	
MAR-M200	Ni-0.15C-9Cr-10Co-12.5W-1.8Cb-2Ti-5Al	300	8520	0.40	12.7	
		600	8430	0.42	14.0	
		900	8330	0.46	16.8	
		1200	8180	0.52	22.8	

\*Data collected from several sources.

Material	Pyrex glass	Amorphous	2520	4.6	$\beta$	Thermal Expansion ( $\text{kg m}^{-3}$ )	Density ( $\text{kg m}^{-3}$ )	Thermal Conductivity ( $\text{W m}^{-1} \text{K}^{-1}$ )	Specific Heat ( $\text{J g}^{-1} \text{K}^{-1}$ )	Emissivity
TiO <sub>2</sub>	Rutile tetragonal	Anatase tetragonal	4250	9.4	8.8 at 400 K	3.3 at 1400 K	0.799 at 400 K	0.920 at 1700 K	0.83 at 450 K (T)	0.75 at 1100 K (N)
Al <sub>2</sub> O <sub>3</sub>	Brookite orthorhombic	4170	3840	9.4	8.8 at 400 K	3.3 at 1400 K	0.799 at 400 K	0.920 at 1700 K	0.83 at 450 K (T)	0.75 at 1100 K (N)
C <sub>4</sub> O <sub>3</sub>	Hexagonal	3970	7.2-8.6	27.2 at 400 K	0.1088	5.8 at 1400 K	0.20 at 1273 K	0.75 at 100 K (N)	0.41 at 1600 K (N)	0.69 (N)
Mullite	Orthorhombic	2800	5.7	5.2 at 400 K	3.3 at 1400 K	0.1046	0.20 at 1200 K	0.87 at 1200 K (N)	0.53 at 1200 K (N)	0.65 at 1500 K (N)
Plasma-stabilized ZrO <sub>2</sub>	Cubic, monoclinic,	5560-6100	13.5	1.7 at 400 K	1.9 at 1600 K	0.502 at 400 K	0.669 at 2400 K	0.82 at 0 K (N)	0.4 at 1200 K	0.5 at 2000 K (N)
ZrO <sub>2</sub>	Cubic	5600-5700	7.6-10.5	0.69-2.4	0.69-2.4	1.9 at 1600 K	0.502 at 400 K	0.669 at 2400 K	0.4 at 1200 K (N)	0.5 at 2000 K (N)
Plasma-sprayed ZrO <sub>2</sub>	Cubic, monoclinic,	7280	13	9.6 at 400 K	1.2 at 1400 K	0.370 at 300 K	0.520 at 1200 K	0.65 at 1300 K (T)	0.25-0.4 at 700 K (T)	0.61-0.68 at 700 K (T)
CeO <sub>2</sub>	Cubic	5600-5700	7.6-10.5	0.69-2.4	0.69-2.4	1.9 at 1600 K	0.502 at 400 K	0.669 at 2400 K	0.4 at 1200 K (N)	0.5 at 2000 K (N)
TiB <sub>2</sub>	Hexagonal	4500-4620	8.1	6.5-12.2 at 300 K	0.632 at 300 K	0.1155 at 1400 K	0.1155 at 1366 K	0.8 at 1000 K (N)	0.85 at 1000 K (N)	0.8 at 2800 K (N)
TiC	Cubic	4920	7.4-8.6	3.3 at 400 K	0.544 at 293 K	0.43 at 1400 K	0.544 at 293 K	0.5 at 800 K (N)	0.4 at 1500 K	0.38 at 2800 K (N)
TiC <sub>2</sub>	Cubic	1440-1450	6.7	3.2 at 400 K	0.167 at 273 K	0.40 at 1400 K	0.167 at 273 K	0.2 at 1600 K (N)	0.33 at 3000 K (N)	0.28 at 4000 K (N)
SiC	a hexagonal	3210	4.3-5.6	6.3-15.5 at 400 K	0.628-0.1046	0.21-33 at 1400 K	0.628 at 273 K	0.837 at 811 K	0.502 at 273 K	0.23-0.4 at 1800 K (N)
SiC (CVD)	b cubic	3210	5.5	19	19	0.293 at 1366 K	0.293 at 1366 K	0.1464 at 2000 K	0.1464 at 1600 K	0.85 at 400 K (N)
Si <sub>3</sub> N <sub>4</sub>	cubic	3180	3.0	9.30 at 400 K	0.400-1.600	0.400 at 400 K	0.400 at 400 K	0.8 at 600 K (N)	0.8 at 1300 K (N)	0.9 at 600 K (N)
TiN	cubic	5430-5440	8.0	24 at 400 K	0.1046 at 1366 K	0.628 at 273 K	0.628 at 273 K	0.5 at 1100 K (N)	0.5 at 2100 K (N)	0.5 at 1400 K (N)
Graphites (with grain)	Hexagonal	2210	0.1-1.94	1.67-518.8	0.711-1.423	0.8 at 1366 K (T)	0.8 at 1366 K (T)	0.33 at 3000 K (N)	0.33 at 3000 K (N)	0.33 at 3000 K (N)

"N" is for normal, and T is for total hemispherical emissivity.  
From L. M. Shieppard and G. Geiger (eds.), *Ceramic Source*, Vol. 6, The American Ceramic Society, Westerville, OH, 1991, p. 345.

618 Appendix B  
Table B.3 Thermal Properties of Selected Polymers Used for Molding and Extrusion

Material	$\rho$ $\text{kg m}^{-3}$	$C_p$ $\text{kJ kg}^{-1} \text{K}^{-1}$	$k$ $\text{W m}^{-1} \text{K}^{-1}$	$\beta^*$ $10^{-3} \text{K}^{-1}$
Polyethylene				
low density	910-925	2.3	0.33	10-22
high density	940-965	2.3	0.46-0.50	11-13
Polypropylene	900-910	1.9	0.12	8.1-10
Polystyrene				
general purpose	1040-1050	1.3	0.10-0.14	6-8
impact resistant	1030-1060	1.3-1.5	0.042-0.13	3.4-21
Poly(methyl)methacrylate	1170-1200	1.5	0.17-0.25	5.9
Polyvinylchloride				
rigid	1300-1580	0.84-1.2	0.15-0.21	5-10
plasticized	1160-1350	1.3-2.1	0.13-0.17	7-25
ABS**	1030-1060	1.3-1.7	0.19-0.33	8-10
Cellulose acetate	1220-1340	0.17-0.33	8-18	
Fluoropolymers				
-CF <sub>2</sub> -CF <sub>2</sub> (teflon)	2140-2200	1.0	0.25	10
-CF <sub>2</sub> -CFCI-	2100-2200	0.92	0.20-0.22	4.5-7.0
Nylon-6,6	1130-1150	1.7	0.24	8
POLycarbonate	1200	2.2	0.20	6.8
Polyulfone	1240	1.3	0.12	5.2-5.6
Epoxy-glass composite	1600-2000	3.3	0.17-0.42	1-5

\* $\beta$  is linear expansion coefficient

\*\*Acrylonitrile-butadiene-styrene

Data selected from M. Chanda and S. K. Roy, *Plastics Technology Handbook*, Marcel Dekker, New York, NY, 1987, Appendix 3.

Table B.4 Thermophysical Properties of Gases at Atmospheric Pressure

$T$ (K)	$\rho$ $(\text{kg m}^{-3})$	$C_p$ $(\text{kJ kg}^{-1} \text{K}^{-1})$	$\eta \times 10^6$ $(\text{Ns m}^{-2})$	$v \times 10^6$ $(\text{m}^2 \text{s}^{-1})$	$k \times 10^3$ $(\text{W m}^{-1} \text{K}^{-1})$	$\alpha \times 10^6$ $(\text{m}^2 \text{s}^{-1})$	$\Pr$
Air							
300	1.1614	1.007	184.6	15.89	26.3	22.5	0.707
400	0.8711	1.014	230.1	26.41	33.8	38.3	0.690
500	0.6964	1.030	270.1	38.79	40.7	56.7	0.684
600	0.5804	1.051	305.8	52.69	46.9	76.9	0.685
700	0.4975	1.075	338.8	68.10	52.4	98.0	0.695
800	0.4354	1.099	369.8	84.93	57.3	120	0.709
900	0.3868	1.121	398.1	102.9	62.0	143	0.720
1000	0.3482	1.141	424.4	121.9	66.7	168	0.726
1200	0.2902	1.175	473.0	162.9	76.3	224	0.728
1400	0.2488	1.207	530	213	91	303	0.703
1600	0.2177	1.248	584	268	106	390	0.688
1800	0.1935	1.286	637	329	120	482	0.683
2000	0.1741	1.337	689	396	137	589	0.672
Carbon Dioxide (CO <sub>2</sub> )							
300	1.7730	0.851	149	8.40	16.55	11.0	0.766
400	1.3257	0.942	190	14.3	24.3	19.5	0.737
500	1.0594	1.02	231	21.8	32.5	30.1	0.725
600	0.8826	1.08	270	30.6	40.7	42.7	0.717
700	0.7564	1.13	305	40.3	48.1	56.3	0.717
800	0.6614	1.17	337	51.0	55.1	71.2	0.716
Carbon Monoxide (CO)							
300	1.1223	1.043	175	15.6	25.0	21.3	0.730
400	0.8421	1.049	218	25.9	31.8	36.0	0.719
500	0.6752	1.065	254	37.7	38.1	53.1	0.710
600	0.56126	1.088	286	51.0	44.0	72.1	0.707
700	0.48102	1.114	315	65.5	50.0	93.3	0.702
800	0.42095	1.140	343	81.5	55.5	116	0.705
Helium (He)							
300	0.1625	5.193	199	122	152	180	0.680
400	0.1219	5.193	243	199	187	295	0.675
500	0.09754	5.193	283	290	220	434	0.668
600	-	5.193	320	-	252	-	-
700	0.06969	5.193	350	502	278	768	0.654
800	-	5.193	382	-	304	-	-
900	-	5.193	414	-	330	-	-
1000	0.04879	5.193	446	914	354	1400	0.654
Water Vapor (steam)							
380	0.5863	2.060	127.1	21.68	24.6	20.4	1.06
400	0.5542	2.014	134.4	24.25	26.1	23.4	1.04
500	0.4405	1.985	170.4	38.68	33.9	38.8	0.998
600	0.3652	2.026	206.7	56.60	42.2	57.0	0.993
700	0.3140	2.085	242.6	77.26	50.5	77.1	1.00
800	0.2739	2.152	278.6	101.7	59.2	100	1.01

**Table B.4** Thermophysical Properties of Gases at Atmospheric Pressure\* (continued)

<i>T</i> (K)	$\rho$ (kg m <sup>-3</sup> )	$C_p$ (kJ kg <sup>-1</sup> K <sup>-1</sup> )	$\eta \times 10^6$ (N s m <sup>-2</sup> )	$\nu \times 10^6$ (m <sup>2</sup> s <sup>-1</sup> )	$k \times 10^3$ (W m <sup>-1</sup> K <sup>-1</sup> )	$\alpha \times 10^6$ (m <sup>2</sup> s <sup>-1</sup> )	<i>P<sub>r</sub></i>
<b>Hydrogen (H<sub>2</sub>)</b>							
300	0.08078	14.31	89.6	111	183	158	0.701
400	0.06059	14.48	108.2	179	226	258	0.695
500	0.04848	14.52	126.4	261	266	378	0.691
600	0.04040	14.55	142.4	352	305	519	0.678
700	0.03643	14.61	157.8	456	342	676	0.675
800	0.03030	14.70	172.4	569	378	849	0.670
900	0.02694	14.83	186.5	692	412	1030	0.671
1000	0.02424	14.99	201.3	830	448	1230	0.673
1100	0.02204	15.17	213.0	966	488	1460	0.662
1200	0.02020	15.37	226.2	1120	528	1700	0.659
1300	0.01865	15.59	238.5	1279	568	1955	0.655
1400	0.01732	15.81	250.7	1447	610	2230	0.650
1500	0.01616	16.02	262.7	1626	655	2530	0.643
1600	0.0152	16.28	273.7	1801	697	2815	0.639
1700	0.0143	16.58	284.9	1992	742	3130	0.637
1800	0.0135	16.96	296.1	2193	786	3435	0.639
1900	0.0128	17.49	307.2	2400	835	3730	0.643
2000	0.0121	18.25	318.2	2630	878	3975	0.661
<b>Nitrogen (N<sub>2</sub>)</b>							
300	1.1233	1.041	178.2	15.86	25.9	22.1	0.716
400	0.8425	1.045	220.4	26.16	32.7	37.1	0.704
500	0.6739	1.056	257.7	38.24	38.9	54.7	0.700
600	0.5615	1.075	290.8	51.79	44.6	73.9	0.701
700	0.4812	1.098	321.0	66.71	49.9	94.4	0.706
800	0.4211	1.122	349.1	82.90	54.8	116	0.715
900	0.3743	1.146	375.3	100.3	59.7	139	0.721
1000	0.3368	1.167	399.9	118.7	64.7	165	0.721
1100	0.3062	1.187	423.2	138.2	70.0	193	0.718
1200	0.2807	1.204	445.3	158.6	75.8	224	0.707
1300	0.2591	1.219	466.2	179.9	81.0	256	0.701
<b>Oxygen (O<sub>2</sub>)</b>							
300	1.284	0.920	207.2	16.14	26.8	22.7	0.711
400	0.9620	0.942	258.2	26.84	33.0	36.4	0.737
500	0.7698	0.972	303.3	39.40	41.2	55.1	0.716
600	0.6414	1.003	343.7	53.59	47.3	73.5	0.729
700	0.5498	1.031	380.8	69.26	52.8	93.1	0.744
800	0.4810	1.054	415.2	86.32	58.9	116	0.743
900	0.4275	1.074	447.2	104.6	64.9	141	0.740
1000	0.3848	1.090	477.0	124.0	71.0	169	0.733
1100	0.3498	1.103	505.5	144.5	75.8	196	0.736
1200	0.3206	1.115	532.5	166.1	81.9	229	0.725
1300	0.2960	1.125	588.4	188.6	87.1	262	0.721

\*Condensation of Table A.4 in F. P. Incropera and D. P. Dewitt, *Fundamentals of Heat and Mass Transfer*, 3rd edition, John Wiley, New York, NY, 1990.

## APPENDIX C Conversion Factors

**Table C.1** Linear measure equivalents

Multiply by value in table to obtain these units →	kilometer (km)	meter (m)	centimeter (cm)	millimeter (mm)	micrometer (μm)	angstrom (Å)	foot (ft)	inch (in)
Given in these units ↓								
kilometer (km)	1	$10^3$	$10^5$	$10^6$	$10^9$	$10^{13}$	$3.2808 \times 10^3$	$3.937 \times 10^4$
meter (m)	$10^{-3}$	1	$10^{-2}$	$10^3$	$10^6$	$10^{10}$	3.2808	$3.937 \times 10^1$
centimeter (cm)	$10^{-5}$	$10^{-2}$	1	10	$10^4$	$10^8$	$3.2808 \times 10^{-2}$	$3.937 \times 10^{-1}$
millimeter (mm)	$10^{-6}$	$10^{-3}$	$10^{-1}$	1	$10^3$	$10^7$	$3.2808 \times 10^{-3}$	$3.937 \times 10^{-2}$
micrometer (μm)	$10^{-9}$	$10^{-6}$	$10^{-4}$	$10^{-3}$	1	$10^4$	$3.2808 \times 10^{-6}$	$3.937 \times 10^{-5}$
angstrom (Å)	$10^{-13}$	$10^{-10}$	$10^{-8}$	$10^{-7}$	$10^{-4}$	1	$3.2808 \times 10^{-10}$	$3.937 \times 10^{-9}$
foot (ft)	$3.048 \times 10^{-4}$	$3.048 \times 10^{-1}$	30.48	$3.048 \times 10^2$	$3.048 \times 10^5$	$3.048 \times 10^9$	1	12
inch (in)	$2.54 \times 10^{-5}$	$2.54 \times 10^{-2}$	2.54	25.4	$2.54 \times 10^4$	$2.54 \times 10^8$	$8.333 \times 10^{-2}$	1

**Table C.2** Volume equivalents

Multiply by value in table to obtain these units →	cubic centimeter (cm <sup>3</sup> )	cubic feet (ft <sup>3</sup> )	cubic inch (in <sup>3</sup> )	cubic meter (m <sup>3</sup> )	gallons (U.S.) (gal)	liters (L)
Given in these units ↓						
cubic centimeter (cm <sup>3</sup> )	1	$3.531 \times 10^{-5}$	$6.102 \times 10^{-2}$	$10^{-6}$	$2.642 \times 10^{-4}$	$10^{-3}$
cubic feet (ft <sup>3</sup> )	$2.832 \times 10^4$	1	$1.728 \times 10^3$	$2.832 \times 10^{-2}$	7.481	28.32
cubic inch (in <sup>3</sup> )	16.39	$5.787 \times 10^{-4}$	1	$1.639 \times 10^{-5}$	$4.329 \times 10^{-3}$	$1.639 \times 10^{-2}$
cubic meter (m <sup>3</sup> )	$10^6$	35.31	$6.102 \times 10^4$	1	$2.642 \times 10^3$	$10^3$
gallons (U.S.) (gal)	$3.785 \times 10^3$	$1.337 \times 10^{-1}$	$2.31 \times 10^2$	$3.785 \times 10^{-3}$	1	3.785
liters (L)	$10^3$	$3.531 \times 10^{-2}$	$6.102 \times 10^1$	$10^{-3}$	$2.642 \times 10^{-1}$	1

Multiply by value in table to obtain these units →	Given in these units ↓	gram (g)	Kilogram (kg)	Pound (lb.)	Ton, long	Ton, short	Ounces (oz)	Tonne (t)	metric
1	$10^3$	$2.205 \times 10^{-3}$	$9.84 \times 10^{-7}$	$1.102 \times 10^{-4}$	$3.527 \times 10^{-2}$	$10^{-4}$			
$10^6$	1	2.205	$9.84 \times 10^{-4}$	$1.102 \times 10^{-3}$	$3.527$	$10^{-3}$			
$4.536 \times 10^2$	0.4536	1	$4.464 \times 10^{-4}$	$5.0 \times 10^{-4}$	16	$4.938 \times 10^{-1}$	1.016	ton, long	
$1.016 \times 10^6$	$1.016 \times 10^6$	$2.24 \times 10^6$	$2.00 \times 10^6$	$8.929 \times 10^6$	1	$3.20 \times 10^6$	0.9074	ton, short	
ounces (oz)	28.35	$2.835 \times 10^{-2}$	$6.25 \times 10^{-2}$	$2.79 \times 10^{-3}$	$3.125 \times 10^{-3}$	1	$1.877 \times 10^{-5}$	tonne (t)	
tonnes (t)	$10^6$	$10^6$	$2.205 \times 10^6$	$9.842 \times 10^5$	$1.102$	$3.527 \times 10^6$	1	tonne (t)	

Multiply by value in table to obtain these units →	Given in these units ↓	g cm <sup>-3</sup>	kg m <sup>-3</sup>	lb. ft <sup>-3</sup>	lb. in <sup>-3</sup>	These units ↓	Given in these units →	g cm <sup>-3</sup>	kg m <sup>-3</sup>	lb. ft <sup>-3</sup>	lb. in <sup>-3</sup>
$g\text{ cm}^{-3}$	1	$10^3$	$10^3$	$62.43$	$3.613 \times 10^{-2}$						
$\text{g L}^{-1}$	$10^{-3}$	1	$10^3$	$6.243 \times 10^{-2}$	$3.613 \times 10^{-3}$						
$\text{kg m}^{-3}$	$10^{-3}$	1	1	$6.243 \times 10^{-2}$	$3.613 \times 10^{-3}$						
$\text{lb. ft}^{-3}$	$1.602 \times 10^{-3}$	$16.02$	1	$6.243 \times 10^{-2}$	$3.613 \times 10^{-3}$						
$\text{lb. in}^{-3}$	27.68	$2.768 \times 10^6$	$2.768 \times 10^6$	$1.728 \times 10^6$	1						

Table C.5 Force equivalents

Multiply by value in table to obtain these units →	Given in these units ↓	dyne (g cm s <sup>-2</sup> )	Newton, N (kg m s <sup>-2</sup> )	Poundal (lb s <sup>-2</sup> )	Pound force (lb.)	Pound force (lb.)
$\text{dyne (g cm s}^{-2}\text{)}$	1	$10^3$	$7.233 \times 10^{-3}$	$2.248 \times 10^{-6}$		
$\text{Newton, N (kg m s}^{-2}\text{)}$	$10^6$	1	$1.3826 \times 10^{-1}$	1	$3.108 \times 10^{-2}$	
$\text{Poundal (lb. ft s}^{-2}\text{)}$	$1.3826 \times 10^4$	$1.3826 \times 10^4$	1	$3.108 \times 10^{-1}$		
$\text{Poundal (lb.)}$	$4.448 \times 10^4$	$4.448$	$32.17$	1		

**Table C.6 Energy equivalents**

Multiply by value in table to obtain these units →	Btu	cal	erg	ft lb <sub>f</sub>	hp h <sup>*</sup>	joule, J	kcal	kW h	L atm
Given in these units ↓									
Btu	1	$2.52 \times 10^2$	$1.055 \times 10^6$	$7.7816 \times 10^3$	$3.93 \times 10^{-4}$	$1.055 \times 10^3$	$2.520 \times 10^{-1}$	$2.93 \times 10^{-4}$	10.41
cal	$3.97 \times 10^{-3}$	1	$4.184 \times 10^3$	3.086	$1.558 \times 10^{-4}$	4.184	$10^{-3}$	$1.162 \times 10^{-6}$	$4.129 \times 10^{-1}$
erg	$9.478 \times 10^{-11}$	$2.39 \times 10^{-8}$	1	$4.376 \times 10^{-8}$	$3.725 \times 10^{-14}$	$10^{-7}$	$2.39 \times 10^{-11}$	$2.773 \times 10^{-14}$	$9.869 \times 10^{-18}$
ft lb <sub>f</sub>	$1.285 \times 10^{-3}$	$3.241 \times 10^{-1}$	$1.356 \times 10^7$	1	$5.0505 \times 10^{-7}$	1.356	$3.241 \times 10^{-4}$	$3.766 \times 10^{-7}$	$1.338 \times 10^{-2}$
hp h <sup>*</sup>	$2.545 \times 10^3$	$6.4162 \times 10^3$	$2.6843 \times 10^3$	$1.98 \times 10^6$	1	$2.6845 \times 10^3$	$6.4162 \times 10^3$	$7.455 \times 10^{-1}$	$2.6494 \times 10^4$
joule, J	$9.478 \times 10^{-4}$	$2.39 \times 10^{-1}$	$10^7$	$7.376 \times 10^{-1}$	$3.725 \times 10^{-7}$	1	$2.39 \times 10^{-4}$	$2.773 \times 10^{-1}$	$9.869 \times 10^{-3}$
kcal	3.9657	$10^3$	$4.184 \times 10^6$	$3.086 \times 10^3$	$1.558 \times 10^{-3}$	$4.184 \times 10^3$	1	$1.162 \times 10^{-3}$	41.29
kW h	$3.4128 \times 10^3$	$8.6057 \times 10^3$	$3.6 \times 10^{13}$	$2.655 \times 10^6$	1.341	$3.6 \times 10^6$	$8.6057 \times 10^3$	1	$3.5534 \times 10^4$
L atm	$9.604 \times 10^{-2}$	24.218	$1.0133 \times 10^6$	74.73	$3.774 \times 10^{-3}$	$1.0133 \times 10^2$	$2.422 \times 10^{-2}$	$2.815 \times 10^{-3}$	1

\*hp h is horsepower hour.

**Table C.7 Pressure equivalents**

Multiple by value in table to obtain these units →	atmosphere (atm)	bar	lb <sub>f</sub> ft <sup>-2</sup>	lb <sub>f</sub> in <sup>-2</sup>	N m <sup>-2</sup> (Pascal, Pa)	Column of Hg at 0°C		Column of H <sub>2</sub> O at 15°C	
						in	mm	ft	mm
atmosphere (atm)	1	1.0133	$2.1162 \times 10^3$	14.696	$1.0133 \times 10^3$	$2.992 \times 10^4$	$7.60 \times 10^3$	33.93	$1.0342 \times 10^4$
bar	0.9869	1	$2.0886 \times 10^3$	14.503	$1 \times 10^3$	$2.9529 \times 10^4$	$7.5002 \times 10^3$	33.48	$1.0206 \times 10^4$
lb <sub>f</sub> ft <sup>-2</sup>	$4.7252 \times 10^{-4}$	$4.7879 \times 10^{-4}$	1	$6.9444 \times 10^{-3}$	$4.7879 \times 10^3$	$1.414 \times 10^{-2}$	$3.591 \times 10^{-1}$	$1.603 \times 10^{-2}$	4.887
lb <sub>f</sub> in <sup>-2</sup>	$6.8043 \times 10^{-3}$	$6.8946 \times 10^{-2}$	144	1	$6.8944 \times 10^3$	2.036	$5.171 \times 10^3$	2.309	$7.0378 \times 10^3$
N m <sup>-2</sup> (Pascal, Pa)	$9.8687 \times 10^4$	$1 \times 10^3$	$2.0886 \times 10^2$	$1.4504 \times 10^4$	1	$2.9529 \times 10^4$	$7.5002 \times 10^3$	$3.3458 \times 10^{-4}$	$1.0198 \times 10^1$
Hg column, in	$3.3421 \times 10^{-2}$	$3.3866 \times 10^{-2}$	$7.0726 \times 10^1$	$4.9124 \times 10^{-1}$	$3.3864 \times 10^3$	1	$2.54 \times 10^1$	1.134	$3.456 \times 10^2$
Hg column, mm	$1.3158 \times 10^{-3}$	$1.3333 \times 10^{-3}$	2.7845	$1.934 \times 10^{-2}$	$1.3332 \times 10^2$	$3.937 \times 10^{-1}$	1	$4.464 \times 10^{-2}$	13.61
H <sub>2</sub> O column, ft	$2.947 \times 10^{-2}$	$2.986 \times 10^{-2}$	62.372	$4.3314 \times 10^{-1}$	$2.9888 \times 10^3$	$8.819 \times 10^{-1}$	22.4	1	$3.048 \times 10^2$
H <sub>2</sub> O column, mm	$9.669 \times 10^{-3}$	$9.797 \times 10^{-3}$	2.046	$1.421 \times 10^{-3}$	9.806	$2.893 \times 10^{-3}$	$7.349 \times 10^{-2}$	$3.281 \times 10^{-3}$	1

Multiply by value in table to obtain these units →	Given in these units ↓	centipoise (CP)	$\text{g cm}^{-1}\text{s}^{-1}$	$\text{lb}_m\text{ ft}^{-1}\text{hr}^{-1}$	$\text{lb}_y\text{ s ft}^{-2}$	$\text{N s m}^{-2}$
centipoise (CP)	1	$6.7197 \times 10^{-4}$	$2.4191$	$2.0886 \times 10^{-5}$	$10^3$	
$\text{g cm}^{-1}\text{s}^{-1}$	$10^3$	$10^{-2}$	$6.7197 \times 10^{-4}$	$2.4191 \times 10^{-5}$	$2.0886 \times 10^{-2}$	$0.1$
(poise, P)				$6.7197 \times 10^{-2}$	$2.4191 \times 10^{-2}$	$2.0886 \times 10^{-3}$
$\text{lb}_m\text{ ft}^{-1}\text{hr}^{-1}$	$4.1338 \times 10^{-1}$	$4.1338 \times 10^{-3}$	$2.7778 \times 10^{-4}$	$1$	$8.6336 \times 10^{-6}$	$4.1338 \times 10^{-4}$
$\text{lb}_y\text{ s ft}^{-2}$	$4.788 \times 10^0$	$4.788 \times 10^0$	$32.174$	$1.1583 \times 10^5$	$1$	$4.7879 \times 10^0$
$\text{lb}_m\text{ ft}^{-1}\text{hr}^{-1}$	$1.4882 \times 10^0$	$14.882$	$1$	$3.6 \times 10^0$	$3.1081 \times 10^{-2}$	$1.4882$
$\text{lb}_y\text{ s ft}^{-2}$						
$\text{N s m}^{-2}$	$10^0$	$10$	$6.7197 \times 10^{-1}$	$2.4191$	$2.0886 \times 10^{-2}$	$1$

Multiply by value in table to obtain these units →	Given in these units ↓	$\text{Btu hr}^{-1}\text{ft}^{-1}\text{opF}^{-1}$	$\text{cal s}^{-1}\text{cm}^{-1}\text{K}^{-1}$	$\text{erg s}^{-1}\text{cm}^{-1}\text{K}^{-1}$	$\text{W m}^{-1}\text{K}^{-1}$
$\text{Btu hr}^{-1}\text{ft}^{-1}\text{opF}^{-1}$	1	$4.1365 \times 10^{-3}$	$1.7307 \times 10^0$	$1.7307$	$1.7307$
$\text{cal s}^{-1}\text{cm}^{-1}\text{K}^{-1}$	$2.4175 \times 10^0$	1	$4.1840 \times 10^7$	$4.1840 \times 10^0$	
$\text{erg s}^{-1}\text{cm}^{-1}\text{K}^{-1}$	$5.7780 \times 10^0$	$2.3901 \times 10^{-4}$	1	$10^{-3}$	
$\text{W m}^{-1}\text{K}^{-1}$	$5.7780 \times 10^{-1}$	$2.3901 \times 10^{-3}$	$10^0$	$10^0$	1

Table C.10 Diffusivity equivalents

Multiply by value in table to obtain these units →	Given in these units ↓	$\text{cm}^2\text{s}^{-1}$	$\text{ft}^2\text{hr}^{-1}$	$\text{m}^2\text{s}^{-1}$
$\text{cm}^2\text{s}^{-1}$	1	$3.8750$	$10^{-4}$	$3.8750 \times 10^0$
$\text{ft}^2\text{hr}^{-1}$	$2.5807 \times 10^{-1}$	1	$2.5807 \times 10^{-3}$	
$\text{m}^2\text{s}^{-1}$	$3.8750$	$10^{-4}$	$10^{-4}$	1

## APPENDIX D

### Description of Particulate Materials

In materials processing there are instances when the material is present as a collection of particles. Properties of the individual particles and more often the properties of the aggregate of all the particles must be measured and ultimately related to the transport of momentum, energy and mass. Metals, ceramics and polymers may all be produced in particulate form by crushing, grinding, precipitation, attrition, spraying, or atomization. The correlation of particulate behavior, either alone or in fluid-solid situations, has not been easy to accomplish because of the difficulty in establishing meaningful parameters describing size, size distribution, shape, and surface characterization. For most engineering purposes, the use of the mean particle diameter has sufficed, but first the particle sizes in a powder have to be measured.

#### Measurement Methods

**Sieving:** The use of sieves is widely used and is the most reliable method for particles greater than 30  $\mu$ m. Various sequences of screen apertures are available; most screen apertures are square. The sequence of openings is usually a geometric progression. If the edge length of a square opening is increased by  $\sqrt{2}$ , the area of the opening is doubled. This is the basis for the U.S. Sieve Series, for which the base is a 1 mm opening (no. 18 screen). The Tyler Series is based on the opening in a 200 mesh sieve, 74  $\mu$ m, or 0.029 inch. The openings and corresponding screen designations for those and four other common screen series are given in Table D.1.

**Elutriation:** By passing air through a bed of particles at various velocities, material of various sizes can be elutriated from the bed and collected separately.<sup>1</sup> The result is separations by weight fraction of the original sample carried off at various air velocities. Then, using Stokes' law for spherical particles, and solving for diameter, the weight fraction

<sup>1</sup>P. S. Roller, *ASTM Bull.* 37, 607 (1932).

Table D.1 Wire mesh sieve series

Mesh number	Aperture dimension, in					AFNOR
	U.S. Std.	Tyler Std.	British Std.	IMM	DIN	
1					0.197	0.197
1½					0.1575	0.1575
2	0.315	0.312			0.118	0.124
2½	0.265	0.263			0.0985	0.0985
3	0.223	0.221			0.0786	0.0786
3½	0.187	0.185				
4	0.157	0.156	0.1320	0.100	0.059	0.063
5	0.132	0.131	0.1107		0.0472	0.0492
6	0.111	0.110	0.0949		0.0394	0.0394
7	0.0937	0.093	0.0810	0.062	0.0295	0.0315
8						
9						
10	0.0787	0.065	0.0660	0.050	0.0236	0.0248
12	0.0661	0.055	0.0553	0.0416	0.0197	0.0197
14	0.0555	0.046	0.0474			
16	0.0469	0.039	0.0395	0.0312	0.01695	
18	0.0394		0.0336		0.01575	
20	0.0331	0.0288		0.025	0.0118	0.0124
22						
24						
25	0.0280	0.0276	0.0275	0.020	0.00985	0.00985
28						
30	0.0232	0.0232	0.0236	0.0197	0.0166	
32						
35	0.0197	0.0164	0.0164	0.0142		
36						
40	0.0165	0.0166	0.0166	0.0125	0.0059	0.0063
42						
44	0.0138	0.0138	0.0136			
45	0.0138					
48						
50	0.0117	0.0116				
52						
60	0.0098	0.0097	0.0116	0.0070	0.00472	0.00492
65			0.0099		0.0083	0.00394
70	0.0083	0.0082	0.0083	0.0071	0.00354	0.00394
72						
80	0.0070	0.0069	0.0083	0.0062	0.00295	0.00315
85						
90						
100	0.0059	0.0058	0.0060	0.0055	0.00236	0.00248
115		0.0049		0.0050		
120						
140	0.0041		0.0049	0.0042		
150						
170	0.0035	0.0041	0.0041	0.0033		
200	0.0029	0.0035	0.0035	0.0030	0.0025	
230	0.0024					
240						
250						
270	0.0021	0.0021	0.0024	0.0026		
300						
325	0.0017	0.0017	0.0017	0.0021		
400					0.0015	

Notes: IMM is Institution of Mining and Metallurgy (British), DIN is the German standard, and AFNOR is the French standard.

$$\omega = \frac{\text{volume of voids}}{\text{bulk density of the porous medium} + \text{true density of the solid material}} \quad (\text{D.1})$$

or

$$\omega = 1 - \frac{\text{volume of voids} + \text{volume of solids}}{\text{bulk density of the porous medium}}$$

The closest possible packing of equal-size spheres gives  $\omega = 0.259$ . This is rarely achieved in practice, since most materials are at least somewhat irregular in shape and exhibit a relatively high degree of friction between particles. Typical values of  $\omega$  lie between 0.35 and 0.5 in a loosely packed medium. In most instances, we must measure  $\omega$  *in situ*, using Eq. (D.1).

Since there are voids in the packing of equal-size spheres, small particles may enter without changing the overall volume of the bed, so clearly, the size distribution of the particles has an effect on the bulk density of the bed. Furas<sup>2</sup> made some classical studies on the void fractions in packed beds, using binary mixtures of particles (two different sizes) in various proportions. He started, in each case, with materials with the same initial (single component) voidages  $\omega^0$ , mixed them, and measured  $\omega$  for the mixture. Figure D.1 shows his results for  $\omega^0 = 0.5$ . It is clear that, as the difference in the particle size increases, lower and lower  $\omega$  values are obtainable, with minimum voidages occurring in the range 55–67 wt% of the larger-size material. Essentially, the same range for minimum voidages is found when  $\omega^0 = 0.6$  and 0.4.

Furas also made calculations of the *minimum* void fractions for three- and four-component mixtures of particles in which each component *alone* exhibits the same voidage. If the coarse and fine particles in a binary mixture are of *equal particle density and equal initial voidage*, then when the voids,  $\omega$ , in the coarse material are saturated with fines, the volume fraction of coarse material is  $1/(1+\omega)$ , and the amount of fine material is  $1 - [1/(1+\omega)]$ . A third, still smaller, component can then be added to the binary mixture, filling the interstices of the second component, etc. The *total volume fraction* of solids in the mixture is then

$$(1 - \omega_n) = \frac{1}{1+\omega} + \left[ 1 - \frac{1}{1+\omega} \right] + \left[ 1 - \frac{1}{1+\omega} \right]^2 + \dots$$

White and Walton,<sup>3</sup> who used geometric considerations and assumed close packing of spheres, computed the number and size of particles needed to fill interspaces in the packing with each addition of a smaller component. This led to a reduction in the overall void fraction as smaller particles are added. With an ideal five-component mixture, the voidage is 0.149, decreased from the initial 0.259. Table D.2 indicates some of the results of their calculations. Experience with foundry sands indicates that this approach, although idealized, is useful.

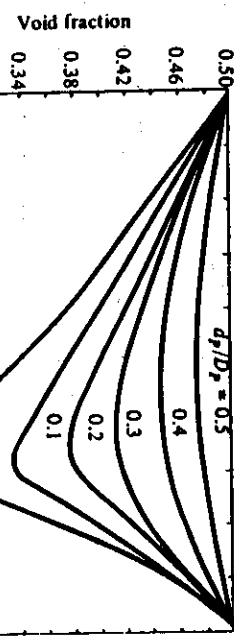


Fig. D.1 Experimental voidage of two-component particle mixtures, both having initial void fractions

of 0.5. The numbers on the curves refer to the ratio of the particle diameters. (From Furnas, *ibid.*)

which simplifies to

$$(1 - \omega) = \frac{1}{1 + \omega} + \frac{\omega}{1 + \omega} + \frac{\omega^2}{1 + \omega} + \dots + \frac{\omega^n}{1 + \omega}. \quad (\text{D.2})$$

When each term in Eq. (D.2) is multiplied by  $100/(1 - \omega)$ , the result is the percentage of each component in a mixture which will produce the minimum voids. Figure D.2 illustrates the results obtained by Furnas for two samples of mixtures with all initial components having  $\omega = 0.4$  and  $0.6$ , respectively. It should be emphasized that Figs. D.1 and D.2 refer only to minimum voids.

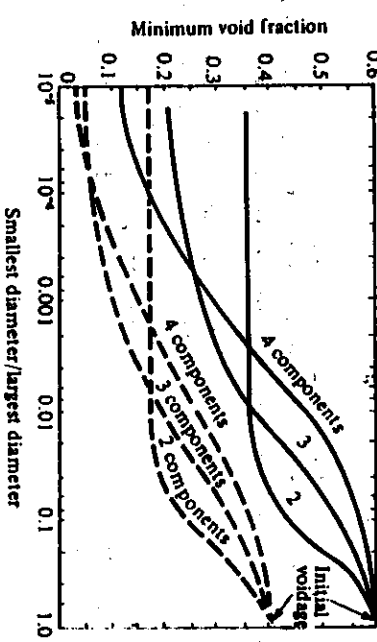


Fig. D.2 Calculated minimum voidage in two-, three-, and four-component particle mixtures. (From Furnas, *ibid.*)

Table D.2 Effect of size gradations on properties of a rhombohedral packing. (From White and Walton, *ibid.*)

Property	Mixture with:				
	Primary	Secondary	Tertiary	Quaternary	Quinary
Diameter	$d$	$0.414d$	$0.225d$	$0.177d$	$0.116d$
Relative number	1	2	8	8	8
Volume of space	$0.524d^3$	$0.037d^3$	$0.006d^3$	$0.0026d^3$	$0.0008d^3$
Volume of spheres added	$0.524d^3$	$0.037d^3$	$0.012d^3$	$0.0021d^3$	$0.0006d^3$
Total solid volume of spheres added	$0.524d^3$	$0.561d^3$	$0.573d^3$	$0.595d^3$	$0.602d^3$
Fractional voids in mixtures	0.2595	0.207	0.190	0.158	0.149
Weight of spheres in final mixture, %	77.08	5.47	1.75	3.31	0.97
Total surface area of spheres in mixture	$3.14d^2$	$3.68d^2$	$4.00d^2$	$4.77d^2$	$5.11d^2$

## APPENDIX E

### Flow Measurement Instruments

#### Area meters

The flow meters discussed in Chapter 4 are based on the principle of placing a restriction on the flowing stream, creating a pressure drop and a corresponding change in flow velocity through the restricted flow area. However, in area meters the pressure drop stays constant and the flow area changes as the velocity changes, rather than *vice versa*. The most common type of area meter—called a rotameter—is illustrated in Fig. E.1. The flow is read by measuring the height of a float in the *slightly tapered column*.

A force balance applied to the float determines the equilibrium position. When a fluid of density  $\rho$  moves past the float and maintains it in suspension, we can use the same force balance that was used several times in Chapters 2 and 3 for particle dynamics. The net buoyant weight of the float is balanced by the upward force created by the moving fluid. This is expressed as

$$(\rho_f - \rho) \frac{m_f}{\rho_f} g = F_k \quad (E.1)$$

where  $m_f$  is the mass of the float, and  $\rho_f$  is the float density.

For a given meter through which a given fluid flows, the left side of Eq. (E.1) is constant and independent of flow rate. Accordingly,  $F_k$  is constant when the float is at equilibrium, and, if the flow rate changes, then the float counters the effect of this change by taking on a new equilibrium position. For example, if the float is at some equilibrium position corresponding to some mass flow rate and then the mass flow rate increases,  $F_k$  becomes larger, and the float rises. However, as the float rises, the tapered tube presents a larger cross-sectional area for flow, and the velocity of the fluid between the float and the tube wall decreases, so that a new equilibrium position is eventually reached, where  $F_k$  returns to the value expressed by Eq. (E.1).

where  $W$  = mass flow rate,  $D_f$  = characteristic diameter of float, and  $D_i$  = diameter of the tube.

The ratio  $D_f/D_i$ , of course, is directly related to the meter reading  $h$ , so that Eq. (E.2) does show the general form  $W = W(h)$ . Equation (E.2) is important because it indicates how the same set of curves generated to fit its functional relationship can be used for all fluids. Thus, if one intends to utilize a rotameter for many different fluids (for example, as a laboratory item), one should know enough characteristics of the rotameter to be able to make it completely versatile.

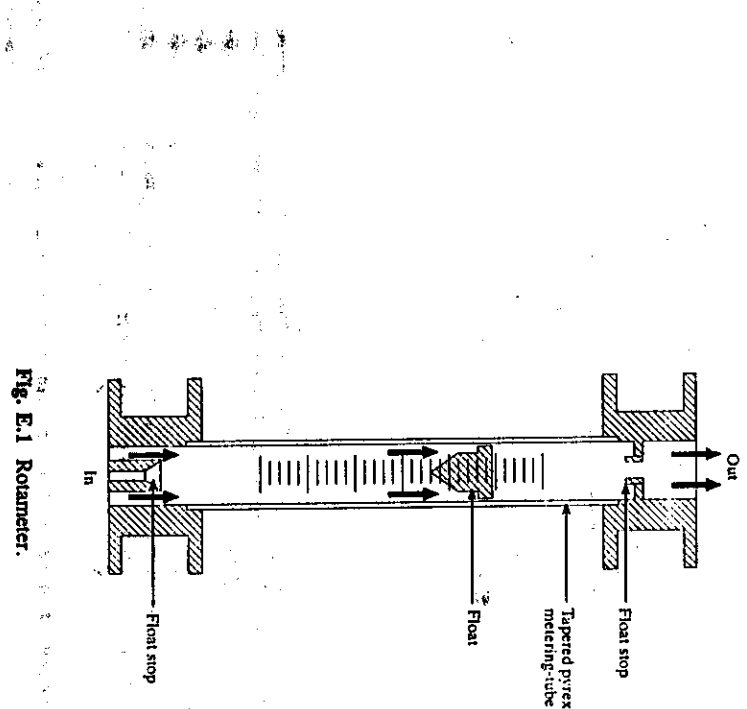
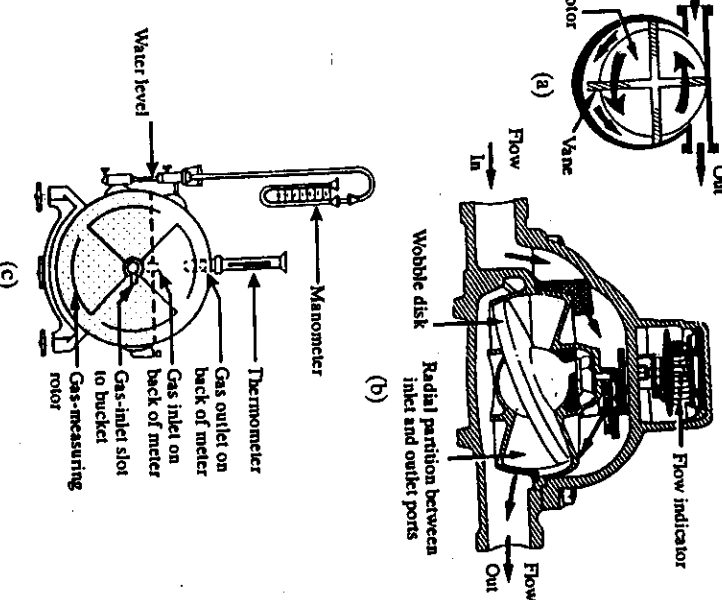


Fig. E.1 Rotameter.

\*The variety in designs of rotameters is so great that there does not exist one relationship valid for all types of rotameters to describe how the mass flow rate varies with height. The manufacturers usually supply calibration data for their devices, each set of data being appropriate for a specific fluid. Thus, if a gas mixture such as He plus 10% O<sub>2</sub> is being passed through a rotameter calibrated for He alone, then the user is fooling himself unless the rotameter is recalibrated for the He plus 10% O<sub>2</sub> mixture. One can also make use of a dimensional analysis of the system that would indicate how the physical parameters interact.<sup>1</sup>

When we apply a dimensional analysis to a float of a given geometry, the following functional relationship between dimensionless groups evolves

$$\frac{W}{D_f^4/m_f g \rho (1 - \rho/\rho_f)} = f \left[ \frac{\sqrt{m_f g \rho (1 - \rho/\rho_f)}}{\eta} \cdot \frac{D_f}{D_i} \right]. \quad (\text{E.2})$$



In some cases, for example, in pilot or bench-scale research work, the total flow through a line is required. There are many flow totalizers available, depending on the magnitude of the flow being studied. A common type is a volumetric meter, called the *rotary vane meter* (see Fig. E.2a), which is applicable for either liquids or gases. Such meters measure flows from approximately  $10^{-3} \text{ m}^3 \text{s}^{-1}$  to  $2 \text{ m}^3 \text{s}^{-1}$  with an accuracy of better than half of a percent.

For metering and totalizing liquids, the *rotating disk meter* is used (Fig. E.2b). It operates over a range from  $6 \times 10^{-5}$  to  $6 \times 10 \text{ m}^3 \text{s}^{-1}$  with an accuracy of one percent.

For totalizing gas flow, the *liquid-sealed gas meter* is employed (Fig. E.2c). This type is designed for the range from  $10^{-4} \text{ m}^3 \text{s}^{-1}$  to  $2 \text{ m}^3 \text{s}^{-1}$  and has an accuracy of about half of a percent.

#### Flow totalizers

## APPENDIX F

### Derivation of Eq. (9.62) for Semi-infinite Solids

From Chapter 9, we recognized that Eq. (9.54) satisfies the boundary conditions of Eqs. (9.60) and (9.61) along with the initial condition of  $f(x') = \theta_i$  (uniform). First, we put Eq. (9.54) in a more convenient form:

$$\theta = \frac{1}{2\sqrt{\pi\alpha x}} \int_0^\infty f(x') \left\{ \exp \left[ \frac{-(x-x')^2}{4\alpha x} \right] - \exp \left[ \frac{-(x+x')^2}{4\alpha x} \right] \right\} dx'. \quad (\text{F.1})$$

Next we change variables,  $\beta = (x' - x)/2\sqrt{\alpha x}$  and  $\beta' = (x' + x)/2\sqrt{\alpha x}$ , and substitute  $f(x') = \theta_i$ :

$$\frac{\theta}{\theta_i} = \frac{1}{\sqrt{\pi}} \int_{\beta=-\infty/\sqrt{\alpha}}^{\infty} e^{-\beta^2} d\beta - \frac{1}{\sqrt{\pi}} \int_{\beta=-\infty/\sqrt{\alpha}}^{\infty} e^{-\beta'^2} d\beta', \quad (\text{F.2})$$

or noting that primes are no longer necessary, we have

$$\frac{\theta}{\theta_i} = \frac{1}{\sqrt{\pi}} \left[ \int_{\beta=-\infty/\sqrt{\alpha}}^{\infty/2/\sqrt{\alpha}} e^{-\beta^2} d\beta + \int_{\beta=\infty/\sqrt{\alpha}}^{\infty/2/\sqrt{\alpha}} e^{-\beta^2} d\beta \right]. \quad (\text{F.3})$$

Figure F.1 schematically indicates these integrals, and shows that their sum results in

$$\frac{\theta}{\theta_i} = \frac{1}{\sqrt{\pi}} \int_{-\infty/\sqrt{\alpha}}^{\infty/2/\sqrt{\alpha}} e^{-\beta^2} d\beta = \frac{2}{\pi} \int_0^{\infty/2/\sqrt{\alpha}} e^{-\beta^2} d\beta. \quad (\text{F.4})$$

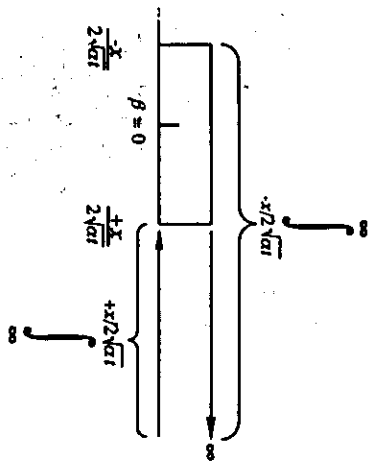


Fig. F.1 Schematic representation of the integral in Eq. (F.3).

The solution in its final form is

$$\frac{T_i - T}{T_i - T_f} = \operatorname{erf} \frac{x}{2\sqrt{\alpha t}}. \quad (9.62)$$

After predeposition the concentration of the dopant is given by the curve marked  $t = 0$  in Fig. 13.8. This becomes the initial distribution for the silicon wafer when it is subjected to drive-in diffusion. Assuming no loss of dopant from the surface, the boundary conditions and the initial condition for  $C(x,t)$  are given by Eqs. (13.52a,b,c). Now if we change the concentration to one that is relative to  $C_0$ , then Eqs. (13.52a,b,c) become

$$\frac{\partial}{\partial x} [C(0,t) - C_0] = 0, \quad (G.1)$$

$$C(\infty,t) - C_0 = 0, \quad (G.2)$$

and

$$C(x,0) - C_0 = f(x') - C_0. \quad (G.3)$$

If we make  $f(x')$  in Fig. 13.8 into an even function (e.g., as in Fig. 9.14b), then Eq. (9.48) applies with  $C - C_0$  substituted for  $T$  and  $D$  substituted for  $\alpha$ . For an even function,  $f(-x') = f(x)$  so Eq. (9.48) is written

$$C - C_0 = \int_{x=0}^{\infty} \frac{f(x') - C_0}{2\sqrt{\pi D t}} \left\{ \exp \left[ -\frac{(x+x')^2}{4Dt} \right] - \exp \left[ -\frac{(x-x')^2}{4Dt} \right] \right\} dx'. \quad (13.53)$$

## APPENDIX G

### Derivation of Eq. (13.53) for Drive-in Diffusion

- Abbaschian, R., 423  
 Absorptivity  
     definition, 370  
     of gases, 402  
 Absorption coefficient, 405  
     for viscous flow, 144  
 Activation energy, 431  
 Aggregate fluidization, 104  
 Alternating direction implicit method, 590  
 Aluminum quenching, 301  
 Analog, electric, 386-390  
 Anderson, A.R., 165  
 Angeles, O.F., 534  
 Archimedes number, 270  
 Area meters, 124, 637  
 Arrhenius equation, 431  
 Auman, P.M., 268  
 Austempering, 298  
 Average velocity, 42  
 Averbach, B.I., 422  
 Azbel, D., 262  
 $\beta$ -alumina, 440  
 Bag house, 138  
 Ball bearings, 324  
 Bamberg, M., 269  
 Banding, 505  
 Bardes, B., 350  
 Barone, R.V., 488  
 Basic oxygen steelmaking, 163  
 Beam lengths for gas radiation, 401  
 Bed, 101  
 Bedworth, R.E., 493  
 Bernoulli's equation, 113, 116-117, 153  
 application to flow from ladles, 131  
 application to pilot tube, 125  
 Bernstein, M., 235  
 Biesenberger, J.A., 34  
 Bills, P.M., 24, 25  
 Bingham plastics, 29  
 Blot number, 293, 299  
 Bird, R.B., 1, 203, 240, 523  
 Black body, 370  
 Black radiator  
     approximation of, 370-371  
     definition, 370  
 Blake-Kozeny equation, 94  
 Blasius, H., 65  
 Blowers, 15  
 Boiling heat transfer, 262  
 Boltzmann-Matano technique, 472  
 Boltzmann's constant, 372  
 Bonilla, C.F., 266  
 Boiret, M., 26, 27  
 Borg, R.J., 425  
 Boundary layer, 62  
     mass transfer, 528-529  
     momentum, 224  
     thermal, 224  
 Brake horsepower, 153  
 Brewster, M.Q., 374  
 Brice, J.C., 355  
 Bridgeman, 203  
 Brinacombe, J.K., 605  
 Brines used for quenching, 264  
 Brody, H.D., 488  
 Bromley, L., 10  
 Buckingham's Pi theorem, 248  
 Buffer layer, 603  
 Buoyant force, 70  
 Burnout, 263  
 Calderbank, P.H., 532  
 Carburation, 504  
     of iron, 551  
 Carburizing, 473, 490-497, 532-536  
     example of, 481-482  
 Carmahan, B., 581, 590  
 Carslaw, H.S., 293, 303, 469, 562  
 Carter, R.E., 440  
 Cast iron, 411  
 Cavitation, 147  
 Centipose, 6  
 Central differencing, 607  
 Centrifugal pump, 145-146  
 axial flow, 145  
 tangential, 145  
 Ceramic materials, 209, 507, 544, 591, 631  
 brick, 326  
 Cess, R.D., 374  
 Chang, P., 447  
 Chapman, T., 16, 18  
 Chapman-Enskog theory, 11, 13, 453  
 Characteristic boiling curve, 263  
 Characteristic energy parameter, 9  
 table of, 11  
 Chemical diffusion coefficient, 428  
 Chemical vapor deposition, 537  
 Chell, solidification against, 334-335  
 Cherenkov, N.P., 106  
 Chilton-Colburn theory, 531-533  
 Churchill, S.W., 255  
 Chvorinov's rule, 332  
 Clauisng factor, 561  
 Cohen, M., 422  
 Cohen, M.H., 447

- Colburn's analogy  
heat transfer, 251
- Collision cross section, 7
- Collision integral  
definition, 10
- graph, 455
- table, 12
- Collur, M.M., 566
- Complementary error function, 302
- Composite cylindrical wall, 286
- Concentration boundary layer, 528
- Conductance coefficient, 564
- Conductance of vacuum system  
components, 170
- definition, 170
- table, 171
- Conduction heat transfer  
through cylindrical walls, 233-235
- Configuration factor, 381
- (*see* View factor)
- Conservation of energy, 114
- Contact heat transfer coefficient, 274
- Contact resistance, during solidification,  
347-348
- Continuous annealing process, 235, 303
- Continuous casting, 342, 350-355
- example problem, 353-354
- fluid flow in, 143
- heat removal by mold, 353
- heat transfer in, 355
- machine, 363
- surface temperature during, 355
- thickness solidified, graph, 354
- Continuity equation
- Convection, natural, 258
- Converging-diverging nozzles, 161
- Cooling rates  
chart for determination of, 310
- Cooling water requirements, 353
- Core, 571
- Coring, 485
- Correlation coefficient,  $f$ , 424
- Crank, J., 469, 487
- Crank-Nicolson method, 580
- Crawford, R.J., 34

- Creeping flow around a solid sphere, 68-74
- Critical radius, 287
- Crystal growth, 355
- heat transfer during, 355
- Curved pipes, friction loss in, 123-124
- Cylinders, solidification times for, 331-332
- Czochralski-type crystal grower, 355
- Damper, 152
- Danckwerts, P.U., 536
- Darcy, 91
- Darcy's law, 90, 93
- Darken, L.S., 428, 430
- Darken's equation, 428
- Davison, J.F., 104
- Debroy, T., 566
- Debye, P., 188
- Deem, H.W., 375
- Deissler, R.B., 212
- De Laval nozzle, 160-162
- Dendrite arms, 485
- Dendritic arm spacing, 485
- Dendrit structures, 329, 485
- Derje, G., 450-451
- Desmond, R.M., 262
- DeWitt, D.P., 262, 375, 380
- Die castings, 334
- Diens, G.J., 425
- Diffuse surfaces, 374
- Diffusion  
in a moving gas stream, 513-516  
in a slab, 478  
in ceramic materials, 435  
in common liquids, 453  
in gases, 453-456  
in liquid metals, 448  
in liquids, 444  
in molten salts and silicates, 450  
in porous media, 457-459  
in solid circular cylinder, 478  
in spheres, 478  
into & falling liquid film, 516-519  
Knudsen, 457  
through a stagnant gas film, 510-513
- Diffusion anneal, 469
- Diffusion coefficient data  
in porous media, 457-459  
in solid ferrous alloys, 433-434
- inter-, in common liquids, 452
- inter-, in gases, 453
- inter-, in liquid ferrous alloys, 450
- inter-, in liquid nonferrous alloys, 449
- self-, in dilute solid alloys, 424
- self-, in liquid metals, 445, 449
- self-, in molten salts, 451
- self-, in pure solid metals, 423, 432
- Diffusion constants in Si, 443
- Diffusion couple, 470-480
- general, 523-526
- Diffusion in solids  
finite systems, 476-480  
intersitial alloys, 425  
steady-state, 463  
through cylinders, 464
- transient, 468
- Diffusion into a falling liquid film, 516-519
- Diffusion pump  
Ho coefficient, 176  
limiting forcepressure, 175  
multi-stage, 175  
speed of, 175-176  
ultimate pressure of, 176  
vapor trap, 176
- Diffusion through gases  
moving gas, 513-516  
stagnant gas, 510-513
- Diffusion through porous media, 457
- Diffusion volume, 456
- Diffusivity  
heat, 330  
momentum, 6
- Dilatant fluids, 29
- Dimensional analysis, 77
- Buckingham's Pi theorem, 248
- similarity technique, 77, 230
- Direct-exchange factor, 381
- (*see* View factor)
- Discharge coefficient, 128
- Dissipation function, 238
- Dissipation rate of turbulence energy, 604
- Dobbins, W.E., 537
- Donald, D.K., 359
- Drag coefficient, 83
- Drag force, 67
- Drag form, 70
- Dopants, 480
- Dougherty, D.L., 256
- Effective heat of fusion, 334
- Effective interdiffusivity, 457
- Effective jet radius, 164
- Effective thermal conductivity of packed bed, 212
- Effect of mold contour on solidification, 332
- Effect of superheat on solidification time, 334
- Efficiency  
of fans, 152
- of pumps, 146-147
- Effusion cells, 561
- Eian, C.S., 212
- Eigenvalues, 292
- Einstein, A., 14, 192, 421, 445
- Electors, 166
- Electro system, 166
- Electric analogs, 386-388
- Electric arcs, 315
- Electrical conduction, 436
- Electron beams, 315, 356
- Electron conduction, 436
- Electron-hole conduction, 436
- Electroslag remelting, 137, 338
- Elliott, J.F., 450, 563
- Elutriation, 108, 631
- Emissive power  
definition, 369
- Emissivity  
as function of view angle, 374  
as function of wavelength, 373  
of ferrous materials, 377  
of gases, 399  
of metal surfaces, 374-377  
of oxides, 376-377  
of several materials, 375  
of some ceramic materials, 376  
reduced, 399-400
- Emittance  
definition, 369
- Emulsions  
used for quenching, 264
- Energy equation, 236-242  
(*see* General energy equation)  
for conduction, 281

Energy transfer by radiation, 369

Epitaxial growth, 545  
Equation of continuity, 50, 51  
in cylindrical coordinates, 57  
in rectangular coordinates, 57  
in spherical coordinates, 57

of  $A$  in various coordinate systems, table, 525

Equation of energy in terms of energy and momentum fluxes, 241

(*see* Navier-Stokes' equation)

in cylindrical coordinates, 59  
in rectangular coordinates, 58  
in spherical coordinates, 60

Equivalent diameter for noncircular conduits, 117

Equivalent length for various fixtures, 123  
Ergun's equation, 93, 97

friction factor associated with, 96  
Error, N., 440

Error function complementary, 302  
definition, 308  
table, 303

Eucken, A., 191  
Euler method, 571, 574

Evans, J. W., 605  
Evaporation, 512

Evaporation constants, 565  
table, 567

Exchange between infinite parallel plates, 378  
figure, 129  
for flow meters, 129  
table, 129

Extended Nernst-Einstein equation, 437  
Eyring, H., 15

Eyring theory, 446  
Eyring's theory of viscosity, 15

Falling film flow, 39-41  
average velocity in, 42  
maximum velocity in, 42  
velocity distribution in, 43

volume flow rate in, 43  
Falling-sphere viscometer, 71  
Fan laws, 155

Fanning equation, 117  
Fan, 118, 137, 151-158  
Fan characteristics, 152

Fan laws, 155  
Fans

characteristic curve, 152  
horsepower of, 153  
interaction with system, 154-158  
pumping limit of, 154  
static efficiency, 153  
total efficiency, 153  
Fermi energy, 196  
Fick's first law, 419  
of diffusion, 420  
Fick's second law, 428, 469  
of diffusion, 525  
*FIDAP* software, 605  
Film boiling, 263, 267  
Film penetration theory, 537  
Film theory, 535  
Finite difference approximation, 571  
method, 578  
First law of thermodynamics, 113  
Flemings, M.C., 350, 485, 488-489  
Floating-zone process, 355  
Flood, S.C., 606  
Flow  
laminar, 3  
streamline, 3  
turbulent, 3  
Flow, creeping, around a sphere, 68  
momentum-flux distribution in, 69  
normal forces in, 70  
pressure distribution in, 69  
velocity components, 69  
Flow between parallel plates, 44  
average velocity in, 45  
maximum velocity in, 45  
shear stress distribution in, 45  
velocity distribution in, 45  
volume flow rate in, 45  
Flow coefficient, for meters, 128  
Flow in noncircular conduits, 81-82  
Flow measurement, 124-131  
area meters, 637  
(*see* Velocity meters, Head meters, and Area meters)

Flow nozzle, 127

Flow of a falling film, 41

flow over a flat plate, 62

boundary layer in, 62-66

drag force in, 67

Reynolds number for, 63, 66

Flow past a sphere, 85-90

Flow through a circular tube, 46

average velocity in, 48

example problem, 48

maximum velocity in, 47  
Newtonian fluids, 46  
Power law non-Newtonian fluids, 49  
velocity distribution in, 47  
volume flow rate in, 48  
Flow through fluidized beds, 101  
Flow through piping networks, 135  
Flow through valves and fittings, 122-123  
Flow totalizers, 639  
Fluctuation theory, 447  
*FLUENT* software, 605  
Fluidity, 15  
Fluidized, 101  
Fluidized beds, 101-112  
applications of, 106-107  
elutriation in, 108  
particulate fluidization, 101, 105  
Reynolds number in, 103  
Fluids  
Newtonian, 29, 42  
Non-Newtonian, 29  
Rheoplectic, 31  
Flux  
Galileo number, 104  
Ganesan, S., 100  
Gas phase transport control, 553  
Gas-solid reactions, 551  
models of, 560  
Gas temperature, 397  
Gases  
absorptivity, 399  
collision diameters in, 455  
diffusion coefficients in, 454  
diffusion in, 453-456  
diffusion in binary gases, 464  
emissivity, 399  
reduce emissivity, 399-400  
thermal conductivity of, 190-192  
transmissivity, 403  
viscosity of, 7-13  
Geiger, G.H., 531  
General energy equation  
components of, 236-240  
in curvilinear coordinates, 240  
in cylindrical coordinates, 240, 242  
in rectangular coordinates, 240, 242  
in spherical coordinates, 240, 242  
General equation of continuity, 524  
Frantz, J.F., 103  
Frenkel defect, 435  
Frenkel, J., 13  
Frequency factor, 431  
Freihahn, R.J., 532  
Friction drag, 85  
Friction factor, 76  
dimensional analysis for, 77-79  
experimental results, 79  
for flow in rectangular ducts, 82  
Glass, thermal conductivity of, 203  
Glasses, 370

- Cosman, A.D., 605  
 Grain-boundary diffusion, 433  
 Graphite, 533  
 Grashof number  
     for heat transfer, 231  
     for mass transfer, 531-532  
     for natural convection, 258  
 Gray bodies, 373, 378  
 Green, H.S., 16  
 Griffiths, D.K., 268  
 Grossmann, M.A., 264  
 Grube solution, 470  
 Gruneisen's constant, 193  
 Gupta, R., 106  
 Gunney-Lure charts, 293  
 Guthrie, R.I.L., 20, 205, 446, 581  
 Hagen-Poiseuille law, 48  
 Harrison, D., 104  
 Hauffe, K., 435  
 Head  
     friction, 146  
     net positive suction, 147  
 horizontal cylinders, 259  
 horizontal surfaces, 261  
 vertical plates, 259  
 Heat transfer during crystal growth, 355  
 Heat transfer for natural convection, 228-  
     233, 258  
 Heat transfer from a sphere to a flowing  
     fluid, 256  
 Heat transfer in fluidized beds, 268  
 Heat treatment, 262, 407, 486, 560  
     of a continuous sheet of steel, 407  
 Heisler charts, 293  
 Higbie, R., 536  
 Hill, D.R., 268  
 Hills, A.W.D., 350, 352,  
     Ho coefficient, 176  
 Hollraum, 371  
 Hole theory of liquids, 13, 446  
 Holman, J.P., 255, 262, 380  
 Homogenization, 486-491  
     of alloys, 485  
 kinetics, 582  
 Hopkins, B.E., 435  
 Horsepower, 147  
 Hoti, H.C., 374, 376, 392, 400  
 Hot-wire anemometer, 257  
 Howell, J., 374  
 Hughmark, G.A., 531  
 Hydraulic radius, 93  
 Hydrodynamical theory, 444  
 Hydrogen, 544  
 Removal from metal, 550  
 for quenching oils, 265  
 for water-spray cooling, 268  
 in aqueous quenching media, 267  
 liquid metals, 251  
 of natural convection from horizontal  
     surfaces, 261

- on the casting side of interface, 347  
 on the mold side of interface, 347  
 over a flat plate, 224-228  
     average, 225  
     local, 225  
 radii, 396  
 total, 396  
 total, across metal-mold interface, 347-  
     349  
 Heat-transfer coefficients for  
     flow over a flat plate, 250  
     flow past a sphere, 255  
     flow through packed beds, 272  
 Heat-transfer coefficients for natural  
     convection for  
         horizontal cylinders, 259  
         horizontal surfaces, 261  
         vertical plates, 259  
 Heat transfer during crystal growth, 355  
 Heat transfer for natural convection, 228-  
     233, 258  
 Heat transfer from a sphere to a flowing  
     fluid, 256  
 Heat transfer in fluidized beds, 268  
 Heat treatment, 262, 407, 486, 560  
     of a continuous sheet of steel, 407  
 Heisler charts, 293  
 Higbie, R., 536  
 Hill, D.R., 268  
 Hills, A.W.D., 350, 352,  
     Ho coefficient, 176  
 Hollraum, 371  
 Hole theory of liquids, 13, 446  
 Holman, J.P., 255, 262, 380  
 Homogenization, 486-491  
     of alloys, 485  
 kinetics, 582  
 Hopkins, B.E., 435  
 Horsepower, 147  
 Hoti, H.C., 374, 376, 392, 400  
 Hot-wire anemometer, 257  
 Howell, J., 374  
 Hughmark, G.A., 531  
 Hydraulic radius, 93  
 Hydrodynamical theory, 444  
 Hydrogen, 544  
 Removal from metal, 550  
 for quenching oils, 265  
 for water-spray cooling, 268  
 in aqueous quenching media, 267  
 liquid metals, 251  
 of natural convection from horizontal  
     surfaces, 261
- on the casting side of interface, 347  
 on the mold side of interface, 347  
 over a flat plate, 224-228  
     average, 225  
     local, 225  
 radii, 396  
 total, 396  
 total, across metal-mold interface, 347-  
     349  
 Heat-transfer coefficients for  
     flow over a flat plate, 250  
     flow past a sphere, 255  
     flow through packed beds, 272  
 Heat-transfer coefficients for natural  
     convection for  
         horizontal cylinders, 259  
         horizontal surfaces, 261  
         vertical plates, 259  
 Heat transfer during crystal growth, 355  
 Heat transfer for natural convection, 228-  
     233, 258  
 Heat transfer from a sphere to a flowing  
     fluid, 256  
 Heat transfer in fluidized beds, 268  
 Heat treatment, 262, 407, 486, 560  
     of a continuous sheet of steel, 407  
 Heisler charts, 293  
 Higbie, R., 536  
 Hill, D.R., 268  
 Hills, A.W.D., 350, 352,  
     Ho coefficient, 176  
 Hollraum, 371  
 Hole theory of liquids, 13, 446  
 Holman, J.P., 255, 262, 380  
 Homogenization, 486-491  
     of alloys, 485  
 kinetics, 582  
 Hopkins, B.E., 435  
 Horsepower, 147  
 Hoti, H.C., 374, 376, 392, 400  
 Hot-wire anemometer, 257  
 Howell, J., 374  
 Hughmark, G.A., 531  
 Hydraulic radius, 93  
 Hydrodynamical theory, 444  
 Hydrogen, 544  
 Removal from metal, 550  
 for quenching oils, 265  
 for water-spray cooling, 268  
 in aqueous quenching media, 267  
 liquid metals, 251  
 of natural convection from horizontal  
     surfaces, 261

- transient heat conduction, 305  
 Ingots, 334  
 Insulation, 287, 321  
     critical radius of, 287  
     effect of, 283  
 Interatomic spacing, 18, 423  
     table, 19  
 Interdendritic liquid, 485  
 Interdiffusion, 448, 450,  
     Interdiffusion coefficient, 428  
     in ferrous materials, 434  
     in nonferrous metals, 432  
 Internal temperature gradients, 290  
 Interface resistance, 342-346  
 Internal temperature gradients, 290  
 Intrinsic diffusion coefficient, 425  
 Intrinsic speed of vacuum pumps, 173  
 Ion implantation, 482, 507  
 Iron ore sinter plant  
     pressure drop across, 98-100  
 Iron oxide  
     effect on slag viscosity, 22, 24-25  
 Isentropic shockless flow, 162  
 Ishida, T., 567  
*j*-factor  
     heat transfer, 251  
     mass transfer, 529  
 Jacobbi, H., 350  
 Jaeger, J.C., 293, 303, 469, 562  
 Jain, V.K., 275  
 Jensen, K.F., 541  
 Jets, supersonic  
     area of interaction with bath, 158  
     impact pressure, 159-165  
     length of core, 164  
     momentum of, 164  
     spreading of jet, 163  
 Johns, F.R., 165  
 Joniny end-quench test, 310  
 Jost, W., 435, 469, 474, 485  
 Jump frequency, 423  
     structure of, 456  
     thermal conductivity in, 197  
 Liquid phase control, example of, 565-566  
 Liquid-sealed gas meter, 639  
 Local mass transfer coefficients, 520  
 Log mean, 512  
 Long horizontal cylinders, 259  
 Long-time solutions, 300
- Kinetic theory of gases, 7, 453  
 Kirchoff's law, 389  
 Kirkaldy, J.S., 431, 513  
 Kirkendall effect, 426  
 Kirkwood, J.G., 16  
 Kitaev, B.I., 273  
 Knudsen, 168, 170  
 Knudsen diffusion, 457  
     coefficient, 457  
 Knudsen effusion cells, 560-562  
 Kofstad, P., 435  
 Kreith, F., 400  
 Kubaschewski, O., 435  
 Kucharski, M., 21  
 Kunii, D., 106  
 Kroger, F.A., 435  
 Kwank, M., 103  
 Ladies  
     discharge coefficient for, 132  
 flow front, 131  
 time to empty, 133  
 Laminar flow, 3  
 Laminar sublayer, 603  
 Langhaar, H., 68  
 Langville, A.H., 636  
 Laplace equation, 282  
     written in cylindrical coordinates, 285  
 Lasers, 309-310, 318  
     beams, 315, 356  
 Laser welding, 566, 569  
 Latent heat, 330  
 Launder, B.E., 603, 605  
 Law of conservation of momentum, 54  
 Lead, diffusion in, 460  
 Lenard-Jones potential, 9, 11, 18, 464  
 Leva, M., 103  
 Leverpiel, O., 106  
 Levitation melting, 412  
     mass transfer during, 543  
 Lewis, W.K., 535  
 Li, J.C.M., 447  
 Lightfoot, E.N., 203, 240, 523  
 Liquid metals, 259  
     diffusion in, 445  
 Liquid phase control, example of, 565-566  
 Liquid-sealed gas meter, 639  
 Local mass transfer coefficients, 520  
 Log mean, 512  
 Long horizontal cylinders, 259  
 Long-time solutions, 300

- Lorenz number, 196  
 Love, T.J., 374  
 Lucks, L.F., 375  
 Luther, H.A., 581, 590  
 Mach number, 160, 164–165  
 Machlin, E.S., 563  
 Manganese vaporization from molten steel, 566  
 Mapother, D., 437  
 Marangoni effect, 521  
 Marchello, J.M., 537  
 Marcusen, L., 215  
 Marshall, W.R., Jr., 256  
 Martonik, L.J., 532  
 Mass flux vector, 524  
 Mass transfer, 509 correlations involving gas bubbles, 532  
 gas-liquid, 531 to spheres, 531  
 average, 520 definition, 519 for laminar flow over a flat plate, 528 local, 520 model, 535–537  
 Mass transfer coefficient film penetration theory, 537 two-resistance theory, 547–551 Mass transfer  $i$ -factor, 529–530 Mass transfer Nusselt number, *Nu<sub>M</sub>*, 520 Mass transfer resistances, 548 Matao interface, 474–475 Maximum velocity, 42 Maxwell-Boltzmann distribution of velocities, 168 McAdams, W.H., 255, 258, 261 Mechanical energy equation, 113 Mechanical vacuum pumps intrinsic speeds, 173 positive displacement, 173 rotary piston, 173 Melt spinning, 366 Metallurgical length, 355 Method of separation of variables, 291 Microsegregation, 485, 582 Microaggregates, 329 Minimum fluidization, 102 Minimum void fractions, 633 Mixed control of reactions gas-liquid, 547–551 gas-solid, 551–560
- Mixed mean temperature, 247 Mobility, 15, 429 in an electrical field, 436, 496 self-diffusion, 422 Models of gas-solid reactions, 560 Molar average velocity, 509 Mold length, 353 Mold material, 361 Molecular flow, 166, 168 Molecular flow mechanics, 168–173 Molecular liquids, viscosity of, 15 Molecular pumps, 178 Molten plastics, 29 Momentum conservation, law of, 54 convective, 52 flux, 42 general equations, 50–56 viscous, 53 Momentum balance, 39 for flow between parallel plates, 44 for flow in a tube, 46 in a falling film, 40, 41 Momentum boundary layer, 226, 229 Momentum diffusivity, 225 Momentum equation cylindrical coordinates, 59 rectangular coordinates, 58 spherical coordinates, 60 Momentum transport, 5 Monochromatic emissive power, 372 Moore, M.R., 350, 352 Morgan, E.R., 267 Moving line source, 319 Moving point source, 315 Mrowec, S., 425 Mutual diffusion coefficient, 428
- Nanda, C.R., 531 Nandapunkar, P.J., 100 Natural convection heat transfer, 259, 261 mass transfer, 529 Navier-Stokes' equation, 50, 55, 56 Nemst-Einstein equation, 429 extended, 437 Net positive suction head, 147 Newtonian fluid, 5 Newtonian heating or cooling, 288 conditions for validity, 288, 299 example problem, 289 Newton's law of viscosity, 6, 55 No-net-flux surfaces, 390
- figure, 392 Noncircular conduits, 81–82 Nonmetallic stoichiometric compounds, 429 mean free path of, 193 Photon contribution to thermal conductivity, 200 Pickling, 157 Pigford, R.L., 254, 518 Pilling and Bedworth constant, 493 Pillig, N., 493 Pitot static tubes, 124–126 Planck's constant, 372 Planck's distribution law, 372 Planck's equation, 372 Poirier, D.R., 100, 488 Poise definition, 6 units, 6 Polyethylene-glycol, 265 Polyethylene, 313, 363 Polymer solutions used for quenching, 264 Polymers, 30, 466, 500, 631 Ostwald power law, 29 Overall evaporation constants, 567 Overall mass transfer coefficients, 547 Overall rate constant, 565 Oxidation parabolic, 497–498 parabolic rate constants, 498 Oxide layers, 491 Oxides defect structures in, 438 thermal conductivity of, 193–194, 200 data, 194 Packed beds, heat-transfer coefficient in, 272 Pape, P.O., 273 Parabolic oxidation constants, 493 Particulate materials, 631 Paul, A., 566 Pauling, L., 445 Pauly, S., 466 Paschkis, V., 266–267, 303 Peak temperature, 317 Peclet number, 317, 520 Pelletizing, 155 Penetration theory, 536 Permanent mold castings, 334 Permeability, 90, 92, 466 data, 466 specific permeability, 91 Peterson, N.I., 485, 513

- Precipitation-hardenable aluminum alloys, 264  
Predisposition, 480  
Pressure drop for flow across a packed bed, 94, 95  
for flow through fittings, 122-123  
for flow through a pipe, 80  
Pressure pouring, 142  
Price, J.B., 438  
Prinz, B., 269  
Product solutions, 313-315  
example of, 313  
figure illustrating, 314  
Pseudoplastics fluids, 29  
Pumpdown time, 177  
Pumping limit of fans, 154  
Pumping speed effective, 172  
of vacuum pumps, 172-173  
units, 173  
Pumps (*see* Vacuum pumps)  
centrifugal, 145-146, 148  
characteristic curve, 148  
diffusion, 175  
efficiency of, 148  
positive displacement, 145-146  
reciprocating, 145  
rotary, 145  
Quenchants, 264  
Quenching aluminum, 266, 289  
heat transfer coefficients in, 264-269  
heat transfer in, 262-268  
of steel sheet, 140, 264  
oils, 264-268  
salt solutions, 264  
Radiance, 369  
Radiant heat transfer, 369  
between infinite parallel plates, 378-381  
electrical analog of, 387  
within furnaces, 383, 384  
Radiant furnace, 407  
Radiant thermal conductivity, 195  
Radiant-flux density, 369  
Radiation from gases, 398-404  
Radiation heat transfer ceramics, 404  
glasses, 404

- Ruddle, R.W., 350  
Radiation heat-transfer coefficient, 396  
Radiation shields, 380  
Radioactive tracers, 459  
Radiosity total, 370  
Ranz, W.E., 256  
Rate-determining step, 417  
Rational rate constant, 495  
Read, C.M., 606  
Recirculating flows, 598  
Reduced emissivity, 399  
of carbon dioxide, 400  
Reduced temperature, 16  
Reduced viscosity, 16  
Reduced volume, 16  
Reed-Hill, R.E., 423  
Reflectivity, 370  
Refractory walls, 391  
Reheat furnace, 413  
Reid, R.C., 454  
Relative interface temperature during freezing, graph, 340  
Relative position, 293  
Relative roughness, 79  
Relative temperature, 293  
Residual segregation index, 488  
Resistance concept, 283  
Reynik, R.J., 447  
Reynolds, 4  
Reynolds, J.E., 422  
Reynolds number, 4, 63, 78, 446  
for flow over a flat plate, 63, 66  
for flow past submerged objects, 87  
for flow through fluidized beds, 103  
for flow through packed beds, 95, 96  
local, 66  
transition from laminar to turbulent flow, 75, 79  
Rheology, 29  
Rheoplectic fluids, 31  
Richardson, F.D., 440  
Ring mechanism, 425  
Rodriguez, F., 34  
Rogers, S., 606  
Roisenow, W.M., 251, 259, 263  
Roots pump, 174  
Rosenthal, D., 317  
Rotary vane meter, 639  
Rotameter, 131-132, 637  
Rotating disk meter, 639  
Roughness effect on heat transfer, 251  
table, 80  
values, 80
- Ruddle, R.W., 350  
Salt solutions, heat transfer in, 264  
Sands diffusion in, 450  
thermal conductivity of, 207  
Sand solidification in, 329-334  
thermal conductivity of, 214-215  
Sarofim, A.F., 374, 376, 394, 400  
Sauterfield, L.N., 458  
Saunders, O.H., 273, 413  
Saxton, H., 448  
Schack, A., 194, 199  
Schmidt number definition, 520  
Schneider, P.J., 309, 407  
Sebastien, D.H., 256  
Sebastien, R.A., 256  
Seed crystal, 356  
Segregation index, 488  
Self-diffusion, 421-424  
in liquid metals, 445  
Self-diffusion coefficients for pure metals, 423  
Self-diffusion mobility, 422  
Semiconductor crystals, 355  
Semiconductors, thermal conductivity of, 200  
Semi-infinite bar, 470  
Semi-infinite body, solution of heat flow equation for, 341  
Semi-infinite plate, steady-state, conduction through, 282  
Semicircularity, 293  
Separation constant, 291  
Separation of variables, 291  
Severity of quench, 264  
Shape factor 4, 96  
Shape factor, 96, 97  
table, 97  
Shape factor for screened particles, 97  
Shape factor for solidification in sand molds, 332-333  
Shear stress, 5  
Sheet glass, 413  
Sheet, heating of with radiation, 407-409  
Shell mold, 413, 577  
Sherby, O.D., 432, 448
- Sherwood number definition, 520  
prediction in gas-liquid transfer, 527  
Sherwood, T.K., 250, 454, 458  
Shewmon, P.G., 423  
Shock wave, 162  
Short-time solutions, 300  
Siegel, R., 374  
Sievert's law, 465  
Sieving, 631  
Silica equivalence of aluminum oxide, 23  
Silicate glass, 441  
Silicate melts, 370  
Silicon, 507, 542, 643  
oxidation of, 556  
Similarity technique, 77-79  
Simnad, M.T., 432  
Singh, S.N., 489  
Sinha, A.K., 264  
Sintering, iron ore, 98  
Slags structure of, 22-24  
thermal conductivity of, 206-208  
viscosity of, 22-29  
Slurries, 29  
Soldering, 367  
Solidification against a chill, 334-338  
convection during, 100  
effect of mold contour on, 332  
in a sand mold, 329-331  
interface resistance during, 342-346  
rate, 329, 335  
time of a casting, 331  
Spalding, D.B., 603, 605  
Spanow, E.M., 374  
Specific permeability, 91  
Specular surfaces, 374  
Sphere (*see* Flow around a sphere)  
buoyant forces on, 70  
form drag on, 70  
friction drag on, 70  
solidification time for, 337-339  
Spray, heat transfer with, 268-269  
Sprays, heat transfer with, 268-269  
Spray-ion pumps, 180  
Stagnation temperature, 165  
Stanton number, 251  
Static efficiency, 153  
Steady-state conduction through

composite cylinder, 286–285  
in a composite wall, 283  
in a flat plate, 282  
in a hollow cylinder, 285  
in an infinite cylinder, 295  
infinite cylinders, 293, 295  
infinite plates, 293–294  
spheres, 293, 296–297  
Steam injectors, 177–179  
pumping capacity, 178  
Stefan-Boltzmann constant, 186  
equation, 372  
Stewart, W., 203, 240  
Stewart, W.E., 523  
Stoke, 6  
Stokes-Einstein equation, 445  
Stokes' law, 71, 445, 631  
Stolz, G., 265–267  
Stream function, 65  
Streamline flow, 3  
Streeter, V.L., 54, 69  
Sun, R.C., 409–410  
Superheat, effect of on solidification time, 324  
Super ionic conductors, 440  
Supersonic core, 164  
Supersonic nozzles  
design of, 158–165  
exit velocity, 162  
mass flow rate from, 159–165  
Surface area of particles  
for irregular particles, 96–97  
per unit volume of bed, 96  
per unit volume of particles, 95  
267  
Surface condition, effect on nucleate boiling, 560–563  
Surface depletion, 433  
Surface diffusion, 433  
Surface renewal theory, 536  
Surface resistance, effect of on temperature distribution in semi-infinite solid, 306–310  
Sutherland-Einstein equation, 445  
Swalin, R., 447  
Szekely, J., 605  
Tammann, G., 493  
Tammann scaling constant, 493  
Taylor, H.F., 332  
TEACH 2-E software, 605  
Temperature distribution  
in infinite solids, 307  
in semi-infinite solids, 308–310  
Thermal diffusivity, 225  
Thermal gradients, 357

Temperature history in a semi-infinite solid with surface resistance, 309  
Temperature profile, fully developed, 221  
Temperature response for infinite cylinders, 293, 295  
infinite plate, 293–294  
spheres, 293, 296–297  
Temperature furnace, 397  
Temporal mean velocity, 4  
Terminal velocity, 71, 89, 103  
Thermal boundary layer, 226, 229  
Thermal conductivity, 187–218  
in aluminum alloys, 197  
of amorphous or molecular solids, 202  
of bulk materials, 208  
carbides, 201  
cermets, 208  
of common gases, 191  
of dielectric materials, 193  
of gases, 190–191  
in glasses, 203  
of graphite, 201  
of highly basic silicate melts, 206  
of insulating materials, 194  
of liquid metals, 197  
of liquids, 203–208  
of materials, 188  
of metal-matrix composites, 208  
of molding sands, 203–205  
of nickel and nickel-base alloys, 198  
of nitrides, 201  
of oxides, 194, 200  
of packed beds, 211–214  
of polyatomic gases, 191  
of polymers, 203  
of powder metal compacts, 211  
of pure iron and iron-base alloys, 199  
of pure metals, 196  
of semiconducting compounds, 200  
of silica sand molds, 214  
of slag, 205, 208  
in solids and alloys, 196  
slags, 207  
of solid and molten  $\text{CaO-SiO}_2\text{-Al}_2\text{O}_3$   
207  
of solid metals, 205  
of solids, 191  
of steels, 199  
of two-phase mixtures, 210, 212  
of various liquids, 205  
Thermal diffusivity, 225  
Thermal gradients, 357

Thermal radiation  
definition, 369  
Thermal resistance, 283, 287  
fluid-solid interface, 285  
infinite cylinder, 285  
infinite slab, 283  
Thermal shock, 410  
Thermal stresses, 409  
Thermocouple, 396  
effect of radiation on indicated temperature, 396  
Thickness of solidified layer in chill molds, 334–338  
in sand molds, 330  
Thixotropic fluids, 31  
Throughput in vacuum technology, 166  
Toor, H.L., 537  
Tortuosity, 457  
Total exchange factor, 391–394  
Total head, 147  
Total heat-transfer coefficient, 396  
Total hemispherical emissivity, 374  
of window glass, 406  
Total hemispherical radiation intensity, 369  
Total irradiation, 370  
Total molar flux, 509  
Total radiosity, 370  
Total solidification time, 330  
Touloukian, Y.S., 375  
Tracer atom, 423  
Tracer, diffusion coefficient with, 424  
Tracers, 469–480  
Transference number, 437, 494  
Transient conduction with radiation, 407–409  
Transition metal oxides, 436  
Transmission probability, 169  
Transmissivity  
definition, 370  
of gases, 402–404  
Tube bundle theory, 93  
Turbulence, 598  
Turbulence layer, 604  
Turbulent flow, 3  
in pipes, transition value of  $Re$ , 75  
Turbulent layer, 603  
Turbulent mass diffusivity, 605  
Turbulent thermal conductivity, 605  
Turkdogan, E.T., 25, 446, 454, 455  
Turnbull, D., 447  
Tuyeres, 106

Umklapp collision, 193  
Units  
diffusion coefficient, 420  
heat flux, 188  
heat-transfer coefficient, 186  
kinematic viscosity, 6  
mass flux, 420  
mass transfer coefficient, 519–523  
molar flux, 420  
thermal conductivity, 188–189  
viscosity, 6  
Universal velocity profile, 603  
Unsteady-state heat conduction, 300  
Up-hill diffusion, 428  
Upwind finite difference method, 608  
Urbain, G., 26, 27

Vacancies, 421  
Vacancy mechanism, 425  
Vacuum arc melting, 338  
Vacuum  
annealing, 166  
arc melting, 338  
degassing, 166, 183  
gauges, 167  
melting, 166  
processes, 166  
pumps, 167  
units of, 166  
Vacuum melting system  
Pump-down speed, 172  
Vacuum melting, 560  
vaporization during, 560, 563–567  
Vapor pumps  
characteristic curve, 174, 176  
diffusion, 175  
intrinsic speed of, 173  
limiting forepressure, 175  
mechanical, 173  
ultimate pressure, 174  
Valves  
equivalent length of, 123  
table, 123  
Vapor deposition, 411  
Vapor diffusion pumps, 166  
Vaporization (see Evaporation constants)  
during melting, 563–567  
from liquid metals, 563  
Knudsen cell, 560

